Proceedings of the International Conference on the Interactions of Neutrons with Nuclei

Technical Information Center
Energy Research and Development Administration

NOTICE

Available from the National Technical Information Service, U. S. Department of Commerce, Springfield, Virginia 22161

Price: Paper Copy $21.25 (domestic)
$23.75 (foreign)
Microfiche $2.25 (domestic)
$3.75 (foreign)

Printed in the United States of America
USERDA Technical Information Center, Oak Ridge, Tennessee

CONF 760715-P1
Distribution Category UC 34c

INTERNATIONAL CONFERENCE ON THE INTERACTIONS OF NEUTRONS WITH NUCLEI

VOLUME I (MAIN SESSIONS)

PROCEEDINGS OF A CONFERENCE
LOWELL, MASSACHUSETTS, U.S.A.
JULY 6 - 9, 1976

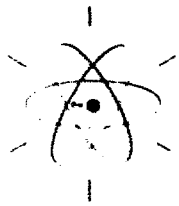

EDITOR:

ERIC SHELDON

ASSOCIATE EDITORS:

GUS P. COUCHELL

SUSAN A. GOODWIN

SURESH C. MATHUR

DAVID J. PULLEN

UNIVERSITY OF LOWELL
LOWELL
MASSACHUSETTS 01854
U.S.A.

SCIENTIFIC SPONSORS

THE INTERNATIONAL UNION OF PURE AND APPLIED PHYSICS

THE AMERICAN NUCLEAR SOCIETY

THE AMERICAN PHYSICAL SOCIETY

THE INSTITUTE OF PHYSICS (U.K.)

U.S. ENERGY RESEARCH AND DEVELOPMENT ADMINISTRATION

U.S. NATIONAL SCIENCE FOUNDATION

UNESCO SUBVENTION - 1976 - DG/2.1/414/4/ (IUPAP)

Dedicated to the Illustrious Memory
of
JAMES CHADWICK and ENRICO FERMI

JAMES CHADWICK
(1891 - 1974)

[Photograph courtesy of The American Institute of Physics, Meggars Gallery of Nobel Laureates]

ENRICO FERMI
(1901 - 1954)

[Photograph courtesy of University of California, Los Alamos Scientific Laboratory, New Mexico]

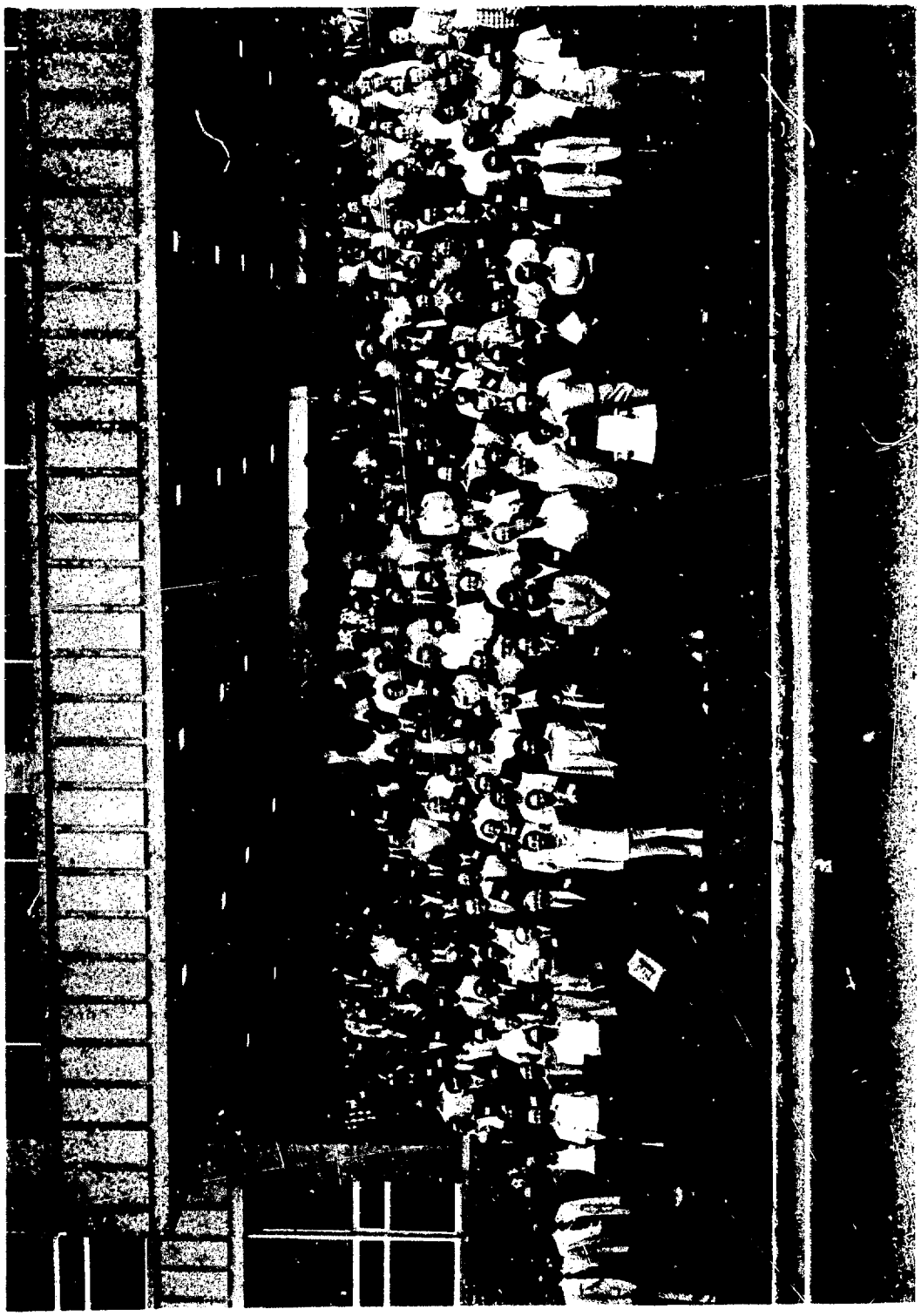

THE WHITE HOUSE

WASHINGTON

June 4, 1976

It gives me great pleasure to extend a warm welcome to the many distinguished participants who will be devoting their knowledge, insight and wisdom to reviewing the latest progress and surveying the prospects for the future of neutron physics at the International Conference on the Interactions of Neutrons with Nuclei to be held at the University of Lowell.

Those who are concerned with this important area of scientific research have contributed significantly to our understanding of the fundamental nature of matter and to the discovery of fission and the harnessing of nuclear energy.

I hope that your sessions will prove stimulating and rewarding for all who attend and that your discussions will pave the way to new scientific progress for the lasting benefit of all mankind.

Gerald R. Ford

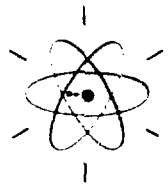

1976 International Conference on the Interactions of Neutrons with Nuclei

Very appreciative thanks are expressed to the following for generous assistance, encouragement, interest and support:

THE UNIVERSITY OF LOWELL

The Board of Trustees
The President, Dr. John B. Duff
The Executive Vice President, Dr. Everett V. Olson
The Provost, Dr. Leon E. Beghian (ICINN Executive Officer)
The Deans, Faculty, Students, Officers and Staff

ICINN LOCAL COMMITTEE

Iris Beghian
Frederick B. Bischoff
C. Daniel Cote
Gus Couchell
M. Brendan Fleming
F. Raymond Hardy
James Phelps
David J. Pullen
Malcolm K. Smith
George J. Toscano

ICINN REGISTRATION COMMITTEE

James H. Doherty, Jr.
Donald T. Donati
James J. Egan
Arthur Mitten
Walter A. Schier
Nancy E. Sullivan

ICINN SECRETARIAL STAFF AND AIDES

Arlene Dillon
Jacquelyn Jones
Claude Dozois

UNIVERSITY OF LOWELL, DIVISION OF CONTINUING EDUCATION

Ernest P. James
David H. Priester

UNIVERSITY OF LOWELL PRESS AND COMMUNITY RELATIONS

Dr. Herman V. LaMark
Linda M. Frawley
John Brus

UNIVERSITY OF LOWELL RESEARCH FOUNDATION

UNIVERSITY OF LOWELL ALUMNI ASSOCIATION

GRANT-AWARDING AGENCIES

International Union of Pure and Applied Physics
Massachusetts Department of Commerce and Development
U. S. National Science Foundation
U. S. Energy Research and Development Administration

COMMERCIAL AND INDUSTRIAL EXHIBITORS, SPONSORS AND CONTRIBUTORS

THE LOCAL COMMUNITY

Co-sponsored by The International Union of Pure and Applied Physics, The American Nuclear Society, The American Physical Society, The Institute of Physics (U K)

1976 International Conference on the Interactions of Neutrons with Nuclei

Conference Chairman:
Dr. Eric Sheldon

Scientific Deputy Chairman:
Dr. Suresh C. Mathur

Administrative Deputy Chairman:
Dr. Susan A. Goodwin

Conference Telephone
(617) 458-9592

ORGANIZING COMMITTEE

H. H. Barschall
(U. Wisconsin)
G. A. Bartholomew
(AECL, Canada)
L. Cranberg
(TDN, Texas)
H. Feshbach
(MIT, Massachusetts)
J.A. Harvey
(ORNL, Tennessee)
M. T. McEllistrem
(U. Kentucky)
A. B. Smith
(ANL, Illinois)

INTERNATIONAL ADVISORY COMMITTEE

K. Abrahams
(Netherlands)
F. Ajzenberg-Selove
(U. S. A.)
I. Bergqvist
(Sweden)
J. R. Bird
(Australia)
S. W. Cierjacks
(Germany)
J. Csikai
(Hungary)
M. El-Nadi
(U. A. R.)
T. E. O. Ericson
(Switzerland)
A. T. G. Ferguson
(U. K.)
I. M. Frank
(U. S. S. R.)
J. Humblet
(Belgium)
P. K. Iyengar
(India)
C. C. Jonker
(Netherlands)
A. M. Lane
(U. K.)
C. Mahaux
(Belgium)
A. Michaudon
(France)
M. Moshinsky
(Mexico)
J. Rossel
(Switzerland)
I. Šlaus
(Yugoslavia)
K. Tsukada
(Japan)
H. A. Weidenmüller
(Germany)
C. Weitkamp
(Germany)
E. Wigner
(U. S. A.)

COMMERCIAL AND INDUSTRIAL EXHIBITORS, SPONSORS AND CONTRIBUTORS

Academic Press (Publishers), Inc.
Addison-Wesley Publishing Company, Inc.
Adcotel Vacuum Products
Brookhaven National Laboratory
Canberra Industries
Commodore Foods, Inc.
Dennis Office Supply Corporation
General Electric Company, Nuclear Energy Divisions
General Ionex Corporation
Gordon and Breach Science Publishers, Ltd.
Harshaw Chemical Company
High Voltage Engineering Corporation
Langan News Company
Laughton Garden Center
Lowell Institution for Savings
Lowell Medical Instrument Company
National Electrostatics Corporation
North-Holland Publishing Company
Ortec
Plenum Publishers, Inc.
Prince Macaroni Manufacturing Company
Raytheon Company
Selcrad - Applied Radiation, Ltd.
Stencil Company
The Lowell Sun
The Spare House Restaurant, Lowell
Union National Bank
University of Lowell Associates (Bookstore), Inc.
University of Lowell Research Foundation
Wang Laboratories (Calculators), Inc.
Western Electric Company
Xerox Corporation

Co-sponsored by The International Union of Pure and Applied Physics, The American Nuclear Society, The American Physical Society, The Institute of Physics (U.K.)

With support from The Massachusetts Department of Commerce and Development.

PREFACE

These Proceedings record the transactions of the International Conference on the Interactions of Neutrons with Nuclei, which was held at the University of Lowell in Lowell, Massachusetts, U.S.A. from Tuesday, July 6 to Friday, July 9, 1976 and was attended by 430 participants from 26 countries.

The Conference was planned for 2 years as an academic and scientific contribution to the U.S. Bicentennial, to take place just after the Fourth-of-July, at the sesquicentennial of the city of Lowell and on the first anniversary of the formation of the University of Lowell. It was conducted on the North Campus of the University, in the Olney Science Center and in Olsen Hall.

The Conference was conceived as a topical successor to earlier meetings, such as those held in 1957 at Columbia University, in 1965 at Antwerp and 1972 at Budapest, in which the aim was to survey the entire realm of basic neutron physics from a nuclear standpoint, reviewing the present status and assessing the potentialities for the future of this field of endeavor. It was somewhat more extensive in scope, both as regards attendance, (215 attendees from the U.S.A. [i.e., 65%], plus representatives from Australia, Austria, Belgium, Brazil, Canada, China [Nationalist Republic], Egypt, France, Germany [G.D.R.], Germany [F.R.G.], Great Britain, Hungary, India, Iraq, Italy, Japan, Mexico, Netherlands, Poland, South Africa, Sweden, Switzerland, Turkey, U.S.S.R., United States and Yugoslavia) and in coverage of topics, which extended over a diversity of theoretical, experimental, technological and general areas. These ranged over the electromagnetic interactions (photoneutrons and radiative capture) and the strong interactions (scattering, reactions, polarization, stripping, transfer, fission, fusion) of neutrons, a review of neutron facilities, instrumentation and applications, intermediate and high-energy neutron physics, and related topics of general interest. Altogether, 34 Invited Papers and 198 Contributed Papers were presented at simultaneous (but staggered) Main and Parallel Sessions, as detailed in the Program Schedule and List of Papers which have been reproduced in these Proceedings. The list of First Authors of these papers comprises 207 names, of whom 83 [i.e., 40%] stem from the U.S.A. and 124 [i.e., 60%] from overseas (same 25 countries as those of the above attendees). This illustrates the international flavor of this event, which together with the distinguished character of its participants, constituted a particularly gratifying feature of the Conference. Also especially pleasurable was the involvement of many younger delegates, graduate students and others, who injected a vivacity and enthusiasm into the atmosphere of this gathering which, together with a very evident, all-prevading spirit of friendliness, imbued this Conference with a memorable and noteworthy cordiality.

The scientific program comprised 26 Invited Papers in the Main Session, each of 30 minutes' duration, followed by up to 15 minutes of discussion (except for a 45-minute Conference summary and Overview, presented by Professor Eugene Paul Wigner of Princeton University, U.S.A. and a 10-minute closing address, delivered by Academician Professor Illya Mikallovich Frank of the Joint Institute for Nuclear Research, Dubna, U.S.S.R.). These were complemented by 8 similar Invited Papers in the Parallel Session, whose content was more applicational or technological in emphasis. The Main Session on Thursday afternoon, July 8, 1976 was devoted to subjects of general interest in which neutron physics plays a dominant role outside the immediate bounds of nuclear physics, e.g., neutron biophysics, neutron solid-state physics, neutron astrophysics, and the use of neutrons for the production and utilization of energy. Certain aspects of neutron

therapy and other medical applications were also examined in some of the talks in the Parallel Session.

Also featured in a Joint Session was a 1-hour Conference Forum, comprising a free-ranging panel discussion among 9 invited prominent neutron physicists (one representative each from Belgium, Hungary, Great Britain, India, Italy, Japan, Poland, U.S.A. and the U.S.S.R.). Interspersed among the Invited Papers of the Main and Parallel Sessions were 8 Special Contributed Papers, individually selected for their topical interest from among those submitted for presentation: these Special Contributed Papers are reproduced in their entirety in these Proceedings as are the Invited Papers, whereas limitations of space imposed a restriction in reproduction to only the Résumés and Abstracts of the remaining 190 Contributed Papers. These latter were delivered orally in simultaneous Papers Sessions of the Parallel Schedule, each paper being allotted a 10-minute span followed by 5 minutes of discussion. In addition, 1½-hour subsequent periods were allocated for the display of data and results in Poster Sessions, at which the opportunities for meetings and discussions between authors and participants were at their best (not to mention the morning and afternoon refreshment breaks - a statistic which we cannot refrain from recording here is the consumption of 35 dozen doughnuts by the participants during the last break of the Conference and comparable quantities at other times).

Throughout the duration of the Conference, an extensive exhibit of equipment, data-handling systems, books, journals and brochures of interest to neutron physicists was arranged in some of the laboratory halls adjacent to the Poster Sessions.

Daily tours were conducted around the physics facilities at the University of Lowell, and especially into the Pinansky Nuclear Center (the only State-supported research center of its kind) housing a 5.5-MV HVEC Model CN Van de Graaff accelerator with Mobley buncher and subnanosecond time-of-flight systems, and a General Electric swimming-pool research reactor, presently operating at a 1-MW power level. Also, on Thursday morning, July 8, 1976 groups were taken to the High Voltage Engineering Corporation in Burlington and to the M.I.T. Bates Linear Accelerator facility at Middleton, Massachusetts. Some additional private scientific visits were also arranged.

The afternoon and evening of Wednesday, July 7 were devoted to a Conference Excursion to Boston, and on the evening of Thursday, July 8 the Conference Banquet was held for 350 participants and guests at the Sheraton Rolling Green Motor Inn, Andover, Massachusetts, the principal Banquet Address being delivered by the Guest of Honour, Professor Edoardo Amaldi of the University of Rome, who spoke on "Personal Recollections of Early Times in Neutron Physics". Also forming part of the social program of the Conference was a Special Reception for Invited Speakers and Committee Members on Monday evening, July 5, and a general Reception for all attendees on Tuesday evening, July 6.

It was an especial pleasure to include a high number of family members accompanying participants, whose presence was greatly appreciated. In all, upward of 80-90 companions also took part in the arrangements. A special Companion Program was established, comprising coach tours to nearby areas of cultural, historical or recreational merit. Thus, an excursion to Old Sturbridge Village was arranged for Tuesday, July 6, a Companion group left for Boston early on Wednesday morning, July 7 in order to visit Concord, Lexington, and

other Revolutionary (Bicentennial) sites in the area before visiting special exhibitions and locations in Boston prior to meeting up with the Scientific participants in the main Conference Excursion later that day. For Thursday, July 8, a drive to the Atlantic Seacoast (notably viewing Marblehead, Salem, Gloucester and Rockport on Cape Ann) was arranged, and on Friday, July 9, a combination walking/bus tour was conducted through Lowell's canal systems and historical or architectural attractions, including the South Campus of the University of Lowell.

The language of the Conference was English throughout, and a complete record on magnetic tape was made of all Invited Talks and discussions. The Invited Speakers were asked to send preliminary Abstracts, followed by the full text of their Invited Papers, prior to the Conference so that by the time the Conference began, all Abstracts of Invited and Contributed Papers could be distributed to each participant in duplicated loose-leaf form in a ring-binder Conference Portfolio. The manuscripts of the full texts were assembled during the Conference, at which time preliminary unedited transcripts of the Discussions were also prepared and made available to the Speakers for revision. The final text of the Proceedings was then assembled in the fortnight after the Conference and despatched for rapid publication.

We sincerely and gratefully appreciate the consideration shown by the Speakers in conveying to us the manuscripts on schedule and in scrutinizing our original transcripts of discussions as rapidly and thoroughly as possible, in the interests of speedy publication. In several instances, it was not possible for participants to review this material, and we ask their indulgence for the fact that we have accordingly taken upon ourselves the final editing and reproduction. Tape transcription is notoriously prone to misunderstanding, and we had to use our discretion whenever it was not obvious what certain unclear remarks had been intended to convey. As time was of the essence, we confined ourselves merely to rendering our interpretation of these statements, correcting obvious slips but retaining those endearing personal characteristics of expression that emerge in verbal discussions and are deserving of preservation. In this regard, future transcribers can take heart from our experience of the reconstruction of a remark by a distinguished Speaker to the effect that he was "partial to the use of the R-matrix" as an avowal that he was "partial to the use of Army tricks"!

The highly compressed nature of the schedules enabled a vast amount of material to be covered in the four days of the Conference, and necessitated the division of these Proceedings into two fairly bulky volumes. For ease of perusal, we have included a Table of Contents and Conference Schedule and in Volume II an Author Index, List of Invited and Contributed Papers (arranged alphabetically according to first author), a List of Participants, and a CINDA Index.

The contents of VOLUME I (MAIN SESSION) comprise the Inaugural Ceremonies, 23 Invited Papers, 4 Special Contributed Papers and Discussions of the Main Session. In VOLUME II (JOINT, PARALLEL AND PAPERS SESSIONS) are presented the texts of the Friday-afternoon Joint Sessions transactions, namely 1 Invited Talk and the Conference Forum in Session MM, and 2 Invited Talks of Session MN. Also contained therein are 8 Invited Papers and 4 Special Contributed Papers that were delivered in the Parallel Sessions, together with the discussions that followed. The Abstracts of 190 Contributed Papers are presented next, and Volume II concludes with 3 Banquet Addresses, a Secretarial Contribution, and the above-mentioned set of Indexes. For the compilation of the CINDA Index we are indebted to the Neutron Cross-Section Center at Brookhaven under the direction of Dr. S. Pearlstein.

For the extensive high-quality secretarial assistance of Mrs. Arlene Dillon, Ms. Jacquelyn Jones, Ms. Elizabeth Connors, Ms. Betty Ryan, Ms. Diane Duggan, Ms. Pam Leczynski and Ms. Ellen Ward, for the ready and able draughtsmanship of Mr. Bernard Killion, for the facilities of the University of Lowell and of the Research Foundation, and for the innumerable instances of helpfulness encountered in the intensive preparation of these Proceedings, we hereby express our lasting deep admiration and gratitude.

The Sponsorship accorded to the 1976 International Conference on the Interactions of Neutrons with Nuclei by the International Union of Pure and Applied Physics, The American Physical Society, The Institute of Physics (U.K.), The American Nuclear Society, The U. S. National Science Foundation and the U. S. Energy Research and Development Administration (whose Technical Information Division is publishing these Proceedings, obtainable from

The National Technical Information Service,
U.S. Department of Commerce,
5285, Port Royal Road,
Springfield,
Virginia 22161
U.S.A.

has been greatly appreciated. To these agencies and to the many other organizations and individuals who have generously provided support to enable this Conference to proceed, and especially to all our ICINN Committee Members and aides we record our warmest thanks. And finally, but none the less sincerely, to the visiting scientists and companions who so greatly stimulated and honored us by their presence and goodwill, we append our very profound gratefulness for a memorable, exhilarating, and altogether wonderful experience.

Eric Sheldon
(Editor)

Gus P. Couchell
Susan A. Goodwin
Suresh C. Mathur
David Pullen
(Associate Editors)

University of Lowell
July 24, 1976

ICINN PROGRAM SCHEDULE : TUESDAY, JULY 6, 1976

TIME	SESSION NO.	MAIN SESSION	TIME	SESSION NO.	PARALLEL SESSION
9.00	MA	CHAIR: L.E. Beghian *(U. of Lowell, USA)*			
		INAUGURAL ADDRESSES: J.B. Duff *(President, U. of Lowell, USA)* T. O'Neill *(Lieutenant-Governor, Commonwealth of Massachusetts, USA)* E. Sheldon *(ICINN Chairman, U.of Lowell)*			
9.30	MA	RECENT ADVANCES IN NEUTRON PHYSICS H. Feshbach *(Massachusetts Institute of Technology, USA)*			
10.15	-	*GROUP PHOTOGRAPH (Main Entrance, Olney)*			
10.25	-	*REFRESHMENTS (Olney Lobby)*			
10.45	MB	CHAIR: K. Abrahams *(Reactor Centrum Nederland, Petten, Netherlands)*	10.45	PA	CHAIR: J. Csikai *(Debrecen, Hungary)*
10.45	MB1	THE HIGH-FLUX REACTOR AT GRENOBLE AND ITS SPECIAL NEUTRON BEAM INSTALLATIONS R.L. Mössbauer *(ILL Grenoble, France)*	10.45	PA1	NEUTRON INSTALLATIONS AND FACILITIES S.W. Cierjacks *(Kernforschungszentrum Karlsruhe, Germany)*
11.30	MB2	RESONANCE NEUTRON CAPTURE J.R. Bird, J.W. Boldeman, B.J. Allen, A.R. deL. Musgrove, M.J. Kenny *(AAEC Lucas Heights, Australia)*	11.30	PA2	ACCELERATOR-PRODUCED NEUTRONS OF HIGH FLUX RATE L. Cranberg *(TDN Inc., Austin, Texas, USA)*
12.15 - 1.45		*LUNCHEON (Student Union Cafetorium)*	*12.15 - 1.45*		*LUNCHEON (Student Union Cafetorium)*
1.45	MC	CHAIR: G.A. Bartholomew *(AECL Chalk River, Canada)*	1.45	PB1	*Parallel Sessions of Contributed Papers:* A1-8: Neutron Properties & Forces (O-115) G1-8: Polarization (O-513) J1-8: Fission and Fusion (O-517) F1-8: Neutron-induced Reactions (O-519) K1-8: Theoretical Neutron Physics (O-521)
1.45	MC1	FAST RADIATIVE CAPTURE I. Bergqvist *(U. of Lund, Sweden)*			
2.30	MC2	ULTRACOLD NEUTRONS V.I. Luschikov *(JINR - Dubna, USSR)*			
3.15	MC3	NEUTRON RESONANCES: NEUTRON REACTION MECHANISMS AND NUCLEAR STRUCTURE J.A. Harvey *(ORNL, Oak Ridge, USA)*	3.45	-	*REFRESHMENTS (Olney Lobby)*
4.00	-	*REFRESHMENTS (Olney Lobby)*			
4.30	MD	CHAIR: J. Rossel *(U. of Neuchatel, Switz.)*	4.15	PB2	*Parallel Sessions of Contributed Papers:* H1-11:Neutron Instrumentation (O-115) D1-7: Photoneutrons & Rad. Capture (O-513) J9-15:Fission and Fusion (O-517) B1-7: Resonance Neutrons (O-519) K9-15:Theoretical Neutron Physics (O-521)
4.30	MD1	FAST NEUTRON SCATTERING FROM SOME MEDIUM MASS NUCLEI M.T. McEllistrem *(U. of Kentucky, USA)*			
5.15	MD2	FAST NEUTRON SCATTERING: REACTION MECHANISMS AND NUCLEAR STRUCTURE A.T.G. Ferguson *(AERE - Harwell, UK)*, I.J. van Heerden *(Southern U. Nuclear Institute, Faure, South Africa)*, P. Moldauer and A. Smith *(ANL, Argonne,USA)*	4.15	PB2	*Poster Sessions in O-102 to O-105:* A1-8: Neutron Properties & Forces F1-14:Neutron-induced Reactions K1-8: Theoretical Neutron Physics K22-27: Theoretical Neutron Physics L1-7: Miscellaneous
6.00	-	*CONCLUSION*	*6.00*	-	*CONCLUSION*

8.30 RECEPTION AT THE SHERATON ROLLING GREEN MOTEL, ANDOVER

COMPANION PROGRAM EXCURSION: STURBRIDGE VILLAGE, MASSACHUSETTS (8.45 A.M. - 4.15 P.M.)

ICINN PROGRAM SCHEDULE : WEDNESDAY, JULY 7, 1976

TIME	SESSION NO.	MAIN SESSION
9.00	ME	CHAIR: J.B. Garg *(State U. of New York at Albany, USA)*
9.00	ME1	*Special Contributed Paper:* FLUCTUATION ENHANCEMENTS OF COMPOUND CROSS SECTIONS FOR ELASTIC, DIRECTLY COUPLED, AND WEAKLY ABSORBED CHANNELS P.A. Moldauer *(ANL, Argonne, USA)*
9.15	ME2	*Special Contributed Paper:* SPIN DETERMINATION OF FISSION RESONANCES G.A. Keyworth *(LASL, Los Alamos, USA)*
9.30	ME3	NEUTRON-INDUCED REACTIONS ON VERY LIGHT AND LIGHT TARGET NUCLEI I. Slaus *(Rudjer Boskovic Nuclear Institute, Zagreb, Yugoslavia)*
10.05	-	REFRESHMENTS (Olney Lobby)
10.25	MF	CHAIR: H.H. Barschall *(U. of Wisconsin,USA)*
10.25	MF1	NEUTRON-INDUCED REACTIONS II: (n,x) REACTIONS ON MEDIUM AND HEAVY NUCLEI N. Cindro *(C.E.N. Bruyères-le-Châtel,France)*
10.45	MF2	NEUTRON-INDUCED CASCADE REACTIONS J. Fréhaut *(C.E.N. Bruyères-le-Châtel,France)*
11.15	MF3	NEUTRON POLARIZATION F.W.K. Firk *(Yale University, USA)*
12.00	-	CONCLUSION

TIME	SESSION NO.	PARALLEL SESSION
9.00	PC	CHAIR: R.L. Macklin *(ORNL, Oak Ridge,USA)*
9.00	PC1	FAST NEUTRON DETECTORS AND INSTRUMENTATION B. Zeitnitz *(U. of Bochum, West Germany)*
9.45	-	REFRESHMENTS (Olney Lobby)
10.15	PD	CHAIR: C. Newstead *(Brookhaven Nat.Lab.,USA)*
10.15	PD1	TECHNOLOGICAL AND INDUSTRIAL APPLICATIONS OF NEUTRONS C. Titkamp *(GKSS, Geesthacht, Germany)*
11.00	PD2	DETERMINATION OF SCATTERING LENGTHS AND MAGNETIC SPIN ROTATIONS BY NEUTRON INTERFEROMETRY H. Rauch *(Atominstitut der Österreichischen Hochschulen, Vienna, Austria)*, G. Badurek, W. Bauspiess, U. Bonse, and A. Zeilinger
11.45	PD3	*Special Contributed Paper:* STRUCTURE STUDIES OF ^{7,8}Li AND ^{11,12}B FROM ELASTIC SCATTERING OF NEUTRONS R.O. Lane, R.M. White, and H.D. Knox *(Ohio University, Athens, USA)*
12.00	-	CONCLUSION

12.00	-	CONCLUSION
12.15 - 1.00		LUNCHEON (Student Union Cafetorium)
1.00		CONFERENCE EXCURSION TO BOSTON

COMPANION PROGRAM EXCURSION: CONCORD, LEXINGTON, CAMBRIDGE, BOSTON 9.00 A.M. - 5.40 OR 9.15 P.M.)

NOTE: SCIENTIFIC WORKSHOPS MAY BE ARRANGED AT 8.00 P.M. IN THE STUDENT UNION BUILDING IF DESIRED.

ICINN PROGRAM SCHEDULE : THURSDAY, JULY 8, 1976

TIME	SESSION NO.	MAIN SESSION
9.00	MG	CHAIR: P.A. Moldauer *(ANL, Argonne, USA)*
9.00	MG1	THEORETICAL NEUTRON PHYSICS I: ELUCIDATION OF NUCLEAR STRUCTURE V.G. Soloviev *(JINR - Dubna, USSR)*

TIME	SESSION NO.	PARALLEL SESSION
9.00	PE	CHAIR: R.E. Chrien *(Brookhaven National Laboratory, USA)*
9.00	PE1	*Special Contributed Paper:* PRODUCTION OF POLARIZED FAST-NEUTRON BEAMS - AN EVALUATION OF SEVERAL METHODS R.L. Walter and P.W. Lisowski *(Duke U.,USA)*

9.45	MG2	THEORETICAL NEUTRON PHYSICS II: MICROSCOPIC CALCULATIONS OF THE OPTICAL-MODEL POTENTIAL J.-P. Jeukenne, A. Lejeune and C. Mahaux *(U. of Liège, Belgium)*	9.15	PE2	*Special Contributed Paper:* AN OPTICAL MODEL POTENTIAL BASED ON THE FOLDED YUKAWA MODEL A. Prince *(National Neutron Cross-Section Center, Brookhaven National Lab., USA)*
10.30	-	*REFRESHMENTS (Olney lobby)*	9.30	PE3	NEUTRON STANDARDS AND THEIR APPLICATION H. Liskien *(B.C.N.M. - Geel, Belgium)*
10.50	MH	CHAIR: J. Humblet *(U. of Liège, Belgium)*	*10.15*	-	*REFRESHMENTS (Olney lobby)*
10.50	MH1	THEORETICAL NEUTRON PHYSICS III: SPECTRUM FLUCTUATIONS AND THE STATISTICAL SHELL MODEL P.A. Mello *(U. Nacional Autonoma de Mexico)* J. Flores, T.A. Brody, J.B. French, and S.S.M. Wong	10.35	PF	CHAIR: F.G.J. Perey *(ORNL, Oak Ridge, USA)*
			10.35	PF1	THE IMPORTANCE OF NEUTRON DATA IN FISSION REACTOR APPLICATIONS E.M. Bohn *(ANL, Argonne, USA)*, H. Henryson, J. Hardy, Jr., R. Roussin and C.Weisbin
11.35	MH2	THEORETICAL NEUTRON PHYSICS IV: NUCLEAR REACTIONS A.M. Lane *(AERE - Harwell, UK)*	11.20	PF2	NEUTRON SOURCES FOR MEDICAL APPLICATIONS K.E. Scheer, K.H. Höver and K.A. Schmidt *(Deutsches Krebsforschungszentrum Heidelberg, West Germany)*
			12.05	PF3	*Special Contributed Paper:* STATUS OF NEUTRON ACTIVATION CROSS SECTIONS FOR REACTOR DOSIMETRY M.F. Vlasov *(IAEA, Vienna, Austria)*, W.N. McElroy and A. Fabry
12.20	-	*C O N C L U S I O N*	*12.20*	-	*C O N C L U S I O N*
12.20 - 2.00		*LUNCHEON (Student Union Cafetorium)*	*12.20 - 2.00*		*LUNCHEON (Student Union Cafetorium)*
2.00	MI	CHAIR: S.H. Chen *(Massachusetts Institute of Technology, USA)*	2.00	PG1	*Parallel Sessions of Contributed Papers:* E1-6: Neutron Scattering (O-115) D8-13: Photoneutrons & Rad. Capture (O-513) J16-18:Fission and Fusion (O-517) I1-3: Standards and Data (O-517) B9-13: Resonance Neutrons (O-519) K16-21:Theoretical Neutron Physics (O-521)
2.00	MI1	USE OF NEUTRON SCATTERING FOR THE ANALYSIS OF BIOLOGICAL STRUCTURES B.P. Schoenborn *(Brookhaven National Laboratory, USA)*			
2.45	MI2	SOLID-STATE ASPECTS OF NEUTRON PHYSICS RESEARCH W. Gläser *(Technisch. " , München, Germany)*			
3.30	-	*REFRESHMENTS (Olney lobby)*	3.30	-	*REFRESHMENTS (Olney lobby)*
4.00	MJ	CHAIR: F. Ajzenberg-Selove *(U. of Pennsylvania, USA)*	4.00	PG2	*Parallel Sessions of Contributed Papers:* E7-12: Neutron Scattering (O-115) D14-19:Photoneutrons & Rad. Capture (O-513) I4-9: Standards and Data (O-517) B14-19: Resonance Neutrons (O-519) K22-28:Theoretical Neutron Physics (O-521)
4.00	MJ1	NEUTRON ASTROPHYSICS R.A. Smith *(State U. of New York at Stony Brook, USA)*			
4.45	MJ2	NEUTRONS AND ENERGY J.L. Fowler *(ORNL, Oak Ridge, USA)*	4.15	PG2	*Poster Sessions in O-102 to O-105:* F1-6: Neutron Scattering F13-23:Neutron Scattering M1-11: Neutron Instrumentation J1-18: Fission and Fusion K9-21: Theoretical Neutron Physics K28-38:Theoretical Neutron Physics
5.30	-	*C O N C L U S I O N*	5.30	-	*C O N C L U S I O N*

7.30 COCKTAILS 8.00 CONFERENCE BANQUET AT THE SHERATON ROLLING GREEN MOTEL, ANDOVER.

ICINN PROGRAM SCHEDULE : FRIDAY, JULY 9, 1976

TIME	SESSION NO.	MAIN SESSION	TIME	SESSION NO.	PARALLEL SESSION
9.00	MK	CHAIR: A.N. Benson (Duke U., USA)	9.00	PM1	*Parallel Sessions of Contributed Papers:*
9.00	MK1	NEUTRONS AND FISSION A. Michaudon (C.E.N.-Bruyères-le-Châtel, France)			E13-17: Neutron Scattering (O-115) D20-24: Photoneutrons & Rad. Capture(O-513) I10-14: Standards and Data (O-517) C 1- 5: Neutron Facilities (O-519) K24-32: Theoretical Neutron Physics (O-521)
9.45	MK2	*Special Contributed Paper:* NEUTRON-INDUCED FISSION OF ^{233}U, ^{235}U AND ^{239}Pu M.A. Hooshyar, B. Compani-Tabrizi and F. Rory Malik (Indiana U., USA)	10.15	-	*REFRESHMENTS (Olney Lobby)*
10.00	MK*	*Special Contributed Paper:* DOUBLY RADIATIVE NEUTRON CAPTURE IN H_2 AND D_2 E.D. Earle (AECL - Chalk River, Canada), A.B. McDonald, M.A. Lone, H.C. Lee, and F.C. Khanna	10.45	PM2	*Parallel Sessions of Contributed Papers:* E18-23: Neutron Scattering (O-115) L 1- 7: Miscellaneous Topics (O-513) F 9-14: Neutron-Induced Reactions (O-519) K33-38: Theoretical Neutron Physics (O-521)
10.15	-	REFRESHMENTS (Olney Lobby)	10.45	PM2	*Poster Sessions in O-105 to O-105:* B 1-19: Resonance Neutrons C 1- 5: Neutron Facilities D 1-24: Photoneutrons & Radiative Capture E 7-12: Neutron Scattering G 1-16: Polarization I 1-14: Standards and Data
10.45	ML	CHAIR: P.K. Iyengar (Bhabha Atomic Research Institute, Trombay, Bombay, India)			
10.45	ML1	NEUTRONS AND FUSION C.W. Maynard (U. of Wisconsin, USA)			
11.30	ML2	NEUTRON PHYSICS AT LAMPF (Clinton P. Anderson Los Alamos Meson Physics Facility) L.C. Northcliffe (Texas A & M University, USA)			
12.15 - 1.45		LUNCHEON (Student Union Cafeteria)	12.15 - 1.45		LUNCHEON (Student Union Cafeteria)
1.45	MM	CHAIR: E. Amaldi (U. of Rome, Italy)			
1.45	MM1	RESEARCH TRENDS IN NEUTRON PHYSICS J.E. Lynn (AERE - Harwell, UK)			
2.30	MM2	CONFERENCE FORUM *Moderator:* H.H. Barschall (U. of Wisconsin, USA) *Panel:* C. Coceva (Comitato Nazionale per l'Energia Nucleare, Bologna, Italy), J. Csikai (Kossuth U., Debrecen, Hungary), A.T.G. Ferguson (A.E.R.E.-Harwell, UK), P.K. Iyengar (Bhabha Atomic Research Centre, Trombay, Bombay, India), C. Mahaux (U. of Liège, Belgium), V.G. Soloviev (J.I.N.R.-Dubna, USSR), S. Tanaka (Japan Atomic Research Establishment, Tokai, Japan), Z.L. Wilhelm (Warsaw U., Poland).			
3.30	-	*REFRESHMENTS (Olney Lobby)*			
4.00	MM	CHAIR: I.M. Frank (JINR - Dubna, USSR)			
4.00	MM1	CONFERENCE SUMMARY AND OVERVIEW E.P. Wigner (Princeton U., USA)			
4.45	MM2	CLOSING ADDRESS I.M. Frank (JINR - Dubna, USSR)			
4.55	MM3	CONCLUDING REMARKS E. Shelton (ICINN Chairman, U. of Lowell, USA)			
5.00	-	*CONCLUSION OF ICINN CONFERENCE*			

LIST OF ICINN GUESTS, SPEAKERS AND PANELISTS

The final ICINN Conference Program, compiled on June 21, 1976, comprises the following Guest of Honour and Banquet Speaker, 34 Invited Speakers, 9 Conference Forum Panelists and 47 Chairpersons, listed in alphabetical sequence according to Conference Session.

GUEST OF HONOUR AND BANQUET SPEAKER (July 8, 1976)

E. AMALDI	University of Rome	Italy	9.00 p.m.

ICINN INVITED SPEAKERS

I. BERGQVIST	University of Lund	Sweden	MC1
J. R. BIRD	AAEC Lucas Heights	Australia	MB2
E. M. BOHN	ANL, Argonne	U.S.A.	PF1
S. W. CIERJACKS	Kernfoschungszentrum Karlsruhe	W. Germany	PA1
N. CINDRO	C.E.N., Bruyères-le-Châtel	France	MF1
L. CRANBERG	TDN, Inc., Austin, Texas	U.S.A.	PA2
A. T. G. FERGUSON	AERE - Harwell	U.K.	MD2
H. FESHBACH	Massachsetts Inst. of Technology	U.S.A.	MA
F. W. K. FIRK	Yale University	U.S.A.	MF3
J. L. FOWLER	ORNL, Oak Ridge	U.S.A.	MJ2
I. M. FRANK	JINR, Dubna	U.S.S.R.	MN2
J. FREHAUT	C.E.N., Bruyères-le-Châtel	France	MF3
W. GLÄSER	Technische Universität München	W. Germany	MI2
J. A. HARVEY	ORNL, Oak Ridge	U.S.A.	MC3
A. M. LANE	AERE - Harwell	U.K.	MH2
H. LISKIEN	B.C.M.N., Géel	Belgium	PE3
V. I. LUSCHIKOV	JINR, Dubna	U.S.S.R.	MC2
J. E. LYNN	AERE - Harwell	U.K.	MM1
C. MAHAUX	Université de Liège	Belgium	MG2
C. W. MAYNARD	University of Wisconsin at Madison	U.S.A.	ML1
M. T. McELLISTREM	University of Kentucky	U.S.A.	MD1
P. A. MELLO	Universidad Nacional Autonoma	Mexico	MH1
A. MICHAUDON	C.E.N., Bruyères-le-Châtel	France	MK1
R. L. MÖSSBAUER	Institut Laue - Langevin, Grenoble	France	MB1
L. C. NORTHCLIFFE	Texas A & M University	U.S.A.	ML2
H. RAUCH	Atominstitut der Oesterreichischen Hochschulen, Vienna	Austria	PD2
K. E. SCHEER	Deutsches Krebsforschungszentrum Heidelberg	W. Germany	PF2
B. P. SCHOENBORN	Brookhaven National Laboratory	U.S.A.	MI1
I. ŠLAUS	"Rudjer Bošković" Nuclear Institute, Zagreb	Yugoslavia	ME3
R. A. SMITH	State University of New York at Stony Brook	U.S.A.	MJ1
V. G. SOLOVIEV	JINR, Dubna	U.S.S.R.	MG1
C. WEITKAMP	G.K.S.S., Geesthacht	W. Germany	PD1
E. P. WIGNER	Princeton University	U.S.A.	MN1
B. ZEITNITZ	University of Bochum	W. Germany	PC1

CONFERENCE FORUM PANELISTS (1976)

H. H. BARSCHALL	*University of Wisconsin at Madison*	*U.S.A.*
C. COCEVA	*C.N.E.N., Bologna*	*Italy*
J. CSIKAI	*Kossuth University, Debrecen*	*Hungary*
A. T. G. FERGUSON	*A.E.R.E. - Harwell*	*U.K.*
P. K. IYENGAR	*Bhabha Atomic Research Institute*	*India*
C. MAHAUX	*University of Liège*	*Belgium*
V. G. SOLOVIEV	*J.I.N.R. - Dubna*	*U.S.S.R.*
S. TANAKA	*J.A.E.R.I., Tokai-mura*	*Japan*
Z. T. WILHELMI	*Warsaw University*	*Poland*

LIST OF ICINN CHAIRPERSONS

K. ABRAHAMS	Reactor Centrum Nederland, Petten	Netherlands	MB
F. AJZENBERG-SELOVE	University of Pennsylvania, Philadelphia	U.S.A.	MJ
E. AMALDI	University of Rome	Italy	MM
B. K. BARNES	University of Lowell and Los Alamos Scientific Laboratory, Los Alamos	U.S.A.	PG2/E
H. H. BARSCHALL	University of Wisconsin at Madison	U.S.A.	MF
G. A. BARTHOLOMEW	A.E.C.L., Chalk River	Canada	MC
C. M. BARTLE	Australian National University, Canberra	Australia	PG2/D
L. E. BEGHIAN	University of Lowell	U.S.A.	MA
C. R. GOULD	Duke University & TUNL	U.S.A.	PH2/F
R. C. BLOCK	Rensselaer Polytechnic Institute, Troy	U.S.A.	PB2/B
H. CAMARDA	Lawrence Livermore Laboratory	U.S.A.	PB2/K
S. H. CHEN	Massachusetts Inst. of Technology	U.S.A.	MI
R. E. CHRIEN	Brookhaven National Laboratory	U.S.A.	PE
G. P. COUCHELL	University of Lowell	U.S.A.	PG1/E
J. CSIKAI	Kossuth University, Debrecen	Hungary	PA
I. M. FRANK	J.I.N.R. - Dubna	U.S.S.R.	MN
F. GABBARD	University of Kentucky	U.S.A.	PG2/I
J. B. GARG	State University of New York at Albany	U.S.A.	ME
D. W. HALDERSON	Queen's University, Kingston, Ontario	Canada	PG2/K
J. HUMBLET	Université de Liège	Belgium	MH
P. K. IYENGAR	Bhabha Atomic Research Centre, Bombay	India	ML
H. JAHN	Kernforschungszentrum Karlsruhe	W. Germany	PB2/J
S. S. KAPOOR	Bhabha Atomic Research Centre, Bombay	India	PG1/J&I
G. H. R. KEGEL	University of Lowell	U.S.A.	PB1/A
G. A. KEYWORTH	Los Alamos Scientific Laboratory	U.S.A.	PG2/B
F. C. KHANNA	A.E.C.L., Chalk River	Canada	PB1/J
R. O. LANE	Ohio University, Athens	U.S.A.	PB1/G
W. M. MACDONALD	University of Maryland	U.S.A.	PG1/K
R. L. MACKLIN	O.R.N.L., Oak Ridge	U.S.A.	PC
V. A. MADSEN	Lawrence Livermore Laboratory and Oregon State University	U.S.A.	PH1/K
F. B. MALIK	Indiana University	U.S.A.	PH2/K
P. A. MOLDAUER	Argonne National Laboratory	U.S.A.	MG
H. W. NEWSON	Duke University	U.S.A.	MK
C. NEWSTEAD	Brookhaven National Laboratory	U.S.A.	PD
F. G. J. PEREY	O.R.N.L., Oak Ridge	U.S.A.	PF
R. B. PEREZ	O.R.N.L., Oak Ridge	U.S.A.	PB1/K
J. PHELPS	University of Lowell	U.S.A.	PB2/H
H. POSTMA	Rijksuniversiteit Groningen	Netherlands	PG1/B
D. J. PULLEN	University of Lowell	U.S.A.	PH1/I
S. M. QAIM	Kernforschungsanlage Jülich	W. Germany	PG1/D
H. RAUCH	Atominstitut der Österreich. Hochschulen	Austria	PB2/B
J. R. RISSER	Rice University, Houston, Texas	U.S.A.	PB1/F
V. C. ROGERS	Ford, Bacon & Davis Utah, Inc.	U.S.A.	PH2/E
J. ROSSEL	Université de Neuchâtel	Switzerland	MD
A. B. SMITH	Argonne National Laboratory	U.S.A.	PH1/E
M. K. SMITH	University of Lowell	U.S.A.	PH2/L
T. TERASAWA	University of Tokyo	Japan	PH1/D
J. TURKIEWICZ	Instytut Badan Jadrowych, Warsaw	Poland	PH1/C

TABLE OF CONTENTS OF VOLS. I AND II

Contents, Volume I	Page
Presidential Letter	v
Acknowledgements I	vii
Acknowledgements II	viii
Preface	ix
ICINN Program Schedules	xiii
List of ICINN Guests, Speakers and Panelists	xvii
List of ICINN Chairpersons	xviii
Table of Contents	xix
OPENING CEREMONIES (JOINT SESSION MA)	1
MA1 - Session Chairman's Introductory Remarks L. E. Beghian	3
MA2 - Inaugural Address J. B. Duff	5
MA3 - Opening Address T. P. O'Neill, Jr.	7
MA4 - Conference Chairman's Opening Address E. Sheldon	9
MA5 - Recent Advances in Neutron Physics H. Feshbach	13
MAIN SESSION MB	63
Chair: K. Abrahams	
MB1 - The High-Flux Reactor at Grenoble and Its Special Neutron Beam Installations R. L. Mössbauer	65
MB2 - Resonance Neutron Capture J. A. Bird, J. W. Boldeman, B. J. Allen, A. R. de L. Musgrove and M. J. Kenny	76

(continued) Page

MAIN SESSION MC 97

Chair: G. A. Bartholomew

MC1 - Fast Radiative Capture 99
I. Bergqvist

MC2 - Ultracold Neutrons 117
V. I. Luschikov

MC3 - Neutron Resonances: Neutron Reaction Mechanisms and Nuclear Structure 143
J. A. Harvey

MAIN SESSION MD 169

Chair: J. Rossel

MD1 - Fast Neutron Scattering from Some Medium Mass Nuclei 171
M. T. McEllistrem

MD2 - Fast Neutron Scattering: Reaction Mechanisms and Nuclear Structure 204
A.T.G. Ferguson, I.J. van Heerden, P. Moldauer and A. Smith

MAIN SESSION ME 241

Chair: J. B. Garg

ME1 - Fluctuation Enhancements of Compound Cross Sections for Elastic, Directly Coupled and Weakly Absorbed Channels 243
P. A. Moldauer

ME2 - Spin Determination of Fission Resonances 254
G. A. Keyworth

ME3 - Neutron Induced Reactions on Very Light and Light Nuclei 272
I. Šlaus

MAIN SESSION MF 345

Chair: H. H. Barschall

MF1 - Neutron Induced Reactions II: (n,x) Reactions on Medium and Heavy Nuclei 347
N. Cindro

MF2 - Neutron Induced Cascade Reactions 365
J. Fréhaut

MAIN SESSION MF (continued) Page

MF3 - Neutron Polarization 389
F.W.K. Kirk

MAIN SESSION MG 419

Chair: P. A. Moldauer

MG1 - Theoretical Neutron Physics: The Elucidation of Nuclear Structure 421
V. G. Soloviev

MG2 - Microscopic Calculations of the Optical-Model Potential 451
J.-P. Jeukenne, A. Lejeune and C. Mahaux

MAIN SESSION MH 493

Chair: J. Humblet

MH1 - Spectrum Fluctuations and the Statistical Shell Model 495
P. A. Mello, J. Flores, T. A. Brody, J. B. French and S.S.M. Wong

MH2 - Neutron Reactions 525
A. M. Lane

MAIN SESSION MI 541

Chair: S. H. Chen

MI1 - Use of Neutron Scattering for the Analysis of Biological Structures 543
B. P. Schoenborn

MI2 - Solid-State Aspects of Neutron Physics Research 562
W. Gläser

MAIN SESSION MJ 595

Chair: F. Ajzenberg-Selove

MJ1 - Neutron Astrophysics 597
R. A. Smith

MJ2 - Neutrons and Energy 611
J. L. Fowler

MAIN SESSION MK 639

Chair: H. W. Newson

MK1 - Neutrons and Fission 641
A. Michaudon

MAIN SESSION MK (continued) Page

MK2 - Neutron Induced Fission of ^{233}U, ^{235}U, and ^{239}PU 725
M. A. Hooshyar, B. Compari-Tabrizzi & F. Bary Malik

MK3 - Doubly Radiative Neutron Capture in H_2 and D_2 777
E. D. Earle, A. B. McDonald, M. A. Lone,
H. C. Lee and F. C. Khanna

MAIN SESSION ML 787

Chair: P. K. Iyengar

ML1 - Neutrons and Fusion 789
C. W. Maynard

ML2 - Neutron Physics at LAMPF 808
L. C. Northcliffe

Contents, Volume II — Page

Acknowledgements I xxix

Acknowledgements II xxx

Preface xxxi

ICINN Program Schedule xxxv

List of ICINN Guests, Speakers and Panelists xxxix

List of ICINN Chairpersons xl

Table of Contents xli

JOINT SESSION MM 825

Chair: E. Amaldi

MM1 - Research Trends in Neutron Physics 827
J. E. Lynn

MM2 - Conference Forum 857
Moderator: H. H. Barschall

JOINT SESSION MN 871

Chair: I. M. Frank

MN1 - Conference Summary and Overview 873
E. P. Wigner

MN2 - Closing Address 887
I. M. Frank

MN3 - Concluding Remarks 889
E. Sheldon

PARALLEL SESSION PA 891

Chair: J. Csikai

PA1 - Neutron Installations and Facilities 893
S. W. Cierjacks

PA2 - Accelerator-Produced Neutrons 926
L. Cranberg

PARALLEL SESSION PC 943

Chair: R. L. Macklin

PARALLEL SESSION PC (continued) Page

PC1 - Fast Neutron Detectors and Instrumentation 945
B. Zeitnitz

PARALLEL SESSION PD 973

Chair: C. Newstead

PD1 - Technological and Industrial Applications of Neutrons 975
C. Weitkamp

PD2 - Determination of Scattering Lengths and Magnetic Spin Rotations by Neutron Interferometry 1027
H. Rauch, G. Badurek, W. Bauspies, U. Bonse and A. Zeilinger

PD3 - Structure Studies of Light Nuclei $7 \leq A \leq 12$ From Elastic Scattering of Neutrons 1042
R. O. Lane, R. M. White and H. D. Knox

PARALLEL SESSION PE 1059

Chair: R. E. Chrien

PE1 - Sources of Polarized Fast-Neutron Beams - A Status Report . 1061
R. L. Walter and P. W. Lisowski

PE2 - An Optical Model Potential Based on the Folded Yukawa Model 1083
A. Prince

PE3 - Neutron Standards and Their Application 1110
H. Liskien

PARALLEL SESSION PF 1125

Chair: F. G. J. Perey

PF1 - The Importance of Neutron Data in Fission Reactor Applications 1127
E. M. Bohn, H. Henryson II, J. Hardy, Jr., R. Roussin and C. Weisbin

PF2 - Neutron Sources for Medical Applications 1162
K. E. Scheer, K. H. Höver and K. A. Schmidt

PF3 - Status of Neutron Cross Sections for Reactor Dosimetry 1186
M. F. Vlasov, A. Fabry and W. N. McElroy

Page

CONTRIBUTED PAPERS

A - Neutron Properties and Forces 1235
Chair: G. H. R. Kegel

B - Resonance Neutrons 1245
Chair: R. E. Block, H. Postma, G. A. Keyworth

C - Neutron Facilities 1267
Chair: J. Turkiewicz

D - Photoneutrons and Radiative Capture 1275
Chair: H. Rauch, S. M. Qaim, C. M. Bartle, T. Terasawa

E - Neutron Scattering 1303
Chair: G. P. Couchell, B. K. Barnes, A. B. Smith, V. C. Rogers

F - Neutron-Induced Reactions 1337
Chair: J. R. Risser, Jr., C.R. Gould

G - Polarization 1353
Chair: R. O. Lane

H - Neutron Instrumentation 1365
Chair: J. Phelps

I - Standards and Data 1381
Chair: S. S. Kapoor, F. Gabbard

J - Fission and Fusion 1397
Chair: F. C. Khanna, H. Jahn, S. S. Kapoor

K - Theoretical Neutron Physics 1425
Chair: R. B. Perez, H. Camarda, W. MacDonald, D. Halderson, V. A. Madsen, F. B. Malik

L - Miscellaneous 1471
Chair: J. K. Smith

BANQUET ADDRESSES 1481

Banquet Introduction 1483
E. Sheldon

Banquet Address 1485
E. V. Olsen

Personal Recollections of Early Times in Neutron Physics 1492
E. Amaldi

SECRETARIAL SURVEY SONNET 1499
B. Ryan

Page

Index of Invited and Contributed Papers 1503

Author Index of Papers 1527

Geographical Distribution of Authors 1545

Index of Speakers and Discussants 1565

Participants 1569

Geographical Distribution of Participants 1597

CINDA Index 1621

ICINN OPENING CEREMONIES

9.00 A.M., TUESDAY, JULY 6, 1976 IN OLNEY 150

MAIN SESSION MA

Chair: L.E. Beghian (University of Lowell, U.S.A.)

SESSION CHAIRMAN'S INTRODUCTORY REMARKS

L. E. Beghian

(ICINN Executive Officer and Provost of The University of Lowell, Mass., U.S.A.)

On behalf of the University of Lowell, I would lik to extend a warm welcome to our distinguished guests and delegates. Before the delivery of the scheduled Inaugural Addresses and the delivery of the opening Scientific Invited Paper in this first Session of The International Conference on the Interactions of Neutrons with Nuclei, I would like to read a message of welcome from Senator Edward M. Kennedy, the Senior Senator of The Commonwealth of Massachusetts:

" I DEEPLY REGRET THAT I AM UNABLE TO BE PRESENT AT THE OPENING CEREMONIES OF THIS INTERNATIONAL CONFERENCE. IT WOULD HAVE BEEN A PARTICULAR PLEASURE FOR ME SINCE IT WOULD HAVE BEEN MY FIRST OPPORTUNITY TO VISIT YOUR CAMPUS SINCE THE UNIVERSITY OF LOWELL WAS FORMED, A LITTLE OVER A YEAR AGO, THROUGH THE MERGER OF LOWELL TECHNOLOGICAL INSTITUTE AND LOWELL STATE COLLEGE.

THE 10,000 STUDENTS AT THE UNIVERSITY OF LOWELL HAVE BEEN ATTRACTED HERE AS MUCH BY THE EXCELLENCE OF THE FACULTY AS BY THE AVAILABILITY OF RESEARCH FACILITIES SECOND TO NONE IN THE STATE UNIVERSITY SYSTEM. THE UNIVERSITY RUNS THE ONLY CENTER FOR NUCLEAR RESEARCH IN THE STATEWIDE SYSTEM, AND OFFERS A UNIQUE OPPORTUNITY FOR DESERVING STUDENTS FROM ALL OVER THE STATE TO OBTAIN AN EXCELLENT SCIENTIFIC EDUCATION AT A COST THEY CAN AFFORD. THE PRESENCE HERE TODAY OF 330 PARTICIPANTS FROM 30 COUNTRIES IS AMPLE TESTIMONY TO THE INTERNATIONAL STATURE WHICH THIS INSTITUTION HAS ALREADY ACHIEVED IN THE SCIENTIFIC WORLD.

PLEASE CONVEY MY BEST WISHES TO ALL THE PARTICIPANTS AT THE CONFERENCE.

EDWARD M KENNEDY UNITED STATES SENATE"

Now I would like to introduce Dr. John B. Duff, the President of The University of Lowell, to open the Conference.

INAUGURAL ADDRESS

John B. Duff

(President, University of Lowell)

Honored Guests, Distinguished Guests, and Fellow Colleagues at the University of Lowell!

All of us here at the University are honored by your presence at launching the International Conference on the Interactions of Neutrons with Nuclei. This represents the first major international conference devoted to basic neutron physics to be held in the United States in nearly 20 years. It also forms another link with the chain of highly successful neutron physics conferences that have been held previously at Antwerp in 1965 and at Budapest in 1972. It is especially gratifying that attendance at our present meeting has appreciably surpassed all previous such gatherings and that we are privileged to include among our numbers so many outstanding scientists.

That a Conference of this magnitude should be held on the day that the United States enters its third century in the midst of our Bicentennial celebrations, and to be held in the newly-formed University over which I was recently given the privilege of presiding makes this a source of enormous personal gratification to me and to all at the University.

We are especially appreciative of the fact that the President of the United States of America has sent us a personal message of goodwill (reproduced in the Frontispiece).

Accordingly, I am happy to declare this Conference open and on behalf of the University family and the Greater Lowell Community, as well as the Conference's Local Executive Committee which did so much to prepare this program and all these arrangements, I bid you a warm welcome and extend to you our friendliest good wishes for a highly stimulating and productive Conference.

OPENING ADDRESS

Thomas P. O'Neill, Jr.

(Lieutenant - Governor, Commonwealth of Massachusetts)

My privilege is to welcome all in this distinguished gathering on behalf of the Commonwealth of Massachusetts. I want to extend special greetings to the many guests from the international scientific community who are here. Science, more so in my opinion than any other human endeavor, speaks a common language and holds to a common loyalty, namely Truth. Our first American physicist, Benjamin Franklin, was welcomed by his scientific contemporaries in both France and Britain, despite his mission on behalf of revolution - was welcomed rather for his sympathy and his contribution toward truth.

In that same spirit, we greet you all here today. I want to acknowledge the presence specifically of three renowned Nobel laureates among the Invited Speakers: Academician Professor I. M. Frank, Professor R. L. Mössbauer, and Professor E. P. Wigner. I dare say that most of what the world knows about basic neutron physics is concentrated in this hall today. What we do not as yet know about the neutron, I expect will be substantially less by the time this Conference concludes. For most of us, the frontier that you are exploring is as remote as the surface of Mars, but that does not mean that we do not appreciate the significance of your work. Whether or not we grasp the subtleties of scientific theories, we have all benefited inestimably from the work of Galileo, Newton, and Einstein. That which is a mystery to us may be a commonplace for our children or grandchildren.

I want to congratulate Dr. Duff, Dr. Sheldon and the Department of Physics at the University of Lowell for the eminently successful realization of this Conference project. The seeds of three years of hard work are now finally coming to fruition. I know that many citizens and organizations in the city of Lowell and in this country have contributed time, effort and resources toward making this Conference a total success. We think that this city was a marvel of the Industrial Revolution and one of the first in the New World to grasp the significance of nineteenth - century science and technology. Some of that same spirit, I think, is reflected in the eagerness of the people of Lowell and of this Commonwealth to encourage the scientific ideas of the present and future centuries.

You have our good wishes for all of your deliberations. We deeply appreciate your presence here today and are truly grateful for your participation in this international meeting of distinguished and authoritative minds. You do us great honor.

Thank you very, very much.

CONFERENCE CHAIRMAN'S OPENING ADDRESS

Eric Sheldon

(University of Lowell, Massachusetts, U.S.A.)

As the Director of this Opening Session points his baton toward me to cue in my voice with those others who have already sounded the *Leitmotiv* of this chorus of welcome, I have to invoke sight as well as sound to convey the restatement of our theme. With a strict injunction from the Conductor that my melody line is marked *"Sostenuto - ma non troppo !"* (since I am allowed only about one mean neutron lifetime for my presentation), I will offer my message to you in visual form *(Figure 1)*, which expresses, better than my halting tongue could encompass, the immense pleasure that your distinguished participation is affording us, and the cordial welcome that we would like to extend, individually and collectively, to each of you.

It is indeed both gratifying and fitting that this gathering should have assembled from all corners of the globe to survey the present status and future prospects of neutron physics, as this is itself a domain that has come into being through the contributions of so many nations and that now draws its unique strength from the co-operative endeavours of so many countries.

To the mighty Greek civilization, through its Ionian school of philosophy as represented by the scholars Anaxagoras, Leucippus and Democritus in the fifth century B.C. we owe the concept of atoms, as reiterated by the Latin poet Lucretius in the first century B.C., and as placed on a scientific basis nineteen centuries later in England, France, Germany and Italy by Dalton and others. This set the stage for the pinpointing of the nucleus within the atom by Rutherford of New Zealand, ushering in the tremendous interpretative nuclear developments of the 1930's.

Toward the end of 1930, Bothe and Becker in Germany published results of investigations on artificially-induced γ-ray emission with weak α-radiation sources, followed in 1931 by data from considerably stronger α-sources as used in France by Irène Curie and Jean Frédéric Joliot. The scene then switches to England, where at the Cavendish Laboratory in Cambridge Webster had in 1932 taken up similar investigations to those pursued by Bothe and Becker and, one month later, James Chadwick was led to the conclusion that a product of the α-irradiation of light target nuclei had to be chargeless particles with a mass closely akin to that of protons, namely that one was dealing with the emission of *neutrons* (and not of hyperenergetic γ-rays, as had previously been postulated). Chadwick's famous paper in the Proceedings of the Royal Society of London [A 136 (1932) 692-708] on "The Existence of a Neutron" concluded with the triumphant and prophetic words:

> *"The neutron hypothesis gives an immediate and simple explanation of the experimental facts; it is consistent in itself and it throws new light on the problem of nuclear structure."*

To follow this splendid quotation with another, more recent statement that eloquently conveyed (in unconscious poetry) the grandeur and centrality of neutron physics, I would like to repeat the way that Dr. Jacob Bronowski expressed himself in "The Ascent of Man":

"At twilight on the sixth day of Creation,
So say the Hebrew commentators to the Old Testament,
God made for man a number of tools
That give him also the gift of creation.
If the commentators were alive today, they would write
' God made the neutron '.

.....

The neutron was therefore a new kind of probe,
A sort of alchemist's flame,
Because, having no electrical charge,
It could be fired into the nuclei of atoms
Without suffering electrical disturbance,
And change them.
The modern alchemist,
The man who more than anyone
Took advantage of that new tool,
Was Enrico Fermi in Rome."

It is to James Chadwick and to Enrico Fermi that we gratefully and respectfully dedicate this Conference today. May our deliberations and contributions to humanity prove worthy of the grandiose legacy that they have bestowed upon us.

Fermi, with his brilliant school of co-workers in Italy, among whose numbers was included this Conference's cherished Guest of Honour, Professor Edoardo Amaldi of the University of Rome, for the first time applied this wondrous and powerful tool to the production of man-made isotopes in 1934. By the end of the decade, synthesis had given way to analysis, as Hahn and Strassmann in Germany, Meitner and Frisch, Bohr and Wheeler in Scandinavia and the United States recognized the phenomenon of nuclear fission induced by neutrons. Worldwide research efforts were devoted to elucidating the characteristics of the fission chain reaction (e.g., by Fermi himself, as well as by von Halban, Kowarski, Szilard, Wigner, Oppenheimer, and many others). It has now been brought to the stage at which it holds immense promise for mankind toward the resolution of its immediate energy requirements in the face of dwindling stocks of fossil fuels.

We now recognize the multifaceted diversity, the exquisitely attractive potentialities and possibilities offered by neutron physics, and it needs no words on my part to emphasize the excitement and captivation of the quest to unravel its mysteries and complexities over the years. Acknowledging this to have been a truly international, collective endeavour involving the mingling of the keenest scientific minds and most-highly developed experimental resources, we look to the continuation of this impetus in splendour and fruitfulness throughout the ensuing years.

It is our fervent hope that this Conference will act as a further spur to international co-operation in scientific research and in the exchange of scientific information. The development of international research centers constitutes a particularly felicitous and promising line of progress in our field, just as in other realms of physics.

Internationalism has been the guiding principle in the selection of our Advisory Committee, who have ensured world-wide representation at this Conference. As you see, even our Executive Committee at Lowell, composed of Drs. Beghian, Goodwin, Mathur and myself, is multinational in origins and composition. We are cognizant and proud of the fact that the international flavour of scholarship has been recognized and encouraged throughout the academic community, and particularly at this new institution, among faculty and students alike. This is a special time, when the United States celebrate the Bicentennial, the city of Lowell its Sesquicentennial, and the University its first anniversary. We are indeed happy that you have come from so far afield to share in it and to participate in this first Conference here.

At about this time a year ago, when the Legislature enacted the merger of The Lowell Technological Institute (the present University's North Campus) and The Lowell State College (constituting our sister South Campus, which you will have an opportunity to visit next Friday) to bring about the formation of The University of Lowell it also made two other separate decisions, seemingly unrelated. These have an effect on the arrangements for our Conference, and in bringing them to your attention, I would also like to try to suggest a possible connection, since after all even random correlations form a legitimate subject of study in our discipline: The first decision was to delete from this year's University budget a line item for the fiscal expenses of this Conference at a time of economic deprivation, obliging us to raise the necessary means from elsewhere; the second initiative was to put into operation a rule that smoking is not permitted in such public places within the Commonwealth as lecture halls, classrooms, seminar rooms, elevators, etc. So please forbear from smoking except in designated areas such as lobbies, lounges or offices. As to the connection between these two rulings, I can only put forward the obvious interpretation that in their inability to provide funds for the Conference, the Legislature made provision for you to save enough from not smoking for the rest of this week to finance the not inconsiderable outlay involved in staging this meeting !

That we were in fact able to find the resources for this Conference is due not only to the generous contributions from sponsoring agencies and organizations, including many industrial and commercial concerns in our local area whom we gratefully acknowledge in our list of donors, but also to the support provided by our University, especially through its Division of Continuing Education, and to a most understanding loan and encouragement from the University Alumni Association. We are truly indebted to countless individuals and institutions for their heartening response to this occasion.

It goes without saying that we hope you will in all respects enjoy this Conference and benefit from it, both now and in the time to come. It has been planned as an academic and scientific contribution to the U.S. Bicentennial by probably the newest University in this country, and it will aim to carry forward the theme of such previous international conferences devoted to fundamental neutron physics as that of 1957 at Columbia University, of 1965 at Antwerp, and of 1972 at Budapest. The challenges and difficulties of pursuing research in neutron physics are more than amply compensated by the marvellous diversity to which it lends itself. To try to compress this wealth of material into but a few days provided us with appreciable problems and you with a highly concentrated program.

The neutron is probably unique in its sensitiveness to all four basic interactions presently recognized in physics: the powerful nuclear interaction, the electromagnetic, weak and gravitational interactions. Even in this last-named category, the neutron has continued to be a subject for investigation, be it in establishing the equality of the attractive gravitational force for neutrons and antineutrons alike or, as in a paper to be published in the July 15, 1976 issue of The Physical Review by L. Koester of the Technische Universität, München, in verifying the equality of

the gravitational and inertial mass of the neutron. Another obvious instance in which the neutron enters into gravitational interactions of profound significance to the physics of our cosmos is the ultra-dense world of neutron stars. I have no doubt that undreamed-of surprises lie in store for us in the domain of neutron astrophysics, even as we prepare to hear of the latest progress in the course of this Conference. Obviously the main thrust of the meeting will be directed toward an examination of electromagnetic and strong nuclear interactions from a fundamental point of view, but we shall also be hearing of developments having an important bearing upon energy production and utilization, we will be updating our knowledge of neutron instrumentation and facilities, particularly in the high-flux field where recent advances seem to offer significant promise toward neutron therapy, as well as in the general realm of neutron biophysics.

But there is one interaction stronger than all of these: the all-redeeming force of Love. May we, through our intense love of neutron physics, use this Conference to forge links of affection, one with another, so that our endeavours now and in the future may serve not only Science but also Humanity, and that they bring about the realization of a world-wide diffusion of knowledge, understanding and friendship.

Figure 1. Multilingual Greetings to ICINN Participants

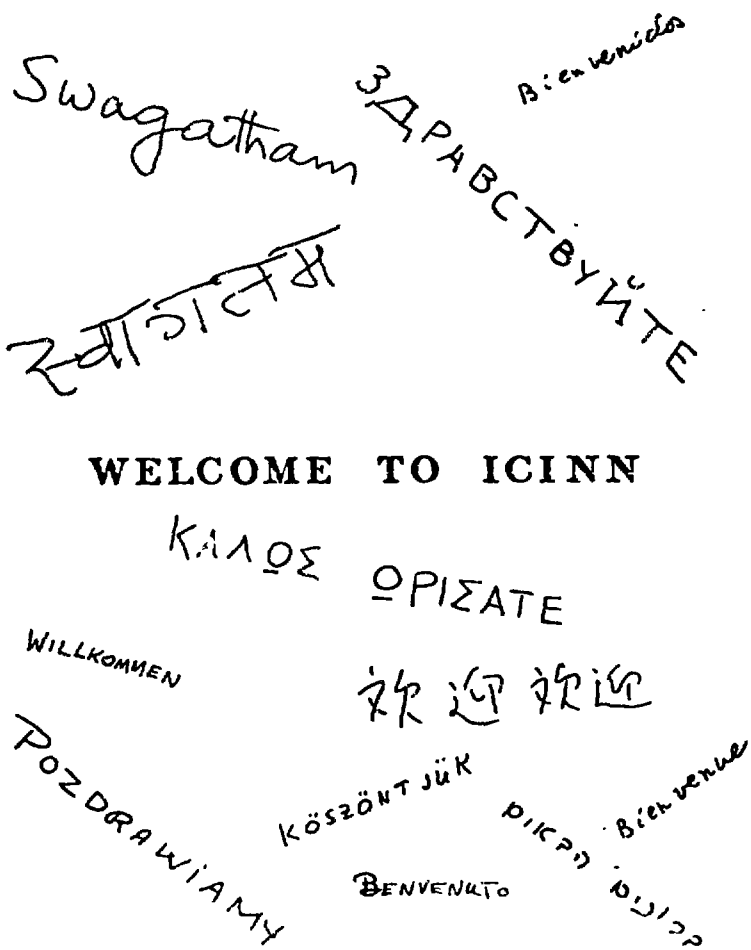

9.30 a.m., Tuesday, July 6, 1976 in Olney 150 Invited Paper: Session MA

RECENT ADVANCES IN NEUTRON PHYSICS

H. Feshbach

Department of Physics, Massachusetts Institute of Technology, Cambridge, MA 02139, U S. A.

RÉSUMÉ

In recent years, and especially over the past decade, significant advances have b en made in numerous fields of experimental and theoretical physics, which will be critically reviewed. Examples of progress in specific areas will be presented, and an overview of the present status of neutron physics will be given.

ABSTRACT

In reviewing the past decade of progress in neutron physics, the importance of the neutron as an uncharged projectile in nuclear interactions is stressed. A preliminary survey of some of the difficulties and developments in neutron instrumentation is presented, and mention is made of the importance of the elucidation of quantum numbers, such as spin, for neutron resonances.

Commencing the main part of the survey with a consideration of elastic neutron scattering and its description in terms of the optical model, and tracing its connection with inelastic scattering, a discussion is given of the latest progress in establishing the parametric form of the optical potential, and of the use of coupled-channel and fluctuation formalisms.

Consideration is also given to multistep processes, with especial reference to the treatment of sequential reactions. An important fairly recent development is the detailed formulation of the effects of pre-equilibrium processes upon measured cross sections, and this is discussed at some length.

An account is given of a general statistical theory developed by Kerman, Koonin and Feshbach from 1972-76, and its consequences are described, several illustrative examples being given.

Finally, some discussion is presented of doorway state effects and related phenomena, and attention is drawn to further theoretical developemnts that will form the subject of Invited Papers to be presented later in the Conference program.

RECENT ADVANCES IN NEUTRON PHYSICS

H. Feshbach

Laboratory For Nuclear Science And Department Of Physics
Massachusetts Institute of Technology
Cambridge, Massachusetts 02139

*This work is supported in part through funds provided by ERDA under Contract E(11-1)-3069.

An invited paper presented at the 1976 International Conference on the Interactions of Neutrons with Nuclei, July, 1976.

Center for Theoretical Physics Publication #566

Although natural radioactivity had been known for some time, and some nuclear reactions had been induced by collisions with alpha particles it wasn't until the neutron had been discovered in 1932 that nuclear physics and nuclear science really began. Only then did it become clear that the fundamental constituents of the nucleus of the atom are the neutron and the proton. Understanding the nature of the forces acting between these elementary constituents, and more generally understanding their interaction when they are inside the nucleus and how these forces act in concert to produce the atomic nucleus is one of the great fundamental challenges faced by modern science. Nuclear forces are one of the four fundamental forces of nature. They play a decisive role in the history of our universe, in astronomical processes such stellar evolution leading to the formation of the various kinds of naturally occuring elements such as those which occur in our own planetary system. Nuclear forces are also ultimately responsible for our energy resources which originate in nuclear processes in the sun. And hopefully nuclear processes will be more directly able to provide energy from fission and fusion reactors. The neutron is the "workhorse" of these terrestrial energy sources. From both the pragmatic point of view and from the point of view of the basic scientific inquiry into the fundamental properties of matter, the neutron and nuclear structure, the title of this conference, is a subject of unusual importance.

A property of the neutron which makes it so useful on both scores is its electric neutrality. The positively charged nucleus exerts a strong repulsive force on other charged particles such as the proton with the consequence that these particles must be energetic if they are to interact via the short range nuclear forces with a nucleus. On the other hand the neutron being neutral has no difficulty in approaching nuclei. Thus the neutron is uniquely endowed for studying the low energy phenomena. It is no accident that fission of nuclei was first discovered using neutrons. Although other techniques have been developed it remains the primary low energy probe of the strong nuclear interactions.

The neutrality of the neutrons, together with their instability against β decay does however pose important technical problems. The second of these means that the only neutrons found in Nature are within nuclei--so that they must be extracted by bombardment by other particles or produced in such a process as fission. Because of their neutrality it is difficult to collimate and direct them to form beams of monoenergetic neutrons, and of course there are attendant detection problems. These problems will be discussed in a parallel session which follows. But perhaps a few examples are in order principally to point to the increased sophistication and sensitivity of experiments which have become feasible in recent years.

At reactors the traditional chopper method has been augmented by the use of filters, a method pioneered at the MTR, but now

in use at many installations such as NBS and BNL(1). The use of a scandium plus titanium filter provides a very clean beam for 2keV neutrons, the Fe + Ti Filter a beam for 25keV neutrons while at 144 keV, a Si filter is used. Improvements associated with the electron linac which is at present the most effective source of neutrons include the recent extension into the MeV range. Experiments involving neutrons with energies up to 20 MeV appear to be possible. At ORELA it has also been proven possible to measure inelastic neutron cross-sections very accurately. These measurements involve being able to determine the energies of both the incident and emergent neutron. Although it is a much older method, first developed by Bertozzi, Paolini and Sargent (2) in 1958, the threshold photoneutron reaction in which low energy neutrons are produced using the high energy end of a brems-strahlung spectrum has been extensively employed.

One of the problems of great importance is the determination of the quantum numbers of neutron resonances, such as their spin. In this connection I would like to mention two developments. One is the use of a photoneutron polarimeter system, which determines the polarization of the emergent neutron, developed at ANL (3). The application of that system to the reaction $^{208}Pb(\gamma,\vec{n}_o)^{207}Pb$ showed that the resonances at photon energies of 7.56, 7.70, 7.92, 7.98, 8.03, and 8.23 MeV are E1 excitations not M1 as originally believed. Another beautiful example is the spin determination of resonances in the neutron interaction

with ^{237}Np and ^{235}U by a Los Alamos-Oak Ridge collaboration (4). A pulsed neutron beam which has been polarized strikes a polarized ^{235}U target. Measurements of the resonance cross-sections are made with these polarizations parallel and anti-parallel permitting the determination of the spins of 65 resonances below 60eV in ^{235}U. Where it can be applied this method is more effective than the traditional methods such as observation of de-excitation gamma rays or the measurement of both total and scattering cross-sections. I won't continue this tabulation. It is not complete. The intent is to provide a feeling as to the quality of measurements and the sophistication of the technique which are now possible. Precision is now beginning to approach that which is achieved in charged particle reactions. More examples will naturally turn up in the course of this report and during the conference.

This increased precision and capability have led to the discovery of new phenomena and an incisive examination of ones thought to be thoroughly understood. This has led at the same time, quite in parallel to the experimental developments, to a more sophisticated theoretical treatment of neutron reactions which has in many cases a more direct dependence on the structure of the nuclei involved.

Let me begin with an old friend--the elastic scattering of neutrons by nuclei and its theoretical description by the optical model which provides the average amplitude to which one

must add the fluctuation cross-section determined empirically or calculated using the statistical model. The optical model, that is the single particle model description for the neutron-nucleus interaction, has proved to be extraordinarily useful, but in its traditional form it takes into account only the global aspects of the interaction as expressed in the smooth dependence upon the mass and atomic number, the radius, skin thickness, deformation parameter etc. for the real and imaginary part of each term in the optical potential of a given spatial symmetry. I shall not describe these, assuming your familiarity with them; nor shall I summarize the various spatial spin and isopin forms nor the energy dependence of the associated empirical constants which have been proposed. Suffice it to say these exist and are given for example in Atomic Data and Nuclear Data Tables by Perey and Perey (5) together with a table of empirical constants determined by various analyses. A deviation from the smooth behavior may be indicative of an effect of some special aspect of the structure of the nucleus interacting with the neutron. There are such deviations, discernible because of higher quality data, and these deviations must be taken into account when the optical model wave functions are used in the discussion of other phenomena involving the same nucleus. Such deviations from the global values are expected if the target is easily polarized by the incident neutron. In that case it is best to use a coupled channel description in which the incident channel, neutron plus target in its ground state is

coupled to an excited state of the system. In the case of a vibrational nucleus for example, that might consist of a neutron and the target in a one-phonon state. Solcviev as well as Beres, Divadeenam, Newson and a number of collaborators have used this approach. If the shell model approach appears appropriate, the second stage would consist of the neutron plus a particle-hole excitation, i.e., a 2p-1h or three quasi-particle state. If only one such excited state is involved this process is referred to as a 2-step process. In the coupled channel description these two steps occur many times coherently with the one-step process. The general case of many steps has been reviewed by Tamura (6).

The concept of the multi-step process is of venerable age so that there are many examples of its use in, for example, reactions induced by charged particles. An interesting recent example is concerned with neutron scattering by the even Sm isotopes (7). It might be useful to give some of the details. A two-stage process, in which the 2+ rotational state was excited was used for ^{152}Sm and ^{154}Sm. The nucleus ^{148}Sm was considered to be a vibrator, the excited level in the second stage is then a 2+ vibration. Both assumptions were tried for ^{150}Sm. Total cross-sections for ^{148}Sm, ^{150,148}Sm, ^{152,148}Sm, ^{154,148}Sm were measured for neutron energies varying from 0.7 to 15 MeV. Differential cross-sections were obtained at 7.0 MeV neutron energy. The calculation of the coupling matrix elements was macroscopic in

nature--i.e. $V_{opt} = V_{opt}(R,A,Z,N,\vec{\sigma},\vec{\ell})$ where $R = R_o [1 + \Sigma_{\lambda\mu} \alpha_{\lambda\mu} Y_{\lambda\mu}(\Omega)]$ for the vibrator and $R = R_o(1 + \Sigma_{\lambda'} \beta_{\lambda'} Y_{\lambda' o}(\theta'))$ in the body fixed system for the deformed case. V_{opt} was obtained by fitting low energy data on these nuclei and by employing empirical V_{opt} valid in this energy and mass number range. The results are shown in Figures 1,2,3,4. We see that the deformation or vibration optical models are quite capable of obtaining good fits for the "obvious" vibrator ^{148}Sm and the "obvious" rotators ^{152,154}Sm. In the latter case the value of the deformation, the parameter β_2, is determined to within 10%. The question of ^{150}Sm is moot although the data favors the vibrational description. Improved data should resolve the issue. The paper did not quote the magnitude of the statistical contribution to the inelastic cross-section.

Coupled channel calculations have in this context, though not in others, employed only the excited states of target nuclei in forming channels. The possibility of the 2nd stage involving particle transfers or charge exchange should also be considered. These could be important whenever the energy expended is not large and if the coupling matrix elements are relatively large, as would be the case if the 2nd stage system resonated at the appropriate energy. The importance of such a process would be suggested if the associated reaction had an appreciable cross-section.

One of the dividends of a coupled channel calculation is the cross-section for inelastic scattering, in the above case

to the 2^+ state of the target. Many of the theoretical discussions of neutron induced reactions have been based on the statistical model. But as the above remarks make clear, the direct process also contributes to the cross-section, a point which has been made by several investigators. It is expected that the direct component will rapidly become more important as the neutron energy increases for excitations to low lying states of the residual nucleus; statistical theory will still be applicable to the low energy part of the emergent particle spectrum. Whether the evaporation model, in which angular momentum considerations appear only in the level densities, is used or whether one employs a model which explicitly conserves angular momentum depends very much upon the density of levels in the residual nucleus. If the levels are sparse the second is appropriate. This point manifests itself quite strongly when reactions involve the emission of a second particle, e.g. (n,2n), (n,nα), (n,nγ) etc. The process occurs sequentially so that the first step involves an inelastic excitation, while the second involves the emission of a neutron, α, or γ, in the three cases specifically mentioned. If the energy available after emission is small so that only low lying levels of the residual nucleus are possible, angular momentum considerations can play a significant role. For example in the case of second stage alpha particle emission the use of the simple evaporation model can lead to errors of the order of magnitude of 20 as exemplified by the $^{63}Cu(n,n\alpha)^{59}Co$ reaction (E_n = 12MeV) to the ground state of the

latter according to Fu and Perey (8). Of course this is a reflection of the sensitivity of the alpha particle transmission factor to the angular momentum barrier. Another example is discussed by Fu (9) namely the $^{40}Ca(n,x\gamma)$. See Figure (6). The superiority of the more detailed model over the evaporation model is apparent. Another example in the same figure is the $(n,np\gamma)$ reaction (unlabelled) in where we see that 2.817 MeV γ-ray to the ground state is more abundant than the γ-rays from the 2.526 or 3.02 levels, a conclusion which one could not obtain using the simple evaporation model. A similar point has been made in regard to γ decay from a nucleus which has been excited to a high spin state. Even after the evaporation of several neutrons the nucleus is left with a high spin which of course has a strong effect on which γ ray transitions will be favored.

These remarks emphasize the care with which sequential processes need to be treated. In particular it is not surprising that the (n,2n) process is not always as simple as was originally thought when this process was considered as two sequential evaporations. In Figure (7) we see an example (10) of how this recipe fails and the need to add in the "pre-equilibrium" component. In another paper, [Figure (8)] a direct component (11) is added in as well.

The pre-equilibrium process was first suggested by Griffin who used some qualitative considerations of Weisskopf and Block. A vast literature has grown up around this topic and I shall not

attempt to summarize it. Suffice it to say that it is in its present form a semi-classical theory with a number of ad-hoc empirical elements. It does not have the ability to calculate angular distributions, nor does the recipe invoked for multi-particle production seem to be entirely satisfactory. But within these limitations it is highly successful, often achieving quantitative understanding of the data.

As it turns out this is a very fundamental problem, and perhaps it is worth a little overall review before we proceed with the discussion. The neutron spectrum in, say, an (n,n′) reaction has the shape shown in Figure (9). The high energy end corresponding to low excitation energies of the residual nucleus is, at sufficiently high energy, dominated by the direct process while the low energy end is for the most part an evaporation spectrum. The angular distribution is strongly anisotropic and asymmetric at the high energy end while it is spherical in the evaporation region. The problem we face is to fill in and understand the "in between". We have already mentioned some important points. In most of this region the evaporation theory is not adequate. Secondly, the Bohr independence hypothesis is not valid. Finally, in the few cases which have been investigated, the angular distribution is symmetric about 90° close to the evaporation region but is asymmetric near the direct interaction region.

Beside the immediate goal of predicting the cross-section in this intermediate region, the resolution of the problem has

an impact on two problems of great importance and generality. The first has to do with the compound nuclear wavefunction. Although Breit and Wigner taught us how to describe a compound nuclear resonance and although a number of theories of nuclear reactions are available, yet a description of the compound nuclear wavefunction does not exist today. The second, as pointed out by Agassi and Weidenmüller, is the problem of the non-equilibrium quantum statistical mechanics of relatively small systems. Nuclear reactions present a unique opportunity for studying this problem.

I shall very briefly present a general statistical theory developed by Kerman, Koonin and myself. Presentations were made in several conferences that were held in 1973 (12, 13), but no full account has yet been published. Of course I cannot give a full account here; just a summary of the concepts, assumptions and results. It is assumed that the reactions proceed through a set of stages of increasing complexity (Figure 10). Complexity is defined in terms of the description appropriate to the nuclear system under investigation. If the shell model is used, as is done in Griffin's model, complexity is defined in terms of the number of particles and holes; the simplest is the incident one-particle state, the next more complex are the 2p - 1h states, the next the 3p - 2h states etc. If a vibrational model is used, the complexity is defined in terms of the number of phonons. The reaction can end at any step in the chain by a transition to the final state. The second assumption is the

chaining hypothesis which states that a given stage can be connected by the residual Hamiltonian only with its nearest neighboring stages, that is those differing at most by unit complexity. Finally the statistical hypothesis is assumed. One immediate consequence is that amplitudes for particles emitted from differing stages do not interfere. But in addition the statistical assumption is used differently according to whether there are particles in the continuum in a given stage or all particles are bound. These two non-interfering contributions to the cross-section are referred to as multi-step direct and multi-step compound. The statistical averaging in the second case asserts that states of differing angular momentum J and parity π do not interfere. To this is added the assumption, which can be verified in a given model, that $\Gamma_n >> D_{n-1}$ where Γ_n is the average width of states in the n'th stage and D_{n-1} is the level spacing in the (n-1)st stage. One obtains the familiar statistical result that the angular distribution is symmetric about 90°. It is expected that the multi-step compound forms the major contribution in the region close to the evaporation region and becomes less and less important as the direct region is approached. The average multi-step compound fluctuation cross-section for a given J and π is

$$\sigma_{fi}^{(fluct)} = \frac{\pi}{k^2} \sum_{n=1}^{r} \frac{\Gamma_n^{(f)}}{\Gamma_n} \left[\prod_{k=1}^{n-1} \frac{\Gamma_k^{\downarrow}}{\Gamma_k} \right] \left(2\pi \frac{\Gamma_1^{(i)}}{D_1} \right) .$$

The terms have a fairly transparent meaning. The first term

measures the probability of going with the first stage, the product gives the attenuation of the incident flux because of emission while en route to the n'th stage and the last factor gives the probability of emission into the final state. This result is very similar to that obtained in the Griffin model.

The statistical approximation in the case of the multi-step direct component is complementary in its nature to that employed for the multi-step compound. It states that

$$\sum V_{\gamma\alpha}(\vec{k}_2,\vec{k}_1)V_{\alpha i}(\vec{k}_1,\vec{k}_2)V^{*}_{i\alpha}(\vec{k}_i,k_1\vec{\Omega}_1')V^{*}_{\alpha\gamma'}(k_1\vec{\Omega}_1',\vec{k}_2') \sim \delta(\vec{\Omega}_1-\vec{\Omega}_1'). \quad (1)$$

In this expression V is the matrix element of the residual interaction using distorted waves between states α of stage 1 and states γ of stage 2; $\vec{k}_1$ etc. give the momenta of the particle in the continuum and $\vec{\Omega}_1$ is a unit vector in the $\vec{k}_1$ direction. With this random phase approximation one obtains for the differential cross-section:

$$\left\langle \frac{d\sigma(\vec{k}_f,\vec{k})}{d\Omega_f dU_f} \right\rangle_f = \sum_{n,\nu} \int \frac{d\vec{k}_1}{(2\pi)^3} \cdots \int \frac{d\vec{k}_\nu}{(2\pi)^3} \left[\frac{\pi\hbar d\omega_{n,\nu}(\vec{k}_f,\vec{k}_\nu)}{d\Omega_n d\Omega_f} \right] \left[\frac{\pi\hbar d\omega_{\nu,\nu-1}(\vec{k}_\nu,\vec{k}_{\nu-1})}{d\Omega_\nu dU_\nu} \right]$$

$$\cdots\cdots \frac{\pi\hbar\, d\omega_{2,1}(\vec{k}_2,\vec{k}_1)}{d\Omega_2\, dU_2} \quad \frac{d\sigma_{1i}(\vec{k}_1,\vec{k}_i)}{d\Omega_1\, dU_1} \,. \qquad (2)$$

The first term on the right gives the differential probability for going from the incident channel to the first stage in which the residual nucleus has an excitation between U_1 and $U_1 + dU_1$.

The factor $d\omega_{21}(\vec{k}_2,\vec{k}_1) / (d\Omega_2 dU_2)$ gives the differential probability per unit time for a transition from $\vec{k}_1$ to $\vec{k}_2$ and the residual nucleus from stage 1 to stage 2. These quantities are essentially direct reaction transition probabilities using distorted waves, and the cross-section is given simply by folding the direct reaction cross-sections over all possible intermediate steps conserving energy at each step. This expression is exactly what one would expect in the kinetic theory classical discussion of the passage of a particle through a Fermi gas model of the nucleus. Though of course it applies more broadly. It thus connects directly with Bertini's cascade theory. But importantly it also establishes a connection with the multiple scattering theory applicable at higher energies. Indeed as the energy increases the contribution of the multi-step compound process will correspondingly decrease.

Two applications will be reported both dealing with the multi-step compounds process. The neutron spectra produced by the reactions, $^{51}V(p,n)\ ^{51}Cr$, are shown in Fig. 11. The experiments were performed by Grimes, Anderson, Wong et al. at the Lawrence Livermore Laboratory. The angular distributions of the neutrons at the low energy end of the spectrum are isotropic while those nearby are symmetric about 90°. The data is fitted by the above theory using two constants, g, measuring the level density in the residual nucleus and, v, the strength of the residual interaction.

A second application is concerned with the (γ,α) reaction. Although it is not directly connected with the subject of this conference, I bring it up because of the insight it gives into the question of the conservation of isospin. The experiment in question is $^{28}Si(\gamma,\alpha)^{24}Mg$ and $^{30}Si(\gamma,\alpha)^{26}Mg$ in the region of the giant dipole. The first of these is isospin forbidden. Nevertheless its cross-section is larger than the second which is isospin allowed. By adapting the multi-step compound analysis discussed above R. L. Feinstein (14) was able to show that isospin was not conserved primarily because of the many steps involved in building the alpha particle whereas isospin conservation should hold in the (γ,p) or (γ,n) process since these are essentially one-step processes. The point I emphasize here is that isospin conservation will generally not hold for multi-step and compound nuclear processes. This issue of isospin conservation may be of importance for the (n,α) reactions discussed by J. Harvey at this conference.

It is often the case, as it was for the (p,n) reactions discussed above, that only a few steps contribute to the pre-equilibrium component. If only one step beyond the incident channel is important, the multi-step compound reaction reduces then to the statistical theory of doorway states as discussed in detail in reference [15]. This was recognized by Grimes, et al. (16) who were able to fit the data using this model, obtaining thereby values for the average doorway state width and spacing. It is amusing to recall that the paper in which the

name "doorway states" was introduced (17) was one which employed the statistical theory of doorway states to explain the S-wave strength function, with particular attention to the deep minimum in the A = 110 region. Figures (12), (13) and (14) provide strength functions for S, P and D waves tabulated by Wilmore and Hodgson (18). Recently that approach to the strength function was renewed and improved by Müller, Rohr [19] and Kirouac [20]. The former authors looked particularly at the 3S resonance region, the latter at the 4S. The structure in the 4S region is shown in Figure (15) where we see a strong odd-even effect, the strength function for the even Z, odd N nuclei lying above that for the even Z-even N nuclei. The changes in the work of Block include (1) a spin cut-off factor rather than a multipole expansion, replacing thereby three empirical parameters by one; (2) an explicit A dependence of the average escape width, namely $(1/A^3)$, and (3) the use of the Fermi gas to estimate the density of 3 quasi-particle states. The results are shown in Fig. (16). Similar results were obtained by Müller and Rohr for the 3S region. However this simple model fails in the regions in between and one then has to return to the more complex model of Block. The $(1/A^3)$ dependence of the width is also obtained in the studies of pre-equilibrium reactions. These results are very tantalizing; the dependence on doorway state density seems to be clear on an empirical basis. More theoretical studies are needed.

The identification of individual isolated doorway states has proven to be difficult except in the case where symmetry effects or a dynamical mechanism operates. The first is exemplified by the isospin analog states, the latter by the giant multipole resonances and by subthreshold fission. Theoretical indications that isolated doorways for neutrons interacting with nuclei exist near closed shell nuclei are borne out by experiment.

The most thorough examination of neutron reactions for identification of doorway state effects has been performed by the Duke group, Bilpuch, Newson, Beres, Divadeenam and their collaborators. The whole effort is made possible by the extraordinary high experimental resolution which the Duke group has obtained. I won't attempt to discuss their results since these were reviewed by Newson (1) at the 1971 Albany Conference. Evidence for doorway structure was found for target nuclei $Pb^{206,207,208,209}$, Tl^{205}, $Ni^{56,58}$, Fe^{54}, $Ca^{40,44,48}$, Si^{28} and ^{88}Sr. Theoretical calculations using the 2p-1h description of doorways or the particle-vibrator model are in qualitative agreement with these identifications. The small value of the strength function for ^{48}Ca for energies ranging up to 1.4 MeV was for example shown to be the consequence of the absence of any doorway state in that region, an effect predicted by the calculations of Beres and Divadeenam. The p wave doorway state in ^{28}Si has since been observed by Jackson and Toohey (22) who studied the reaction $^{29}Si(\gamma,n)\ ^{28}Si$ and find a very strong correlation

between the partial neutron and gamma-ray widths [Fig. (17)]. Similarly the Australian-Oak Ridge group verified the doorway in ^{89}Si (23). On the other hand the Oak Ridge Group (24) upon investigation of the reaction $^{206}Pb(n,\gamma)$ do not corroborate the doorway state in $^{206}Pb + n$. This does not necessarily mean that this doorway state does not exist. It could be explained if the structure of the state were such as to make gamma transitions unfavored. One result, in agreement with Payne's and other calculations, is that the width of the doorways as one proceeds away from closed shell nuclei rapidly increases and they become impossible to observe if indeed one can say they exist at all.

It is by now some eight years since the phenomenon of intermediate structure in sub-threshold fission as illustrated in Figure (18) for $^{240}Pu(n,f)$ was discovered. It should be recalled that the total neutron cross-section in the same energy domain does not show this clustering phenomenon. By this time other examples of this phenomenon have been found. A recent review has been given by Michaudon (26) and he also reports to this conference. The phenomenon is understood on the basis of the double humped barrier as proposed by Strutinsky and applied to this situation by Weigmann and Lynn (see Fig. 19). From the point of view of reaction this may be regarded as an example of an exit doorway. The picture has been verified by the observation of electromagnetic transitions in the class II region. It has been suggested that rotational levels built

upon these vibrational levels may exist. These levels seem to have been observed in the case of $^{232}Th(n,f)$ as reported by Blons et.al. (27). From these data the moment of inertia associated with the second region can be determined. A similar result has been surmised for ^{238}U by an Oak Ridge group. They found a number of fission clusters whose average spacing is too small for vibrational clusters (28). Parenthetically Perez and de Saussure (29) observe an entrance channel doorway in the reaction $^{238}U(n,\gamma)$. See also Spencer and Karppeler confirming results (30).

The doorway state can often decay into several channels. If the branching ratios for a number of channels are substantial, the channels are said to have a common doorway, a phrase coined by Lane. He employed it in connection with radiative neutron capture (or its inverse, the threshold photoneutron reaction) where the doorway is common to both the neutron and gamma-ray channels. The consequences are that there can be a strong correlation between the partial neutron width and the partial gamma ray width and also with (d,p) spectroscopic factor. As the careful experiment of Chrien, Cole, Slaughter and Harvey (31) on $^{98}Mo(n,\gamma)^{99}Mo$ has shown, the correlation is strong when the ground state of the residual nucleus has a strong single particle character and the resonant state in $^{98}Mo+n$ can be excited by absorption of a gamma ray. Such a transition picks out the single-particle component of the resonant state. A valence model such as that of Lane and Lynn (32) suggests itself.

This model has had quantitative success in these correlated transitions. However, it is not clear why the complex nature of the resonant state can be neglected, a problem which has been discussed by Lane (33).

A second phenomenon which has been the source of much concern relates to the photon strength function for the heavy elements $73 \leq Z \leq 82$. A typical example (34) is shown in Fig. (20) in which the photo-strength function for ^{197}Au and ^{198}Au is given. The broken curve is the Lorentzian from the giant dipole resonance in Au. We see a strong dip in the data below 5 MeV. Originally it was suggested that these data could be understood on the basis of a single doorway state. However, according to the shell model calculations on ^{208}Pb by Khanna and Harvey such a description is not tenable and that one must assume that several doorway states contribute. The calculation does provide an explanation of the dip below 5 MeV which arises from the presence of a parity gap, that is a gap of (ph) states with the correct parity.

I shall not discuss a number of theoretical investigations which will be presented to this conference. There is the familiar problem of the statistical properties of the resonance parameters to be discussed by Mello and Flores. There is the paper of Jeukenne, Lejeune and Mahaux to be presented by Mahaux. In all of the previous discussion very little attention is paid to the relationship between the phenomena and the underlying nuclear forces. In this paper the calculation of the real and

imaginary part of the optical potential in the Brueckner-Hartree-Fock framework is performed with very encouraging results. And finally there is the paper of Soloviev who considers the strength functions using the quasi-particle formalism.

REFERENCES

1. For a review see C. D. Bowman, p. 119 "Nuclear Cross Sections and Technology" NBS Special Publication NBS 425 (Oct. 1975).

2. W. Bertozzi, F. R. Paolini, C. P. Sargent Phys. Rev. 110, 790 (L), (1958).

3. R. J. Holt and H. E. Jackson Phys. Rev. Letters 36, 244, (1976).

4. G. A. Keyworth, C. E. Olesen, F. T. Seibel, J. W. J. Dabbs, N. W. Hill Phys. Rev. Letters 31, 1077, (1973).

5. C. M. Perey and F. G. Perey Atomic and Nuclear Data Tables 13, 293, (1974).

6. T. Tamura Physics Reports, 14C, 61, (1974).

7. R. Shamu, G. Haouat, J. Lachkar, Ch. Lagrange, M. McEllistrem, Y. Patin, J. Sigaud, F. Cocu, E. Bernstein and J. Ramirez presented at the National Soviet Conference on Neutron Physics (Kiev, June 9-13, 1975).

   J. P. Delaroche, Ch. Lagrange, and J. Salvy presented at a conference held Dec. 8-12, 1975 at the ICTP, Trieste on "The Use of Nuclear Theory in Neutron Data Evaluation."

8. C. Y. Fu and F. G. Perey Jl. of Nuclear Materials, to be published.

9. C. Y. Fu "Nuclear Cross Sections and Technology", NBS Special Publication 425 (Oct. 1975) p. 329.

10. D. Hermsdorf, G. Kiessig, and D. Seeliger presented at a conference held Dec. 8-12, 1975 at the ICTP, Trieste on "The Use of Nuclear Theory in Neutron Nuclear Data Evaluation".

11. H. Jahn, C. H. M. Broeders and I. Broeders p. 353, "Nuclear Cross Sections and Technology", NBS Special Publication 425 (Oct. 1975).

12. H. Feshbach Rev. Mod. Phys. 46, 1, (1974).

13. H. Feshbach Proceedings of the International Conference on Nuclear Physics, Munich, Aug. 27 - Sept. 1, 1973. J. de Boer and H. J. Mang editors. North Holland (1973).

14. R. L. Feinstein M.I.T. Thesis (1975).

15. H. Feshbach, A. K. Kerman, R. H. Lemmer Ann. Phys. (N.Y.) 41, 230 (1967).

16. S. M. Grimes, J. D. Anderson, R. A. Pohl, J. W. McClure and C. Wong Phys. Rev. C3, 645, (1971) Phys. Rev. C4 607 (1971).

17. B. Block and H. Feshbach Ann. Phys. (N.Y.) 23, 47, (1963).

18. D. Wilmore and P. E. Hodgson presented at a conference held Dec. 8-12, 1975 at the ICTP, Trieste on "The Use of Nuclear Theory in Neutron Nuclear Data Evaluation".

19. K. N. Müller and G. Rohr Nucl. Phys. A164, 97 (1971).

20. G. J. Kirouac p. 338 "Nuclear Cross Sections and Technology" NBS Special Publication 425, (Oct. 1975).

21. H. W. Newson "Strength Functions and Intermediate Structure: in Statistical Properties of Nuclei, edited by J. B. Garg Plenum Press, New York (1972).

22. H. E. Jackson and R. E. Toohey Phys. Rev. Letters 29, 379, (1972).

23. J. W. Boldeman, B. J. Allen, A. R. deL. Musgrove and R. L. Macklin submitted to Nuclear Physics.

24. B. J. Allen, R. L. Macklin, C. Y. Fu, and R. R. Winters Phys. Rev. C. 7, 2598, (1973).

25. E. Migneco and J. P. Theobald Nucl. Phys. A112, 603, (1968).

26. A. Michaudon Advances in Nuclear Physics 6, 1, (1973).

27. J. Blons, C. Mazur and D. Paya p. 642 Nuclear Cross Sections and Technology NBS Special Publication 425 (1975).

28. F. C. Difilippo, R. B. Perez, G. de Saussure, D. K. Olsen and R. W. Ingle contributed paper PB1/J3 this conference.

29. R. B. Perez and G. de Saussure p. 623 Nuclear Cross Section and Technology NBS Special Publication 425 (1975).

30. R. R. Spencer and F. Karppeler p. 620 Nuclear Cross Sections and Technology NBS Special Publication 425 (1975).

31. R. E. Chrien, G. W. Cole, C. G. Slaughter and J. A. Harvey Phys. Rev. C. 13, 578, (1976).

32. A. M. Lane and J. E. Lynn Nucl. Phys. 17, 563 & 586, (1960).

33. A. M. Lane Ann. Phys. (New York) 63, 171, (1971).

34. G. A. Bartholomew, E. D. Earle, A. J. Ferguson, J. W. Knowles, and M. A. Lane Advances in Nuclear Physics 7, 229, (1973).

FIGURE CAPTIONS

Figure 1 The total cross section of ^{148}Sm for neutron scattering. The error bars indica e statistical errors only. The curves are obtained from coupled channel calculations for the assumptions given in the figure. (See Ref. 7)

Figure 2 Elastic scattering angular distributions for ^{148}Sm and ^{150}Sm at 7.0 MeV incident neutron energy. The curves are obtained from coupled channel calculations for the assumptions given in the figure. (See Ref. 7)

Figure 3 Angular distributions given the sum of the elastic cross section and the cross section for the excitation of the first 2^+ level for ^{152}Sm and ^{154}Sm for 7 MeV incident neutron energy. The curves are obtained from coupled channel calculations for the assumptions given in the figure. (See Ref. 7)

Figure 4 The measured total cross-section difference divided by the ^{148}Sm total cross-section for $^{150,148}Sm$, ^{152}, ^{148}Sm and $^{154,158}Sm$. All shown are coupled channel calculations assuming rotational (full line) or vibrational (dashed line) models. The quadrupole deformations were $\beta_2 = 0.14, 0.17, 0.22, 0.24$ for ^{148}Sm, ^{150}Sm, ^{152}Sm, respectively. (See Ref. 7)

Figure 5 Calculated helium production cross-section for ^{63}Cu. "Total" is the sum of (n,α), (n,αx), and (n,nα). Dots are calculations for (n,nα) in which the spins of the states of ^{59}Co are set equal to 1/2 instead of the correct values of 7/2, 3/2, 5/2, 3/2, 1/2, 9/2, 5/2 and 7/2. (See Ref. 8)

Figure 6 Pronounced gamma rays arising from ^{40}Ca (n,xγ) reactions for 18.5 MeV incident neutrons. The levels excited in $^{40}Ca(n,np)^{39}K$ reaction are shown. (See Ref. 9)

Figure 7 Evaluation of neutron emission spectrum from $^{93}Nb+n$ at 14 MeV incident energy. Full line represents calculation with the program, Glune, dash-dotted curve shows the pre-equilibrium contribution. (See Ref. 10)

Figure 8 Comparison between measured and calculated angular integrated inelastic cross-sections where the fit includes the direct part. The reaction is $^{56}Fe(n,n')$, at a neutron energy of 14 MeV. (See Ref. 11)

Figure 9 Schematic spectrum of particles emitted in a nuclear reaction.

Figure 10 Stages in a nuclear reaction.

Figure 11 Comparison of theory with experiment $^{51}V(p,n)\ ^{51}Cr$. Calculated values are denoted by o = pre-compound, □ = evaporation, x = total values. The experimental data was provided by Grimes et al. (See Ref. 13)

Figure 12 Experimental data on neutron s-wave strength functions compared with spherical and deformed optical-model results. (See Ref. 18)

Figure 13 Experimental data on p-wave strength functions compared with calculations with a non-local potential. (See Ref. 18).

Figure 14 Experimenta data on d-wave strength functions compared with calculations with a non-local potential. (See Ref. 18)

Figure 15 s-wave neutron strength functions of even Z - odd N nuclei (open symbols) and even Z - odd N nuclei (closed symbols) in the first peak of the 4S resonance. Three odd Z isotopes (x) are shown. (See Ref. 20)

Figure 16 Calculated fluctuations in s-wave neutron strength functions $143 < A < 158$. (See Ref. 20)

Figure 17 Ground state radiation widths Γ_{γ_0} and reduced neutron widths γ_n^2 for resonances in the ^{29}Si compound nucleus with $J^\pi = \frac{3}{2}^-$. ρ gives the correlation coefficient. (See Ref. 22)

Figure 18 High resolution subthreshold fission cross-section for $^{240}Pu(n,f)$. (See Ref. 25)

Figure 19 Potential energy of deformation as a function of the deformation parameter β; taken from A. Mekjian, Advances in Nuclear Physics, 1, 1, (1973).

Figure 20 Strength functions for Au. a) The solid circles are from $\sigma_{\gamma\gamma}$ while the points above 8 MeV are from $\sigma_{\gamma n}$. (b) The points O, ▲ and ● are from the spectrum fitting method - thermal (n,γ) data, the sequential extraction method $(d,p\gamma)$ data, and the high resolution method. (c) The open circles are from the spectrum fitting method. (See Ref. 34)

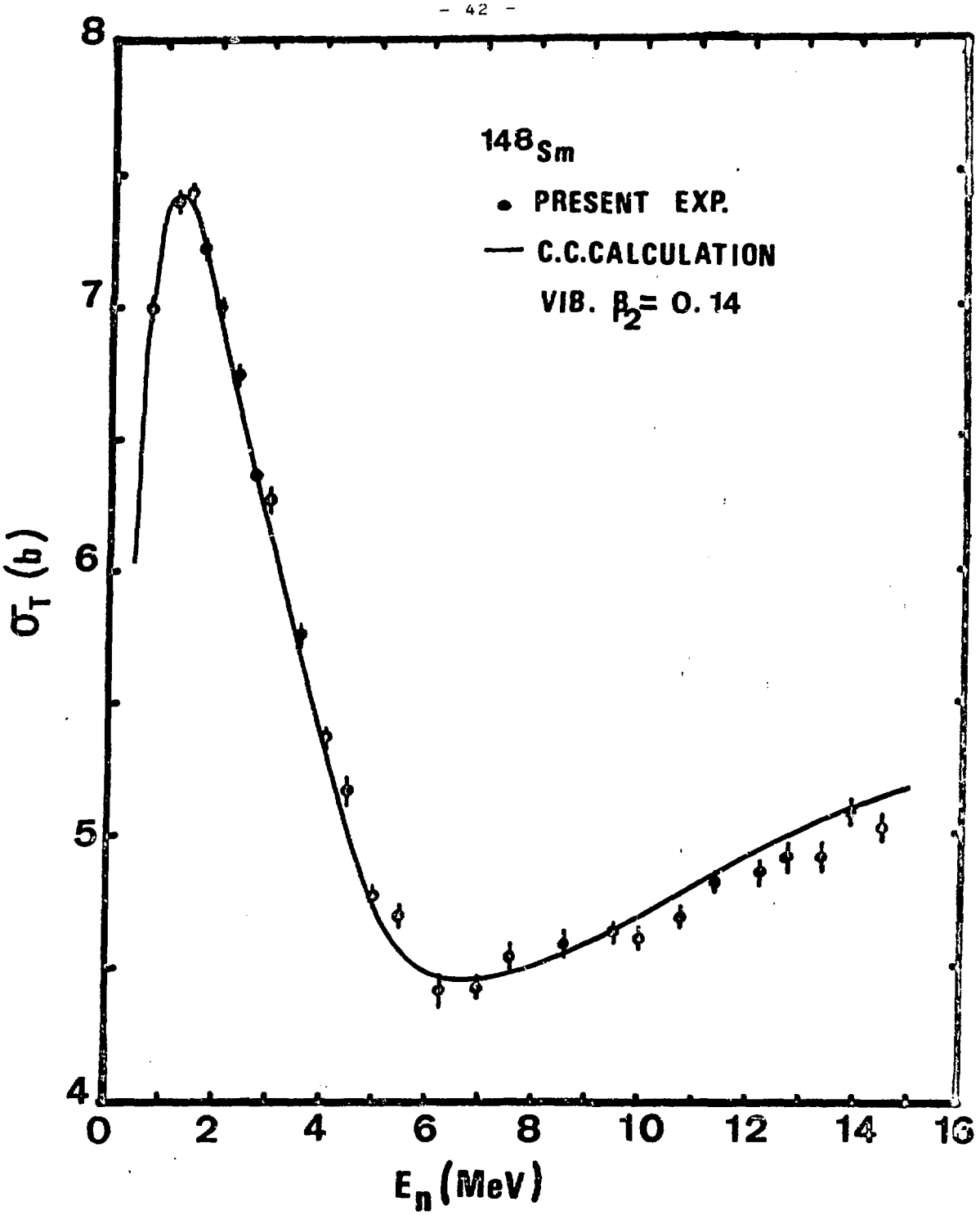

FIG. 1 - The total cross section of ^{148}Sm for neutron scattering. The error bars indicate statistical errors, only . The solid curve was determined using deformed-potential optical-model coupled-channel calculations assuming ^{148}Sm was a vibrational nucleus with $\beta_2 = 0.14$

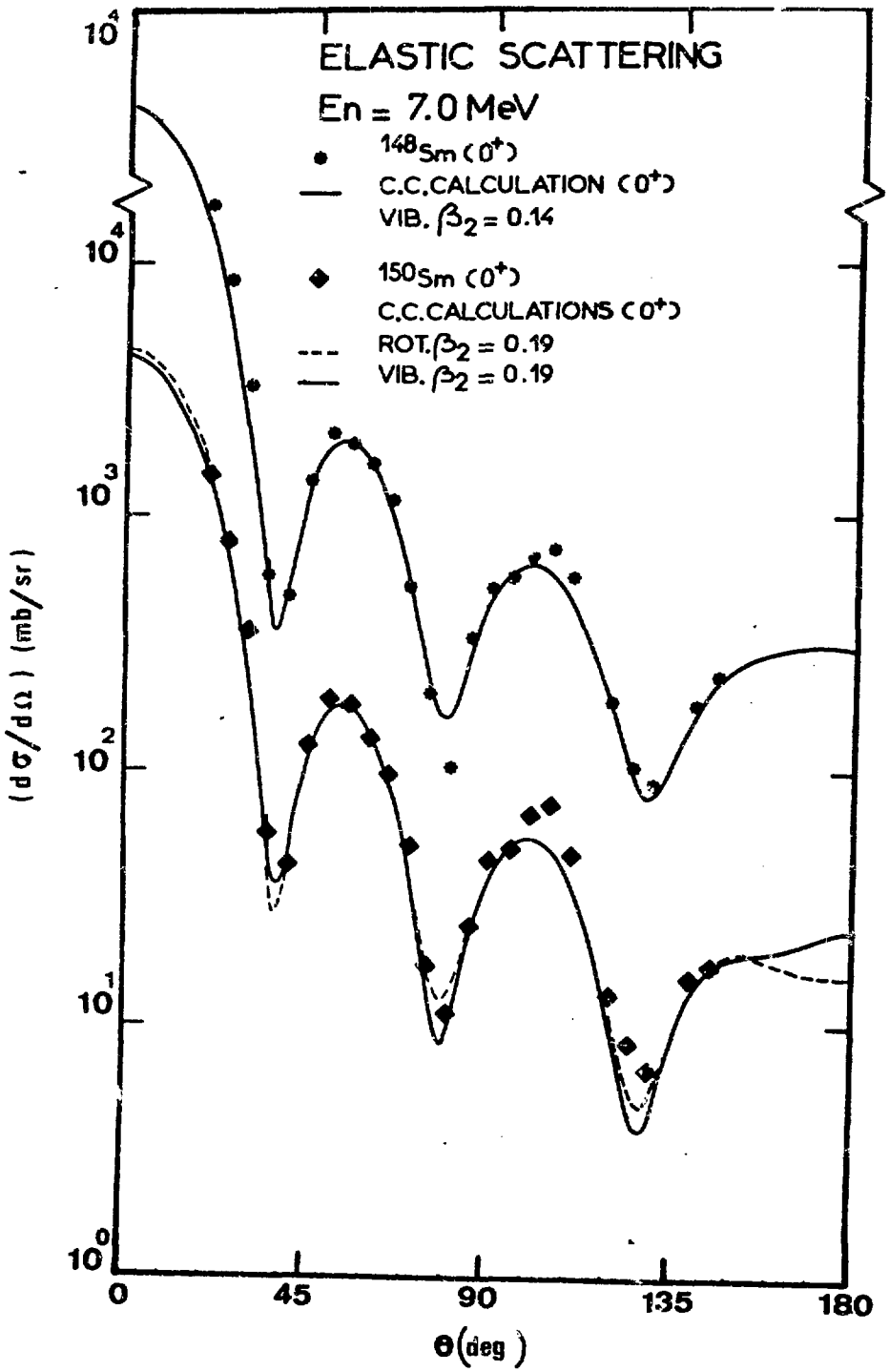

FIG. 2 - Elastic scattering angular distributions for ^{148}Sm and ^{150}Sm at 7.0 MeV incident neutron energy . The curves are the results of coupled-channel calculations for the assumptions given in the figure .

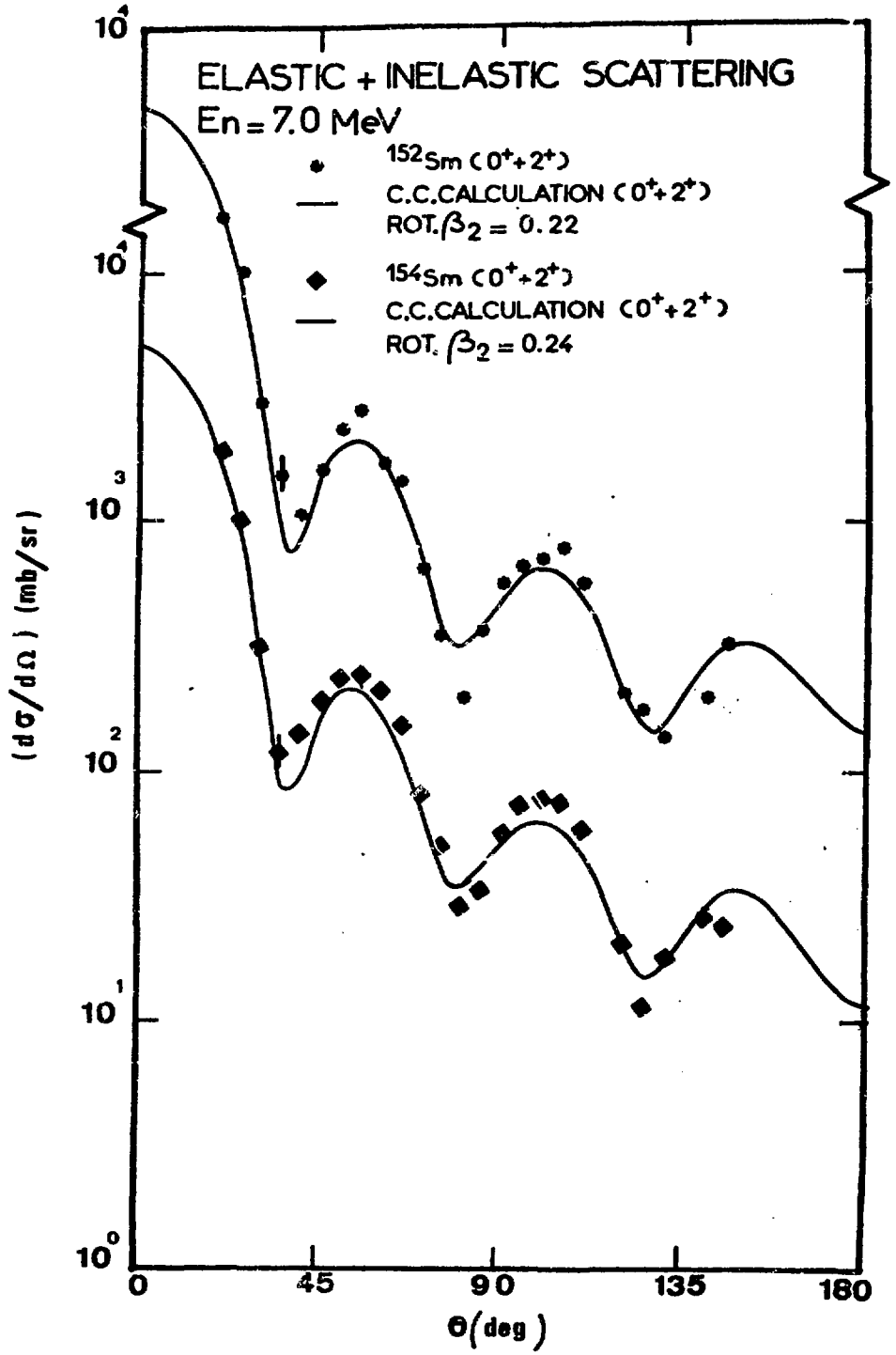

FIG. 3 - Angular distributions for the sum of elastic and inelastic (first 2^+ state) cross sections for ^{152}Sm and ^{154}Sm at 7.0 MeV incident neutron energy . The two solid lines represent the calculated cross sections for elastic plus inelastic (2^+) scattering by ^{152}Sm and by ^{154}Sm .

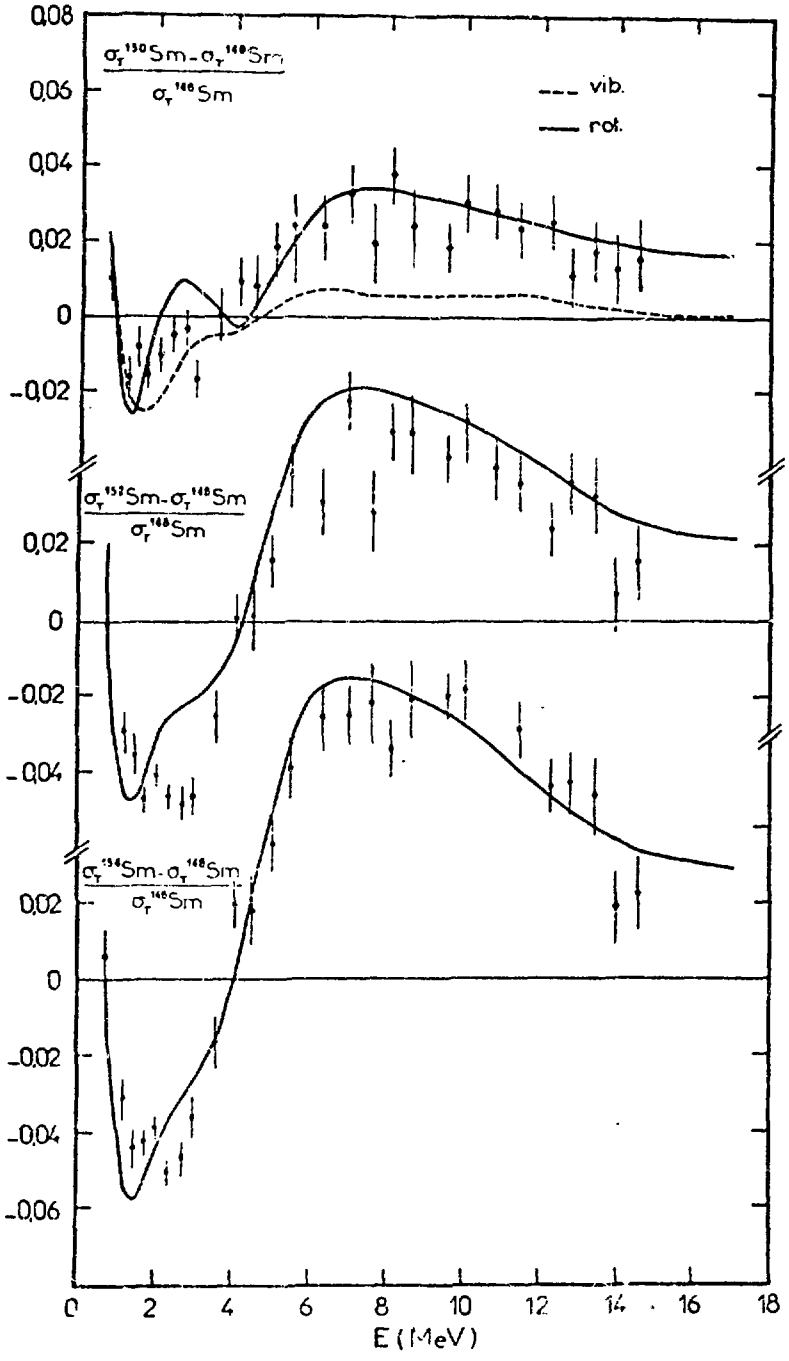
0,08
0,06
0,04
0,02
0
-0,02
$\frac{\sigma_\gamma^{150}Sm-\sigma_\gamma^{148}Sm}{\sigma_\gamma^{148}Sm}$
--- vib.
— rot.
0,02
0
-0,02
-0,04
$\frac{\sigma_\gamma^{152}Sm-\sigma_\gamma^{148}Sm}{\sigma_\gamma^{148}Sm}$
0,02
0
-0,02
-0,04
-0,06
$\frac{\sigma_\gamma^{154}Sm-\sigma_\gamma^{148}Sm}{\sigma_\gamma^{148}Sm}$
0
2
4
6
8
10
12
14
16
18
E (MeV)

Figure 4.

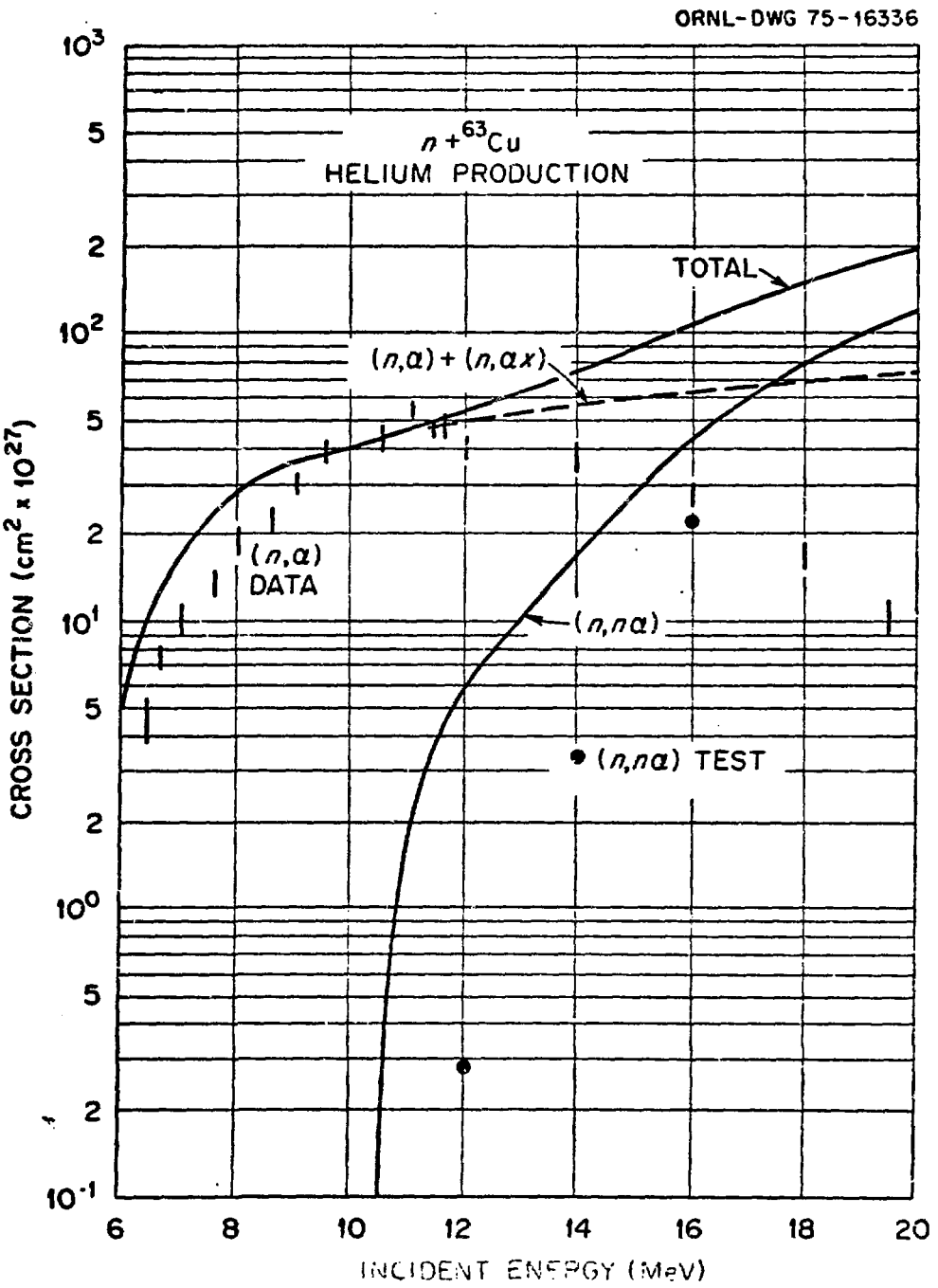
ORNL-DWG 75-16336
$n + {}^{63}Cu$
HELIUM PRODUCTION
TOTAL
$(n,\alpha) + (n,\alpha x)$
(n,α)
DATA
$(n,n\alpha)$
$(n,n\alpha)$ TEST
CROSS SECTION ($cm^2 \times 10^{27}$)
INCIDENT ENERGY (MeV)
10^3
5
2
10^2
5
2
10^1
5
2
10^0
5
2
10^{-1}
6
8
10
12
14
16
18
20

Figure 5.

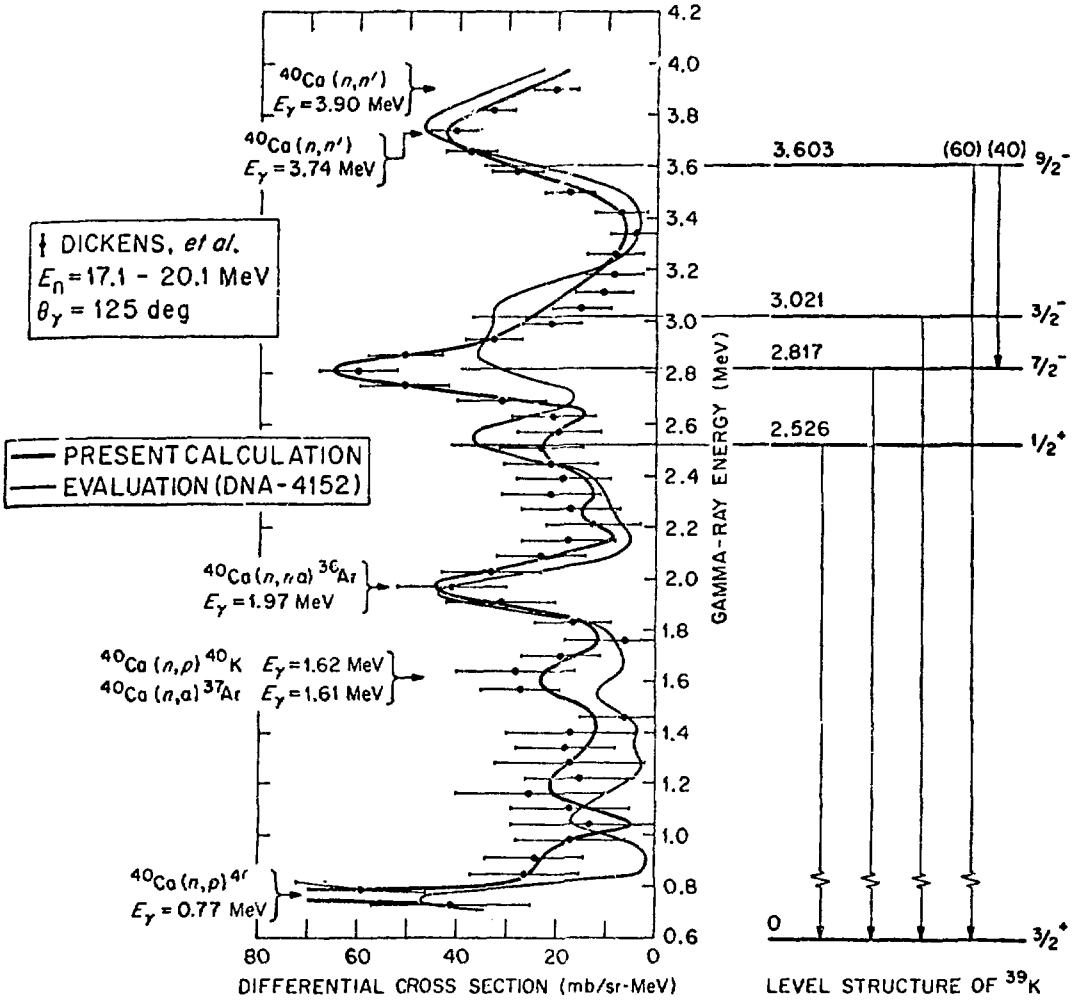
^{40}Ca (n,n') E_γ = 3.90 MeV
^{40}Ca (n,n') E_γ = 3.74 MeV
DICKENS, et al.
E_n = 17.1 - 20.1 MeV
θ_γ = 125 deg
PRESENT CALCULATION
EVALUATION (DNA-4152)
^{40}Ca (n,nα) ^{36}Ar E_γ = 1.97 MeV
^{40}Ca (n,p) ^{40}K E_γ = 1.62 MeV
^{40}Ca (n,α) ^{37}Ar E_γ = 1.61 MeV
^{40}Ca (n,p) ^{40} E_γ = 0.77 MeV
GAMMA-RAY ENERGY (MeV)
DIFFERENTIAL CROSS SECTION (mb/sr-MeV)
3.603
(60) (40)
9/2⁻
3.021
3/2⁻
2.817
7/2⁻
2.526
1/2⁺
0
3/2⁺
LEVEL STRUCTURE OF ^{39}K

Fig. 6

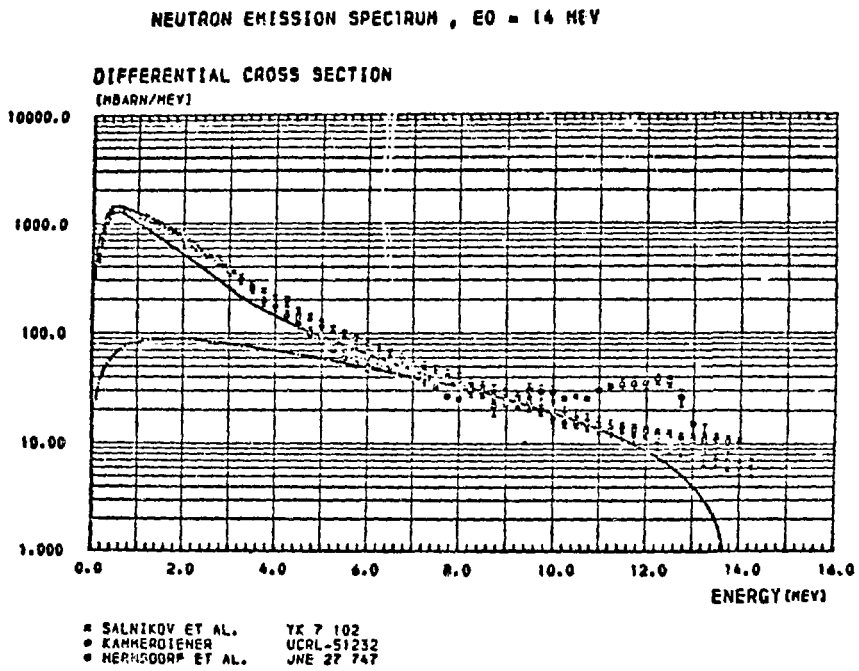
NEUTRON EMISSION SPECTRUM , E0 = 14 MEV
DIFFERENTIAL CROSS SECTION
(MBARN/MEV)
10000.0
1000.0
100.0
10.00
1.000
0.0
2.0
4.0
6.0
8.0
10.0
12.0
14.0
16.0
ENERGY (MEV)
* SALNIKOV ET AL. YK 7 102
• KAMMERDIENER UCRL-51232
• HERMSDORF ET AL. JNE 27 747

Fig. 7

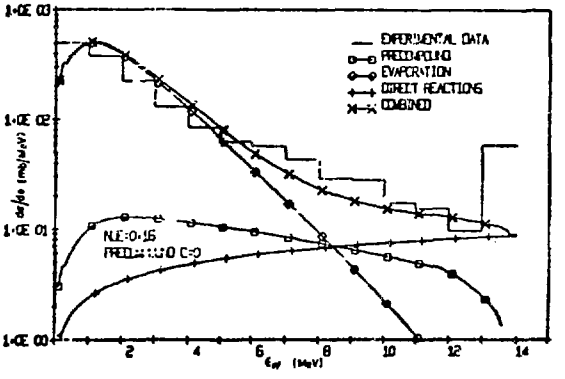
EXPERIMENTAL DATA
PREEQUILIBRIUM
EVAPORATION
DIRECT REACTIONS
COMBINED
1.0E 03
1.0E 02
1.0E 01
1.0E 00
2
4
6
8
10
12
14

Fig. 8

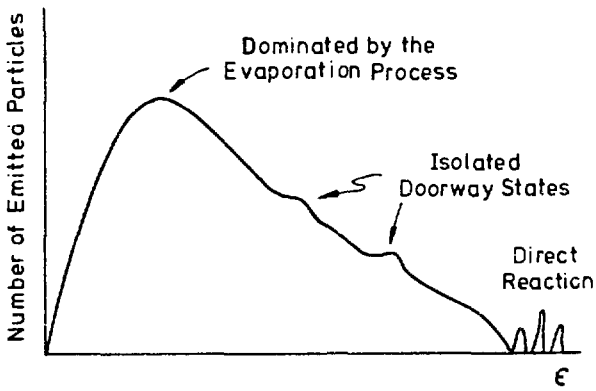
Number of Emitted Particles
Dominated by the
Evaporation Process
Isolated
Doorway States
Direct
Reaction
ϵ

Fig. 9

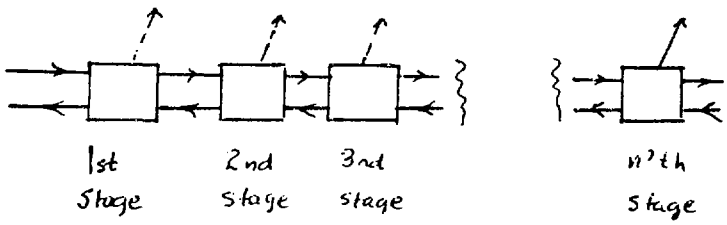

Fig. 10

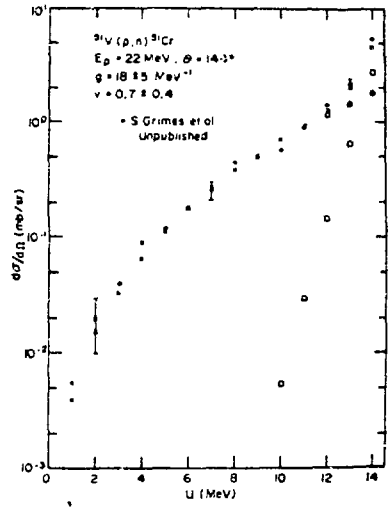

Comparison of theory with experiment $^{51}V(p,n)^{51}Cr$.

Fig. 11

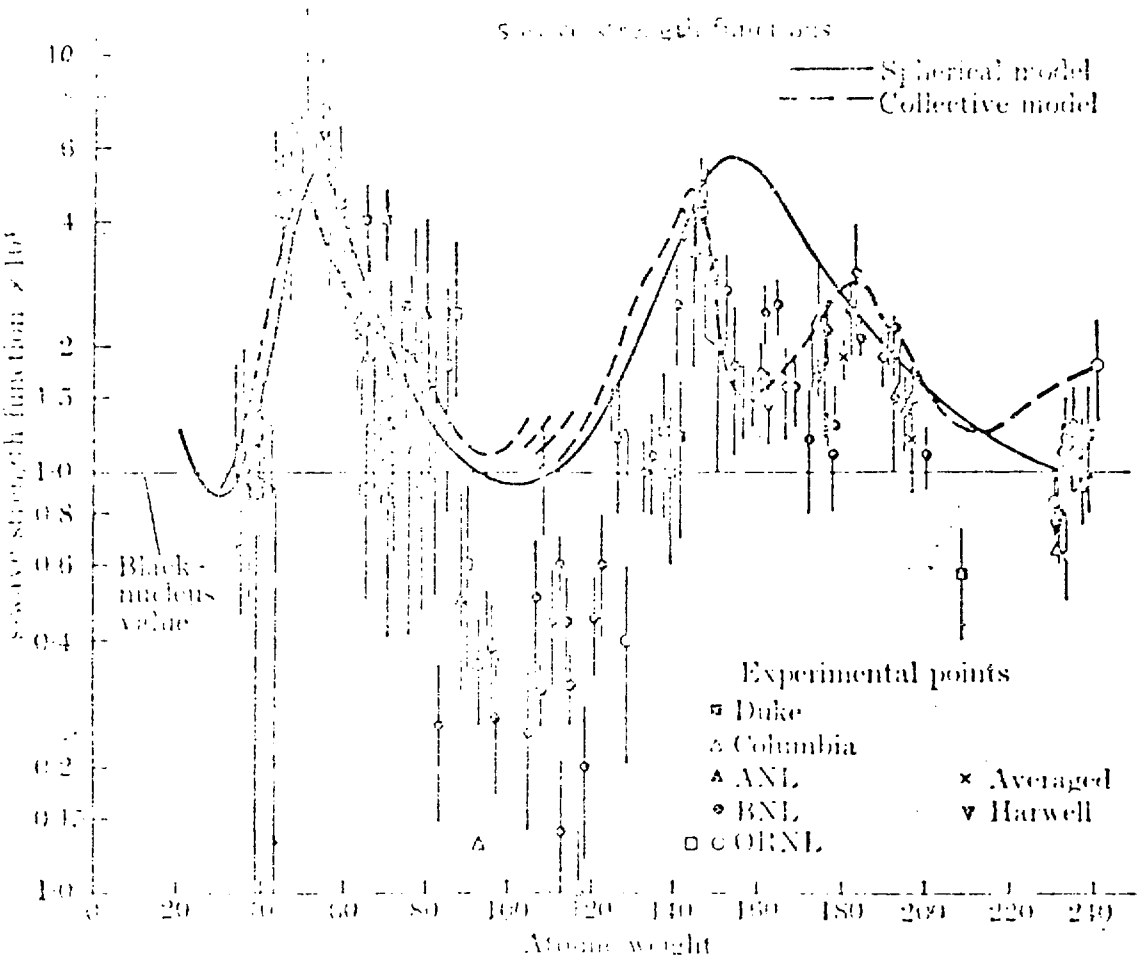
Spherical model
Collective model
Black-nucleus value
Experimental points
Duke
Columbia
ANL
BNL
ORNL
Averaged
Harwell
Atomic weight

Fig. 12

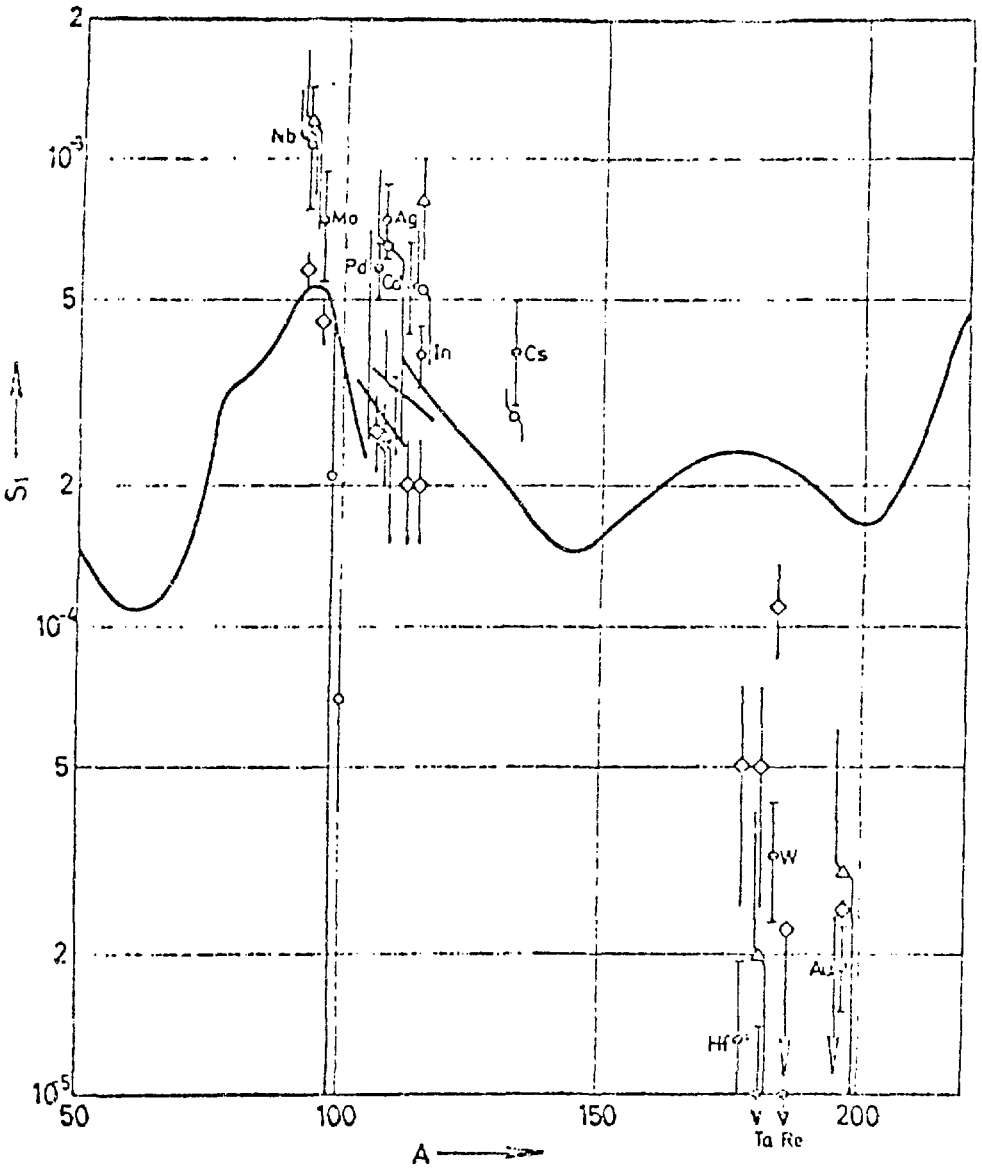
2
10⁻³
5
2
10⁻⁴
5
2
10⁻⁵
Si
Nb
Mo
Ag
Pd
Cd
In
Cs
W
Au
Hf
50
100
150
200
A
Ta Re

Fig. 13

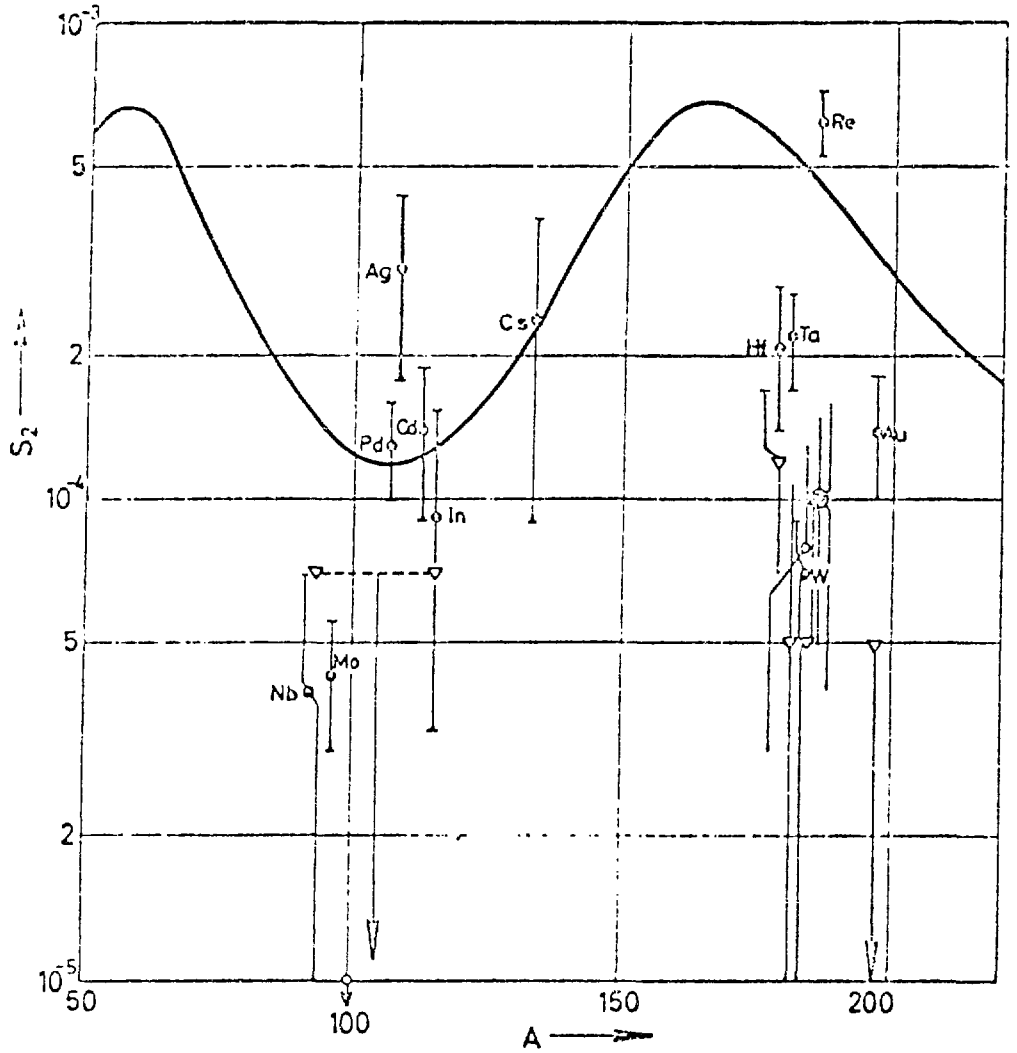

Fig. 14

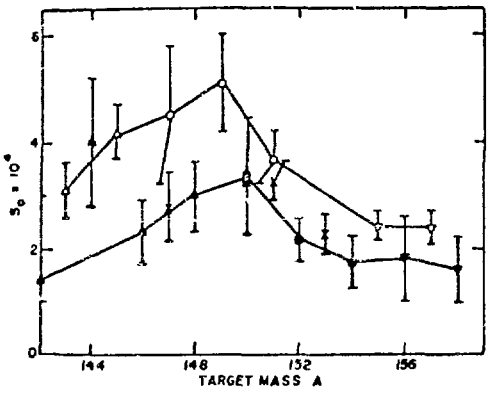

Fig. 15

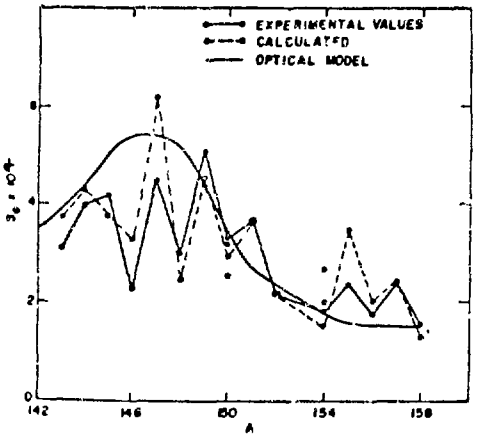
EXPERIMENTAL VALUES
CALCULATED
OPTICAL MODEL
8
4
2
0
142
146
150
154
158
A

Fig. 16

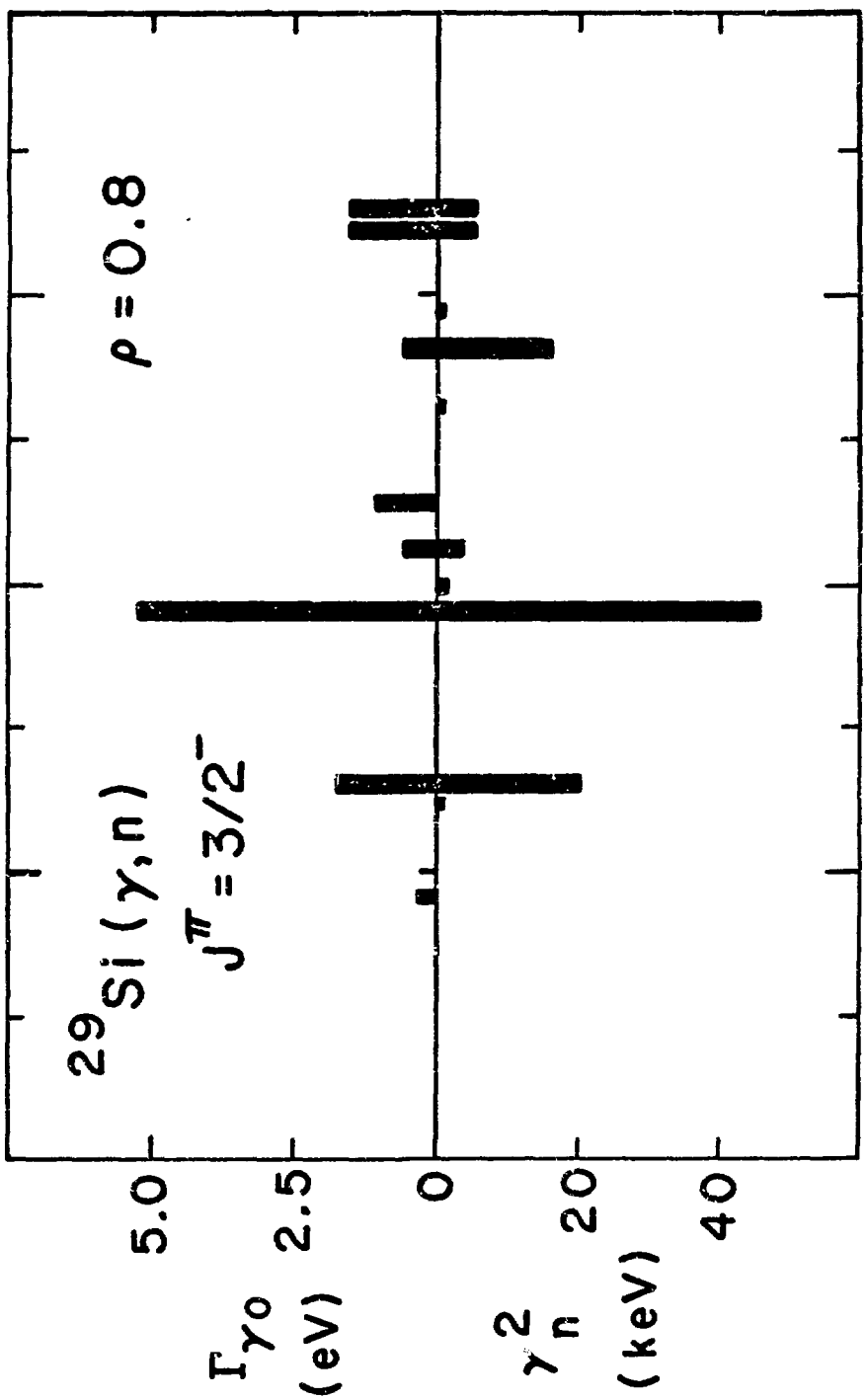
^{29}Si (γ,n)
$J^{\pi} = 3/2^-$
ρ = 0.8
Γ_{γ_0} (eV)
5.0
2.5
0
γ_n^2 (keV)
20
40
0
0.4
0.8
1.2
E_n (meV)

Fig. 17

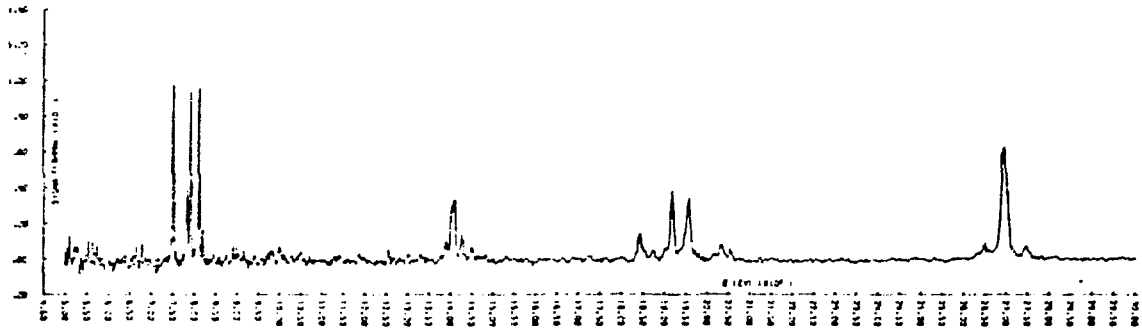

Fig. 18

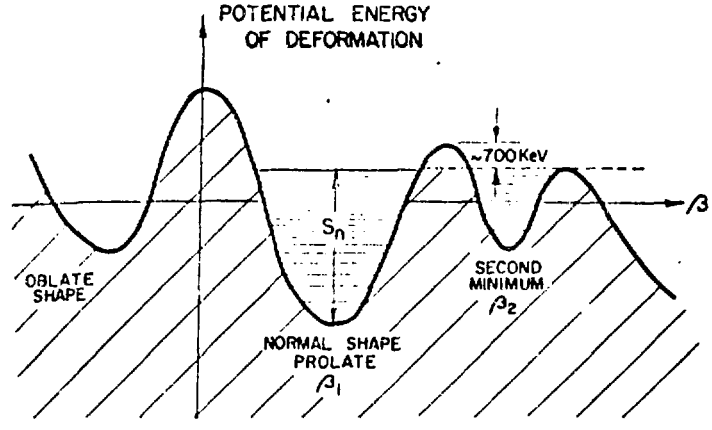
POTENTIAL ENERGY
OF DEFORMATION
~700 KeV
S_n
β
OBLATE
SHAPE
NORMAL SHAPE
PROLATE
β_1
SECOND
MINIMUM
β_2

Fig. 19

Gamma-Ray Strength Functions

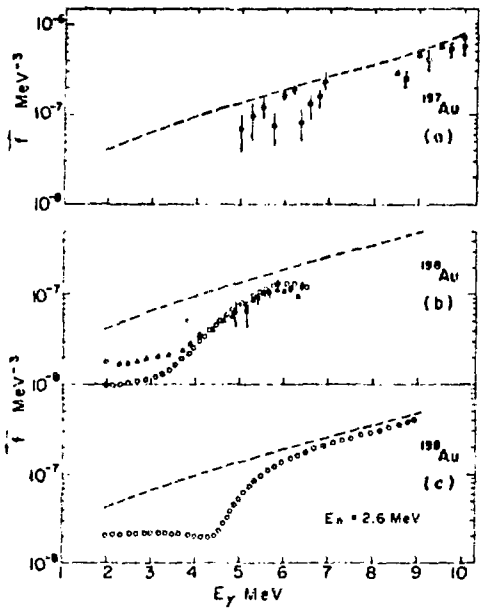

Fig. 20

MA 1 -- RECENT ADVANCES IN NEUTRON PHYSICS. H. FESHBACH, (M.I.T.)

Newstead (Brookhaven National Laboratory):
You've had quite a remarkable track record in predicting terms in the optical potential which physicists have subsequently verified experimentally. I wonder if we can tempt you into prognosticating further as to what other terms there might be?

Feshbach:
I think it has enough terms as it stands. I prefer to go on to coupled channels to describe the other degrees of freedom of the system.

Khanna (Chalk River):
I would like to ask a question about this coupled channel calculation you just mentioned. The microscopic calculation of the optical potential suggests that low-lying collective states can contribute as much as 50% to the strength of the optical potential at the same time you employ a couple d-channel calculation, don't you think there is a certain amount of over-counting going on?

Feshbach:
If you do it wrong there surely is. You have to do it right and that's all there is to it. If you put into the optical potential the effect, for example, of the imaginary term and the effect of coupling to these other modes, then of course you are counting twice. You should of course not do that, you should eliminate that. On the other hand, that does not necessarily mean that it must be all real. There are, after all, other modes of inelasticity -- or if you wish, the fluctuation cross sections -- all of which give a contribution to the imaginary terms of the diagonal components of the optical potential. There is one thing I wanted to say at the end with regard to microscopic calculations of the optical potential which I'm reminded of by this discussion. So I'll entertain a question about that. I have already asked it so now I should answer it. Namely that there have been a number of attempts to do microscopic calculations of the parameters of the optical potential and I won't go through the history of that: Professor Soloviev is one of the practitioners of that art and is at this conference. There is also at this conference a paper from a group from Liège by Jeukenne, Lejeune and Mahaux (MG 2), which I recommend to all of you, in which the Brueckner-Hartree-Fock method is applied quite successfully to the problem.

10:45 A.M., TUESDAY, JULY 6, 1976, IN OLNEY 150

MAIN SESSION MB

Chair: K. Abrahams (Reactor Centrum Nederland

Petten, Netherlands)

10.45 a.m., Tuesday, July 6, 1976 in Olney 150 Invited Paper: Session MB1

THE HIGH-FLUX REACTOR AT GRENOBLE AND ITS SPECIAL NEUTRON BEAM INSTALLATIONS

R.L. Mössbauer

Institute Max von Laue - Paul Langevin

38 Grenoble, France

RÉSUMÉ

The high-flux reactor of the Institute Max von Laue - Paul Langevin at Grenoble, equipped with cold source, hot source, neutron guides and a large variety of neutron spectrometers, serves as a unique central facility for a large number of laboratories in many different areas of research. The paper describes the Institute, its Reactor and the associated neutron beam installations.

ABSTRACT

The 57 MW high-flux reactor of the Institute Max von Laue - Paul Langevin at Grenoble serves as a central neutron beam facility for laboratories and research institutes in the three member countries, Great Britain, France and the Federal Republic of Germany. The heavy water moderated and cooled reactor is equipped with hot, thermal and cold moderators, providing neutrons with high intensity over an unusual wide range of energies (wave-lengths) extending from some 0.1 meV (30 Å) up to some 500 meV (0.4 Å). An extensive system of neutron guides with different curvatures permits the transport of neutrons over distances ranging up to 140 m with hardly any loss of intensity within linear apertures as they are typical for neutron spectrometers within their scattering planes. The transported beams, in addition, exhibit only very low background contaminations by fast and epithermal neutrons and γ-radiation. A large variety of different types of neutron spectrometers mounted on reactor faces or on neutron guides provide unique research opportunities in fields such as nuclear physics, crystallography, solid state physics, chemistry, metallurgy and biology. The paper describes the Institute and its operational mode, its reactor and the associated neutron beam installations.

THE INSTITUTE MAX VON LAUE - PAUL LANGEVIN (ILL)

The high-flux reactor of the Institute Max von Laue - Paul Langevin (ILL) at Grenoble, France, serves as a central neutron beam facility for universities and research laboratories in France, Great Britain and West-Germany. The aim is to provide the scientific community of the affiliated countries with unique neutron beam measuring facilities applicable in fields such as the physics of condensed matter, chemistry, biology, nuclear physics and material sciences. The purpose of the ILL thus differs fundamentally from that of most other Research Institutes. The Institute is in fact largely operating as a user's facility, with about 70% of its neutron beam time being reserved for experiments proposed by external laboratories. The majority of these experiments originate in the three member countries, with scientists from other countries frequently collaborating. The Institute is carrying out an extensive development program of advanced neutron instrumentation, besides its principal task to operate the reactor and its associated neutron beam facilities and to carry out the comprehensive measuring program, mainly in collaboration with external users.

The ILL operates under the jurisdiction of a Steering Committee, with a Scientific Council advising the Director on the Scientific Program and on practical aspects relating to its execution. The Scientific Council has 8 Subcommit-

tees, which specialize in specific scientific domains and which meet bi-annually in order to review the submitted experimental proposals. The requests for measuring time are presently exceeding the experimental possibilities by factors between 2 and 3, requiring rather rigid selection procedures.

THE HIGH-FLUX REACTOR (HFR)

The HFR was constructed with the single purpose to serve as a neutron beam reactor, making compromises due to other operational tasks unnecessary. The whole design was governed by the desire to incorporate special installations such as cold and hot neutron sources and neutron guides, in an effort to achieve the largest possible flexibility with respect to experimental conditions and possibilities. Special efforts were undertaken to achieve the following goals :

1) a neutron spectrum substantially extending above and below the range of wavelengths which are normally available in thermal neutron reactors

2) the possibility to accomodate at the reactor a very large number of neutron spectrometers

3) a level at the experimental sites of a fast neutron background, which is as low as possible

4) an economical operation, both with respect to fuel consumption, operational flexibility and repair flexibility. We note in this context, that the whole construction of the reactor has been laid out on the basis of individual detachable units. Any major part of the reactor, in particular the beam tubes and individual parts of the cold and hot sources can be separately replaced

5) a lay-out which renders the use of the neutron beams as simple as possible, especially with respect to radiation hazards and health physics requirements. We note in this context, that the experimental facilities are physically separated from the functional areas of the reactor operation.

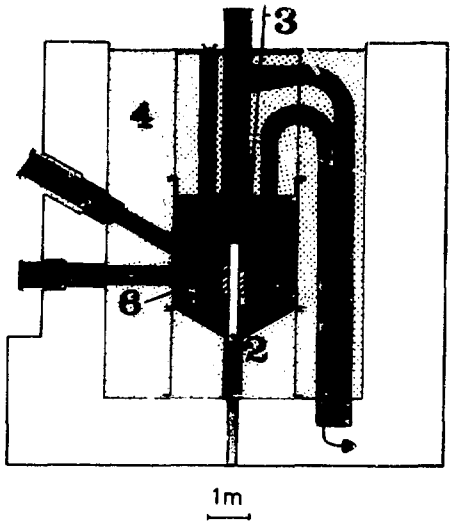

Fig.1 Assembly of the neutron beam tubes inside the reactor tank.(1)fuel element (2)control rod (3)safety rods (4)light water pool (5)heavy water tank (6)hot neutron source

We specify in the following some major design features of the HFR. The reader is referred for details to the pertinent ILL reports [1,2]. Fig.1 illustrates the general arrangement of the core and its environment in the HFR. 40 t of heavy water are used for the thermalisation of the neutrons and for cooling in the primary cooling circuit.

The use of only a single fuel element greatly facilitates its exchange, which is made every 42 days, after a mean burn-off of 30% of the initial charge of ^{235}U. The fuel element contains 8,6 kg of ^{235}U enriched to 93% in the form of UAl_3 dispersed into an aluminium matrix. It is made up of 280 plates, welded by electron bombardement between two coaxial cylinders, as shown in Figure 2. A total power of 57 MW is generated, giving rise to a peak power density of 3 kW/cm^3. The surface of the fuel element experiences a maximum temperature of 147°C. Cooling is achieved by a central unit, which pumps 2010 m^3/h of heavy water through the fuel element, with a speed of 15.5 m/sec in

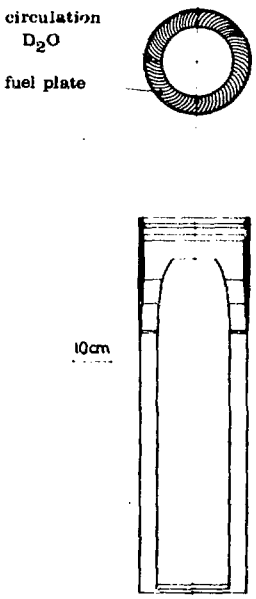

Fig.2 Fuel element cross-section

the space between the fuel plates and at a static pressure of 14 bars at the entrance side. The central bore of the fuel element serves to accomodate the Ni control rod employed in the operation of the HFR. Fig.3 shows the flux distribution inside the reflector. The neutrons generated in the fission process and slowed down in the reflector, yield a maximum flux of 1.2×10^{15} of thermal neutrons/cm^2/sec at a distance of 15 cm from the core. The noses of the neutron tubes are placed at this position which has the additional advantage that the flux of fast neutrons is already reduced by a factor of 40 relative to the flux in the fuel element. The heat production rate, likewise, is lower by a factor 7 to 8. The beam tubes, furthermore, are oriented tangentially with respect to the core, yielding a reduction factor of 10 for the fast neutrons and the γ-rays in the neutron beams. The arrangement of the beam tubes is shown in Fig.4. The use of heavy water for moderation and reflection on the one hand causes a low background of γ-rays, on the other hand initiates the production of tritium, amounting to some 4 Curie/dm^3/year. For operational reasons, the tritium content is limited to 2 Curie/dm^3. A special plant has been set up to extract tritium and hydrogen from the heavy water, using a catalytical exchange procedure between the polluted heavy water vapor and pure deuterium gas, followed by a fractional distillation procedure.

It may finally be of interest to note, that the reactor was operated in 1975 at 70,5% of the total time, with only a 2% loss of time due to unforeseen shut-downs.

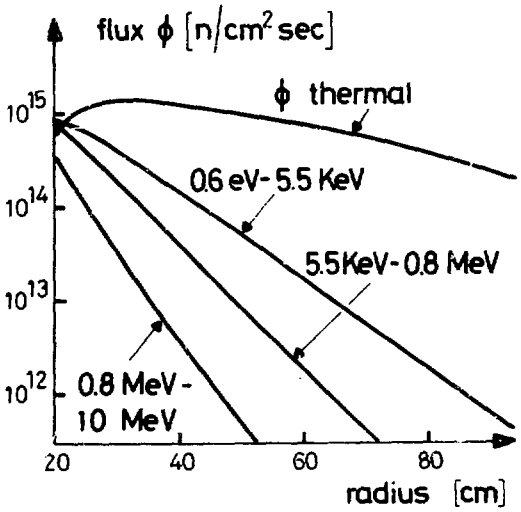

Fig.3 Flux distribution inside the moderator

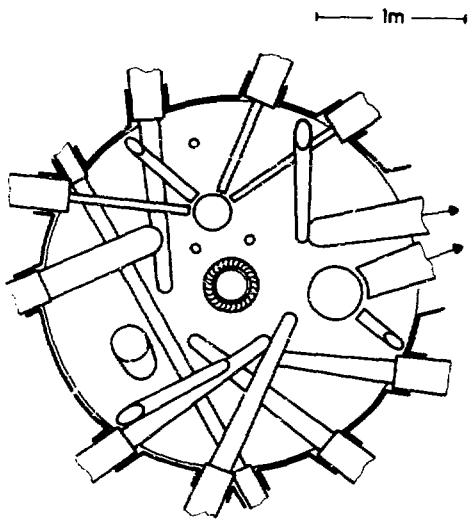

Fig.4 Arrangement of the beam tubes around the reactor core

NEUTRON BEAM FACILITIES

The HFR is equipped with special facilities, which render the application of its neutron beams particularly versatile :

1) A low temperature moderator, the socalled "cold source", is composed of a

spherical vessel of 38 cm diameter with thin aluminium walls filled with 25 litres of deuterium boiling at 25 K. The deuterium is condensed in a heat exchanger which in turn is cooled by gaseous helium from a refrigerator. If complete thermal equilibrium could be reached in such a moderator, one could for instance with the moderator at 30 K gain an increase in the cold neutron flux by a factor of 100 as compared to a moderator at 300 K. The finite size of the moderator and its absorbing properties somewhat reduces the real gain, which nevertheless remains still very significant, as shown in Fig.5.

2) A high temperature moderator, the socalled "hot source", consists of a cylindrical block of graphite of 20 cm diameter and 30 cm length, insulated by graphite wool and heated to 2200 K by nuclear reactions. The presence of the hot source substantially extends towards higher energies the usable part of the neutron spectrum, as shown in Fig.5. Energies up to 500 meV are available with intensities sufficient for experimental applications.

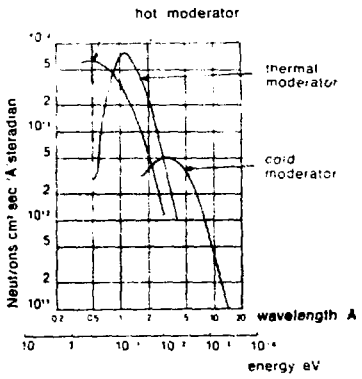

Fig.5 Spectral neutron brightness for different moderators at the HFR

3) Neutron guides. The HFR has been equipped with an extensive system of neutron guides, which transport neutrons over long distances, avoiding the usual loss in intensity with the square of distance. These guides employ the principle of total reflection which applies to neutrons incident in vacuum onto a flat surface at glancing angles below a critical angle γ_c which is defined by the relations

$$\cos \gamma_c = n = \sqrt{1-\lambda^2 Nb/\pi}$$

where n is the refraction index and λ the wavelength of the incident neutrons, while N is the atomic density and b the scattering amplitude of the totally reflecting atoms. For nickel, which is the reflecting material of the neutron guides installed at the ILL, one has $\gamma_c \simeq 0.1\ \lambda$, if γ_c is measured in degrees and λ in Ångström. Neutrons with sufficiently long wavelengths, especially those originating in the cold source, therefore become totally reflected within angular ranges, as they are typical for neutron spectrometer collimators. Such guide tubes, in addition, can be curved, so that there is at a certain distance non longer a direct view of the source. This way most of the fast neutrons, which are not totally reflected and therefore do not propagate along the guide, are effectively eliminated. The residual fast flux, in fact, decreases approximatively as the inverse of the fourth power of the length of the guide tube, whereas the losses of thermal neutrons are merely proportional to the length. The latter losses are due partly to macroscopic defects,such as poor alignment of some sections of the guide,angular misalignements,curvature or waviness of the guide walls. Another source of losses are microscopic defects,such as the roughness of the reflecting surfaces which cause diffuse reflexions aside from the specular reflexions.By these defects a certain fraction of the neutrons become scattered outside of the critical angle and thereby are lost for the following reflexions.The HFR at Grenoble is equipped with 10 neutron guides,mostly with lengths between 30 and 100m, a radius of curvature between 25 m and 27000 m, and with a rectangular cross section of 3 x 20 cm. They consist of optically polished glass plates, covered with a thin layer (1500 Å) of vacuum evaporated nickel, which serves as the totally reflecting material. The overall intensity losses, employing mechanical precisions of a few hundredths of a mm and angular adjustements of about 10^{-4} radian amount to some 0.5 to 1% intensity loss per meter guide length. Typical values for the total neutron flux at the exit of neutron guides with large radii of curvature are of order $10^9 n/cm^2/sec$. Each neutron guide can accomodate up to 6 different experi-

mental set-ups, in part by feeding only a fraction of the rather large beam cross section to an individual instrument, in part by multiple use of particular beams. Such multiple use becomes possible if several spectrometers are operated in series and whereby each instrument uses different narrow wavelength ranges which are filtered out by monochromator crystals. The neutron guides at the ILL thus provide three major advantages : (1) they more than double the number of instruments which can be accomodated around the HFR, (2) they provide particularly clean neutron beams with unusually small background contaminations by fast neutrons and γ-rays, (3) they provide well collimated neutron beams which, according to the guide curvatures, are preselected in their wavelength ranges.

NEUTRON INSTRUMENTATION

The high flux and the advantageous properties of the neutron beams of the ILL are primarily used to extend the range of applicability of neutrons, in particular by increasing energy resolution and by increased use of spin polarization and analysation techniques. The ILL in this connection engages in a large and already quite successful development program on crystal monochromators, spin polarizers and analyzers and multidetector units.

There exist at present a total of 29 different neutron spectrometers which are routinely operated. In addition, some 15 special measuring positions are in use for on-line experiments on cold and thermal neutron guides. Design and construction work on another 9 instruments is in progress. Fig.6 gives a survey of the location of the various spectrometers around the reactor and on the neutron guides, facing either cold, thermal or hot moderators. Table 1 gives a short specification of instruments. Space permits only a few general remarks on the instrument portfolio and the reader is referred to various reports of the ILL[3,4]. We shall make a few remarks concerning exclusively some of the more exotic instruments :

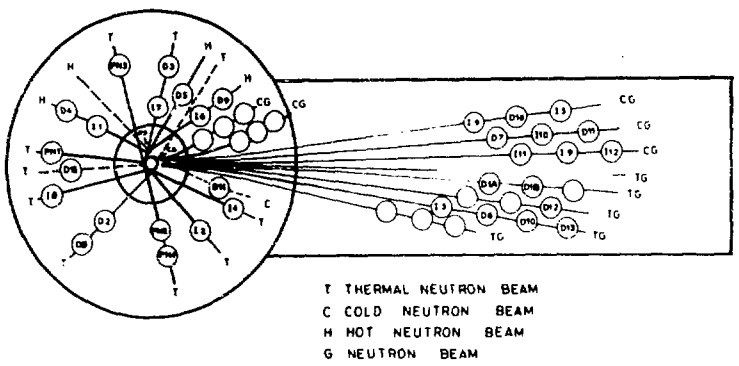

Fig.6 Distribution of instruments

1) Multi-chopper time-of-flight spectrometer[5] IN5 : The instrument is used for high resolution low energy transfer studies, in particular by quasi-elastic scattering. It comprises four disc-choppers, two defining the wavelength, the other two eliminating higher orders and preventing frame overlap. An energy resolution of 24 meV (FWHM) is obtained at λ = 10 Å and with the 4 choppers running at 165 Hz. This high resolution was achieved by using high rotation frequencies, by using neutrons from the cold source and by employing a distance of 6 m between the outermost choppers, which became possible by placing intensity saving neutron guides between the chopper discs. Neutrons are scattered from the specimen into a 4 m helium filled flight path and detected by a banc of 400 ^{3}He counters.

2) High Energy Resolution Backscattering Spectrometer[6] IN10 : This spectrometer eliminates one of the prime sources for the loss in energy resolution, i.e. the wavelength spread $\Delta\lambda$ in a beam reflected from a monochromator crystal due to the finite divergence $\Delta\theta$ in the incident polychromatic beam. Consideration of the Bragg equation and of its derivative, respectively, yields :

TABLE 1

SURVEY OF NEUTRON SPECTROMETERS AT ILL

Instrument classification used : D ≡ Diffractometer ; IN ≡ Inelastic spectrometer ; PN ≡ Nuclear physics spectrometer ; S ≡ special beam installation.
Beam classification used : HB ≡ hot source direct beam, TB ≡ thermal source direct beam, CB ≡ cold source direct beam, TG ≡ thermal guide, CG ≡ cold guide.

Position		Specification
D1A	TG	Two axis high resolution diffractometer
D1B	TG	Two axis diffractometer with multi-detector
D2	TB	Two axis high flux diffractometer
D3	TB	Two axis diffractometer using polarized neutrons, without polarization analysis
D4	HB	Two axis diffractometer for liquids
D5	HB	Three axis spectrometer using polarized neutrons and polarization analysis
D6	TG	Single crystal diffractometer with 100 spherically oriented detectors, using a modified Laue-method
D7	CG	Elastic diffuse scattering spectrometer
D8	TB	Conventional four circle diffractometer
D9	HB	Four circle diffractometer
D10	TB	Four circle diffractometer with energy analyser
D11A	CB	Small angle scattering camera with multi-detector
D11B	CB	Long wavelength diffuse scattering spectrometer
D12	TB	Photographic detection diffractometer, "Modified Laue-Method"
D13	TG	Double crystal neutron diffractometer
D14	-	Television camera multi-detector system under development
D15	TB	Four-circle Mark VI diffractometer on inclined beam tube
D16	CB	Four circle Mark VI diffractometer
D17	CG	Small and large angle scattering camera with multidetector
D18	TG	Neutron interferometer
IN1	HB	Three axis spectrometer for high incident energies
IN2	TB	Three axis spectrometer with double crystal monochromator
IN3	TG	Three axis high resolution spectrometer
IN4	TB	Rotating crystal spectrometer with multidetector banc
IN5	CG	Multichopper time-of-flight spectrometer with multidetector banc
IN7	TB	Mechanical statistical chopper
IN8	TB	High intensity three axis spectrometer
IN9	CG	Time of flight polarization spectrometer
IN10	CG	Backscattering Doppler-spectrometer with high energy resolution
IN11	CG	Neutron spin echo spectrometer with very high energy resolution
IN12	CG	Three axis spectrometer for high energy resolution at low energy transfers
PN1		Mass separator for nuclear fission products
PN2		High resolution conversion electron spectrometer with in-pile target
PN3		High resolution bent crystal gamma ray spectrometers with in-pile target
PN4		Anti-Compton γ-ray spectrometer and pair-formation γ-ray spectrometer

$$2d \sin\theta = \lambda$$

$$2d \cos\theta \, \Delta\theta = \Delta\lambda$$

where θ is the Bragg angle, d is the lattice constant characteristic of the particular reflection and λ is the neutron wavelength. The wavelength spread apparently vanishes for a scattering angle of $2\theta = 180°$. Backscattering consequently is used in both the monochromator and analyser crystals of the instrument, while simultaneously employing Doppler-shift techniques to compensate for energy differences between incident and scattered neutrons due to inelastic scattering in the sample under study. Energy resolutions as small as 0.25 meV have been achieved, with energy transfers in the range of $\pm$ 2 x 10^{-5}eV.

3) Small Angle Scattering Camera[7] D11 A : This instruments uses neutron wavelengths in the range of 2 to 20 Å. The angular resolution of the instrument can be varied by changing the distance between monochromator and sample in steps between 60 cm and 40 m. The distance sample-detector equals the distances chosen on the entrance side of the instrument, thus matching entrance and exit collimations. The scattered neutrons are measured by a two-dimensional multidetector unit with 64 x 64 elements of 1 cm^2 surface each. The analysis of the small angle scattering distribution provides information on large structures, typically between 10 and 10000 Angströms. Such studies have proven most revealing in a variety of fields, ranging from metallurgy to polymer science and to biology. These experiments have turned out to be particularly informative due to the fact, that H and D as well as H_2O and D_2O have coherent scattering amplitudes of opposite sign, thus permitting to vary or even cancel the scattering contributions from solvent material, crystal water or from certain subgroups of a composite system with the consequence that scattering contributions from certain specified domains or units become emphasized.

4) Neutron Spin Echo Spectrometer[8] IN 11 : Neutrons polarized parallel to a guide field enter the spectrometer and have their spin direction turned by 90° in a specific direction perpendicular to the guide field. They then process in the guide field while travelling down the entrance arm of the spectrometer. A second symmetric part of the spectrometer with equal but opposite magnetic field directions leads to a back-reeling of the spin directions, causing each neutron at the exit to arrive with the same spin orientation as had been present at the entrance, independent of the velocity of the neutrons. This is the spin echo principle. It may be used for neutron spectroscopy by placing a sample at the center position, which destroys the perfect precession symmetry for those neutrons, which undergo velocity changes due to inelastic scattering processes. Such neutrons experience a different number of Larmor precessions in both spectrometer arms and can be observed by the change in the exit polarization. The instrument, which is nearing completion, utilizes the neutron spin-echo principle to determine the Fourier-transform of the sample scattering function at a given detector setting. The high resolution of the instrument for small energy changes is a consequence of the large number of precessions which the neutrons undergo during their passage along the instrument. The spectrometer has been designed to operate in the wavelength range between 4 and 16 Å with an energy resolution ranging from 500 meV to 2 neV.

THE MEASUREMENT PROGRAM

Space does not permit to describe in any sense the comprehensive experimental program of the ILL. In 1975 at total of 535 experiments have been carried out, individually ranging in time from a few hours up to the entire year. Some 1100 scientists from 136 different institutions and from 16 different countries had been engaged in this program. The reader is referred to the Annual Reports of the Institute, which contain condensed summaries of the experimental results and complete literature references[9]. We shall here confine ourselves to give in Table 2

T A B L E 2

EXPERIMENTAL PROGRAMME JANUARY 1 TO DECEMBER 31, 1975

Major areas of Scientific interest	Number of Instrument days	Number of Experiments	Number of Instruments Involved
Biology	216	49	4
Chemistry	237	41	6
Crystal Structure	623	60	8
Liquids and Amorphous	466	52	10
Diffuse Scattering	307	59	10
Phonons	388	38	7
Phase Transitions	121	11	4
Magnetic Structure	658	71	8
Magnons	190	20	4
Crystal Field Effects	125	14	3
Nuclear Physics	947	62	6
Scientific Test and Feasibility Experiments	284	58	21
Total	4562	535	27

some statistical information reflecting the main areas of research and shall then conclude with a few more specific remarks on the nuclear physics program in the spirit of the main topic of this conference.

MEASUREMENTS IN THE DOMAIN OF NUCLEAR PHYSICS

The ILL performs an extensive research effort in the domain of neutron capture spectroscopy, employing high resolution bent crystal gamma-ray spectrometers[10], internal conversion electron spectrometers[11] combined with anti-compton and pair-spectrometers. The nuclear fission process is being studied by means of a huge parabola-type mass spectrometer[12]. This instrument separates on-line the heavy fission fragments from a foil of fissionable material placed in the pile. The instrument is used in a two-fold way. Firstly, the available high resolution serves to measure the fission yield as function of mass, nuclear charge and kinetic energy. Complete mass separation became possible up to masses around 150. Efforts to extend the measurements into the heavy mass range are in progress.

A second major application of the fission spectrometer is nuclear spectroscopy on neutron rich nuclei far off the stability line. Such studies involve β and γ spectroscopy, lifetime measurements as well as measurements of delayed emission processes. Continuous tape transport systems[13] and helium-jet are employed in the collection and measuring procedures. An example for a measurement is shown in Fig.7. The nuclear physics program comprises besides the measurements on the spectrometers many experiments, which make use of the high intensity and low background neutron beams of the ILL. Of particular interest are here the studies on the neutron itself, such as the search for an electric dipole moment of the neutron[15], studies of time-reversal invariance[16] and of parity conservation. In the latter case, a study is in progress of the anisotropy of γ-radiation following polarized neutron capture in the reaction $n + \gamma = d + \gamma$. The installation of a source of ultra-cold neutrons, which is scheduled for the fall of this year, will permit an improved renewal of the search for an electric dipole moment of the neutron, a remeasurement of the neutron lifetime, as well as interesting studies of nuclear and solid state effects in a rather new and unknown wavelength range.

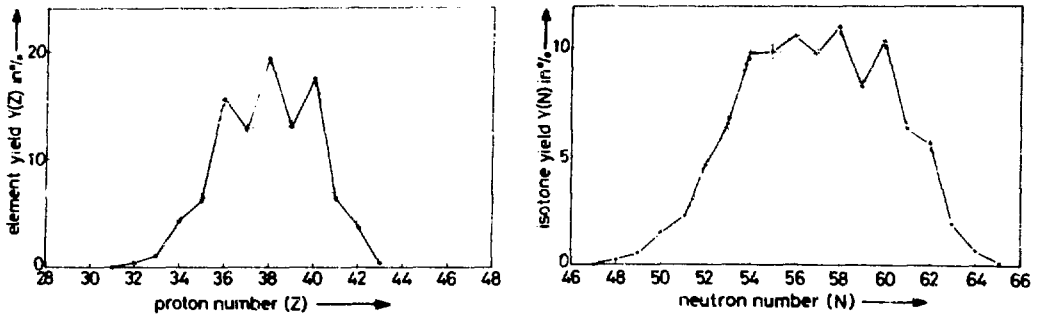

Fig.7 Proton and neutron yields (summed over masses and kinetic energy) originating from the fission of ^{235}U. With the fissioning nucleus, i.e. $^{235}U + n$, being doubly even, odd neutron or odd proton numbers are only created by breaking a pair. They therefore exhibit a lower yield. The effect is less pronounced and less constant for neutrons, since it is smeared out to some extent by neutron evaporation[14].

APPLICATION PROCEDURE FOR THE USE OF ILL FACILITIES

All research proposals should be sent to the Office of the Scientific Secretary:

B. MAIER
Institut Laue-Langevin
156 X
38042 Grenoble Cedex, France

Tel. (76) 97.41.11 poste 82.44

Appropriate forms are obtainable on request from this office.
The closing dates for acceptance of applications are as follows :

August 31 and February 15.

All proposals are submitted to the Scientific Council for approval.

It should be noted that the ILL in general provides free of charge the neutron beams and stantard measuring equipment, such as existing spectrometers, counters, standard cryostats and shielding equipment. Other special equipment, in particular samples, must be provided by the user.

REFERENCES

1) Commissariat à l'Energie Atomique, BIST Nr.165, December 1971.

2) Commissariat à l'Energie Atomique, BIST Nr.166, January 1972.

3) Neutron Research Facilities at the high flux reactor of the ILL, ILL January 1975.

4) Neutron Beam Facilities at the HFR, available for users ; issued annually.

5) F. Douchin, R.E. Lechner and R. Scherm, Nucl. Instr. and Methods (1976), to be published.

6) M. Birr, A. Heidemann, B. Alefeld, Nucl. Instr. Methods 95, 435 (1971) ; B. Alefeld, Kerntechnik 14, 15 (1972).

[7] K. Ibel, Journ. Applied Cryst. (1976), in print.

[8] F. Mezei, Z. Physik 255, 146 (1972).

[9] Annual Reports 1973, 1974 and 1975 of the Institute Max von Laue-Paul Langevin.

[10] H.Börner, Instrument MANUAL PN3, ILL.

[11] W. Mampe, P. Jeuch, T. v.Egidy, K. Schreckenbach, F. Braumandl, J. Larysz, Nucl. Instr. and Meth. 128, 585 (1975).

[12] E. Moll, H. Schrader, G. Siegert, M. Asghar, J.P. Bocquet, G. Bailleul, J.P. Gautheron, J. Greif, G.I. Crawford, C. Chauvin, H. Ewald, H. Wollnik, P. Armbruster,G. Fiebig, H. Lawin, K. Sistemich, Nucl. Instr. Meth. 123, 615 (1975).

[13] G. Bailleul, J.P. Bocquet, H. Schrader, R. Stippler, B. Pfeiffer, M. Asghar, C. Chauvin, J.P. Gautheron, J. Greif, G. Siegert, P.Armbruster, H. Ewald, J. Blachot, E. Monnand, F. Schussler, Z. Physik A 273, 283 (1975).

[14] G. Siegert, J. Greif, H. Wollnik, G. Fiedler, R. Decker, M. Asghar, G. Bailleul, J.P. Bocquet, J.P. Gautheron, H. Schrader, P. Armbruster, H. Ewald, Phys. Rev. Letters 34, 1034 (1975) ; G. Siegert et al., Phys. Rev., in print.

[15] B. Dress, A. Miller, M. Pendlebury, P.E.J. Perrin and N. Ramsey, to be published.

[16] R.I. Steinberg, P. Liaud, B. Vignon, V.W. Hughes, Phys. Rev. Letters 33, 41 (1974).

MB 1 - THE HIGH FLUX REACTOR AT GRENOBLE AND ITS SPECIAL NEUTRON BEAM INSTALLATIONS - R. L. Mössbauer (ILL, Grenoble)

Block (R.P.I.):

In neutron scattering there has always been a debate between people with pulsed neutron sources, who say they can do very well with high momentum transfers, and people with reactors, who can do well with very low momentum transfers. Now you mention you have a high energy source running at 2200 degrees K. Will you please comment on what energy you feel is the crossover point where the pulsed sources would become superior and below which the Grenoble reactor would be superior?

Mössbauer:

There is a big debate going on at the moment about this, because there will probably be a European effort to build a pulsed source as well. When I say European, I'm not talking about the Russian pulsed reactor which will soon go into operation at Tokobad, a tri-national effort in connection with Grenoble. We think that the crossover point is probably around 300 millielectron volts. Our source goes up to 500 millielectron volts, but nevertheless the intensities there already drop substantially. We have done experiments up to 500 millielectron volts, but the intensity leaves something to be desired. Now there is, of course, the question of a pulsed source, and there will soon be a conference about this. We are thinking about a spallation source at the moment, but there are other possibilities. The question concerning a pulsed source is that it will be rather expensive, and are there enough applications to justify the major financial engagement? I think this will depend crucially on how far we can come down in energy with such a source. It is quite clear that at the higher energies such a hot neutron source will be far superior to what we presently have; in other words, anything above 500 millielectron volts. But are there enough important experiments which justify the very major financial expenses, and how far can we go down in energy? We think we can probably cover most of the thermal range, and since there is tremendous pressure at the Grenoble facility, I would be most happy to relieve our reactor from much of the thermal and all of the hot work, and maybe put a second cold source into our reactor so that we would have a double operation then. That's a special feature of this station. I think it's really a question of how much physics is there still to be done at the higher energies.

11.30 a.m., Tuesday, July 6, 1976 Paper Subject: Session MB 2

RESONANCE NEUTRON CAPTURE

J. R. Bird, J. W. Boldeman, B. J. Allen, A. R. de L. Musgrove and M. J. Kenny

Physics Division, AAEC Research Establishment, Lucas Heights,

Private Mailbag, Sutherland, NSW 2232, Australia

RÉSUMÉ

Many results are now available showing large variations in radiative widths, correlations between Γ_γ and Γ_n as well as preferred E1 and M1 transitions to single particle final states. These can be explained by assuming that Γ_γ contains a compound nucleus component (well defined from earlier work on complex nuclei) plus valence nucleon transitions (dependent on Γ_n and S_f) plus particle-hole components (dependent on S_f).

ABSTRACT

Resonance studies at low neutron energies often involve complex nuclei which, in the main, provide verification of the statistical theory of neutron interactions. However, much of the recent work on resonance neutron capture has taken advantage of the availability of improved facilities for studying interactions at neutron energies up to 1 MeV. Sufficient data have now been obtained on nuclei with low level densities (including many odd-neutron and near magic compound nuclei) to obtain systematic information on departures from the statistical model.

High resolution capture cross section measurements give radiative widths which vary markedly from resonance to resonance, from nucleus to nucleus, and for different neutron angular momenta. The largest values are usually associated with strong initial state correlations (Γ_γ,Γ_n^ℓ) as well as final state correlations ($\Gamma_{\gamma f}$,S_f). The most striking results occur near closed neutron shells and provide confirmation of the valence model which reproduces these results quantitatively. The success of the valence model indicates that valence transitions are fully decoupled from the giant dipole resonance for s-, p- and possibly d-wave neutron interactions.

Gamma ray spectra from neutron capture at energies up to the order of 1 MeV show intermediate structure involving preferred transitions which follow closely the systematics of single-particle configurations as measured with (d,p) interactions. Structure has also been observed in threshold photonuclear measurements of $\Gamma_{\gamma 0}$ although detailed agreement between these and neutron capture results is not always obtained. The widespread occurrence of final state correlations, even when valence transitions are weak, points to the importance of additional doorway-state mechanisms. Radiative widths are thus most usefully viewed as the sum of a statistical component, a valence component and terms representing doorway-state effects. However, an adequate quantitative theory for partial radiative widths in such models is still needed. From this work it is possible to develop more realistic systematics for radiative widths and the shape of capture gamma ray spectra than are given by the statistical theory.

RESONANCE NEUTRON CAPTURE

ICINN, Lowell 1976

J.R. Bird, B.J. Allen, J.W. Boldeman, M.J. Kenny, A.R. deL. Musgrove

Physics Division, AAEC Research Establishment

Lucas Heights, NSW, 2232, Australia

1. INTRODUCTION

Resonance studies at low neutron energies preferentially involve complex nuclei and in the main, provide verification of the statistical theory of neutron interactions. However, much of the recent work on resonance neutron capture has taken advantage of the availability of improved facilities for studying interactions at neutron energies up to 1 MeV. Sufficient data have now been obtained on nuclides with large resonance spacings, including many odd-neutron and near-magic nuclei, for it to be worthwhile to explore the systematic trends of the departures from the statistical model. A discussion of models and the data available for distinguishing between them is followed by consideration of a framework for including non-statistical effects in the parametrisation of neutron resonance capture.

2. MODELS

THE STATISTICAL MODEL

Early work on neutron capture showed the existence of narrow resonances and led to Bohr's compound nucleus hypothesis. This, in turn, was the basis of the statistical theory of nuclear reactions which was very successful in the following decades - so much so that, to many nuclear physicists, neutron cross sections and statistical theory are synonymous. This is not surprising in view of the confirmation of many of the main consequences of statistical theory which appears in the reviews and textbooks.

Statistical theory is based on the assumption that a very large number of configurations randomly contribute to the reduced width amplitude for a particular resonance state. This assumption is expected to apply accurately only at high excitations in the more complex nuclei. Although the early studies in neutron capture were necessarily concentrated in such regions, enough evidence of non-statistical effects has now been accumulated to establish patterns of behaviour from mass 20 upwards.

In resonance capture there are a number of results of statistical theory which must be qualified in the light of new information. These are illustrated by the following examples.

Width Distributions

The statistical assumption leads to the expectation that partial radiation widths ($\Gamma_{\gamma if}$) will follow a Porter-Thomas distribution. Experimental difficulties have limited the amount of evidence on their distribution but it is generally accepted that the Porter-Thomas distribution applies in most statistical nuclei. Departures from the statistical model are demonstrated by the occurrence of correlations between partial radiation widths and reduced neutron widths of initial and final states.

In complex nuclei, radiative capture leads to the emission of many different

gamma-ray cascades. The total radiation width (Γ_γ) is then the sum of many partial widths and has a correspondingly narrower distribution. This is illustrated by the results[1] for ^{167}Er in Figure 1. By contrast, the widths for p3/2 resonances in ^{88}Sr are dominated by a few transitions and have a very broad distribution.[2] Correlations with reduced neutron widths, and energy dependent structure are also observed.

Partial Radiation Widths

Resonance averaged reduced widths ($\bar{k}_{if}$) for electric dipole transitions[3] are shown in Figure 2. Although the overall average value ($\bar{k}_{E1} = 2.5 \times 10^{-9}$ MeV^{-3}) applies from mass 50 to 250, there are systematic departures - for example, when $\Gamma_{\gamma if}$ is correlated with the single-particle widths of final states.

Magnetic dipole transitions are a factor of 7 weaker than electric dipole transitions[4] and the average reduced width ($\bar{k}_{M1} = 18 \times 10^{-9}$ MeV^{-3}) applies over a similar mass range. However, again, departures have been reported in some mass regions.

Radiation Widths

Average radiation widths show a relatively smooth variation with mass number[1,5] which can be partially explained, in statistical theory, by changes in level density and binding energy. Much of this data consists of measurements made on nuclides with enough low energy resonances, for which capture exceeds scattering, to give reliable and accurate average values. These values usually provide good support for statistical theory. However, non-statistical effects are observed in nuclides with lower level densities for which average radiation widths may vary with mass number, neutron angular momentum (ℓ) and neutron energy.

Gamma Ray Spectra

The envelope of the spectrum of primary gamma rays from neutron capture is given, in the statistical model, by[6]:

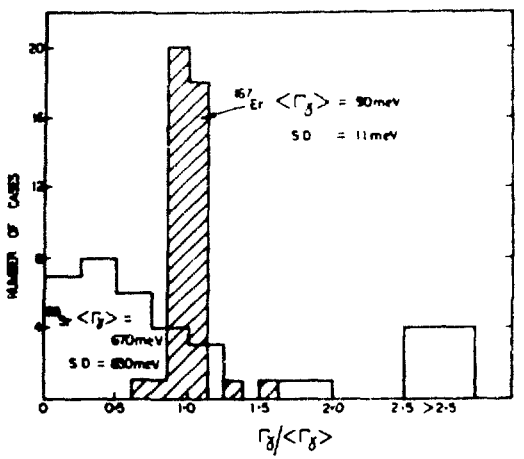

Figure 1. Distributions of radiation widths for a statistical nucleus (^{167}Er) and a non-statistical (^{88}Sr).

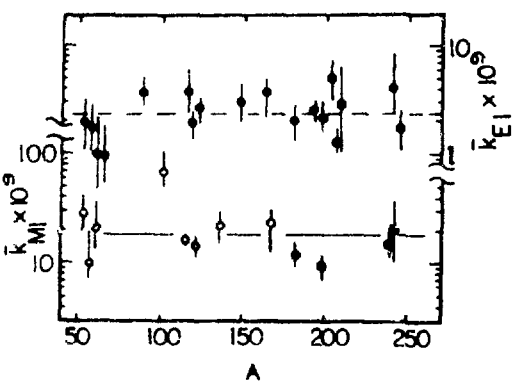

Figure 2. Resonance averaged reduced widths[3] for E1 transitions (upper) and M1 transitions (lower).

$$(I_\gamma)_s = K E_\gamma^3 f(E_\gamma) \bar{D}_i [\bar{D}_f \bar{\Gamma}_\gamma]^{-1} \quad (1)$$

where I_γ is the intensity of gamma rays of energy E_γ, $\bar{D}_i$ and $\bar{D}_f$ are the average spin-zero level spacings at initial and final state energies, and $f(E_\gamma)$ is any additional dependence on gamma-ray energy such as may be imposed by the giant dipole resonance. The competition between level density and gamma-ray energy factors leads to an asymmetric bell-shaped spectrum and this shape is occasionally observed. However, departures from this shape are both striking and common. Such departures were first observed as groups of strong high energy gamma rays in thermal capture spectra. Resonance capture spectra show similar results for s-wave resonances in the regions of the 3s and 4s strength function maxima and additional structure for p-wave resonances in the 2p and 3p regions.

Giant Dipole Resonance

The giant dipole resonance (GDR) occurring in photon strength functions is commonly described by either a smooth Lorentzian distribution or the sum of two such distributions. However, the GDR is often more complex in shape - particularly in the region near the neutron threshold where resonance capture studies are carried out. The Brink-Axel treatment, which assumes that the E_γ dependence of partial radiation widths can be determined from the shape of the low energy tail of the appropriate Lorentzian[4], makes no allowance for local structure near threshold. Structure is frequently observed in photoneutron yields but it may, in part, be introduced by the emission of neutrons to excited states which do not participate in neutron capture reactions. However, other measurements confirm the presence of structure near threshold[6,7].

VALENCE AND DOORWAY MODELS

The importance of simple reaction mechanisms in neutron capture was considered by Lane and Lynn[5,8] who introduced hard sphere or direct capture, and channel or valence capture. These processes arise from the overlap of initial and final state wave functions in the external region of the target nucleus, which acts as an inert core. However, such single particle effects are not sufficient to explain all the observations on resonance capture[9] and it has been necessary to consider each partial radiation width as derived from a reduced width amplitude which contains a number of components[10].

$$\gamma_{if}^2 = C_1 \gamma_v(\theta_i, \theta_f) + C_2 \gamma_d(\theta_f) + C_3 \gamma_t(\theta_i) + C_4 \gamma_c. \quad (2)$$

The first term arises from valence nucleon capture which is proportional to both the resonance reduced neutron width amplitude (θ_i) and the final state reduced width amplitude (θ_f). The second term involves doorway interactions which create a particle-hole pair and depend only on θ_f, while the third term arises from particle-hole configurations in the initial and final states and depends on θ_i only. The fourth term represents all the remaining forms of interaction lumped together as compound nucleus formation and decay. The amplitude components may interfere either constructively or destructively for a particular transition, but the interference terms should average to zero for measurements summed over many resonances or many final states.

The number of terms in equation (2) depends on the number of distinguishable processes occurring and information on these may come from the study of intermediate structure or of correlations between different reaction channels. Not only do correlations occur for partial radiation widths to specific final states but also for total radiation widths when a small number of partial widths are dominant. This means that capture cross sections, as well as gamma ray spectra and threshold photoneutron experiments, can be used in the study of non-statistical effects.

A variety of correlation coefficients are useful:

Initial State Correlations

Many Resonances - One Final State $\rho_i = \rho(\Gamma_{\gamma if}; \Gamma^{\ell}_{ni})$

Many Resonances - Many Final States $\bar{\rho}_i = \rho(\bar{\Gamma}_{\gamma f}; \Gamma^{\ell}_{ni})$

Many Resonances - All Final States $\rho_I = \rho(\Gamma_{\gamma}; \Gamma^{\ell}_{ni})$

Final State Correlations

One Resonance - Many Final States $\rho_f = \rho(k_{if}; (2J+1)\theta^2_f)$

Many Resonances - Many Final States $\bar{\rho}_f = \rho(\bar{k}_f; (2J+1)\theta^2_f)$

Total Correlations

Many Resonances - Many Final States $\rho_T = \rho(\Gamma_{\gamma if}; \Gamma^{v}_{\gamma if})$

Valence Capture

The valence component ($\Gamma^{v}_{\gamma if}$) of a partial radiation width can be calculated from the optical model[11-14]:

$$\Gamma^{v}_{\gamma if} = q_{if}(E_\gamma) \quad \theta^2_f \, \Gamma^{\ell}_{ni} \, E^3_\gamma \, Z^2/A^2 \qquad (3)$$

where Γ^{ℓ}_{ni} is the resonance reduced neutron width and $q_{if}(E_\gamma)$ is the overlap intergral (including geometric factors) obtained using optical model wave functions normalised in the internal region of the nucleus. An average valence component is obtained by summing equation (3) over final states:

$$\langle\Gamma^{v}_{\gamma}\rangle = Q_i \, \langle\Gamma^{\ell}_{n}\rangle = Q_i \, S_\ell \, \bar{D} \qquad (4)$$

where S_ℓ is the ℓ-wave strength function and $\bar{D}$ the average level spacing.

Evidence for valence capture is illustrated in Figure 3 where measured radiation widths[2,15] for p3/2 resonances in ^{88}Sr and ^{90}Zr are compared with values calculated from equation (4). Most of the points cluster along a line which represents the sum of $\langle\Gamma^{v}_{\gamma}\rangle$ and a statistical component of 150 MeV, with $\rho_I = 0.85$. This provides strong evidence for the presence of valence transitions. For resonances with large radiation widths, the calculation gives quantitative agreement with the observed widths.

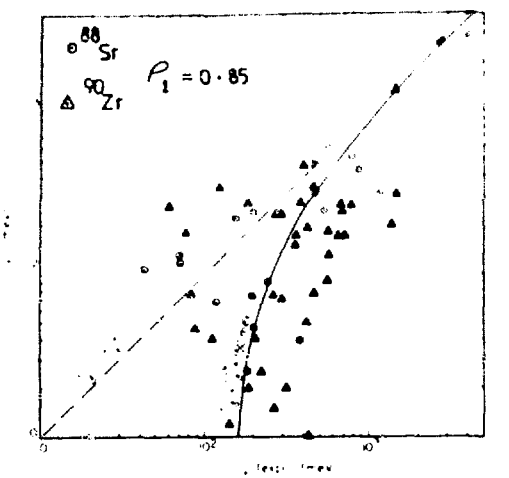

Figure 3. Comparison of measured radiation widths[2,15] for p-wave resonances in ^{88}Sr and ^{90}Zr with reduced neutron widths as expressed by calculated valence widths.

Particle-Hole Interactions

Valence capture involves correlations between partial radiation widths and reduced neutron widths of both initial and final states. If one of these correlations is observed

without the other, and if correlations, or intermediate structure, occur for nuclei in which valence components are small, then a different form of interaction must be involved. For example, if the incoming neutron interacts with either a neutron or proton in the target nucleus to form a 2p-1h compound state, this interaction will not convey a dependence on the initial state neutron widths. However, de-excitation by annihilation of the particle-hole will still depend on the availability of suitable single-particle final-state configurations. This form of interaction will therefore be characterised by final state correlations but no initial state correlations. An example occurs for neutron capture in ^{43}Ca where 24 s-wave resonances give an initial state correlation coefficient of 0.2 and valence model calculations predict that only 7% of the average radiation width arises from valence capture[16]. However, for the 1.48 keV resonance which dominates thermal capture, the final state correlation coefficient for 22 transitions is 0.75[17].

Initial state correlations occur more frequently than predicted by the valence model, and other forms of particle-hole interaction must be considered to explain these results. For example, the presence of common particle-hole configurations in both the initial state and final state can lead to additional transition strength which is correlated with Γ_n^2 but uncorrelated or even anti-correlated with θ_f^2. Thus strong transitions may be observed to states not populated in stripping reactions.

Particle-hole configurations in both initial and final states but with the same parity may give rise to enhanced M1 transitions - often corresponding to spin-flip transitions between shell-model configurations with the same orbital angular momentum.

Calculations of the contributions to transition rates from particle-hole interactions require model wave functions of low lying states and methods for calculating initial state configurations in terms of such wave functions. Some success has been achieved in such calculations for spherical nuclei[18-20] but in general, the phases and amplitudes of suitable configurations and their spreading width near the particle separation energy are not well enough known. Neutron capture measurements can therefore be of considerable value in exploring the extent to which simple configurations occur.

3. DATA

RADIATION WIDTHS

The determination of all the parameters of low energy resonances requires measurements of whichever is the smaller of scattering or capture cross sections. Scattering measurements are very difficult and have received only limited application. On the other hand there have been a number of continuing projects making accurate measurements of capture cross sections. Prominent in this area in recent years has been the project developed at ORELA by R.L. Macklin and numerous collaborators. High resolution capture cross section measurements at energies up to the order of 1 MeV have considerably increased the number of values of resonance parameters available[21] - particularly for nuclides with level spacings in the range 1 to 100 keV.

Average values of s and p-wave radiation widths are plotted in Figure 4. Most results have been taken from the BNL-325 compilation[1] and these have been supplemented by more recent values where available. Also shown in Figure 4 is a schematic level scheme indicating the positions of single particle states and neutron shell closures. Regions where strong E1 transitions are known to occur are shown and the presence of these transitions can be seen to influence the radiation

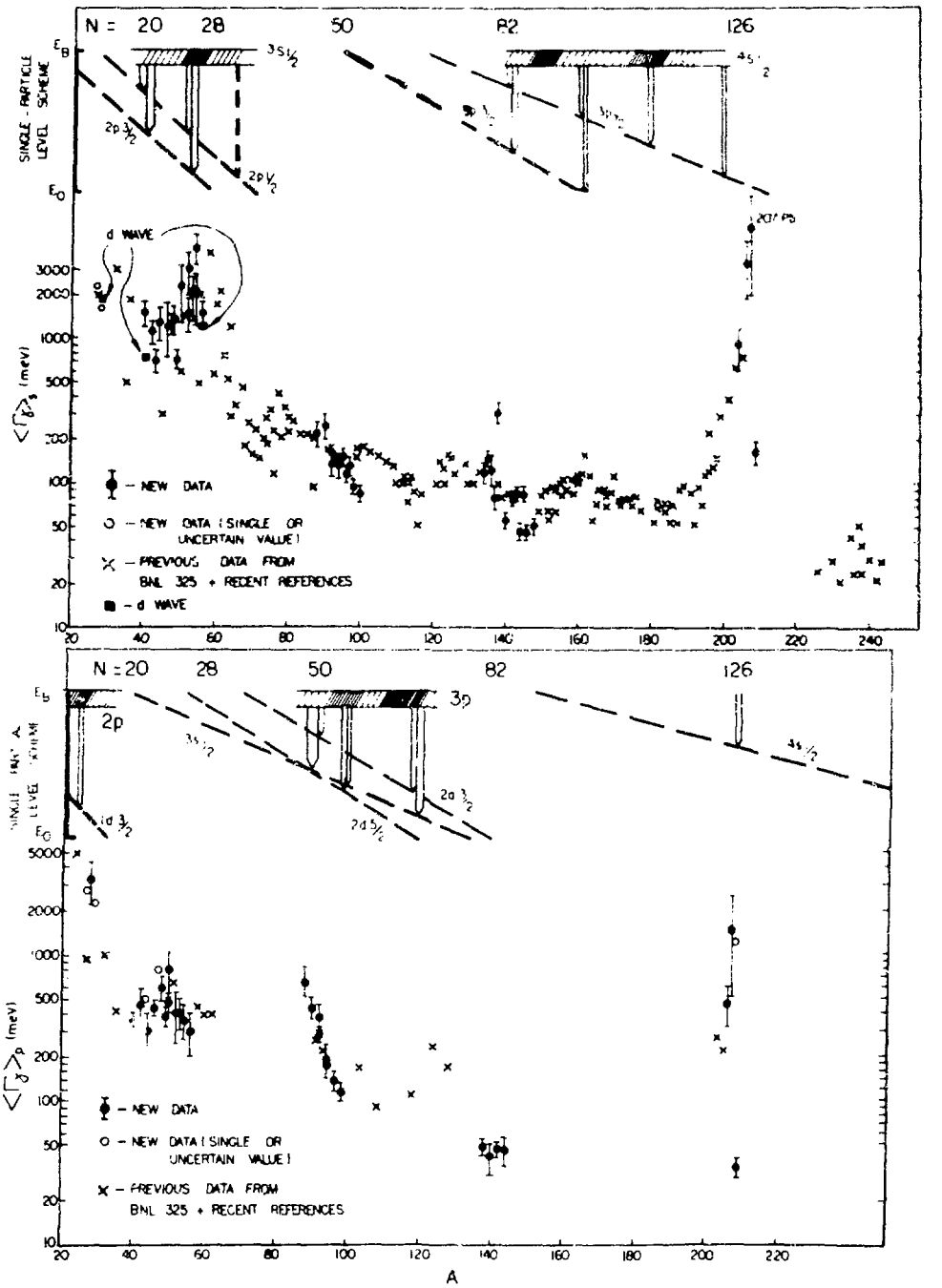

Figure 4. Radiation widths for s-wave (upper) and p-wave (lower) resonances as a function of mass number. Single particle E1 transitions between relevant capturing and final states are shown in each case.

widths. In the 3s region, s-wave widths can be 3 to 4 times the p-wave widths whereas in the 3p region the situation is reversed, with p-wave widths being approximately twice the average s-wave widths. Near N=82 s-wave widths are again enhanced and for ^{138}Ba a ratio of 6 has been reported[22]. A similar ratio has been observed for ^{209}Bi[23].

Although the major feature for s-wave radiation widths is the large peak at A=208 (N=126), there is no sign of any comparable effect at N=20 or 50. Also the 4s strength function maximum, which is broadened and split by the effects of deformations, appears to have only a very small influence on radiation widths. Clearly the availability of low-lying p-states is a prerequisite for strong s-wave capture and this is reinforced by the influence of neutron shell closure. Thus, while semi-empirical formulae which are based on the statistical assumption have been moderately successful in accounting for the structure observed in $\langle\Gamma_\gamma\rangle$ as a function of A[24,25], the structure is in fact the result of non-statistical effects and the contributions from simple reaction mechanisms.

There is evidence for peaks in p-wave radiation widths at A ~ 30, 90 and 208 although data is sparse in intervening regions. It is of interest that there is also a small peak near A = 50 and limited evidence for high values near A = 120. These are regions where strong M1 transitions have been observed[26-29] which may influence the radiation widths when E1 transitions are not favoured. Measurements are needed at intermediate neutron energies for many more nuclei to provide further information on p-wave interactions.

It is reasonable to assume that d-wave radiation widths will follow a similar pattern to that for s-wave resonances, although there is a possibility that additional structure may be introduced because E1 transitions can occur to f-states as well as to p-states. Evidence has been found for the presence of d-wave resonances in the 2d and 3d regions[30-32]. For example, gamma-ray transitions have been observed to the 7/2$^-$ ground state of ^{41}Ca and to 5/2$^-$ and 7/2$^-$ states throughout the region A = 40 - 70. Although 5/2$^-$ states may be populated by p-wave M1 transitions as well as d-wave E1 transitions, both ℓ-values must be considered in the analysis of cross-sections in the region of the strength function maxima even at energies below 100 keV. Three values of average radiation widths have been obtained[21] which are a little below the s-wave values in the same mass region (see Figure 4).

INITIAL STATE CORRELATIONS

Initial state correlation coefficients for s and p-wave capture are plotted in Figure 5 as a function of mass number. The vertical bars indicate only the effects of varying sample size on the uncertainty in coefficients[33]. Additional uncertainties arise from experimental errors in measured widths. The observed scatter of points in any one mass region presumably gives some indication of the overall uncertainties - except that, near magic numbers, changes can occur quite quickly in the contributions from valence capture.

Positive correlations are observed for s-wave resonances in nuclei near A = 55, 140, 165 and 200 and for p-wave resonances near A = 30 and 90. The number of nuclides for which correlations are observed is quite impressive. It is also of interest that one or two large widths often dominate the calculation of correlation coefficients, outweighing a lot of small but poorly correlated results.

Calculated values of $\langle\Gamma_\gamma^v\rangle$ vary by many orders of magnitude as the reduced neutron widths and level spacings change. Typical values are included in Figure 5, plotted as ratios to the corresponding average radiation widths. Again peaks occur near mass 30, 55, 90 and, to a minor extent, near 140. Even in these regions the

valence process does not fully explain the observed correlations or the observed radiation widths.

The varying success of valence predictions in the 3p region is illustrated by the following results for p-wave resonances:

TABLE 1

Resonance Parameters and Correlation Coefficients

Nuclide		^{88}Sr	^{90}Zr	^{92}Zr	^{92}Mo	^{98}Mo
Reference		2	15	21	11	11
$\langle\Gamma_\gamma\rangle_s$	(meV)	220	250	136	160	93
$\langle\Gamma_\gamma\rangle_p$	(meV)	670	440	380	290	117
$\langle\Gamma_\gamma^v\rangle_p$	(meV)	420	140	165	40	32
ρ_I	p3/2	0.96	0.58	0.88	0.62	0.4
ρ_I	p1/2	0.78	0.24	0.61	0.96	

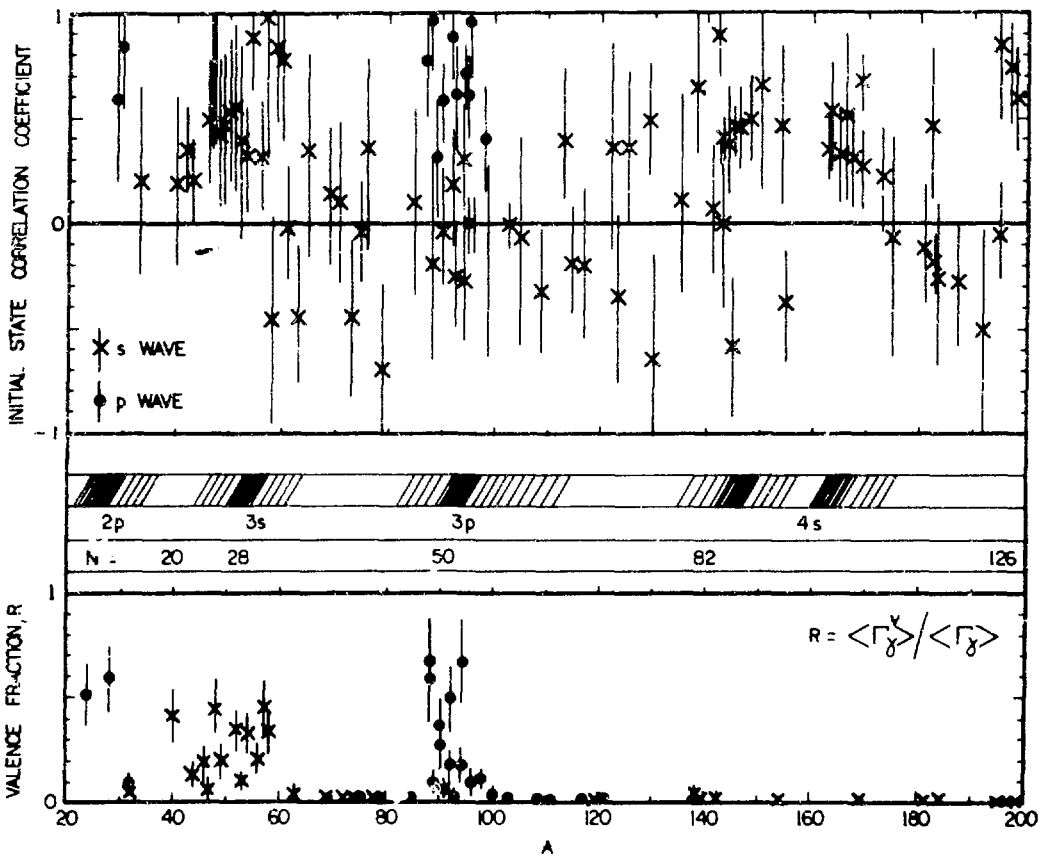

Figure 5. Initial state correlation coefficients (mostly ρ_I) for s and p-wave resonances (upper) and calculated valence fractions (lower). The positions of strength function maxima and magic neutron numbers are shown in the centre.

The s-wave radiation widths can be taken to indicate an approximate upper limit to the magnitude of the statistical component in each nuclide, since only M1 transitions can then occur to low-lying single particle states. Thus, the calculated valence components are to be compared with $\langle\Gamma_{\gamma p}\rangle - \langle\Gamma_{\gamma s}\rangle$. In ^{88}Sr, the predicted valence component is almost twice the statistical component and the larger radiation widths are within 25% of the estimates from the optical model formulation of the valence theory[2]. This close agreement is reflected in the large observed correlation coefficient.

In ^{90}Zr, the valence component needs to be supplemented by another mechanism in order to explain the magnitudes of the radiation widths and the moderate correlation coefficients[15]. Measurements of ground state transitions lead to the same conclusion[34]. In ^{92}Zr, the valence component increases because of an increase in p-wave strength function and the observed correlation also increases[21]. In ^{92}Mo and ^{98}Mo, the small level spacing leads to low neutron widths and hence small valence estimates[11] although, in the latter case, the estimated valence component is still a significant fraction of the observed $\langle\Gamma_{\gamma p}\rangle$. For these two isotopes ρ_I behaves in the opposite manner to the valence fraction and again other mechanisms are needed to explain the results.

Soloviev and Voronov[35] have calculated the energies of single-particle and 2p-1h states for nuclei in the 2p region. They find that the positions of these states vary markedly with respect to the neutron separation energy. The number of such states which can contribute to E1 or M1 decay of observed resonances therefore varies from isotope to isotope and this provides at least a partial explanation of the observed results. For example, they find that the valence model should be more significant in ^{92}Zr and ^{98}Mo than in ^{92}Mo in agreement with the observed results.

Valence capture contributes up to 50% of the gamma strength for large resonances in the 3s region. For example, the 192 keV resonance in ^{54}Fe has a radiation width of 16 eV and the calculated valence component is 10 eV[21]. In other isotopes such as ^{40}Ca, ^{52}Cr and ^{56}Fe, the average valence component is of the order of 30% of the observed s-wave widths and only moderate correlation coefficients are observed. Calculations by Soper[36] indicate that a considerable portion of the dipole strength in this mass region can be decoupled from the giant resonance to provide additional strength in E1 gamma decays from the threshold region. This dilutes the initial state correlations predicted by the valence model.

A similar situation exists in the 4s region where many examples of initial state correlations are observed (see Figure 5). The values plotted in Figure 5 are mostly ρ_I and the positive values differ from those for $\bar{\rho}_i$ which have been reported to be zero in this region[10]. However, here, valence estimates account for less than 10% of the observed Γ_γ values and particle-hole contributions which depend on Γ_n are needed to explain the observations. Information is needed on gamma-ray spectra to explore the nature of these interactions and this is discussed further in a later section.

It is clear from these examples that the valence model works well in those cases near closed shells where it is expected to dominate. Elsewhere it contributes smaller components to the observed radiation widths. There are no cases in which the valence model over-predicts the average radiation widths and thus no evidence for depletion of the valence strength by the giant dipole resonance.

There are a number of examples of over-prediction of individual radiation widths and of partial radiation widths. To some extent these can be attributed to uncertainties in experimental data, but there is also evidence for two sources of interference amongst reduced width amplitudes. Figure 3 shows that a considerable

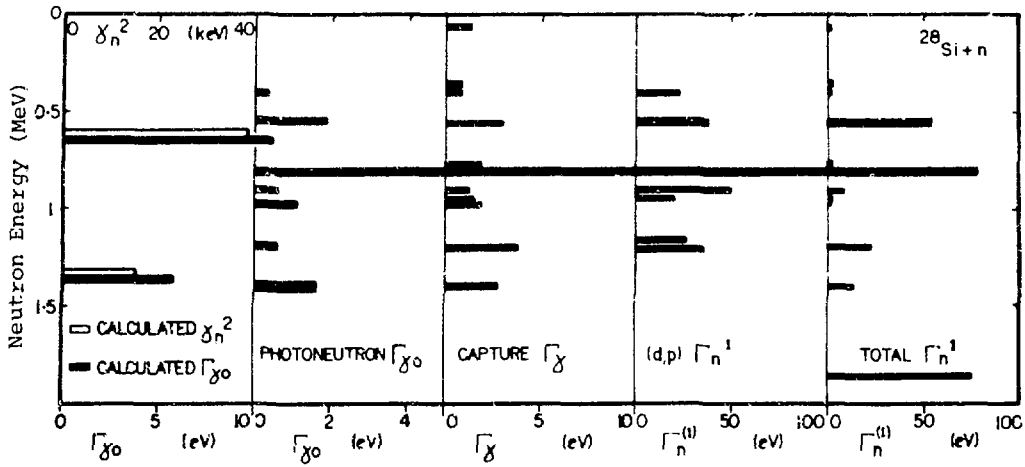

Figure 6. Measured and calculated resonance parameters[1,18,37-39] in ^{28}Si + n.

range of Γ_γ values are observed for resonances for which Γ_γ^ν is relatively small. This can be attributed to interference between the terms in equation (2). Varying phases should lead to some cancellation of this interference in the case of total radiation widths. However, there are so few partial widths contributing strongly to the nuclides concerned that interference can still be expected to be important.

In ^{28}Si[18] and ^{98}Mo[11] it has been shown that additional excited target configurations, which carry no E1 strength, can be important through their effect on Γ_n values. Such configurations may interfere constructively or destructively in the neutron channel, leading to incorrect values of Γ_n^ℓ for use in estimating valence components. Destructive interference is required to explain the results in ^{28}Si whereas constructive interference is required for ^{98}Mo.

INTERMEDIATE STRUCTURE

Because of the major contributions to resonance neutron capture from simple reaction mechanisms it is of considerable interest to look for a neutron energy dependence of the valence and particle-hole effects. A number of capture experiments have reported intermediate structure and additional results are provided by threshold photoneutron measurements using time-of-flight techniques. The most complete body of evidence has been obtained for ^{29}Si and the results are summarised in Figure 6. Reduced neutron widths of resonances at neutron energies up to 1.5 MeV have been measured in total cross section experiments[1] and by the (d,p) reaction[37]. Ground state radiation widths have been measured by the photoneutron technique[38] and total radiation widths by neutron capture measurements[39]. These all show the presence of large Γ_n and Γ_γ values between 500 and 1000 keV and the correlation for 20 p-wave resonances is ρ_I=0.84. Halderson et al.[18] have used a phonon-particle model, which gives good results for low lying levels in ^{29}Si, to calculate the expected position and strength of p3/2 states in the resonance region. The results are included in Figure 6 and provide a satisfactory explanation of the strength seen in p-states in this energy region.

Photoneutron measurements on ^{57}Fe show a few dominant ground state transitions for neutron energies near 200 and 600 keV[40]. However, neutron capture measurements[21] give a much more complex picture (Figure 7). The specific resonances seen in the photoneutron measurements have large radiation widths, but so do many other

resonances in the energy range up to 800 keV. The possibility that d-wave resonances are important in this energy region has already been mentioned and further work is needed to establish conclusively whether there is intermediate structure arising from p-wave M1 effects.

Large radiation widths for p-wave resonances have been observed in localised regions of neutron energy for capture in ^{88}Sr, ^{90}Zr and ^{92}Zr (Figure 8). Similar structure occurs for neutron widths which are correlated with the radiation widths. Measurements are needed over a wider energy range to fully establish the existence of this structure. Other examples of energy dependent radiation widths have also been found (for example in ^{19}F[41] and ^{205}Tl[42]).

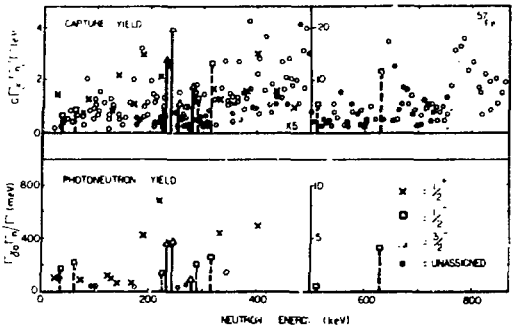

Figure 7. Comparison of resonance areas from capture cross sections[21] (upper) and threshold photoneutron measurements (lower)[40] for ^{56}Fe + n.

Measurement of resonance averaged transition rates has been a very useful technique at low neutron energies[4]. Results obtained using a similar technique to study p-wave resonances in Cd and Sn isotopes[43] indicate that p-wave E1 transitions from capture in the odd isotopes do not show unexpected structure in the neutron energy range from 10 to 100 keV. Structure may be more likely to occur for capture in the even isotopes but a much larger energy range is needed to study this.

Although structure has been reported in all the mass regions in which non-statistical effects are prominent, there is still insufficient evidence to determine the spreading width for single-particle and particle-hole configurations with any accuracy. The cases that have been reported involve widths of 100 keV or less.

PARTIAL RADIATION WIDTHS

Structure in gamma ray spectra from thermal neutron capture was the first evidence found for non-statistical processes in neutron capture. Similar structure is observed in resonance capture spectra - involving preferred transitions to final states which are usually those observed in ℓ_n = 0, 1 or 2 stripping reactions. Transitions to ℓ_n = 3 states have also been observed[44]. Results for individual resonances are subject to Porter-Thomas fluctuations which make it difficult to establish sytematic trends. This is illustrated in Figure 9 where results[45] for two resonances in ^{92}Mo are com-

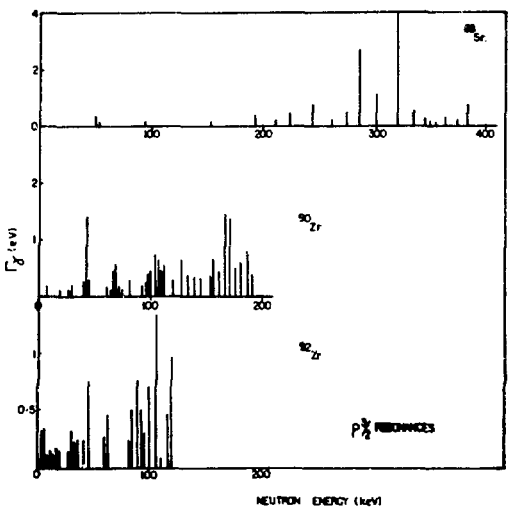

Figure 8. Measured radiation widths[2,15,21] for p-wave resonances in ^{88}Sr, ^{90}Zr and ^{92}Zr as a function of neutron energy.

pared with the (d,p) strengths as contained in calculated values of $\Gamma^{v}_{\gamma if}$. No correlation is found for these two resonances even though the averaged coefficient for 16 p-wave resonances is $\bar{\rho}_f = 0.96$ for s1/2 final states and 0.70 for d3/2, 5/2 final states. On the other hand, the two resonances in ^{98}Mo which are included in Figure 10 have high correlation coefficients[46] whereas only 5 out of 17 resonances give large values of $\bar{\rho}_f$ and 3 out of 10 final states give large values of $\bar{\rho}_i$. Other difficulties in obtaining a reliable interpretation of the results which are available can be illustrated for the case of capture in ^{142}Nd. Three (d,p) experiments and two thermal measurements can be combined in various ways to obtain values of ρ_f which vary from 0.05 to 0.6.

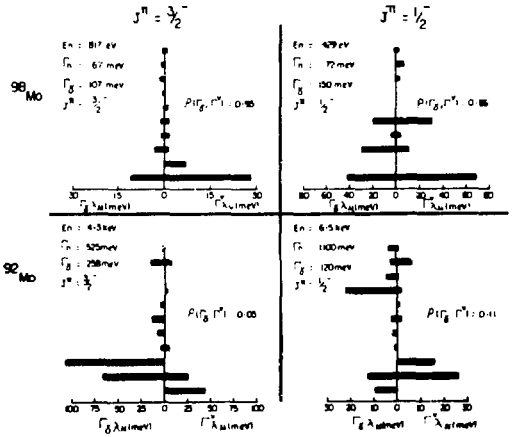

Figure 9. Comparison of partial radiation widths ($\Gamma_{\gamma\lambda\mu}$) with final state reduced widths as expressed by the calculated valence component ($\Gamma^{v}_{\gamma\lambda\mu}$)[45,46].

The averaging of partial widths over many resonances with the same J,π overcomes the difficulty with fluctuations but with a present limitation to nuclides with average level spacings of the order of 1 keV or less. In many cases it is important to separate s-wave and p-wave effects by making measurements for many resolved resonances when both ℓ-waves contribute. An additional method for seeking information on non-statistical effects in gamma-ray spectra is to study the systematics of the occurence of strong transitions as a function or mass number.

Final State Correlations

Reported values of final state correlation coefficients are plotted in Figure 10 as a function of A. Results from resonance studies are supplemented by those

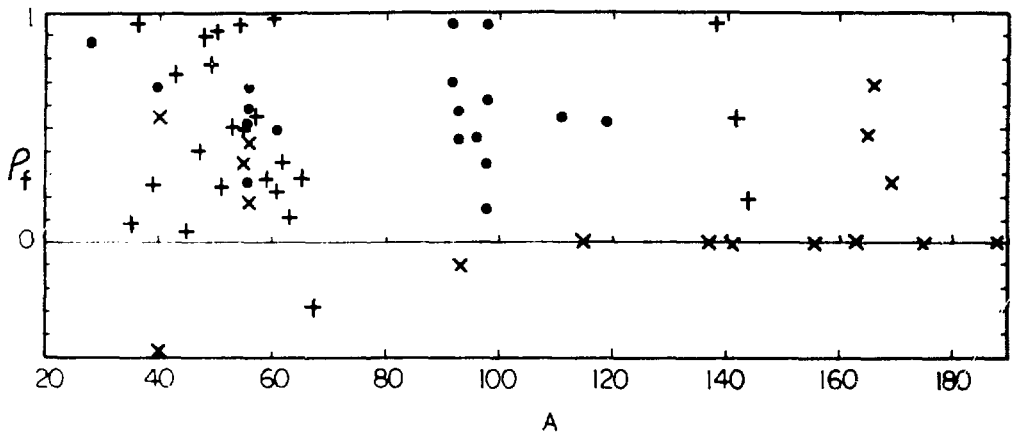

Figure 10. Final state correlation coefficients from s-wave (x) and p-wave resonances (•) and from thermal capture (+).

from thermal capture when this is dominated by resonances[33]. There is a marked lack of information in some regions - arising from a shortage of both (n,γ) and (d,p) results. However, some high values have been reported in each of the non-statistical regions.

In the 3s region, final state correlations support the evidence from initial state correlations on contributions from valence capture. For example, both correlation coefficients are 0.9 for capture in ^{54}Fe which has N = 28 and has an important valence component[21]. The coefficients and the estimated valence component are much reduced in ^{56}Fe. It is of interest that final state correlations are observed in ^{56}Fe for M1 transitions from p-wave resonances[47] and the coefficients are comparable (0.2 - 0.6) with those for s-wave resonances.

A number of detailed experiments have been carried out in the 3p region and the averaged correlation coefficients are compared in Table 2.

TABLE 2

Average Correlation Coefficients for p-Wave Resonances

Nuclide	^{92}Mo	^{92}Mo	^{93}Nb	^{93}Nb	^{94}Mo	^{96}Mo	^{98}Mo	^{98}Mo
Reference	45	49	48	50	49	49	46	49
Number of:								
Resonances	16	~1	~40	10	~4	~5	17	~5
Final States	12	11	45	20	9	10	10	10
$\bar{\rho}_i$	0.51;0		0	0			0.3	
$\bar{\rho}_f$	0.8	0.69	0.47	0.38	0.67	0.47	0.4	0.97

The results support the varying role which has already been discussed for valence and doorway interactions in this mass region. Generally, final state correlations are observed to be higher than initial state correlations - implying that the second term in equation (2) plays a significant role.

Some final state correlations have been reported in the 4s region where neither these nor initial state correlations can be attributed entirely to valence capture. In some cases it would seem that $\bar{\rho}_i$ is higher than $\bar{\rho}_f$ - implying a role for the third term in equation (2). This can be attributed to the presence of particle-hole configurations in the final states which are coupled to the incident neutron and can be fed directly from the entrance channel.

Strong gamma ray transitions have been observed[44] to ℓ_n = 3 final states following capture in ^{139}La, and these transitions cannot be accounted for by statistical or valence processes. A 2p-1h mechanism has been invoked to explain the observed gamma-ray spectra, but it remains to be seen whether initial state correlations are present or absent in this case.

Strong Transitions

There are many gamma ray spectra measurements in which too few transitions are observed for meaningful correlation coefficients to be calculated. Nevertheless, non-statistical effects are often apparent from the fact that a few dominant transitions may account for at least 50% of Γ_γ. For capture in even-even nuclides, strong high energy transitions occur to final states whose energies and stripping widths are relatively smooth functions of mass number from 20 to 70 and 85 to 140[51]. The intensities of strong transitions from s-wave capturing states to p3/2 and p1/2 final states follow closely the stripping widths.

A comparison of gamma-ray intensities from p-wave capture, with (d,p) ℓ_n = 0,2 results for s½, d3/2 and d5/2 final states is shown in Figure 11. The gamma ray reduced widths were obtained from relative gamma ray intensity measurements

normalised where necessary to the non-statistical part of the average radiation widths. The normalisation for ^{91}Zr is to the photoneutron ground state results[34]. Only the strongest transition for each final state spin is included and the (n,γ) data follow the same trends as the stripping results which demonstrate the effects of the filling of sub-shells.

The evidence for systematic behaviour of strong transitions is sufficiently widespread, and supported by evidence from correlations, for there to be no need to restrict the analysis of neutron capture results to analogies with stripping reactions. The capture results can be used in their own right to establish single-particle properties of many nuclides.

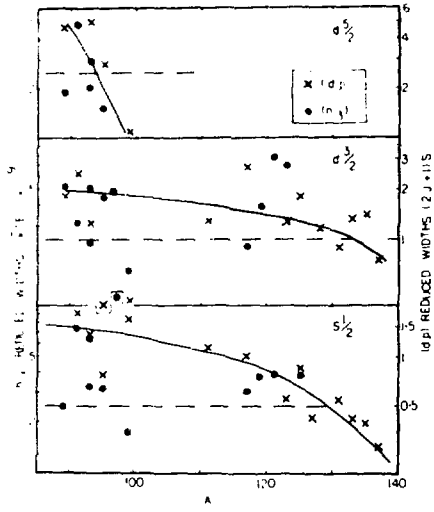

Figure 11. Comparison of (n,γ) and (d,p) reduced widths for s1/2, d3/2 and d5/2 final states

M1 Transitions

High average values of M1 reduced widths have been reported in the non-statistical regions (e.g. A ~ 30, 55, 90, 140 and 208) although in some cases (such as ^{56}Fe and ^{208}Pb) there are difficulties in reconciling conflicting experiments[3]. Particularly high values, which are to be compared with the overall average, $\bar{k}_{M1} = 18 \times 10^{-9}$ MeV^{-3}, are listed in Table 3.

TABLE 3

Enhanced M1 Reduced Widths

Nuclide	^{19}F	^{27}Al	^{101}Ru	$^{117,118}Sn$	^{138}Ba
Reference	26	26	27	28	29
No. of Transitions	3	6	7	3	
$\bar{k}_{M1} \times 10^{9}$ (MeV^{-3})	164	164	191	270	90

It is possible that such high values have an influence on total radiation widths but insufficient information is available to confirm the giant M1 resonances found in photon excitation experiments[7].

4. SYSTEMATICS

Average radiation widths show a smooth trend with mass number which can be attributed to compound nucleus interactions, but many effects from simpler reaction mechanisms are superimposed on this trend. At low masses there is a considerable variation in results because of the small number of transitions which are involved for many nuclei. Peaks occur near specific masses for each ℓ-wave and, in the regions of these peaks, average radiation widths may vary systematically with neutron energy. Correlations with reduced neutron widths are also observed, especially for capture in even-even nuclides throughout much of the mass range.

Semi-empirical formulation of the effects of level density need to be reconsidered separately for each ℓ-wave. The quantitative prescription for valence

capture could be used, plus estimates of the strength of doorway state contributions (which at this stage must be established experimentally) and a relatively smooth statistical contribution.

Electric dipole transitions from capture in most even-even nuclides (except those in the regions of large deformations) follow closely the systematics in excitation energy and reduced neutron widths of single-neutron states. Average M1 transition rates, which are normally about one seventh of those for E1 transitions[4], also show some increased values but the systematics of these are not fully established.

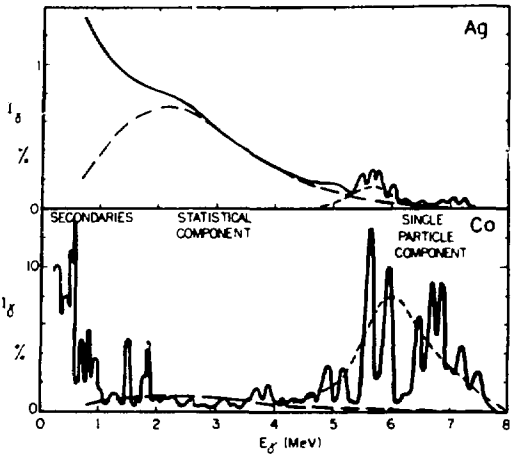

Figure 12. Schematic representation of spectra with a dominant single particle component (lower) and a dominant statistical component (upper).

Values of reduced radiation widths should be subdivided into groups, at least for even-odd nuclides. The strongest transitions which populate final states with single particle configurations have a considerably higher average reduced width than do E1 transitions to states with more complex configurations. They also follow specific trends with mass number for each spin and parity of the final states. In considering the E_γ dependence of reduced widths it is necessary to allow for the presence of intermediate structure near the neutron threshold, based on decoupling of single-particle effects from the giant resonance as well as possible fine structure in the giant resonance itself.

Structure in neutron capture spectra arises from preferred high energy transitions to low-lying single-particle states as well as favoured low energy transitions from the decay of those states. This is illustrated schematically in Figure 12 for two cases - one with a dominant contribution from statistical interactions and the other with a dominant contribution from single-particle processes (including particle-hole interactions).

The expression for the envelope of primary gamma rays can be modified to include single-particle effects:

$$I_\gamma = (I_\gamma)_s + K\, F(W, E_R, E_\gamma) \qquad (5)$$

where E_R and W are the centre position and width of a single-particle peak. The function F will not necessarily have a common form for all nuclei. However, a suitable function, such as a skew gaussian, may be satisfactory in many cases. It should be possible to use empirical information already available to define suitable values of W and E_R.

Although there is now much firm evidence for the importance of these non-statistical effects, there is still a great deal of work to be done to define the models and parameters fully. Some of the problems of special interest include:

(i) Intermediate Structure - measurements over an extended energy range on target nuclides such as ^{88}Sr, ^{90}Zr, etc., to substantiate evidence on the localisation of valence and doorway strength.

(ii) Models - further detailed comparisons in multiple experiments (as described for ^{28}Si) on light nuclides and closed-shell nuclides and comparison with calculations from realistic nuclear structure models.

(iii) Doorway States - study of nuclides immediately following closed subshells, where particle-hole states may be of particular importance.

(iv) Partial Radiation Widths - absolute measurements of gamma-ray spectra for many more nuclides in the 3p and 4s regions to determine the systematics of reduced widths and correlations.

(v) d-Wave Resonances - a study of $7/2^-$ transitions in the mass 140 region and further search for d-wave resonances in isotopes of Cr, Fe, Ni, Pb, etc.

These and other aspects of resonance neutron capture should produce interesting physics and useful data for some time to come.

5. ACKNOWLEDGEMENTS

Much of the work reported here was been made possible through a collaborative program with R.L. Macklin at ORNL. We are pleased to acknowledge this as well as stimulating discussions and correspondence with A.M. Lane and R.F. Barrett.

6. REFERENCES

1) S.F. Mughabghab and D.I. Garber, BNL 325 3rd Ed. 1973, 1.

2) J.W. Boldeman, B.J. Allen, A.R. deL. Musgrove, R.L. Macklin and R.R. Winters; (^{88}Sr) Nucl. Phys. 1976, in press.

3) H.E. Jackson, JAERI-M5984, 1975, p.119; Proc. 2nd Int. Symp. on Neutron Capture Gamma Ray Spectroscopy Petten, 1975, p.437.

4) L.M. Bollinger, Proc. Asilomar Conf. on Photonuclear Reactions and Applications, CONF 730301, 1973, p.783.

5) J.E. Lynn, Theory of Neutron Resonance Reactions (Clarendon, Oxford 1968).

6) G.A. Bartholomew, E.D. Earle, A.J. Ferguson, J.W. Knowles and M.A. Lone, Advances in Nuclear Physics (Plenum, 1974) 7, p.229.

7) R.L. Bramblett, S.C. Fultz, B.L. Berman, Proc. Asilomar Conf. on Photonuclear Reactions and Applications, CONF 730301, 1973, p.13.

8) A.M. Lane and J.E. Lynn, Nucl. Phys. 1960, 17, pp.563, 586.

9) A.M. Lane, Proc. 2nd Int. Symp. on Neutron Capture Gamma Ray Spectroscopy, Petten, 1975, p.31; S.F. Mughabghab, ibid. p.53; R.E. Chrien, ibid, p.247.

10) M. Beer, Ann. of Phys. 1971, 65, p.181.

11) A.R. deL. Musgrove, B.J. Allen, J.W. Boldeman and R.L. Macklin; (Mo), Nucl. Phys. 1976, in press.

12) A.M. Lane and S.F. Mughabghab, Phys. Rev. 1974, C10, p.412.

13) R.F. Barrett and T. Terasawa, Nucl. Phys. 1975, A240, p.445.

14) J. Cugnon, C. Mahaux, Proc. 2nd Int. Symp. on Neutron Capture Gamma Ray Spectroscopy, Petten, 1975, p.81.

15) J.W. Boldeman, B.J. Allen, A.R. DeL. Musgrove and R.L. Macklin, Nucl. Phys. 1975, A246, p.1.

16) A.R. deL. Musgrove, B.J. Allen, J.W. Boldeman and R.L. Macklin; (^{42,43,44}Ca), Nucl. Phys. 1976, in press.

17) D.H. White and R.E. Birkett, Phys. Rev. 1972, C5, p.513.

18) D. Halderson, B. Castel, I.P. Johnstone and M. Divadeenam, Phys. Rev. Lett. 1976, 36, p.760.

19) V.G. Soloviev, Proc. 2nd Int. Symp. on Neutron Capture Gamma Ray Spectroscopy, Petten, 1975, p.99.

20) V.A. Knat'ko and E.A. Rudak, Sov. Nucl. Phys. 1972, 15, p.626.
M. Divadeenam, W.D. Beres and H.W. Newson, Ann. of Phys. 1972, 69, p.428.

21) AAEC/ORNL Collaboration - Results for the following nuclides are in the course of publication: ^{28}Si, $^{40-44}$Ca, $^{46-50}$Ti, $^{50-54}$Cr, $^{54-57}$Fe, ^{88}Sr, $^{90-94}$Zr, $^{92-98}$Mo, $^{134-138}$Ba, ^{140}Ce, $^{142-148}$Nd.

22) A.R deL. Musgrove, B.J. Allen, J.W. Boldeman and R.L. Macklin, Nucl. Phys. 1975, A252, p.301.

23) R.L. Macklin and J. Halperin, Phys. Rev. 1976.

24) A.G.W. Cameron, Can. J. Phys. 1959, 37, p.322.

25) V. Benzi, G. Reffo and M. Vaccari, Proc. Panel on Fission Product Nuclear Data, Bologna, 1974, III, p.123.

26) M.J. Kenny, P.W. Martin, L.E. Carlson and J.A. Biggerstaff, Aust. J. Phys. 1974, 27 p.759.

27) K. Rimawi, J.B. Garg, R.E. Chrien, G.W. Cole and O.A. Wasson, Phys. Rev. 1974, C9, p.1978.

28) M.R. Bhat, R.E. Chrien, O.A. Wasson, M. Beer and M.A. Lone, Phys. Rev. 1968, 166, p.1111.

29) R.J. Holt and H.E. Jackson, Phys. Rev. 1974, C12, p.56.

30) J.R. Bird, B.J. Allen and M.J. Kenny, Proc. 1st Int. Symp. on Neutron Capture Gamma Ray Spectroscopy, Studsvik, 1969, p.587.

31) D.M.H. Chan and J.R. Bird, Aust. J. Phys. 1971, 24, p.671.

32) R.F. Barrett, B.J. Allen, M.J.Kenny, and A.R. deL. Musgrove, Phys. Lett. 1976, 61B, p.441.

33) B.J. Allen, et al., To be published.

34) R.E. Toohey and H.E. Jackson, Phys. Rev. 1974, C9, p.346.

35) V.G. Soloviev and V.V. Voronov, JINR-E4-8834, 1975.

36) Reported in: A.M. Lane, Ann. of Phys. 1971, 63, p.171.

37) L.R. Medsker, H.E. Jackson and J.L. Yntema, Phys. Rev. 1974, C9, p.1851.

38) H.E. Jackson and R.E. Toohey, Phys. Rev. Lett. 1972, 29, p.379.

39) J.W. Boldeman, B.J. Allen, A.R. deL. Musgrove and R.L. Macklin, Nucl. Phys. 1975, A252, p.62.

40) H.E. Jackson and E.N. Strait, Phys. Rev. Lett. 1971, 27, p.1654; Phys. Rev. 1971, C4, p.1314.

41) R.L. Macklin and R.R. Winters, Phys. Rev. 1973, C7, p.1766.

42) E.D. Earle, M.A. Lone, G.A. Bartholomew, B.J. Allen, G.G. Slaughter and J.A. Harvey, Proc. Albany Conf. on Statistical Properties of Nuclei (Plenum, 1972) p.263.

43) Hla Pe, B.J. Allen, M.J. Kenny and J.R. Bird, Proc. 2nd Int. Symp. on Neutron Capture Gamma Ray Spectroscopy, Petten, 1975, p.115, and also this Conference.

44) B.J. Allen, M.J. Kenny, R.F. Barrett and K.H. Bray, Phys. Lett. 1976, 61B, p.161.

45) O.A. Wasson and G.G. Slaughter, Phys. Rev. 1973, C8, p.297.

46) R.E. Chrien, G.W. Cole, G.G. Slaughter and J.A. Harvey, Phys. Rev. 1976, C13, p.578.

47) M.J. Kenny, Aust. J. Phys. 1971, 24, p.803.

48) R.E. Chrien, K. Rimawi and J.B. Garg, Phys. Rev. 1971, C3, p.2054.

49) K. Rimawi and R.E. Chrien, Proc. 2nd Int. Symp. on Neutron Capture Gamma Ray Spectroscopy, Petten, 1975, pp.364, 368.

50) T.J. Haste and B.W. Thomas, J. Phys. G, 1975, 1, pp.967, 981.

51) J.R. Bird and F. Hille, Proc. 2nd Int. Symp. on Neutron Capture Gamma Ray Spectroscopy, Petten, 1975, p.160.

MB 2 - RESONANCE NEUTRON CAPTURE - J. R. Bird (AAEC, Lucas Heights)

Newstead (B.N.L.):

Roger, one of the features of this correlation business seems to be that when you expand the energy range and include more resonances, the correlation goes away. At least that was the case a few years ago when I was last involved with this subject. Do I understand that the situation is now changed -- that there is definite evidence for these correlations in the various mass regions?

Bird:

Yes, that's correct. It's the measurements at several hundred kilovolts energy which help to provide confidence in this, I believe. I showed you the case of strontium where the correlation comes in strongly once you have made measurements to four or five hundred keV. It certainly seems true that there are regions in which correlations are limited, and other regions where they are greater, but you have to remember that the very effects we are looking for are not smooth statistical effects. By their very nature they appear as a few dominant transitions from a few dominant resonances, and you may or may not observe it in some experiments. It takes a lot of data to build up the picture.

Chrien (B.N.L.):

In one of the first slides you showed concerning the strontium-88 total radiation widths, you compared the distribution with those from erbium-167. It seemed to me as though the strontium distribution was even broader than the Porter-Thomas distribution. I wonder if you'd care to comment on that feature?

Bird:

We haven't made a Porter-Thomas fit, but since there is a correlation with neutron widths of .9 or more, then the distribution is presumably the same as the neutron width distribution.

1:45 P.M., TUESDAY, JULY 6, 1976, IN OLNEY 150

MAIN SESSION MC

Chair: G.A. Bartholomew (A.E.C.L. Chalk River, Canada)

1.45 p.m., Tuesday, July 6, 1976 Invited Paper: MC1

FAST RADIATIVE CAPTURE

I. Bergqvist

Department of Physics, University of Lund,

Lund, Sweden

RÉSUMÉ

Recent studies of fast neutron capture processes in the energy range 5 - 15 MeV are focused on investigations of the validity of the direct-semidirect capture theory. Considerable effort has also recently been made to improve the activation technique for neutron capture cross section measurements.

ABSTRACT

A review of recent developments in theory and experiment of fast neutron radiative capture will be presented. The experimental data on heavy nuclei in the neutron energy range of 5 - 15 MeV strongly support the interpretation in terms of direct and semidirect capture processes. However, difficulties have been encountered in the theoretical description of the interaction between the incident neutron and the target nucleus. These difficulties are most conspicuous for light nuclei. For these nuclei recent measurements indicate a relatively strong contribution of compound nuclear reactions in this energy range. This observation would help to find an appropriate formulation of the particle-nucleus interaction.

Several problems remain unsolved in fast neutron capture at energies below 5 MeV. Unfortunately, little new information is available in this energy range. Previous studies on γ-rays from neutron capture and (d,pγ) reactions on heavy nuclei (A > 90) have shown that the results can be interpreted in terms of a γ-ray strength function for E1 transitions. Some aspects of this strength function will be discussed.

Recent activation measurements of fast neutron capture cross sections have revealed serious errors in former activation cross section values caused by low-energy secondary neutrons from reactions such as (n,2n) and (n,n') in target and sample material. The most notable errors occur for deformed nuclei at a neutron energy of 14 - 15 MeV, but the influence of secondary neutrons can be significant also at considerably lower neutron energies.

I. INTRODUCTION

This review on fast neutron capture will be confined to aspects relating to γ-ray strength functions, direct and semidirect capture and experimental problems in cross section measurements. The situation can be illustrated by the yield curve for the reaction $^{40}Ca(n,\gamma_0)^{41}Ca$, i.e. the yield of γ-rays to the $1f_{7/2}$ ground state of ^{41}Ca. Figure 1 shows the results from experiments performed at Los Alamos by Bergqvist, Drake and McDaniels [1] and at Uppsala by Nilsson ec al [2]. The curves represent calculations based on the compound nucleus (CN) and direct-semidirect (DSD) models. The solid line is the sum of the predicted cross sections.

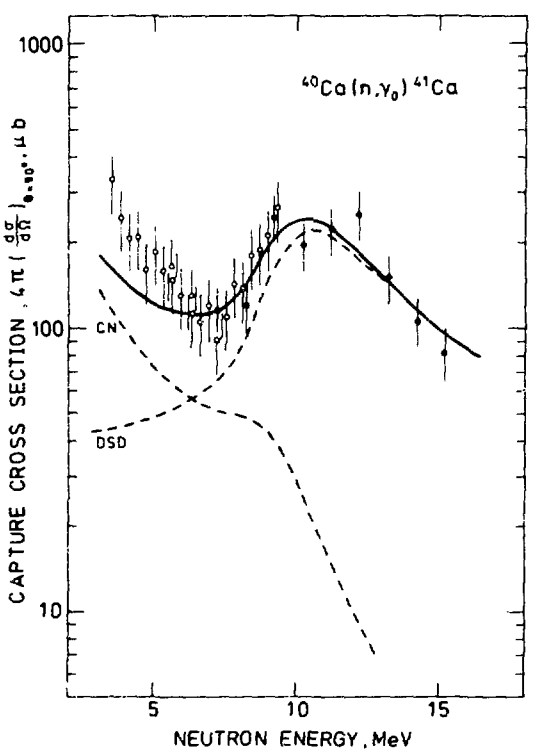

Fig. 1. Cross section for the $^{40}Ca(n,\gamma_0)^{41}Ca$ reaction. Experimental results are taken from ref. [1] (filled circl and ref. [2] (open circles). The dashed curves show the compound nucleus (CN) and direct-semidirect (DSD) cross sections.

The most crucial parameter in the compound-nucleus calculations is the radiation width. An estimate of the E1 γ-ray strength can be obtained by relating it to the photoabsorption cross section. This method, outlined in Section II, has recently been comprehensively discussed for A > 90 nuclei by Bartholomew et al [3]. For lighter nuclei, almost no information on the γ-ray strength function is available. Nevertheless, the same procedure for the estimate of the γ-ray strength was followed in the calculations of the $^{40}Ca(n,\gamma_0)$ cross section. The estimate will, of course, be very uncertain but the agreement with the experimental results indicates that the method might be applicable also to light nuclei.

The predicted direct-semidirect cross section is taken from a calculation by Nilsson and Eriksson [4]. In this calculation it was assumed that the giant dipole resonance of ^{41}Ca is split into two isospin components, of which only the $T_<$ component can be excited in neutron capture reactions of direct type. The interaction between the incident neutron and the target nucleus was represented by a volume form function with the strength of the real isospin part of the optical potential. A more general formulation of the coupling will be discussed in Section III.

The agreement is quite good between the observed cross section and the sum of the predicted cross sections over the giant resonance region, i.e. for $E_n >$ 6 MeV. Strictly speaking, the compound and direct-semidirect cross sections should not be added in such a simple way. Mantzouranis [5] has shown that the usual Hauser-Feshbach theory fails in an energy region where both compound and direct processes contribute. The effect of this interference is not known in the present case.

Finally, in Section IV, we shall briefly discuss experimental problems in capture cross section measurements using the activation technique. The main problem is the influence of secondary low-energy neutrons in measurements of fast neutron cross sections which is often very large and difficult to correct for.

II. THE γ-RAY STRENGTH FUNCTION FOR E1 TRANSITIONS

We define the γ-ray strength function as the average reduced width for transitions of a particular multipole type. For an E1 transition of energy E_γ from a level at E_λ with spin and parity J^π, the strength function is

$$f(E_\gamma) = \frac{< \Gamma_{\gamma i \lambda} >}{E_\gamma^3} \rho_J(E_\lambda), \qquad (1)$$

where $< \Gamma_{\gamma i \lambda} >$ is the partial γ-ray width averaged over states with spin and parity J^π in the neighbourhood of E_λ and $\rho_J(E_\lambda)$ is the level density for such states.

The strength function for ground state transitions can, as shown by Axel [6], be related to the photoabsorption cross section, $< \sigma_{\gamma a}^J >$. Following ref. 3 we write

$$f(E_\gamma) = 26 \cdot 10^{-5} \frac{< \sigma_{\gamma a}^J(E_\gamma) >}{g_J E_\gamma} \quad \text{MeV}^{-3}, \qquad (2)$$

where $g_J = \frac{2J+1}{2J_0+1}$ and $< \sigma_{\gamma a}^J(E_\gamma) >$ is the average absorption cross section (in barn) of a nucleus with ground state spin J_o for the excitation of levels with spin J at energy $E_\lambda = E_\gamma$. The total observed absorption cross section, $< \sigma_{\gamma a} >$, is the sum of all contributing $< \sigma_{\gamma a}^J >$. For E1 transitions one usually assumes [7] that

$$< \sigma_{\gamma a\ E1}^J > = \frac{g_J}{3} < \sigma_{\gamma a\ E1} > .$$

In this case the strength function

$$f(E_\gamma) = 8.7 \cdot 10^{-5} \frac{<\sigma_{\gamma a}(E_\gamma)>}{E_\gamma} \text{ MeV}^{-3} \qquad (3)$$

is independent of spins J_o and J.

In applications to neutron capture reactions a further assumption has to be made to describe γ-ray transitions to excited states. This assumption, referred to as the Brink hypothesis [7], states that each excited state has built on itself a giant resonance identical to that for the ground state but shifted upward in excitation energy by the energy of the particular state. The application of the strength function also to excited states implies that all levels are treated equally and that only the average statistical properties of the levels are considered. Single-particle effects, for example, which are of dominating importance in reactions of direct type have to be dealt with separately.

The photoabsorption cross sections are generally well established at energies above the neutron binding energy. Generally, one or two Lorentz curves describe the observed cross sections quite well, i.e.

$$\sigma_{\gamma a}(E_\gamma) = \sum_{i=1}^{2} \frac{\sigma_i E_\gamma^2 \Gamma_i^2}{(E_\gamma^2 - E_i^2)^2 + E_\gamma^2 \Gamma_i^2}, \qquad (4)$$

where E_i, Γ_i and σ_i are the resonance energy, width and maximum cross section, respectively, which are adjusted to fit the experimental data. This form can be used to obtain an estimate of the photon strength in the energy region around and below the neutron binding energy, where very little information is available from photonuclear work.

Experimental methods and results to test the validity of the strength function concept have recently been reviewed by Bartholomew et al [3]. For nuclei with A > 90, the experimental results on the γ-ray strength functions show an overall energy dependence in fair agreement with that predicted from the Lorentzian curve. A strong departure from this curve is observed in the mass range A ≈ 190 - 208, i.e. near the closed shells Z = 82 and N = 126. Evidence for a similar substructure is found also in the range A ≈ 110 - 140, i.e. near the Z = 50 and N = 82 closed shells.

We shall now focus on two nuclei in these mass regions, namely ^{198}Au, which has been studied in a recent experiment by Earle, Bergqvist and Nilsson [8] in order to resolve a discrepancy evident in earlier measurements, and ^{116}Sn, for which theoretical calculations have now been performed by Csernai and Zimányi [9].

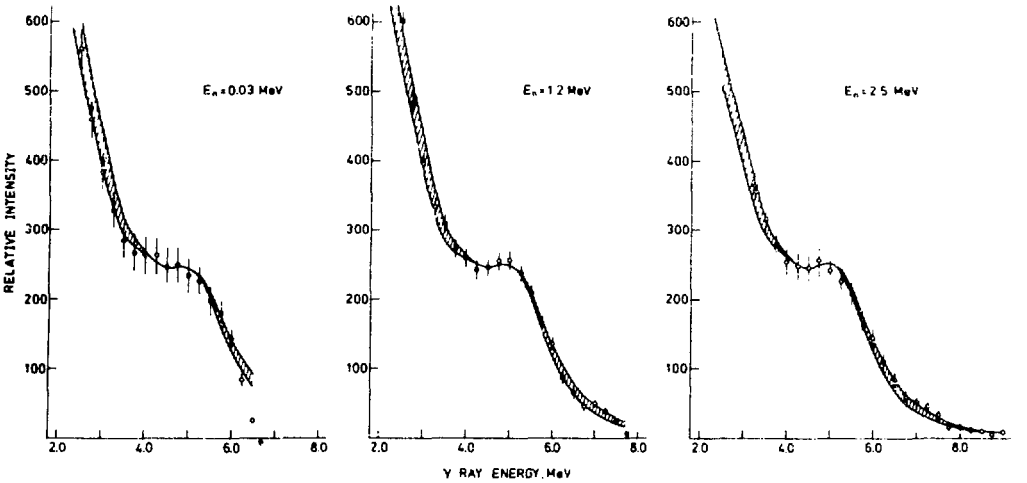

Fig. 2 Experimental and calculated γ-ray spectra from $^{197}Au(n,\gamma)^{198}Au$ (see text).

In the experiment, the γ-ray spectra from the reaction $^{197}Au(n,\gamma)^{198}Au$ were measured at several incident energies between 30 keV and 2.5 MeV. The γ-ray detector was a 5" NaI (Tl) spectrometer and time-of-flight technique was used to reduce background. Preparatory work on the experimental arrangement, shielding and timing electronics resulted in considerable improvement in the signal-to-background ratio compared to earlier measurements. The results for three neutron energies are shown in Fig. 2. These γ-ray spectra have been obtained by unfolding the detector response function from the observed pulse distributions.

The shapes of the spectra are nearly the same at all neutron energies. The γ-ray intensity decreases with energy up to $E_\gamma \approx 3.5$ MeV, becomes roughly constant in the range $E_\gamma \approx 4.0 - 5.2$ MeV and falls off at higher energies. The similarity of the spectral shapes (the variations can probably be attributed to statistical errors and uncertainties in γ-ray energy calibrations) indicates that a γ-ray strength function can be found which would give calculated spectral distributions in satisfactory agreement with all the observed spectra. Such calculated spectra are shown as solid curves in Fig. 2 with shaded areas to indicate approximately the variations of the spectral shapes. The 2.5 MeV results disagree significantly with earlier measurements [10] at approximately this energy. The signal-to-background ratio in the previous measurements was rather unfavorable, which implied difficulties in the determination of the background.

The γ-ray strength function extracted from the spectra of Fig. 2 is represented in Fig. 3 as solid curves again with the shaded areas to indicate the variation of the results at different neutron energies. The shape of the γ-ray spectra is reflected in the strength function by the bends of the curve near $E_\gamma = 3.5$ MeV and 5.5 MeV and the rather sharp increase with E_γ between these energies. Comparison with the results quoted in the review of Bartholomew et al [3] obtained from analyses of spectra from thermal neutrons (open circles), and from the reaction $^{197}Au(d,p\gamma)^{198}Au$ (filled triangles) shows good agreement except at

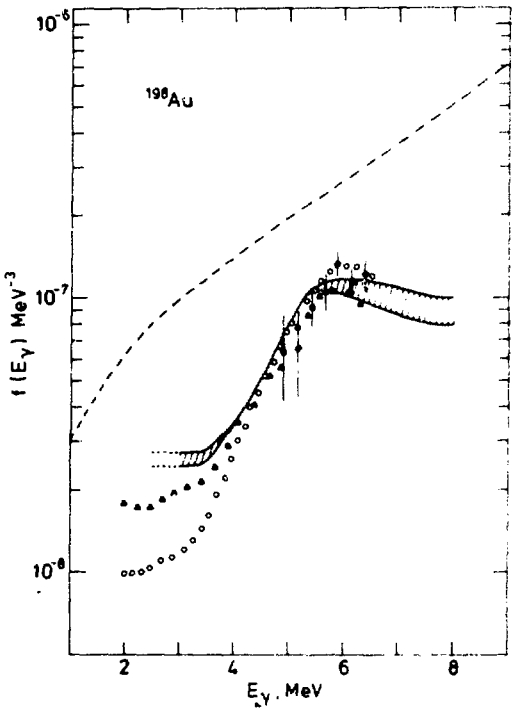

Fig. 3 Gamma-ray strength function for ^{198}Au (for symbols, see text).

lower γ-ray energies which is difficult to determine in neutron capture experiments. Absolute normalization of the present curve has been made to the high resolution γ-ray results of Leper, Bollinger and Thomas using a ∿ 2 keV broad neutron beam (filled circles). The experimental results fall significantly below the Lorentzian curve (dashed line).

The serious discrepancy between the strength functions previously deduced for ^{198}Au is primarily due to differences in the assumed level density distributions. This was illustrated by Bartholomew et al [3], who showed that different level densities assumed for ^{198}Au produce differences of about an order of magnitude for $f(E_\gamma)$ around E_γ = 6 MeV. The level density formula connected to all the results presented in Fig. 3 is

$$\rho_0 = A\, e^{E/T} \qquad (5)$$

with a constant temperature T = 0.753 MeV.

Early analyses of the γ-ray spectra following neutron capture in ^{197}Au indicated a peak at E_γ = 5.7 MeV ("pygmy resonance") in the strength function. The new results support the observation by Bartholomew et al that there is a decrease from E_γ = 5.5 MeV to 3.5 MeV which is stronger than that of the Lorentzian extrapolation of the giant dipole resonance. Above 6 MeV, there might also be a decrease but the dip is certainly not so deep as that suggested by Lundberg and Starfelt [13]. In some other nuclei, e.g. Tl, the pygmy resonance stands out more clearly.

The observation of the clustering of strength around 5.5 MeV in nuclei near closed shells suggests an interpretation in terms of particle-hole excitations. Such excitations would for most orbitals, but not all, introduce a parity change. The unperturbed particle-hole energies for neutrons cluster around 5.5 MeV and those for protons somewhat higher. Some early calculations for ^{208}Pb indicated that most of the strength for the $4s3p^{-1}$ neutron state would be decoupled from the giant resonance. However, later calculations by Harvey and Khanna [14] show that the particle-hole states near the unperturbed energies are collective, i.e. the $4s3p^{-1}$ and $3d3p^{-1}$ states are coupled to other particle-hole configurations and fragmented in states distributed over several MeV.

Numerical calculations have now been performed by Csernai and Zimányi [9] on ^{116}Sn which has neutron $3p_{1/2}$, $3p_{3/2}$ and $2f_{7/2}$ single particle states near the threshold. The unperturbed energies of the five particle-hole states $p_{1/2}s^{-1}_{1/2}$, $p_{3/2}s^{-1}_{1/2}$, $p_{3/2}d^{-1}_{5/2}$, $f_{7/2}g^{-1}_{7/2}$, and $f_{7/2}d^{-1}_{5/2}$ are around 8 MeV.

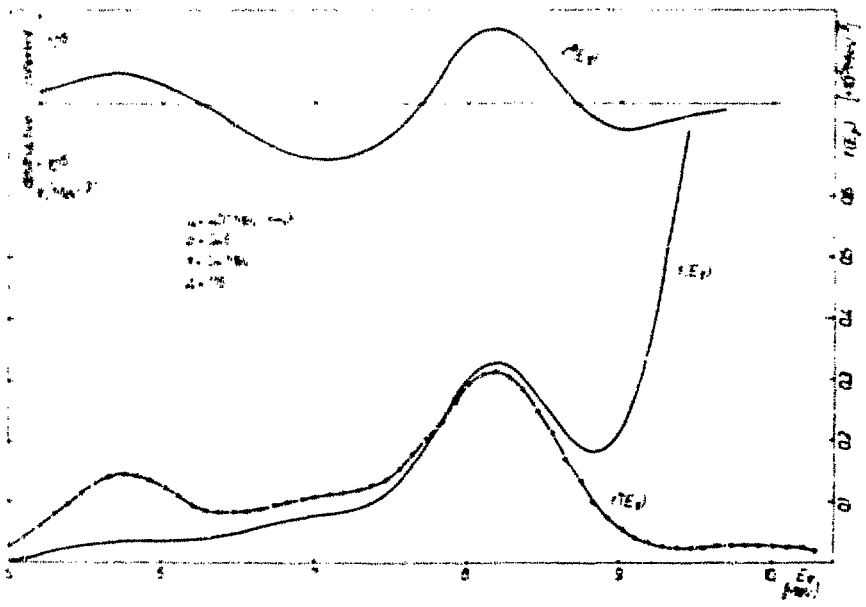

Fig. 4 Gamma-ray strength function for ^{116}Sn from threshold calculations in ref. 8. The contribution from neutron states near threshold is represented by the curve with points. The insert shows the collectivity of the threshold states.

The calculations give the eigenvalues and corresponding transition probablilities to the ground state. The strength function is obtained by representing each line of the discrete spectrum with a Gaussian function to simulate the spread of the strength over many background levels. One of the resulting strength functions is shown in Fig. 4. The dotted curve indicates the contribution of the five particle-hole states mentioned above, and it can be seen that this is dominating around 8 MeV. Hence, it is shown that neutron single-particle states near threshold are able to produce an independent collective state decoupled from the giant resonance.

A new source of decoupling some strength from the giant dipole resonance has been found by Gyarmati, Lane and Zimányi [15]. The effect arises when the particle-hole states are combined with a dense set of complicated background states. The strongly varying boundary condition at the nuclear surface leads to an anomaly. It is thus a threshold effect which operates most strongly for neutron waves of low ℓ-values.

Although some progress has been made in this field very much remains to be done. Experimentally, the mass region below A ≈ 90 should be investigated. Different methods as reviewed by Bartholomew et al [3] should be applied to test the validity of the strength function concept. Theoretically, we need calculations also for nuclei in other mass regions, e.g. A = 190 - 208. The fact, that the Lorentzian extrapolation of the giant dipole resonance strongly overestimates the strength in the low-energy region of nuclei near closed shells, is disturbing. Attempts to find more appropriate formulas for the extrapolation should be made.

III. DIRECT-SEMIDIRECT CAPTURE IN THE GIANT RESONANCE REGION

The direct-semidirect (DSD) cross section for the capture of a neutron with angular momentum ℓ' and spin j' into a bound single-particle orbit with quantum numbers $n\ell j$ can be written

$$\sigma^{DSD}_{\ell'j',n\ell j} = \sigma^{D}_{\ell'j',n\ell j} \; F_{eff}(\ell'j',n\ell j), \tag{6}$$

where σ^{D} is the direct cross section and F_{eff} an effective charge factor

$$F_{eff}(\ell'j',n\ell j) = \left| 1 - \frac{1}{E_R - E_\gamma - i\frac{\Gamma}{2}} \cdot \frac{\int u_{n\ell j}(r) h(r) u_{\ell'j'}(r)}{\int u_{n\ell j}(r) r \, u_{\ell'j'}(r) dr} \right|^2. \tag{7}$$

This factor describes the enhancement caused by the semidirect process in which the incident neutron excites the target nucleus into the giant dipole state. The parameters E_R and Γ are the energy and width of the giant resonance; $u_{\ell'j'}$ is the radial wave function of the incident neutron, $u_{n\ell j}$ that of the captured neutron and h(r) the coupling function which is proportional to the neutron-nucleus vibration coupling interaction.

Various formulations of the DSD model can be related to different functions, h(r). A summary of these different functions has previously been given [16]. Here we shall be more specific and recommend the use of the complex coupling function derived by Potokar [17]

$$h(r) = \text{const} \; r \left\{ V_1 f(r) - iW_1 4b \frac{df(r)}{dr} \right\}, \tag{8}$$

where V_1 and W_1 are the strengths of the real and imaginary part of the optical symmetry potential, f(r) the Wood-Saxon form of the potential and b is the diffuseness parameter. This form allows the use of V_1 and W_1 determined from other experiments for predictions of DSD cross sections. Conversely, we can treat V_1 and W_1 as free parameters to be determined from the fitting of the experimental capture results and then compare with optical model parameters obtained from analyses of other experimental data.

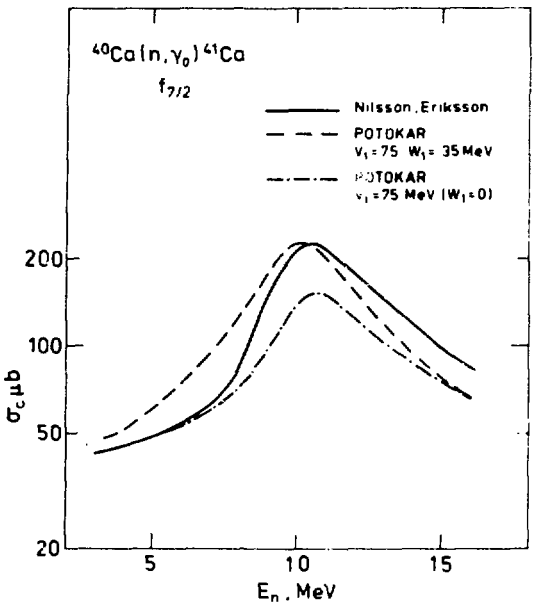

Fig. 5 Comparison of DSD cross sections with real (solid and dot-dashed curves) and complex (dashed curve) coupling functions.

The effect of the complex coupling function on the capture cross section is illustrated in Fig. 5 for the reaction $^{40}Ca(n,\gamma_0)^{41}Ca$. The values of V_1 = 75 MeV and W_1 = 35 MeV are taken from analysis by Carlson, Lind and Zafiratos [18] of charge exchange reactions on medium-weight nuclei. Comparison with the cross section curve calculated with a real coupling function (Nilsson and Eriksson [4]) shows a more symmetric curve around the peak at $E_n \approx 10$ MeV. This is primarily due to the effects of interference between direct and semidirect capture. With the real coupling function the interference is constructive above the giant resonance peak and destructive below. The interference term is relatively large and makes the curve much steeper on the low-energy side of the peak than on the high-energy side. The experimental cross sections do not generally show this asymmetry. The imaginary part of the complex coupling function has opposite signs of the interference term compared to the real part and, thus, removes much of the asymmetry. It was found [17] that the complex coupling function gives a significant improvement in the fit of the experimental data for the reaction $^{208}Pb(n,\gamma)^{209}Pb$. For $^{40}Ca(n,\gamma_0)^{41}Ca$ the new experimental results indicate a rather strong contribution of compound nucleus processes on the low-energy side of the peak and it is not obvious that the inclusion of the imaginary part in the coupling function will improve the fit.

The combination of the complex coupling function in the DSD calculations and the compound nucleus cross section gives, however, a remarkable improvement in the description of the cross curve for γ-rays to excited levels between 1.9 MeV and 2.7 MeV in ^{41}Ca (Fig. 6).

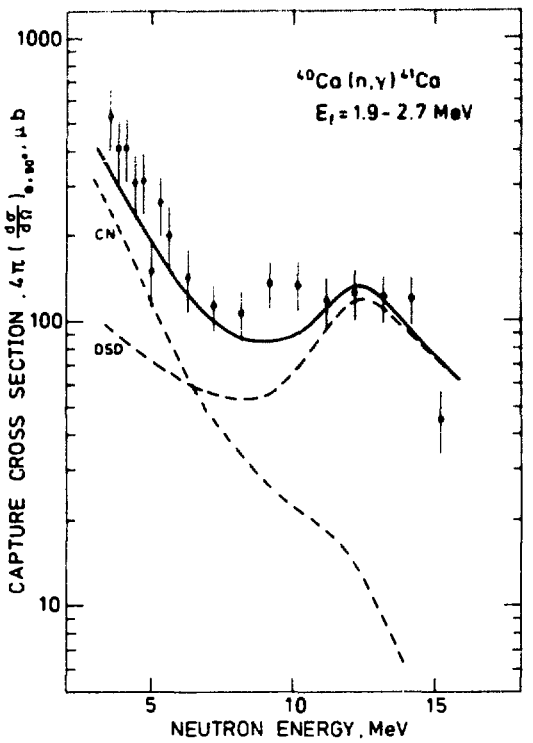

Fig. 6 Cross section of the $^{40}Ca(n,\gamma)^{41}Ca$ reaction for γ-rays to excited levels between 1.0 and 2.7 MeV. Experimental results are taken from ref. 1 (filled circles) and ref. 2 (open circles). The dashed curves show the compound nucleus (CN) and direct-semidirect (DSD) cross sections.

Potokar [17] found in hi. analysis of the $^{208}Pb(n,\gamma)^{209}Pb$ reaction that the experimental results are well reproduced with strength values V_1 = 75 MeV and W_1 = 140 MeV of the symmetry potential. The same parameters have been applied also for $^{89}Y(n,\gamma)^{90}Y$ and found to give good agreement. An example is the cross section for γ-rays to the $d_{5/2}$ doublet - the ground state and the first excited state of ^{90}Y - which is shown in Fig. 7. The experimental results are from measurements performed at Uppsala (open circles) and at Los Alamos (filled circles). The solid curve is the DSD prediction with the complex coupling (V_1 = 75 MeV, W_1 = 140 MeV) and the dashed curve that with the real (W_1 = 0) coupling function. It is obvious that the imaginary part of the complex coupling here is of dominating importance both in magnitude and shape of the cross section curve. It seems likely that the inclusion of compound nucleus reactions will change the situation somewhat. Experiments in the neutron energy range below 6 MeV are in progress to determine the cross section in this range. For the total capture cross sections recent calculations by Longo, Reffo and Saporetti [19] indicate a relatively large compound nucleus contribution below E_n = 8 MeV.

The shapes of the γ-ray spectra can often be used to determine roughly the relative importance of the compound nucleus and direct-semidirect reactions. This is illustrated in Fig. 8, taken from ref. 19. The predicted shapes of the spectra from the two types of reactions are quite dissimilar. The single-particle structure is not known in the excitation energy region just below the binding energy. and, of course, the intensity of γ-rays from direct-semidirect reactions is uncertain in this region. Further uncertainties are related to the γ-ray strength function and level densities of ^{90}Y. Nevertheless, the spectra can serve the purpose of making a rough distinction between the compound nucleus and direct-semidirect processes.

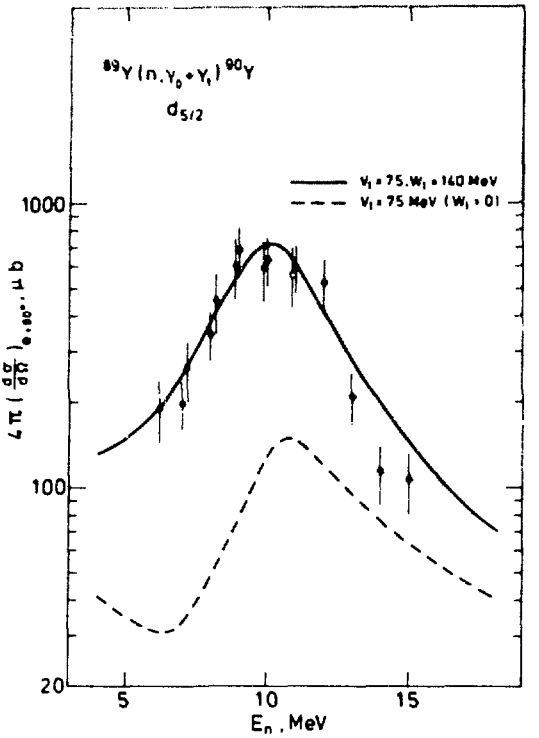

Fig. 7 Cross section for the $^{89}Y(n,\gamma_0+\gamma_1)^{90}Y$ reaction. Theoretical cross sections are from direct-semidirect calculations with complex coupling function, V_1 = 75 MeV and W_1 = 140 MeV (solid curve) and with W_1 = 0 (dashed curve).

These examples show that the compound nucleus contribution first must be determined before the systematics of the strengths V_1 and W_1 can be obtained from neutron capture cross sections. Furthermore, we need, to measure angular distributions of the γ-rays at several neutron energies. This is a very time-consuming work but it is rewarded by its importance to a better understanding of the capture mechanism. This latter point has been emphasized by Potokar and Likar, e.g. in a contribution to this conference [20]. Of particular interest is the contribution of E2 radiation in energy regions just below the E1 giant resonance for the isoscalar part and above for the isovector part. New theoretical calculations on the E2 contributions are reported to this conference by Potokar [21] and Longo and Saporetti [22].

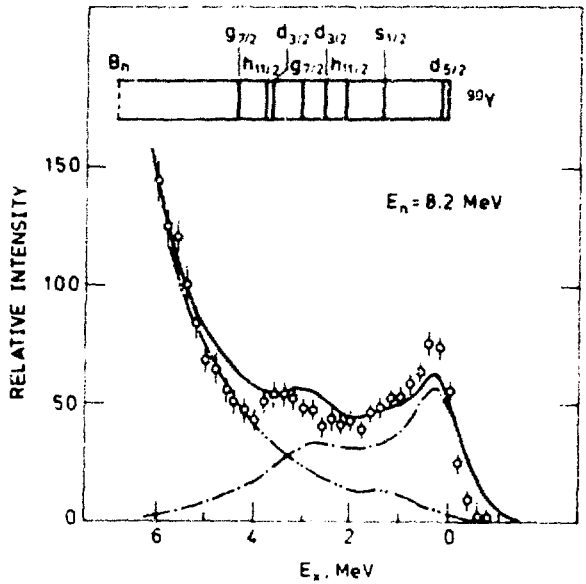

Fig. 8 Comparison of experimental and theoretical shapes of the γ-ray spectrum from $^{89}Y(n,\gamma)^{90}Y$. Theoretical spectra - dot-dashed curve from direct-semidirect and dot-dot-dashed from compound nucleus calculations - are taken from ref. 19.

IV CAPTURE CROSS SECTION MEASUREMENTS WITH THE ACTIVATION METHOD

The activation technique is a relatively simple method to measure fast neutron cross sections. Applied to (n,γ) cross sections, however, it is easy to overlook inherent difficulties. One such difficulty arises from the presence of low-energy neutrons produced in reactions like (n,n'), (n,2n) and (n,pn) in the target backing, the sample itself and surrounding material.

This problem was recognized some years ago when the 14 - 15 MeV cross sections deduced from measurements of the capture γ-ray spectra were found to disagree with the activation results. Several measurements have since then been performed and the results clearly demonstrate the influence of the secondary low-energy neutrons. The experimental arrangements have been improved in order to reduce this influence; the tritium target heads have been redesigned to reduce the mass of material near the beam spot and aluminium has been used because of its low cross section for neutron production. Even with these improvements the production of secondary neutrons is relatively large and the corrections are difficult to determine.

The correction for secondary neutrons produced in the sample itself is generally obtained from a study of the dependence of the activation yield on the sample thickness and diameter. As an example, Fig. 9 shows the dependence for the reaction $^{115}In(n,\gamma)^{116m}In$ [23] on the sample thickness. The observed activation

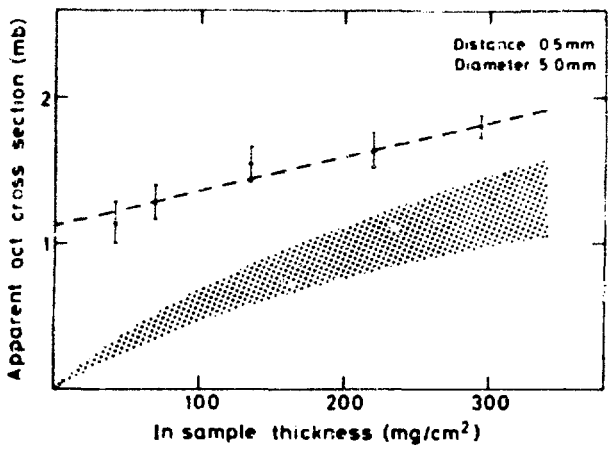

Fig. 9 Dependence of the apparent activation cross section for the reaction $^{115}In(n,\gamma)^{116}In$ on the sample thickness. The shaded area shows the theoretically calculated contribution of secondary neutrons.

yield (here defined as the apparent cross section) is found to be roughly linearly dependent on the thickness. An estimate of the contribution to the activation yield of secondary neutrons has been made by applying a method similar to that described in ref. [23].

The result of this estimate is represented in the figure by the shaded area to indicate the uncertainties of the cross section values used in the calcualtion.

The influence of secondary neutrons from sources outside the sample can be determined from the dependence of the activation yield on the distance between the tritium target and the sample. One encounters difficulties when the corrections for all the dependencies are to be determined. The extrapolations to zero distance, to zero thickness and diameter are not straightforward and coupling effects are present between observed dependencies.

Another method was used by Schwerer et al.[24] who determined the flux of low-energy neutrons at the sample position using gold foils with and without cadmium cover for thermal and epithermal neutrons and threshold reactions for higher energy neutrons.

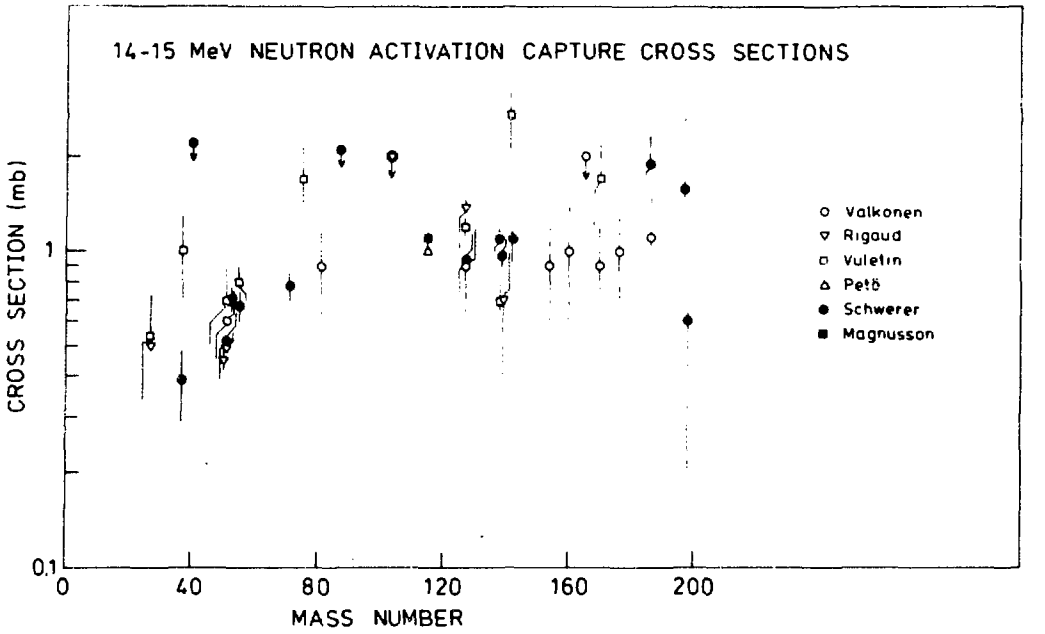

Fig. 10 Neutron capture cross section as a function of mass number.

The results of these new measurements [23, 25-29] are summarized in Fig. 10. The old results exhibited large fluctuations with mass number with maxima up to about 10 mb for deformed nuclei and minima for closed shell nuclei. These fluctuations are now gone - the scattering of the points reflect experimental uncertainties rather than a real variation of the capture cross sections.

The importance of secondary low-energy neutrons has, thus, been established in activation measurements of the 14 - 15 MeV capture cross sections. Secondary neutrons do certainly play a rôle in activation measurements also at lower neutron energies. This remains to be studied.

REFERENCES

1) I. Bergqvist, D.M. Drake and D.K. McDaniels, Nucl. Phys. 1974, A231, 29.

2) L. Nilsson, A. Lindholm, B. Pålsson and I. Bergqvist, to be published.

3) G.A. Bartholomew, E.D. Earle, A.J. Ferguson, J.W. Knowles and M.A. Lone, Advances in Nuclear Physics 1973, 7, 229;

G.A. Bartholomew and F.C. Khanna, Proc. Second Int. Symposium on Neutron Capture Gamma-Ray Spectroscopy and Related Topics, Petten, The Netherlands, September 2-6, 1974, p. 119 (1975).

4) L. Nilsson and J. Erikssen, Phys. Lett. 1974, 49B, 165.

5) G. Mantzouranis, Z. Physik 1973, 264, 405.

6) P. Axel, Phys. Rev. 1962, 126, 671.

7) D.M. Brink, Doctoral Thesis, Oxford University (1955).

8) E.D. Earle, I. Bergqvist and L. Nilsson, to be published.

9) L.P. Csernai and J. Zimányi, Central Research Institute for Physics, Budapest, 1976, Report KFKI-76-16.

10) E.D. Earle, M.A. Lone, G.A. Bartholomew, W.J. McDonald, K.H. Bray, G.A. Moss and G.C. Nelson, Can. J. Phys. 1974, 52, 989.

11) E.G. Fuller, H.M. Gerstenberg, H. Vander Molen and T.C. Dunn, Photonuclear Reaction Data, 1973, NBS Special Publication 380.

12) G.D. Loper, L.M. Bollinger and G.E. Thomas, Argonne National Laboratory Progress Report, ANL 1972, 7971.

13) B. Lundberg and N. Starfelt, Nucl. Phys. 1965, 67, 321.

14) M. Harvey and F.C. Khanna, Nucl. Phys. 1974, A221, 77.

15) B. Gyarmati, A.M. Lane and J. Zimányi, Phys. Lett. 1974, 50B, 316.

16) I. Bergqvist, Proc. Second Int. Symposium on Neutron Capture Gamma Ray Spectroscopy and Related Topics, Petten, The Netherlands 1974, p. 199.

17) M. Potokar, Phys. Lett. 1973, 46B, 346.

18) J.D. Carlson, D.A. Lind and C.D. Zafiratos, Phys. Rev. Lett. 1973, 30, 99.

19) G. Longo, G. Reffo and F. Saporetti, Lett. Nuovo Cimento 1976, 16, 193.

20) A. Likar and M. Potokar, Contribution PB2/K9 to this conference.

21) M. Potokar, Contribution PB2/K10 to this conference.

22) G. Longo and F. Saporetti, Contribution PG1/D8 to this conference.

23) G. Magnusson and I. Bergqvist, to be published.

24) O. Schwerer, M. Winkler-Rohatsch, H. Warhanak and G. Winkler, to be published.

25) J. Kantele and M. Valkonen, Phys. Lett. 1972, 39B, 625;
M. Valkonen, private communications.

26) F. Rigaud, M.G. Desthuilliers, G.Y. Petit, J.L. Irigaray, G. Longo and F. Saporetti, Nucl. Sci. Eng. 1974, 55, 17.

27) G. Petö, Int. Symposium on Interactions of Fast Neutrons with Nuclei, Gaussig, GDR, 1975.

28) J. Vuletin, P. Kulisic and N. Cindro, Lett. Nuovo Cimento 1974, 10, 1.

MC 1 - FAST RADIATIVE CAPTURE - I. Bergqvist (Univ. of Lund, Sweden)

Newstead (B.N.L.):

Well, I'm very pleased to see that the (n,γ) analysis also supports the need for a complex isospin potential such as we first found necessary in the explanation of certain strength function systematics and in the (p,n) experiments. But I'm a little surprised at the magnitude of the imaginary term W_1, particularly in the case of yttrium, where W_1 = 140 MeV, which is quite enormous compared to the usual values found from scattering experiments, typically 12 to 16 MeV. Perhaps part of the explanation is that there is a normalization constant of four here such as you have in the Lane expression for $(\vec{t}.\vec{T})/A$, which would bring the value down to 35 MeV. But still, 35 MeV seems rather high for yttrium-89 and I wonder if you have a comment about that?

Bergqvist:

I think the inclusion of a compound nucleus contribution (which we know to be present) to this yield curve -- a calculation we're currently performing -- will decrease W_1 more than the real strength. But still, there will probably be a rather high value of W_1 and I don't understand that. I know that for lead this very large value of W_1 seems to be required, and I think Tony Lane has an explanation for that. Would you care to comment on the rather large values of W_1, for instance in lead?

Lane (A.E.R.E.):

In the heavier nuclei like lead, where at the energies we're talking about the W for the $T_>$ states is zero because there just are none, than you find that when you translate that zero value for the $T_>$ and some suitable value for the $T_<$ states into W_1 and W_0, a value for W_1 of this order-of-magnitude is absolutely reasonable. I mean, there is a factor of something like A/N-Z that comes in that multiplies it out. So I don't regard it as ridiculously large -- at least not in a heavy nucleus.

Potokar (Inst. Josef Stefan, Ljubljana):

I would like to remark that in the analysis of the data, several effects are ignored: for example, first of all the a_1 contributions and the quadrupole contributions, then the type of correlations in the final state, and the energy dependence of the symmetry potential. These effects lead to lower values of W_1 and there are also other effects which I'll discuss in my report.

Chrien (B.N.L.):

Could you clarify the situation with regard to the gamma-ray strength function in gold? I had thought, at the last one of these eminent conferences in Budapest, that it was very carefully explained to us that the absolute value of the photon strength function, as derived from thermal neutron capture experiments, agreed very well with the giant resonance extrapolation at 6 MeV, and then as one went to lower energies a deficiency appeared. Your curve seemed to indicate a deficiency even at 6 MeV.

Bergqvist:

That's right. In the review paper by Bartholomew and collaborators there still is a difference between the Lorentzian and the experimental data. In the

Lorentian they used, the parameters were based on rather early work. There is some new photonuclear work on ^{197}Au in which the new parameters just give a larger difference between the Lorentian and the experimental points.

Lane:

While on that same subject of the gold strength function, I remember that when the original Bergqvist-Starfeld data were taken there were a number of items of special interest there. One was that the knee that we saw in the strength functions seemed to disappear at 7 MeV. So one question that I have is, if you take the experimental strength functions that you infer from the lower energy data and then calculate what you should observe at 7 MeV neutron energy, does the knee persist or is it ironed out by level density considerations? That's point number one. Point number two is simply to note that at these energies we have statistical type effect -- the knee in the strength function -- is probably associated with other non-statistical effects in neutron capture such as correlations and so forth, which are, I think, almost without exception associated with s- and p-transitions. However, as Bartholomew pointed out years ago, at energies around 2.5 MeV the cross sections are certainly dominated by higher partial waves. So, then, we have to get used to the idea of non-statistical effects in higher partial waves.

Bergqvist:

Concerning the first point, I think you are referring to our work on inelastic $(n,n'\gamma)$ scattering of neutrons and the gamma rays following the reaction. Is that right?

Lane:

I thought in that work of some years ago there was 2-MeV, 4,5-MeV and 7-MeV data.

Bergqvist:

Right. We went up to 7 or even 8.5 MeV, I think, but then we couldn't study any knee in the (n,γ) reaction in that gamma ray spectrum, because that's masked by the much more intense gamma rays from (n,n') reactions. We did look for the effect also in the gamma rays from inelastic scattering processes but we couldn't find anything there. The explanation for that, I think, is still open. It could be a level density effect or, of course, it could be a reaction mechanism effect. I do plan to take up these experiments again.

Vonach (Univ. of Vienna):

How well could one use the method outlined to calculate the total (n,γ) cross section, for example, as compared with activations for which there are available a large number of good data at 14 MeV? Is it possible to sum up over all the final states?

Bergqvist:

Oh, yes, it is possible.

Potokar:

I have another remark. Your newest spectra for yttrium are flat in the low energy region, so in this respect the reliability of the results of statistical calculations is questionable and also carries some angular dependence of the spectra. I don't know how to explain this by such simple statistical theory.

Bergqvist:

You made this comment before this session started and I haven't had time to check this point. I'm sure you checked it. The figure on the spectrum and the decomposition of the spectrum into two reactions was used here just to provide an illustration. I don't now recall the actual details. I know we have made angular distribution measurements for yttrium and I know that you are referring to those measurements, but I did not include them here.

Paper Subject : Session MC 2

2.30 p.m., Tuesday, July 6, 1976

ULTRACOLD NEUTRONS

V.I.Luschikov

Laboratory of Neutron Physics, Joint Institute for Nuclear Research, Dubna, USSR

RÉSUMÉ

The paper gives a review of theoretical and experimental works on the extraction, transportation and storage of ultracold neutrons.

ABSTRACT

In 1959 Zeldovich[1] pointed out to the possibility of storage in a closed vessel of very slow neutrons with energies below $\lesssim 10^{-7}$eV noting that one may achieve the storage time up to the life-time of a free neutron before β-decay ($\sim 10^3$ sec). This possibility is due to the effective repulsing potential which describes the interaction of slow neutrons with many substances employing a strong suppression of inelastic processes in the reflection of ultracold neutrons (UCN). In a series of experiments beginning 1968[2] the effective methods were developed of obtaining pure UCN beams from the maxwellian spectrum of thermal neutrons. The UCN beams of intensity about 10^3 n/sec and density up to 10^2 n/liter were obtained at the reactors with thermal neutron flux of 5×10^{13} n/cm^{2}sec. Such UCN beam parameters allow to measure easily the UCN storage time in different vessels and under different conditions. Maximum UCN storage time achieved in the experiments is about 400 sec and it is much shorter than that theoretically estimated. Both theoretical and experimental search for the explanation of this discrepancy was undertaken but no satisfactory result had been obtained as yet. Nevertheless the already obtained value of the UCN storage time permits to perform at high flux reactors experiments on the search for the electric dipole moment of the neutron and on the determination of the life-time of a free neutron before β-decay. Moreover, one may consider ultracold neutrons as a specific quantum gas of elementary particles, which properties are an interesting field for investigation.

1) Ya.B.Zeldovich, JETF, 36, 1952(1959).
2) F.L.Shapiro, Report at the International Conference on Nuclear Structure Study with Neutrons, Budapest, 1972.

FAST NEUTRON SCATTERING FROM SOME MEDIUM MASS NUCLEI

Scattering studies between 1 and 14 MeV incident neutron energy have been and are being done to meet a variety of nuclear structure interests. Some of the more prominent are: to continue the examination of i-spin dependence or neutron excess dependence of scattering potentials, a topic of interest for many years, and to assess those properties of particular nuclei which noticeably effect scattering from them, such as properties which would influence the absorption of the scattering, or small angle elastic scattering cross sections. In the incident energy range between 1 and 4 MeV, inelastic scattering studies are a powerful means of studying nuclear levels in a wide range of nuclei, at least those presumed to be spherical. These are some of the topics which will be featured in this review.

Questions about the behavior of neutron scattering, or the phenomenological description of scattering, often depend for solution on reasonably precise comparisons of scattering by different nuclei, or comparisons of scattering from one nucleus but at different neutron energies. For example, the examination of ξ dependence in neutron scattering, where ξ is the neutron excess defined as $\xi \equiv N - Z/A$, often requires examination of scattering potentials which differ by $\lesssim 1$ MeV in 50, or 2%. To have confidence in such comparisons the data examined must be reasonably precise and accurate. The use of inelastic scattering cross sections to determine properties of nuclear levels depends on measured values which can be viewed with confidence. The study of fast neutron inelastic scattering is receiving must attention recently, partly as a means of studying nuclear excited levels, and partly because good descriptions of elastic scattering make possible the study of inelastic excitation mechanisms. Good descriptions of elastic scattering are important as a point of departure for the examination of inelastic scattering.

Two complementary methods are available for neutron inelastic scattering cross section measurements, at least at fairly low neutron energies. One involves direct detection of the scattered neutrons, and the other involves detection of γ rays deexciting levels excited by neutron inelastic scattering; that is, the measurement of $(n,n'\gamma)$ production cross sections. The comparison of cross sections measured in both (n,n') and $(n,n'\gamma)$ studies gives us an estimate of the confidence we can associate with the measurements of inelastic scattering cross sections. The neutron detection experiments have the advantage that the process of interest is directly detected. The $(n,n'\gamma)$ method suffers from being indirect, which in practice means one must know the branching ratios for γ-ray decay of all excited levels before the scattering cross sections can be obtained. But the 2 keV energy resolution of a Ge(Li) detector means that γ-ray detection will enable the study of levels which could never be resolved with present neutron detection methods. This is a point which will be especially important near the end of this paper, in reference to the study of scattering by deformed nuclei. A systematic description of techniques for these two kinds of experiments would be a lengthy review in itself; this will not appear here. Fortunately, at least for neutron detection experiments, the techniques have been described in considerable detail.[1,2] Some reviews of $(n,n'\gamma)$ experiments[3,4] have described methods in use for those experiments. A few detection systems will be illustrated so that important characteristics of them can be discussed. Especially for the $(n,n'\gamma)$ experiments, whose techniques have been less emphasized in the literature, some critical points effecting cross section accuracy will be emphasized.

After a comparison of cross sections from (n,n') and (n,n'γ) experiments, a comparison will be presented of results from different laboratories, all using neutron detection. Both of these comparison reviews should give us a basis for evaluating the degree of success to be expected in using scattering studies to determine nuclear properties, or to examine the influences of nuclear properties on elastic and inelastic scattering.

A few examples of the use of low energy neutron inelastic scattering to study properties of nuclear levels will be presented, to illustrate the use of these studies in nuclear spectroscopy, one of the major thrusts of low energy experiments. Another major topic will be updating the studies of the ξ dependence of scattering potentials, with some information provided for the imaginary parts, as well as the review of the real parts of the potentials. Most of the material mentioned above will refer to spherical nuclei which are not very deformable. Some information will be added for nuclei presumed spherical, but soft against deformation.

The next topic will be a recent extensive survey of small angle elastic scattering; through its introduction we can see vividly the effects of deformation on neutron scattering. Some additional scattering studies, from the transitional nuclei between spherical and deformed, will again highlight the influence of deformation on scattering, or at least the differences between scattering from spherical and deformed nuclei. It should be clear that this review will be entirely phenomenological, with essentially no discussion of reaction theory. We will present applications of standard models to measurements as a means of interpreting them, but will not examine model details.

The system shown in Figure 1 is that in use at Kentucky for neutron detection experiments. It was developed originally by J. D. Brandenberger and his students[5] and subsequently extended by A. Obst and J. L. Weil[6]. The essential elements are the massive shield surrounding the liquid scintillation detector, to protect it from radiation scattered in the room, and the shadow bar near the neutron source. This bar, made from a machinable form of tungsten, directly shadows the liquid scintillation detector from the neutron source and also shadows the entrance to the collimator from the source, so that that part of the detector collimator does not itself become a source of scattered background for the detector. An important element also is the heavy metal entrance aperture to the collimator, which prevents the scintillator from seeing anything except the region of the scatterer. All of these points and many others are stressed in the review of L. Cranberg[7], whose pioneering work on closed geometry shielding for neutron detection was the basis for the designs at many laboratories.

The second figure shows a design completed by D. W. Glasgow, et al.[2], and shows very careful attention to detail in its design. One sees again the important elements: the tungsten shadow bar, the Cu entrance baffle to the detector collimator, and a massive detector shield. This system was originally designed and used at the Aerospace Research Laboratories (ARL) of Wright Patterson AFB, and was later moved to its present location at Triangle Universities Nuclear Laboratories (TUNL).[8] Both this and the Kentucky systems were developed for neutron time-of-flight detection with flight paths ranging to between 4 m and 6 m. For work at flight paths longer than 5 m it is often convenient to have a multi-detector system, such as that in use at the Centre d'Etudes de Bruyeres-le-Chatel[9] (BLC) and shown in Fig. 3. These four detectors, spaced 20° apart, have all the essential components multiplied by 4. The extra problems of having four or more detectors, each carefully adjusted, stabilized, and detector efficiency measured,

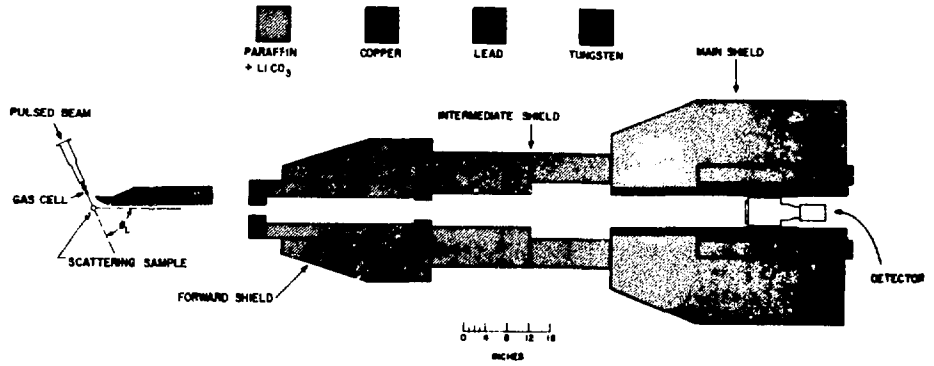

Figure 1. Kentucky detection system, designed[5] for detection distances of 2 to 4 meters. Modular design allows the shields to be used with detectors of various types and sizes. Important elements are the W shadow bar and the Cu baffles.

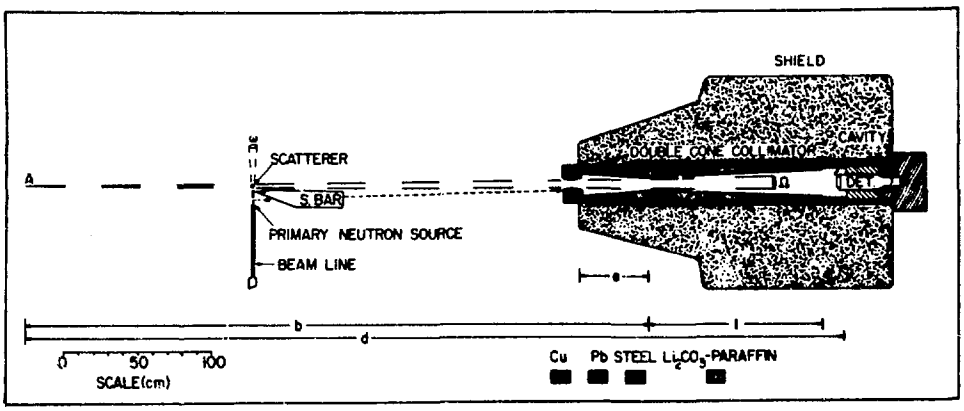

Figure 2. ARL-designed[2] detection system. Double-cone collimator reduces backgrounds scattered from collimator walls. The Cu plug behind the detector reduces back-scattering into the detector.

are probably more than compensated for by the gains in data collection time for experiments with long flight paths and correspondingly small data collection rates. One special difficulty of a multi-detector system is in the use of the shadow-bars. Each one shields a single detector, but the additional three only present extra material to scatter background into that detector. To minimize their role as scatterers, they are withdrawn somewhat from the proximity of the scattering sample, and then an auxiliary wedge of heavy metal is placed near the source to shadow the bars themselves from the source. This is a compromise in a multi-detector system which reduces a little the effectiveness of those early shields. This and similar multi-detector systems show their real worth in high detector-resolution experiments.

The pulsed beam from either single-ended Van de Graaffs or tandems usually has a burst width of between 0.7 and 1.3 ns. When this is combined with an intrinsic detector time resolution of about 0.8 ns, the total system resolution for scattered neutron detection usually ranges between 1.7 and 2.4 ns. For example, recent experiments at BLC use an overall resolution of 1.8 ns. An experiment is in progress at 3.4 MeV incident energy, and a flight path of 10 m. By keeping the neutron source thin in energy, a detected energy resolution of 25 keV is obtained. This is quite valuable for separating excited levels of heavy nuclei, but the run time is 20 hours per point! It is in experiments of this kind that multi-detector systems are truly appreciated.

An alternate but indirect way of separating closely spaced levels in neutron inelastic scattering is the use of $(n,n'\gamma)$ reactions. Two attitudes toward γ-ray detection are in current use. One is the use of a Ge(Li) detector surrounded by an annular detector of NaI(Tℓ) and operated in anti-coincidence with the central Ge(Li) detector. This system was emphasized[4] in an earlier review of $(n,n'\gamma)$ experiments, and has the advantage of reducing Compton-scattering in the detected γ-ray spectrum, usually by a factor of about 4. However, the large annulus of NaI(Tℓ) has high detection efficiency for background radiation, and therefore must have a massive shield surrounding it. In practice this limits detector distances to about 1.5 m or more. An alternative and simpler system is to use a single Ge(Li) detector in a small shield, and employ it at distances of about 0.6 m or more. The Kentucky arrangement is shown in Fig. 4. For distance perspective, the tungsten wedge is the shadow bar of Fig. 1, and the sample to Ge(Li) detector distance is 0.6 m. All of the detection systems from the different laboratories are designed to be easily re-positioned in angle, to facilitate angular distribution measurements.

A comparison of neutron inelastic scattering cross sections from (n,n') and $(n,n'\gamma)$ experiments has been developed by McDaniels, et al.[10] based on experiments carried out at Argonne National Laboratory (ANL) and Kentucky. There are several differences between these methods, in addition to the fact that different radiations are detected. The neutron detection data are usually normalized to the p(n,n)p scattering cross section, since it is a very well known standard.[11] The Kentucky measurements of $(n,n'\gamma)$ cross sections have been normalized to a compilation of measurements for the $^{56}Fe(n,n'\gamma)^{56}Fe$ production cross sections for the 0.847 MeV transition begun by D. B. Nichols,[4] and periodically brought up-to-date by others. The compilation[12] was revised in 1973, and a portion of it is shown in Fig. 5. This presents differential γ-ray production cross sections for the 0.847 MeV line of ^{56}Fe between incident energies of 1.0 and 4.7 MeV. The solid curve is a series of polynomial segments which have been least-squares-fitted to the measurements in 0.5 MeV incident energy intervals. A deviation region of ± 8% from that curve would include more than 2/3 of the measured points.

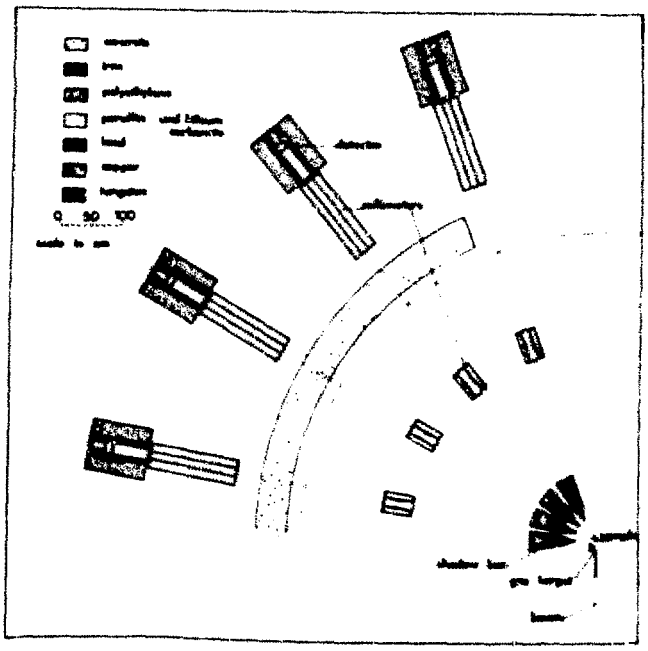

Figure 3. Intermediate version of the BLC four unit detection system. Later versions have more massive collimators and detector shields.

all of which have been selected to correspond to measurements with an energy spread of 50 to 90 keV. This compilation is presently being updated again to include measurements published since 1973.

The γ-ray detection method has high sensitivity, because the detector can be placed fairly close to the scattering sample, as illustrated in Figure 4. The time-of-flight procedures instituted by L. Cranberg[13] and adopted by R. B. Day[14] are used to separate the desired γ rays from undesired backgrounds. This is illustrated in Fig. 6, which shows the time distribution of radiation in the Ge(Li) detector for scattering in an Fe sample. This figure is taken from a pulsed-beam TOF experiment at the Kentucky accelerator.[10] The prompt γ rays from inelastic scattering are separated from backgrounds by setting a time-gate around the γ-peak and accepting only those events. These events in the Ge(Li) detector are

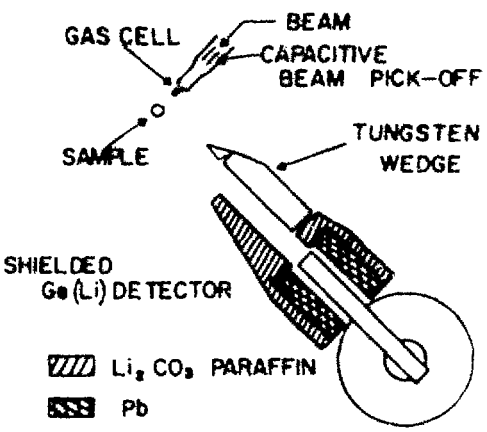

Figure 4. Single Ge(Li) detector in a small shield, for use at small detection distances, <1 m.

then energy analyzed in the conventional way to separate transitions from different excited levels. A time gate around the γ-peak of Fig. 6 gives a 20 fold reduction in time uncorrelated background and avoids all backgrounds caused by fast neutrons scattered into the detector, the neutron peak of Fig. 6. To achieve this separation between neutron and γ-ray peaks, 0.6 m is a sufficiently long flight path. That and other background eliminations provide enough sensitivity to measure transitions corresponding to cross sections of only a few mb.[4,12]

An important consideration in both neutron and γ-ray detection experiments is that given to sample-size effects. Corrections for these effects have been extensively discussed in the literature for neutron detection. They are calculated using approximate but analytic recipes[15,16] or Monte Carlo methods[17,18], and these two methods have recently been shown to be in good agreement.[18] Much less has been written about similar corrections for (n,n'γ) measurements. For many years an approximation introduced by Day[4,19] allowed one to ignore both neutron attenuation in the sample and multiple scattering, making corrections only for γ-ray attenuation.[20] Tessler and Glickstein showed that in general all three corrections were important, at least in geometries similar to that of Fig. 4, which use small cylindrical scatterers.[21] The University of Lowell group has also been concerned with the importance of these corrections,[22] and most recently D. L. Smith at ANL has developed Monte-Carlo methods[23] for making these corrections. The analytic methods of Engelbrect[15] are easily adapted to making sample-size corrections to inelastic scattering cross sections for either neutron or γ-ray detection, and have been used in a recent study[10] of the effects of such corrections for (n,n'γ) measurements. Some results from that study are shown in Fig. 7 for two elements, Fe and Pb. Plotted here are apparent cross sections, in relative units, for the 847-keV line of ^{56}Fe and the 2615-keV line of ^{208}Pb as a function of the size of the scattering sample. The results are shown at three incident energies for Fe and one neutron energy for Pb. The plots show measurements for scatterers of three different diameters; in each case the sample height was about the same as the diameter; both were varied. The lower data points in each panel are corrected only for γ-ray absorption; they would provide sample-size independent results if the Day approximation was accurate for this geometry. One sees instead that errors of the order of several percent would be present, the size error depending upon the size of the sample. The upper data points and curve show the effects of correcting for neutron flux attenuation and γ-ray absorption, assuming that multiple scattering can be ignored. Finally the solid data points and central curves result from making corrections for all three effects, incident neutron attenuation, multiple elastic scattering, and γ-ray absorption in the sample. The results of those calculations are then reasonably sample independent.

Neutron inelastic scattering cross sections inferred from (n,n'γ) measurements are shown in Table I for neutron energies near 3 MeV incident on ^{92}Zr. They are compared to neutron inelastic scattering cross sections measured in neutron detection experiments at ANL[24] and at Kentucky.[25] The agreement amongst the three sets of results is good. The average deviation between the two (n,n') experiments is 18% and that between the (n,n'γ) results and the (n,n') results of Ref. 24 is 17%. A similar comparison[26] of (n,n') and (n,n'γ) cross sections for 3.5 MeV neutrons incident on ^{92}Mo shows an average deviation for four inelastic groups of 7%, and a comparison of cross sections for just the first excited 2^+ levels of four Mo isotopes shows an average deviation of 4%. For the Mo comparisons, both

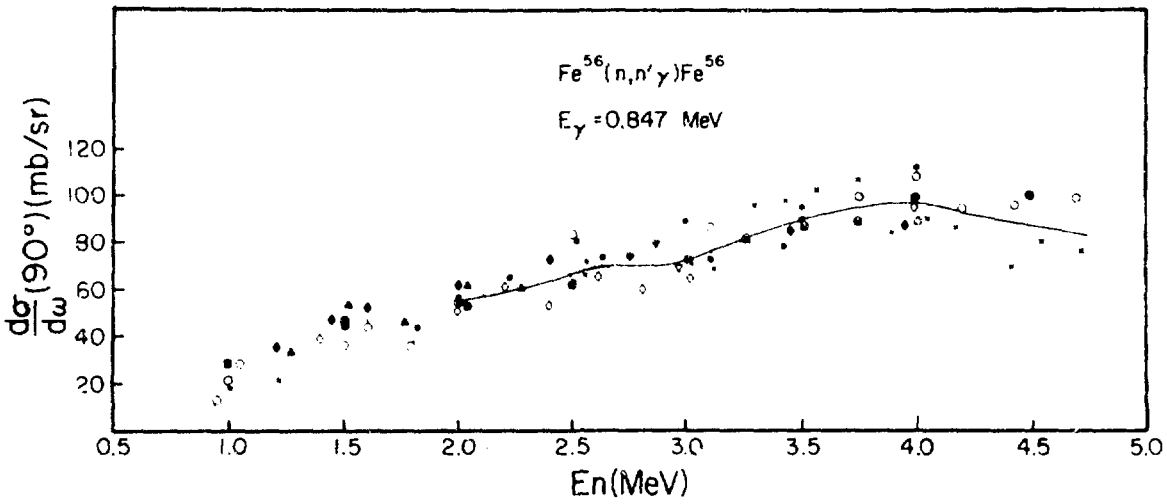

Figure 5. A compilation of differential γ-ray production cross sections for the 847-keV transition in ^{56}Fe. Points are corrected for anisotropy and isotopic abundance of ^{56}Fe where necessary. All correspond to measurements with an energy spread of 50-90 keV, except the dotted curve. Symbols are identified in Ref. 10 and 12.

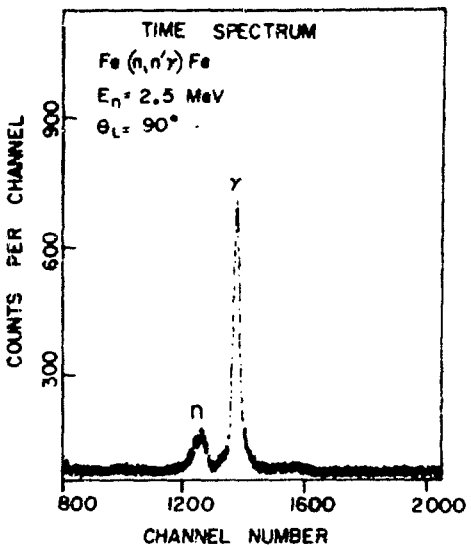

Figure 6, Time-of-flight spectrum in Ge(Li) detector of Fig. 4 at a detector distance of 0.7 m.

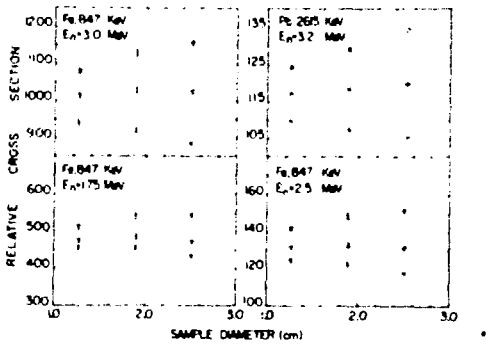

Figure 7. Sample-size dependence of corrected γ-ray production cross sections. Lower curve, γ-ray absorption corrected only. Upper curve, both γ-ray absorption and neutron attenuation corrections were made. Central curve also includes neutron multiple scattering corrections.

the (n,n') and (n,n'γ) measurements were made at Kentucky. These comparisons give us an estimate of the confidence to be associated with measured inelastic scattering cross sections.

Table I

A comparison of neutron inelastic scattering cross sections in ^{92}Zr from (n,n') and (n,n'γ) measurements. A direct comparison of complete γ-ray measurements and interpolated n-detection results is given in 3.2 MeV. The 90° γ-ray excitation functions were used to extrapolate the γ-ray results to energies where n-detection data were available, 2.75 and 3.5 MeV.

	2.75 MeV			3.20 MeV			3.50 MeV	
Level Energy	(n,n'γ)	Ref. 25 (n,n')	Ref. 24 (n,n')	(n,n'γ)	Ref. 24 (n,n')	(n,n'γ)	Ref. 25 (n,n')	Ref. 24 (n,n')
934.1	633	606	560	477	416	421	283	290
1381.9	108	109	145	101	112	84	58	96
1494.8	183	254	230	155	196	130	153	175
1846.4	240	340	280	245	220	192	172	190
2066.1	240	160	275	207	224	181	157	162
2339.0				134	168	126	234	150
2398.0				98	121	89		112

Inelastic neutron scattering in the few MeV incident energy range has been developed into a very fruitful method of determining nuclear level and decay schemes. The high nuclear penetrability for neutrons means that nuclear levels can be studied with incident neutron energies little higher than the excitation energies of the levels to be studied. Ambiguities are virtually absent when level energies and γ-ray decay schemes are determined by these methods.[4] A couple of examples will illustrate the methods, both drawn from studies of neutron scattering in the A ∿ 90 region. These were part of a systematic study of neutron scattering in the A ∿ 90 region initiated by J. D. Brandenberger and the author, together with other colleagues who developed various phases of the study. Figure 8 shows neutron spectra scattered by ^{94}Mo. The detection system of Fig. 1 was used, and the separated isotope scattering sample contained about 0.4 moles.

Interest here centers on the small group labeled 1740 keV in the ^{94}Mo spectrum. This level is at twice the energy of the first excited 2^+ level, and decays to it. Its decay energy so well matches that of the strongly excited 2^+ level that the γ-rays cannot be separately observed! But the scattered neutron angular distribution, shown in Fig. 9a, shows a very strong anisotropy. This forward and backward peaking was predicted by L. Wolfenstein[27] to be the special signature of a 0^+ level. This angular distribution, together with the magnitude of the inelastic scattering cross section, uniquely fixes[28] the level as 0^+. The upper panel of the figure shows the yield of the combined γ-ray decays from the 1.74 MeV 0^+ and the 0.87 MeV 2^+ levels as a function of incident neutron energy. It shows the expected abrupt increase as threshold is crossed for excitation of the 1.74 MeV level.

The second example shows reliance upon measured (n,n'γ) angular distributions, this time in ^{92}Zr. Measured angular distributions for three decays from the 2742.6-keV level of ^{92}Zr are shown in Fig. 9b. When these data are carefully analyzed, and large M2/E1 mixing ratios are rejected, the level is definitely

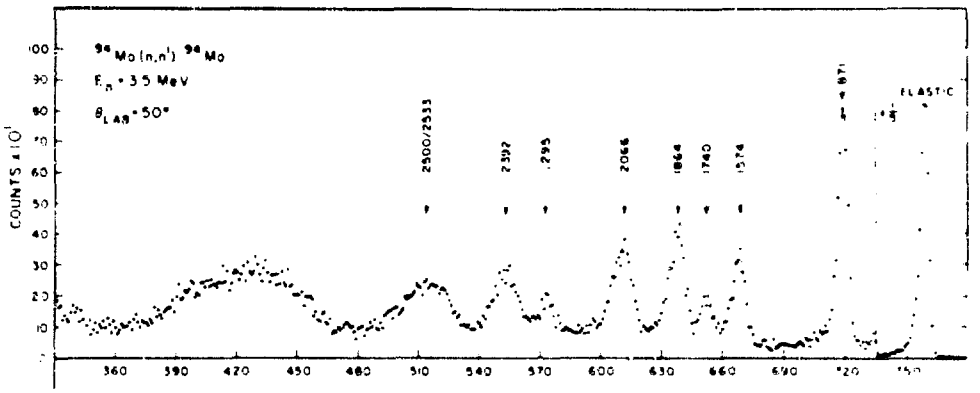

Figure 8. Scattered neutron spectrum at 3.9 m. The numbers above the arrows are level excitation energies in keV.

assigned[12] as 4^-. The 1248-keV line is shown to be an E1 and the 257.3-keV line an M1 transition.[12] These two illustrations show the use of neutron and γ-ray angular distributions to determine properties of levels. The magnitudes of inelastic scattering cross sections in spherical nuclei can also be of assistance in fixing spin assignments. For example, we have measured 53 cross sections for levels excited in two isotopes, ^{92}Zr and ^{94}Zr, and then calculated them with the Wolfenstein-Hauser-Feshbach (WHF) model[27] as modified by the fluctuation corrections of Moldauer.[29] The average deviation of measurements from calculations is ∿ 30%, but variations for particular excited levels range almost to a factor of 2. Thus cross sections are not an especially stringent test; they can be used only at the factor of 2 level. The curves shown in Figs. 9a and 9b are all WHF calculations. Neutron inelastic scattering studies employing both neutron and γ-ray detection, especially angular distribution measurements, provide a powerful means of studying properties of nuclear levels when analyzed within the framework of the statistical model.[27,28] These methods are especially useful because in spherical nuclei the cross sections and angular distributions have no dependence on dynamical nuclear properties, or intrinsic structures of levels. Only spins, parities, and excitation energies play a role.

As noted before, one of the central issues in studies of neutron scattering has been the confidence with which the measured and reported cross sections could be viewed. To explore this question further, it is useful to present several comparisons of cross sections measured in different laboratories. The first of these is shown in Fig. 10, which presents a comparison between older Kentucky measurements[30] for A and newer results from Velkley, et al.[31] at ARL. The precision and accuracy of the two data sets is fairly impressive, indicating quite good agreement, well within the quoted accuracy of 5% and precision of about 2% for the ARL elastic data. The inelastic results are in good agreement for groups to low excited levels, near 1 to 2 MeV excitation energy, but drift apart by about 20% for the group near 3 MeV excitation energy. The overall agreement for the inelastic scattering is quite impressive.

A comparison between measurements from three laboratories is available in Figures 11 and 12. These are drawn from a large carbon scattering study[32] at BLC. The BLC data overlap a similar experiment of Perey and Kinney[33] at ORNL, and the comparison of data from the two groups is shown at 8.5 MeV bombarding energy. One can see that the comparison is excellent, well within the normalization uncertainties of about 5% on either experiment. A scattering study for carbon was also completed recently at ARL laboratories, between 7 and 9 MeV incident energies.[34] The 9 MeV data of Figs. 11 and 12 show results from both

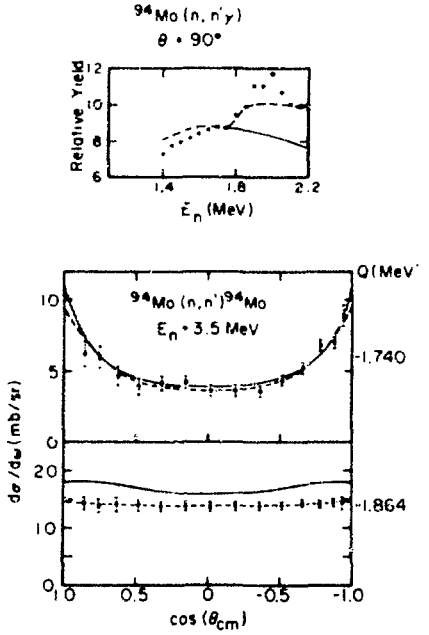

Figure 9a. Neutron angular distributions to a 0^+ and 2_2^+ level. Upper panel shows γ-ray excitation function for $0^+ + 2_1^+$ γ rays.

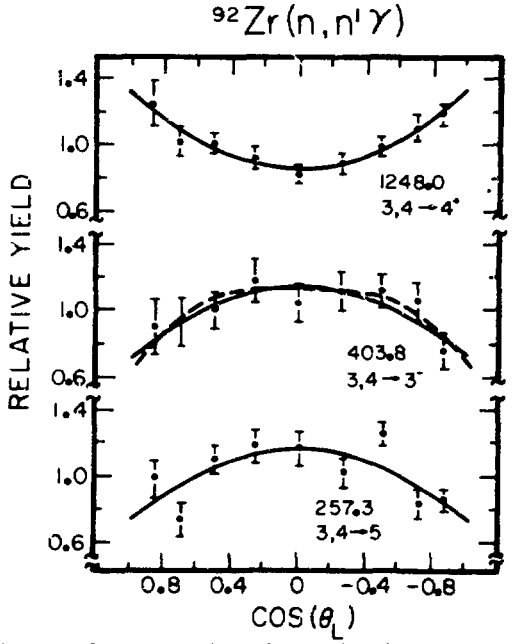

Figure 9b. Angular distributions for decays from 2742.6 keV. A test for large M2/E1 admixtures eliminates J=3.

the ARL[34] data and BLC studies.[32] Once again excellent agreement is obtained between results of the two laboratories. These figures link together three different experiment, showing the good agreement which exists amongst them. The measurements shown at 14.0 and 14.5 MeV include comparisons with much older measurements of lower precision; in these cases the comparisons are not as satisfactory. A more expanded comparison is presented in Fig. 13 of neutron scattering cross sections for carbon at 9 MeV incident energy. Data from the ARL experiment[33] are compared with very recent measurements made at TUNL.[35] The entire TUNL study is about as extensive as that shown in Figs. 11 and 12 from BLC, and the data from those two studies are in very good agreement. The agreement shown in Fig. 13 is the ARL and TUNL studies are being met. It may be worth noting that in Figs. 10 and 13 one sees comparisons which are excellent for elastic scattering cross sections but are less perfect for inelastic scattering to highly excited levels. These relative shifts of normalization with changes in scattered neutron energies probably reflects the difficulty in knowing well the energy dependence of the neutron detection efficiency. Careful determination

of the neutron detection efficiency for the detector actually used is one of the most critical tasks to be performed in a high precision, high accuracy neutron scattering study.

One of the tests of the adequacy of local, energy dependent potentials to describe neutron scattering has been the test for ξ dependence, or neutron excess dependence, and whether or not the ξ dependence reflects the i-spin dependence expected by Lane.[36] The last major review of this question for neutron scattering[37] in 1972 seemed to reach the conclusion that the ξ dependence of the real part of the potential was only about half or less that expected on the basis of proton scattering. At any incident neutron energy one writes the depth of the real scattering potential as: $V(r) = (V_0 \pm V_1 \xi)\ f(r)$, with $f(r)$ a Saxon-Woods form factor. Similarly, one writes $W_D(r) = (W_0 \pm W_1 \xi)\ g(r)$, with $g(r)$ a derivative Saxon-Woods form factor for the imaginary part of the potential, W_D. For proton scattering the coefficients derived from global fits seem to be[38] $V_1 \sim 24$ MeV, and $W_1 \sim V_1/2$. On the other hand neutron scattering surveys seemed to suggest[37] $V_1 \leq 13$ MeV, half the value implied by global proton scattering analyses. Since this would appear to violate the notion of i-spin dependence for scattering potentials, it is worthwhile to re-examine this question in the light of newer experiments.

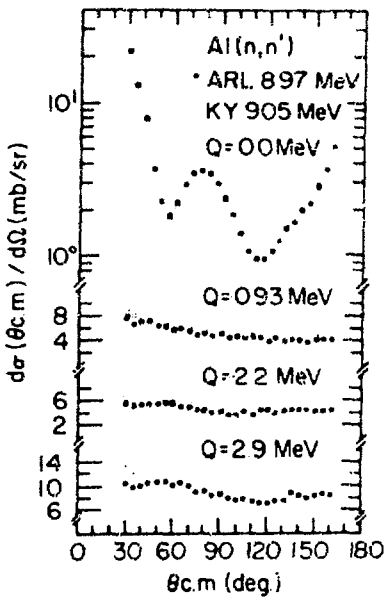

Figure 10. Comparison of ARL and Kentucky cross section measurements in Al.

A particularly effective method of testing the notion of i-spin dependence of scattering potentials is the simultaneous analysis of proton and neutron scattering from the same nuclei, a procedure adopted for 14 MeV neutron scattering from ^{59}Co and ^{209}Bi quite some years ago.[39] The result for these two nuclei was in the range $V_1 = 23$-24, depending on other assumptions in the analysis. The recent 9 MeV scattering experiment of Velkley, et al.[31] included differential elastic scattering cross sections for three nuclei near A=60. The measurements and potential analyses are shown in Fig. 14, and the potential depths determined are plotted in Fig. 15. From the slope of V vs. ξ one finds $V_1 = 22$. Although this was an analysis of neutron scattering, the potential determined with ξ dependence was tested for 9.8 MeV proton scattering by ^{59}Co. The fits to proton scattering cross sections and polarization data are shown in Fig. 16, a very nice confirmation of the notion of i-spin dependence. Both of the studies cited involved only a few nuclei, hardly a substantial test, however. A more extensive set of scattering data has just been obtained by Ferrer, et al. at a neutron energy of 11 MeV.[40] Their analysis of this data together with older (p,p) data on the same nuclei, also at 11 MeV, is shown in Fig. 17. One sees that good fits are obtained, and they suggest $V_1 = 22$ MeV. Instead of analyzing the data at equal bombarding energies, one may elect to analyze at energies shifted by the Coulomb displacement energy[41] and using standard energy dependencies[42] for the scattering potentials. Ferrer, et al.[40] have been able to do this for three nuclei included in their 11 MeV neutron scattering study, and the results are

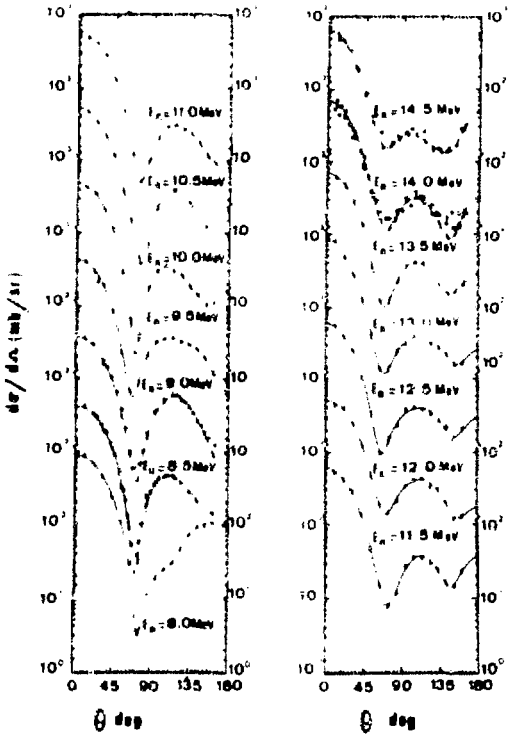

Figure 11. Elastic scattering by ^{12}C.

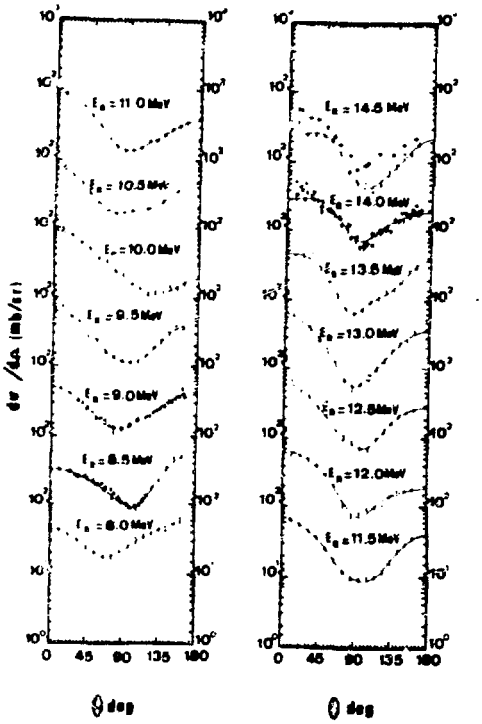

Figure 12. Inelastic scattering to the 4.43 MeV level of ^{12}C.

shown in Fig. 18. The fits to one of the nuclei, ^{120}Sn, are not comparable to the fits of Fig. 17, but are still fair. When all of the combined (n,n) and (p,p) analyses are included, they determine V_1 to be very close to 22, the value Velkley, et al.[31] had found at 9 MeV.

The Ohio University group also analyzed their extensive set of 11 MeV neutron scattering angular distributions separately, to see what ξ dependence that data by itself would indicate.[43] Distributions of differential cross sections had been measured for 21 nuclei. For ξ dependence tests, 16 of them were divided into four groups of comparable A, one group being four of the even-A Mo isotopes. The five light isotopes, ranging from Mg to Ca, were excluded, since each of their angular distributions were quite distinct; no systematic development of scattering seems evident amongst those elements. The groups analyzed included one very similar to the set included in the ARL 9 MeV experi-

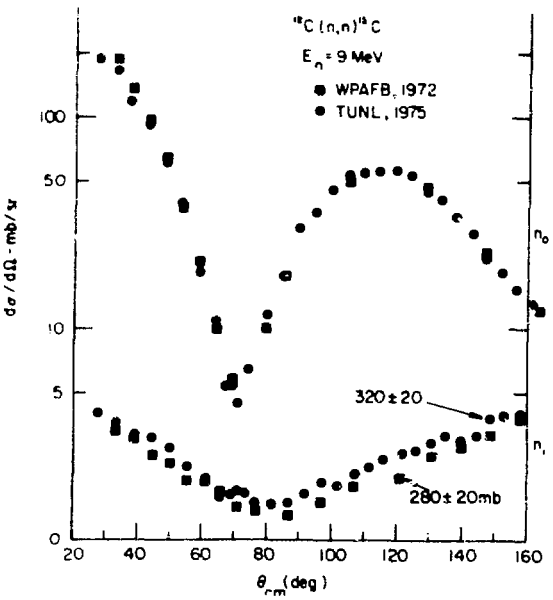

Figure 13. Comparison of ARL and TUNL data for C. Elastic (n_0) and inelastic (n_1) groups are shown.

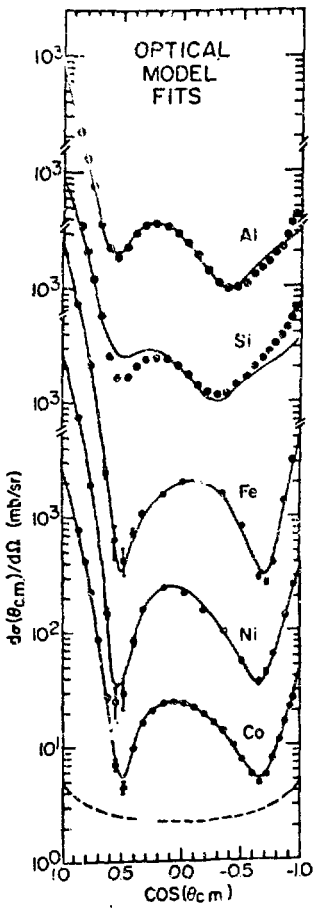

Figure 14. Elastic scattering and optical model fits for 9 MeV neutrons incident. Measurements are from Ref. 31.

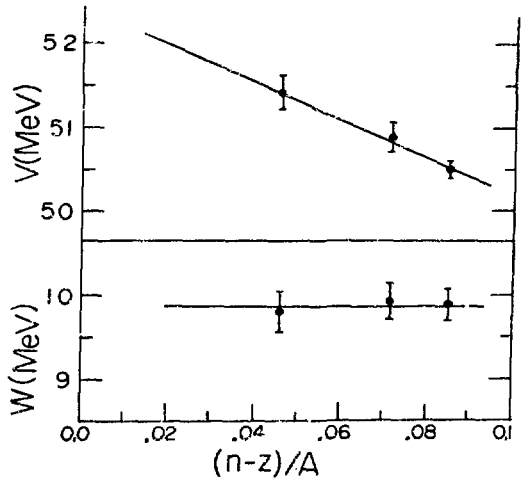

$$V = 55.30 - 0.32E + 0.27(Z/A^{\frac{1}{3}}) \pm 22(n-z)/A$$

Figure 15. The ξ dependence of V and W for Fe, Ni, and Co data of Fig. 14.

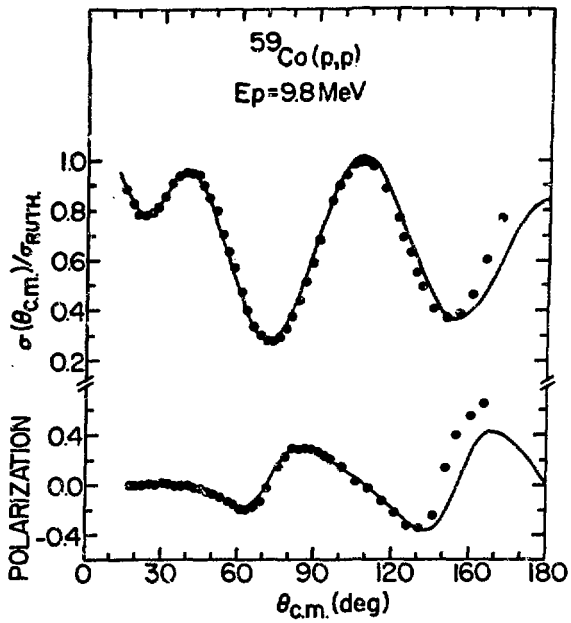

Figure 16. Elastic scattering data and fits using potential strengths of Fig. 15.

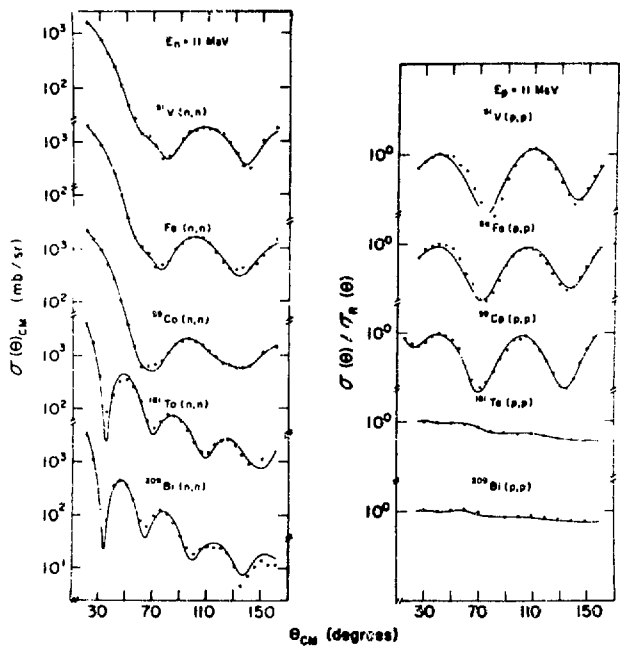

Figure 17. Elastic neutron and proton scattering cross sections and potential analyses for 11 MeV incident energy.

and other weaknesses of fits shown in Figs. 19 and 20 may reflect detailed structural differences which cannot be represented in an analysis which includes many nuclei.

A good deal of information is available from experiments at lower energies. The Kentucky study of scattering by nuclei in the A~90 region includes measurements on four Mo isotopes at 6 MeV incident energy. The scattering neutron TOF spectra are shown in Fig. 21, where one sees strong excitation of the ground state and low-lying levels. The differential cross sections for elastic scattering are shown in the right-hand panel, as well as the potential fits. The analysis of the scattering is presently incomplete, but

ment,[31] one of the four Mo isotopes, and one including heavy elements. The interesting observation is that the ξ dependence obtained from analysis of all four groups is the same. The coefficient $V_1 = 24$, with variations of less than 0.2 MeV from one group to another. The fits obtained to the nuclides of the different groups are shown in Figs. 19 and 20, where one sees that the systematic development of the scattering angular distributions seems to be well represented by the analysis. One notes also that in systematic analyses of this kind the fits are not uniformly excellent for all nuclei. For example the fit to ^{92}Mo in Fig. 19 is not good; this may call into question the confidence with which the potential parameters are greeted for the set of Mo isotopes, or it

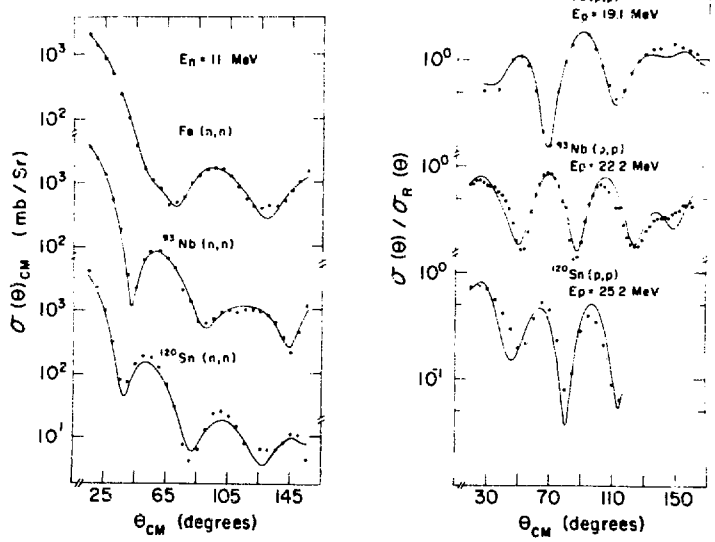

Figure 18. Neutron and proton scattering data and analyses, with the proton incident energy shifted by the coulomb displacement energy.

has progressed enough to make clear the fact that $V_1 = 24$. This result had also been obtained by Smith, et al.[45] in their analysis of neutron scattering from the Mo isotopes between 1.8 and 4.1 MeV incident energies. For the rigid, spherical Mo isotopes it seems clear that the ξ dependence is just that obtained from a survey over a large range of nuclei, and also that the same ξ dependence applies to scattering potentials for measurements made at all energies between 2 MeV and 11 MeV. In addition the coefficient V_1 appropriate for a set of isotopes is also the coefficient for a global analysis.[43] Examination of Figs. 19 and 20 shows that most of the nuclides included in the survey are also rigid, spherical nuclei, however. It is possible that this result applied particularly to such nuclei.

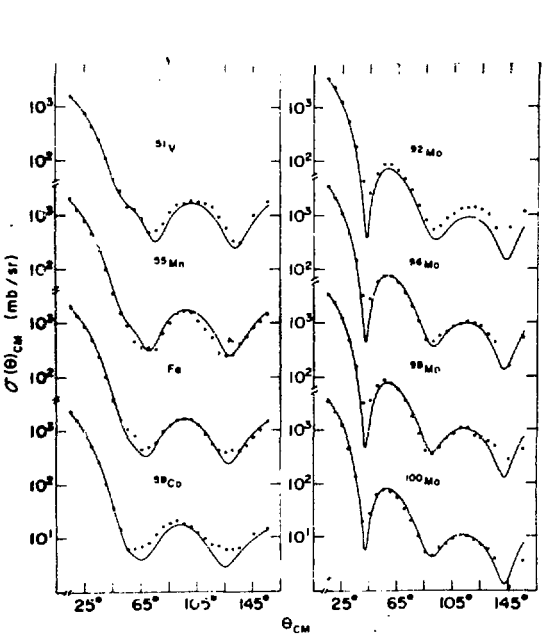

Figure 19. Data from 11 MeV neutron scattering survey analyzed in two groups for two mass regions.

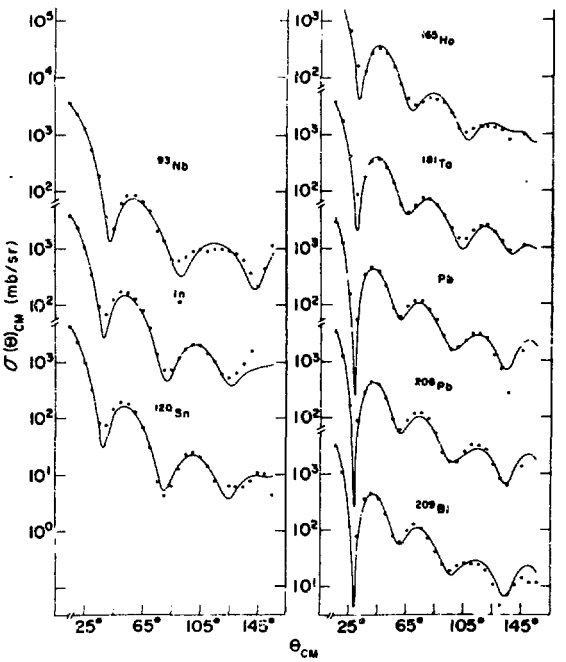

Figure 20. Elastic scattering cross sections for each panel have been separately analyzed to determine a potential.

More information about this last point comes from a scattering study of the soft, deformable Se isotopes. Elastic and inelastic scattering cross sections to first excited 2^+ levels were measured for four isotopes at incident energies of 6 and 8 MeV by Lachkar, et al. at BLC.[46] Their potential analysis of the data found that reasonable fits to the data could only be obtained for $V_1 = 9 \pm 2$ MeV! This was reminiscent of results from earlier scattering surveys[37] which had indicated small coefficients for ξ dependence, of this size or less. A possible reason for this anomalous behavior might lie in the fact that the deformation amplitudes β_2 ranges from 0.2 to 0.3 as determined from Coulomb excitation studies.[47] These are large values for nuclei not regarded as deformed. To test the hypothesis that the large and varying β_2-vibrational amplitudes were the cause of the small V_1, the

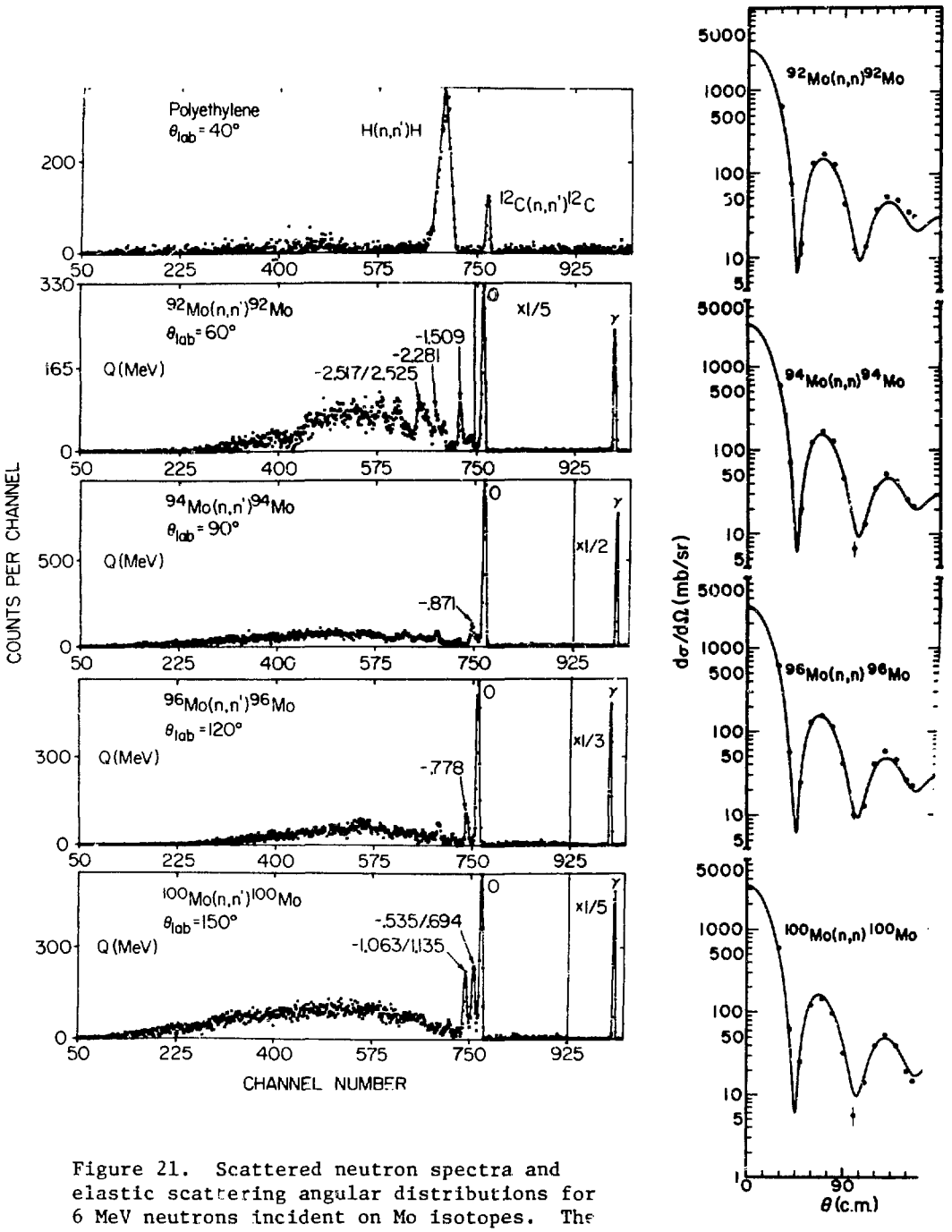

Figure 21. Scattered neutron spectra and elastic scattering angular distributions for 6 MeV neutrons incident on Mo isotopes. The top spectrum of the left panel shows that from the normalization sample.

measurements were re-analyzed in a calculation which explicitly coupled the ground and 2^+ levels.[9] Both elastic and inelastic cross sections are shown in Figs. 22 and 23 for an incident neutron energy of 8 MeV. The coupled channels analysis provides excellent fits to the data for the four Se isotopes, and with the coefficient $V_1 \lesssim 20$ MeV in the new analysis. The real part of the scattering potential has the same ξ dependence for these deformable isotopes as for the more rigid nuclei of Figs. 19-21 when the deformation effects are explicitly included in the analysis.

What can be said about the coefficient of ξ in the imaginary part of the potential, W? The analysis of s-wave strength functions (S_o) some years ago by Delaroche and Newstead[48] showed two trends. The gradual progression of S_o from element to element was consistent with global analyses in which $W_1 \sim 0$. On the other hand within sets of isotopes S_o decreases very rapidly with ξ, a behavior requiring large W_1 values, ranging from 40-62 MeV for different isotope sets.[48] The Se+n scattering study,[9] including both the elastic and inelastic scattering cross sections of Figs. 22 and 23, fix W for each nuclide. From those determinations $W_1 \simeq 38$, a large value consistent with the fits to low energy strength functions. The mass survey at 11 MeV also seems to fix W_1. Both from the combined neutron and proton scattering analysis[43] and from the separate analysis of neutron scattering[44]. Ferrer, et al. conclude that $W_1 \sim 10$-15 MeV, which would give

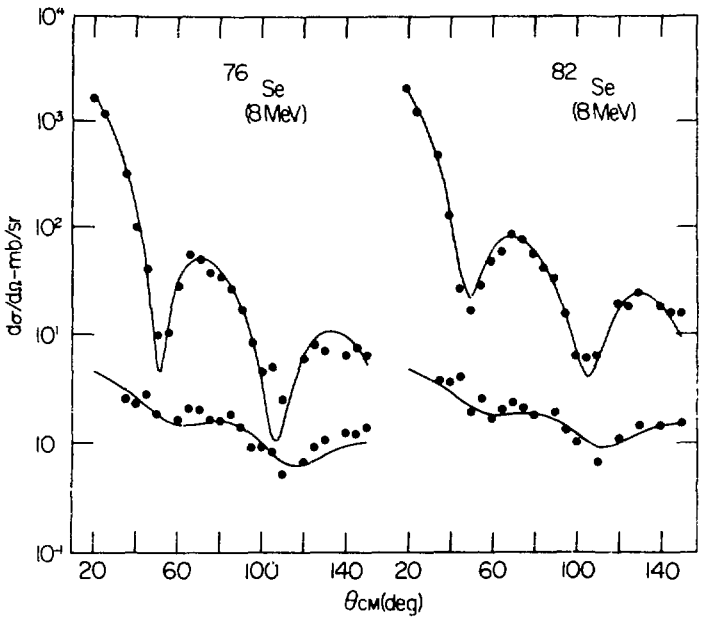

Figure 22. Measurements and coupled channel (cc) analyses for elastic and inelastic scattering at 8 MeV.

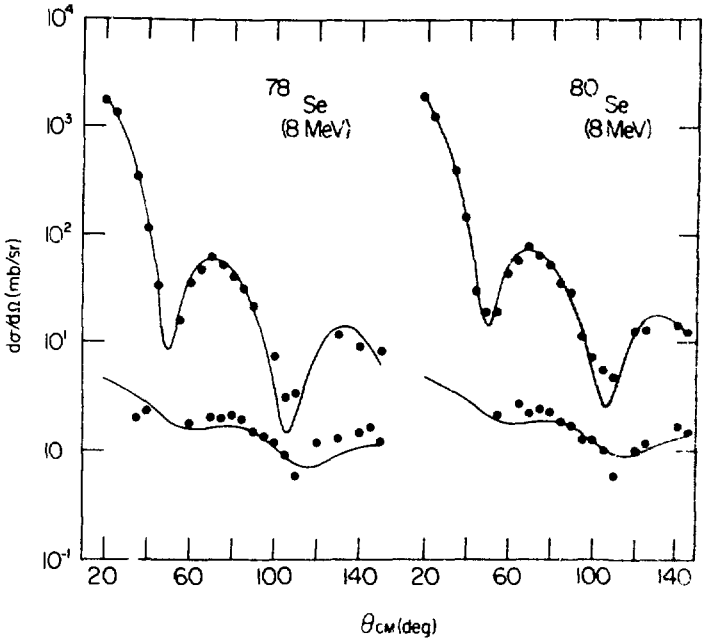

Figure 23. See caption for Fig. 22.

values for V_1 and W_1 consistent with the expectations of Bechetti and Greenlees,[42] who projected $W_1 \sim V_1/2$. On the other hand in their analysis of a selected set of the 11 MeV scattering data, those for isotopically pure scattering samples and with minimum inelastic contributions to the elastic scattering data, they determined $W_1 \sim 2$ MeV. The analysis of Velkley, et al.[31] and that shown in Fig. 21 are for $W_1 = 0$.

A clear and general statement about W_1 does not seem possible at this time. For V_1, a definitive statement can be made. Both for analyses of sets of isotopes and for those including many elements, $V_1 \simeq 22$-24 MeV. That this coefficient is consistent with the strength of i-spin potentials used in the analysis of isobaric-analog resonances has been noted by Brandenberger and Schrils.[49] Some years ago G. R. Satchler pointed out that all potentials of whatever form which satisfy the condition VR^n = constant are at least approximately phase equivalent. With this condition and a series expansion for $V(r+\delta r)$ in terms of r, the strength of volume and surface potentials can be related if n is known.[50] The scattering potential derived from forms used for analog resonance analysis is:[49] $V_1(r) = (1/4)(N-Z)U_1\ g(r)$, with U_1 ranging from 1.3 - 1.8 for analyses with different surface forms for g(r). The coefficient U_1 which characterizes the scattering data of Velkley, et al.[31] is $U_1 = 1.4$, which is equivalent to the volume coefficient $V_1 = 22$. Thus the presently determined coefficients $V_1 = 22$-24 are completely consistent with strengths implied by analog resonance analysis.[49]

The determination of scattering systematics seems to be rendered more difficult by the variations in deformability and deformations encountered in different mass regions; but these variations can be at least partially accounted for, and the systematics restored, through use of coupled channel calculations. This was illustrated by the neutron scattering study of the Se isotopes discussed above. That the coupled-channel framework would be a good one for the development of systematics was projected by S. Tanaka, who completed a massive analysis of neutron total and scattering cross sections[51] with coupled channel models. He began by determining an energy dependent scattering potential to fit ^{209}Bi and ^{207}Pb data. Then adding a ξ dependent term to the real potential with $V_1 = 24$, he calculated results throughout the periodic table without altering any potential parameters. He simply adjusted coupling strengths to reflect deformation properties of the target nuclei as revealed in Coulomb excitation and charged particle scattering studies. An obvious success of this approach was in the calculation of total cross sections for the light deformed nuclei between ^{23}Na and ^{40}Ca, and at incident energies between 1 and 3 MeV. In fact the coupled channel approach gave better results than a one-channel, spherical potential model for many nuclei at low bombarding energies. Another striking success was the fit to the energy dependence of the total cross sections for the deformed rare earths. Foster and Glasgow[52] has been unable to reproduce those cross sections with a one-channel analysis. An example of a success of this global analysis is shown in Fig. 24, which shows fit to neutron scattering by ^{120}Sn. The measurements are from the Japan Atomic Energy Research Institute (JAERI).[53] The elastic scattering data are quite well fit, considering that the potentials have not been adjusted for this nucleus. The difference between the one-channel model fits, shown as dashed curves, and coupled channel model results is modest for this rather rigid nucleus. The difference between solid and dashed curves for the first excited level is the direct inelastic contribution. As is often the case for spherical nuclei, that contribution is small enough so that even its existence may not be evident in the data, but the fits which combine WHF and direct contributions represent the measurements well.

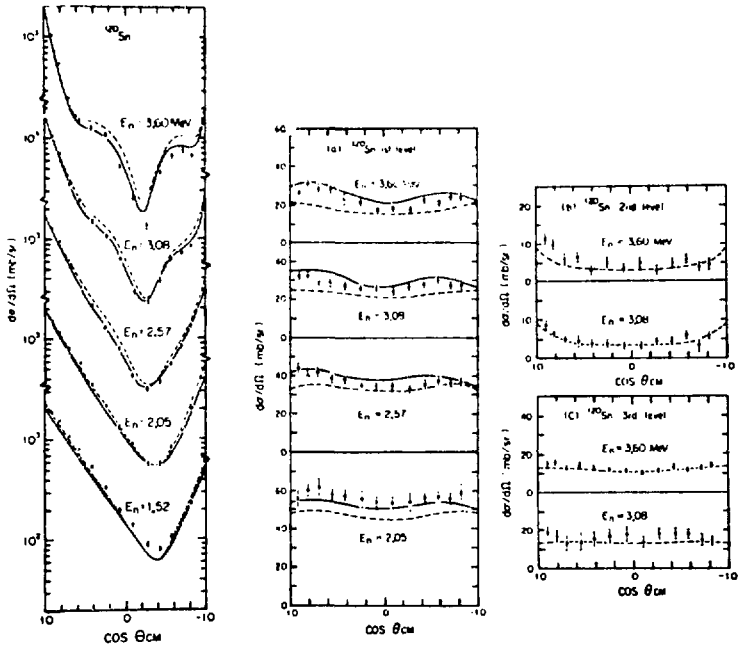

Figure 24. Measurements and cc analysis for ^{120}Sn. Dashed curves are statistical model (WHF) calculations.

Before delving further into modifications of scattering caused by deformations or nuclear softness, it will be useful to examine a recent large scale study of small angle elastic scattering completed by Bucher, Hollandsworth, and others[54] at the Edgewood Arsenal tandem accelerator. These data were taken to provide an extensive and accurate survey of small scattering, to help define the information available in such data. The experimental apparatus for the measurements[54] is shown in Fig. 25. The detection system is designed to shield the detector from direct flux from the source, and from scattered background, but admit scattered neutrons from four azimuthal sections at a fixed (small) angle. The effort is to maximize shielding for neutrons at angles other than the scattering angle while also maximizing transmission for neutrons scattered at the desired angle. To examine data from this system, very different than those of Figs. 1-4, Fig. 26 shows a comparison of small angle data with that from the BLC study of carbon, completed by Haouat, et al.[32] The triangles are BLC data, and the curve is their least squares Legendre polynomial fit to the full angular distribution, shown in Fig. 10. The agreement is truly excellent at 9.5 and 14.0 MeV incident energies, and fair at 11.0 MeV. The confidence gained from this comparison helps us as we examine the small angle data of Figs. 27-29. The points shown in these and in all figures dealing with results of this survey[54] are differential cross sections after subtraction of the incoherent contribution caused by the neutron's magnetic moment.[55] The arrows along the left ordinate axis are lower limits or Wick's limits from the accurately measured total cross sections.[56] The curves are calculations with the Wilmore-Hodgson potential.[57] These data span almost the entire range of nuclei. In every case they extrapolate to 0° a little above or at Wick's limit. For elements Be through Fe the extrapolated 0° values are enough to indicate small real parts for the forward scattering amplitude. For elements Ni-Bi the cross sections seem to be very

close to the Wick's limit values. Except for the light elements, the Wilmore-Hodgson potential in a standard optical model calculation does a good job of representing the angular dependence of small angle scattering. The only really anomalous behavior is that for W at 7.55 and 11.0 MeV, which we will attribute to deformation effects.

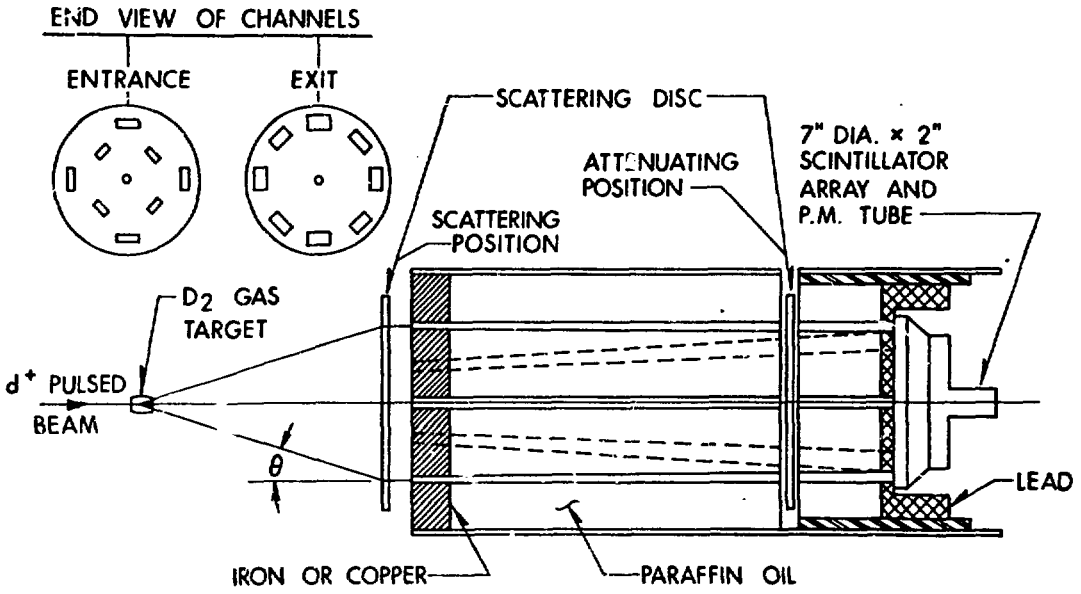

Figure 25. Small angle scattering detection system of Bucher, Hollandsworth, and Lamoreaux. Designed for measurements from 1 to 15°.

The first report and analysis of deformation enhanced small angle scattering was that of G. Palla,[58] who showed the effects on neutron scattering from U. Subsequently, Benenson, et al.[59] showed that no such enhancement at all appeared at 14.8 MeV incident energy. The data were well fit with a spherical potential model. The reconciliation of these and other conflicting reports about enhancements of small angle scattering may be contained in the data of Bucher and Hollandsworth[60] for Pb and U, shown in Fig. 30. The solid dots are the measurements, and the solid curves are fits to the energy and angle dependence they have found for small angle scattering. Other symbols represent measurements by other investigators, most of which deviate seriously[60] from the data of Bucher and Hollandsworth. The arrows on the left ordinate for U are again Wick's limit values, so that the extrapolated 0° values contain only information already present in the total cross sections. To emphasize the effects of deformation for U, the ratios of U and Pb values are shown in Fig. 31, together with some model calculations. We see in the measurement ratios at 1° and 15° a very strong energy dependence. One might conclude from measurements a little below 6 MeV or somewhat above 14 MeV[59] that U scatters like spherical Pb, no anomaly would be evident. But between 7 and 12 MeV very strong departures from spherical

nucleus behavior are evident. The solid and dashed curves shown to the right are from coupled channel calculations of Lagrange and Mondon[61] for U. These show the ratios attributed to the deformation, represented by β_2 in the model. The energy shift between the calculated and measured ratios reflects the fact that the calculations are done entirely for U, with β_2 = 0 and 0.3, but the measurements are ratios of cross sections for U and Pb. Part of the problem of conflicting reports about small angle scattering enhancements may be traced to disagreements of measurements,[61] but part can also be traced to the fact that measurements are made for deformed nuclides at different bombarding energies.

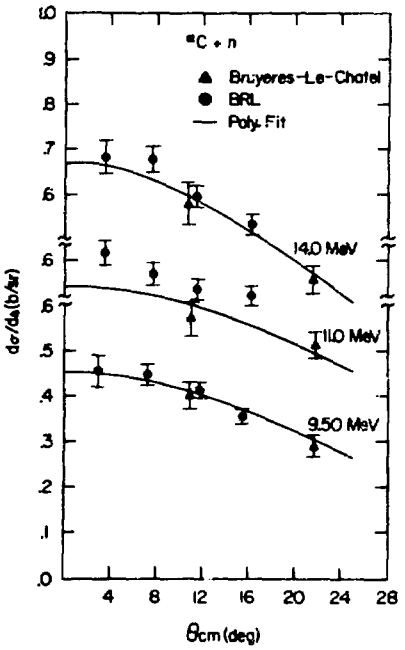

Figure 26. Comparison of data from two laboratories at small angles.

The strong energy dependence of deformation related effects in total cross sections (σ_t) was explicitly demonstrated in the measurements of Shamu, et al.[62] at Western Michigan University (WMU). The differences between σ_ts for deformed and presumably spherical ^{148}Sm, normalized to σ_t for ^{148}Sm, are shown in Fig. 32. In the meantime Lagrange and Mondon[61] had prepared a coupled channel analysis of Sm + n scattering for several isotopes, based on low energy strength functions and total cross sections for natural Sm between 0.6 and 14 MeV incident energies. The subsequent successful analysis of Ch. Lagrange[63] of the WMU measurements is also shown in Fig. 32. The data and analyses are are quite similar to those shown in Fig. 31 for small angle cross sections. For these transitional Sm isotopes one sees two energy regions of pronounced effects, near 2.5 MeV and a broad region from 7 to 10 MeV. Different scattering cross section measurements were completed for these isotopes at Kentucky[64] and at BLC.[65] The elastic and inelastic scattering cross sections to the first excited 2^+ level are shown in Fig. 33 for one of the isotopes, ^{152}Sm. These measurements and analyses were completed at BLC for 7 MeV incident energy. The detailed fit to the elastic scattering results is quite good, and the magnitude of the inelastic scattering cross sections is also well represented in the analysis.[9] Thus the coupled channel model, which treats the excited level of ^{152}Sm as those of a rotational nucleus, provides a good description of neutron total, elastic, and inelastic scattering cross sections to the 2^+ level as well as describing the low energy scattering properties.

The other energy region of apparently pronounced effects is near 2.5 MeV incident energy. These same isotopes have been studied by D. F. Coope, et al., who saw remarkably large enhancements of inelastic scattering for deformed isotopes.[66] The inelastic scattering cross sections to the first 2^+ levels of three isotopes, ^{148,150,152}Sm, are shown in Fig. 34. One sees there the featureless, almost isotropic data for ^{148}Sm. This is typical of results for spherical nuclei. The strong structure for ^{152}Sm is quite atypical of neutron inelastic scattering angular distributions, and presents clear evidence of strong collective enhancements at low bombarding energies. That these enhancements involve not only the first 2^+ states but a large part of the ground state rotational band is

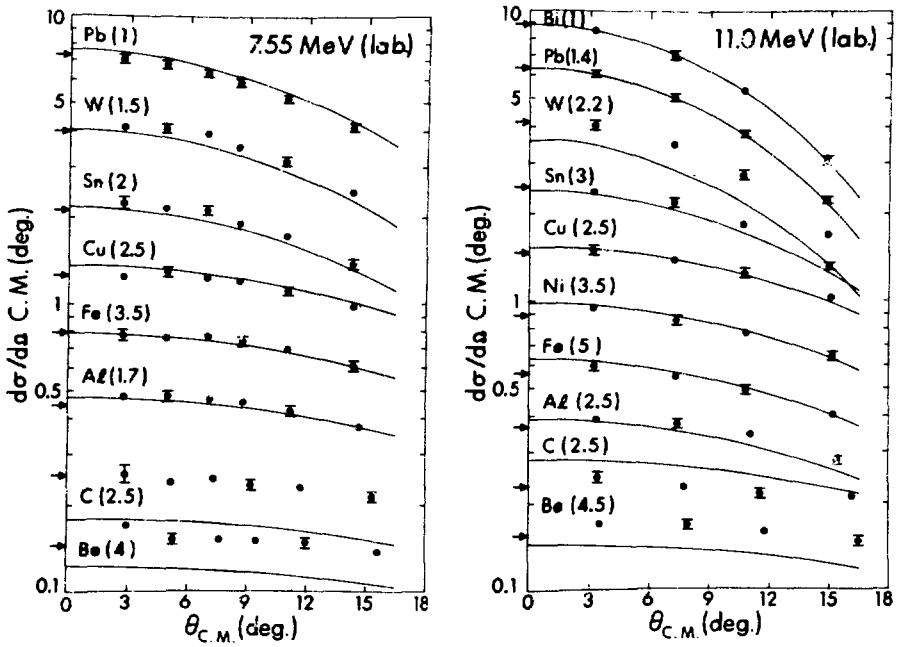

Figures 27 and 28. Small angle measurements and calculations (curves) with a spherical optical model. Numbers in parentheses denote off sets (in bars) for plotting purposes. Arrows denote Wick's limit values.

demonstrated in Fig. 35, which shows strong γ rays de-exciting the 4^+ and 6^+ levels of ^{152}Sm. For these states, collective enhancements produce cross sections about 4 times as strong as would be predicted with WHF or statistical model calculations, or with coupled channel calculations. The potential used for the latter was that which had worked well for scattering to the ground and first excited levels.[9,63,64]

In summary, comparisons of elastic scattering cross sections measured in different laboratories show good agreement, supporting the accuracy claims of about 5% on measurements when special care to achieve this is developed in the experiments. For inelastic scattering, measurements from different groups suggest consistency within about 10-15% and this includes results inferred from γ-ray production cross sections as well as those from neutron detection. The results for γ-ray production at bombarding energies ≤ 3.5 MeV indicate that that method reliably extends neutron inelastic scattering studies to nuclei whose levels cannot be resolved in neutron detection.

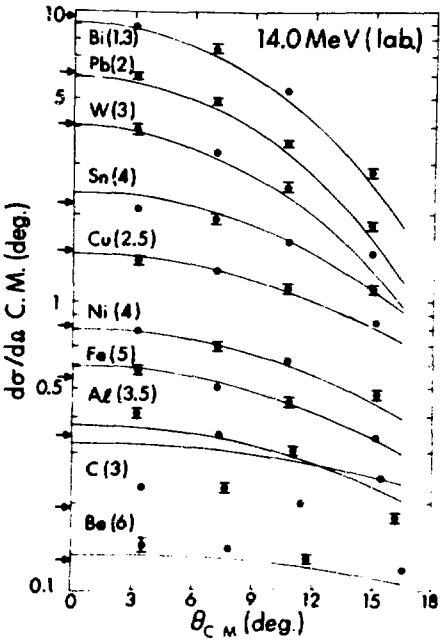

Figure 29. See caption for Figs. 27 and 28.

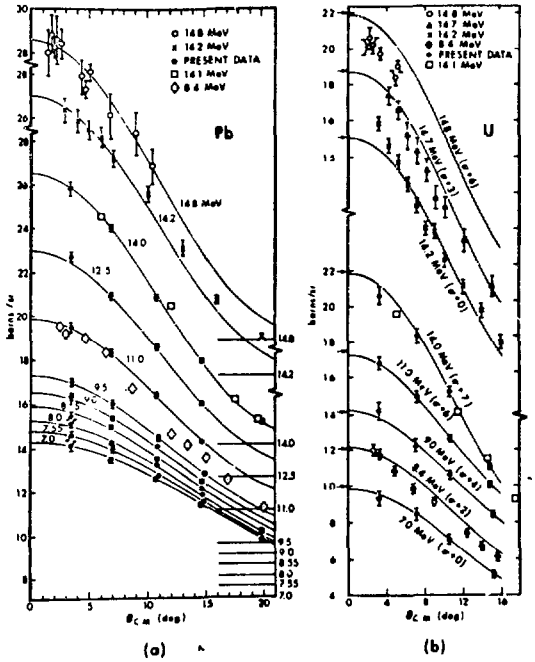

Figure 30. Small angle data for Pb and U.

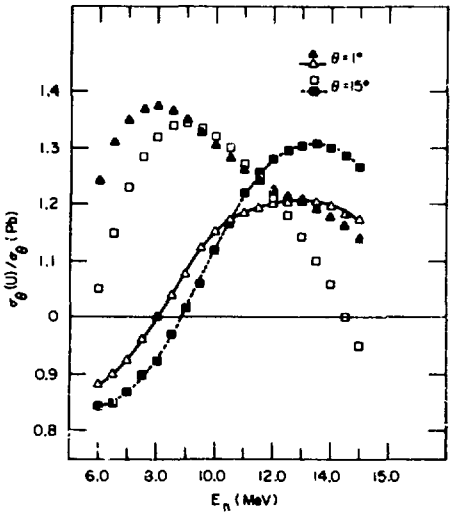

Figure 31. Ratios of small angle scattering cross sections for deformed U and spherical Pb. The curves are cc calculations as described in the text.

Recent scattering studies and surveys at incident energies between 3 and 11 MeV seem to clarify that the neutron excess dependence of the real part of the neutron scattering potential is just that expected from an i-spin dependent potential whose strength is consistent with that used in analyses of i-spin analog resonances. These studies all apply most clearly to spherical nuclei which are not very deformable, and include one set of isotopes. Extension of this result to a set of soft or deformable isotopes requires that most important of the deformation effects be explicitly included in the analysis, a coupled channels analysis. Without explicit inclusion of deformation effects an anomalous i-spin dependence is observed. Global coupled channel analyses of total cross sections have shown that scattering potential systematics apply over most of the periodic table, successfully including deformed and spherical nuclei. These studies also confirm the i-spin dependence of the real part of the scattering potential.

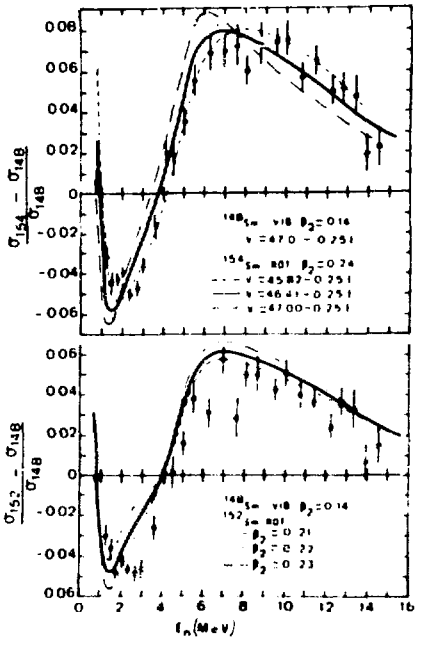

Figure 32. Total cross section differences and cc calculations.

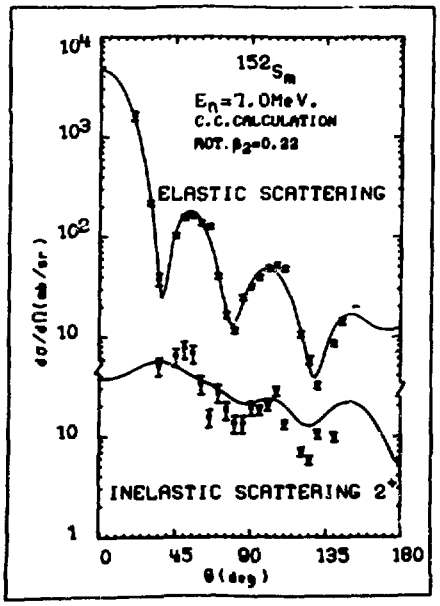

Figure 33. Measurements and coupled channel (cc) fits for elastic and inelastic scattering.

For many years inelastic scattering cross sections measured at incident neutron energies $\lesssim$ 3 MeV have been satisfactorily described with statistical models. These are for experiments carried out with spherical nuclei, since the small energy level separation in deformed nuclei made their study especially difficult. When scattering potentials were carefully determined to fit total and elastic scattering cross sections for the nucleus being studied, the WHF model or modified forms of it represented inelastic scattering cross sections usually to within 25-30%. Thus neutron inelastic scattering in these nuclei is an effective tool for the study of static properties of excited nuclear levels.

Just recently, and especially at this conference, many groups are reporting inelastic scattering cross sections for strongly deformed nuclei for low incident neutron energies. These experiments report cross sections in even A nuclei which are much larger than those consistent with the WHF model, making clear for the first time that very strong collective enhancements occur for neutron inelastic scattering at low bombarding energies and in deformed nuclei.

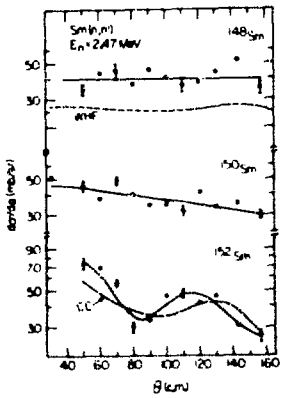

Figure 34. Neutron inelastic scattering to 2$^+$ levels of three Sm isotopes at 2.47 MeV.

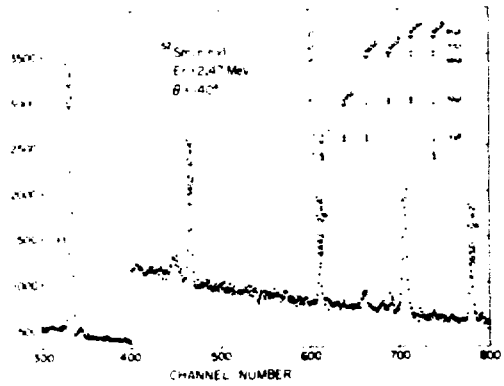

Figure 35. The enhanced $4^+ \rightarrow 2^+$ and $6^+ \rightarrow 4^+$ transitions dominate the ^{152}Sm (n,n'γ) spectrum at 2.47 MeV.

A recent and extensive survey of small angle elastic scattering shows no anomalously large cross sections, except that differential cross sections for deformed nuclei are large compared to spherical potential model predictions. This deviation of small angle cross sections from spherical model expectations is quite dependent on incident neutron energy, being particularly pronounced between 7 and 12 MeV incident energies. Even this deformation-dependent effect

is contained implicitly in the total cross sections, since the extrapolated 0° cross sections approach Wick's limit values.

A characteristic of neutron scattering systematics seems to be that the systematics separates spherical from deformed nuclei; neutron scattering behaves quite differently for the two classes of nuclei, even at rather low bombarding energies. While coupled channel calculations developed to date do not accurately describe inelastic scattering in deformed nuclei, particularly at low bombarding energies, they *do* provide a framework which unifies the description of neutron scattering from both spherical and deformed nuclei.

ACKNOWLEDGEMENTS

The author is deeply in debt to his colleagues at Kentucky, and particularly to Prof. J. D. Brandenberger, for helping him to understand and adopt methods used in neutron scattering studies. He is also indebted to his colleagues at Kentucky and BLC for many discussions about the interpretation of scattering data. Gratitude is also expressed here to the many investigators who willingly supplied experimental results and analyses prior to their publication. In this connection particular debts are owed to C. E. Hollandsworth, W. Bucher, J. Rapaport, J. Lachkar, and S. Tanaka.

REFERENCES

1. L. Cranberg and J. S. Levin, Phys. Rev. 103, 343 (1956); A. B. Smith, in Nucl. Res. with Low Energy Accels., edited by J. B. Marion and D. M. Van Patter (Academic Press, New York, 1967) p. 359; D. W. Glasgow, et al., Nucl. Instr. and Methods 114, 541 (1974); A. Adam and J. Cabé, Nucl. Instr. and Methods 121, 339 (1974).
2. A. Langsdorf, Jr., in Fast Neutron Physics, Vol. I, edited by J. Marion and J. L. Fowler (Interscience Pub. Inc., New York, 1960); D. W. Glasgow, et al., Nucl. Instr. and Methods 114, 521 (1974).
3. R. B. Day, in Progress in Fast Neutron Physics, edited by G. C. Phillips, J. B. Marion, and J. R. Risser (Univ. of Chicago Press, Chicago, 1963).
4. M. T. McEllistrem, in Nucl. Res. with Low Energy Accels., edited by J. B. Marion and D. M. Van Patter (Academic Press, New York, 1967) p. 167.
5. J. D. Reber and J. D. Brandenberger, Phys. Rev. 163, 1077 (1967); J. D. Reber, Ph.D. Dissertation, University of Kentucky, 1967 (unpublished).
6. A. Obst and J. L. Weil, Phys. Rev. C7, 1076 (1973).
7. L. Cranberg, R. K. Beauchamp, and J. S. Levin, Rev. Sci. Instr. 28, 89 (1957).
8. F. O. Purser, et al., in Proc. Nucl. Cross Sections and Tech., edited by R. A. Schrack and C. D. Bowman (NBS Spec. Pub. 425, 1975) p. 866.
9. J. Lachkar, M. T. McEllistrem, G. Haouat, Y. Patin, J. Sigaud, and F. Coçu, submitted to The Physical Review.
10. F. D. McDaniels, G. P. Glasgow, and M. T. McEllistrem, to be submitted to Nuclear Instruments and Methods.
11. J. C. Hopkins and G. Breit, Nucl. Data A9, 137 (1971).

12. G. P. Glasgow, F. D. McDaniel, J. L. Weil, J. D. Brandenberger, and M. T. McEllistrem, to be submitted to The Physical Review.

13. L. Cranberg and J. S. Levin, "Neutron Cross Sections-Angular Distributions", compiled by Donald J. Hughes and Robert S. Carter (BNL-400, 1956).

14. R. B. Day, Phys. Rev. 102, 767 (1956).

15. C. A. Engelbrecht, Nucl. Instr. and Methods 80, 187 (1970); Nucl. Instr. and Methods 93, 103 (1971).

16. M. Walt and H. H. Barschall, Phys. Rev. 93, 1062 (1953); M. Walt, Ph.D. Dissertation, University of Wisconsin (1953)(unpublished); L. Cranberg and J. S. Levin, Los Alamos Scientific Laboratory Report No. LA-2177 (1959).

17. J. B. Parker, et al., Nucl. Instr. and Methods 14, 1 (1961); ibid. 30, 77 (1964); ibid., 60, 7 (1968); B. Holmquist, B. Gustavsson, and T. Wiedling, Arkiv fur Fysik 34, 481 (1967); W. E. Kinney, Nucl. Instr. and Methods 83, 15 (1970).

18. D. E. Velkley, J. D. Brandenberger, D. W. Glasgow, and M. T. McEllistrem, Nucl. Instr. and Methods 129, 231 (1975).

19. K. Nishimura, K. Okano, and S. Kikuchi, Nucl. Phys. 70, 421 (1965).

20. J. W. Boring, Ph.D. Dissertation, University of Kentucky (1960)(unpublished).

21. G. Tessler, S. S. Glickstein, and E. E. Carroll, Jr., Phys. Rev. C2, 2390 (1970).

22. Lowell Technological Institute, Progress Report, February, 1972 (unpublished).

23. Donald L. Smith, Argonne National Laboratory Report ANL/NDM-17 (1975).

24. P. Guenther, A. Smith, and J. Whalen, Phys. Rev. C12, 1797 (1975); Argonne National Laboratory Report No. ANL/NDM-7 (1974).

25. F. D. McDaniel, et al., Bull. Am. Phys. Soc. 18, 1402 (1973), and to be submitted to The Physical Review.

26. G. P. Glasgow, K. Sinram, J. D. Brandenberger, and M. T. McEllistrem, Bull. Am. Phys. Soc. 17, 901 (1972).

27. L. Wolfenstein, Phys. Rev. 82, 690 (1951); W. Hauser and H. Feshbach, Phys. Rev. 87, 366 (1952).

28. M. T. McEllistrem, J. D. Brandenberger, K. Sinram, G. P. Glasgow, and K. C. Chung, Phys. Rev. C9, 670 (1974).

29. P. A. Moldauer, Rev. Mod. Phys. 36, 1079 (1964); Phys. Rev. C11, 426 (1975).

30. J. D. Brandenberger, A. Mittler, and M. T. McEllistrem, Nucl. Phys. A196, 65 (1972).

31. D. E. Velkley, et al., Phys. Rev. C9, 2181 (1974).

32. G. Hoauat, J. Lachkar, J. Sigaud, Y. Patin, and F. Coçu, Proc. Conf. Nucl. Cross Sections and Tech., edited by R. A. Schrack and C. D. Bowman (NBS Spec. Pub. 425, 1975); C.E.A. Report No. R4641 (1975).

33. F. G. Perey and W. E. Kinney, Oak Ridge National Laboratory Report ORNL-4441 (1969).

34. D. E. Velkley, et al., Phys. Rev. C7, 1736 (1973).

35. F. O. Purser, et al., Proc. Conf. Nucl. Cross Sections and Tech., edited by R. A. Schrack and C. D. Bowman (NBS Spec. Pub. 425, 1975).

36. A. M. Lane, Nucl. Phys. 35, 676 (1962).

37. G. R. Satchler and F. G. Perey, Nuclear Structure Study with Neutrons, edited by J. Erö and J. Szücs, Budapest (Plenum Press, New York, 1974) p. 133.

38. C. M. Perey and F. G. Perey, Atom. Data and Nucl. Data Tables 13, 293 (1974).

39. H. J. Erramuspe, Nucl. Phys. A105, 569 (1967).

40. J. C. Ferrer, J. D. Carlson, and J. Rapaport, to be published in Physical Review Letters.

41. W. J. Courtney and J. D. Fox, Atom. Data and Nucl. Data Tables 15, 141 (1975).

42. F. D. Bechetti and G. W. Greenlees, Phys. Rev. 182, 1190 (1969).

43. J. D. Ferrer, J. D. Carlson, and J. Rapaport, to be submitted to Nuclear Physics.

44. F. D. McDaniel, private communication.

45. A. B. Smith, P. Guenther, and J. Whalen, Nucl. Phys. A244, 213 (1975).

46. J. Lachkar, et al., Proc. Conf. Nucl. Cross Sections and Tech., edited by R. A. Schrack and C. D. Bowman (NBS Spec. Pub. 425, 1975), p. 897.

47. P. H. Stelson and L. Grodzins, Nucl. Data A1, 21 (1965); J. Barrette, M. Barette, G. Lamoureux, S. Monaro, and S. Marzika, Nucl. Phys. A235, 154 (1974).

48. C. M. Newstead and J. P. Delaroche, Nuclear Structure Study with Neutrons, edited by J. Erö and J. Szücs, Budapest (Plenum Press, New York, 1974) p. 142.

49. J. D. Brandenberger and R. Schrils, Phys. Rev. C13, 2559 (1976).

50. G. R. Satchler, Isospin in Nuclear Physics, edited by D. H. Wilkinson (North Holland Pub., Amsterdam, 1973).

51. Shigeya Tanaka, Japan Atomic Energy Research Institute Report No. JAERI M-5984 (1974).

52. D. G. Foster and D. W. Glasgow, Phys. Rev. C3, 576 (1971).

53. S. Tanaka, Y. Tomita, Y. Yamanonti, and K. Ideno, Nuclear Structure Study with Neutrons, edited by J. Erö and J. Szücs, Budapest (Plenum Press, New York, 1974).

54. W. P. Bucher, et al., Ballistic Research Laboratories Report No. BRL-2099; ibid., BRL-1562; W. Bucher, C. Hollandsworth, and R. Lamoreaux, Nucl. Instr. and Methods 111, 237 (1973); W. Bucher and C. E. Hollandsworth, Phys. Letters 58B, 277 (1975).

55. J. Schwinger, Phys. Rev. 73, 407 (1948).

56. R. B. Schwartz, R. A. Schrank, H. T. Heaton, II, NBS Spec. Pub. 138 (1974); Brookhaven National Laboratory Compilation, ENDF/BIV.

57. D. Wilmore and P. E. Hodgson, Nucl. Phys. 55, 673 (1964).

58. G. Palla, Phys. Letters 35B, 477 (1971).

59. R. E. Benenson, K. Rimauri, E. H. Sexton, and B. Center, Nucl. Phys. A212, 147 (1973).

60. W. P. Bucher and C. E. Hollandsworth, Phys. Rev. Letters 35, 1419 (1975).

61. Ch. Lagrange and N. Mondon, Centre d'Etudes de Limeil, CEA Report No. DO-114 (1973).

62. R. E. Shamu, E. M. Bernstein, D. Blondin, J. J. Ramirez, and G. Rochau, Phys. Letters 45B, 241 (1973).

63. Ch. Lagrange, Lett. J. de Physique 35, 111 (1974).

64. Ch. Lagrange, et al., Phys. Letters 58B, 293 (1975).

65. M. T. McEllistrem, et al., Proc. Conf. Nucl. Cross Sections and Tech., edited by R. A. Schrack and C. D. Bowman (NBS Spec. Pub. 425, 1975) p. 942.

MD 1 - FAST NEUTRON SCATTERING FROM SOME MEDIUM MASS NUCLEI
M. T. McEllistrem (University of Kentucky, U.S.A.)

Mahaux (Liège):

I have three questions. First, did you see any evidence for an imaginary part in the I-component of the optical potential?

McEllistrem:

Let me comment on that question first because it was interesting for us to look for that. Years ago, Newstead and De la Roche had shown that if you look at the behavior of s-wave strength functions at low energies from element to element you didn't need any I-spin component in order to describe that dependence. But if you looked at a set of isotopes for a particular element, like a set of tellurium isotopes or a set of tin isotopes, then there was a very strong dependence required in the imaginary part of the potential. The I-spin coefficient was something like 40- to 60-MeV, depending upon isotope se. In the case of selenium, we found a very strong I-spin dependence in the imaginary part of the potential. On the other hand, in analyzing the spherical nuclei, the molybdenum isotopes, we didn't need that at all. And other people constructing analyses have found that the I-spin coefficient they need is either zero or, what Bechetti and Greenlees proposed from proton scattering analysis years ago, about one-half the magnitude of the I-spin coefficient in the real part of the potential; that is, about 12- or 13-MeV. So I am not able to see a systematic trend in the coefficient of I-spin dependence in the imaginary potential.

Mahaux:

That's from elastic scattering because from (p,n) direct charge exchange reactions it seems that you need some imaginary part. I come to the second part of my question: you have shown a Coulomb correction of $.27Z/A^{1/3}$. Where is this .27 coming from, because usually I think peopl- take .4?

McEllistrem:

I think some early estimates had suggested .4 and then someone later, I've forgotten who now, reanalyzed some data carefully and found that they could get a better fit with .27. The Ohio University group, I think, used .27 also, but that's a detail I don't recall.

Rapaport (Ohio University):

Bechetti and Greenlees, I understand, found a value of .27 in their work. We have found on analysis of T=0 nuclei, using both (p,p) and (n,n) data, a value of .48 ± .07 assuming the same form factor for that term and that the real part of the potential is more suitable.

Mahaux:

Finally, you quote numbers like 24 MeV for the I-component of the potential. This is not too meaningful if one does not say, for instance, what the range of the potential is. What you measure is something that is related with the volume integral of the potential per nucleon. My question here is whether you find a slope for this quantity, as a function of neutron excess, which is different from the one which was found, for instance, by Holmqvist and Wiedling a number of years ago?

McEllistrem:

Let me answer that question indirectly by saying that for almost all of the analyses used here, the radius for the Saxon-Woods potential for all parts of the real part of the potential -- the I-spin dependent part and other parts -- is approximately 1.25 $A^{1/3}$ fermis. But I believe Rapaport has actually looked at the slope of that integral. Am I correct in saying that the slope is different from the Holmqvist-Wiedling analysis which determined an I-spin coefficient of 12.5 or 13 MeV.

Rapaport:

Are you referring to the dependence on energy of V_1 or W_1?

McEllistrem:

No. The dependence on neutron excess of J_1, the volume integral of the real part of the scattering potential.

Rapaport:

Okay. Yes, the value that we are finding there is .8 plus or minus roughly 10%. So in other words, if one does a volume integral and plots that versus $\varepsilon = (N - Z)/A$, one finds a slope of about $.8 \pm 0.1$.

McEllistrem:

I believe the earlier analysis, and Francis Perey can probably correct me if I'm wrong, showed very little dependence on neutron excess.

Rapaport:

Well, the proton dependence is not there at all, or I guess only neutron data shows some dependence and our values agree with the Wiedling 2- to 8-MeV neutron elastic scattering results.

Newstead, (Brookhaven N. L.):

I would like to comment on Professor Feshbach's suggestion and Claude Mahaux's question. Now, Professor Feshbach has pointed out that to properly analyze for the real part of the isospin strength V_1, it's necessary to do a full-scale analysis taking into account collective effects -- that is, a coupled-channels calculation -- and I think this is a very important remark that he's made, and you've proved that experimentally. But by carrying Feshbach's suggestion a step further, I think it's possible to understand another aspect of this problem and answer Mahaux's question concerning evidence for W_1. In the analysis of elastic and inelastic scattering for a chain of isotopes, that is, as you add pairs of neutrons, the results so far have been rather inconclusive. Sometimes you find you require an imaginary strength W_1, and sometimes, such as in molybdenum, it just washes out. Now, extending Professor Feshbach's suggestion, we can see that even though a coupled-channels calculation of the elastic and inelastic scattering has been carried out, if this analysis did not use the proper deformation parameters, and these are sometimes not well known, then that would certainly very much affect the result and could, if the parameters went the wrong way, wash out the isospin effects that one is looking for.

McEllistrem:

I guess that's really a comment. I think the deformation parameters are well enough known so that it shouldn't make a difference between an I-spin coefficient of 40 MeV, which seems to be implied from analysis of strength functions in some sets of isotopes, and zero. I don't think that the deformation parameters are so badly known as that.

Newstead:

Yes, I'm sure in some cases it's probably true that the parameters are known very well. But in other cases, in fact, it seems they're really not that well known. Unless one is really quite sure about those parameters, I still think that this is a real possibility. I think in the molybdenum isotopes this may be the case.

Mughabghab (Brookhaven N. L.):

I have two questions, but first I would like to point out that there is some recent experimental evidence from the B(E2) values that ^{100}Mo, for example, is deformed, and the β_2 value derived is about 0.2. What would this do to your fit of ^{100}Mo and systematics for molybdenum isotopes? Secondly, did you carry out ^{100}Mo $(n,n'\gamma)$ measurements?

McEllistrem:

Well, let me answer the last question first. We have ^{100}Mo $(n,n'\gamma)$ measurements, and the inelastic cross sections are not consistent with, for example, the cross sections we have for samarium. They do not show strong enhancements of collective states over the cross sections that one would expect on the basis of a statistical calculation. So I do not see in the neutron inelastic scattering at low bombarding energies the kinds of enhancements that you would associate with a well deformed nucleus. If you look at the levels of ^{100}Mo and attempt to represent them, say, with a variable moment-of-inertia model, it suggests that the ground state moment-of-inertia is zero. In other words, that model would not project a deformed character for ^{100}Mo at low excitation energies. The analysis which we made and that I showed here is not a coupled-channel analysis for those isotopes at this time. We want to do that, but we haven't reached that point yet. I know the deformation parameter is large for ^{100}Mo, and there is a big change in the level separations between ^{100}Mo and the other isotopes, but that seems to be accounted for quite well in the statistical model calculations. There is nothing dramatically evident in the cross sections at low bombarding energies.

Soloviev (J.I.N.R.):

There is a very interesting point concerning the nuclear shape in excited compound states. It is possible to say from our own data that ^{148}Sm is spherical in the excited state and ^{152}Sm is deformed in the excited compound state. It is possible to reach this conclusion.

McEllistrem:

In the case of ^{152}Sm it has a rotational spectrum. It has the character that one expects for a deformed nucleus. In ^{154}Sm ----

Soloviev:

It's clear for low-lying states that this is deformed. But what is the shape near the neutron binding energy? Is it possible to say that it is deformed in the compound state?

McEllistrem:

The neutron analysis, the coupled-channel analysis, really does't need to take cognizance of whether or not it's deformed at the excitation energy of the incoming neutron. The energy transferred is small. The samarium states are all below 700 kilovolts, you see, so you're really only talking about states that are very near the ground state, and there I think for ^{152}Sm it's clear. Now, ^{154}Sm is a very good question. I said, presumed spherical. I don't know that it is really a spherical isotope.

[Note added in Discussion: Several authors and another speaker have argued that the volume integral per nucleon of the real potential (J/A) is a better index of the symmetry dependence, or I-spin dependence, than the real potential coefficient, V_1. If that index had been adopted here, no conclusions from scattering comparisons within this review would be altered, since all analyses reported use geometrical parameters which differ from one another by only a few percent. Rapaport has stated (above) that J/A values from the 11 MeV neutron scattering show the same (N-Z)/A dependence as those found in earlier scattering surveys. Thus the symmetry dependence found in earlier reviews and that reported here would be in agreement, if J/A is compared rather than V_1. M. T. M.]

5.15 p.m., Tuesday, July 6, 1976 in Olney 150 Invited Paper: Session MD2

FAST NEUTRON SCATTERING: REACTION MECHANISMS AND NUCLEAR STRUCTURE

A. T. G. Ferguson

Atomic Energy Research Establishment, Harwell, England

I. J. van Heerden

Southern Universities Nuclear Institute, Faure, Republic of South Africa

P. Moldauer and A. Smith

Argonne National Laboratory, Argonne, Ill. U.S.A.

RÉSUMÉ

Contemporary experimental and theoretical understanding of (n;n), (n;n') and (n;n',γ) processes is outlined with emphasis on a unified physical view of reaction mechanisms and nuclear structure parameters of medium (fluctuating), and heavy (deformed-actinide) nuclei at energies where both compound-nucleus and direct-reaction mechanisms are prominent.

ABSTRACT

The experimental and theoretical understanding of fast neutron (n;n), (n;n') and (n;n',γ) processes is outlined in the context of reaction mechanisms and nuclear structure. The objective is a unified physical representation of the properties of medium (fluctuating) and heavy-deformed nuclei at relatively low energies ($\lesssim$ 5 MeV) where compound-nucleus and direct reactions are prominent and where inelastic neutron processes provide insight into nuclear structure not otherwise easily available. The correlation of physical concepts and experimental observation is illustrated by selected studies of neutron scattering and associated processes (e.g., total neutron cross sections, strength functions) employing both high and average experimental energy-resolutions. Present and potential experimental capability to provide quantitative physical information is noted including techniques and sources. Model concepts and parameters relevant to energy-averaged properties (optical model), compound-nucleus reactions (statistical model and fluctuations), collective phenomena (couple-channel model) and nuclear structure are discussed. Applications of these models to measured cross sections and associated properties are made to determine structural properties of nuclear states. The sensitivities of cross sections to various physical model parameters are discussed.

FAST NEUTRON SCATTERING: REACTION MECHANISMS AND NUCLEAR STRUCTURE

A. T. G. Ferguson

Atomic Energy Research Establishment, Harwell, England

I. J. van Heerden

Southern Universities Nuclear Institute, Faure, Republic of South Africa

P. Moldauer and A. Smith

Argonne National Laboratory, Argonne, Ill. U.S.A.

I. INTRODUCTION

It has long been appreciated that inelastic neutron scattering was potentially a powerful tool for the study of nuclear structure. On any objective view however its quantitative contribution to that field has been small by comparison with alternative charged particle techniques. During the last years there has been steady progress in the development of both the experimental techniques for the study of inelastic scattering and of the theoretical framework which enables nuclear structure information to be derived from such measurements. Much of the motivation for such improvements has come from the need for cross section data for use in applications and the need for its theoretical understanding to enable such data to be predicted for nuclei for which there is no possibility of measurement. It will emerge that the main differentiating advantage of neutron inelastic scattering for purposes of spectroscopy are to be found in the domain below four or five MeV. It is therefore with this energy range that we shall principally be concerned. The questions we will attempt to review are

a. What progress has been made in experimental techniques that support our objective?

b. Is there a body of theory that is internally consistent and satisfactory from the theoretical point of view?

c. What evidence have we that current theories give a satisfactory description of experimental observations.

We will first look briefly (Sec.II) at the current theoretical position and then go on (Sec. III) to make some comments on techniques. The main substance of the paper consists of comparisons of experimental observations and theoretical predictions in the general context of (n;n') processes (Sec.IV) and in the special case of the (n;n'γ) reactions with attention to the complimentary nature of the processes and their implica-

tions on nuclear structure and compound-nucleus and direct-reaction mechanisms. Finally, we will attempt to summarize our overview of the situation.

II. BASIC THEORIES AND PRACTICAL POTENTIALS

Neutron scattering proceeds by two mechanisms, direct and compound, described by the unitary S-matrix

$$\underset{\sim}{S} = \underset{\sim}{S}^{d} + \underset{\sim}{S}^{cn} \qquad (1)$$

The direct scattering cross sections exhibit gradual energy variations over several hundred keV and the corresponding neutron-angular distributions are peaked in the forward direction. Compound processes proceed through distinct resonances at low energies and exhibit cross section fluctuations produced by overlapping and interfering resonances at higher energies. The corresponding fluctuating S-matrix energy dependence takes the form

$$S_{cd}^{cn} = -i \sum_{\mu} \frac{\Gamma_{\mu c} \Gamma_{\mu d}}{(E-E_{\mu}) + \frac{1}{2} i \Gamma_{\mu}} \qquad (2)$$

and, in the energy average,

$$\bar{S}^{cn} = -(\pi/\bar{D}) \langle \rho_{\mu} \times \rho_{\mu} \rangle \quad .$$

Energy averaged compound-nucleus cross sections that are smoothed over resonances or fluctuations have gradual energy variations and a fore-to-back symmetry of the associated angular distributions. The interrelation of direct and compound-nucleus processes is prominent in neutron interactions at energies of $\sim$ several MeV particularly where the excitation of collective modes is strong. This is also a region rich in structure information and particularly suited to neutron studies. It is this region that is primarily addressed here.

The energy-averaged cross sections are described by the optical model (O.M.) in which the interaction between the neutron and target nucleus is described by a complex potential well (1). Much of the power of the optical model lies in its simplicity which implies limitations that should be kept in mind. Solutions of the Schrödinger equation with such a complex potential yield the energy-averaged S-matrix, $\bar{S}$, which determines the direct shape-elastic scattering cross section and average-compound-absorption cross sections or transmission coefficients, T, as well as average total cross sections. In principle a relatively small number of measurements should fit the values of the S-matrix. Of these measured values only the average total cross section is directly related to $\bar{S}$ and its precise measurement and interpretation should be a part of any general analysis. This basic fact is too often ignored. Unfortunately the total cross section determines only the real part of $\bar{S}$ and no observable gives a direct determination of its imaginary component. Indirect recourse must be made to the average elastic cross section above several MeV or the

resonance structure at low energies. In the case of deformed or deformable nuclei one must add to the complex potential well certain coupling potentials between neutron channels involving rotationally or vibrationally related levels of the target. The result is a set of coupled Schrödinger equations--the Coupled Channels Optical Model (C.C.O.M.) (2)--which yields direct scattering cross sections not only in the elastic channels but also in all directly coupled inelastic channels, in addition to the average absorption and total cross sections. In these cases $\bar{S}$ is non-diagonal and this is the rule rather than the exception for wide ranges of target nuclei.

The average absorption cross sections provided by the O.M. permit us to calculate the statistical properties of the compound nucleus cross sections. The average compound cross sections are conventionally obtained by means of the Hauser-Feshbach formula (3)

$$\bar{\sigma}^{cn}_{cc'} = \pi\lambda^2 \frac{T_c T_{c'}}{\sum_{c''} T_{c''}} \qquad (3)$$

In many cases this expression must be multiplied by the width-fluctuation correction factor

$$F_{cc'} = \left\langle \frac{\Gamma_c \Gamma_{c'}}{\Gamma} \right\rangle \Big/ \frac{\langle \Gamma_c \rangle \langle \Gamma_{c'} \rangle}{\langle \Gamma \rangle} \, . \qquad (4)$$

which has the effect of enhancing the average compound elastic cross section by factors of up to 3 at low energies and up to 2 at higher energies. Average inelastic cross sections are reduced correspondingly. The origin of this correction lies in the correlation between the fluctuations in the entrance and elastic exit channels.

Detailed calculations have led to somewhat more complicated expressions for the average compound cross section whose evaluation depended upon statistical effects that were difficult to determine. One plausible set of statistical assumptions led to a correction depending upon a parameter Q (4) which we refer to below as the Moldauer-Q-parameter. More recent studies have shown that these additional corrections to the Hauser-Feshbach formula are not widely applicable because of a phenomenon called R-matrix cancellation (5).

In the case of the C.C.O.M. where one has direct inelastic scattering, the calculation of the average compound cross section is complicated by the fact that there may exist correlations in the fluctuations between any directly coupled channels, leading to correlation enhancements of inelastic as well as elastic average cross sections. To calculate average compound cross sections in these cases one must first diagonalize the C.C.O.M. average S-matrix by means of the Engelbrecht-Weidenmüller (E.W.) transformation (6), then compute the fluctuation-corrected Hauser-Feshbach cross sections in this transformed channel space, and finally apply the inverse E.W. transformation to obtain the average compound cross sections connecting the physical coupled channels. For this purpose one needs the complete

C.C.O.M. S-matrix, not just the usually computed elements that connect to the entrance channel.

Average compound inelastic enhancements due to direct coupling are sensitive not only to the transmission coefficients but also to the relative phases of the average S-matrix elements. Large effects are expected only in the vicinity of the causality limit where the determinant of Satchler's penetration matrix $P=\bar{S}\bar{S}^{\dagger}$ vanishes (7). There, enhancements comparable to elastic enhancements can occur.

The statistical theory underlying the calculation of γ-ray angular distributions has been described in detail in the classic paper by Sheldon and Van Patter (8). They assume a Hauser-Feshbach formalism for calculation of the level population. This treatment can readily be modified to include the Moldauer correction factor discussed above (5). An alternative to this which is equally effective is the multiplicative factor proposed by Tepel et al. (9). Neutron inelastic scattering at neutron energies just slightly above the threshold for excitation of a particular level are dominated by S-wave outgoing neutrons and one can obtain model independent limits for the angular distribution of the associated transition. For example consider the excitation of a 3⁻ state from a 0+ ground state. Near threshold the ingoing neutron waves will have $\ell_1 = 3$ with $\ell_2 = 0$. This yields a model independent angular distribution of the ground state transition with angular asymmetry of 2.37. If the state were 3+ the limiting angular distribution would give an angular asymmetry of 3.2. Thus there is clear parity dependence near threshold.

The experimental application of the above concepts requires a suitable model-potential and there are a number of "global" optical models that are qualitatively satisfactory (10). The basic nature of the two nucleon reaction mechanism implies, in the equivalent local approximation, an energy dependence of the real potential strength (11,12,13). This is consistent with the consensus of experimental evidence indicating an approximately linear decrease in real strength of about 0.3 MeV/MeV. With increasing energy, surface absorption gives way to volume absorption. It is odd that many interpretations of neutron processes to tens of MeV tend to ignore this effect. Recent calculations show that the small absorptions at low energies are consistent with observed strength functions (14,15,16) and that increasing values are required for quantitative description of observed neutron cross sections in the few MeV range. Physically this is reasonable as the absorption should be qualitatively proportional to the product of the matrix governing the interaction and the density of states and the latter is roughly proportional to energy. It should be remembered that calculations of nonelastic cross sections can be sensitive to inverse transmission coefficients deduced from a model at energies several MeV removed from the incident energy and that their determination thus will be influenced by the energy dependence of the model parameters. Beyond the problem of energy dependence and the onset of volume absorption there are additional ambiguities in the determination of the surface absorption. Outstanding of these is the inability to accurately identify the components of the product $W \times b$. This is sensitive to deformation as a crude spher-

ical approximation of the deformation leads to increasing values of the surface absorption width, D. Small closure will effect both real and imaginary potential terms (17) and there is a $\frac{N-Z}{A}$ dependence of, at least, the real potential strength (18). Looking in detail at S_0 and S_1 strength functions suggests that both l-dependence and deformation are factors in determining absorption magnitudes (19). In short, even in the lower energy range where the absorption is largely confined to the surface the details of the models are complex and far from easily separable.

Both static and dynamic deformations are a prominent characteristic of the neutron interaction with a wide range of nuclei. Deformations are commonly deduced from (p;p'), (α;α') and coulomb excitation results using first order single approximations and extensive tables of the resulting β_λ coefficients are available (20). More accurate approximations considering the higher order terms (i.e., quadrupole and hexadecapole) lead to smaller β_λ values and inclusion of β_4 gives improved agreement with the measured neutron values (16,21). Pragmatic neutron calculations often consider only the β_2 term and in these cases even smaller values tend to be indicated as the result of the omission of the β_4 term. Considering these factors it is doubtful that the neutron results indicate general substantive differences between deformations deduced from neutron and charged-particle measurements. An exception is near the closed shells where dynamic deformations due to neutron vibrations have been observed (22) to be considerably larger than those due to the corresponding proton vibrations. These widely-present deformations can strongly influence both real and imaginary potential selection by amounts large compared to those attributed to other mechanisms, e.g., parameter variations due to deformation can be several times those attributed to the $\frac{N-Z}{A}$ term of the potential (10). In view of this widespread and relatively strong impact of various types of collective deformations it is probably unfortunate that they have received so little attention until relatively recently.

III. COMMENTS ON TECHNIQUES AND METHODS

Neutron scattering studies have largely employed the pulsed-beam monoenergetic-source time-of-flight techniques originated by Cranberg et al. (23) nearly two decades ago. Over the years this technique has been developed into a good spectroscopic tool with fine resolutions as illustrated, for example, by the studies of the actinide region by Haouat et al. reported elsewhere at this conference. The rate of development in this field has been slow over the last ten years with an improvement of at best a factor two in burst width and little significant increase in peak intensity. Accelerator and source techniques developed in the context of high energy physics could greatly contribute here. The latter offer order-of-magnitude increases in intensity and intensity remains the problem. A limitation of the method is the incident energy resolution of 10-100 keV which prevents the high resolution study of highly fluctuating cross sections. In this problem area intense white-source techniques as employed, for example, by Kinney et al. (24) have had a profound impact that is only now being fully appreciated. In selected cases, such as scattering from ^{56}Fe at energies of < 2.0 MeV, the resolutions are superlative as

illustrated elsewhere in these remarks) and provide a new basis for physical interpretation of both fluctuating elastic and inelastic channels.

Conventional small-sample and ring-geometry (n;n',γ) studies with monoenergetic neutron sources are widely pursued using the high-resolutions and good sensitivities of the large GeLi detectors (25,26). The source is often pulsed for background suppression and resolutions are typically 2-3 keV at 1 MeV. Representative of the measured gamma-ray spectra is that of ^{75}As shown in Fig. 1 obtained at Southern Universities Nuclear Institute (27). A wealth of structure information is available from threshold to several MeV. The exact transitional energies can be precisely determined and the resolution far surpasses that available in the complimentary (n;n') studies. Detector sensitivities can be accurately calibrated using reference standards and neutron flux determined from a reference cross section such as ^{235}U(n;f) or ^{7}Li(n;n',γ) (28) or using a standard counter.

Many of the more interesting (n;n',γ) problems require isotopically separated materials of which only small samples are available. A technique has therefore been developed by Elbakr et al. (29), in which a small 0.01 mole scatterer is placed as close as possible to the neutron source. The observed yield of a particular γ-ray is therefore an average over the incident neutron energy distribution and intensity as well as over the γ-ray angular distribution. Consequently it is described in terms of an average production cross section at an effective neutron energy, and the analytical procedures required for determining these two quantities have been developed (29). Using these techniques the overall errors in the deduced differential cross sections are estimated to be $\lesssim$ 25%. The method has been verified by studies of the "well known" 846.8 keV state in ^{56}Fe with results in agreement with those obtained with conventional larger-sample methods.

As elsewhere in nuclear physics, the small digital computer has had a profound impact. It is widely used in data acquisition and reduction with repertoires of software for use in both (n;n') and (n;n',γ) studies. However, only recently has generally careful attention been given to correction procedures essential to highly quantitative results. It has become all too evident that many of the widely used and simple prescriptions for correcting finite-sample results are deficient and can easily introduce systematic errors of 5-10%. More accurate procedures are warranted (30,31). This fact is evident in the historical trend of well known cross sections (e.g., (n;n',γ) of the 846 keV state of ^{56}Fe) particularly in the region of fluctuations and effects both normalization and angular distributions (32). In the broader and powerful contexts, it is not evident that the digital systems have been employed in a simulation manner correlating physical theory and experimental mockup in a manner common to other high-technology endeavors. The capability exists and should be fully exploited.

IV. SCATTERING CROSS-SECTIONS-THEORY AND EXPERIMENT

A. Global Fits

There have been numbers of attempts to obtain a global fit to all data

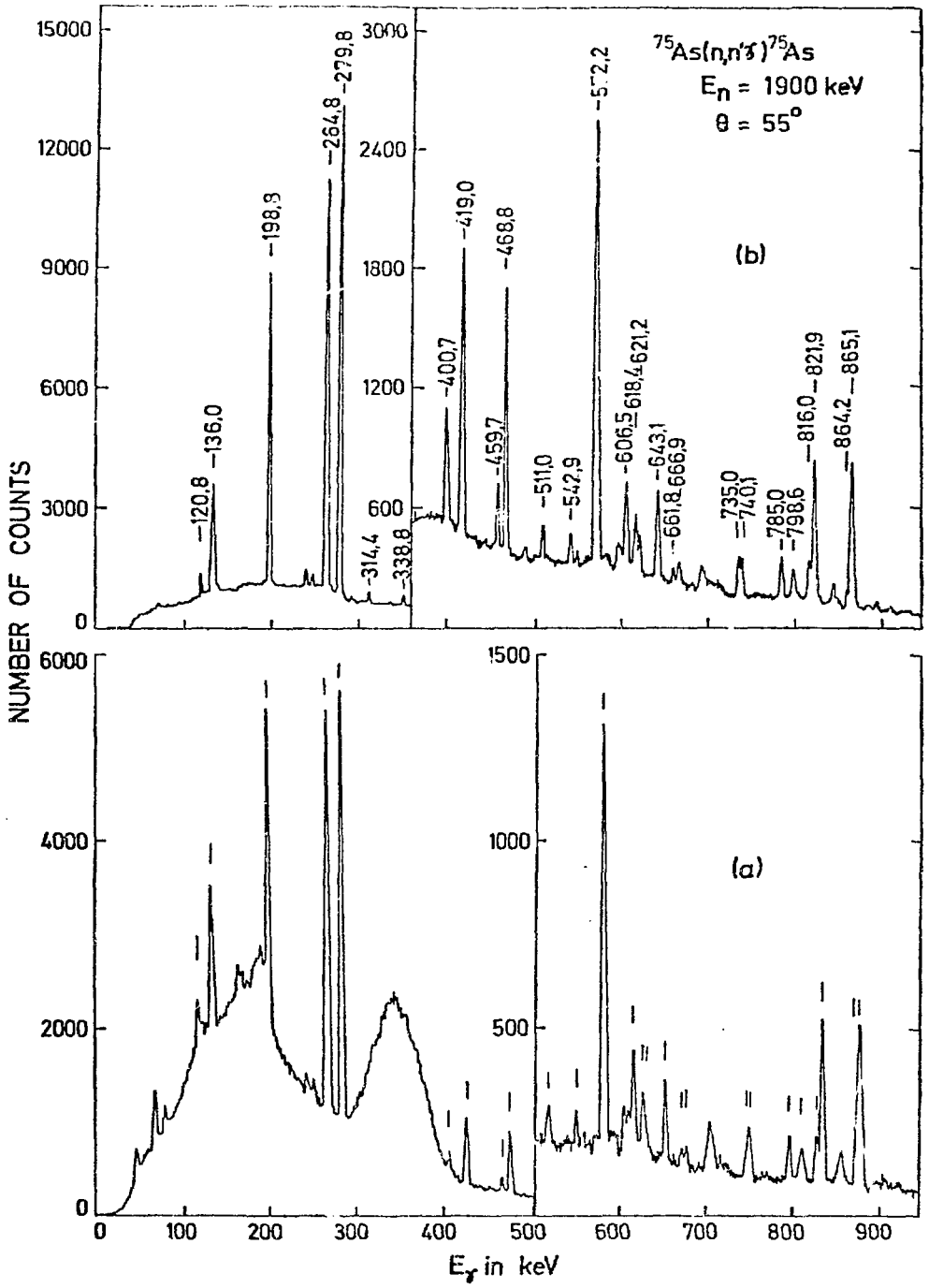

Fig. 1. The gamma-ray spectrum from ^{75}As measured at an incident neutron energy of 1900 keV. The gamma-ray energies are in keV. Spectrum 'A' was obtained with a $^{7}Li(p,n)$ source whereas 'B' was obtained with a $^{3}T(p,n)$ source.

on total, elastic and inelastic cross sections within a defined neutron energy range. At the Antwerp Conference in 1966, Smith et al. (33) presented an analysis of data on inelastic scattering cross sections of neutrons in the energy range 0.3-1.5 MeV. This covered 30 nuclei from A=23 to A=238. Using a spherical optical model and Molduaer-corrected Hauser-Feshbach theory they obtained good qualitative fits across the board with only a few local difficulties. At higher energies dominated by direct processes the model of Perey and Buck has become a classic "bench mark" (11). Over a very wide energy range the model of Engelbrecht and Fiedeldey is notable for its successful description of total cross sections (13).

Recently a similar global view of inelastic scattering has been taken by Almen-Ramström (34) who has made a systematic study in the range 2.0 - 6.5 MeV. She looked at elements ranging from Aℓ to Bi not, however, including any of the strongly deformed rare earths or actinides. The data were compared with the predictions of the fluctuation-corrected Hauser-Feshbach model. The optical model parameters were taken from a global fit to their elastic scattering data by Holmqvist and Wiedling (35). This data set included the same range of elements and energies as the inelastic data. For most of the levels studied in the even-even nuclei, a good fit (within 15%) was obtained with the Moldauer Q parameter set to zero. The exceptions were the first 2+ levels in Fe^{54}, ^{56}Fe, ^{50}Cr, ^{54}Cr and certain sequences of levels in ^{89}Y, ^{93}Nb, ^{115}In and ^{209}Bi where disagreements between measurement and calculation can exceed a factor of two. It is suggested that this may be related to the collective motion-particle coupling character of the states concerned giving significant direct components. None of the strongly deformed nuclei were included in this survey. In the sections that follow we will concentrate mainly on these areas of difficulty such as the region of fluctuating cross sections, the region of strong vibrational phenomena, and the region omitted from this global fit namely the heavy deformed nuclei.

B. Fluctuating Cross Sections

Theoretical estimates indicate large fluctuations in both angle and energy of scattered neutron distributions from mid-weight nuclei (e.g., A=50-70) into the several MeV range (36). Recent very fine resolution studies of neutron scattering from ^{56}Fe by Kinney et al. (37) support the theoretical predictions. These results, illustrated in Fig. 2, are very impressive. The fine resolution of $\sim$ 1 keV clearly shows very large fluctuations in the elastic channel well into the MeV range and the measurements probably still represent some energy averaging over the fluctuations. It is not trivial to compare these high resolution results with broader resolution (e.g., $\Delta E \sim 50$ keV) values as the comparisons are sensitive to the exact energy scales and resolution functions which are not generally well known. Discrete-resonance analysis of this wealth of information is an awesome prospect. However, statistical analysis, now in progress, has the potential for new insight into the compound-nucleus process.

Fluctuations, such as illustrated in Fig. 2, are characteristic of this mass-energy region and they will strongly effect the character of the

more common broad-resolution elastic scattering measurements as illustrated by Ni, V and Co elastic distributions shown in Fig. 3. Even though determined with relatively broad resolutions (25-50 keV) the distributions do not smoothly vary with energy below 3-4 MeV. Any single distribution, regardless of accuracy, does not provide a reliable basis for an O.M. potential. This is illustrated in Fig. 4 where conventional Xi-square O.M. fits to the data give a reasonable representation with O.M. potential parameters that vary considerably from energy to energy--by amounts large compared to detailed aspects of the potential (e.g., $\frac{N-Z}{A}$ dependence).

The above fluctuations persist into the non-elastic channels with very strong effects and attendant problems as illustrated by the recent (n;n',γ) and (n;n') studies of Kinney et al. (37), D. Smith (38) and A. Smith (39) outlined in Fig. 5. White-source techniques show strong fluctuations to $\tilde{\sim}$ 2.0 MeV. The normalization relative to the ^{7}Li(n;n',γ) standard has been confirmed using broad ($\tilde{\sim}$ 50 keV) resolutions and ^{235}U(n,f) standards and by direct determination of the corresponding (n;n') cross section relative to the basic H(n,n) cross section. When taken in a broad scope, the results obtained with $\tilde{\sim}$ 50 keV resolutions are very consistent with the average values of the high resolution results. However, again the energy-averaged measurements are sensitive to exact energy scales and experimental resolutions and thus comparisons at isolated energies can be very deceptive not only between experiments but also in comparisons with energy-averaged theory. This remains true even when the experimental resolutions are large ($\tilde{\sim}$ 100 keV). This is a particular concern when reactions such as ^{56}Fe inelastic processes are employed as reference standards in the few MeV region. Moreover, Kinney et al. have observed large fluctuations in the angular distributions of gamma-rays emitted in the (n;n',γ) process in ^{56}Fe and these include relatively strong P_4 terms. The strength of the latter have been verified in broader-resolution measurements by D. Smith. In these instances the common practice of assuming P_2 distributions and limiting measurements to angles corresponding to P_2 nodes will not yield quantitatively accurate angle-integrated cross sections.

The capability of energy-average theory to describe the trends of the fluctuating cross sections are illustrated in Fig. 4. The conventional Hauser-Feshbach calculation characteristically leads to too large average cross sections. Width fluctuation corrections in the manner of Moldauer (4) lead to a much more appropriate description of the measured values. An alternative use of the "correlation enhancement correction" of Tepel et al. (9) leads to essentially the same result in practical applications and the method has well described the energy-average angular distributions of the emitted quanta.

Deformation can influence the fluctuating structure in a characteristic manner as shown by calculations of Moldauer et al. (40). The character of the fluctuating cross sections can be estimated from the energy average parameters. Such an approach has been applied to the calculation of total and inelastic scattering cross sections of titanium. Cross sections calculated with a spherical model and a vibrational-coupling model are qualitatively different with the ellipsoidal (vibrational-coupling)

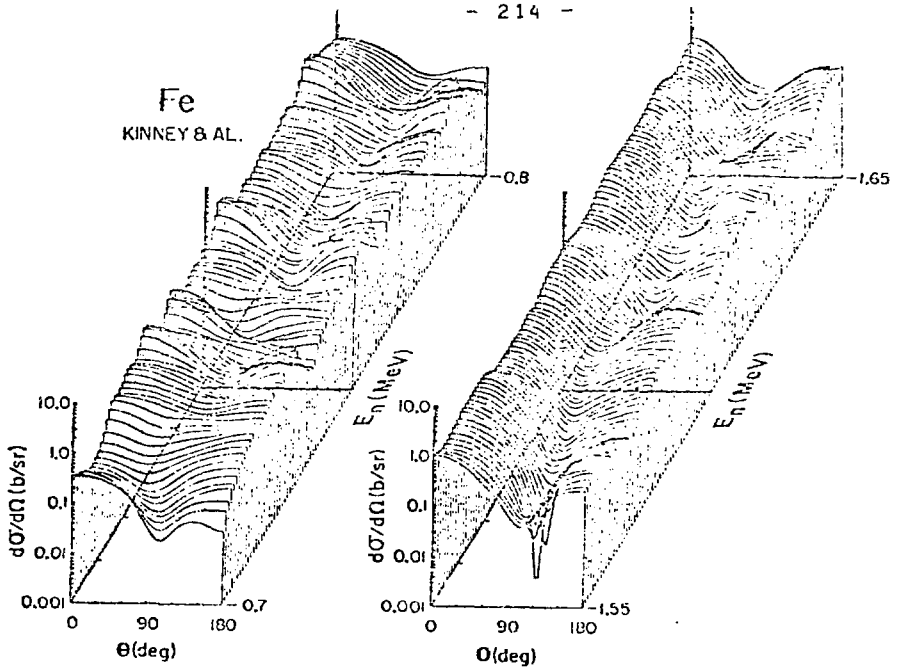

Fig. 2. High resolution elastic scattering cross sections of iron measured by Kinney et al. (37).

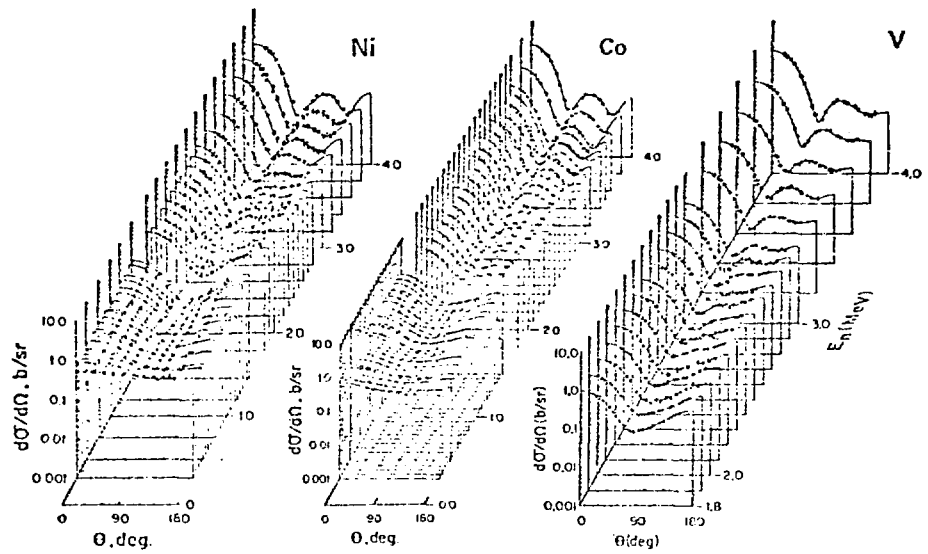

Fig. 3. Differential elastic neutron scattering cross sections of Ni, Co and V (39,41 and 43).

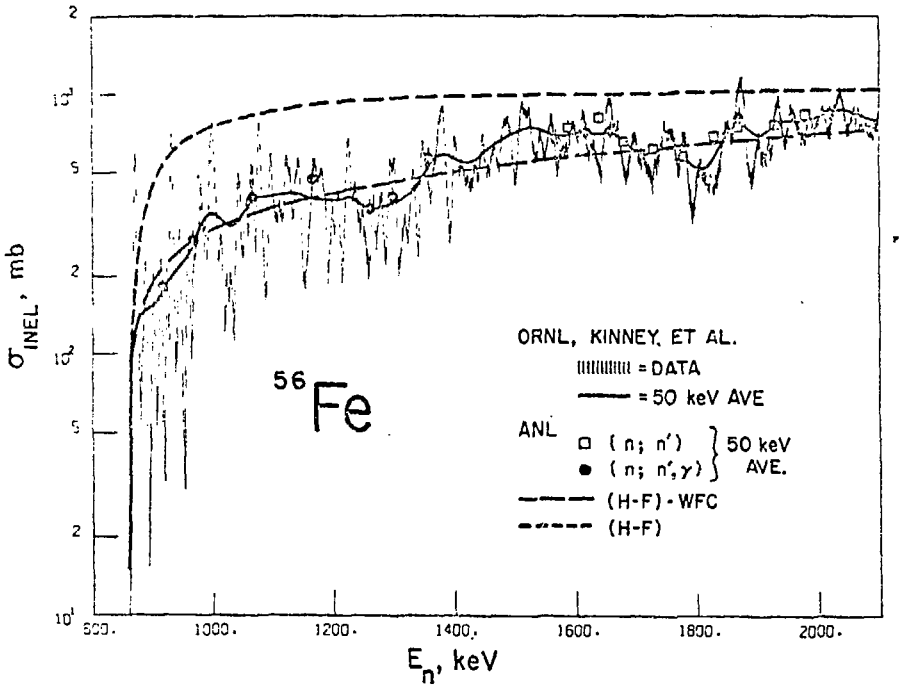

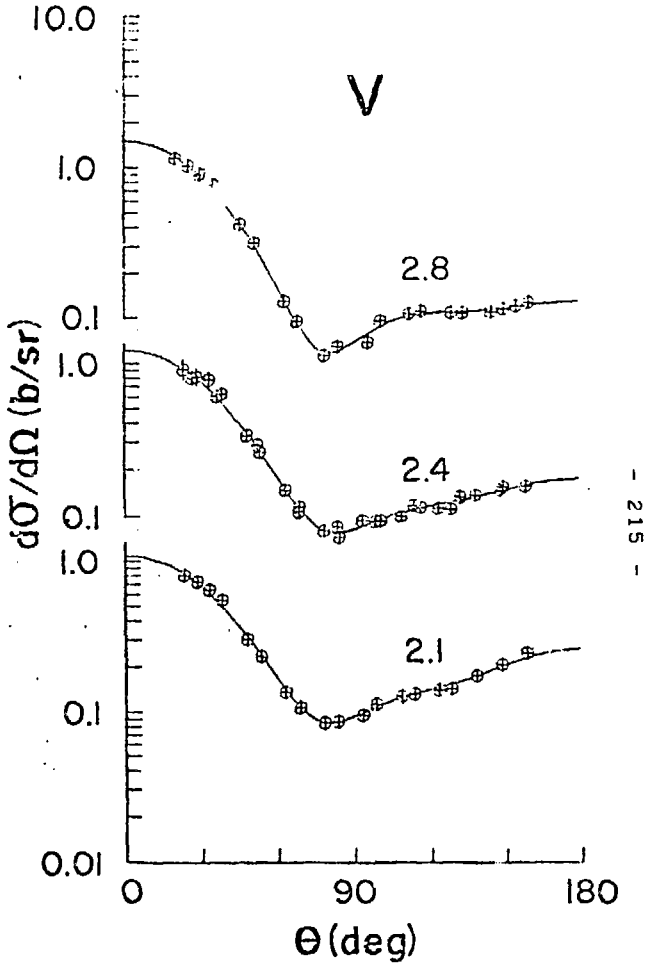

Fig. 4. (right) Measured differential elastic scattering cross sections of vanadium (39) and curves indicating the results of six parameter Xi-square optical model fit to the data.

Fig. 5 (up) Inelastic neutron excitation of the 846 keV state of Fe-56. High resolution results of Kinney et al. (24) are compared with broad resolution (n;n') and (n;n',gamma) results of refs. 38 and 39. Energy-averaged cross sections calculated with the Hauser-Feshbach formula with and without corrections are indicated by dashed curves.

model yielding results much more descriptive of experiment. This titanium example is an extreme case. However, other nuclei in this region have appreciable vibrational coupling with consequently similar behavior of fluctuating structure. The present calculations are qualitative, the computational techniques approximate and costly but the relatively strong and qualitative influence of the vibrational reaction on the fluctuating structure gives emphasis to the importance of the direct reaction mechanism and can guide the choice of energy-average potentials.

The more common knowledge of inelastic scattering in this region is based upon energy averaged results lacking the resolution of the above ^{56}Fe example. There is a characteristic rapid transition over the few MeV range from single or few open channels with attendant uncertainties in channel correlations to a complexity of channels that cannot at present be resolved experimentally. The result is a relatively narrow energy "window" most favorable for the analysis of the associated structure. Even with these limitations, analysis of measured (n;n') cross sections has given new structure insight. For example, studies of ^{59}Co have resolved alternate spin assignments in the few MeV range consistent with the concept of a proton hole in the $f_{7/2}$ shell (41) assuming deformation in the manner of Mottelson and Nilsson (42).

C. Potentials and Deformation near A≈100

Elastic neutron scattering measurements over a relatively broad energy range in this mass region provide a basis for models subsequently applicable to structure assay. Illustrative of such comprehensive results is elastic scattering from the isotopes of molybdenum shown in Fig. 6. (44). Measurements such as these give good definition of the parameters of a conventional spherical optical potential. The sampling is sufficiently large to mitigate the effects of fluctuations which remain appreciable in this region (45). However, there are ambiguities in the interpretation. At energies of 3-5 MeV compound elastic contributions remain significant. Their quantitative calculation is uncertain due to a lack of knowledge of channel competition and recourse must be made to statistical-average properties. At lower energies with only a few open compound-nucleus channels, resonance-correlation enhancement of selected channels can be large (see Sec.II). We do not know how to calculate rigorously such contributions. Contemporary practice amounts to little more than a renormalization of width-fluctuation-corrected Hauser-Feshbach estimates (e.g., use of the Moldauer "Q" parameter) with adjustments of Q to obtain agreement with experiment as illustrated in Fig. 7. The angular distributions of neutrons corresponding to the excitation of certain states have characteristic signatures; for example, those concave distributions corresponding to the 0+ states shown in Fig. 7. An additional factor is the known large deformation of many of the isotopes in this mass region which can strongly affect the above simple spherical models. For example, the heavier molybdenum isotopes are strongly deformed (20) with characteristics of both vibrational and rotational phenomena (e.g., ^{100}Mo). Such deformation effects can strongly influence the interpretation as illustrated in Fig. 8. Potential parameters deduced from deformed and spherical bases are con-

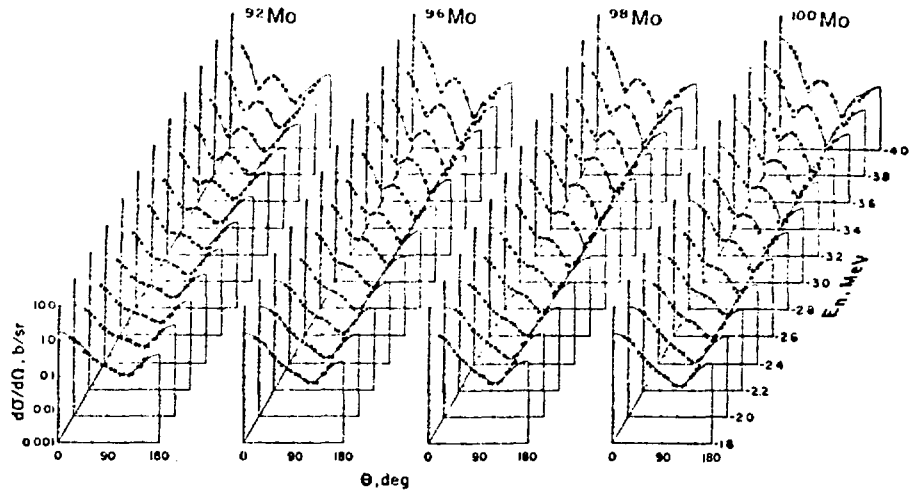

Fig. 6. Differential elastic neutron scattering cross sections of Mo-92,96,98 and 100. Curves indicate the results of a spherical optical model fit to the data using a single potential (44).

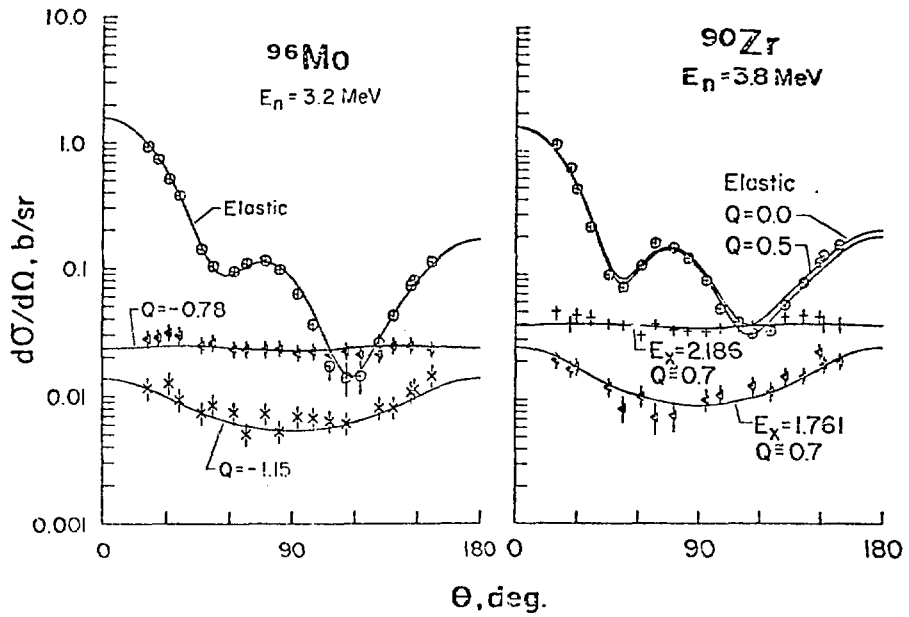

Fig. 7. Right--The differential scattering of 3.8 MeV neutrons from Zr-90. Data points indicate the results of ref. 48. Excitation energies are given in MeV. Curves were obtained with the corrected H-F formula using the indicated correlation parameter,Q, values.

Left--The differential scattering of 3.2 MeV neutrons from Mo-96(44). Curves indicate calculated results, excitation energies, Q, are give in MeV.

siderably different and by amounts large compared to those attributed to other potential properties (e.g., $\frac{N-Z}{A}$ dependence).(46 and 18). Similar importance of deformation in these molybdenum isotopes has been noted in (p;n) studies (47). Certainly, deformation should be a consideration in the physical interpretationiin this region and with it comes additional parameters and computational complexity that tend to destroy simplicity and uniqueness.

In some cases, such as ^{90}Zr, the excited structure is reasonably known and with the above potentials and measured (n;n') cross sections a qualitative test of physical understanding is possible as a transition is made from single to many compound-nucleus exit channels (48). Such comparisons are illustrated in Fig. 9. All calculations employed the width-fluctuation-corrected Hauser-Feshbach formula. Near the first few thresholds this result lies pronouncedly lower than the measured values (lower curves) but the discrepancy decreases with increasing energy and the opening of many additional channels. Enhancement of the first inelastic group is particularly strong (934 keV, 2+ state) and similar enhancement has been noted in the compound-elastic component. However, there remains a consistent discrepancy between enhancement factors indicated by the (n;n) and the (n;n') measurements. This example is probably illustrative of the current shortcomings in compound-nucleus computational capability. Well above the first few thresholds with many open channels comparison of calculation and measurement is more rewarding and has led to better understanding of the spins of a number of the excited states of this nucleus. Other (n;n') cross section results are somewhat better described by theory as indicated by the ^{100}Mo values of Fig. 9 (44). Neutrons corresponding to the excitation of more than ten "states" in ^{100}Mo have been observed (many corresponding to multiplets of states). This nucleus is strongly deformed and, as noted above, potential selection is sensitive to that deformation. However, at these illustrated energies deformation has small qualitative impact upon discrete inelastic cross sections. The first two states (0.54 MeV, 2+; 0.69 MeV, 0+) are well known and cross sections calculated with the width fluctuation corrected Hauser-Feshbach formula are reasonably consistent with observation. The measured values and associated interpretation support the suggested doublet character of higher lying states (e.g., 1.766 and 1.770 MeV) and give some guidance as to suggested spins.

Recent (n;n) and (n;n') studies by Reitmann et al. (49) suggest a strong parity dependence of the optical potential in the region of isomerism near A=100. Neutron scattering and associated (n;n',γ) studies of the interaction of fast neutrons with ^{103}Rh could not be described by a single potential and there was observed a strong parity conservation associated with the (n;n',γ) transitions. This is illustrated by the measured and calculated (n;n') cross sections of Fig. 10. A potential giving a good description of the elastic reaction and the negative parity inelastic cross sections was grossly different from that found suitable for the excitation of positive parity states even when careful attention was given to theoretical correction factors (9). The interpretation suggests a 10% parity dependence of the real potential and nearly a factor of two for the imaginary potential. These are very large changes. Retrospective examination of similar scattering processes in this mass-energy region suggest a

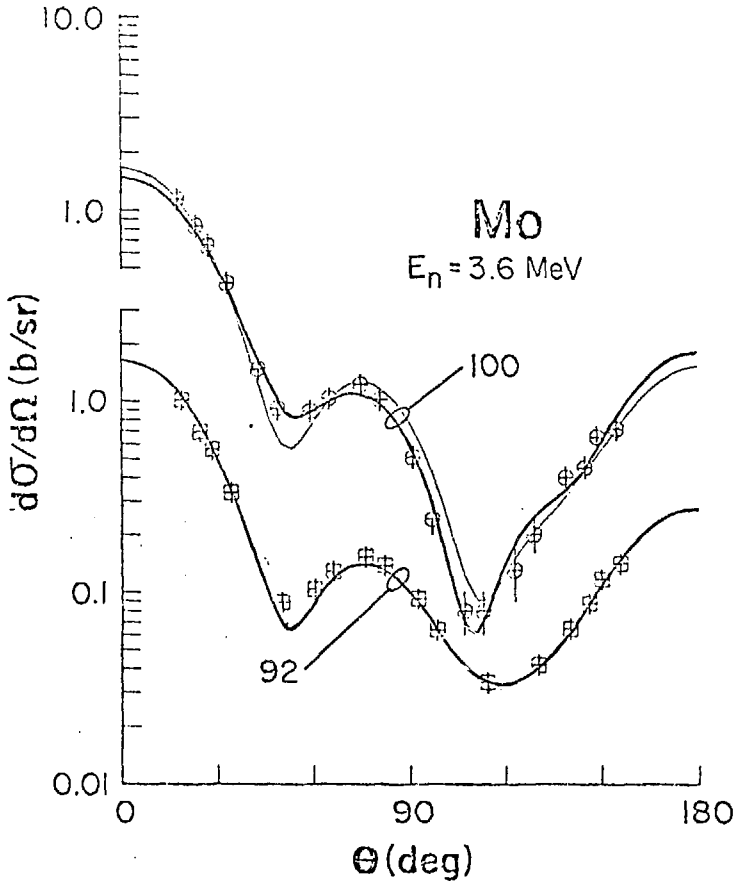

Fig.-8. Measured and calculated neutron elastic scattering from Mo-92 and Mo-100 at 3.6 MeV (44). The heavy curves were obtained using the same potential and known variations in deformation. The light curve indicates the results obtained with the addition of the (N-Z)/A term in the potential.

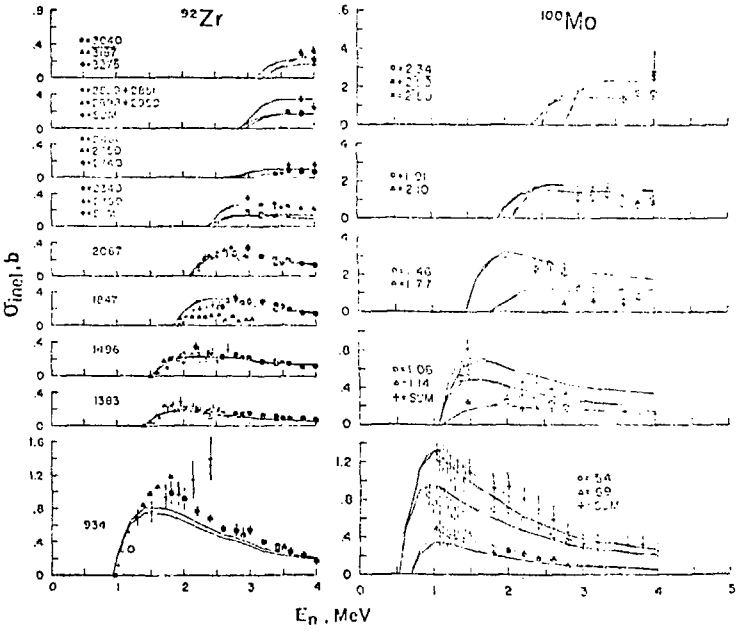

Fig.-9. Left--Inelastic neutron excitation cross sections of Zr-92. Excitation energies are given in keV. Data points indicate results of both (n;n') and (n;n',gamma) measurements as defined in ref.48. Curves denote the results of calculation; where there are two curves the upper one is inclusive of the correction factors to the H-F formula.

Right--Inelastic neutron excitation cross sections of Mo-100. Measured values are from ref. 44. Dotted curves are "eye-guides" to the data, solid curves the results of corrected H-F calculations.

similar strong parity dependence of the potential (e.g., ^{93}Nb and ^{115}In; (50 and 34)) and it is noted that historically "global" parameter sets tend to have difficulties in this region. A possible explanation is a strong l-dependence of the potential in this region of minimal s-wave and maximal p-wave strength functions and this is suggested by some recent strength function interpretations (51). An alternative is a basically different character of the positive and negative parity states and this may be more consistent with the strong observed parity conservation in the (n;n',γ) processes. As another alternative, the two classes of state may also have different deformations.

D. Statically Deformed Rotational Nuclei

In the region A=180-190 the statically deformed nuclei start the transition to sphericity with rapid changes in deformation and collective structures. The even isotopes of tungsten are in this region and attractive experimentally as the low-lying rotational structure can be clearly resolved using time-of-flight techniques. Detailed elastic-and inelastic-neutron scattering and total-neutron cross sections have recently been obtained for the three isotopes ^{182}W, ^{183}W and ^{186}W over a wide energy and angle range as illustrated in Figs.11,12 and 13 (52). These results provide a good foundation for model and structure interpretations extending from low-energies where compound-nucleus processes are major factors to 3-4 MeV where elastic and low-lying inelastic components are essentially entirely due to direct reactions.

The inelastic processes generally fall into two categories. The first is associated with the ground-state rotational band predominently excited by direct processes at several MeV energies. The second is the excitation of the many higher lying states proceeding largely through the compound-nucleus mechanism. In this latter category are 15-30 observed "states" in each of these three isotopes, many of them undoubtedly multiplets. The experimental time distributions are complex. The observed inelastic neutrons are generally emitted approximately isotropically excepting those associated with 0+ states characteristic of the onset of the β-vibrational band. As the energy increases the number of open channels grows very rapidly and the corresponding individual cross sections become very much smaller. Some of the aspects of these inelastic processes are illustrated in Fig. 12. The low-lying states are well defined over a large energy range. The higher-lying levels rapidly increase resulting in a cumulative inelastic cross section of $\tilde{\sim}$ 3.9 b at 2.5 MeV. That magnitude is consistent to within $\tilde{\sim}$ 10% with the observed elastic and total neutron cross sections. The cumulative sum of inelastic cross sections has steps which suggest the onset of band structure.

At energies of a few MeV a coupled-channel model assuming quadrupole and hexadecapole static deformation (or alternately, reduced quadrupole strength alone) well describes elastic and ground-state-rotational-band inelastic distributions (see Fig. 11) and the total cross section. At

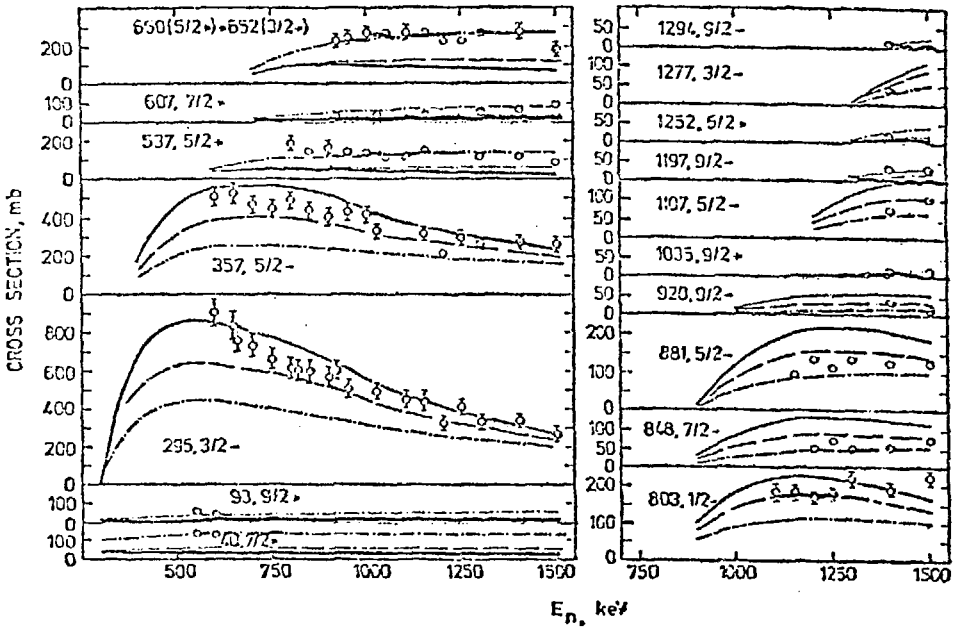

Fig.-10, (up) Inelastic neutron scattering cross sctions of Rh-103 from ref. 49, Reitmann et al. Data points indicate measured values. The -.-.-.-.- curve indicates results calculated with the "positive parity" potential and the ------ curve those with a negative parity potential as described in ref. 49.

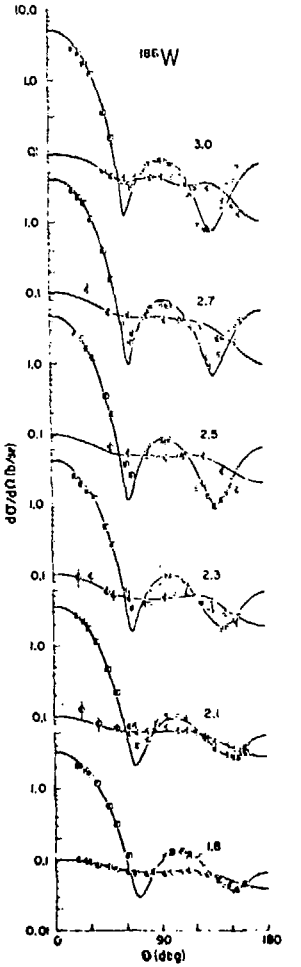

Fig.-11, (right) Differential cross sections for elastic and inelastic (E_x=0.122 MeV) scattering from W-186. Measured values are indicated by data points. The curves indicate the results of coupled-channel calculations as described inthe text and ref. 52.

lower energies compound-nucleus contributions are large, width-fluctuation-corrections significant and an enhancement of the compound-elastic contribution is indicated. The same model is also suitable for describing angle-integrated inelastic cross sections (Fig. 12). The direct excitation of the first two members of the ground-state rotational band is large above several MeV. Theoretical prediction of the higher-excited states is less certain particularly above $\sim$ 1.6 MeV comparison of measurement and calculation suggests the assignment of prominent band heads systematically correlated with similar ^{184}W and ^{182}W results.

The above interpretations were primarily developed in the context of ^{186}W and led to β_2 values of 0.180. The model was then examined in the context of ^{184}W and ^{182}W limiting parameter variations to the magnitude of the deformation. An illustrative result is shown in Fig. 13. The neutron measurements indicate $^{182}\beta_2$ is about 10% larger than $^{186}\beta_2$. This is very similar to the relative change deduced from coulomb excitation studies (20) but the magnitude of β_2 deduced from the neutron results is approximately 20% lower than that indicated from coulomb excitation studies. As noted above (Sec.II), this difference is expected from approximations commonly employed in coulomb excitation interpretations and probably does not reflect any true measurable difference in deformation as derived from the neutron and charged-particle processes. From Fig. 13, it is also evident that the neutron sensitivity to deformation is most significant in the elastic process at large scattering angles in this mass-energy region. The same angular area is sensitive to the relative contributions of β_2 and β_4 components. Thus measurements at very large scattering angles seem to have a possible potential for better identifying the character of deformation in this region including the relative importance of β_2 and β_4 terms and possible differences between results obtained with neutron and charged-particle probes.

E. The Even-Even Actinides

Neutron scattering from the even-even actinides has much the same character as that from the above rotational nuclei but is experimentally more formidable due to the closer spacing of the collective structures. However, excellent experimental resolutions are providing quantitative results as illustrated by the work of Haouat et al., reported at this conference (53). The prominent excitation is that of the first rotational state (2+) at $\sim$ 50 keV yet the experimental resolution is sufficent to reasonably resolve this and associated components at a number of angles. Such results obtained at Bruyeres-le-Chatel, Lowell and Argonne are reasonably consistent and confirm the large angular anisotropies predicted by theory as illustrated in Fig. 14. At these energies the processes are essentially all direct reaction. Calculations based upon this assumption and using the model developed in the context of the tungsten isotopes (see above) are qualitatively descriptive of the measured values. They also give detailed quantitative agreement with the subsequent measurements while concurrently well describing total and elastic scattering cross sections. Alternate models give different results (53) particularly for the excitation of the 4+(148 keV) state and there are large uncertainties at forward

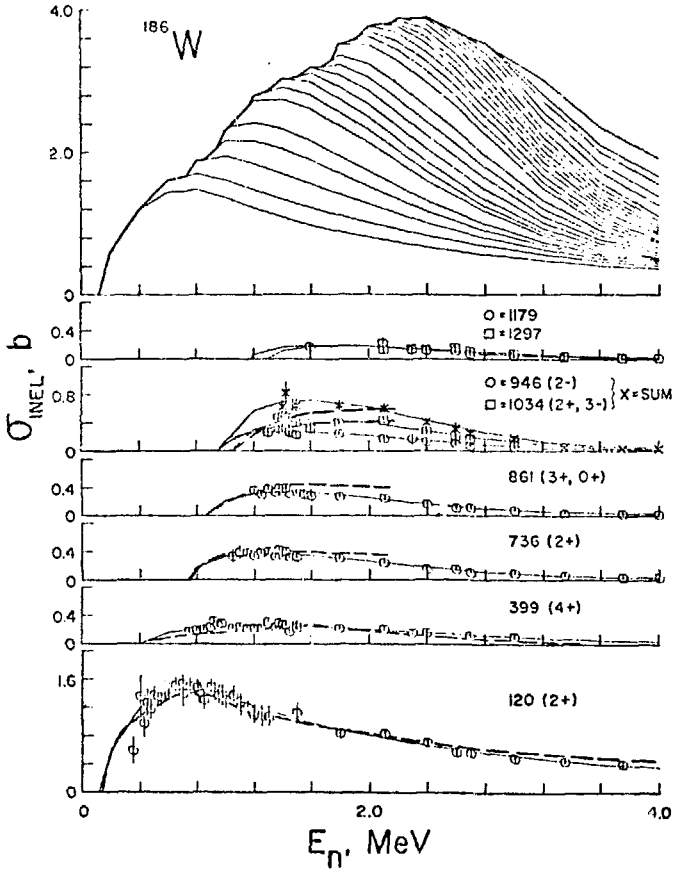

Fig.-12. Inelastic neutron scattering cross sections of W-186 (52). Measured values for the first observed six states are shown. Solid curves are "eye-guides" and dashed curves the results of calculations as described in the text. The upper curve indicates the cummulative inelastic scattering cross section due to the excitation of 24 observed "states".

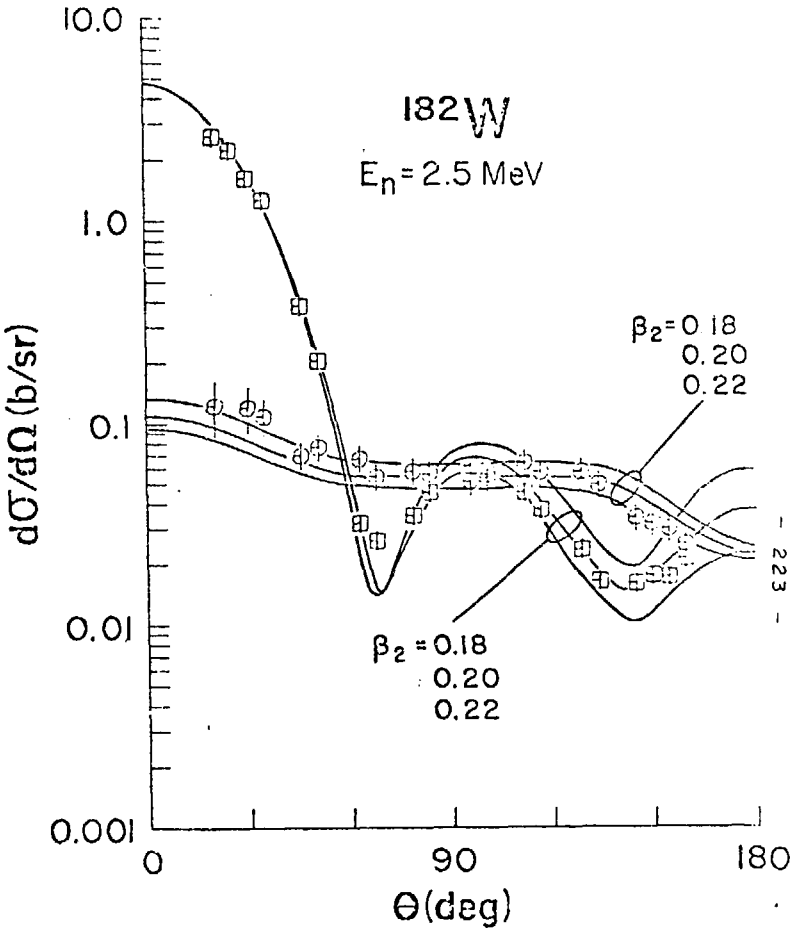

Fig. 13. Measured and calculated elastic and inelastic (E_x=0.120 MeV) neutron scattering from W-182. Calculations are explicitly based on the model developed from W-186 (see Fig.-11) with the indicated variations in the deformation parameter, beta-2. Larger beta-2 results in smaller back-angle elastic scattering and conversely for the inelastic process.

angles. Even given these shortcomings these results suggest a qualitative understanding of these direct-inelastic processes sufficient for the reasonable deduction of angle-integrated values as illustrated in Fig. 15.

As the energy decreases the compound-nucleus mechanism becomes prominent and our understanding deteriorates. Total cross sections present some theoretical difficulties. Good agreement with measured strength functions is achieved by reduced absorption which adversely effects inelastic compound nucleus contributions tending to under-predict the measured values. In addition there is indication of strong enhancement of the inelastic channels. In the few 100 keV region the measured excitations of the first state tend to show persistent structure that has not been theoretically explained (56). With these complexities and uncertainties it is attractive to quantitatively define a model in the simpler spherical region near A=208 then extend it to the actinide region introducing only the concept of deformation. Such an approach has the additional advantage of similar values of $\frac{N-Z}{A}$ at A$\sim$208 and for the common actinides. This avenue has been pursued using ^{206}Pb, ^{207}Pb, ^{208}Pb, ^{209}Bi and ^{238}U with the results shown in Fig. 16 (57). A relatively good description of the measured ^{238}U elastic distribution at 554 keV was obtained. Extrapolations to higher energies and to the total cross sections to 10 MeV are also good. The model is at least as good in many aspects as those specially tailored to ^{238}U (16). However, the troublesome problem of channel correlations remains and, typically, the compound-elastic enhancement indicated by experiment is $\sim$ 40%. Moreover, there is a consistent tendancy for experiments to yield a stronger forward peaking of the inelastic cross section than predicted by C.C.O.M. theory. An interesting characteristic of the potentials developed near A$\sim$208 is an apparent minimum in the real potential strength at A=208 and there is the known minimum in the imaginary potential near shell closures (58,59). These effects appear relatively stronger than the general overall $\frac{N-Z}{A}$ dependence of "global" model sets.

The compound-nucleus process continues to dominate inelastic neutron scattering in the actinides to higher excitations and incident energies of more than an MeV. The requisite measurements are difficult but complimentary use of (n;n') and (n;n'γ) techniques is now providing a new insight into the structure of deformed actinides. This is perhaps best illustrated by the recent studies of ^{232}Th by McMurray et al. (60). The neutron scattering aspects of this study are indicated in Fig. 17 and the corresponding (n;n'γ) measurements and associated structure interpretation are discussed below.

V. THE (n;n'γ) PROCESS

A. Correlation with the (n;n') Process and Structure

During the last ten years there has been a steady increase in the amount of research being carried out on γ-rays from neutron inelastic scattering and the nuclei studied cover the entire mass region to Pu. Some ^{232}Th(n,n'γ) results (60) recently obtained at the Southern Universities Nuclear Institute, can serve as an example of how such measurements are

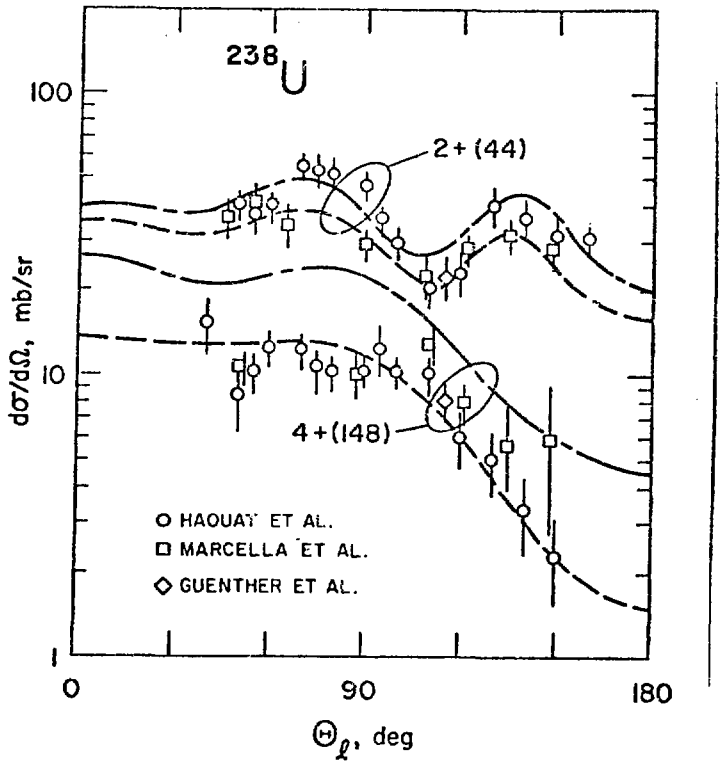

Fig.-14. Differential cross sections for the excitation of the 45 keV (2+) and 148 keV (4+) states of U-238 by 2.5 MeV neutrons. Results of Haouat et al. (53), Guenther et al.(54) and Marcella et al. (55) are given as indicated. Curves indicate results of coupled-shannel calculations; the upper set from ref. 53 and the lower from ref. 54.

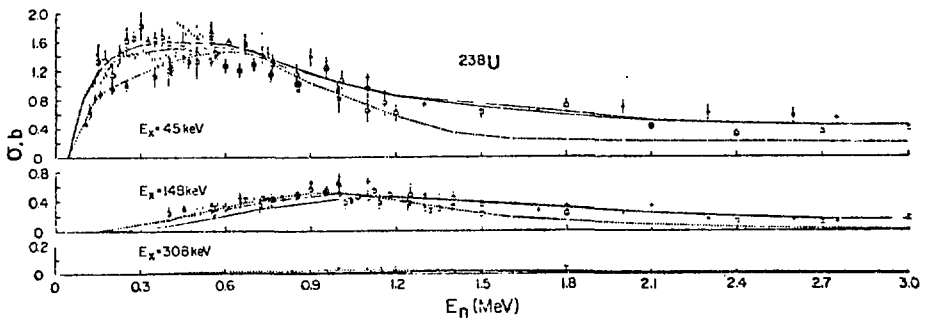

Fig.-15. Cross sections for the inelastic neutron excitation of the ground-state rotational band of U-238. Data values are defined in ref. 54. The solid and coarse-dashed curves indicate two evaluated data sets. the fine-dashed curve is the result of model calculations including both compound-nucleus and direct-reaction components as described in ref. 54.

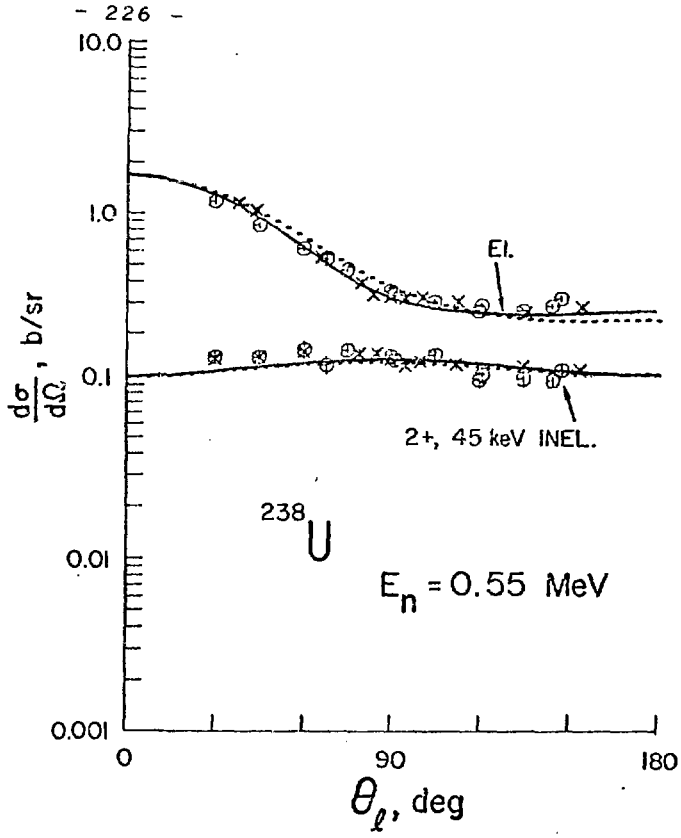

Fig.-16.(right) Scattering of 550 keV neutrons from U-238. Data values taken from refs. 54 and 71. The solid curves are the result of deformed model calculations based upon a potential developed in the spherical region of A=208 (57). The dashed curve indicates a similiar calculation based upon the potential of LaGrange.(16).

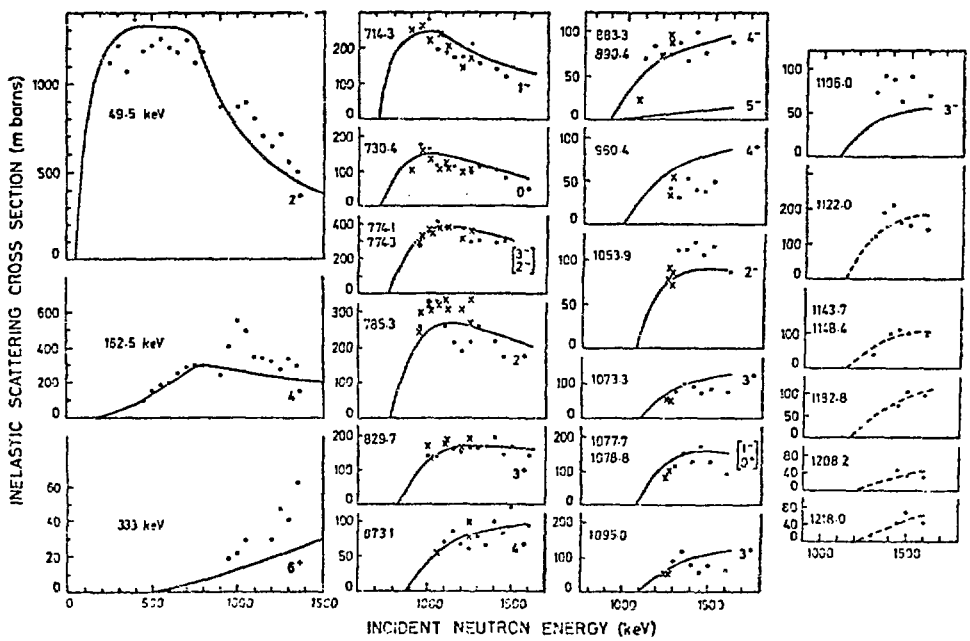

Fig.-17. Neutron inelastic excitation cross sections of Th-232 as determined by McMurray et al. (50). Measured values are indicated by data points. Curves denote the results of statistical (H-F) calculations using the indicated spins and parities.

interpreted. In these measurements γ-ray spectra produced at $\theta_\gamma = 90°$ by neutron inelastic scattering from the ^{232}Th nucleus were obtained at neutron energies ranging from 750 to 2100 keV. Fig. 18 illustrates the results obtained. The strength of the (n,n'γ) method in providing data on the relative cross sections of closely spaced levels, previously unresolved in (n,n') studies, can be illustrated by reference to the close lying doublet of states at 774.1 and 774.3 keV. The 774.1 keV level decays directly to the ground-state and the decay γ-ray has an entirely different excitation shape from the two decay γ-rays of the 774.3 keV level. The level and decay scheme shown in Fig. 19 has been deduced from the measured γ-ray energies, the energy thresholds, excitation shapes and the existence of any branch decays. Preliminary γ-ray angular distributions have been determined and the angle-integrated cross sections compared with the directly observed (n;n') values shown in Fig. 17. The indicated theoretical values were obtained using the Hauser-Feshbach formula with the variable enhancement corrections of Tepel et al. (9). For those levels with spin and parity values known from Coulomb excitation studies, the predicted curves show good agreement with the excitation curves directly obtained from neutron time-of-flight measurements. However, it is obvious that in this case the (n;n'γ) reaction studies cannot provide directly comparable (n,n') cross section data, presumably due to the existence of EO transitions not involving γ-ray emission, internal conversion, etc. Electric monopole transitions (EO) have, in fact, been observed in coulomb excitation studies (72) for the 730.4, 774.3, 785.3 and 873.1 keV levels in ^{232}Th. These results show that for the K = 0 band about one-third of the population of levels in this band, viz., the 730.4 (0^+), 774.3 (2^+) and 873.1 (4^+) keV levels, decay via electric monopole de-excitation to the ground-state band. Taking these EO transitions into account, there is a much closer agreement between the directly measured neutron inelastic scattering cross sections and those obtained from (n;n'γ) measurements.

The close neutron source-to-scatterer geometry, outlined in Sec. III, has been used to study the ^{114}Cd and ^{116}Cd nuclei (61), two nuclei in the rare earth region, ^{154}Sm (62,63) and ^{160}Gd (Ref. (66) and also the ^{203}Tℓ and ^{205}Tℓ nuclei (64). For each nucleus studied, γ-ray spectra from neutron inelastic scattering were obtained over a wide range of incident neutron energies. Fig. 20 shows a typical "scatterer-in minus scatterer-out" γ-ray spectrum obtained from ^{154}Sm with incident neutrons of maximum energy 1.7 MeV. Gamma-ray spectra such as these were used to determine level positions and decay modes for all the nuclei studied. For spin assignments the (n,n') excitation curves experimentally obtained were compared with Hauser-Feshbach theory and Fig. 21 shows the experimental and theoretical cross sections that have been obtained for the 1351, 1378 and 1381 keV levels in ^{160}Gd.

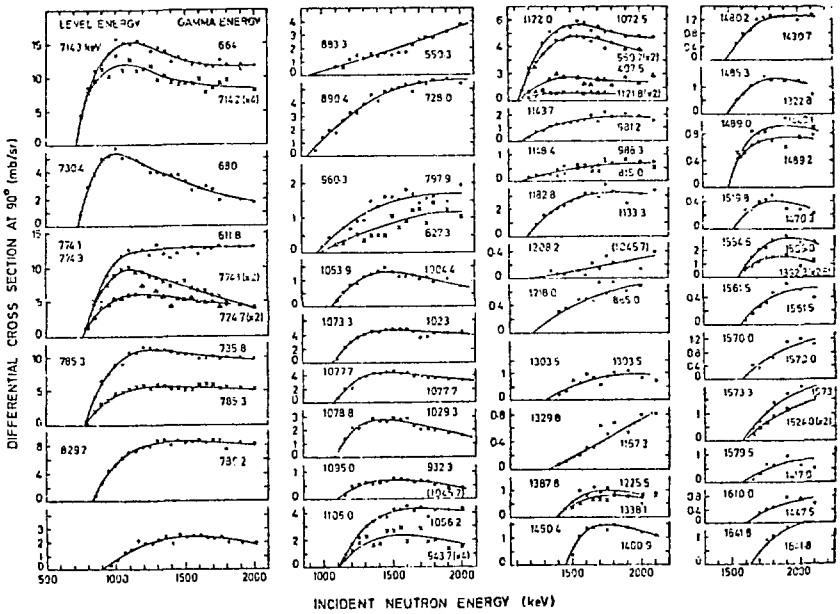

Fig.-18. Differential gamma-ray production cross sections for the Th-232 (n;n',gamma) reaction (60). The gamma-ray energies are given on the right and the deduced level energies on the left of each figure section.

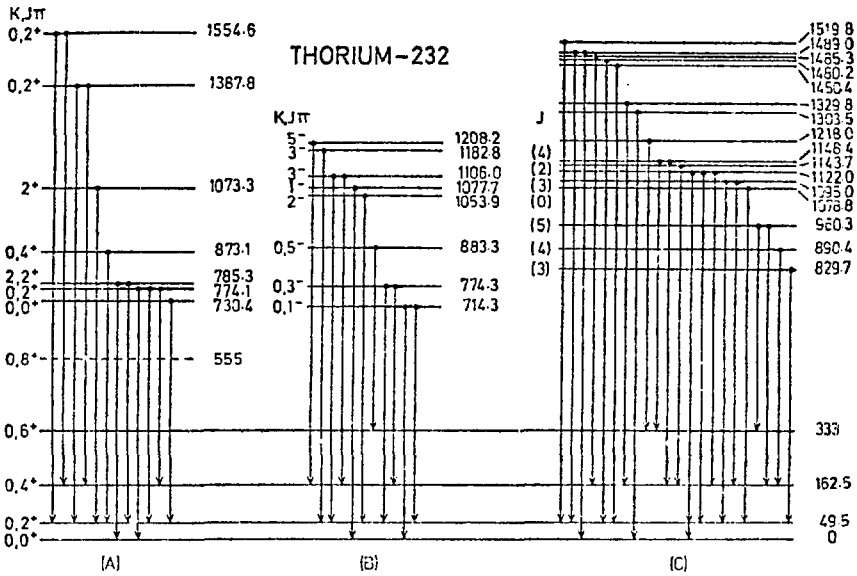

Fig.-19. The Th-232 level energies and decay transitions deduced from (n;n',gamma) measurements (60). The levels marked (A) and (B) are the positive and negative parity levels that have also been observed in coulomb excitation studies.

B. Determination of Spin Values and Mixing Ratios From Angular Distributions

Accurate (n;n'γ) angular distribution results have now been obtained for a large number of nuclei over the entire mass region. In many cases a comparison of the experimental results with statistical model predictions of Sec. II has been very useful for determination of spin assignments. Due to the rapid rise of the (n;n') cross section above threshold, it is also possible to measure the angular distribution of a particular transition γ-ray just slightly above its threshold. It is well known that, if the spin J_i of the emitting level is greater than the ground-state spin J_o, the γ-ray anisotropy depends very sensitively on the spins of the initial and final states and on the multipole character of the γ-ray. For levels with $J_i > J_o$, it is therefore often possible, using procedures developed by Sheldon and van Patter (8), to use angular distribution measurements to obtain the nuclear level spins and the mixing ratios of mixed multipole γ-ray transitions.

As an example of the utilization of (n;n'γ) angular distributions for spin assignments involving transitions of mixed multipolarity, one can refer to the recent ^{120}Sn results of Kikuchi and Sugiyama (65). Their distributions are shown in Fig. 22. Analysis as a function of the multipole mixing ratio has been performed for these γ-ray transitions and the calculated angular distributions giving minimum χ^2 values for each illustrated $J_i \rightarrow J_f$ transition. The 412 keV γ-ray is a transition from a level at 2.699 MeV to a 5^- level at 2.267 MeV. The angular distribution seems to indicate a spin of 4 for this level, and a mixing ratio of 0.31 ± 0.15 for a suggested E1/M2 admixture. For all the other γ-ray transitions the observed angular distributions seem to indicate spins of either 2 or 3 for the initial levels. For some of these levels it was, however, possible to decide between these two spin values by comparing the observed branching ratios with those derived from single particle estimates.

The small sample method can also be used for studying γ-ray angular distributions from the (n;n'γ) reaction (66). Here the γ-ray angular distribution, $W(\bar{E}_n,\bar{\theta}_\gamma)$ can be expressed as:

$$W(\bar{E}_n,\bar{\theta}_\gamma) = g(\bar{E},\bar{\theta}_\gamma)W_{exp}(E_p,\theta_\gamma) \qquad (5)$$

where $\bar{\theta}_\gamma$ denotes the average γ-ray angle with respect to the incident neutron direction and $g(\bar{E},\bar{\theta}_\gamma)$ is a geometric factor for correcting the experimental γ-ray angular distribution, $W_{exp}(E_p,\theta_\gamma)$. In this technique

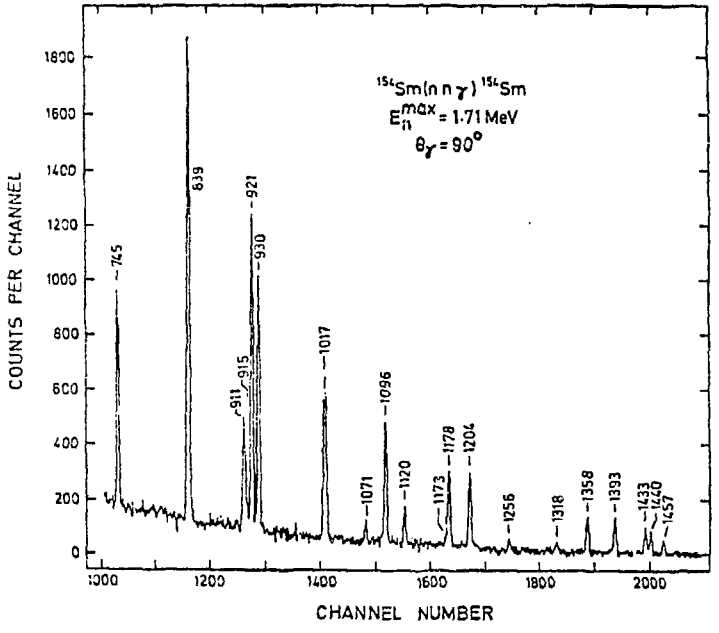

Fig.- 20. The spectrum of gamma-rays following the (n;n',gamma) reaction in Sm-154 at E_n(max)=1.71 MeV. Background has been subtracted using data from a no-sample run.

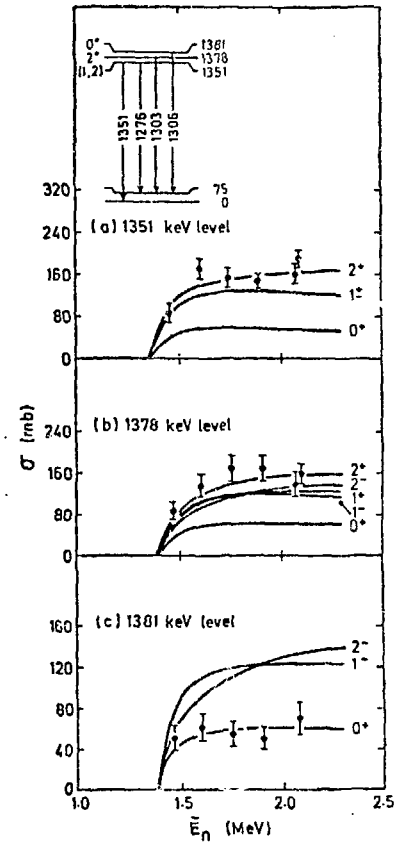

Fig.- 21. Excitation curves for the 1351,1378 and 1381 keV levels in Gd-160 together with the results of Hauser-Feshbach calculations using the indicated spin and parity values.

it is however impossible to determine this correction factor unless the spin J_i of the level and the mixing ratio of the γ-ray transition are already known. To overcome this difficulty Davidson, et al. (66) have developed a computer code EVA in which the geometric corrections are applied to the theoretical angular distributions for various J_i and δ values. These can then be directly compared with the measured distributions.

The usefulness of the above approach for the determination of level structure and for spin assignments can be seen from the $(n;n'\gamma)$ results for ^{203}Tl. This nucleus is near a closed shell, and can therefore be represented by a fairly simple model.

Previous experimental studies (64) have established spin and parity values for only the ground-state and for the first and second excited states. Possible candidates for the theoretically predicted 7/2+ level at about 1 MeV excitation are the 1045, 1066, 1073 and 1075 keV levels observed in the $(n;n'\gamma)$ reaction (67). The 1045 level can be eliminated on the basis of its γ-ray branching (68). Davidson, et al. have measured the angular distributions for the γ-ray transitions from these levels to the first excited state at 279 keV, and these are shown in Fig. 23, together with the χ^2 plots. As can be seen, the 1073 keV level is the most probable choice for the predicted $7/2^+$ state with the other two at 1066 and 1075 keV eliminated at the 98% confidence level.

C. Interpretation of Branching Ratios

In many $(n;n'\gamma)$ studies the spin assignments made by comparing the γ-ray angular distributions or the inferred $(n;n')$ cross sections with statistical model predictions, are not unique. In such cases the observed branching ratios can place some further restrictions on the possible spin values.

A large amount of reliable data now exists on the γ-ray strengths for transitions with well established multipolarity, γ-ray strength denoting the γ-ray width for the transition divided by the Weisskopf single particle width, that is $\Gamma_\gamma/\Gamma_{\gamma W}$. These have been compiled (69,70) and from these experimental distributions it is now possible to place some upper limits on the γ-ray strengths for the various multipole transitions. From the empirical data it is obvious that, except for E2 transitions, the transition speed is much below the Weisskopf single particle estimate. The branching ratios calculated on the basis of the single particle estimate can therefore be used for approximate spin assignments. For example in the $^{120}Sn(n;n'\gamma)$ studies of Kikuchi and Sugiyama (65) the 2096 keV level decays to the ground-state and to the first excited state at 1171 keV. The branching ratio of the 2096 keV transition relative to that of the 925 keV was 0.99. From the measured γ-ray angular distribution and excitation function, a spin value of 2 or 3 is indicated for this level. The calculated branching ratios for 2^+, 3^- and 3^+ assignments are 0.070, 4.4×10^{-8} and 4.4×10^{-8} respectively. For a 3^+ assignment this means that the 1096 keV M3 and the 925 keV M1 transitions should be so enhanced and hindered respectively that the combined effect is to increase the relative branching ratio by a factor of almost 10^8. The 3^- assignment can be excluded on the

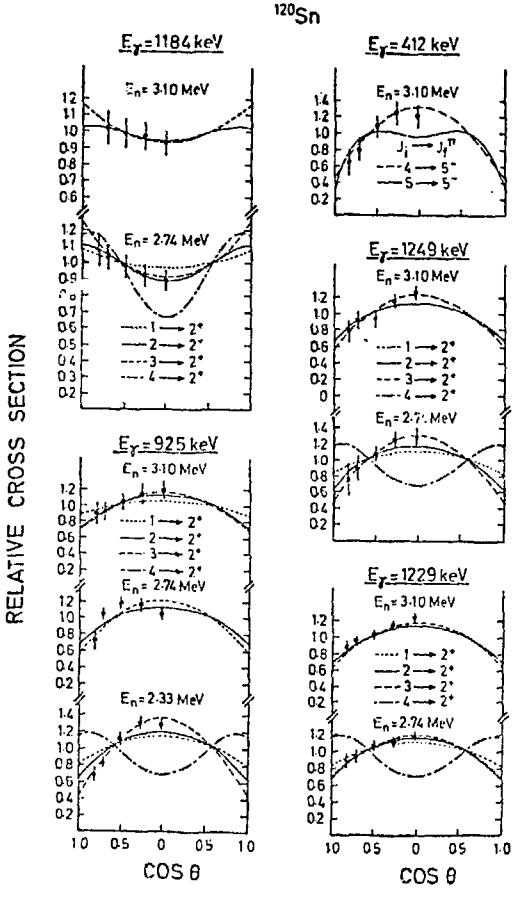

Fig.-22. Measured gammay-ray angular distributions for the Sn-120(n;n',gamma) reaction. The curves indicate the results of calculations based upon the illustrated spin and parity values.

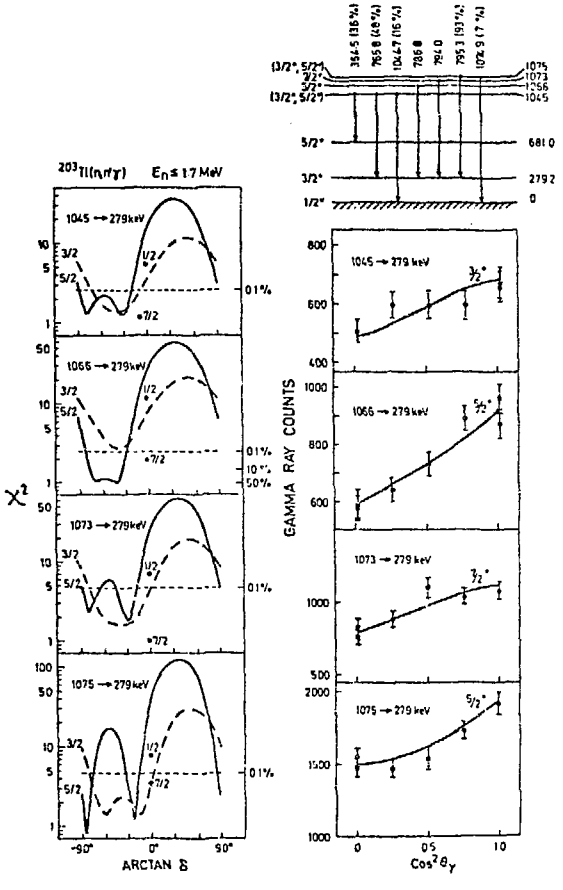

Fig.-23. Experimental and theoretical gamma-ray angular distribution results for the Tl-203(n;n',gamma) reaction for a maximum neutron energy of 1.7 MeV. In the X^2 vs arc-tan-delta plots, shown on the left side for different spin values, the 0.1% confidence levels are denoted by dashed lines.

grounds that the lowest 3^- level in ^{120}Sn is around 2400 keV. A spin value of 2 therefore seems to be indicated for this level.

According to the collective model (42) the ratios of reduced transition probabilities to states of a rotational band can be expressed simply in terms of ratios of Clebsch-Gordon coefficients. The relationship also holds when the initial and final states belong to the same rotational band.

The branching ratios obtained from ^{154}Sm and ^{160}Gd studies (62,63) have, for example, been used to calculate the B(E1) ratios of the γ-rays depopulating the octupole band. In Table 1 these ratios are compared with this prediction. Good agreement is obtained for a K = 0 assignment for the octupole band.

TABLE 1

Experimental and theoretical ratios of transition probabilities from members of the octupole band in ^{154}Sm and ^{160}Gd to members of the ground-state (g) rotational band.

Nucleus	$\frac{J_o \to J_g}{J_o \to J'_g}$	B(E1; $J_o \to J_g$)/B(E1; $J_o \to J'_g$) Experiment	Theory
^{154}Sm	$\frac{1^- \to 2^+}{3^- \to 4^+}$	1.83 ± 0.1	1.997
	$\frac{3^- \to 4^+}{3^- \to 2^+}$	1.19 ± 0.06	1.33
^{160}Gd	$\frac{1^- \to 2^+}{3^- \to 4^+}$	2.07 ± 0.1	1.997
	$\frac{3^- \to 4^+}{3^- \to 2^+}$	1.32 ± 0.07	1.33

VI. CONCLUSIONS

In the beginning we set forth three general questions that we have attempted to answer.

We have asked if the body of the theory is internally consistent and satisfactory from a theoretical point of view. The answer is affirmative. The work of Moldauer (5) and Engelbrecht and Weidenmüller and associates (6) has placed on a sound theoretical footing the corrected Hauser-Feshbach theory particularly defining the nature of the correction factors, their regions of applicability and providing approximations for their practical application. The coupled-channel optical model is theoretically sound and can give exact descriptions of the reactions providing the requisite coupling parameters are provided. In practice, however, attempts to treat

more than the simplest coupling schemes (e.g., those associated with the ground-state rotational band) rapidly become very complex with attendant increases in parameters, ambiguities and computational complexity. Ground-state-associated couplings are by far the most significant, particularly those associated with the rotational band. In the heavy deformed nucleus the next set of couplings is to and within the various collective vibrations--the several octupole bands, the β- and γ- vibrations, etc. All of these are probably of comparable strength. To understand all of these complexities is indeed a formidable task. The question is--are these really significant matters? We will return to this point below.

Turning to the question--"does the theory reasonably describe experiment?". Generally, the overwhelming evidence is that it does excepting very local and generally small and detailed exceptions. In those regions where the compound-nucleus treatment is appropriate a very large body of experimental data can be well described. However, the continuing necessity to treat the corrections to the Hauser-Feshbach formula to a more or less extent as a free parameter is unsatisfying and reduces our ability to use the model for predictions and for the definition of nuclear structure. For the latter purpose there is no obvious solution from the theoretical side and the alternative appears to be the minimization of the problem by extending the studies to increased energies where the uncertainties are greatly reduced. Thus improved experimental techniques providing good resolution of levels at higher incident neutron energies would be an important development.

While, in the strongly statically deformed nuclei, there can be no doubt that the coupled channels model describes the data on the ground state rotational band reasonably well. There is however little or no experimental evidence to compare with such a theory for the vibrational levels. One would feel intuitively that the inter and intra band couplings are likely to be of such importance that the excitation of a given level could follow a complex path. That would be not too different from what we suppose happens in the compound nucleus case. The contemporary success of coupled-channels interpretations of the ground-state band and associated statistical interpretations at higher energies is consistent with this view. However, the question remains open and deserves computational-experimental examination.

Much of the interpretation of the $(n;n'\gamma)$ process can be model independent--e.g., angular distributions near threshold, branching ratios can all be interpreted on the basis of well established electromagnetic theory. This is a very strong situation and one that should be exploited above all in the mass region where it has few serious competitors i.e., among the heavy nuclei.

On the question of technique development progress has been modest. The great need is for another increase of intensity comparable to that achieved by the introduction of bunching but without the side effects of energy and angular spread attendant upon the latter. There also appears to exist a large shortfall between computational and theoretical capability

and what is actually employed in the concept, execution and analysis; the concept of system-analysis has not arrived.

Clearly inelastic scattering is a very live field with much promise though some problems. We hope when others review its progress over the next five years they will have some exciting progress to report.

REFERENCES

1. H. Feshbach, C. E. Porter, V. F. Weisskopf, Phys. Rev. 96, 448 (1954).
2. Taro Tamura, Revs. Mod. Phys. 37, 679 (1965).
3. W. Hauser and H. Feshbach, Phys. Rev. 87, 366 (1952).
4. P. A. Moldauer, Phys. Rev. 135, B642 (1964).
5. P. A. Moldauer, Phys. Rev. C11, 426 (1975).
6. C. A. Engelbrecht and H. A. Weidenmüller, Phys. Rev. C8, 859 (1973).
7. P. A. Moldauer Phys. Rev. C12, 744 (1975).
8. E. Sheldon and D. M. van Patter, Rev. Mod. Phys. 38, 143 (1966).
9. J. W. Tepel, H. H. Hoffmann and H. A. Weidenmüller, Phys. Lett. 49B, 1 (1974).
10. For example, F. Becchetti and G. Greenlees, Phys. Rev. 182, 1190 (1969).
11. F. Perey and B. Buck, Nucl. Phys. 32, 353 (1962).
12. K. Brueckner et al., Phys. Rev. 100, 891 (1955).
13. C. Engelbrecht and H. Fiedeldey, Ann. Phys. 42, 262 (1967).
14. C. Newstead and C. Cierjacks, NEANDC Report JAERI-M-5984 (1975).
15. S. Tanaka, NEANDC Report JAERI-M-5984 (1975).
16. Ch. LaGrange, NEANDC Report JAERI-M-5984 (1975).
17. A. Lane et al., Phys. Lett. 2, 424 (1958); see also Smith et al., private com. (1976).
18. A. Lane, Phys. Lett. 8, 171 (1962); Also see M. McEllistrem at this conference.
19. J. Sierra and P. Turinsky, NEANDC Report JAERI-M-5984.
20. P. Stelson and L. Grodzins, Nucl. Data 1A, 21 (1965).
21. K. Harada and S. Igarasi, private com. (1975).
22. J. Anderson, private com. (1976).
23. L. Cranberg and J. Levin, Phys. Rev. 109, 2063 (1958).
24. W. Kinney and F. Percy, Priv. Com. (1976).
25. R. B. Day, Prog. in Fast Neutron Physics, ed. G. Philips, J. Marion and J. Risser, Univ. Chicago Press, Chicago (1963).
26. D. L. Smith, Argonne Natl. Lab. Report ANL/NDM-12 (1975), see also ANL/NDM-17.
27. W. McMurray, P. Colliers and P. Saayman, Nucl. Phys. A225 37 (1974).
28. D. L. Smith, to be published.
29. S. Elbakr, I. van Heerden, W. Dawson, W. McDonald and G. Nielson, Nucl. Instr. and Methods 97 283 (1971).
30. J. Routti and S. Prussin, Nucl. Instr. and Methods 70 125 (1969).
31. D. L. Smith, Argonne Natl. Lab. Report ANL/NDM-17 (1975).
32. D. L. Smith, Argonne Natl. Lab. Report ANL/NDM-20 (1976), See also A. Smith, priv. com. (1976).
33. A. Smith and P. Guenther, Proc. of Conf. on Nuclear Structure Study With Neutrons, Antwerp, (1966) North-Holland Pub. Co.

REFERENCES (Contd.)

34. E. Almen - Ramström, Aktiebolaget Atomenergi Report AE-503 (1975).
35. B. Holmqvist and T. Wiedling, Aktiebolaget Atomenergi Report AE-430 (1971).
36. P. Moldauer, priv. com. (1976).
37. W. Kinney et al., priv. com.
38. D. L. Smith, Argonne Nat'l Lab. Report ANL/NDM-20 (1976).
39. A. B. Smith, private com. (1976), see also E. Barnard et al., Nucl. Phys. A118, 321 (1968).
40. E. Barnard et al., Argonne Nat'l Lab. Report ANL/NDM-3 (1974).
41. P. Guenther et al., Argonne Nat'l Lab. Report ANL/NDM-1 (1973).
42. B. Mottelson and S. Nilsson, K. Danske Vedersk, Selsk. mat-fys. Skr. 1, No. 8 (1958).
43. P. Guenther et al., Argonne Nat'l Lab. Report ANL/NDM-11 (1975).
44. A. Smith et al., Nucl. Phys. A244 213 (1975).
45. A. Langsford et al., priv. com.
46. F. Becchetti and G. Greenlees, Phys. Rev., 182 1190 (1969).
47. V. Madsen et al., priv. com. (1976).
48. P. Guenther et al., Phys. Rev., C12, 1797 (1975).
49. D. Reitmann et al., Proc. Conf. on Neutron Cross Sections and Technology, (1975), Nat'l Bur. Stds. pub., NBS-425.
50. P. Guenther et al., Argonne Nat'l Lab. Report, ANL/TM/CTR-4 (1973).
51. H. Canarda, Phys. Rev., C9, 28 (1974).
52. P. Guenther et al., Priv. Com. (1976).
53. G. Haouat et al., see Session MD-II.
54. P. Guenther et al., Argonne Nat'l Lab. Report ANL/NDM-16 (1975).
55. T. Marcella et al., priv. com. (1976).
56. E. Barnard et al., Proc. 2nd Inter. Conf. on Nucl. Data for Reactors, IAEA Press, Vienna (1970).
57. P. Guenther et al., to be published.
58. W. Vonach et al., Phys. Lett. 11, 351 (1964).
59. A. Lane et al., Phys. Rev. Lett. 2, 424 (1959).
60. W. R. McMurray, I. J. van Heerden, E. Barnard and D. T. L. Jones, Report SUNI 41, Southern Universities Nuclear Institute (1975) 4.
61. D. R. Gill, N. Ahmed, W. J. McDonald, G. C. Nielson, S. A. Elbakr, I. J. van Heerden and W. K. Dawson, Nucl. Phys. A229 (1974) 397.
62. S. A. Elbakr, I. J. van Heerden, D. R. Gill, N. Ahmed, W. J. McDonald, G. C. Nielson and W. K. Dawson, Phys. Rev. C10 (1974) 1864.
63. S. A. Elbakr, I. J. van Heerden, B. C. Robertson, W. J. McDonald, G. C. Nielson and W. K. Dawson, Nucl. Phys. A211 (1973) 493.
64. N. Ahmed, D. R. Gill, W. J. McDonald, G. C. Nielson and W. K. Dawson, Phys. Rev. 11 (1974) C869, which also contains earlier references.
65. S. Kikuchi and Y. Sugiyama, Nucl. Phys. A223 (1974) 1.
66. J. M. Davidson, H. R. Hooper, D. M. Sheppard and G. C. Nielson, Report UAE NPL-1082, Nuclear Research Centre, University of Alberta (1975) and private communication.
67. N. Azziz and A. Covello, Nucl. Phys. A123 (1969) 681.
68. E. Barnard, N. Coetzee, J.A.M. deVilliers, D. Reitmann and P. van der Merwe, Nucl. Phys. A157 (1969) 130.

REFERENCES (Contd.)

69. D. H. Wilkinson, Nuclear Spectroscopy Part B, ed. Fay Ajzenberg-Selove, Academic Press, New York and London (1960) 852.
70. P. M. Endt and C. van der Leun, Atomic Data and Nuclear Data Tables 13 (1974) 67.
71. E. Barnard et al., Nucl. Phys., 80 46 (1966).
72. F. S. Stephens, B. Elbek and R. M. Diamond, Proc. Conf. on Reactions between Complex Nuclei, Asilomar, ed. A. Ghiorso, R. M. Diamond and H. E. Conzett, University of California Press, Berkeley and Los Angeles (1963) 303.

MD 2 -- FAST NEUTRON SCATTERING FROM SOME MEDIUM MASS NUCLEI — A.T.G. Ferguson (A.E.R.E. -- Harwell)

Lagrange (Bruyères):
Please, can you tell me what kind of parameters you have taken for the inelastic scattering cross section for uranium?

Ferguson:
Well, these calculations were carried out by Dr. Smith, and I think perhaps that it would be most appropriate if he answered that question directly.

Smith (A.N.L.):
The model does not differ appreciably from the one you proposed some time ago. It does have a larger absorption and a somewhat larger radius. There will be a publication out on an A.N.L.-N.D. document, No. 23, which is routinely sent to your laboratory. It is developed by fitting a spherical model to the four isotopes lead-206,-207,-208 and bismuth —209, and then introducing from this extensive fit just the deformation. It has some advantages over your model and it also has some shortcomings, particularly at low energies -- it does not give as good a description of the strength function.

Feshbach (M.I.T.):
I am struck by the success the deformed model has had in the various cross sections we've seen displayed both in your talk and in the preceding one. And I'm struck particularly because the model is a rather special one. You take a potential and you introduce the deformation to the radius parameter. Heaven knows why that works so well, but it is true it works! And it also works quite well when you do electron scattering from deformed nuclei. Except there are hints now that when you get up to the higher multipoles it does break down. But I think one should remark on the remarkable agreement one obtains with this very simple model. The second question is, has anybody looked into the question -- particularly in the molybdenum isotopes -- what effect the vibrational levels would have in the description of the scattering, i.e., of inelastic scattering, and so on ?

Ferguson:
Yes, there have been some calculations in which, instead of introducing rotational wave functions, one introduced vibrational-type wave functions. These appear to work reasonably well in the region where one has strong vibrational aspects of the nucleus. But I think that to some extent much of this comparison work is done by experimenters who tend to take the model that is available. Usually the models that are available have only the facility for having vibrational levels or rotational levels. There are some rather sophisticated ones available in a number of laboratories in which there is a place to introduce detailed wave-functions at one's own choice. But I feel that this option has been exercised too rarely.

Horen (O.R.N.L.)
In charged-particle inelastic scattering, of course, the interaction mainly takes place on the surface, whereas in the neutron scattering I would imagine it can take place over the whole volume. My question is whether you would take into account the difference between an excitation of a vibrational state which is concentrated on the surface and a rotation in a deformed nucleus, which you could bang at any point

in the nucleus, essentially. So, in a naive way, one might expect a larger cross section for exciting rotational spectra in deformed nuclei than you might get from a vibrational excitation of a spherical nucleus. Maybe someone could tell me if this naive picture is good or bad.

Ferguson:
I think that to some extent this goes back to Dr. Feshbach's comment. It's amazing what a simple picture we could get away with. Perhaps he would like to add some further comment. He says "no".

Wigner (Princeton University):
I think in the higher energy region all models give the same result. And this is to some degree a mystery to me. But I know that if one thinks crudely about the R-matrix model, which we all believe is fundamentally correct, at first instance it looks as if it were impossible to explain the results in which the elastic cross section changes by a factor of 40 in different directions, which means that the intensity of emission in those directions at every energy is very low. Now, in this case, I did play around with it and I showed that it's rather independent of the details of the R-function, what happens eventually. And I suspect that this independence of the model persists so that the simple models will work well also in this case. Dr. Feshbach looks unhappy, perhaps he wants to contradict.

Feshbach:
Yes, when I'm just thinking I look unhappy. I was trying to understand your remarks and I'm not sure what the statement of "independence" with respect to the model really means. For example, it is clear that for deformed nuclei one had to put in the deformation - so it's not independent of the model. Hence, why "independence"?
Wigner:
I mean that it doesn't matter much whether one uses a coupled-channel model, or an R-matrix model, one gets the same result. And I woke up to this a short time ago so I don't know the full explanation, but I think we should find it. You don't look unhappy anymore.

Newstead (B.N.L.):
Isn't it true that if you do both a vibrational or a deformed coupled-channels calculation that there's only one term that's actually different between the vibrational calculation and the rotational calculation? There's an additional term which comes in, that sometimes can be small. So although obviously the physics is quite different, in fact the calculation can be done with either one independently.

Ferguson:
There is not a great deal of difference in it. And by adjustment of parameters undoubtedly one can make it fit with one model or the other. Thinking about some of this discussion, I wonder if I might be permitted to put a question from the chair to Dr. Soloviev? Could he, for example, tell us whether there are any really spherical nuclei?

[Background Remark (amid laughter): God knows!]

Soloviev:
Yes. - Magic nuclei are of course spherical.

Benenson (S.U.N.Y. Albany):

I had a question, and that was whether it would be possible that forward-angle inelastic scattering would give comparable information about deformation parameters as does the back-angle elastic scattering?

Ferguson:

Well, I have not seen an extensive survey of computation in that regard, but from the computations I have seen on tungsten isotopes, which seem quite typical, there was no greater sensitivity in the inelastic channel at forward angles than there was at any other angle. It seemed quite flat with angle. But in the elastic scattering, while there was no sensitivity at all at forward angles there was very significant sensitivity at back angles. You may go back to the slide if you'd like to see it. You can see that the band of predictions for the inelastic scattering is very little wider at a quite inaccessible forward angle — at least inaccessible by normal techniques - compared with the width of this band at angles around 150-160 degrees, which one would normally regard as the limit of experimental accessibility in the backward direction. On the other hand, one can see that in the case of elastic scattering there's a big differentiation between the forward angles and back angles, and quite a reward to be got from struggling to get to as near as possible to 180 degrees.

Sheldon (University of Lowell):

There is a quick corollary to this as well, if one goes on to consider polarization. Then the scattering at back angles becomes a very much more sensitive criterion for diagnosis than some of the forward angle polarizations.

9:00 A.M., WEDNESDAY, JULY 7, 1976, IN OLNEY 150

MAIN SESSION ME

Chair: J.B. Garg (State University of New York at Albany, U.S.A.)

9.00 a.m., Wednesday, July 7, 1976 Special Contributed Paper: ME 1

FLUCTUATION ENHANCEMENTS OF COMPOUND CROSS SECTIONS FOR ELASTIC, DIRECTLY COUPLED, AND WEAKLY ABSORBED CHANNELS*

P. A. Moldauer

Argonne National Laboratory, Argonne, Ill. 60439, U.S.A.

* *Work performed under the auspices of the Energy Research and Development Administration.*

RÉSUMÉ

The qualitative and quantitative behavior of average compound nucleus cross section enhancements relative to the Hauser-Feshbach prediction are discussed and are compared with the results of real and computer experiments.

ABSTRACT

Most average compound nucleus cross sections are well specified by the Hauser-Feshbach formula which requires only a knowledge of all channel transmission coefficients. There are, however, three types of compound cross sections whose values may be enhanced compared to Hauser-Feshbach. Corresponding reductions affect cross sections for competing channels. Compound elastic cross sections are enhanced by a factor depending upon the distribution of partial widths. The maximum elastic enhancement is by a factor of 3 in the limit of isolated resonances and by a factor of 2 in the limit of overlapping resonances. Compound reaction cross sections between directly coupled channels may be enhanced by a factor not exceeding the elastic enhancement. Its value depends both on the strength of the direct interaction and the relative phase of the direct S-matrix element. Large effects are limited to cases where the determinant of Satchler's penetrability matrix is near zero (causality limit.) Both of the above effects arise from correlations of entrance and exit channel partial widths. The fluctuation of total widths may cause very large enhancements of small compound cross sections between weakly absorbed channels that compete with a few strongly absorbed channels. In the case of one or two competing strong channels the magnitude of this enhancement factor is theoretically unlimited. For N competing strong channels (N>2), the maximum enhancement is $(1-2/N)^{-1}$. The theoretical values and methods of computation of these three types of enhancement are discussed and are compared with the results of real and computer experiments.

Average compound nucleus cross sections are important for all kinds of applications of neutron interactions, from nuclear physics to the design and operation of fission and fusion reactors. Let me start by giving a very brief historical review of the subject.

In the earliest days of neutron resonance physics [1] it was recognized that the energy average of a resonance cross section could be explained in terms of the average level spacing D and the average partial widths $\langle \Gamma_{\mu c} \rangle$ and the average total widths $\langle \Gamma_{\mu} \rangle = \sum_c \langle \Gamma_{\mu c} \rangle$. In units of $\pi\lambda^2$ the energy averaged compound nucleus cross section between channels c and d was given by

$$\bar{\sigma}_{cd}^{C.N.} = \frac{2\pi}{D} \frac{\langle \Gamma_{\mu c} \rangle \langle \Gamma_{\mu d} \rangle}{\langle \Gamma_{\mu} \rangle} \quad . \tag{1}$$

With the advent of the neutron optical model [2] and the identification of the partial-width-to-spacing ratio for isolated resonances with the optical model transmission coefficient

$$T_c = 2\pi\Gamma_{\mu c}/D, \tag{2}$$

Eq. (1) became the Hauser-Feshbach formula [3]

$$\bar{\sigma}_{cd}^{C.N.} = \sigma_{cd}^{H.F.} = \frac{T_c T_d}{\sum_e T_e} \quad . \tag{3}$$

A little later it was realized that in Eq. (1) the average should have been taken as follows:

$$\bar{\sigma}_{cd}^{C.N.} = \frac{2\pi}{D} \left\langle \frac{\Gamma_{\mu c} \Gamma_{\mu d}}{\Gamma_{\mu}} \right\rangle \quad , \tag{4}$$

leading to the width-fluctuation-corrected Hauser-Feshbach formula [4]

$$\bar{\sigma}_{cd}^{C.N.} = \sigma_{cd}^{H.F.} \times W_{cd} \quad . \tag{5}$$

I shall return to a discussion of the width fluctuation correction factor W_{cd} below.

The problem becomes a great deal more complicated when one wishes to calculate average cross sections in the domain of interfering resonances [5], because of the complicated demands imposed by the unitarity requirement. Taking unitarity explicitly into account, one obtains an expression of the following type [6]

$$\bar{\sigma}_{cd}^{C.N.} = \left\langle \frac{\theta_{\mu c} \theta_{\mu d}}{\theta_{\mu}} \right\rangle - M_{cd} \tag{6}$$

where

$$\langle \theta_{\mu c} \rangle = T_c + \sum_d M_{cd} \tag{7}$$

while

$$\langle \theta_{\mu} \rangle = \sum_c \langle \theta_{\mu c} \rangle \tag{8}$$

and M_{cd} depends in a complicated way upon correlations among the S-matrix pole parameters.

If one assumes that all these correlations vanish, then one finds that the matrix M is diagonal and that it and $\langle \Theta_{\mu c} \rangle$ can be expressed in terms of the transmission coefficients T_c and certain resonance interference parameters Q_c. Formulas based on this assumption were put forward a dozen years ago. [6] However, these formulas are not correct because, as has been shown [7, 8], the correlations in M do not vanish but become very appreciable.

At the same time another kind of simplification was discovered [8]. Writing

$$\Theta_{\mu c} = G_{\mu c} + X_c$$

where
$$\langle G_{\mu c} \rangle = T_c \tag{9}$$

and
$$X_c = \sum_d M_{cd}$$

we get from Eq. (6),

$$\bar{\sigma}_{cd}^{C.N.} = \frac{T_c T_d}{\Sigma(T+X)} W_{cd} + \left[\frac{(T_c X_d + T_d X_c + X_c X_d) W_{cd}}{\Sigma(T+X)} - M_{cd} \right] . \tag{10}$$

It turns out [8] that a rather complicated consequence of unitarity is that the second term in square brackets in Eq. (10) vanishes. I have called this M-cancellation. As consequence we are left with a width-fluctuated Hauser-Feshbach formula.[8]

Let me now turn to a discussion of the width fluctuation correction. It has the form

$$W_{cd} = \left\langle \frac{G_{\mu c} G_{\mu d}}{\sum_e G_{\mu e}} \right\rangle \Bigg/ \frac{\langle G_{\mu c} \rangle \langle G_{\mu d} \rangle}{\left\langle \sum_e G_{\mu e} \right\rangle} , \tag{11}$$

where $\langle G_{\mu c} \rangle = T_c$ and the $G_{\mu c}$ fluctuate in μ in a way which we assume can be adequately represented by a chi-squared distribution with ν_c degrees of freedom. In fact ν_c varies between the values of 1 for isolated resonances, to the value of 2 for strongly overlapping resonances [8]. A useful approximate formula for the dependence of the ν_c upon T_c has been given by Hofmann et al.[9]

It is useful to separate the width fluctuation correction into two factors:

$$W_{cd} = C_{cd} \times F_{cd} , \tag{12}$$

where the "covariance factor" C_{cd} is

$$C_{cd} = \frac{\langle G_{\mu c} G_{\mu d} \rangle}{\langle G_{\mu c} \rangle \langle G_{\mu d} \rangle} \tag{13}$$

and the "fluctuation factor" F_{cd} is

$$F_{cd} = \left\langle \frac{G_{\mu c}\, G_{\mu d}}{\sum_e G_{\mu e}} \right\rangle \approx \frac{\langle \sum_e G_{\mu e} \rangle}{\langle G_{\mu c}\, G_{\mu d} \rangle} .$$

Let me first discuss the covariance factor C. For the elastic channel this can be calculated to give

$$C_{cc} = \frac{\langle G_{\mu c}^2 \rangle}{\langle G_{\mu c} \rangle^2} = 1 + \frac{2}{\nu_c} , \qquad (15)$$

which varies from an elastic enhancement factor of 3 for $\nu_c = 1$ to a factor of 2 for $\nu_c = 2$. Then C_{cd} can be expressed in terms of ν_c, ν_d and the correlation coefficient ρ_{cd} between $G_{\mu c}$ and $G_{\mu d}$,

$$C_{cd} = 1 + \rho_{cd} \sqrt{(C_{cc}-1)\ (C_{dd}-1)}$$

$$= 1 + \frac{2\,\rho_{cd}}{\sqrt{\nu_c\ \nu_d}} \qquad (16)$$

In the absence of direct reactions we have in general $\rho_{cd} = \delta_{cd}$ and so $C_{cd} = 1$ for $c \neq d$. However where channels c and d are coupled by a direct reaction, then ρ_{cd} can differ from zero. To see this, we note that causality [10] requires that $\det P \geq 0$ where P is the Satchler penetration matrix $P = 1 - \bar{S}^{+}\bar{S}$ where $\bar{S}$ is the average S-matrix. This causality requirement is entirely analogous to the requirement that $T_c \geq 0$ in the absence of direct reactions.

At the causality limit the condition $\det P = 0$ reduces the free parameters describing the channels by one. So in the case of n channels, only n-1 can be linearly independent at the causality limit and there must be correlations. In particular, in the case of two channels at the causality limit, there must be complete correlation and therefore the inelastic enhancement C_{12} must equal the elastic enhancement C_{11}. This is illustrated in Fig. 1, where [10] $\det P = 0$ when the parameter $D = 0.5$. Detailed calculations show that the enhancement drops off very fast when one moves away from the causality limit [10].

The general method for computing the direct enhancement employs the Engelbrecht-Weidenmüller transformation matrix U which diagonalizes the average S-matrix [11]

$$S' = U^{T} S U$$

$$\left(\tilde{S}' \text{ diagonal}\right) \qquad (17)$$

The width-fluctuation-corrected Hauser-Feshbach cross sections $\bar{\sigma}^{C.N.}_{cd}$ are then calculated in the transformed channel space and the result is that [10,11]

$$\bar{\sigma}^{C.N.}_{cd} = \sum_{ef} C_{cdef}\ \bar{\sigma}^{C.N.}_{ef} , \qquad (18)$$

where the coefficients C_{cdef} are products of the elements of the transformation matrix U. In equation (18) enhanced elastic cross sections in the primed space are mixed into the nonelastic cross sections, giving rise to the enhancements of compound cross sections which compete with direct reactions.

Turning now to the fluctuation factor F we see that it will go to unity when $G_\mu = \sum_c G_{\mu c}$ does not fluctuate, that is when nν is large (n = no. of channels, ν = average ν_c). This is the general situation for large numbers of channels.

Most frequently F is less than unity by just enough to compensate for the elastic enhancement by a reduction of both elastic and nonelastic cross sections. The resulting width fluctuation corrections for certain classes of two and three channel situations are illustrated in Fig. 2.

The effect on the neutron inelastic cross section in iron is shown in Fig. 3.

Finally, F_{cd} can be greater than unity if both T_c and T_d are small but compete with strongly absorbed channels [12]. In that case G_μ and $G_{\mu c} G_{\mu d}$ will become effec ively uncorrelated and

$$F_{cd} \approx \left\langle \frac{1}{G_\mu} \right\rangle \left\langle G_\mu \right\rangle = \infty \quad (n\nu \leq 2)$$
$$= \frac{n\nu}{n\nu - 2} \quad (n\nu > 2). \tag{19}$$

This possibly severe enhancement of small compound nuclear cross sections affects mostly charged particle cross sections that compete with strong neutron channels.

References

1. H. A. Bethe, Rev. Mod. Phys. 9, 69 (1937)
2. H. Feshbach, C. E. Porter, V. F. Weisskopf, Phys. Rev. 96 448 (1954)
3. W. Hauser and H. Feshbach, Phys. Rev. 87, 366 (1952)
4. A. M. Lane and J. E. Lynn, Proc. Phys. Soc., London A70, 557 (1957)
5. P. A. Moldauer, Phys. Rev. 123, 968 (1961)
6. P. A. Moldauer, Phys. Rev. 135, B642 (1964)
7. H. A. Weidenmüller, Phys. Rev. C9, 1202 (1974)
8. P. A. Moldauer, Phys. Rev. C11, 426 (1975)
9. H. M. Hofmann, J. Richert, J. Tepel, and H. A. Weidenmüller, Ann. Phys. 90. 403 (1975)
10. P. A. Moldauer, Phys. Rev. C12, 744 (1975)
11. C. A. Engelbrecht and H. A. Weidenmüller, Phys. Rev. C8, 859 (1973)
12. P. A. Moldauer, Phys. Rev. C (1975) to be published

Figure Captions

Fig. 1. Elastic and Inelastic enhancements for a class of directly coupled two channel S-matrices.

Fig. 2. Width fluctuation correction for some types of two and three channel cases.

Fig. 3. Excitation cross section for the 845-keV level in ^{56}Fe. Data are compared with Hauser-Feshbach and width-fluctuation-corrected Hauser-Feshbach results.

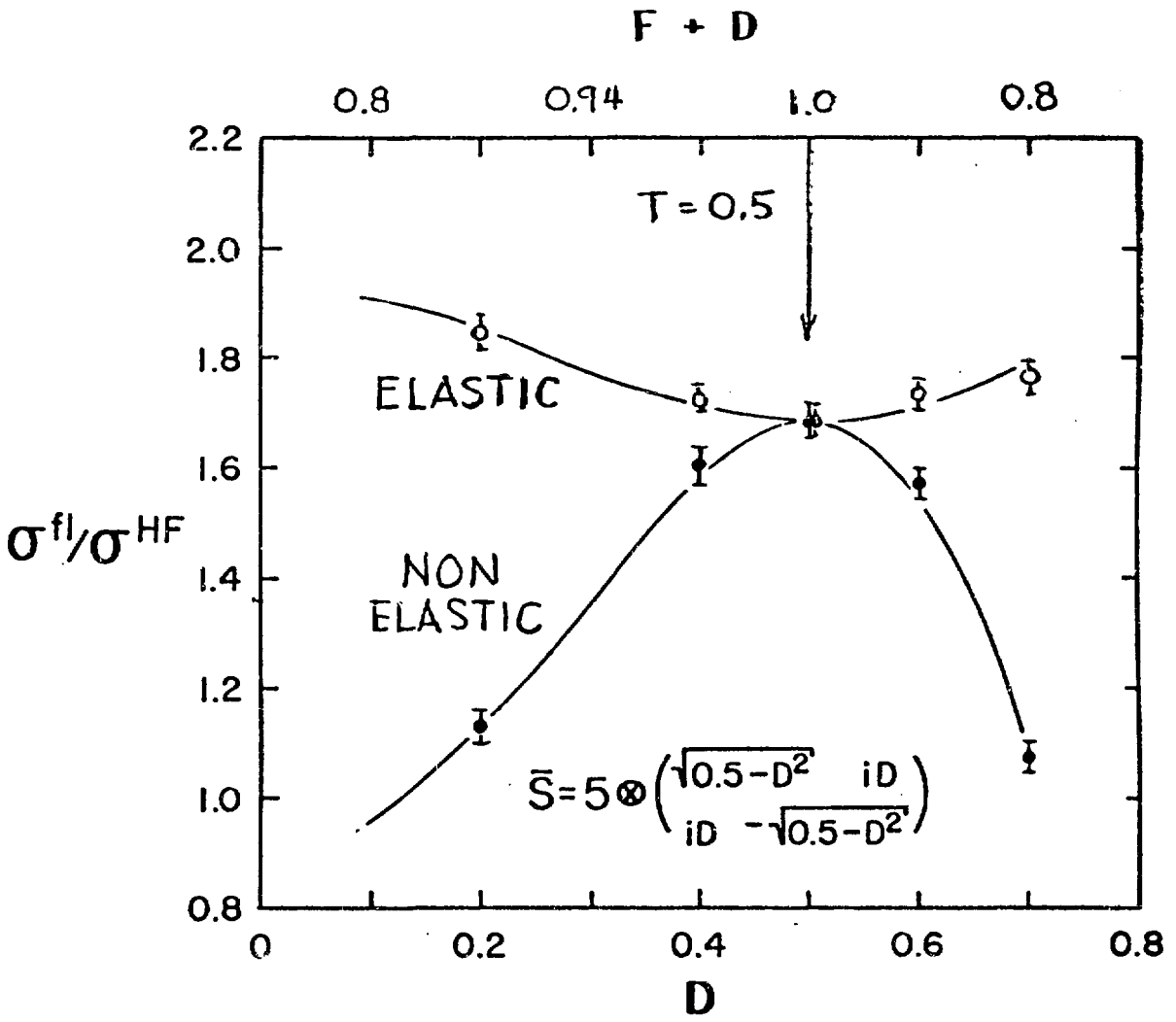

Fig. 1. Elastic and inelastic enhancements for a class of directly coupled two channel S-matrices.

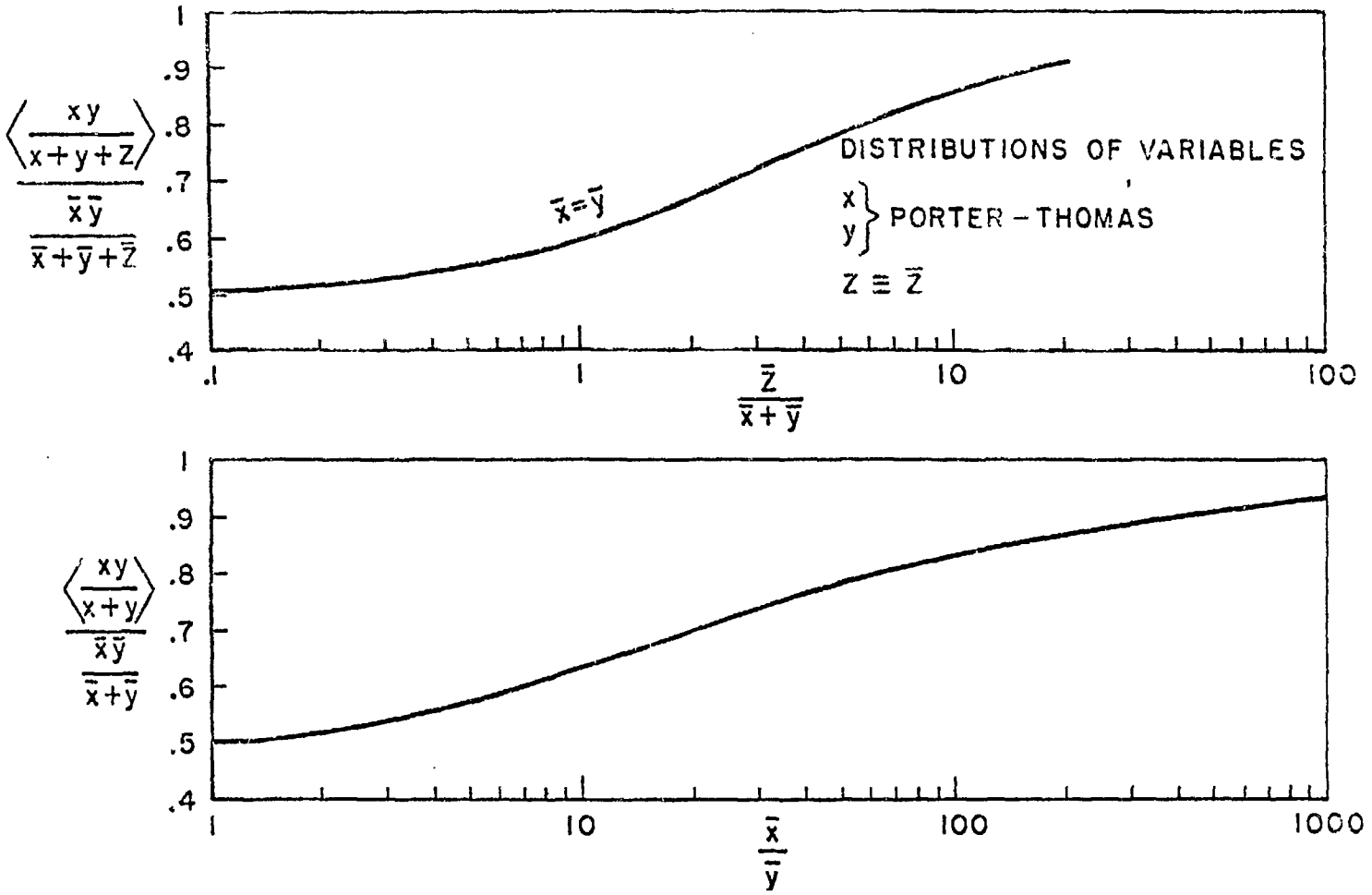

Fig. 2. Width fluctuation correction for some types of two and three channel cases.

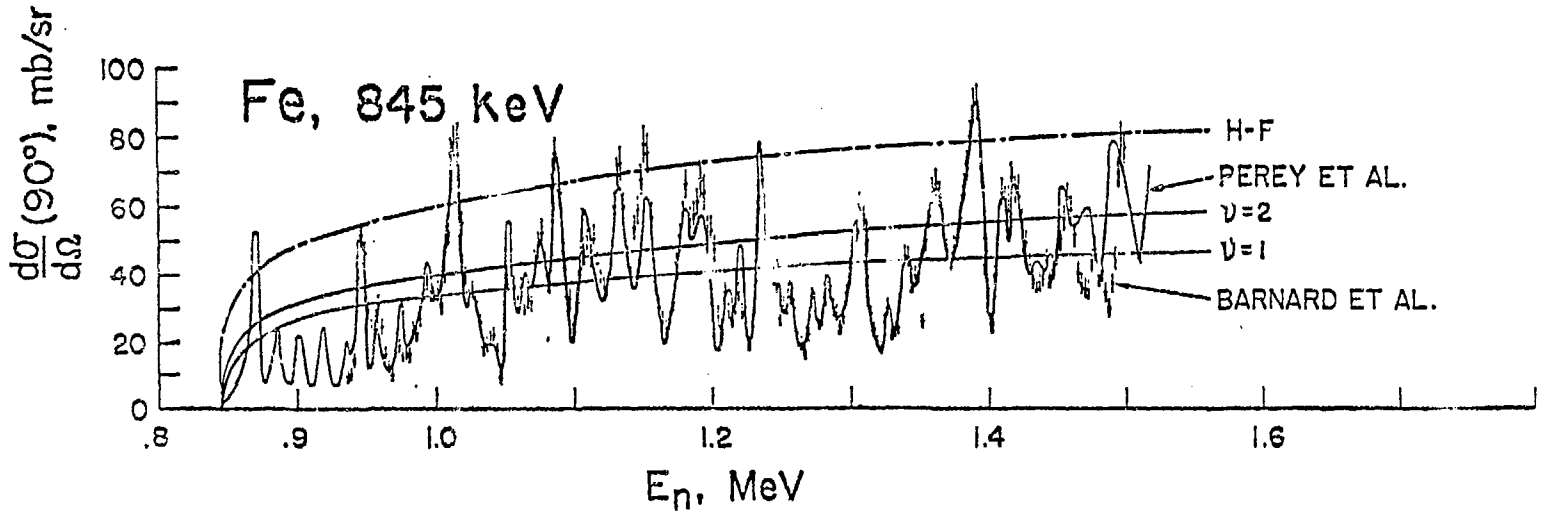

Fig. 3. Excitation cross section for the 845-keV level in ^{56}Fe. Data are compared with Hauser-Feshbach and width-fluctuation-corrected Hauser-Feshbach results.

ME 1 - FLUCTUATION ENHANCEMENTS OF COMPOUND CROSS SECTIONS FOR ELASTIC, DIRECTLY COUPLED, AND WEAKLY ABSORBED CHANNELS - P. A. Moldauer (ANL, Argonne, USA)

Lone (Chalk River):

How does the statistical fluctuation factor, or, as you say, the enhancement factor, depend on the averaging interval?

Moldauer:

Everything depends on the averaging interval. There are a great many assumptions involved in any statistical theory. You have to assume that you have something called a stable averaging interval, and if you make the averaging interval smaller, your sample will represent different distributions.

Lone:

So the enhancement could be more than two, for a limited sample.

Moldauer:

The enhancement could be as large as three for isolated resonances. In fact, the maximum enhancement is three for isolated resonances, and goes down to two in the limit of overlapping resonances.

Lone:

What I have in mind is some Monte Carlo calculations I did on a sample size of less than 100. I saw a sort of skewed symmetry which goes up to five and even higher.

Moldauer:

Unfortunately that was in the part of the talk that I did not get to. There were two factors, and the other factor, the fluctuation factor, can give you essentially unlimited enhancements. And let me just say that that can happen when you have either an elastic cross-section or a non-elastic between two channels where both of the channels involved have very small transmission factors, so that they do not contribute appreciably to the total widths. There also have to be channels with large transmission factors present. But yes, you're right, the enhancement due to this other factor can in fact be unlimited.

McEllistrem (Kentucky):

One of the formulas you presented showed the compound elastic enhancement written as $1 + 2/\nu$. The number of degrees of freedom, and the values of ν you have, would allow elastic enhancements ranging between two and three. But the last slide you presented showed elastic enhancements of about 1.6 to 1.7. I am interested in this because analyses of very careful experiments which have to fix the compound elastic scattering carefully from data analyses seem to imply enhancements slightly less than 2, about 1.6 to 1.7.

Moldauer:

I am sorry. One has to be careful about one means by "enhancement." The enhancement that I showed on the curve was the enhancement relative to Hauser-Feshbach. The enhancement that I talked about when I talked about the correl-

ation enhancement was the numerical factor that is given by the correlation factor alone; that is usually diminished by the fluctuation factor that I did not get to. So the net enhancement over Hauser-Feshbach is very often around 1.5.

Special Contributed Paper: ME 2

9.15 a.m., Wednesday, July 7, 1976

SPIN DETERMINATION OF FISSION RESONANCES*

G. A. Keyworth

Los Alamos Scientific Laboratory, University of California, Los Alamos, NM 87545

*Work performed under the auspices of the United States Energy Research and Development Administration

RÉSUMÉ

The use of a polarized neutron beam to bombard a polarized target appears to be the most definitive method among those employed hitherto to determine the spin of neutron-induced fission resonances. A review is presented of this technique and of experiments currently in progress, as well as those projected for future study.

ABSTRACT

Spin determination of neutron induced fission resonances is important to the basic understanding of the fission process and, in particular, to understanding both the role and the nature of the fission transition states. Of the several experimental techniques which have been used in the past for determining spins in fissionable nuclei, only the technique using a polarized neutron beam and a polarized target seems to be definitive. For the fissionable isotopes it is assumed that certain fission resonance properties, such as ν, the number of neutrons emitted in fission, and the kinetic energy and mass distribution of the fragments are strongly correlated with either the spin J or the spin projection K on the nuclear symmetry axis. However, the question of whether J or K plays the definitive role remains unanswered. Although it has also long been assumed that K = J for nuclear ground states, even this assumption has never been experimentally verified. In this paper, we review experimental techniques and results using polarized neutrons and polarized and aligned targets and describe the program we are currently pursuing in this area. We also make recommendations for future measurements which we see as most important in contributing to an understanding of the fission process.

SPIN DETERMINATION OF FISSION RESONANCES

G. A. Keyworth

Los Alamos Scientific Laboratory, University of California
Los Alamos, New Mexico 87545, U.S.A.

INTRODUCTION

Ten years ago, Eric Lynn noted[1] that understanding of the neutron cross sections of the non-fissile nuclei seemed fairly complete through measurements and complex potential models. He then explored the question of how far a similar program could be carried out for fissionable nuclei. Since the theory most fundamental to the understanding of fission cross sections at low neutron energies is the channel theory of A. Bohr,[2] Lynn examined the energies and nature of those internal nuclear states associated with the transition of the nucleus through the fission barrier, the fission channels. He concluded at that time that understanding of this basic theory was far from complete, if not even somewhat superficial, due largely to a lack of pertinent measurements. Unfortunately, although considerable effort has been expended to make relevant measurements and to pursue complex models, our understanding of the properties of the fission channels has been only little improved in the last ten years.

In the Bohr theory, the transition states or fission channels are collective in nature and characterized by the total angular momentum J, the parity π, and the projection K of J on the nuclear symmetry axis, assuming that the nuclear shape during the passing of the saddle point remains axially symmetric. These channels are assumed to occur in bands, corresponding to particular modes of collective motion, and each band is characterized by the same K value and parity. Within each band, there are a number of different J values. An open fission channel is one which is both energetically available and has the same J^{π} as the compound nucleus.

Probably the most straightforward approach to understanding the nature and the role of these fission channels is in the direct observation of slow neutron fission resonances. Ideally, one needs to determine the channel quantum numbers, J^{π} and K, the resonance parameters, E_o, Γ_n, Γ_f, and Γ_γ, and the detailed behavior of the fission products. In particular, one should study the prompt neutrons, the distribution of fragment masses and energies, and even the total neutron and γ-ray energies, for each fission resonance. Although broad in scope, these measurements are presently feasible for a variety of fissionable nuclei. Availability of intense pulsed neutron sources and, as we will show later, advances in cryogenic technology presently permits observation of the most elusive of these quantities, the channel quantum numbers. In this paper, we will examine both the present state of available information on the channel quantum numbers for resonance fission and the most urgently needed additional experiments. Although a wealth of information pertaining to resonance parameters in fissionable nuclei exists, very

few measurements pertaining to channel quantum numbers have been made. The discussion in this paper will necessarily rely heavily upon the alignment measurements of Pattenden and Postma and upon the polarization results from an experimental program conducted jointly by Los Alamos and Oak Ridge scientists.

EXPERIMENTAL TECHNIQUES

A rather vast amount of effort has been expended in the past to determine the spins of fission resonances. Any detailed and complete discussion of the techniques employed would necessarily be lengthy. Briefly, the various techniques used may be divided into two basic classifications. The first includes the direct methods, which encompass both the polarization techniques where a polarized target and a polarized beam are used and the method of using the total and scattering cross sections to determine the statistical weight factor, g_J. The class of indirect methods includes all other techniques used to infer the spin of the fission resonances. Among those techniques are: 1) level interference effects in elastic scattering and radiative capture, 2) γ-ray transitions and multiplicities, 3) fission width distributions, 4) prompt neutron and γ-ray emission, 5) fission fragment mass asymmetry and kinetic energy distributions, and 6) the ratio of ternary to binary fission

Of the two direct methods, each has a disadvantage. The main disadvantage of the polarized target and polarized beam technique is its extreme complexity. Although the results are simple to interpret, i.e. resonances of one J value are diminished while the resonances of the other are enhanced, the experimental techniques and apparatus are formidable. Although this method is a virtually infallible method for distinguishing between s-wave resonances of different spin, care must be taken to determine the correct absolute spin values. The single method which has been successfully employed to produce significant polarization in fissionable targets uses the hyperfine splitting in ferromagnetic systems. This hyperfine field, which may be several MOe, interacts with the nuclear magnetic moment, μ, to produce the nuclear polarization. However, the sign of the magnetic moment is frequently unknown and the direction of the hyperfine field may be either parallel or antiparallel to the applied field. Usually, sufficient information exists, either from Mössbauer measurements or from model calculations, to determine the signs of μ and the hyperfine splitting. In addition, the behavior of the observed resonances, such as the spacing or width distribution, may permit absolute determination of spin values. A further indication of the absolute spin is found in the approximate expression relating the polarized cross section, σ_p, to the unpolarized cross section, σ_o:

$$\sigma_p = \sigma_o(1 + f_I f_N f_n) \tag{1}$$

Here f_n is the polarization of the incident neutron beam, f_N is the polarization of the target, and f_I is a spin-dependent factor given by:

$$f_I = \frac{I}{I+1} \text{ for } J = I + 1/2$$

$$f_I = -1 \text{ for } J = I - 1/2.$$

Clearly, the enhancement or diminution of a resonance is greater for the $J = I - 1/2$ case. With sufficient nuclear polarization and with a reasonably low value of the target spin I, this distinction permits determination of the absolute value of J.

The method of using the total and scattering cross sections is difficult if $\Gamma_n/\Gamma << 1$, a common occurrence for fissionable nuclei. Comparisons between spin assignments in ^{235}U[3] and in ^{237}Np[4] by the two direct methods show little better than random agreement, due presumably to the low ratio of Γ_n/Γ.

A general lack of consistent spin assignments for resonances in fissionable nuclei by the various indirect methods would by itself lead one to doubt these techniques. However, an excellent example for a detailed comparison between such assignments and those from a polarized beam and target experiment exists in the heavily studied system ^{235}U + n. This comparison is detailed in Ref. 3 but we will review the basic results. Generally, agreement between the spin assignments from the indirect techniques and from the polarization experiments are nearly random with a single interesting exception. Four groups[5-8] of experimenters attempted to assign spins to low energy radiative capture resonances in ^{235}U by examining the de-excitation γ-rays. Three of these four measurements are in poor agreement with the polarization experiment while the work of Corvi et al[5] is in perfect agreement, for those limited cases which they studied. The remaining indirect techniques appear to be less fruitful, except in special cases such as ^{239}Pu where the ground state spin is 1/2. Only two K-bands exist, 0^+ and 1^+, with the 0^+ channel being fully open and the 1^+ only partially open.

The K-value of a fission resonance of known J may be directly determined by measuring the angular distribution of fission fragments from an aligned target. Such a measurement was attempted originally by Dabbs et al[9] and later by Pattenden and Postma[10] on ^{235}U in crystals of UO_2 $Rb(NO_3)_2$, and by Kuiken et al[11,12] on ^{233}U and ^{237}Np in the same crystal. All these experiments were handicapped by the low thermal conductivity of the host crystals with a resultant low degree of alignment. This problem may be surmounted by using an intermetallic compound which exhibits antiferromagnetism. In such a compound, the relatively high thermal conductivity will permit one to reduce the temperature low enough to achieve a sufficient degree of alignment to unambiguously assign K-values to fission resonances. In principle, this measurement should be considerably simpler than the spin determination experiment which requires both a polarized beam and a polarized target.

EXPERIMENTAL RESULTS

Presently, unambiguous spin assignments for resonances in slow neutron-induced fission exist only for ^{235}U, ^{237}Np, and although somewhat more ambiguous, for ^{239}Pu.

Because of the scope and number of measurements on ^{235}U, the remainder of this paper will primarily address this single nucleus. We will examine the information available in the resolved region, say below 60 eV, and describe briefly the status of the unresolved region. In both regions the role of spin will be discussed, with help from some new results from an experiment using a polarized neutron beam and polarized ^{235}U target.

The results from a preliminary measurement made at the Oak Ridge Electron Linear Accelerator (ORELA) reported by Keyworth et al[3] in 1973 assigned spins to 65 resonances below 60 eV. The more recent measurement, with increased polarization and statistical accuracy, permit assignments to all known resonances in this energy region. In these measurements, the neutron beam was polarized by transmission through single crystals of $La_2Mg_3(NO_3)_{12} \cdot 24H_2O$ (LMN) in which the protons in the waters of hydration were dynamically polarized. The target was the intermetallic ferromagnetic compound US, which was polarized in a ^3He-^4He dilution refrigerator operated at $\sim$ 0.02°K and in a magnetic field $\sim$ 5 kOe. The details of the methods used are described in Refs. 3 and 4.

The data consist of time-of-flight spectra of fission events occurring in the target with the neutron beam polarized parallel and antiparallel to the target polarization, and of the transmission under the same conditions. The degree of polarization of the neutron beam and of the target was approximately 50% and 15%, respectively. For the analysis of the more recent data, M. S. Moore has devised a new technique of separating the components of the cross section due to J = 3 and J = 4. If N_3 and N_4 are the J = 3 and J = 4 ennanced count rates, i.e. the spin antiparallel and parallel data, then we can write

$$N_3 = A_3\sigma_3\phi + A_4\sigma_4\phi \tag{2a}$$

and

$$N_4 = B_3\sigma_3\phi + B_4\sigma_4\phi, \tag{2b}$$

where σ_3 and σ_4 are the cross sections for J = 3 and J = 4, ϕ is the neutron flux, and the constants A_3, A_4, B_3, and B_4 are determined from f_n, f_N, and I as defined in Eq. (1). Solving for the appropriate spin-dependent components, we get

$$\sigma_3\phi = (B_4N_3 - A_4N_4)/(A_3B_4 - B_3A_4) \tag{3a}$$

and

$$\sigma_4\phi = (A_3N_4 - B_3N_3)/(A_3B_4 - B_3A_4) \tag{3b}$$

In Figs. 1-4 these quantities are plotted for the energy ranges 8-44 eV, where the resonances are resolved, and 200-260 eV, where the resonances are unresolved. This analytical technique has greatly facilitated the analysis in both regions. One can simply assign spins from examination of the plots. Using this technique, these recent data show clearly the existence of previously unresolved overlapping levels of different spin, as exemplified by the structure near 35 eV.

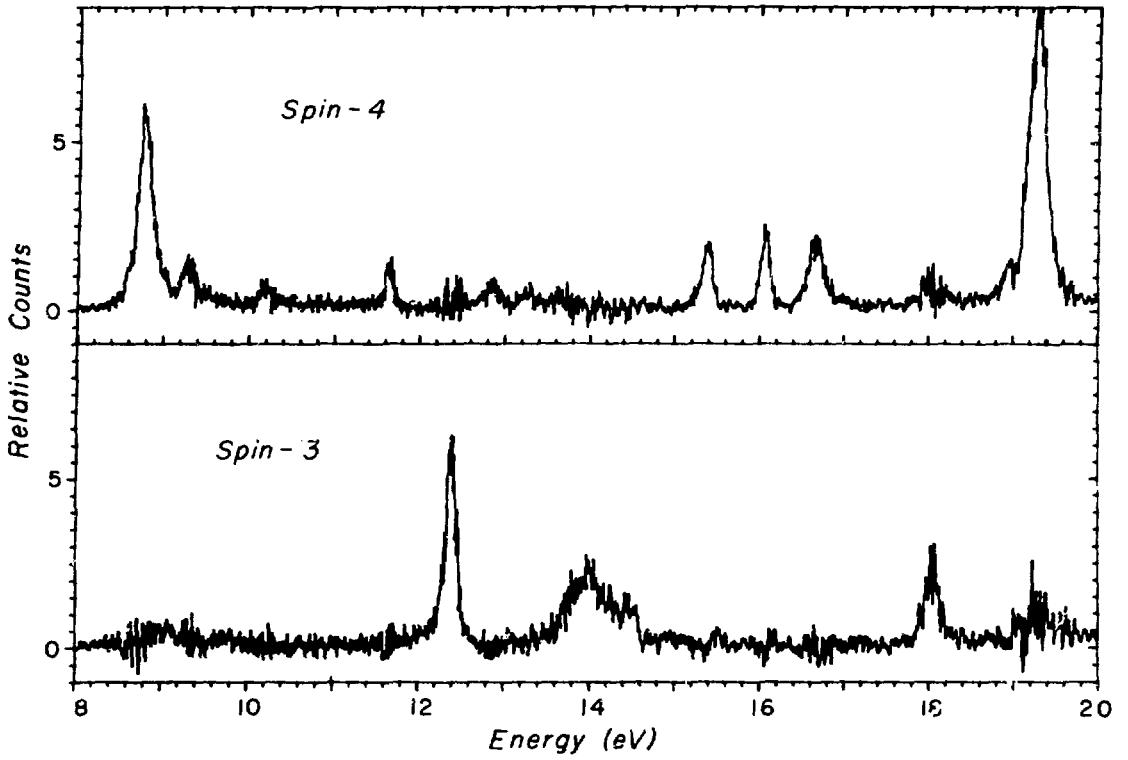

Fig. 1. Spin-separated resonance structure in the fission of $^{235}U + n$ versus neutron energy in the energy range from 8 to 20 eV. Note the presence of the very weak resonance with J = 3 at 9 eV. This resonance has not been seen previously due to the masking effect of the two resonances at 8.8 and 9.3 eV, each with J = 4.

In Fig. 5, we have plotted a stairstep distribution of spacings for resonances with J = 3 and J = 4 below 360 eV. The distributions have constant slope up to 60 eV, and the ratio of the slopes is close to what one expects if the level densities are proportional to (2J + 1). This suggests that few levels are missed below 60 eV. We applied the Δ_3 test of Dyson and Mehta[13] which also indicated that few levels are missed. By requiring that the Δ_3 statistic agree with the value predicted using the Gaussian Orthogonal Ensemble of Dyson,[14] we found probable positions for these few missing levels. With this technique, we arrived at the recommended average spacing of 1.153 eV and 0.896 eV for the J = 3 and J = 4 cases, respectively. This implies a total of 119 levels below 60 eV. As an independent check, we applied a missing level test which is based upon two assumptions:

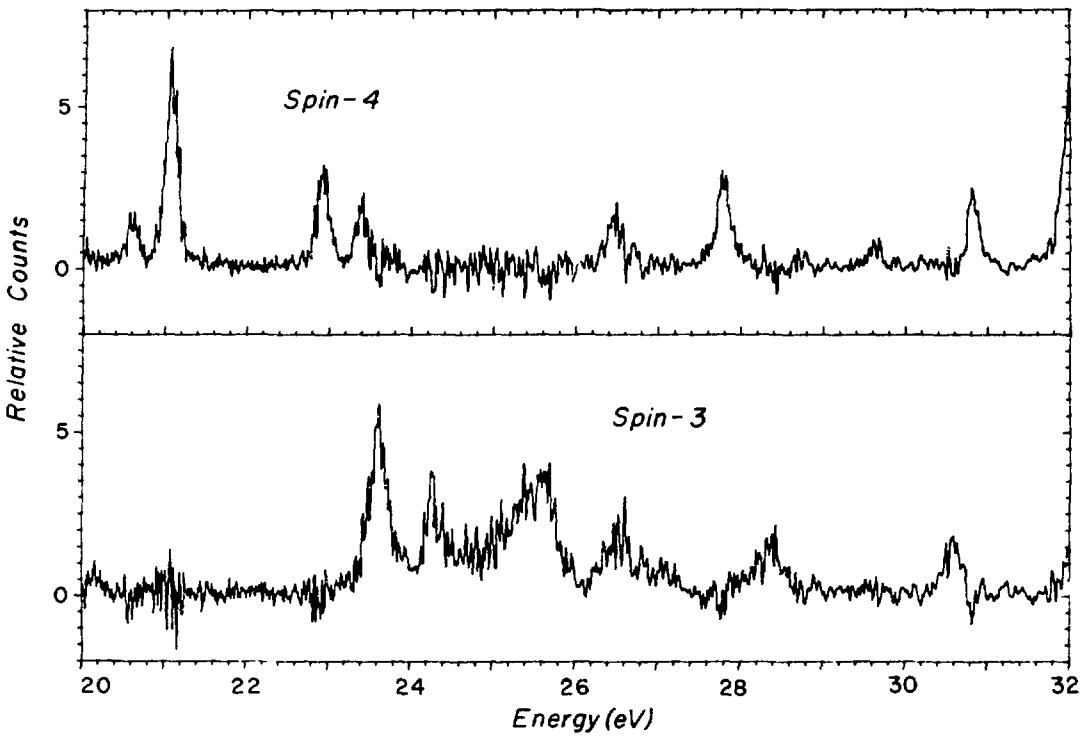

Fig. 2. Spin-separated resonance structure in the fission of ^{235}U + n versus neutron energy in the energy range from 20 to 32 eV. Note the doublet composed of a resonance with J = 4 at 26.4 eV and another with J = 3 at 26.55 eV. Although a comparison of the capture and fission cross sections does indicate two slightly displaced levels, this doublet has not been previously reported.

1) the neutron width distribution is Porter-Thomas, and 2) the widths larger than $\langle \Gamma_n^o \rangle/4$ are accurately known. With these assumptions, and the resonance parameters for ^{235}U of Reynolds,[15] we estimate that there are 110 ± 10 levels below 60 eV, in reasonable agreement with the estimate from the Δ_3 test. We thus feel confident that we have identified and assigned spins to a complete set of resonances in ^{235}U below 60 eV. The number of levels which are missed in the usual type of measurement, in which the spins are not separated, seems to be substantially lower than the statistical analysis of Garrison[16] would indicate. We also see no evidence for a very large number of missing levels as suggested by Felvinci et al.[17] For energies up to 350 eV we have assigned spins to most of the observed structure, although most individual resonances above 200 eV are unresolved.

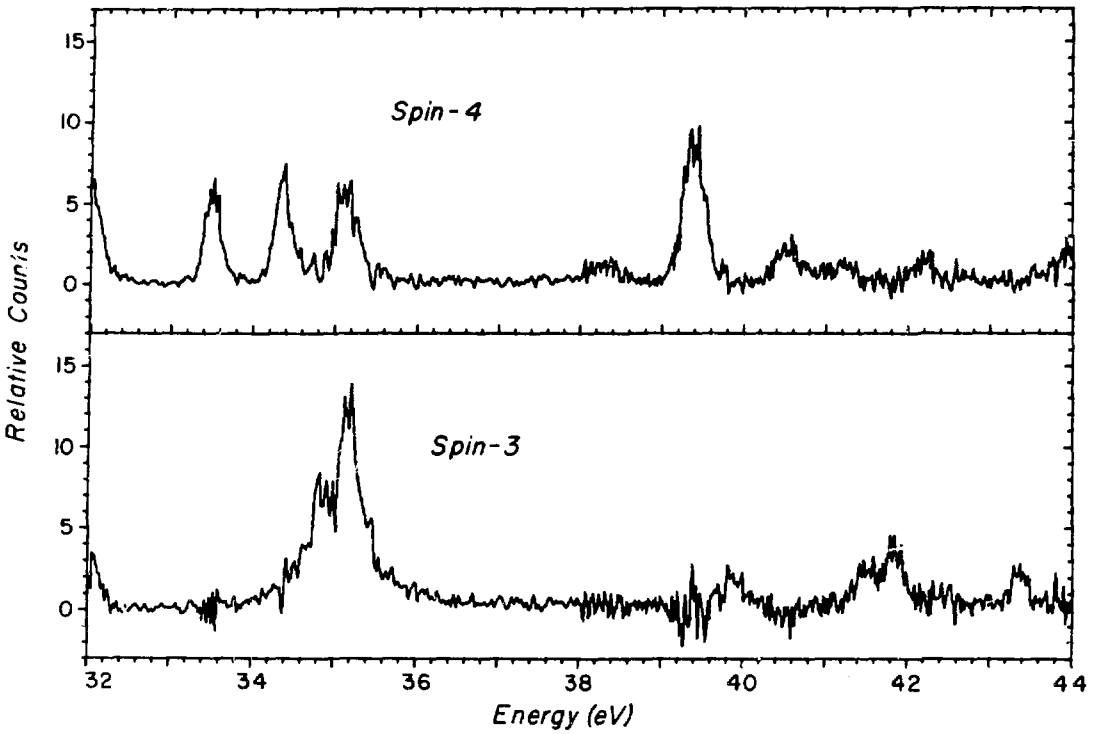

Fig. 3. Spin-separated resonance structure in the fission of ^{235}U + n versus neutron energy in the energy range from 32 to 44 eV. Note the separation of the complex structure in the vicinity of 35 eV.

Two sets of resonance parameters resulting from multilevel analysis of total and all measured partial cross sections are available: 1) those of Smith and Young[18] for ENDF/B-III, and 2) those of Reynolds for ENDF/B-V. Using the Smith and Young fission widths, we calculate $\langle \Gamma_f \rangle_{3^-} = 0.179$ eV and $\langle \Gamma_f \rangle_{4^-} = 0.090$ eV, whereas from Reynold's parameters we get $\langle \Gamma_f \rangle_{3^-} = 0.220$ eV and $\langle \Gamma_f \rangle_{4^-} = 0.098$ eV. This discrepancy can be attributed to the different values for the radiation widths of $\langle \Gamma_\gamma \rangle = 0.0355$ eV determined by Smith and Young and $\langle \Gamma_\gamma \rangle = 0.042$ eV assumed by Reynolds. The Bohr-Wheeler estimate, modified for a double-humped barrier, is expressed by

$$\langle \Gamma_f \rangle = \frac{n\langle D \rangle}{4\pi} \qquad (4)$$

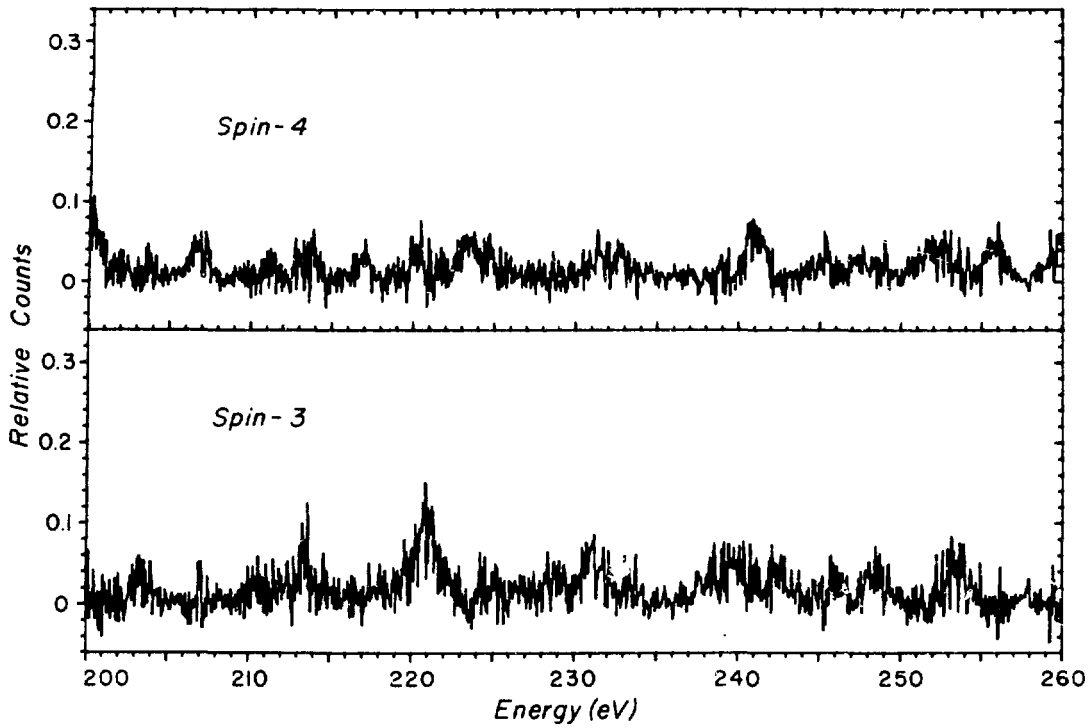

Fig. 4. Spin-separated structure in the fission of ^{235}U + n versus neutron energy in the energy range from 200 to 260 eV.

where n corresponds to the number of open channels. Using this expression, we arrive at fission widths of $\langle \Gamma_f \rangle_{3^-} = 0.092$ eV and $\langle \Gamma_f \rangle_{4^-} = 0.071$ eV for each open channel. The results of the two multilevel analyses are consistent with approximately two open channels for J = 3, or more if the channels are only partially open, and with no more than one fully open channel for J = 4 resonances.

Additional information regarding the configuration of those fission channels may be gleaned from the Pattenden and Postma[10] data on the angular distribution of fission fragments from aligned ^{235}U. This angular distribution may be expressed as

$$W(\theta) = 1 + \sum_{\substack{n \text{ even} \\ n \leq 2I}} A_n f_n(I) P_n(\cos \theta) \qquad (5)$$

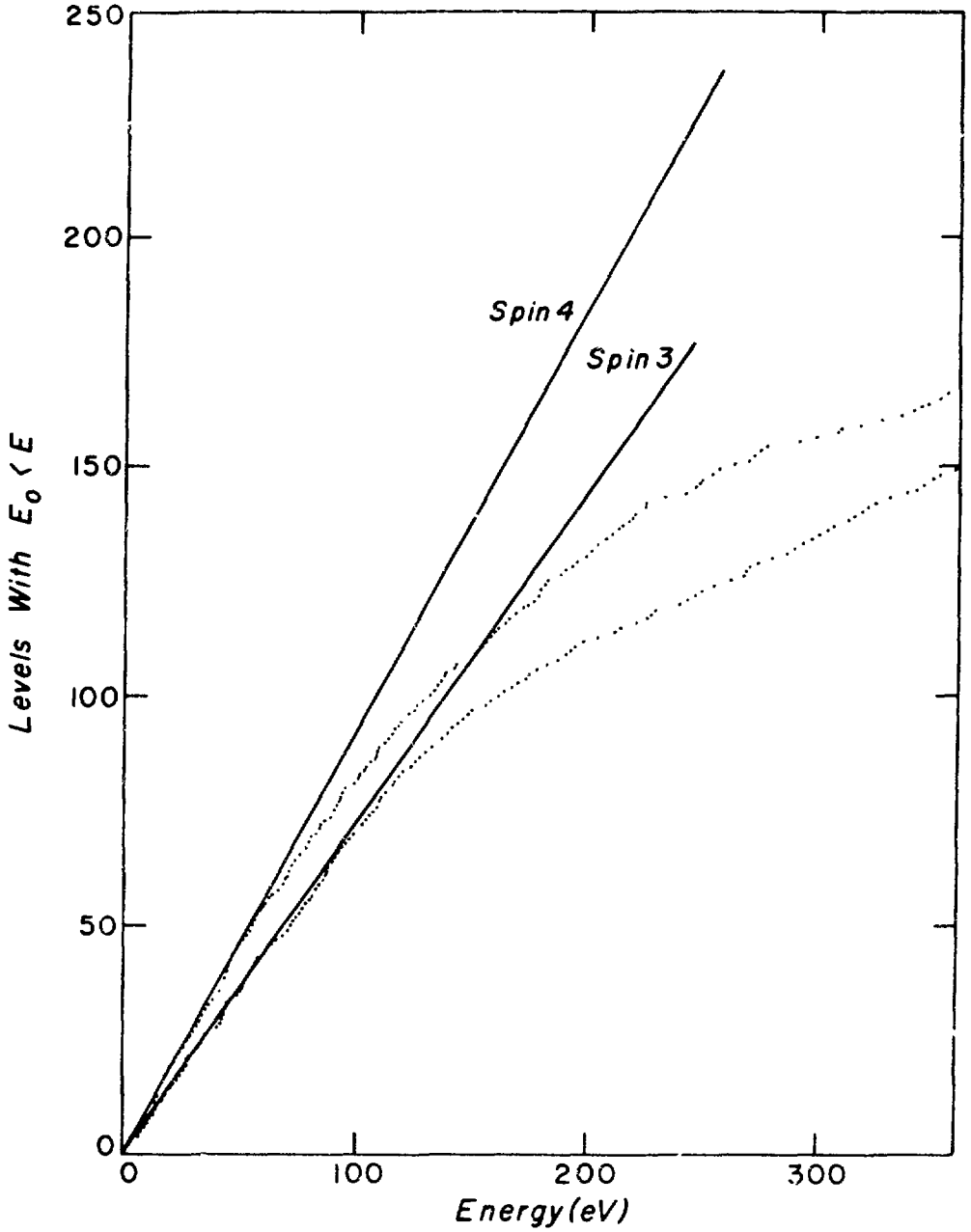

Fig. 5. Observed resonance spacing distribution in (^{235}U + n) below 360 eV. Data points give the number of levels having a resonance energy less than the energy shown on the abscissa, and correspond to the tips of the stairs in the usual stairstep plot. The solid lines represent a fit to the data points below 60 eV, and show the expected (2J + 1) slope.

Where the A_n parameters contain the geometric factors, the f_n are the alignment parameters, and P_n are the Legendre polynomials. In the Pattenden and Postma measurements, only the A_2 terms are measured. For a well-resolved resonance with known spin and unique K, measurement of A_2 should determine K. Because of the use of a fission booster target with a relatively long pulse of 230 ns and a short (10 m) flight path, few of the resonances in the Pattenden and Postma experiment were well resolved. Thus, we define an average or effective J value for $^{235}U + n$ as

$$J_{eff} = 3 + \frac{\sigma_4}{\sigma_3 + \sigma_4} \tag{6}$$

where σ_3 and σ_4 are the spin-3 and spin-4 cross sections used in Eqs. (2a) and (2b). A plot of A_2 versus J_{eff} is shown in Fig. 6. The solid line in the figure represents a least-squares fit to the data and may be used to infer the average value of A_2 for pure spin-3 resonances ($J_{eff} = 3.0$) and for pure spin-4 resonances ($J_{eff} = 4.0$). We thus obtain $\langle A_2 \rangle_{J=3} = 1.22$ and $\langle A_2 \rangle_{J=4} = 2.01$. Knowing that the (J,K) = (4,0) channel is forbidden because of parity conservation and recalling the assumptions from above on the number of open channels for each spin state, we may assume that the two lowest channels, (J,K) = (4,1) and (4,2), are open. Knowing the A_2 value for each (J,K), we may calculate the contribution from each channel. If for the average fission widths we take the mean of the averages from the two multilevel analyses, we get $\langle \Gamma_f \rangle_{J=3} = 0.20$ eV and $\langle \Gamma_f \rangle_{J=4} = 0.094$ eV. For the J=4 resonances, we determine $\langle \Gamma_f \rangle_{J,K=4,1} = 0.075$ eV and $\langle \Gamma_f \rangle_{4,2} = 0.019$ eV. This implies that since the (J,K) = (4,1) channel is fully open, the (3,1) channel should also be fully open with a fission width of .096 eV. Solving for the K = 0 and 2 channel widths, we get $\langle \Gamma_f \rangle_{J,K=3,0} = 0.020$ eV and $\langle \Gamma_f \rangle_{3,2} = 0.084$ eV. However, the assumption of $\langle \Gamma_f \rangle_{3,0} = 0$ and thus $\langle \Gamma_f \rangle_{3,1} = \langle \Gamma_f \rangle_{3,2} = 0.100$ eV is not inconsistent with the errors involved. The surprising fact is that, although it has long been assumed that the channels open in order of ascending K, following the sequence of octupole bands observed near the ground states of even-even nuclei. Why the (J,K) = (3,0) channel is either completely or nearly completely closed can presently only be answered hypothetically.

Although we know that the average behavior is consistent with the above explanation based on the fission channel concept, we do not yet know whether K is a conserved quantum number in fission. One notes in Fig. 6 that the points are nearly uniformly distributed over a broad range of A_2 values. This implies that the observed angular distribution is not consistent with integer K-values, but rather there is an admixture of the fission channels. However, one must be wary of overinterpreting the Pattenden and Postma results due to the lack of well-resolved resonances in this data.

The preceding discussion addresses only the resolved region in ^{235}U. It has been suggested [20,21] that the fluctuations in the unresolved region result from local enhancement due to broad states in the second well of the double-humped fission barrier. Keyworth et al[41] showed that for $^{237}Np + n$, the subthreshold fission resonances corresponding to a single state in the second well all have the same spin. If the structure in $^{235}U + n$ involves a similar mechanism, then one would expect a spin dependence.

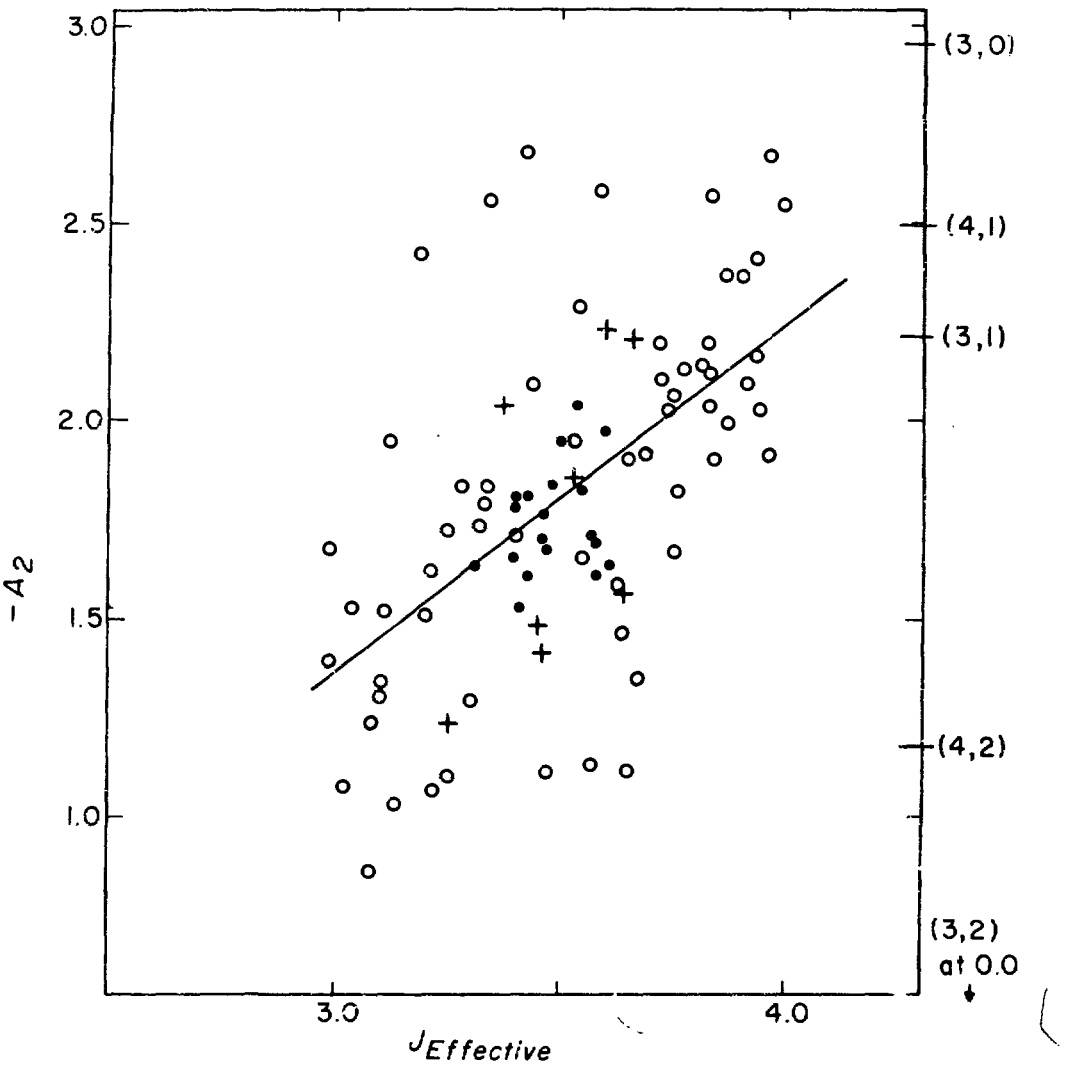

Fig. 6. The variation of A_2 from Pattenden and Postma versus $J_{effective} = 3 + \sigma_4/(\sigma_3 + \sigma_4)$. The straight line shows a linear least-squares fit to these data. The open circles show A_2 data for resonance structure, the closed circles data for the unresolved region below 2 keV, and the plus signs data for the between-resonance background regions reported by Pattenden and Postma.

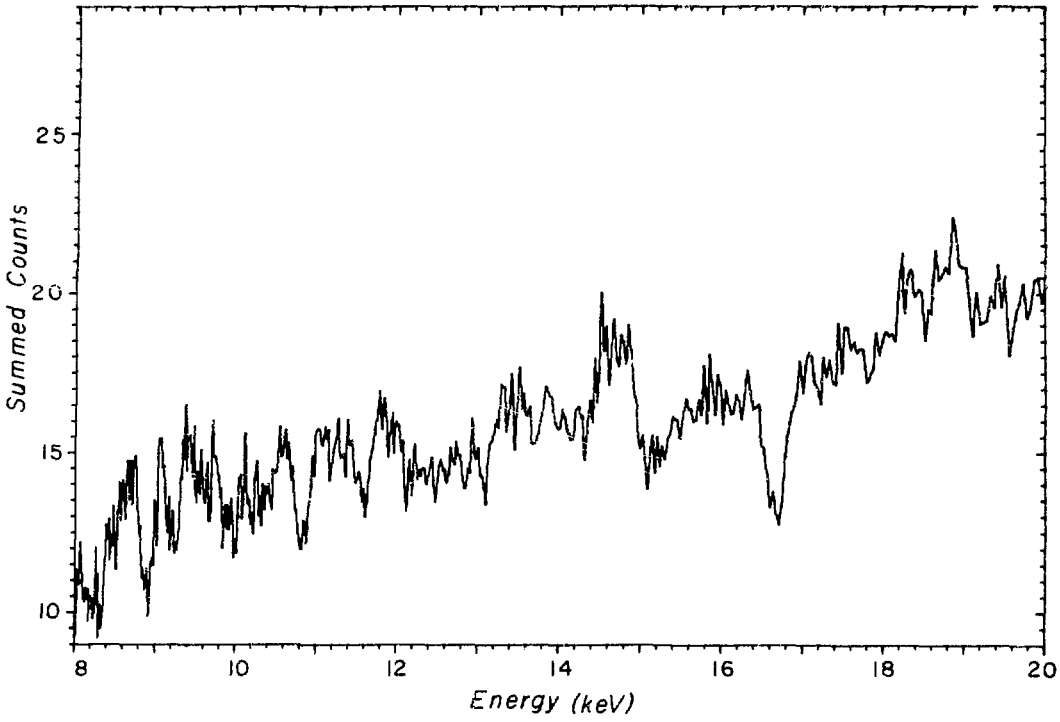

Fig. 7. Summed counts (spin-3 enhanced plus spin-4 enhanced count rates) observed in the fission of (^{235}U + n) versus neutron energy in the energy range from 8 to 20 eV.

The fission cross section of ^{235}U + n in the range 8 - 20 keV is shown in the plot of summed counts, $N_3 + N_4$, in Fig. 7. The large fluctuations are clearly evident. However, the spin-separated data over the same energy region, shown in Fig. 8, show minimal evidence for any spin dependence in the fluctuation, possibly due to the poor statistical accuracy. To test quantitatively for intermediate structure, we then pursued statistical tests on broad-bin averages. Following Migneco et al,[20] we initially carried out a Wald-Wolfowitz runs-distribution test from 0.1 to 25 keV on $J_{eff} - \langle J_{eff} \rangle$ using bins of 240 and 400 eV, and from 0.1 to 10 keV with bins of 85 eV. Although Migneco et al reported that this test gave significant results when applied to σ_f for ^{235}U, the test applied to the polarization data gave results consistent with a random distribution of spin. A similar calculation of the serial correlation coefficients of J_{eff} followed by a Wald-Wolfowitz test on these coefficients again showed no significant departure from a random distribution.

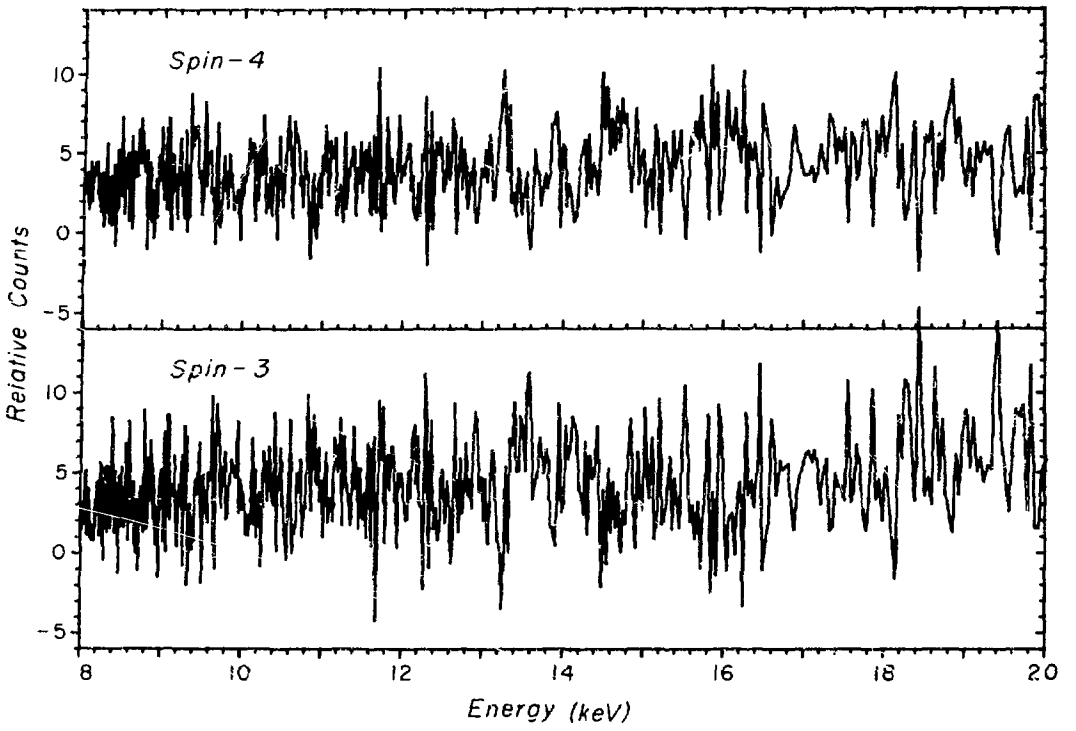

Fig. 8. Spin-separated count rates in the fission of (^{235}U + n) versus neutron energy in the energy range from 8 to 20 keV. Except for the cluster between 14 and 15 keV, which is clearly spin 4, it is not obvious that either of these curves correlates with that shown in Fig. 7.

Another test, however, showed a more interesting result. We calculated the correlation coefficient between the spin-3 data and the summed counts and between the spin-4 data and the summed counts, for broad-bin averages. The results, shown in Table I, imply that the observed structure is attributable to spin 4. Apparently, there is still enough statistical error associated with the broad-bin averages that it masked the effect when we used the usual tests for intermediate structure. We do feel, however, that the results shown in Table I are definitive and show that essentially all the fluctuating part of the ^{235}U fission cross section in the region analyzed has J=4. We thus conclude that these polarization data give strong support to the hypothesis that the fluctuations in the ^{235}U fission cross section are a second-well phenomenon.

CONCLUSIONS

Knowledge of the ^{235}U + n system has been substantially enhanced by removing uncertainties in the resonance spins. For an understanding of the average properties, division of the resonances into the appropriate spin groups permits an accurate description of the cross section. However, understanding of the underlying fission process remains incomplete.

For example, with this spin information, one may search for a dependence upon J and K of the fission fragment mass distribution, fragment kinetic energy distribution, and $\bar{\nu}$. Although available measurements of these quantities are limited in resolution and scope, there is no clear evidence for dependence upon spin alone. In fact, measurements[21,22] of $\bar{\nu}$ over several of the larger resonances in ^{235}U clearly preclude a dependence of this quantity upon J alone. However, it has been demonstrated[23] that the (n,γf) process can account for the relatively large fluctuations of $\bar{\nu}$ in ^{239}Pu. Although the evidence[24] is less persuasive in the case of ^{235}U, this process is probably involved in the $\bar{\nu}$ variations. One may well expect that the fragment mass and kinetic energy distributions are dependent upon J and K but the poor state of knowledge of K values coupled with the poor resolution in existing measurements makes detailed interpretation tenuous.

What is needed is a coherent approach toward answering these questions, initially in ^{235}U alone. Using the new time-of-flight facility being implemented at the Los Alamos Meson Physics Facility (LAMPF), the Weapons Neutron Research Facility (WNR), we are pursuing such an approach. Using an antiferromagnetic intermetallic compound of uranium rather than the paramagnetic crystals used by Dabbs and Pattenden and Postma, we hope to achieve sufficient alignment of ^{235}U with sufficient resolution to determine the K-value, or the admixture of K-values, for each J-value assigned in the measurements using a polarized target and beam. Concurrently, we will use the intense low energy neutron flux at the WNR facility to determine the fragment kinetic energy distribution and the fragment mass distribution for the larger resonances in ^{235}U. We expect that the results of these proposed measurements, in conjunction with existing data, will provide answers to those questions on ^{235}U addressed earlier in this paper.

TABLE I

Correlation coefficients and significance levels for the correlation of spin-3 and spin-4 data with structure in ^{235}U σ_f, from 8 - 25 keV. In this table, the significance level is the probability that the observed correlation or larger would occur with a randomly selected sample.

Energy Range (keV)	Bin Width (keV)	$\rho(N_3,\Sigma)$	Significance of $\rho(N_3,\Sigma)$	$\rho(N_4,\Sigma)$	Significance of $\rho(N_4,\Sigma)$
8.0 - 10.4	0.12	-0.01617	~0.50	0.7048	0.0003
10.4 - 12.8	0.12	0.2148	0.18	0.6148	0.002
12.8 - 15.2	0.12	0.0889	0.35	0.3815	0.05
15.2 - 20.0	0.24	0.1996	0.20	0.7111	0.0002
20.0 - 24.8	0.24	0.2336	0.16	0.7443	0.0001
24.8 - 34.4	0.48	0.2864	0.11	0.8194	<0.00001

REFERENCES

1. J. E. Lynn, Proc. Int. Conf. on Nuclear Data for Reactors, Paris, vol. 2, (1966), p. 89.

2. A. Bohr, Proc. 1st Conf. on Peaceful Uses of Atomic Energy, Geneva, vol. 2, (1956), p. 151

3. G. A. Keyworth, C. E. Olsen, F. T. Seibel, J. W. T. Dabbs, and N. W. Hill, Phys. Rev. Lett., 31, 1077 (1973).

4. G. A. Keyworth, J. R. Lemley, C. E. Olsen, F. T. Seibel, J. W. T. Dabbs, and N. W. Hill, Phys. Rev. C8, 2352 (1973).

5. F. Corvi, M. Stefanon, C. Coceva, and P. Giacobbe, Nucl. Phys. A203, 145 (1973).

6. R. G. Graves, R. E. Chrien, D. J. Garber, G. W. Cole, and O. A. Wasson, Phys. Rev. C8, 787 (1973).

7. H. Weigmann, J. Winter, and M. Heske, Nucl. Phys. A134, 535 (1969).

8. W. R. Kane, Phys. Rev. Lett. 25, 953 (1970).

9. J. W. T. Dabbs, F. J. Walter, and G. W. Parker, Proc. Symposium on Physics and Chemistry of Fission 1, Salzburg (1965), p. 39.

10. N. J. Pattenden and H. Postma, Nucl. Phys. A167, 225 (1971).

11. R. Kuiken, N. J. Pattenden, and H. Postma, Nucl. Phys. A190, 401 (1972).

12. R. Kuiken, N. J. Pattenden, and H. Postma, Nucl. Phys. A196, 389 (1972).

13. F. J. Dyson and M. L. Mehta, J. Math. Phys. 4, 703 (1963).

14. F. J. Dyson, J. Math. Phys. 3, 140 (1962).

15. J. T. Reynolds, KAPL-M-7396 (1975).

16. J. D. Garrison, Phys. Rev. Lett. 29, 1185 (1972).

17. J. Felvinci, E. Melkonian, and W. W. Havens, Jr., Nuclear Cross Sections and Technology, NBS Special Publication 425, 580 (1975).

18. J. R. Smith and R. C. Young, ANCR-1044 (1971).

19. G. D. James, G. de Saussure, and R. B. Perez, Trans. Am. Nuc. Soc. 17, 495 (1973).

20. E. Migneco, P. Bonsignore, G. Lanzanò, J. A. Wartena, and H. Weigmann, Nuclear Cross Sections and Technology, NBS Special Publication 425, 607 (1975).

21. R. E. Howe, T. W. Phillips, C. D. Bowman, Phys. Rev. C13, 195 (1976).

22. R. L. Reed, Ph. D. Thesis, Rensselaer Polytechnic Institute, 1973 (unpublished).

23. D. Shackleton, J. Trochon, J. Fréhaut and M. Le Bars, Phys. Lett. 42B, 344 (1972).

24. G. Simon, D. Sc. Thesis, Paris (1975).

ME 2 - SPIN DETERMINATION OF FISSION RESONANCES - G. A. Keyworth (LASL, Los Alamos, USA)

No discussion.

[illegible] a.m., Wednesday, July [illegible]

NEUTRON INDUCED REACTIONS ON VERY LIGHT AND LIGHT NUCLEI

Ivo Šlaus

Institute "Rudjer Bošković", Zagreb, Yugoslavia

RÉSUMÉ

A critical survey of (n,p), (n,d), (n,t), (n,α) reactions on light nuclei (A 40) and of multiparticle breakup processes D(n,2n)p, ^{6}Li(n,dα)n, ^{7}Li(n,tα)n, ^{10}B(n,$\alpha\alpha$t), ^{10}B(n,$\alpha\alpha$d)n, ^{12}C(n,3α)n, and ^{14}N(n,3αt) is presented.

ABSTRACT

This review paper outlines the information on current progress of neutron interactions with light nuclei. The following topics are discussed: d+n: total breakup, n-n and n-p quasifree scattering and final state interactions; n+d $\longrightarrow$ t+γ radiative capture; t+n elastic scattering and breakup data; (n,p) angular distributions on ^{3}He, ^{6}Li, ^{7}Li, ^{10}B, ^{12}C, ^{14}N, ^{16}O, ^{19}F, ^{27}Al, ^{32}S, and ^{40}Ca; (n,d) angular distributions on ^{3}He, ^{6}Li, ^{7}Li, ^{10}B, ^{11}B, ^{14}N, ^{15}N, ^{16}O, ^{19}F, ^{27}Al, ^{32}S, ^{34}S, ^{35}Cl and ^{36}Ar; (n,t) angular distribution on ^{6}Li, ^{7}Li, ^{10}B, ^{11}B, ^{14}N and ^{19}F and (n,α) angular distributions on ^{9}Be, ^{11}B, ^{14}N and O^{16}. A summary of n+^{12}C is presented.

A 4π type study of multiparticle particle breakup processes ^{6}Li(n,dα)n, ^{7}Li(n,tα)n, ^{10}B(n,$\alpha\alpha$t), ^{10}B(n,d$\alpha\alpha$)n, ^{12}C(n,3α)n, and ^{14}N(n,3αt) provide insight into reaction mechanisms: sequential decays and quasifree scatterings.

Most of the data are obtained at E_{inc} 14 MeV. However, the development of neutron facilities at Van de Graaff, isochronous cyclotrons and meson facilities have provided data also at other energies.

Information on nuclear interaction and nuclear structure obtained from these studies is discussed.

NEUTRON INDUCED REACTIONS ON VERY LIGHT AND LIGHT NUCLEI

Ivo Šlaus

Institute "Rudjer Bošković", Zagreb, Yugoslavia

1. Introduction

The aim of this paper is to outline the information on current progress of neutron interaction with light nuclei. We will concentrate on neutron induced reactions and consequently we will almost completely omit discussing the elastic and inelastic neutron scattering.

Most of the neutron data have been obtained at $E_{inc} \sim 14$ MeV (Si 68). However, neutron facilities developed at Van de Graaff accelerators, at isochronous cyclotrons, particularly at Crocker Nuclear Laboratory, UC Davis and at Kernforschungs Zentrum, Karlsruhe, and at meson facilities have now provided significant data at other energies.

2. The n-d breakup reaction

2.1. The total breakup cross section has been measured: i) "directly" by detecting breakup products and ii) "indirectly" by subtracting the integrated elastic differential cross section from the total n-d cross section (the cross sections for n-d Bremsstrahlung and for radiative capture are negligible. The cross section for radiative capture becomes significant only below 100 eV).

The indirect measurements have been performed using both p-d (Ho 68) and n-d (Se 70, Se 72, Ro 70) elastic scattering angular distributions. The p-d angular distributions have been corrected for Coulomb effects. The uncertainties in these indirect measurements are represented by results at 18.55 and 23 MeV (Se 72).

Early direct measurements have been confined to energies around and below 14 MeV (Ca 61, Ho 69, Gr 71). Pauletta and Brooks have recently (Pa 75, Pa 73) measured the n-d breakup cross section from $E_{inc} = 8$ to 22 MeV by integrating the energy distribution of breakup

protons and recoil deuterons observed in the deuterated scintillator used both as a detector and as a deuterium target. (see Fig. 1.)

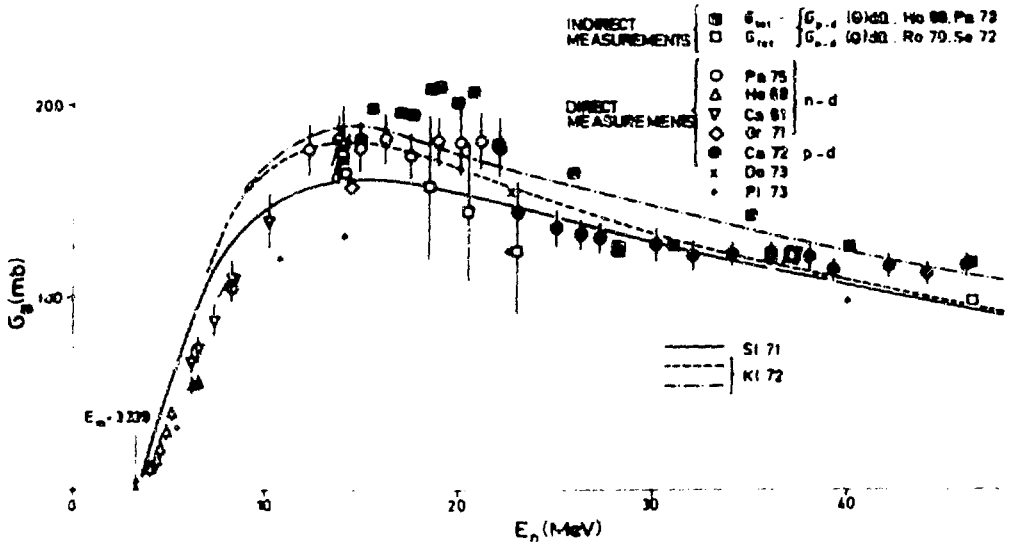

Fig. 1.

The energy of charged particles have been deduced from the integrated scintillation output (L). A pulse shape discrimination has been used to obtain a pulse (S) characteristic of the scintillation decay time and hence of the nature of the ionizing particle. The schematic representation of the experiment is shown in Fig. 2. An isometric representation of an LS spectrum obtained for 22 MeV neutrons incident on deuterated benzene is shown in Fig. 3. Letters: e, p, d, and alpha indicate the ridges due to electrons, protons, deuterons and alphas. One can clearly see the minimum in the deuteron ridge; which corresponds to the minimum in the n-d elastic differential cross section. The feature of this setup is the simultaneous measurement of proton and deuteron energy spectra. Therefore, it is not necessary to know either the number of target nuclei or the

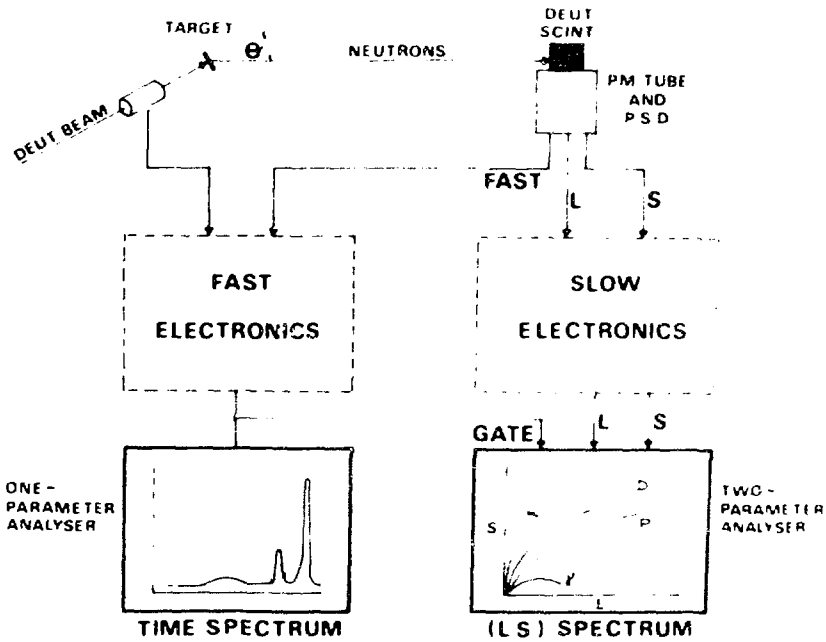

Fig. 2.

number of incident neutrons. Fig. 4. shows the measured proton energy distribution at E_{inc} = 22 MeV. The enhancements are associated with n-p and n-n final state interactions (FSI). The crosses at low energies have been obtained by subtracting the contribution from the reaction $^{12}C(n,p)^{12}B$. The low energy portion of the proton spectrum is estimated by assuming that it is given by the phase space normalized to the data at $0.4\ E_p^{max} \leq E_p \leq 0.7\ E_p^{max}$. The

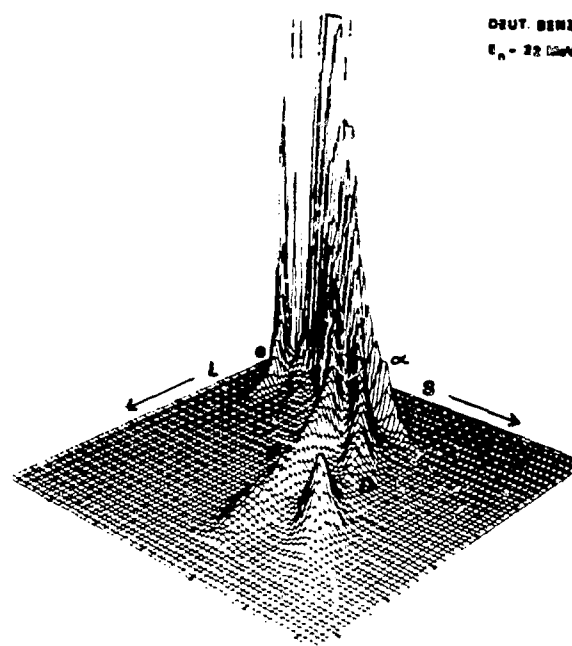

Fig. 3.

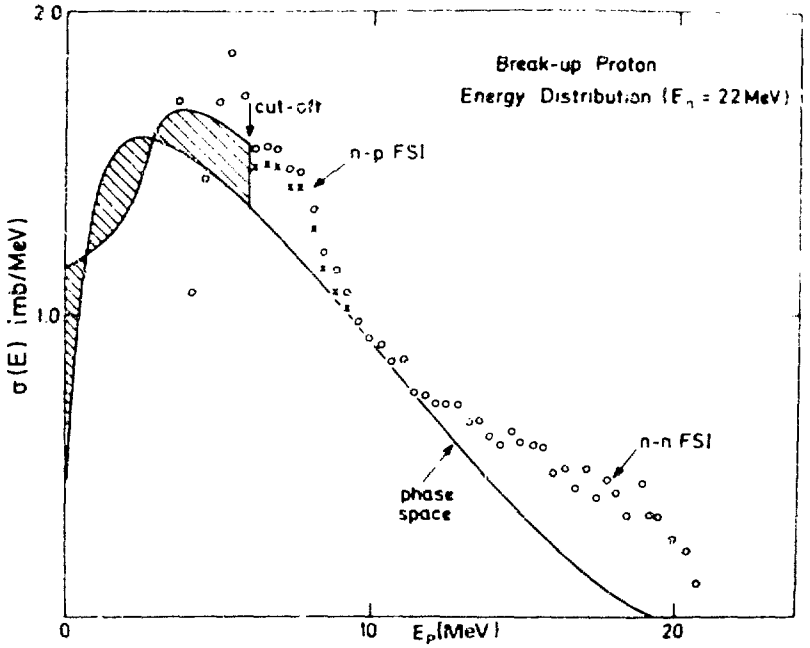

Fig. 4.

measured energy spectra have been corrected for edge effects, multiple scattering and proton spectra also for the contribution of recoil protons. The contribution due to n-n quasifree scattering (QFS) is localized at low proton energies, whereas that due to n-p QFS is distributed over all proton energies. Since n-n FSI angular distribution is peaked at small proton angles, the enhancement due to n-n FSI is localized at higher proton energies, and the n-p FSI around 4/9 E_p^{max}. The uncertainties in the cross section due to extrapolation of the proton energy spectra are of the order of the n-n QFS contribution, which is estimated to be less than the n-n FSI contribution (at $E_{inc} \leq 30$ MeV).

The breakup cross section σ_B has been determined by two methods:

a) $\sigma_B = \sigma_{peak} \frac{Ip}{Ipeak}$ where Ipeak is obtained by integrating the measured deuteron energy distribution from the minimum, σ_{peak} is the corresponding integral obtained from N-d angular distribution, and Ip is the integral of the proton energy distribution extrapolated to zero energy assuming the phase space shape.

b) use n-d elastic data to obtain the total deuteron integral Id from Ipeak : $\sigma_B = \sigma_T/(1 + Id/Ip)$, where σ_T is the total cross section.

The results obtained by two the methods agree and the mean values are given in Fig. 1.

The n-d total breakup cross section data are compared in Fig.1. with p-d data from 22 to 46 MeV (Ca 72) and with the calculations based on the Faddeev formalism:

i) Kloet and Tjon (Kl 72) have used local S wave potentials. Dashed curve in Fig. 1. is for Malfliet - Tjon potential I-III (repulsive cores in both singlet and triplet N-N interaction), while the dashed-dotted is for Malfliet - Tjon potential I-IV (repulsive core only in singlet states).

ii) Sloan (Sl 71) has used the separable S wave interaction (solid curve).

iii) Doleschall (Do 73) has included in the exact calculation also the P wave separable interaction (x's).

iv) Pieper (Pi 73) has included both P and D waves separable interaction, but only perturbatively (crosses).

One can conclude:

1) The total breakup cross section for N+d is measured up to $E_{inc} \sim 50$ MeV with an accuracy which varies from 7 to 25%.

2) The data agree with the calculations based on the Faddeev formalism using rather simple N-N force.

3) The total breakup cross section is a sensitive observable to distinguish various features of the nuclear force.

2.2. The n-n QFS

Two measurements of the D(n,2n)p reaction at QFS kinematic conditions have been performed at $E_{inc} = 14.1$ MeV at $\theta_{n1} = \theta_{n2} = 30^\circ$, $\phi_{12} = 180^\circ$ (Fig.5., left hand side, open circles Sl 71a, points Bo 75) and $\theta_{n1} = \theta_{n2} = 40^\circ$, $\phi_{12} = 180^\circ$ (right hand Bo 75) and have been compared with the predictions of the calculation based on the Faddeev formalism using the S wave separable interaction with Yamaguchi (Y) and exponential form factors (E) in both singlet and triplet states.

These measurements are faced with considerable technical

difficulties due mainly to the rather severe background from gamma rays, direct and scattered neutrons, to low intensities of incident neutrons, and to the modest efficiency of neutron counters. The experimental setup used in (Sl 71a, Th 73): incident neutrons, collimated by the associated alpha-particles, strike a C_6D_6 target-

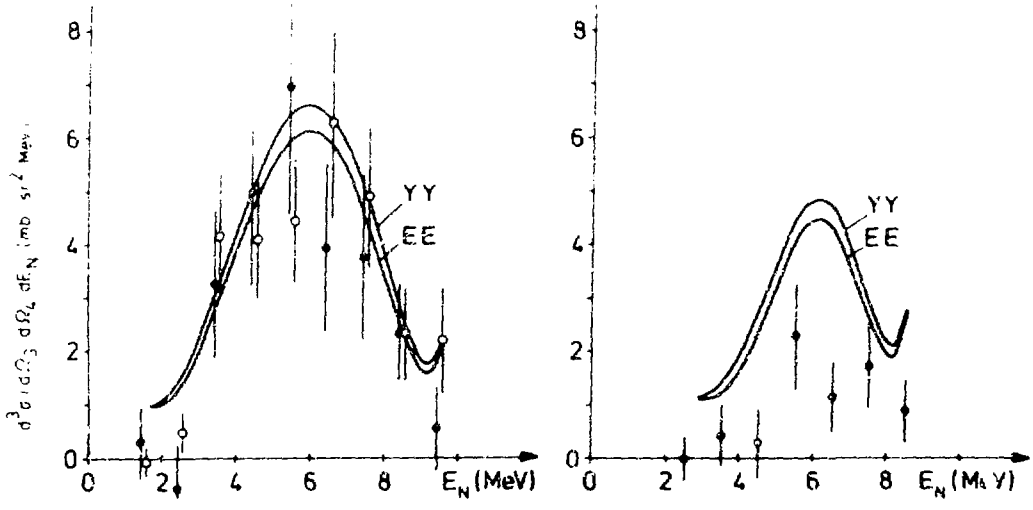

Fig. 5.

scintillator. The proton from the deuteron breakup is detected in this counter and it provides the start for a T.O.F. measurements of two neutrons scattered in fixed directions Θ_{n1} and Θ_{n2}. Requirement of the coincidence (few ns) between the C_6D_6 and the alpha counter virtually eliminates the fraction of the counting rate in the C_6D_6 due to gamma rays. To further reduce the accidental coincidences "reject" alpha counters have been introduced at 180° in the line joining the neutron source to the neutron counters. In addition, pulse shape discriminations have been used in the C_6D_6 and in the neutron counters. This experimental setup enables the measurement of seven independent kinematic variables: energies of two neutrons (E_{n1},E_{n2}), proton energy (E_p), the directions of two neutrons (Θ_{n1},Θ_{n2},ϕ_{12}) and

the incident neutron energy (E_{inc}). The cross section for the multiparticle reaction resulting into N particles in the final state depends on $3N-4$ independent kinematic variables (IKV). Since for N=3, there are 5 IKV, this set... kinematically overdetermines the measurement providing two additional constraints. For QFS kinematic conditions the energy of the spectator proton is very low (typically $0 \leq E_p \leq 1$ MeV) and successful measurements have been reported (Bo 75) even without information about the breakup proton.

The n-p QFS has been measured at E_{inc}= 14.4 at $\Theta_n = \Theta_p = 30^\circ$, $\phi_{12} = 180^\circ$ (Va 70) and the data have been compared with the Faddeev type calculations (Sl 71a).

2.3. The n-n FSI

The contribution of the n-n FSI to the total breakup cross section has been determined by measuring the n-n FSI enhancement over the phase space (Pa 73) and by integrating over energy and angle the upper end of the proton energy spectra (De 66). Fig. 6. shows this contribution, δ, as a percentage of σ_B.

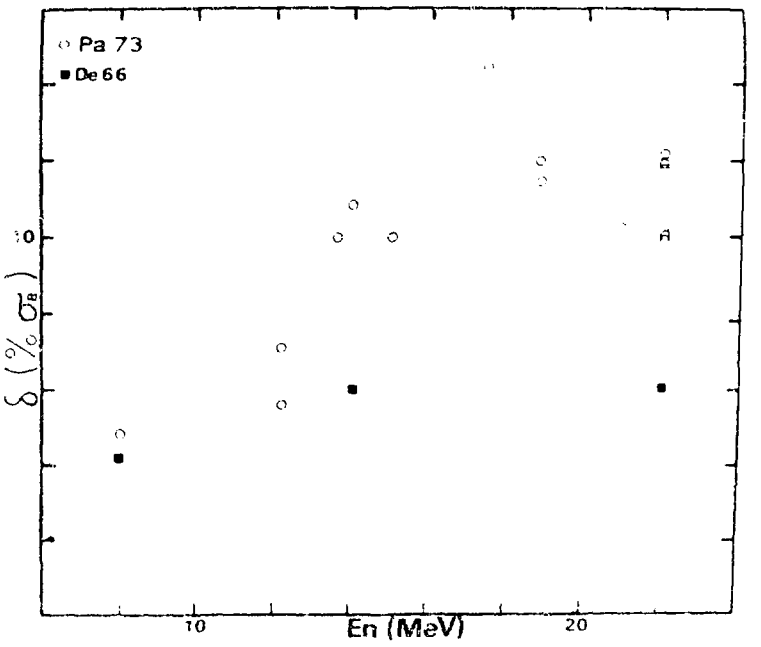

Fig. 6

Three different geometries have been used to study the n-n FSI in the reaction nd $\rightarrow$ nnp:

i) detecting breakup protons at forward angles. One measures three variables: E_p, θ_p, and E_{inc} and thus the process is not kinematically determined. Proton energy spectra measured at several incident energies and at several forward angles (Il 61, Ce 64, Vo 65, Ba 67, Bo 68, Pr 70, St 72, Sh 73) reveal a pronounced enhancement at E_p^{max} due to n-n FSI at $E_{nn} \sim 0$ and therefore, it is in principle possible to extract n-n effective range parameters: a_{nn} and r_{nn}. It has been shown (Ca 74) that in this geometry the analyses based on Watson-Migdal model, Born approximation, impulse approximation and the Komarov-Popova treatment are not correct. It is necessary to perform the analysis based on the Faddeev theory. An additional disadvantage of this geometry is the strong dependence on the energy resolution (if an experimental resolution is 400 keV it is necessary that the statistical accuracy is $\sim$ 3% (Da 73)). The FSI enhancement depends on a_{nn} and only weakly on r_{nn} (varying r_{nn} from 2.2 to 3.4 fm does not change a_{nn} more than the uncertainty due to the present statistical accuracy of the data). The values of a_{nn} extracted from these measurements are listed in Table 1. Recently this reaction has been measured a) at Grenoble (Bo 76) using multiwire counters giving each proton trajectory a 1° accuracy. The shape of the FSI enhancement and its absolute magnitude did not give so far a definite value for a_{nn}. b) at Lawrence Livermore Laboratory (Ha 75) using a charged particle magnetic quadrupole spectrometer with 200 keV energy resolution (twice as good as in any of the previous measurements). A 14 MeV neutron source producing 4×10^{12} n/s has been used. The analysis is in progress.

ii) measuring the momenta of two outgoing neutrons and the energy of the breakup proton providing together with the knowledge of the incident energy seven IKV and thus kinematically overdetermining the process (Ze 72, Ze 74, Bo 72, Br 74, Ho 68a, Gr 69a, Mc 75a). Simultaneous study of n-n FSI ($\theta_{n1} = \theta_{n2} = 30^\circ$, $\phi_{n1} = 180^\circ$, $\phi_{n2} = 165^\circ$) and of n-p FSI ($\theta_{n2} = 30^\circ$, $\theta_{n3} = 84.3^\circ$, $\phi_{n2} = 165^\circ$, $\phi_{n3} = -7.5^\circ$) allows to determine the n-n effective range, r_{nn}, from the ratio of two

Table 1.

a_{nn} from D(n,p)2n measurements

E_{inc} (MeV)	Θ_p	a_{nn} (fm)	used r_{nn} (fm)	analysis	Ref.
14.4	4°	-22 ± 2	2.84	Born+Watson-Migdal	Il 61
14.4	4.8°	-21.7 ± 1	2.8	Born+Watson-Migdal	Ce 64
14	0°	$-23.6 \pm 2 \pm 1.6$		Komarov-Popova	Vo 65
14		-14 ± 3		Impulse Appr.	Ba 67
		-16 ± 3		Born Appr.	Ba 67
8-28	5°,20°	-15.9 ± 1.1	2.8	Impulse Appr.	Bo 68
		-30		Watson-Migdal	
14.1	0°	-16.2 ± 2.2		Born Appr.	Gr 69a
14.1	0°	-23.2 ± 1.9	2.65	Komarov-Popova	Pr 70
14	0°	$-16.7 \pm 2.6 \pm 3.0$	2.63	Comparison proc.	Sl 68a
14.06	3.5°	$-23 + 3.6 - 4.2$	2.65	Komarov-Popova	Sk 72
50	3.8°	-21.7 ± 1.2	2.6	Impulse Appr.	St 72
14.1	4°	-19.3 ± 0.8	2.84	Impulse Appr.	Sh 73
		-18.3 ± 0.22	2.84	Cahill (Faddeev)	Sh 73

cross section (which can be measured much more accurately than the absolute cross section).

The shape of the FSI enhancement depends predominantly on the n-n scattering length, a_{nn} (Kl 73, Ze 74) and in fact the simple Watson-Migdal model already gives a good description of the shape with the correct a_{nn} (Br 74, Eb 72, Ca 74). However, the absolute cross section for n-n and n-p FSI strongly depends on r_{nn}, on the form factor and on the type of calculation (see Fig. 7a and b). In most analyses the N-N force has been approximated using S wave interaction with Yamaguchi form factors (Y). Calculations with several different S wave rank-one separable potentials have shown (Br 74a) that the better treatment of the high energy repulsion in the N-N force improves the agreement with the D(p,2p)n data and that one of the best form factors which fits the known N-N phase shifts at higher

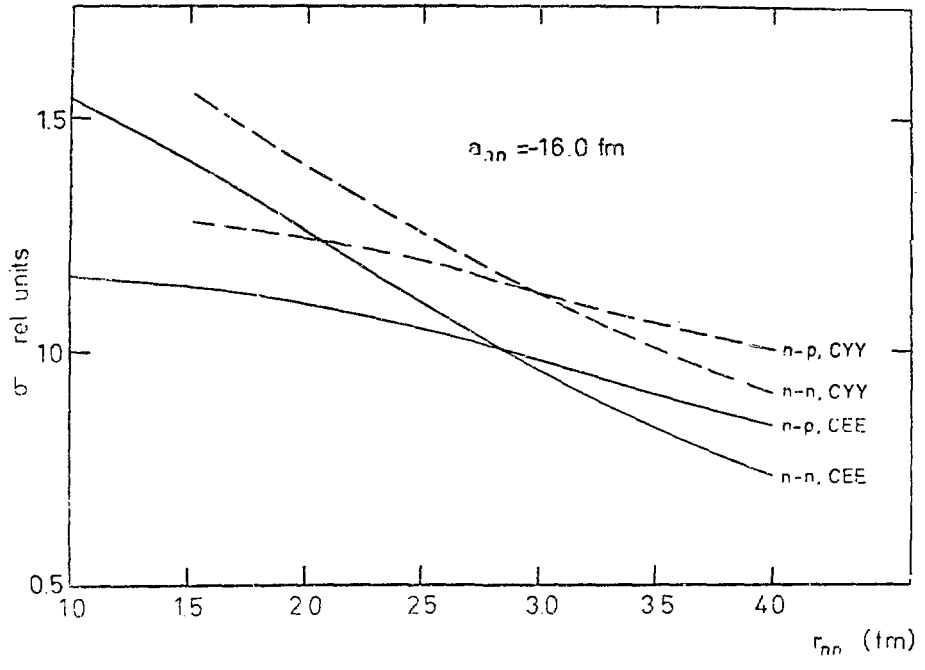

Fig. 7a. Relative dependence of the calculated cross section on r_{nn} for two form factors and two types of calculations (Ze 74).

energies is the exponential one (E). Earlier analyses based on the Faddeev theory have used the average of the n-p and n-n singlet potential in the kernel of the integral equation and have allowed for charge dependence only in the inhomogeneous term. This method is often called hybrid (H) to be distinguished from the correct procedure (C) when the charge dependence is introduced both in the inhomogeneous term and in the kernel.

Table 2. summarizes the values of a_{nn} obtained in various kinematically complete measurements. The n-p FSI has been studied (Lu 70) and gives for a_{np}= -23.0 ± 1.7 using the Watson-Migdal model.

iii) In the three body breakup reaction where two of the outgoing particles are neutral and one of them is detected at Θ_1= 0,

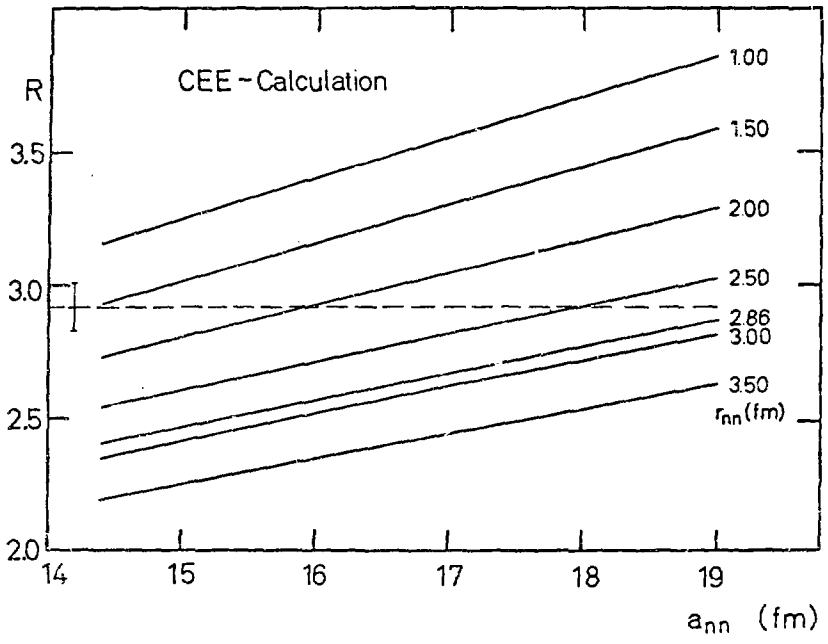

Fig. 7b. Ratio of the integral of the n-n to n-p FSI as a function of a_{nn} and r_{nn}. The dashed line denotes the experimental result (Ze 74).

the measurement of the incident energy, and the energies of two outgoing particles provides five IKV (E_{inc}, E_1, E_2, and since $\Theta_1 = 0$ the process does not depend on any azimuthal angle: $\vec{p}_{inc} - \vec{p}_1$, $\vec{p}_2$ and $\vec{p}_3$ form a triangle). The disadvantage of this setup is the lack of constraints to reduce the background. The advantages are: the kinematically allowed region covers an area shown in Fig. 8. and one can simultaneously study n-p and n-n FSI and regions far from quasi two body processes. In particular, one can investigate processes along the constant relative energy locus (dashed-dotted line in Fig. 8; dashed line is the symmetry axis) where the cross section is sensitive to the off-energy shell effects (Ja 73). An experimental advantage of this method is that one of the particles is detected in a 4π solid angle with a 100% efficiency and one has to use only one neutron detector. The experimental distribution of deuteron breakup

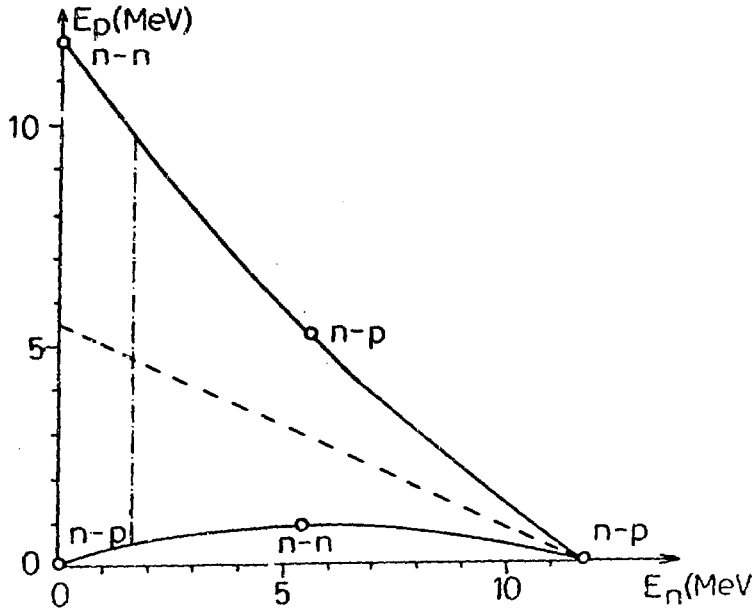
Ep(MeV)
n-n
10
5
n-p
n-p
n-n
n-p
0
0
5
10
En(MeV)

Fig. 8.

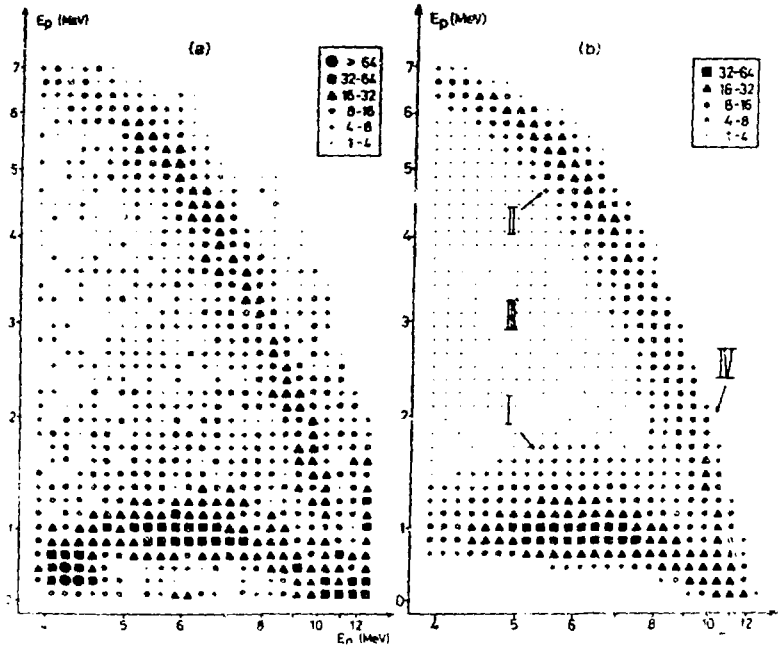
Ep (MeV)
(a)
> 64
32-64
16-32
8-16
4-8
1-4
Ep(MeV)
(b)
32-64
16-32
8-16
4-8
II
III
I
IV
En (MeV)

Fig. 9.

Table 2.

a_{nn} determined from kinematically complete measurements

a_{nn}	Analysis	Nuclear interaction	E_{inc}	Ref.
-16.3 ± 1.0	Faddeev, n-n shape	CEE	18.4	Ze 74
-16.6 ± 1.0	Faddeev, both n-n and n-p FSI	CEE	18.4	Ze 74
-15.8 ± 0.9	same	HYY	18.4	Ze 72
-16.0 ± 1.0	Watson-Migdal		18.4	Ze 72
-16.2 ± 1.2	Faddeev, n-n shape	HYY	14.2	Br 74
-16.8 ± 1.3	Watson-Migdal		14.2	Br 74
-25 ± 3*	Ch 67		14.3	Sa 72
-17.1 ± 0.8	Watson-Migdal		120-140	Mc 75a
-15.7 ± 2.0	Faddeev, n-n shape	CEE	14.1	Ke 75
-16.3 ± 1.6	Faddeev, n-n and n-p	CEE	14.1	Ke 75

* This value can be criticized both an experimental and theoretical grounds (Ku 75).

events in the E_p vs E_n plane is given in Fig. 9a. compared with the simulation of the spectrum using the CEE calculation (Fig. 9b) with a_{nn}= -16 fm, r_{nn}= 2.86 fm. Qualitative features of the data are well reproduced in the calculation. However, the theory predicts a significantly lower cross section in region III(far from FSI). Since this discrepancy could not be eliminated by any choice of the input n-n force, the n-n parameters have been determined by analysing separate parts of the spectra: a) n-n FSI (region I) is sensitive to a_{nn}, but not to r_{nn}. Using r_{nn}= 2.86 fm, one obtains a_{nn}= -15.7 $\pm$ 2.0 fm. b) the ratio of magnitudes of the distributions in regions I and II (n-p FSI) depends on a_{nn} and r_{nn}. A simultaneous fit to both distributions yields: a_{nn}= -16.3 $\pm$ 1.6 fm, r_{nn}= 3.15 $\pm$ 0.7 fm. c) the comparison between distributions in regions I and IV

(n-p FSI) has not given a_{nn} or r_{nn}.

2.4. The n-n effective range parameters

Information concerning a_{nn} have been obtained so far from the studies of D(n,2n)p, ^{3}H(n,d)2n, ^{3}H(t,^{4}He)2n, D(π^-,γ)2n, ^{3}H(d,^{3}He)2n and D(d,2p)2n reaction. There are two classes of studies presently suitable for quantitative consideration:

1. D(π^-,γ)2n yielding a_{nn}= -16.4 ± 1.6 fm (Sa 72a)
2. D(n,2n)p kinematically complete experiments analyzed using the Faddeev theory. CEE should be considered superior to HYY analysis.

We choose:

a_{nn}= -16.3 ± 1.0 fm (Ze 74)
-16.6 ± 1.0 fm (Ze 74)
-15.7 ± 2.0 fm (Ke 75)
-16.3 ± 1.6 fm (Ke 75)

The average of these values is

a_{nn}= -16.26 ± 0.66 fm

can be compared with the previously recommended values:

a_{nn}= -16.7 ± 0.6 fm (Ve 71)
a_{nn}= -16.4 ± 0.9 fm (He 72)
a_{nn}= -16.61 ± 1.45 fm (Ku 75)
a_{nn}= -16.2 ± 0.6 fm (Ze 75)

Information concerning r_{nn} have been obtained i) from the reactions ^{3}H(d,^{3}He)2n and ^{3}He(d,t)2p using the comparison procedure (Ba 66), ii) comparing the ratio of the experimental cross sections for n-n and n-p FSI with the ratio calculated using the Faddeev theory (Ze 74, Ke 75), iii) from the n-n QFS (Sl 71a).

Results: i) r_{nn}= 3.2 ± 1.6 fm. However, in view of the limitation of the comparison procedure (Va 67) the uncertainties should be increased.

ii) r_{nn}= 3.6 ± 0.4 at E_{inc}= 18.4 using HYY (Ze 72)
r_{nn}= 2.13 ± 0.4 using CEE (Ze 74)
r_{nn}= 1.95 ± 0.4 using CYY (Ze 74)
r_{nn}= 3.15 ± 0.7 at E_{inc}= 14.1 using CEE (Ke 75)

The extracted values depend on the assumed form factor. The FSI cross section depends on the-off-the-energy nuclear interaction.

iii) r_{nn}= 2.4 ± 1.6 using the spectator model (Sl 71a)
r_{nn}= 2.5 ± 0.8 using HYY and the absolute cross section data (Sl 71a) (Vr 75)

The average of the results obtained using the Faddeev theory gives r_{nn}= 2.67 ± 0.6 fm
It has been shown (Sl 76) that QFS magnifies on-shell differences between potentials and it is insensitive to off-shell variation. If the ratio of the cross sections around QFS at $E_{inc} \sim 25$-30 MeV is measured with an accuracy of 2-3%, then r_{nn} can be determined with the accuracy of ~ 3-4%. One cannot use the present data at E_{inc}= 14.1 MeV data since the only available measurement at $\theta_{n1}=\theta_{n2}=40^{o}$ (Bo 75) has large errors, the cross section is too low and it would give unrealistic values for a_{nn} and r_{nn}.

3. The n-d Bremsstrahlung

Only an upper limit has been quoted for n-d Bremsstrahlung cross section at E_{inc}=14.1 MeV:
$d^2\sigma(\theta_n=\theta_\gamma=30^{0}, \phi=180^{o})/d\Omega_n d\Omega_\gamma < 2 mb/sr^2$ (Sl 71a)

4. Radiative capture n+d ⟶ t+ γ

The experimental cross section at thermal energies is 0.6 ± 0.05 mb (Ju 63). The cross section calculated using the probability of the ^{3}H S' state, P_S, , of 1% is 0.15 mb (Ph 72). The discrepancy decreases as P_S, increases, but since it is unlikely that P_S, is larger than 2%, it is necessary to represent meson exchange effects more realistically.

At higher energies data exist only at 14 MeV: σ_T=29.4±5.8 μb (Ce 61) and a preliminary result using a more sophisticated experimental setup σ_T=10±3 μb (Tu 76a).

Since the energy of the outgoing triton is a linear function of the angle θ of the gamma ray emission, the measurement of the triton energy spectrum yields the angular distribution:

$$\frac{d\sigma}{d\Omega} = a + b \sin^2\theta (1 + \beta\cos\theta + \gamma\cos^2\theta)$$

A preliminary analysis (Tu 76a) gives $a \sim 5$ μb/sr, $b \sim 90$ μb/sr, $\beta \sim 0.5$, and $\gamma = 0$.

There are no data on triton photodisintegration.

The charge symmetric process $D(p,\gamma)^3He$ and its inverse reaction have been studied at several energies (e.g. Ch 72, Ti 73, Be 70).

5. The nucleon-trion interaction

5.1. Elastic scattering

Angular distributions have been measured at E_{inc}= 6, 9, around 14-15, 18, 19.5, 21 and 25 MeV (Co 51, De 76, Bl 66, Da 68a, Ko 68, Fu 67, Se 72, De 68, Sh 75). In general, the data are consistent and in agreement with the data on the charge symmetric process: p-^{3}He scattering. However, results of several measurements done around 14-15 MeV are mutually inconsistent (Figs. 10 and 11): i) The results at 14.3 MeV (Co 51) should be renormalized by 14% because the cross section has been determined assuming 50 mb/sr for the n-p differential cross

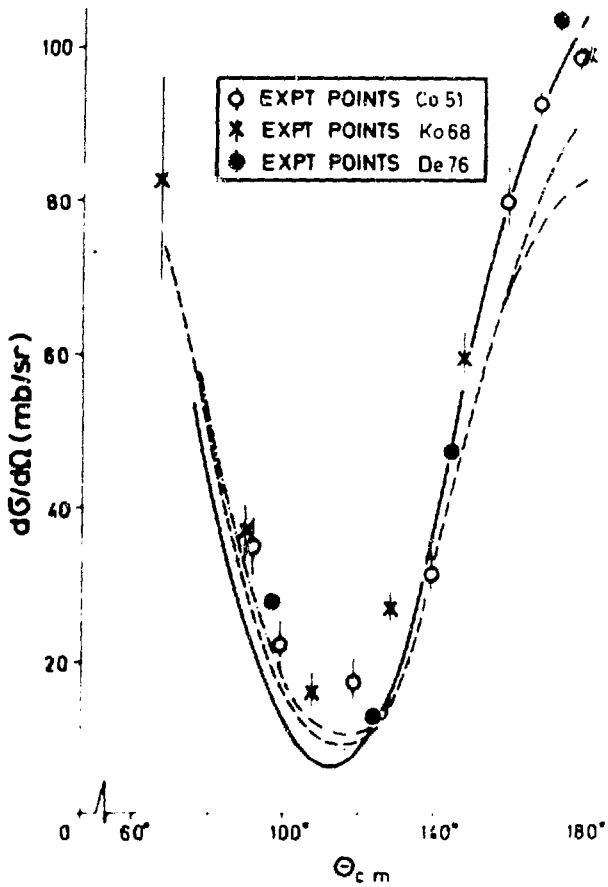

Fig. 10. Angular distribution of the n-t elastic scattering at E_{inc} 14 MeV. Dashed curve represents the p -^{3}He data (Hu 71) at 13.9 MeV: Theoretical calculations (Ha 71): Solid curve - S wave [illegible], dashed-dotted curve - with tensor and spin orbit force.

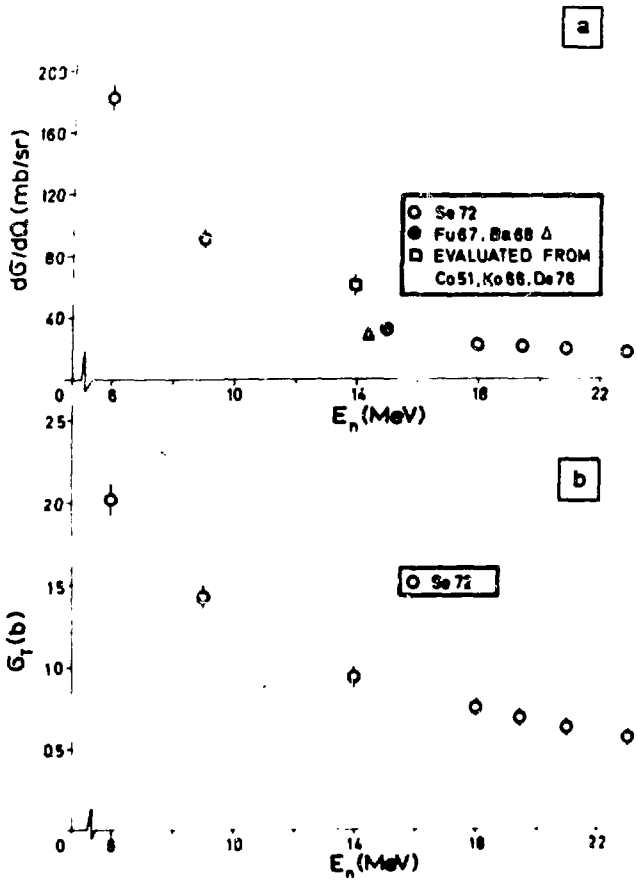

Fig. 11.

section at 180°, while the new value is 57.2 mb/sr (Ho 71). ii) Data at 14.1 MeV (Ko 68) match the renormalized Coon's data (Co 51) as well as the data at 13.85 MeV (De 76). iii) Data at 14.4 MeV for $\Theta \geq 160^{\circ}$ (Ba 68) are about a factor of two lower than the data i) - ii). iv) Data at 14.1 MeV (Sh 75) and 15.2 MeV (Fu 67) are in agreement with the data at 14.4 MeV (Ba 68). v) Data by (De 68) and (Bl 66) are situated in between.

The experimental $d\sigma/d\Omega$ ($\Theta_{cm}=149^{\circ}$) and total n-t cross section as function of E_{inc} are given in Fig. 11. The backward n-t elastic scattering studies (Pa 76) at E_{inc}=13.94, 14.4 and 14.94 MeV have shown that the cross section does not change by more than ~15%.

Considerable progress has been achieved (Al 70, Tj 75) in extending the exact treatment to four particle systems. Tjon (Tj 76) has recently applied the Faddeev-Yakubovskii equations to the N-T scattering. The results of his calculation compared with the data in Fig. 12. demonstrate the importance of including higher partial wave components in the (3+1) subamplitude.

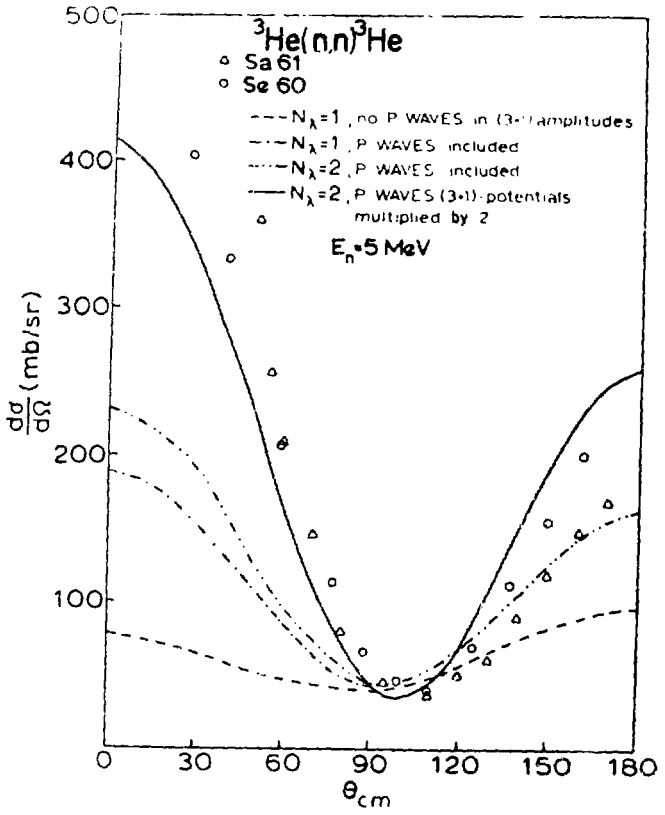

Fig. 12. The results of the theoretical calculations (Tj 76) using N-N S wave Malfliet-Tjon I-III potential and neglecting Coulomb forces. N_λ is the number of terms in the two nucleon subamplitude. Data are from (Sa 61) and (Se 60).

5.2. The n+t breakup

The reaction ^{3}H(n,d)2n has been studied at E_{inc} ~14 MeV (Aj 65, Th 66, Fu 68, Ad 71) and a pronounced peak due to n-n FSI has been observed. The extracted value for a_{nn} depends on the reaction mechanism and on the triton wave function employed in the calculation (Va 67, Ad 71).

Recently an improved measurement of the n-t interaction has been performed (De 76) using large acceptance angle (20°) multiwire and ΔE-E silicon detectors. Long runs have been performed at E_{inc}=14 MeV, at Θ=6.5° accumulating ~10^5 elastic tritons (320 mb/sr), and ~10^4 deuterons from the reaction ^{3}H(n,d)2n (35 mb/sr). A proton spectrum shows several peaks (Fig. 13): ^{3}He(n,p)^{3}H (14.7), n-p

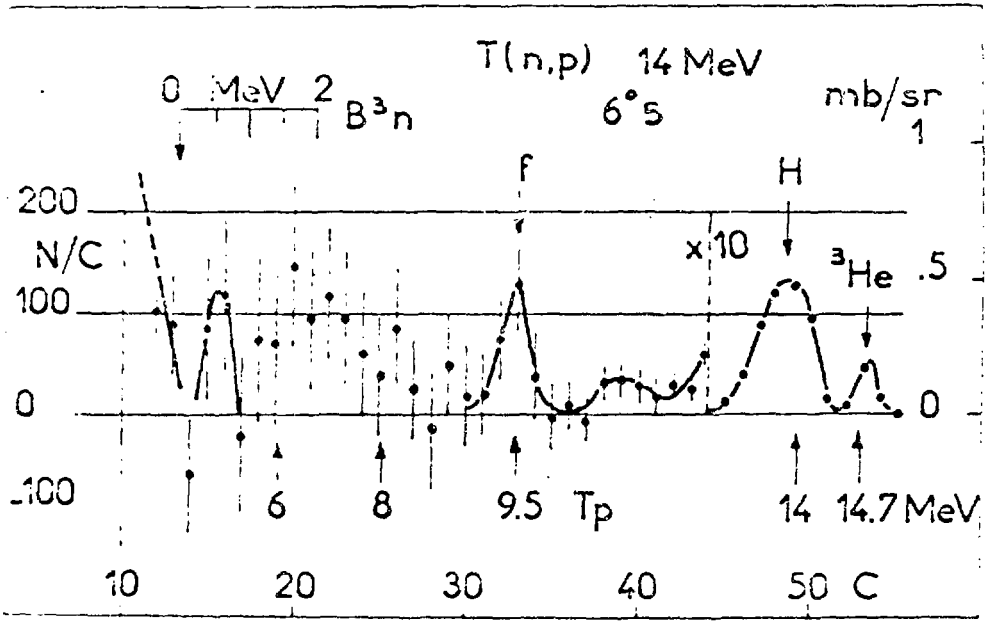

Fig. 13.

scattering (14) fortuitous coincidences with the elastic triton peak (f:9.5) and also a group around $E_p \sim 6$ MeV with the cross section ~ 1 mb/sr. It represents a possible resurrection of a similar group found earlier (Aj 65) and interpreted as a possible state of ^{3}n. However, all other studies that should have revealed the analogs of this state have not provided conclusive evidence for excited states in A=3 nuclei (Fi 75).

5.3. The reactions ^{3}He(n,p)T and ^{3}He(n,d)d

The cross sections for the reactions ^{3}He(n,p)T and ^{3}He(n,d)d have been obtained from the inverse reactions using the reciprocity theorem (Pa 74). Fig. 14. shows the evaluated total cross sections for these reactions. Though the graph for the reaction ^{3}He (n,p)T starts at 0.2 MeV, the data are also available from thermal energies (Al 67).

The differential cross section for the reaction ^{3}He(n,d)d

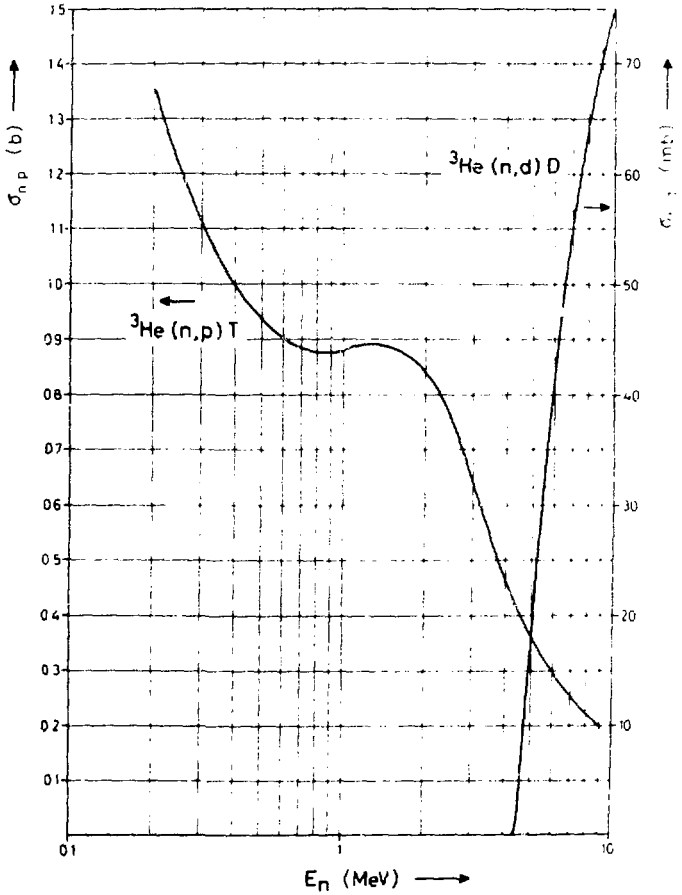

Fig. 14.

can be expressed as: $\sigma(\theta)=\frac{\sigma_T}{4\pi}\sum_L A'_L P_L(\cos\theta)$, $A'_o = 1$ and the Legendre coefficients are given in Fig. 15. (Pa 74). The ratio of the differential cross section to the total cross section for the reaction ^{3}He(n,p)T is given in Fig. 16. (Pa 74). The 14.4 MeV data are compared in Fig. 17. with the calculation (El 66) (solid curve) done assuming proton knock out (K) and heavy particle (n+d → t) stripping (H): $\sigma(\theta) \sim |AK + BH|^2$. Complex parameters A and B are adjusted to produce the best fit to the data: $|B|^2/|A|^2 = 0.2$ and the interference term $|AB^* + A^*B|/|A|^2$ is - 2/3. The angular distribution can be represented as a sum of Legendre polynomials up to L=7 (dashed curve in Fig. 17. (An 67).

6. The n-^{12}C interaction

Accurate n+^{12}C data are required in several applications: i) nuclear energy - calculation of neutron transport in shielding material, ii) neutron radiotherapy, iii) n+^{12}C data are proposed as standards for neutron flux measurements and energy calibration (IN 74), iv) ^{12}C + n reaction cross sections are necessary to calculate neutron detection efficiencies for scintillators containing

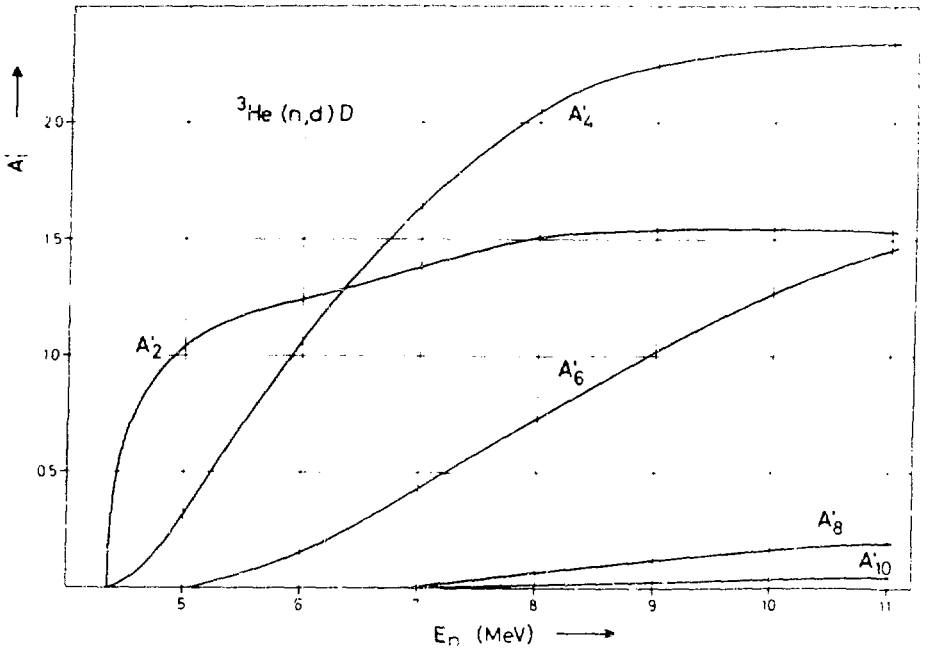
^{3}He (n,d) D
A'
A'4
A'2
A'6
A'8
A'10
20
15
10
05
5
6
8
9
10
11
En (MeV)

Fig. 15.

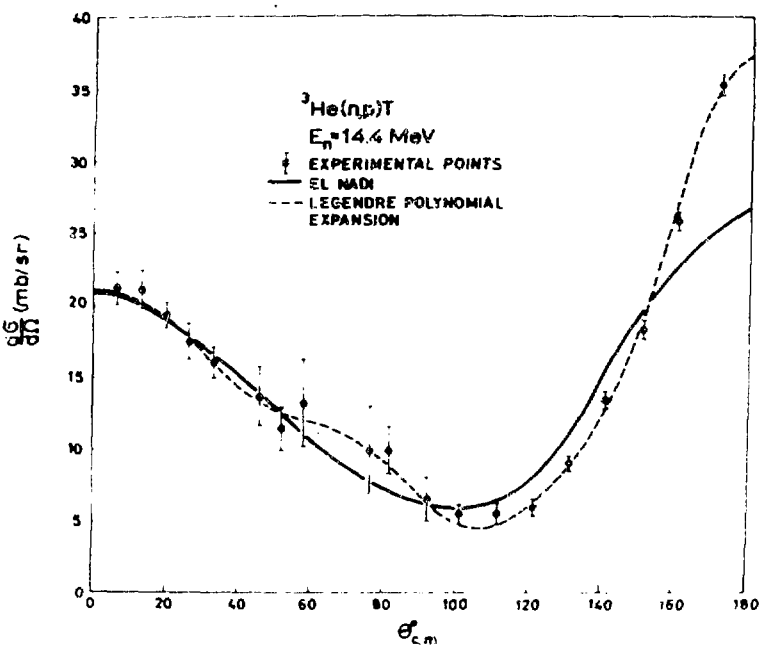
^{3}He(n,p)T
En=14.4 MeV
EXPERIMENTAL POINTS
EL NADI
LEGENDRE POLYNOMIAL EXPANSION
dσ/dΩ (mb/sr)
40
35
30
25
20
15
10
5
0
0
20
40
60
80
100
120
140
160
180
θc.m

Fig. 17.

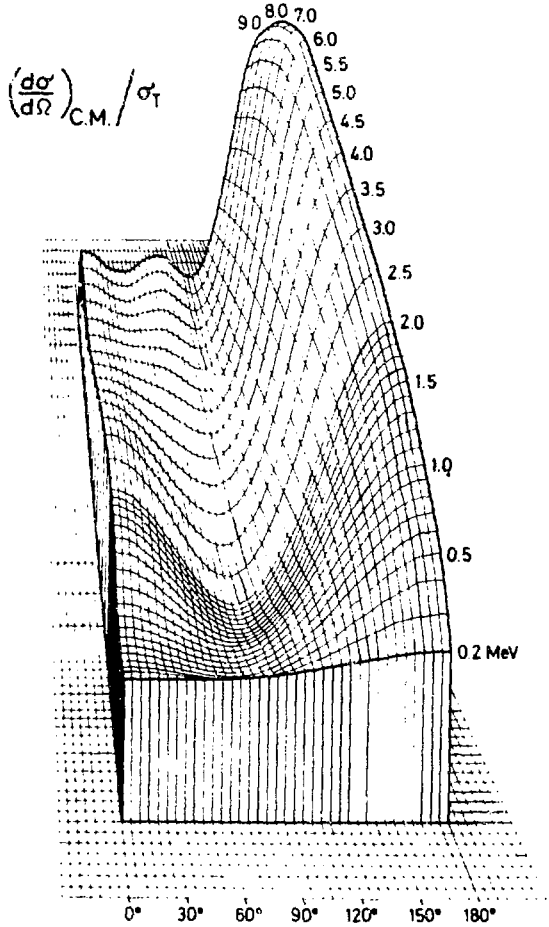

Fig. 16.

carbon. An evaluation of the cross sections for ^{12}C + n reactions in the range E_{inc} = 0 to 20 MeV have been recently perform d (La 75). We will present here the evaluations for the reactions (n,α), (n,3α), (n,p) and (n,d).

6.1. $^{12}C(n,\alpha)^{9}Be_{gs}$

Cross sections shown in Fig. 18. include $^{12}C(n,\alpha)^{9}Be_{gs}$ (Gr 55, Da 63, Ki 69) and $^{9}Be(\alpha,n)^{12}C_{gs}$ (Ve 68, Re 60, Ob 72) data. All (α,n) cross sections below 15 MeV are consistent and the value corresponding to E_n = 13.7 MeV (Ve 68) is in good agreement with the absolute measurement of the (n,α) at 14 MeV: σ = 80±10 mb (Br 68, Al 62). The (n,α) data at $E_{inc} \sim$ 8-9 MeV (Da 63) are consistent in shape but smaller in magnitude. The evaluation of Lachkar et al. (La 75) includes also the (n,α) data of (Ch 64, Br 68, Hu 66) and (α,n) data (Ni 62) at $E_n \sim$ 14-17 MeV, while the (n,α) (Sa 71) and (α,n) data (De 63) are by a factor of two too low.

6.2. $^{12}C(n,n')3\alpha$

Fig. 19. shows the cross section data from three measurements (Va 58, Fr 60, Gr 49) together with the recommended cross section (La 75) based on a recent measurement (Cr 74) which suggests a broad structure at $E_n \sim$ 12 MeV.

The mechanism of the reaction $^{12}C(n,n')3\alpha$ has been studied

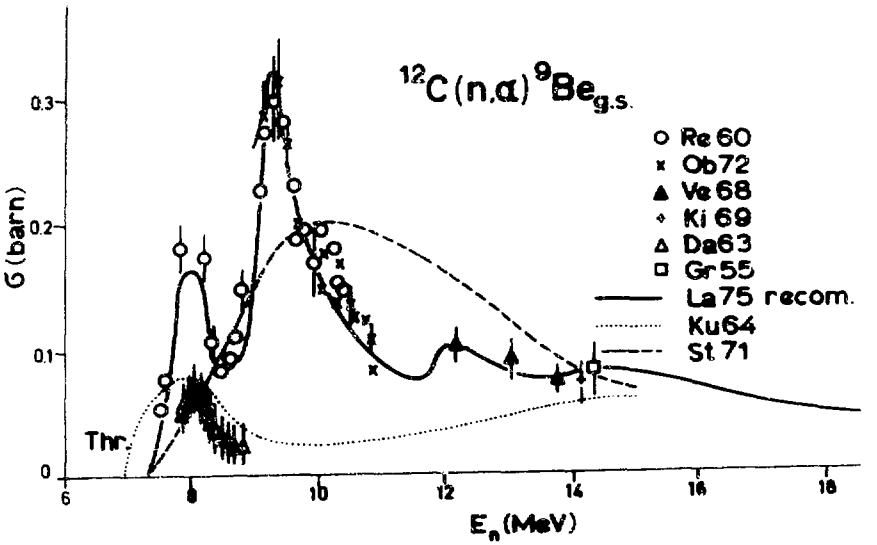

Fig. 18. The $^{12}C(n,\alpha)^{9}Be_{gs}$ data. The solid curve is the recommended cross section (La 75), dotted and dashed curves are the cross sections used in Kurz's (Ku 64), and Stanton's (St 71) programs, respectively.

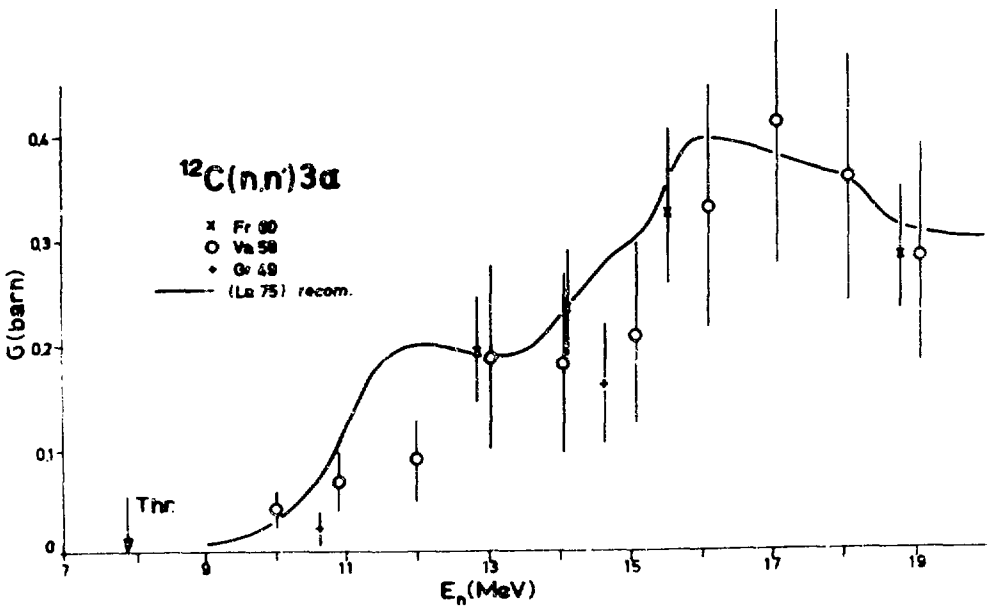

Fig. 19.

mainly in kinematically complete studies and it has been concluded that the reaction proceeds predominantly (~ 80%) through sequential decays involving $^{12}C^{*}$. Similar conclusions have been drawn from the studies of the reaction $^{12}C(p,p')3\alpha$. Table 3. summarizes the contribution of each partial cross section $^{12}C(n,n')^{12}C^{*}$ to the total $^{12}C(n,n')3\alpha$ cross section (La 75).

6.3. $^{12}C(n,p)^{12}B$ and $^{12}C(n,d)^{11}B$

The (n,p) cross section measured using the activation technique (Ri 68, Kr 59) is shown in Fig. 20. together with the recommended cross section (La 75).

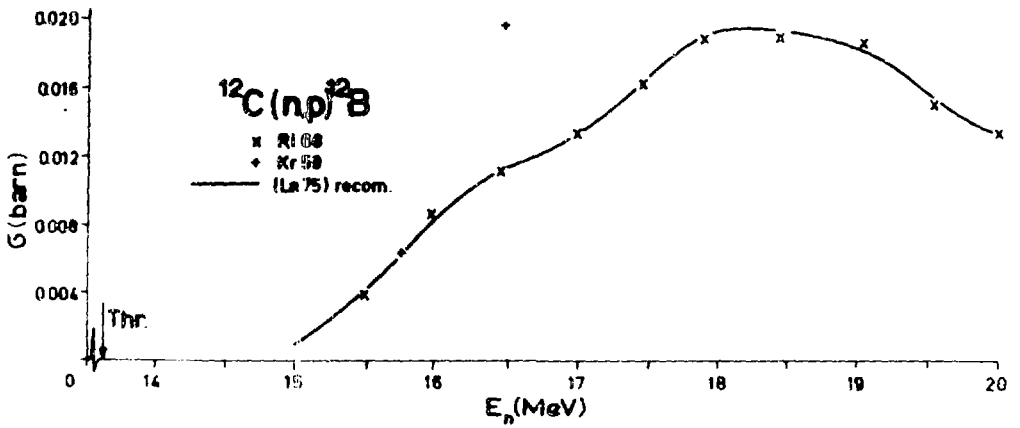

Fig. 20.

The experimental cross sections for the reaction $^{11}B(d,n)^{12}C_{gs}$ (Am 57, Cl 65) have been converted to the $^{12}C(n,d)^{11}B_{gs}$ cross sections and are shown in Fig. 21. together with the recommended values (La 75).

The cross section for the reaction $^{12}C(n,np)^{11}B$ at E_{inc}= 22 MeV has been estimated to be 0.03 b (Sh 70).

Differential cross sections for the reactions $^{12}C(n,p)$ and $^{12}C(n,d)$ have been measured at E_{inc}= 56 MeV (Mc 75). The results compared with the (p,d) data are given in Fig. 22. The notation (n,p) includes all final states in which a free proton occurs i.e. $^{12}C(n,p)^{12}B$, $^{12}C(n,np)^{11}B$, double contribution from $^{12}C(n,2p)^{11}Be$

Table 3.

Partial cross sections $^{12}C(n,n')^{12}C^{*}$ in mb (La 75)

Q (MeV)	$\Gamma_{tot.}$ (keV)	E_{inc} (MeV)								
		10	11	12	13	14	15	16	18	20
- 7.653	9.7	5	10	20	11	10	10	10	5	5
- 9.638	34		40	70	64	65	83	100	70	45
- 10.3	3000			10	10	15	15	20	15	5
- 10.84	320			5	20	35	50	70	45	30
- 11.83	274				5	20	41	70	80	70
- 12.71	2					10	30	50	75	80
- 13.35	400						5	15	30	55
$\alpha + {}^{9}Be^{*}$		25	80	90	75	80	60	60	40	10
$(n,n'3\alpha)$		30	130	195	185	235	294	395	360	300

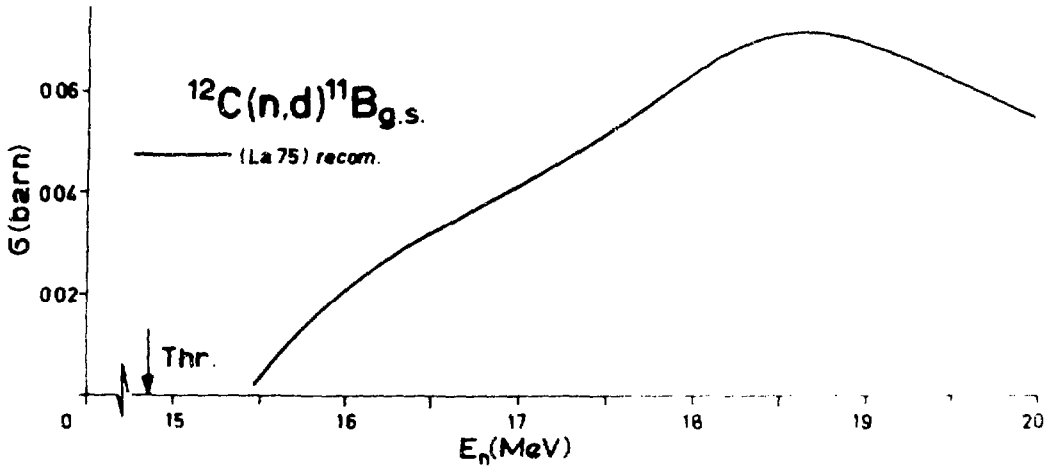

Fig. 21.

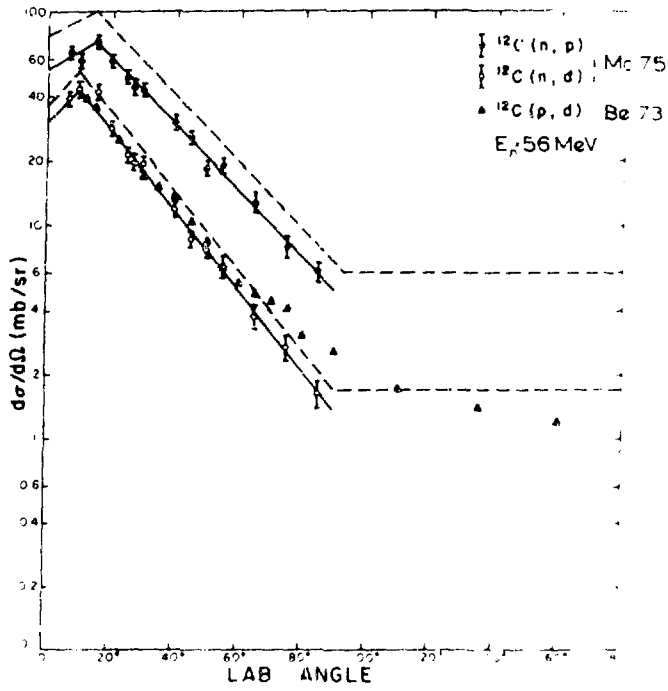

Fig. 22. $^{12}C(n,p)$ and $^{12}C(n,d)$ data. Solid lines represent the data. Dashed curves include the estimate for the emission of protons and deuterons below the detecting threshold and are extrapolated to $\theta > 90^{o}$ assuming the isotropic angular distributions.

and $^{12}C(n,pd)^{10}Be$, the last one being included in both (n,p) and (n,d) cross sections. The cross sections for these processes at 56 MeV are: $\sigma(^{12}C(n,p)) \sim 219$ mb and $\sigma(^{12}C(n,d)) \sim 78$ mb (no uncertainties are quoted due to a number of assumptions included in these estimates). The integrated cross sections for reactions leading to individual states of the residual nuclei are: $^{12}C(n,p)^{12}B_{gs}$ $\sigma = 3.4 \pm 0.6$ mb, $^{12}C(n,p)^{12}B^*(4.3\ MeV)\sigma = 3.2 \pm 0.6$mb, $^{12}C(n,p)^{12}B$ (7.4 MeV) $\sigma = 4.3 \pm 0.6$ mb, $^{12}C(n,d)^{11}B_{gs}$ $\sigma = 20 \pm 2$ mb, $^{12}C(n,d)^{11}B^*(2.12\ MeV)\sigma = 3 \pm 1$ mb.

The recommended cross sections for n + ^{12}C reactions from E_{inc} = 2 to 20 MeV are summarized in Fig. 23. The estimated errors are given in Table 4.

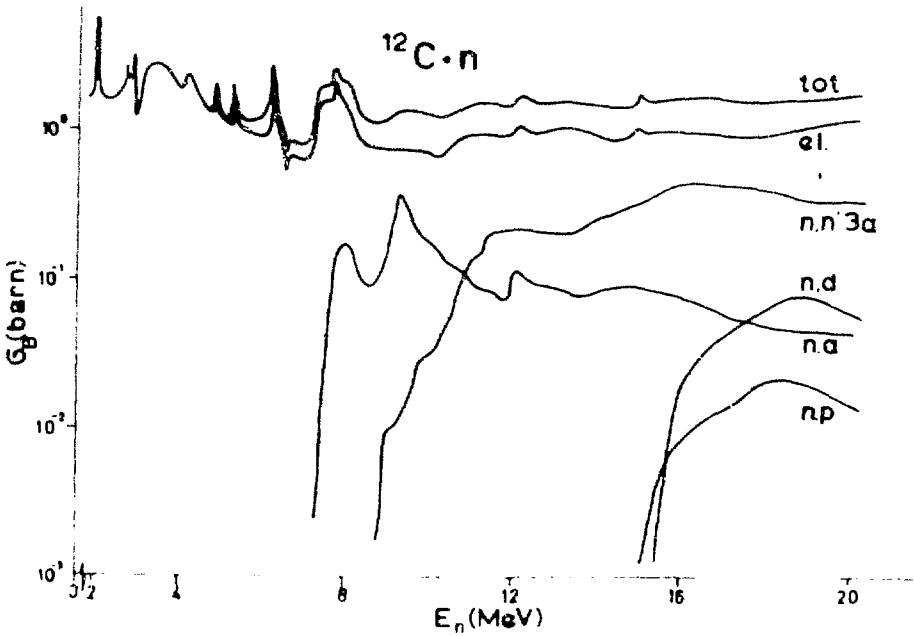

Fig. 23.

Table 4.

Estimated errors in the recommended ^{12}C + n data (La 75)

Process	Neutron Energy (MeV)				
	Thermal	0-4.8	4.8-8	8-15	15-20
Total	1%	1-2%	4%	4%	6%
Elastic	1%	4%	5%	5-7%	10%
(n,α_o)			12%	12%	20%
(n,n')3				20%	25%
(n,p)					15%
(n,d_o)					15%

7. (n,p) reactions

The total reaction cross sections for $^{6}Li(n,p)^{6}He$, $^{16}O(n,p)^{16}N$, $^{19}F(n,p)^{19}O$ and $^{27}Al(n,p)^{27}Mg$ are given as function of E_{inc} in Figs 24 a-f) (Bo 74, Ma 75 and references therein).

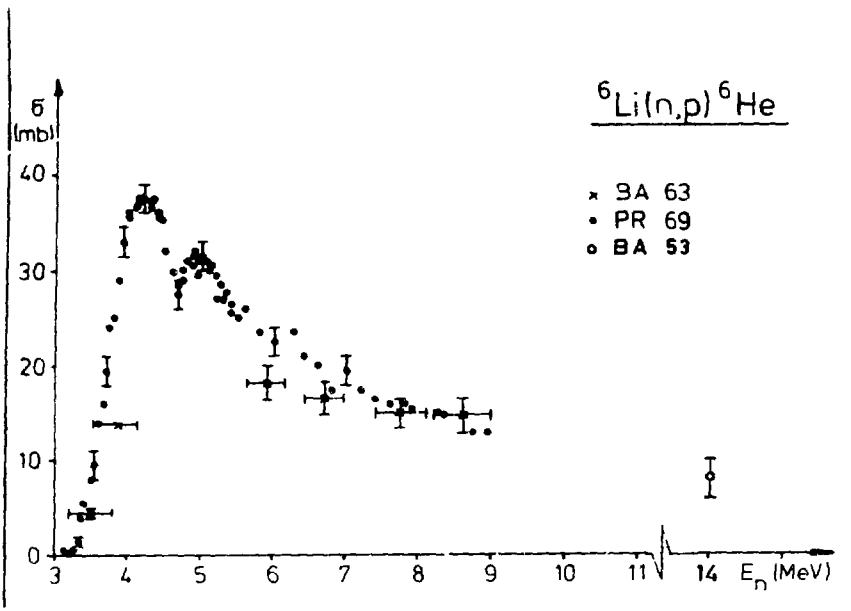

Fig. 24a.

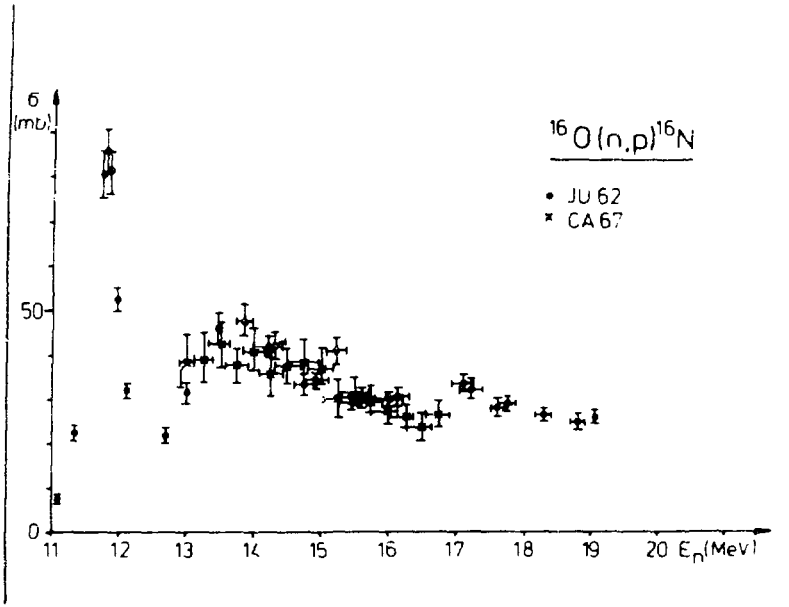

Fig. 24b.

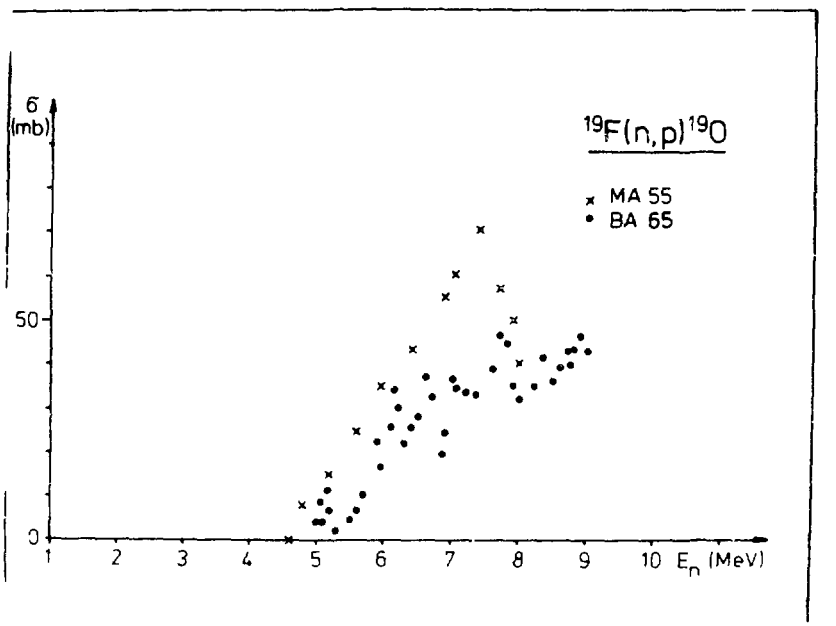

Fig. 24c.

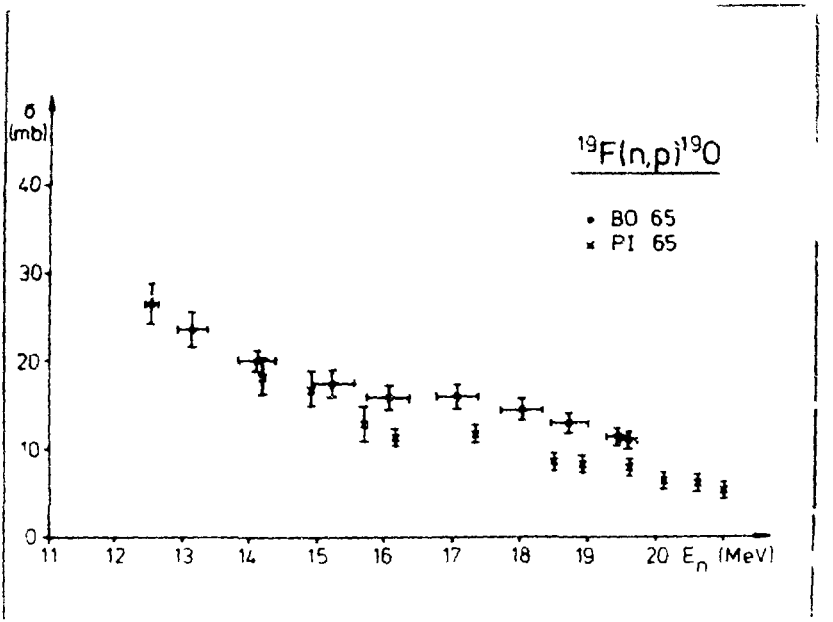

Fig. 24d.

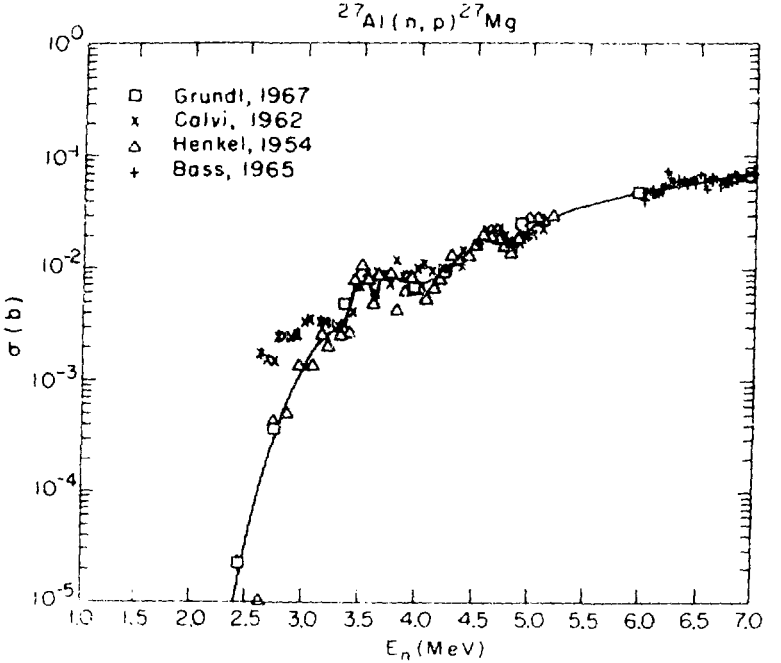

Fig. 24e.

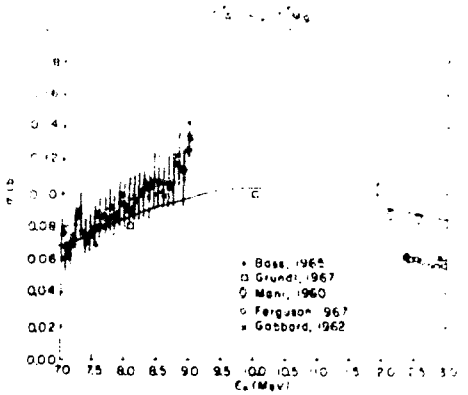

Figure 2

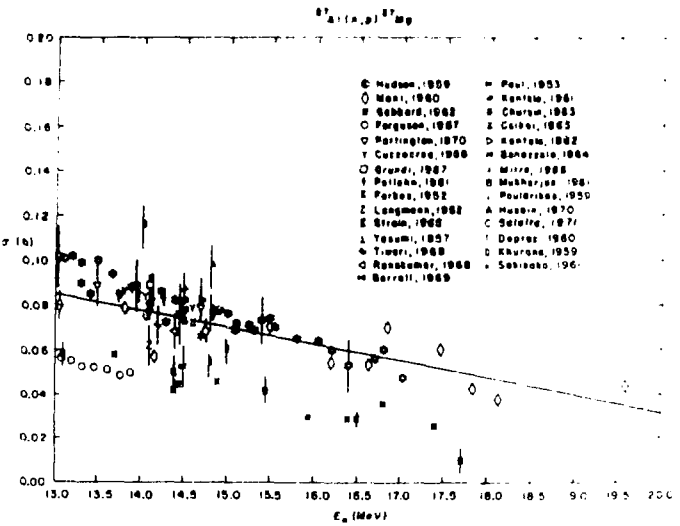

Fig. 24f.

The recommended values for the reaction $^{27}Al(n,p)^{27}Mg$ reaction are given as solid curves in Figs. 24e-f). The energy dependence of the curve below 3 MeV is approximated by an L=0 penetrability function. Most of the data are mutually consistent (the data of (Fe 67) are relative data and they should be renormalized to 77 mb at 14.1 MeV, instead of 55 mb at 13 MeV).

Table 5. summarizes the measurements of (n,p) reactions on light nuclei.

Charge exchange reactions (n,p), (p,n), (h,t) and (t,h) and radiative pion capture have been used to populate analogs of giant resonances. A series of experiments have been undertaken at Crocker Nuclear Lab. (UC 75) and investigations have so far included ^{6}Li, ^{7}Li, ^{12}C, ^{14}N, ^{16}O, ^{20}Ne, ^{27}Al and ^{209}Bi at E_{inc} = 43, 56.3 and 64 MeV (UC 75, Ki 76). The reactions $^{6}Li(n,p)^{6}He$ and $^{12}C(n,p)^{12}B$ populate T=1 analogs to collective M1 transitions. The angular distributions for (n,p) reactions (UC 75) together with the existing (p,p') and (p,n) data to the members of the same isotriplet are given in Fig. 25. The DWBA calculations based on the macroscopic collective model form factor are also shown in Fig. 25 (dashed and solid curves)

Table 5.

Available data on (n,p) reactions on light nuclei

Reaction	E_{inc}(MeV)	$\sigma_{max}(\theta)$(mb/sr)	References
$^{3}H(n,p)^{3}n$	14.1	0.7 ± 0.3	De 76
$^{3}He(n,p)^{3}H$	14.4	35.4 ± 0.8	Au 67, Pa 64
$^{6}Li(n,p)^{6}He_{gs}$	56.3	11	UC 75
$^{7}Li(n,p)^{7}He_{gs}$	56.3		UC 75
$^{10}B(n,p)^{10}Be_{gs}$	14.4	0.26 ± 0.04	Pa 64
$^{10}B(n,p)^{10}Be^{*}_{1.e.s.}$	14.4	1.6 ± 0.1	Pa 64
$^{12}C(n,p)^{12}B_{gs}$	56.3	3	UC 75
$^{14}N(n,p)^{14}C_{6.09}$	14.4	1.0 ± 0.8	Pa 64
$^{14}N(n,p)^{14}C^{*}_{6.6-7.3}$	14.4	5.1 ± 1.4	Pa 64
$^{14}N(n,p)^{14}C^{*}_{8.3}$	14.4	0.7	Pa 64
$^{14}N(n,p)^{14}C^{*}_{9.8}$	14.4	0.7	Pa 64
$^{14}N(n,p)^{14}C^{*}_{10.43,\ 10.47}$	14.4	7.8 ± 1.2	Pa 64
$^{16}O(n,p)^{16}N_{gs,0.1,0.3,0.4}$	14.4	8.5 ± 0.6	Pa 64
$^{19}F(n,p)^{19}O_{gs,1.e.s.}$	14.4	0.8 ± 0.08	Re 68
$^{19}F(n,p)^{19}O^{*}_{2.e.s.}$	14.4	0.5 ± 0.05	Re 68
$^{19}F(n,p)^{19}O^{*}_{3,4,5\ e.s.}$	14.4	0.85 ± 0.05	Re 68
$^{27}Al(n,p)^{27}Mg^{*}_{6}$	56.3	1.0 ± 0.3	Br 75
$^{27}Al(n,p)^{27}Mg^{*}_{14.4}$	56.3	2.2 ± 0.3	Br 75
$^{32}S(n,p)^{32}P_{gs,1.e.s.}$	5.85	15 ± 2	Fo 72
$^{32}S(n,p)^{32}P_{2.e.s.}$	5.85	6 ± 2	Fo 72
$^{40}Ca(n,p)^{40}K_{gs,1.e.s.}$	5.85	400	Fo 72

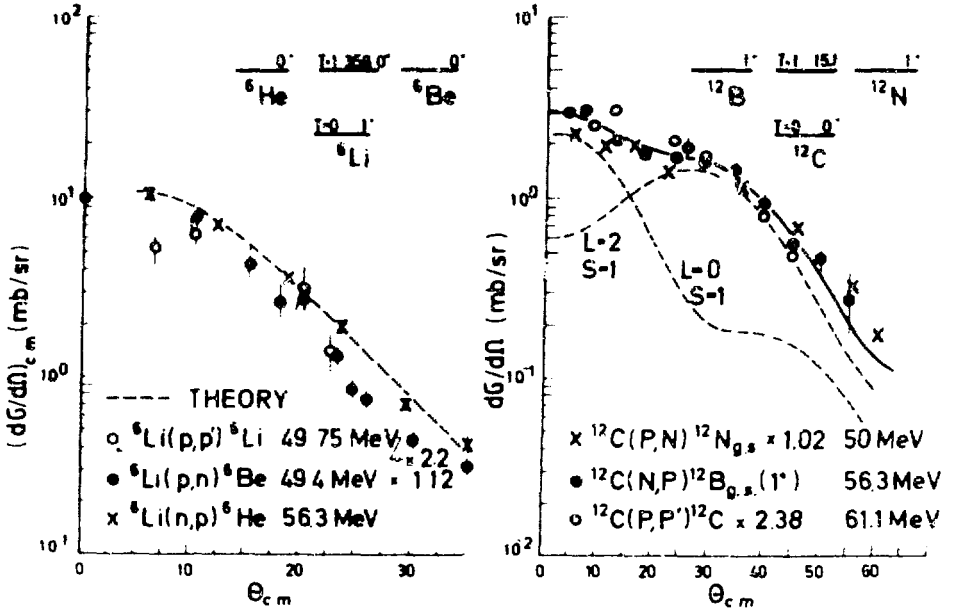

Fig. 25.

Proton spectra from the reaction $^{12}C(n,p)^{12}B$ have also shown evidence for a giant magnetic quadrupole 2^- state at 4.3 MeV excitation in ^{12}B and a giant electric dipole 1^- state at 7.7 MeV. There is no evidence for strong collective excitations in $^7Li(n,p)^7He$. Proton spectra reveal a peak corresponding to the $^7He_{gs}$ unbound against n+^{6}He decay by 440 keV. Proton spectra from the reaction $^{27}Al(n,p)^{27}Mg$ (Br 75) are characterized by peaks corresponding to 6, 10 and 14.4 MeV excitation in ^{27}Mg. The angular distribution of the 6 MeV resonance is consistent with L=0, S=1 (lower portion of Fig. 26.) indicating that it can be an M1 analog. The angular distribution of the 14.4 MeV resonance (upper portion of Fig. 26.) is compared with the DWBA predictions for L=1 and L=2 using a macroscopic form factor based on the Goldhaber-Teller model.

The differential cross sections for the reactions $^{10}B(n,p)^{10}Be^{0+}_{gs}$ and $^{10}B(n,p)^{10}Be^{2+}_{1.e.s.}$ at 14.4 MeV (Pa 64) (Fig. 27.) suggest that the n-p interaction is spin-dependent. Fig. 28. shows the angular distribution of the reaction $^{16}O(n,p)^{16}N$ leading to four unresolved states in ^{14}N: ground (2-), 0.126 (0-), 0.296 (3-)

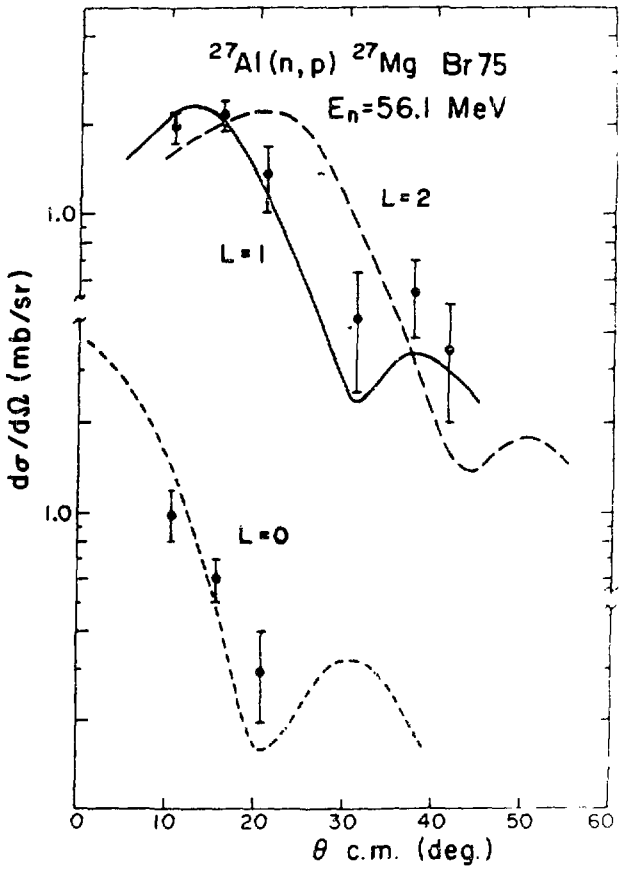

Fig. 26.

and 0.396 MeV (1-) states compared with the PWBA predictions where L=1 and L=3 transitions have been incoherently added with weighting factors of 3 and 8, respectively (Pa 64). The angular distributions of the reactions ^{19}F(n,p)^{19}O (Re 68) are shown in Fig. 29. Integrating the proton spectra from 4 MeV up and from $\Theta=0^{\circ}$ to 120° one obtains 32 mb, to be compared with ~ 20 mb (Ka 62, Mi 66, Pi 65, see Fig. 23d) and with the 50 ± 10 mb (Fa 68).

8. <u>(n,d) reactions</u>

Table 6. summarizes available data on (n,d) reactions. Experimental angular distributions indicate the dominance of direct mechanism. The zero range DWBA calculations assuming the proton pickup has been performed (Mi 67, Mi 71, Pa 76). Data from ^{3}He to ^{19}F are compared with the DWBA predictions using one average neutron optical model potential with surface absorption and three average deuteron potentials: A (surface absorption, dashed-dotted curve), B (surface absorption, solid) and C (volume absorption, dashed). Some results are shown in Fig. 30a-e). Data for chlorine and argon have been analyzed using the neutron potential (Ro 65) and two deuteron potentials: set A (Mi 67, Mi 68a) and set B which gives a somewhat better fit to the elastic scattering data. Both deuteron potentials have surface absorption, and set B has also a spin-orbit term (see Fig. 31.) The neutron and

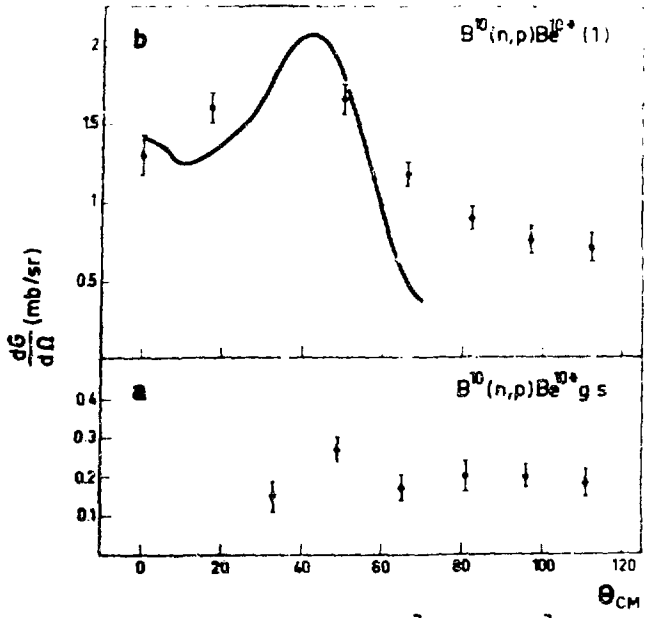

Fig. 27. Angular distributions for $^{10}B(n,p)^{10}Be_{gs}$ (a) and $^{10}B(n,p)^{10}Be^{*}_{1.e.s.}$ (b). The solid curve is the PWBA prediction using L=2 and a weak L=0 transition (Pa 64)

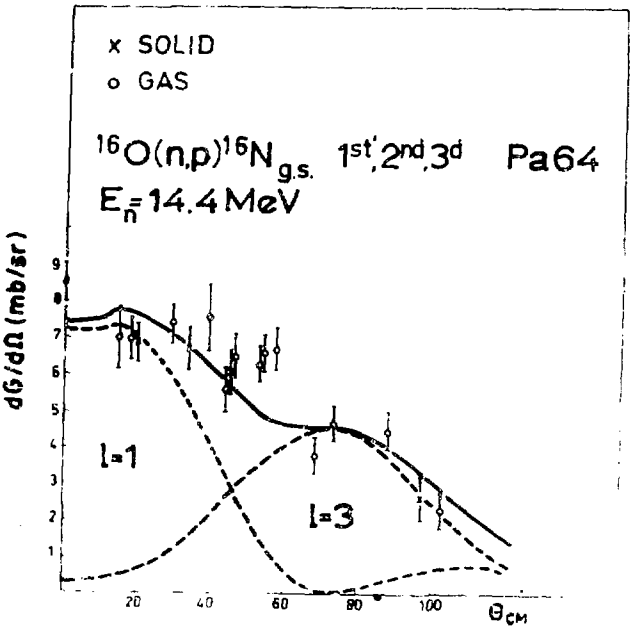

Fig. 28.

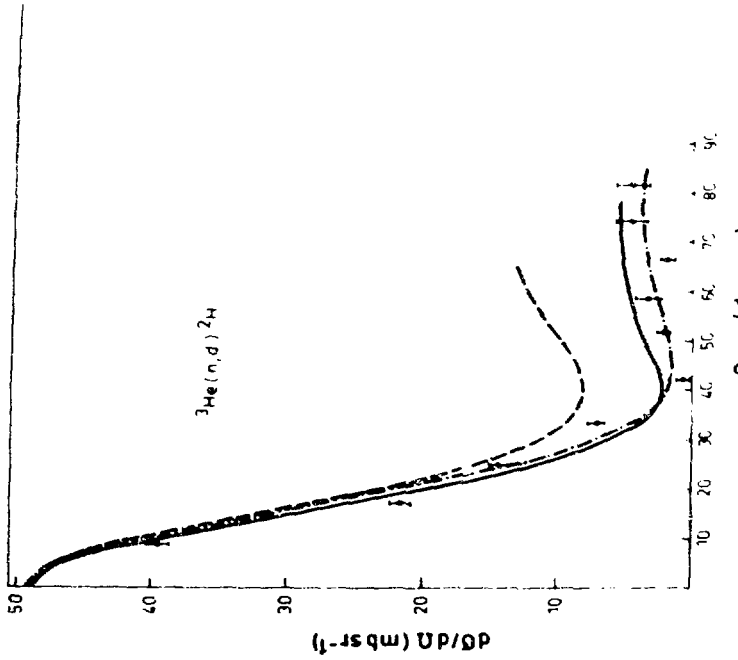

Fig. 30a.

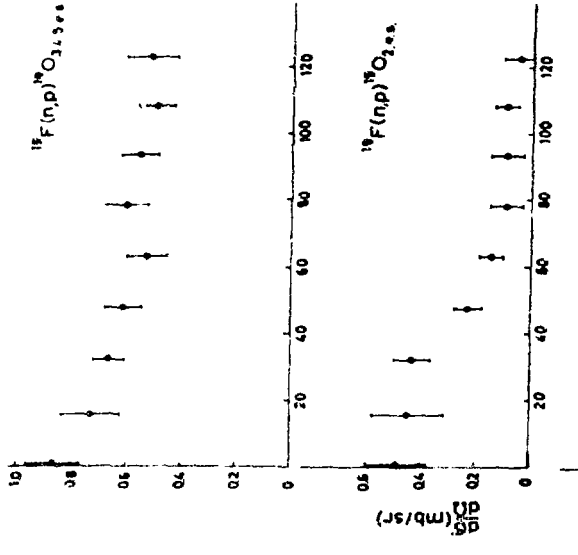

Fig. 29.

Table 6.

Available data on (n,d) reactions on light nuclei

Reaction	$\sigma_{max}(\theta)$ (mb/sr)	Transferred orb. ang. mom.	Reference
$^{3}He(n,d)d$	39.6 ± 0.8	0	Au 67
$^{6}Li(n,d)^{5}He_{gs}$	51.3 ± 4; 45 ± 4	1	Va 65, Fr 54
$^{7}Li(n,d)^{6}He_{gs}$	2.2 ± 0.35	1	Mi 70
$^{10}B(n,d)^{9}Be_{gs}$	8.6 ± 0.4; 8.4 ± 0.4	1, (3,5)	Va 65, Ri 54
$^{10}B(n,d)^{9}Be^{*}_{2.43}$	5.8 ± 0.3; 5.0 ± 0.3	1, (3,5)	Va 65, Ri 54
$^{11}B(n,d)^{10}Be_{gs}$	2.1 ± 0.1	1	Mi 68
$^{14}N(n,d)^{13}C_{gs}$	7.3 ± 0.5; 9.2 ± 1	1	Fe 67, Mi 68
	9.0 ± 1 ; 10.4 ± 1.9		Ca 57, Za 63
$^{14}N(n,d)^{13}C^{*}_{3.68}$	4.9 ± 1.9; 12.5 ± 1	1	Fe 67, Ca 57
	8.5 ± 1.5		Za 63
$^{15}N(n,d)^{14}C_{gs}$	3.3 ± 0.45	1	Fe 67
$^{16}O(n,d)^{15}N_{gs}$	4.7 ± 0.7	1	Pa 64a
$^{19}F(n,d)^{18}O_{gs}$	23 ± 1, 24 ± 1.5	0	Re 68, Ri 57
$^{19}F(n,d)^{18}O^{*}_{1.9}$	1.6 ± 0.6, 1.5 ± 0.1	2	Ri 57, Pa 64
$^{19}F(n,d)^{18}O^{*}_{3.68}$	2.8	0	Pa 64
$^{23}Na(n,d)^{22}Ne_{gs}$	1 ± 0.2		Sa 65
$^{23}Na(n,d)^{22}Ne^{*}_{1.3}$	3.5 ± 0.4		Sa 65
$^{23}Na(n,d)^{22}Ne^{*}_{3.3}$	3.0 ± 0.3		Sa 65
$^{31}P(n,d)^{30}Si_{gs}$	15 ± 1.5; 20 ± 2	0	Co 60, Sa 65
$^{32}S(n,d)^{31}P_{gs}$	15 ± 1 ; 18.2 ± 2.6	0	Co 60, Ve 60
$^{35}Cl(n,d)^{34}S_{gs}$	1.5 ± 0.35; 2.73 ± 0.42	2	Pa 76, Mi 67
$^{35}Cl(n,d)^{34}S^{*}_{2.13}$	4.5 ± 0.5	0,2	Pa 76
$^{35}Cl(n,d)^{34}S^{*}_{3.3}$	6.96 ± 0.5	0	Mi 67
$^{37}Cl(n,d)^{36}S_{gs}$	1.65 ± 0.55	2	Pa 76
$^{36}Ar(n,d)^{35}Cl_{gs}$	1.85 ± 0.35	2	Pa 76
$^{36}Ar(n,d)^{35}Cl^{*}_{1.22, 1.76}$	8 ± 1		Pa 76

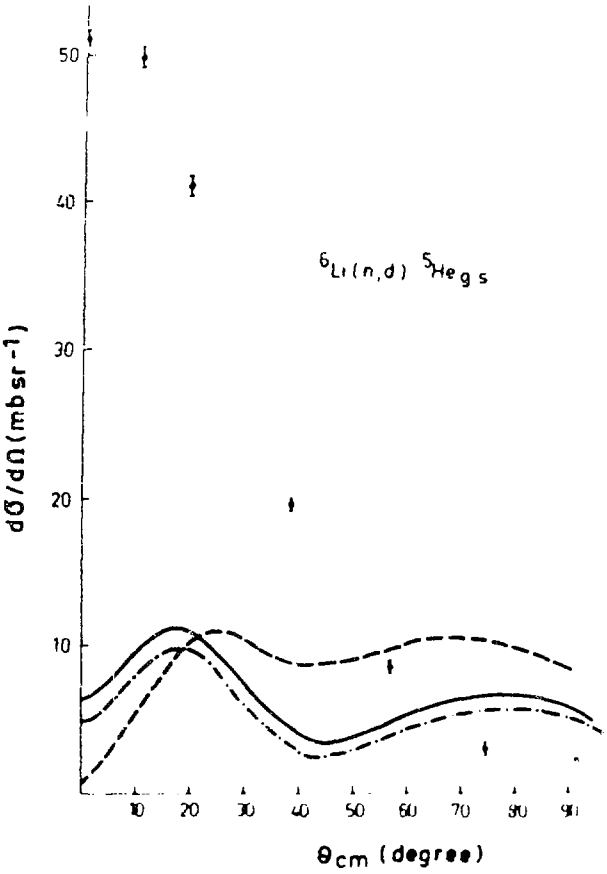

Fig. 30b.

Fig. 30e.

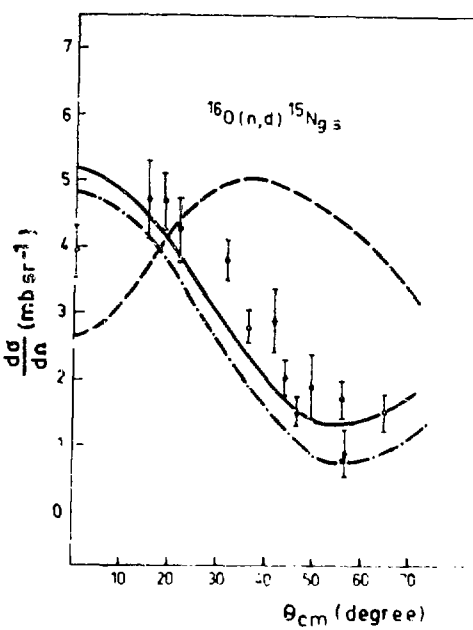

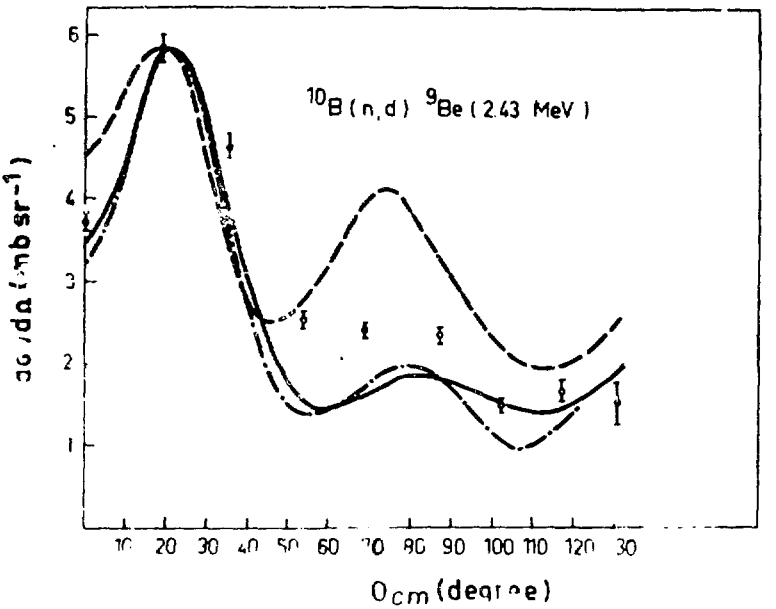

Fig. 30c.

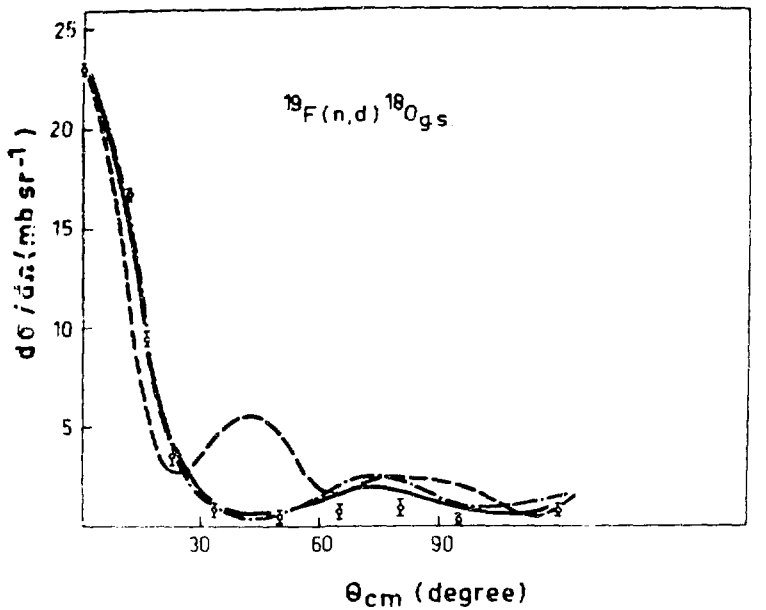

Fig. 30d.

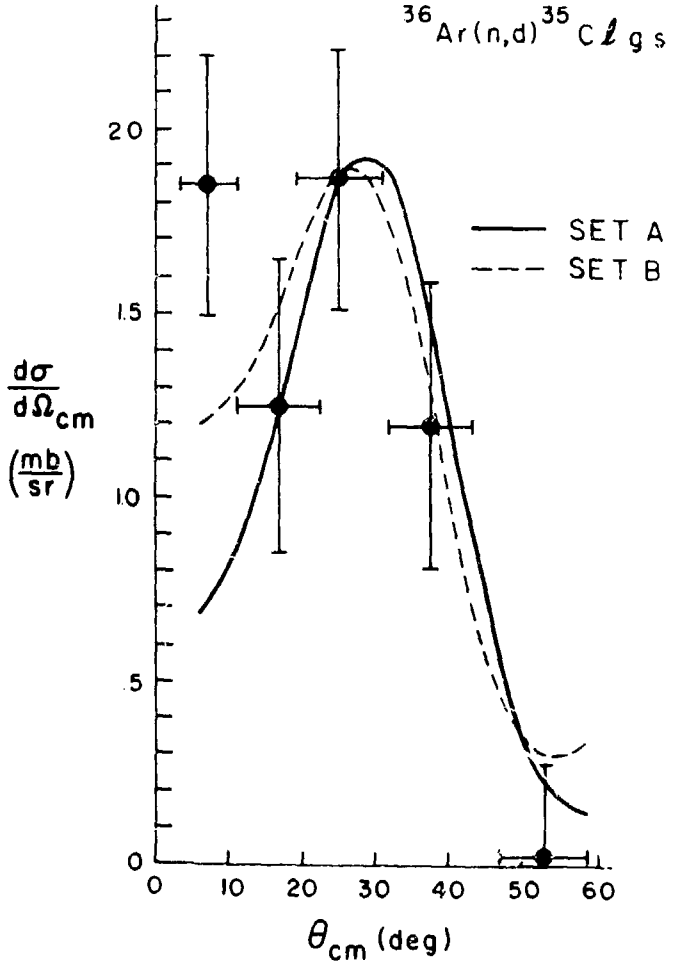
$^{36}Ar(n,d)^{35}Cl\ g.s.$
SET A
SET B
$\frac{d\sigma}{d\Omega_{cm}}$ $\left(\frac{mb}{sr}\right)$
θ_{cm} (deg)

Fig. 31.

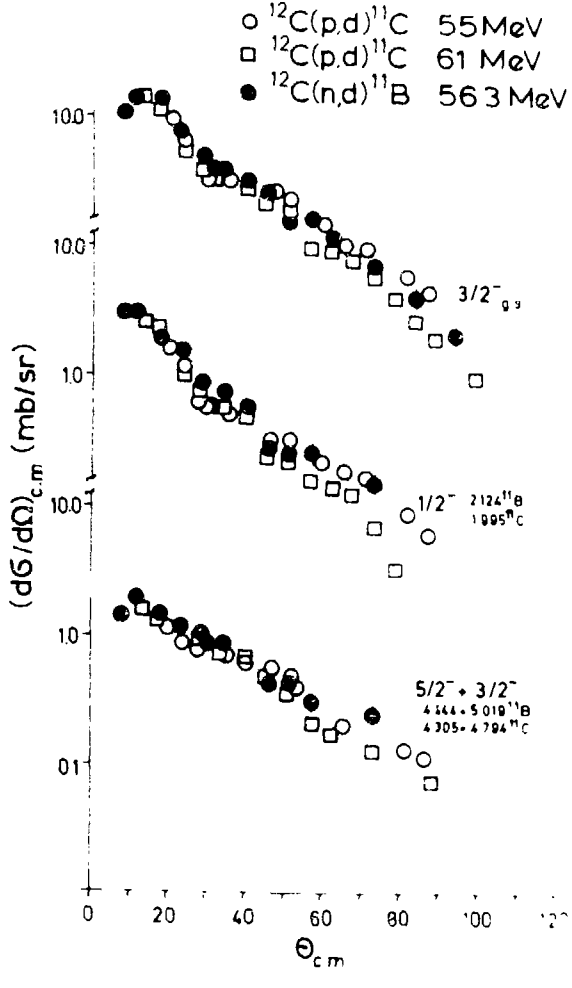
$^{12}C(p,d)^{11}C$ 55MeV
$^{12}C(p,d)^{11}C$ 61 MeV
$^{12}C(n,d)^{11}B$ 56.3 MeV
$3/2^-_{g.s.}$
$1/2^-$
$5/2^- + 3/2^-$
$(d\sigma/d\Omega)_{c.m.}$ (mb/sr)
$\Theta_{c.m.}$

Fig. 32.

Table 7.

Spectroscopic factors

A, B and C in parenthesis denote deuteron potentials (Mi 71, Pa 76)

Reactions	(n,d)	(p,d)	(d,t)	(d,^{3}He)	(^{3}He,α)	(p,2p)	Theory
^{3}He(n,d)d	1.7 (A) 2.4 (B) 1.7 (C)						S_{max}=1.5
^{6}Li(n,d)^{5}He$_{gs}$	~10						1.36
^{7}Li(n,d)^{6}He$_{gs}$	1 (A) 0.6 (B) 0.8 (C)	1.1a				2.1 n	0.85r
^{10}B(n,d)^{9}Be$_{gs}$	1.2 (A) 1.1 (B) 1.3 (C)	0.76b 0.88d	0.80c 0.96e	0.76c 1.02e			1.2p 1.06r
^{10}B(n,d)^{9}Be$^*_{2.43}$	1.3 (A) 1.3 (B) 1.7 (C)	0.76b 1.2d	0.66c				1.14p 1.02r
^{11}B(n,a)^{10}Be$_{gs}$	1.1 (A) 1.3 (B) 0.7 (C)	0.48d	1.35c	1.28c			0.64p
^{14}N(n,d)^{13}C$_{gs}$	3.8 (A) 2.5 (B) 1.3 (C)	1.52d	1.8d	1.76d	1.66h		1.39p 1.98q
	2.0 f						
^{15}N(n,d)^{14}C$_{gs}$	1.8 (A) 1.3 (B) 0.8 (C)	1.5g		1.5i	1.5i		1.5 jj limit 1.23p
	1.6 f						
^{16}O(n,d)^{15}N	4.5 (A) 4.1 (B) 4.0 (C)	4.4d 2.9b	3.0j 2.58d	4.6k 2.51			3.05s
^{19}F(n,d)^{18}O	0.4 (A) 0.4 (B) 0.8 (C)				0.57m		0.51t
^{35}Cl(n,d)^{34}S$_{gs}$	1.04 (A) 1.18 (B) 1.58 v 1.07 z			1.26v 1.50j 1.29y			1.1ss 0.94tt
^{35}Cl(n,d)^{34}S$^*_{2.13}$ (I=0)	0.34 (A) 0.45 (B) 0.29v 0.36z			0.37j 0.35y			0.58ss

Reactions	(n,d)	(p,d)	(d,t)	(d,^{3}He)	(^{3}He,)	(p,2p)	Theory
$^{35}Cl(n,d)^{34}S^{*}_{2.13}$ (L=2)	0.28 (A)			0.93 v			0.21 ss
	0.26 (B)			0.55 j			
	0.51 z			0.39 y			
$^{37}Cl(n,d)^{36}S_{gs}$	1.8 (A)			4.21 v			1.136ss
	2.04 (B)			1.64 j			1.22 x
	0.35 z			1.32 x			
$^{36}Ar(n,d)^{35}Cl_{gs}$	3.62 (A)			4.4 w			3.89ss
	3.82 (B)						4 tt

References:
a (Li 69), b (To 69), c (Fi 67), d (Ba 69), e (Ga 68), f (Fe 67), g (Sn 69), h (Kn 70), i (Bo 70), j (Pu 69), k (Hi 67), l (Do 69), m (Ka 70), n (Ja 67), o (Mi 68), p (Co 67), r (Ba 64), q (Na 63), s (Br 66), t (El 70), v (Cu 62), w (Do 74), x (Gr 69), y (Mi 68), z (Fa 67), ss (Gd 64), tt (Wi 71).

deuteron potentials used for chlorine and argon differ from those used for ^{3}He to ^{19}F.

Table 7. summarizes the spectroscopic factors obtained from (Mi 71) and (Pa 76) and compares them with spectroscopic factors extracted from other reactions and with theoretical predictions.

The DWBA gives a satisfactory fit to the data and yields spectroscopic factors in reasonable agreement with the theoretical predictions. The only exception is the reaction $^6Li(n,d)^5He_{gs}$ (Fig. 30b.) where the shape of the angular distribution is not reproduced by the pickup model. If one would normalize the DWBA prediction to the maximum experimental cross section, one would obtain S~10 as compared to the theoretical value of S=1.36. It has been pointed out (Va 65) that the reason for the discrepancy is the large contribution of the deuteron knock out process.

The (n,d) reactions have been also studied at E_{inc}= 56.3 MeV (UC 75). Fig. 32. shows the $^{12}C(n,d)^{11}B$ data compared with the $^{12}C(p,d)^{11}C$ data at 55 and 61 MeV.

9. (n,t) reactions

Table 8. summarizes the measurements of (n,t) reactions on light nuclei. Measured angular distributions suggest the importance of direct mechanisms (Fig. 33a-d). Data are compared with the zero range DWBA calculations assuming a two nucleon pickup mechanism. Nuclear structure factors have been calculated using wave functions from (Bo 64). The neutron optical model potentials are the same as in the study of (n,d) reactions on ^{3}He to ^{19}F (Mi 71). Two sets of triton potentials have been used both with volume absorption: D - which fits ^{3}He - ^{12}C and E - which fits t + ^{12}C elastic scattering. In Figs. 33 the DWBA predictions using potential D are given by solid curves and those using potential E by dashed curves. The absolute values of the experimental cross sections are larger than the theoretical. The ratios are given in Table 8. and differ for two triton optical model potentials.

In some (n,t) reactions other mechanisms could be important, e.g. in the reaction ^{7}Li(n,t)^{5}He the contribution of the knock-out process is obviously important, as is also supported by the fact

Table 8.

(n,t) reactions on very light nuclei

Reaction	$\sigma_{max}(\theta)$ (mb/sr)	Exp/theory	Reference	E_n (MeV)
^{6}Li(n,t)^{4}He$_{gs}$	22.6 ± 2.8		Re 67	2.7
	8.38 ± 0.27	1.4 (D) 6.1 (E)	Re 67	14.4
^{7}Li(n,t)^{5}He$_{gs}$	15.6 ± 0.5	2.4 (D) 13.2 (E)	Mi 70	14.4
^{10}B(n,t)^{8}Be$_{gs}$	0.79 ± 0.06	4 (D) 20 (E)	Va 64	14.4
^{10}B(n,t)^{8}Be$^{*}_{2.9}$	1.62 ± 0.08	5.4 (D) 17 (E)	Va 64	14.4
^{11}B(n,t)^{9}Be$_{gs}$	2.57 ± 0.08	4 (D) 12 (E)	Mi 70	14.4
^{14}N(n,t)^{12}C$_{gs}$	2.6 ± 0.25	3.5 (D) 16 (E)	Re 67 Mi 70	14.4
^{14}N(n,t)^{12}C$^{*}_{4.4}$	5.6 ± 0.4	4.5 (D) 13 (E)	Re 67 Mi 70	14.4
^{19}F(n,t)^{17}O$_{gs}$	1.2 ± 0.07		Re 67	14.4
^{19}F(n,t)^{17}O$_{0.87}$	2.45 ± 0.13		Re 67	14.4

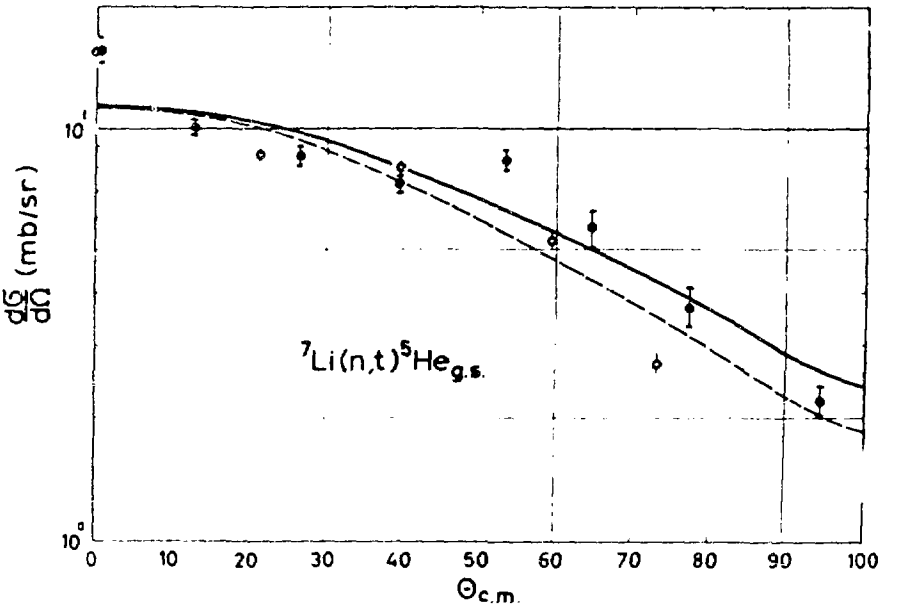

Fig. 33a.

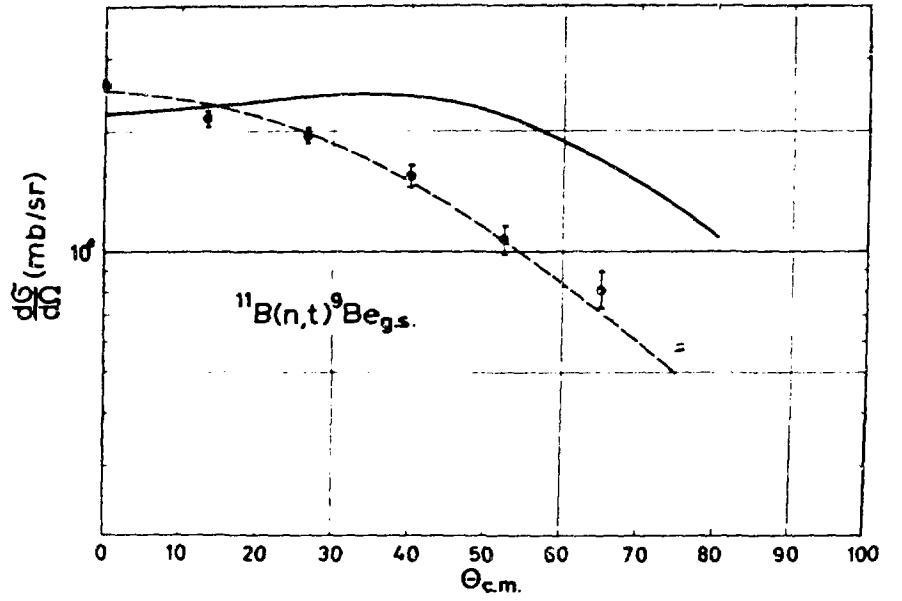

Fig. 33b.

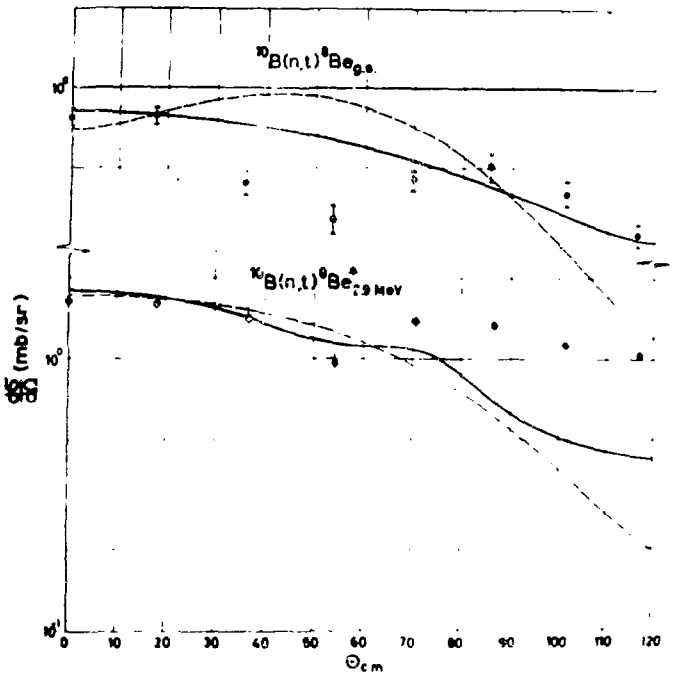

Fig. 33c.

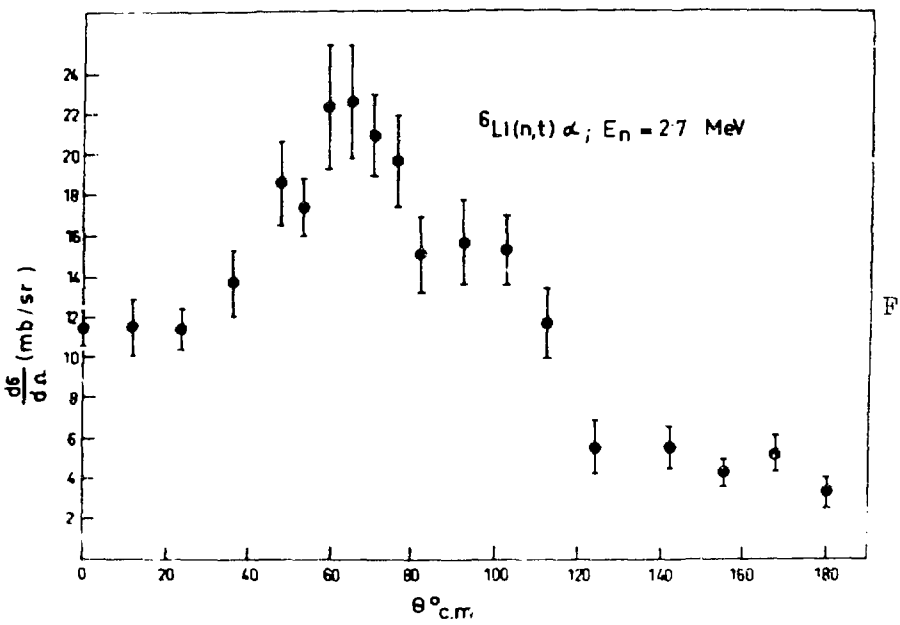

Fig. 33d.

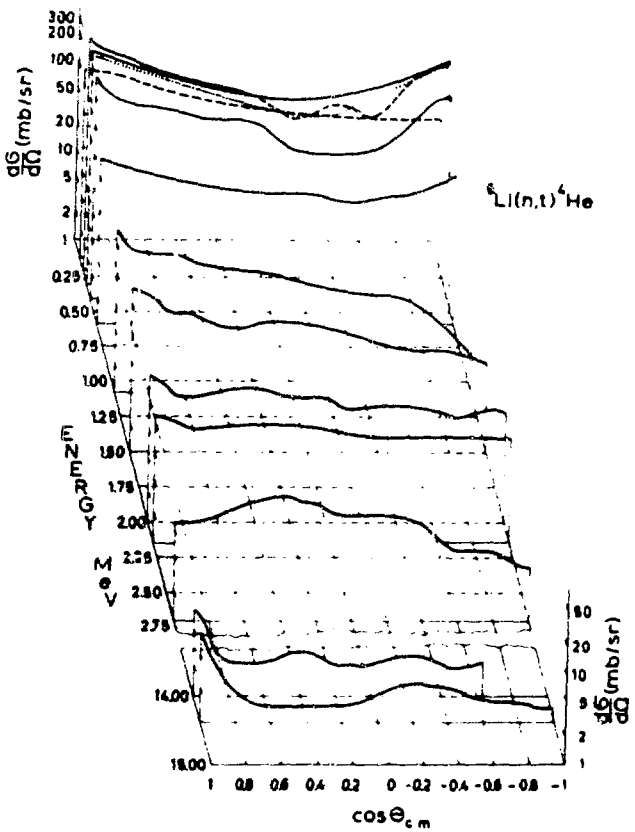

Fig. 34.

that the cross sections for the reaction $^{7}Li(p,t)$ is twice as large as for the $^{7}Li(p,^{3}He)$ reaction (Ce 56).

The reactions $^{7}Li(n,t)xn$ and $^{10}B(n,t)\alpha x$ result in a three body final state. Angular distributions are meaningful only if one can reliably extract the contribution due to the sequential mechanism involving a well defined intermediate state. For example, it has been established that the sequential decays through $^{8}Be_{gs}$, $^{8}Be^{*}_{2.9}$ and $^{7}Li^{*}_{4.63}$ are present in the reaction $^{10}B(n,t)\alpha\alpha$, but the last two partially overlap in the triton energy spectra.

The total cross section for the reaction $^{6}Li(n,t)$ obtained by integrating the angular distribution in Fig. 33d. is 166 ± 21 at E_{inc} = 2.7 MeV (Re 67) compared with 26 ± 3 mb at E_{inc} = 14.4 MeV, both in good agreement with other measurements (St 64). The broad maximum observed at $\theta \sim 65^{\circ}$ (Fig. 33d.) is also seen in the reaction $^{6}Li(p,^{3}He)$ at E_{inc} = 2.91 MeV (Ma 56). Excitation curve reveals a resonance at E_{p} = 1.85 MeV corresponding to the formation of the compound nucleus $^{7}Be^{*}$ (7.19 MeV). Similarly, there is a resonance in the reaction $^{6}Li(n,t)\alpha$ at E_{n} = 0.3 MeV ($^{7}Li^{*}_{7.48}$). Angular distributions at various incident neutron energies are shown in Fig. 34.

10. (n,α) reactions

The excitation functions for some (n,α) reactions are given in Figs. 35, 36, 37a, and b) (Bo 74, Yo 75, Ar 56, Sc 70, Ba 65, Pi 65). Solid curves in Figs. 37 are recommended cross sections (Yo 75). The energy dependence of the recommended curve below 6 MeV is given by an L = 0 penetrability function. The recommended value for $^{27}Al(n,\alpha)^{24}Nb$ cross section at 14.1 MeV is 124 mb.

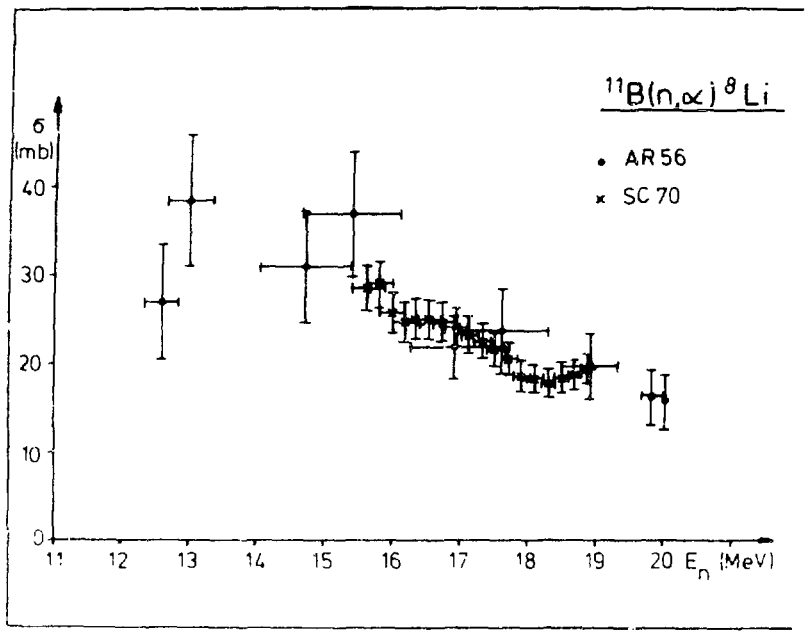

Fig. 35.

10.1. The reaction $^{9}Be(n,\alpha)^{6}He$

Differential cross sections have been measured from $E_{inc} \sim 8$ to 30 MeV (Kr 72), in particular at 12.2, 14.1 (Sm 76), 14.4 (Pa 67a) and 18 MeV (Sm 76). The Karlsruhe isochronous cyclotron has been used to produce a continuous spectrum of $\sim 4 \times 10^{7}$ neutrons/s-cm^2 by bombarding the internal carbon target with 54 MeV deuterons. Experimental apparatus: time-of-flight in

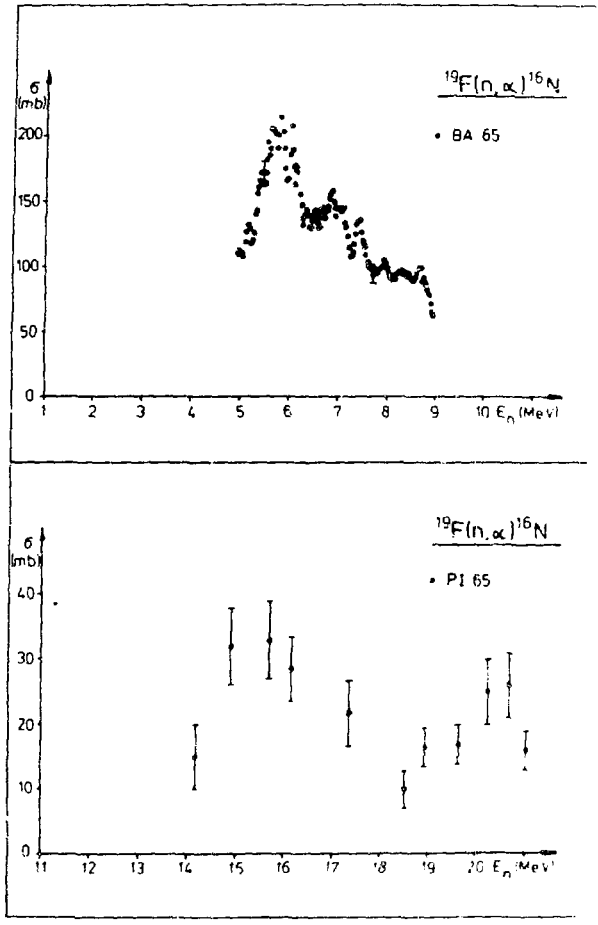

Fig. 36.

conjunction with a set of counter telescopes provides a simultaneous measurement of angular distributions at many incident energies. Fig. 38. shows the angular distributions for a) $^{9}Be(n,\alpha)^{6}He_{gs}$ and b) $^{9}Be(n,\alpha)^{6}He^{*}_{1.8}$ (see also Sm 76). Dashed curves are eye guides only. Neutron energy is written besides each curve. Angular distributions at 12.2, 14.1, 14.4 and 18.0 MeV are given in Fig. 39. In these measurements (Pa 67a, Sm 76) both ^{4}He and ^{6}He have been detected thus providing a full angular distribution. The backward peaking of the angular distribution persisting at least from 12 to 18 MeV and the smooth excitation function (Fig. 40) strongly argue that the direct mechanism is responsible for the reaction $^{9}Be(n,\alpha)^{6}He_{gs}$. Dashed curves are the predictions of the PWBA calculation assuming coherent addition of heavy particle stripping and pickup mechanisms. Requiring the best fit to the data determines the ratio pickup vs heavy particle stripping to be ~ 0.001. The heavy particle stripping dominates over the ^{3}He pickup in the entire angular region. This is obviously unrealistic. The analysis of the charge symmetric process $^{9}Be(p,\alpha)^{6}Li$ (De 72) using zero range and exact finite range DWBA shows that the contribution of the heavy particle stripping at forward angles decreases by an order of magnitude by introducing

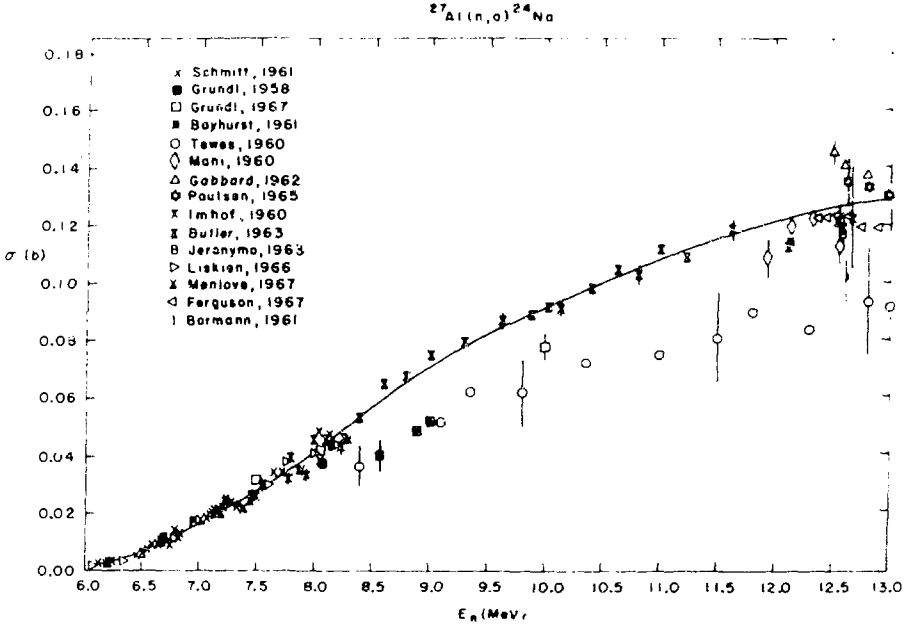

Fig. 37a.

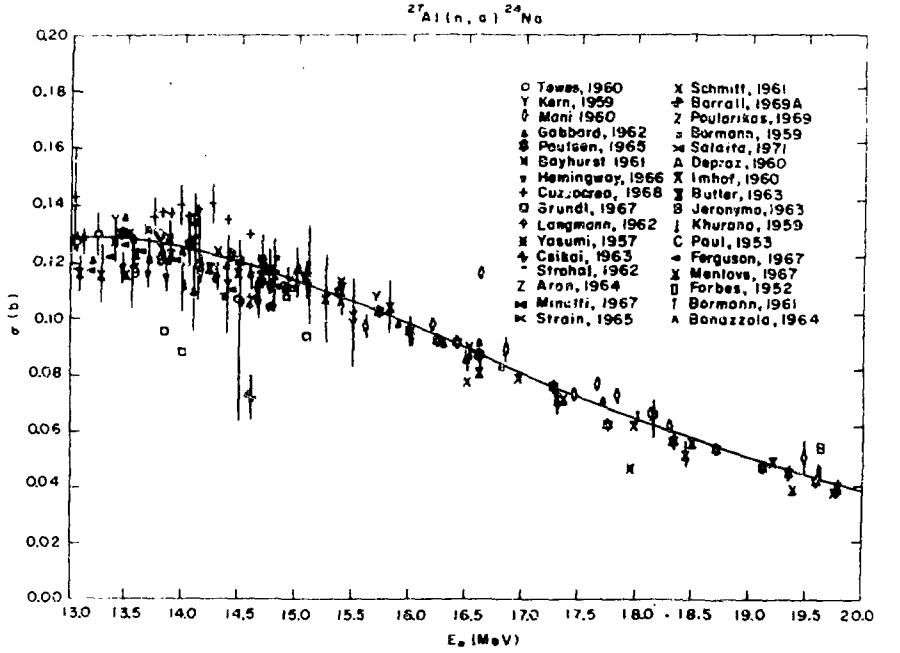

Fig. 37b.

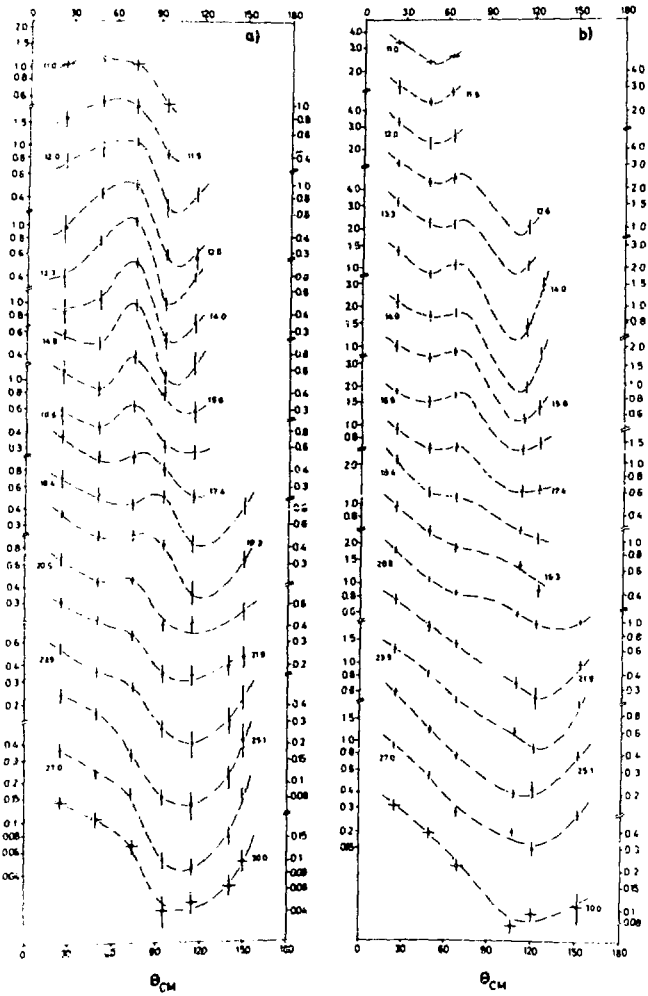

Fig. 38.

the exact finite range. Estimates of the knock out process have shown that its contribution is substantially smaller than the pickup cross section

10.2. The reaction $^{11}B(n,\alpha)^{8}Li$

The reaction $^{11}B(n,\alpha)^{8}Li$ has been investigated at 13.9 (We 71), at 14.1 MeV using the CsI(Tl) detector (Bo 73) and at 14.4 MeV using nuclear emulsions where these events are visualized as events resulting into an alpha particle and ^{8}Li which beta decays into $^{8}Be \rightarrow \alpha+\alpha$ (An 76). Figs. 41a (We 71, Bo 73) and b (An 76) show angular distributions leading to $^{8}Li_{gs}$ and $^{8}Li^{*}_{0.975}$ states. Three measurements disagree. The data of (Bo 73) suggest a symmetric angular distribution in agreement with the Hauser-Feshbach model (Fig. 41a).

The structure of ^{11}B is mainly $t+^{8}Be$ (see also De 72). The spectroscopic factors for $^{8}Li+\alpha$ and $^{7}Li+h$ are ~two orders of magnitude smaller and therefore it is reasonable that the pickup and knockout mechanisms do not contribute significantly to the reaction $^{11}B(r,\alpha)^{8}Li$. The cross sections for the reactions $^{11}B(n,\alpha)^{8}Li_{gs}$ and $^{11}B(n,\alpha)^{8}Li^{*}_{0.975}$ are 17.7 ± 5.5 mb and 9.2 ± 3.0 mb, respectively (An 76, Ar 56, Se 70, He 56).

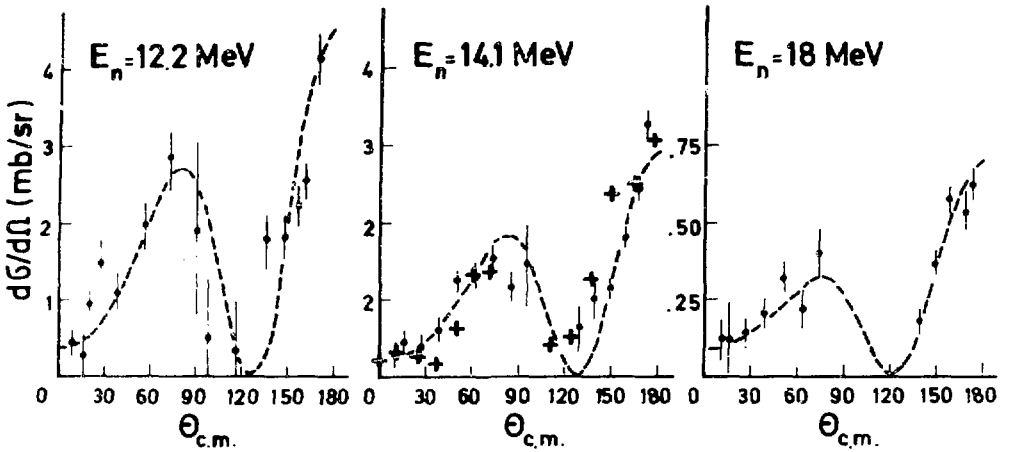

Fig. 39. Data: points (Sm 76), crosses (Pa 67a) at 14.4 MeV

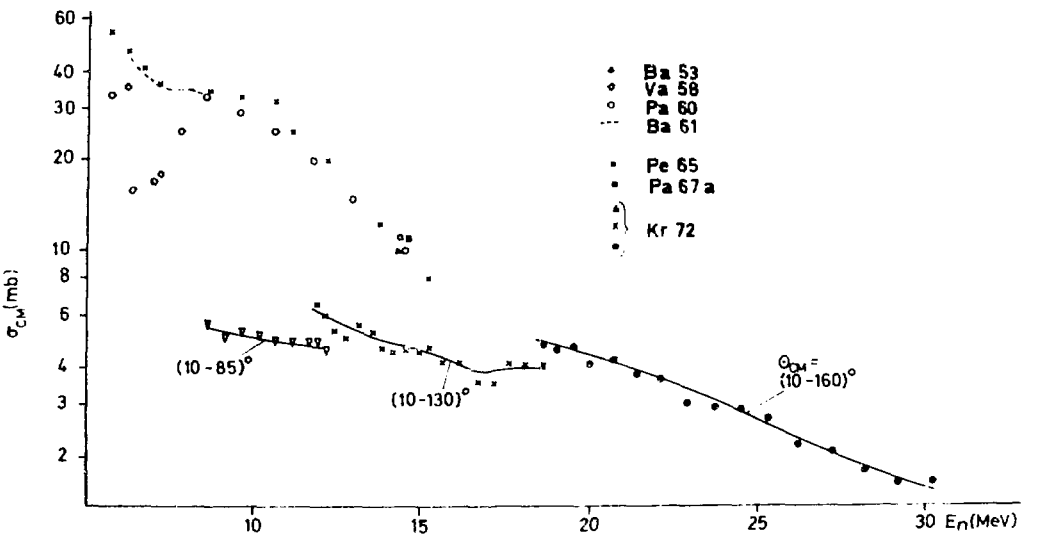

Fig. 40. Energy dependence of the $^{9}Be(n,\alpha)^{6}He_{gs}$ cross section obtained by integrating the angular distributions over the region indicated in parentheses (Kr 72).

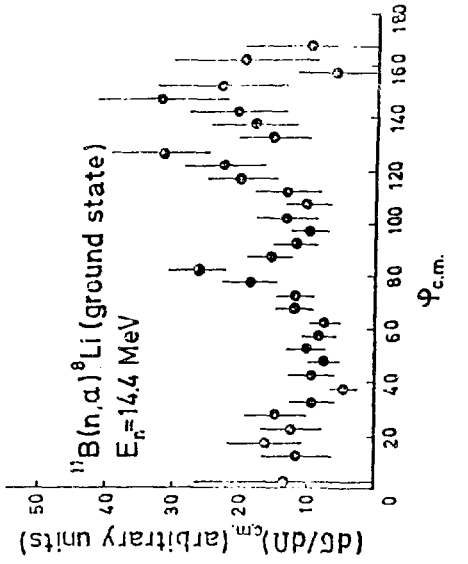

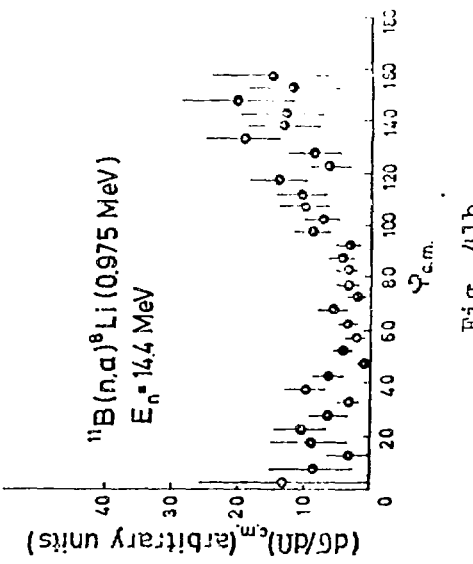

Fig. 41b.

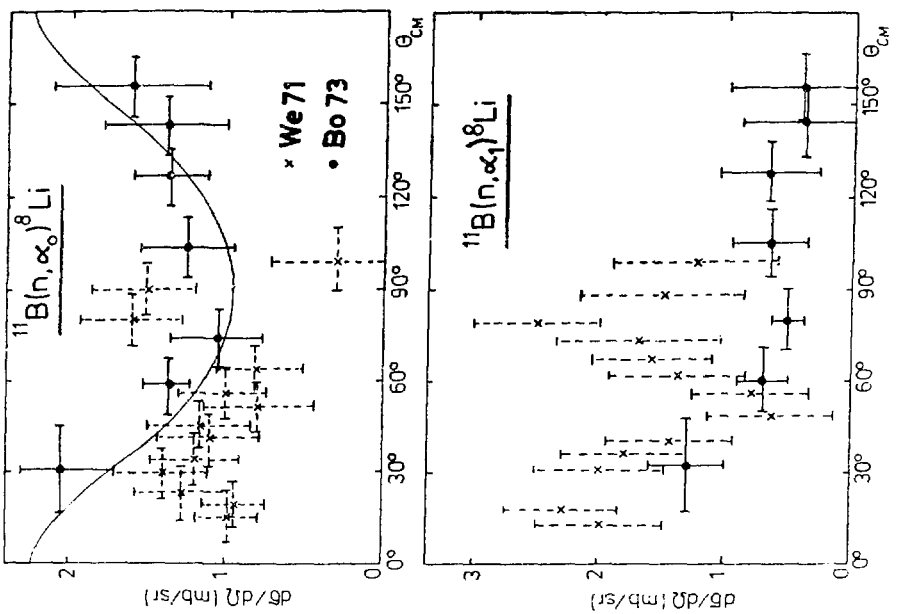

Fig. 41a.

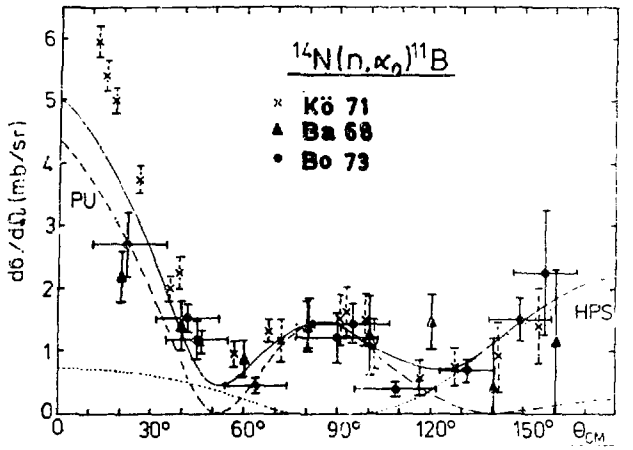

Fig. 42.

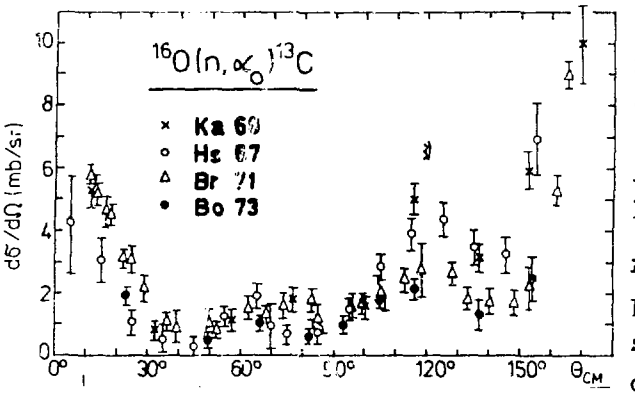

Fig. 43.

10.3. The reactions $^{14}N(n,\alpha)$, $^{16}O(n,\alpha)$ and $^{19}F(n,\alpha)$

The reaction $^{14}N(n,\alpha)^{11}B$ has been measured at 14 MeV (Bo 73, Le 68, Ba 68, Ma 68, Kö 71). Measurements (Fig.42) indicate the presence of direct mechanisms: pickup (dashed curve) and heavy particle stripping (dotted curve - PWBA). The solid curve is the incoherent addition of the two processes. There is evidence that at E_{inc}=15-19 MeV (Sa 71) this reaction proceeds through compound nucleus formation.

Even the early qualitative studies of the reaction $^{16}O(n,\alpha)^{13}C_{gs}$ revealed pronounced forward and backward peaking. The structure observed in recent measurements of the angular distribution (Ka 69, Br 71, Ma 68a, Hs 67, Mc 66, Bo 73) (Fig. 43) corresponds to similar structures observed in the studies of the reactions $^{13}C(\alpha,n)^{16}O_{gs}$ and $^{16}O(p,\alpha)^{13}N_{gs}$ (Br 71). Various PW and DWBA calculations (Le 68, Ma 68a, Hs 67, Mc 66, La 67) indicate that the backward alpha emission is mainly due to heavy particle stripping. Pickup and knockout mechanisms are also present. However, the measurements in the range E_{inc}= 14.8 to 18.8 MeV (Si 68) indicate a pronounced energy dependence and the compound nucleus mechanism is suggested.

In the study of the reaction $^{19}F(n,\alpha)^{16}N$ it has not been possible to resolve groups leading to low lying states in ^{16}N. The

measured angular distribution agrees with the Hauser-Feshbach model.

11. Neutron induced multiparticle processes

Visual detectors (e.g. bubble chambers, nuclear emulsions) used simultaneously as targets provide an almost 4π detection geometry. The breakup into 3, 4, ... particles appears as a star with as many prongs as there are charged particles involved in the decay and therefore, the counting rate in the correlation measurement does not depend on the number of detected particles. Multiparticle reactions leading to N particles have 3N-4 IKV. i) If all particles in the final state are charged, their momenta can be determined, (3N data) and the process is overdetermined: 4 constraints. If the incident neutron spectrum is continuous, one can use the available information to determine the energy of the neutron causing the reaction. ii) If one particle in the final state is neutral (3N-3 measurements), the process is only once overdetermined. iii) If two particles in the final state are neutral (3N-6 measurements) the process is underdetermined. It is desirable to overdetermine the process so as to be able to use the additional constraints to uniquely identify particles and to reduce the background.

Table 9. lists elements present in nuclear emulsions, their densities, dominant nuclear reactions with their cross sections and Q values. The last column gives the relative frequency of these reactions with respect to n-p elastic scattering (An 62). Emulsions loaded with lithium and boron are also available.

In multiparticle reactions it is desirable to represent data in terms of those variables which have a simple physical meaning, e.g. relative energy of two outgoing particles, E_{ij}, and momentum transfer, p. The representation of the data in terms of such variables is meaningful only when a large portion of the phase space is explored. The density distributions of such generalized Dalitz diagrams exhibit dynamical features of specific reaction mechanisms if appropriate variables are used. Dalitz plots for the reaction ^{7}Li(n,tα)n are shown in Fig. 44.: a) $E_{\alpha n}$ vs $E_{\alpha t}$ with bands corresponding to sequential decays, b) $E_{\alpha n}$ vs p_t. Single particle

Table 9.

Elements present in nuclear emulsions

Element	ρ(g/cm^3)	Reaction	σ(mb)	Q(MeV)	$(n\sigma)_{rel}$
Ag	1.817	^{109}Ag(n,p)	12.5	-0.328	29.8
Br	1.324	^{79}Br(n,α)	10.0	1.798	24.3
		^{81}Br(n,α)	100.0	0.631	237.8
I	0.052	^{127}I(n,p)	230.0	0.092	26.6
		^{127}I(n,α)	180.0	4.291	20.8
C	0.277	^{12}C(n,3α)	230.0	-7.28	1523.0
H	0.053	H(n,p)n	650.0		10000.0
O	0.249	^{16}O(n,p)	89.0	-9.603	401.5
		^{16}O(n,α)	310.0	-2.202	1398.4
N	0.074	^{14}N(n,α)	100.0	-0.155	152.7
		^{14}N(n,2α)	58.0	-8.823	88.5
S	0.007	^{32}S(n,p)	370.0	-0.926	22.0

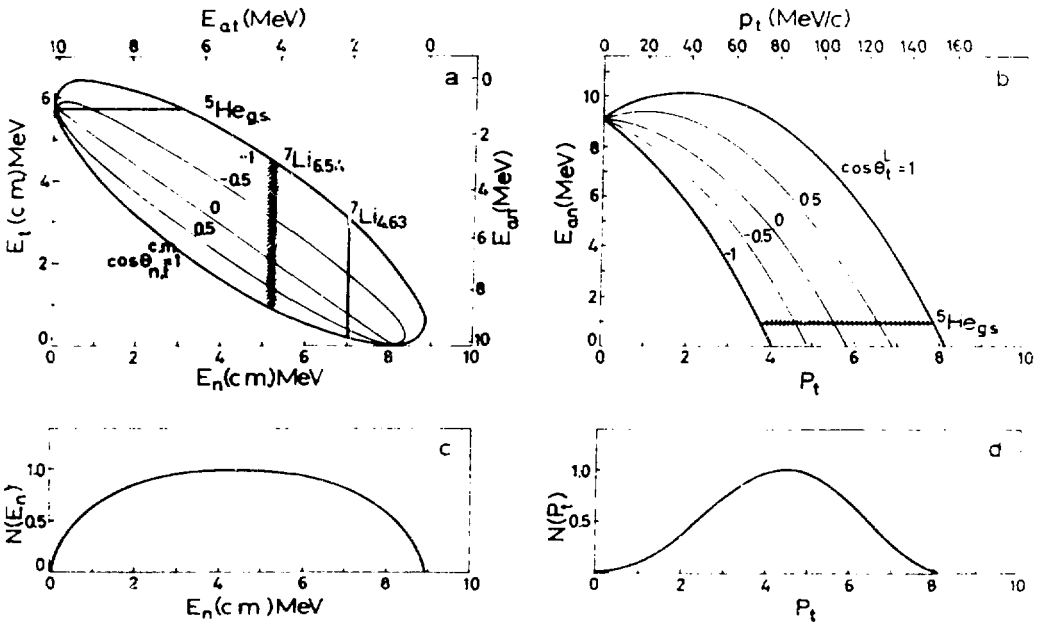

Figs. 44a-d.

phase space distributions as a function of neutron energy, E_n, and triton momentum, p_t, are shown in Fig. 44 c) and d), respectively. Data from reactions leading to 4 body final states (particles i, j, k, l) can be displayed in a triangular plot E_{ij} vs E_{kl}. Bands perpendicular to E_{ij} correspond to sequential decays through i-j states, thus enabling the identification of 2 body resonances in a 4 body breakup. When such resonances are established, the 4 body process can be reduced to a quasithree body process: (ij) + k + l.

11.1. The reaction ^{7}Li(n,tα)n (An 74)

At E_{inc} = 14.4 MeV the reaction proceeds mainly through inelastic neutron scattering followed by the decay of ^{7}Li into α + t. The contributions of the sequential decays through $^7Li^*_{4.63}$, $^7Li^*_{6.56}$ and $^5He_{gs}$ are 150 ± 20 mb, 54 ± 10 mb and 49.5 ± 9 mb, respectively, using 300 mb for the total cross section (Ro 62).

The contributions of the QF n-α scattering has been investigated through experimental $E_{\alpha n}$ vs p_t plots imposing the condition $E^*(^7Li) > 7$ MeV (Fig. 44e). Thin lines in the p_t distribution

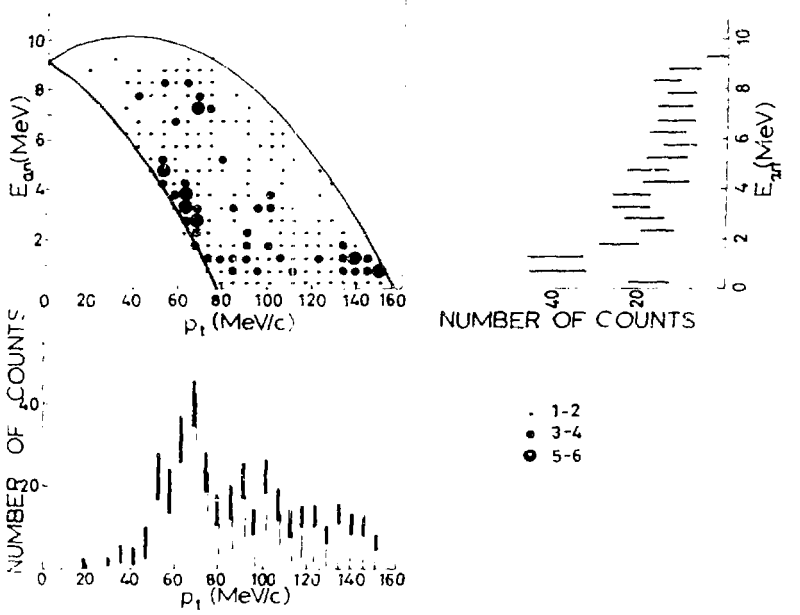

Fig. 44e.

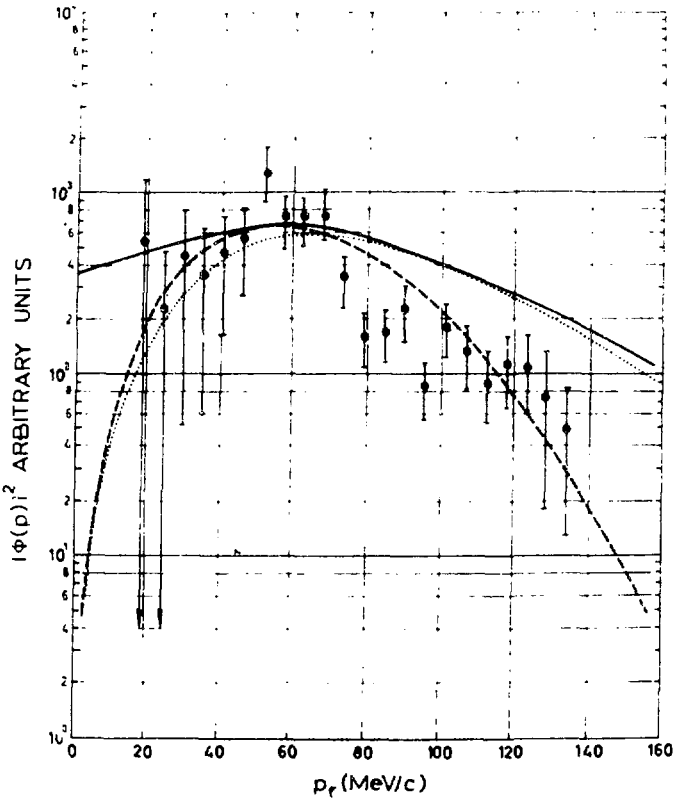

Fig. 44f.

represent the spectrum after the subtraction of the events proceeding via $^5He_{gs}$ sequential decay. Fig. 44f. shows the extracted square of the Fourier transform $|\phi(p)|^2 = d^3\sigma/(\sigma_{n\alpha} \cdot PSF)$ compared with $|\phi(p)|^2$ deduced from the study of the $^7Li(p,p\alpha)t$ reaction (solid curve - Ja 70) and with the theoretical calculations assuming ^7Li composed of two clusters: α and t in L=1 described by a Hankel wave function with a cutoff of 2.87fm (dotted) and a harmonic oscillator function (dashed). The total contribution of the QF n-α scattering amounts to 46 ± 10 mb.

11.2. The reactions $^6Li(n,\alpha d)n$ and $^6Li(n,\alpha p)2n$

Cross sections for these reactions are given in Fig. 45. The solid curves represent the recommended values (EN 75).

Evidence for n-α QFS has been found in the reaction $^6Li(n,\alpha d)n$ and the extracted Fourier transform can be described by Hankel function for the L=0 relative motion of α-d clusters in ^6Li (An 75).

11.3. The reactions $^{10}B(n,\alpha\alpha d)n$ and $^{10}B(n,\alpha\alpha t)$ (An 72)

About 5-6% of the total four body breakup can be attributed to the double FSI: $n+^{10}B \longrightarrow (\alpha d)_{^6Li^*_{2.18}} + (\alpha n)_{^5He_{gs}}$. The four body

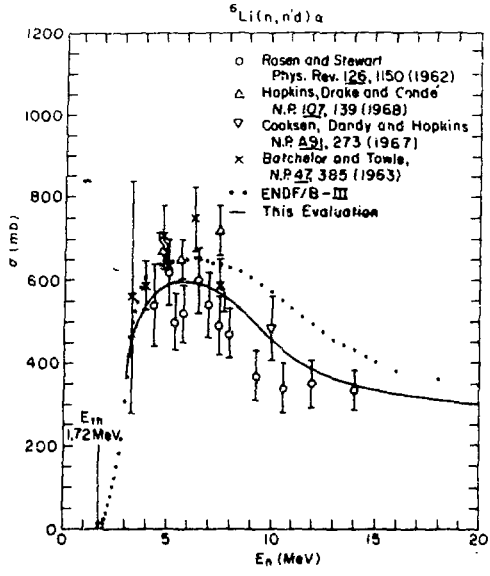

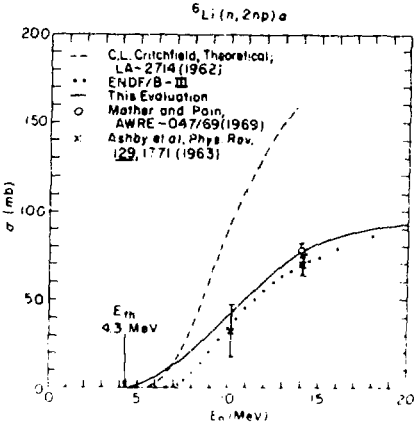

Fig. 45.

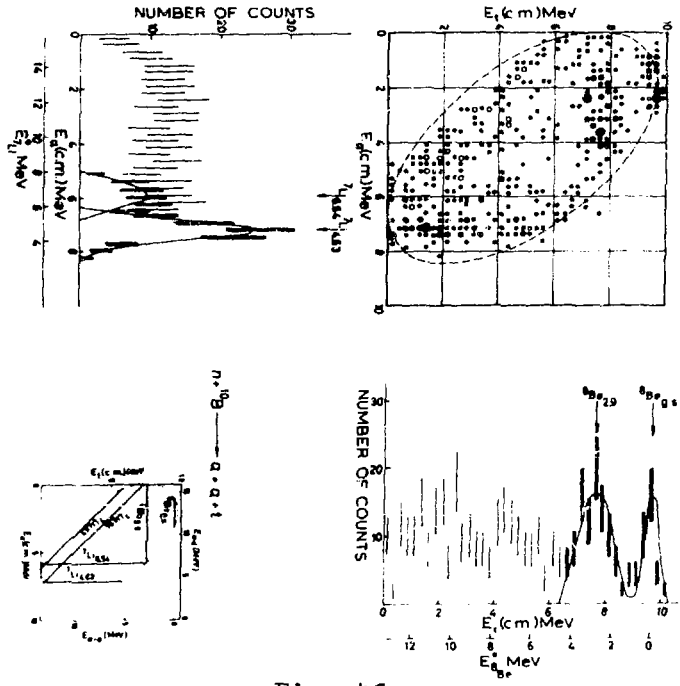

Fig. 46.

The reaction ^{10}B(n,ααt) proceeds through intermediate states reaction also proceeds as a QF interaction between the incident neutron and a correlated αα or αd group in ^{10}B. Information about the presence of ^{8}Be and ^{6}Li unstable states in ^{10}B can be obtained investigating the contribution of higher relative angular momentum components in the wave functions d-^{8}Be and α-^{6}Li*. Defining the percentage of events beyond 100 MeV/c one obtains results which are not unreasonable in the spectator model picture.

$^{8}Be_{gs}$, $^{8}Be^{*}_{2.9}$, $^{7}Li^{*}_{4.63}$ and even $^{7}Li^{*}_{6.54}$ (Fig. 46). Since there are two alphas in the final state there are two sets of bands involving intermediate states of $^{7}Li^{*}$. It seems that there is no contribution of a simultaneous 3 body breakup.

11.4. The reaction $^{12}C(n,3\alpha)n$

This process has been studied at E_{inc}=14.4 MeV (An 75a, An 75b), 18.2 MeV (An 76) and with a continuous neutron spectrum extending to ~ 40 MeV (An 76b). The reaction can proceed through sequential decays:

$^{12}C + n \rightarrow n' + {}^{12}C^{*}(\rightarrow \alpha + {}^{8}Be(\rightarrow \alpha\alpha))$ (1)

$\rightarrow \alpha + {}^{9}Be^{*}(\rightarrow n + {}^{8}Be(\rightarrow \alpha\alpha))$ (2.1)

$\rightarrow \alpha + {}^{9}Be^{*}(\rightarrow \alpha + {}^{5}He(\rightarrow \alpha n))$ (2.2)

$\rightarrow {}^{8}Be(\alpha\alpha) + {}^{5}He(n\alpha)$, (3) double FSI

and through QF processes where neutron interacts with an alpha or a correlated $\alpha\alpha$ pair ($^{8}Be_{gs}$, $^{8}Be^{*}$).

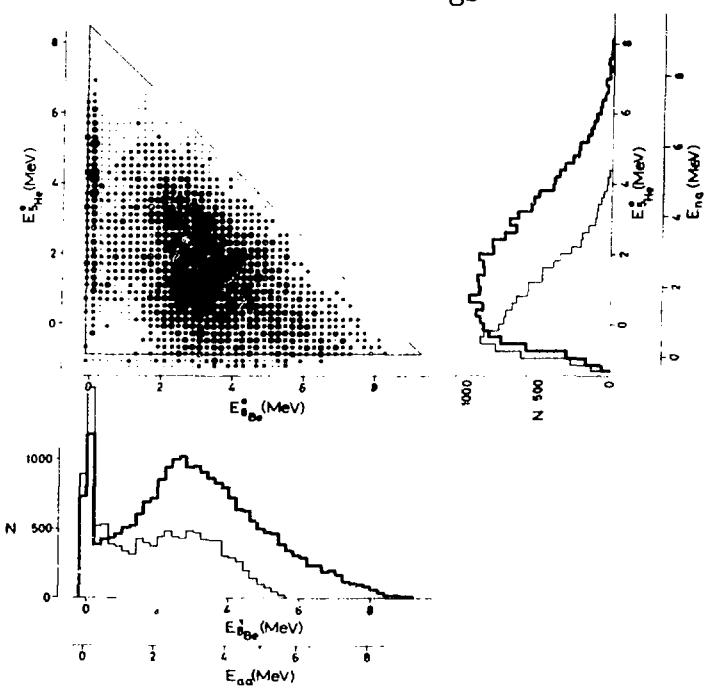

Fig. 47.

Fig. 47. shows the density distribution of experimental events in the E (^{5}He) vs E (^{8}Be) plot for E_{inc}=18.2 MeV. The right and lower histograms are projections on each axis. Thin line histograms are the corresponding spectra at E_{inc}= 14.4. Each event is represented by 3 data points in the plot, since any of 3 different but indiscernible pairs of three final state alphas may constitute the ^{8}Be nucleus. If alphas i and j interact, then $\alpha_i - \alpha_j$ and α_k - n produce correct excitations of ^{8}Be and ^{5}He, while other

two combinations give "spurious events". The two spurious events are well separated from the correct one only for events representing two alphas forming a narrow $^{8}Be_{gs}$. Hence, these spurious events were omitted. Data show strong enhancements due to $^{8}Be_{gs}$, a broad peak due to $^{8}Be^{*}_{2.9}$, but no structure due to $^{5}He_{gs}$. There is no indication of double FSI: $^{8}Be + {}^{5}He_{gs}$. Since ^{8}Be is formed in this 4 body reaction, we can treat it as a quasithree body process $n+\alpha+{}^{8}Be$, e.g. in a Dalitz plot $E(^{9}Be^{*})$ vs $E(^{12}C^{*})$. The analyses of various Dalitz plots at 14.4 and 18.2 MeV show (An 75, An 76a) that i) the process proceeds mainly through $^{12}C(n,n')^{12}C^{*}$ involving 9.63, 10.84, 11.83 and 12.71 MeV excited states of ^{12}C ($\sim$ 80% of the $^{12}C(n,3\alpha)n'$ cross section at 14-18 MeV, see also Table 3); ii) the process $^{12}C(n,\alpha)^{9}Be^{*}_{2.43}(\rightarrow n\,2\alpha)$ contributes $\sim$ 10% at 14.4 MeV and $\sim$ 5% at 18.2 MeV and there is an indication of the decay through $^{9}Be^{*}_{4.75}$ state; iii) there are no events corresponding to a possible simultaneous breakup; iv) the density distributions of the Dalitz plots at E_{inc}=14.4 MeV indicate that a) the process $^{12}C^{*}_{9.63}\rightarrow 3\alpha$ proceeds only through $^{8}Be_{gs}$ (of course, since the 9.63 MeV state is 0.64 MeV lower than the $\alpha+{}^{8}Be_{2.9}$ system); $^{12}C^{*}_{10.8}\rightarrow 3\alpha$ branches 69% through $^{8}Be_{gs}$ and 31% through $^{8}Be^{*}_{2.9}$; $^{12}C^{*}_{12.71}\rightarrow 3\alpha$ proceeds only through $^{8}Be^{*}_{2.9}$. These results are in agreement with the spin-parities of the corresponding states in ^{12}C, i.e. 3-, 1- and 1+ respectively; the process $^{12}C^{*}_{11.83}$ proceeds $\sim$32% via $^{8}Be_{gs}$. This already questions the spin-parity J^{π} assignment of 2- for $^{12}C^{*}_{11.83}$. The density distributions calculated assuming that the excited state of ^{12}C with J^{π} = 1- and 2- decays via $^{8}Be_{2.9}(2+)$ for orbital angular momenta L=1 and 3 have been compared with the data and have suggested that the 11.83 MeV should have J^{π} = 1- (An 75b). This result has been also supported by the study at E_{inc}= 18.2 MeV (An 75c).

The reaction $^{12}C(n,3\alpha)n$ can also proceeds via QF n-α and n-($\alpha\alpha$) interaction, the last one can be either the QFS or QF reaction. The extensive study of these processes is under way at $E_{inc}\leq$ 40 MeV. There is no conclusive evidence for the presence of QF processes at 14.4 MeV. Fig. 48. shows the extracted momentum distribution $|\phi(p)|^{2}$ for the n-α QFS compared with the calculated

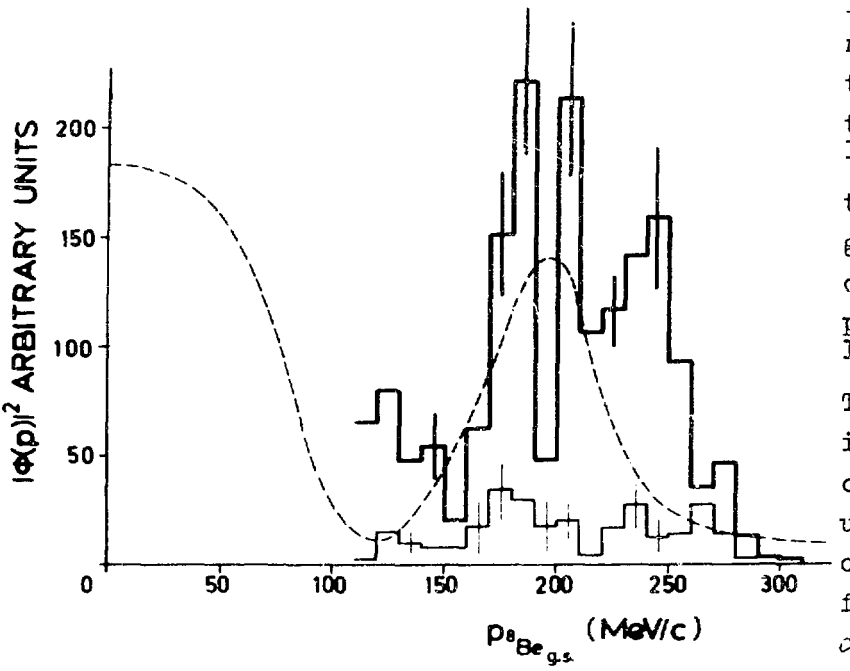

Fig. 48. The momentum distribution $|\phi(p)|^2$ of the $^{8}Be_{gs}$ in the ^{12}C nucleus. The thin line histogram presents only data which proceeds via $^{12}C^{*}_{9.63}$ state. The dashed curve is the theoretical distribution using a harmonic oscillator wave function with $\alpha - ^{8}Be_{gs}$ relative angular momentum L = 0.

distribution (dashed curve). It seems that at $E_{inc} \sim 18$ MeV the reaction $^{12}C(n,3\alpha)n$ proceeds at least partly via QF process, but it has not been possible to quantitatively determine its contribution to the total cross section.

11.5. The three and four body n induced ^{14}N breakup

The dominant reaction mechanism for the process $^{14}N(n,\alpha\alpha)^{7}Li_{gs}$ (or $^{7}Li^{*}_{0.468}$) at $E_{inc} \sim$ 14-18 MeV is the sequential decay via the $^{8}Be_{gs}$ and to excited states of ^{11}B (Tu 75, Tu 76, Sc 71). The relative contribution of the established intermediate states, ^{8}Be and ^{11}B, is given in Table 10. Fig. 49. shows the E(^{8}Be) vs E($^{11}B^{*}$) Dalitz plot at 18.2 MeV.

The four body process $^{14}N(n,3\alpha)t$ has been studied at 18.2 MeV (Tu 76). Fig. 50a. shows the E($^{7}Li^{*}$) vs E($^{8}Be^{*}$) plot, which demonstrates that the reaction proceeds via $^{8}Be_{gs}$ ($\sim$50%). Projecting all data on E($^{7}Li^{*}$) one can also see the enhancement due to the decay through $^{7}Li^{*}_{4.63}$ state and in particular the contribution

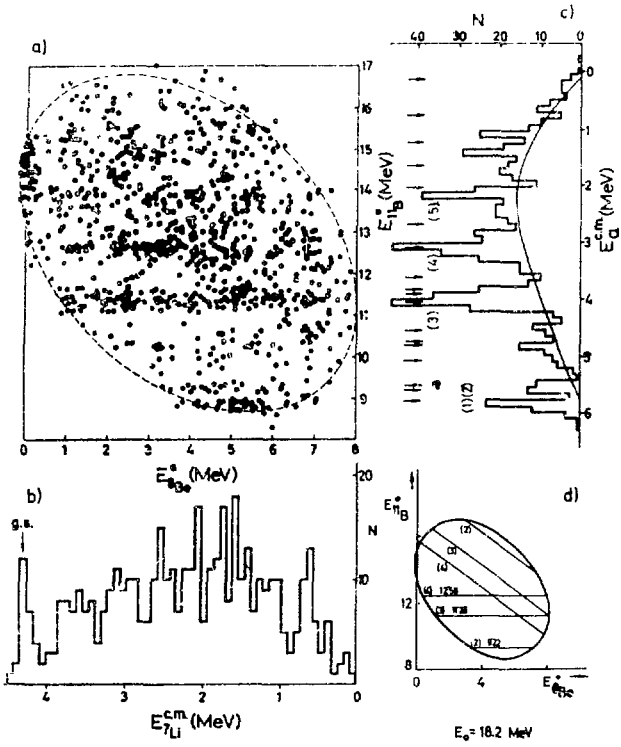

Fig. 49. $E(^{8}Be)$ vs $E(^{11}B^{*})$ plot at E_{inc}=18.2 MeV (a) and the projected spectra (b and c). Arrous indicate the known levels in ^{11}B. The solid curve in c) represent the continuum due to spurious events (two alphas). Diagram d is a sketch of the loci corresponding to relevant states in ^{11}B.

Table 10.

Relative contributions to the reaction $^{14}N(n,\alpha\alpha)^{7}Li$

Intermediate state	E_{inc} (MeV)	^{8}Be	^{11}B						
Peak number (Fig. 49)			1	2			3	4	5
Excitation Energy (MeV)		gs	8.925	9.185 9.274	10.33	10.59	11.27 11.46	12.56	14.04
Relative contribution (%)	18.2	6±1	10±2	5±1			22±2	17±2	9±2
	14.4	13±1	16±2	13±2	6±1	9± 1	15±2		

(right hand spectrum) of the process $^{14}N+n \rightarrow {}^{8}Be_{gs}(\alpha\alpha)+{}^{7}Li^{*}_{4.63}(\alpha t)$ amounts to ~18% of the total four body yield. Since the reaction is a quasithree body process $^{8}Be+\alpha+t$ we can construct the E_t vs E_α plot (Fig. 50b), where from one concludes that the reaction proceeds

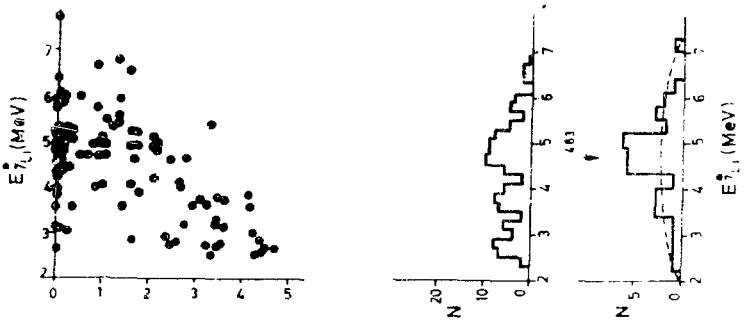

Fig. 50a. $E(^{7}Li^{*})$ vs $E(^{8}Be)$ plot after subtracting spurious events associated with true events proceeding via $^{8}Be_{gs}$.

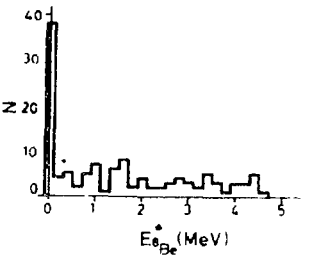

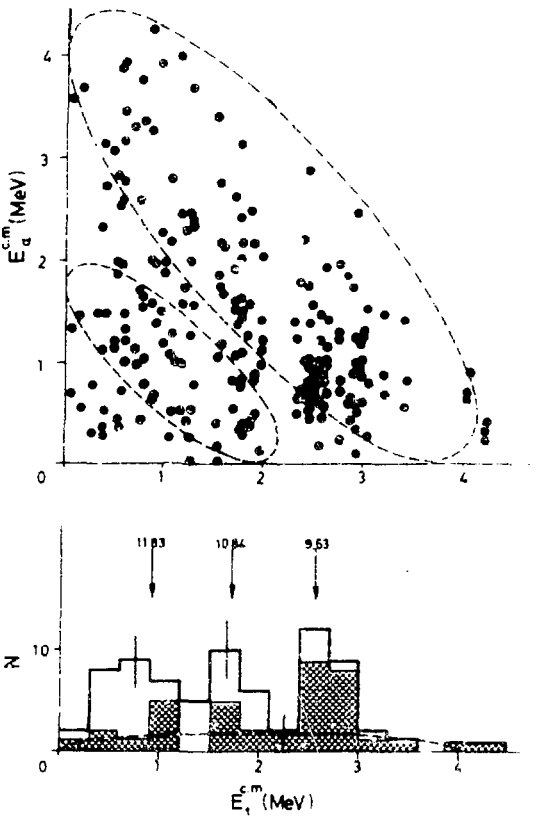

Fig. 50b. E_t vs E_α plot. Events group along bands of fixed E_t i.e. $E(^{12}C^{*})$. Dashed curves in the upper portion of the figure indicate the loci corresponding to $^{8}Be_{gs}$ and $^{8}Be^{*}_{2.9}$ intermediate states. Since there are three indiscernible alphas each event is represented by three dots in the figure, only one being correct. They have different E but the same $E(^{12}C^{*})$. Therefore, the excitation energy has three values whenever the intermediate state consists of either one or two alphas, but only one if all three alphas are involved. Spurious events as well as those corresponding to the process $^{14}N(n,\alpha)^{11}B^{*}(\rightarrow\alpha\,^{7}Li^{*}(\rightarrow\alpha,t)$ can fall outside the ^{8}Be loci. The shaded area of the spectrum represents events proceeding via the $^{8}Be_{gs}$.

~ 80% as $^{14}N(n,t)^{12}C^{*}_{9.6,10.8,11.8}$ ($\alpha + {}^{8}Be$ (mainly Be_{gs}). The process $^{14}N(n,\alpha)^{11}B^{*}(\rightarrow\alpha\alpha t)$ has not been observed.

At E_{inc} = 18.2 MeV the total four body cross section is 0.96 ± 12 mb, the cross sections for the reactions: $^{14}N(n,{}^{8}Be_{gs})^{7}Li^{*}_{4.63}$ = = 0.19 ± 0.04 mb, $^{14}N(n,t)^{12}C^{*}$ = 0.77 ± 0.11 mb, while the three body cross section $^{14}N(n,\alpha\alpha)^{7}Li_{gs + 0.468}$ is 12.7 ± 1.5 mb and $^{14}N(n,{}^{8}Be_{gs})^{7}Li_{gs + 0.468}$ cross section is 0.76 ± 0.1 mb. The uncertainties represent only relative errors which are quite small because the measurements have been done under identical conditions for all these reactions.

Acknowledgements

It is a pleasure to thank Drs. B. Antolković, F.D. Brooks, J. Csikai, R.C. Haight, N.S.P. King, B.A. Magurno, D.R. Maxson, M. Mizanul Islam, S.M. Qaim, J. Rossel, W. Scobel, D.L. Smith, J. Tudorić-Ghemo, and B. Zeitnitz for providing the author with their latest published and unpublished work.

References:

(Ad 71) G. Adam, E. Bar Avraham, R. Fox, Y. Porat, Nucl. Phys. (1971) A178, 321
(Aj 65) V. Ajdačić, M. Cerineo, B. Lalović, G. Paić, I. Šlaus, P. Tomaš, Phys. Rev. Lett. (1965) 14, 442 and 444
(Al 62) R.A. Al Kital, R.A. Peck, Jr., Phys. Rev. (1962) 130, 1500
(Al 67) J. Als-Nielsen, ENEA, Neutron Data, CCDN (1967) No 6
(Al 70) E.O. Alt, P.Grassberger, W. Sandhas, Phys. Rev. (1970) C1, 85
(Am 57) O. Ames, G.E. Owen, C.D. Schwartz, Phys. Rev. (1957) 106, 775
(An 62) B.Antolković, Ph.D. thesis (1962) Univ. of Zagreb
(An 67) B. Antolković, G. Paić, P. Tomaš, D. Rendić, Phys. Rev. (1967) 159, 777
(An 72) B. Antolković, Nucl. Instr. Methods (1972) 100, 211
(An 74) B. Antolković, Nucl. Phys. (1974) A219, 332
(An 75) B. Antolković, M. Turk, Clustering Phenomena in Nuclei II, ORO-4856-26 (ERDA, TIC (1975) 307)
(An 75a) B. Antolković, Z. Dolenec, Nucl. Phys. (1975) A237, 235
(An 75b) B. Antolković, J. Hudomalj, Nucl. Phys. (1975) A237, 253
(An 75c) B. Antolković, Few Body Problems in Nuclear and Particle Physics, eds. R.J. Slobodrian et al (1975) 428
(An 76) B. Antolković, priv. com.
(Ar 56) A.A. Armstrong, G.M. Frye, Phys. Rev. (1956) 103, 335
(Ba 53) M.E. Battat, F.L. Ribe, Phys. Rev. (1953) 89, 80

(Ba 61) R. Bass, T.W. Bonner, H.P. Haenni, Nucl. Phys. (1961) 23,122
(Ba 63) J. Barry, J. Nucl. En. (1963) AB 17, 273
(Ba 64) V.I. Balashov, A.N. Boyarkina, I. Rotter, Nucl. Phys. (1964) 59, 417
(Ba 65) R. Bass et al, Rep. EANDC(E) 66 "U", NEA (1966) 64
(Ba 66) E. Baumgartner et al, Phys. Rev. Lett. (1966) 16, 105
(Ba 67) E. Bar Avraham et al, Nucl. Phys. (1967) B1, 49
(Ba 68) R. Backinger, M. Uhl, Nucl. Phys. (1968) A116, 673
(Ba 68a) I. Basar, Few Body Problems, Light Nuclei, Nucl.Inter. eds. I. Šlaus, G. Paić, Gordon-Breach (1968) 867
(Ba 69) D. Bachelier, et al, Nucl. Phys. (1969) A126, 60
(Be 58) E.F. Bennet, D.R. Maxson, Phys. Rev. (1958) 110, 131
(Be 70) B.D. Belt, C.R. Bingham, M.L. Halbert, A. van der Woude, Phys. Rev. Lett. (1970) 24, 1120
(Be 73) F.E. Bertrand, R.W. Peele, (1973) ORNL 4799
(Bl 68) D. Blanc et al, J. Phys. Colloq. (1966) No 1, CI-98
(Bo 64) A.N. Boyarkina, Izv. Akad. Nauk SSSR (1964) 28, 337
(Bo 65) M. Bormann et al, Nucl. Phys. (1965) 63, 438
(Bo 68) A. Bond, Nucl. Phys. (1968) A120, 183
(Bo 70) W. Boline, H. Homeyer, H. Lettau, H. Morgenstern, J. Scheer, F. Sickelschmidt, Nucl. Phys. (1970) A154, 105
(Bo 72) R. Bouchez et al, Nucl. Phys. (1972) A185, 166
(Bo 73) M. Bormann, D. Kaack, V. Schröder, W. Scobel, L. Wilde, Z. Physik (1973) 258, 285
(Bo 74) M. Bormann, H. Neuerst, W. Scobel, Handbook on Nucl. Activation Cross Sections (1974), Tech. Rep. Ser. No 156, IAEA
(Bo 75) E. Bovet, F. Foroughi, J. Rossel, Helv. Phys. Acta (1975) 48, 137
(Bo 76) R. Bouchez, Few Body Dynamics (1976) eds. A.N. Mitra (North Holland Publ. Comp.) 194
(Br 66) G.E. Brown, A.M. Green, Nucl. Phys. (1966) 75, 401
(Br 68) M. Brendle et al, Z. Naturforschung (1968) 23a, 1229
(Br 71) H.J. Brede et al, Z. Physik (1971) 245, 1
(Br 74) W.H. Breunlich et al, Nucl. Phys. (1974) A221, 269
(Br 74a) J. Bruinsma et al, Phys. Lett. (1974) B49, 137
(Br 75) F.P. Brady, N.S.P. King, M.W. Mc Naughton, G.R. Satchler, (1975) Crocker Nucl. Lab., Annual Rep. UCD-CNL 186, p. 4C
(Ca 57) R.R. Carlson, Phys. Rev. (1957) 107, 1094
(Ca 61) H.C. Catron, M.P. Goldberg, R.W. Hill, J.M. LeBlanc, J.P. Stoering, C.J. Taylor, M.A. Williamson, Phys. Rev. (1961) 123, 210
(Ca 67) W. Carstens, Diplomarbeit, Hamburg (1967)
(Ca 72) R.F. Carlson et al, Few Particle Problems in the Nucl. Inter. eds. I. Slaus et al. (North Holland, 1972) 475
(Ca 74) R.T. Cahill, Phys. Rev. (1974) C9, 473; Phys. Lett. (1974) B49, 150
(Ce 61) M. Cerineo, K. Ilakovac, I. Šlaus, P. Tomaš, Phys. Rev. (1961) 124, 1947
(Ce 64) M. Cerineo et al, Phys. Rev. (1964) 133, B948
(Ce 66) J. Cerny, C. Detraz, R.H. Pehl, Phys. Rev. (1966) 152, 950
(Ch 64) M.L. Chatterjee, P. Sen, Nucl. Phys. (1964) 51, 583
(Ch 67) Yu I. Chernukhin, R.S. Shuvalov, Sov. J. Nucl. Phys. (1967) 4, 197

(Ch 72) C.C. Chang, E.M. Diener, E. Ventura, Phys. Rev. Lett. (1972) 29, 307
(Cl 65) C.M. Class, J.E. Price, J.R. Risser, Nucl. Phys. (1965) 71, 433
(Co 51) J.H. Coon et al, Phys. Rev. (1951) 81, 33
(Co 60) L. Colli et al, Nuovo Cim. (1960) 16, 991
(Co 67) S. Cohen, D. Kurath, Nucl. Phys. (1967) A101, 1
(Co 64) L. Colli et al, Nucl. Phys. (1964) 54, 253
(Cr 74) S.N. Cramer, E.M. Oblow, ORNL (1974) TM 4494
(Cu 62) B. Cujec, Phys. Rev. (1962) 128, 2303
(Da 63) E.A. Davis, T.W. Bonner, D.W. Worley, Jr., R. Bass, Nucl. Phys. (1963) 48, 169
(Da 73) J.C. Davis et al, Phys. Rev. (1973) C8, 863
(De 63) G. Deconninck, M. DeVroey, J.P. Meulders, J. Simonet, Nucl. Phys. (1963) 49, 424
(De 66) K. Debertin, K. Hofmann, E. Rössle, Nucl. Phys. (1966) 81, 220
(De 68) K. Debertin et al, Few Body Problems, Light Nuclei, Nucl. Inter., eds. I. Slaus, G. Paić, Gordon Breach (1968) 857
(De 72) R.M. DeVries, J.L. Perrenoud, I. Slaus, J.W. Sunier, Nucl. Phys. (1972) A178, 424
(De 76) S. Desremaux, A. Chisholm, P. Perrin, R. Bouchez, Few Body Dynamics (1976) eds. A.N. Mitra et al, (North Holland Publ. Comp.) p. 220
(De 76a) S. Desremaux (1976) thesis, Univ. Grenoble
(Do 69) H. Doubre et al, Phys. Lett. (1969) 29B, 355
(Do 73) P. Dolleschall, Nucl. Phys. (1973) A201, 266 and priv.com.
(Do 74) P. Doll, H. Mackh, G. Mairle, G.J. Wagner, Nucl. Phys. (1974) A230, 329
(Eb 72) W. Ebenhöh, Nucl. Phys. (1972) A191, 97 and Few Particle Problems in Nucl. Interactions (1972) eds. I. Slaus et al. (North Holland Publ. Comp.) p. 325
(El 66) M. El Nadi, A. Rabbie, Atomkernenergie II (1966) 233
(El 70) P.J. Ellis, T. Engeland, Nucl. Phys. (1970) 144, 161
(Fa 67) M. Fazio et al, Nuovo Cimento (1967) 51B, 459
(Fa 68) M. Fazio et al, Nucl. Phys. (1968) A111, 255
(Fe 67) P. Fessenden, D.R. Maxson, Phys. Rev. (1967) 158, 948
(Fi 67) W. Fitz, R. Jahr, R. Santo, Nucl. Phys. (1967) A101, 449
(Fi 75) S. Fiarman, S.S. Hanna, Nucl. Phys. (1975) A251, 1
(Fo 72) F. Foroughi, J. Rossel, Helv. Phys. Acta (1972) 45, 439
(Fr 54) G.M. Frye, Phys. Rev. (1954) 93, 934
(Fr 60) G.M. Frye, L. Rosen, L. Stewart, Phys. Rev. (1955) 99,1375
(Fu 67) E. Fuschini et al, Nuovo Cim. (1967) 48B, 190
(Fu 68) E. Fuschini et al, Nucl. Phys. (1968) A109, 465
(Ga 68) M. Gaillard et al, Nucl. Phys. (1968) A119, 161
(Gl 61) R.N. Glover, E. Weingold, Nucl. Phys. (1961) 24, 630
(Gl 64) P.W.M. Glaudemans, G. Wieckers, P.J. Brussard, Nucl. Phys. (1964) 56, 529
(Gr 49) L.L. Green, W. Gebson, Proc. Phys. Soc. (1949) A62, 296
(Gr 55) E.R. Groves, R.W. Davis, Phys. Rev. (1955) 97, 1205
(Gr 69) W.S. Gray et al, Nucl. Phys. (1969) A140, 494
(Gr 69a) H. Grässler, R. Honecker, Nucl. Phys. (1969) A136, 446
(Gr 71) E.R. Graves, J.D. Seagrave, (1971) NcSAC 38, 116

(Ha 71) H.H. Hackenbroich, P. Heiss, Z. Physik (1971) 242, 352
(Ha 75) R.C. Haight, S.M. Grimes, B.J. Tuckey, J.D. Anderson (1975) UCRL-77151 preprint and priv. com.
(He 56) S.A. Heiberg, Phys. Rev. (1956) 96A, 856
(He 72) E.M. Henley, D.H. Wilkinson, Few Particle Problems in Nucl. Interact. 1972 (eds. I. Slaus et al, North Holland Publ. Comp.) p. 242
(Hi 67) J.C. Hiebert, E. Newman, R.H. Bassel, Phys. Rev. (1967) 154, 898
(Hs 67) Y. Hsu, C. Huang, C. Chang, Nucl. Phys. (1967) A104, 679
(Ho 68) A. Horsley, Nucl. Data Tables (1968) A4, 321
(Ho 68a) R. Honecker, H. Grässler, Nucl. Phys. (1968) A107, 81
(Ho 69) M. Holmberg, Nucl. Phys. (1969) A129, 327
(Hu 66) A. Huck et al, J. Phys. (1966) C-1, 88
(Hu 71) R.L. Hutson et al, Phys. Rev. (1971) C4, 17
(Il 61) K. Ilakovac et al, Phys. Rev. (1961) 124, 1923
(IN 74) INDC, Rep. Subcom. Standards (1974) Sydney
(Ja 67) B.K. Jain, D.F. Jackson, Nucl. Phys. (1967) A99, 113
(Ja 70) M. Jain, Univ. of Maryland Techn. Rep. (1970) 70-086
(Ja 73) M. Jain, J.G. Rogers, D.P. Saylor, Phys. Rev. Lett. (1973) 31, 838
(Ju 62) J.A. de Juren et al, Phys. Rev. (1962) 127, 1229
(Ju 63) F.T.Jurney, N.T. Motz, ANL (1963) 6797, 236
(Ka 62) J. Kantele, D.G. Gardner, Nucl. Phys. (1962) 35, 353
(Ka 69) H. Karge, Wiss. Zeitschr. Univ. Jena, Math-Nat Reihe (1969) 18, 51
(Ka 70) G.Th. Kaschl et al, Nucl. Phys. (1970) A155, 417
(Ke 75) J. Kecskemeti, T. Czibok, B. Zeitnitz, Nucl. Phys. (1975) A254, 110
(Ki 69) H. Kitazawa, N. Yamamuro, J. Phys. Soc. Japan (1969) 26,500
(Ki 76) N.S.P. King et al, contribution to this conference
(Ki 72) W.M. Kloet and J.A. Tjon, Few Nucleon Problems in the Nuclear Interaction (ed. I. Slaus et al, North Holland Publ. Comp. 1972) 376 and 380
(Kl 73) W.M. Kloet, J.A. Tjon, Nucl. Phys. (1973) A210, 380
(Kn 70) A.R. Knudson, F.C. Young, Nucl. Phys. (1970) A149, 323
(Ko 68) J.M. Kootsey, Nucl. Phys. (1968) A113, 65
(Ko 71) H.G. König, Frühjahrstagung der DPG, Würzburg (1971)
(Kr 72) L.Kropp, P. Forti, Nucl. Instr. Methods (1972) 104, 381
(Ku 64) R.J. Kurz, LRL Report UCRL (1964) 11339; S.T. Thornton, J.B. Smith, Nucl. Instr. Methods (1971) 96, 551
(Ku 75) B. Kühn, Fiz. Elem. Cast i Atom Jadr. (1975) 6, 347
(La 67) G.H. Lamot et al, Nucl. Phys. (1967) A99, 633
(La 75) J. Lachkar, F. Coçu, G. Haouat, P. le Floch, Y. Patin, J. Sigaud, NEANDC(E) 168 "L", Com. a l'Energie Atomique France (Nov. 1975, preprint)
(Le 68) B. Leroux et al, Nucl. Phys. (1968) A116, 196
(Li 69) Y.L. Li, S.K. Mark, Nucl. Phys. (1969) A123, 147
(Lu 70) C. Lunke, J.P. Egger, J. Rossel, Nucl. Phys. (1970) A158, 278
(Ma 55) J.B. Marion, R.M. Brugger, Phys. Rev. (1955) 100, 69
(Ma 56) J.B. Marion, G. Weber, F.S. Mozer, Phys. Rev. (1956) 104, 1402

(Ma 68) D.R. Maxson et al, Nucl. Phys. (1968) A110, 609
(Ma 68a) D.R. Maxson et al, Nucl. Phys. (1968) A110, 555
(Ma 75) B.A. Magurno, ENDF/B-IV (1975) BNL-NCS-50446
(Mc 66) W.N. McDicken, W. Jack, Nucl. Phys. (1967) A104, 677
(Mc 75) M.W. McNaughton, N.S.P. King, F.P. Brady, J.L. Ullmann, Crocker Nucl. Lab. Annual Report (1975) UCD-CNL 186, 2B
(Mc 75a) M.W. McNaughton et al, Nucl. Phys. (1975) A239, 29
(Mi 66) B. Mitra, A.M. Ghose, Nucl. Phys. (1966) 83, 157
(Mi 67) Đ. Miljanić, M.Sc. thesis (1967), Univ. of Zagreb
(Mi 68a) Đ. Miljanić, G. Paić, B. Antolković, P. Tomaš, Nucl. Phys. (1968) A106, 401
(Mi 68) Đ. Miljanić, M. Furić, V. Valković, Nucl. Phys. (1968) A119, 379
(Mi 70a) Đ. Miljanić, Ph.D. thesis, 1970, University of Zagreb
(Mi 70) Đ. Miljanić, M. Furić, V. Valković, Nucl. Phys. (1970) A148, 312
(Mi 71) Đ. Miljanić, V. Valković, Nucl. Phys. (1971) A176, 110
(Na 63) M.A. Nagarajan, Nucl. Phys. (1963) 42, 454
(Ni 62) A. Nilsson, J. Kyellman, Nucl. Phys. (1962) 32, 177
(Ob 72) A.W. Obst, T.W. Grandy, J.L. Weil, Phys. Rev. (1972) C5, 738
(Pa 60) K.Parker, AWRE - Rep. (1960) O-27/60
(Pa 64) G. Paić, Ph.D. thesis (1964) Univ. of Zagreb
(Pa 64a) G. Paić, I. Šlaus, P. Tomaš, Phys. Lett. (1964) 9, 147
(Pa 67a) G. Paić, D. Rendić, P. Tomaš, Nucl. Phys. (1967) A96, 476
(Pa 73) G. Pauletta, Ph.D. thesis (1973) Univ. of Cape Town
(Pa 74) A. Paulsen, H. Liskien, Neutron Standard Ref. Data (1964) IAEA-PL-242-2/21, p. 135
(Pa 75) G. Pauletta, F.D. Brooks, Nucl. Phys. (1975) A255, 267
(Pa 76) D.C. Palmer, D.R. Maxson, J.R. Bading, reprint (1976)
(Pa 76a) G. Paić, D. Rendić, V. Pečar (1976) Fizika, to be published
(Pe 65) S.T. Perkins, TID-22446 (1965)
(Ph 72) A.C. Phillips, Nucl. Phys. (1972) A184, 337
(Pi 65) J. Picard, C.F. Williamson, Nucl. Phys. (1965) 63, 673
(Pi 73) S.C. Pieper, priv. com.
(Pr 69) G. Presser, R. Bass, K. Krüger, Nucl. Phys. (1969) A131, 679
(Pr 70) A.N. Prokof'ev, G.M. Shklyarevskii, Sov. J. Nucl. Phys. (1970) 11, 318
(Pu 69) K.K. Purser et al, Nucl. Phys. (1969) A132, 75
(Pu 69a) N. Puttaswamy, J. Yntema, Phys. Rev. (1969) 177, 1624
(Re 60) T. Retz-Schmidt et al, Bull.Am.Phys.Soc. (1960) 5, 110
(Re 67) D. Rendić, Ph.D. thesis (1967) Univ. of Zagreb
(Re 68) D. Rendić, B. Antolković, G. Paić, M. Turk, P. Tomaš, Nucl. Phys. (1968) A117, 113
(Ri 54) F.L. Ribe, J.D. Seagrave, Phys. Rev. (1954) 94, 934
(Ri 57) F.L. Ribe, Phys. Rev. (1957) 106, 767
(Ro 62) L. Rosen, L. Stewart, Phys. Rev. (1962) 126, 1150; also LA 2643 report
(Ro 70) J.L. Romero, J.A. Jungerman, F.P. Brady, W.J. Knox, Y. Ishizaki, Phys. Rev. (1970) C2, 1153
(Sa 65) B. Salki, Nucl. Phys. (1965) 73, 631
(Sa 71) W. Salatke, E. Baumgartner, P. Huber, Helv. Phys.Acta (1971) 44, 815

(Sa 72) A.I. Saukov et al, Sov.J. Nucl. Phys. (1972) 14, 157
(Sa 72a) R.M. Salter et al, Few Particle Problems in the Nuclear Interact. (1972) (eds. I. Šlaus et al, North Holland Publ. Comp.) p. 112
(Sc 70) W. Scobel, M. Bormann, Z. Naturforschung (1970) 25a, 1406
(Sc 71) G. Schmidt et al, Nucl. Phys. (1971) A173, 449
(Se 59) J.D. Seagrave, Nucl. Forces and the Few Nucleon Problem (1959) (eds. T. Griffith, E.A. Power)
(Se 60) J.D. Seagrave, L. Cranberg, J.E. Simmons, Phys. Rev. (1960) 119, 1981
(Se 70) J.D. Seagrave, Three Body Problems in Nuclear and Particle Physics (ed. J.S.C. McKee and P.M. Rolph, North Holland Publ. Comp. 1970)
(Se 72) J.D. Seagrave, J.C. Hopkins, D.R. Dixon, P.W. Keaton Jr., E.C. Kerr, A. Hüller, R.H. Sherman, R.K. Walter, Ann. Phys. (1972) 74, 250
(Sh 70) D. Shackleton, thesis, Univ. of Cape Town, 1970
(Sh 73) S. Shirato, K. Saitoh, N. Koori, Nucl. Phys. (1973) A215, 277
(Sh 75) S. Shirato et al, Few Body Problems in Nuclear and Particle Physics, eds. R.J. Slobodrian (Les Presses de l'Univ. Laval, 1975) 547
(Sl 68) I. Šlaus, G. Paić, Solid State Physics, Nuclear Physics and Particle Physics (1968) (ed. I. Saavedra, Benjamin, N.Y.) p. 471
(Sl 68a) R.J. Slobodrian, H.E. Conzett, F.G. Resmini, Phys. Lett. (1968) B27, 405
(Sl 71) I.H. Sloan, Nucl. Phys. (1971) A168, 211 and priv. com.
(Sl 71a) I. Šlaus et al, Phys. Rev. Lett. (1971) 26, 789
(Sl 76) I. Šlaus, Few Particle Dynamics (1976) (eds. A.N. Mitra et al, North Holland Publ. Comp.) p. 584
(Sm 76) W. Smolec et al, Nucl. Phys. (1976) A257, 397
(Sn 69) J.L. Snelgrove, E. Kshy, Phys. Rev. (1969) 187, 1259
(St 64) J.R. Stehn, M.D. Goldberg, B.A. Magurno, R. Wiener-Chasman, Neutron Cross Sections, BNL 325, Sigma Center Brookhaven, 1964
(St 71) N.R. Stanton, Univ. Colorado, Boulder, COO-1545-92 (1971)
(St 72) A. Stricker et al, Nucl. Phys. (1972) A190, 284
(Th 70) S.T. Thornton et al, Phys. Rev. Lett (1970) 17, 701
(Th 74) G.E. Thompson, I. Šlaus, J.W. Sunier, J.W. Verba, D.J. Margaziotis, J.C. Young, Nucl. Instr. Methods (1974) 114, 439
(Ti 73) G. Ticcioni, S.N. Gardiner, J.L. Matthews, R.O. Owens, Phys. Lett. (1973) 46B, 369
(Tj 75) J.A. Tjon, Phys. Lett. (1975) 56B, 217
(Tj 76) J.A. Tjon, reprint (1976)
(To 69) I.S. Towner, Nucl. Phys. (1969) A126, 97
(Tu 75) M. Turk, B. Antolković, D. Winterhalter, Fizika (1975) 7, 23
(Tu 76) M. Turk, B. Antolković, D. Winterhalter, to be published
(Tu 76a) J. Tudorić-Ghemo, Ph.D. thesis, Univ. of Zagreb (1976)
(UC 75) UCD-CNL-186 Crocker Nucl.Lab., Annual Rep. (1975)

(Va 58) S.S. Vasilev, V.V. Komarov, A.M. Popova, J.E.T.P. (1958) 6, 1016
(Va 64) V. Valković, Ph.D. thesis, Univ. of Zagreb (1964)
(Va 65) V. Valković, G. Paić, I. Šlaus, P. Tomaš, M. Cerineo, G.R. Satchler, Phys. Rev. (1965) 139, B331
(Va 67) W.T.H. van Oers, I. Šlaus, Phys. Rev. (1967) 160, 853
(Va 70) V. Valković, M. Furić, Đ. Miljanić, P. Tomaš, Phys. Rev. (1970) C1, 1221
(Ve 60) G.E. Veljukov et al, JETP (1960) 39, 563
(Ve 68) V.V. Verbinski, F.G. Perey, J.K. Dickens, W.R. Burrus, Phys. Rev. (1968) 170, 916
(Ve 71) E. Verondini, Nuovo Cim. Riv. (1971) 1, 33
(Vo 65) V.K. Voitovetskii, I.L. Korsunskii, Yu F. Pazhin, Nucl. Phys. (1965) 69, 513
(Vr 75) D. Vranić, M.Sc. thesis, Univ. of Zagreb, 1975
(Wa 66) R.R. Wagner, R.A. Peck, Bull.Am.Phys.Soc. (1966) 11, 349
(We 71) F. Weng et al, Frühjahrstagung der DPG, Würzburg (1971)
(Wi 68) B.H. Wildenthal, E. Newman, Phys. Rev. (1968) 175, 1431
(Wi 71) B.H. Wildenthal et al, Phys. Rev. (1971) C4, 1266 and 1708
(Yo 75) P.G. Young, D.G. Forster, ENDF/B-IV (1975) p. 21
(Za 63) M.R. Zatzick, D.R. Maxson, Phys. Rev. (1963) 129, 1728
(Ze 72) B. Zeitnitz et al, Phys. Rev. Lett. (1972) 28, 1656; Few Particle Problems in Nucl.Int., eds. I. Slaus et al. (North Holland Publ. Comp. 1972) p.117
(Ze 74) B. Zeitnitz, R. Maschaw, P. Suhr, W. Ebenhöh, J. Bruinsma, J.H. Stuivenberg, Nucl. Phys. (1974) A231, 13
(Ze 75) B. Zeitnitz, Proc. Int. Symp. on Interaction Studies in Nuclei, Mainz (1975), to be published

ME 3 - NEUTRON INDUCED REACTIONS ON VERY LIGHT AND LIGHT TARGET NUCLEI - I. Šlaus, (R.B.N.I., Zagreb, Yugoslavia)

Khanna (Chalk River):

In the early part of your talk you referred to the neutron-neutron scattering length and neutron-neutron effective range. If I recall correctly, for the (n,p) singlet scattering length the value is about -23 fermis, while for the proton-proton scattering length the value is about -8 fermis. After I take out the charge dependent part, or the Coulomb effects, from the p-p scattering length, I come out with a number between seventeen and eighteen fermis. Now, if these numbers are correct and we accept the value that you have given us today, namely, -16.26 ± 0.66 fermis, it would imply that there is a certain amount of charge dependence and charge asymmetry for nuclear potential. Would you care to comment about it?

Šlaus:

First, a comment concerning the nuclear part of the proton-proton interaction. You said correctly that a_{p-p} is -7.7 fermis, and then you have to extract the nuclear part. It has recently been shown by Sauer that the nuclear part of the proton-proton scattering length depends on the off-the-energy shell freedom, and as a matter of fact Sauer argues that we should proceed the other way around, namely, assume the charge symmetry and use that as a constraint for the off-the-energy shell. So, by changing the off-the-energy shell one can obtain for p-p scattering lengths a value which is different from -17 fermis. However, if one does not do that, but rather uses our conventional potential, then as you have said, you obtain something like -17 fermis, which is somewhat different from the value of -16.3, and therefore it might imply some degree of charge symmetry breakdown which is very small. However, let me also say that one has to carefully compare the hydrogen-3 and helium-3 binding energies, and whereas for a long time we believed there to be a discrepancy of the order of 100 keV, this has now been considerably reduced. I would say that at present we have no clear evidence for the breaking of charge symmetry. It would be very important to determine $r_{n,n}$ more accurately, which would then give some additional information on charge symmetry.

Khanna:

Since you have brought up the subject of the triton and helium-3, I would like to add that I think there is still a discrepancy of about 50 keV in the Coulomb energy of these two nuclei, and I think that can perhaps be explained only if you assume a charge dependent interaction which is of the order of half a percent of the strong nuclear interaction which one normally assumes.

Šlaus:

I agree.

Wigner (Princeton Uni[illegible]):

I wonder whether you could make some comments on charge independence also.

Šlaus:

Charge independence is obviously broken to the order of about 4% as derived

from the difference between a_{n-p} & a_{n-n} . The differerce is so large because the scattering length is a magnifying glass and one can see very fine differences in the potentials.

Garg (Albany):

The data on $^{9}Be(n,\alpha)^{6}He$ seem to indicate that heavy particle stripping is the most dominant process that you see. In fact, the ratio is very small for pickup. Could you please explain how the heavy-particle stripping process is taking place in this reaction.

Šlaus:

In the case of pickup, the ^{9}Be target is pictured as $^{3}He + ^{6}He$ and the neutron picks up the helium-3. In heavy particle stripping it is pictured as $^{5}He + \alpha$ and the neutron picks up ^{5}He to form ^{6}He. Now, Smolec's result for the ratio of pickup to heavy particle stripping of 0.1% is obviously unrealistic. As I said, we have also done the calculation and experiment on $^{9}Be(p,\alpha)$, using the finite range Born approximation. There the situation is completely different: one still gets the predominance of the heavy particle stripping but it is not three orders of magnitude greater.

10:25 A.M., WEDNESDAY, JULY 7, 2976, IN OLNEY 150

Main Session MF

Chair: H.H. Barschall (University of Wisconsin, U.S.A.)

10.25 a.m., Wednesday, July 7, 1976 Paper Subject : Session MF 1

NEUTRON INDUCED REACTIONS II : (n,x) REACTIONS ON MEDIUM AND HEAVY NUCLEI

Nikola Cindro*

Service de Physique Nucléaire, Centre d'Etudes de Bruyères-le-Châtel,
B.P. 61, 92120 Montrouge, France.

Permanent address : Institute Rudjer Boskovic, Zagreb, Yugoslavia

RESUME

The recent interest in (n,x) reactions in the MeV and above range is concentrated on two main subjects : the mechanism of nucleon emission (preequilibrium in particular) and the possible role of clustering in the emission of complex particles.

ABSTRACT

(1) It has been known for some time that the statistical model in its simple form was unable to account in detail for the single nucleon emission following fast neutron bombardment of nuclei. The discrepancy between models and experiment was more pronounced for proton than for neutron emission. The theoretical cross sections predicted for the former were off by up to an order of magnitude; the shape of the spectra did not correspond to experimental results either. To account for these discrepancies various nonequilibrium processes were proposed : the direct transitions to low lying states of residual nuclei and different modes of preequilibrium emission. We present a critical comparison of the above models with particular attention to the analysis of the role of the different physical parameters employed. At the end we analyse a unified model of equilibrium and preequilibrium emission.

(2) The emission of complex particles in fast neutron induced reactions is a long-standing problem. The similarity of, e.g., alpha particle emission with the alpha radioactive decay has led to conclusions about the preformation of alpha clusters in nuclei indicating a very high degree of preformation. On the other hand, comparison with (p,α) reactions has rendered these conclusion more ambiguous. We investigate the recent experimental data in view of the need for a preformation factor and its possible relation to nuclear structure.

NEUTRON INDUCED REACTIONS II : (n,x) REACTIONS ON MEDIUM AND HEAVY NUCLEI

N. CINDRO

Service de Physique Nucléaire, Centre d'Etudes de Bruyères-le-Châtel
B.P. 61, 92120 Montrouge, France

Permanent address : Institute Rudjer Boskovic, Zagreb, Yugoslavia

ABSTRACT

Recent interest in (n,x) reactions in the MeV and above range of energies is concentrated on two main subjects : the mechanism of nucleon emission (precompound in particular) and the possible role of clustering in the emission of complex particles. Hence the first two sections of this paper will be devoted to these two subjects. In the last section we shall briefly deal with some other subjects that have recently emerged in the field.

THE MECHANISM OF (n,p) REACTIONS

It has been known for some time that the statistical model in its simple form was unable to account in detail for the single nucleon emission following fast neutron bombardment of nuclei. The discrepancy between model and experiment was more severe for proton then for neutron emission as illustrated in fig. 1 : the experimental points lie at least an order of magnitude higher than the calculated ones. It is thus clear that the evaporation process can account for only a small part of the (n,p) total cross section. This part becomes negligible as the atomic mass (and charge) increase. We can understand this trend by keeping in mind that particles emitted by the evaporation process will have an average energy of the order of the nuclear temperature ($\sim$ 1 MeV) ; the penetrability of such particles through the Coulomb barrier in heavy nuclei is negligible. Hence the small calculated $\sigma(n,p)/\sigma(n,n')$ ratio. In order to bring this ratio in accord with experiment we have to devise a mechanism that favours the emission of higher energy particles; the precompound process provides such a mechanism.

In the closed form expression developed by the Rochester (2,3) and Milano (1) groups the absolute cross section for precompound emission of nucleons integrated over the solid angle is given by (1)

$$\frac{d\sigma(\varepsilon)}{d\varepsilon} = \frac{4\pi}{3}(2s+1)\frac{m\varepsilon}{\pi^2\hbar^3}\sigma_{inv}(\varepsilon)\frac{\hbar}{2\pi}\frac{1}{D(E)}\frac{1}{\omega(E)}\sum_{n=n_0,\Delta n=2}^{\bar{n}}\left(\frac{V}{V_0}\right)^{n-2}(n+1)^2\omega(U,n+1), \quad (1)$$

where s = 1/2 is the nucleon spin, m is the nucleon mass, σ_t is the optical model reaction (nonelastic) cross section for neutrons of energy E_n, ε and $\sigma_{inv}(\varepsilon)$ are, respectively, the kinetic energy of the emitted nucleons and the corresponding inverse cross section, E is the excitation energy of the compound nucleus, U that of the residual nucleus and g is the average single particle spacing in the Fermi gas model. The factor 2/3 in the formula comes from charge conservation (protons and neutrons) in the nucleus.

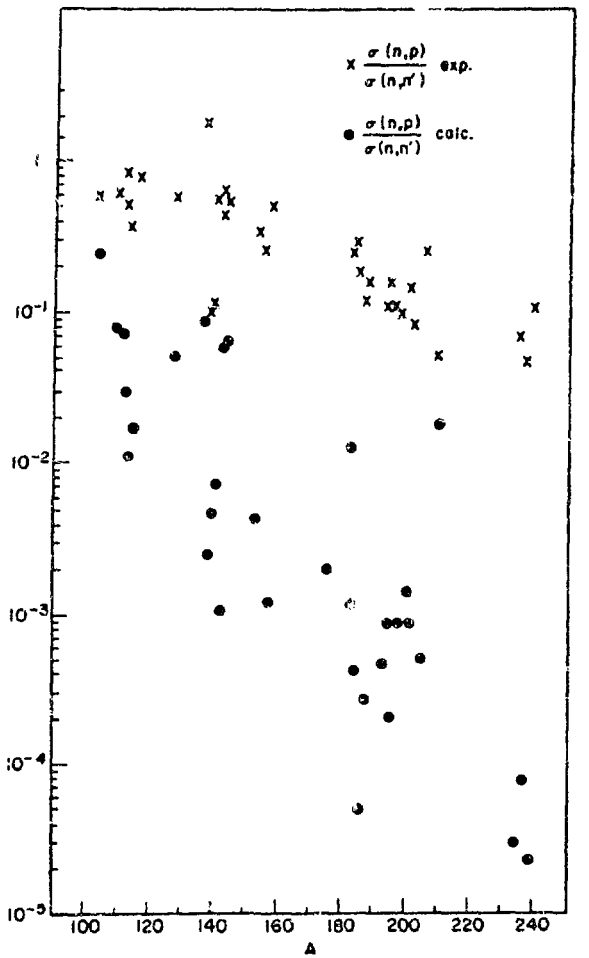

Fig. 1 Plot of experimental (x) and calculated (•) ratios between σ(n,p) and σ(n,n') as a function of mass number for 100 < A < 240. The calculated values were obtained using a conventional statistical evaporation model (from ref. 1).

A stage in the equilibration process is characterized by the number n of excitons (particles and holes); $\bar{n} = \sqrt{2gE}$. The transition between states with n differing by $\Delta n = 2$ (summation over n in steps of 2 from $n_0 = 3$ to $\bar{n}$) is determined by the two body transition matrix element M, whose square $|M|^2$ enters directly into the formula.

Although criticisms and objections stemming from various sources can be formulated as to the validy of the expression (1), the essential features of the physics of the process appear clearly from the discussion of this expression. We find that the cross section for the emission of particles of a given energy ε is a sum of several terms, each of them representing a stage in the equilibration process. As U < E, the contribution of the consecutive terms decreases. In fact, for higher energy particles (ε large hence U small) the contributions of all the terms but the first one ($n_0 = 3$) are negligible. This is physically understandable : the emission of high energy particles occurs in the very early stages of the equilibration process. This fact is responsible for the preponderance of the precompound mechanism in the (n,p) reaction (as opposed to (n,n')); due to the Coulomb barrier, only high energy protons can leave the nucleus; these protons can be produced only in processes preceding the compound nucleus equilibration.

A few samples of the need for preequilibrium processes in (n,p) reactions at MeV energies are shown in Figs. 2 - 4. We see that both the

energy spectrum and the excitation function for a typical nuclear system (CsI) as well as a set of 75 (n,p) total cross sections for medium and heavy nuclei are fitted with a calculation based on the expression (1). It should be pointed out that the scatter of the ratio points in fig. 4 is of the order of the real experimental errors and need not mean a discrepancy between the used precompound model and experiment.

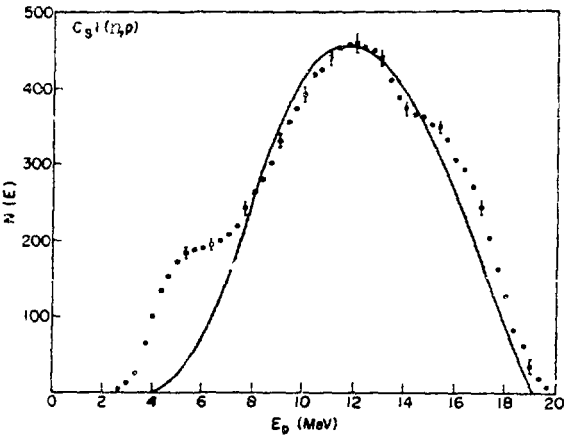

Fig. 2 The spectrum of protons emitted by 21.5 MeV bombardment of CsI. The solid line represents the precompound emission calculated by means of formula (1) (relative units); (from ref. 1).

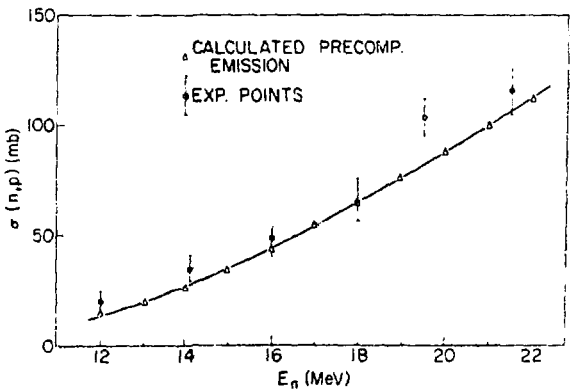

Fig. 3 The excitation function of the (n,p) reaction on CsI calculated from the expression (1) (relative units) ; (from ref. 1).

The reader has certainly noticed that we have restricted our analysis to medium and heavy nuclei. For lighter nuclei, the cutting of the Coulomb barrier is less severe, and lower energy protons may be emitted too. Thus the contribution of the compound emission is not negligible and we have to add it to the precompound contribution. This addition, although in principle straightforward, presents some problems when it comes to its carrying into effect.

Naively represented, the precompound processes are the first stages of a development leading to final equilibration, i.e. to the compound nucleus formation. The compound nucleus should then be the many exciton state where the total energy is shared among many particles and many holes. It is obvious, however, that representations of the equilibration process like that given by the expression (1) do not describe this situation. As we have already seen, the contribution of stages with large values of n (number of excitons), as given by expression (1), drops off very sharply and cuts off the precompound contribution at a very early stage. It is true that this contribution can be calculated using more sophisticated expressions, but the common usage is to fit the physical data (e.g. angle integrated particle spectra) by an uncoherent sum of a precompound and a scaled compound component :

$$\left(\frac{d\sigma(\varepsilon)}{d\varepsilon}\right)_{exp} = \sigma_{pc}(\varepsilon) + R\,\sigma_c(\varepsilon) \qquad (\ )$$

Such combinations with plausible values of R have succeeded in giv-

ing reasonable fits to experimental data. Their physical basis remains, however, rather questionable. An obvious criticism concerns the ingredients of the compound nucleus cross section $\sigma_c(\varepsilon)$: what are the values of the inverse cross sections to be used ? Certainly not the $\sigma_r(\varepsilon) = \sigma_{ne}(\varepsilon)$ obtained from the optical model, as one part of the total flux has already been taken into account by the preequilibrium process.

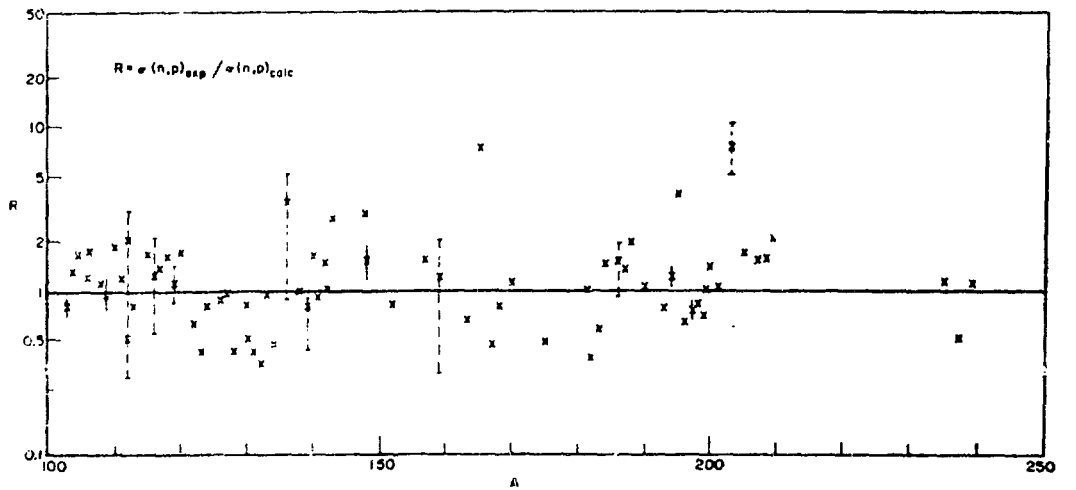

Fig. 4 A global fit to 75 (n,p) total cross sections around 14 MeV for nuclei with A > 100. The calculation gave absolute values once the value of $|M|^2$ was empirically determined (from ref. 1).

A way out is to follow the evolution of the composite nucleus towards equilibrium as a function of time by solving a set of coupled equations, the so called master equations. These equations describe the oscillations of a system near equilibrium ; applied to precompound processes (5) they describe the transition from a stage with n excitons to stages with (n - 2) and (n + 2) excitons respectively (including a finite particle emission probability). In the work of Cline (6) and Blann (7) these equations are solved numerically by the method of finite differences and a set of curves describing the time evolution of the emitted cross sections can be obtained. Fig. 5 shows that most of the precompound emission takes place very early in the reaction (according to ref. 4, after about 2000 iterations, corresponding to about 2×10^{-20}s), while the emission of the total particle spectrum (full reaction cross section exhausted) takes an estimated time of about 1.5×10^{-18}s. In this picture the reaction process divides naturally into two parts : the precompound part emitted very early in the reaction and the compound nucleus part which grows in a very much longer time scale (4).

It is fair to say that precompound emission is not the only mechanism that provides higher energy particles in the spectrum. Arndt and Reif (8) have suggested

that the higher energy part of the spectrum should originate from direct reactions leading to states in nuclei at high energy of excitation. Their calculation is performed using DWBA with form factors computed from a microscopic 1 particle - 1 hole description of collective states in even-even nuclei up to about 7 MeV. Although calculations of (n,p) spectra are not available, 14 MeV (n,n') spectra calculated by this method show fair agreement with experiment. For $^{40}Ca(n,n')$ the agreement with experiment is somewhat better then when using the geometry dependent hybrid model (Fig. 6).

Summarizing the present status of our knowledge of the (n,p) reaction mechanism we can say that there is little doubt that for nuclei with A > 100 the non-compound emission is preponderant. The various preequilibrium models give a satisfactory overall description of the experimental data; this description, moreover, fits with the overall description of other neutron induced reactions. It is, however, fair to say that there exist also other ways by which these data can be accounted for.

THE EMISSION OF ALPHA PARTICLES

This is a long -standing problem in nuclear physics. It is known that nuclei, when bombarded by energetic projectiles, emit many more alpha particles then pre-

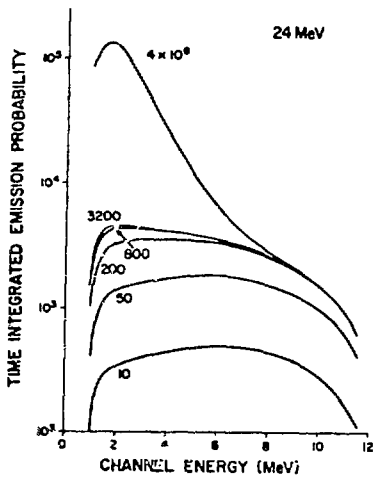

Fig. 5 Results of coupled channel calculations for a system with A = 100 and 24 MeV excitation. The numbers next to the curves indicate the number of elapsed time increments (1 time increment ~ 10^{-23}s); (from ref. 4).

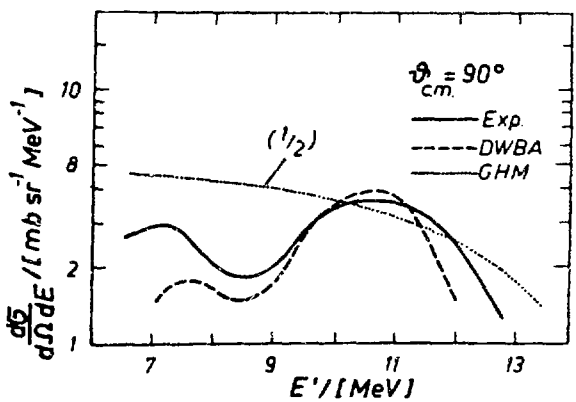

Fig. 6 Comparison of experimental (full curve) and calculated spectra for ^{40}Ca (n,n') at 90° for 14 MeV neutrons. GHM stands for calculations using the geometry dependent hybrid model ; DWBA stands for DWBA calculations to excited states in nuclei (from ref. 8).

dicted by pure statistical considerations. We like to think of this problem in terms of alpha particle sub-structures, called, at times, by musically sounding names* . A new zest to these considerations was added by the discovery of peculiar resonances in the continuum near the particle emission threshold observed in slow neutron induced (n,α) reactions (9). In this paper we shall, however, restrict ourselves to (n,α) reactions in the MeV bombarding energy region.

The (n,α) cross section systematics at 14 MeV has been reviewed several years ago (10). This systematics showed that while compound nucleus emission was able to account for the total cross sections for nuclei with mass number A between roughly 20 and 80, it failed completely to account for the alpha emission in heavy nuclei, the difference with experiment reaching orders of magnitude around A = 200. It thus became soon visible that mechanisms other then compound nucleus formation are present in the emission of alpha particles.

The precompound emission of alpha particles was first studied in terms of the Griffin exciton model (5). Two approaches could be distinguished. The first of them was based on the assumption that the alpha particle is preformed in a target nucleus and may be represented by a single exciton (11). The second approach assumed that a complex particle, represented by a number of excitons equal to its mass number, is formed from the excited nucleons of the composite nucleus (12). While the former approach was applied to a more extensive set of 14 MeV (n,α) data, the latter approach had the advantage that it could be applied to the emission of any type of complex particles.

A third, independent, approach to the (n,α) emission in heavy nuclei was suggested by the Warsaw (13) and Zagreb (14)groups. This approach is based on the observation that similarities exist between some 14 MeV (n,α) spectra and the corresponding single neutron level densities. To explain these similarities, it was assumed that the knock-out mechanism, proceeding by the ejection of an alpha cluster from the surface, is followed by the capture of a neutron by the remaining (usually unperturbed) core (13). The neutron fills up the single particle states of the core. Accordingly, the alpha particle spectrum should show a predominant excitation of single neutron states in the final nucleus. This model is somewhat simpler than the one developed by Milazzo-Colli et al. (11) but the physical bases of the two models are quite similar.

The controversy is centered here around the so called preformation factor of complex particles in nuclei. Do complex structures exist in a prefabricated state in excited nuclei ? If so, where and to what extend could they be found in nuclei ? And what kind of states are excited in nuclei by the emission of complex particles ?

Let us first analyze the answers given in the frame of the precompound models. The method used by the Milano (11) and Zagreb (15) groups gives the energy spectrum of alpha particles emitted by the precompound process in the following closed form :

* Quartets, for the non initiated.

$$\frac{d\sigma(n,\alpha)_{p.eq.}}{d\varepsilon} = \sigma_r \frac{m_\alpha \varepsilon o_{inv}(\varepsilon) g_R}{4\pi^3 \hbar^2 |M|^2 g_c^5 E^3} \sum_{\substack{n=3 \\ (\Delta n = +2)}}^{\bar{n}} \left(\frac{g_R U}{g_c E}\right)^{n-2} (n-1)(n+1)^2 \frac{\phi K_n^\alpha}{\phi K_n^\alpha + (1-\phi) K_n^\nu} \qquad (3)$$

The meaning of the physical quantities is the same as in expression (1) except for the coefficients K_n and ϕ. The value $K_n^\alpha = K_{p,h}^\alpha$ is the percentage of states containting an excited α-particle and an "α-particle" hole in the state assembly corresponding to p + h = n excitons ($K_n^\alpha \times \rho_n$ is the level density of the particular kind of states obtained by the excitation of an α cluster). The values $K_n^\nu = K_{p,h}^\nu$ correct for charge conservation.

Once the values of K_n^α and K_n^ν are calculated (11) the essential free parameter in the expression (3) is the probability ϕ that the incoming neutron will strike an alpha cluster preformed in the nucleus. Leaving aside some difficulties in choosing appropriate values of $|M|^2$ and g_c (around closed shells for the latter), it is a fact that expression (3) fits a number of energy spectra and excitation functions of (n,α) reactions (Fig. 7).

Crucial to this analysis is the value of the preformation factor ϕ. The A dependence of this factor is shown in fig. 8. The values of ϕ vary from 0.1 to 0.8 showing a wide fluctuation around A = 150.

It is difficult to attribute a realistic physical meaning to this parameter, as it is hard to believe that preformed alpha clusters occur in nuclei at such a high rate. Other nuclear phenomena suggest a much lower rate (if any) of alpha clusters in nuclei. It is, however, fair to say that in a subsequent analysis Milazzo-Colli et al. (16) have obtained consistent values of ϕ by a combined analysis of radioactive alpha decay and (p,α) and (n,α) reactions.

The model used by Kalbach - Cline (17) to account for the precompound emission of complex particles is an extension of the Griffin's model (5) that does not contain an explicit preformation factor. Rather, an empirical factor equal to the factorial of the mass number of the emitted particle has been introduced into the rate expressions for particle emission. The value of all parameters have, however, been fixed in order to fit proton emission spectra and the model was then applied to complex particle emission. Quite satisfactory fits were obtained for (p,α) spectra but the model was not (to our knowledge) applied to (n,α) reactions.

The approach of Oblozinsky (18) is midway between the two ; for its absence of an empirical preformation factor it follows, however, the more general pattern of ref. (17). Its precompound basis is the Blann's hybrid model (2) rather then the Griffin's exciton model (as in ref. (17)) or in the earlier work of Ribansky and Oblozinski (19)) . In this model the probability $P_x(\varepsilon)d\varepsilon$ to emit a nucleon x in the energy channel ε, ε + dε is given by :

$$P_x(\varepsilon)d\varepsilon = \sum_{\substack{n=n_o \\ \Delta n=+2}}^{\bar{n}} \left[\frac{p_x}{p} \frac{\omega_{p-1,h}(E - B_x - \varepsilon)}{\omega_{p,h}(E)} \rho_{1,0}(B_x + \varepsilon) d\varepsilon \right] \left[\frac{\lambda_c^x(\varepsilon)}{\lambda_c^x(\varepsilon) + \lambda_+^x(\varepsilon)} \right] D_n \cdot \qquad (4)$$

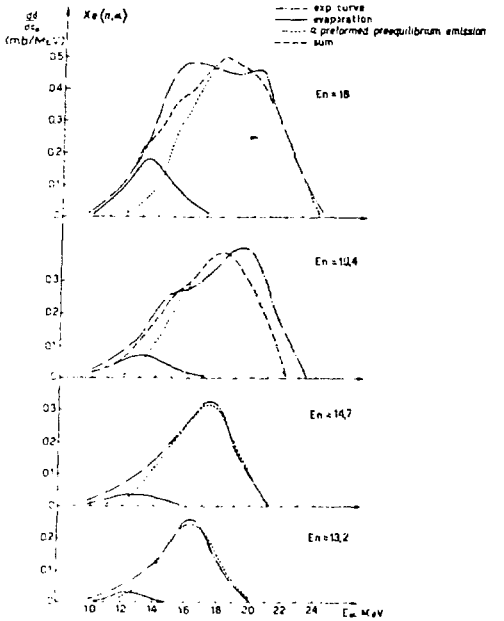

Ref. ? Energy spectra of $X_e(n,\alpha)$ at different neutron energies compared with the predictions for evaporation and α preformed precompound emission.

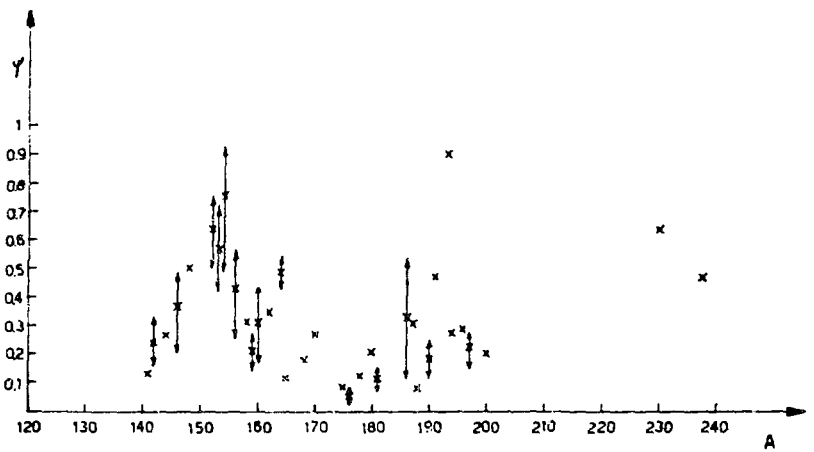

Fig. 8 The A dependence of the preformation factor ϕ (ref. 11).

where B_x is the binding energy of the nucleon and E the excitation energy of the composite nucleus. The value p_x denotes the number of nucleons of type x present in the state with n = p + h nucleons ; ρ is the intermediate density of states.

The structure of expression (4) is quite straightforward. The first set of square brackets represents the probability to find a nucleon of the required type and energy in a p-particle, h-hole state ; the second set of brackets contains the probability that the excited particle of interest will decay into the continuum at the rate λ_c^x before it interacts internally at the rate λ_+^x to give a (n + 2) exciton state. D_n is the depletion factor representing the fraction of the initial population surviving the excitation by particle emission prior to the formation of the considered n-exciton state. Oblozinski (18) has modified the above expression to derive the probability $P_\beta(\varepsilon)d\varepsilon$ of emitting a complex particle β formed from p_β excited nucleons in the energy channel ε, $\varepsilon + d\varepsilon$:

$$P_\beta(\varepsilon)d\varepsilon = \sum_{\substack{n=n_0 \\ \Delta n=+2}}^{\bar{n}} \left[R_\beta(p) \frac{\omega_{p-p_\beta,h}(E - B_\beta - \varepsilon)}{\rho_{p,h}(E)} \omega_{p_\beta,0}(B_\beta + \varepsilon)\, d\varepsilon \right] \tag{5}$$

$$\left[\frac{\gamma_\beta \lambda_c^\beta(\varepsilon)}{\gamma_\beta \lambda_c^\beta(\varepsilon) + \gamma_\beta \lambda_+^\beta(\varepsilon) + (1 - \gamma_\beta)\,(\overline{\lambda_c^x(\varepsilon) + \lambda_+^x(\varepsilon)})} \right] D_t \,.$$

It is rather instructive to compare the expressions (4) and (5) . While their structure is identical, changes occur in the form of the two square brackets. The factor $R_\beta(p)$ in the first is a simple combinational correction, introduced already by Kalbach - Cline (17), which assures the right combination of neutrons and protons to form the outgoing complex particle β. The main modification is in the second square bracket, where a factor γ_β was introduced. This factor gives the fraction of time that a given configuration of p_β nucleons can be treated as a complex particle β. Hence $\gamma_\beta < 1$.

Let us now discuss this factor more in detail. As introduced in ref. (18), this factor is an adjustable parameter. The usual procedure is to adjust all the other parameters of expression (5) to fit nucleon emission with $\gamma_\beta = 1$ (in which case expression (5) becomes identical with expression (4)) and then to chose γ_β in such a way as to fit experimental (n,α) and (p,α) spectra.

Fig. 9 shows the fits to the ^{93}Nb(n,α) spectrum at 14.2 MeV obtained with various methods. The dotted curve represents a conventional equilibrium calculation, the solid curve is the precompound calculation obtained using the expression (3), ref. (11) and the dashed curve is the precompound calculation obtained using the expression (5), ref. (18). The values of ϕ (ref. 11) and γ_α (ref. 18) were, respectively 0.17 and 0.0015. The evaporation component (dotted curve) should, normally, be added to the two calculations. The dashed-dotted curve is the result of a complete equilibration calculation by Bersillon and Faugère (20) following the method of Kalbach-Cline (17) with no adjustable parameter included. These calculations were performed by solving the set of master equations (5) with particle emission included ; for the latter, the probability $W_\beta(p,h,\varepsilon)$ for emitting a complex

particle β with energy ε from a state with n = p + h excitons given by Kalbach - Cline were taken (see eqs. (1) and (6) of ref. 17). These expressions do not contain any adjustable A - dependent preformation factor. Rather, they contain a unique factor P_β ! (= 4 ! for alpha particles) which corrects empirically for the emission of complex particles. The calculation of Faugere and Bersillon (20) used parameters fixed by fitting the 14.4 MeV neutron spectrum of ^{93}Nb ($g = \frac{A}{13}$, $|M|^2$ = 20 keV^2) ; once these parameters were fixed and P_β ! taken as 24, no other parameter was introduced to fit the alpha spectrum. Although the calculated values overestimate the experiment (P_β ! appears to be too large a correction factor), the shape of the alpha spectrum is reasonably reproduced (see fig. 9).

What information about the alpha clustering probability in nuclei can be extracted from the above calculations ? Although values of the factors ϕ and γ_α can not be directly compared, their physical meaning should not be very dissimilar, as seen from expressions (3) and (5). In this context it is worth noting that the method of Oblozinsky (18) based on the hybrid model (2), requires a much smaller value of the "preformation" (or whatever it is) factor then the method of Milazzo-Colli (11) based on the exciton model (5). In view of the relative consistency of the values of ϕ extracted from different kinds of experiments (16), it may be argued that the somewhat unrealistic values of ϕ needed in ref. (11) are a consequence of a deficiency of the basic precompound model used. The large values of ϕ would then implicitly cover this deficiency. We know, on the other hand, that the exciton model in its various versions was quite successful in fitting nucleon spectra (4) ; moreover the results of ref.(20) show that this model can qualitatively account for the emission of alpha particles without an A - dependent preformation factor. All the models, however, require for the alpha particle an empirical emission probability larger then the one based on considerations of pure statistics.

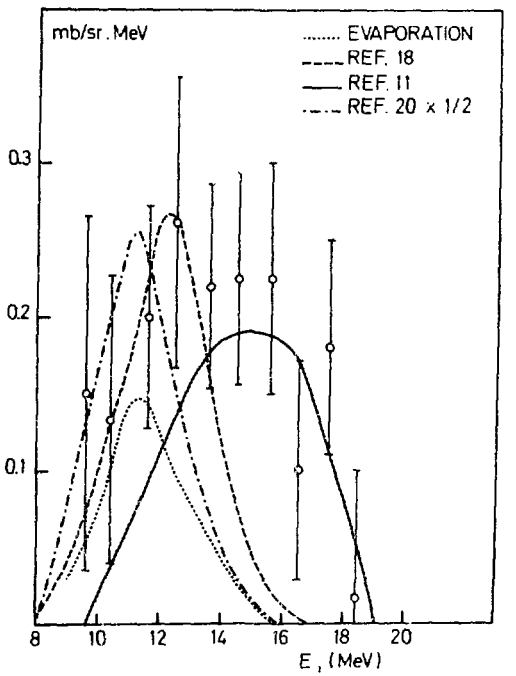

Fig. 9 The experimental spectrum of $^{93}Nb(n,\alpha)$ at 14.2 MeV and the fits obtained with an evaporational formula (dotted curve), with the precompound expressions (3) (solid curve) and (5) (dashed curve) and from ref. (20) (dashed-dotted curve).

Concluding this section, we should briefly present the recent results of the Warsaw group on the direct knock out of alpha clusters. Glowacka et al. (21) have refined the arguments outlined earlier in this section, by the use of the Shapiro's dispersion theory. Their method can be summarized as follows : A direct reaction excites by definition a small number of degrees of freedom ; thus the removal of a group of nucleons becomes feasible. In contrario, the excitation on many degrees of freedom would mean sharing the energy among many nucleons and "group emission" would be negligible. In their formalism

Glowacka et al. (21) assume that the amplitude of a direct reaction is described by a set of nonrelativistic Feynman diagrams ; for a (n,α) reaction, experimental considerations restrict the choice to a single triangular diagram describing the knock out of an alpha particle from the target nucleus. There again the reduced width for the dissociation of the target nucleus T into (T - α) and α appears as an adjustable parameter. The results of a calculation of spectra of $^{151}Eu(n,\alpha)^{148}Pm$ and $^{169}Tm(n,\alpha)^{166}Ho$ at 18.15 MeV are shown in Fig. 10 (solid lines) together with the results of a precompound calculation using the formulas of ref. (22) (dotted lines). While the precompound calculation reproduces the average pattern of the spectra, the use of the dispersion theory introduces structure in the calculated spectra. Indeed, experimental spectra show considerable structure, but it is not obvious that the calculated structure is always correlated with the observed one. On the other hand, the dispersion theory calculations predict adequate angular distributions ; the existing precompound calculations do not give angular information on the emission of complex particles.

Summarizing this section, it is my impression that we have not yet understood the mechanism of (n,α) reactions on heavy nuclei. None of the existing models is able to account for the relatively large number of particles emitted following the neutron bombardment of nuclei without introducing some sort of more or less justified empirical multiplying factor. The hypothesis of the abundant presence of alpha clusters on the nuclear surface is an attractive one ; we should, however be able to understand it starting from first principles. For the moment, we are not.

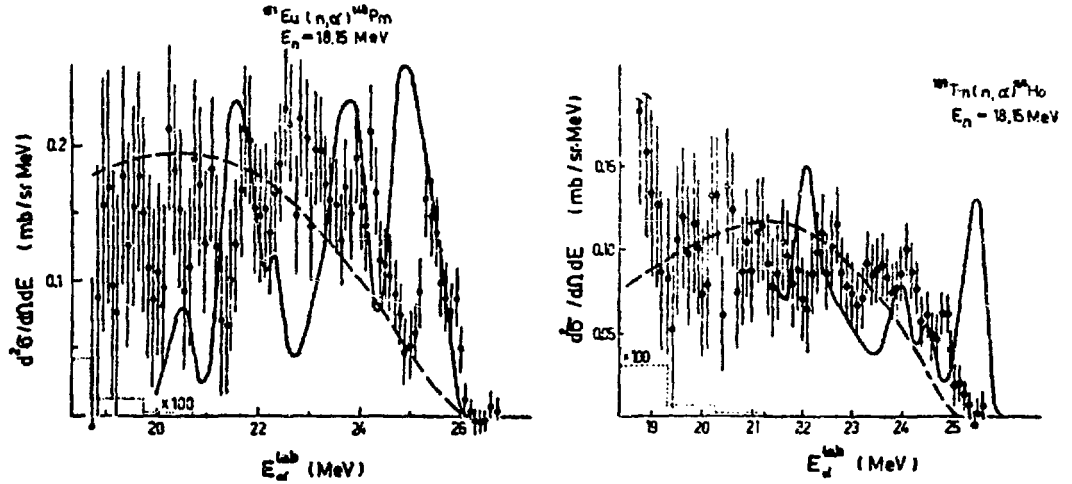

Fig. 10 Comparison of the angle integrated experimental spectra of $^{151}Eu(n,\alpha)^{148}Pm$ (left) and $^{169}Tm(n,\alpha)^{166}Ho$ (right) with preequilibrium calculations (dashed curves) and the dispersion theory calculations of ref. (21) (solid curves). The light dotted curves represent (clearly inadequate) evaporation calculations (from ref. 21).

NEW LINES OF INVESTIGATION

We shall now deal with two separate problems which are mutually connected only by the role of the isospin quantum number and by the fact that they represent new and somewhat unusual lines of investigation in fast neutron induced reaction studies.

Isospin Conservation

Nature has ordered nuclear levels in such a way that the lowest lying states will be those of the lowest possible isospin. Thus in a nucleus with a neutron excess the lowest states will have the isospin of the ground state (i.e. $T = T_z = (N - Z)/2$), while at some higher excitation energies a set of states with one additional unit of isospin, the so called $T_>$ states will appear. Owing to this fact, at moderate excitation energies more $T_<$ states will, in general, be available then $T_>$ states. Now, in proton induced reactions on a target with isospin T_o the fractions of states with $T_<$ and $T_>$ formed in the intermediate nucleus are, respectively, $2\ T_o/(2\ T_o + 1)$ and $1/(2\ T_o + 1)$. As, normally, $T_o >> 1$, many more $T_<$ states are formed. On the other hand in a neutron induced reaction, only $T_<$ states are formed.

Kalbach - Cline et al. (23) have discussed this problem and, in particular, the question to what extent is the isospin conserved as a good quantum number. If the isospin is mixed and all composite states are populated with an equal probability, the decay pattern for proton and neutron induced reactions will be identical and characteristic of the more abundant $T_<$ states. If, on the contrary, isospin is conserved, there is a chance to observe the $T_>$ decay. Proton and neutron emission spectra will be different for neutron and for proton induced reactions respectively. An interesting suggestion (4) will be, e.g. to compare (n,p) and (p,p') spectra on an isotopic chain. In reactions at moderate energies ($E_{exc} \sim 20$ MeV) where precompound processes are important, the rate of emission of protons from a neutron rich nucleus like ^{120}Sn to the $T_<$ states decreases rapidly in the course of the equilibration process. Thus, while most of the $T_<$ cross section involves equilibrium particle emission, essentially none of the $T_>$ cross section survives the equilibration process (4,23). The preequilibrium component would, thus, be richer in $T_>$ states then the equilibrium component. While comparison between calculations and experiment were made for (p,p') spectra (23), it would be interesting to extend such a comparison to (n,p) spectra too (4).

Analogs of the Dipole Giant Resonance via the (n,p) Reaction.

Another example of a new line of investigation is the recent report by Brady et al.(24) of the excitation of the giant dipole resonance analogs via the (n,p) reaction. The (n,p) reaction produces a change of $\Delta T_z = \Delta T = +1$ in target nuclei with $N > Z$; thus we expect it to excite only analogs of $T_>$ states of the target. For the ^{27}Al(n,p)^{27}Mg reaction studied by Brady et al., these are the isobaric analogs of the $T_>$ ($T = 3/2$) components of the giant dipole resonance in ^{27}Al. Fig. 11 shows the 15.5° lab. spectrum of ^{27}Al(n,p)^{27}Mg at 56.1 MeV together with the ^{27}Al(p,p') spectrum for 61.5 MeV incident protons. The excitation energy scales were adjusted for the Coulomb energy and (n,p) mass differences between ^{27}Mg and ^{27}Al (6.9 MeV) ; the peaks around 14.4 MeV in ^{27}Mg and 21.3 MeV in ^{27}Al correspond to each other rather well. They are also aligned to the photoneutron and total photonuclear cross section peak positions (see bottom of fig. 11).

In addition to the major component of the giant dipole resonance analog at 14.4 MeV Brady et al. report two other peaks in the spectrum, visible around, respectively, 10 and 6 MeV of excitation in ^{27}Mg. The first (at ∿ 10 MeV) may correspond to a splitting of the $T_>$ dipole resonance into a major (14.4 MeV) and a smaller (10 MeV) component. The intensity ratio of the two components is not inconsistent with the predictions of the hydrodynamic model of the giant dipole resonance (predicted ratio ∿ 2.5). Using the same model to estimate the intrinsic quadrupole moment Q_o of the ^{27}Al ground state from the ratio of the excitation energies in ^{27}Al corresponding to these two components, Brady et al. obtained a value of Q_o = 0.45 ± 0.05 barns. The second peak (around 6 MeV) may possibly be an M1 analogue, as its exhibits an angular distribution consistent with ℓ = 1 and is not visible in the photonuclear spectra (24).

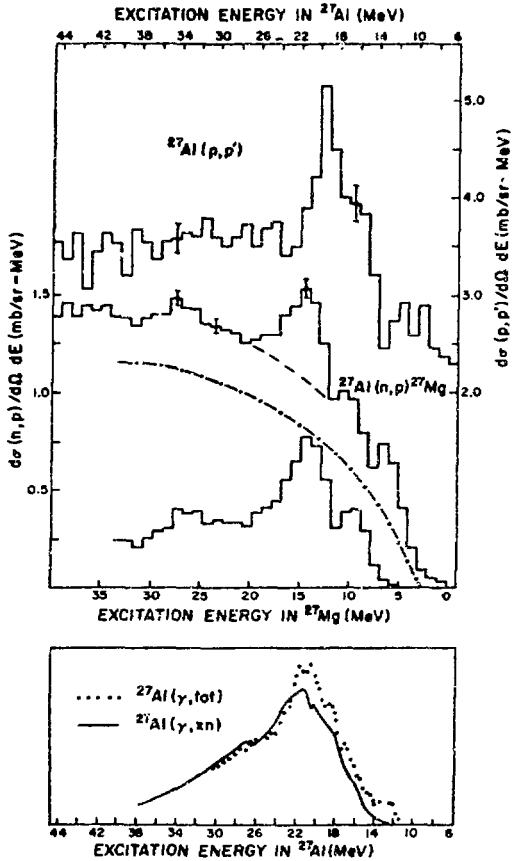

Fig. 11 Top part : The $^{27}Al(n,p)^{27}Mg$ spectrum at 15.5° lab. and 61.1 MeV incident neutron energy (middle curve) compared to the $^{27}Al(p,p')$ spectrum at 15° lab. and 61.5 MeV incident proton energy (top curve); the lowest curve is the background (dash-dotted curve) subtracted (n,p) spectrum. Bottom part : the corresponding $^{27}Al(\gamma,xn)$ and ^{27}Al (γ,tot) photonuclear spectra.

It would be interesting to perform similar experiments on other nuclei and see whether analogous results can be obtained.

CONCLUSION

While it is hard to compete in the field of fast neutron induced reactions with the experimentally much more rewarding and richer in spectroscopic information charged particle induced reactions, the former still present some unique features as complementary studies. The extension of the bombarding energy range to higher energies (up to 50 MeV) may open new lines of investigation. Unfortunately, only few laboratories have facilities for producing high energy neutrons.

The author acknowledges the kind hospitality of the Service de Physique Nucléaire, C.E.N. Bruyères-le-Châtel, where this work was performed. He is also indebted to several authors cited in this paper for kind permission to liberally use their results.

REFERENCES

1) G.M. Braga Marcazzan, E. Gadioli-Erba, L. Milazzo-Colli and P.G. Sona, Phys. Rev. C6 (1972) 1398.

2) M. Blann, Phys. Rev. Letters 21 (1968) 1357.

3) F.C. Williams, Phys. Letters 31B (1970) 184.

4) C. Kalbach, Acta Phys. Slovaca 25 (1975) 100.

5) J.J. Griffin, Phys. Letters 17 (1966) 478.

6) C. Kalbach - Cline, Thesis, Univ. of Rochester 1971, unpublished.

7) M. Blann, Lecture Notes in Physics, Vol. 22, ed. by N. Cindro, P. Kulisic and T. Mayer - Kuckuk, p. 43, Springer Verlag, Berlin 1973.

8) E. Arndt and R. Reiff, Zentralinstitut für Kernforschung (Rossendorf), Report ZfK 295 (1975) p. 67.

9) Yu. P. Popov, M. Prztyla, R.F. Rumi, M. Stepinski and M. Frontasyeva, Nucl. Phys. A188 (1972) 212.

10) N. Cindro, Rev. Mod. Phys. 38 (1966) 391.

11) L. Milazzo - Colli and G.M. Braga-Marcazzan, Nucl. Phys. A210 (1973) 297.

12) C. Kalbach - Cline, Nucl. Phys. A193 (1972) 417.

13) M. Jaskola, W. Osakiewicz, J. Turkiewicz and Z. Wilhelmi, Nucl. Phys. 110 (1968) 11.

14) P. Kulisic and N. Cindro, Acta Phys. Polonica A38 (1970) 621.

15) R. Caplar, M. Sc. Thesis, Univ. of Zagreb (Yug.) 1974, unpublished ; R. Caplar and P. Kulisic, Fizika 6 (1974) 41.

16) L. Milazzo - Colli, G.M. Braga-Marcazzan, M. Milazzo and C. Signorini, Nucl. Phys. A218 (1974) 274.

17) C. Kalbach - Cline, Nucl. Phys. A193 (1972) 417.

18) P. Oblozinsky, Acta Phys. Slovaca 25 (1975) 214.

19) I. Ribansky and P. Oblozinsky, Phys. Letters B45 (1973) 318.

20) O. Bersillon and L. Faugère, Priv. Comm.

21) L. Glowacka, M. Jaskola, J. Turkiewicz, L. Zemlo, M. Kozlowski and W. Osakiewicz, Nucl. Phys. A244 (1975) 117; ibid. A262 (1976) 205.

22) L. Colli-Milazzo and G.M. Marcazzan-Braga, Phys. Letters 33B (1972) 155.

23) C. Kalbach-Cline, J.R. Huizenga and H.K. Vonach, Nucl. Phys. A222 (1974) 405.

24) F.P. Brady, N.S.P. King, M.W. McNaughton and G.R. Satchler, Phys. Rev. Letters 36 (1976) 15.

MF 1 - NEUTRON INDUCED REACTIONS II: (n, x) REACTIONS ON MEDIUM AND HEAVY NUCLEI - N. Cindro (C.E.N. Bruyères-le-Châtel, France)

Barschall (Wisconsin):

Discussion on this paper will be deferred till the end of Dr. Fréhaut's paper.

10.45 a.m., **Wednesday, July 7, 1976** Paper subject : session **MF 2**

NEUTRON INDUCED CASCADE REACTIONS

J. Fréhaut

Service de Physique Nucléaire, Centre d'Etudes de Bruyères-le-Châtel

B.P. 61, 92120 Montrouge, France

RÉSUMÉ

The present state of experimental data for neutron induced cascade reactions, and in particular data on (n,2n) cross sections, provides a good basis for cross section systematics and nuclear reaction model testing. It is shown that the existing experimental data can be accounted for by using models including both compound nucleus and preequilibrium decay modes.

ABSTRACT

In the energy range below ∿ 18 MeV, the (n,2n) reaction is the predominant cascade reaction, particularly for medium and heavy nuclei. Cascade reactions involving charged particle emission are less probable and have not been as thoroughly investigated. Thus this paper will be primarily concerned with discussing the progress in understanding (1) the mechanism of the (n,2n) reactions and (2) the systematic trends that appear in the energy and mass dependence of the (n,2n) cross sections.

It has been known for several years that the compound nucleus evaporation model can account for the total (n,2n) cross sections in a wide range of energies and nuclei within 20-30% of experiment. It has been also pointed out that the predictions of this model tend to systematically over-estimate the experiment in the energy range below the (n,3n) threshold. Several mechanisms have been proposed to account for this difference : (1) The competition of the gamma decay of unbound states near the neutron emission threshold ; this is supported by the experimental observation that (n,2n) and (n,3n) reactions appear at a significant rate at bombarding energies higher by 0.5-1 MeV than their reaction thresholds. (2) The presence of non-equilibrium processes, such as direct transitions to collective states of the nucleus and preequilibrium processes. These processes act to harden the primary neutron spectrum, as experimentally observed ; thus they reduce the fraction of neutrons capable of giving rise to the emission of secondary neutrons. At energies above the (n,3n) threshold, however, preequilibrium processes contribute to a reduction of the (n,3n) cross section and subsequently to an increase of the (n,2n) cross section, as compared with the statistical model calculations. With increasing incident energy, the evidence grows for the necessity to include non-equilibrium contributions in order to adequately represent the experimental data.

The newly obtained values of (n,2n) cross sections for a wide range of incident energies, and in particular the measurements on series of isotopes, permit a critical revaluation of the trends observed in cross section systematics. It appears now that the regularity previously observed in the (N-Z) dependency of (n,2n) cross sections for constant N and for a given excess energy over the reaction threshold has not a general character, and cannot be straightforwardly used for evaluation purposes.

Paper subject : session MF

NEUTRON INDUCED CASCADE REACTIONS

J. FRÉHAUT

Service de Physique Nucléaire, Centre d'Etudes de Bruyères-le-Châtel

B.P. 61, 92120 Montrouge, France

INTRODUCTION

A cascade reaction can be defined as a reaction in which more than one particle emerges in addition to the final nucleus. Because neutrons have much greater penetrabilities than charged particles, the (n,2n) and (n,3n) reactions are, with few exceptions, the most probable neutron induced cascade reactions in the energy range below 20 MeV. Cross sections for (n,2n) reactions have been extensively measured and analyzed around 14 MeV incident neutron energy. Excitation functions for a large number of nuclides have recently been measured accurately over a wide energy range [1,4], and a brief survey of the techniques employed is given. These data now provide a good basis for the study of the reaction mechanism which is discussed in some detail. Systematic effects such as isotonic and isotopic effects will also be discussed.

Very little information has been published on cascade reactions involving charged particle emission. Measurements have only been performed around 14 MeV incident neutron energy for the [(n,d) + (n,n'p) + (n,pn)] and the [(n,n'α) + (n,αn)] reaction cross sections on a limited number of nuclides. They will be briefly reviewed.

TECHNIQUES OF CROSS SECTION MEASUREMENTS

In most of the published (n,2n) cross section measurements, use has been made of the activation technique. A method based on the large loaded liquid scintillator has been recently developed [5,6]. Because it is a direct method, it overcomes the limitations of the activation technique.

The activation method.

The activation method relies on the determination, after neutron bombardment, of the activity produced in a sample. Although all types of counting methods have been employed, the γ-ray spectrometry is now generally used, particularly because of the recent development of high resolution Ge(Li) detectors. Nevertheless NaI(Tl) scintillation detectors are still widely used [4].

Besides its sensivity to uncertainties in decay schemes, this method is limited to nuclides which leave a suitably active residual isotope. This limitation rules out the possibility of systematic measurements on the different isotopes of a given element. Such measurements are however of prime interest for studying the reaction mechanism.

The large loaded liquid scintillation method.

This technique, which has been recently improved [6], involves the detection of

the emitted neutrons. It relies on two properties of the neutron detector, a large gadolinium loaded liquid scintillator : 1. its high neutron efficiency and 2. the relatively long lifetime of neutrons in the scintillator. This allows identification of an (n,2n) event by 2 separate pulses within a period of about 30 µs following the event.

This method can be used for any nuclide, provided that several grams of material are available for a sample. Thus any separated isotope or natural element of interest for fusion technology can be measured.

REACTION MECHANISM

The title of the present paper "Cascade Reactions" suggests a successive emission of particles. It was deliberately choosen for that reason. Indeed, it has been known for a long time that the (n,2n) reaction, in particular, proceeds mainly through the formation of a compound nucleus, followed by the evaporation of the neutrons. In our discussion of the reaction mechanism, we will begin with a brief description of the evaporation model. The differences which appear between the predictions of this model and experimental data will be examined, and a number of mechanisms which can account for these deviations will be discussed. Some of them, such as the introduction of angular momentum effects and of γ-decay competition with particle emission, remain in the frame of the evaporation model. However new reaction mechanisms, such as direct reactions or preequilibrium emission, are necessary to account also for the observed hardening of the primary neutron spectrum and for the cross section behaviour for incident neutron energies above 15 MeV.

The evaporation model.

Under the Bohr assumption of compound nucleus formation, and with the restriction that the compound and the residual nuclei have such a large density of levels at their excitation energy that a statistical description can be used, the following expression can be derived [7] for the energy distribution of an outgoing particle :

$$I(\varepsilon)\, d\varepsilon \sim \varepsilon\, \sigma_c(\varepsilon)\, \omega(E_n - \varepsilon) \qquad (1)$$

where E_n is the energy of the incident neutron, ε the energy of the emitted particle, $\sigma_c(\varepsilon)$ the cross section for formation of the compound nucleus by a particle of energy ε, and $\omega(E_n - \varepsilon)$ the density of energy levels in the product nucleus with excitation energy $(E_n - \varepsilon)$.

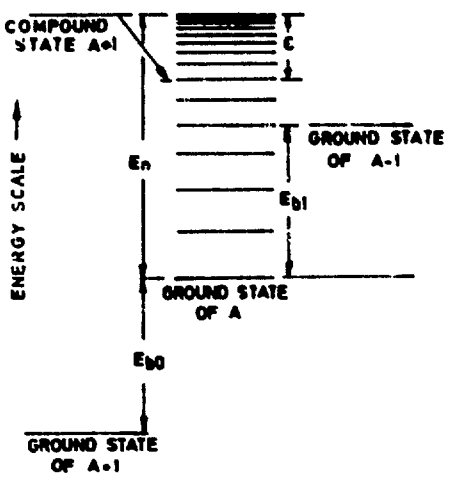

Fig. 1 Compound nucleus decay scheme.

A schematic picture of the compound nucleus decay is shown in fig.1 for the case of the (n,2n) reaction. If we assume that the residual nucleus A always emits a second neutron whenever it is energetically possible and if we neglect cascade reactions involving charged particle emission, then we obtain the following relations for incident energies below the (n,3n) threshold :

$$\frac{\sigma(n,2n)}{\sigma(n,M)} = \frac{\int_0^{E_n - E_{b1}} I(\varepsilon)\, d\varepsilon}{\int_0^{E_n} I(\varepsilon)\, d\varepsilon} \qquad (2)$$

$$\frac{\sigma\ (n,n')}{\sigma\ (n,\ M)} = \frac{\int_{E_n - E_{bl}}^{E_n} I\ (\varepsilon)\ d\varepsilon}{\int_{0}^{E_n} I\ (\varepsilon)\ d\varepsilon} \qquad (3)$$

where $\sigma\ (n,M) = \sigma\ (n,n') + \sigma\ (n,2n)$, and where E_{bl} is the neutron binding energy in the target nucleus A.

A priori calculations are often performed on the basis of these expressions, using appropriate level density formulae and σ_c cross sections obtained from optical model calculations.

This formalism can be easily generalized to the case where emission of charged particules is possible. Further extensions including γ-ray emission and angular momentum effects are also possible.

Defining the nuclear temperature θ as :

$$\frac{1}{\theta\ (E)} = \frac{d}{dE} \left[\log\ \omega\ (E) \right] \qquad (4)$$

and introducing a first order Taylor expansion for the logarithm of the level density around $E = E_n$ in expression (1), Weisskopf [7] obtained a Maxwellian form for the energy distribution of the outgoing first neutron :

$$I\ (\varepsilon)\ d\varepsilon \sim \varepsilon\ \sigma_c\ (\varepsilon)\ \exp\left(-\frac{\varepsilon}{\theta}\right). \qquad (5)$$

Assuming σ_c constant with energy, he derived from equations (2) and (3) the following expressions :

$$\frac{\sigma\ (n,2n)}{\sigma\ (n,\ M)} = 1 - \left(1 + \frac{E_n - E_{bl}}{\theta}\right) \exp\left(-\frac{E_n - E_{bl}}{\theta}\right) \qquad (6)$$

$$\frac{\sigma\ (n,n')}{\sigma\ (n,\ M)} = \left(1 + \frac{E_n - E_{bl}}{\theta}\right) \exp\left(-\frac{E_n - E_{bl}}{\theta}\right). \qquad (7)$$

The assumptions made to derive the above formulae have their greatest validity several MeV above the (n,2n) threshold. It is thus understandable than they give a good overall representation of the bulk of experimental data available around 14 MeV incident neutron energy [8].

Comparison of the statistical model predictions with experimental results.

As can be seen from expression (4), the (n,2n) cross section is mainly governed by the quantity $U_R = B_n - E_{n1}$ which is generally called the excess energy and corresponds to the total kinetic energy available for the two emitted neutrons. Many nuclei have a Q - value for the (n,2n) reaction of about 6 - 9 MeV, and most of the experimental data are for incident energies between 14 and 15 MeV. This corresponds to an excess energy of 5 - 7 MeV, which is well above the (n,2n) threshold, but still below the (n,3n) threshold, a region where the assumptions leading to the evaporation formula have the maximum validity.

A. Gilbb and N. Cindro have recently shown [9] that in this energy range (U_R = 5 ± 1 MeV) the experimental data are systematically overestimated by the Pearlstein calculations [8]. However the Pearlstein expression is not a purely statistical one, since it contains a scaling factor determined by comparison of the calculations with experimental results. An a priori statistical model calculation was also undertaken by the same authors [10]. Furthermore, they showed that in the energy region U_R = 5 ± 1 MeV the calculated cross sections are not very sensitive to the value of the neutron inverse cross sections $\sigma_c(\varepsilon)$ and the level density parameter, a, which are of crucial significance at lower energy. The results of their calculation plotted in fig. 2 show again that the calculation overestimates the experiment by about 8 %. The peak observed in the mass region A = 150 for the ratio $\sigma_{exp}/\sigma_{cal}$ seems to correspond to an underestimate of the calculated cross sections. In this region (deformed nuclei), some nuclei have a (n,3n) threshold around 14 MeV. At $U_R \sim 6$ MeV, the (n,2n) cross sections are thus calculated just above the (n,3n) threshold for the

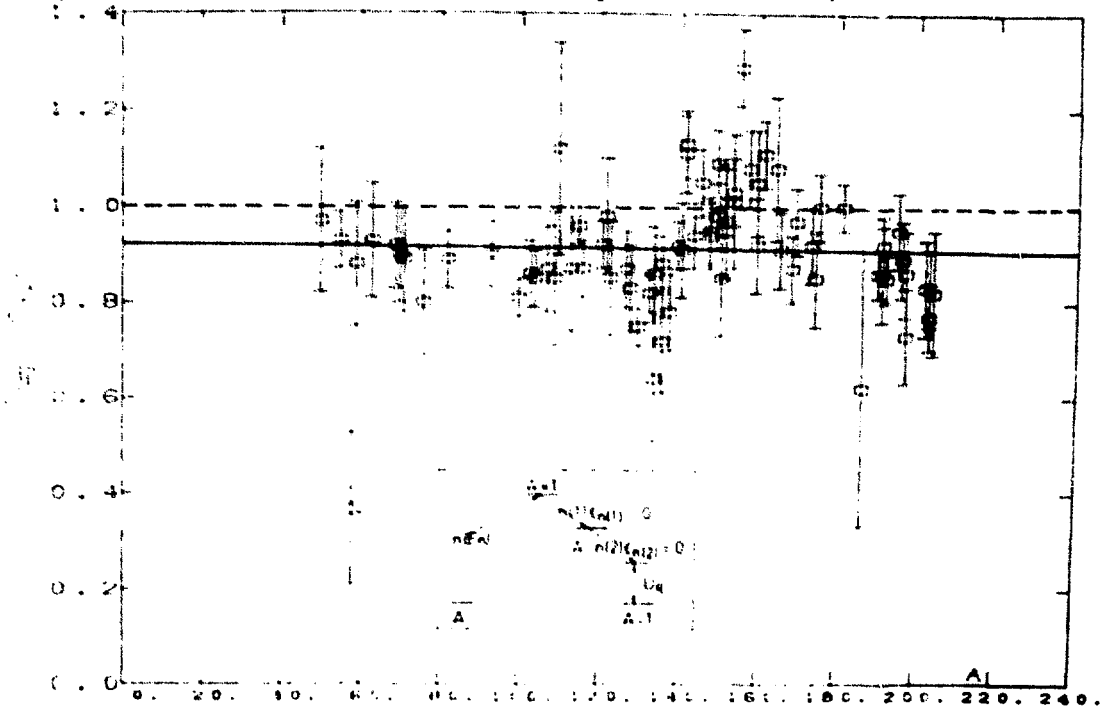

Fig. 2 Comparison of experimental and calculated (n,2n) cross sections for U_R = 5 ± 1 MeV (ref.10). The solid line is a least-square fit to the data : $\sigma_{exp}/\sigma_{cal}$ = - 0.000061 A + 0.92.

corresponding nuclei. As will be discussed later, because the γ-decay competition and the preequilibrium emission are not included in the model, the calculated values are then systematically underestimated, leading to an overestimate of the ratio $\sigma_{exp}/\sigma_{cal}$.

A somewhat different approach was adopted by Lu and Fink [11]. Using a statistical model allowing for neutron and charged particle emission, they calculated the (n,2n) cross sections at 14.4 MeV for a series of nuclei for which they had previously made measurements using the activation method. The upper part of fig. 3 shows the comparison of the calculation with experiment : calculated values are generally ∿ 10% larger than the experimental ones. Arguing that the competition between γ-ray and particle emission should result in an apparent increase of the reaction threshold, they performed new calculations using effective threshold higher by 0.5 and 1 MeV respectively for the (n,2n) and (n,3n) reactions. As seen in the lower part of fig. 3, the agreement is much improved, especially for nuclei having a high (n,2n) threshold (^{58}Ni, ^{92}Mo) and for nuclei having a (n,3n) threshold below 14.4 MeV (^{142}Ce). This latter case demonstrates the rôle that the γ-decay competition (and probably other mechanisms) might play just above the (n,3n) reaction threshold in the existence of a peak around A = 150 in fig. 2. It should also be pointed out that using such effective thresholds has little effect (∿ 3%) well above the (n,2n) threshold, and the conclusions of Holub et al. [10] remain valid. The large discrepancies remaining in fig. 3b for ^{96}Ru, ^{102}Pd and ^{103}Rh, attributed to direct interactions by the authors [11], are more probably due to uncertainties in the decay scheme of the product nuclei : the (n,2n) cross sections recently obtained using the liquid scintillator technique [1] for ^{103}Rh are in good agreement with the predictions of [11].

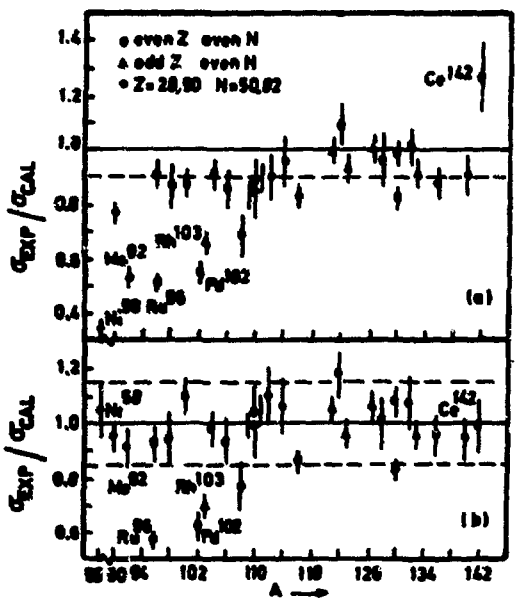

Fig. 3 Comparison of predicted (n,2n) cross sections with experiment at 14.4 MeV. (a) Using ground state thresholds. (b) Using effective thresholds higher by 0.5 and 1 MeV respectively for (n,2n) and (n,3n) reactions. Taken from [11].

A third evidence of the failure of the simple evaporation model in predicting the (n,2n) cross sections is given by the experimental results obtained at incident neutron energies above ∿ 20 MeV. As can be seen in the lower part of fig. 4 taken from reference [4], the evaporation model cannot account for the high energy tail in the excitation function.

Two mechanisms have been proposed to account for the differences between experiment and the predictions of the simple compound nucleus evaporation model. The first which allows for angular momentum effects and for competition between γ-ray and particule emission is an extension of the statistical model. The second mechanism, by which direct or preequilibrium particle emission can occur, lies outside the statistical model. Both will be reviewed successively.

Competition between γ-ray and particle emission. Angular momentum effects.

One of the approximations generally used in the statistical model calculations is that de-excitation of an excited nucleus by γ-ray emission may be neglected if the nucleus can also decay by particle emission. The validity of this assumption is doubtful just above the reaction threshold [12]. At the incident energies considered here, the compound nucleus may be formed with relatively high spin values. The particles evaporated from the compound nucleus have an average energy of the order of 1 to 2 MeV and thus carry away small orbital angular momenta. Therefore, only relatively high spin states of the final residual nuclei can be populated. Because of the low density of high spin levels in the residual nuclei at low excitation energy, the γ-ray emission can compete favourably with the particle emission. Such a situation may occur for an excitation energy up to several MeV in the residual nucleus. This is particularly true in the case of (n,2n) and (n,3n) reactions for the compound nuclei obtained respectively after the emission of a first and a second neutron. It should also be pointed out that the statistical approximation is not valid just above the (n,2n) and the (n,3n) thresholds since the number of exit channels available to the last emitted neutron is generally limited.

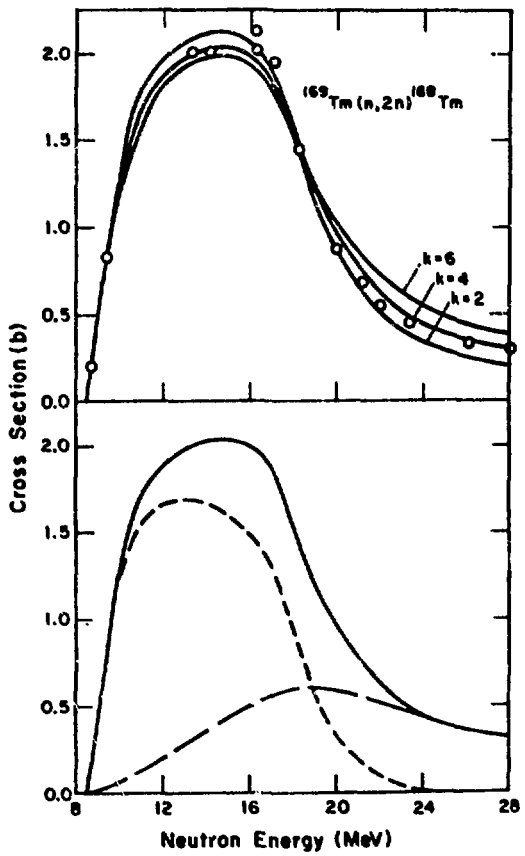

Fig. 4 Calculated and experimental cross sections for $^{169}Tm(n,2n)^{168}Tm$. The upper part shows the fit of an equilibrium plus preequilibrium component using different values of k, the scaling factor for the transition rate λ_{n+2} in the preequilibrium model. The lower part shows the decomposition of the total (n,2n) cross section (full line) into an equilibrium (short-dashed curve) and a preequilibrium component (long-dashed curve), calculated with k = 4. Taken from [4].

One of the effects of the γ-decay competition should be a strong reduction of the (n,2n) and (n,3n) cross sections around the reaction thresholds. This is supported by the experimental observation that (n,2n) reactions do not become significant until the incident neutron energies exceed the (n,2n) ground state thresholds by 0.5 - 1 MeV. Similarly the shift is of the order of 1 to 1.5 MeV for (n,3n) reactions, and the (n,2n) cross sections do not appreciably diminish in this energy interval [1,4]. The overall effect of neglecting the γ-ray decay competition in evaporation model calculations should be an apparent shift of calculated excitation functions toward low energies [8,13]. Such a shift has little influence on (n,2n) cross sections calcu-

lated well above the (n,2n) threshold but still below the (n,3n) thresholds. It is one of the reasons why the statistical model has been quite successful in predicting the (n,2n) cross sections around 14 MeV.

Angular momentum effects may have a more complex rôle. They can modify the relative fraction for primary neutron emission leading to unbound states of the residual nucleus (secondary emission allowed) versus that leading to bound states of the residual nucleus (secondary emission not allowed). When charged particle emission competes favourably with neutron emission, the relative branching ratios can also be affected. The net result could be an enhancement as well as a reduction of the calculated (n,2n) cross section.

Decowski et al. [14] have performed compound nucleus calculations including the γ-decay competition and angular momentum effects. Fig. 5 shows that the calculation fits reasonably well their experimental results for ^{113}In and ^{204}Pb. Unfortunately these authors do no indicate the importance of the γ-decay of unbound states and of angular momentum effects for (n,2n) cross sections. However these effects are shown to increase the calculated cross section for the formation of the isomeric state by inelastic scattering, leading to a better agreement with experiment.

A good illustration of angular momentum effects is given in fig. 6 where are presented the results of a calculation by J.Jary [15] for ^{89}Y and ^{93}Nb in three different cases :

1 - Simple evaporation model allowing for charged particle emission, without γ-decay competition and angular momentum effects. The nuclear level density distributions are taken from Gilbert and Cameron [16]. The inverse reaction cross sections

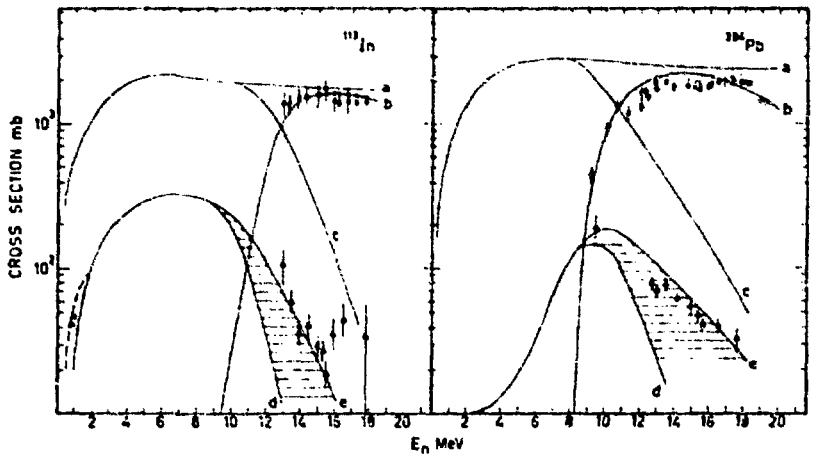

Fig.5 Comparison of the experimental cross sections for the $^{113}In(n,n')^{113m}In$, $^{204}Pb(n,n')^{204m}Pb$ (triangles) and the $^{113}In(n,2n)^{112}In$ and $^{204}Pb(n,2n)^{203}Pb$ (circles) reactions with the calculated ones : (a) the compound nucleus formation cross section, (b) the (n,2n) cross section, (c) the total (n,n') cross section, (e) and (d) the cross section for formation of the isomeric state by inelastic scattering with and without the γ-decay of unbound states, respectively. The shadowed area corresponds to the contribution of the γ-decay of unbound states. Taken from [14].

σ_c are obtained by optical model calculations [17] using the SPRT method [18].

2 - Same as in 1., but with nuclear level density parameters determined from available experimental data using a fitting procedure similar to that of Gilbert and Cameron [10].

3 - Same as in 2., but taking into account the angular momentum effects (not the γ-decay competition). The transmission coefficients T_{lj} are calculated according to the SPRT method [17,18].

For both nuclei, the charged particle rate always remains small. For incident neutron energies up to $\sim$ 4 MeV above the (n,2n) threshold, angular momentum effects strongly limit transitions towards bound states of ^{89}Y in the de-excitation of the compound nucleus ^{90}Y, which leads to an enhanced (n,2n) cross section, in fairly good agreement with experimental results (fig.6). In the case of ^{93}Nb, angular momentum effects act now in the opposite direction and tend to reduce the (n,2n) cross section. The resulting predicted curve fits the experiment [1] very well (Fig.6).

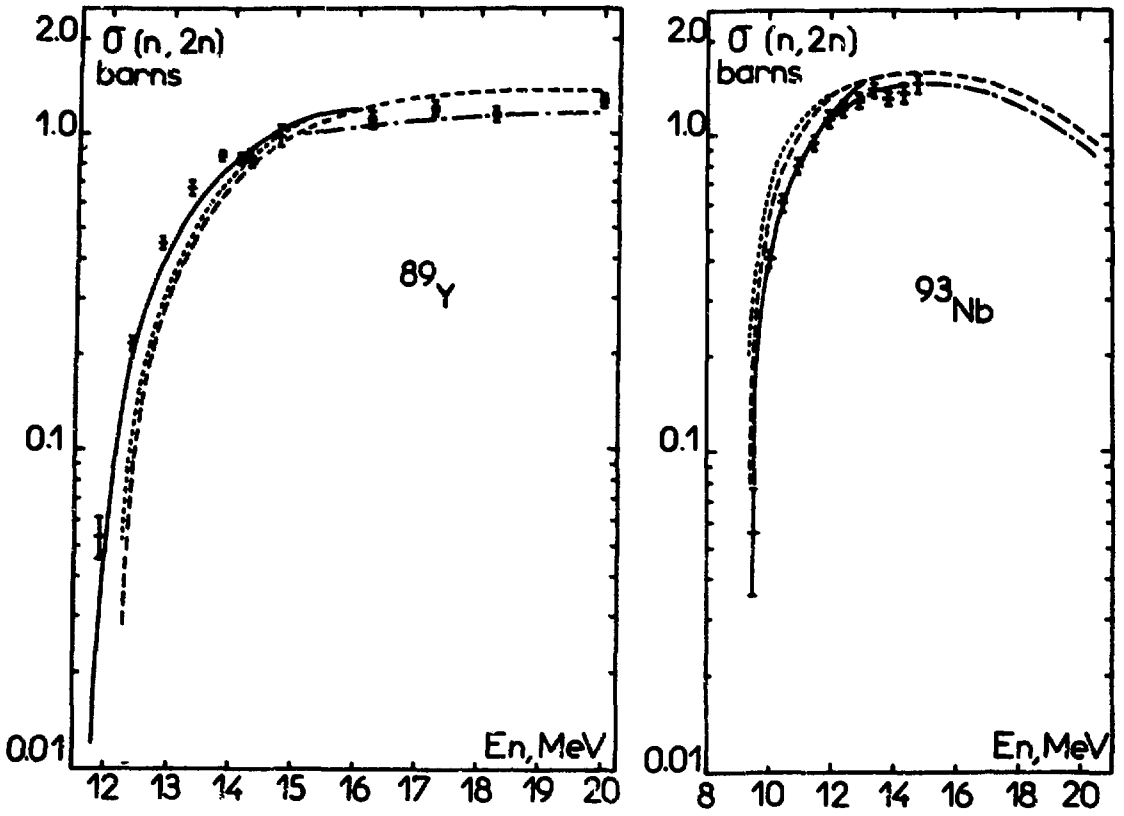

Fig.6 Comparison of experimental and calculated [15] (n,2n) cross sections for ^{89}Y and ^{93}Nb ; dotted curve : simple evaporation model ; dashed curve : adjusted level densities ; full line : angular momentum effects included ; dotted-dashed curve : preequilibrium emission included above 12 MeV for ^{93}Nb and above 15 MeV for ^{89}Y ; symbols + and ● : experimental results of [1] and [4] respectively.

For both nuclei, the use of adjusted level density distributions results in a reduction of the calculated cross section which is not negligible up to ∿ 3 MeV above the reaction threshold. However its influence is smaller than the angular momentum effects by a factor of about 3. In both cases, there is no special need for including γ-decay competition in order to fit the experimental results.

In conclusion, it should be kept in mind that besides the competition between γ-ray and particle emission, which certainly is not negligible in certain cases, the angular momentum effects and the level density distributions are also strongly influencing the (n,2n) cross section calculations up to several MeV above the reaction threshold.

Preequilibrium contribution to (n,2n) reactions.

In the compound nucleus evaporation model, the interaction of the incident neutron with a nucleus is considered to occur in two steps, 1. the formation of the compound nucleus, and 2. the subsequent statistical decay of the compound nucleus, which is considered independant of its mode of formation (the Bohr hypothesis). In the formation step, the assumption is made that the total energy (binding + kinetic) of the incoming neutron is immediately shared with all other nucleons. We now wish to considerer the effects of dropping this assumption and are interested in what happens during the equilibration time. A model has been recently proposed by Griffin [18] in an attempt to calculate the decay probabilities of an excited nucleus at every stage of its approach to statistical equilibrium. Further developments and applications have been investigated by Williams [20], Blann et al. [21,22] and Cline et al. [23,24]. It is out of the scope of the present paper to discuss in detail the preequilibrium processes. We shall only show what may be their contribution to (n,2n) and (n,3n) reactions.

Time dependant calculations show that preequilibrium particle emission occurs mainly in the early stage of the reaction, in a time interval much smaller than the compound nucleus life time [24]. This behaviour results in a natural division of the emitted neutron spectrum into two components :

1-the preequilibrium component which can be approximated by the closed form expression :

$$N(\varepsilon) = K \; \varepsilon \; \sigma_c(\varepsilon) \sum_{n=3,5,7\ldots} n(n-1) \left(\frac{E_n - \varepsilon}{E_n + E_{bo}} \right)^{n-2} \qquad (8)$$

where E_n and ε stand for respectively the incident and the outgoing neutron energy, $\sigma_c(\varepsilon)$ for the inverse reaction cross section, E_{bo} for the neutron binding energy in the compound nucleus A + 1 (see fig.1). The parameter n is the number of excited particles and holes, and K is a normalisation factor.

2 - the equilibrium component, given by equation (5).

Fig. 7 shows a decomposition of the total neutron spectrum resulting from bombardment of ^{93}Nb with 14.6 MeV neutrons [i.e. neutrons from (n,n'γ), (n,2n), (n,np) and (n,pn) reactions], obtained using a least square fit analysis [25]. The preequilibrium component fits rather well the high energy tail of the spectrum. It should be pointed out that the part of the spectrum lying above 5.8 MeV (secondary neutron emission not possible) corresponds to the primary emitted neutrons only. As a result, the effect of preequilibrium emission concerns mainly the first emitted neutron and is quite negligible in the secondary emission. This is a recurring feature of the analysis of data obtained at ∿ 14 MeV incident neutron energy.

The hardening of the primary neutron spectrum caused by the preequilibrium emission reduces the fraction of neutrons capable of giving rise to the emission of secondary neutrons, and thus leads to a reduction of the (n,2n) cross section, as predicted by the simple compound nucleus evaporation model. At incident neutron energies around 14 MeV, the reduction can be estimated to be of the order of 10%, in good agreement with the analysis of Holub et al. [9,10]. At higher energies (above the (n,3n) threshold) preequilibrium emission now favours the (n,2n) reaction, at the expense of the (n,n') reaction, as observed by Bayhurst et al. [4] (fig. 4).

Different approaches are possible in calculating the preequilibrium contribution to (n,n') cross sections. J. Jary [15] uses essentially the energy integrated preequilibrium spectrum (equation 5) in which the constant K is calculated using the complete expression given by Cline and Blann [24]. The squares of the average two-body matrix elements $|M|^2$ appearing in the complete expression are determined by fitting the experimental primary neutron spectra [26] using an equilibrium plus a preequilibrium component as described above [equations (5) and (8)]. The compound nucleus formation cross section σ_c used to calculate the equilibrium component is that obtained by optical model calculations [17,18], but reduced by an amount corresponding to the calculated preequilibrium term. The level density parameters are determined by fitting the available experimental data using the procedure described by Gilbert and Cameron [19]. The model allows for charged particle emission and takes into account angular momentum effects, but the γ-decay is not included. The calculations for ^{89}Y and ^{93}Nb (fig. 4) agree fairly well with the experimental results. The preequilibrium contribution is found to be negligible below 15 MeV incident neutron energy for ^{89}Y, and below 17 MeV for ^{93}Nb. Bayhurst et al. [4] adopted the hybrid model formalism [21] to evaluate the preequilibrium component they added to the evaporation term. The absolute value of the preequilibrium contribution was calculated by adjusting the transition rates λ_{n+2} so as to reproduce the experimental data for ^{169}Tm (see fig. 4). The best fit was obtained by using $\lambda^{III}/4$, where λ^{III} is the value evaluated in [21] by fitting the average mean free path of excited nucleons in nuclear matter as calculated by Kikuchi and Kawai [27]. Their calculation also differs from the one of Jary [15] in the values σ_c for in-

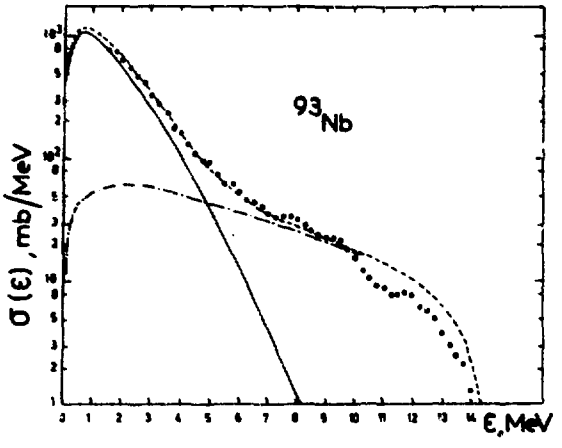

Fig. 7 Experimental total neutron spectrum obtained by bombardment of ^{93}Nb with 14.6 MeV neutrons (full circles). The cross sections for neutron emission from equilibrium and preequilibrium states according to equations (5) and (8) are denoted by the solid and the dotted-dashed lines respectively. The sum of both (dashed line) fits the experimental points. Taken from [25].

verse cross sections and in the choice of a different set of level densities. Moreover, the γ-decay competition is included and angular momentum effects are taken into account only for neutron decay to levels below 2 MeV excitation energy. These authors obtain in general good agreement between calculated and observed (n,2n) and (n,3n) cross sections in the energy range from threshold to 28 MeV. Generally, the contribution of preequilibrium emission is substantial and increases with energy. For ^{169}Tm (fig. 4) the contributions of equilibrium and preequilibrium emission to the (n,2n) cross section are equal at ∿ 19 MeV and preequilibrium emission is the only appreciable mode above 24 MeV.

Direct reaction contribution to (n,2n) reactions.

Most of the available experimental data on (n,2n) cross sections and on energy distributions of emitted neutrons are satisfactorily understood in the frame of the compound nucleus plus preequilibrium theories. There is however some evidence that direct reactions may also play a non negligible rôle. The most trivial indication is that we know they exist in the inelastic scattering of intermediate energy neutrons. Typical values of angle integrated cross sections for inelastic scattering to the first 2^+ state of some Se, Nd and Sm isotopes [28,35,36] are given in table I. Such large values cannot be accounted for by Hauser Fesbach type calculations. They result mainly from a strong coupling of the ground state (0^+) to the first excited level (2^+). It thus appears that direct scattering of neutrons of intermediate energy to the low lying collective states amounts to a few hundred millibarns. These direct transitions to bound states of the residual nucleus will partially deplete the low energy part of the evaporation spectra and thus will reduce the possibility of emission of a second neutron. However, as far as (n,2n) cross section calculations are concerned, this effect is properly taken into account when a coupled channel calculation is used to derive the compound nucleus formation cross sections used in evaporation models [18].

A general feature of direct reactions is that the energy spectrum of emitted particles is harder than the Maxwellian spectrum predicted by the evaporation theory. Unfortunately this feature is shared with the preequilibrium emission, and it is hardly possible to determine the relative part of both processes in the high energy tail observed in the experimental spectra.

Nucleus	^{76}Se	^{78}Se	^{80}Se	^{82}Se	^{142}Nd	^{144}Nd	^{146}Nd	^{148}Nd	^{150}Nd	^{148}Sm	^{150}Sm	^{152}Sm
E_n, MeV	8	8	8	8	7	7	7	7	7	7	7	7
$\sigma(2^+)$,mb	184	201	202	209	65	106	196	224	255	178	213	286

TABLE I

Angle integrated cross sections for inelastic scattering of medium energy neutrons to the first 2^+ state of some Se, Nd and Sm isotopes [28,35,36].

A more specific feature is that the angular distributions of product particles, particularly those of higher energy, are peaked in the forward direction. Now compound nucleus and preequilibrium processes tend to give angular distributions which are isotropic or symmetrical about 90 degrees [29,30]. H. Jahn et al.[31] have taken advantage of this trend in an attempt to interpret the inelastic scattering of 14.7 MeV neutrons on ^{56}Fe. Using a plane-wave-Born-approximation (PWBA) analysis of the angular distribution measured by Hermsdorf et al. [32], they showed that the forward directed anisotropy observed for energies of the scattered neutrons above ∿ 7 MeV had the typical shape of direct reactions which is closely related to the shape of the square of the spherical Bessel functions. Furthermore, they showed that the energy spectrum of the inelastically scattered 14.7 MeV neutrons measured by Hansen et al. [33] for ^{56}Fe could not be fitted by a sum of an evaporation spectrum and of a preequilibrium component calculated in the frame of Blann's model [22] using realistic parameters. They concluded that a third component accounting for direct reactions should be added and derived it from their PWBA analysis. As shown in fig. 8, they obtain overall good agreement between calculations and experiment.

A similar theoretical approach was adopted by Lukyanov et al. [34] to fit the experimental forward peaked angular distribution they obtained from bombardment of 9.1 and 14.4 MeV neutrons on two groups of nuclei around A = 56 and A = 90. Neglecting preequilibrium effects, they showed that for all the nuclei studied the energy dependence of the angle integrated spectra was well approximated by the expression :

$$\sigma(\varepsilon) = \alpha\ \varepsilon\ \exp\left(-\frac{\varepsilon}{\theta}\right) + \gamma \sqrt{\frac{\varepsilon}{E_n}}\ (E_n - \varepsilon) \qquad (9)$$

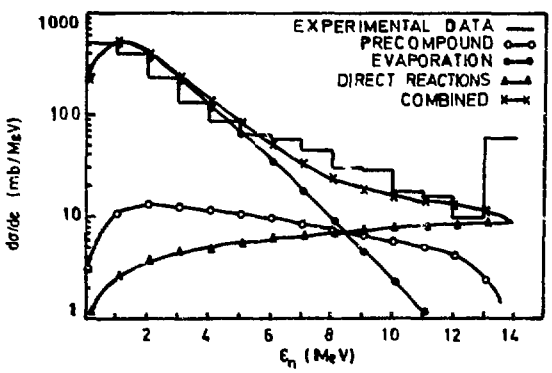

Fig.8 Comparison of measured and calculated energy spectra of inelastically scattered 14.7 MeV neutrons on ^{56}Fe. Taken from [31].

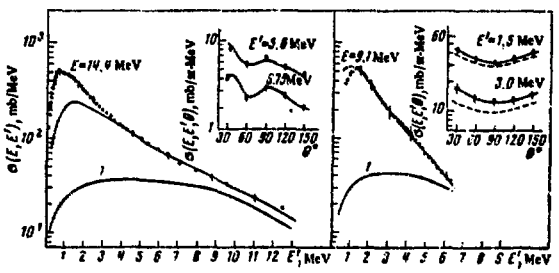

Fig.9 Comparison of measured (points) and calculated (solid lines) energy spectra of inelastically scattered 9.1 and 14.4 MeV neutrons on ^{56}Fe. The curve 1 represents the contribution of direct processes. Selected angular distributions are also given ; dashed curves are for angular distributions of evaporated neutrons. Taken from [34].

where E_n and ε stand for the energy of the incident and the outgoing neutron respectively, θ for the nuclear temperature, and where α and γ are adjustable parameters. The first term corresponds to an evaporation spectrum, while the second one stands for the contribution of direct processes and fits the forward peaked part of the spectrum. The results of their investigation for ^{56}Fe is shown in fig. 9. For E_n = 14.4 MeV, the fit was performed only for excitation energies of the first residual nucleus below the (n,2n) threshold (E_{th} = 11.2 MeV), i.e. for the first emitted neutron (ε > 3.2 MeV).

Comparison of fig. 8 and of fig. 9 (for 14.4 MeV incident neutron energy) shows that the sum of the preequilibrium and direct reaction components in the former one is about one half of the direct reaction component in the latter one, whereas the overall fit to experimental data is acceptable in both cases. This illustrates the crudity of the calculations, and analysis similar to that discussed above are no more than indicative. The facts are that the high energy tail of the experimental spectra can be accounted for either by preequilibrium or by direct emission, as well as by a mixture of the two effects. The existence of a forward peaked angular distribution for the high energy part of the inelastically scattered neutron spectra is indicative of the presence of direct reactions. More quantitative predictions call for an extension of the existing models.

SYSTEMATICS OF (n,2n) CROSS SECTIONS

In 1966 Csikai and Petö [37] observed that the (n,2n) cross sections at a constant excess energy U_R above threshold vary linearly with (N-Z) if either N or Z is constant. They derived an empirical formula :

$$\sigma (Z \pm \Delta Z, N) = \sigma (Z,N) \mp m (U_R) \Delta Z \qquad (10)$$

with m = 231 mb for U_R = 3 MeV and for all values of N except N = 28. This expression was extensively used by evaluators to provide recommended values of (n,2n) cross sections where experimental data were not available [38].

A revaluation of this observation has been recently carried out [39] on the basis of the experimental results given in compilations by Bödy [40] and Kondaiah [41] and of more recent measurements [1-4,42], in particular on several series of isotopes [1-3]. Fig. 10 shows the results of this investigation for a number of isotones around N = 50 and 82 respectively. The measured cross sections are plotted against (N-Z) for several values of the excess energy U_R. The extreme right of the figure shows the Csikai Petö trend calculated from expression (10) at U_R = 3 MeV for the isotones N = 44 and N = 90. It appears that the cross sections have a mounting tendency for given values of N and U_R , but the curves are rather irregular and their shapes vary with both N and U_R. The scatter of experimental points is such, however, that substantial changes in the apparent behaviour are possible. For U_R = 3 MeV, the slope of the average lines is generally less steep than that proposed by Csikai and Petö.

Fig. 11 shows the (n,2n) cross sections recently measured for some even Nd and Sm isotopes [3] plotted against (N-Z) for different values of U_R. Again we observe a mounting tendency, but it is difficult to propose a single simple expression accounting for the behaviour of the two isotopic chains, even for U_R = 3 MeV. Thus it appears now that the trend observed by Csikai and Petö [37] for U_R = 3 MeV is not regular and has not a general character. Hence, it cannot be used for evaluation purposes.

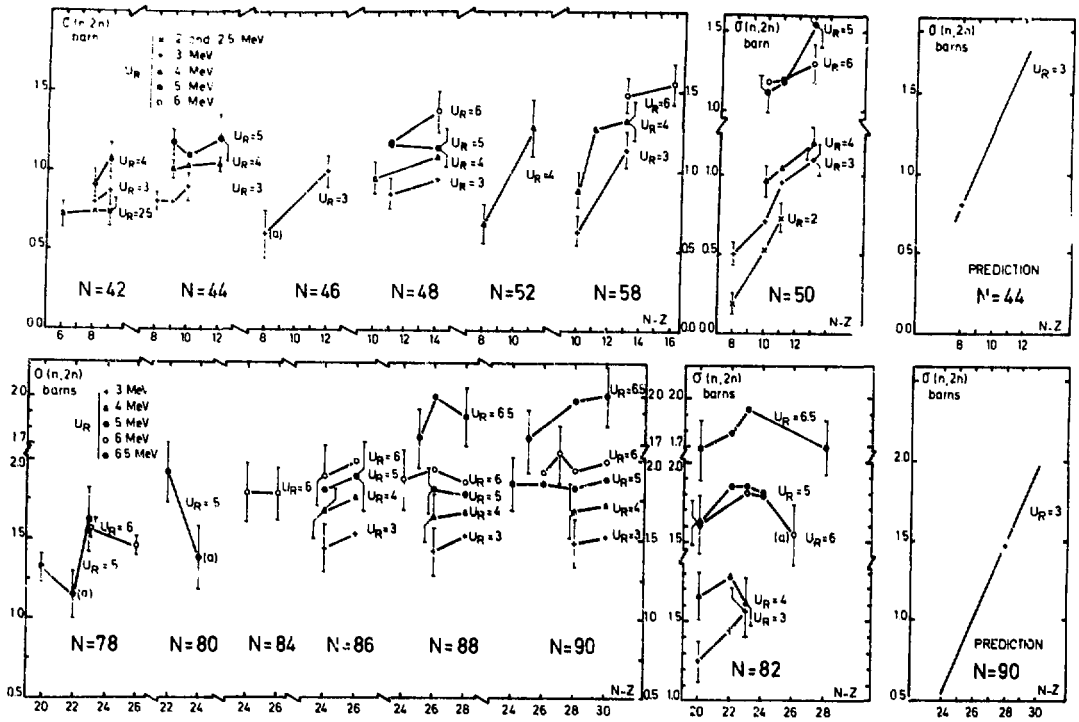

Fig.10 The (N-Z) dependence of the (n,2n) cross section at various values of the excess energy U_R for several isotones around N = 50 and N = 82. Points marked (a) were obtained from measurements to a metastable state (σ^m) to which a calculated value of σ^g was added. The extreme right of the figure shows the Csikai Petö trend calculated from expression (10) at U_R = 3 MeV for the isotones N = 44 and N = 90. Taken from [39].

It should be pointed out that simple evaporation formulae such as (6) do not allow explicitly for any (N-Z) dependence at constant U_R. When the simple energy dependence of the nuclear temperature [7]:

$$\theta = \sqrt{\frac{E_n}{a}}$$

is introduced in (6), one obtains :

$$\frac{\sigma\,(n,2n)}{\sigma\,(n,M)} = 1 - \left(1 + \frac{U_R\sqrt{a}}{\sqrt{U_R+E_{b1}}}\right)\exp\left(-\frac{U_R\sqrt{a}}{\sqrt{U_R+E_{b1}}}\right) \qquad (11)$$

The ratio $\sigma(n,2n)/\sigma(n,M)$ as given by (11) depends only on the values of U_R

and of E_{b1}, the binding energy of the last neutron in the target nucleus. On the other hand, for constant values of N, E_{b1} decreases generally with (N-Z) for (N-Z) values larger than the value corresponding to the stability valley (which is the case for most of the nuclei in fig. 10). Thus, for a given value of U_R, a simple phase space argument [39] shows that $\sigma(n,2n)/\sigma(n,M)$ should increase with (N-Z) at constant N. However quantitative calculations show that this effect accounts only for about 10% of the observed increase.

We believe that the Csikai Petö trend results rather from the behaviour of $\sigma(n,M)$, the sum of the (n,n'), (n,2n), (n,3n), etc... cross sections. Following Pearlstein [8], the (n,2n) cross section can be written as :

$$\sigma(n,2n) = \sigma_{ne} \frac{\sigma(n,M)}{\sigma_{ne}} \frac{\sigma(n,2n)}{\sigma(n,M)} \qquad (12)$$

where $\sigma(n,2n)/\sigma(n,M)$ is given by expression (6) and σ_{ne}, the nonelastic cross section, can be considered as constant in the energy range of interest here and is approximated by the empirical relation of Flerov and Talyzin [43]:

$$\sigma_{ne} = \pi (0.12 A^{\frac{1}{3}} + 0.21)^2 \qquad (13)$$

The ratio $\sigma(n,M)/\sigma_{ne}$ represents the fraction of the reaction cross section involving only neutron emission. This ratio is close to one for heavy nuclei, for which the Coulomb barrier hinders the emission of charged particles. For lighter nuclei, however, charged particle emission becomes more probable and the ratio is smaller. The ratios $\sigma(n,M)/\sigma_{ne}$ as determined by Pearlstein [8] are plotted versus (N-Z)/A in fig. 12, together with the empirical formula given by Barr et al. [44]:

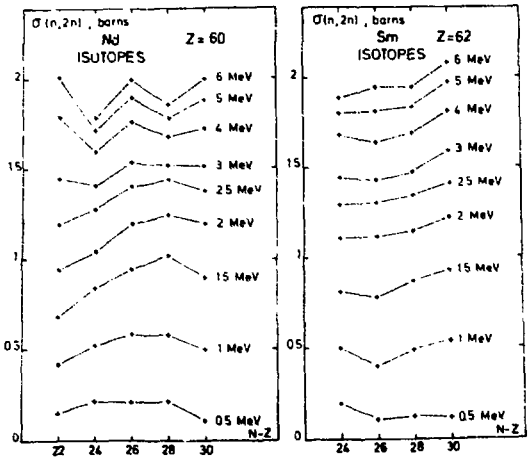

Fig. 11 The (N-Z) dependence of the (n,2n) cross section at various values of the excess energy U_R for the Nd and Sm isotopes [3].

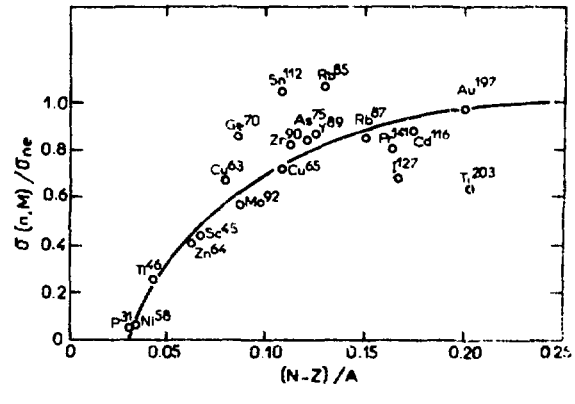

Fig. 12 Fraction of the reaction cross section involving only neutrons emission as a function of the neutron excess (N-Z)/A. Taken from [8].

$$\frac{\sigma(n,M)}{\sigma_{ne}} = 1 - 1.764 \exp\left(-18.14 \frac{N-Z}{A}\right) \qquad (14)$$

In the case of medium and heavy nuclei, the value of σ_{ne} is approximatively constant for a given set of isotones or of isotopes, according to expression (13). Also (N-Z)/A varies appreciably for the same set. As a final result $\sigma(n,M)/\sigma_{ne}$, and thus $\sigma(n,2n)$, are increasing functions of (N-Z) for a given value of N or Z and at constant excess energy U_R. Calculations according to equations (11) through (14) can account farly well for the observed increasing trend of $\sigma(n,2n)$ with (N-Z). In particular, the predicted average slope is less steep for higher values of A, in good agreement with experiment (fig. 10). It is also understandable that large deviations from the general trend may occur, since the values of $\sigma(n,M)/\sigma_{ne}$ are somewhat scattered around the average curve (fig. 12). On the other hand local effects, such as angular momentum, level density or direct inelastic scattering effects will also smear out the regularity of the predicted trend. The net result to be expected is a persistent but rather irregular increase of $\sigma(n,2n)$ with (N-Z), as shown in figs. 10 and 11.

CASCADE REACTIONS INVOLVING

CHARGED PARTICLE EMISSION

In addition to (n,2n) and (n,3n) reactions, there exist for most nuclei other cascade reactions which are energetically possible with 14-15 MeV neutrons. However these reactions involve the emission of charged particles and are generally much less probable than (n,2n) reaction for medium and heavy nuclei, because of the existence of the Coulomb barrier inhibition. Therefore, they are difficult to investigate and very little information has been published on the subject. Most of the studies in recent years have been carried out using activation techniques for cross section measurements at 14-15 MeV incident neutron energy.

The most interesting results concern the (n,n'p), (n,pn) and (n,d) reactions, which cannot be distinguished by the activation method. Lu and Fink [11] have observed that the $|(n,n'p) + (n,pn) + (n,d)|$ cross sections for the lightest stable isotope of even Z elements in the region Z = 28 to 50 are linearly related to both Z and A (fig. 13). Their observation relies on measurements on ^{58}Ni, ^{96}Ru, ^{106}Cd and ^{112}Sn. However this apparent linearity might be fortuitous, since their predicted value of ∿ 350 mb for ^{84}Sr is not confirmed by the value of 120 ± 10 mb

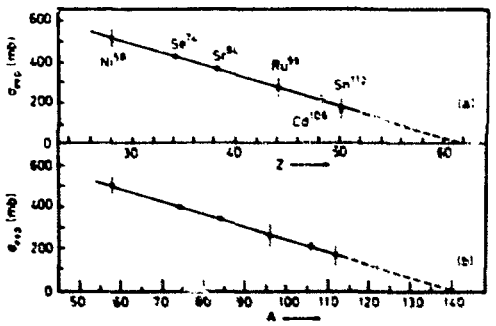

Fig. 13 The $|(n,n'p) + (n,pn) + (n,d)|$ experimental cross sections for the lightest stable isotope of even Z elements are shown. They are linearly related to (a) Z and (b) A of the target nucleus. The predicted cross sections for ^{74}Se and ^{84}Sr are also shown. Taken from [11].

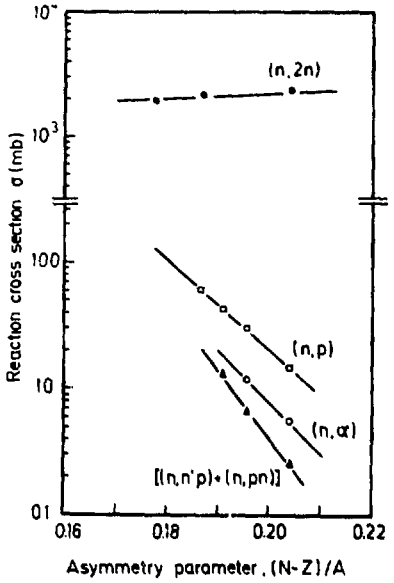

Fig.14 Trends in (n,2n), (n,p), (n,α) and [(n,n'p) + (n,pn)] reaction cross sections for isotopes of tungsten. The cross sections are plotted versus the asymmetry parameter (N-Z)/A of the target nucleus. Taken from [46].

recently measured by Qaim and Stöcklin [45].

Qaim and Graça [46] have recently measured some (n,2n), (n,p), (n,α) and [(n,n'p) + (n,pn) + (n,d)] cross sections at 14.7 MeV on tungsten isotopes. The results of their investigation are plotted on fig.14 as a function of the asymmetry parameter (N-Z)/A. The cross sections for charged particle emission are much smaller than the (n,2n) cross sections and present the well-known decreasing trend with the increasing relative neutron excess of the target nucleus, a consequence of the competition between neutron and charged particle emission. For the first time, a similar correlation is observed for the [(n,n'p) + (n,pn) + (n,d)] reaction.

Very little information is available for other reactions. Cross sections have been measured using the activation technique for the [(n,n'α) + (n,αn)] reactions [45] on ^{65}Cu, ^{70}Zn, ^{71}Ga, ^{76}Ge and ^{99}Tc. They lie in the millibarn region. The (n,2p) reaction has been investigated at 14.6 MeV by Lulic et al. [47]. They found cross sections ranging between 20 and 60μb for a set of eleven nuclei from ^{41}K to ^{139}La.

The common feature of all these cascade reactions involving charged particle emission is that the measured cross sections are generally much larger than the predictions of the evaporation model [11,47]. Thus the reactions are likely to proceed by direct interaction or preequilibrium emission. However, further experimental studies are necessary to investigate properly the reaction mechanisms.

REFERENCES

[1] J. Fréhaut and G. Mosinski, Proc. Conf. on Nuclear Cross Sections and Technology (Washington) 1975, 2, 897.

[2] J. Fréhaut and G. Mosinski, to be published in the Proc. of the National Soviet Conference on Neutron Physics (Kiev) 1975.

[3] J. Fréhaut and G. Mosinski, paper presented at the 5th International Symposium on the Interaction of Fast Neutrons with Nuclei (Gaussig, DDR) 1975.

[4] B.P. Bayhurst, J.S. Gilmore, R.J. Prestwood, J.B. Wilhelmy, N. Jarmie, B.H. Erkkila and R.A. Hardekopf, Phys. Rev. 1975, C12, 451.

[5] D.S. Mather and L.F. Pain, AWRE Report 047/69, 1969.

[6] J. Fréhaut, to be published in Nucl. Inst. and Methods 1976.

[7] J.M. Blatt and V.F. Weisskopf, Theoretical Nuclear Physics (John Wiley and Sons, New York, 1952), p. 367 ff.

[8] S. Pearlstein, Nucl. Sci. Engng. 1965, 23, 238.

[9] E. Holub and N. Cindro, Phys. Lett. 1975, 56B, 143.

[10] E. Holub, O. Bersillon, N. Cindro and J. Jary, contribution to the 5th International Symposium on the Interaction of Fast neutrons with Nuclei (Gaussig DDR) 1975.

[11] W. Lu and R.W. Fink, Phys. Rev. 1971, C4, 1173.

[12] J.R. Grover, Phys. Rev. 1962, 127, 2142.

[13] M. Bormann, H.H. Bissem, E. Magiera and R. Warnemünde, Nucl. Phys. 1970, A157, 481.

[14] P. Decowski, W. Grochulski, J. Karolyi, A. Marcinkowski, J. Piotrowski, E. Saad and Z. Wilhelmi, Nucl. Phys. 1973, A204, 121.

[15] J. Jary, Contribution to this Conference and private communication.

[16] A. Gilbert and A.G.W. Cameron, Can. J. Phys. 1965, 43, 1446.

[17] Ch. Lagrange, to be published in the proc. of the National Soviet Conference on Neutron Physics (Kiev) 1975.

[18] J.P. Delaroche, Ch. Lagrange, J. Salvy, Review Paper, IAEA Consultant Meeting, Trieste (8-12 Dec. 1975).

[19] J.J. Griffin, Phys. Rev. Lett. 1966, 17, 478.

[20] F.C. Williams, Nucl. Phys. 1971, A166, 231.

[21] M. Blann and A. Mignerey, Nucl. Phys. 1972, A186, 245.

[22] M. Blann, Nucl. Phys. 1973, A213, 570.

[23] C.K. Cline, Nucl. Phys. 1972, A186, 173 ; 1972, A193, 417 ; 1972, A195, 353.

[24] C.K. Cline and M. Blann, Nucl. Phys. 1971, A172, 225.

[25] D. Hermsdorf, S. Sassonoff, D. Seeliger and K. Seidel, J. Nucl. Energy 1973, 27, 747.

[26] P. Decowski, W. Grochulski, Report ZfK 271, 1974.

[27] K. Kikuchi and M. Kawai, Nuclear Matter and Nuclear Reactions (North Holland, Amsterdam, 1966), p. 36 ff.

[28] J. Lachkar, G. Haouat, M.T. McEllistrem, Y. Patin, J. Sigaud and F. Coçu, Proc. Conf. on Nuclear Cross Sections and Technology, Washington 1975, 2, 897.

[29] S.M. Grimes, J.D. Anderson, J.W. McClure, B.A. Pohl and C. Wong, Phys. Rev. 1971, C3, 645.

[30] H. Goldstein, Fast Neutron Physics, Part II, J.B. Marion and J.L. Fowler Eds. (Interscience Publishers, New York, 1963), p. 1525 ff.

[31] H. Jahn, C.H.M. Broeders and I. Broeders, Proc. Conf. on Nuclear Cross Sections and Technology, Washington 1975, 1, 350.

[32] D. Hermsdorf, S. Sassonoff, D. Seeliger and K. Seidel, Kernenergie 1974, 17, 259.

[33] L.H. Hansen, J.D. Andersen, P.S. Brown, R.J. Howerton, J.L. Kamenerdiener, C.M. Logan, E.F. Plechaty and C. Wong, Nucl. Sci. Engng. 1973, 51, 278.

[34] A.A. Lukyanov, O.A. Salnikov and E.M. Saprykin, Sov. J. Nucl. Phys. 1975, 21,35.

[35] M.T. McEllistrem, J. Lachkar, G. Haouat, Ch. Lagrange, Y. Patin, R.E. Shamu, J. Sigaud and F. Coçu, Proc. Conf. on Nuclear Cross Sections and Technology, Washington 1975, 2, 942.

[36] G. Haouat, J. Lachkar, Ch. Lagrange, M.T. McEllistrem, Y. Patin, R.E. Shamu, and J. Sigaud, B.A.P.S. 1975, 20, 1196.

[37] J. Csikai and G. Petö, Phys. Lett. 1966, 20, 52.

[38] Z.T. Bödy and J. Csikai, Atom. Energy Rev. 1973, 11, 153.

[39] N. Cindro and J. Fréhaut, Phys. Lett. 1976, 60B, 442.

[40] Z. Bödy INDC Report 10, 1973.

[41] E. Kondaiah, J. of Phys. 1974, A7, 1457.

[42] S.M. Qaim, Nucl. Phys. 1974, A224, 319.

[43] N.N. Flerov and V.M. Talyzin, J. Nucl. Energy 1957, 4, 529.

[44] D.W. Barr, C.I. Browne and J.S. Gilmore, Phys. Rev. 1961, 123, 859.

[45] S.M. Qaim and S. Stöcklin, Proc. 8th Symp. on Fission Technology, Noordwijkerhout (The Netherlands) 1974, EUR 5182 e, 939.

[46] S.M. Qaim and C. Graça, Nucl. Phys. 1975, A242, 317.

[47] L. Lulic, P. Strohal and I. Slaus, Nucl. Phys. 1970, A154, 273.

MF 2 - NEUTRON-INDUCED CASCADE REACTIONS - J. Fréhaut (C.E.N. Bruyères-le-Châtel, France)

Barschall (Wisconsin):

Dr. Cindro's and Dr. Fréhaut's papers are now open for discussion.

Khanna (Chalk River):

I would like to ask a question of Professor Cindro, actually, and this really concerns the fact that whether the alpha particles are pre-formed in the nucleus or not, and I find it very hard, and the reason is that the Pauli Exclusion Principle plays enormous tricks on us. I think, even if you take a look at a very simple nucleus like beryllium-8, or the first excited state of carbon-12, which almost everyone believes is essentially very much like the 3-alpha-particle state, however, if you write down the wave function and you antisymmetrize it, that wave function has very little overlap with 3-alpha particles. Now I have no idea as to what the calculation of ϕ that was shown in one of the slides implied; however, the later calculation in which one tried to include some effects of the core must be very imprecise, because I'm sure one cannot include all the ninety-four nucleons present inside the nucleus. And unless you do include all the ninety-four nucleons, I am not sure you can take into account the fact of the Pauli Principle and therefore any estimate that you will get for pre-formation has to be tremendously in excess of what it really is.

Cindro:

Was that a question or a comment? I can answer the part of your comment which appeared to be a question. I think that you are quite right in saying that the values of ϕ necessary to fit the experimental spectra by using the pre-compound model in its simplest form are quite unrealistic; I think I have said it repeatedly in the talk. As to your comment about the alpha states in light nuclei, like beryllium or carbon, I would be inclined to take it the other way around and say that from the fact that the calculations cannot reproduce the overlap of the wave functions of four nucleons that may be deduced from experiment, I would rather be inclined to look into the calculations.

Mughabghab (Brookhaven Natl. Lab.):

I ask a question of Dr. Fréhaut. What pre-equilibrium fraction was required, for example, to fit the yttrium (n, 2n) data, and did you use a constant value throughout the energy region, or did you have to vary it?

Fréhaut:

The fraction is about ten percent and it was varied, but I think on Friday there will be a presentation of the calculation in a parallel session.

Wigner (Princeton Univ.):

First, I have a very simple question which may have been answered already, but I would like to hear it once more. When you have these two or three mechanisms, is their ratio given experimentally or theoretically?

Fréhaut:

I think up to now it is experimentally. We fit the experimental spectra and

angular distributions using formulas which contain terms accounting for the different mechanisms.

Wigner:

So that when you introduce a second mechanism you give yourself the freedom of an additional constant?

Fréhaut:

Yes.

Wigner:

Thank you. You know what Poincaré said?

Cindro:

Could I perhaps elaborate on Fréhaut's interpretation? In the case that has been shown here, the direct part has been introduced as the missing part in the forward peaked angular distribution. Now, I think it would be wrong to consider that the pre-compound emission need not be forward peaked, too. In fact, I think it is; we just don't know how to calculate it. So the division between direct and pre-equilibrium is rather a very arbitrary one at this stage.

Wigner:

Arbitrary?

Cindro:

Yes, not even on the ground of experiment; this division is rather questionable both on conceptual and practical grounds.

Wigner:

Thank you. That essentially confirms. May I ask, or make a comment; I don't quite agree with the statement about the absence of alpha particles. It is true that if I take, for instance, and this I have calculated myself for the oxygen-16, the independent particle model, and think of it as four-alpha particles, the probability is very small, but the probability to find one alpha particle in it is enormously high. In fact, I think the way I remember it, two alpha particles are quite frequently present. It is a fact that the wave function of the shell model is the right one, the shell model is not far from the wave function of the alpha particle model. For closed nuclei, for nuclei like oxygen-16, probably also carbon-12, it is not.

Seeliger (Dresden):

I would like to make a comment on the question of distinction between direct and pre-equilibrium mechanisms. As it was said on Tuesday by Feshbach that they are really not different mechanisms, because the first part in the pre-equilibrium theory is a statistical treatment of a direct process in a single particle approximation, and therefore one should distinguish between direct collective interaction that is not included at all in pre-equilibrium models, and direct single particle excitations. The latter are included in the pre-equilibrium model also. But the existing models, the pre-equilibrium models,

do not explain and have no formulation for the angular distributions. And therefore, it is better to make calculations by a direct theory for the single particle direct excitation also, and take the higher terms by the existing pre-equilibrium models. I think that it is not right to say, here is one mechanism and there is another mechanism. One should have more clarity on this question. That was the first comment. The second comment is the following: Dr. Fréhaut has said that the (n, 2n) cross section in general is decreased by the presence of pre-equilibrium emission. It's not generally so. It's true in a special energy region and for a special mass number region, but there is also some other mass number region where the pre-equilibrium decay does not change the (n, 2n) cross section or even increase it. We have made a lot of systematic calculations on this point which are presented in a contributed paper. Thank you.

Cindro:

I would like to add to your first point, with which I am partly in agreement. I think it's quite clear that the collective transitions are not included. Now as to the point that direct components are included into the pre-equilibrium, that is something that has to be taken with great care since it might be misleading and in particular it might be misleading if one thinks that the first term in the pre-equilibrium is the direct part.

Wigner:

Sorry to interrupt; could you give a definition of "direct"?

Cindro:

Yes. What we mean here by "direct" is the transition matrix element in the DWBA.

Vonach (Vienna):

I'd like to support Dr. Seeliger's conclusion. I have also discussed it in detail with Weidenmüller a half year ago. The single particle part of the direct interaction is certainly contained in the usual pre-equilibrium model. This is also supported by the fact that Weidenmüller actually calculated the angular distribution of the pre-equilibrium part and he gets about the same answer as Seeliger got for his statistical DWBA characterization. So it's really identical and the first part essentially does represent the direct single particle.

Cindro:

Are you saying that the first term in the pre-equilibrium expansion is identical to the direct part?

Vonach:

It is contained. I am sure that the single particle direct is in a rough way, because the exciton model is certainly a rougher approximation that DWBA. But in a rough way it's contained.

Moldauer (Argonne):

I think this argument between you two revolves around the definition of "direct" and I think DWBA is a rather unsatisfactory definition of a reaction mechanism.

It's a theoretical approximation but not a definition, and I think the first term of the pre-equilibrium series could be a much better definition of what we mean by "direct", provided one chooses the appropriate quasi-particle basis.

Malik (Indiana Univ.):

I have a brief comment. I find it very interesting that a pre-formation probability of one-half is required to fit (n, α) data in the actinide region. I would like to note that pre-formation probability required to understand the alpha decay is about 10^{-2}.

Cindro:

(Note added to the discussion):

A part of Dr. Malik's comments refers to preliminary calculations not presented orally, but included in the paper (Faugère and Bersillon, CEN Bruyères-le-Châtel, priv. comm.) The point of these calculations is to include the possibility of complex particles being created from core nucleons also. The contribution of core nucleons is, however, reduced by an arbitrary "penalizing" factor.

Jahn (Karlsruhe):

(Note added to the discussion):

I would like to remark that one should be careful in making statements about "the pre-equilibrium model" since there are several versions due to M. Blann. Two of these versions, the so-called pure-hybrid, and the geometry-dependent-hybrid versions, claim to reproduce absolute values for the high energy tail of the angle-integrated energy distributions of the inelastic nucleon cross sections. In our "Washington paper", whose results have been mentioned by Dr. Fréhaut and Professor Feshbach, we tried to reproduce the 14-MeV ^{56}Fe (n,n') angle-integrated energy distribution of the inelastic cross section by means of the pure-hybrid model with the equidistant Fermi gas one-nucleon level density as the basis for the exciton statistic, and had obtained only a fraction of the experimental data of the Livermore group. We then found that a certain averaged experimental angular distribution of the Dresden group would be represented quite well by adding a plane-wave Born term which we consequently called a direct component. We have now very recently been able to incorporate this direct component into the pre-equilibrium description by using the so-called geometry dependent hybrid with realistic Fermi gas one-nucleon level density as the basis for the exciton statistics. The results are presented in our contributions to this conference and are in reasonable agreement with the experimental results of the Livermore and Dresden groups.

11.15 a.m., Wednesday, July 7, 1976 Invited Paper: Session MF3

NEUTRON POLARIZATION

F. W. K. Firk

Electron Accelerator Laboratory, Yale University, New Haven, Ct. 06520

RÉSUMÉ

Some recent experiments involving polarized neutrons are discussed; they demonstrate how polarization studies provide information on fundamental aspects of nuclear structure that cannot be obtained from more traditional neutron studies.

ABSTRACT

Until recently, neutron polarization studies tended to be limited either to very low energies or to restricted regions at higher energies, determined by the kinematics of favorable $(p,\vec{n})$ and $(\vec{d},n)$ reactions. With the advent of high intensity pulsed electron and proton accelerators and of beams of vector polarized deuterons, this is no longer the case. We have entered an era in which neutron polarization experiments are now being carried out, in a routine way, throughout the entire range from thermal energies to tens-of-MeV. The significance of neutron polarization studies is illustrated in discussions of a wide variety of experiments that include i) the measurement of T-invariance in the β-decay of polarized neutrons ii) a search for the effects of meson exchange currents in the photo-disintegration of the deuteron iii) the determination of quantum numbers of states in the fission of aligned ^{235}U and ^{237}Np induced by polarized neutrons and iv) the double- and triple-scattering of fast neutrons by light nuclei.

INTRODUCTION

Studies of polarization effects in nuclear reactions involving neutrons provide information of a basic nature that can be obtained only indirectly (or sometimes not at all) using traditional experimental methods. We recall the work of Adair et al[1] at Wisconsin in the early 50's in which the sign and magnitude of the nuclear spin-orbit potential was first established by studying the polarization of neutrons scattered from various nuclei.

Polarization is a consequence of interference effects between the amplitudes associated with a particular process. In neutron induced reactions, such effects can arise in many ways, for example: i) in non-resonant scattering at those energies where many different partial waves are allowed ii) from interference between certain resonant and non-resonant scattering iii) from resonance - resonance interference iv) from interference from the cumulative effect of distant levels (which may be interpreted using an optical model) v) from the presence of a spin-spin term. In photon induced reactions,[2,3] polarization effects can arise from interference between multipoles of appropriate angular momentum and parity and between photonucleon decay channels (either from different states or from an isolated state which is a superposition of base states of different relative orbital angular momentum). The results of such studies can therefore elucidate fundamental questions of nuclear structure.

Perhaps the best-known examples of the essential part played by polarization studies in Nuclear Physics involve tests of P- and T-invariance of quantum systems [4,5] and of the basic features of the nucleon-nucleon interaction.[6]

The following examples have been chosen to illustrate the wide variety of information that has been obtained in this field lately. (Several detailed reviews of neutron polarization have been given in the past [see Haeberli[7], Barschall[8] and Walter[9]]).

PRINCIPLES OF POLARIZATION

We shall limit the discussion to spin 1/2-spin 0 elastic scattering. Before scattering, the spin-part of the neutron wave function is

$$\chi_1 = \begin{pmatrix} \alpha_1^{\uparrow} \\ \alpha_1^{\downarrow} \end{pmatrix}$$

where $\alpha_1^{\uparrow}$ and $\alpha_1^{\downarrow}$ are the complex amplitudes for the spin to be "up" or "down", respectively.

After scattering (states which we label with primes), the amplitudes are changed, giving

$$\chi_1' = \begin{pmatrix} \alpha_1^{\uparrow'} \\ \alpha_1^{\downarrow'} \end{pmatrix}$$

where $\tilde{M}_1 \chi_1 = \chi_1'$

If the scattering matrix $\tilde{M}_1$ is to be invariant under rotations and reflections

(conservation of angular momentum and of parity) it must have the form[10]

$$\tilde{M}_1 = g_1 \tilde{1} + h_1 \vec{\sigma} \cdot \hat{n}_1 \qquad (1)$$

where $\tilde{1} = \begin{pmatrix} 1 & 0 \\ 0 & 1 \end{pmatrix}$, $\vec{\sigma}$ is the Pauli spin (vector) matrix

and $\hat{n}_1 = \vec{k}_1 \times \vec{k}' / |\vec{k}_1 \times \vec{k}_1'|$ is a unit vector normal to the scattering plane. Here, $\vec{k}_1$ and $\vec{k}_1'$ are the momenta before and after the (first) scattering, respectively.

We shall see that the state of polarization after the first scattering can be determined by scattering from a second nucleus of known analyzing power. This process results in yet another change in the amplitudes:

$$\chi_2' = \begin{pmatrix} \alpha_2^{\uparrow\prime} \\ \alpha_2^{\downarrow\prime} \end{pmatrix}$$

where $\tilde{M}_2 \chi_2 = \chi_2'$

and $\chi_2 = \chi_1'$

The scattering matrix $\tilde{M}_2$ has the form

$$\tilde{M}_2 = g_2 \tilde{1} + h_2 \vec{\sigma} \cdot \hat{n}_2 \qquad (2)$$

where $\hat{n}_2 = \vec{k}_2 \times \vec{k}_2' / |\vec{k}_2 \times \vec{k}_2'|$ is a unit vector normal to the second scattering plane

and $\vec{k}_2 = \vec{k}_1'$

The two planes are rotated with respect to each other by the angle ϕ, so that

$$\hat{n}_1 \cdot \hat{n}_2 = \cos \phi$$

If the initial beam is unpolarized ($< |\alpha_1^{\uparrow}|^2 - |\alpha_1^{\downarrow}|^2 > = 0$ etc.),

the differential cross section after the first scattering is

$$\frac{d\sigma_1}{d\Omega} = |g_1|^2 + |h_1|^2$$

and the state of polarization of the beam after the first scattering is

$$\frac{|\alpha_1^{\uparrow'}|^2 - |\alpha_1^{\downarrow'}|^2}{|\alpha_2^{\uparrow'}|^2 + |\alpha_1^{\downarrow'}|^2} = \left(\frac{g_1 h_1^* + g_1^* h_1}{|g_1|^2 + |h_1|^2} \right) \cos \phi \qquad (3)$$

$$= p_1 \cos \phi$$

where $\vec{p}_1 = p_1 \hat{n}_1$

The beam is seen to be polarized if $h_1 \neq 0$.

(The complex amplitudes g_1 and h_1 are called the non-spin-flip and spin-flip amplitudes, respectively. If $h_1 \neq 0$, it means that there is a non-central part to the potential (eg: a spin-orbit part)).

If this partially polarized beam is scattered a second time, the differential cross section is found to be

$$\frac{d\sigma_2}{d\Omega} = (|g_1|^2 + |h_1|^2)(1 + \vec{p}_1 . \vec{A}_2) \qquad (4)$$

where $\vec{A}_2 = A_2 \hat{n}_2$ is the analyzing power of the second scatterer

and $$A_2 = \frac{g_2 h_2^* + g_2^* h_2}{|g_2|^2 + |h_2|^2} \qquad (5)$$

therefore $$\frac{d\sigma_2}{d\Omega} = \left(\frac{d\sigma_2}{d\Omega} \right)_{unpol} (1 + \vec{p}_1 . \vec{A}_2) \qquad (6)$$

and $\vec{p}_1 . \vec{A}_2 = p_1 A_2 \cos \phi$

The method of measuring p_1 is therefore to observe the left-right symmetry, in scattering from a second target (2), in the same plane as the first reaction ie: the angle ϕ is 0 or π. In this case

$$\frac{d\sigma_2}{d\Omega} = \left(\frac{d\sigma_2}{d\Omega} \right)_{unpol} (1 \pm p_1 A_2) \qquad (7)$$

and $$\frac{d\sigma^R - d\sigma^L}{d\sigma^R + d\sigma^L} = p_1 A_2 = R . \qquad (8)$$

The sign convention is as shown [11]

[Looking down on the scattering plane]

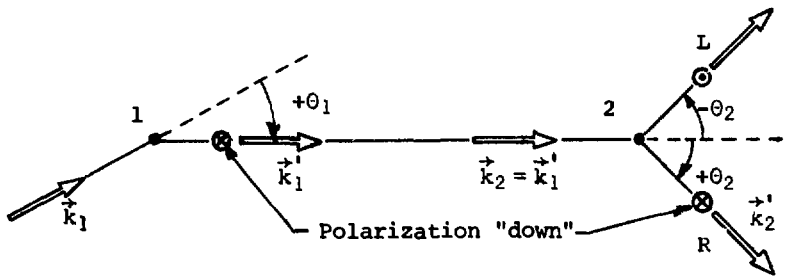

In elastic scattering, the polarization is equal to the analyzing power (p=A).

In order to measure p_1, we require a measurement of R and of A_2 (= p_2).

Application of the above principles will be presented in later sections.

In this brief outline, we have not used the general methods involving the density matrices of the unscattered and scattered beams. Such an approach becomes most useful in those experiments involving more complex spin configurations. The general principles are presented and illustrated in detail by Welton.[12]

TESTS OF FUNDAMENTAL SYMMETRIES

A TEST OF T-INVARIANCE IN THE β-DECAY OF POLARIZED NEUTRONS

A greatly improved experimental upper limit for D, the triple-correlation coefficient in the β-decay of the polarized free neutron, has recently been reported by Steinberg et al.[13] This coefficient appears in the expression for the decay rate in the form[14]

$$D\vec{P}_n \cdot (\vec{p}_e \times \vec{p}_{\bar{\nu}}) / E_e E_{\bar{\nu}} \qquad (9)$$

Here, $\vec{P}_n$ is the neutron polarization and $\vec{p}_e$, $\vec{p}_{\bar{\nu}}$, E_e and $E_{\bar{\nu}}$ are the momenta and energies of the leptons. This expression is odd under time reversal; a non-zero value of D therefore implies a breakdown of T-invariance. The value obtained by Steinberg et al. is

$$D = -(1.1 \pm 1.7) \times 10^{-3}$$

which is consistent with T-invariance. The quoted error is largely statistical and is based upon the observation of 5×10^6 events. The phase angle ϕ between the coupling constants g_V and g_A is

$$\phi = 180.14 \pm 0.22^{o}$$

In neutron β-decay, the Coulomb interaction is the only important final state interaction and its contribution to D vanishes in a pure V-A theory. Possible weak magnetism effects contribute less than 2×10^{-5}.

The experiment was carried out at the high flux reactor at Grenoble. The cold neutrons had a mean velocity of 1100 m/s and they were polarized by a magnetized curved guide; their mean polarization was (70 ± 7)%. The beam intensity leaving the polarizer was 10^{9} neutron/s and its profile was 5 cm high by 0.6 cm wide. The neutron polarization vector was turned into the beam direction and was periodically changed to be either parallel or anti-parallel to the momentum vector of the neutron.

The magnitude of the neutron momentum may be neglected so that the term (9) can be rewritten

$$D\vec{P}_n \cdot (\vec{p}_p \times \vec{p}_e) / E_e E_\nu \qquad (10)$$

where $\vec{p}_p$ is the momentum of the recoil proton. The experimental geometry was chosen to maximize the triple product as shown.

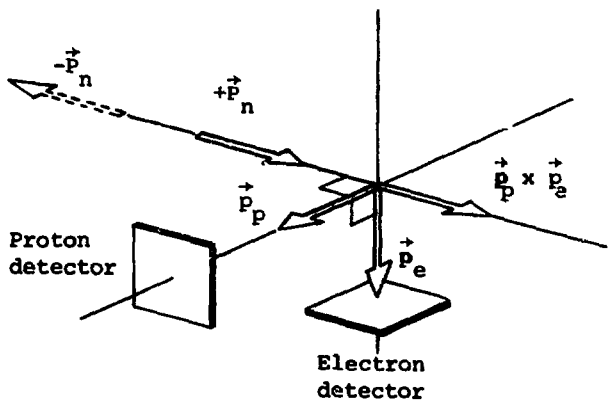

The electrons were detected in a conventional plastic scintillator biased to accept electron energies between 100 and 500 keV. The recoil protons were accelerated to 20 keV and counted in a thin (4000 Å) layer of NaI(Tl). Sixteen time-delayed spectra of coincidences between electron and proton (4 electron detectors, 4 proton detectors and two directions of the incident neutron polarization vector) were recorded. The data were collected during a 2½-month period.

NEUTRON POLARIZATION EFFECTS IN TWO- AND THREE-NUCLEON SYSTEMS

New experiments on $\vec{n}$ - p and $\vec{n}$ - d elastic scattering have been reported recently and all of them are at the forefront of experimental technique. A particularly innovative experiment is that of Brooks and Jones[15,16] whose method opens up interesting possibilities in studies of $\vec{n}$ - p and $\vec{n}$ - d reactions at energies above a few MeV. Before presenting some of their results, a few comments on their method will be useful. In 1964, Tsukada and Kikuchi[17] demonstrated that the scintillation decay of an anthracene crystal excited by 3.7 MeV protons is direction-dependent, relative to the crystal axes. They showed that the fast component is more direction-dependent than the slow component. Brooks and Jones carried out a detailed study of this effect in many different scintillators and, in the course of this work, they invented a new polarimeter suitable for studies of $\vec{n}$ - p and $\vec{n}$ - d interactions. Consider a neutron incident at an angle α with respect to an axis c', normal to an (a,b) plane in the crystal:

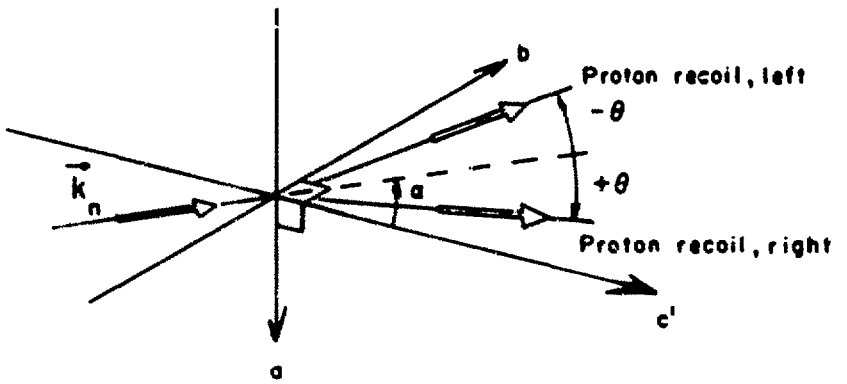

For a proton that recoils through an angle (-θ) towards the b-axis, the values of the integrated light output $\mathcal{L}(-\theta)$ and of the ratio of the slow- to total-light component $\mathcal{S}(-\theta)$ are different from the values obtained when a proton recoils through an angle (+θ) towards the c'-axis. In general,

$$\mathcal{L}(-\theta) < \mathcal{L}(+\theta)$$

and

$$\mathcal{S}(-\theta) > \mathcal{S}(+\theta)$$

The measured two-parameter $(\mathcal{L},\mathcal{S})$ data can be analyzed to give the left-right asymmetry in $\vec{n}$-p scattering[18] in an anthracene crystal ($C_{14}H_{10}$) and in $\vec{n}$-d scattering[19] in a deuterated crystal. The $\vec{n}$-d results at neutron energies of 16.4 and 21.6 MeV are shown in Fig. 1.

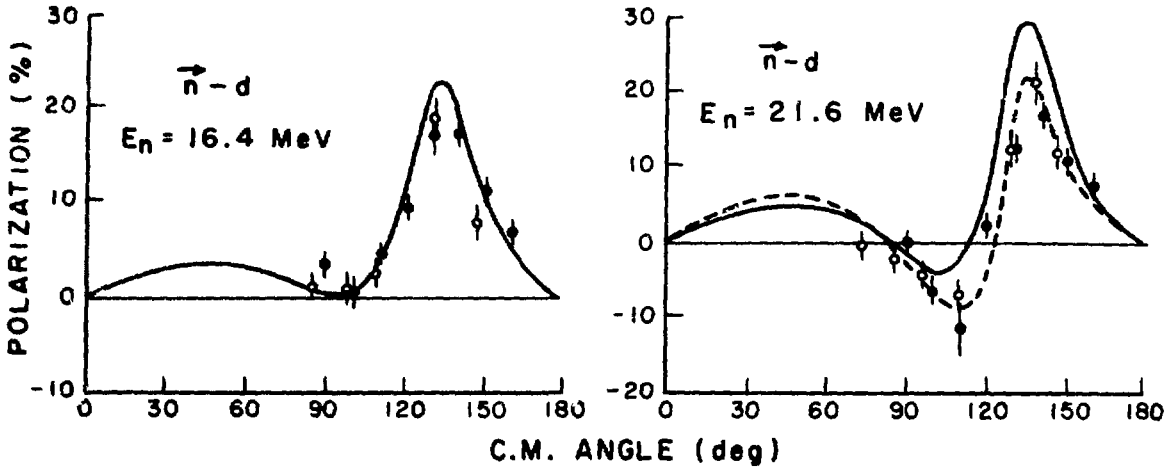

Fig. 1. The $\vec{n}$-d results, at two energies, obtained by Steinbock et al [19] and Morris et al [20] [open circles] compared with the calculations of Pieper [21] [solid curve] and with the p-d measurements [22] [dashed curve].

The work of Morris et al [20] is also shown together with the theoretical calculations of Pieper [21], and with the general trend of the $\vec{p}$-d measurements (the dashed curve). [22] No measurable difference is observed between the polarized neutron and proton induced reactions at these energies. The present status of 3-body theory is discussed in a recent review by Doleschall. [23]

In a demanding experiment, Johnsen et al [24] [see also the contribution to this conference [25]] have measured the spin correlation parameter A_{yy} in $\vec{n}$-$\vec{p}$ scattering at 50 MeV. Their apparatus is shown schematically in Fig. 2.

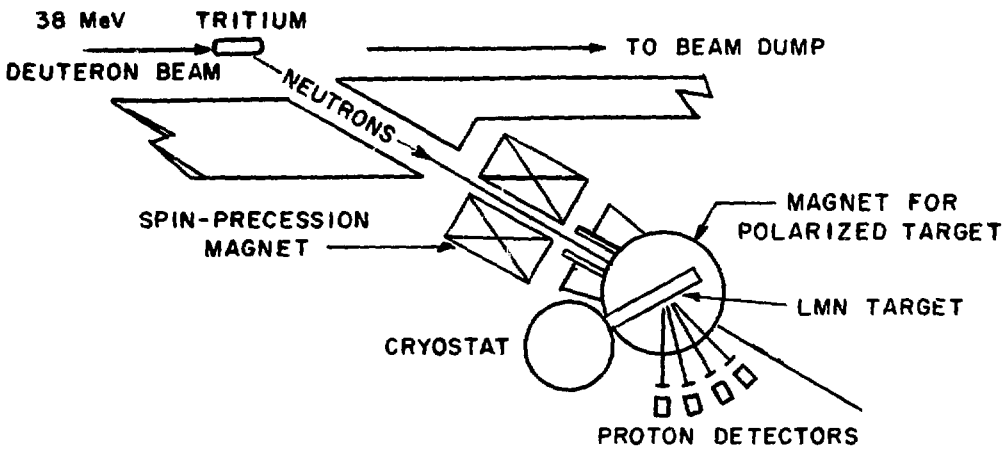

Fig. 2. An arrangement for stydying the spin correlation parameter, A_{yy}, in $\vec{n}$-$\vec{p}$ scattering at 50 MeV. [24]

The partially polarized beam from the T-d reaction, is scattered from an aligned LMN proton target. The incident spin direction can be changed with a solenoidal field. Their results are shown in Fig. 3 where they are compared with the

parameters of a recent analysis.[26]

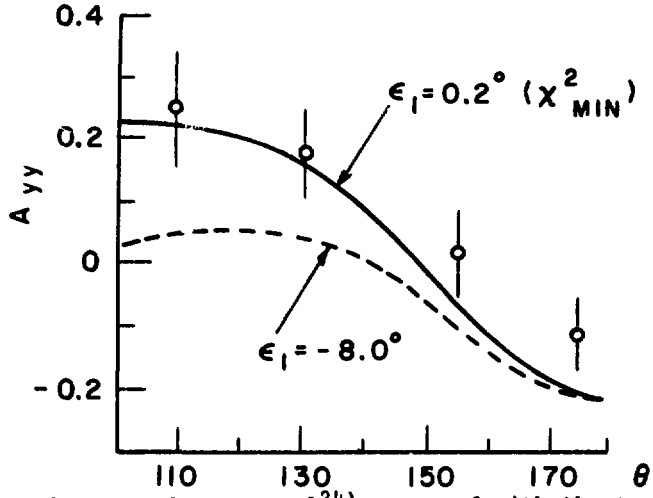

Fig. 3. The results of Johnsen et al[24] compared with the two possible values of ϵ_1 (≈0 or -8°), that gave equally good fits to all n-p data at 50 MeV prior to the present work.[26]

Neutron triple scattering experiments are notoriously difficult. However, they can provide unique information on the interaction and therefore it is important that they should not be overlooked in future research programs. Ahmed et al[27] have carried out a measurement of the depolarization parameter D(θ) in $\vec{n}$-d scattering at low energy [see also the contribution to this conference[28]]. Their method is outlined in Fig. 4.

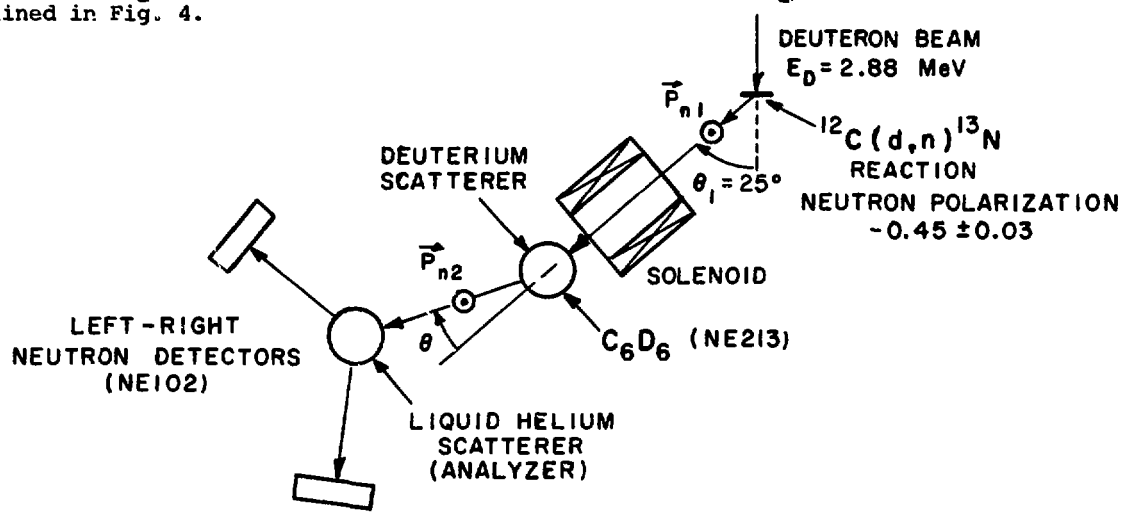

Fig. 4. Apparatus for an $\vec{n}$-d triple-scattering study reported by Ahmed et al.[27]

Their results are compared with theory in Fig. 5.

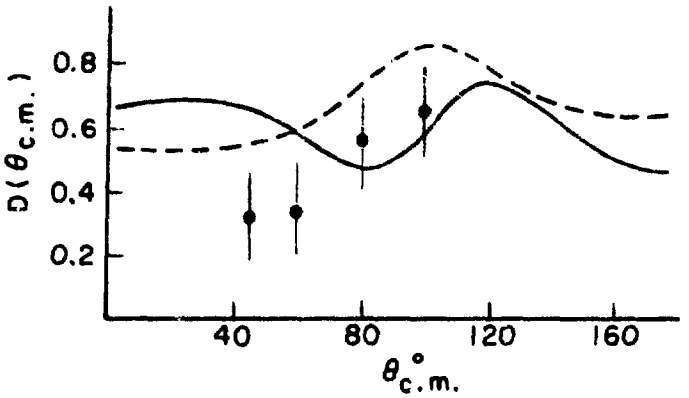

Fig. 5. The results of Ahmed et al[27] compared with two parameterizations of the ERA model.

Clearly, more work remains to be done both experimentally and theoretically before this basic interaction is sufficiently well-understood, even at these low energies.

An important new technique for producing polarized neutrons, particularly in the energy range 10 to 20 MeV, uses the polarization transfer mechanism in $\vec{D}(\vec{d},\vec{n})$ and $\vec{T}(\vec{d},n)$ reactions at forward angles.[29] Walter and his colleagues at Duke University have recently reported measurements on $(n,\vec{p})$ scattering at 90° (c.m.) for neutron energies of 13.5 and 16.0 MeV using the $D(\vec{d},\vec{n})$ reaction as a source.[30] Their results set new standards of precision in neutron polarization studies in the difficult energy region under study; typical statistical accuracy reported is 0.001. Their results are systematically smaller than the LRL$\bar{X}$ predictions but are consistent with values calculated with the new phase shifts of Arndt et al.[31]

THE DOUBLE-SCATTERING OF FAST NEUTRONS BY LIGHT NUCLEI

For many years, neutron double-scattering experiments were not considered practicable [32,33] and the first n-^{4}He double-scattering experiment reported[34] did not change the general view. However, in 1972, a program of studies of the polarization of neutrons scattered from light nuclei was successfully initiated at the Yale Electron Accelerator Laboratory, using the double-scattering technique.

The method involves the polarization of an unpolarized flux of neutrons by elastic scattering from ^{12}C. The polarization of the flux scattered at a given angle is measured using true double-scattering in which the polarized flux is scattered again from an identical ^{12}C target at an identical scattering angle. The asymmetry in the doubly scattered flux is measured and, after taking into account the (known) energy-loss at the first scattering, the results are analyzed to give the absolute polarization p of the flux.[35,36] Having established the polarization of the source, the analyzing powers of other nuclei can be obtained by replacing the second scatterer with an appropriate target.[37,38,39]

The initial flux of unpolarized neutrons is generated via the (γ,n) reaction in a heavy nucleus and therefore the spectrum is Maxwellian with a maximum intensity at an energy of about 1 MeV. The intensity decreases rapidly at energies above 5 MeV; this is a necessary feature in making measurements of polarization that results from elastic scattering of neutrons in light nuclei. The neutron energies are measured with good resolution (typically 0.7 ns.m^{-1}). A generalized neutron spin-precession method is used that is well-suited to a continuous energy spectrum of neutrons; this method greatly reduces the systematic errors that would otherwise occur in the experiment.[40,41]

A typical layout of the experiment when used to measure the analyzing power of a light nucleus is shown in Fig. 6. Here, the first reaction angle is 50° and the second scatterer is a cylinder of liquid helium viewed by an array of fast neutron detectors. The observed (source) polarization of neutrons, obtained in a true n-^{12}C double-scattering experiment, is shown in Fig. 7.

The essential points in obtaining the analyzing power when using the generalized spin-precession solenoid are:

The integrated magnetic field required to precess a neutron of measured energy E_π through 180° is

$$\int H.d\ell = 2.37 \times 10^5 \times \sqrt{E_\pi(\text{MeV})} \quad \text{Oe-cm}$$

and the angle of precession, ϕ, of a non-relativistic neutron of measured energy E_ϕ is

$$\phi = \pi\sqrt{E_\pi/E_\phi}$$

The product of the polarization p of the source and the analyzing power A of the second scatterer is

$$pA = \pm(1-R_\pm)/(R_\pm - \cos\phi)$$

where + and - refer to the right and left detector, respectively and

$$R_\pm = \left[N_\pm(H)/N_\pm(0)\right]\left[C(0)/C(H)\right]$$

where $N_\pm(H)$ and $C(H)$ are the corresponding detector count rates and monitor count rate with the field on and $N_\pm(0)$ and $C(0)$ the corresponding rates with the field

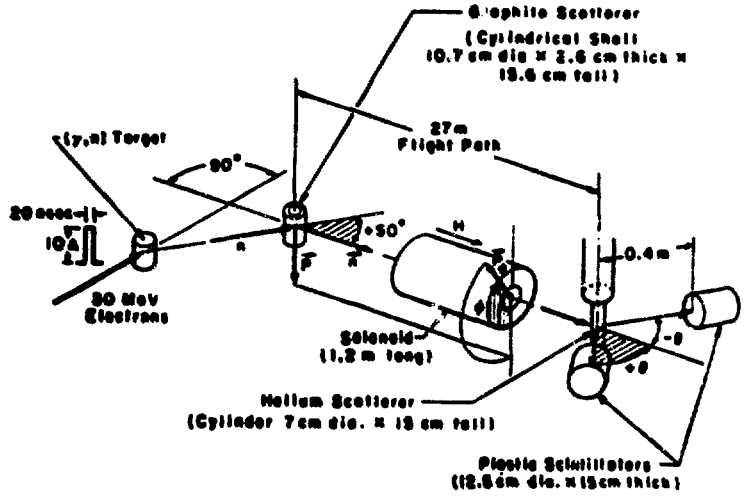

Fig. 6. Schematic diagram of the neutron double-scattering arrangement.

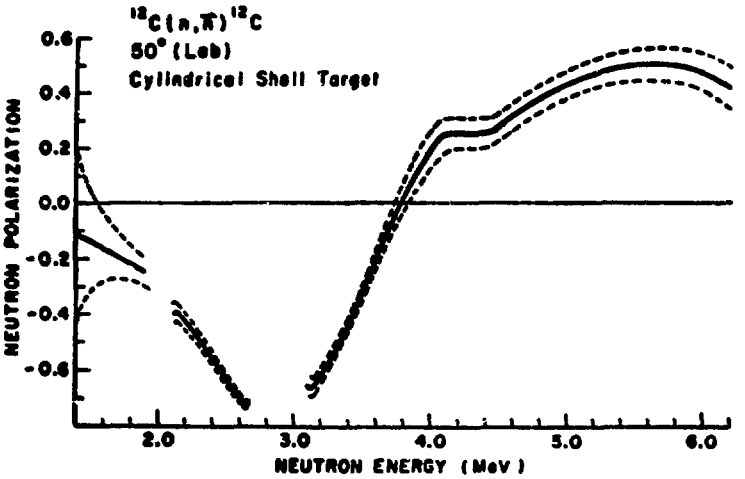

Fig. 7. The observed polarization for neutrons scattered from the graphite target at 50° (lab).

off. It is now straightforward to deduce pA independently of the monitor rates.[41]

Phase-shift and R-matrix Analyses

The measured polarizations were analyzed using iterative grid search techniques to give definitive sets of phase-shifts and R-matrix parameters. The inclusion of partial waves higher than d-waves did not alter the quality of the fits significantly. Expressions for the differential cross section, polarization and total cross section used are:

$$\sigma(\theta) = (1/k^2)\sum_{L=0}^{4} B_L P_L(\cos\theta)$$

$$\sigma(\theta)p(\theta) = (1/k^2)\sum_{L=1}^{4} C_L \bar{P}_L^1(\cos\theta)$$

$$\sigma_T = (4\pi/k^2)\sum_{L=0}^{2}\left[\ell\sin^2\delta_\ell^- + (\ell+1)\sin^2\delta_\ell^+\right]$$

where $P_L(\cos\theta)$ and $\bar{P}_L^1(\cos\theta)$ are the Legendre and associated Legendre polynomials. Values for the expression B_L and C_L in terms of phase-shifts have been derived by Blatt and Biedenharn and Simon and Welton.[42,43]

The elastic scattering of neutrons from spin-zero nuclei is the simplest application of R-matrix theory.[44,45] Only one channel is open so that

$$R_{\ell J} = \sum_\lambda \gamma^2_{\lambda\ell J}/(E_{\lambda\ell J}-E)$$

where $\gamma^2_{\lambda\ell J}$ and $E_{\lambda\ell J}$ are the reduced widths and energies, and the states are denoted by λ, and also

$$R_{\ell J} = (f_\ell - B_{\ell J})^{-1};\ f_\ell(E) = a u_\ell^{-1}(a)(du_\ell/dr)_a$$

where a is the channel radius, u_ℓ is the radial part of the wave function and $B_{\ell J}$ is the boundary condition. The collision function $U_{\ell J}$ can be expressed in terms of a single, real phase-shift, $\delta_{\ell J}$ thus

$$U_{\ell J} = \exp(2i\delta_{\ell J})$$

The phase-shifts are related to the R-function as follows

$$\delta_{\ell J} = -\phi_\ell + \arctan\{P_\ell R_{\ell J} / [1 - R_{\ell J}(S_\ell - B_{\ell J})]\}$$

where S_ℓ, P_ℓ and ϕ_ℓ are the well-known shift function, penetrability, and hard-sphere phase-shift. We define the resonance energy E_R as the energy at which the resonant phase-shift is an odd integral multiple of $\pi/2$. The width of the resonance is

$$\Gamma_{\lambda\ell J} = 2P_\ell \gamma^2_{\lambda\ell J}$$

Distant levels are taken into account using the method given in Ref. 46, i.e.

$$R^{\infty}_{\ell J} = R_{O\ell J} + R_{\ell J} E$$

A fit was made to the polarization measurements by minimizing the quantity

$$S = \sum_{j=1}^{M} \sum_{i=1}^{N} \frac{\left[p_{cal}(\theta_i, E_j) - p_{exp}(\theta_i, E_j)\right]^2}{\left[\Delta p(\theta_i, E_j)\right]^2}$$

where N is the number of angles (between 4 and 9, depending on the experiment) and M is the total number of energy points used. The optimum R-matrix parameters derived from this procedure, were used to predict the differential and total cross sections, and additional polarizations throughout the entire energy range up to about 5 MeV.

Details of the analysis of the polarization data in the case of $\vec{n}$-^{6}Li scattering are given in a recent paper.[47] This is a complex problem because the target nucleus no longer has spin zero and the (n,α) channel must be properly taken into account. Examples of the measurements and of the analyses of the neutron double-scattering program reported above are shown in Fig. 8. (the observed asymmetry in $^{12}\vec{C}(50^{\circ})$ - ^{4}He(60°) scattering[39]), in Fig. 9. (the phase-shift analysis of the ^{16}O$(\vec{n},n)^{16}$O reaction, measured at nine angles between 1 and 4 MeV) and in Fig. 10 (the total scattering cross section predicted from an analysis of the polarization data for the $^{16}\vec{O}(n,n)^{16}$O reaction[38]).

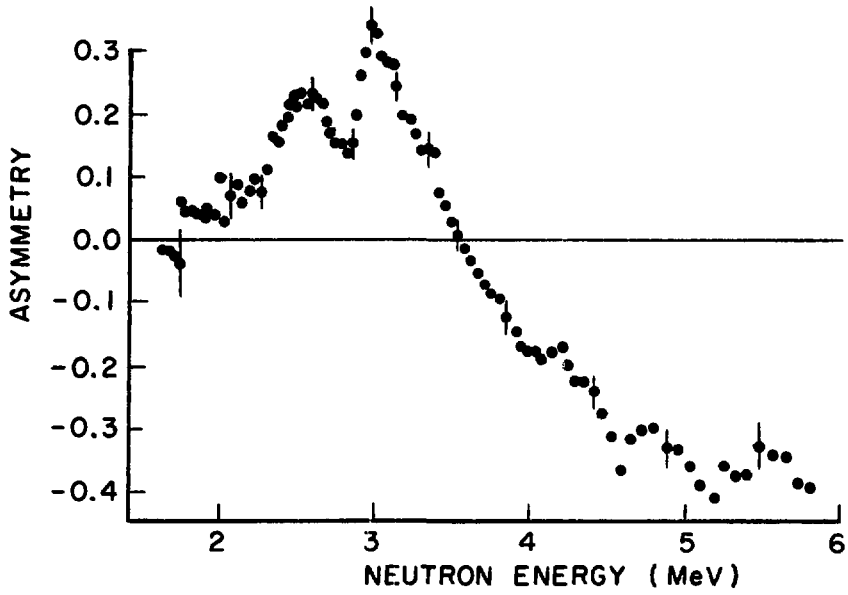

Fig. 8. The observed asymmetry product for ^{12}C(50°) - ^{4}He(60°) neutron double-scattering.[39]

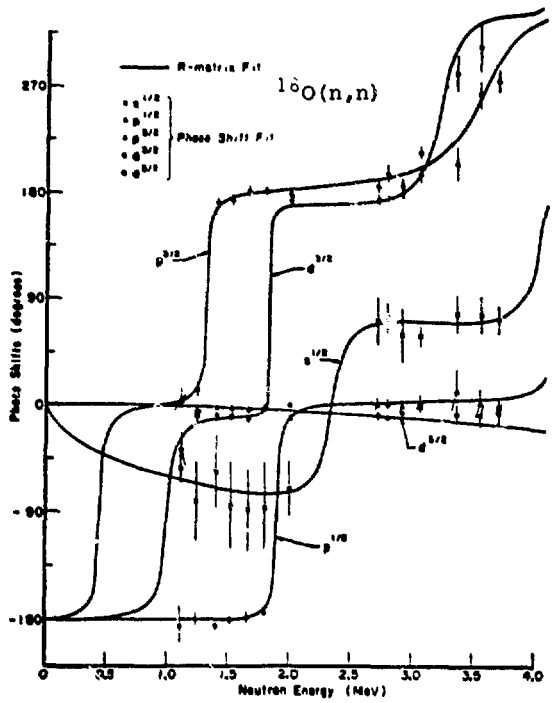

Fig. 9. Phase shifts resulting from the analysis plotted in the first and fourth quadrants. The continuous curve is the *R*-matrix fit while the discrete points are the result of the phase-shift analysis.

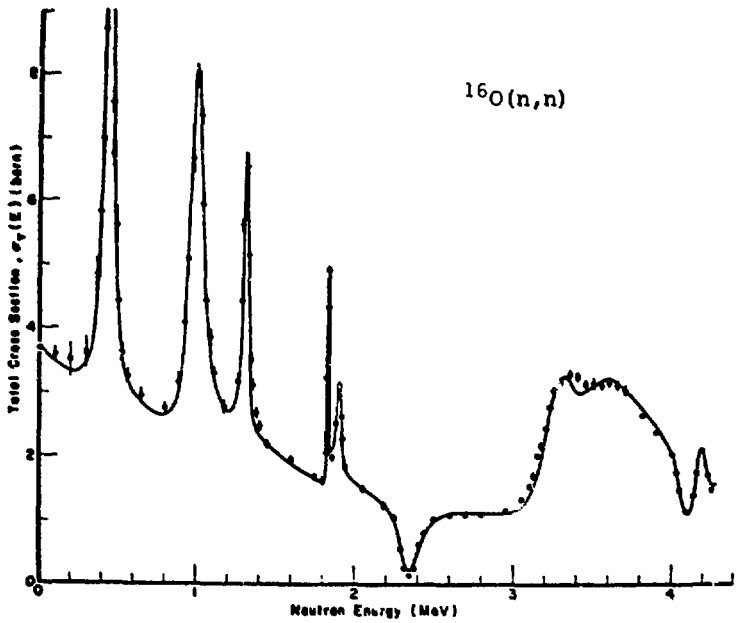

Fig. 10 The *R*-matrix prediction of the total cross section.

THE TRANSMISSION OF POLARIZED NEUTRONS THROUGH POLARIZED TARGETS

Although it has been known for many years that the measurement of the transmission of polarized neutrons through a polarized target can give the values of the spins of low energy (s-wave) resonances directly, few such measurements have been performed.[48,49,50] This situation is somewhat surprizing in view of the well-established low temperature techniques that form the basis for producing polarized proton targets (the polarizers) and polarized targets. There is, however, one outstanding example of the method, due to Keyworth et al[50] who measured the spins of many resonances in $^{237}Np + n$ and $^{235}U + n$; their work will be discussed in the hope that it may encourage others to take advantage of this powerful technique.

If a beam of polarized neutrons (polarization p_n) is passed through a polarized target (polarization p_T) and the directions of the vectors $\vec{p}_n$ and $\vec{p}_T$ are parallel, then the transmission $T_J^{\uparrow\uparrow}$ is given by[51]

$$T_J^{\uparrow\uparrow} = e^{-n\sigma_J} \{\cosh(\rho_J p_T n\sigma_J) - p_n \sinh(\rho_J p_T n\sigma_J)\}$$

where n is the number of nuclei/cm^2 in the target, σ_J is the unpolarized cross section and

$$J = I \pm 1/2,$$

is the spin of the resonance, and I is the target spin.

If we write $J_+ = I + 1/2$ and $J_- = I - 1/2$, the values of ρ_J are

$$\rho_{J_+} = I/(I+1) \text{ and } \rho_{J_-} = -1$$

The transmission $T_J^{\uparrow\downarrow}$, corresponding to the vectors $\vec{p}_n$ and $\vec{p}_T$ being anti-parallel, is

$$T_J^{\uparrow\downarrow} = e^{-n\sigma_J} \{\cosh(\rho_J p_T n\sigma_J) + p_n \sinh(\rho_J p_T n\sigma_J)\}$$

For a $J_+ = I + 1/2$ state, the difference in transmission for parallel and anti-parallel polarization vectors is therefore

$$T_{J_+}^{\uparrow\uparrow} - T_{J_+}^{\uparrow\downarrow} = \Delta T_{J_+} = -2\, p_n e^{-n\sigma_{J_+}} \cdot \sinh\left[\left(\frac{I}{I+1}\right) p_T n\sigma_{J_+}\right] \qquad (11)$$

which is always negative.
If, however, a state has $J_- = I - 1/2$, the difference in transmission is

$$T_{J_-}^{\uparrow\uparrow} - T_{J_-}^{\uparrow\downarrow} = \Delta T_{J_-} = +2p_n e^{-n\sigma_{J_-}} \cdot \sinh\left[p_T n\sigma_{J_-}\right] \qquad (12)$$

which is always positive.

Keyworth et al [50] used a high intensity, unpolarized, pulsed neutron beam from ORELA and obtained a polarized neutron beam by passage through a polarized LMN target ($p_n = 0.55$). The direction of the vector $\vec{p}_n$ could be reversed with a magnetic field. The transmission of this beam through a polarized ^{237}Np (or ^{235}U) target ($p_T = 0.2$) was measured for the two incident polarization directions. In addition, the yield of fast fission neutrons was measured in an array of detectors around the (second) polarized target. The clear-cut determination of resonance spins in $^{237}Np + n$, using Eqs. (11 and 12) is shown in Fig. 11 (In this case, I = 5/2, therefore $J_+ = 3$ and $J_- = 2$)

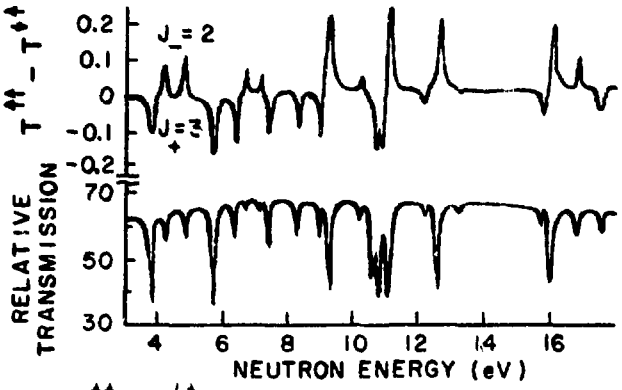

Fig. 11. Values of $T^{\uparrow\uparrow} - T^{\uparrow\downarrow}$ and the relative transmission for $^{237}Np + n$ showing the clear-cut determination of the resonance spins.[50]

A most interesting conclusion from their experiment is that the fine-structure resonances in a given intermediate-structure group in the fission yield have the same spin.

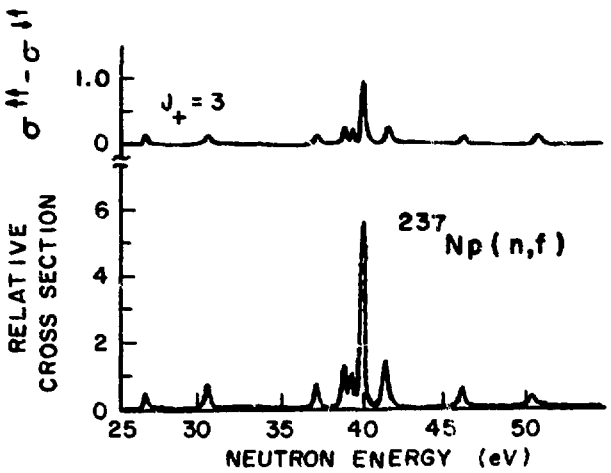

Fig. 12. Measurement of the spins of resonances in the fission of ^{237}Np in the vicinity of the intermediate structure at 40 eV.[50]

NEUTRON POLARIZATION EFFECTS IN NUCLEAR PHOTO-DISINTEGRATION

The shell model forms the basis of nuclear structure theory so that any attempt to provide a more quantitative understanding of the model is a matter of fundamental importance. The interaction between photons and nuclei affords a sensitive probe of certain features of nuclear structure. At photon energies below about 30 MeV, the interaction is predominantly electric dipole in character, so that the incident photon only excites a limited number of states which have the correct spins and parities (consistent with the addition of one unit of angular momentum and a change in parity). The following qualitative description of the photon-nucleus interaction illustrates the major points of the problem. Consider a light nucleus with a ground state configuration which is well-described by the shell model. The most straightforward examples are those nuclei which have closed shells of neutrons and protons eg: ^{16}O, ^{40}Ca and ^{208}Pb.

An E1 photon excites a nucleon into a higher energy state; if the photon energy E_γ is sufficiently high then the nucleon becomes unbound and is emitted (in light nuclei, $E_\gamma \gtrsim 15$ MeV for neutron emission to occur). A 1 particle -1 hole (1p-1h) state is thereby created; in the case of E1 absorption in ^{16}O, five such 1p-1h states are possible. The final "electric dipole states" Ψ_D^* are considered to be linear combinations of the five base states:

$$\Psi_D^* \propto \sum_{i=1}^{5} c_i \phi_i$$

If the combination happens to be coherent then a strong transition will be observed. In ^{16}O, there are two such transitions which, between them account for more than 90% of the total dipole absorption strength. These states, at 22 and 25 MeV were predicted, in a calculation of this type, by Elliott and Flowers[52] in 1957 and were subsequently observed in the reactions $^{15}N(p,\gamma_0)^{16}O$, $^{16}O(e,e',p_0)^{15}N$, and $^{16}O(\gamma,n_0)^{15}O$ between 1959 and 1962.

A signigicant test of the shell model used in the Elliott-Flowers calculation requires a determination of the amplitudes c_i which are associated with the five base states. It will be shown that it is not possible to answer these questions simply by measuring the angular distributions of the outgoing photonucleons - a measurement of their differential polarizations is also necessary.

In general, the angular distribution of the photonucleons is of the form:

$$\frac{d\sigma}{d\Omega} = \sum_{L=0}^{N} A_L P_L (\cos\theta)$$

where $P_L(\cos\theta)$ is the Legendre polynomial of order L and N is the maximum allowed value of L (consistent with the conservation of angular momentum).

In the present case of E1 absorption in ^{16}O, the differential cross section for photoneutrons emitted to the ground state of ^{15}O has the form:

$$\frac{d\sigma}{d\Omega} = \frac{3}{16}\pi_\gamma^2 \{2(a_s^2 + a_d^2) + (2\sqrt{2}\, a_s a_d \cos\Delta_{sd} - a_d^2) P_2(\cos\theta)\} \qquad (13)$$

Here, a_s and a_d are the real magnitudes of the s^- and d^- wave emission amplitudes respectively and $\Delta_{sd} \equiv \delta_s - \delta_d$, where δ_s and δ_d are their respective phases. The only reaction matrix elements which contribute in this case are:

$$\langle \ell = 0,\ s = 1,\ \alpha' | R^{1-} | E1\alpha \rangle \equiv a_s e^{i\delta_s} \qquad (14)$$

and $$\langle \ell = 2,\ s = 1,\ \alpha' \left| R^{1^-} \right| E1\alpha \rangle \equiv a_d e^{i\delta_d} \qquad (15)$$

where s is the channel spin and α,α' specify the ground state ($J^\pi = 0^+$) and excited states ($J^\pi = 1^-$) respectively. The coefficients, A_L are given by:

$$A_o \sim a_s^2 + a_d^2$$

and

$$A_2 \sim (a_s a_d \cos\Delta_{sd} - a_d^2)$$

Now $4\pi A_o$ is the total cross section and is insensitive to interference effects between the different components (the $\ell = 0$ and $\ell = 2$ partial waves associated with the outgoing nucleons). Although the A_2 - coefficient contains an interference term, it is nonetheless finite if the state only emits d-wave ($\ell = 2$) nucleons. The differential polarization of photonucleons has the form

$$\frac{d\vec{P}}{d\Omega} = \hat{k} \sum_{L=1}^{N} B_L \bar{P}_L (\cos\theta) \qquad (16)$$

where $\hat{k}$ is a unit vector normal to the scattering plane and $\bar{P}_L(\cos\theta)$ is the associated Legendre polynomial. The significant difference between the expressions for the angular distribution and polarization of photonucleons is the absence of the $L = 0$ term in the summation in Eq. (16). This reflects the fact that any polarization produced is due to interference effects between different channels. In the present example, it is found that:

$$\frac{d\vec{P}}{d\Omega} = k\lambda^2_\gamma (0.205\ a_s a_d \sin\Delta_{sd})\ \bar{P}_2^1(\cos\theta) \qquad (17)$$

which shows that the differential polarization is zero (for all values of θ) if either $a_s = 0$ or $a_d = 0$.

Another important point emerges from the expression for $d\vec{P}/d\Omega$ given in Eq. (17): the associated Legendre function of second order is:

$$\bar{P}_2^1(\cos\theta) = -\sqrt{\frac{15}{16}} \sin 2\theta \qquad (18)$$

which means that, at a reaction angle of $\theta = 90^o$, the polarization $d\vec{P}/d\Omega = 0$. Conversely, the appearance of any polarization at $\theta = 90^o$ is clear evidence of the intrusion of M1 or E2 multipoles in the absorption process.

With these points in mind, three groups[53,54,55] have measured the polarization of photoneutrons from a number of nuclei at appropriate angles. The most recent work involves studies of the reactions $d(\gamma,\vec{n})p$ [56], $^{16}O(\gamma,\vec{n}_o)^{15}O$ [57] and $^{208}Pb(\gamma,\vec{n})^{207}Pb$ [58], using the method developed at Yale in which an intense pulsed source of electrons produces a bremsstrahlung photon spectrum (in a tungsten converter) with a maximum energy set to avoid exciting non-ground state transitions in ^{16}O and ^{208}Pb. The neutron energies are determined with good resolution (<1 ns.m^{-1}) and the neutron polarization determined by measuring the left-right asymmetry in scattering from a suitable light nucleus (^{24}Mg at neutron energies between 0.1 and 0.5 MeV, ^{16}O between 0.3 and 1.5 MeV, ^{12}C between 1 and 10 MeV and ^4He between 1 and 20 MeV).

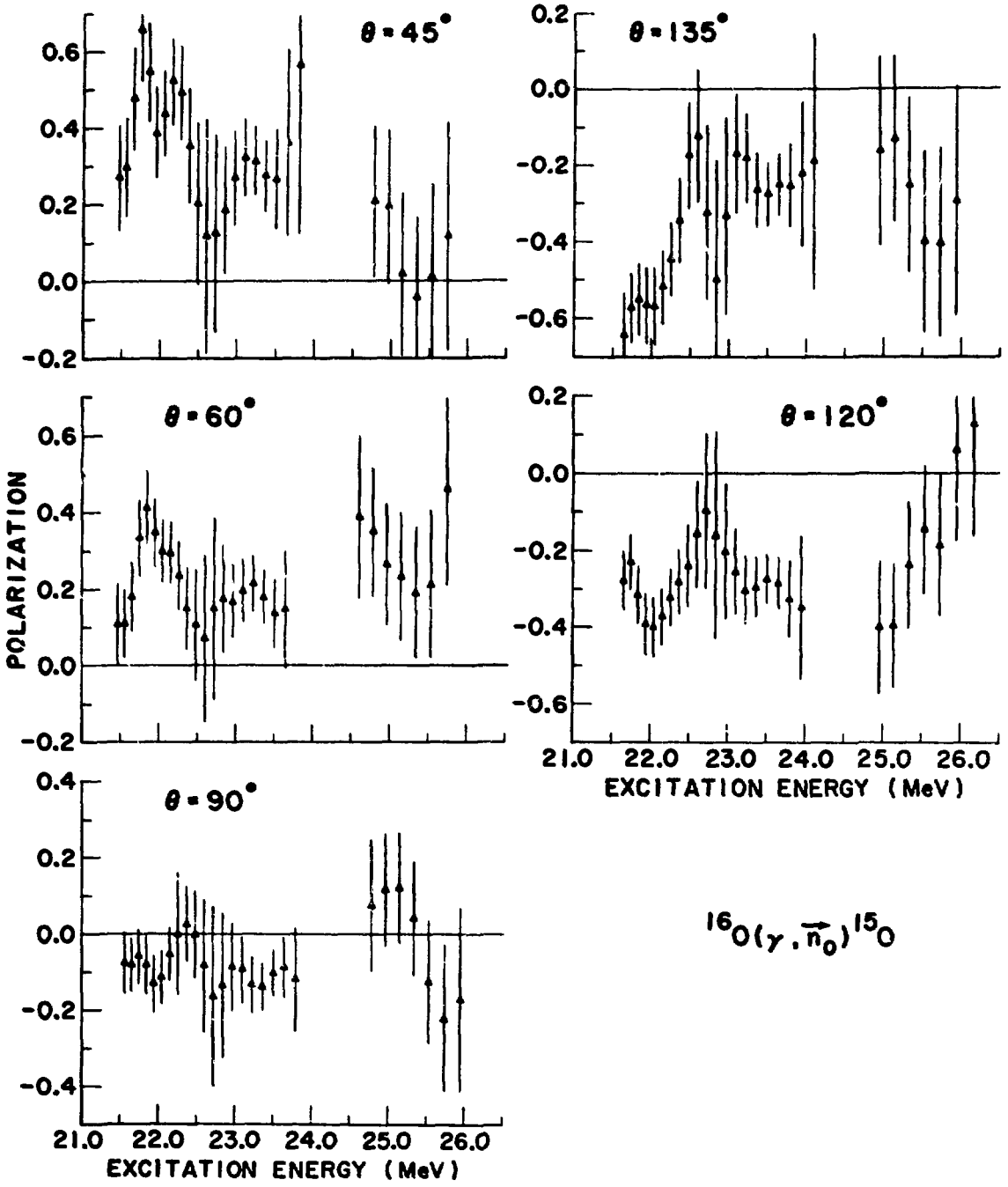

Fig. 13. The angular distribution of polarization of photoneutrons in the $^{16}O(\gamma,\vec{n}_0)^{15}O$ reaction in the region of the main dipole states.[57]

The measured $^{16}O(\gamma,\vec{n}_o)^{15}O$ polarizations are shown in Fig. 13. The energy region covers the main giant dipole states. The most noticible features are the energy-dependence of the polarization (which is not observed in the $^{16}O(\gamma,\vec{p}_o)^{15}N$ data, deduced from studies of the inverse reaction [59]) and the non-zero polarization at 90°. These results are now being analyzed, together with the angular distribution data of Syme et al [60] in order to deduce the s- and d-wave amplitudes and the possible E2 contributions to the absorption process.

Holt et al [61] have used the same technique to measure the polarization of photoneutrons from the $^{208}Pb(\gamma,\vec{n}_o)^{207}Pb$ reaction just above threshold. They have shown that all of the states previously reported to have spin and parity 1^+ are in fact 1^- states except for the one at 613 keV. This is a most interesting result that has clearly shown the need for polarization studies in this field. The question now requiring an answer is: where is the M1 strength located in ^{208}Pb? We shall have to wait for the answer.

The $D(\gamma,\vec{n})p$ results [62] provide information not only on the absorption process in this basic interaction but also on the role of meson currents at energies well below the meson threshold. This aspect of the work is discussed in the next section.

A SEARCH FOR THE EFFECTS OF MESON CURRENTS IN THE $d(\gamma,\vec{n})p$ REACTION AT LOW ENERGIES

Several calculations have appeared recently that illustrate clearly the need to include meson exchange currents in the theories of certain fundamental features of few-nucleon systems (such as the magnetic moments of 3-body systems and the β-decay rate of the triton [63]). Riska and Brown [64] have explained the long-standing discrepancy between the experimental value for the thermal n-p capture cross section of 334.2 ± 0.5 mb and the "best" theoretical estimate of 302.5 ± 4.0 mb by demonstrating the importance of pion exchange, excitation of the N^*_{33} state and the process $\omega \rightarrow \pi\gamma$ in this reaction. Another interesting theoretical development that has emerged from this new approach is concerned with calculations of the cross sections for photo-disintegration of the deuteron from threshold to about 100 MeV. Hadjimichael and Arenhövel et al [65,66] have shown that, whereas the energy dependence of the total and differential cross section for the $d(\gamma,n)p$ reaction remain almost unchanged by the inclusion of meson exchange currents and nuclear isobars the differential polarization of the photo-nucleons is changed appreciably. The essential difference between the calculations of Hadjimichael and Arenhövel et al is that Hadjimichael did not include the contributions of nuclear isobars in the description of the ground state of the deuteron. In both calculations, the effect of meson currents and of isobars is to increase the magnitude of the neutron polarization compared with the values predicted by the Schrödinger-type calculations as typified in the work of Partovi [67] and Nunemaker [68]. Typical diagrams included in the work of Hadjimichael are

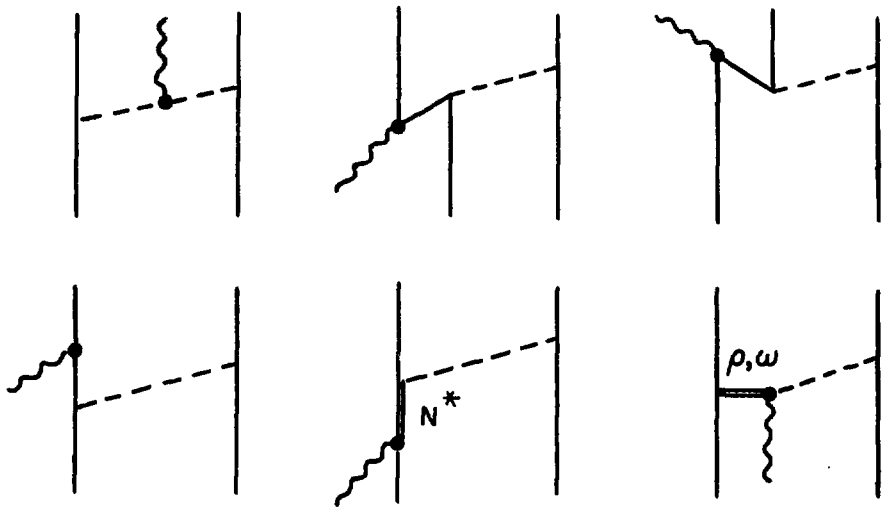

The reason that meson exchange currents do not make any appreciable contribution to the total cross section is to be found in the predominance of E1 absorption below 100 MeV. The E1 amplitudes are about an order-of-magnitude larger than the amplitudes for the spin-flip transitions $^3S_1 \rightarrow {}^1S_0$ and $^3D_1 \rightarrow {}^1D_2$. The two-body magnetic moment operator has non-zero matrix elements only for these spin-flip transitions and therefore it is only in such transitions that meson exchange currents can make themselves felt. Therefore, when these relatively small amplitudes are squared, as required in calculating the total cross section, they give rise to negligibly small contributions.

The differential cross section has the form

$$\frac{d\sigma}{d\Omega} = a + b \sin^2\theta + c \cos\theta \qquad (19)$$

where the third term is due to E1 - M1 interference. The M1 amplitudes that enter here, however, are all of the spin-conserving variety so that the contributions of meson exchange currents are again negligible. If we look at the expression for the differential polarization, a different picture emerges

$$p \cdot \left(\frac{d\sigma}{d\Omega}\right) = A \sin\theta + B \sin\theta \cos\theta \qquad (20)$$

where the first term now represents E1 - M1 interference that contains M1 amplitudes of the spin-flip variety and these are changed by the inclusion of meson effects. It is also important to note that the first and second terms in (20) are of comparable absolute value so that the term containing meson effects is not overwhelmed by the remaining term.[65]

We have searched for meson effects in the $d(\gamma,\vec{n})p$ reaction at photon energies between 6 and 14 MeV and at reaction angles of 60, 90, and 120° by measuring the polarization of the photoneutrons with an absolutely calibrated polarization analyzer of ^{12}C.[62] The target consisted of a cylinder of liquid deuterium in a thin-walled

cryostat. The unpolarized photons were generated by stopping a 32-MeV energy analyzed pulsed beam of electrons from the Yale LINAC in a thick bremsstrahlung converter. The results are shown in Fig. 14.

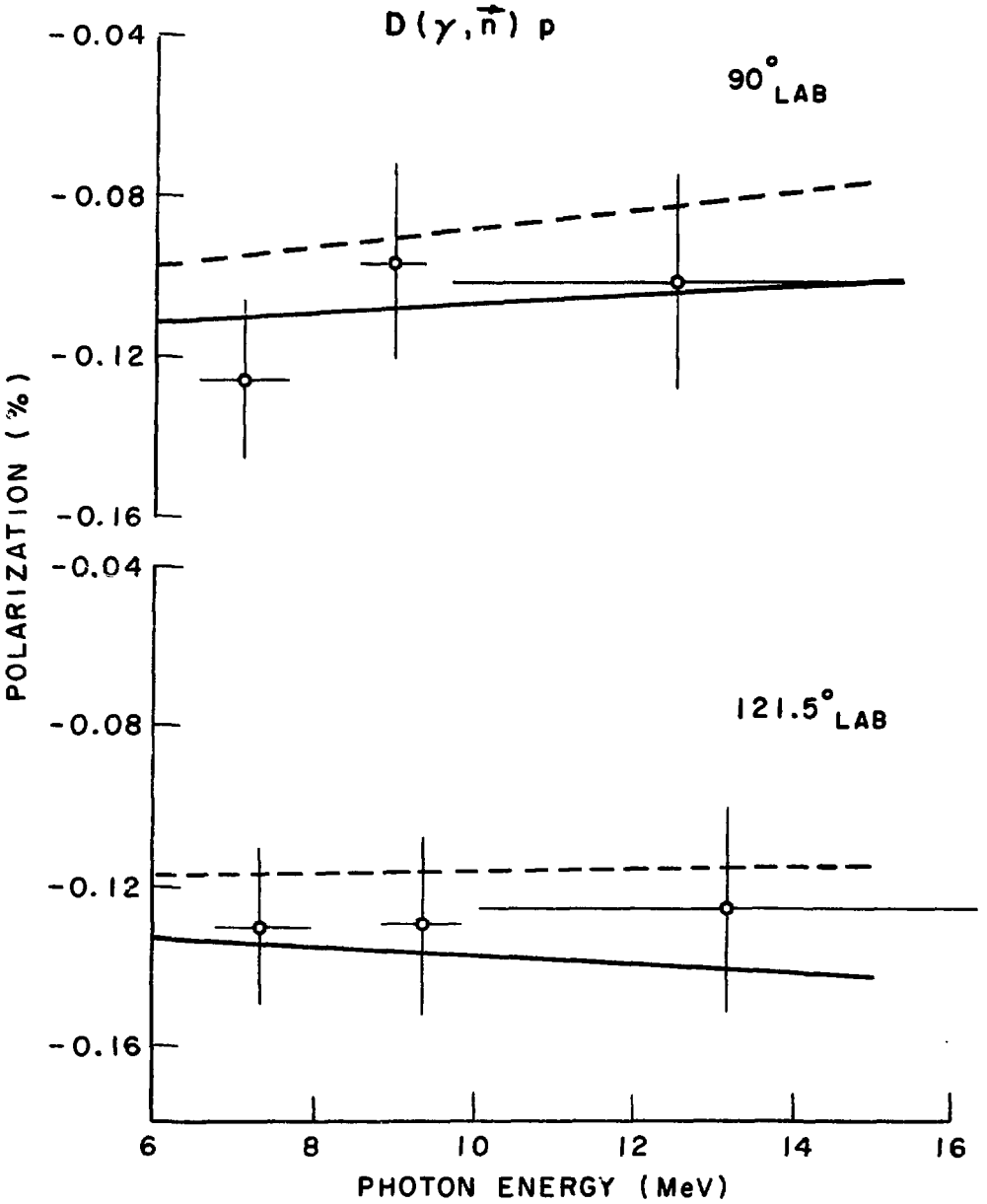

Fig. 14. The observed polarization in the $D(\gamma,\vec{n})p$ reaction at two angles compared with the theory of Hadjimichael[65]; the dashed curves without meson corrections and the full curves with meson corrections.

A considerable effort was made in this experiment to reduce the systematic uncertainties to negligible amounts. The most important effect was found to be depolarization of the photoneutrons due to n-d elastic scattering in the liquid deuterium target. A full-scale Monte Carlo calculation was performed to correct for this effect, and the results shown in Fig. 14 are therefore considered to be the true "point" polarizations. The measurement at 60^{o} (lab) exhibits the same trend as those at 90^{o} and 121.5^{o} namely, a systematic shift towards the predicted values of Hadjimichael and Arenhövel et al that include meson exchange currents. Although the combined effects of such exchange currents and of nuclear isobars are predicted to increase at higher energies, it should be noted that there are no polarization analyzers available above neutron energies of 20 MeV that are absolutely calibrated. The immediate efforts in this field must therefore continue to rely upon the use of ^{12}C and ^{4}He as analyzers below 20 MeV (corresponding to photon energies below about 40 MeV).

CONCLUSIONS

The objective of this review has been to demonstrate the essential part played by neutron polarization studies in furthering our knowledge of nuclear structure, from tests of T-invariance to clear-cut determinations of the spins of highly excited states observed in neutron reactions.

Several important aspects of this burgeoning branch of Neutron Physics have not been covered; they include: polarization studies in medium and heavy nuclei that can provide information on the neutron-nucleus optical potential, including the elusive spin-spin term; studies of Mott-Schwinger scattering; studies of $(\vec{p},n)$, $(\vec{d},n)$, $(\vec{^{3}He},n)$, $(\vec{\alpha},n)$ reactions etc. All of these topics are discussed in detail in the proceedings of the recent Zurich Conference on polarization phenomena; in particular, the review by Walter[9] gives a complete, up-to-the-minute account of these experiments.

It is important to carry out new and improved tests of P-invariance; the old result of Lobashov[4,5] is not consistent with that obtained in the spectacular measurement of $\vec{p}$-p scattering at 15 MeV[69] in which the invariance is shown to be a few parts in 10^{7}. There are sound reasons for carrying out such tests with neutrons - we must continue to forge ahead!

REFERENCES

1) R. K. Adair, S. E. Darden and R. E. Fields, Phys. Rev. 96 (1954) 503.

2) A. M. Baldin, V. I. Goldanskii and I. L. Rozental', Kinematics of Nuclear Reactions, Oxford Univ. Press, 1961.

3) M. I. Shirokov, Zhur. Eksp. i Teoret. Fiz. 32 (1957) 1022.

4) E. M. Henley, Ann. Rev. Nucl. Science 19 (1969) 367.

5) H. A. Weidenmüller, Polarization Phenomena in Nuclear Reactions, Univ. of Wisconsin Press, 1971.

6) L. Wolfenstein, Ann. Rev. Nucl. Science 6 (1956) 43.

7) W. Haeberli, Fast Neutron Physics, Vol. II, Interscience, 1963.

8) H. H. Barschall, 2nd Inter. Polarization Conf. Karlsruhe, 1965.

9) R. L. Walter, 4th Inter. Symposium on Polarization Phenomena in Nuclear Reactions, 1976 (in press).

10) N. F. Mott and H. S. W. Massey, The Theory of Atomic Collisions, Oxford Univ. Press, 1965.

11) The "Basel" Convention.

12) T. A. Welton, Fast Neutron Physics, Vol. II, Interscience, 1963.

13) R. I. Steinberg, P. Liaud, B. Vignon and V. W. Hughes, Phys. Rev. Lett. 33 (1974) 41.

14) J. D. Jackson, S. B. Treiman and H. W. Wyld Jr., Phys. Rev. 106 (1957) 517.

15) F. D. Brooks and D. T. L. Jones, Nucl. Inst. 121 (1974) 69.

16) D. T. L. Jones and F. D. Brocks, Nucl. Phys. A222 (1974) 79.

17) D. Tsukada and S. Kickuchi, Nucl. Inst. 17 (1964) 286.

18) F. D. Brooks and D. T. L. Jones, Nucl. Inst. 121 (1974) 77.

19) M. Steinbock, F. D. Brooks and I. J. van Heerden, 4th Inter. Symposium on Polarization Phenomena in Nuclear Reactions, 1976 (in press).

20) C. L. Morris, R. Rotter, W. Dean, and S. T. Thornton, Phys. Rev. C9 (1974) 1687.

21) S. C. Pieper, Nucl. Phys. A193 (1972) 519.

22) J. C. Faivre, D. Garreta, J. Jungerman, A. Papineau, J. Sura and A. Tarrata, Nucl. Phys. A127 (1969) 169.

23) P. Doleschall, 4th Inter. Symposium on Polarization Phenomena in Nuclear Reactions, 1976 (in press).

24) S. W. Johnsen, F. P. Brady, N. S. P. King and M. W. McNaughton, ibid.

25) J. L. Romero, F. P. Brady, N. S. P. King and M. W. McNaughton, contribution to this conference.

26) J. Binstock and R. Bryan, Phys. Rev. D9 (1974) 2528.

27) M. Ahmed, D. Bovet, P. Chatelain and J. Weber, 4th Inter. Symposium on Polarization Phenomena in Nuclear Reactions, 1976 (in press).

[28] D. Bovet, P. Chatelain, S. Jaccard, Y. Onel, J. Piffaretti, R. Vinet and J. Weber, contribution to this conference.

[29] J. E. Simmons, W. B. Broste, G. P. Lawrence, J. L. McKibben and G. C. Ohlsen, Phys. Rev. Lett. 27 (1971) 113.

[30] W. Tornow, P. W. Lisowski, R. C. Byrd, S. E. Skubic and R. L. Walter, B.A.P.S. 21 (1976) 636.

[31] R. A. Arndt, private communication to R. L. Walter and M. H. MacGregor, R. A. Arndt and R. M. Wright, Phys. Rev. 182 (1969) 1714.

[32] W. Haeberli, Fast Neutron Physics, Vol. II, Interscience, 1963.

[33] J. M. Daniels, Oriented Nuclei: Polarized Targets and Beams, Academic Press, 1965.

[34] R. B. Perkins and C. Glashausser, Nucl. Phys. 60 (1964) 433.

[35] R. J. Holt, F. W. K. Firk, R. Nath and H. L. Schultz, Phys. Rev. Lett. 28 (1972) 114.

[36] R. J. Holt, F. W. K. Firk, R. Nath and H. L. Schultz, Nucl. Phys. A213 (1973) 147.

[37] G. T. Hickey, F. W. K. Firk, R. J. Holt, R. Nath and H. L. Schultz, Phys. Lett. 47B (1973 348.

[38] G. T. Hickey, F. W. K. Firk, R. J. Holt and R. Nath, Nucl. Phys. A225 (1974) 479.

[39] J. E. Bond and F. W. K. Firk, Nucl. Phys. A258 (1976) 189.

[40] P. Hillman, G. H. Stafford and C. Whitehead, Nuovo Cimento, 4 (1956) 67.

[41] R. Nath, F. W. K. Firk, R. J. Holt and H. L. Schultz, Nucl. Inst. 98 (1972) 385.

[42] J. M. Blatt and L. Biedenharn, Rev. Mod. Phys. 24 (1952) 258.

[43] A. Simon and T. A. Welton, Phys. Rev. 90 (1953) 1036.

[44] E. P. Wigner and L. Eisenbud, Phys. Rev. 72 (1947) 29.

[45] A. M. Lane and R. G. Thomas, Rev. Mod. Phys. 30 (1958) 257.

[46] F. W. K. Firk, J. E. Lynn and M. C. Moxon, Proc. Phys. Soc. (Lond) 82 (1963) 477.

[47] R. J. Holt, F. W. K. Firk, G. T. Hickey and R. Nath, Nucl. Phys. A237 (1975) 111.

[48] H. Postma, H. Marshak, V. L. Sailor, F. J. Shore and C. A. Reynolds, Phys. Rev. 125 (1962) 979.

[49] F. L. Shapiro, Nuclear Structure Study with Neutrons, North-Holland, 1966.

[50] G. A. Keyworth, J. R. Lemley, C. E. Olsen, F. T. Seibel, J. W. T. Dabbs and N. W. Hill, Phys. Rev. C8 (1973) 2352.

[51] A. Stolovy, Phys. Rev. 118 (1960) 211, and 134B (1964) 68.

[52] J. P. Elliott and B. H. Flowers, Proc. Roy. Soc. A242 (1957) 57.

[53] W. Bertozzi, P. T. Demos, S. Kowalski, C. P. Sargent, W. Turchinetz, R. Fullwood and J. Russell, Phys. Rev. Lett. 19 (1968) 396.

54) G. W. Cole Jr., F. W. K. Firk and T. W. Phillips, Phys. Lett. 30B (1969) 91 and R. Nath, F. W. K. Firk and H. L. Schultz, Nucl. Phys. A194 (1972) 49.

55) R. J. Holt and H. E. Jackson, Phys. Rev. Lett. 36 (1976) 244.

56) L. Drooks, F. W. K. Firk, H. L. Schultz and R. J. Holt, B.A.P.S. 91 (1976) 534.

57) R. Nath, Y-H. Chiu and F. W. K. Firk, to be published.

58) R. J. Holt, R. M. Laszewski and H. E. Jackson, to be published.

59) H. F. Glavish, Inter. Conf. on Photonuclear Reactions and Applications, Vol. II, Lawrence Livermore Laboratory, Univ. of California, 1973.

60) D. B. C. B. Syme and G. I. Crawford, ibid.

61) R. J. Holt, private communication, 1976 and refs. 55 and 58.

62) L. Drooks, Ph.D. Thesis, Yale University (1976).

63) J. Blomquist, Phys. Lett. 32B (1970) 1.

64) D. O. Riska and G. E. Brown, Phys. Lett. 38B (1972) 193.

65) E. Hadjimichael, Phys. Lett. 46B (1973) 147 and private communication.

66) H. Arenhövel, W. Fabian and H. G. Miller, Phys. Lett. 52B (1974) 303.

67) F. Partovi, Ann. of Phys. 27 (1964) 79.

68) R. D. Nunemaker, Ph.D. Thesis, Yale University, 1968.

69) J. M. Potter, J. D. Bowman, C. F. Hwang, J. L. McKibben, R. E. Mischke, D. E. Nagle, P. G. Debrunner, H. Frauenfelder and L. B. Sorenson, Phys. Rev. Lett. 33 (1974) 1307.

MP 3 - NEUTRON POLARIZATION - F.W.K. Firk (Yale University, U.S.A.)

King (Univ. of California, Davis):

I have a comment concerning the A_{yy} spin correlation parameter measurement. Your slide indicated a preferred value of 0.2 degrees for ε_1 in fact, recent phase shift analysis studies by Peter Signell of Michigan State indicates that a value much closer to the 2.5 degrees is preferred, rather than 0.2 degrees. The essence of your comments is still the same, however. By systematically excluding various parts of the data set, around 50 MeV, Signell found that a 90 degree center of mass datum should be excluded from the Oak Ridge differential cross section measurements. This results in a much more stable solution near 2.5 degrees.

Malik (Indiana Univ.):

I was happy to see that the polarization data is suggesting the presence of M1 and E2 in the giant dipole region, which was suspected about four or five years ago because of the angular distribution.

Firk:

Yes. It's also encouraging to know, I recall one of your students' theses on this question, that you can in fact account for the 25 MeV upward region in a pure direct interaction model, but now you see the problems are down at 22 and 3 MeV, where one sees considerable structure. That, by the way, I didn't comment on. You have structure in the (gamma-n) polarization, but not in the (gamma-p) polarization as measured in the inverse reaction. And yet the cross sections are identical in shape, energy dependence; magnitudes are good, the differential cross sections agree, but the polarizations don't; so again, it's telling us something rather subtle about the actual process. And we do need, of course, bigger and better multi-particle-multi-hole calculations.

Jain (Texas A&M Univ.):

This is just a comment regarding the beautiful work on the neutron polarization and polarization transfer at medium energy from Texas A & M which you did not draw attention to.

Firk:

Yes. One of the reasons, apart from lack of time, is that Lee Northcliffe is dealing with the intermediate energy range and I wasn't quite sure whether he was coming down to meet us at 10 MeV or what, so I hope that he will, in fact, cover that work.

Jain:

Lee's talk would be concerned with the work at LAMPF. The work which I'm drawing attention to is from Texas A & M cyclotron.

Firk:

Yes, I'm aware of the work, and I'm sorry if I didn't fit it in, along with all the dozens of other deserving cases.

Jain:

Okay, thank you.

Walter (Duke):

As you know, when we produce polarized neutrons via the polarization transfer on deuterium gas targets, we can transfer about ninety percent of the polarization of the deuteron to the neutron. Furthermore, if one used a thick gas target, one can produce a continuous distribution of polarized neutrons this way also. Depending on the deuteron polarization, one may reach about sixty-five percent polarization. I haven't done the calculation, but I was wondering if you have ever calculated a comparison between a flux produced with a polarization transfer reaction and the polarized flux that you produce by scattering the intense (γ,n) flux.

Firk:

I haven't made a direct comparison, Dick. I'm not aware of your thick target type fluxes and work. Presumably that's the kind of thing, if you are going to pulse it, which you would probably have to do to separate off the continuum problem, then it'll be a matter of probably the duty factor on your machine. You see, that's the difficulty with the electron machines. If we had a megacycle rep rate, we'd be in great shape, straight factor of ten to the fifth or something would be very useful right now, and that's what's missing, as we all know.

9:00 A.M., THURSDAY, JULY 8, 1976, IN OLNEY 150

MAIN SESSION MG

Chair: P.A. Moldauer (ANL, Argonne, U.S.A.)

9.00 a.m., Thursday, July 8, 1976 in Olney 150 Invited Paper: Session MG1

THEORETICAL NEUTRON PHYSICS: THE ELUCIDATION OF NUCLEAR STRUCTURE

V. G. Soloviev

Joint Institute for Nuclear Research (JINR) - Dubna, Head Post Office Box 79, Moscow

RÉSUMÉ

Analysis of radiative neutron-capture data permits information to be extracted on many aspects of nuclear structure, and particularly on nuclear configurations. The interpretation of such evidence, and other findings in neutron physics, is surveyed, indicating the scope of recent advances in theoretical neutron physics in shedding light upon nuclear characteristics.

NUCLEAR-STRUCTURE ASPECTS OF THEORETICAL NEUTRON PHYSICS

V.G.Soloviev

Joint Institute for Nuclear Research, Dubna, SSSR

International Conference on the Interactions of Neutrons with Nuclei (July 6-9, 1976)

RÉSUMÉ

The structure of neutron resonances is studied on the basis of the semimicroscopic nuclear theory. Few-quasiparticle components of the wave functions of neutron resonances are calculated which determine the neutron and radiational strength functions. It is stated that it is necessary to clarify the role of their many-quasiparticle components.

ABSTRACT

The structure of neutron resonances is studied within the framework of the general approach based on the operator form of the wave functions. The role of three-quasiparticle components in the wave functions of neutron resonances is studied and the cases of validity of the valence neutron model are pointed out. It is shown that the experimental information about the structure of neutron resonances is limited to few-quasiparticle components which are of 10^{-3}-10^{-6} part of the normalization of their wave functions. To study the structure of neutron resonances it is necessary to find the values of many-quasiparticle components of the wave functions. The ways of experimental finding of these components based on the study of γ -transitions between highly excited states are discussed. The fragmentation of single-particle states in deformed nuclei is studied within the framework of the model based on the quasiparticle - phonon interactions. The S ,- p ,- and d -wave neutron strength

functions are calculated, and a good agreement with experiment is obtained.

1. The aim of our investigations which have been performed during several recent years is to construct such a variant of the semi-microscopic theory of atomic nucleus which could serve as base for a detailed description of low-lying states. It should give a general structure of the wave functions for the states of intermediate and high excitation energies. Based on it, one should construct some averaged description of few-quasiparticle components of the wave functions of these states in terms of various strength functions. It is shown[1] that there are grounds for the development of the unified desciption of low, intermediate and high excitation states of atomic nuclei. Such a description is realized for few-quasiparticle components of the wave functions of these states.

The structure of highly excited states arose interest long ago. Progress in the study of the structure of neutron resonances is due to the construction of resonance reaction theory[2], the study of non-statistical effects[3] and wide development of neutron spectroscopy[4,5].

Our investigation of the state structure of intermediate and high excitation energies is performed along two lines: general consideration based on the operator form of the wave function[6,7] and calculation of the state characteristics within the model based on the quasiparticle phonon interactions[8].

In this report we shall discuss the properties of neutron resonances. It should be noted that the neutron resonances are in a peculiar position among highly excited states is due to the availability of complete and exact experimental data rather than to their physical meaning. Our treatment of neutron resonances is based on the generalization of methods describing low-lying states[9] to the states of intermediate and high excitation energy.

2. Let us present the basic statements of the semi-microscopic approach based on the operator form of the wave function of a highly excited state and evaluate the contribution of simplest configurati-

ons in the wave functions of neutron resonances.

Now we construct the wave function of a highly excited state within the framework of the semi-microscopic approach of the superfluid nuclear model. The wave function can be represented as the expansion in number of quasiparticles. With increasing excitation energy the state structure becomes complicated because in the wave function a more important role is played by the components with larger and larger number of quasiparticles. The wave function, for instance, of the highly excited state of an odd-mass spherical nucleus is:

$$\Psi_i(I^\pi M) = b_I^i \mathcal{Q}^+_{IM} \Psi_0 + \sum_{\substack{j_1 j_2 j_3 \\ m_1 m_2 m_3}} b_i^i(j_1 m_1 j_2 m_2 j_3 m_3) \mathcal{Q}^+_{j_1 m_1} \mathcal{Q}^+_{j_2 m_2} \mathcal{Q}^+_{j_3 m_3} \Psi_0 + \sum_{\substack{j_1 j_2 j_3 j_4 j_5 \\ m_1 m_2 m_3 m_4 m_5}} b_i^i(j_1 m_1 j_2 m_2 j_3 m_3 j_4 m_4 j_5 m_5) \mathcal{Q}^+_{j_1 m_1} \mathcal{Q}^+_{j_2 m_2} \mathcal{Q}^+_{j_3 m_3} \mathcal{Q}^+_{j_4 m_4} \mathcal{Q}^+_{j_5 m_5} \Psi_0 + \dots \quad (1)$$

This expression is added by the operators of the pairing vibrational phonons which replace the operators $(\mathcal{Q}^+_{jm}\ \mathcal{Q}^+_{j-m})_{I\ 0}$. Besides, the operators of any phonons can be explicitely introduced into eq.(1).

When constructing the wave function (1) we assume that the density matrix is diagonal for the ground state of the nucleus. In this representation the wave function of a highly excited state should contain thousands of different components. The use of this representation for the wave function of highly excited state is physically justified. In most of the cases the formation of highly excited states proceeds due to capture of a slow neutron or a high-energy γ-ray by a target nucleus in the ground zero-quasiparticle or one-quasiparticle state. Thus, the expansion of eq.(1) seems to be performed in the basis functions of the target-nucleus.

The operator form of the wave function is used in refs.[6,7] to express the reduced neutron, radiational and alpha widths in the neutron resonances in terms of the coefficients b_I^i. The coefficients b_i^i can be found from the spectroscopic factors of the reactions of the

type (dp) and (dt), from the β -decay probabilities, from the probabilities of gamma-transitions between the excited states and so on.

Let us consider, for example, a reduced neutron width which can be approximately written as:

$$\Gamma_{ni}^{0} = \Gamma_{s.p}^{0} \, |b^{(n)}(j)\, U_j|^2, \qquad (2)$$

where the function U_j indicates that the state j should be particle state. Using the experimental values of $\langle \Gamma_{ni}^{0} \rangle$ averaged over a number of resonances one may easily find $|\bar{b}|^2$. For $\mathcal{E} \approx B_n$ they are found to be the following: for nuclei $Ca - Ni$ $|\bar{b}|^2 \sim 10^{-3}$, for $Zn - Ba$ and some isotopes of Au and Hg $|\bar{b}|^2 \sim 10^{-4}$–10^{-5}, for the Pb isotopes $|\bar{b}|^2 \sim 10^{-3}$–10^{-4}, for deformed nuclei $|\bar{b}|^2 \sim 10^{-6}$–10^{-7}.

In the framework of this approach one can make general conclusions about the structure of neutron resonances. Thus, in ref.[10] is shown that the magnetic moments of neutron resonances should be close to the single-particle values. The experiments performed following the suggestion of F.L.Shapiro[11] confirmed these conclusions. The peculiarities of α -decay of neutron resonances were studied, and it is shown that the reduced probabilities of α -decays into the first 2^+ vibrational states should be equal or should exceed those for the transitions to the ground states[6,7]. These peculiarities of neutron resonances were confirmed by the experiments of Ju.P.Popov[14]. There is presented a clear treatment the correlations between the neutron and radiational widths[6] as well as for those between the partial radiational widths[15]. The above correlations were considered in a number of talks at the conferences[3,16]. This method allows the peculiarities of radiational widths to be analysed. For instance, in ref.[17] the causes of irregularity the behaviour of $E1$ -radiational strength function in ^{238}U was investigated.

3. Based on the general semi-microscopic approach in ref.[18], it is studied in which cases the neutron valence model is valid.

Now, we consider δ -transitions from highly excited states described by the wave functions(1)to the one-quasiparticle component of the low-lying states with the wave function

$$\Psi_f(J_f m_f) = C_f \alpha^+_{j_f m_f} \Psi_0 + \ldots \qquad (3)$$

The radiational width calculated with the wave functions (1) and (3) is the following:

$$\Gamma_{\gamma i f}(\lambda) = \frac{8\pi\lambda(\lambda+1)}{\lambda[(2\lambda+1)!!]^2} \Gamma_\gamma^{2\lambda+1} \Gamma^0_{\gamma i f}(\lambda) , \qquad (4)$$

$$\Gamma^0_{\gamma i f}(\lambda) = C_f^2 \Big| b_I^i \frac{\vartheta^{(\mp)}_{j_f I}}{\sqrt{2I+1}} \langle j_f \| \Gamma(\lambda) \| I \rangle \pm \frac{1}{2} \sum_{j_1 j_2} b_I^i (j_f j_1 j_2) \frac{U^{(\mp)}_{j_1 j_2}}{\sqrt{2\lambda+1}} \langle j_1 \| \Gamma(\lambda) \| j_2 \rangle \Big|^2 . \qquad (5)$$

Here $\langle j_1 \| \Gamma(\lambda) \| j_2 \rangle$ is the single-particle matrix element of $E\lambda$ (for which one should take the upper sing in eq.(5)) and $M\lambda$ (for which one should take the lower sign in eq.(5)) transitions;

$$U^{(\mp)}_{j_1 j_2} = U_{j_1} \vartheta_{j_2} \mp U_{j_2} \vartheta_{j_1} , \quad \vartheta^{(\mp)}_{j_1 j_2} = U_{j_1} U_{j_2} \mp \vartheta_{j_1} \vartheta_{j_2} ,$$

where U_j , ϑ_j are the Bogolubov canonical transformation coefficients. The first term in eq.(5) gives reduced radiational width in the neutron valence model[2].

Based on general regularities of the fragmentation of one- and three-quasiparticle states and expressions for the partial radiational widths as (4),(5), one may confirm that the neutron valence model works well at the following conditions:

i) the one-quasiparticle components of the wave functions of

neutron resonances should be the largest, what can be seen in the nuclei near the maxima of S - and p -wave neutron strength functions;

ii) near the neutron binding energy there are no such three-quasiparticle states from which $E1$ -transitions can proceed to the one-quasiparticle components of the wave functions of low-lying states;

iii) the low-lying states to which $E1$ -transitions proceed from the neutron resonances should have large one-quasiparticle components.

The analysis of partial readiational widths, given in ref.[18], for the nuclei $^{91,93,95,97}Zr$, $^{93,95,97,99}Mo$ allowed one to make the following conclusions:

1) One-quasiparticle components clearly manifest themselves in the wave functions of neutron resonances in the Zr isotopes with A =91,93,95 and 97, and the neutron valence model should work well;

2) A large radiational $E1$ -width in ^{91}Zr indicates a considerable contribution to the wave functions of p -resonances of three-quasiparticle configurations;

3) A large radiational $M1$ -width in ^{93}Zr indicates a considerable contribution to the wave functions of s -resonances of the components $d_{3/2}$, $s_{1/2}$ plus I^+ collective phonon;

4) the neutron valence model for $E1$ -ransitions from p -resonances should work well in ^{99}Mo and somewhat worse in ^{95}Mo and ^{97}Mo . In ^{95}Mo an important role is played by $E1$ -transitions from three-quasiparticle components of the wave functions of p -resonances;

5) The enhancement of $M1$ -transitions observed in $^{93,99}Mo$ can be by the presence of the corresponding three-quasiparticle configurations in the wave functions of S -resonances.

Recent experiments[19] have confirmed our prediction[18] that the neutron valence model should work well for $E1$ -transitions

from p -resonances in ^{99}Mo . The analysis of experimental data on zirconium and molibdenum isotopes performed in ref.[16] to justify the validity of the neutron valence model is consistent, on the whole, with our conclusions.

In ref.[20] there were studied γ -transitions from the resonances to the low-lying $s_{1/2}$ and $d_{3/2}$ states in ^{117}Sn and ^{125}Sn , and it was shown that the neutron valence model fails to describe the experimental values of partial widths of $E1$ -transitions (see, also, ref.[16]). Let us consider $E1$ -transitions from the resonances $I^{\pi} = 3/2^{-}$ in ^{117}Sn . Fig. 1 represents the positions of the subshell $3p_{3/2}$ and those three-quasiparticle states from which $E1$ -transitions proceed to the low-lying states $s_{1/2}$ and $d_{3/2}$. The presence of such three-quasiparticle states near the neutron binding energy results in the violation of the neutron valence model and allows one to explain a number of peculiarities of γ -transitions. Thus, from the resonance 147,9 eV there proceeds an intensive $E1$ -transition to the state $s_{1/2}$ and does not proceed to the state $d_{3/2}$ what can be easily explained by a relatively large component $\{s_{1/2}, f_{7/2}, g_{7/2}\}$ in the wave function of this resonance. From the resonance 632 eV there proceeds the transition to the state $d_{3/2}$ and there is no transition to the state $s_{1/2}$ what indicates the presence of a large component $\{d_{3/2}, f_{7/2}, g_{7/2}\}$ in the wave function of this resonance. The three-quasiparticle components, given in the figure, are near S_n in ^{125}Sn too. The presence of these components makes it possible to understand large values of the partial γ -widths as compared to the predictions of the neutron valence model for $E1$ -transitions from the resonance 106,9 eV in ^{123}Sn .

Thus, the use of formulae of the general semi-microscopic approach to the highly excited states and calculation of the position of three-quasiparticle states allows one to analyse simple configurations in the capture states.

It should be noted that in the deformed nuclei due to the richness of the collective excitation branches at the energy $\varepsilon \approx B_n$, the wave functions are so complex that nonstatistical effects connected with few-quasiparticle components appear very seldom.

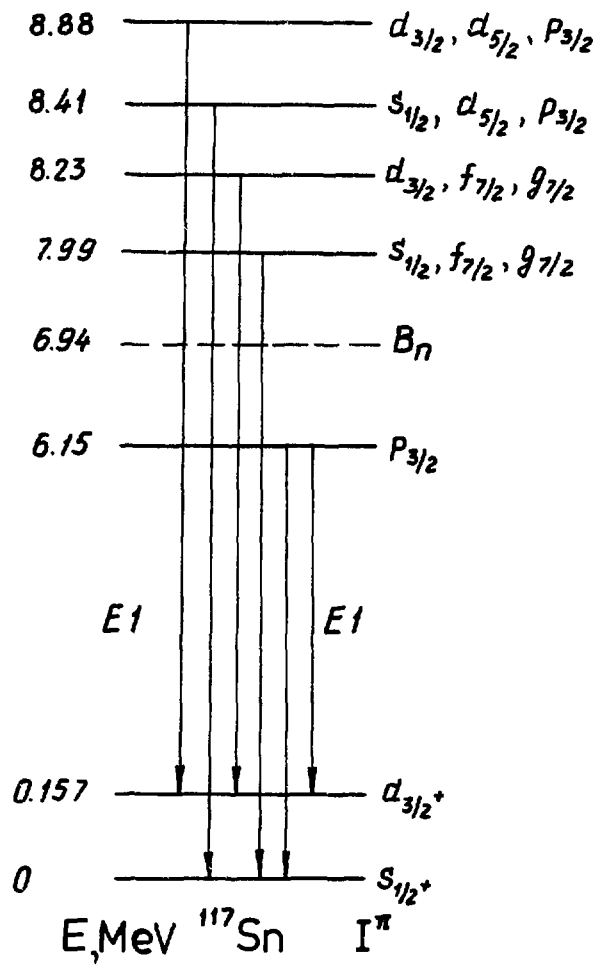

Fig.1. *E1* -transitions in ^{117}Sn from one- and three-quasiparticle components of the wave functions of the states with $I^\pi = 3/2^-$.

So, one can observe the correlations for $E1$ -transitions from I^- S -wave resonances to the ground and first 2^+ rotational state in ^{158}Gd, ^{160}Dy, ^{172}Yb, ^{184}W. The correlations between the neutron and $E1$ radiational widths in the transition tc the states with $K^\pi = 2^+$ from the resonances 2^- in the reaction $^{173}Yb(n,\gamma)^{174}Yb$ are also observed. There are experimental indications to the existence of such correlations[21].

The general semi-microscopic approach allows one to study the rotational properties of highly excited states. In ref.[15] it was suggested to study to what extent the quantum number K (the projection of the angular momentum into the nucleus symmetry axis) is a good quantum number for the wave functions of neutron resonances. In ref.[15] γ -transitions from the resonances were assumed to be K - forbidden, if the following condition is fulfilled for them

$$|I - K_f - \lambda| > 0, \qquad (6)$$

where I is the resonance spin, and λ is the multipolarity of γ -transition. One can judge about the role of the quantum number K by the degree of retardation of K -forbidden γ -transitions from the neutron resonsnces as compared to the similar but K - allowed transitions. The available experimental data allowed one to conclude that the selection rules over K are violated at high excitation energies. This indicates the fact that in highly excited states the rotational motion is not explicitly separated but distributed among other nuclear motions.

The study of the fragmentation of two-, three-, and four-quasiparticle states is of great interest. It is important to study experimentally the two-, three- and four- nucleons transfer reactions. Much attention should be paid, for example, to the measurement of neutron and partial radiational widths for the neutron resonances in the reactions of the type $^{176}Lu(n,\gamma)^{177}Lu$ and $^{177}Lu(n,\gamma)^{178}Lu$ if one uses the three-quasiparticle isomer $23/2^-$ in ^{177}Lu as a target. In the first case one can obtain the values of three- and in the second case of four-quasiparticle components of the wave functions of neutron resonances.

The use of unstable targets in the neutron spectroscopy, the importance of which was pointed out in ref.[6], will make it possible to obtain information about the values of three,- and four-quasiparticle components. It is necessary to support such measurements the first of which have been already performed[22].

4. Concerning the available experimental information on the nuclear structure obtained in the study of the characteristics of neutron resonances, we may say the following:

i) From the reduced neutron widths mainly the information about certain one-, or two-quasiparticle components of their wave functions is obtained;

ii) From the partial radiational widths for γ -transitions to the ground states, one can extract the data on one- and three-quasiparticle or two-quasiparticle components of their wave functions;

iii) From the neutron and radiational strength functions the information about averaged over a number of neutron resonances values of the above components can be obtained;

iv) In the processes of α -decays of neutron resonances and γ -transitions from them to the excited states there take part the components of the neutron resonances wave functions with larger number of quasiparticles. However, from these processes we can obtain the data only on the integral contribution of such components.

Therefore, almost the whole experimental information about the structure of neutron resonances is the information on the few-quasiparticle components of their wave functions only . In complex nuclei the few-quasiparticle components are of 10^{-3}-10^{-6} part of the normalization of their wave functions. Indeed, we have a very insignificant part of the experimental information about the wave functions of neutron resonances. Therefore, we can make the following conclusions:

1) Statistical regularities concern only the few-quasiparticle components of the wave functions of neutron resonances.

2) Nonstatistical effects manifesting themselves in neutron

resonances concern only the behaviour of few-quasiparticle components of their wave functions. These effects allow one to assert, as it was done by R.E.Crien et al.[19], the violation of the Bohr hypothesis on the compound states.

3) If one has no right to extent the regularities concerning only a small part of the wave function to the whole wave function. Such an extensiton is in fact made in the statistical description of the structure of neutron resonances.

4) One may state that there is no experimental confirmation of the validity applicability of the N.Bohr hypothesis on the compound states to the neutron resonances.

5. Up to now the processes connected with few-quasiparticle components of the wave functions of neutron resonances have been discussed. In ref.[7] the problem on the magnitude of many-quasiparticle components of the wave functions was raised. The assumption was also made that the wave functions of the intermediate excitation energy and neutron resonances have sufficiently large many-quasiparticle components. This is due to the fact that the interactions between quasiparticles and the quasiparticle-phonon interaction at these energies can not fragmentate many-particle states so strongly as the single-particle states.

The ways of experimental detection of large many-quasiparticle components of the wave functions of neutron resonances were discussed in refs.[7,23,24]. Presently, the most available way of determination of the values of the largest many-quasiparticle components is the study of $E1$ -, $M1$,- and $E2$ - transitions from the neutron resonances tothe states with energy by (1.0-1.5) MeV less than their. The probabilities of such transitions can be evaluated in the study of the subsequent α -decay of an excited state, fission or neutron emission. The observation of such γ -transitions or γ -cascades, the reduced probabilities of which are close to the single-particle ones, gives evidence to the existence of large many-quasi-particle components in the wave functions of neutron resonances. The study of γ -transitions from the neutron resonances to the states of intermediate excitation energy gives the information on the values of in-

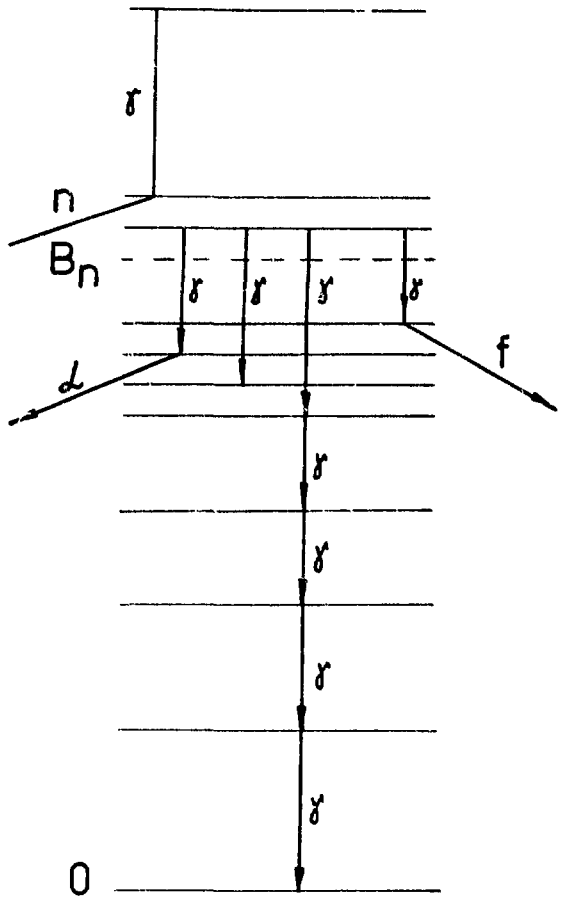

Fig.2. Symbolic representation of the ways of experimental detection of large many quasiparticle components in the wave functions of highly excited states.

vidual four- and six-quasiparticle components. Possible ways of detection of large many-quasiparticle components of the wave functions of neutron resonances are schematically represented in Fig.2.

The most promising method of measuring of the values of the largest components of neutron resonance wave functions is the study of the reaction (n, f, α) with the subsequent evaluation of intensities of f -transitions between the neutron resonances and states lying by (1-2) MeV lower. The experimental results of Popov and collaborators[25] show that there are relatively large components in the wave functions of these states.

I should like to emphasize that from the viewpoint of the study of the structure of intermediate and high excitation energy states, the answer to the question whether these are large many-quasiparticle components in the wave functions of neutron resonances is of fundamental importance.

6. In the study of the state structure of intermediate and high excitation energies in atomic nuclei the important role is attributed to the fragmentation, i.e. the distribution of the strength of single-particle or many-particle states over many nuclear levels. In the independent particles and quasiparticles models the single-particle strength is concentrated on a single level. In the extreme statistical model it is randomly distributed over all nuclear levels. For the construction of neutron strength functions Lane, Thomas and Wigner[26] introduced a model of intermediate coupling. However, the direct calculations of the fragmentation were not performed in the framework of this model.

To describe the complication of the state structure with increasing excitation enerty and to study general regularities of fragmentation, we use the model based on the quasiparticle phonon interaction. In the framework of the model the characteristics of low-lying levels are described, and the strength functions for the neutron or proton transfer reactions of the type (dp) or (dt) are calculated for the states of intermediate excitation energy. The description of S -, p -, and d -wave neutron strength functions is given and the method of calculation of radiational strength

functions is developed. The energies of giant multipole resonances are calculated and the method of calculation of their widths and fine structure is developed. The model is described in ref.[8], in ref.[27] the approximate methods of solving its equations were developed. In ref.[28] the model was generalized to the case of the introduction of spin-multipole forces, in ref.[29] it is applied for the description of doubly even deformed nuclei, while in ref.[30] for odd-A spherical nuclei. Preliminary results of our investigations on the single-particle fragmentation were reported for deformed nuclei in refs.[24,31] for spherical nuclei in ref.[32].

The wave function of the model in the variant corresponding to odd-A deformed nucleus is:

$$\Psi_i(K^\pi) = \frac{1}{2}\sum_\sigma \Big\{ \sum_\rho C_\rho^i a_{\rho\sigma}^+ + \sum_g D_g^i (a^+ Q^+)_g + \frac{1}{2}\sum_G F_G^i (a^+ Q^+ Q^+)_G \Big\} \Psi_0 , \tag{7}$$

where i is the number of the state, $g = \nu t$, $G = \nu t$, t_2 $(\rho\sigma)$, $(\nu\sigma)$ denote the quantum numbers of single-particle states. Using the variational principle we find the system of main equations and also for $\rho \neq \rho_c$ (ρ_c is a selected single-particle state)

$$\frac{C_\rho^i}{C_{\rho_c}^i} = \frac{\theta_{\rho\rho_c}(\rho)}{\theta_{\rho\rho_c}(\eta_i)} , \tag{8}$$

where the denominator of (8) is the determinant of the system and the numerator is the determinant in which ρ -th column is replaced by that of free terms. The quantity $(C_{\rho_c}^i)^2$ is determined from the wave function normalization. The secular equation for defining the energies η_i symbolically can be written as:

$$\mathcal{F}_{\rho_c}(\eta_i) = 0. \tag{9}$$

To describe highly excited states within the framework of the model, the phonons of multipole and spin-multipole type with $\lambda = 1,...7$ and higher as well as a large number of phonons of each multipolarity are taken into account. Alongside with the known low-lying collective quadrupole and octupole phonons, we consider many weakly collectivized phonons as well as high-lying phonons like the giant resonances. The configurational space of the model is large, the wave functions of highly excited states comprise millions of different components. Good description (taking into account many-phonon components) of the density of highly excited states proves the completeness of the configurational space[33].

To study the fragmentation of single-particle states, one should calculate the energies and wave functions of many states, and sum up $(C_{p}^{i})^2$ in some energy interval. Thus, only a small part of the obtained results is used. Therefore, let us use the direct calculation method of averaged characteristics without a detailed calculation of each state. We construct the function

$$\Phi_{p_0}(\eta) = \sum_i (C_{p_0}^i)^2 \rho(\eta_i - \eta), \tag{10}$$

where

$$\rho(\eta_i - \eta) = \frac{1}{2\pi} \frac{\Delta}{(\eta - \eta_i)^2 + (\Delta/2)^2}. \tag{11}$$

The energy interval of averaging Δ is a free parameter. We rewrite the function $\Phi_{p_0}(\eta)$ as

$$\Phi_{p_0}(\eta) = -\sum_i \left(\frac{\partial \mathcal{F}_{p_0}(\eta)}{\partial \eta} \right)^{-1}_{\eta = \eta_i} \rho(\eta_i - \eta). \tag{10'}$$

The function (10') may be written as a contour integral around the poles which are the roots of eq.(9). Considering that the contour integral over infinite radius circle in the complex plane η is

equal to zero, we pass to two contour integrals around the poles $z_{1,2} = \eta \pm i\frac{\Delta}{2}$. After some transformations we get:

$$\varphi_{\rho_0}(\eta) = \frac{1}{\pi} Im\left(\frac{1}{\mathcal{F}_{\rho_0}(\eta + i\frac{\Delta}{2})}\right). \qquad (12)$$

For a simplified model with $F = 0$ after calculations, we obtain

$$\varphi_{\rho}(\eta) = \frac{\Delta}{2\pi} \frac{\Gamma(\eta)}{(\varepsilon(\rho) - \gamma(\eta) - \eta)^2 + (\frac{\Delta}{2})^2 \Gamma^2(\eta)}. \qquad (13)$$

The Breit-Wigner form is strongly distorted due to the depen- on $\eta\Gamma(\eta)$ and $\gamma(\eta)$ which explicit form is given in ref.[34]. This results in an essential difference from the accepted description of neutron strength functions[2].

The peculiarities of the fragmentation of single-particle states in deformed nuclei were studied in refs.[24,31,34]. Fig.3 represents the fragmentation in ^{159}Gd of the state 624↑ lying 2 MeV higher than the Fermi-level and of high particle states 633↑ and 640↑. It is seen from the figure that the shape of the fragmentation curve differs from the Gauss one. The strength of the state far from the Fermi-level is distributed in a wide energy interval.

7. The possibility of calculation the fragmentation of single-particle states resulted in a new semi-microscopic method of calculation of the neutron strength functions (see ref.[31,34]). The neutron strength function is defined as:

$$S_\ell = \frac{\langle \Gamma_n^\ell \rangle}{\langle D \rangle}, \qquad (14)$$

where Γ_n^ℓ is the reduced neutron width, D is the spacing between the levels with the given I^π. Using neutron strength function as in ref.[35] and the wave function of the neutron resonances in the form (7) we get the S -wave neutron strength function, in the form

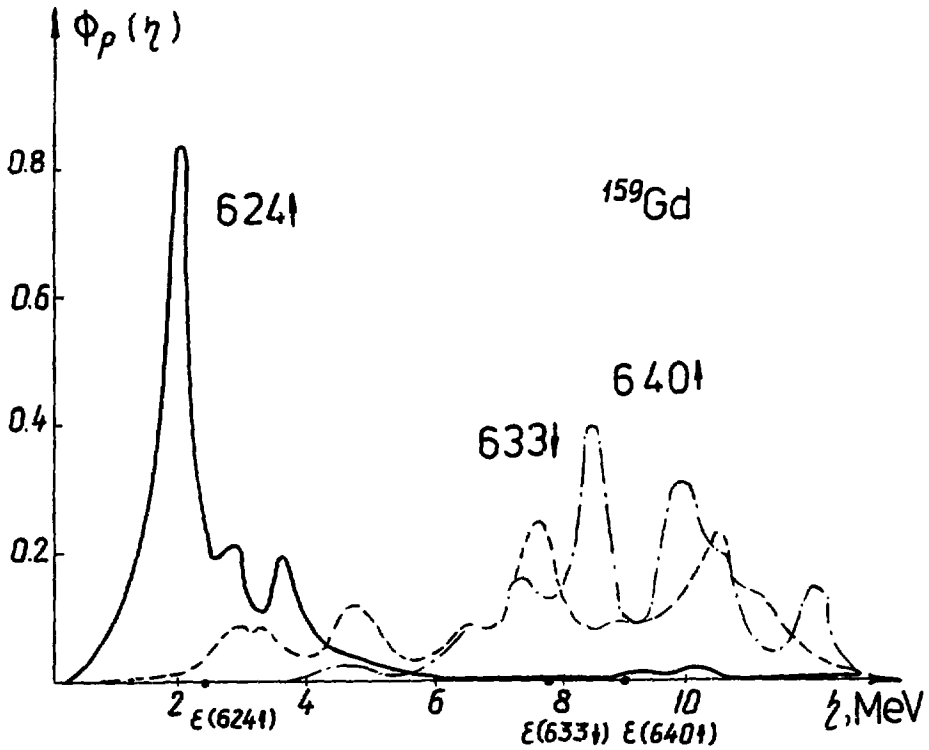

Fig.3. The fragmentation of single-particle states 624↑ (solid line), 633↑ (dotted line) and 640↑ (dot-dashed line) in ^{159}Gd . The quasiparticle energies are denoted by $\mathcal{E}(\rho)$

$$S_o = \frac{15(\text{keV})}{\Delta E(\text{keV})} A^{-1/3} \sum_i \Delta E \left| \sum_\rho a_{c\,1/2}^{\rho\,1/2} U_\rho C_\rho^i \right|^2, \qquad (15)$$

where ΔE is the energy interval over which the averaging is taken, the summation over ρ is performed over single-particle states with $K^\pi = 1/2^+$. According to ref.[36] the single-particle wave function φ_ρ^K is represented as an expansion in the spherical basis

$$\varphi_\rho^K = \sum_{nlI} a_{nlI}^{\rho K} \varphi_{nlI}, \quad a_{lI}^{\rho K} = \sum_n a_{nlI}^{\rho K}. \qquad (16)$$

We introduce the strength functions:

$$S_{lI}^{\rho K}(\eta) = \sum_i \rho(\eta - \eta_i) \left| \sum_\rho a_{lI}^{\rho K} U_\rho C_\rho^i \right|^2. \qquad (17)$$

Proceeding in the same way as when deriving the expression $\Phi_{jc}(\eta)$ we get:

$$S_{lI}^{\rho K}(\eta) = \frac{1}{\pi} \sum_\rho (a_{lI}^{\rho K} U_\rho)^2 \operatorname{Im}\left\{ \frac{1}{\mathcal{F}_\rho(\eta + i\Delta/2)} \right\} +$$

$$+ \frac{2}{\pi} \sum_{\rho > \rho'} a_{lI}^{\rho K} a_{lI}^{\rho' K} U_\rho U_{\rho'} \operatorname{Im}\left\{ \frac{\theta_\rho(\rho'; \eta + i\Delta/2)}{\theta_\rho(\eta + i\Delta/2)} \right\}. \qquad (18)$$

In our notations the expressions for s-, p - and α -wave neutron strength functions for the deformed nuclei are the following:

$$S_o = (15\,\text{KeV}) A^{-1/3} S_{0\,1/2}^{\rho\,1/2}, \qquad (19)$$

$$S_1 = (5\,KeV)A^{-1/3}\left\{S^{P_{1/2}}_{1,1/2} + S^{P_{1/2}}_{1,3/2} + S^{P_{3/2}}_{1,5/2}\right\}, \qquad (20)$$

$$S_2 = (9\,KeV)A^{-1/3}\left\{S^{P_{1/2}}_{2,3/2} + S^{P_{1/2}}_{2,5/2} + S^{P_{3/2}}_{2,3/2} + S^{P_{3/2}}_{2,5/2} + S^{P_{5/2}}_{2,5/2}\right\}, \qquad (21)$$

where $S^{PK}_{\ell,\ell\pm1/2}$ is defined by eq.(18) and given in units $(KeV)^{-1}$. For spherical nuclei S_0 is defined by eq.(19), and

$$S_1 = (5\,KeV)A^{-1/3}\left\{S^{P}_{1,1/2} + 2S^{P}_{1,3/2}\right\}, \qquad (22)$$

$$S_2 = (9\,KeV)A^{-1/3}\left\{2S^{P}_{2,3/2} + 3S^{P}_{2,5/2}\right\} \qquad (23)$$

In these formulae the multiplier δ_ℓ is equal to I for $\ell = 0$ and $(2\ell-1)/(2\ell+1)$ for $\ell \neq 0$ appearing in the calculation of the single single-particle neutron width for the square well.

The S - and P - wave neutron strength functions were calculated for some tin and tellurium isotopes. A good description of the S -wave strength function in its minimum was obtained. In the tellurium isotopes the subshell $3S_{1/2}$ is below the Fermi level and with increasing A some increase of C^2_p is compensated by decrease of U^2_j. A satisfactory description of the p -wave neutron strength function in the region close to its maximum is given (in ref.[32]) in eqs.(10)(10') the multiplier 1/3 is omitted). One should note that when calculating the fragmentation and strength functions in spherical nuclei it is necessary to use the model where the quasiparticle plus two phonons are taken into account in the wave function.

The numberical results for the S -, P -, and d -wave neutron strength functions are given in table 1. The experimental data are taken from refs.[37,38]. The calculations were performed with Δ =0.4 MeV, in many cases the results slightly depend on the

Table 1

Neutron strength functions at $\eta = B_n$.

Compound nucleus	B_n MeV	$S_0 \cdot 10^4$ Exp.	$S_0 \cdot 10^4$ Calc.	$S_1 \cdot 10^4$ Exp.	$S_1 \cdot 10^4$ Calc.	$S_2 \cdot 10^4$ Calc.
^{155}Sm	5.819	1.8 ± 0.5	1.0		1.1	1.2
^{159}Gd	6.031	1.5 ± 0.2	1.1	$2.8^{+1.4}_{-1.0}$	1.6	1.0
^{161}Gd	5.650	1.8 ± 0.4	1.0	$0.88^{+0.84}_{-0.47}$	1.1	1.2
^{161}Dy	6.448	2.0 ± 0.36	1.5	-	0.5	1.5
^{163}Dy	6.253	1.88	1.8	1.4	0.7	3.7
^{165}Dy	5.635	1.7	1.8	1.3	0.6	3.6
^{169}Er	5.997	1.5	3.4	0.7	0.5	6.8
^{171}Er	5.676	1.54	3.5	0.8	0.7	5.2
^{183}W	6.187	2.1 ± 03	4.6	0.3 ± 0.1	0.8	2.0
^{231}Th	5.09	1.3	1.1	-	0.7	4.0
^{233}Th	4.96	0.9	0.8	0.5-1.6	0.6	6.0
^{233}U	5.88	0.95	0.9	-	0.8	4.0
^{235}U	5.27	1.13 ± 0.4	1.3	-	1.2	5.8
^{237}U	5.30	1.3 ± 0.2	1.2	2.3 ± 0.6	1.1	4.6
^{239}U	4.78	1.1 ± 0.1	1.5	1.7 ± 0.3	0.8	3.8
^{241}Pu	5.41	0.94 ± 0.9	0.9	2.8	1.0	3.4
^{243}Pu	5.05	0.9 ± 0.1	1.4	-	1.4	4.0
^{245}Cm	5.696	1.1 ± 0.2	1.6	-	0.7	3.0

quantity Δ . But if the energy $\varepsilon = B_n$ is near the local maximum or minimum, the change of Δ may result in the change of S_ℓ by a factor up to 1.5. The calculation results strongly depend on the coefficients $a^{\lambda\kappa}_{\ell I}$ in the expansion of the single-particle wave function in the spherical basis (see formula(16)). The calculation of these coefficients should be made more accurately for the quasi-bound states.

Table 1 shows that a rather good description of the s - and p -wave neutron strength functions is obtained. We also present the calculation results of the d -wave strength functions for which there are only very preliminary experimental data. The agreement of our description with experimental data is not trivial as the calculations are based on the fragmentation of single-particle states and have no free parameter.

The method of calculation of averaged characteristics was applied in ref.[39] for the calculation of γ -transition probabilities. This method can be used for the calculation of partial radiational widths. One may hope that in this way the influence of the giant dipole resonance on the strength radiational functions will be clarified.

8. In conclusion I should like to note that our study of the structure of neutron resonances is performed within the semi-microscopic theory pretending to the unified description of few-quasiparticle components of the wave functions at low, intermediate and high excitation energies. In ref.[40] the possibilities of the unified description from the low-lying states to the neutron resonances and further to the giant multipole resonances are demonstrated. The description of each individual level is obtained for the low-lying states. For the states of intermediate and high excitation energies the few-quasiparticle components are represented as the corresponding strength functions.

In conclusion I am grateful to L.A.Malov and V.V.Voronov for useful discussions and help.

REFERENCES

1) V.G.Soloviev, Izv.Akad.Nauk SSSR (ser.fiz.)1974, 38, 1580.

2) J.E.Lynn, The Theory of Neutron Resonance Reactions (Clarendon Press, Oxford, 1968)
H.Feshbach, Ann.of Phys. 1958, 5, 357; 1962, 19, 287
C.Mahaux, H.A.Weidenmüller, Schell-Model approach to nuclear reactions (North-Holland, Amsterdam, 1969)

3) C.Mahaux, in J.Eröand J.Szücs (ed.), Nuclear Structure with Neutrons (Adamèniai Kiadó, Budapest, 1974),p.197
A.M.Lane, in Neutron Capture Gamma-Ray Spectroscopy (Reactor Centrum Nederland, Petten, the Netherlands, 1975),p.31
S.F.Mughabghab, in Neutron Capture Gamma-Ray Spectroscopy (Reactor Centrum Nederland, Petten, the Netherlands, 1975),p.81

4) I.M.Frank, in J.Erö and J.Szücs (ed.), Nuclear Structure with Neutrons (Adadémiai Kiadó, Budapest, 1974),p.17
L.M.Bollinger, Nuclear Structure with Neutrons (Akadémiai Kiadó, Budapest, 1974),p.347
I.Bergqvist, Nuclear Structure with Neutrons (Akadémiai Kiadó, Budapest, 1974),p.427

5) P.M.Endt, in Neutron Capture Gamma-Ray Spectroscopy (Reactor Centrum Nederland, Petten, the Netherlands, 1975),p.17
G.A.Bartholomew, F.C.Khanna, in Neutron Capture Gamma-Ray Spectroscopy (Reactor Centrum Nederlands, 1975),p.119
R.E.Chrien, in Neutron Capture Gamma-Ray Spectroscopy (Reactor Centrum Neederlands, 1975), p.247
O.W.B.Schult, in Neutron Capture Gamma-Ray Spectroscopy (Reactor Centrum Nederlands, 1975), p.505

6) V.G.Soloviev, Yad.Fiz.1972, 15, 733;
V.G.Soloviev, Phys.Lett 1971, 35B, 109; Phys.Lett. 1972, 39B,605

7) V.G.Soloviev, Part. and Nucl., 1972, 3, 770
V.G.Soloviev, Phys.Lett. 1972, 42B, 409
V.G.Soloviev, in J.Eröand J.Szücs (ed.), Nuclear Structure with Neutrons (Akadémiai Kiadó, Budapest, 1974), p.85

[8] V.G.Soloviev, Izv.Akad.Nauk SSSR (ser.fiz.) 1971, 35, 666
V.G.Soloviev, L.A.Malov, Nucl.Phys. 1972, A196, 433

[9] V.G.Soloviev, Theoria Slozhnych Jader, Nauka, (Moscow, 1971)

[10] V.V.Voronov, V.G.Soloviev, Yad.Fiz. 1972, 16, 1188

[11] F.L.Shapiro in Research Applications of Nuclear Pulsed Systems (IAEA, Vienna, 1967), p.176

[12] K.U.Berckurts, G.Brunhart, Phys.Rev. 1970, C1, 726
V.P.Alfimenkov et al. Yad.Fiz. 1973, 17, 13

[13] V.P.Alfimenkov et al. Phys.Lett. 1975, 53B, 429
L.B.Pikelner in Selected Topics in Nuclear Structure, v.II (JINR D-9682, Dubna, 1976)

[14] J.Kvitek, Yu.P.Popov, Nucl.Phys.1970, A154, 177
Yu.P.Popov et al. Nucl.Phys. 1972, A188, 212

[15] V.G.Soloviev, Phys.Lett. 1971, 36B, 199

[16] O.W.B.Schult in Selected Topics in Nuclear Structure v.II (Publ. Department JINR D-9682, Dubna, 1976)

[17] V.V.Voronov, V.G.Soloviev, Zh.Exsp.Theor Fiz. Pis'ma. 1976, 23, 84

[18] V.V.Voronov, V.G.Soloviev, Yad.Fiz. 1976, 23, 942
V.G.Soloviev, V.V.Voronov, Contributed Paper PBI/K4 ICINN, Lowell, Mass. USA, 1976

[19] R.E.Chrien et al. Phys.Rev. 1976, C13, 578

[20] M.R.Bhat at al. Phys.Rev. 1975, C12, 1457

[21] S.F.Mughabghab, in J.Erö and J.Szücs (ed.), Nuclear Structure with Neutrons (Akadémiai Kiadó, Budapest, 1974), p.167
L.Aldea et al. Trudy III Vsesoyuznogo Soveshchaniya po Neitronnoj Fizike (Obninsk, 1974), v.2, p.85

[22] V.P.Vertebny at al. in Neitronnaya Fizika (Obninsk, 1974) v.I, p.70

[23] V.G.Soloviev in Neitronnaya Fizika (Obninsk, 1974),v.2, p.70

[24] V.G.Soloviev in Neutron Capture Gamma-Ray Spectroscopy (Reactor Centrum Nederland, Petten, the Netherlands, 1975), p.99

25) Yu.P.Popov in Neutron Capture Gamma-Ray Spectroscopy (Reactor Centrum Nederland, Petten, the Netherlands, 1975), p.379
Yu.P.Popov in Selected Topics in Nuclear Structure, v.II (JINR D-9682, Dubna, 1976)

26) A.M.Lane, R.G.Thomas and E.P.Wigner, Phys.Rev. 1966, 98, 693

27) L.A.Malov, V.G.Soloviev, Preprint JINR P4-7639,(1973)
Yad.Fiz., 1975, 21, 502; Teor.Mat.Fiz.,1975, 25, 132
S.V.Akulinichev, L.A.Malov, Communication JINR P4-8433 (1974)
L.A.Malov, G.Orchirbat, Preprint JINR P4-8492 (1974)
L.A.Malov, V.O.Nesterenko, Preprint JINR P4-8206 (1974)

28) V.G.Soloviev, Teor.Mat.Fiz., 1973, 17, 90

29) G.Kyrchev, V.G.Soloviev, Teor.Mat.Fiz. 1975, 22, 244

30) A.I.Vdovin, V.G.Soloviev, Teor.Mat.Fiz. 1974, 19, 275.

31) L.A.Malov, V.G.Soloviev, Yad.Fiz. 1976, 23, 53

32) D.Dambasuren et al. Journ.Phys. G: Nucl.Phys. 1976, 2, 26

33) A.I.Vdovin et al., Yad.Fiz. 1974, 19, 516
V.G.Soloviev, Ch.Stoyanov and A.I.Vdovin, Nucl.Phys. 1974 A224, 411
L.A.Malov, V.G.Soloviev, and V.V.Voronov, Nucl.Phys. 1974, A224, 396; Phys.Lett. 1975, 55B, 17
V.V.Voronov, L.A.Malov, V.G.Soloviev, Yad.Fiz. 1975, 21, 40; Preprint JINR E4-9236 (1975)

34) L.A.Malov, V.G.Soloviev, Preprint JINR P4-9652 (1976)

35) K.Seth, Nucl.Data 1966 A2, No.3, 299

36) Ph.A.Gareev et al., Part. and Nucl., 1973, 4, 357

37) S.F.Mughabghab, D.I.Garber, Brookhaven National Lab.report BNL-325 (3 rd ed.) 1973

38) F.Rahn et al. Phys.Rev. 1974, C10, 1904; Phys.Rev. 1972, C6, 1854
H.I.Lion et al. Phys.Rev. 1975, C11, 462

39) S.V.Akulinichev, L.A.Malov, Preprint JINR P4-9672 (1976)

40) V.G.Soloviev, in Selected Topics in Nuclear Structure v.II(JINR D-9682, (Dubna, 1976)

MG 1 - THEORETICAL NEUTRON PHYSICS I: ELUCIDATION OF NUCLEAR STRUCTURE - V. G. Soloviev (JINR, Dubna, USSR)

Wigner (Princeton Univ.):

I have two questions. The first one is: for the bulk of the wave function, let us say at the neutron resonances of uranium, how many quasi-particles does it have?

Soloviev:

If we consider the whole wave function I show that for uranium we have many components; for example, ^{239}U, we have about ten single quasi-particle components; about 10^4 quasi-particle phonons and about 10^6 quasi-particle two-phonons. Yes, but of course we know there are many quasi-particle three-phonons and it means that our wave function is not the true wave function. We are only thinking that we could describe one quasi-particle's components in language of strength function, but our wave function is not the real wave function for neutron resonance because we don't take components with larger number of quasi- particles and phonons.

Wigner:

I understand that. But if I look at the whole wave function, what is the majority of it? The majority is five quasi-particles, or ten quasi-particles, or how many?

Soloviev:

It's possible to sum if we consider the number of poles. For example, in the uranium region, most poles are quasi-particles plus two-phonons and quasi-particles plus three-phonons. But the quasi-particles plus four-phonon contribution is much smaller, because the binding energy is 4.8 MeV. At such energy, most poles are quasi-particles+two-phonons and quasi-particles plus three-phonons.

Wigner:

Most of it is only three phonons.

Soloviev:

Yes, two and three.

Wigner:

I see. I would have thought many more.

Soloviev:

If we consider larger energy, in this case more will have components with four or five phonons.

Wigner:

But you have hundreds of thousands of states and the hundreds of thousands of states must be all orthogonal to each other. With ten holes and particles

I don't know whether you can make hundred thousand or fifty thousand states orthogonal to each other.

Soloviev:

Yes, but the wave function is orthogonal, of course. We get an equation with all our excited states orthogonal.

Wigner:

And most of the wave functions consist of two or three quasi-particles?

Soloviev:

Yes. Three quasi-particles or five quasi-particles.

Wigner:

Three to five?

Soloviev:

Yes.

Wigner:

Oh, thank you. That increases it very much. Now, my second question is: I did not, and I think many others did not, fully understand what you mean by Bohr's hypothesis, which you say is not really confirmed. What is that hypothesis?

Soloviev:

I stress that our experimental information is only experimental information about a few quasi-particle components of the wave function. Secondly, these few quasi-particle components are only a small part of the whole wave function. These are only two points and I think it is necessary to obtain experimental information for the other parts.

Wigner:

But, you said that some hypothesis of Bohr is not confirmed. Which is that hypothesis?

Soloviev:

Yes, but it is possible to imagine a compound nucleus that has many millions of components and the components are small and fluctuate randomly. It seems to me we have experimental information about only a few quasi-particle components and it does not seem right to come to a conclusion about the whole wave function if you know only a small part of wave function. Maybe there are many components, maybe the Bohr hypothesis is true for such a wave function with many components randomly distributed.

Wigner:

Which hypothesis of Bohr which is incorrect?

Soloviev:

Not incorrect, but unconfirmed.

Wigner:

Which hypothesis is unconfirmed?

Soloviev:

My conclusion is only about two points. We have experimental information about few quasi-particle components. The few quasi-particle component is only a small part of the whole wave function.

Wigner:

I concur absolutely, but you did not say which hypothesis of Bohr is unconfirmed.

Newstead (Brookhaven):

Do you mean, for example, when you have a correlation between the entrance channel and the gamma ray decay, that that means you have a memory of the entrance channel and therefore that's a non-confirmation of the Bohr hypothesis, because the Bohr hypothesis says that you don't remember how the state was formed?

Soloviev:

Yes, but it's only a specific case, only a specific non-statistical effect, it's only a specific case belonging to a few quasi-particle components. But what I like to stress is that it is necessary to get experimental information about the whole wave function, or maybe a more important part of it.

Moldauer:

I think we should get off that subject. May I just make the final comment on this historic occasion? It might behoove us occasionally to go back to history and see what Bohr actually said and perhaps agree on what we mean by various hypotheses. I think we understand what you mean, that in fact we don't know the whole wave function from looking at neutron resonances and I think we all agree on that and we can then go back and read Bohr and decide all for ourselves what, in fact, bearing this has on Bohr's hypothesis. Can we go on, perhaps, to another topic?

Khanna (Chalk River):

Since you have that slide on, essentially my question concerns that one. What you have got is a system in which there are quasi-particles and phonons. You have replaced a system of all quasi-particles in terms of quasi-particles and phonons. The question is, are there any Pauli principle effects which you are ignoring which are important, that is, exclusion effects?

Soloviev:

Yes, we take into account the Pauli principle only in a rather simple way. In deformed nuclei, if the phonon is collective, it means that its wave function has many two quasi-particle components. This case, of very few two-phonon

states, is only a very special case where the Pauli Principle has not worked. Only if the two-phonons are not collective, it is the same, but we excluded such cases. The Pauli principle is important if we consider many phonon states, for example, five-phonons states, six-phonons states; these are the cases where the Pauli Principle is very important. But for two-phonons states in deformed nuclei it is not important, although in light nuclei it is very different. In deformed nuclei, because we have a very large configuration space, Pauli Principle effects are not so important. There are many other problems which we don't take into account in our consideration and they are more important, compared with the Pauli Principle.

Khanna:

But earlier you said that important components in these wave functions come from three to five phonon states. That would imply that there will be Pauli effects, which are quite important. Will you give an estimate?

Soloviev:

In our calculation we take into account only quasi-particles and two-phonon state and not more. In this case our wave function has a million components and I stress that it is not the real wave function of neutron resonances. Our wave function only describes one quasi-particle component. And it means that we can only calculate neutron strength function and in future radiative strength function. It is different. These are small components which affect the normalization and the averaging which increases the fragmentation. But one quasi-particle and two quasi-particle phonons are the real terms and they determine fragmentation. This is only some background in our calculations.

Mughabghab (Brookhaven):

From your theoretical studies of valence capture in molybdenum-92 or -98, what would be your expectation for heavier Molybdenum isotopes, for example? Can you tell us about that?

Soloviev:

We investigated, as I remember, Voronov and I investigated only molybdenum-93, 95, 97 and 99. But we didn't consider heavier nuclei which are possible to consider, but in this region, we are more or less into a transition to deformed molybdenum isotopes -- because molybdenum isotopes 100, 102 may be deformed. If we assume they are spherical, it is possible to make some conclusions, but if it is in a transition region to deformed nuclei, it is difficult to make some prediction. Such simple considerations are possible for spherical nuclei only, but not for transitional nuclei.

Feshbach (M.I.T.):

I wonder if you thought at all about the connection between your description and the statistical theory of nuclear reactions? In particular, do you have anything to say about the so-called evaporation region, or about the quasi-equilibrium region?

Soloviev:

It seems to me it's difficult to say anything about this connection. This is a stationary description. No questions are asked about how the states are produced; it is a little different from other approaches.

Feshbach:

It's not the time dependence. I mean the theory that Kerman, Khanna and myself have is not a time dependent theory, it's a stationary state theory in which these things occur. But never mind that. I mean, just let's look at the evaporation region where there are, after all, many papers which are not time dependent in their approaches, which gives rise to the Maxwellian distribution of particles, and there has been a very successful application of that kind of thinking, so I am curious as to whether you can approach this from your formalism. Perhaps it's too early to ask that question.

Soloviev:

But the evaporation region is at very high excitation. Our description is better at low energies. In neutron resonances this description is better for intermediate excitation energy; with giant resonance description we have difficulty with unbound states but evaporation region I don't know how, it's a long way to go to this region, it seems to me.

Newstead, Brookhaven:

It's interesting to see this comparison between your theoretical calculations of the s- and p- wave strength functions and the experimental values. Your calculation shows the same strength functions for the several gadolinium isotopes and here we know experimentally there is a difference in fact, though one could argue about the statistics. So what about the trends? Why don't they come out in your calculations?

Soloviev:

Yes, it's difficult to explain how to change from one nucleus to another. It's only a factor of two or three. It seems to me no parameter is good enough, but it is impossible to explain why specifically, just now, specifically from one deformed nucleus to another.

9.45 a.m., Thursday, July 8, 1976 in Olney 150 Invited Paper; Session MG2

MICROSCOPIC CALCULATIONS OF THE OPTICAL-MODEL POTENTIAL

J.-P. Jeukenne, A. Lejeune

University of Liège at Sart Tilman, 4000 Liège 1, Belgium

and C. Mahaux*

Nuclear Physics Laboratory, Oxford

* *Presented by C. Mahaux, on leave of absence from University of Liège.*

RÉSUMÉ

We present a critical survey of several recent microscopic calculations of the optical-model potential for nucleons. Special emphasis is laid on those calculations which are sufficiently realistic to impose meaningful constraints on the parametric expressions used in the analysis of the experimental data.

ABSTRACT

If it is sufficiently realistic, a microscopic calculation of the optical-model potential (OMP) for nucleons is of fundamental and of practical interest : (1) It is of fundamental interest because the rendering of the empirical OMP from a realistic nucleon-nucleon interaction is intimately related to the theoretical understanding of the success of the shell model ; conversely, this can serve as a test of the underlying many-body theory and of the nucleon-nucleon interaction. (2) It is of practical interest because the analysis of the experimental data is unable to fully determine the OMP, which is complex, nonlocal, energy dependent, ... : some theoretical constraints are therefore needed to restrict the freedom in the parametrization of the phenomenological OMP ; it is important to derive these constraints from a realistic calculation, since otherwise they may be meaningless and might then generate spurious trends in the parameters of the empirical OMP. For these reasons, we believe that a microscopic calculation of the OMP is really useful only if it is sufficiently "realistic", in the sense that it uses as much information as possible on the nucleon-nucleon interaction, on the theoretical properties of the OMP, on nuclear structure, and if it is based on a reliable approximation scheme. Therefore, it is mainly with this criterion in mind that we discuss the relative merits of several recent calculations of the OMP. These calculations are based on a variety of theoretical approaches : low energy nuclear reaction , multiple scattering, Green functions, Hartree-Fock or Brueckner-Hartree-Fock theories ; they involve either effective or realistic nucleon-nucleon interactions. We discuss the imaginary as well as the real part of the OMP.

1. INTRODUCTION

Practically all empirical analyses of the interaction of neutrons with nuclei make essential use of the optical model. The fact that high quality fits are obtained from optical-model potentials (OMP) which vary smoothly with energy and target mass number indicates that these OMP are physically meaningful and thus carry useful information. In order to extract this information, one must relate the phenomenological OMP (POP) to the theoretical OMP (TOP). Hence, the main aim of a theoretical study of the optical model is threefold :

(a) Explain the success of the optical model, which at first sight appears to be at variance with the strong nature of the nucleon-nucleon interaction. Note that by its very nature this problem requires the use of realistic (i.e. strong) nucleon-nucleon forces. As is well-known, the Pauli principle plays an essential role in this respect ; it must therefore be a prime ingredient of any reliable theory of the optical model.

(b) Give a definition of the OMP. This problem is somewhat ambiguous since a potential is not an observable ; it is rather an auxiliary quantity from which observables can be calculated. However, the almost universal success of the model suggests that the ambiguity is very much reduced if the TOP is required to be consistent with the use that is made of optical-model phase shifts and - more importantly - of optical-model wavefunctions. In other words, the definition must express the requirement that the OMP describes the evolution of that part of the incident wavepacket which decays exponentially in time. We recall in sect. 2 that this requirement is fulfilled if the TOP is identified with the mass operator (or self-energy).

(c) Find a reliable way of computing this mass operator (TOP) or at least find theoretical constraints that must be fulfilled by the POP. Several theoretical techniques for calculating the mass operator are briefly described in sect.3.A number of numerical results recently obtained for the real and for the imaginary parts of the OMP are critically surveyed in sects. 4 and 5, respectively. Our conclusions are contained in sect. 6.

2. DEFINITION

Details on the present section can be found in ref. [1]). Let us denote by $|0\rangle$ the (exact) target ground state. The probability amplitude of finding at point r' and at time t (> 0) a nucleon that has been created at point $\vec{r}$ and at time t = 0 is given by the "one-body Green function" :

$$G(\vec{r},\vec{r}',t) = -i \langle 0| a(\vec{r}',t)\, a^{+}(\vec{r}',t=0) |0\rangle \quad . \tag{1}$$

We have omitted the spin and isospin variables.

Let us now consider the simplified case of infinite, symmetric and uncharged nuclear matter. Then, the Green function depends on the variables $|\vec{r}-\vec{r}'|$, t and on the medium density ρ : $G_\rho(|\vec{r}-\vec{r}'|,t)$. We shall often omit the index ρ, which is related to the Fermi momentum

k_F by

$$\rho = \frac{2}{3\pi^2} k_F^3 \quad . \tag{2}$$

By successive Fourier transformations, we can construct various representations for the Green function :

$$G_\rho(|\vec{r}-\vec{r}'|,t) \leftrightarrow G_\rho(k,t) \leftrightarrow G_\rho(k,E) \quad , \tag{3}$$

where, for simplicity, we keep the same notation for G. As mentioned in sect. 1, the optical model deals with that part of the wave packet which decays exponentially in time, and has thus a well-defined (complex) frequency. In other words, we write ($\hbar = 1$)

$$G(k,t) = -iR(k)\exp(-ie(k)t)\exp(-\frac{1}{2}t/\tau) + G^{CN}(k,t) \quad , \tag{4}$$

and it is only the first term on the rhs of eq. (4) that the optical model can describe. The second term accounts for the fact that the nucleon can excite complicated compound nuclear states immediately after its creation [2]). The Fourier transform of the first term on the rhs of eq. (4) reads

$$G(k,E) \approx \frac{R(k)}{E - e(k) + iW(k)} \quad , \tag{5}$$

where

$$W(k) = (2\tau)^{-1} \quad , \qquad e(k) = \frac{k^2}{2m} - V(k) \quad . \tag{6}$$

In the case of a gas of noninteracting nucleons in an external potential $(-)U^{(o)}(k)$, the Green function reduces to

$$G^{(o)}(k,E) = \{E - \frac{k^2}{2m} + U^{(o)}(k)\}^{-1} \quad . \tag{7}$$

The comparison between eqs. (5) and (7) shows that the complex quantity

$$M(k) = - V(k) - iW(k) \tag{8}$$

is the mean potential energy of a nucleon with momentum k.

From eqs. (5), (6), we have

$$G(k,E) \approx \frac{R(k)}{E - \frac{k^2}{2m} - M(k)} \quad . \tag{9}$$

This suggests to identify the OMP with the mass operator M(k,E) which is defined by the following equation (actually we should extend definition (1) to negative time [1]))

$$G(k,E) = \frac{1}{E - \frac{k^2}{2m} - M(k,E)} \quad . \tag{10}$$

Several representations of the mass operator are obtained by successive Fourier transformations

$$M_\rho(|\vec{r}-\vec{r}'|,c) \leftrightarrow M_\rho(k,t) \leftrightarrow M_\rho(k,E) \quad . \tag{11}$$

Note that the dependence of M(k,E) on k reflects the nonlocal character of the OMP, while its dependence on E is associated with the time dependence (i.e. with the dynamical character) of the mean field. We write

$$M(k,E) = - V(k,E) - iW(k,E) \quad . \tag{12}$$

The following subtracted dispersion relation and asymptotic behaviour hold

$$V(k,E) = f(k) + \pi^{-1}\int_{-\infty}^{\infty} dE' \, \frac{W(k,E')}{E' - E} \quad , \tag{13}$$

$$W(k,E) \xrightarrow[E \to \varepsilon_F]{} c^2(E - \varepsilon_F)^2 \quad , \tag{14}$$

where ε_F is the Fermi energy

$$\varepsilon_F = \frac{k_F^2}{2m} + M(k_F,\varepsilon_F) \quad . \tag{15}$$

The identification of the mass operator with the mean field is also valid in the case of a finite nucleus [3,4]. Then, however, the mass operator is a more complicated function : $M(\vec{r},\vec{r}',E)$. Moreover, it is a wild function of energy in the region of isolated resonances : it can thus be necessary to identify the OMP with the energy-average $M(\vec{r},\vec{r}',E+iI)$, where I is the averaging interval [5]. Since the direct calculation of the mass operator in a finite nucleus is quite complicated, the calculations are often carried out in nuclear matter and then extrapolated in finite nuclei by means of the following "local density approximation" (LDA), whose accuracy admittedly still requires to be further tested : In nuclear matter, the mass operator $M_\rho(|\vec{r}-\vec{r}'|, E)$ is a function of the density ρ. By identifying ρ with the experimental matter distribution $\rho(r)$ of a finite nucleus, one obtains M as a function of the distance r from the nuclear centre, of the nonlocality variable $|\vec{r}-\vec{r}'|$ and of the energy E.

In most empirical analyses, the POP is parametrized either in the form of a local, energy-dependent field or else (and more rarely so) of a nonlocal, energy-independent field as in the pionneering work of Perey and Buck [6]. The TOP, i.e. the mass operator, is nonlocal and complex. Before comparing it with the POP, it is thus necessary to construct potentials that are "equivalent" to the TOP but are either nonlocal and energy independent or purely local and energy dependent. This can be achieved by means of the "local energy approximation" [7,8,9]. The latter amounts to taking the value of the mass operator M(k,E) at the pole of the Green function. The real part of this pole is approximately given by the energy-momentum relation

$$e(k) = \frac{k^2}{2m} + \mathrm{Re}\, M(k,e(k)) \quad . \tag{16}$$

Since k and e are related by eq. (16), one may consider M(k,e(k)) either as a function of k, in which case we write

$$M_\rho(k,e(k)) = M_\rho(k) = - V_\rho(k) - iW_\rho(k) \quad , \tag{17}$$

or else as a function of the energy e, in which case we write

$$M_\rho(k,e(k)) = M_\rho(e) = - V_\rho(e) - iW_\rho(e) \quad . \tag{18}$$

The potential $M_\rho(e)$ is local and energy dependent ; the Fourier transform of $M_\rho(k)$ over k is a nonlocal but energy-independent field. The equivalent OMP (17) or (18) can now be directly compared with the POP.

We note that the dependence of M(e) on e differs from the "true" energy dependence of the TOP (M(k,E)) on the energy E, since it contains a spurious energy dependence due to the true nonlocality. In practice, the true nonlocality and the true energy dependence of the TOP can only be disentangled by means of theoretical considerations. Attempts in this direction have been made on the basis of the subtracted dispersion relation (13) which, however, only yields semi-quantitative information [10]. The two effects can be distinguished in a theoretical calculation provided that the latter involves no adjustable parameters, since otherwise the variability of the parameters can blur the distinction between true nonlocality and true energy dependence. This problem is not only of fundamental but also of practical interest. Indeed, the "Perey effect" [6] (attenuation of the scattering wave function in the nuclear interior) and the Coulomb correction [11] are both due to the nonlocality. We shall see that they are underestimated if, as in all calculations to-date, they are evaluated from the nonlocality of the energy-independent nonlocal field (17).

3. CALCULATIONAL APPROACHES

3.a. Perturbation theory

The mass operator can be expanded in powers of the nucleon-nucleon interaction v if the latter is sufficiently weak. Some of the lowest order terms of this perturbation expansion are represented in Fig. 1. We attached a hat on each contribution to emphasize that the expansion is meaningful only in the case of a very weak, and thus usually "effective", nucleon-nucleon force.

The first order term is the Hartree-Fock (HF) contribution $\hat{M}^{(HF)} = \hat{M}^{(1a)}$. Its expression reads

$$\hat{M}^{(HF)}(k) = \sum_{j<k_F} \{\langle \vec{k},\vec{j}|v|\vec{k},\vec{j}\rangle - \langle \vec{k},\vec{j}|v|\vec{j},\vec{k}\rangle\} \tag{19}$$

$$= \sum_{j<k_F} \langle \vec{k},\vec{j}|v|\vec{k},\vec{j}\rangle_A \quad , \tag{20}$$

where the index A refers to antisymmetrization, and where we used the simplified notation

$$\sum_{j<k_F} = \sum_{\vec{j},j<k_F} \quad . \tag{21}$$

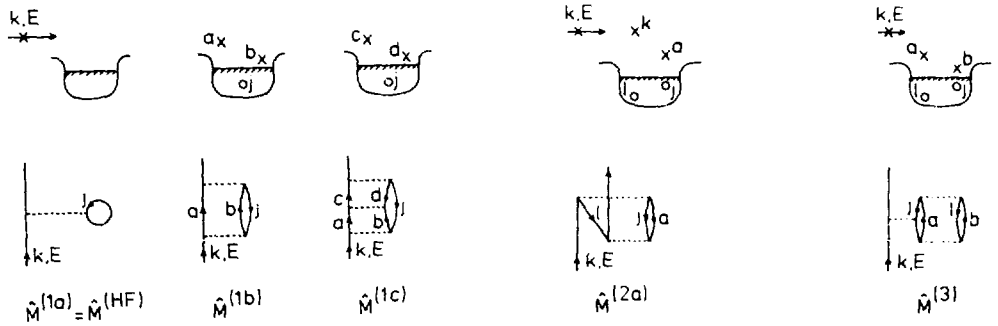

Fig. 1. Some of the lowest order terms of the expansion of the mass operator M(k,E) in powers of the nucleon-nucleon interaction. The Fermi surface is represented by a shaded line.

In a finite nucleus, the action of the HF field (19) on the scattering wave function $\chi_E(r)$ takes the following form, in the coordinate space representation,

$$\hat{M}^{(HF)}(\vec{r},\vec{r}')\chi_E(\vec{r}) = \sum_{j=1}^{A} \int \psi_j^{*}(\vec{r}')\, \psi_j(\vec{r}')\, v(|\vec{r}-\vec{r}'|)\, \chi_E(\vec{r})\, d^3r'$$

$$- \sum_{j=1}^{A} \int \psi_j^{*}(\vec{r}')\, \psi_j(\vec{r})\, v(|\vec{r}-\vec{r}'|)\, \chi_E(\vec{r}')\, d^3r' \quad , \qquad (22)$$

In terms of the one-body density matrix, eq. (22) reads

$$\hat{M}^{(HF)}(\vec{r},\vec{r}')\chi_E(\vec{r}) = \int \rho(\vec{r}')\, v(|\vec{r}-\vec{r}'|)\, d^3r'\, \chi_E(\vec{r})$$

$$- \int \rho(\vec{r},\vec{r}')\, v(|r-r'|)\chi_E(\vec{r}')\, d^3r' \quad . \qquad (23)$$

We see that in the HF approximation the mass operator is real, independent of energy and nonlocal. The nonlocality arises from the exchange (Fock) term, which can be replaced by an equivalent local (but energy dependent) field, as discussed in sect. 2. In the HF approximation, the incoming particle simply feels the mean potential created by the target which is assumed to be inert (no correlation : independent particle model). This is depicted in Fig. 1 (top left) and is the origin of the static (independence of energy) character of the HF field.

There exist two second-order contributions ; they are represented by graphs $\hat{M}^{(1b)}$ and $\hat{M}^{(2a)}$ in Fig. 1. Their expressions read

$$\hat{M}^{(1b)}(k,E) = \sum_{j<k_F} \sum_{a,b>k_F} \frac{\langle \vec{k},\vec{j}|v|\vec{a},\vec{b}\rangle \langle \vec{a},\vec{b}|v|\vec{k},\vec{j}\rangle_A}{E + e(j) - e(a) - e(b) + i\delta} \quad , \qquad (24)$$

$$\hat{M}^{(2)}(k,E) = \sum_{\ell,j<k_F} \sum_{a>k_F} \frac{\langle \vec{k},\vec{a}|v|\vec{j},\vec{\ell}\rangle \langle \vec{j},\vec{\ell}|v|\vec{k},\vec{a}\rangle_A}{E + e(a) - e(j) - e(\ell) - i\delta} \quad , \tag{25}$$

where

$$e(d) = \frac{d^2}{2m} + U(d) \quad . \tag{26}$$

The "auxiliary" potentiel U(d) is a parameter which can be chosen in such a way as to improve the convergence of the perturbation series. The self-consistent HF choice consists in taking

$$U(d) = \hat{M}^{(HF)}(d) \quad ; \tag{27}$$

for $d < k_F$, this choice is the nuclear matter counterpart of the requirement that the bound eigenstates of the HF hamiltonian

$$H^{(HF)} = -\frac{1}{2m}(\vec{\nabla})^2 + \hat{M}^{(HF)}(\vec{r},\vec{r}') \tag{28}$$

be identical to the single particle wave functions ψ_j in eq. (22). Note that $\hat{M}^{(1b)}$ and $\hat{M}^{(2)}$ are energy dependent and complex. The imaginary part of $\hat{M}^{(1b)}$ differs from zero for $E > e(k_F)$; it gives the lowest-order contribution to the imaginary part of the OMP. The imaginary part of $\hat{M}^{(2)}$ differs from zero for $E < e(k_F)$; it gives rise to the first nonvanishing contribution to the width of the hole states. The physical meaning of $\hat{M}^{(1b)}$ is that the incident nucleon can excite a two-particle - one hole (2p-1h) intermediate state, whence the name "core polarization graph" coined for it by Bertsch and Kuo [12]. The contribution $\hat{M}^{(2)}$ arises because the existence of the incident nucleon k suppresses the contribution of those 2p-2h target configurations where one of the particle is in state k, whence the name "Pauli blocking graph" [12].

There exist several third-order contributions. One of them, represented by graph $\hat{M}^{(3)}$ in Fig. 1, is static. It can be added to the HF term ; the resulting sum being called the "renormalized Hartree-Fock" (RHF) approximation :

$$\hat{M}^{(RHF)}(k) = \sum_{j<k_F} f(j) \langle \vec{k},\vec{j}|v|\vec{k},\vec{j}\rangle_A \quad . \tag{29}$$

Here, 1-f(j) is the probability that the momentum state j is depleted because of the existence of 2p-2h admixtures in the target.

3.b. Brueckner expansion

Interactions which fit the nucleon-nucleon scattering are usually so strong that the perturbation expansion of sect. 3.a badly diverges. This can be understood as follows. While the Pauli principle imposes that nucleons a and b (see $\hat{M}^{(1b)}$) lie above the Fermi surface, and thus somewhat quenches the strength of the interaction between the incident nucleon k and the target nucleon j, it does hinder the excited nucleons a and b to interact repeatedly. Hence, it appears appropriate to allow for repeated scattering between a and b, i.e. to group all

contributions with particle-particle ladders, namely $\hat{M}^{(1b)}$, $\hat{M}^{(1c)}$,... Another justification consists in noting that all these graphs contain only one hole line, i.e. involve only one integration from 0 to k_F over an intermediate momentum. Hence, it appears that a regrouping of the graphs of the perturbation series according to their number of hole lines roughly amounts to building an expansion where the density plays the role of a small parameter (see eq.(2)). More precisely, the "small parameter" of the expansion is believed to be approximately given by the cube of the ratio of the hard core of the nucleon-nucleon interaction to the average internucleon distance [13].

The leading term of this low-density expansion is usually called the Brueckner-Hartree-Fock (BHF) approximation ; it is denoted by $M^{(1)}$ in Fig. 2, and reads

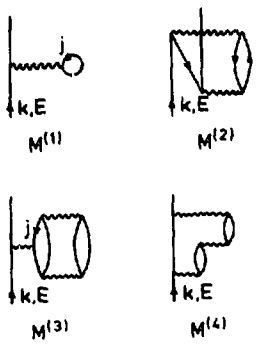

Fig. 2. Some of the lowest-order terms of the low-density Brueckner expansion for the mass operator.

$$M^{(BHF)}(k,E) = M^{(1)}(k,E) = \sum_{j<k_F} \langle \vec{k},\vec{j}\,|\,g[E+e(j)]\,|\,\vec{k},\vec{j}\,\rangle_A \quad , \qquad (30)$$

where the "reaction matrix" g[w] is a solution of the Bethe-Goldstone integral equation

$$g[w] = v + v \sum_{a,b>k_F} \frac{|\vec{a},\vec{b}\rangle\langle\vec{a},\vec{b}|}{w - e(a) - e(b) + i\delta}\, g[w] \quad . \qquad (31)$$

It is immediately verified that the first iteration of (31) corresponds to the approximation

$$M^{(1)}(k,E) = \hat{M}^{(1a)}(k) + \hat{M}^{(1b)}(k,E) \quad . \qquad (32)$$

It also appears appropriate [13] to replace the value (27) for the auxiliary potential U(d) by the BHF choice

$$U(d) = \mathrm{Re}\, M^{(1)}(d,e(d)) \quad , \qquad (33)$$

although, actually, the complex choice $U(d) = M^{(1)}(d,e(d))$ would be somewhat better.

The addition of particle-particle ladders to $\hat{M}^{(2)}$ (Fig. 1) leads to the two-hole line contribution $M^{(2)}$ (see Fig. 2) ; in the same way, $\hat{M}^{(3)}$ is the progenitor of a series of graphs whose sum is represented by $M^{(3)}$ in Fig. 2. As in sect. 3.a, $M^{(1)}$ and $M^{(3)}$ can be summed to yield the renormalized BHF (RBHF) approximation

$$M^{(RBHF)}(k,E) = M^{(1)}(k,E) + M^{(3)}(k,E) = \sum_{j<k_F} f(j) \langle \vec{k},\vec{j} | g[E+e(j)] | \vec{k},\vec{j} \rangle_A \qquad (34)$$

Note that, in the BHF approximation, the OMP is both nonlocal and energy-dependent, while it is static in the HF case. The dependence of $M^{(1)}(k,E)$ on k yields the true nonlocality of the BHF field, while its dependence on E corresponds to its true (dynamical) energy dependence. This is discussed in detail in ref. [1]). Note also that the BHF field is complex, while the HF approximation is real.

3.c. Multiple scattering expansion

If the Pauli principle is omitted in eq. (31), i.e. if the summation over a and b is allowed to extend over the states below the Fermi surface, and if furthermore e(a) and e(b) are replaced by pure kinetic energies, the reaction matrix reduces to the transition matrix t[w] for free nucleon-nucleon scattering amplitude. If one neglects the values of U(j) and U(k) as compared to $k^2/(2m)$, which may be justified for large values of k, one obtains the following approximation for the OMP :

$$M^{(IA)}(k) = \sum_{j<k_F} \langle \vec{k},\vec{j} | t \left[\frac{k^2}{2m} + \frac{j^2}{2m}\right] | \vec{k},\vec{j} \rangle_A \quad . \qquad (35)$$

Expression (35) is the leading term of the multiple scattering series ; it is sometimes called the impulse approximation, although this expression is also used to denote some improved expressions. The nature of the approximations that lead from (31) to (35) (neglect of Pauli principle and of binding energy effects) indicates that (35) is valid only at high energy. Its main interest is that it only involves the free nucleon-nucleon scattering amplitude, i.e. a quantity that can be directly obtained from nucleon-nucleon scattering data (one can rewrite (35) in terms of nucleon-nucleon phase shifts) : There is no need to introduce a nucleon-nucleon potential, although this or an equivalent ambiguity (off-shell extension) cannot be avoided if one wants higher order terms of the multiple scattering series.

3.d. Nuclear reaction theory

In the framework of nuclear reaction theory, the OMP is introduced as follows. Let Ψ_E denote the exact scattering wave function at the energy E, with the boundary condition that incoming waves are present only in the channel where the target is in its ground state $|0\rangle$. By projecting Ψ_E onto $|0\rangle$, one obtains a single particle wave function $\chi_E(\vec{r})$. The latter is the eigenstate of a one-body Schrödinger equation where the potential is the mass operator $M(\vec{r},\vec{r}',E)$ [14,15]). As mentioned in sect. 2, it may be necessary to average $M(\vec{r},\vec{r}',E)$ over energy in the region of isolated resonances before identifying it with

the usual OMP [5]). Although these manipulations are of quite general validity, the physical content of the theory and its practical applications or difficulties can best be discussed by making reference to the perturbation expansion (sect. 3.a).

In a finite nucleus the first-order term is given by eq. (22), where the ψ_j's are to be determined self-consistently from the HF hamiltonian. Once this single-particle basis $(\psi_j, \chi_E(\vec{r}))$ is adopted, one can in principle calculate the second order corrections $\hat{M}^{(1b)}$ and $\hat{M}^{(2)}$ (see Fig. 1).

Let us first consider the core polarization graph $\hat{M}^{(1b)}$. In a finite nucleus, it is useful to make a distinction between two types of contributions to $\hat{M}^{(1b)}$ (eq. (24)), namely those where nucleons a and b are in bound orbitals on the one hand, and those where a or b is in the continuum. Important difficulties appear when both a and b are in the continuum. In the first case, the summations over a and b are discrete ; in the second case one of the summations is replaced by an integral :

$$\hat{M}^{(1b)}(k,E) = \frac{1}{2} \sum_{j<k_F} \sum_{a,b=k_F}^{k_B} \frac{|\langle \vec{k},\vec{j}|v|\vec{a},\vec{b}\rangle_A|^2}{E + e(j) - e(a) - e(b)}$$

$$+ \frac{1}{2} \sum_{j<k_F} \sum_{b=k_F}^{k_B} \int_{k_B}^{\infty} da \frac{|\langle \vec{k},\vec{j}|v|\vec{a},\vec{b}\rangle_A|^2}{E + e(j) - e(a) - e(b) + i\delta} \quad , \qquad (36)$$

where k_B denotes the wave number of the last bound unoccupied orbital. The first term on the rhs of eq. (36) is a discrete sum of real quantities. It corresponds to the excitation of quasibound 2p-1h states by the incident nucleons, i.e. to the excitation of resonances [16]). Although it is real, it contributes to the imaginary part of the OMP when one performs an energy average ($E \to E + iI$) over the resonances. This interpretation can easily be carried over to the excitation of more complicated compound states : the first term on the right-hand side of eq. (36) can then be written somewhat symbolically in the more general form (which goes beyond second order perturbation theory)

$$\frac{1}{2} \sum_n \frac{\langle \chi_E(\vec{r})\phi_o(1,\ldots,A)|v|\phi_n(0,1,\ldots A)\rangle_{AA}\langle\phi_n|v|\phi_o\chi_E(\vec{r}')\rangle}{E + e_o - e_n} \quad , \qquad (37a)$$

where χ_E is the HF scattering single particle wave function, ϕ_o the target wave function in the HF approximation, and e_o its energy, while the ϕ_n's are the quasibound states obtained by diagonalizing the full hamiltonian in the subspace of the bound eigenstates of the HF hamiltonian for the system with A+1 nucleons. The integration runs over all coordinates 1...A of the target nucleons. Thus, (37a) expresses the influence of compound nucleus formation on the OMP. The antisymmetrization sign in (37a) gives no problem. However, note that the wave function ϕ_o in (37a) is not the exact target wave function $|0\rangle$: it is the uncorrelated HF ground state. It is possible to replace in (37a) the quantity $|\phi_o\rangle$ by a more correct model target wavefunction, obtained by

diagonalizing the full hamiltonian among the bound eigenstates of the HF hamiltonian for the system with A nucleons [16]. This amounts to stating that the contribution of that part of graph $\hat{M}^{(3)}$ (Fig. 1) where nucleons a and b are in bound orbitals can be included in expression (37a). Indeed, we saw in sect. 3.a that the role of $\hat{M}^{(3)}$ is to take into account the existence of 2p-2h excited states in the target.

We now turn to the second term on the right-hand side of eq. (36). Since a (or b) now lies in the continuum, the 2p-1h intermediate states can more appropriately be associated to channels, and the summation over a and b corresponds to a summation over intermediate channels. This term reads then, in a somewhat sketchy notation,

$$\frac{1}{2} \sum_{c \neq 0} \int_{\varepsilon_c} dE' \frac{\langle \chi_E(\vec{r}) \phi_o(1,..,A) | v | \psi_E^c, (0,1,..,A) \rangle_{AA} \langle \psi_E^c, | v | \chi_E(\vec{r}') \phi_o \rangle}{E + e_o - E' + i\delta} \quad (37b)$$

where ψ_E^c is the wave function of the inelastic channel c, with threshold energy ε_c. The term (37b) corresponds to the direct feeding of inelastic or of reaction channels c. It is complex if $E + e_o$ is larger than the threshold energy of the lowest inelastic channel. The result (37b) can be extended by taking for ϕ_o the model target wavefunction that corresponds to the lowest configuration obtained by diagonalizing the full hamiltonian in the subspace of the bound eigenstates of the HF hamiltonian for A nucleons. Likewise, the ψ_E^c,'s can be replaced by channel wavefunctions where the residual nuclei are described by model wavefunctions obtained by diagonalizing the full hamiltonian in the subspace of the bound eigenstates of the HF hamiltonian for A nucleons [16].

It is quite difficult to extend (36) or (37a,b) to the case where the two nucleons a and b are in the continuum or to the case where ϕ_o contains configurations where one or more nucleons are in scattering states. Indeed, one then encounters difficulties analogous to those met in the three-body problem ; moreover, double-counting problems appear, due to antisymmetrization [14]. These difficulties are intimately related to the other second order contribution, namely $\hat{M}^{(2)}$. Indeed, we saw in sect. 3.a that the physical origin of graph $\hat{M}^{(2)}$ is that the true target wavefunction $|0\rangle$ may contain 2p-2h excited states where one nucleon is in the continuum. Thus, graph $\hat{M}^{(2)}$ and more generally all "backward-going graphs" were excluded from the shell-model approach to nuclear reactions, where at most one nucleon is allowed to be in the continuum [16]. Some configurations with two nucleons in scattering states can be included in the shell-model formalism in the framework of the random-phase approximation (RPA) [17]. In that case, however, it appears more convenient not to use the techniques of nuclear reaction theory proper, but rather to return to the definition of the OMP as being the mass operator. Indeed, it can be shown that a selected infinite number of graphs of the perturbation theory can be summed up in closed form ; they include the backward going graphs characteristic of the RPA. This was demonstrated by N. Vinh Mau [18], who made use of a suitable truncation of the hierarchy of coupled equations which relate the one-, two-,...body Green functions [19].

3.e. Martin-Puff-Schwinger approaches

We just mentioned the existence of an infinite system of coupled equations which relate the one-, two-, three-,...body Green functions [19]. The RPA is obtained from this set by a truncation that amounts to introducing a ladder approximation for the particle-hole two-body Green function [20]. This approximation appears well adapted for the treatment of long-range correlations. Other possibilities of truncation exist, which seem more appropriate for handling short-range correlations. They have been proposed by Puff [21] and by Falk and Wilets [22] and are usually called the $\Lambda_{00}, \Lambda_{01}, \Lambda_{11}$ approximations. They have been reviewed in ref. [23]. They lead to expressions for the mass operator which are formally analogous to the BHF approximation (30). However, the propagator in the integral equation fulfilled by the corresponding reaction matrix is different from that which appears in (31) : both the form of the Pauli projection operator $|\vec{a},\vec{b}><\vec{a},\vec{b}|$ and the energy denominator (choice of the auxiliary potential U(a)) are altered.

3.f. Discussion

We have seen that many different theoretical approaches exist for the calculation of the OMP. The particular method that one selects depends on the input that one wants to use. For instance, a calculation based on "realistic"(i.e. strong) nucleon-nucleon forces in practice restricts the choice to the Brueckner, multiple scattering or Martin-Schwinger-Puff approaches. On the contrary, a calculation where one wishes to make maximum use of nuclear structure information will usually be performed in the framework of nuclear reaction theory (sect.3.d).

4. CALCULATIONS OF THE REAL PART OF THE OMP

4.a. Meaningfulness of theoretical constraints

Lerner and Redish [24] emphasized that "the utility of a theory of the OMP can only be investigated by calculating the OMP directly, without free parameters". This is so because the variability of some parameters might amount to mocking up processes in a manner that can correspond to imposing unphysical constraints on the calculated OMP. We illustrate this point by briefly discussing the example of the "reformulated optical-model potentiel" [25,26]. This model consists in approximating the mass operator by the first term on the rhs of eq. (23), i.e.

$$\hat{M}(r) = \int \rho(\vec{r}') \; v \; (|\vec{r}-\vec{r}'|) \; d^3r' \quad . \tag{38}$$

As before, the spin and isospin variables are implicit, and the hat on $\hat{M}(r)$ reminds one that expression (38) can be meaningful only if used in connection with a weak - and thus in practice "effective" - interaction v. Attempts have been made to apply (38) to obtain information on the nuclear density $\rho(r)$, by considering v as known. Conversely, one can try to obtain information on the effective interaction v by inserting an empirical value of ρ in (38). The existence of these two possibilities already shows that the physical information derived from (38) is of limited accuracy. There are two main reasons for this ambi-

guity. Firstly, expression (38) is a rather crude approximation since exchange and higher order terms are neglected. Secondly, the effective interaction v is poorly known.

The magnitude of the exchange contributions (second term on the rhs of eq. (23)) has been the subject of some debate [27,28,29]). Recent estimates [29]) show that this nonlocal term is too small to account for the observed nonlocality of the empirical OMP. This may indicate that higher order corrections are important, or else that the effective interaction v should depend on energy or be nonlocal. Moreover, any sensible microscopic model for the effective interaction v leads to a density-dependent force. It was emphasized by Myers [30]) that this density-dependence strongly influences the geometrical characteristics of the OMP calculated from (38) [31]). Furthermore, the imaginary part of the OMP is usually still treated phenomenologically in the empirical fits and this further blurs the interpretation of this type of analysis. In view of all these uncertainties, it appears dangerous to attach much significance to the information obtained from the use of the reformulated OMP (38) in the analysis of the experimental data.

This discussion illustrates the necessity of reducing the number of adjustable parameters if one wants a theoretical calculation of the OMP to impose meaningful constraints on empirical analyses or, conversely, if one wants to extract physical information from phenomenological OMP. This is the reason why below we group the various calculations of the OMP according to the number and to the nature of the parameters that they involve. We first discuss the theoretical works which are based on a realistic nucleon-nucleon force and involve no adjustable parameter (sect. 4.b). Then, we review calculations which involve an interaction which is effective but whose parameters are determined by fitting other nuclear properties than the OMP (sect. 4.c), and are therefore not adjustable. Finally, we describe two recent works where adjustable parameters appear but which nevertheless seem to provide useful physical information (sect. 4.d).

4.b. Realistic nucleon-nucleon interactions

4.b.1. Martin-Schwinger-Puff approach. Strong nucleon-nucleon interactions have been used by Reiner [32]) and more recently by Ho-Kim and Khanna [33]), by Gall and Weigel [34]) and by Marville [35]) to calculate the real part of the OMP in nuclear matter in the frame of the Λ_{oo} approximation (sect. 3.e). The results are qualitatively similar to those obtained from Brueckner's theory and described below. Since, moreover, these authors did not construct the OMP in finite nuclei and used only semi-realistic forces, we do not discuss these works in detail here.

4.b.2. Multiple scattering series. The multiple scattering series has mainly been used at intermediate and at high energies, since it is believed to be inaccurate at low energy. Its leading term is the impulse approximation (IA), eq. (35). The energy dependence of the real and imaginary depths of the OMP as calculated from (35) is shown in Fig. 3 (dashed curves), for the Fermi momentum $k_F = 1.35$ fm^{-1} which corresponds to the nuclear centre. For the horizontal scale, we have defined energy e that corresponds to the momentum k by

$$e^{(IA)} = \frac{k^2}{2m} + \mathrm{Re}\ M^{(IA)}(k) \quad . \tag{39}$$

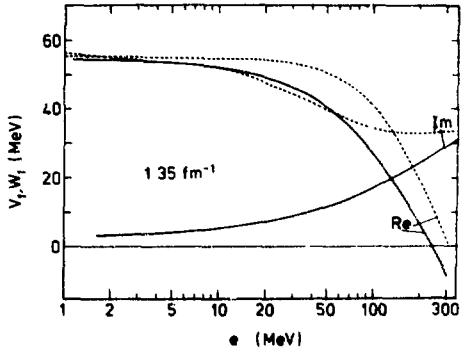

Fig. 3. The dashed lines represent the dependence on the energy e (eq. (39)) of the absolute value of the real and of the imaginary parts of the OMP, as computed in symmetric nuclear matter from the impulse approximation (35). The full curves show the dependence on e (defined now by eq. (40)) of the absolute value of the depths in the BHF approximation. In all cases, Reid's hard core interaction [36] was used [37].

The full curves represent the energy dependence of the real and imaginary parts of the BHF approximation $M^{(BHF)}(k,e(k))$ (see eqs.(30),(33)) where now $e^{(BHF)}(k)$ is defined by

$$e^{(BHF)}(k) = \frac{k^2}{2m} + \mathrm{Re}\ M^{(BHF)}(k) \quad . \tag{40}$$

In both cases, Reid's hard core interaction [36] was used.

For a fixed value of k, one has

$$|\mathrm{Re}\ M^{(IA)}(k)| < |\mathrm{Re}\ M^{(BHF)}(k)| \quad , \tag{41}$$

since the IA neglects the repulsive effects of the Pauli principle ($|\vec{a},\vec{b}><\vec{a},\vec{b}|$ in eq. (31)) and of the dispersion (U(a) in eq. (31)). However, Fig. 3 shows that these omissions are largely compensated by the difference between the definitions (39) and (40) of the nucleon energy, whence the fair agreement between the IA and BHF approximations as far as the real potential depth is concerned.

It is usually stated that the IA yields a local potential which is strictly proportional to the density. In the framework of the local density approximation (sect. 2), this statement holds true when the energy of the incoming nuclei is taken equal to its kinetic energy ($e(k) = k^2/(2m)$). On the contrary, the potential well extends beyond the matter distribution if definition (39) is adopted. This is so because the relation (39) between e and k is density-dependent. This will be discussed in detail elsewhere [37].

The IA (35) has been used by Dabrowski et al. [38,39]) to evaluate the symmetry part of the OMP, i.e. the difference between the depths of the OMP for neutrons and for protons, due to the existence of a neutron excess.

Higher order corrections to the impulse approximation in finite nuclei have been estimated by many authors. In particular, Lerner and Redish [37]) evaluate some off-shell effects in the framework of a three-body model (the projectile, one active bound nucleon and one inert core) ; they use Reid's soft core interaction [6]) and conclude that off-shell effects are significant in the case of the scattering of 65 MeV protons by ^{14}O, ^{17}O and ^{18}O. Note that their calculated OMP is in good agreement with the empirical one only at the nuclear surface ; it is much too deep in the nuclear interior. Nevertheless, good fits to the scattering cross sections are obtained if a phenomenological imaginary part is added to the calculated real part of the OMP. This points to the usefulness of a simultaneous calculation of the real and of the imaginary part of the OMP if one wants to establish the "utility of a theory of the OMP".

The impulse approximation (35), with a correction to include Pauli and binding effects in an approximate way, has recently been used by Dabrowski and Haensel [39]) to calculate the isospin, spin and spin-isospin components of the OMP in polarized infinite nuclear matter. The spin-spin component is found to be somewhat larger than in an estimate by Satchler [40]), based on the folding model (eq. (38)) corrected for core polarization. The latter effect leads to a significant quenching of the spin-spin component. In ref. [39]) the core polarization is essentially represented by uncorrelated two-particle - one hole states (graph $\hat{M}^{(1b)}$ in Fig. 1), while in ref. [40]) the core polarized states are described by collective excitations.

4.b.3. Perturbation expansion. We noted in sect. 4.a that interactions that are "realistic" are usually too strong to allow the use of the perturbation expansion described in sect. 3.a. However, some interactions exist which are weak and are semi realistic in the sense that they reproduce nucleon-nucleon scattering data at low and medium energies.

Slanina and McManus [27]) constructed a sum of two Yukawas (for both the central and the spin-orbit components) which fits the nucleon-nucleon scattering amplitudes at 40 MeV. They calculated the OMP from the first order expression (23) for the targets ^{40}Ca, ^{58}Ni, ^{120}Sn and ^{208}Pb. The density $\rho(r)$ in (23) was taken from experiment while the exchange contribution was evaluated from a Hartree-Fock calculation of the one-body density matrix. The latter HF calculation was performed with a different interaction than v, since the force v used by Slanina and McManus would not saturate nuclear matter. The volume integral and the root mean square radius of the calculated OMP are both significantly smaller than the empirical values. This indicates the importance of higher order terms (core polarization graph $\hat{M}^{(1b)}$...). These can in part be mocked up by adopting an effective interaction. Thus, Slanina and McManus were led to use the reformulated OMP (38) in connection with a number of effective density dependent interactions (see sect. 4.c).

Tabakin's separable nucleon-nucleon interaction [47]) is believed to be sufficiently weak to apply the perturbation expansion, but to be too strong to justify the neglect of second and higher order terms. It was adopted by MacKellar, Reading and Kerman [47]) who studied the scattering by ^{16}O of low energy (a few MeV) neutrons. These authors were thus interested in reproducing the low energy scattering cross section, including the $d_{3/2}$ single particle resonance, rather than the OMP proper.

It would be of interest to calculate the OMP from the perturbation expansion, with one of the very soft but still realistic interactions that have recently be constructed, for instance by Gogny, Pires and de Tourreil [48]) or by de Tourreil and Sprung [49]). These soft forces have been used with fair success for ground state calculations in the framework of second-order perturbation theory.

4.b.4. Brueckner expansion. In the present section, we discuss in some detail recent calculations that have been performed in the framework of Brueckner's approach.

Kidwai and Rook [46]) used the Hamada-Johnston [44]) interaction ; their numerical solution of eqs. (30), (31) is marred by three somewhat inaccurate approximations, which concern : (i) The discretization of the integral over j in eq. (30) ; (ii) The omission of the auxiliary potential, namely of U(j), U(a) and U(b) in eqs. (30), (31) ; (iii) The use of a modified version of the reference spectrum method to solve eq. (31). The latter point was later on cured by Rook [47]) who, however, had to use the simpler Tabakin's interaction [43]). The latter yields too large binding and saturation density in nuclear matter. This, together with points (i) and (ii) above [1]), is probably the main origin of the too strong attraction obtained by Rook. This author also evaluated the symmetry potential ; he obtains good agreement (24 MeV) with the usually quoted empirical value. However, this may be a coïncidence, because of two main facts : (a) Rook neglected the effects of rearrangement and of nonlocality, which are rather large (but have opposite signs) ; (b) Points (i) and (ii) above should be improved.

We now turn to a somewhat detailed presentation of our results. We used the BHF approximation (30), with the self-consistent choice (33) for the auxiliary potential U(d), for all momenta d. No adjustable parameter appears in the calculation, whose sole input in the case of nuclear matter is Reid's hard core nucleon-nucleon interaction [51]). The case of finite nuclei is treated in the framework of the local density approximation (LDA) described in sect. 2. The experimental density distributions were taken from refs. [48,49]).

The calculated energy dependence of the potential depth is represented by the full curve in Fig. 3, for $k_F = 1.35$ fm^{-1}. We recall that the energy is defined by eq. (40). We apologize for the fact that the figures below don't always share the same notation. Thus, the bombarding energy e (eq. (40)) is sometimes denoted by E or E_p ; the potential depths are called V_1, V or $V_0^{(1)}$ and may differ by a sign.

In Fig. 4, we compare the calculated potential depth at $k_F = 1.40$ fm^{-1} ($\rho = 0.185$ fm^{-3}) to empirical values of the OMP at the nuclear centre, in the case of proton scattering by ^{40}Ca and ^{58}Ni. Taking the more realistic value $k_F = 1.36$ fm^{-1} ($\rho = 0.166$ fm^{-3}) would somewhat

decrease the theoretical curve, but this would be largely compensated by the Coulomb correction (see below). The empirical points in Fig. 4 are derived from variable geometry. This explains their scatter and, at the same time, attaches more significance to the comparison between theoretical and empirical depths.

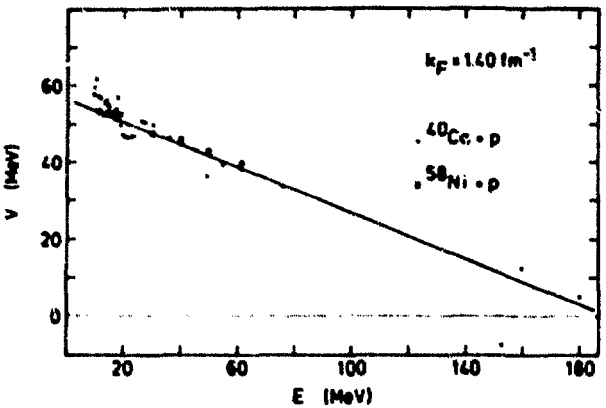

Fig. 4. Comparison between the depth of the OMP as calculated from the BHF approximation (full line) and empirical values in the case of proton scattering by ^{40}Ca [50] (dots) and by ^{58}Ni [51] (crosses), respectively (from ref. [52]).

The nonlocality of the theoretical OMP can be obtained by computing the Fourier transform U(s), with $s = |\vec{r}-\vec{r}'|$, of the self-consistent field U(k) (see eq. (33)). This quantity is plotted in Fig. 5 (dashed curve), for $k_F = 1.35\ fm^{-1}$. The full curve is a Gaussian with nonlocality range 1.02 fm. The small deviation between the two curves for $s > 1.5$ fm indicates that the phenomenological Gaussian model of Perey and Buck [6]) is not exactly confirmed by the calculation or, equivalently, that the theoretical nonlocality range slightly depends on energy. We calculated that it is equal to 0.84 fm at 7 MeV [1]), to be compared with the empirical value 0.85 fm given by Perey and Buck. Note that the nonlocality range discussed here is that of the equivalent nonlocal but energy-independent OMP (see sect. 2). The "true" nonlocality range is determined by the Fourier transform of Re M(k,E) over k, for fixed E. This true nonlocality range is somewhat larger than the values quoted above : it is found equal to 1.07 fm at 7 MeV. As we mentioned in sect. 2, this difference between true and "global" nonlocality is important for the discussion of the Perey effect.

In order to construct the OMP in a finite nucleus from the LDA, we calculated the OMP in nuclear matter with seven different densities. In Fig. 6, we show the calculated energy dependence of the OMP depth for the Fermi momenta 1.35 fm^{-1} ($\rho = 0.166\ fm^{-3}$), 1.10 fm^{-1} ($\rho = 0.090\ fm^{-3}$) and 0.82 fm^{-1} ($\rho = 0.037\ fm^{-3}$).

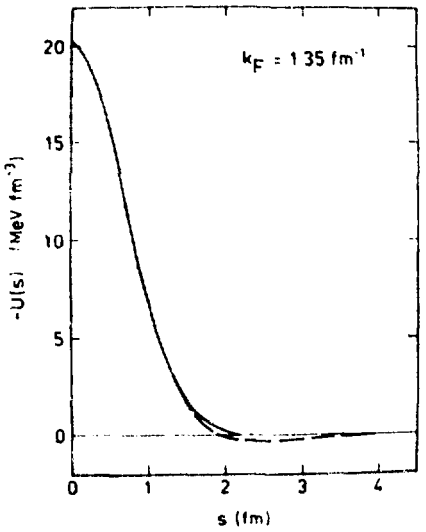

Fig. 5. The dashes show the dependence on the nonlocality parameter $s = |\vec{x}-\vec{x}'|$ *of the calculated equivalent energy-independent, nonlocal OMP. The full line is a Gaussian fit, with nonlocality range 1.02 fm. (From ref.* [1]).

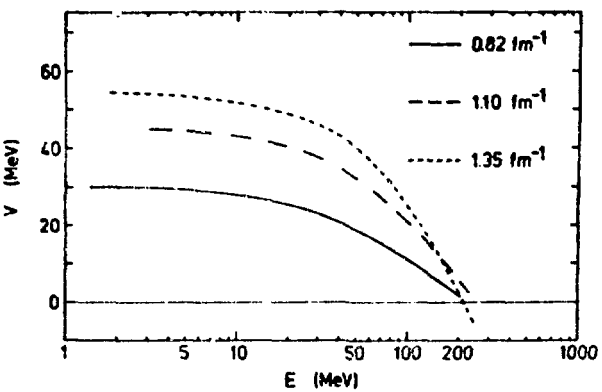

Fig. 6. Dependence on the bombarding energy (eq. (40)) of the calculated depth of the OMP in symmetric nuclear matter, for three values of the Fermi momentum.

As expected, the depth decreases with decreasing density, at least below 150 MeV. The potential changes sign at a lower energy (230 MeV) in the nuclear interior than at the surface. In the energy range 240 < E < 275 MeV, the theoretical OMP will thus be slightly attractive in the surface region and slightly repulsive in the internal region [53]). Some empirical evidence exists for an effect of this type, albeit at a somewhat smaller energy [54]).

We now turn to the case of finite nuclei, and discuss the example of ^{208}Pb. We first neglect the role of the symmetry potential. The full curve in the upper part of Fig. 7 represents the Fermi density distribution of ^{208}Pb, as taken from ref. [49]). The half-maximum density ra-

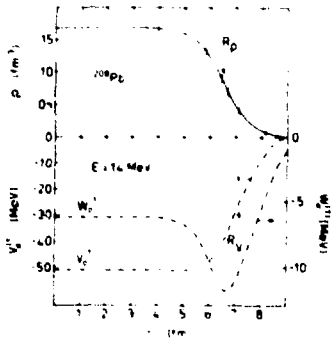

Fig. 7. The full curve represents the empirical density distribution in ^{208}Pb, the Fermi law given in ref.[49]). The dashed curves show the calculated real and imaginary parts of the OMP at 14 MeV. The symmetry part of the OMP is not included.

dius is equal to 6.51 fm. Its location is indicated by the arrow labelled R_ρ . The dashed curves in the lower part of Fig. 7 represent the calculated real ($V_o^{(1)}$) and imaginary ($W_o^{(1)}$) parts of the OMP, at 14 MeV. The half-maximum potential radius is located at R_V = 7.15 fm.

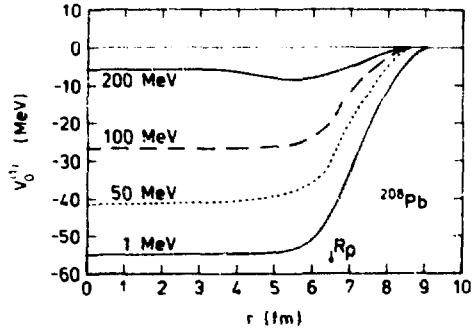

Fig. 8. Radial dependence of the calculated OMP of ^{208}Pb at 1, 50, 100 and 200 MeV. The symmetry potential is omitted. The arrow labelled R_ρ indicates the location of the half-density radius.

In Fig. 8, we show the calculated real part of the OMP for a number of energies. Note that at 200 MeV the calculated potential well is slightly more attractive at the surface than in the nuclear interior, in keeping with our previous remark.

The calculated half-maximum potential radii are represented by the full dots in Fig. 9. They lie on the straight line

$$R_V = 1.204\ A^{1/3} \quad (\text{fm}) \quad . \tag{42}$$

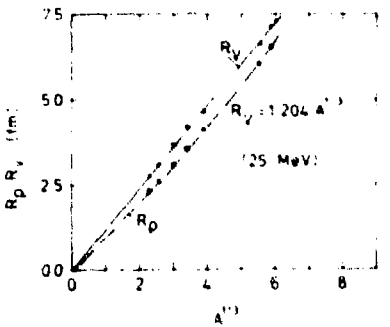

Fig. 9. The full dots give the calculated half-maximum potential radius [37]. The full straight line corresponds to the linear law $R_V = 1.204\ A^{1/3}$. The open dots and the dashed line represent the half-maximum density radius R_ρ (eq. (43)).

This is remarkable since our calculation is based on a density distribution [49] whose half-maximum density radius is not a linear function of $A^{1/3}$:

$$R_\rho = (0.978 + 0.0206\ A^{1/3})A^{1/3} \quad (\text{fm}) \quad . \tag{43}$$

Before comparing the calculated OMP with empirical ones, we must still include the effects of neutron excess (and of the Coulomb field, in the case of protons). We calculated [37] the symmetry component aU_1 of the OMP in the framework of the BHF approximation, including the effect of the density-dependence of the reaction matrix [55,56] and a correction due to the nonlocality of the OMP. The final result is significantly smaller than the usually quoted empirical value, as derived from proton scattering, namely $U_1 = 24$ MeV [57]. However, the latter empirical number is very sensitive to the value adopted for the Coulomb correction, and which we believe to be an underestimate. This point will be discussed below.

Holmqvist and Wiedling [58] have estimated the symmetry potential to be $U_1 = 12.5$ MeV from the analysis of the scattering of 8 MeV neutrons by a series of 22 targets. In Fig. 10, we compare our calculated symmetry part (aU_1) of the OMP in the case of ^{208}Pb (full curve) to the

empirical value of ref. [58]). The corresponding volume integrals agree within one percent.

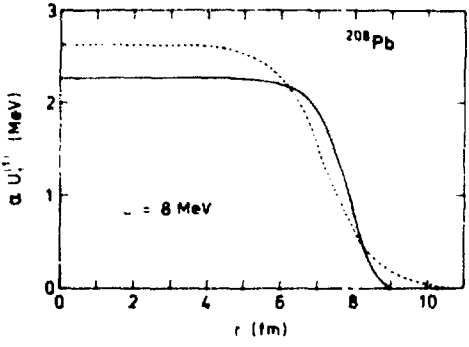

Fig. 10. Comparison between the calculated symmetry component of the OMP (full curve [37]) and the empirical one [58]), for the scattering of 8 MeV neutrons by ^{208}Pb.

The agreement displayed in Fig. 10 might still be considered not completely convincing. Indeed, Hodgson [59]) emphasized that the empirical value of the symmetry potential sensitively depends on the assumption that is made concerning the dependence on mass number of the half-maximum potential radius R_V. The fact that our calculated R_V varies linearly with $A^{1/3}$ (eq. (43)), as assumed in ref. [58]) ($R_V = 1.22\ A^{1/3}$ fm), already indicates that our calculated symmetry potential is in good agreement with experimental evidence. This is further established by Fig. 11, where we compare the dependence on $\alpha = (N-Z)/A$ of the volume integral per nucleon of our calculated total (including the symmetry part) OMP to the empirical values (open dots) of Holmqvist and Wiedling [58]).

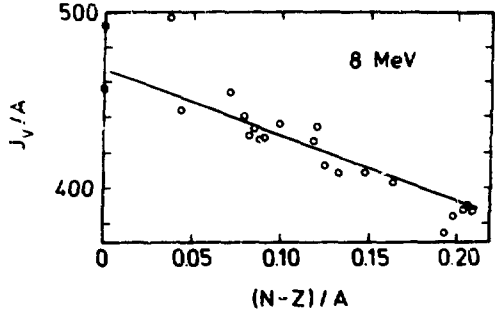

Fig. 11. Comparison between the volume integral per nucleon of the calculated OMP (full line) [37]) and the empirical values (open dots) of Holmqvist and Wiedling [58]).

In the case of protons, one must include the effect of the Coulomb potential on the OMP. In first approximation, this amounts to adding to the OMP calculated for neutrons the Coulomb field created by a uniformly charged sphere with a charge radius that is equivalent [60] to that of the target nucleus. However, the nonlocality of the OMP introduces a "Coulomb correction" Δ_c . The latter is usually included in the phenomenological analyses by adding $0.4\ Z/A^{1/3}$ (MeV) to the absolute value of the depth of the OMP [11]. In ref. [61], we argued that this "standard" value is an underestimate because the true nonlocality of the OMP is larger than hitherto believed. Although we maintain this statement, the reasoning carried out in ref. [61] is erroneous.⁂ The origin of our error is that we had assumed [61] that when the Coulomb potential V_c is turned on, the mass operator $M(k,E)$ is replaced by $M(k,E) + V_c$, while in reality it becomes $M(k,E - V_c) + V_c$. We since corrected this error ; this amounts to replacing $\hat{m}_\rho$ by $m_\rho^{\ddagger}$ in eq. (11) of ref. [61]. We computed the Coulomb correction Δ_c in the case of the scattering of 25 MeV protons by ^{208}Pb. The result is represented by the full curve in fig. 12, where the dashes show the "standard" value adopted in refs. [57,114]. We see that the calculated Coulomb correction is larger than the standard one.

It is the sum $\alpha U_1 + \Delta_c$ of the symmetry and of the Coulomb correction components of the OMP that appears in the expression of the OMP : these two components cannot be separated in the analysis of proton scattering data. In fig. 13, we compare the calculated sum $\alpha U_1 + \Delta_c$ (full curve) to the empirical one [57], in the case of the scattering of 25 MeV protons by ^{208}Pb.

In Figs. 14 and 15, we compare the volume integral per nucleon and the root mean square radius of the empirical OMP [62] with calculated values, including the effects of the Coulomb correction and of the symmetry potential. The agreement is quite good in view of the absence of any adjustable parameter. It appears that the calculated root mean square radius is systematically slightly smaller than the empirical one.

We also estimated the effect of some higher order corrections,

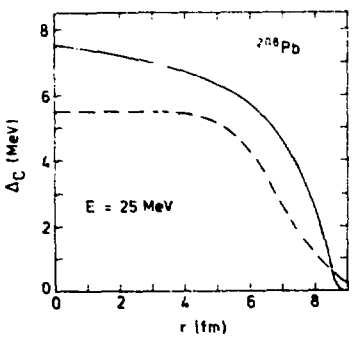

Fig. 12. Comparison between the calculated (full curve) and the standard [57] (dashed curve) Coulomb correction, for the scattering of 25 MeV protons by ^{208}Pb (preliminary).

⁂ *We gratefully acknowledge a very useful discussion with Professor A.K. Kerman which led to the latter conclusion.*

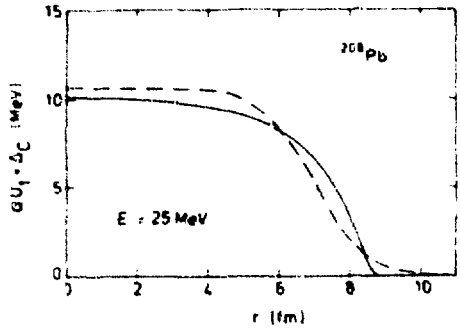

Fig. 13. Comparison between the calculated (full curve) [37] and the empirical (dashed curve) [57] values of the sum of the symmetry and of the Coulomb correction components of the OMP (preliminary).

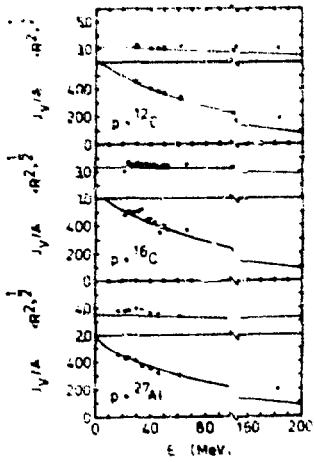

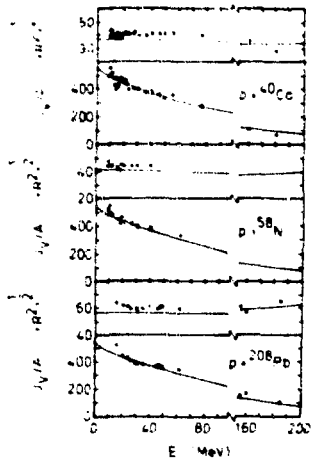

Fig. 14.

Fig. 15.

Fig. 14. Comparison between the calculated (full curves) [37] and the empirical (full dots) [62] volume integral per nucleon (in MeV fm^3) and root mean square radius for the scattering of protons by ^{12}C, ^{16}O and ^{27}Al.

Fig. 15. Same as Fig. 14, for ^{40}Ca, ^{58}Ni and ^{208}Pb.

namely of graphs $M^{(2)}$ and $M^{(3)}$ in Fig. 2. Preliminary results have been reported in ref. [63]). It appears that the magnitude of these corrections is too small to spoil the good agreement displayed in Figs. 10-15.

4.c. Effective interactions

In the present section, we review some calculations which are based on effective nucleon-nucleon interactions but which do not involve adjustable parameters. In practice, most of these effective interactions have been constructed to fit the properties of the ground and of low-lying bound states. Hence, one should normally not expect them to yield accurate results for the OMP above several tens MeV. Moreover, the use of effective interactions does not allow to separate in a meaningful way the nonlocality from the energy dependence of the OMP. We saw in sect. 4.b.4 that this distinction is not only of fundamental but also of practical interest.

Slanina and McManus [27]) have calculated the OMP from the folding formula (38) ; they used for v density-dependent effective interactions proposed by Kuo and Brown [64,65]) and by Green [66]). The resulting volume integrals per nucleon and root mean square radii are in better agreement with empirical values than those obtained from their density-independent semi-realistic nucleon-nucleon force (sect. 4.b.3). This result shows the importance of using density-dependent forces in connection with approximation (38) [30,31]). It also indicates that effective interactions that have been adjusted to the properties of the ground or low excited states meet with semi-quantitative success in the calculation of the OMP.

Exchange corrections to expression (38) (see eq. (23)) have been estimated in refs. [27,28]). These authors find (see, however, ref. [29])) that exchange effects account for approximately 80 percent of the observed energy dependence of the empirical local OMP. However, this result should not be interpreted as indicating that 80 percent of the phenomenological energy dependence arises from nonlocality. Indeed, we have seen in sect. 4.b.4 that the true nonlocality corresponds to an energy dependence of the local equivalent OMP that is larger (by about 30 percent) than the phenomenological energy dependence. The same conclusion is reached on the basis of the dispersion relation (13) [10,67,68,69]). The exchange (Fock) term is only <u>one</u> source of the nonlocality of the OMP. In particular, the polarization graph $M^{(1b)}$ (Fig. 1) is nonlocal (and energy dependent) ; it was not included in the works of Slanina and McManus [27]) and of Owen and Satchler [28]). This type of correction could in principle be included in the expression (23) but would then require to replace v by a <u>nonlocal</u> (and also density and energy-dependent) effective interaction $v(\vec{r},\vec{r}')$. Approximation (38) for instance would then read

$$M(\vec{r},\vec{r}') = \int \rho(\vec{r}_o)\; v(\vec{r}-\vec{r}_o,\; \vec{r}'-\vec{r}_o)\; d^3r \quad . \tag{44}$$

In other words, the "direct" term (38) would then be nonlocal.

Dover and Van Giai [70,71]) have used the Skyrme three-body contact interaction to calculate the real part of the OMP in the framework of the Hartree-Fock approximation (sect. 3.a). Their approach is entirely

self-consistent, in the sense that they generate the one-body density matrix $\rho(\vec{r},\vec{r}')$ from the Skyrme interaction. The volume integrals per nucleon of their calculated results are represented by the dashed lines in Fig. 16, where the full straight lines are least square fits to the empirical values [62] (full dots, the same as in Figs. 14 and 15). We see that the calculated energy dependence is somewhat too large.

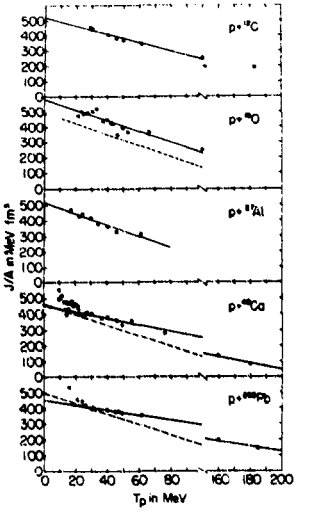

Fig. 16. Comparison between the volume integrals per nucleon calculated by Dover and Van Giai [71] (dashed lines) with the empirical values (full dots). The full lines are least square linear fits to the full dots (from ref. [62]).

Manweiler [72] also used a Skyrme force in a recent calculation of the OMP, similar to that of Dover and Van Giai [71].

4.d. Adjusted interactions

Following the pionneering work of Greenlees, Pyle and Tang [25], it became fashionable to fit the data with a "reformulated" OMP, i.e. the folding formula (38), where v is a phenomenological effective interaction which contains a number of adjustable parameters. A review of many works based on this kind of approach has recently been given by Sinha [26]. As we briefly argued in sect. 4.a, it appears that little reliable information or constraints can be obtained in this way, in view of the lack of accuracy of approximation (38) on the one hand and of the limited knowledge of the residual interaction on the other hand. Therefore, we shall not discuss this approach further here.

It can happen that instructive findings emerge from attempts to reproduce scattering data from an expression of the OMP which involves adjustable parameters. We discuss two such examples.

The first example is the recent work by Manweiler [73]. This author extends to the continuum a model that had previously been deve-

loped by Elton and Webb [74]) to fit bound state properties, including bound single-particle energies. The model consists in a Schrödinger equation with a nonlocal potential of the Perey-Buck form [6]), namely

$$V(\vec{r},\vec{r}') = U(\frac{\vec{r}+\vec{r}'}{2}) \exp[-\frac{(r-r')^2}{b^2}] \quad . \tag{45}$$

In addition to the nonlocality range b, several parameters appear in the parametrization of U and of its spin-orbit part. The interest outcome of the model is that it was found possible to fit fairly well the bound single-particle energies and the scattering data below 50 MeV with the same nonlocal potential.

The same type of results emerge from the second example, namely the recent work by Giannini and Ricco [75]). These authors also find that the bound single-particle energies and the elastic scattering cross sections can be fairly well reproduced by a nonlocal potential with a real part of the form (45), for N = Z nuclei with A < 40. They constructed the equivalent local potential (ELP) to (45). The full line in Fig. 17 shows the dependence on energy of the depth of their parametrized ELP. Note that the energy scale extends from -60 to +130 MeV, i.e. that bound states are included. The radius of the ELP slight-

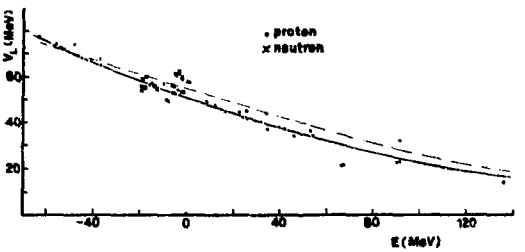

Fig. 17. The points represent the depth of the local potential that would yield the experimental single particle energies and scattering cross sections for protons (full dots) and for neutrons (crosses), for N = Z nuclei with A ≤ 40 and with the energy dependent radius of ref. [75]). The full curve is drawn through the points. The dashed curve is the result of our BHF approximation, at k_F = 1.35 fm^{-1}.

ly decreases with energy. The full dots represent the depth of the local potential which has the same geometry as the ELP to (45) and reproduces the bound single-particle states and the scattering data for protons. The crosses refer to neutrons.

It is striking that all these points lie in the vicinity of a smooth curve. The scatter around -8 MeV is an indication of configuration mixing. However, we note that the scatter is not random ; there is a clear tendency for the low energy points to lie below the high energy ones. This indicates an increase of the level density at the

Fermi surface or, equivalently, a local enhancement of the effective mass near the Fermi surface. The existence of such an effect had been pointed out by Brown, Gunn and Gould [76]. The theoretical interpretation proposed by Bertsch and Kuo [12], by our group [77] and by Hamomoto and Siemens [78,79,80] relies on the importance of graphs $\hat{M}^{(1b)}$ and $\hat{M}^{(2)}$ in Fig. 1. In physical terms, it arises from the fact that the "true" energy dependence of the OMP is enhanced at the Fermi surface, while the true nonlocality remains smooth [77,1]. An effect of this type cannot be contained in a simple parametric form like (45).

The dashed curve in Fig. 17 is the result of our BHF calculation (see small dashes in Fig. 6) ; the effect of the enhanced energy dependence alluded to above has not been included in this dashed curve. Note that the two curves in Fig. 17 are not directly comparable since they refer to slightly different geometries. Nevertheless, we are somewhat puzzled by the smoothness of the phenomenological (full) curve and by its fair agreement with the BHF approximation. Indeed, the latter is usually believed to be inaccurate at negative energy because of the importance of the "rearrangement" graph $M^{(2)}$ (Fig. 2), which is repulsive and thus decreases the potential depth.

Finally, we emphasize that the empirical success met in the fitting of the bound and scattering data with the parametric form (45) does not imply that the arguments given in refs. [73,75] are valid. For instance, the various approximations made in ref. [75] appear to be unjustified at low energy, and the "true" energy dependence is not explicitly included in ref. [73].

5. CALCULATIONS OF THE IMAGINARY PART OF THE OMP

5.a. Meaningfulness of theoretical constraints

The calculation of the imaginary part of the OMP is more delicate than that of its real part V, because it is a fairly reasonable first approximation to take for V the static Hartree-Fock field (23), while W is by its very nature a dynamical quantity. Indeed, the imaginary part W of the OMP accounts for the loss of flux from the entrance channel. Part of this flux corresponds to the feeding of the compound nucleus (eq. (37a)) ; the other part arises from direct transitions into inelastic or reaction channels (eq. (37b)). The microscopic description of these processes requires the configurations of the compound nuclear states, of the residual states in the inelastic channels and of the effective interaction v, or else that of the matrix elements which appear in eqs. (37a), (37b). Reliable calculations of this type are thus very difficult to perform. Some attempts will be described in sect. 5.c. They have the main advantage of being able to include nuclear structure effects, such as for instance the fact that some residual nuclei are in excited vibrational states. If these collective effects are quantitatively important, the use of these finite nucleus calculations is necessary. However, we note that in practice they must involve effective interactions ; accordingly, some details are partly lost, such as the true nonlocality of the imaginary part. Indeed, the effective interaction is usually assumed to be local, while it could in reality very well be nonlocal (see eq. (44)). Another problem is that these calculations are specific to each tar-

get, while the practical definition of the OMP only requires that it represents the average trend of the mean field over the whole periodic table.

From the systematics of available OMP, it has recently been shown that the volume integral of the imaginary part W of the empirical OMP is a fairly well defined function of energy and of mass number [81,82], although with more scatter around the average than in the case of the volume integral of the real part V. Hence, it appears appropriate to apply, for the calculation of the average trend of W, a nuclear matter plus local density approach similar to the one that we described in sect. 4.b for the real part of the OMP. The aim of this type of calculation should thus be the reproduction of the main trends of the imaginary part of the OMP. On the other hand, the marked deviations from the average behaviour are probably due to finiteness effects (collective states) and their explanation requires a calculation which is more specific to the nucleus. Thus, the two types of approaches are complementary. They are described in sects. 5.b and 5.c, respectively.

5.b. Realistic nucleon-nucleon interactions

5.b.1. Martin-Schwinger-Puff approach. The imaginary part W of the OMP was calculated in the framework of the Λ_{oo} approximation of Green's function theory (see sects. 3.e, 4.b.1) by Reiner [83] and more recently by Ho-Kim and Khanna [33], Gall and Weigel [34] and Marville [35], in the case of symmetric nuclear matter. These authors used simplified but nevertheless semi-realistic nucleon-nucleon interactions. The imaginary part W calculated in ref. [33] is disturbingly small (2.4 + 0.009 E, in MeV). The value of W obtained in refs. [83,34,35] has about the same magnitude as the empirical one above several tens MeV. At lower energies, however, the calculated values are too small. This can be ascribed to the failure of the Λ_{oo} approximation to fulfil the asymptotic behaviour (14) [35].

5.b.2. Multiple scattering approach. The impulse approximation (35) does not contain the effect of the Pauli principle which is the main origin of the decrease of the imaginary part of the OMP at low energy. Hence, it can only be used in the intermediate and high energy domains, which fall somewhat outside the scope of this Conference. Even at medium energy, off-shell, Pauli and binding energy effects are sizable [84].

At low energy, the phase space restriction due to the Pauli principle can be included in an approximate way by using the frivolous model of Clementel and Villi [85] or an improved version thereof [86,87,88]. This, however, still neglects off-shell effects. This approach has recently been used by Dabrowski and Haensel [39,89] to study the spin, isospin and spin-isospin dependent terms of the imaginary part of the OMP for infinite nuclear matter.

5.b.3. Perturbation expansion. Soft interactions that fit the low-energy scattering data have been used in a few early calculations of the imaginary part W of the OMP in nuclear matter [90,91,92,93]. Ripka [93] paid special attention to the nonlocality of W. It would be of interest to compute W from second order perturbation theory, using one of the recently constructed soft but nevertheless realistic nu-

cleon-nucleon forces [43,44]).

5.b.4. Brueckner expansion. Rook has applied the Brueckner-Hartree-Fock approximation (30) in the case of Tabakin's interaction. His calculation suffers from the computational defects mentioned in sect. 4.b.4. The resulting inaccuracy is worse in the case of the real part of the OMP [1]).

Therefore, we mainly describe here the results that we obtained from the BHF approximation, using Reid's hard core nucleon-nucleon interaction and eqs. (30)-(33). As we noted right after eq. (33), a complex choice for the auxiliary potential would actually be preferable. Work along these lines is in progress [94]). We do not believe that this would significantly alter the results since it amounts to average over energy a quantity that is smoothly energy-dependent.

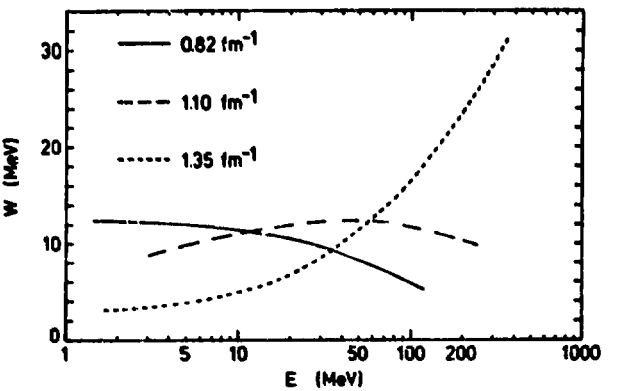

Fig. 18. Energy dependence of the imaginary part of the calculated OMP in symmetric nuclear matter, for the Fermi momenta k_F = 1.35, 1.10 and 0.82 fm^{-1}, respectively [37]).

In Fig. 18, we show the dependence on the energy E (≡ e, eq.(40)) of the imaginary part of the OMP for infinite and symmetric nuclear matter, with the Fermi momenta (see eq. (2)) k_F = 1.35, 1.10 and 0.82 fm^{-1}, respectively. At low energy, the absorption is largest at low density (surface peaked absorption). Above 60 MeV, on the contrary, the absorption is largest in the nuclear interior (volume absorption).

In Fig. 19, we show the value of W for various energies, in the case of ^{208}Pb. The arrow labelled R_ρ indicates the location of the half-maximum density radius. We see that at low energy the maximum of W occurs somewhat beyond R_ρ.

The nuclear matter + LDA approach can at best yield only the overall trend of W, since it does not contain nuclear structure (collectivity) effects, which may be important for some nuclei [95,96,97]). In this respect, it is gratifying that it has recently been observed that

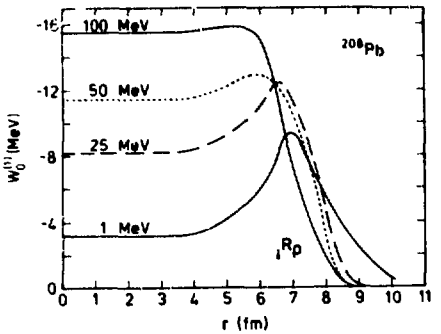

Fig. 19. Calculated imaginary part of the OMP of ^{208}Pb for the energies 1, 25, 50 and 100 MeV [37]. The symmetry component of the OMP is not included.

the imaginary part W of the empirical OMP has a smooth overall dependence on mass number A and energy E. This is exhibited in Fig. 20, where the full dots show the volume integral of W per nucleon for various nuclei with A $\geq$ 40 [81]. The dash-and-dots, the full curve and the dashes represent the volume integral calculated from the BHF approach, for ^{208}Pb, ^{169}Tm and ^{58}Ni, respectively. We see that the

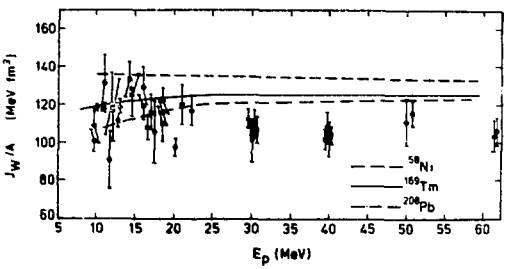

Fig. 20. The full dots represent the energy dependence of the volume integral of the imaginary part of the OMP (averaged over A for fixed energy E) [81]. The long dashes, the full curve and the dash-and-dots show our calculated values for ^{58}Ni, ^{169}Tm and ^{208}Pb, respectively. The symmetry component of the OMP has been included.

agreement is rather satisfactory. A more recent compilation [82], based on a much larger and more recent set of empirical OMP, shows more scatter than the points in Fig. 20 but confirms the existence of a general trend. The latter is even in better agreement with our calculation because the points above 25 MeV lie somewhat higher than those

shown in Fig. 20. Moreover, this more complete compilation [82]) confirms our theoretical finding that the volume integral per nucleon increases with decreasing A, in particular for A < 40.

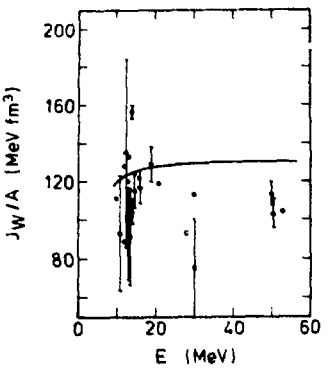

Fig. 21

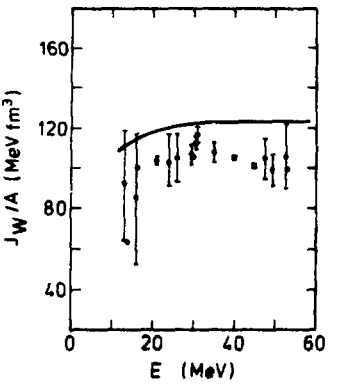

Fig. 22

Fig. 21. Comparison between our calculated values of J_W/A for ^{169}Tm and a compilation of empirical values [82]) for nuclei with 100 ≤ A ≤ 210, the case of ^{208}Pb being excluded (see Fig. 22).

Fig. 22. Comparison between the volume integral per nucleon J_W/A of the empirical OMP (full dots, from ref. [82]) and our calculated value [37]), in the case of proton scattering by ^{208}Pb.

In Fig. 21, we compare our values of J_W/A for A = 169 with a compilation of empirical values [82]) for 100 ≤ A ≤ 210, the case of ^{208}Pb being excluded. In Fig. 22, we show a detailed comparison between empirical and calculated values of the volume integral (J_W/A) per nucleon of the imaginary part of the OMP, in the case of proton scattering by ^{208}Pb.

Finally, we show in Fig. 23 the calculated imaginary part of the symmetry component of the OMP for ^{208}Pb at 14 and 50 MeV. We recall that $\alpha = (N-Z)/A$. The full curves correspond to the assumption that the neutron and proton density distributions have the same half-maximum density radius ; the dashes result from the assumption that the neutron density radius is larger by 0.15 fm than the proton density radius. The arrow points to the radius at half-maximum of the real part of the OMP. The comparison between Figs. 10 and 23 shows that the calculated real and imaginary symmetry components of the OMP have approximately the same depth.

5.c. Effective interactions

The calculation of the imaginary part of the OMP from effective interactions which had been constructed to reproduce the properties of nuclear bound states presents more interest than in the case of the real part. Indeed, the imaginary part is usually believed to be more

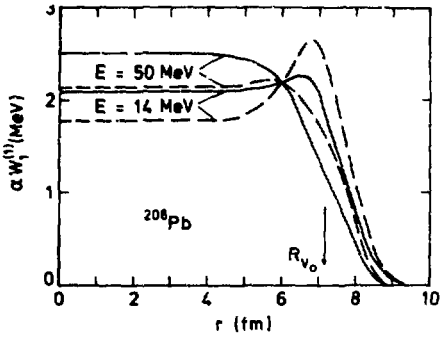

Fig. 23. Calculated imaginary part of the symmetry component of the OMP for ^{208}Pb at 14 and 50 MeV [37]. The full curves derive from the assumption that the proton and neutron distributions have the same radius. The dashes result from a neutron skin with a thickness equal to 0.15 fm.

sensitive to nuclear structure, in particular to collectivity effects [95,96,97]. In practice, the theoretical method is based on a more or less elaborate version of the nuclear reaction theory (sect. 3.d).

Very few calculations exist of that fraction of the imaginary part of the OMP that is due to compound nucleus formation (eq. (37a)). The main reason is that little is known concerning the structure of the compound resonances (ϕ_n), in particular at high energy. Hence, most calculations of this component have been limited to low or negative energy. The compound states ϕ_n are usually described by means of a particle-vibration coupling model. This is the case for the study of ^{58}Ni (refs. [98,99]) and ^{208}Pb (refs. [100,101,102]). Since these calculations only involve several compound states and a few degrees of freedom, the calculated imaginary part W has a wild energy dependence and an awkward nonlocality. It can therefore not be readily compared with empirical values. For instance, the solid curve in Fig. 24 represents the calculated value of W for the scattering of s-wave neutrons by ^{208}Pb [102] (full curve) ; the dashed line is a typical empirical value.

The contribution of compound nucleus formation to the imaginary part of the OMP at somewhat higher energy was evaluated by Cugnon [103] in the case of the ^{39}K target. He described the compound states ϕ_n as one particle-one hole configurations, thus neglecting collectivity effects. Cugnon [103] also evaluated the contribution of direct transitions into inelastic channels (eq. (37b)), assuming that the residual states are one hole excitations of ^{39}K. This probably leads to an underestimate of the value of (37b). Cugnon finds that the contributions of compound nuclear formation and of direct inelastic absorption are of about the same magnitude, in the case of his model. This appears to be the only work where these two modes of absorption have been studied simultaneously.

The contribution to W of direct inelastic transitions has been

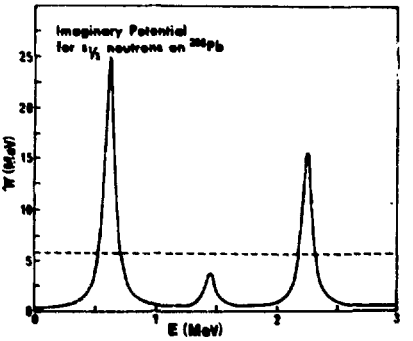

Fig. 24. The solid curve represents the imaginary part of the OMP as calculated in the framework of a particle-vibration coupling model. The dashed line is a typical empirical value (from ref. [102]).

evaluated by Rao, Reeves and Satchler [104]) in the case of the scattering of 30 MeV protons by ^{40}Ca and ^{208}Pb. The calculation is macroscopic, in the sense that the target excited states are described by the collective deformed potential model. The calculated absorption cross sections are in fair agreement with experiment provided that one adds the contribution of unobserved excited states (as evaluated by means of sum rules) and provided that one includes an estimate of the effect of pick-up channels. The latter appear to play a significant role in the absorption [105]). The angular distributions derived from the OMP calculated in ref. [104]) are in poor agreement with experimental data.

A detailed microscopic calculation of the contribution of direct transitions into inelastic channels has recently been made by N. Vinh Mau and Bouyssy [106]), in the case of the scattering by ^{40}Ca of protons with an energy ranging from 20 to 60 MeV. These authors used an improved version of expression (37b), which treats the Pauli principle with particular care and describes the target excited states in the framework of the random phase approximation. The calculated imaginary part is nonlocal. N. Vinh Mau and Bouyssy construct an equivalent local potential by means of the local energy approximation of Perey and Saxon [7]) (sect. 2). We note incidentally that the authors of ref. [104]) were unable to find a local OMP that would yield the same differential cross sections as their calculated OMP. The local imaginary part $W_L(r)$ obtained by N. Vinh Mau and Bouyssy [106]) at E = 20 MeV is shown in Fig. 25. The calculated W_L can be decomposed in a volume and a surface contribution. It is seen from Fig. 25 that most of the surface absorption is due to inelastic scattering to odd parity states, while the even parity states dominate at the nuclear centre. This trend becomes more pronounced as the energy increases. The energy dependence of the calculated volume (W_V^e) and surface (W_S) absorptive strengths is represented by the full dots in Fig. 26. The upper index e on W_V^e refers to the fact that the geometry of the volume component obtained by N. Vinh Mau and Bouyssy differs from the adopted empirical one (smaller radius

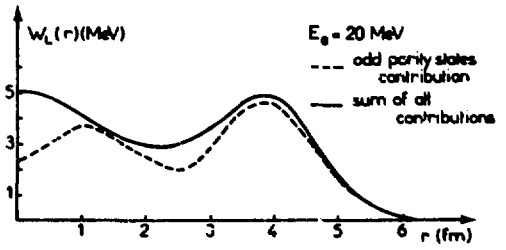

Fig. 25

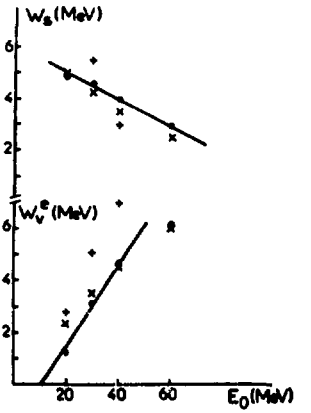

Fig. 26

Fig. 25. Local equivalent of the imaginary part of the OMP calculated by N. Vinh Mau and Bouyssy in the case of the scattering of 20 MeV protons by ^{40}Ca (from ref. [106]).

Fig. 26. Comparison between the surface and effective volume strengths calculated by N. Vinh Mau and Bouyssy (full dots) and the empirical values of refs. [57] (plusses) and [107] (crosses). In the latter case, the empirical surface strength has been divided by two in order to take into account a geometrical difference (from ref. [106]). The full straight lines have been drawn through the calculated dots.

and larger diffuseness). The "effective" volume strength W_V^e in Fig. 26 has been renormalized to account for this geometrical difference. The empirical values in Fig. 26 are represented by plusses [57] or by crosses [107]. In the latter case, the empirical surface strength has been divided by two, again in order to take into account a geometrical difference (smaller empirical diffuseness assumed in ref. [107]) to fit the observed s-wave neutron strength function [108]). The agreement between calculated and empirical values displayed in Fig. 26 is impressive. One of the main interests of this type of calculation is to yield the contribution of specific inelastic channels, thereby allowing a study of nuclear structure effects. The aspects of the calculation which appear to deserve closer study are the neglect of compound nuclear absorption, the modifications that would result from replacing the zero-range effective interaction [109,110]) by a finite range force, the construction of the local equivalent potential and the use of plane waves for the description of the scattered nucleon in the inelastic channels. Work on some of these points is in progress [111]).

5.d. Adjusted interactions

Perey and Buck [6]) had been able to fit the elastic scattering

cross section with a surface-peaked complex phenomenological OMP, with a fixed nonlocality range. The imaginary part of the corresponding local equivalent potential is essentially independent of energy. This finding appears to contradict the asymptotic behaviour (14). This had led to the surmise that the Fermi gas model is inapplicable, because of the importance of direct inelastic transitions into vibrational excited states [112]). However, it was pointed out by Frahn [113]) and demonstrated by Engelbrecht and Fiedeldey [107]) that equally good fits can be obtained with an energy dependent imaginary part that fulfils (14). We have moreover seen in sect. 5.c that the calculation by N. Vinh Mau and Bouyssy, where the vibrational states are explicitly included, leads to an imaginary part that increases in absolute magnitude with increasing energy.

This trend is confirmed by empirical analyses that cover a wider energy range than that investigated by Perey and Buck [6]). For instance, Manweiler [73]) and Giannini and Ricco [75]) both had to add an energy-dependent imaginary part to their nonlocal OMP.

6. CONCLUSIONS

We have seen that many theoretical approaches exist for calculating the OMP. We argued that those calculations which do not involve any adjustable parameter are of particular interest, for two main reasons. Firstly, they can establish the accuracy of the theoretical approximations. Secondly, they can provide meaningful theoretical information or constraints on the OMP. Some of this information cannot be obtained from the analysis of the scattering data alone, and therefore require a theoretical estimate. One example is the true nonlocality of the OMP, which is needed for calculating the Coulomb correction and the "Perey effect" (sect. 4.b.4).

One of us (C.M.) is grateful to Dr. P.E. Hodgson and to his colleagues of the Nuclear Physics Laboratory for their kind hospitality and for useful discussions.

REFERENCES

1) J.-P. Jeukenne, A. Lejeune and C. Mahaux, Phys. Reports, in press 1976.
2) D.J. Thouless, Reports on Progr. in Phys., 1964, 27, 53.
3) J.S. Bell and E.J. Squires, Phys. Rev. Lett. 1959, 3, 96.
4) J.S. Bell, in E.R. Caianiello (ed.), Lectures on the Many-Body Problem (Academic Press, New York, 1962) p. 91.
5) R. Lipperheide, Z. Phys. 1967, 202, 58.
6) F. Perey and B. Buck, Nucl. Phys. 1962, 32, 353.
7) F.G. Perey and D.S. Saxon, Phys. Rev. 1964, 10, 107.
8) W.E. Frahn, Nucl. Phys. 1965, 66, 358.
9) F. Capuzzi, in Proc. of the Conference on the Optical Potential in Nuclear Physics, Pavia (Italy), April 8-9, 1976 (INFN, Italy, 1976).
10) M. Bertero and G. Passatore, Z. Naturforsch. 1973, 28A, 519.
11) F.G. Perey, Phys. Rev. 1963, 131, 745.
12) G.F. Bertsch and T.T.S. Kuo, Nucl. Phys. 1968, A112, 204.
13) J. Hüfner and C. Mahaux, Ann. Phys. (N.Y.) 1972, 73, 525.
14) H. Feshbach, Ann. Phys. (N.Y.) 1962, 19, 287.

15) R. Lipperheide, Nucl. Phys. 1966, 89, 97.
16) C. Mahaux and H.A. Weidenmüller, Shell-Model Approach to Nuclear Reactions (North-Holland Publ. Comp., Amsterdam, 1969).
17) J.N. Ginocchio, T.H. Shucan and H.A. Weidenmüller, Phys. Rev. 1969, C1, 55.
18) N. Vinh Mau, in Theory of Nuclear Structure (Trieste Lectures 1969), (International Atomic Energy Agency, Vienna, 1970) p. 931.
19) P.C. Martin and J. Schwinger, Phys. Rev. 1959, 115, 1342.
20) G.E. Brown, Many-Body Problems (North-Holland Publ. Comp., Amsterdam, 1972).
21) R.D. Puff, Ann. Phys. (N.Y.) 1961, 13, 317.
22) D.S. Falk and L. Wilets, Phys. Rev. 1961, 124, 1887.
23) M. Weigel and G. Wegmann, Forts. der Physik 1971, 19, 451.
24) G.M. Lerner and E.F. Redish, Nucl. Phys. 1972, A193, 565.
25) G.W. Greenlees, G.J. Pyle and Y.C. Tang, Phys. Rev. 1968, 171, 1115.
26) B. Sinha, Phys. Reports 1975, 20C, 1.
27) D. Slanina and H. McManus, Nucl. Phys. 1968, 116, 271.
28) L.W. Owen and G.R. Satchler, Phys. Rev. Lett. 1970, 25, 1720.
29) W.G. Love and L.W. Owen, Nucl. Phys. 1975, A239, 74.
30) W.D. Myers, Nucl. Phys. 1973, A204, 465.
31) D.K. Srivastava, N.K. Ganguly and P.E. Hodgson, Phys. Letters 1974, 51B, 439.
32) A.S. Reiner(Rinat), Phys. Rev. 1964, 133, B1105.
33) Q. Ho-Kim and F.C. Khanna, Ann. Phys. (N.Y.) 1974, 86, 233.
34) H. Gall and M.R. Weigel, Z. Physik 1976, A276, 45.
35) C. Marville, preprint (Liège, 1976).
36) R.V. Reid, Ann. Phys. (N.Y.) 1968, 50, 411.
37) J.P. Jeukenne, A. Lejeune and C. Mahaux, to be published.
38) J. Dabrowski and A. Sobiczewski, Phys. Letters 1963, 5, 87.
39) J. Dabrowski and P. Haensel, Can. J. Phys. 1974, 52, 1768.
40) G.R. Satchler, Phys. Letters 1971, B34, 37.
41) F. Tabakin, Ann. Phys. (N.Y.) 1964, 30, 51.
42) A.D. MacKellar, J.F. Reading and A.K. Kerman, Phys. Rev. 1971, C3, 460.
43) D. Gogny, P. Pires and R. de Tourreil, Phys. Letters 1970, 32B, 591.
44) R. de Tourreil and D.W.L. Sprung, Nucl. Phys. 1973, A201, 193.
45) H.R. Kidwai and J.R. Rook, Nucl. Phys. 1971, A169, 417.
46) T. Hamada and I.D. Johnston, Nucl. Phys. 1962, 34, 382.
47) J.R. Rook, Nucl. Phys. 1974, A222, 596.
48) M.A. Preston, Physics of the Nucleus (Addison-Wesley Publ. Comp., Inc., Reading, Mass., 1962).
49) J.W. Negele, Phys. Rev. 1970, C1, 1260.
50) W.H.T. Van Oers, Phys. Rev. 1971, C3, 1550.
51) G.L. Thomas and E.J. Burge, Nucl. Phys. 1969, A128, 545.
52) J.-P. Jeukenne, A. Lejeune and C. Mahaux, Phys. Rev. 1974, C10, 1391.
53) J.-P. Jeukenne, A. Lejeune and C. Mahaux, in G. Ripka and M. Porneuf (eds.), Proc. of the International Conference on Nuclear Self-Consistent Fields (Trieste, Febr. 1975) (North-Holland Publ. Comp., Amsterdam, 1975) p. 155.
54) L.R.B. Elton, Nucl. Phys. 1966, 89, 69.
55) K.A. Brueckner and J. Dabrowski, Phys. Rev. 1964, 134, B722.

56) N. Azziz, Nucl. Phys. 1970, A147, 401.
57) F.D. Becchetti and G.W. Greenlees, Phys. Rev. 1969, 182, 1190.
58) B. Holmqvist and T. Wiedling, Nucl. Phys. 1972, A188, 24.
59) P.E. Hodgson, Nucl. Phys. 1970, A150, 1.
60) L.R.B. Elton, Nuclear Sizes (Oxford Univ. Press, 1961) p. 36.
61) J.-P. Jeukenne, A. Lejeune and C. Mahaux, Phys. Letters 1976 (in press).
62) W.H.T. Van Oers, et al., Phys. Rev. 1974, C10, 307.
63) J.-P. Jeukenne, A.Lejeune and C. Mahaux, Nukleonika 1975, 20, 181.
64) T.T.S. Kuo and G.E. Brown, Phys. Letters 1965, 18, 54.
65) T.T.S. Kuo and G.E. Brown, Nucl. Phys. 1966, 85, 40.
66) A.M. Green, Phys. Letters 1967, 24B, 384.
67) G. Passatore, Nucl. Phys. 1967, A95, 694.
68) G. Passatore, Nucl. Phys. 1968, A110, 91.
69) R. Lipperheide and A.K. Schmidt, Nucl. Phys. 1968, A112, 65.
70) C.B. Dover and Nguyen Van Giai, Nucl. Phys. 1971, A[illegible], 559.
71) C.B. Dover and Nguyen Van Giai, Nucl. Phys. 1972, A190, 373.
72) R.S. Mackintosh, Nucl. Phys. 1972, A192, 80.
73) R.W. Manweiler, Nucl. Phys. 1975, A240, 373.
74) L.R.B. Elton and S.J. Webb, Phys. Rev. Lett. 1970, 24, 145.
75) M.M. Giannini and G. Ricco, preprint Genova, November 1975.
76) G.E. Brown, J.H. Gunn and P. Gould, Nucl. Phys. 1963, 46, 598.
77) J.-P. Jeukenne, A. Lejeune and C. Mahaux, Phys. Letters 1975, 59B, 208.
78) I. Hamamoto, in G. Alaga, V. Paar and L. Sips (eds), Problems of Vibrational Nuclei (North-Holland Publ. Comp., Amsterdam, 1975).
79) I. Hamamoto, in G. Ripka and M. Porneuf (eds.), Proc. of the International Conference on Nuclear Self-Consistent Fields (Trieste, Febr. 1975) (North-Holland Publ. Comp., Amsterdam, 1975), p. 171
80) I. Hamamoto and P. Siemens, Nucl. Phys. (in press).
81) D.C. Agrawal and P.C. Sood, Phys. Rev. 1974, C9, 2454.
82) P.E. Hodgson, 1976 (private communication).
83) A.S. Reiner, Phys. Rev. 1965, 138, B389.
84) R.C. Johnson and D.C. Martin, Nucl. Phys. 1972, A192, 496.
85) E. Clementel and C. Villi, Nuovo Cimento 1955, 2, 176.
86) G.L. Shaw, Ann. Phys. (N.Y.) 1959, 3, 509.
87) I.R. Afnan and Y.C. Tang, Nucl. Phys. 1970, A141, 653.
88) J. Cugnon, Nucl. Phys. 1971, A165, 393.
89) P. Haensel, Nucl. Phys. 1975, A245, 29.
90) L. Verlet and J. Gavoret, Nuovo Cimento 1958, 10, 505.
91) B. Jancovici, Nucl. Phys. 1960, 21, 256.
92) B. Jancovici, Progr. Theor. Phys. (Kyoto) 1960, 23, 76.
93) G. Ripka, Nucl. Phys. 1963, 42, 75.
94) F. Brieva and J.R. Rook, 1976 (private communication).
95) G.E. Brown, Comments Nucl. Part. Phys. 1970, 4, 75.
96) A. Sugie, Phys. Rev. Lett. 1960, 4, 286.
97) D. Gross, Z. Physik 1967, 207, 251.
98) T.F. O'Dwyer, M. Kawai and G.E. Brown, Phys. Letters 1972, 41B, 259.
99) N. Azziz and R. Mendez-Placido, Phys. Rev. 1973, C8, 1849.
100) A. Lev, W.P. Beres and M. Divadeenam, Phys. Rev. Lett. 1973, 31, 555.
101) A. Lev, W.P. Beres and M. Divadeenam, Phys. Rev. 1974, C9, 2416.
102) A. Lev and W.P. Beres, Phys. Letters 1975, 58B, 263.

[103]) J. Cugnon, Nucl. Phys. 1973, A208, 333.
[104]) C.L. Rao, M. Reeves III and G.R. Satchler, Nucl. Phys. 1973, A207, 182.
[105]) R.S. Mackintosh, Nucl. Phys. 1974, A230, 195.
[106]) N. Vinh Mau and A. Bouyssy, Nucl. Phys. 1976, A257, 189.
[107]) C.A. Englebrecht and H. Fiedeldey, Ann. Phys. (N.Y.) 1967, 42, 262.
[108]) P.A. Moldauer, Nucl. Phys. 1963, 47, 65.
[109]) V. Gillet and E.A. Sanderson, Nucl. Phys. 1964, 54, 472.
[110]) V. Gillet and E.A. Sanderson, Nucl. Phys. 1967, A91, 292.
[111]) N. Vinh Mau, private communication.
[112]) M. Bruneau and N. Vinh Mau, in J.E. Bowcock (ed.), Methods and Problems of Theoretical Physics (North-Holland Publ. Comp., Amsterdam, 1970) p. 333.
[113]) M.P. Fricke, E.E. Gross, B.J. Morton and A. Zucker, Phys. Rev. 1967, 156, 1207.

MG 2 - THEORETICAL NEUTRON PHYSICS II: MICROSCOPIC CALCULATIONS OPTICAL MODEL POTENTIAL - Mahaux (Liège)

D. Divadeenam (B.N.L.):

Does your calculation include the effects due to target excitations?

Mahaux:

Yes, it does. It does in an average sense, since we use nuclear matter it is necessarily in an average sense, but we include via the use of Wigner's theory the particle hole excitations of the targets, so we include target polarizations in an average sense: we don't include shell effects, and so we miss the fact that some targets, to use the expression used by Professor Feshbach the other day, are particularly soft and so easily polarized and some other ones are so much harder to polarize so that we should expect to miss shell effects for instance and indeed in the case of calcium-40 we get too large an absorption, while it works very well for the other nuclei.

Divadeenam:

In addition to predicting the ground state binding energy, do you also predict the excited states of the target?

Mahaux:

No, because this is not a finite nuclear calculation so we don't look at excited states except for the single particle state which is described by the optical model. So, the only work where, not the only one, but the most detailed one, is the one by Nichol, Vinmo and Boissi who explicitly introduced the excited states of calcium, but these theoretical excited states of calcium seem to work very well for lowest ones.

V. A. Madsen (Livermore Laboratory and Oregon State University):

I have a comment on the value of V_1 that you calculated. Whereas there is an ambiguity in the optical model calculations, the (p,n) reaction requires a value of V_1 that is consistent with the Becchetti and Greenlees parameters, and a value half that would be much too low.

Mahaux:

Yes, the value of V_1 itself is not very meaningful because it should be associated with geometrical properties of this coupling, that's one point. A second point is that as I indicated, one should include the fact that there is a so-called Perey effect, to say that the wave function in a normal local field and inside the nucleus is not the same as the wave function in the local field. Now it was shown some 10 years ago by Francis Perey and Anna Maria Salouise that this is very important if you want to study precisely charge exchange reactions. This may effect the value of U_1 by easily 50% or factor 2 and this is not often enough taken into account, excepting that by Perey, and some work by Egel, I don't know about other ones. Now the third point is that a number of other recent empirical fits indicate that the value of V_1 which fits well charge exchange reactions is something like 17 MeV. This is quoted for instance by Galownski and collaborator in the last issue of Nuclear Physics and I was told that this is also the value they take. I think that these differences may have to do with the geometry that one assumes for the coupling.

Madsen:

Just one additional comment. The Perey Effect would further reduce the cross-section in the calculations.

Mahaux:

Yes, I agree, it should be included, but it's a problem.

Rapaport (Ohio University):

I have a comment and a question and the comment is as follows: One can get a handle on the so called Coulomb correction term by doing both proton and neutron elastic scattering on T=0 nuclei. We have done that work with Carlson et. al to be presented in paper PG2/E10, and the value that we are getting is not .4 but .48 which agrees very well with the ones you have indicated. What I find is that this value also depends on what formal factor, what radial dependence you are using for that part of the potential. Could you say how much is the volume integral contribution to the Coulomb correction term in the case of Pb-208, the curve you showed?

Mahaux:

Could I explain the shape of the curve?

Rapaport:

No, the volume integral of the Coulomb correction term.

Mahaux:

Yes, the volume integral is 25% larger than the one you would get from the Bechetti-Greenleas.

Rapaport:

You don't recall the value?

Mahaux:

The value I have, but not ----

Rapaport:

Is it proportional to Z?

Mahaux:

It is essentially proportional to Z, yes. We have made calculations for calcium, lead and so on. I have just shown one example here.

Cindro (Bruyères-le-Châtel):

My comment concerns the magnitude of the isospin term for which we have seen many numbers here. Now if one would start from simple physics, one would say that the presence of the isospin term comes from the fact that the interaction of nucleons with a nucleus is sensitive to the fact whether the nucleus is composed of neutrons or protons, or in other words, is sensitive to the small difference between the (n,p) and the (n,n) forces. Now, this difference is small, so at first sight I would expect that this term would be small. Why, then have physicists been seeing very big terms? Is it perhaps due to the fact that we have been using the isospin term as an additional parameter to fit things realted to other effects? I would like people who have different opinions to comment on my comment if time permits.

Mahaux:

Well, this is a point where I think that the theory can be useful and from the theoretical point of view you do expect an effect and you do expect an effect which is roughly between 5 and 50 MeV. Dr. Lane several years ago had made a number of estimates using various known facts of experimental physics, for instance, the semi-directory data of capture is one where this coupling comes in. Now it is in fact a small term because you multiply it by (N-Z/A), so it does indicate, as I have shown, it is maximum in the case of lead and it is 2 MeV in the depths of the potential. This indeed is also a reason why it is very hard to pin down an exact value for that term. Now, your question also reminds me that what one measures here is not V_1 or U_1, not the symmetry potential itself, but the expectation value of this quantity in a certain state which is the state occupied by the excess neutron. And this is subject to shell effects certainly, so indeed one should expect fluctuations in these values and when one gives a number, it's an average number of a nuclei. Now, I should also perhaps mention that we have studied the imaginary part of this coupling, but I don't have time to discuss that.

Moldauer (Argonne):

May I just ask one quick question? What is the interpretation of the imaginary part that you get when you calculate the real potential?

Mahaux:

The imaginary part of which potential?

Moldauer:

Well, when you calculate the real potential you get a complex answer and then you take the real part of that and throw away the imaginary part. What does that mean? What's the interpretation of that imaginary part?

Mahaux:

Oh, the interpretation is that if you take a nucleus, since we are serious, we can imagine experiments, and take a big nucleus and put the nucleon on top of it. When you put a nucleon on top of it, it has some potential energy. Right at the beginning when you create this nucleon, take a time dependent description, it doesn't have a well defined energy, but after a very short time you get this way, the packet gets stabilized and you can define a potential energy. The real part of the optical model potential is that potential energy of that part of the wave packet which decays exponentially in time, which is that part of the wave packet that the optical model has to do with. The imaginary part of the potential has to do with life time of this wave packet.

Moldauer:

Should that contribute to the observed imaginary potential, that is to the imaginary part of the optical potential?

Mahaux:

I think yes, I think this is what is observed.

Moldauer:

That's not how you calculated the imaginary potential?

Mahaux:

Oh, yes, we calculate the imaginary potential part at the same time as the real part.

Moldauer:

One last question.

Newstead (B.N.L.):

Claude, this is very impressive progress you've made in these microscopic calculations of the optical potential, particularly the imaginary part, W_0, but I wonder, have you any results for the imaginary isospin potential W_1?

Mahaux:

Yes, we do. It's very dangerous to give numbers because one should also give the form factor of that thing. But roughly speaking, it is about as large, a bit larger in fact as the real part at small energies that is, say below 15 MeV and significantly larger, in fact a factor two larger, than the real part at 50 MeV. But take these numbers with caution because one should really give the shape of the potential as well.

10:50 A.M., THURSDAY, JULY 8, 1976, IN OLNEY 150

MAIN SESSION MH

Chair: J. Humblet (Universtiy of Liège, Belgium)

10.50 a.m., Thursday, July 8, 1976

SPECTRUM FLUCTUATIONS AND THE STATISTICAL SHELL MODEL*

P. A. Mello[+], J. Flores[+], T. A. Brody[+], J. B. French[°], and S. S. M. Wong[△]

[+] Instituto de Física, Universidad Nacional Autónoma de México, México 20, D.F.

[°] Department of Physics and Astronomy, University of Rochester, Rochester, N.Y.

[△] Department of Physics, University of Toronto, Toronto, Ontario M5S 1A7, Canada.

* *Work supported by the Instituto Nacional de Energía Nuclear, México, by the U.S. Atomic Energy Commission (Energy Research and Development Administration), and the National Research Council of Canada. Work to be published in "Advances in Nuclear Physics".*

RÉSUMÉ

A survey is presented of the main recent advances in the theory and experimental data of spectrum fluctuations. It is shown that level fluctuations, and in particular spacing distributions, follow certain general rules, which are reviewed in detail.

ABSTRACT

We review the main advances in the theory of spectrum fluctuations and its comparison with experiment that have been achieved in the past few years. We first show that level fluctuations, in particular spacing distributions, are of a very general character[1]: the same distribution is observed in the slow-neutron resonance domain, in the fine structure near isobaric analogue states, in realistic shell-model calculations and, surprisingly enough, also in the ground-state region. This evidence allows us to consider the nuclear table as a physical realization of an ensemble of Hamiltonians, thus reaffirming the ideas of random-matrix theory, in particular in its two-body random Hamiltonian ensemble (TBRE) version[2], defined by a random two-body force in a given shell-model space. We then study the properties of the TBRE: the level density is Gaussian when the number of particles is large, in accordance with what obtains in realistic shell-model calculations; the nearest-neighbor spacing distribution is close to Wigner's, except in the ground-state region, where it shows slightly less repulsion, in accordance with experimental evidence, which unfortunately is scarce; for k-th neighbor spacings, after an appropriate unfolding[3] is performed, the distribution is the same as that predicted by the Gaussian orthogonal ensemble and coincides with experiment in almost all cases; the distribution of widths, even thought the TBRE is not an orthogonal ensemble, follows the Porter-Thomas law[4]. All these results have been obtained via Monte Carlo calculations since, from an analytical point of view, the problem is not tractable. However, there is evidence that simplified versions of TBRE[4,5], which are mathematically more tractable, share its properties. Using these ensembles, it has been possible to show that the density is Gaussian for almost all members of the ensemble[6] (internal ergodicity) and to study some properties of the two-point correlation function.

1) T.A.Brody, E.Cota, J.Flores and P.A.Mello, Nucl. Phys. (in press).
2) J.B.French and S.S.M.Wong, Phys. Lett. 33B (1970) 449.
O.Bohigas and J.Flores, Phys. Lett. 34B (1971) 261.
3) S.S.M.Wong and J.B.French, Nucl. Phys. A198 (1972) 188.
4) E.Yépez, Ph.D. Thesis, Universidad Nacional Autónoma de México, 1975 (unpubl.).
5) J.B.French, Rev. Mex. Fís. 22 (1973) 221.
6) K.K.Mon and J.B.French, Ann. Phys. (N.Y.) 95 (1975) 90.

SPECTRUM FLUCTUATIONS AND THE STATISTICAL SHELL MODEL*

P.A.Mello, J.Flores, T.A.Brody
Instituto de Física, Universidad Nacional Autónoma de México, México 20, D.F.

J.B.French
Department of Physics and Astronomy, University of Rochester, Rochester, N.Y. 14627

S.S.M.Wong
Department of Physics, University of Toronto, Toronto, Canada

The nuclear shell model has traditionally dealt with the determination of individual eigenstate properties, mainly in the low-energy region of spectra. In this paper we discuss a different application of the shell model : the statistical properties of nuclear spectra. Statistical methods are often resorted to only because it is not feasible to obtain the individual properties of levels, due to experimental problems or theoretical difficulties. It is the purpose of this paper to show, for the particular case of nuclear spectra, that these methods are able to reveal features of considerable interest which are not accessible to studies of individual properties.

*An extended version of this paper is to be published elsewhere. This work has been supported in part by the Instituto Nacional de Energía Nuclear and the Consejo Nacional de Ciencia y Tecnología, México, by the U.S. Energy Research and Development Administration, Contract No. E(11-1)-2171, and by the National Research Council of Canada.

1. THE STATISTICAL APPROACH

Parts of three spectra, obtained in rather different conditions, are shown in fig. 1 : the slow-neutron resonances·) of ^{167}Er, the states near an isobaric analogue state[2]) in ^{49}V, and the results from a large realistic shell-model calculation[3]) for ^{24}Mg. In the three cases all the 50 levels shown have the same total angular momentum J and parity π ; the scales have been so chosen that the average spacing D between nearest neighbours is the same in the three spectra.

Although the individual levels in the three spectra are placed very differently, some of their statistical properties are indeed very similar. Consider, for instance, the number of spacings smaller than $D/2$; as is made clear by fig. 1, where they are marked with asterisks, this number is nearly the same in the three cases. This regularity, of statistical origin, is even more evident in fig. 2, showing the histogrammes of the nearest-neighbour spacings ; the histogrammes agree rather well with the continuous curve, which corresponds to Wigner's distribution[4])

$$p_W(x) = \frac{\pi}{2} x \exp\left(-\frac{\pi}{4}x^2\right) \qquad (1)$$

where $x = s/D$, that is, the nearest-neighbour spacing s measured in units of its average D.

One should note that features of statistical nature (such as the spacing distribution) are apparent only when a whole stretch of levels is taken into account ; this situation is similar to that in statistical thermodynamics, where properties such as the temperature make sense only on a macroscopic scale.

The three spectra of figs. 1 and 2 are taken from a region of high excitation energy. Unfortunately it is difficult to assign J^π values to levels in an intermediate energy region ; so in order to examine the spacing distribution in this energy range, we must resort to large shell-model calculations[3]) which, even if not correct in their detailed predictions, may be expected to reproduce correctly

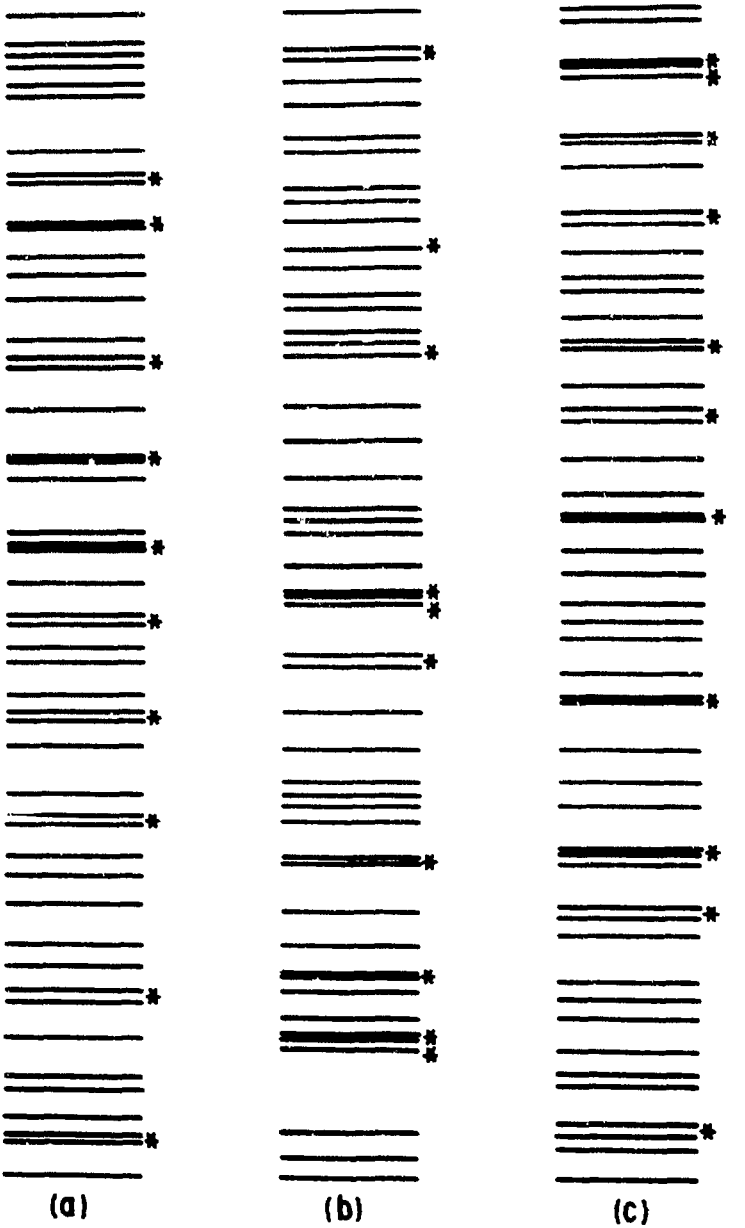

Fig. 1. Fifty levels from three representative spectra. Spacings smaller than half the average spacing D for each spectrum are marked by asterisks.

a) Slow-neutron resonances[1]) for ^{167}Er.

b) States of ^{49}V near the 2.7 MeV isobaric analogue state[2]).

c) Levels from a shell-model calculation[3]) for ^{24}Mg.

the statistical features - as is evidenced by fig. 2c for the high-energy region. The resulting spacing histogrammes for two groups of levels from intermediate energies are given in fig. 3 ; the shape of the distribution is clearly very close to that of fig. 2.

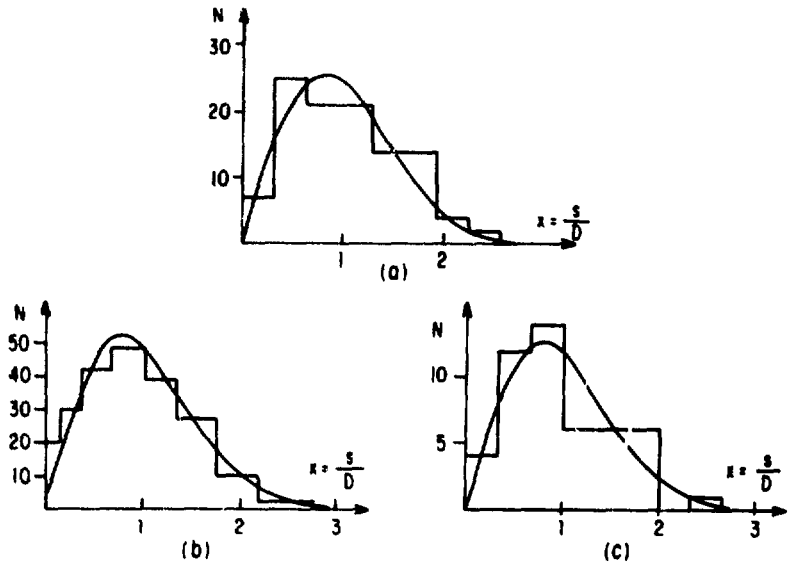

Fig. 2. Histogrammes of the distributions of the nearest-neighbour spacings for the three spectra of Fig. 1.

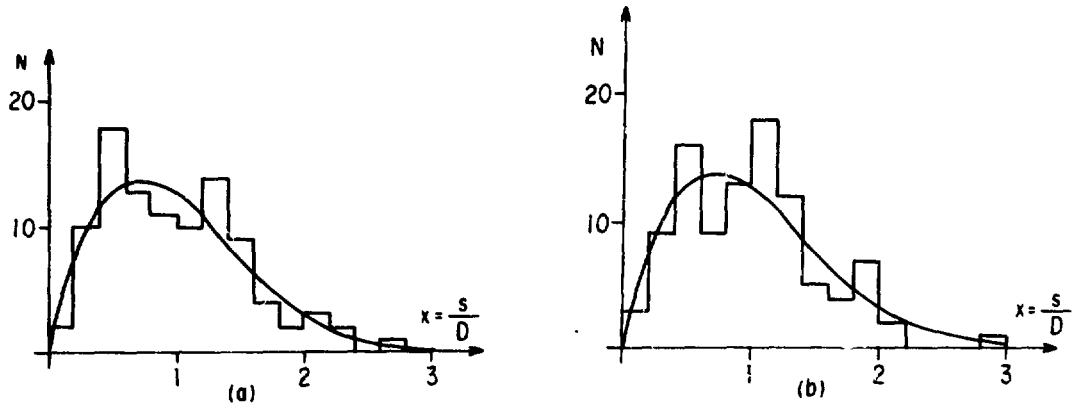

Fig. 3. The nearest-neighbour spacing distribution for a sequence of 100 levels obtained from the 1206-dimensional matrix computed by Chang and Zuker[3]) for ^{24}Mg. a) Level 401 to level 500 ; b) Level 501 to level 600.

What happens when we go as far down as the ground-state region ? Here any attempt at defining an average spacing D for an individual nucleus fails, since the position of the first few levels fluctuates so wildly. An answer to the question can be found, however, if we consider many nuclei : plot the spacing between the first pair of levels with the same J and π for different nuclei, as a function of A. If very light nuclei, say with $A < 18$, are ignored, an average spacing $D(A)$ can be determined quite consistently and turns out to be proportional to A^{-1} ; furthermore, the resulting data fall cleanly into two classes[5] : the "systematic" group, to which belong the even-even, rotational, magic and doubly magic nuclei, with spacings that deviate very little from $D(A)$; and the "statistical" group, comprising the remainder. After dividing the spacings of the latter by $D(A)$ so as to normalise them, the histogramme of fig. 4 is obtained[6] : this, together with the histogrammes shown earlier, suggests that the nearest-neighbour spacing distribution is of a rather general character[7].

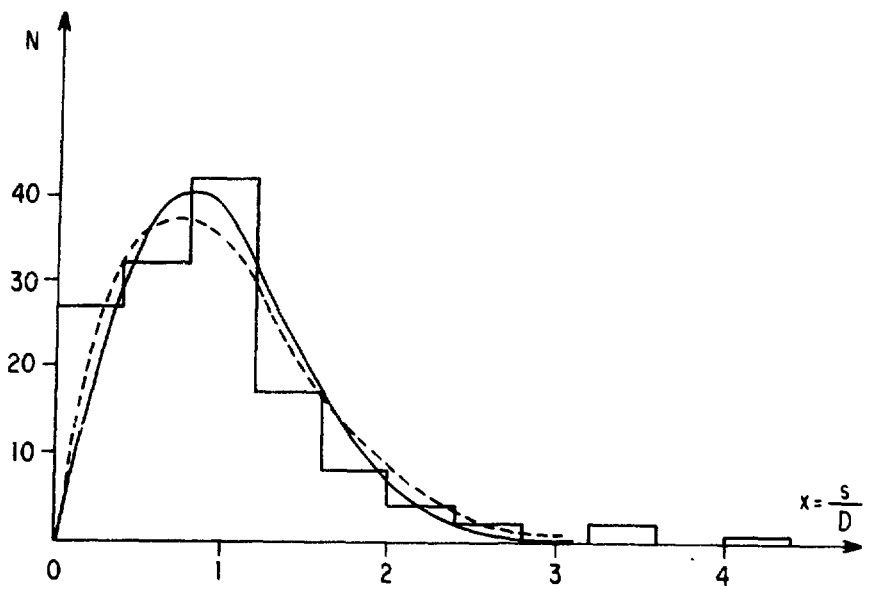

Fig. 4. Histogramme of the energy difference between the lowest two states having the same values of J and π for the "statistical" group in the nuclear table. The solid line represents eq. (1), the dotted one corresponds to eq. (15) with $\omega = 0.8$.

The procedure for obtaining fig. 4 is similar to that followed in statistical mechanics : whenever the time average of a function for an individual system cannot easily be calculated, a large set of (theoretical) replicas of the system, all described by the same macroscopic properties but corresponding to different microscopic initial conditions, is introduced under the name of *ensemble*, and averages taken over it ; if such an ensemble average can be used instead of the time average, the ensemble is *ergodic*[8]). The statistics of the nuclear case differ, however, in two respects : instead of the time, it is the energy that one averages over, and the ensemble consists of systems that instead of having different initial conditions are described by different Hamiltonians. The data in fig. 4 then constitute a finite sample from an experimental realisation of such an ensemble.

A theory intended to account for such features as the wide applicability of the spacing distribution will then partake of the general nature of statistical mechanics in using ensembles as its basic concept, however much the details may differ ; and just as in statistical mechanics much of the underlying detail features are irrelevant, so one hopes that here the theory will not require answers to the many questions in nuclear physics that are still open. The theoretical work to be presented in this paper will have a further limitation : since we deal only with spectra composed of discrete states or very narrow resonances, we shall limit ourselves to the matrix representation of the Hamiltonians making up the ensemble ; these will then be constructed in the spirit of the shell model, and will thus furnish the building blocks for what we shall call the *statistical shell model*[9]).

So far we have only mentioned the nearest-neighbour spacing distribution ; but the same statistical theory should allow us to analyse other statistical properties, such as the n^{th}-neighbour spacing distributions, or that of the reduced widths of nuclear resonances ; these are examples of *local properties* or *fluctuations*[10,11]). The statistical shell model should also account for global properties such as the secular or long-range variation of the level density or the strength function.

II. THE TWO-BODY RANDOM HAMILTONIAN ENSEMBLE

We shall discuss three different ensembles under the heading of the statistical shell model, which we now proceed to define more precisely. Consider m particles in a set of N single-particle states, the same for all members of the ensemble. Then the residual two-body interaction is completely defined if its matrix elements, say $V_{\alpha\beta}$, with respect to antisymmetrised two-particle states α and β are given. For the m-particle states $|m;i\rangle$ the matrix elements are then found by standard shell-model techniques as the linear combinations

$$\langle m;i|H|m;j\rangle = \sum_{\alpha,\beta} C_{\alpha\beta}^{ij} V_{\alpha\beta} \qquad (2)$$

The matrices with these elements then constitute an ensemble of random matrices if the $V_{\alpha\beta}$ are stochastic variables ; any member, in other words, is given by choosing these quantities as random numbers sampled from an appropriate distribution. If m is sufficiently large, the particular form of the distribution is not crucial, so long as the $V_{\alpha\beta}$ are statistically independent : the central-limit theorem will ensure the same form of distribution for the matrix elements (2). The ensemble so obtained is the two-body random Hamiltonian ensemble (TBRE) ; it is marked by strong statistical correlations among the matrix elements (2), since their number is usually very much larger than that of the $V_{\alpha\beta}$.

In its original form[9], both the total angular momentum J and its projection J_z were taken to be good quantum numbers ; the evaluation of the coefficients $C_{\alpha\beta}^{ij}$ in (2) then requires the full resources of shell-model theory, and if N and m are at all large is excessively complicated and time-consuming. Yépez[12] showed that as regards the statistical behaviour of the ensemble one can ignore J ; he studied an ensemble with only J_z as a good quantum number. Although this is calculationally far simpler than the original TBRE, it is still too difficult to handle analytically, and thus almost all results for it were obtained from Monte Carlo calculations.

In an attempt to define a mathematically tractable ensemble without losing the physical relevance of the TBRE, one of the authors[13]) proposed ignoring altogether the presence of good quantum numbers ; the two-body character of the force - giving rise to the correlations we have mentioned - is then the essential feature that characterises this ensemble, which, for reasons described in ref. 13, we shall call an embedded ensemble (EE). Its algebraic structure is much simpler, since the coefficients $C^{ij}_{\alpha\beta}$ for it reduce to simple phase factors.

The ensembles mentioned up to now are all built on two-body forces ; to generalise to k-body forces, with $k > 2$, is difficult in the original TBRE, somewhat easier for Yépez' version, and immediate for the EE : one need merely use k-body matrix elements as the basic stochastic variables and combine them to give m-particle matrix elements by means of phase factors which are easily derived. Since as a consequence the EE results are little more difficult to obtain for $k > 2$ than for $k = 2$, we shall consider in what follows the more general k-body EE.

In the past, much attention has been paid to the particular ensemble for which $k = m$. In this case the linear combination (2) disappears, the distribution we sample is the final one and its choice thus not a matter of indifference. The actual value of k (or m) is irrelevant for characterising the ensemble, since it no longer appears in the definition. To specify completely the distribution of the matrix elements, a further assumption is needed : the joint probability distribution of all the $d(d + 1)/2$ matrix elements (d is the size of the matrix, which as is usual is taken to be real and symmetric) is assumed to be invariant under the operations of the rotation group R_d in d dimensions. Under these conditions one obtains the well-known Gaussian orthogonal ensemble[10]) (GOE), for which many useful analytical results have been derived[11]). Its predictions agree well with experimental results for many of the fluctuation properties such as the spacing distributions, but tend to fail for global properties such as the level density or the strength function.

III. THE LEVEL DENSITY AND ITS FLUCTUATIONS IN THE EMBEDDED ENSEMBLE

It is not yet possible to give a complete account of the level density and the corresponding fluctuations in the k-body EE ; we shall restrict ourselves largely to a physically significant limiting case, namely large "dilute" systems, where $m \to \infty$, $N \to \infty$, but $m/N \to 0$. In this limit the Pauli principle plays no further role, and calculations are consequently much simplified[14].

The level density in an individual matrix with eigenvalues E_i is a sum of delta functions,

$$\rho(E) = \sum_{i=1}^{d} \delta(E - E_i) \tag{3}$$

If the matrix dimensionality d is large, one can consider instead a smoothed-out approximation $\tilde{\rho}(E)$. For non-interacting particles, i.e. for $k = 1$, this smoothed-out density becomes a Gaussian in the dilute limit, because the matrix element given by (2) is a sum of independent terms and the central-limit theorem comes into action. This is true no matter how peculiar the single-particle spectrum may be, provided $\sum E_i^p < \infty$ for $p = 1$, 2 and 3. For $k \geq 2$ this is no longer so ; nevertheless the ensemble-averaged density $\overline{\rho(E)}$ should yield a characteristic form, and the question how far this is also valid for individual spectra (i.e. the ergodic problem) may also be tackled.

We proceed as follows[14] : H is a k-body operator, and we write as before its defining k-particle matrix elements as $V_{\alpha\beta}$, where α and β now denote two of the $\binom{N}{k}$ orthogonal states of k particles in the N single-particle levels which constitute the shell-model space. We take, as before, the $V_{\alpha\beta}$ to be real and statistically independent random numbers, with

$$\begin{aligned} V_{\alpha\beta} &= V_{\beta\alpha} \\ \overline{V_{\alpha\beta}^{2\lambda+1}} &= 0, \qquad \lambda = 0, 1, 2, \ldots \\ \overline{V_{\alpha\beta}^{2}} &= (1 + \delta_{\alpha\beta})\nu^2 \end{aligned} \tag{4}$$

We need not specify any further details of the distribution of the matrix elements. The constant v^2 is chosen to be $\binom{N}{k}^{-1}$, so that in the limit of large N the average expectation value of H^2 in the k-particle spectroscopic space tends to unity. This normalisation simplifies the algebra without affecting the essential results. The behaviour of $\overline{\rho(E)}$ will be determined from its moments, defined as

$$M_p(m) = \int_{-\infty}^{\infty} E^p \overline{\rho(E)}\, dE$$

We have that

$$M_p(m) = \binom{N}{m}^{-1} \overline{\mathrm{Tr}\ (H^p)} = \overline{\langle H^p \rangle_{\{m\}}} \qquad (5)$$

where the bar, as throughout this paper, denotes ensemble averaging, and the subscript $\{m\}$ is a reminder that H acts in the m-particle spectroscopic space. As is clear from (4), all moments M_p of odd order vanish, and $\overline{\rho(E)}$ is therefore symmetric about the mean energy, which can without loss of generality be taken to be 0. This result appears at first sight to be unphysical, since in actual nuclei the level density rises[15], roughly as $\exp \sqrt{E}$, until the continuum is reached ; yet here it will rise only until $E = 0$, and then fall in exactly the same manner. But it must be remembered that we have deliberately not taken into account the existence of the continuum, and therefore all the upper part of the spectrum yielded by a finite matrix will be unrealistic ; it can be argued[16], in fact, that only the superposition of several such lower halves of spectra, one for each shell, will account for the observed nuclear level density, though the validity of this model is not yet established. The question to be asked, therefore, is whether the energy variation of $\overline{\rho}$ for low energies reproduces adequately the observed behaviour.

For even orders, $p = 2\nu$, we can distinguish two limiting cases : $k = m << N$ and $k << m << N$. In the first case,

$$M_{2\nu}(m=k) \xrightarrow[N\to\infty]{} \frac{1}{\nu+1} \binom{2\nu}{\nu} \left(M_2(m=k)\right)^{\nu} = \frac{1}{\nu+1} \binom{2\nu}{\nu} \qquad (6)$$

which are the moments of Wigner's well-known "semicircular" law[10]

$$\overline{\rho(E)} = \frac{1}{2\pi}(4 - E^2)^{\frac{1}{2}} \tag{7}$$

which, as our derivation shows, is valid more generally than the GOE to which it is usually applied. As we mentioned, it is not a good approximation to the experimental nuclear level densities ; not even the curvature has the right sign. On the other hand, for the second case, i.e. the dilute EE, it can be shown that a central-limit theorem operates, so that the moments become those of a Gaussian

$$\overline{\rho(E)} = (2\pi\sigma^2)^{-\frac{1}{2}}\exp(-\frac{E^2}{2\sigma^2}), \qquad \sigma^2 = \binom{m}{k} \tag{8}$$

a result first obtained by numerical calculations for the TBRE[9]. The lower extreme of a Gaussian is a much better representation of the experimental data than the semicircular law.

For other values of m, between these two extremes, $\overline{\rho(E)}$ is intermediate between a semicircle and a Gaussian.

How much does the density for an individual matrix differ from the ensemble average given by (7) or (8) ? The method of moments gives an answer through the evaluation of the variance

$$\Sigma_p^2(m) = \overline{\langle H^p \rangle_{\{m\}}^2} - (\overline{\langle H^p \rangle_{\{m\}}})^2 \tag{9}$$

which gives the fluctuations of the p^{th} moment around its ensemble value $M_p(m)$. It may be shown that $\Sigma_p^2(m) \sim \binom{N}{k}^{-2} \longrightarrow 0$ as $N \longrightarrow \infty$. Thus for the embedded ensemble the level density becomes ergodic in the limit of large N, since the probability that any member deviates from the ensemble average becomes vanishingly small. Monte Carlo calculations indicate that this property carries over to the TBRE. The $k = m$ case was studied analytically by Olson and Uppuluri[19].

One can also evaluate the covariances $\Sigma_{pq}(m)$, of which the variances (8) are special cases : $\Sigma_{pp}(m) = \Sigma_p^2(m)$. They are found as

$$\Sigma_{pq}(m) = \overline{\langle H^p\rangle_{\{m\}}\langle H^q\rangle_{\{m\}}} - \overline{\langle H^p\rangle_{\{m\}}}\;\overline{\langle H^q\rangle_{\{m\}}} \qquad (10)$$

and are the moments of the two-point correlation function

$$C(E_1,E_2) = \overline{\rho(E_1)\rho(E_2)} - \overline{\rho(E_1)}\cdot\overline{\rho(E_2)} \qquad (11)$$

This correlation function is directly related to the fluctuations in level density. When E_1 and E_2 are very different, it gives an indication of the presence of long-range order, for it only goes to 0 if there is none ; and its integral with respect to both arguments over a finite interval yields the fluctuation in the number of levels to be found within that interval.

For large N in the case $k = m$, the covariance (10) becomes

$$\Sigma_{pq}(k=m) = 2\binom{N}{k}^{-2} \sum_{\zeta\geq 1} \zeta \binom{p}{\frac{p-\zeta}{2}} \binom{q}{\frac{q-\zeta}{2}} \qquad (12)$$

and vanishes unless p and q have the same parity ; the sum goes over all ζ of that parity, up to $\min(p,q)$. This result can be used to approximate the actual density function $\rho(E)$ of (3) for an individual matrix by

$$\rho'(E) = \overline{\rho(E)} + \sum_{\zeta} \eta_\zeta \rho^{\{\zeta\}}(E) \qquad (13)$$

if the η_ζ and the auxiliary functions $\rho^{\{\zeta\}}(E)$ are chosen in such a way that the moments of $\rho'(E)$ coincide with the values given by eqs. (5), (9) and (12). This can be achieved if the p^{th} moment of $\rho^{\{\zeta\}}(E)$ is

$$\binom{N}{k}^{-1} \sqrt{2\zeta}\binom{p}{\frac{p-\zeta}{2}}$$

and the η_ζ (which must of course be random variables to reproduce the variation of $\rho'(E)$ over the ensemble) satisfy

$$\overline{\eta_\zeta} = 0, \qquad \overline{\eta_\zeta \eta_{\zeta'}} = \delta_{\zeta\zeta'}$$

Thus we obtain an explicit level density, eq. (13), which reproduces those properties of the real density that derive from the two-point correlation (11) for the case $k = m$. One important result found in this way is that the fluctuation of the mean value of the number of levels n in a finite energy interval is

$$\text{var } (n) = \frac{2}{\pi^2} \ln n \qquad (14)$$

and is therefore very much smaller than var $(n) \sim n$, the value to be expected if there were no long-range rigidity in the spectrum of the kind first discussed by Dyson and Mehta[17]). This rather unexpected result is not at all evident from visual inspection of any spectrum, but is confirmed, as we shall see, both by experimental data and by Monte Carlo results. In fact, the presence of some sort of long-range structure hidden by short-range disorder is characteristic of the physically interesting random-matrix ensembles and not merely of the GOE, for which it was first discovered. (Note, incidentally, that these results are not in conflict with the ergodicity mentioned above : as N increases, the energy interval containing n levels decreases, and the fluctuations we are discussing are only seen after a suitable change of scale.)

For large values of $E_1 - E_2$, the correlation function (11) can be deduced explicitly ; the value coincides with that found by Mehta[11]) for the central region of Wigner's "semicircle", but is valid for any part of the semicircle, as had already been indicated by Monte Carlo studies[18]).

In the "dilute" case of the EE, where $m >> k$, no such complete results have yet been obtained. Σ_{pq} can be decomposed in a form similar to (12),

$$\Sigma_{pq} = 2\binom{m}{k}^2 \binom{N}{k}^{-2} \sum_{\zeta} \zeta\,(p-\zeta-1)!!\binom{p}{\zeta}\binom{m}{k}^{\frac{p-\zeta}{2}}(q-\zeta-1)!!\binom{q}{\zeta}\binom{m}{k}^{\frac{q-\zeta}{2}}$$

but the expression for the terms in this sum is only valid when $\zeta < m/k$; for ζ larger than this ratio modifications would be required, but their exact nature is not yet known. It has been established, however, that there is not the same long-range rigidity as

in the GOE, though there is some reason to believe that it is far from negligible.

The method of moments, some of whose results we have described, is clearly rather powerful ; how far it can be extended beyond its presently known limits is, however, quite unknown. Higher-order correlations (three-point correlation functions and so on) remain to be studied, as does the derivation of the spacing distributions. Only in the limiting case $k = m$ and the particular case of the GOE has this been achieved analytically ; for $k \neq m$ only Monte Carlo results are available.

IV. THE THEORETICAL SPACING DISTRIBUTION

The distribution of the level spacings is usually described by giving the probability density $p(n;x)$ for finding a spacing of size x with n levels in between ; as before, x is normalised so that the average nearest-neighbour spacing (for $n = 0$, that is to say) is $\mathcal{D} = 1$. The existence of long-range correlations, discussed in the preceding section, means that $p(n;x)$ is not simply the convolution of $p(n-1;x)$ with $p(0;x)$; it also constitutes one of the reasons why it has not yet proved possible to deduce the spacing distributions from the results on fluctuations of the preceding section. Only for the case of the GOE, where $k = m$, is the analytical form of $p(n;x)$ known. In particular, Mehta and Gaudin[20] showed that in the central part of the "semicircle" the exact nearest-neighbour distribution $p(0;x)$ is almost indistinguishable from Wigner's distribution $p_W(x)$ of eq. (1).

In other energy regions the level density is not even approximately constant, and this variation must be corrected for by "unfolding" the spectrum in such a way that it is reduced to constant level density without the essential nature of the fluctuations being affected. When $k = m$, it has been shown[21] that this is always possible ; the result probably carries over to the general case,

but has been proved only for large m. We shall nevertheless suppose that unfolding is always achievable in a consistent and satisfactory way, as is indeed borne out by Monte Carlo calculations for several types of ensembles. For the case of the GOE, these results show that the nearest-neighbour spacing distribution is the same for all energies : in the language of stochastic processes, the spacing distribution is stationary[22].

This result may be made more precise by looking at a remarkable property of this distribution, namely the so-called "level repulsion" : the fact that, as will be observed in fig. 2, small spacings are very unlikely. This effect is measured by the statistic ω, obtained by fitting to the spacing histogramme a distribution function which generalises eq. (1) and adjusting ω by least squares ; this function is[23]

$$p_\omega(0;x) = Ax^\omega \exp(-\alpha x^{\omega+1}) \qquad (15)$$

(A and α are determined by requiring the area under the curve and the average $\bar{x} \equiv D$ to be both = 1.) When the positions of successive levels are completely random and independent, the spacings are exponentially distributed and $\omega = 0$; for Wigner's distribution $\omega = 1$; and for the exact GOE distribution $\omega = 0.9525$. In fig. 5 we plot the

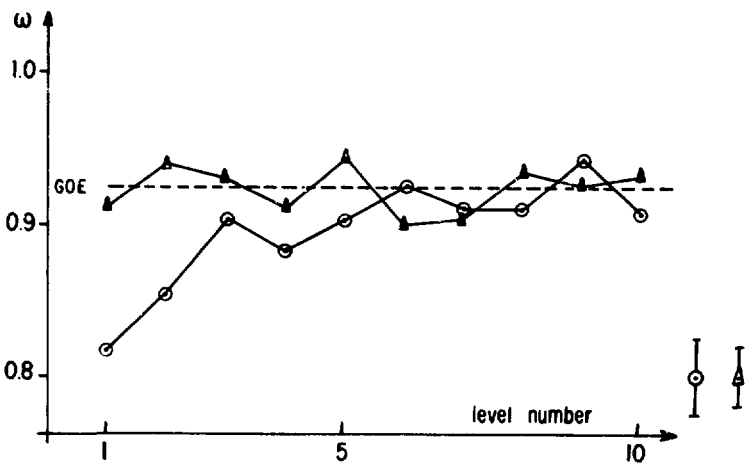

Fig. 5. The statistic ω as a function of energy for the GOE and the TBRE, obtained from Monte Carlo calculations.

value of ω, found from Monte Carlo calculations, as a function of the energy in the GOE ; the stationarity property we have mentioned is seen from the fact that at no energy does ω differ significantly from its central value.

The repulsion parameter ω can also be used to examine another ergodic property of the GOE, namely whether the nearest-neighbour spacing distribution for individual matrices converges to the ensemble one for large enough dimensionality. Fig. 6 shows the answer to be yes : the dispersion of the ω values for individual matrices about the ensemble average diminishes as $d^{-\frac{1}{2}}$, and thus the GOE is ergodic for this particular property.

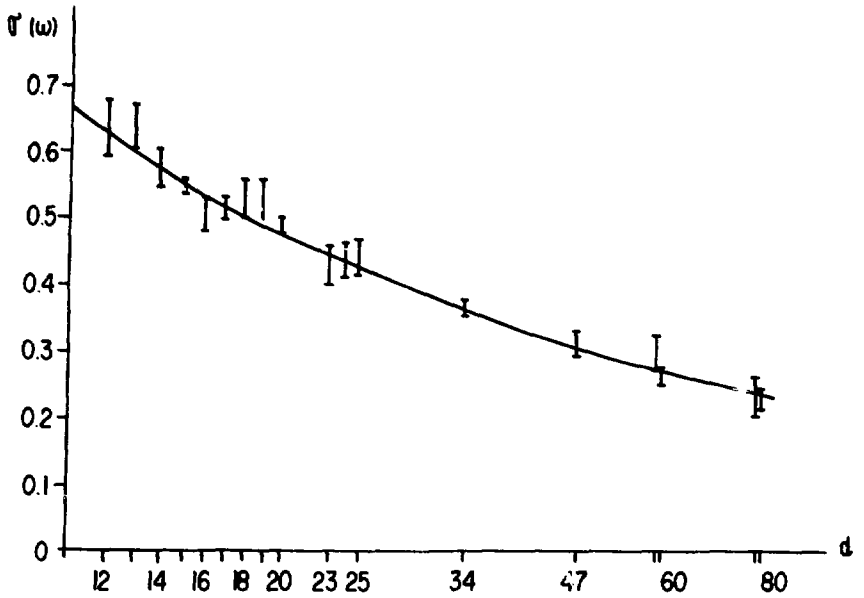

Fig. 6. The dispersion of the ω values for individual matrices from the GOE, as a function of the dimensionality d.

Mehta and des Cloizeaux[24]) have obtained analytic expressions for the $p(n;x)$ of the GOE when $n > 0$ in terms of spheroidal functions. For n large enough, $p(n;x)$ tends to Gaussian shape ; since the average must of course have the ensemble value $n + 1$, the width $\sigma(n)$ of the distribution is enough to specify it completely. We plot the values of $\sigma(n)$ as a function of n in fig. 7, which includes for comparison the values of $\sigma_p(n) = \sqrt{n+1}$ which correspond to a sequence

of levels with completely independent distributions. In such a sequence the spacing x of order n is the sum of $n + 1$ independent

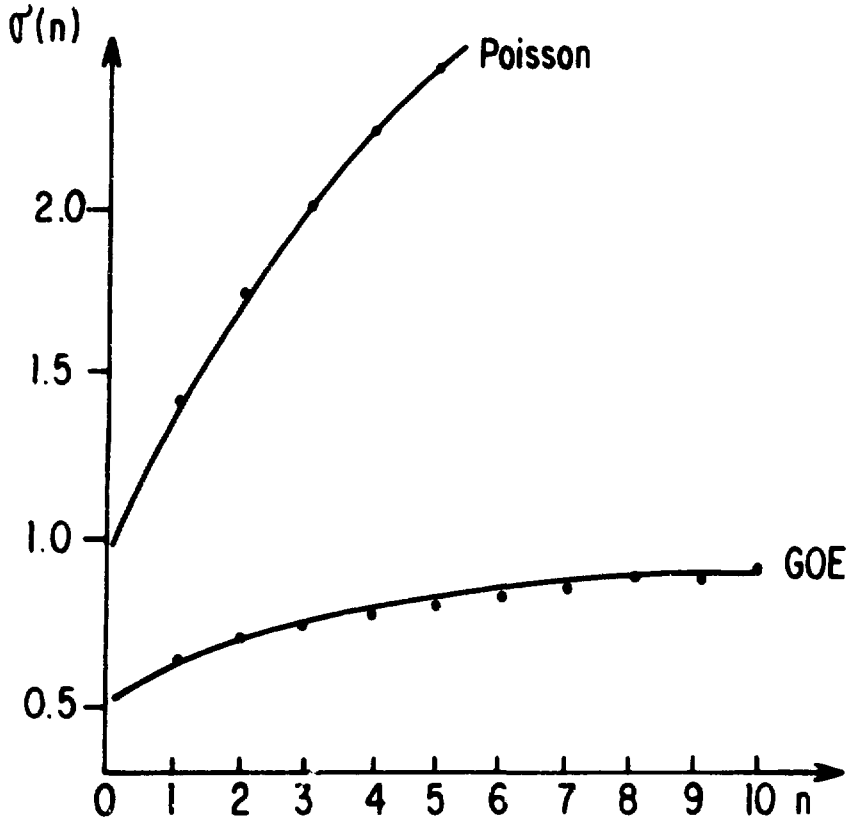

Fig. 7. The standard deviation $\sigma(n)$ of the n^{th}-order neighbour spacing distribution $p(n;x)$ for the GOE and the completely random case (Poisson).

random variables, and the Gaussian nature of $p(n;x)$ for large n is thus a direct result of the central-limit theorem. For the GOE the origin of the Gaussian shape of the higher-order $p(n;x)$ is much less obvious, because of the tendency to long-range order we have discussed, which for instance brings about a correlation of - 0.27 between successive zero-order spacings.

For the TBRE in both its versions, rather complete Monte Carlo calculations have been carried out over the last few years, with the following results : for $n = 0$ and in the central region, $p_{TBRE}(0;x)$ coincides with the GOE result ; but, as fig. 5 shows, the distribution is not stationary, and in the ground-state region the

repulsion has diminished to 0.8. The lack of stationarity is even more marked for $n > 0$, as can be seen in fig. 8. For $\sigma(n)$ in the central region the results are again the same as for the GOE.*

Except for the GOE, no analytical results are known, and this renders more difficult the comparison of theory and experiment, the point to be taken up in the next section.

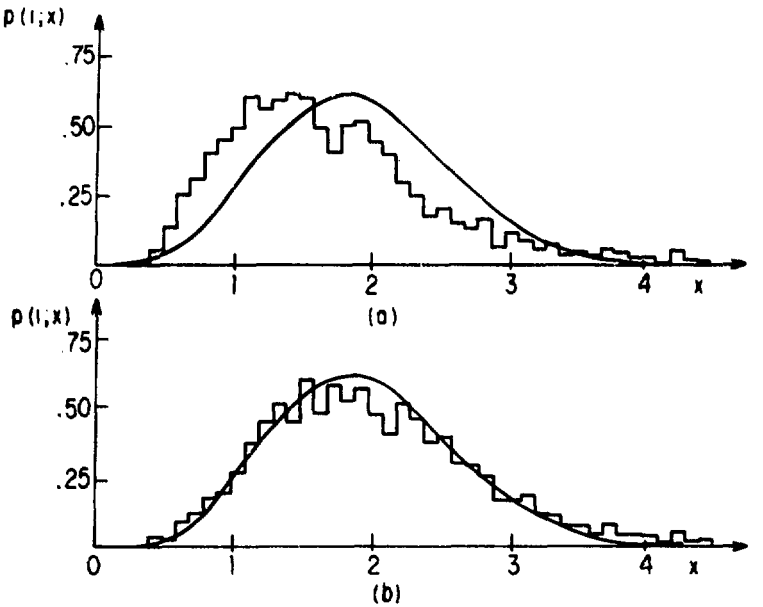

Fig. 8. The distribution $p(1;x)$ for the TBRE in the ground-state region (a) and in the central region (b).

*The discrepant results published earlier[25]) have been shown[26]) to be due to the fluctuations of the average spacing $\mathcal{D}$ between members of the ensemble ; these fluctuations are much more important for the TBRE than for the GOE, a result in agreement with the reduced rigidity of the EE, which as mentioned is expected to have statistical properties closely paralleling those of the TBRE.

V. COMPARISON OF THEORY AND EXPERIMENT

We have focussed attention in this paper on the fluctuations in level sequences that belong all to the same angular momentum and parity. It is for these so-called "pure" sequences that the theoretical results and Monte Carlo calculations we have discussed are valid. The reason is simple : spectra belonging to different J^{π} values are essentially independent of each other ; it is thus natural that the superposition of a number of such spectra makes the spacing distribution move towards the exponential type which results when there is no structure due to correlations and which no longer carries any information of interest to nuclear physics. When two such spectra are superimposed, the analysis is still in principle possible, and certain results are known for such situations[27] ; we shall not discuss them here, however, because our knowledge concerning them is still too incomplete.

The requirement that the series should be pure places much emphasis on the need for high-quality experimental data, in an area where the experimental techniques are not simple. On the one hand, no levels with differing J^{π} should be included, on the other hand none with the same J^{π} should be missed out. Adequate level sequences are provided by three types of experimental results : firstly there are a number of excellent series from slow-neutron resonance scattering[1,28-36], the best ones probably coming from even-even targets in the rare-earth region ; secondly there are good results[2,37] for proton resonances on targets such as ^{44}Ca and ^{48}Ti ; lastly there are the data from the nuclear-table ensemble[7] we discussed in section I.

It is evidently necessary that some checks be made of the quality of the data, which arise from different experiments carried out for different purposes. Several statistical parameters are available for this ; but it should be remembered that the underlying theory derives from specific models, so that their validity cannot be separated from the question of the validity of these models. The distinction between "purity-test" parameters and those used to

verify the theoretical description is thus quite relative ; moreover the six parameters for which we quote results are by no means statistically independent of each other, though any detailed theory is lacking. But it is known, chiefly from Monte Carlo work, that certain parameters are much more sensitive to the presence of any "foreign" levels or the absence of missed-out levels ; these are the parameters we use to check the purity of level series. Other parameters are much less sensitive to impurities, and these are then more relevant to testing the validity of theoretical models.

The three purity-test parameters are the following :

(*i*) The Δ_3 statistic, due to Dyson and Mehta[17]), which is based on a very wide class of ensembles as theoretical model ; what they have in common is that they predict a considerable long-range correlation of the type we have discussed ; certainly the GOE and probably the EE belong to this class. The value of Δ_3 is given by the least-squares residual obtained upon fitting a straight line to the staircase plot of the number of levels below an energy value as function of that energy. For n levels in the series, its expectation value and dispersion are

$$\overline{\Delta}_3 = \frac{1}{\pi^2}(\ln n - 0.0687) \qquad \sigma_{\Delta_3} = 0.11$$

(*ii*) The F test was originally designed by Dyson[38]) to examine shorter-range correlations, over energy intervals containing, say, n levels. Computational tests on Monte-Carlo generated ensembles and on sections of large shell-model calculations have shown that the standard deviation of the F values, σ_F, is rather more sensitive to the presence of impurities of either kind, and accordingly we include values for it, computed with $n = 10$ levels, to be compared with the theoretical value

$$\sigma_n^2(F) = \ln \pi n \qquad \text{i.e.} \quad \sigma_{10}(F) = 1.856$$

(*iii*) The dispersion of the number of levels in a fixed energy interval. For large n, the result of eq. (1) is valid ; we choose an energy interval such that on the average it will contain 10 levels

(a number that makes practical computations possible), and therefore use instead of (14) an expression which contains "small" terms[17])

$$\text{var } (n) = \frac{2}{\pi^2}(\ln 2\pi n + 1 + \gamma - \frac{\pi^2}{8})$$

For 10 levels this yields a theoretical value of 0.953 for the standard deviation of n.

The three parameters used to examine the validity of the theoretical structure we have described are :

(*i*) The value of the repulsion parameter ω, determined by adapting (15) to the data, as already described. The least-squares process also yields an estimate of the confidence interval for ω ; this is also quoted, since it indicates how well (15) fits the data (the χ^2 test is observed in Monte Carlo calculations to have too wide a spread to be very useful).

(*ii*) The standard deviations $\sigma(n)$ of the spacing distributions of order n which we discussed in the preceding section. Only those for n = 0, 3, 6 and 10 are given, in order to indicate the general trend.

(*iii*) The correlation coefficient ρ_o between successive nearest-neighbour spacings. In a sense, this coefficient (whose expectation value for the GOE is - 0.27, as we have seen) is related to the $\sigma(n)$, since these are reduced well below the value for independent levels because of the long-range order of which this correlation is an expression.

The data, both experimental and theoretical, for these six parameters, together with other relevant information are presented in Table I. It will be seen that not only the experimental results but also those from large shell-model calculations agree on the whole with the theoretical predictions both of the GOE and the TBRE, as far as fluctuations are concerned. There are, however, some exceptions ; one of these are the two sets of data from plutonium isotopes[36]), where the values of the three purity-test parameters shed some doubt on the quality of the data - unless the results must be

TABLE I

Target and projectile		ref.	n	E_{min}-E_{max}	$\mathcal{D}$	σ_F	$\sqrt{var(n)}$	Δ_3 exp	Δ_3 theo	ρ_o	σ_0	σ_3	σ_6	σ_{10}	ω	notes
^{166}Er	n	1	109	0-4200	38.4	1.8	0.96	0.46	0.47	-0.22	0.53	0.76	0.81	0.93	0.85±0.19	
^{168}Er	n	1	50	0-4700	95.3	1.9	0.78	0.29	0.39	-0.29	0.50	0.73	0.65	0.61	1.03±0.12	
^{152}Sm	n	28	70	0-3665	51.8	1.9	0.91	0.40	0.42	-0.26	0.56	0.77	0.81	0.78		
^{152}Sm	n	35	70	0-3665	51.8			0.40	0.42						0.96±0.10	
^{232}Th	n	29	178	0-3000	16.8	2.2	1.05	0.39	0.51	-0.19	0.54	0.83	0.86	1.03	0.83±0.14	
^{238}U	n	29	146	0-3015	20.8	1.7	0.80	0.42	0.49	-0.24	0.50	0.60	0.62	0.79	1.21±0.09	
^{172}Yb	n	30	55	0-3900	70.3	1.7	1.04	0.41	0.40	-0.24	0.55	0.88	1.00	0.89	0.79±0.12	
^{182}W	n	31	41	0-2650	66.3	1.6	0.73	0.26	0.37	-0.37	0.47	0.61	0.68	0.73		
^{112}Cd	n	32	52	0-7000	137	2.7	0.67	0.30	0.39	-0.32	0.38	0.65	0.69	0.53	0.62±0.17	
^{158}Gd	n	33	47	0-4000	86			0.29	0.38	-0.14						
^{162}Dy	n	34	48	0-3000	64.6			0.34	0.39	-0.29	0.39	0.53	0.65	0.78	0.99±0.13	
^{239}Pu	n	36	91	0- 300	3.2	4.9	1.60	2.25	0.45	-0.23	0.59	0.96	1.25	1.56	0.76±0.21	a
^{240}Pu	n	36	43	0- 680	15.8	3.1	1.27	0.65	0.37	-0.23	0.56	1.09	1.17	1.00	0.79±0.19	
^{44}Ca	p	37	39	1990-2390		3.2	1.03	0.34	0.35	-0.35	0.52	0.68	0.87	0.77	0.96±0.22	b
^{48}Ti	p	2	66	2150-3100		3.4	1.20	0.51	0.38	-0.21	0.57	0.87	1.03	0.98	0.95±0.12	b
N.T.E.		6	135												0.69±0.21	c
^{24}Mg (S.M.)		3	120			1.3	0.81	0.33		-0.30	0.50	0.67	0.68	0.73	0.91±0.07	d
GOE (∞)			100			1.9	0.95		0.46	-0.27	0.53	0.75	0.82	0.87	0.9526	e
GOE (294)			100			1.9±0.3	0.88	0.48		-0.27	0.54	0.75	0.84	0.89	0.94±0.08	e,f
TBRE (294)						2.0±0.4	0.96	0.46		-0.26	0.52	0.73	0.80	0.85	0.95±0.06	
TBRE-J_z			126							-0.27	0.52	0.70	0.77		0.96±0.05	e
TBRE (294)															0.80±0.05	e,g
Poisson (294)			100			7.6±1.8	2.81	5.78	6.67	-0.03	1.00	1.92	2.48	2.97	-0.07±0.12	e,f

interpreted to mean that the statistical shell model is not applicable to these two nuclei. Another exception worthy of note is the high value of the repulsion parameter ω observed for ^{238}U : while low values can easily be understood as due to admixtures of independent level series, no physically significant ensemble is at present known that predicts a value larger than 1. A third one is furnished by the nuclear-table data, where the low value of the repulsion agrees better with the ground-state region of the TBRE than with the GOE ; the error limits are, however, rather wide.

Notes for Table I

The number n is the number of levels in the spectrum used to derive the quantities given. E_{min}, E_{max} and D are indicated in eV. The meaning of the listed variables is explained in the text. N.T.E. refers to the nuclear-table ensemble, also discussed in the text.

a) The levels identified as 1^+ by the authors[36]) were used.

b) The positive-parity levels were used.

c) Since the nuclear-table ensemble is not constituted by a single level sequence, only the value of ω is relevant.

d) Results of a large shell-model calculation. The value of ω was derived from the nearest-neighbour spacings between level 401 and level 600 in the total of 1206 levels ; the other quantities were calculated for the central 120 levels.

e) Theoretical ensembles ; the number in parentheses in the first column indicates the dimensionality of the matrices used in the computations.

f) The value of ω was obtained in an independent computation with matrices of size 120×120.

g) The value of ω corresponds to the ground-state region.

VI. CONCLUSIONS

The statistical shell model yields, as we have seen, numerical predictions that agree rather well with experimental results, but certainly no better than do those of the GOE ; the difference between the two is rather that such ensembles as the TBRE or the EE are based on much more realistic and physically justifiable suppositions.

However, while the theory thus clearly accounts for the essential features of such fluctuations as the level-spacing distributions, there are still a considerable number of gaps in our theoretical understanding, some of which we have pointed out. Further work will no doubt reveal aspects in the body of the theory where the predictions derived depend sensitively on the type of ensemble, so that we can discriminate between them.

Perhaps the most astonishing feature is that a relatively general theory should be able to explain such a wide range of phenomena, taken from both the ground-state region and high excitations of a large number of different nuclei.

REFERENCES

1. H.I.Liou, H.S.Camarda, S. Wynchank, M. Slogowitz, C. Hacken, F. Rahn and J. Rainwater, Phys. Rev. C5 (1972) 974.
2. E.G.Bilpuch, N.H.Prochnow, R.Y.Cusson, H.W.Newson and G.E. Mitchell, Phys. Lett. **35B** (1971) 303.
3. A. Zuker, private communication.
4. E.P.Wigner, Gatlinburg Conference on Neutron Physics, ORNL-2309 (1957) 59 ; reprinted in ref. 10.
5. J. Flores and P.A.Mello, Rev. Mex. Fís. **22** (1973) 185.
6. E. Cota, J. Flores, P.A.Mello and E. Yépez, Phys. Lett. **53B** (1974) 32.
7. T.A.Brody, E. Cota, J. Flores and P.A.Mello, Nucl. Phys. **A259** (1976) 87.
8. A.I.Khinchin, *Mathematical Foundations of Statistical Mechanics*, Dover Publ. Inc., New York 1949.
9. J.B.French and S.S.M.Wong, Phys. Lett. **33B** (1970) 449 ; O. Bohigas and J. Flores, Phys. Lett. **34B** (1971) 261.
10. C.E.Porter (ed.), *Statistical Theories of Spectra*, Academic Press, New York 1965.
11. M.L.Mehta, *Random Matrices*, Academic Press, New York 1967.
12. E. Yépez, Ph.D. thesis, Universidad Nacional Autónoma de México (1975).
13. J.B.French, Rev. Mex. Fís. **22** (1973) 221.
14. K.K.Mon and J.B.French, Ann. Phys. (N.Y.) **95** (1975) 90.
15. J.E.Lynn, *The Theory of Neutron-Resonance Reactions*, Clarendon Press, Oxford 1968.
16. J.B.French, Rev. Mex. Fís. **23** (1974) 189.
17. F.J.Dyson and M.L.Mehta, J. Math. Phys. **4** (1963) 701 ; reprinted in ref. 10.
18. O. Bohigas and J. Flores, Phys. Lett. **35B** (1971) 5.
19. W.H.Olson and V.R.Uppuluri, Proceedings of the Sixth Berkeley Symposium on Probability and Statistics (June 1970), ORNL-4603.
20. M.L.Mehta, Nucl. Phys. **18** (1960) 395 ; M. Gaudin, Nucl. Phys. **25** (1961) 447 ; both articles are reprinted in ref. 10 ; see

also ref. 11, chapter 5.

21. J.B.French and P.A.Mello, to be published.
22. A.M.Yaglom, *An Introduction to the Theory of Stationary Random Functions*, tr. Richard A. Silverman, Prentice-Hall, Englewood Cliffs, N.J. 1962.
23. T.A.Brody, Lett. Nuovo Cim. **7** (1973) 482.
24. M.L.Mehta and J. des Cloizeaux, Ind. J. Math. **3** (1971) 329.
25. O. Bohigas and J. Flores, in *Statistical Properties of Nuclei*, ed. J. Garg, Plenum Press, New York 1972, p. 195.
26. S.S.M.Wong and J.B.French, Nucl. Phys. **A198** (1972) 188.
27. I.I.Gurevich and M.I.Pevsner, Nucl. Phys. **2** (1956-57) 575 ; N. Rosenzweig and C.E.Porter, Phys. Rev. **120** (1960) 1698 ; both papers are reprinted in ref. 10.
28. F. Rahn, H.S.Camarda, G. Hacken, W.W.Havens, Jr., H.I.Liou, J. Rainwater, M. Slogowitz and S. Wynchank, Phys. Rev. **C6** (1972) 251.
29. F. Rahn, H.S.Camarda, G. Hacken, W.W.Havens, Jr., H.I.Liou, J. Rainwater, M. Slogowitz and S. Wynchank, Phys. Rev. **C6** (1972) 1854.
30. H.I.Liou, H.S.Camarda, G. Hacken, F. Rahn, J. Rainwater, M. Slogowitz and S. Wynchank, Phys. Rev. **C7** (1973) 823.
31. H.S.Camarda, H.I.Liou, G. Hacken, F. Rahn, W. Makofske, M. Slogowitz, S. Wynchank and J. Rainwater, Phys. Rev. **C8** (1973) 1813.
32. H.I.Liou, G. Hacken, F. Rahn, J. Rainwater, M. Slogowitz and W. Makofske, Phys. Rev. **C10** (1974) 709.
33. F. Rahn, H.S.Camarda, G. Hacken, W.W.Havens, Jr., H.I.Liou and J. Rainwater, Phys. Rev. **C10** (1974) 1904.
34. H.I.Liou, G. Hacken, J. Rainwater and U.N.Singh, Phys. Rev. **C11** (1975) 462.
35. G.I.Kirouac and H.M.Eiland, Phys. Rev. **C11** (1975) 895.
36. A.P.Jain and J. Blons, Nucl. Phys. **A242** (1975) 45.
37. W.M.Wilson, E.G.Bilpuch and G.E.Mitchell, Nucl. Phys. **A245** (1975) 285.
38. F.J.Dyson, unpublished work described in H.I.Liou, H.S.Camarda and F. Rahn, Phys. Rev. **C5** (1972) 1002.

MH 1 - THEORETICAL NEUTRON PHYSICS III: SPECTRUM FLUCTUATIONS AND THE STATISTICAL SHELL MODEL - P. A. Mello (U. Nacional Autonoma de Mexico)

Newstead (Brookhaven):

If I understand you, it's not possible to distinguish between the two-body random ensemble and the Gaussian orthogonal ensemble, is that correct?

Mello:

Yes, I would say so. As far as fluctuations are concerned, the results are the same for the Gaussian orthogonal ensemble as for the two-body random ensemble. You may find some differences if you do not eliminate, in the two-body random ensemble, fluctuations in scale, from matrix to matrix of the ensemble. If you take them out, then the results of the two-body random ensemble coincide, as far as numerical calculations are concerned, with those predicted by the Gaussian orthogonal ensemble. But of course, the density is quite different, as you saw.

Coceva (CNEN, Italy):

I should like to make a comment on the possibility of making experimental purity tests. We have made some calculations on the influence of missed or spurious levels on the Δ_3 statistic, which is a statistic sensitive to long-range correlations. We have found that even in some cases in which the purity is almost complete, the distribution of Δ_3 becomes so large that when you find a Δ_3 value in agreement with the theoretical one, or when you find a Δ_3 value much larger than the theoretical one, you may not be sure whether it is a pure series or a departure from statistical theory. This is because the distribution quickly becomes very large, compared with the ideally pure case.

Mello:

It is not possible, of course, to make a neat separation between purity test parameters and those parameters which are used to test the validity of the theory, because they all originate from the same theory. However, so far as these departures from theory are concerned, we can perhaps learn more when we find discrepancies with the theoretical predictions. The plutonium data may indicate some underlying dynamical situation which is not clear to us at the moment. This probably also applies to the case of uranium, where the value of W is too high. One more comment concerning Dr. Newstead's question. As I showed before, there is one difference, which I would like to call a second-order difference, between the two ensembles, namely in the ground state region. In the ground state region, both the Gaussian orthogonal ensemble and the two-body random ensemble show a repulsion of energy levels, of course. But the two-body random ensemble has a slightly smaller repulsion. This effect seems to be present in the 135-spacings histogram obtained from the nuclear table. So if that is to be believed, then there is slightly better agreement with the two-body random ensemble than with the GOE as far as that region is concerned. However, we have to remember that the number of spacings in this case is only 135, and it is not possible to make a definite statement.

Khanna (Chalk River):

One really knows not only the distribution and spectrum of the nuclear levels

but also something about the gamma-ray strength of those levels. The question I would like to ask you is, can one carry out an analysis and make any statement about how the strength of gamma rays might be distributed in this spectrum?

Mello:

You mean in one given spectrum, or in the nuclear table?

Khanna:

Either one.

Mello:

I do not know about the extension of the theory to describe the distribution of gamma strength. However, I would like to comment on fluctuations in gamma widths: there are quite old comparisons made in the time of Porter and Thomas which are comparable with the theoretical results based on the Porter-Thomas distribution. Now, as far as the nuclear table is concerned, that's a very interesting problem which we would like to tackle. It might be very interesting to see whether the Porter-Thomas distribution is realized when you consider, for instance, transitions between the first excited and the ground state throughout the nuclear table ensemble. But that's still an open problem which we have still not done. It's nevertheless a very interesting one.

Wigner (Princeton Univ.):

I have two questions. You mentioned, or you demonstrated, a very clear behavior of the ^{240}Pu compound nucleus. How common is such an unusual or irregular behavior? Is ^{240}Pu alone in this, or is every second nucleus that way?

Mello:

Well, I can answer that by showing you the more complete table. You can see that for Pu you have $\sigma_F = 4.9$ as compared to the theoretical result of 1.9, and the others are quite regular. There are only a few cases which are slightly low. Now, concerning the σ_0, σ_3, σ_6 and σ_{10}, the Pu data are systematically higher, and the others, except for small fluctuations, coincide rather well with the GOE results. So I would say there are only a few spots in which experiment does not agree with theory.

Wigner:

About one-fifth of the nuclei misbehave?

Mello:

Probably, yes.

Wigner:

I have one other question, if you don't mind. Has anybody investigated whether there is a connection between neutron widths and spacing of the next level? That is something I have asked before?

Mello:

Do you mean whether there is any correlation?

Wigner:

Yes.

Mello:

Well, there is a calculation which was done by Gary Mitchell at Duke University for the fine structure in an isobaric analogue resonance in V, in which he calculated the correlation coefficient between the proton width of each level and the spacing between that level and the next one. The result was very small, of the order of one percent.

11.35 a.m., Thursday, July 8, 1976 in Olney 150 Invited Paper: Session MH2

NEUTRON REACTIONS

A. M. Lane

UKAEA, Harwell, Didcot, Oxon. OX11 ORA

RÉSUMÉ

A survey of neutron reactions is presented, including established phenomena and recent developments. Special mention is made of developments in the theory of radiative capture as a process involving the interplay of various mechanisms (direct, semi-direct, and compound) and manifesting the close relation between nuclear reactions and nuclear structure.

ABSTRACT

Most of the main phenomena of neutron reactions were identified and labelled before 1962: low-energy resonances and the compound nucleus, Barschall giant resonances, doorway states, optical potential, direct reactions (pick-up, inelastic scattering), direct radiative capture. Apart from the phenomenon of pre-equilibrium processes, most recent developments have been improvements and extensions to older theories; for instance, the optical model has been refined by the inclusion of T.t and I.i terms, and applied to ultra-high energies (> 1 GeV) and to negative energies (hole states).

On the purely theoretical side, developments have been: increasingly accurate evaluation of the optical potential starting from two-body forces; explicit calculation of individual resonances in simple nuclei at low excitations where resonances can be identified; the analysis of the observed parallel behaviour of the excitation curve of X(n,n)X and the spectrum of X(d,p) for the same excitation region of the system (X + n); Calculation of neutron strength functions for deformed nuclei by microscopic methods; establishment of a satisfactory joint theory of direct and compound nucleus reactions.

Developments in the theory of radiative capture merit special mention, since this subject displays beautifully the interplay of various mechanisms (direct, semi-direct, and compound), and also the close relation between nuclear reactions and nuclear structure.

A. LANDMARKS IN THE HISTORY OF NEUTRON REACTIONS

Taking a panoramic view of the subject, there are five landmarks: resonances and the compound nucleus, optical model, direct reactions with DWBA, doorways and pre-equilibrium processes. Almost all developments in the subject come under these headings. First I will briefly review these landmarks, then I will discuss items of interest that have appeared in the last few years, say since 1970, then I will mention neutron capture as a specific example.

1. Resonances and the compound nucleus

Neutron resonances were first seen in the 1930's, and a huge number have been documented since. These showed, as Bohr told us, that a part at least of neutron reactions proceed through a long-lived intermediate state - the "compound nucleus". This fitted in with the idea of very strong neutron-target interaction, implying that any neutron crossing the target surface is absorbed - if not always to a reaction channel (which may be impossible on energetic grounds), at least in the sense that coherence with the incident particles is lost for a short-lived wave packet. This means that the energy-averaged S-matrix for elastic scattering, $\langle S_{nn} \rangle$, is given by the boundary condition of ingoing waves at the nucleon surface. From this quantity, one obtains the energy-averaged total cross-section, essentially $(1-\mathrm{Re}.\langle S_{nn} \rangle)$. The ingoing wave boundary condition implies a monotonically decreasing cross-section.

2. Optical Model

This last feature was denied by the data (Barschall resonances) in 1952. This leads to a more flexible approach, the optical model, in which $\langle S_{nn} \rangle$ is the S-matrix for a complex potential $V_{opt} \equiv (V+iW)$. If W is strong enough and V is smooth at the nuclear edge, then the earlier Bohr picture is reproduced, corresponding to the mean free path of the entering nucleon being very small. For smaller W, the mean free path is larger, comparable with the nuclear radius. This means that any single-particle resonant effects in V alone will not be entirely washed out. Thus we expect that cross-sections are no longer smooth, but can have the observed modulated behaviour.

Note that the optical model potential V_{opt} is formally defined as the potential whose S-matrix equals $\langle S_{nn} \rangle$. In the absence of exchange, it was shown by Feshbach[1] and by Brown and co-authors[2] that one can derive from this definition the form:

$$V_{opt} = \langle o | (\Sigma v) - (\Sigma v) \frac{1}{QHQ - E^{+}} (\Sigma v) | o \rangle$$

where Σv is the nucleon-target interaction, $|O\rangle$ is the target, $Q \equiv 1 - |O\rangle\langle O|$ and H is the total Hamiltonian. The matter of the comparison between observed and calculated forms of V_{opt} is discussed by Dr. C. Mahaux[3].

3. Direct Reactions and DWBA

An important generalisation[4] of this result is as follows: Suppose that the target has a number of excited states $|A\rangle$ that are directly coupled to the ground state in inelastic processes, then the averaged S-matrix $\langle \underline{S} \rangle$ is given by the coupled-channels solution to the optical-potential matrix $\underline{V}_{opt}$ with elements given by the last formula with $\langle O | --- | O \rangle$ replaced by $\langle A | --- | B \rangle$, and Q replaced by $(1 - \Sigma_A |A\rangle\langle A|)$.

This is valid whether the channels are open or closed. In the case of one excited state that is weakly coupled to the ground state, one finds, with $|a\rangle \equiv |Ou_\ell\rangle$, $|b\rangle \equiv |Au_{\ell'}\rangle$

$$\langle S_{ab} \rangle = \langle Au_{\ell'} | \Sigma v | Ou_\ell \rangle$$

where u_ℓ, $u_{\ell'}$ are the single-particle solutions to the two diagonal elements in V_{opt}. This result is DWBA. When the coupling is stronger, $\langle S_{ab} \rangle$ is obtained from solution of the coupled-channel problem, which is the CCBA.

We see that the spirit of the optical potential, demanded by the Barschall resonances, implies that $\langle S_{ab} \rangle \neq 0$, i.e. that direct reactions occur. This fits in with the simple physical picture, viz. when the incident nucleon has an appreciable m.f.p in the target, it can excite it and then escape directly (assuming that it has enough energy) i.e. it can give rise to a direct reaction.

4. Doorways[5]

So far, no nuclear structure properties have been assumed. If we now appeal to the shell-structure of the target (an approach which is consistent with the appreciable m.f.p against collision that has just been mentioned), then we may naturally identify those target states that are directly excited as 1p-1h states. These play an important role even if the available energy allows no reactions. Along with the incident nucleon, they give rise to 2p-1h states. In the formula for V_{opt} these and only these are directly excited by (Σv). They are contained in the intermediate states corresponding to QHQ. If other states are ignored or serve only to spread then, writing these states as d, they contribute to V_{opt}:

$$\sum_d \frac{\langle O | \Sigma v | d \rangle^2}{Ed - E - \frac{i\Gamma_d \downarrow}{2}}$$

The effect of this on a single particle state in $\langle S_{nn} \rangle$ is to split it up into substates d. The absorption into the compound nucleus occurs necessarily via states d, hence the term "doorway". When a 2p-1h state is excited, it can decay in three ways: return to the 1p state, decay to 3p-2h state, or (if energy is available) by particle escape. (Obviously the picture can be continued to higher levels in the hierarchy of particle-hole excitation). If the decay to 3p-2h states (represented as $\Gamma_d \downarrow$) is slow enough that states d do not overlap, then we may expect to see "intermediate structure" in single particle states corresponding to the presence of doorways. There are still very few cases where such structure is observed. (For a 1973 summary, see the review by C. Mahaux[6]). Here are three recent cases:

(i) Structures are observed[7] in $^{89}Y(p,\gamma)$ superposed on the upper side of the GDR. There are seven bumps with a spacing of $\sim$ 1MeV, and widths $\sim$ few 100 keV. These are identified as $T_>$= 6 states in photo-absorption on ^{90}Zr. They extend up to $E^*(^{90}Zr)$ = 23.7 MeV, where the excitation in the T=6 states is $\sim$ 11MeV, so they almost certainly represent systematic intermediate structure.

(ii) Twenty five $p_{3/2}$ resonances[8] in $^{88}Sr(n,n)$ up to 500keV are such that two levels at 287, 321keV have as much reduced width as all the others together.

(iii) In $^{98}Mo(n,n)$, there are about sixty p-levels[9] below 23 keV; the 30 levels below 12 keV have over three times as much width as those above. Although impressive, this evidence should be treated with caution in view of similar cases in the past which have evaporated eg in $^{53}Cr(n,n)$, there are 4 strong levels below

9 keV, then almost nothing[10,11] to 60keV (for ℓ=0). More recent data shows that the levels below 9keV are two J=1, two J=2 and strong levels occur between 60 and 100keV.

In a complete description of doorways, one not only observes them, but also identifies them eg as particular 2p-1h states. This has been done in some cases, such as in the paper[9] on the above case (2). Sometimes it is necessary to resort to statistical testing[12] to see if evidence for doorways is statistically significant or not.

5. Pre-Equilibrium Processes

Once one accepts the idea of a heierarchy of doorway states, 2p-1h, 3p-2h, etc. then one must be prepared to observe corresponding types of reaction product. At each doorway level, there is the possibility of escape of a particle if enough energy is available. Thus, for high incident energies, the spectrum of inelastic particles contains contributions from one-step (i.e. direct), two-step, three-step, etc. processes besides the compound nucleus (CN) part. Typically, with 60 MeV incident energy, the direct process is calculated to give inelastic processes with energy losses 0 - 40 MeV, while the CN part gives energy losses in the range 55-60 MeV. The observed angle-integrated spectrum is flat from 0-50 MeV, beyond which it rises. The absence of a gap at 40-55 MeV is attributed to particles from two step processes involving 3p-2h intermediate states. At higher energies, three, four, etc - step processes contribute. It has become clear through the work of M. Blann[13] and others thaz the observed spectra definitely require these contributions. In that case, they offer indirect evidence for the existence of the closely-related doorway states. For a summary of pre-equilibrium also, for recent applications to (p,n) spectra, see Blann et al[14]. In these studies, the angle-integrated spectrum is an incoherent sum over J values and levels in the doorway hierarchy, each level being characterised by the relative probabilities of decaying to levels above, below and by natural decay. The formula is set up on the basis of physical intuition. For an attempt to construct a formula from S-matrix theory by making statistical dynamical assumptions, and to enable angular distributions to be covered, see Agassi et al[15].

B. OPTICAL POTENTIAL: NEW FEATURES

1. Spin-Spin Interaction

Although the gross features of the optical potential have been clear for many years, there continue to be developments on detailed features. One of these is the possible spin-spin term that can occur when the target has a spin. By scattering polarised neutrons on polarised targets, one can isolate any spin-spin effect. Also, by taking spins parallel to and perpendicular to the beam, one can distinguish possible interaction forms like $\sigma.I$ and $(\sigma.r)(I.r)$. Recent data[16,17] on ^{59}Co (n,n) at 0.4 - 3 MeV indicate the former. The energy-dependence of the effects is unexplained.

2. Deformation in the Optical Potential

Recently evidence on this has been obtained from the energy-dependence of the total (n,n) cross-section from 0.75 to 14 MeV on $^{148,152,154}Sm$ isotopes. The coupled-channel fit[18] in terms of an energy-dependent optical potential gives deformation values β_2 = 0.14, 0.22, 0.24 for the three isotopes. These values agree quite closely with data from angular distributions of (p,p), (e,e) and (α,α') scattering and Coulomb excitation.

3. Microscopic Calculation of Strength Functions

Once an optical potential is given, corresponding strength-functions can be derived. However it is not necessary to use the optical potential; rather one can evaluate the strength-function more directly by diagonalising H in a basis of states containing 1p, 2p-1h, 3p-2h etc. excitations. Nowadays, very ambitious shell-model diagonalisations are available and, in principle, these could be used for providing a microscopic theory of strength-functions. In the mass-regions 35 and 45, the Michigan State University results[19] of Wildenthal et al. can be used to provide strength-distributions. A qualitative feature is that, despite the wide dispersion of the shell-model states by interaction, the strength for a shell model orbit that is filling (like the $1.f_{7/2}$ for $A \simeq 45$) is very little dispersed, but remains concentrated[20] in a few low-lying states.

Another approach is that pioneered by Soloviev[21] and co-workers. They set up bases of states that are so extensive (up to 10^4) that they produce densities of eigen-states comparable with those observed. They discuss s,p and d states in deformed nuclei ^{163}Dy, ^{169}Er, ^{239}U. States are described in terms of excitation of quasi-particles ($\alpha^+_{\rho\sigma}$) and zero, one or two phonons ($Q_{\lambda\mu}^+{}_j$) in the even-even core nucleus. $\rho\sigma$ labels Nilsson levels, ($\lambda\mu$) labels multipolarity and j labels various phonons of the same multipole order. The eigenstates are intrinsic states, i.e. they have K as a quantum number. Evaluation is made of the spreading of Nilsson orbits in ^{163}Dy, ^{169}Er and ^{239}U, and, from these, the strength-functions of s,p,d waves are obtained. Typically most of the strength is within a range of 3 MeV, with the rest mostly in an extensive high-energy tail. Further, within the 3MeV range, there may be two or three maxima. It is tempting to describe these as doorways, but it is not certain that they will persist if the basis of states is increased. A further application is to the zero energy strength function for s,p,d waves in a wide range of nuclei from ^{117}Sn to ^{255}Fm. Both data and theory show some fluctuation for adjoining nuclei of about the same type, but not always in exact parallel.

4. Strength-Functions for Hole States

In the most formally satisfactory definition of the optical potential, hole, as well as particle, strength is included. (This corresponds to a fully anti-symmetric theory). Recently some attention has been given to the spreading of hole states. The above work of Soloviev includes pairing effects, which blur the distinction between hole and particle states, and some of the calculated strength functions are for Nilsson orbits which are occupied, i.e. holes. Recently attention has been focussed on deep-lying hole states by the data on (e,e'p) reactions on ^{12}C, ^{40}Ca, etc. These reveal[22] the $1s_{1/2}$, $1p_{3/2}$, $1p_{1/2}$, etc. hole states, and can be used to check Koltun's theorem relating total B.E. and hole spectra of nuclei. Actually the observed spectra do not obey the theorem. The consensus seems to be that this is because of missing high-energy (i.e. deeply bound) strength. Although only a few per cent of strength, this has a much larger effect on the energy-weighted strength in the theorem[23,24].

C. DIRECT REACTION FEATURES

1. Parallel of (d,p) Spectrum and (n,n) Excitation Curve on Same Target

The first case to be studied was that [25] of the target ^{15}N. The (n,n) total cross-section data between En = 2.2 and 3.2 MeV show several resonances including s-waves ones which appear as a characteristic dip, instead of a peak.

The remarkable thing about the (d,p) excitation curves to the same regions of excitation is that, not only do they show structures at the expected energies corresponding to the (n,n) resonances, but that they have the roughly same character and relative size; in other words, the background - resonance interference is the same in the two cases. It has been pointed out that this is expected if the (d,p) process is described in plane-wave Born Approximation (PWBA), which gives:

$$S(\vec{k}_d,\vec{k}_p) = \langle {}^{15}N,\vec{k}_n|V_n|\psi({}^{16}N,\varepsilon)\rangle$$

where $\vec{k}_n$ represents a neutron plane-wave, exp $i\vec{k}_n\vec{r}$, with $\vec{k}_n \equiv \vec{k}_d - \vec{k}_p$, and $\psi({}^{16}N,\varepsilon)$ is the scattering solution of $^{15}N+n$ at neutron energy $\varepsilon=(E_d-E_p-2.2MeV)$. V_n is the $(n-{}^{15}N)$ interaction. This matrix element is just an off-shell version of the (n,n) matrix element, which carries the restriction $\hbar^2k_n^2 = 2M\varepsilon$. Thus, the observed rough parallel of (d,p) and (n,n) arises in PWBA if off-shell effects are small. Some attention has been given to the corrections arising from DWBA and off-shell effects, and generally this explains the small differences between (d,p) and (n,n). Other recent examples are ^{24}Mg (Ref 26), ^{23}Na (Ref 27) and a paper submitted to this conference on ^{12}C (Ref 28). The last paper allows for coupled channel effects (CCBA) in its analysis of the cross-section for the 6.86 (5/2+) state (width 6keV).

2. Joint Theory of Direct and Compound Nucleus Reactions

When the presence of both processes became clear, cross-sections were fitted in an ad hoc fashion by adding together two expressions, the Hauser-Feshbach (HF) expression for the compound nucleus part and the DWBA for the direct reaction part, thus:

$$\langle\sigma_{ab}\rangle = \langle|\delta_{ab}-S_{ab}|^2\rangle = \sigma_{ab}(\text{dir}) + \sigma_{ab}(\text{fluc})$$

$$\sigma_{ab}(\text{dir}) = |\delta_{ab}-\langle S_{ab}\rangle|^2 \rightarrow \text{DWBA}$$

$$\sigma_{ab}(\text{fluc}) = \langle|S_{ab}-\langle S_{ab}\rangle|^2\rangle \rightarrow \text{HF}$$

This procedure is not satisfactory. It was recognised at an early stage that the existence of direct reactions implies that quantities that are assumed random in M.F. theory are not random. Specifically, direct reactions imply correlations between reduced-width amplitudes:

$$[\gamma_{\lambda a}\gamma_{\lambda b}]_{\text{av. on }\lambda} \neq 0. \quad \text{(See Ref 29)}$$

This raises the important problem of setting up a satisfactory joint theory of both pricesses. An incidental problem is to see if, given $\langle S_{ab}\rangle$ or $\sigma_{ab}(\text{dir})$ one can find a prescription for $\sigma_{ab}(\text{fluc})$ in terms of $\langle S_{ab}\rangle$ alone. Clearly, since $\sigma(\text{dir})$ and $\sigma(\text{fluc})$ are mathematically distinct in general this cannot be done without assumptions. Hopefully one can make "reasonable" assumptions of a statistical nature that will relate $\sigma(\text{fluc})$ to $\langle S\rangle$. From what has already been said, this will <u>not</u> be randomness of amplitudes $\gamma_{\lambda a}$ if direct reactions occur. If they do not occur, then this assumption is acceptable and leads to the H.F. result that $\sigma_{ab} \propto T_aT_b$ where $T_a \propto (1-|\langle S_{aa}\rangle|^2)$

There have been three main attacks on this problem: Kawai, Kerman and

Mc Voy[30], Weidenmüller[31] and co-authors and Moldauer[32]. The essential difference between the last two and the first is that the latter maintain unitarity of the S-matrix (actually by working with the K-matrix, which is real). This is a definite merit if the number of channels is limited. For high energies however, where a huge number of channels are open, this merit is neutralised by the need to invert vast matrices to pass from $\underline{K}$ to $\underline{S}$.

Let us first discuss the case of few channels, where unitarity is vital and the Weidenmüller-Moldauer approach is better. There is no problem in the one-channel case, since $\sigma(\text{fluc})$ is given in terms by $\langle S\rangle$ by unitarity: $\sigma(\text{fluc})=1-|\langle S\rangle|^2$. (The same is true for many channels if $\sigma(\text{fluc})$ is summed over channels). The first non-trivial case is two open channels, as happens eg for a deformed even target with incident neutron energy between that of the 2+ and 4+ rotational states; alternatively for proton elastic and inelastic scattering near an analogue state.

The essence of the Weidenmüller approach[31] is exploitation of the fact that the unitary matrix, $\underline{U}$ say that diagonalises the transmission matrix $\underline{T}$:

$$\underline{T} \equiv \underline{1} - \langle \underline{S}^* \rangle \langle \underline{S} \rangle$$

$$\underline{U}^\dagger \underline{T}\, \underline{U} = \text{diagonal}$$

also has the property

$$\underline{U}^T \langle \underline{S} \rangle\, \underline{U} = \text{diagonal}$$

Further the phases of $\underline{U}$ can be chosen to make the r.h.s. real. Now we may define:

$$\underline{S} \equiv \underline{U}^T \underline{S}\, \underline{U}$$

$\underline{S}$ has the properties that $\langle \underline{S} \rangle$ is real, diagonal and $\underline{S}^\dagger \underline{S} = \underline{1}$. Thus it has the features of a Hauser-Feshbach S-matrix. The quantity $\sigma_{ab}(\text{fluc})$ can be expressed in terms of $\langle S^*_{\alpha\beta}\, S_{\gamma\delta} \rangle$. The usual H.F. theory prescribes $\langle |S_{\alpha\beta}|^2 \rangle$ and says that all other terms except $\langle S^*_{\alpha\alpha}\, S_{\gamma\gamma} \rangle$ are negligible. Not only does it not prescribe this last quantity, but its prescription for $\langle |S_{\alpha\beta}|^2 \rangle$ is imperfect since it suppresses the width-fluctuation correction factor (WFC). This arises even in the simple case of isolated resonances since

$$\left\langle \frac{\Gamma_{\lambda a}\Gamma_{\lambda b}}{\Gamma_{\lambda a}+\Gamma_{\lambda b}+\cdots} \right\rangle \neq \frac{\langle \Gamma_{\lambda a}\rangle\langle \Gamma_{\lambda b}\rangle}{\langle \Gamma_{\lambda a}\rangle+\langle \Gamma_{\lambda b}\rangle+\cdots}$$

Thus a supplementary study has been made of the H.F. situation (no direct reactions). One relates S to the corresponding K-matrix, then chooses the real amplitudes in this to be random in sign, and of magnitude to reproduce the prescribed $\langle \underline{S} \rangle$. Computer experiments on this basis then give forms for $\langle S^*_{\alpha\beta}\, S_{\gamma\delta} \rangle$. One finds that, for $\Gamma \gg D$ (where the WFC is $\approx$ unity), that $\langle |S_{\alpha\beta}|^2 \rangle$ is separable in the way suggested by HF theory $T_\alpha T_\beta (\Sigma T_\gamma)^{-1}$. However, as Moldauer has emphasised, when one interprets this result in terms of the parameters in the pole-expansion of the S-matrix, it seems miraculous. These parameters have very strong and unexpected properties eg level-level correlations, channel-channel correlations in widths (not amplitudes) and large fluctuation in total level widths. The H.F. factorisation when $\Gamma \gg D$ emerges as a result of subtle interplay of these effects.

Some important results when $\langle \underline{S} \rangle$ = diagonal are:

(i) the cross-section correlation width (as deduced from an Ericson analysis) is identified with the most probable width which, as a result of the skew distribution, is considerably less than the average width.

(ii) The correction to H.F. separability for σ(fluc) - the generalisation of the WFC factor - is significant when < twenty or so channels are open.

(iii) Sometimes fluctuation cross-sections are strongly enhanced by the WFC factor. This happens especially when one channel has a weak transmission and is in competition with some channels with strong ones. When direct reactions occur, one expects:

(a) correlations between amplitudes
(b) cross-correlations in the fluctuations of cross-sections
(c) enhancement of σ(fluc)

Although Moldauer's method did not exploit the above transformation property of $\langle S \rangle$ by U, it contains the same essentials as the Weidenmuller method, viz. one sets up a K-matrix whose (real) amplitudes are such that the prescribed $\langle S \rangle$ is reproduced, but are random apart from this condition. The two methods correspond to two methods of making the randomness assumptions.

When the results of the Weidenmüller and KKM theories are compared in the case $\Gamma \gg D$, one finds that the equations for the WFC factors are very similar, despite the absence of explicit unitarity in KKM. This encourages one to set up theories in terms of the S-matrix instead of the K-matrix, at least when there are many channels open and matrix inversion becomes impractical. This has recently been done by Agassi et al[15], and used as the basis of a microscopic theory of pre-equilibrium processes.

Applications of the Weidenmüller-Moldauer theory include

(i) Cross correlations[33] between ^{88}Sr(p,p) and ^{88}Sr(p,p') near the 3/2+ analogue at 7.5 MeV.

(ii) Inelastic neutron scattering: ^{89}Y, reported at this Conference[34].

(iii) Cross-correlations[35] between ^{92}Mo +p and ^{92}Mo(2+)+p' channels at the 3/2+ analogue State, as seen implicitly in average $\sigma_{pp'}(\theta)$, $P_{pp'}(\theta)$ and $\sigma_{p,p'\gamma}(\theta_p,\theta_\gamma)$ data. In all three cases the usual HF treatment of σ(fluc) fails to fit the data but the improved treatment gives good fits.

Note that the corrections to the HF formula that are verified in these examples arise from two sources. One is the WFC effect that, as we have seen, occurs even for isolated resonances. The other is the correlations (in sign as well as magnitude) between channels that is implied by the presence of a direct process (the analogue in cases (i) (iii)). In the case of the polarisation, the first effect does not change the HF prediction of zero polarisation, but the second effect does. Thus the two effects appear differently in different data.

D. RESONANCES: NEW FEATURES

1. Analogue States

A qualitatively new experimental feature is the observation of analogue states in neutron data. In ^{207}Pb +n (total cross-section) at E_n = 16.8 MeV, a small (4% of background) resonance is seen[36], corresponding to the expected position of the analogue of the 0.8 MeV state of ^{208}Tl. In ^{24}Mg(n,n), analogue states of the first three states of ^{25}Na are seen[37] at E_n = 475(5/2+), 555(3/2+) and 1567(1/2+) keV. The value of Γ_n^0 for the last (s-wave) level is 3.4eV, compared to 10,19, 26eV for three normal s-wave levels. For the d-wave levels, Γ_n^2 is 1.1, 3.6eV compared to normal values 53,59,158,160,627.

2. Correlations of Widths in Resonance Neutron Capture

In terms of the number of relevant papers, this is a vast field. To focus on essentials, let us first note that two kinds of correlation are found (i) resonance correlations between neutron and El capture widths (for a given final state f), $\Gamma_{\lambda n}$ and $\Gamma_{\lambda f}$, over resonances λ (ii) final state correlations between El capture widths (for a given resonance λ) and neutron spectroscopic factors, $\Gamma_{\lambda f}$ and S_f, over final states f. There is a tendency for a given target and neutron partial wave to show both or neither. The best correlations are with A=40-65 (s-wave) and A=88-100 (p-wave). The most striking resonance correlations are:

^{90}Zr, p-wave: $\rho(\Gamma_{\lambda n}, \Gamma_{\lambda f}) = 0.58$ for 37 resonances[38,39] of J = 3/2- for f = ^{91}Zr g.s.

^{88}Sr, p-wave: $\rho(\Gamma_{\lambda n}, \Gamma_{\lambda f}) = 0.96$ for 20 resonances[40] of J = 3/2-, 0.77 for 13 resonances of J = 1/2- for f = ^{89}Sr g.s.

^{42}Ca, s-wave: $\rho(\Gamma_{\lambda n}, \Gamma_{\lambda f}) = 0.35$ for 24 resonances[41] of J = 1/2+ for all f together.

The most striking final state correlations are for thermal capture in A=40-65, where about a dozen cases are known with $\rho > 0.90$. In several cases, it is believed that thermal capture is dominated by tails of nearby resonances, in other cases not. Thus the evidence suggests that both resonant and non-resonant (direct) capture show final state correlations. The best cases of capture on resonances showing final state correlations are:

^{92,94,96,98}Mo, p-wave: in all cases, there is a final 1/2+ state with large spectroscopic factor ($S_f > 0.5$) and two or more weak 1/2+ states. The average capture taken over resonances near E_n = 24 keV all show dominant capture[43] to the former state. For 3/2+ final states, there is no evidence for correlations. ^{93}Nb, p-wave: both the average capture over resonances near 24 keV[44] and individual resonance studies[45] indicate $\rho(\Gamma_{\lambda f} E_\gamma^{-3}, S_f) \sim 0.4$ for about 40 final states f. These includes all spins and parities allowed for El radiation (2+ -- 7+), so part of the correlation may simply reflect the $(2J_f+1)$ factors and the fact that states f with spins 4+,5+ allow $\ell_n=0$ transfer while others allow only $\ell_n=2$. In the second study[45], the correlation was evaluated for 20 states f below 1.5 MeV of positive parity, at least 6 of these being 4+.

The observed correlations are associated with a direct capture component[46]. This is identified as valence capture, involving primarily $\ell_n=0,1$ orbits, and is believed to be due, at least in part, to the fact that a large part of the El integral arises from outside the nucleus. This enables this valence transition to be decoupled from the GDR.

This area has been evolving for several years and it is impossible in this survey to go inzo details of the degree of understanding that has been reached. Instead I will indicate two areas where attention has been concentrated lately:

(i) asymmetry between resonance and final state correlations. According to the valence model, these should have about the same size, but there are experimental signs that, in some nuclei (eg ^{92}Mo, ^{93}Nb, Refs. 43,44), that the final state correlation may be larger. A tentative description of this can be obtained[47] by appealing to the presence of core transitions involving ℓ_n=0,1 orbits, e.g. for ^{92}Mo, the transitions 2p → 3s. These give an asymmetry in the observed sense, and are covered by the valence assumption of decoupling of ℓ_n=0,1 E1 strength from the GDR.

(ii) the occurrence of M1 final state correlations. There are experimental signs of this for s-wave capture in several nuclei in the range A=20-40 (Ref. 48) and A=90-106 (for 1/2+ final states) Ref. 49. Since direct capture does not exist for M1 transitions, one is forced to interpret the results in terms of semi-direct M1 transitions[50] in which the incident neutron excites the collective 1+ state of the target, which then decay by an M1 transition. This picture appears to fit the observed facts. Note that it predicts final state correlazions, but not resonance correlations. Another prediction is that the effect should be most pronounced where there is a bound ℓ_n=0 state whose binding energy is roughly equal to the 1+ collective energy (5-7 MeV). This corresponds precisely to the mass-regions, A=20-40, A=90-106 where effects are found.

REFERENCES

1) H. Feshbach, Ann.Phys. 5, 357 (1958), 19, 287 (1962)
2) G.E. Brown & C.T. de Dominicis Proc.Phys.Soc. A72, 70 (1958)
3) J.P. Jeukenne, A. Lejeune & C. Mahaux, paper MG 2 (this Conference)
4) M. Sano, S. Yoshida & T. Terasawa, Nucl.Phys. 6, 20 (1958)
5) H. Feshbach, A.K. Kerman & R.H. Lemmer, Ann.Phys. 41, 230 (1967)
6) C. Mahaux, Ann.Rev.Nucl.Sci. 23, 193 (1973)
7) Askin, Hicks, Allen, Petty & Thompson, Nucl.Phys. 204 209 (1973)
8) Malan, Pineo, Divadeenam, Choi, Bilpuch & Newson, Ann.Phys. 89, 284 (1975)
9) A. Musgrove, B. Allen, J. Boldeman & R. Macklin, preprint
10) Good, Paya, Wagner & Tamura, Phys.Rev. 151, 912 (1966)
11) K.N. Muller & G. Rohr, Nucl.Phys. 164 97 (1970)
12) J. Baudinet-Robinet & C. Mahaux, Phys.Rev. C9, 723 (1974)
13) M. Blann, Ann.Rev.Nucl.Sci. 25, 123 (1975)
14) M. Blann et al. Nucl.Phys. A257, 15(1975)
15) D. Agassi, M.A. Weidenmüller & G. Mantzanouris, Phys.Rep. 22C, No. 3(1975)
16) W. Heeringa & H. Postma, Phys.Lett 61B, 350 (1976)
17) T.R. Fisher et al. Nucl.Phys. A179, 241 (1972)
18) Shamu, Lagrange, Bernstein, Ramirez, Tamura & Wong, Phys.Lett 61B 29 (1976)
19) Wildenthal, Halbert, McGrory & Kuo, Phys.Rev. C4, 1266 (1971)
20) C.F. Clement & S.M. Perez, to be published
21) V.G. Soloviev "Neutron Capture Gamma Ray Spectroscopy", Petten Conference 1974 (RCN Petten 1975) p.99
22) M. Bernheim et al. Phys.Rev. Lett 32, 898 (1974)
23) W. Fritsch, R. Lipperheide & U. Wille, Nucl.Phys. A241, 79 (1975)
24) A.E.L. Dieperink & T. de Forest, Ann.Rev.Nucl.Sci. 25, 1 (1975)
25) Fuchs, Homeyer, Oeschler, Lipperheide & Mehring, Nucl.Phys. 196, 286 (1972)
26) Bommer et al., Phys.Lett. 52, 421
27) Blanpied et al., Phys.Rev. C12. 1726 (1975)
28) M. Tanifuji, O. Mikoshiba & T. Terasawa, this Conference, Paper A5.

29) J. Hüfner, C. Mahaux & H.A. Weidenmüller
30) M. Kawai, A.K. Kerman & K.W. McVoy, Ann. Phys. 75, 156 (1973)
31) Hofmann, J. Richert, J.W. Tepel & M.A. Weidenmüller, Ann. Phys. 90, 403 (1975)
32) P.A. Moldauer "Statistical Properties of Nuclei"
Albany Conference 1972 (Plenum, 1973) p.335, Phys.Rev. C11, 42B (1975),
C12, 744 (1975); preprint (1976)
33) Blanke, Genz, Rechter & Schreider, Phys.Lett 58B, 289 (1975),
Richert, Simbel & Weidenmüller, Z.Phys. A273, 195 (1975)
34) B.H. Duchemin, this conference, paper K20
35) S. Davis et al., Phys.Rev.Lett 34, 215 (1975)
36) Benetsky, Nefedov, Frank & Stranich, paper C8, Conference on Nuclear
Structure with Neutrons, Budapest 1972
37) H. Weigmann, R.L. Macklin & J.A. Harvey, preprint 1976
38) R.E. Tookey & H.E. Jackson, Phys.Rev. C9, 346 (1974)
39) Boldeman, Allen, Musgrove & Macklin, Nucl.Phys. A246, 1 (1975)
40) Boldeman, Allen, Musgrove & Macklin, preprint 1976
41) Musgrove, Allen, Boldeman, Chan & Macklin, preprint 1976
42) J. Kopecky & C. Plug, RCN-75-004, Petten, Holland 1974
43) K. Rimawi & R.E. Chrien, "Neutron Capture Gamma Ray Spectroscopy",
Conference, Petten, Holland 1974, p.364
44) As ref 43, p.368
45) T.J. Haste & B.W. Thomas, J.Phys.Soc. G1, 967 (1975)
46) A.M. Lane, "Neutron Capture Gamma Ray Spectroscopy" Conference, Petten,
Holland 1974, p.31
47) B.J. Allen, J. Boldeman, A.M. Lane, & A. Musgrove, 1976 unpublished
48) J. Kopecky, this conference, D9
49) Seyfarth, Kardon & Guven, this conference, D6
50) Clement, Lane & Kopecky, to be published

MH 2 - THEORETICAL NEUTRON PHYSICS IV: NUCLEAR REACTIONS - A. M. Lane (AERE, Harwell, UK)

Mughabghab (B.N.L.)

There are indications in the ^{92}Mo and ^{98}Mo data that there is a correlation between the reduced neutron widths and the partial radiative widths for M1 transitions.

Lane:

As I understand it, generally in that mass region the final state correlations tend to be stronger than the initial state correlations.

Mughabghab:

What I am referring to are the M1 transitions.

Lane:

Well, I hope I haven't got my lines crossed. I'm thinking of data that Bob Chrien reported at Petten, where he used 22 kilovolt neutrons averaged over resonances, and found rather strong final state correlations. And I think in niobium also there was evidence of final state correlations but only weak initial state correlations.

Mughabghab:

No, what I'm talking about is the M1 transitions.

Lane:

Oh, I'm sorry, I missed the M1.

Mughabghab:

There is such type of a correlation?

Lane:

Yes, in the mass 90 region. So you are really making a comment.

Mughabghab:

Yes, I'm making a comment. You said that this might bring some headaches to the theoreticians.

Moldauer (Argonne):

Tony, I don't understand what you mean by the distinction between initial state and final state correlations. I mean, there are neutron widths and there are partial radiation widths and whether they occur in the initial or the final state of a particular interaction, they are still either correlated or not, and how does that distinction come in? You sort of assumed we knew all about it, but I don't. Could you explain that a little more thoroughly?

Lane:

Are we talking now about the matter of definition? I mean, are you happy about

the definition of the two entities, initial correlations and final correlations? In initial correlations, or sometimes called resonance correlations, one fixes a final state and then you look for a correlation between partial radiation widths over the set of resonances to that final state, and neutron widths over that same set of resonances. That's initial state correlation. And in the final state correlation you fix a resonance, or possibly you'll fix thermal energy between resonances, and then take a set of final states, low lying states, and look for a correlation between radiation widths to those final states and spectroscopic factors as measured in (d,p) studies to those final states. That's a matter of definition.

Newstead (B.N.L.):

It's interesting that these newly discovered magnetic dipole correlations also occur in the region of strength function maxima; that is the mass 90 region for $\ell = 1$ and the mass 30 region for $\ell = 0$. That is quite analagous to the more usual electric dipole correlations. I wonder if you would comment on that? Also, I would like to ask whether you have any idea as to why the states would be so confined in energy in strontium?

Lane:

No! In strontium I think that's a rather amazing result, and in thallium as I also mentioned, there is a contribution at the conference showing again one huge state, which in the Porter-Thomas distribution would be so far out in the wings as to be, I think, impossible. So I don't have any ideas there. I think the work of Perez and Divadeenam has come closest to analyzing the situation theoretically, and they at least have put tentative identifications as doorways on some of these discontinuities. But they have not really checked into the question of what spreading width they expect for these objects.

Newson (Triangle Univ.'s Nuclear Lab):

You pointed out the similarity between a total s-wave neutron cross-section and the (d,p) reaction. Now, in my simple minded way I've thought of this interference effect as due to interference between the compound nucleus and the hard sphere scattering, and I don't quite imagine hard sphere scattering to have an analog in the (d,p) process. Could you help me out there?

Lane:

Well, that is exactly the reason why people were so astonished when the parallel was so close, and I tried to indicate in those simple equations one way in which we might understand it. But put into words, I think the simplest way of expressing those equations is that we can regard the (d,p) process as just bringing in a neutron, as in a neutron bombardment, but with the extra freedom that we're off energy shell. The k of the neutron and the energy are not related. Therefore anything that you see in neutron scattering you would expect to have a counterpart in the (d,p) spectrum. I don't think I can do better than that.

Block (I.P.I.):

Tony, I'd like to expand on the ^{16}N total cross section curve. It didn't look to me like a normal interference dip in front of a resonance. I'm not familiar with the work, but it looked similar to the resonance in ^{16}O at 2 MeV where

the phase shift is such that you just happen to get a negative point. So I'm wondering, is this really an interference dip to that resonance? It looks very peculiar; it goes down, comes up, and is then horizontal with a peak to the right. That's quite different from anything I've ever seen. Also, is the line an R-matrix fit, or what is it?

Lane:

I think we probably have two separate levels there. It's not the whole structure that's an interference, it's just that the dip itself is caused by interference between a Breit-Wigner amplitude and a background, and the other level is a regular type of level; that is, the Breit-Wigner amplitude has a different phase, and so it stands up instead of digging a hole there. I think there are two levels there. But sometimes, of course, you certainly can get the intermediate situation where you get half a dip and half a level, as it were, in a single structure. There don't appear to be any such examples here, but certainly it can happen. Here, I think, we are dealing with two separate levels, probably different spins and parities.

Cierjacks (Karlsruhe):

May I comment on Dr. Block's question. The results for neutron scattering are data which we measured in Karlsruhe. The solid curve is in fact an s-wave R-matrix multi-level fit to the experimental data. The dip between the two broad peaks belongs to an s-wave resonance and arises from interference from the s-wave resonance and potential scattering.

Khanna (Chalk River):

You referred to the correlations in zirconium-91. I am curious, because we know very well that the dipole strength gets shifted away to much higher energies and, if it does, is it going to make much difference to your argument that the correlations exist in zirconium-91?

Lane:

Yes, I'm glad you raised this point. It's already, of course, amazing that the valence strength survives in its natural energy location in the way that it does in some nuclei, as evidenced by all the correlation phenomena, because generally the giant dipole resonance steals all strength from all particle-hole transitions and moves it 7 MeV away into the giant dipole resonance. But we've got used to that as a fact of life. We still don't really understand it. There are almost no theoretical calculations that indicate the valence strength in s-p transitions should be exempt from the robbery. Even more true is what you say about the two particle-one hole state. So it is just an ad hoc hypothesis. I note only that it still involves s- and p- waves, so it could be included with the previous valence situation by saying that generally all s-p wave states are exempt from giant dipole robbery. But it is a very important point and I think also it applies in some degree to Dr. Soloviev's talk this morning, because one has to be careful about assigning any states as particle, or two particle-one hole. Their natural electric dipole strength, because of the massive robbery of strength by the giant dipole, has to be taken into account in a satisfactory theory.

Khanna:

Yes! But I think you would agree that this is a hypothesis that the s-p strength essentially remains wherever it is in the unperturbed state. There is no theory or calculation that indicates this should happen.

Lane:

Very little. As I say, one or two fragments. In lead, if you use zero-range forces, it happens the s-p strength is rather de-coupled, and calculations by Rowe of Toronto recently on nickel have indicated some de-coupling of s-p strength, but nothing terribly convincing. So it is a problem.

2:00 P.M., THURSDAY, JULY 8, 1976, IN OLNEY 150

MAIN SESSION MI

Chair: S.H. Chen (Massachusetts Institute of Technology, U.S.A.)

.00 p.m., Thursday, July 8, 1976

USE OF NEUTRON SCATTERING FOR THE ANALYSIS OF BIOLOGICAL STRUCTURES

Benno P. Schoenborn
Brookhaven National Laboratory, Upton, New York 11973

RÉSUMÉ

A review is presented of methods for the analysis of biological structures, such as membranes, viruses, protein complexes and structures, etc., by neutron scattering data, based upon the differential scattering for hydrogen versus deuterium. Deuteration of, e.g., proteins, has led to the elucidation of structure in large complexes, having molecular weights in the hundred thousands.

ABSTRACT

The first application of neutron scattering for biological macromolecular analysis is just over seven years old. In this short time, this field has rapidly expanded with applications to protein complexes, membranes, viruses and protein structures. Generally, the advantage of using neutrons instead of x-rays for such structural problems lies in the scattering difference between hydrogen and deuterium. In protein crystallography, this scattering difference permits the elucidation of exchangeable hydrogen atom locations apart from the location of hydrogen atoms themselves. H_2O/D_2O exchange experiments also allow detailed analysis of protein hydration. Phasing of such protein structures with several thousand atoms can be done by anomalous dispersion techniques, or approximate phases can be derived from the "x-ray structure" using non-hydrogen atoms only.

For analysis of membrane structures, the replacement of hydrogen with deuterium provides contrast variation similar to the heavy metal staining used in electron microscopy without, however, the limitations due to distortion and resolution. Since most of these structures have a considerable water content, a simple H_2O/D_2O exchange will often provide phases; this is similar to the heavy atom technique of protein crystallography.

Specific deuteration of proteins has led to a novel approach in quaternary structure analysis of large protein complexes like ribosomes, aspartate transcarbamylase, etc. These complexes are mostly uncrystallizable and have molecular weights of several hundred thousand. The general shape and distribution of constituents of these particles is obtained by specific deuteration of some of its components. With two components deuterated, the problem reduces to a diatomic gas type analysis, yielding data on protein separation and protein shape. Systematic deuteration of different proteins does yield a low resolution map depicting relative arrangements of components like nucleic acids and proteins in complexes like ribosomes, the protein factory of living cells.

INTRODUCTION

Neutron scattering experiments for the analysis of biological structures is a useful addition to the numerous physical techniques used to unravel the comple ities of living things since they allow the determination of structural features not revealed by x-ray methods (1,2,3). The theories of neutron (3) and x-ray (4) scattering are rather similar; the main difference arising from the fact that x-rays are scattered by the electron cloud while neutrons are scattered by the atomic nucleus. For x-rays, the scattering magnitude is proportional to the electron density and the scattering factor, which relates the magnitude of the scattered wave to the incident wave amplitude for a given atom, increases with atomic number. For neutrons the magnitude of the scattering factor depends on the physical size of the nucleus and on the permissible nuclear energy changes caused by the incident neutron while it is momentarily bound to the target nuclei. These energy changes cause resonance effects which vary the scattering factors seemingly haphazardly from atom to atom and from isotope to isot even within the same element (3,5). This resonance scattering effect is seen for the hydrogen isotopes with scattering factor values of $b_H = -.38 \cdot 10^{-12}$cm and $b_D = .65 \cdot 10^{-12}$ cm. The negative scattering amplitude of hydrogen and other elements like titanium and manganese is due to an additional resonance phase change of π that is not observed for most other elements. Generally, however, neutron scattering factors are all of the same order of magnitude and do not show the large variation observed for x-rays (Table 1).

This narrow range of neutron scattering factors prevents the use of the "heavy atom" phasing method, but fortunately there are a number of isotopes

that exhibit strong anomalous scattering behavior which can be used to determine phases (6). The magnitudes of the scattering factors of hydrogen and deuterium and the large difference between them are of particular importance since they are responsible for the large scattering contrasts between the individual components of complex biological molecules that make neutron scattering experiments so powerful. Due to the negative scattering factor, hydrogen will appear as negative densities on a Fourier map with a magnitude sufficient for identification. Apart from this useful aspect, hydrogen atoms unfortunately also exhibit large incoherent scattering that is due to the unpaired spin of the hydrogen nucleus. This incoherent radiation does not contain any structural information but adds considerably to the background. To reduce this background, it is often desirable to reduce the number of hydrogen atoms present by replacing them with deuterium. Apart from the differences in scattering factors, neutrons exhibit a number of other physical properties important to the molecular biologist. The electrically neutral neutron does not produce free radicals as x-rays do and therefore does not cause significant radiation damage, thus enabling the collection of all diffraction data from one sample. Unfortunately though, neutron beams have relatively low flux and even the most intense neutron beams are about 10^5 less intense than common x-ray sources. This handicap can, however, be partly overcome by the use of larger specimens and longer exposures. Larger samples cause few problems since absorption factors for neutrons are considerably smaller than those found for x-rays (Table 1).

PROTEIN CRYSTALLOGRAPHY

The main advantage of using neutrons instead of x-rays in the analysis of proteins is the ability to determine hydrogen atom position. Hydrogen accounts for about 1/3 of all atoms of a protein. They are intimately involved in enzymatic reactions and play a large role in maintaining the 3D structure of the protein (8). Exchangeable hydrogen positions can be determined by crystallizing the protein in D_2O. Exchangeable hydrogens will thus be replaced with deuterium and then indicated by positive instead of negative features on the Fourier map. Particular molecular groups can be titrated by changing the pH, thus establishing local charge and reactivity parameters. The orientation of groups such as histidine can be established since the scattering factor of nitrogen ($9.4 \cdot 10^{-13}$ cm) is significantly larger than that for either O or C; amide groups are therefore also distinguishable from carboxyl groups.

Neutron diffraction analysis is particularly useful in the determination of the location of water of hydration. For proteins crystallized in D_2O, scattering by the water molecule is directly comparable with the scattering from the protein itself, providing more clearly defined Fourier peaks than observable in x-ray maps. Experiments in H_2O and in D_2O further enhance contrast in the map, enabling detailed study of the water of hydration as well as of exchangeable hydrogen positions. A difference map calculated from data with a protein in H_2O and then in D_2O results in localizing hydrogen (deuterium) atoms only. This approach is particularly suitable in distinguishing water from other small molecules since changes in Fourier density features can be assessed in terms of atomic compositions.

Since no crystal damage is expected as observed in myoglobin studies, neutron crystallography dispenses with cumbersome crystal to crystal data scaling and should yield information on individual crystal differences as well as the type and location of radiation damage caused by x-rays. Phasing of neutron protein data is best done by using the x-ray structure (9). Phases are calculated from the x-ray derived structure without postulating H atom positions, e.g. phases are calculated from C, N and O atoms only since this reduces any bias in possible H atom location. The resultant Fourier map will depict H and D atom locations at approximately 1/2 weight. It can be easily demonstrated by model calculations that neutron phases calculated from a protein with and without H atoms exhibit an average deviation of only $\sim 32^{\circ}$ (9). If no x-ray data are available, phases can be determined by using anomalous scattering from isotopes such as samarium, gadolinium or cadmium. Even heavy atom type phasing is possible if molecules rich in hydrogen/deuterium are used (neopentane, etc.). Refinement techniques using real space or least squares techniques interspersed with new phase calculations based on all located atoms do improve the map and enable the location of all atoms. Present experience is, however, rather limited but the author is confident that significant improvements in the understanding of protein structures and function will result from such neutron studies.

SCATTERING FROM ORIENTED SYSTEMS

Problems in this category deal with the structural motive of larger assemblies such as membranes, muscle, collagen, etc. In these cases, where the location of subfragments within a matrix is wanted, it is helpful to consider the average scattering densities of the major components (Table 2). The data in

Table 2 lists such group scattering factors. These scattering densities vary by nearly three orders of magnitude compared to a factor of two for the equivalent x-ray scattering densities. This illustrates why neutrons are ideally suited for such structural investigations. It also should be noted that deuteration of any component drastically alters the scattering density while relative contrast variations can be achieved by altering the aqueous environment of these systems by mixing H_2O with D_2O.

Significant advances in the elucidation of membrane structures have been made by x-ray diffraction (3,11). However, the phasing of the x-ray diffraction data has often been based on controversial methods (13-15).

The large difference between the neutron scattering of hydrogen and deuterium can be used like the heavy atom of protein crystallography and provides a convenient solution to the phase problem. Since all biological membranes contain water, a simple isomorphous replacement of H_2O with D_2O is sufficient to determine at least a low resolution structure. The exact positions of the water molecules within the membrane will determine the resolution achievable by this simple method (12). The necessary diffraction data is collected for the membrane soaked in H_2O and in D_2O Ringer's solution. The intensities are corrected for absorption and extinction with account taken of the quite different absorption corrections for H_2O and for D_2O due to the large incoherent scattering of hydrogen. The Lorentz function corrected structure factors are then used in a difference Patterson function with $(\Delta F)^2 = (|F|_{H_2O} - |F|_{D_2O})^2$ as coefficients. The difference Patterson function thus contains the information regarding distribution of water.

The above definition of $(F)^2$ uses the absolute values of the observed structure factors ignoring possible changes in phase of any diffraction orders. A gradual H_2O/D_2O exchange permits, however, direct observation of phase changes of particular reflections. Such a phase change observed for h=2 in a dipalmitoyl lecithin (DPL) cholesterol sample is shown in Fig. 1.

The presence of exchangeable hydrogen on lipid head groups and in proteins poses a problem by introducing multiple minor sites which add to the difficulty of interpreting the Patterson function, particularly for high resolution structures. To determine phases for a high resolution structural analysis it is therefore best to use a specially deuterated constituent especially if data are obtained for both the H and D versions. Determination of phases by the heavy atom technique is straightforward and follows the methods developed for protein crystallography (16). In the isomorphous replacement method the calculated structure factor (f_c) is obtained for the "heavy group" from the positions given by the Patterson map interpretation. The "heavy group" scattering factor in this case is the difference between the H and D versions ($b_D - b_H$). Since the scaling of f_c relative to the observed structure factor is often difficult, changes in magnitude and sign for F_D and F_H are best detected by following the gradual change in the scattering magnitude of the heavy group, which is easily brought about by mixing the H and D versions of the heavy group (it is particularly easy in the case of H_2O/D_2O exchange).

Specific deuteration and relative contrast variations by H_2O/D_2O exchange are not only useful for phase determination but can easily be used to locate particular constituents in known structures. This approach should prove valuable in binding site studies of inhibitors, activators and drugs.

SOLUTION SCATTERING

X-ray scattering (17-19) from proteins in solution has long been used to determine general shape parameters but has otherwise been of little help. The large difference in scattering densities for groups in which hydrogen is replaced by deuterium and the ease of adjusting scattering contrast by H_2O/D_2O mixing has opened up unique applications in the analysis of protein shapes (20-23) and quaternary structures of complexes (24-26). The low angle scattering profile F(s) of macromolecules in solution is determined by the difference in scattering density $\Delta\rho$ between the solvent and the solute and the Fourier transform of its shape functions (f(r)) with $F(\vec{s}) = \Delta\rho\int\rho(\vec{r})\exp(2\pi i\ \vec{r}\cdot\vec{s})dV$. As a first approximation Guinier (17) has shown that at very small angles the scattering intensity is a linear function of the scattering angle squared, yielding directly the radius of gyration; measuring the distribution of scattering density.

In particles such as viruses, ribosomes, vesicles, etc., which are composed of different macromolecules (proteins, nucleic acids, lipids, etc.), the determination of the radii of gyration R_g of individual components will allow conclusions on their relative distribution (20). The parallel axis theorem of classical mechanics shows that the total radius of gyration (R_T) of a two particle system is given by $R_T^2 = \rho_1 R_1^2 + \rho_2 R_2^2 + \rho_1\rho_2\Delta^2$ where ρ = scattering density and Δ = separation between the two mass centers of radii R_1 and R_2. The radii of gyration of individual components can be determined by contrast variation. In a two particle system the solvent scattering density is adjusted by varying the H_2O/D_2O concentration to match the average scattering density of one of the

acromolecules in order to determine the R_g of the second particle. The procedure s then reversed to measure R_g for the first particle. To increase scattering ontrast and therefore increase the signal to background ratio specific deuteration ight be necessary (27).

At larger angles the scattering profile is determined by the general hape and density fluctuations within the sample (20,21). An interesting case rises when an object possesses two centers with scattering densities different rom its surrounding (24). The scattering function will then contain an intererence term equivalent to the scattering form fr.. diatomic molecules as developed y Debye (28) and described by James (5). $(F(s))^2 = (\rho)^2 \left(\frac{\sin 2\pi sd}{2\pi sd}\right)$ here d is the separation of the two scattering centers. This simple form applies deally only to spherical scatterers and departures from the ideal will modify ie shape somewhat.

Nevertheless this diatomic type scattering theory can be applied to the lucidation of the quaternary structure of protein complexes (24-26). In this ase the solvent is density matched to the complex resulting in a featureless cattering profile. Tw> components are then replaced by their deuterated counterparts mposing a sinx/x type scattering profile on the "background" scattering of the ensity matched complex in solution. The experiment is then repeated with two ther constituents as the focal scatterers eventually yielding by triangulation location map of the different components of the complex. Further analysis of h scattering transform by spherical harmonics, Patterson technique or simple odel calculations will provide information on the shape of the individual particles.

CONCLUSION

While analysis of biological structures by neutron scattering experiment has just begun, the papers in this symposium demonstrate the successful use of neutron scattering techniques to solve many different structural problems. The rapid advancement of this field has been due in part to the ingenious use of old techniques and in part to the development of new experimental techniques, particul those using two-dimensional counters. Most present experiments are however still hindered somewhat by the relatively low flux of present day neutron sources. While little direct increase in reactor flux can be expected, flux can often be improved by using radiation at the optimal wavelength (λ) for the resolution required using either hot or cold moderations to maximize flux. Improvements in beam geometry using efficient monochromators with a proper $\Delta\lambda$ and the use of focussing devices will also often improve the effective flux. Significant gain can still be achieved by the development of still larger high efficiency and high resolution two-dimensional counters. The final degree of success will however always depend on the skill of producing good biological samples specially where selective deuteration is required.

REFERENCES

1. Schoenborn, B., and A. C. Nunes, Ann. Rev. Biophysics and Bioeng. 1, 529 (1972).

2. Blow, D. M., and T. A. Steitz, Ann. Rev. Biochem. 39, 63 (1970).

3. Shipley, G. G. In: Biological Membranes, Chapman (ed.) Academic Press, pp. 1-89 (1973).

4. Bacon, G. E., Neutron Diffraction, Oxford University Press (1962).

5. James, R. W. The Optical Principles of the Diffraction of X-rays, Bell, London (1948).

6. Egelstaff, P. A. Thermal Neutron Scattering, Academic Press, London (1965).

7. Schoenborn, B. P. In: Anomalous Scattering, Ramaseshan and Abrahams (eds), Munksgaard, Copenhagen, pp. 407-421 (1975).

8. Schoenborn, B. P. Nature 224, 143 (1969).

9. Schoenborn, B. P. Cold Spring Harbor Symp.Quant. Biol. 36, 569 (1971).

10. Norvell, J. C., A. Nunes and B. P. Schoenborn, Science (1975).

11. Luzzati, V. In: Biological Membranes, Chapman (ed.), Academic Press, pp. 71-124, (1968).

12. Zaccai, G.,J.K.Blasie and B. P. Schoenborn, Proc. Nat. Acad. Sci. 72, 376 (1975).

13. Schwartz S., J. Cain, E. Dratz and J. K. Blasie, Biophysical J. (1975) in press.

14. Wilkins, M. H. F., A. E. Blaurock and D. M. Engelman, Nature New Biol. 230, 72-76 (1971).

15. Caspar, D. L. D., and D. Kirschner, Nature 231, 46 (1971).

16. Green, D. W., V. M. Ingram and M. F. Perutz, Proc. Roy. Soc. London, A 225, 287 (1954.

17. Guinier, A. X ray Diffraction, W. H. Freeman (ed.), San Francisco, pp. 319-348 (1963).

18. Kratky, O., and I. Pilz, Quart. Rev. Biophys. 5, 481-537 (1972).

19. Beeman, W. W., P. Kaesberg, J. W. Anderegg and M. B. Webb, Handbook Phys. 32, 321-442 (1957).

20. Engelman, D. M. and P. B. Moore, Ann. Rev. Biophys. and Bioeng. 4, 219-241 (1975).

21. Kirste, R. G., H. B. Stuhrmann, Z. Phys. Chem. 56, 338-341 (1967).

22. Stuhrmann, H. B., J. Mol. Biol. 77, 363-369 (1973).

23. Schelten, J., P. Schlecht, W. Schwartz, and A. Mayer, J. Biol. Chem. 247, 5436-5441 (1972).

24. Engelman, D. M., and P. B. Moore, Proc. Nat. Acad. Sci. 69, 1997 (1972).

25. Hoppe, W., Israel J. Chem. 10, 321 (1972).

26. Moore, P. B., D. M. Engelman and B. P. Schoenborn, Proc. Nat. Acad. Sci. (197

27. Moore, P. B., D. M. Engelman and B. P. Schoenborn, Proc. Nat. Acad. Sci. 71, (1974).

28. Debye, P., Ann. Phys. 46, 809-823 (1915).

TABLE I. Cross Sections And Scattering Factors For Elements Occuring In Biological Systems

	Cross section (10^{-24} cm^{+2})			Scattering length 10^{-12} cm^{+1}	
Element	Total	Coherent	Neutron mass absorption coefficient (μ/ρ, cm^2/g)	Neutrons	X rays (sin θ = 0)
H	81.5	1.8	.11	-.38	.28
D	7.6	5.4	.0001	.65	.28
C	5.5	5.5	.0002	.66	1.7
N	11.4	11.0	.048	.94	2.0
O	4.2	4.2	.0	.58	2.3
Na	3.4	1.6	.008	.36	3.14
Mg	3.7	3.6	.001	.53	3.4
P	3.6	3.5	.002	.51	4.2
S	1.2	1.2	.006	.28	4.5
Cl	15.2	12.3	.3	.96	4.8
Ca	3.2	3.0	.004	.46	5.6
Mn	2.0	1.6	.083	-.36	7.0
Fe	11.8	11.4	.015	.95	7,3
Ni	18.0	13.4	.03	1.0	7.9
Zn	4.2	4.2	.006	.56	8.3
Ge	9.0	8.8	.01	.84	9.0

*Neutron scattering data after Shull, MIT, 1971; Neutron cross sections BNL 325, 1955 and Bacon, Int. Tables for X-Ray Cryst. Vol. III, Kynoch Press, Birmingham, 1962

TABLE II. The average neutron scattering length per unit volume of some common biological constituents given in their hydrogenated and deuterated form. The exact volumetric scattering densities depend on the actual atomic compositions and densities.

	Scattering length in 10^{-14} cm per A^3	
	hydrogen form	deuterium form
Water	-.6	6.3
Hydrocarbon	-.3	7.0
Lipid polar head group	1.7	2.6
Proteins	3.0	9.0
RNA	4.2	7.2

FIGURE LEGEND

FIG. 1. Structure factor amplitudes for multilayers of dipalmitoyl lecithin (DPL) cholesterol at 95% humidity. Structure factors were measured as a function of H_2O/D_2O concentration for samples with cholesterol with a hydrogenated and a deuterated hydrocarbon chain (d). The reflection orders are indicated. The data has only been corrected for absorption and sample geometry. The data between the hydrogen vs the deuterated sample has been scaled to equal shapes since the structure factor changes due to the H_2O/D_2O exchange have to be equal for both isomorphous samples.

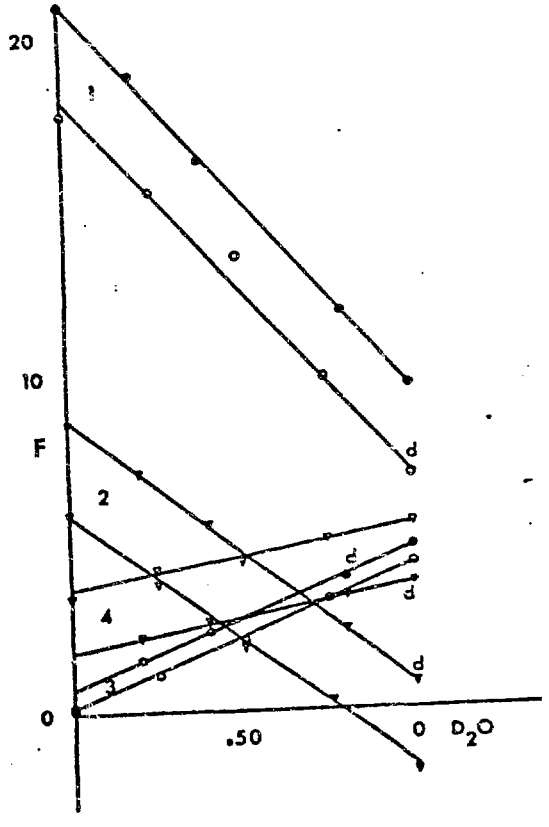
20
10
F
0
1
2
3
4
d
d
d
d
.50
0
D_2O

MI 1 - USE OF NEUTRON SCATTERING FOR THE ANALYSIS OF BIOLOGICAL STRUCTURES - B. P. Schoenborn (Brookhaven National Lab., USA)

Mössbauer (Grenoble):

Are you now actually using the anomalous dispersion method for determining the phase shifts at Brookhaven, especially taking into account that you are somewhat limited in the wave length range which you can use?

Schoenborn:

The data we collected on cadmium was at .8 and 1.2 Ångstroms and obviously would have been much better with a hot source which we don't have at Brookhaven. About 500 reflections were phased by the anomalous state; we have not collected any more cadmium data. We are, however, looking at a gadolinium derivative which has a more suitable resonance, at about 1.7 Ångstroms, which will be easier to handle and we can collect data on both sides of the absorption sheets.

Mössbauer:

If I might still elaborate on this question. How many phases do you actually plan to determine by the anomalous dispersion method? I'm sure you don't want to determine as many phases as you want to measure intensities, but what is the ratio which you see? How many phases does one want, and does one want a few phases with a high accuracy or many phases with a low accuracy?

Schoenborn:

I think in a structure like myoglobin where we have the X-ray structure it is really of no value to get anomalous phases. It was purely a demonstration that it actually works. But if you have a protein with an X-ray structure then you would get as many phases as you possibly can, and I would say you need at least 50% to 2/3 to make it worthwhile. So you need in the order of about 8,000 phases for a structure of the molecular size of myoglobin.

Ajzenberg-Selove (Penn.):

On that last slide, what is the uncertainty of the distances you measured, typically?

Schoenborn:

It's a couple of Ångstroms.

Rostenbach (N.S.F.):

In your résumé you mentioned biological structures such as membranes, and viruses. What is your plan with regard to viruses?

Schoenborn:

Our main work so far has been with membranes, protein and ribosome. We have looked at viruses and Dr. Jacques at I.L.L. has been actually studying some viruses. Again, similar to ribosome it is true that you can distinguish the nucleic acid from the protein very well. And one of the major applications at present is on nuclei or chromosome structure where neutron diffraction analysis, I think, can solve some of the problems the molecular biologists

have been after for a long time. Some of that work is being done by Dr. Bradbury at I.L.L., who is from Portsmouth, England.

Chen (M.I.T.):

What is the upper limit of this triangulation technique and variable contrast?

Schoenborn:

I don't quite understand the question; if you have spherical molecules you can determine it quite well. If the proteins are interwoven like we think s-7 might be, then we do not quite know how to deal with the data yet, but I think by introducing a spherical-harmonic type of analysis we probably will be able to extend it by determining the internal structure of the protein as well as its intermeshing. We are not quite sure as to how to deal with that data yet.

Chen:

With availability of these two dimensional detectors, say in a high flux reactor, what is the practical upper limit of the molecular weight of a compound, for which you can determine the structure?

Schoenborn:

Well, the ribosome has a molecular weight of about two million. I don't know offhand of many biological structures which are larger than that. It depends to what resolution you want to go. If you do a protein structure analysis where you want individual atomic positions, then I would say at present about 50,000 molecular weight is a reasonable one, probably even 80,000. It depends on the quality of the crystal and of the crystal size.

Chen:

The question of damage of the neutron on the biological system, is this absolutely clear?

Schoenborn:

Completely clear? No, but it's reasonable that X-rays produce free radicals and it's free radicals really that do damage to the structure. With neutrons you don't really get free radicals, so that's one type of damage we don't have. Even in the cadmium myoglobin where we expected maybe some damage from the gamma rays, we did not observe any.

Mössbauer:

Concerning the damage problem, I would like to ask a question a little outside of the conference. There was a report recently from Stanford by Phillips and co-workers in which they claimed that synchrotron radiation, in contrast to X-rays, gives much less damage. I find this very perturbing and don't understand it. Would you have any comment on this?

Schoenborn:

X-ray damage has worried us for a long time, and it has been known that it's not so much the dose as the length of time you're exposed. In the old X-ray

protein work where you had relatively weak generators and exposure times of maybe eight to ten hours, more extensive damage occurred for an exposure of one or two hours at maybe ten times the flux. So the damage seems to be flux-dependent. I think it depends on the interaction of the free radical with the structure. Furthermore, we know from experiment that if you go to lower temperature the damages are reduced, again, I think, because the free radicals can't move within the structure. But the question of why and how this damage occurs is obviously not solved; there's probably more than one mechanism, I would expect.

2.45 p.m., Thursday, July 8, 1976 Invited Paper: Session MI2

SOLID-STATE ASPECTS OF NEUTRON PHYSICS RESEARCH

W. Gläser

Physik-Department der Technischen Universität München, West Germany

RÉSUMÉ

The possibilities and advantages of slow neutron probes for solid-state physics research will be surveyed, and recent developments in experimental techniques outlined, such as high resolution diffractometry, spectroscopy and interferometry. Some results of current interest from small-angle scattering and inelastic scattering investigations will be presented, and neutron damage studies briefly considered.

ABSTRACT

The investigation of physical properties of condensed matter with neutrons has rapidly developed into a broad field of research.

Scattering of slow neutrons from solids can reveal many details of structural, magnetic and dynamical properties of these many-particle systems.

Faster neutrons can be used to create defined defects in solids.

In this paper, we endeavour to illustrate the possibilities and advantages of slow neutron probes for solid state research. A few of the more recent developments in experimental techniques, including high-resolution diffractometry, spectroscopy and interferometry will be outlined.

A few prominent examples of results of current interest in solid-state physics from small-angle scattering and inelastic scattering experiments will be discussed, in order to illustrate the success which has been achieved with the neutron technique so far.

Recent results of neutron damage studies will be mentioned.

Some Solid-State Aspects of Neutron Physics Research

W. Gläser

Physik-Department der Technischen Universität München, Germany

Abstract: The investigation of physical properties of condensed matter with neutrons has rapidly developed into a broad field of research. Scattering of slow neutrons from solids can reveal many details of structural, magnetic and dynamical properties of these many particle systems. Faster neutrons can be used to create defined defects in solids. In this paper it will be tried to illustrate the possibilities and advantages of slow neutron probes for solid-state research. A few newer developments of experimental techniques including high resolution diffractometry, spectroscopy and interferometry will be outlined. A few prominent examples of results of current interest in solid-state physics from small angle scattering and inelastic scattering experiments will be discussed, in order to illustrate the success which has been achieved with the neutron technique so far. Recent results of neutron damage studies will be mentioned.

I. Introduction

There are essentially two aspects of neutron interaction with solids which are of general interest for solid-state research, namely the diffraction or elastic and inelastic scattering of slow neutrons and the generation of radiation damage with fast neutrons.
Especially the study of condensed matter by elastic and inelastic neutron scattering has grown into a broad field of research. This is of course due to the unique properties of slow neutrons, in particular their favourable energy-wavenumber relation. For solid-state research neutrons are in a sense super X-rays. Because of their specific interaction with nuclei and due to their magnetic interaction with unpaired electrons they can reveal structures not accessible to X-rays. However in addition, due to the energy wavenumber relation they can reveal the time behaviour of structures (atomic motions) and therefore add a new dimension to structure research.
Today standard techniques like two axis and three axis spectrometry are used for many applications in solid-state physics, crystallography, chemistry and biology. The progress made in this field has been covered in several topical conferences, e.g. the IAEA conference on Neutron Inelastic Scattering at Grenoble in 1972[1], the tenth International Congress of Crystallography at Amsterdam in 1975[2] and the Conference on Neutron Scattering in 1976[3] at Gatlinburg.
It is impossible to summarize all the achievements in a paper like the present one. Instead of we will try to focus our attention to some newer developments which are mainly methodical developments but which demonstrate how the possibilities of the neutron probe as a research tool in solid-state physics can be still extended. The selection remains of course subjective.
We will cover some aspects of neutron diffraction, describe some newer possibilities in neutron spectoscopy and finally mention a particular problem where progress has been made in radiation damage research.

II. Neutron diffraction

1. High resolution diffraction

Structure investigations with neutrons have up to now mainly been performed with two axis diffractometers. The last paper has given us a review on the neutron contribution towards revealing static structures. One of the shortcomings in the use of neutrons for structure work is sometimes the restricted resolution in $\vec{x}$-space. But with neutrons different from X-rays the Bragg relation $\lambda = 2d\sin\theta$ can be applied in a second way. One can measure the wavelength of neutrons scattered by the sample into a fixed direction out of a pulsed white beam. This is the time-of-flight method of neutron diffraction which in principle allows to achieve a higher resolution and was first applied by Buras[4]. A modern spectrometer designed for this purpose and built by Steichele and Arnold[5] at the reactor in Munich is illustrated in Fig.1. The main features are:

a) a three chopper system with which the wavelength region of incoming neutrons can effectively be adapted to the part of the diffraction pattern to be studied and

b) a 150 m neutron guide tube flight path which together with the backscattering geometry allows a lattice parameter resolution $\Delta d/d$ down to $2 \cdot 10^{-4}$.

Fig.2 shows a typical powder diffraction pattern of Al_2O_3 which demonstrates that very high orders can be resolved.

The resolution available in this way allows, e.g., the study of grain sizes in solids and the separation of thermal diffuse and static diffuse (Huang) scattering from Bragg scattering. The main interest in this technique presently is however the possibility to measure diffraction patterns at higher momentum transfers which together with new analysing techniques allows a substantial refinement of structure determination in powder diffractometry. This improved time-of-flight technique together with the accelerator driven intense neutron sources presently under development will certainly extend the range of

applications of neutron diffraction. It should just be mentioned that for determining the structure of liquids, especially of molecular liquids it is crucial to measure at higher momentum transfers than available with present techniques.

2. Small angle scattering

Another technique which during recent years has become an important tool for studies in solid-state physics, metallurgy, chemistry and biology is the small angle scattering of neutrons. This technique which was mainly developed at Jülich and Grenoble[6] is designed for the investigation of heterogeneities in condensed matter with dimensions considerably greater than interatomic distances(30 ... 3000 Å)

The advantages of neutrons compared to X-rays for this purpose are essentially the same as in conventional neutron diffraction. The variation of the nuclear scattering length through the periodic table allows to tackle problems not amenable to X-rays. This is particular important for the study of polymers and biological systems. Because neutrons are also scattered by magnetic moments of atoms magnetisation fluctuations can be studied which is impossible with X-rays and finally a serious drawback of X-ray small angle scattering the double Bragg scattering - which is due to the short X-ray wavelengths only available - can be avoided by using neutrons with wavelengths of 10 Å and more.

It is perhaps worthwhile to point out that in spite of the higher brightness of a modern X-ray power tube compared to a reactor neutron source by about 5-7 orders of magnitude an optimized small angle scattering apparatus for neutrons can be made also superior in scatter intensity compared to an X-ray apparatus.

Fig. 3 shows a scheme of the small angle scattering apparatus at Jülic

One of the fields of solid-state physics where small angle scattering investigations lead to considerable progress is the understanding of the mixed state in type II superconductors. The structure of single vortex lines and the morphology of vortex line lattices in niobium

have been investigated by the Saclay[7] and Jülich[8] group in detail. Also the motion of vortex lines and the pinning forces, which are so important for applications of superconductivity could be determined[9]. Fig.4 shows as an example a 3-dimensional plot of the microscopic magnetic field distribution in niobium for a certain mean magnetic flux as derived from the small angle scattering pattern by Schelten et al.[8]. Such data could not be made available with the decoration technique for flux lines in superconductors used before. Another interesting aspect of vortex lines is that they can move if they are not pinned and cause energy dissipation. This motion has also recently been measured directly in a neutron scattering experiment by Schelten[9].

An other quite different field of condensed matter where neutron small angle scattering experiments could answer old questions should be mentioned at least, namely the physics of solid polymers. Several models had been proposed for the shape or configuration of the chain molecules in the solid amorphous state of polymers. Fig.5 illustrates these models: d) is the cluster model of Flory proposing the same behaviour as in liquid solution, c) is the so called meander model of Pechhold and b) is the collapsed cluster model. In each of these pictures a single chain molecule has been marked. Such marking sensible for neutrons can be achieved by a few hydrogenized molecules in an otherwise deuterated matrix or vice versa. The small angle scattering experiment measuring the scattering from the marked molecules has been performed on polymethylemetacrylate in the glasy state by Schelten et al.[10] Fig. 6 shows the result, the $\varkappa$-dependent scattering cross section ($\varkappa$ is the momentum transfer) measured, compared to the cross sections calculated for several proposed models. The experimental points are in favour of the statistical distribution of clusters as proposed by Flory. So much for neutron small angle scattering. An excellent recent review on this new method has been given by Schmatz et al.[11]

Ultracold neutrons: It should at least be mentioned that with the availability of ultracold neutrons, neutrons with a wavelength of a few hundred Å, a different approach for studying larger inhomogeneities in materials is possible. With ultracold neutrons only the transmission of the sample has to be measured. The deviation of the cross section from the $1/v$ absorption and incoherent inelastic scattering contributions is due to scattering from magnetic and non-magnetic inhomogeneities and can be analyzed with suitable models for these properties. Fig.7 shows as an example the total cross section of an AlZn alloy versus neutron velocity for different heat treatments measured by Steyerl[12]. Whereas the solid line is due to absorption and inelastic scattering the extra cross section is caused by precipitates, by so called Guinier-Preston zones in the material. It turns out, that in many respects this method can be equivalent to small angle scattering[13].

Neutron interferometry: At this place also the perspectives of neutron interferometry in solid-state research should be indicated. A versatile neutron interferometer splitting a neutron beam coherently into two beams by diffraction from a perfect silicon crystal has been successfully tested recently by Bonse and Rauch[14]. This technique opens the possibility to measure phase shifts very accurately and several applications in the direction of solid state physics, e.g. small angle scattering at extreme small angles, or precise measurements of magnetizations in connection with phase transitions, to mention only a few possibilities, can be foreseen.

III Neutron Spectroscopy

1. Measurement of phonon dispersions

The standard technique for studying collective excitations in solids, phonons, magnons etc. by coherent inelastic neutron scattering today is the triple axis method, which is illustrated in Fig.8. A monochromatic neutron beam impinges on the single crystal under investigation. The analysis of energy and direction of neutrons scattered by excitation or annihilation of a phonon determines energy and wavevector

of the phonon and consequently the phonon dispersion of the crystal in a unique way. Phonons at larger wavevectors corresponding to reciprocal lattice distances can be measured only with neutrons. Besides phonon energy determinations intensity measurements yield information on the phonon eigenvectors and line shape and shift analysis which are now feasible contribute to an understanding of anharmonic effects in solids.

In this way phonon dispersions of many solids including some with more elaborate structures have been measured. It is the analysis of this data which gives very detailed information on potentials or generaly speaking on chemical binding in solids.

In order to illustrate the capability of coherent inelastic neutron scattering we list some problems which were in the center of recent interest in solid-state physics and where measurements of phonons contributed significantly.

Firstly the problem of structural phase transitions in solid ought to be mentioned. Here the suggestion that the phase transitions in certain solids are triggered by an instability in a normal vibrational mode of the lattice, a soft mode, has been established and studied in great detail in many examples by now[15-18].

The investigation of the lattice dynamics of several high temperature superconductors like Nb_3Sn[19] and TaC[20] revealed details on the importance of electron-phonon interaction and of electronically driven lattice instabilities in these crystals. Further work along these lines will certainly elucitate the mechanism in question.

Great effort has been made to explain the interesting properties of almost 1-dimensional solids, e.g. 1-dimensional conductors. Here with neutrons the possibility of a Peierls transition or charge density wave in such unusual solids has been discovered [21,22].

Other classes of materials which have been studied during the last few years are superionic conductors, layer structures and low symmetry crystaline solids with the aim to explain the interatomic forces in these rather anisotropic systems. Finally the growing interest in

studying the lattice dynamics of molecular crystals should be mentioned. Coherent inelastic neutron scattering is now a well established research tool for solid-state physics and will be applied in the future to a great variety of special problems of solid-state dynamics.

2. Phonon density of states measurements

There is however the other aspect of inelastic neutron scattering from condensed matter, namely the incoherent scattering. It is well known that the one-phonon term in the so called phonon expansion of the double differential incoherent scattering cross section is proportional to the phonon density of states. The phonon density of states determines many properties of a solid. In fact the first inelastic neutron scattering experiments on solids aimed for the determination of the phonon density of states. Unfortunately there are only a few nuclei, e.g. hydrogen and vanadium which scatter dominantly incoherent so the application of incoherent scattering in solid-state physics was rather limited. But recently it has been shown, that phonon density of states can be measured also for coherent scatterers. The essential point in incoherent scattering is that the wavevector selection rule vanishes. The physical meaning of this is that in an incoherent scattering experiment a sampling of all motions in the solid on which the single scattering atom participates is performed. The idea is therefore to simulate this sampling also in the case of coherent scatterers by summing experimentally over all scattering events in the Brillouin zone which roughly means integrating the scattered intensity over a sufficient large solid angle. Fig.9 illustrates the idea in reciprocal space: The circles represent surfaces of constant phonon energy. The triangle is the wavevector diagram for an one phonon process. Rotating the triangle corresponds to scattering from a powder. This is not sufficient for averaging over all possible scalar products $\vec{\kappa}\cdot\vec{q}$. But allowing a certain κ-range for a fixed energy transfer gives the desired average over the Brillouin zone. This sampling method

which has a much wider range of applications than incoherent inelastic scattering has been worked out systematically during the last years at Karlsruhe and at the high flux reactor in Grenoble[23]. Fig. 10 shows for the simple example of aluminum that the method works. The solid curve has been obtained by fitting a tedious point by point measurement of phonons in a sufficient part of the Brillouin zone[24]. The points are the result of the experimental sampling method. The sampling method has been used to determine the phonon densities of states of a series of high temperature superconductors which is a needed information for understanding the high transition temperatures of these systems.
Fig.11 shows as an example the phonon density of states of Nb_3Sn at two temperatures[25]. The shift of the density of lower frequencies with decreasing temperature is opposite to what one expects in normal solids and is intimately related to a strong electron phonon coupling. By comparing this data with other properties of the superconductor details on the electron phonon interaction can be derived.
Another broad field where the incoherent inelastic neutron scattering method has brought during recent years a large number of new data is concerned with crystal field effects, crystal field splittings in metals and alloys, but this can only be mentioned[26].

3. High resolution backscattering spectroscopy

The search for improved resolution of neutron spectroscopy in order to cover also very small energy transfers lead to the development of the backscattering Bragg reflexion technique. This technique has been successfully demonstrated by Alefeld[27]. Fig. 12 shows a scheme of the backscattering spectrometer installed at a neutron guide at the cold source of the Grenoble high flux reactor.
In this spectrometer perfect silicon single crystals are used in thrue backscattering geometry as monochromator and analyzer crystals. The incident energy is varied by the Doppler effect at the periodical moving monochromator crystal. If, e.g., the (111) lattice planes

of Si are used, the mean incident energy is 2.076 meV and an energy resolution of 0.2 μeV can be reached. The accessible energy range is about ± 10 μeV. The low incident neutron flux of 10^4 n/cm^2 is partly compensated by a large solid angle of the analyzer. Fig.13 illustrates the resolution achieved with this instrument in a measurement of the hyperfine field splitting in fcc cobalt.
This high resolution neutron spectroscopy can be used to study diffusive and tunneling motions of atoms or molecular groups and very low lying collective modes in solids. Fig.14 shows as an example a more complex spectrum, namely the sprectrum of rotational tunneling of NH_4 ions in NH_4ClO_4 at 4K[28]. This spectrum can be explained by assuming transitions between four energy levels. From such data details of the potential of the NH_4 group in the solid can be derived. The investigation of rotational tunneling motions in molecular systems is of growing interest[29].
Finally an experiment should be mentioned which is related to an open question in the context of structural phase transitions. With the experimental proof of soft phonon modes it was believed that the mechanism of structural phase transitions is understood in principle. But more detailed inelastic neutron scattering experiments[30] revealed besides the soft modes increasing extra intensity - critical scattering - at the wavevector of the soft mode around energy transfer zero as the temperature approached the transition temperature of the phase transition. This so called central peak attracted considerable theoretical interest but sofar it withstand any consistent explanation. A key information would be the detection of a finite energy width of this peak. The highest resolution sofar achieved in this problem was by Alefeld and Heidemann[31] with the backscattering technique. Their result is shown in Fig.15 . Fig. 15 shows essentially the resolution of the instrument, no broadening could be detected. From this data they conclude that the width should be less than 0.1μeV, which certainly is hard to understand on the basic of present theories on this phenomenon.

These few examples may be sufficient to illustrate that the back-scattering technique has interesting applications and that neutron spectroscopy has closed the gap to NMR and Mößbauer spectroscopy in solids.
Other high resolution neutron techniques are under development like the spin echo method of Mezei[32] using polarized neutrons and perhaps a future spectroscopy with ultracold neutrons which seems to be feasible will push the limits further down.

IV Neutron Radiation Damage in Metals

The study of radiation damage in solids with fast neutrons and also following thermal neutron capture is also a broad field of research. The understanding of radiation damage is essential for the development of advanced materials necessary in nuclear technology. There are of course many research programs which we cannot discuss in this review. We cannot even touch all aspects of more basic research in this field instead of this we will mention only a few recent experiments which illustrate the kind of progress which has been made in the research on the microscopic properties of radiation defects produced by neutrons in solids, especially in metals.
It is well kown that irradiation of a metal with fast neutrons produces Frenkel defects, namely self-interstials and vacancies which are stable only at very low temperatures, e.g., below 20K in aluminum. Therefore low temperature irradiation facilities in research reactors are needed for this type of research.
Recently it has been shown mainly by diffuse X-ray scattering[33] that in irradiated Al and Cu the stable configuration of the interstitial atom is the 100 -"split" or dumbbell configuration, which is illustrated in Fig.16. These dumbbell can perform low frequency resonant vibrations, which are of librational type. First experimental evidence for these resonant vibrations came from Mößbauer spectroscopy with ^{57}Fe in Al. Vogl et al.[34] studied systematically the influence of the fast neutron irradiation dose on the trapping of defects at Co impurities in Al. They found a new Mößbauer line. From the isomer

shift and quadrupole splitting of this line they could conclude that the Co impurity has trapped an interstitial and both atoms formed a dumbbell complex. Further the Debye-Waller factor of the interstitial Mößbauer line revealed a strong temperature dependence of the mean local displacement of the Mößbauer atom which can be explained assuming a low lying resonance frequency of the dumbbell of about one tenth of the Debye frequency of Al.
These low lying resonance frequencies can explain many well known facts on irradiated fcc metals like the softening of the elastic constants and the low activation energies necessary for interstitial diffusion. The importance of this dynamical process for the basic understanding of the properties of irradiated metals lead to a more detailed search for the dumbbell modes. Theoretical considerations[35] suggested that the coupling of the librational modes should lead to resonant like perturbations of the transverse acoustic phonon dispersion. Such an effect should be detectable by coherent inelatic neutron scattering on an irradiated single crystal although the low concentrations of point defects achievable by neutron irradiation make the experiment difficult.
Phonon measurements on an irradiated single crystal of copper were performed by Nicklow et al.[36] at Oak Ridge and of irradiated aluminum crystals by Böning et al.[37] at Grenoble. The results are shown in Fig.17. The Frenkel defect density in Nicklow's experiment was only 40 ppm, in Böning's experiment 800 ppm. Although there seem to be still some discrepancies between theoretical models and these first experimental results they clearly proof the existence of low lying resonance modes in irradiated fcc metals.

These experiments once more demonstrate the power of the neutron scattering method for solid-state research. Up to now it was believed to be unlikely that such low defect concentrations could be seen with the neutron probe.

Conclusions

By now slow neutrons have been used to investigate a variety of physical properties of condensed matter. Most of these experimental data were unobtainable with other methods. This is particularly thrue for the detailed information on collective excitations in solids.

The success is largely due to the availability of intense neutron sources and the development of special devices like cold neutron sources, neutron guides and hot sources tayloring neutron beams for defined ranges of applications.

Some of the experimental methods have reached high accuracy and are standardized by now so that they can be used more and more routinely for solving special problems concerning structures and dynamics in the broad field of solid-state research.

Although, in this paper, we were only able to discuss a few more recent and novel applications, we can conclude that the development of slow neutron research techniques goes on. This is especially thrue for high resolution spectroscopy, neutron interferometry and the use of ultra cold neutrons. It is not yet possible to survey the full range of possible applications of these new methods.

The use of polarized neutrons as probes will increase with the availability of more effective polarizers. Also the forseeable development of intense pulsed neutron sources in the o.1 to 1 eV energy range will extent the useful range to higher momentum transfer and energy transfers.

Certainly the study of structures, phonon dispersion relations, phonon density of states, other types of collective excitations and diffusive type of motions in more complex materials will be tackled in the future.

Accurate double differential scattering cross section measurements seem to be feasible now and open promising perspectives for revealing e.g. microscopic properties of dense gases, liquids and amorphous solids.

With the growing understanding of simple neutron radiation defects in metals activities in this field will move towards investigating the more complex agglomerated defect structures.

References

1) "Neutron Inelastic Scattering",Proc.Conf. at Grenoble, IAEA Vienna (1972).

2) Proc. Tenth Int.Congr.Crystallogr., Amsterdam (1975).

3) Proc.Conf. on Neutron Scattering at Gatlinburg (1976).

4) B. Buras, Nukleonika 1963, 8, 259

5) E.Steichele and P.Arnold, Phys.Letters 1973, 44A, 165.

6) K.Ibel, W.Schmatz and T.Springer, Atomkernenergie 1971, 17, 15.

7) D.Cribier, B.Jacrot, L.Madhov-Rao, B.Farnaux, Phys.Letters 1964, 9, 106.

8) J.Schelten, H.Ullmaier and G.Lippmann, Z.Physik 1972,253, 219.

9) J.Schelten, H.Ullmaier and G.Lippmann, Phys.Rev. 1975, B12, 1772

10) J.Schelten, W.A.Kruse and R.G.Kirste, Kolloid-Z. 1973, 251, 919.

11) W.Schmatz, T.Springer, J.Schelten and K.Ibel, J.Appl.Cryst. 1974 7, 96.

12) A.Steyerl,Nucl.Instr. and Meth. 1975, 125, 461.

13) R.Lermer and A.Steyerl, phys.stat.sol. 1976, (a)33, 531.

14) W.Bauspieß, U.Bonse, H.Rauch and W.Treimer, Z.Physik 1974,271, 177.

15) G.Shirane in "Structural Phase Transitions and Soft Modes",Proc. NATO Adv.Study Inst.,(Universitetsforlaget Oslo,1971),217.

16) R.Comès and G.Shirane, Phys.Rev. 1972, B5, 1886.

17) J.D.Axe, S.M.Shapiro, G.Shirane, T.Riste in "Anharmonic Lattices Structural Transitions and Melting", (Noordhoff Leiden, 1974).

18) R.Currat, R.Comès, B.Dorner and E.Wiesendanger, J.Phys.C: Solid State Phys. 1974, 7, 2521.

19) G.Shirane and J.D.Axe, Phys.Rev. 1971, B4, 2957.

20) H.G.Smith and W.Gläser, Phys.Rev.Letters 1970, 25, 1611.

21) R.Comès, B.Renker, L.Pintschovius, R.Currat, W.Gläser and G.Scheiber, phys.stat.sol., 1975, (b)71, 171.

22) J.W.Lynn, M.Iizumi, G.Shirane, S.A.Werner and R.B.Saillant, Phys.Rev. 1975, B12, 1154.

23) F.Gompf, H.Lau, W.Reichardt and J.Salgado, "Neutron Inelastic Scattering", IAEA Vienna 1972, p.137.

24) E.R.Cowley, Can. J. Phys. 1974, 52, 1714.

25) E.Schneider, P.Schweiss and W.Reichardt, to be published.

26) Proc.Conf. on "Crystalline Electric Field Effects in Metals and Alloys, Montreal 1974.

27) B.Alefeld, M.Birr, A.Heidemann, Naturwissenschaften 1969, 56, 410.

28) A.Heidemann, to be published.

29) A.Heidemann, to be published.

30) K.Otnes, T.Riste, J.Feder and G.Shirane, Solid State Comm.1971, 9, 1103.

31) B.Alefeld and A.Heidemann, to be published.

32) F.Mezei, Z.Physik 1972, 255, 146.

33) B.v.Guerard, Thesis, Technische Universität München 1975.

34) G.Vogl, W.Mansel and W.Vogl, J.Phys.F: Metal Phys. 1974, 4,2321.

35) P.H.Dederichs, C.Lehmann and A.Scholz, Phys.Rev.Lett. 1973, 31, 1130.

36) R.M.Nicklow, R.R.Coltman, F.W.Young,Jr. and R.F.Wood, Phys.Rev. Letters 1975, 35, 1444.

37) K.Böning, G.Bauer, H.J.Fenzl, R.Scherm and W.Kaiser, to be published.

Figure Captions

Fig.1 Scheme of the neutron time-of-flight diffractometer at the reactor FRM Garching.

Fig.2 High resolution TOF diffraction pattern from an Al_2O_3 powder sample.

Fig.3 Scheme of the small angle scattering apparatus at the reactor FRJ-2 Jülich.

Fig.4 Microscopic magnetic field distribution in the mixed state of niobium as derived from the small angle scattering pattern.

Fig.5 Proposed models for the conformation of polymer chain molecules a) in solution, b) to d) in the solid phase.

Fig.6 Measured scattering cross section for PMMA of molecular weight 250 000 compared to calculated cross sections for different models. Neutron data confirm the statistical cluster model.

Fig.7 Total cross section of an $Al_{.92}Zn_{.08}$ alloy at small neutron velocities for different heat treatments. The solid line is due to absorption and inelastic scattering. The extra cross section is due to the formation of Guinier-Preston zones.

Fig.8 Scheme of the triple axis method for phonon measurements by coherent inelastic neutron scattering.

Fig.9 Illustration of the sampling method for phonon density of states measurements on coherent scatterers.

Fig.10 Phonon density of states of aluminum measured with the sampling technique compared to the density calculated from dispersion curves.

Fig.11 Phonon density of states of the high temperature superconductor Nb_3Sn at two different sample temperatures

Fig.12 Scheme of the high resolution neutron backscattering spectrometer at the high flux reactor in Grenoble.

Fig.13 Hyperfine splitting in fcc cobalt as measured with the backscattering spectrometer.

Fig.14 Spectrum of rotational tunneling modes in NH_4ClO_4 at 4K obtained with the backscattering spectrometer.

Fig.15 Energy width of the central peak in $SrTiO_3$. The measured width is determined by spectrometer resolution and gives an upper limit for the width of the central peak of 0.1 μeV.

Fig.16 Configuration of interstitial dumbbells in fcc metal lattices.

Fig.17 Deviations of phonon frequencies of the TA branch in a) irrad. Cu[36] b) irrad. Al[37] from the frequencies in the not-irradiated samples.

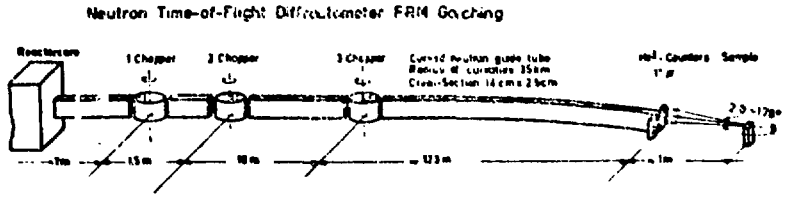
Neutron Time-of-Flight Diffractometer FRM Garching
Reactorcore
1 Chopper
2 Chopper
3 Chopper
Curved neutron guide tube
Radius of curvature 350m
Cross-Section 14 cm x 2.5cm
Sample
15m
11m
123m
1m

Fig. 1

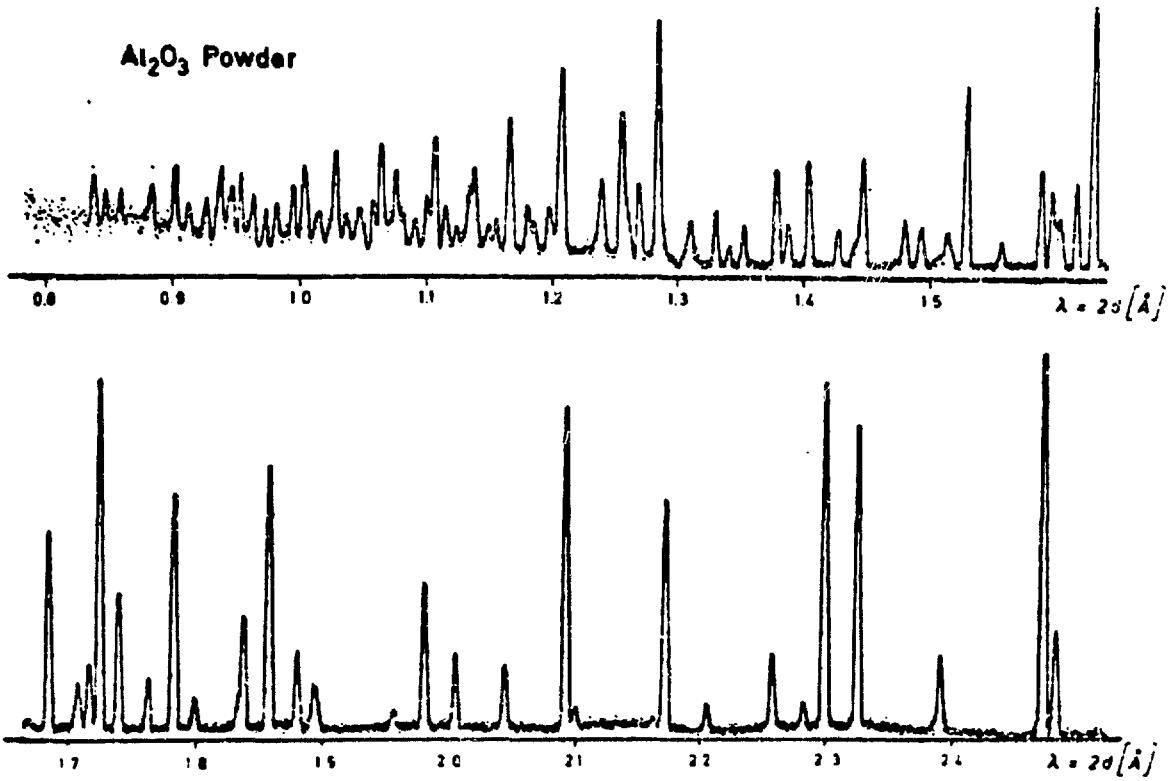
Al_2O_3 Powder
0.8
0.9
1.0
1.1
1.2
1.3
1.4
1.5
$\lambda = 2d[\AA]$
1.7
1.8
1.9
2.0
2.1
2.2
2.3
2.4
$\lambda = 2d[\AA]$

Fig. 2

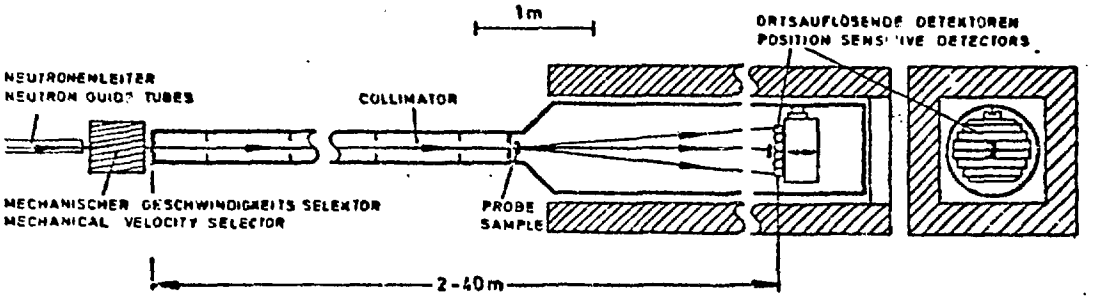

Fig.3 Scheme of the small angle scattering apparatus at the FRJ-2 Jülich

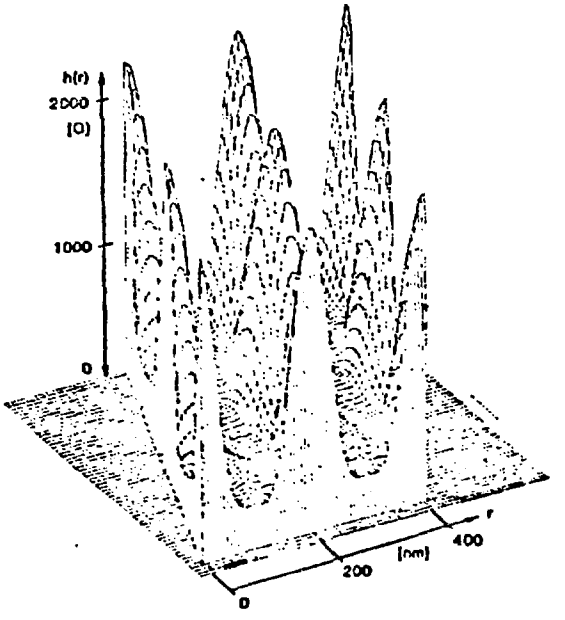

Fig. 4 Microscopic magnetic field distribution in the mixed state of niobium as derived from the small angle scattering pattern[8]

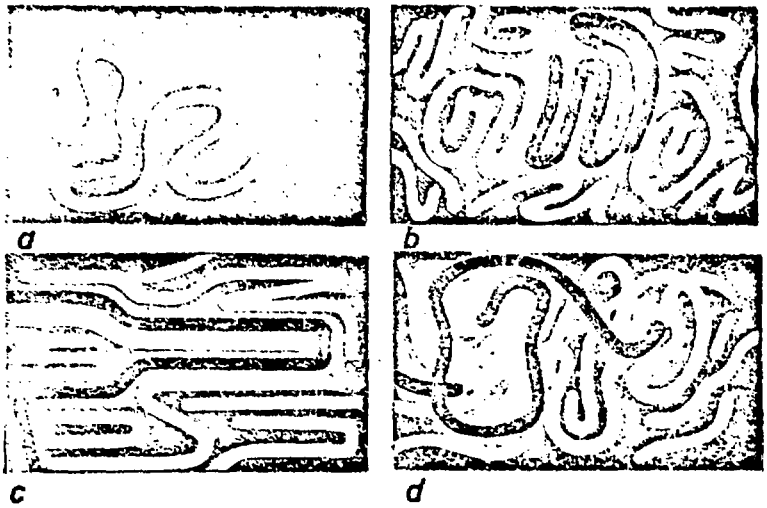

Fig. 5 *Proposed models for the conformation of polymer chains*
a) in solution, b) to d) in the solid phase

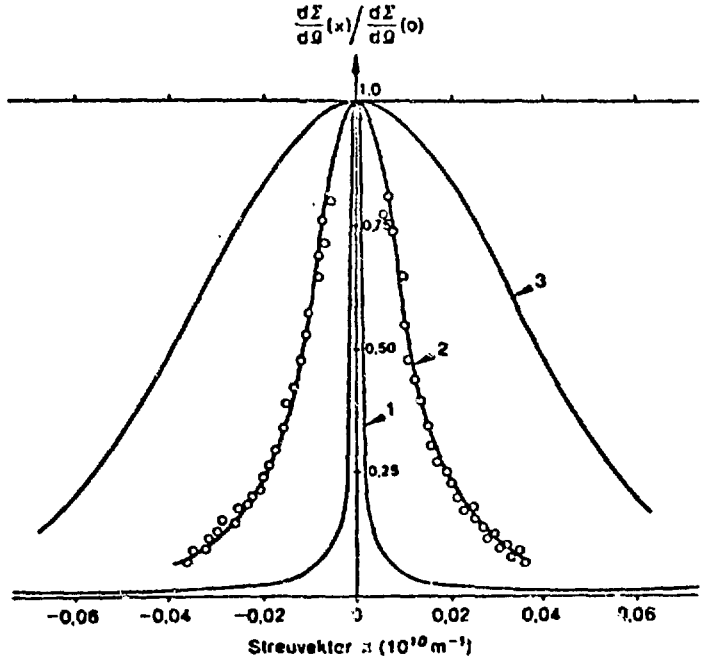

Fig. 6 *Measured scattering cross section for PMMA of molecular weight 250 000 compared to calculated cross sections for different models.*
Neutron data confirm the stastical cluster model.

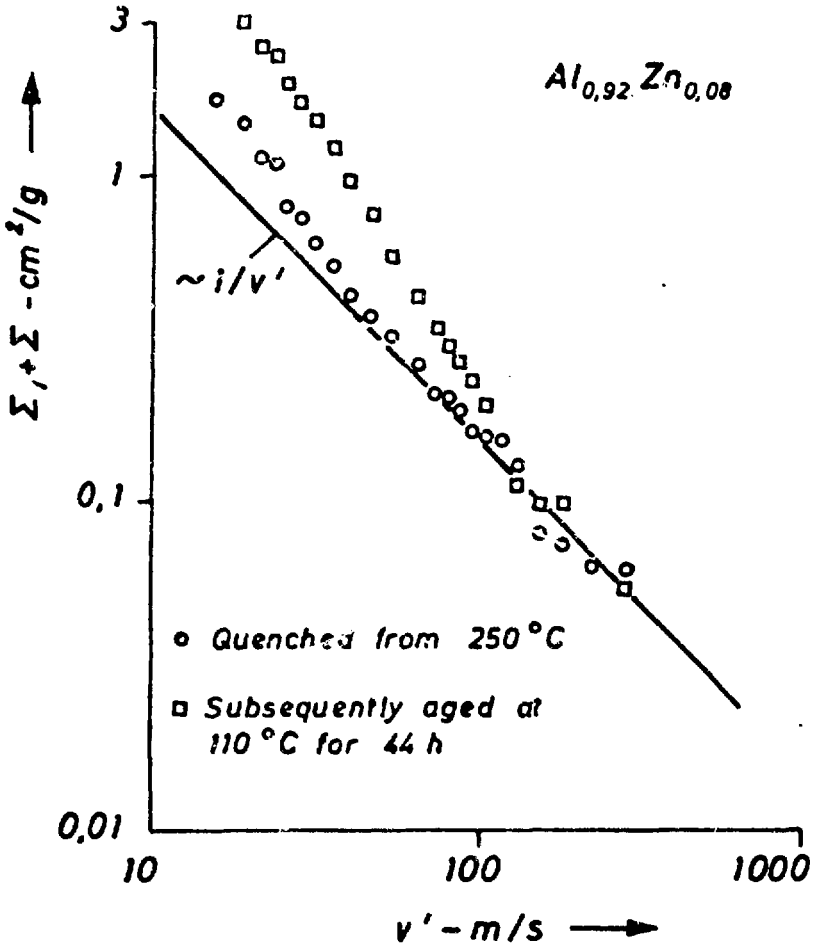

Fig 7 *Total cross section of $Al_{.92}Zn_{.08}$ at small neutron velocities and different heat treatments. Solid line is due to absorption and inelastic scattering. o, □ extra cross section due to Guinier-Preston zones.*

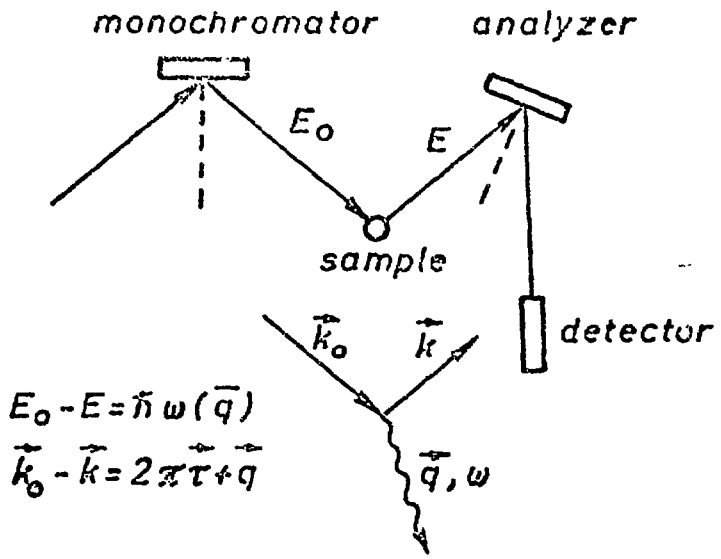

Fig.8 *Scheme of the triple axis method for phonon measurements by coherent inelastic neutron scattering*

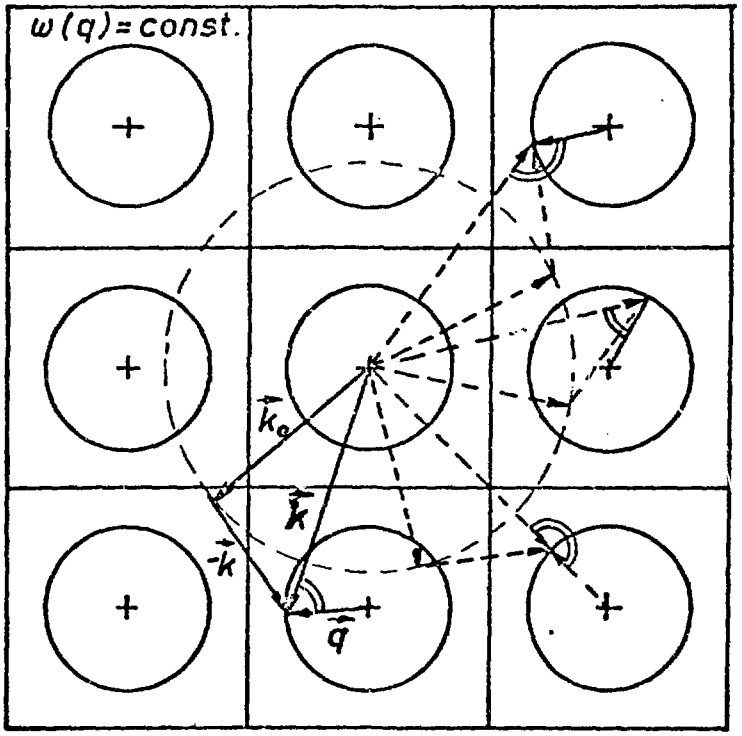

Fig.9 *Illustration of the sampling method for phonon density of states measurements on coherent scatterers*

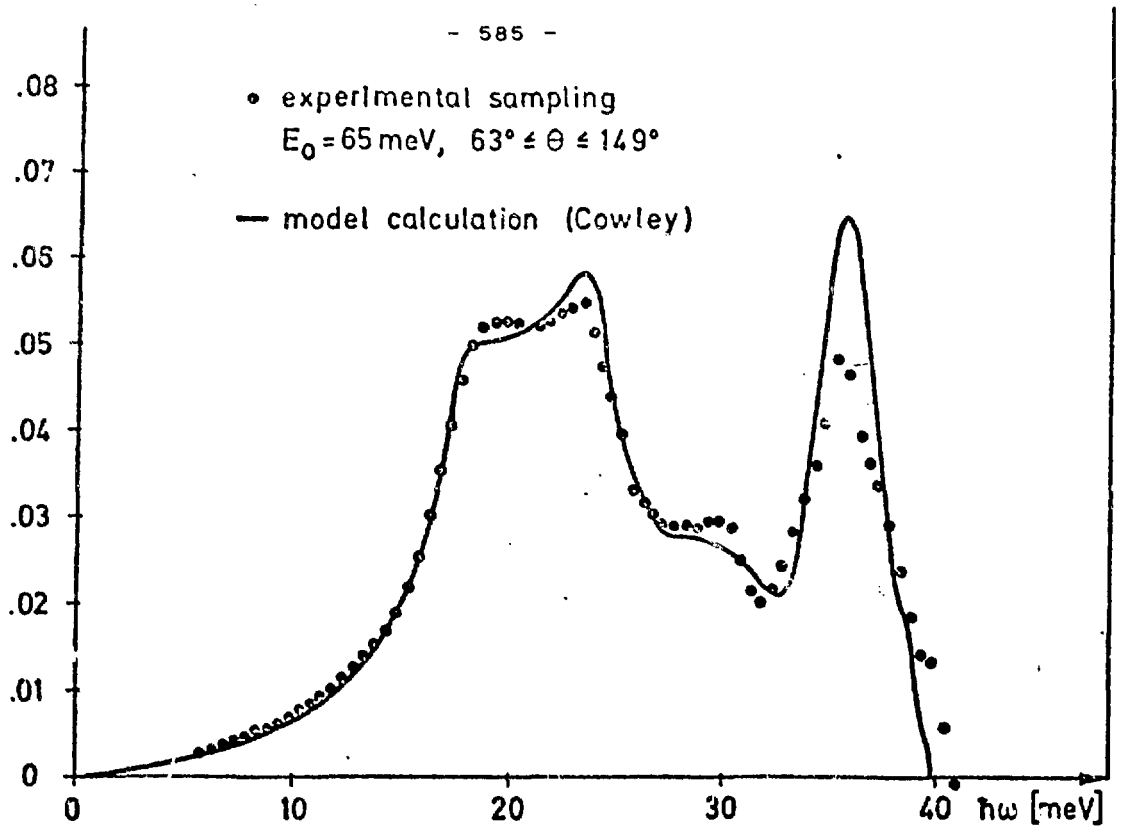

Fig. 10 Phonon Density of States of Aluminum T= 297 K

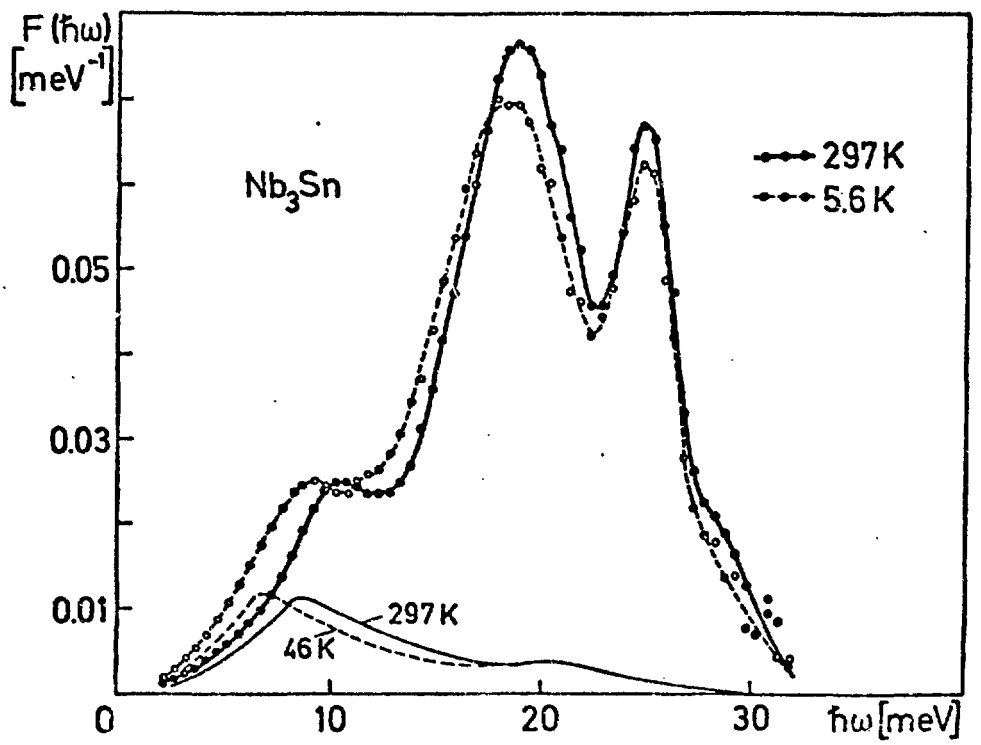

Fig.11 Phonon density of states of the hightemperature superconductor Nb_3Sn

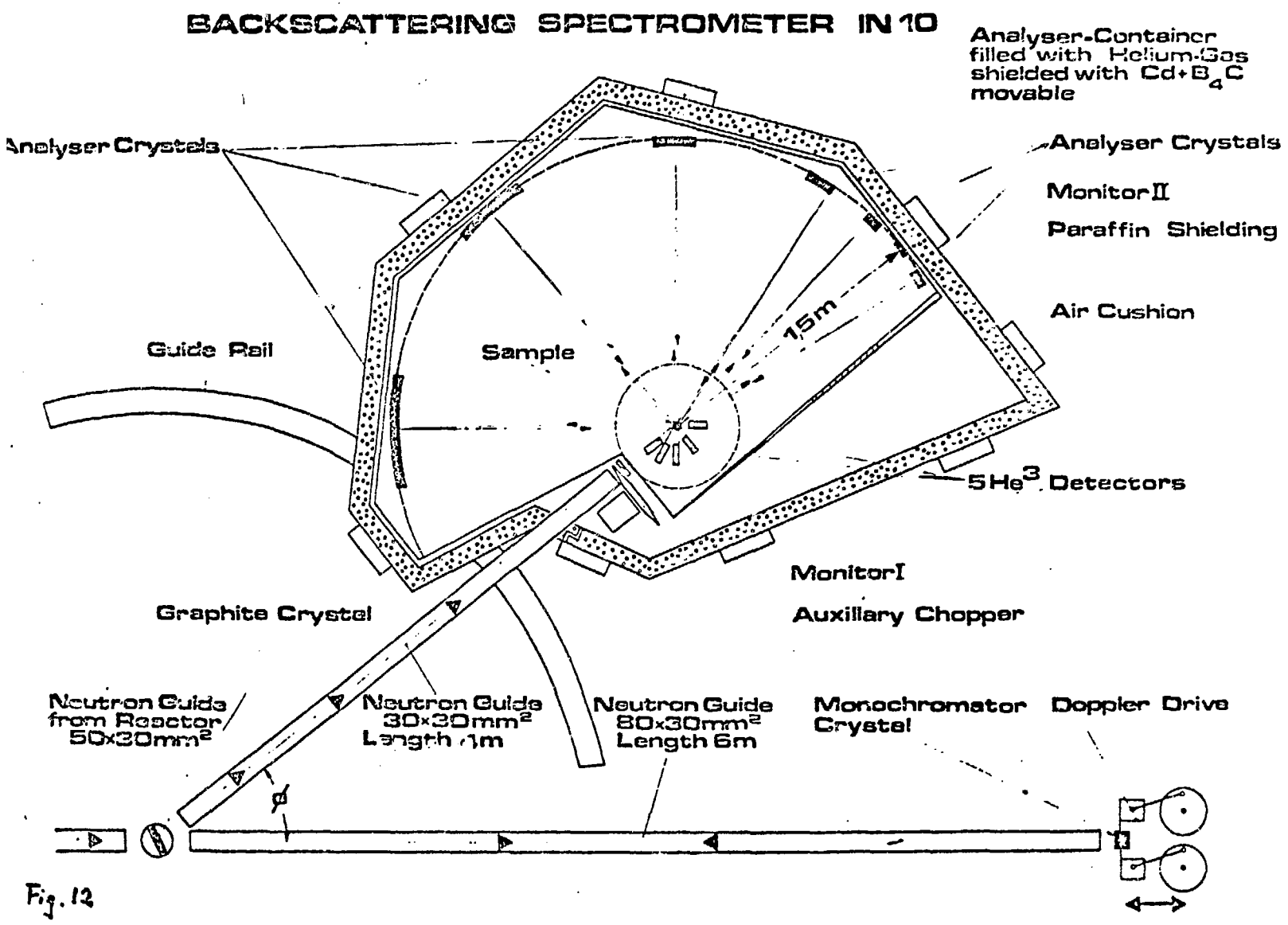
BACKSCATTERING SPECTROMETER IN 10
Analyser-Container filled with Helium-Gas shielded with Cd+B4C movable
Analyser Crystals
Analyser Crystals
Monitor II
Paraffin Shielding
Air Cushion
Guide Rail
Sample
1.5m
5 He3 Detectors
Monitor I
Auxillary Chopper
Graphite Crystal
Neutron Guide from Reactor 50x30mm²
Neutron Guide 30x30mm² Length 1m
Neutron Guide 80x30mm² Length 6m
Monochromator Crystal
Doppler Drive

Fig. 12

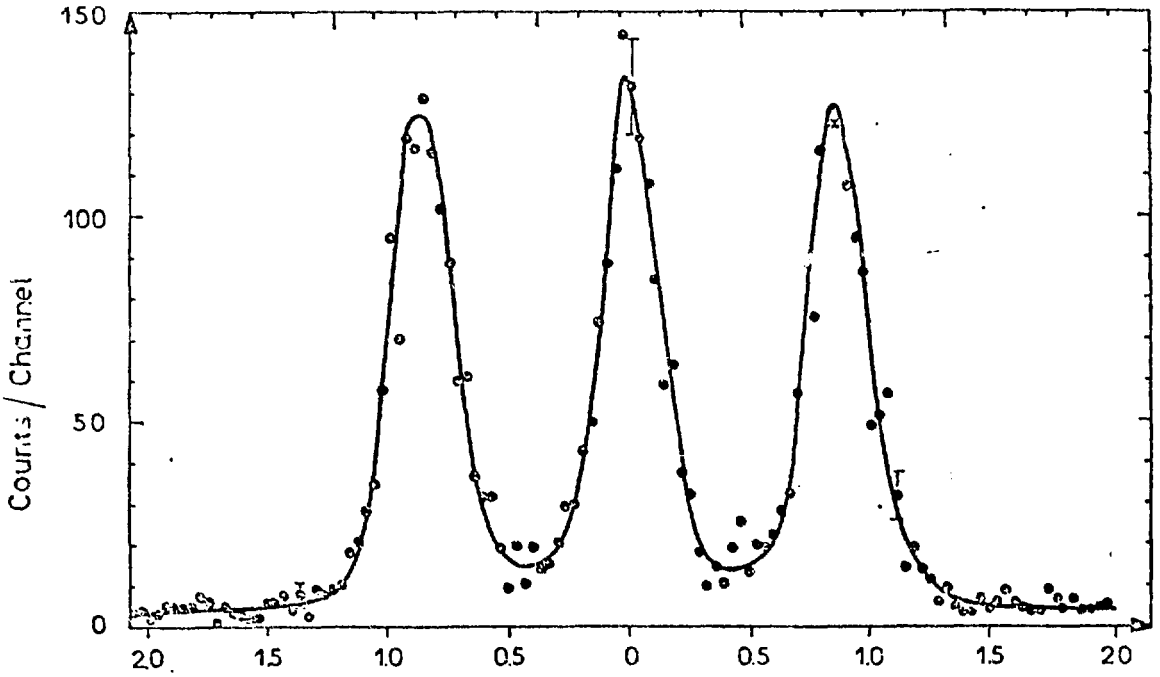

Fig. 13 Hyperfine Splitting in Cobalt fcc

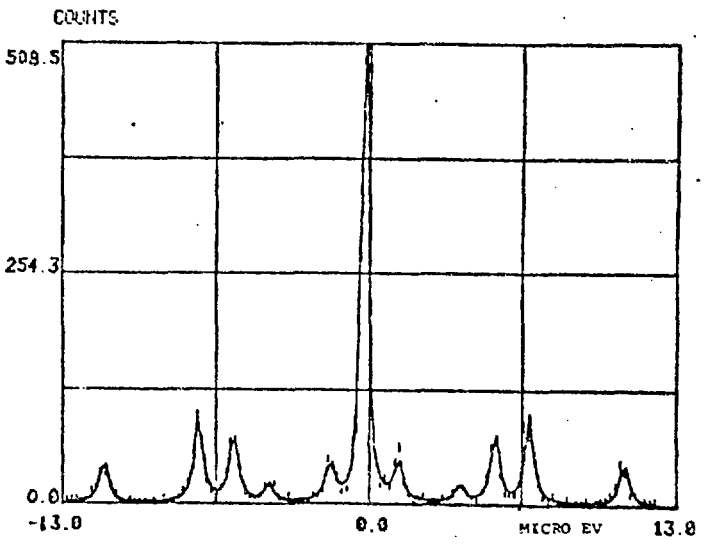

Fig. 14 Spectrum of tunneling modes in NH_4ClO_4 at 4 K (A. Heidemann[28])

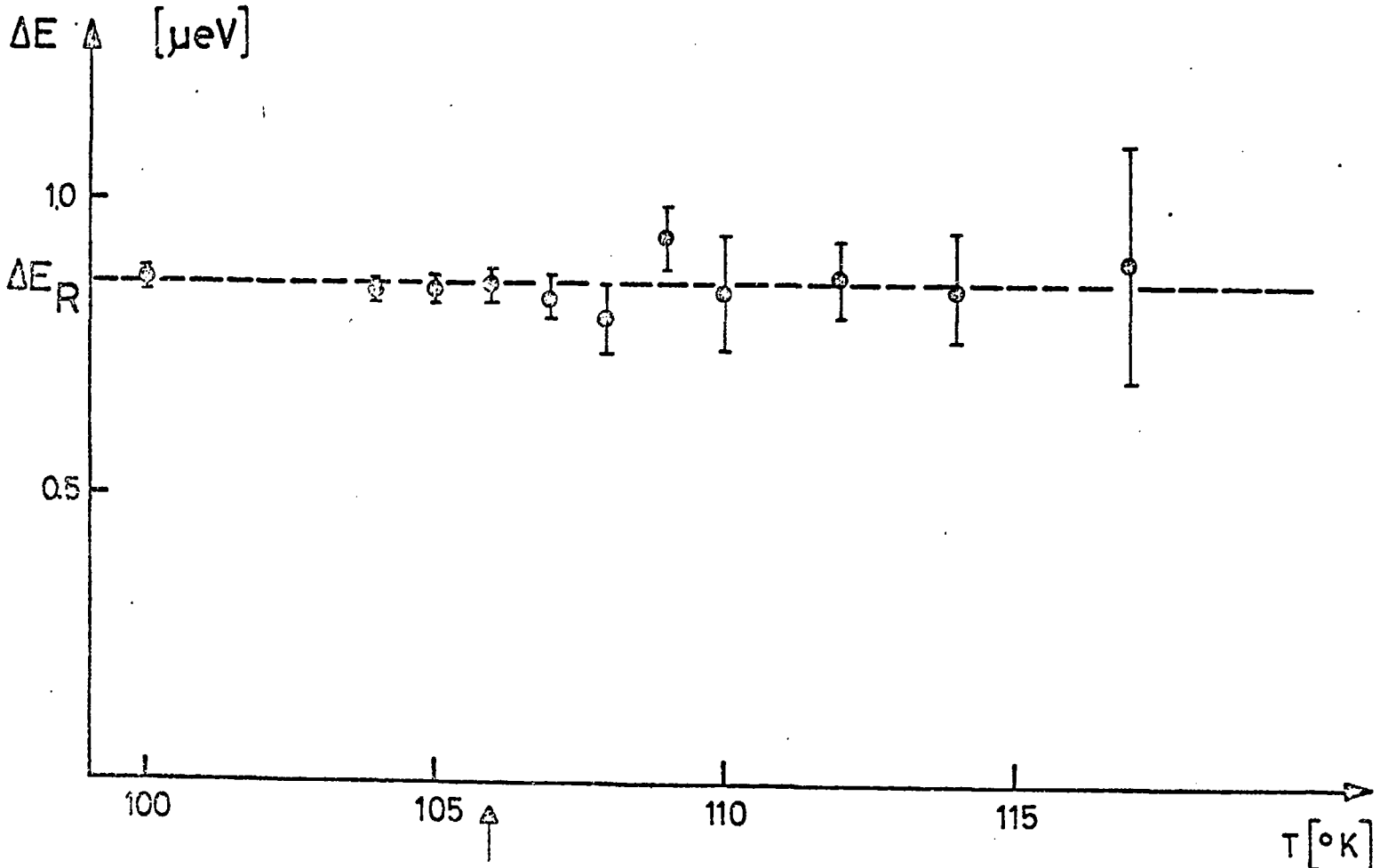

Fig.15 Energy width of the central peak in $SrTiO_3$ (Alefeld et al.[31])

configuration of the 100 split interstitial (fcc -lattice)
atomic displacements in a(100) plane

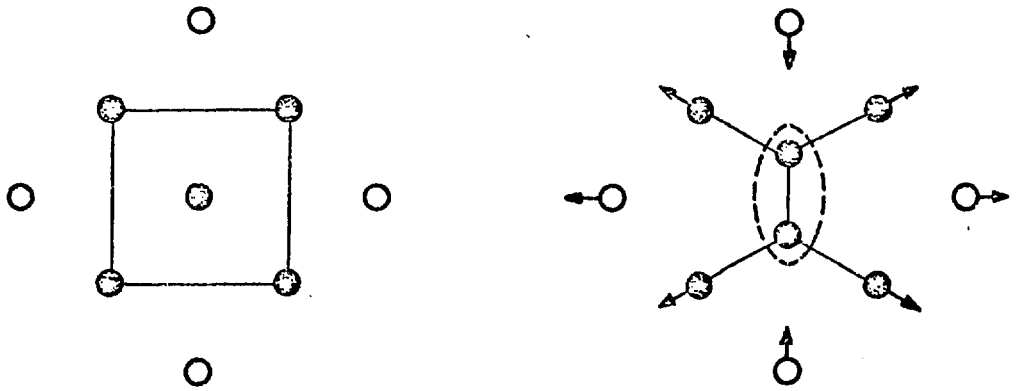

resonant vibrations

E_g' $\frac{\omega}{\omega_{max}} \approx 0.16$

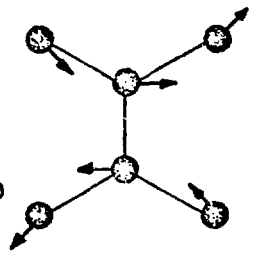

A_{1u} $\frac{\omega}{\omega_{max}} \approx 0.16$

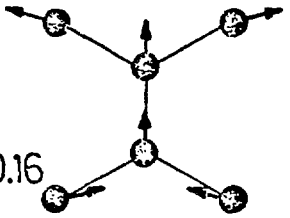

Fig. 14

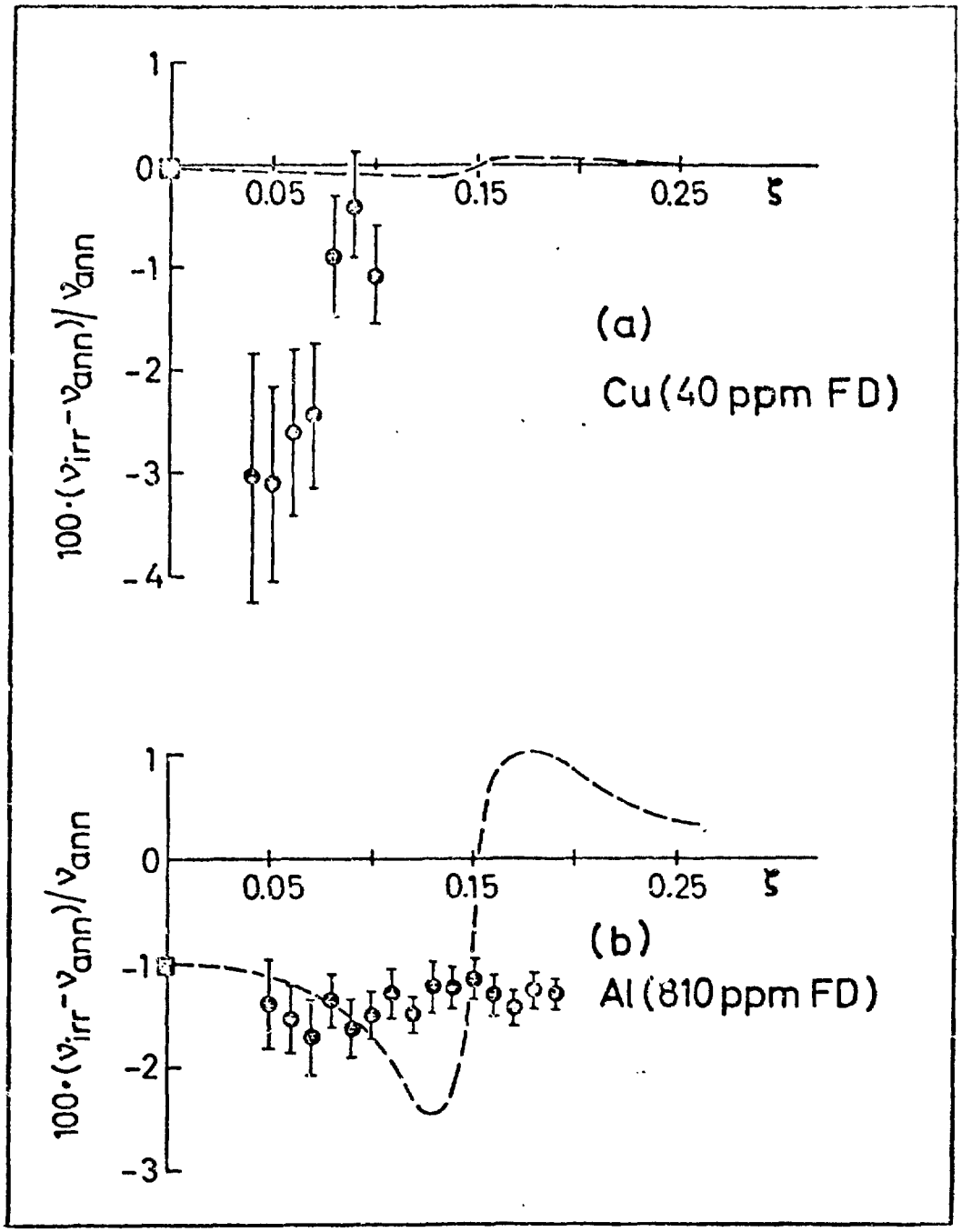

Fig. 17 *Deviations of phonon frequencies of the TA branch in a) irrad. Cu and b) irrad. Al from the frequencies in the not irradiated samples.*

MI.' - SOLID STATE ASPECTS OF NEUTRON PHYSICS RESEARCH - W. Gläser (Technische U., München, Germany)

Newstead (Brookhaven):

Why is the density of phonon vibrations, which you showed in one of your figures, the same at 300°K and 6°K?

Gläser:

Well, actually the anomalicity is a rather small effect if you go from high temperatures to lower temperatures, since the force constants are not changing very much. But the point which I tried to make here is that the change went in the other direction. Normally going to lower temperatures the forces should be stiffer, and this means the density of states should shift to higher frequencies. Now it goes the other way around -- or one could put it in other words -- the negative Grüneisen constant which shows up here is really an indication of the electron-phonon interaction.

Wigner (Princeton Univ.):

What you had was not the density of phonons but the density of states, and that is what confused us.

Gläser:

It's the phonon density of states. That's what one calls the frequency distribution of phonons, for example.

Wigner:

But there are no phonons with high frequency at 6°K.

Gläser:

I'm sorry, this is really the available states for phonons and the tunnel occupation is corrected out. One has to introduce the Bose factor to obtain the occupation of the density.

Wigner:

Thank you very much. I have another question: I was very surprised that the annealed inhomogeneity in $Al_{0.92}$ $Zn_{0.08}$, as shown in your Fig. 7, was greater in the annealed state than in the quenched state.

Gläser:

Yes, this is really the problem of Guinier-Preston zones in these alloys. The cross section went up, and it was not the number of precipitates I had shown, just the total cross section for neutrons transmitting through this sample. And this is changing as it depends on the size of the precipitates in the sample.

Wigner:

But isn't it true that some of the inhomogeneities disappear because the atoms wander from interstitial positions to vacancies if you are annealing?

Gläser:

Yes, but in this particular case of the aluminum-zinc alloy, the experimental studies show that the annealing temperature obviously was not high enough to get these precipitates to vanish.

Wigner:

But the annealing -- what effect did this have?

Gläser:

This really depends on the alloy that you start with, but in this case it seems that you still get clusters of considerable size at the temperatures which have been used here.

Wigner:

May I just ask -- I don't know the solubility of zinc in aluminum. Is it soluble to that extent, or is this a precipitate?

Gläser:

What we have seen here was really a precipitate.

Wigner:

I see, and zinc is not 8% soluble in aluminum at normal temperatures?

Gläser:

That really depends on the treatment of the alloy.

Wigner:

Is it soluble or not?

Gläser:

No.

Chen (M.I.T.):

I would like to ask a question about this sampling technique in coherent scattering. In order to have sampling in the Brillouin zone, don't you have to know the force constant of the metal or, equivalently, you have to know the dispersion curve before you can calculate the cross section to compare with experiment?

Gläser:

No. It has been shown by several theoretical papers that the sampling near the Brillouin zone is really equivalent to what you would call the incoherent approximation. You know in coherent scattering you always get the incoherent approximation if you go to high momentum transfers. But the physical point is not so much the high momentum transfer, but it is really that in scattering one covers a sufficiently large part of the reciprocal lattice. This, of course, can also be achieved with lower momentum transfers if you select your

scattering geometry properly. This is essentially what has been done in the sampling technique.

Chen:

I'm concerned about constructing the initial state from the coherent scattering data. It's a powder sample, right?

Gläser:

Right.

Chen:

So you do it over many q's, then you calculate essentially from this state and then compare with the experiment?

Gläser:

Yes.

Chen:

But then you have to have a certain kind of force model to do that.

Gläser:

No. If you do the experiment on a system, like aluminum for example, you get essentially the density of states by adding up all the inelastic scattering at different angles and this has to be corrected, of course, for multi-phonon processes and perhaps for multiple scattering. But if one can do the correction, and this can be done in a self-consistent way, for example, starting from the experimental data, you don't need any additional information. It's different if you go to more complicated systems like Nb_3Su, where you know one introduces a partial density of states; then one has to introduce, of course, an additional model to make these corrections in order to go from the partial density of states to the density of states of the system.

Coughlin (Harvard Univ.):

Is this small angle scattering method suitable for the actual detection of inhomogeneities in unknown substances i.e., verification of physical separations of complicated unknown substances, e.g., detection of mixtures?

Gläser:

Well, in principle it is possible to detect unknown inhomogeneities in solids by this method. It depends, of course, whether you get contrast in the system for neutrons; whether the scattering lengths or the density of these different regions in the solids, is really different to make any contrast, like Dr. Schoenborn told us about in biological systems. If this is known, then the rest is just calculation from the angular distribution of the scattered intensity.

4:00 P.M., THURSDAY, JULY 8, 1976, IN OLNEY 150

MAIN SESSION MJ

Chair: F. Ajzenberg - Selove (University of Pennsylvania, U.S.A.)

:00 p.m., Thursday, July 8, 197[illegible] in Sidney [illegible] Invited Paper: Session MJ1

NEUTRON ASTROPHYSICS

R. A. Smith

Department of Physics, SUNY at Stony Brook

Stony Brook, New York 11794

RÉSUMÉ

The composition and structure of neutron stars and their relationship to served properties of neutron stars are reviewed.

ABSTRACT

The nominal role of neutron stars is to spin, pulse, and gradually slow down. rtunately, some neutron stars display behavior which provides considerably more formation about their structure. The structure, in turn, reflects the equation state of dense matter in its ground state; not long after the supernova plosion, the bulk of the star is cold (by local standards) and in hydrostatic uilibrium. As a result, the structure and properties of a neutron star are termined by the equation of state and its mass. Neutron stars conventionally are vided into five regions: surface, outer crust, inner crust, liquid interior, and re. For each region, the composition and contribution to the observable aspects stellar structure are reviewed. Since different models of the nucleon-nucleon teraction imply stellar models with very different structures, some inferences interaction models may be drawn. At present, equations of state appreciably iffer than that using the Reid potential seem to be in accord with observations.

NEUTRON ASTROPHYSICS

R. A. Smith

Department of Physics, SUNY at Stony Brook

Stony Brook, New York 11794

RESUME

The composition and structure of neutron stars and their relationship to observed properties of neutron stars are reviewed.

ABSTRACT

The nominal role of neutron stars is to spin, pulse, and gradually slow down. Fortunately, some neutron stars display behavior which provides considerably more information about their structure. The structure, in turn, reflects the equation of state of dense matter in its ground state; not long after the supernova explosion, the bulk of the star is cold (by local standards) and in hydrostatic equilibrium. As a result, the structure and properties of a neutron star are determined by the equation of state and its mass. Neutron stars conventionally are divided into five regions: surface, outer crust, inner crust, liquid interior, and core. For each region, the composition and contribution to the observable aspects of stellar structure are reviewed. Since different models of the nucleon-nucleon interaction imply stellar models with very different structures, some inferences on interaction models may be drawn. At present, equations of state appreciably stiffer than that using the Reid potential seem to be in accord with observations.

INTRODUCTION

Interactions of neutrons with nuclei play an important role in several aspects of astrophysics: nucleosynthesis, supernova explosions, and neutron star structure. In the latter field, we are at the stage of relating observed properties of neutron stars to specific features of the structure of neutron stars. I want to explain how this connection is made and how theory and observation can be used to place qualitative restrictions on the equation of state (EOS) of dense matter.[1)]

Neutron stars are formed in supernova explosions when the central core of 1.4 $M_\odot$ ($1\ M_\odot = 2.0 \times 10^{33}$ g) of a much heavier normal star reaches an evolutionary stage where it can no longer support itself against gravitational collapse by thermal and electron degeneracy pressures. As the core collapses, the matter is compressed by a factor as large as 10^7 until the internal pressure rises sufficiently and halts the infall. In the process, which lasts only milliseconds, a large fraction of the electrons in the star are captured by protons in the nuclei and the matter undergoes some radical phase changes. The neutrinos released serve to blow off the surrounding stellar material. When the dust settles (rather fast, since $GM/R^2 \approx 10^{14}$ cm/s^2), there remains a neutron star with a radius of roughly 15 km, a rotational frequency of perhaps 10^3 rad/s, and a surface dipolar component of the magnetic field around 10^{12} gauss.

Astrophysical objects identified as neutron stars fall into two classes: pulsars and pulsating X-ray sources in binary systems. The model of a pulsar is

shown in fig. 1. Radio-frequency electron synchrotron radiation beamed out from a

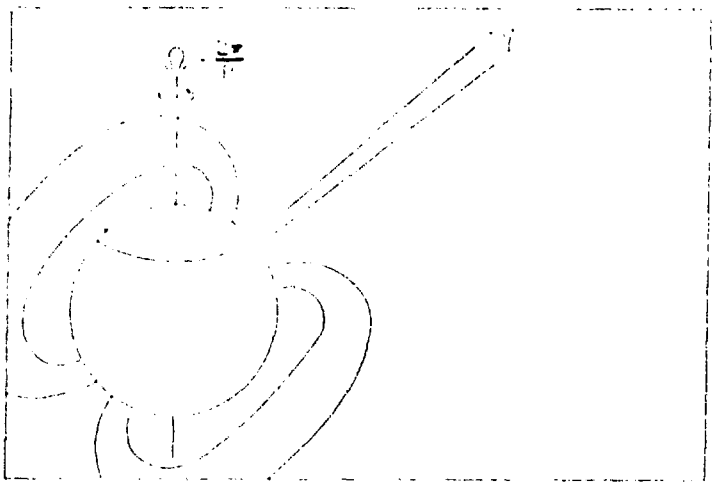

Fig. 1. A pulsar model.

region near the magnetic pole is observed once every rotational period as the beam passes through the observer's line of sight. In the pulsating X-ray sources, the geometry is similar but the X-rays are attributed to the accretion of matter from the (normal) companion star. The identification of these objects with neutron stars is based primarily on the short and highly stable period, P[2] (33 ms to 4 s, measured to as many as 12 significant figures). For pulsars, another very useful measured quantity is the slowdown, $\dot{P}$, typically 10^{-15} s/s . The slowdown results from the loss of angular momentum to the electromagnetic radiation generated by the rotating dipole field. If all stars slowed down uniformly, one could learn very little about their structure. However, due to the rapid rotation of the stars, the stars are somewhat oblate. It is this distortion combined with the rigidity of the crust that makes inferences about the stellar structure possible. Let me first describe the composition and structure of a typical star. A much more detailed discussion may be found in the recent review by Baym and Pethick[3].

STRUCTURE AND COMPOSITION

Calculation of most properties of a neutron star is vastly simpler than for a normal star because energy transport plays a negligible role in determining hydrostatic equilibrium. Most of the star is at a temperature which although hot by normal standards (10^7-10^8 ^{o}K) corresponds to an energy (10^{-3} - 10^{-2} MeV) which is much smaller than the local Fermi energy. A cross-section of a neutron star is shown in fig. 2. The star is naturally divided into five zones of different composition. The basic feature as one proceeds in from th surface is an increase in density with a concomitant average decrease in proton to neutron ratio, corresponding to increased capture of electrons by protons in the original collapse. The penalty for large electron densities is simply the kinetic energy of an electron at the top of the Fermi sea which is much larger than the kinetic energy of a massive nucleon at the same density.

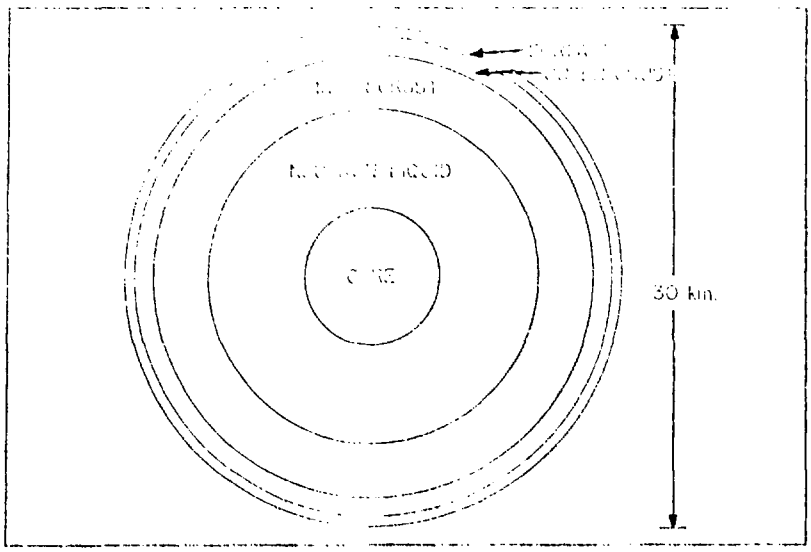

Fig. 2. The regions of a neutron star.

The surface layer. typically 10 m thick, is the only region where the magnetic field and temperature play an important role in determining the phase of the matter. The temperature is no longer small compared with Fermi energies and the presence of very strong magnetic fields profoundly changes atomic structure and molecular binding[4]. While these effects may be important in understanding details of the radiation mechanism, they have no influence on the bulk properties of the star. By the time the density rises to 1×10^6 g/cm^3, the temperature and magnetic field have little effect on the properties of matter and we may consider the material to be in its ground state at the given density.

The outer crust, about 1 km thick, consists of a solid crystalline lattice surrounded by an electron gas. At low densities, the bcc lattice sites are occupied by ^{56}Fe nuclei; this nuclear species minimizes the nuclear energy and the lattice minimizes the Coulomb energy. As the density increases, the matter becomes more neutron rich in discrete steps, due to a playoff between electron capture by protons (saving a large electron Fermi energy) and nuclear structure effects. The optimal nuclear N and Z are assumed to have been reached during the hot supernova explosion. The result is concentric shells of matter, each with a different nuclear species. The nuclear species flits from ^{56}Fe to ^{62}Ni through a total of 12 different nuclei ending at ^{118}Kr.[5] Most of these nuclei are too neutron rich to exist in vacuum, but their energies may be calculated quite well from semi-empirical models.

At 4.3×10^{11} g/cm^3, it becomes energetically favorable for neutrons to "drip" out of the nuclei and lower their kinetic energy enough to compensate for the loss of nuclear attraction. In this inner crust region, on the order of 5 km thick, there is a lattice of nuclei surrounded by neutron fluid and an electron gas. With increasing density, neutronization progresses and the nuclear species continues to change in discrete steps. Here one really has interactions of neutrons with nuclei! Calculations of the equilibrium phase are sensitive to the Coulomb energy and the surface energy of the nuclei in the neutron fluid. The

best calculations indicate that the number of protons per nucleus does not exceed 50, although there may be as many as 1500 neutrons per unit cell.[6] Due to the lattice structure, the material supports shear; the shear modulus depends sensitively on the charge per nucleus and the density of nuclei. The pressure comes mainly from electron degeneracy at low densities and from the neutron fluid at higher densities. Finally, at a density on the order of 2×10^{14} g/cm^3, the lattice disappears smoothly, leaving a pure fluid.

The liquid zone consists primarily of neutrons with a small admixture of protons and electrons. The EOS, which relates the pressure to the energy density, is accessible only through microscopic calculations, which fall into two major categories. In one method, an interaction model for the nucleon-nucleon (NN) interaction, constrained to fit the NN scattering phase shifts, is used as the basis for a many-body calculation of the ground state of neutron matter. In the other, one extrapolates from a model which reproduces the binding energy, saturation density, and symmetry energy of nuclear matter. Ideally, one would use a framework which satisfactorily accounted for both phase shifts, nuclear matter, and general field-theoretic ideas about the NN force. Considerable progress is being made in this direction, but we are not yet at that stage. The neutron liquid is probably superfluid at low densities in $^1S_0$ pairs and at higher densities in $^3P_2$ pairs; protons present are superconducting. At still higher densities, the core repulsion of the NN interaction restores the neutrons to a normal phase. At some density, Λ and Σ hyperons may be present, but they probably have relatively little effect on the equation of state.

The core region, if present in a star, describes some exotic phase of dense matter. A number of possibilities have been advanced, including a π^- condensate[7], a π^0 condensed solid[8], an abnormal state[9], and quark matter[10]. Recent calculations[11] of π^- condensation indicate that onset may be at around twice nuclear matter density. The greatest effect of this phase would be enhanced cooling by antineutrino emission at the early cooling stages of the neutron, including the possibility of an antineutrino burst.[12] The π^0 condensed solid is a possibility and would be interesting primarily because of possible observational consequences of a solid core. The existence and detailed properties of this phase depend sensitively on the interaction model. Simple models of an abnormal state seem to be inconsistent with normal matter[13]. Recent preprints[14,15] suggest that quark matter, at least in the MIT bag model[16], does not appear at neutron star densities.

MODELS

For calculating stellar models, one needs the EOS for matter in its ground state at densities ranging from 10 to 10^{16} g/cm^3 (energy density/c^2). General relativity's (GR) importance in determining the structure of the star is expressed entirely through the equations of equilibrium; GR plays no part in calculations of the EOS. In order to be specific, I will discuss three different EOS's. The first is the EOS of non-interacting neutrons, in which pressure arises solely from neutron degeneracy. This EOS is stiffer than a realistic EOS up to about nuclear matter density, due to the binding energy of nuclei, and much softer at higher densities, due to the absence of short-range repulsion. The other two EOS's roughly span the range of stiffness currently advocated. The second EOS has the general features discussed above under structure and composition and relies on microscopic calculations of neutron matter based on the Reid soft-core phenomenological potentials[17]. The third is similar, but with neutron liquid properties based on a tensor interaction model (TI) of the NN interaction which

includes isobars due to Green and Haapakoski[18]. In this model[8] there is the possibility of a phase transition to a solid π^0 condensed core. As is apparent from fig. 3, these EOS's do span a wide range.

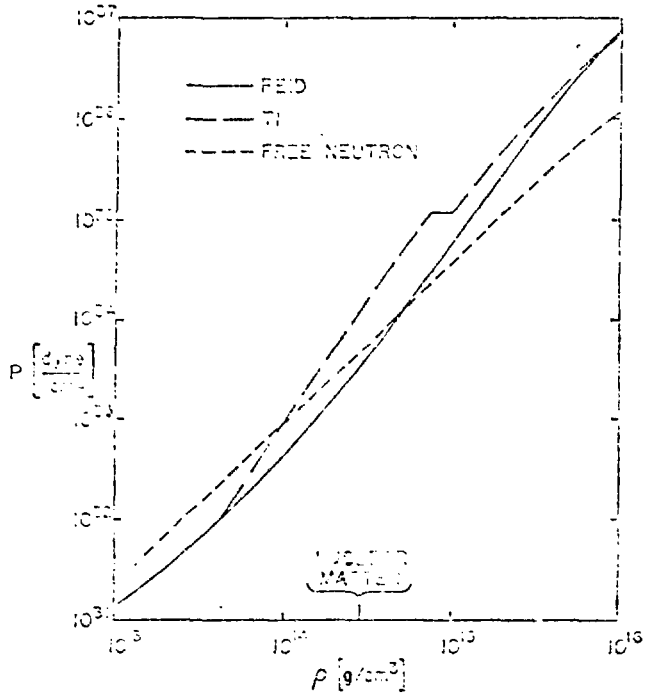

Fig. 3. Representative equations of state.

For a given EOS, a star is specified completely by the central density. Fig. 4 shows this relationship between mass and central density for the three EOS's.

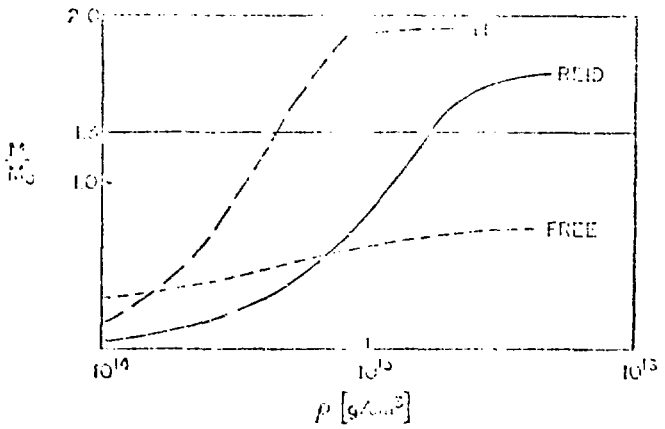

Fig. 4. Mass versus central density.

Only a certain mass range is stable against radial perturbations. Stars with higher central densities than those shown would collapse given the slightest of inward pushes. This mass range is not appreciably affected by the slow rotational speeds observed in pulsars and X-ray sources. Direct and indirect estimates of some neutron star masses are in the range 1.3 - 1.4 $M_\odot$. This indicates that the central repulsion of the NN interaction is important, because non-interacting neutrons only support a star up to .7 $M_\odot$. Unfortunately, other equations of state are not sufficiently distinguished by the maximum mass criterion.

In fig. 5, I have plotted profiles for 1.3 $M_\odot$ Reid (R) and TI stars.

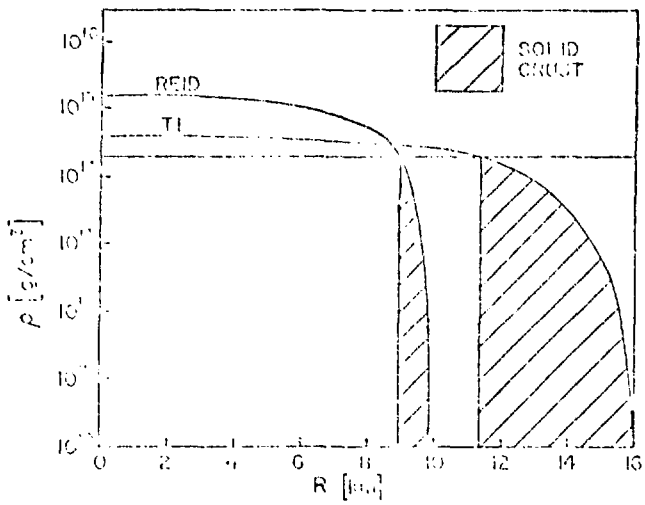

Fig. 5. Density profiles.

Comparison of the two shows that the overall size and proportions of the various regions of the star are quite sensitive to the EOS. These structural differences show up quite strongly in two parameters which describe the influence of rotation on the energy of a star. Following Baym and Pines[19], the total energy due to rotation of a neutron star with angular momentum L is expressed as

$$E_{rot} = L^2/2I + A\epsilon^2 + B(\epsilon-\epsilon_o)^2 \quad , \tag{1}$$

where the ellipticity ϵ is defined as the fractional increase of moment of inertia of the crust due to rotation. The parameters A and B give respectively the decrease in gravitational binding energy and the strain energy built up in the crust due to deformation away from an ellipticity ϵ_o. The first term is simply the rotational kinetic energy and I is the moment of inertia. For the 1.3 $M_\odot$ R (TI) star, A = 9.4(5.2) x 10^{52} erg, B = 0.5(14.2) x 10^{48} erg, and I = 0.93(2.09)x10^{45} g cm^2. Qualitatively, these may be easily understood from the larger size and crustal volume of the TI star. The actual ellipticity of the star is one which minimizes E_{rot} for a given ϵ_o. In liquid core stars, which I will discuss here, B is generally much less than A. The parameters A and B have been related to observables in two situations: starquakes and stellar wobble.

STARQUAKES

In 1969, the rotational frequency of the Crab pulsar suddenly increased by $\Delta\Omega_\infty/\Omega = 9 \times 10^{-10}$, as illustrated in fig. 6. This event is interpreted as a

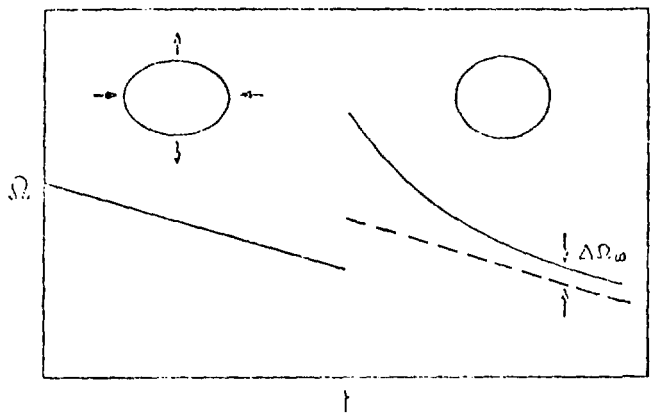

Fig. 6. The change in Ω.

starquake. As the star slows down, it would like to reduce its ellipticity but is hindered by the rigidity of its crust. Ultimately, sufficient strain builds up in the crust that it fractures and reduces its ellipticity enough to relieve some of the stress. The decrease in ellipticity means a decrease in moment of inertia, so the star speeds up. The time between quakes in this model depends on A and B and is given roughly by

$$t_q = -(\Delta\Omega_\infty/\Omega^2\dot{\Omega})(2A^2/BI) \quad , \tag{2}$$

where $\dot{\Omega}$ is the average rate of change of frequency between quakes and $\Delta\Omega_\infty$ is the change in rotational frequency attributable to the quake after internal torques bring the entire star back into corotation. The amount of the initial increase in angular velocity of the crust which is ultimately lost in speeding up the neutron fluid depends on the ratio of crust to neutron liquid moments of inertia.

The term A^2/BI in 1.3 $M_\odot$ stars is very sensitive to the EOS; the R and TI models give t_q of 2100 years and 10 years, respectively. For the Reid EOS to produce a return period of 10 years would require a .5 $M_\odot$ star. This light a star is contraindicated by evolutionary considerations of the pre-supernova star and the non-observation of significant amounts of processed heavy elements in the Crab nebula[20]. A second frequency change observed in 1975 gives a t_q of 6 years. The TI model is also consistent with the observed ratio of crust to liquid moments of inertia.

Three speedups of appreciably larger magnitude have occured for the Vela pulsar ($\Delta\Omega/\Omega \sim 2 \times 10^{-6}$). These, however, seem inconsistent with crustquakes because of the large time required for strain to build up between quakes. It is possible that these represent quakes in a solid core, but determination of this possibility requires a better understanding of what actually goes on inside a star

with a solid core.

WOBBLE

The matter in a liquid neutron star would never be far from having axial symmetry, since non-symmetric perturbations would be damped rather quickly. An isolated neutron star, liquid at formation, would not likely have the opportunity to build up appreciable distortion. However, a neutron star in a binary system is subject to additional torques which could maintain and build non-symmetric perturbations. In this case, rotation does not just involve the symmetry axis; there is in addition a wobble. Fig. 7 shows a body symmetric about an axis which is not parallel to the instantaneous rotation axis.[21]

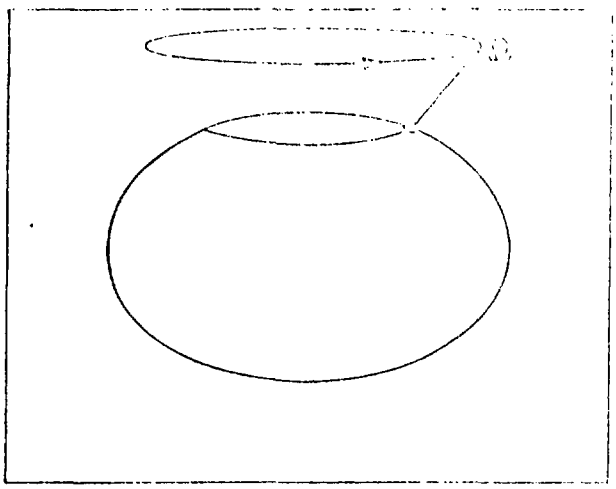

Fig. 7. The mechanics of wobble.

In the star's reference frame, the instantaneous axis of rotation precesses slowly about the body symmetry axis as shown. One neutron star is an attractive candidate for a wobbling star.

The neutron star Her X-1 is a pulsating X-ray source in a binary system. Its rotational period is 1.24 s, the orbital period is 1.7 days, and ingenious methods have been used to determine the mass as $1.33 \pm .13\ M_\odot$.[22] The really interesting feature of this object is the multiple periodicity of the observed X-ray flux[23]. There is a 1.24 s period, corresponding to the rotation of the star, a 1.7 day period of eclipses, as the neutron star disa-pears from sight behind its companion, and a 35 day periodicity which represents an overall on/off cycle. These are represented schematically in fig. 8.

The X-rays are produced as matter originating on the companion star is accreted onto the surface of the neutron star. Brecher[24] suggested that this 35 day periodicity could be interpreted as stellar wobble. Subsequent work by Pines and Shaham[25] shows how the wobble period is related to the same structure parameters A and B involved in the quake theory. The accretion of matter produces a torque on the neutron star. If the wobble in turn couples to the accretion mechanism, then the wobble can be driven and sustained by accretion.

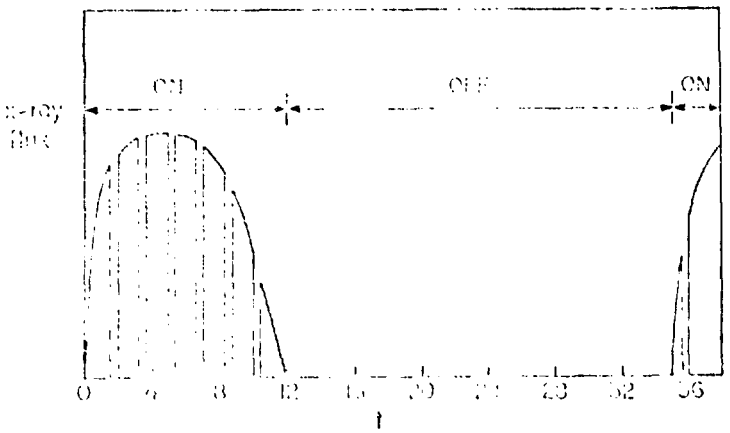

Fig. 8. The X-ray flux for Her X-1.

Accepting this point of view, we can study the relationship between the rotational and wobble periods[25] for different equations of state,

$$P_r/P_w = (3/2)(B/A)\,\epsilon_o. \tag{3}$$

Since the mass is determined, the EOS determines A and B. The ellipticity ϵ_o, at which there would be no strain, is then known. This places a lower bound on the rotational speed at the time of formation, where there was no strain, and on the critical strain angle, which determines how much strain can be withstood before fracture occurs. For the R (TI) model, the rotational speed at formation is at least 4600 (320) rad/s and ϵ_o is .05 (.001). The Reid star was then formed at at least a third of its breakup speed, which is quite unlikely. The critical strain angle is also larger than is comfortable in comparison with terrestrial materials which have similar binding mechanisms. The TI model presents no problem in either respect. This is a further indication that the EOS should be stiff at high densities, at least appreciably stiffer than the Reid potential EOS.

CONCLUSIONS

I have tried to indicate how the composition and properties of the ground state of baryonic matter are determined over the entire density range found in neutron stars. The uncertainties in calculating the EOS at higher density correspond to neutron star models which look and behave quite differently. The comparison with the behavior of real neutron stars points to the need for a quite stiff equation of state in the density range around or above nuclear matter density. In the future, we can look for better calculations of dense matter and presumably for new and interesting observations. In the meantime, we can work for a more thorough understanding of the current observations.

ACKNOWLEDGEMENTS

Much of the work described here was performed in collaboration with Prof. V. R. Pandharipande and Prof. D. Pines. This work has been supported in part by NSF grant MPS 74-22148 and US ERDA grant E(11-1)-3001.

REFERENCES

1) V. R. Pandharipande, D. Pines, R. A. Smith, Ap. J., 1976, in press.

2) T. Gold, Nature, 1969, 218,731.

3) G. Baym, C. Pethick, Ann. Rev. Nucl. Sci., 1975, in press.

4) R. Cohen, J. Lodenquai, M. Ruderman, Phys. Rev. Lett., 1970, 25, 467.

5) G. Baym, C. J. Pethick, P. S. Sutherland, Ap. J., 1971,170,299.

6) J. W. Negele, D. Vautherin, Nucl. Phys., 1973, A207, 298.

7) R. F. Sawyer, D. J. Scalapino, Phys. Rev, 1973, D7, 953.

8) V. R. Pandharipande, R. A. Smith, Nucl. Phys.,1975,A237,507.

9) T. D. Lee, Rev. Mod. Phys., 1975, 47, 267.

10) J. C. Collins, M. J. Perry, Phys. Rev. Lett., 1975, 34, 1353.

11) G. E. Brown, W. Weise, to be published.

12) W. S. Pallister, A. W. Wolfendale, Nature, 1974, 251, 485.

13) V. R. Pandharipande, R. A. Smith, Phys. Lett., 1975, 59B, 15.

14) G. Baym, S. A. Chin, to be published.

15) G. Chapline, Jr., M. Nauenberg, to be published.

16) A. Chodos, R. L. Jaffe, K. Johnson, C. B. Thorn, V.F. Weisskopf, Phys. Rev., 1974,D9, 3471.

17) R. V. Reid, Ann. of Phys., 1968, 50, 411.

18) A. M. Green, P. Haapakoski, Nucl. Phys., 1974,A221, 429.

19) G. Baym, D. Pines, Ann. of Phys., 1971, 66, 816.

20) W. D. Arnett, Ap. J., 1975, 195, 727.

21) H. Goldstein, Classical Mechanics (Addison Wesley, Reading, 1965),p. 162.

22) J. Middleditch, T. Mast, J. Nelson, 1974, 7th Texas Symp. on Rel. Ap., Dallas

23) R. Giaconni, Proc. of 16th Solvay Conf. on Phys. (Editions de l'Univ. Bruxelles), 1974.

24) K. Brecher, Nature, 1972, 239, 325.

25) D. Pines, J. Shaham, Phys. Earth Plan. Int., 1972, 6, 103.

MJ I - NEUTRON ASTROPHYSICS - R. A. Smith (State Univ. of New York, Stony Brook)

Newstead (B.N.L.):

What is the scenario for a neutron star to turn into a black hole? Could you also summarize the current status of experimental evidence for the existence of black holes?

Smith:

So far as turning a neutron star into a black hole, it is necessary to either have a neutron star spinning fast enough at formation so that when it slows down it no longer is able to support itself, or, if you have a neutron star which is accreting mass from another star, sufficient mass must be transferred for the neutron star to become unstable. Now, typical mass transfer rates, I think, are on the order of 10^{-7} solar masses per year, so you'd expect this to take a fairly long time. As far as observational evidence for black holes, I'm perhaps not the best person to talk about this. The main thing one needs to know here is the maximum mass that a neutron star can have, because then if one can make a strong statement that the mass of an object like Cyg X-1 has to be greater than six solar masses, then one can reject it as a neutron star. Now the primary thing that comes in here is the density up to which you are willing to accept the calculated equation of state. A number of years ago Ruffini et al. did a calculation which assumed that up to some density the equation of state was known and beyond that the pressure was limited only by causality, so that the speed of sound in the material shouldn't be greater than c. This gave a maximum mass of 3.2 solar masses. But the exact point at which you do this matching is the critical thing. I've heard people at conferences doing this matching low enough to give up to eight solar masses as the maximum mass. So at that point it's more or less a matter of opinion, I think. The highest mass I've been able to calculate with the stiffest equation of state I've generated is 2.6 solar masses.

Malik (Indiana University):

If I understand correctly, in order to get the equation of state one has to solve the many-body problem in dense matter. Would you care to comment on how good these calculations are, because one would like to know this before we throw away the Reid potential. Also, I am unaware of the reasons for using the T.I. model. How does one choose the parameters for this potential?

Smith:

Let me go back to the first part on the methods used. The equations of state here were based on variational calculations, dating back before 1973. The Reid interaction E.O.S. was based on an LOCV calculation done by Pandharipande. Now in comparison with Bose systems, the LOCV method gives slightly higher energy per particle than Monte Carlo calculations, as demonstrated in the "homework problem." And so the Reid calculation would correspond to a stiffer equation of state than one would obtain by Monte Carlo means. That's for the Bose case and you can't immediately generalize to the Fermion case: but I think the many-body calculations are getting fairly good. Things are less critical for neutron matter than for nuclear matter because you aren't so sensitive to cancellation. So I think probably the many-body theory is reasonable at least,

and small alterations to the energy would make little difference. Secondly, as far as the tensor interaction model goes, I wouldn't want to place too much emphasis on this particular model, even though I did work on it. The main thing is to show that there is a range of equations of states available in the literature, and to show what happens when going from one extreme, the Reid, to the other extreme, the T. I. model. Actually, the T. I. model is based on the NN interaction of Green and Haapakoski who fitted the ^1S_o phase shifts using a tensor interaction which coupled NN states to NΔ states and then back down again. This was generalized to extend to other partial waves as well.

Khanna (Chalk River):

At one time one used to talk of a neutron solid. Is the term "neutron solid" not legitimate any more ?

Smith:

This depends again on your interaction model. If you take the Reid potential, then essentially everybody agrees now that neutron matter does not crystallize using either the Reid central interaction or including the tensor part of the interaction, at least at densities that you would find in neutron stars. Now in the TI model you have an enhanced tensor coupling because the coupling between NN states and NΔ states is a tensor interaction. By arranging the particles with their spins in appropriate directions, Pandharipande and I were able to obtain a neutron solid. But the transition density to this solid state is very sensitive to the interaction model and the many-body calculations. This is what I referred to as a π^0 condensed solid; I do not think other kinds of solids exist, but this one could exist.

Khanna:

But if we assume that we have an interaction model which can give us a solid, can it explain all the known features of the neutron stars ?

Smith:

One thing I didn't mention in the talk was the quake history of the Vela pulsar: there have been three of them, and they're much larger in magnitude than the Crab quakes. It may be possible to explain them on the basis of the quake of a solid core. But one problem there seems to be that enough energy would be released in a core quake that you would expect to see the surface temperature of the star rise enough to be visible in the X-ray region, and yet one hasn't seen X-rays from the Vela pulsar during the quakes. Unless you have an efficient mechanism for getting rid of energy, for example a π-condensate, then it's hard to say at this point.

Golub (Sussex Univ.):

All these potentials you're talking about are two-body forces. Yet some years ago there was some work which indicated that many-body forces would be very important. Do you know if anything's come of that or did it just die by the wayside?

Smith:

Well, they certainly could be. Essentially, what that would give you is a free

parameter, because aside from fitting nuclear matter, the other thing you have to go on is phase shifts, and many-body forces don't show up in the scattering problem.

Golub:

So not much has been done, you would say?

Smith:

Well, if we got desperate trying to fit the properties of nuclear matter we might have to turn to something like that. But other than that it's just introducing a free parameter at this point, I think.

Invited Paper: Session MJ 2

4.45 p.m., Thursday, July 8, 1976

NEUTRONS AND ENERGY*

J. L. Fowler

Oak Ridge National Laboratory and the University of Tennessee

*Research sponsored by the U. S. Energy Research and Development Administration under contract with Union Carbide Corporation.

RÉSUMÉ

Speakers at the conference on "Nuclear Cross Sections and Technology" (1975) have identified the nuclear physics pertinent to the energy problem. The neutron physics discussed, which was most of the pertinent nuclear physics, can form the basis for research programmes not only important for energy but which also contribute to the fundamental understanding of nuclei.

ABSTRACT

In an article "Nuclear Physics and Energy" to be published in "Physics Today" J. L. Fowler and W. W. Havens, Jr. have summarized the nuclear physics required for the energy problem. Measurements in neutron physics constitute the major needs from nuclear physics. There is a large economic pay off for precision in the cross sections needed to optimize the design and operation of power reactors. In particular, there is a pressing need for accurate standards to determine neutron flux at all energies from thermal and 14 MeV. The R matrix formalism has shown that some of the reactions used to measure neutron flux are questionable standards. Since the safety of fast reactors depends to a large extent on doppler broadening of narrow neutron resonances in the keV energy region much more basic research is required on neutron resonances and in particular on multi level effects. The management of long lived radioactive waste arising from build up of transuranium isotopes in power reactors requires the measurement of the neutron cross sections of these highly radioactive isotopes. The design of fusion reactors producing 14 MeV neutrons demand detailed knowledge of the interaction of fast neutrons with nuclei in the thermal to 14 MeV energy range.

NEUTRONS AND ENERGY*

J. L. Fowler

Oak Ridge National Laboratory and the University of Tennessee

ABSTRACT

In an article "Nuclear Cross Sections and Nuclear Energy" to be published in "Physics Today" J. L. Fowler and W. W. Havens, Jr. have summarized the nuclear physics required for the energy problem. Measurements in neutron physics constitute the major needs from nuclear physics. There is a large economic pay off for precision in the cross sections needed to optimize the design and operation of power reactors. In particular, there is a pressing need for accurate standards to determine neutron flux at all energies from thermal to 14 MeV. The R-matrix formalism has shown that some of the reactions used to measure neutron flux are questionable standards. Since the safety of fast reactors depends to a large extent on doppler broadening of narrow neutron resonances in the keV energy region much more basic research is required on neutron resonances and in particular on multi-level effects. The management of long lived radioactive waste arising from build up of transuranium isotopes in power reactors requires the measurement of the neutron cross sections of these highly radioactive isotopes. The design of fusion reactors producing 14 MeV neutrons demand detailed knowledge of the interaction of fast neutrons with nuclei in the thermal to 14 MeV energy range.

*Research sponsored by the U. S. Energy Research and Development Administration under contract with Union Carbide Corporation.

INTRODUCTION

The 1975 international conference on "Nuclear Cross Sections and Technology"[1] was concerned primarily with the the role of nuclear physics for nuclear energy[2], although it dealt also with nuclear physics for other technologies. A review of the Proceedings of the Conference reveals that neutron physics makes up the largest fraction of nuclear physics required for energy technology.[2] The subject matter of this paper, therefore, is the role of neutron physics in energy.

Even for operating nuclear power plants additional measurements in neutron physics can have large economic payoffs.[3] For example, in a typical light water reactor, if improved precision of neutron data can decrease the uncertainty of neutron multiplication near the end of the life of fuel elements by 1%, it could reduce the required compensating adjustment of the enrichment of the ^{235}U fuel with a savings of the order of $2,000,000 per reactor. Similarly an uncertainty in neutron cross sections that leads to an uncertainty in power peaking in fuel elements which limits the power output by 1% may cost the utility company $1,000,000 annually in replacement power. In these typical power reactors, neutron capture by fission products such as ^{135}Xe, ^{147}Pr, ^{148}Pm, and ^{148}Nd reduces the reactivity so that compensation by enriched fuel must be made. A 1% error in the capture cross section of the fission products results in a .09% uncertainty in neutron multiplication which amounts to $200,000 in equivalent ^{235}U enrichment. Thus for the present generation of nuclear power plants reliable neutron cross sections certainly pay off.

NEUTRON FLUX STANDARDS

Precision in neutron measurements depends on precision in neutron flux determination and neutron flux standards. Yet papers presented a year ago

at the "Conference on Nuclear Cross Sections and Technology" cast considerable doubt on the reliability of cross sections of several nuclear reactions, such as the $^{6}Li(n,\alpha)^{3}H$ and the $^{10}B(n,\alpha)^{7}Li$ reactions, commonly used as neutron flux standards. A 1975 summary of neutron standards[4] showed the $^{6}Li(n,\alpha)^{3}H$ cross section, which is known to ∿1% at one keV and to 2-3% at 10 keV, was uncertain to 15-20% around the 246 keV resonance [Fig. 1]. The $^{10}B(n,\alpha)^{7}Li$ cross section measurements also deviated by about 15-20% in the 200 keV energy region[4]. Recent work of G. P. Lamaze,

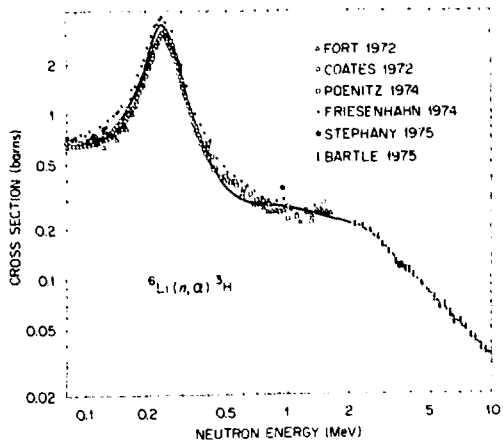

Fig. 1. The $^{6}Li(n,\alpha)T$ cross section as of March 1975. Cross sections from .08 MeV to 2.0 MeV[5,6,7,8,9] are from a review by A. D. Carlson.[4] Cross sections from 2.0 MeV to 10 MeV are measurements of C. M. Bartle.[10]

O. A. Wasson, R. A. Schrack and A. D. Carlson,[11] has reduced the uncertainties in the $^{6}Li(n,\alpha)^{3}H$ and $^{10}B(n,\alpha)^{7}Li$ cross sections considerably, but independent confirmations of these important cross sections by new measurements are required. Between 2 and 10 MeV Bartle,[10] using the associated particle method to determine neutron flux, has measured the absolute $^{6}Li(n,\alpha)^{3}H$ cross section

to ∿3% [Figure 1]. The energy spread (f.w.h.m.) varied from ∿100 keV at 2 MeV to ∿500 keV at 9.7 MeV. He recorded the $^{6}Li(n,\alpha)^{3}H$ reaction products, induced in a $^{6}LiI[Eu]$ scintillator by neutrons from the $D(d,n)^{3}He$ reaction, in coincidence with associated ^{3}He particles.

The application of multilevel, multichannel R-matrix theory to the analysis of the nuclear reactions of light elements has proven to be well suited to evaluate standard cross sections.[12] In the case of the ^{7}Li system the R-matrix analysis not only included data on the $^{6}Li(n,n)^{6}Li$ and $^{6}Li(n,\alpha)^{3}H$ reactions but it also included differential and polarization data on $^{4}He(t,t)^{4}He$ scattering. For the most recent $^{6}Li(n,\alpha)$ results[11] the R-matrix analysis indicates there is still an uncertainty of ∿5% in the $^{6}Li(n,\alpha)^{3}H$ cross section in the 100-700 keV range. Limited data on the various reaction channels of the ^{11}B system restricts the application of the R-matrix analysis in evaluation the $^{10}B(n,\alpha)^{7}Li$ and the $^{10}B(n,\alpha')^{7}Li^{*}$ reactions. Some of the resonant level assignments in the literature are inconsistent. Further measurements on the ^{11}B system are necessary.

In the multi-MeV neutron energy range the most accurate neutron cross sections are those for n,p scattering, but a limitation on their accuracy is the lack of firm experimental information on the differential cross sections for forward scattering of neutrons above ∿10 MeV.[4] At 14 MeV, for example, a proton recoil telescope measurement of neutron flux by detection of forward scattering of protons is uncertain by ∿1% depending upon whether or not the n,p differential cross section is peaked in the C. M. system at forward scattering angles for neutrons. Thus, for practical purposes as well as for theoretical reasons it is urgent that the basic (n,p) differential cross sections be measured in the 10-30 MeV energy range.

The (n,p) total and differential scattering cross sections enter into the calculations of the efficiencies of organic scintillators. Because of their high efficiencies (∿5%) and the fast rise time of their pulses these scintillators are extensively used as MeV neutron detectors. Their calculated efficiencies, however, differ from efficiencies measured with absolute neutron flux determined by associated particle techniques by ∿10%.[13,14] Fig. 2. These differences[14] are present whether one calculates

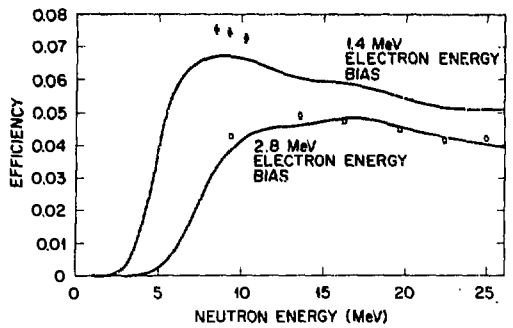

Figure 2. Central efficiency of a 2.5 cm thick 10 cm dia. NE213 scintillator[13] compared with average efficiency calculated with analytical computer program.[15]

the efficiencies with an analytical computer program [15] or a Monte-Carlo efficiency code.[16] Furthermore these differences, in general, can not be corrected by a normalizing factor, as is evident in Fig. 2, so that the calculated efficiences can not be depended upon for relative measurements at different energies. Since organic scintillators are so often used as secondary standards for MeV neutrons, more effort should be put into improving the efficiency calculations.

LIGHT WATER POWER REACTORS

As mentioned in the introduction precision in neutron cross sections at thermal energies can have considerable economic impact on the operation

of light water power reactors. In particular, the capture cross sections of fission products become important near the end of the life of a set of fuel elements, and knowing these cross sections accurately saves a great deal of money in designing the fuel cycles.[3]

In an uranium thermal reactor initially the higher actinide isotopes, ^{239}Pu, ^{241}Pu, ^{242}Am, ^{244}Am, ^{243}Cm, ^{245}Cm are present in relatively small quantities. These actinide isotopes however, are continually being formed through multiple neutron capture starting with ^{238}U and are continually being destroyed through fission. Thus the inventory of these highly radioactive isotopes becomes stabilized at a value several times the quantity produced in the first fuel cycle. They constitute the major portion of the long lived (>1000 years) radioactive waste from a ^{235}U-^{238}U fission reactor. Managing this waste has become one of the central problems in the application of nuclear energy.

To adequately evaluate various schemes for disposing of actinide waste requires better data on their fission and capture cross sections for both thermal and fast neutrons energies (Th to 14 MeV). At the higher energies (n,2n) and (n,3n) cross sections are important. Since some of the actinides are extremely radioactive, special techniques have to be devised to obtain the nuclear data required. For example, in order to measure the fission cross section of ^{245}Cm and ^{243}Cm with their intense α activity, J. W. T. Dabbs et al designed a fission chamber which allows much better discrimination against α particles than is possible with a conventional fission chamber.[17] This is accomplished by depositing the fissionable material on a convex spherical surface and using a concentric spherical surface of slightly larger radius as the ion collector. The outer electrode limits the path of an alpha particle emitted tangentially to the inner surface and thereby discriminates against the longer range alpha particles compared to fission fragments. With the

chamber coated with 10 μg of 30-year ^{243}Cm, which emit 10^7 alphas per second, the background counts due to alpha pileup above the fission fragment bias setting was less than one count per minute. Using the time-of-flight facility of Oak Ridge National Laboratory's Electron Linear Accelerator, Dabbs et al[18] have investigated the fission cross section of ^{243}Cm with preliminary results shown in Fig. 3. Fig. 3b, which gives the response of

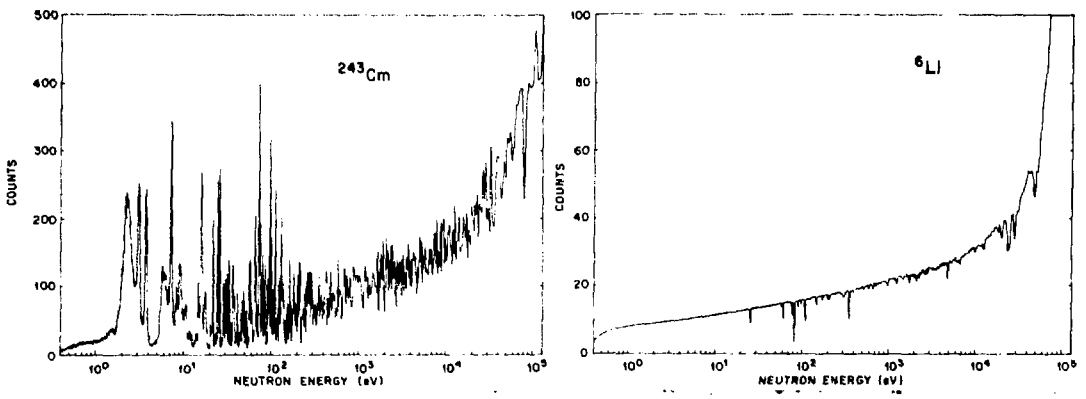

3a 3b

Figure 3. Ten meter time-of-flight measurement of fission of ^{243}Cm. $^{6}Li(n,\alpha)$ results give neutron fluxes for reducing ^{243}Cm data to fission cross sections.[18]

a $^{6}Li(n,\alpha)$ detector, allows a neutron flux determination for the ^{243}Cm fission data in Fig. 3a.

FAST BREEDER REACTORS

The development of the plutonium fast neutron breeder reactors is at the stage thermal neutron reactors were a decade or so ago. Starting off

with the best microscopic neutron data file such as ENDF/B III or IV the reactor engineer designs a series of simulated critical assemblies which give him bias factor corrections which account for the combined errors of the nuclear data and of the analysis method. Measurements with a large number of mockups of critical assemblies allow an evaluation of the uncertainty in the ratio of a particular experimental parameter to that calculated.[19] For the 250 megawatt (MWe) PHENIX Reactor, the French hold that this integral approach is adequate for design purposes. J. Y. Barré et al[20] claim the results obtained during the PHENIX startup (critical mass, power distribution, control rod, reactivity coefficients and shielding) and during one year of normal operation (reactivity loss during burn up) prove the validity of the integral approach to reactor design.

In the case of a fast reactor transient, the doppler coefficient of reactivity is one of the major contributors to the safety of the system. In a ceramic fuelled [PuO_2 and UO_2] fast reactor the doppler effect is the only mechanism that yields an immediate negative reactivity feed back.[19] The negative temperature coefficient from the ^{238}U doppler effect arises principally as a consequence of self protection at neutron capture resonances in ^{238}U. The neutron intensity at an energy of a capture resonance is reduced by the capture process as well as by resonant scattering. Increased temperature of the ^{238}U following an increased power production in the reactor broadens the resonance through thermal motion of the ^{238}U atoms. This reduces the self protection at the ^{238}U capture resonances and increases the loss of neutrons due to capture. Fewer neutrons are then available to carry on the chain reaction so that the power level of the reactor decreases. A great deal of experimental and theoretical work has gone on to show the doppler coefficient is negative.[21] It is now known definitely that in any fast breeder composition of interest the negative

^{238}U doppler coefficient will completely dominate other components of the doppler effect (that due to fission, for example).

The doppler coefficient must be sufficiently negative to more than compensate for all possible positive temperature coefficients such as that due to coolant voids. In a large sodium-cooled fast reactor a void near the center due to boiling of the sodium adds to the reactivity of the reactor.[21] It does this by shifting the neutron energy spectrum toward higher energies where there is relatively more fission than capture and by reducing slightly the effect of capture of neutrons in the sodium coolant. Sodium voids near the outer region of the core, however, increase the neutron leakage and thus tend to reduce the reactivity. Since the very important negative doppler coefficient depends on neutron resonances of all elements likely to be in a fast reactor, much more experimental and theoretical study must go into the treatment of multi-level resonant effects.[22] The doppler broadening of neutron resonances should also be investigated from the point of view of a solid state physicist concerned with vibrations of atoms in solids.

There are a number of cross sections which have considerable impact on the performance of the Liquid Metal Fast Breeder Reactor (LMFBR), and for which the present data are inadequate.[19] Neutron capture and inelastic scattering cross sections of ^{238}U need to be measured more accurately because the breeding performance of the LMFBR is very sensitive to these cross sections. Recent measurements from the University of Lowell on the angular distribution of neutron scattering for the first three states of ^{238}U indicate the importance of such experimental data.[23] The value of $\bar{\nu}$, the number of neutrons per fission of ^{252}Cf, which is uncertain to ~2% has to be pinned down, since this is the standard for the determination of ν for the actinides, in particular the isotopes ^{237}Np, ^{242}Cm, ^{244}Cm, ^{241}Am

and ^{243}Am. These nuclei, as mentioned earlier, are of considerable importance to studies of radioactive waste management and disposal. Furthermore the neutron source strength in the LMFBR is related to the buildup and burn-up of these transuranium elements.[19] Since some of the alloys, which have been developed for fuel cladding and which show relatively low radiation damage, have a substantial Ni content (26-44%),[19] more precise neutron cross section data on the Ni (n,γ), Ni(n,p) and Ni(n,α) reactions are required.

The Nuclear Regulatory Commission of the U.S.A. regards nuclear reactor safety as the key item in considerations of the feasibility of power reactors. In the case of light water reactors twenty years of experience with thermal power reactors and many decades of experience with the technology associated with steam power plants has enabled a Reactor Safety Group, under Norman Rasmussen, to realistically evaluate the probability of accidents and therefore the risk to the general public from commercial thermal nuclear power plants.[24] Since there is a very limited experience with fast reactor power systems, the evaluation of their risks is considerably less certain than that from thermal reactors.

In some ways the sodium cooled fast reactor is fundamentally safe. The sodium coolant is near atmospheric pressure well below its boiling point and has excellent heat transfer properties. There is, however, considerable concern with regard to some other characteristics of a fast reactor. The core in its normal state is not necessarily in its most reactive configuration, so that in the case of a core melt down reactivity may be added from fuel or fuel cladding relocation or from coolant voiding.[21] The course a melt down accident might take depends upon a large number of variables and thus the prediction of the effects of a melt down requires

detailed knowledge of a number of physical phenomena: heat flow, the behavior of materials at high temperatures, the hydrodynamics of the coolant and the molten core material, as well as the neutronic characteristics of the relocated fuel of the core. Although at present the determination of the probable configuration of core material following melt down is so uncertain that nuclear data with large errors are adequate;[20] nevertheless, as the technology of fast reactors develops more precise nuclear data will be required to bring the safety analysis of fast fission power reactors to the level of the recent analysis of the safety of thermal fission power reactors.

Since the status of nuclear data and calculational techniques is such that one has to go through integral experiments for fast reactor design,[20] innovations in reactor concepts are greatly inhibited. Indeed E. P. Wigner in commenting on the significance and accomplishments of the 1975 conference on "Nuclear Cross Sections and Technology"[25] deplored the lack of new ideas even "crazy new ideas." In the fast breeder reactor field he found only one really new proposal. L. H. Tang[26] suggested the incorporation of a removable "moderation jacket" between the inner ^{238}U blanket and the fast neutron core. By optimizing the rate of capture of neutrons by ^{238}U to produce ^{239}Pu this concept could decrease the fuel cycle time by 15 - 35%. While the present cross section data are adequate to indicate merit for this idea, more precise data and calculational techniques are necessary to carry out the design of a practical safe breeder incorporating this idea in order to compare the advantages of this reactor with the presently planned Pu breeding reactors.

THERMAL BREEDING REACTORS

Fuel breeding takes place in a thermal breeder reactor through capture of thermal neutrons by ^{232}Th to form ^{233}U.

$$^{232}Th(n,\gamma)^{233}Th \xrightarrow[22\ min]{\beta^-} {}^{233}Pa \xrightarrow[27\ days]{\beta^-} {}^{233}U$$

According to recent evaluations the value of thermal η^{233}, the number of fission neutrons per neutron absorbed for ^{233}U, as measured directly is 2.30 ± 0.01.[27,28] This is large enough to ensure thermal breeding at least theoretically. But η^{233}, calculated from the average value of neutrons per fission, ν^{233}, is some 1% lower than that given by direct measurements. This discrepancy is attributed to the uncertainty in $\bar{\nu}$ for ^{252}Cf which is the standard for neutrons per fission measurements. Since $(\eta^{233} - 1)$ must exceed one in order to allow for at least one neutron to be captured in ^{232}Th to renew the fuel with neutrons left over to take care of neutron leakage and capture in structural material and coolant, the precise value of η^{233} is of prime importance.

The light water breeder reactor (LWBR) being developed by the Bettis Atomic Power Company is in many respects a conventional pressurized water reactor, but with the core redesigned to operate on the ^{232}Th-^{233}U cycle. As it is conceived it has a low breeding ratio, perhaps such that it just breaks even, that is, it just produces enough ^{233}U fuel to satisfy its own need and to compensate for chemical loses in fuel reprocessing.[29] Thus it requires strict neutron economy. To satisfy this requirement a zirconium alloy, Zircaloy 4, has been developed with low neutron capture cross section to clad the ^{233}U and the ^{232}Th. The designers need accurate data for the capture cross sections of all the materials in the reactor, in particular ^{232}Th, ^{233}U and Zr, as well as data on the capture cross sections of the products of the chain reaction such as fission products and the 27 day ^{233}Pa involved in the ^{232}Th-^{233}U chain.

Thermal reactors moderated and cooled with D_2O or cooled with He gas eliminate neutron capture by hydrogen in H_2O and thereby improve neutron

economy, which makes them attractive as breeders. Elimination of fuel cladding in gas cooled reactors, such as those being developed in the United Kingdom, France, and the United States has the possibility of reducing fuel reprocessing cost to the extent that they might run economically as ^{232}Th - ^{233}U breeders. The addition of BeO to the fuel enhances the neutron economy through the ^{9}Be (n,2n) reaction.[29]

In a fluid-fuel thermal breeder the ^{233}U fuel and the ^{232}Th circulate as a solution, a slurry, or as a molten salt through the active core of the reactor which may be moderated with graphite or BeO. These breeders have a distinct advantage over solid fuel thermal breeders in that the fission products and ^{233}Pa are continually being removed from the high neutron flux region and can be extracted from the fuel stream in a chemical plant associated with the reactor. The ^{233}Pa is allowed to decay to ^{233}U before it is returned to the fuel stream. Preventing capture of a neutron by a ^{233}Pa atom has a double purpose in so far as breeding is concerned. Not only does it conserve the neutrons which would have been captured by the ^{233}Pa atoms but is also prevents the removal of a ^{233}U atom from the fuel chain since the absorption of a neutron by a ^{233}Pa destroys a ^{233}U atom the ^{233}Pa would have formed. Because the margin for thermal breeding is small, the continuous removal of neutron poisons from the reactor has a major effect on the breeding gain. In the Netherlands, the KEMA laboratory is investigating a D_2O slurry concept which uses a homogeneous suspension of spherical $(U,Th)O_2$ particles in the D_2O fluid. In the U.S.A. the Oak Ridge National Laboratory has worked out many of the engineering problems in a molten salt system in which ThF_4 and UF_4 are desolved in a $LiF\text{-}BeF_2$ fuel carrier.[29]

Optimizing the economics of these various types of thermal breeder reactors heavily involves all facets of nuclear engineering in the reactor design as well as advanced chemical engineering in the design of the fuel reprocessing plants. Optimizing the neutron economy in the different designs depends on the nuclear physics of the systems and requires very detailed information on the nuclear processes involved.

For two major problems facing the nuclear energy program, 1) the safeguard problem, and 2) the problem of radioactive waste disposal, thermal breeders have distinct advantages over both light water reactors and fast breeder reactors. T. B. Taylor [30] has pointed out that the fissionable material safeguard problem is simplified for reactors using the ^{232}Th - ^{233}U cycle. In the first place ^{239}Pu is not involved in the fuel cycle. In the second place the reactor fuel ^{233}U contains ^{232}U from the ^{233}U (n,2n) reactions. Since 70 year ^{232}U in its decay chain gives off a number of γ-rays it constitutes "spiking" of the ^{233}U fuel. Handling and shipping ^{233}U fuel requires heavy shielding which together with the radioactive hazard makes diversion of the reprocessed fuel for illegal purposes more difficult than is the case for ^{235}U or ^{239}Pu fuel. Indeed for the fluid fuel thermal breeders, which have their fuel reprocessing plants closely associated with the power reactor, illegal diversion of the fuel by outsiders is all but impossible.

The fissile and fertile materials, ^{233}U and ^{232}Th, in a thermal breeder are some 5 to 6 nucleons removed from ^{238}U, so that continued production of higher actinides through multiple neutron capture is greatly reduced (by factors > 10^6).[31] Consequently, a breeder power system based on the ^{232}Th-^{233}U cycle eliminates many of the

problems of long lived radioactive waste due to actinides. Indeed Raman et al have proposed the ^{233}U-^{232}Th reactor as a burner for the actinide waste from the light water nuclear power system.[31]

FUSION REACTORS

During the last several years magnetic confinement of fusion plasmas has shown such encouraging results that there is optimism with regard to achieving thermonuclear power from d,t plasmas. To be economically feasible, a fusion power reactor operating on the d,t cycle must breed enough tritium fuel to replace that burned in the reactor. This requires that Li be in the blanket surrounding the reactor [Fig. 4]. The 14 MeV d,t neutrons produce tritium through the $^{6}Li(n,\alpha)t$ or the $^{7}Li(n,n\alpha)t$ reactions. Alsmiller et al[32] have calculated the tritium breeding ratio (the ratio of the number of tritium atoms produced per thermonuclear neutron) for three proposed fusion reactor designs and found this ratio to vary from 1.04 to 1.54. While they find that the uncertainty in the $^{6}Li(n,\alpha)t$ cross section (Fig. 1) contributes less than 1% to the uncertainty in the breeding ratio, they find that the uncertainty in the $^{7}Li(n,n\alpha)t$ cross section is somewhat more serious. For the designs with low breeding ratios this latter uncertainty contributes $\sim$2% uncertainty to the breeding ratio, whereas for the designs with high breeding ratio it contributes $\sim$6%. The d,t fusion program, therefore, requires better data on the $^{7}Li(n,n\alpha)t$ cross section from its threshold, 2.8 MeV, to 14 MeV. The uncertainties in the cross section of other elements included in the reactor blanket designs such as C, Be, Al, Ni and F lead to uncertainties of the order of a few percent in the breeding ratio.[32] There is an immediate need for an evaluated file of neutron cross sections relevant to tritium breeding[33] as well as a growing

need for a vigorous program to supply measurements to fill the gaps in knowledge.

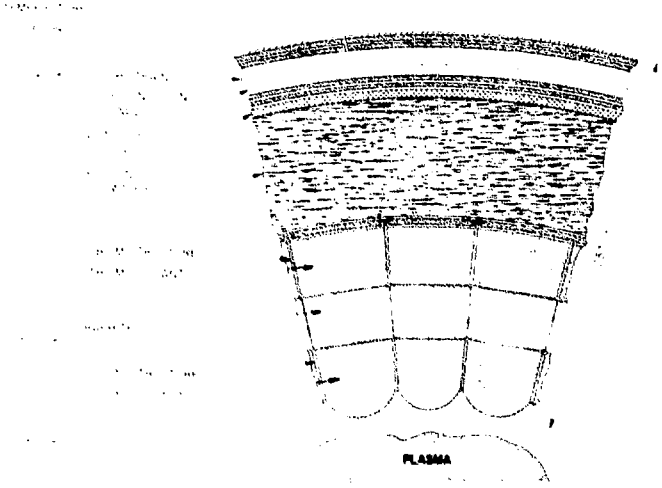

Figure 4. A segment of a blanket and shield region of a fusion reactor. In this design lithium serves both as a coolant and as a tritium breeding medium. Neutrons from the (d,t) plasma are absorbed by the lithium and converted to tritium and heat. Graphite is utilized for neutron moderation and reflection. Niobium provides structural support. Lead and water are used as shielding materials to protect the superconducting magnetic coils from neutrons and gamma rays.

The technical problems of containing a plasma at hundreds of millions of degrees temperature while surrounding the reactor with superconducting coils near 0° are truly formidable (Fig. 4). The blanket which is located between the plasma and the field coils, besides slowing down neutrons from 14 MeV in order to allow for capture in Li to form tritium, also extracts energy from the neutrons and from the $^{6}Li(n,\alpha)t$ reactions. This blanket not only must breed tritium with a breeding ratio greater than one but it must also act as a partial shield for the superconducting coils. In the process of slowing down, neutrons will be inelastically scattered and in some cases will undergo radiative capture, with both reactions leading to secondary γ rays. As much as 30% of the total energy deposited in the blanket can arise from these secondary γ rays and over 90% of the energy deposited in the superconducting magnetic coil system can come from such γ rays.[33] Radiation shielding, therefore, is a crucial problem for the fusion reactor. At present, nuclear data uncertainties limit the possibilities to optimize the shielding in the minimum space between the central reactor and the coils.

Experimental information on secondary γ rays particularly from high energy neutrons is very fragmentary. At 14 MeV radiative capture varies by more than a factor of 10 even for adjacent nuclei, so that systematics of radiative capture cross sections are of little use in predicting cross sections. Systematics of inelastic scattering $(n,n'\gamma)$ cross sections at 14 MeV do not show such rapid variations and are therefore somewhat more useful. The data on such inleastic scattering γ rays, however, are rather sparse.[34] A measurement program to provide a secondary γ ray data base in the one to 20 MeV energy range is strongly recommended to fill the needs of the fusion program. Preliminary results from such a

program have been reported[35].

For a 1000 MWe fusion power reactor the calculated level of induced radioactivity generally is in the 10^9 to 10^{10} curie range.[33] This imposes technological problems for system maintenance, for reactor safety, and for waste disposal, so that the level and characteristics of the induced radioactivity must be known. For (n,2n), (n,p) and (n,α) reactions there is a great deal of data at 14 - 15 MeV and nuclear systematics are such that one can estimate unknown cross sections for nuclei in this energy range to $\sim$30%.[34] Other activation cross sections and those at lower energies cannot be estimated so well from systematics. Use of nuclear models in theoretical calculations can reduce the uncertainties in estimating cross sections to the extent that some engineering preliminary evaluations can be made without the use of experimental information.[36] Of course much experimental information has been incorporated in the models and, as more experimental data comes in, the models will be refined further. Besides activation cross sections the design applications require data on half lives and decay schemes. Measurements of critical cross sections and decay properties should be undertaken immediately.[33]

RADIATION DAMAGE

Technologies involving fast neutrons have revealed serious problems in connection with radiation damage of structural materials.[37] In fast reactors neutron-recoils of atoms of the fuel pins and fuel pin cladding produce vacant lattice sites, an appreciable number of which collect to form voids (probably on impurity gas atoms). These can produce swelling of the fuel pins of $\sim$20% and in a nonuniform neutron flux result in nonuniform swelling. This swelling in stainless steels is a matter of major importance in the development of breeder reactors.

Emperical methods, using Ni ions accelerated with Van de Graaff machines to simulate the void formation due to neutron recoils from Ni nuclei, have facilitated the selection of alloys for further test in the fast neutron flux of a reactor. There are other effects of radiation damage on mechanical properties, such as reduction of ductility and radiation induced creep which must be investigated with fast neutrons.

In a fusion reactor the first wall enclosing the hot plasma [Fig. 4] is expected to be subjected to more radiation damage than has been experienced previously in any nuclear power device, including fast reactors. Besides the surface damage caused by bombardment of particles and radiation from the plasma, there will be considerable volume damage produced by the intense flux of 14 MeV neutrons.[37] The mechanism for radiation damage by high energy neutrons is very poorly understood, and since there is as yet no intense source of 14 MeV neutrons to mock up the flux from a fusion reactor, engineering studies of radiation damage are impractical. It is necessary, therefore, to gain fundamental understanding of this type of radiation damage. Basic studies in the most intense 14 MeV flux available[38] allow a start in the research aimed at this understanding. To satisfy the critical need for more intense neutron sources Armstrong et al[39] have proposed a supersonic jet of deutron gas as a target for a 1.5 A ampere beam of 270 keV tritium ions to produce a 14 MeV neutron flux of $>10^{14}$ neutrons/cm^2·sec. Others propose mocking up the 14 MeV flux with (d,n) neutrons produced by ~30 MeV deuterons on target such as Li[40,41] Here the target problem is somewhat simplified, but much effort has to go into development of a high current high energy accelerator. The required basic understanding of radiation damage by fast neutrons offers immediate challenges to neutron physics as well as to solid state physics.

NEUTRON PHYSICS FOR NON-NUCLEAR ENERGY

Oil well "logging" is perhaps the most prominent application of neutron techniques for non-nuclear energy.[2] The "log" is a continuous recording of the value of some physical parameter as a function of the depth in an oil well drill hole. An instrument package, known as a sonde, is lowered to the bottom of a drill hole at the end of a cable. The cable transmits power to the sonde and signals from it to the surface as the sonde is drawn out of the bore hole. The information carried by the signals is processed and recorded as the "log".

Neutron logging may consist of measuring the scattering of neutrons by the material of the formation through which the sonde is passing. In this case the neutron source is usually a plutonium beryllium source and the scattered neutrons are detected by a counter in the sonde which is well shielded from the source. The counting rate, suitably corrected for the bore hole diamater, rock formation, etc. gives information on the porosity of the formation. A pulsed (d,t) neutron source in the sonde allows a determination of the macroscopic neutron cross section of the formation surrounding the sonde. The main objective of this type of logging is to monitor the chlorine content of the water surrounding the bore hole. In the sonde at a fixed distance from the pulsed source thermal neutrons or capture gamma rays are recorded as a function of time after the pulse. The decay constant of the thermal neutrons so obtained is inversely proportional to the macroscopic neutron cross section of the material in the formation. Chlorine, which has a large capture cross section, reduces the decay constant of the thermal neutrons. This logging method is widely used in the search for petroleum reserves in old oil wells which have been capped.

Gamma ray spectroscopy logging consists of the measurement of the gamma ray spectra from material surrounding the oil well. The most practical techniques use pulsed (d,t) neutron sources and time gated detectors. If the neutron burst is short enough ($\sim\mu$s) the gamma rays following inelastic neutron scattering can be analyzed to give the carbon and oxygen content of the formation. A delayed gate to pick up the gamma rays following thermal neutron capture permits an analysis also of the hydrogen, chlorine, calcium, silicon and iron content. Nuclear techniques in oil well logging, which in 1975 amounted to $\sim$200 million dollars, can be expected to expand significantly in the near future.

The use of nuclear techniques in manufacturing processes by reducing wastage can produce large savings in industrial energy consumption. The availability of intense neutron sources such as plutonium-beryllium and ^{252}Cf fission sources has made activation analysis for feed-back control feasible for some current manufacturing processes. In fact a neutron gamma technique has been developed to determine the hydrogen, calcium, silicon and carbon contents of calcareous aggregate concrete.[42] This could be adapted for feed back control. Further applications of radioactive techniques in the control of the manufacture of chemicals offers opportunities to the chemical industry for significant savings in energy.

REFERENCES

1. "Proceedings of International Conference on Nuclear Cross Sections and Technology," Ed. by Schrack and C. D. Bowman, NBS Spcial Publ. 425 (1975).
2. J. L. Fowler and W. W. Havens, Jr., to be published in "Physics Today" (1976).
3. V. O. Uotinen, J. D. Robertson and J. S. Tukenko, Proc. Int. Conf. Nuclear Cross Sections and Technology, Vol. I, p. 7 (1975).
4. A. D. Carlson, Proc. of Int. Conf. on Nuclear Cross Sections and Technology, Vol I, p. 293 (1975).
5. E. Fort and J. P. Marquette, EANDC (E) 148 "U" 1972.
6. M. S. Coates, G. J. Hunt and C. A. Uttley, Proc. Second IAEA Panel on Neutron Standard. Reference Data, Vienna 1972.
7. W.P. Poenitz, Z. Phys. 268, 359 (1974).
8. S. J. Friesenhahn, V. J. Orphan, A. D. Carlson, M. P. Fricke and W. M. Lopez, USAEC Report INTEL-RT 7011-001 (1974).
9. W. P. Stephany and G. F. Knoll, Proc. Int. Conf. Nuclear Cross Sections and Technology, Vol. I, 236 (1975).
10. C. M. Bartle, Proc. Int. Conf. Nuclear Cross Sections and Technology, Vol. II, 688 (1975).
11. G. P. Lamaze, O. A. Wasson, R. A. Schrack and A. D. Carlson, Proc. this conference.
12. G. M. Hale, Proc. Int. Conf. Nuclear Cross Sections and Technology, Vol. I, 302 (1975).
13. J. A. Cookson, M. Hussian, C. A. Uttley, J. L. Fowler, R. B. Schwartz, Proc. Int. Conf. Nuclear Cross Sections and Technology,Vol. I, 66 (1975).

14. S. A. Elbakr, J. W. Watson and C. A. Miller, Nuclear Inst. and Methods 115, 115 (1974).

15. R. J. Kurz, Lawrence Radiation Lab. Report UCRL-11339 and Errata 1964.

16. N. R. Stanton, Ohio State University Preprint COO-1545-93 Feb. 1971.

17. J. W. T. Dabbs, N. W. Hill, C. E. Bemis and S. Raman, Proc. of Int. Conf. Nuclear Cross Sections and Technology, Vol. I, 81 (1975).

18. J. W. T. Dabbs, N. W. Hill, C. E. Bemis and S. Raman, Contributed Paper PG1/J16 this conference.

19. N. C. Paik, Proc. of Int. Conf. on Nuclear Cross Sections and Technology, Vol. I, p. 39 (1975).

20. J. Y. Barré, J. Bouchard, J. P. Chaudat, "Proc. of Int. Conf. on Nuclear Cross Sect. and Tech.," Vol. I, p. 51 (1975).

21. Robert Avery, "Proc. of Int. Conf. on Neut. Cross Sect. and Tech.," Vol. I, p. 45 (1975).

22. M. W. Dyos, p. 175, "Physics and the Energy Problem," ed. by M. D. Fiske and W. W. Havens, Jr., American Physical Society, Topical Conference on Energy, p. 175, 1974.

23. T. V. Marcella, J. J. Egan, C. H. R. Kegel, C. P. Couchell, A. Mittler, W. A. Schier, D. J. Pullen, B. K. Barnes, A. Jean-Pierre and N. B. Sullivan, Bull. of Amer. Phys. Soc. Vol. 21, 537 1976.

24. "Reactor Safety Study," Draft. Wash. 1400, Aug. 1974.

25. E. P. Wigner, "Round Table Discussion of the Significance of the Conference," Proceedings of International Conference on Nuclear Cross Sections and Technology, Vol. II, p. 964, 1975.

26. L. H. Tang, "Proc. of Int. Conf. on Nuclear Cross Sections and Technology," Vol. 1, p. 422, 1975.

27. J. J. Ullo and M. Goldsmith, "Proc. of Int. Conf. on Nuclear Cross Sections and Technology," Vol. II, p. 553 (1975).

28. M. Goldsmith and J. J. Ullo, Proc. of Int. Conf. on Nuclear Cross Sections and Technology, Vol. II, p. 557 1975.

29. A. M. Perry and A. M. Weinberg, Annual Review of Nuclear Science, 22, 317 (1972).

30. T. B. Taylor, Bull. of Amer. Phys. Soc. 20, 700 (1975).

31. S. Raman, C. W. Nestor, Jr., and J. W. T. Dabbs, Proc. of Int. Conf. on Nuclear Cross Sections and Technology, Vol. I, p. 222, 1975.

32. R. G. Alsmiller, R. T. Santoro, J. Barish, T. A. Gabriel, Nuclear Sci. & Eng. 57, 122 1975.

33. Don Steiner, Nuclear Cross Sections and Technology, Vol. II, 646, 1975.

34. S. J. Qaim, "Nuclear Cross Sections and Technology," Proc. Vol. II, p. 664, 1975.

35. G. T. Chapman, J. K. Dickens, T. A. Love, G. L. Morgan and E. Newman, "Nuclear Cross Sections and Technology," Vol. II, 758, 1975.

36. D. G. Gardner, "Nuclear Cross Sections and Technology", Vol. II, 651, 1975.

37. F. L. Vook, Physics Today, p. 34, Sept. 1975.

38. R. Booth and H. H. Barschall, Nucl. Instrum. and Methods, 99, 1, 1972.

39. D. O. Armstrong, C. R. Emigh, K. L. Mieir, E. A. Meyer, J. D. Schneider, paper submitted to Int. Conf. on Radiation Test Facilities for C.T.R. Surface and Materials Program, Argonne National Lab. 261, July 15-18, 1975, ANL/CTR-75-4.

40. Batchelor, Chasman, Fewell, Lankshear, Sheehan, and Witkover, IEEE Trans. on Nuclear Science, Vol. NS 22, p. 1772, 1975.

41. M. J. Saltmarsh and J.A. Horak, paper submitted to Int. Conf. on Radiation Test Facilities for C.T.R. Surface and Materials Program, Argonne Nat'l Lab. 380, July 15-18, 1975, ANL/CTR-75-4.

42. M. C. Taylor and J. R. Rhodes, Instrumentation Technology, p. 32, 1974; M. C. Taylor, J. R. Rhodes and D. L. Bernard, Proc. of Int. Conf. on Nuclear Cross Sections and Technology, Vol. II, p. 496, 1975.

MJ 2 - NEUTRONS AND ENERGY - J. L. Fowler (Oak Ridge, USA)

Newstead (B.N.L.):

Joe, I certainly would completely agree with you that the ability to predict end of cycle reactivity is of trememdous economic importance for industrial reactor development. Incidentally, I think perhaps your figure about power peaking has too low an economic importance attached to it, because indirectly, of course, power peaking affects reactor safety and if you improperly predict the peaking you may have to reduce the power of the reactor to seventy percent, or sixty percent, which is a terrific economic penalty. Unfortunately, this does not lead in a straightforward way to the necessity for improved nuclear data, and it's this dilemma I want to address. You see, the uncertainties in these quantities are controlled more by our ability to model the reactor, that is by the analytical calculations, than by cross section precision. In present generation diffusion theory calculations utilizing perhaps 50,000 mesh points and a large computer, such as a CDC7600, we still are several percent off in accuracy. Now, first one has to improve these calculational methods and this is the point that the industrial people make. But what they don't appreciate is that once they've improved the calculational ability then they will need the cross sections. Since there is a long lead time on producing these cross sections, both industry and government must continue to support the cross section activity now so they have the cross sections five years from now. This point cannot be emphasized too strongly!

Fowler:

You are certainly right, and I glossed over the fact that there was the uncertainty in the analytical procedures for using more precise cross sections. On the other hand, I did quote industrial people; my numbers on the economic values of precision were from Votinen, Robertson and Tukenko in a paper from the "Neutron Cross Section Technology Conference." So at least three industrial people believe you need more precision in cross sections!

Khanna (Chalk River):

Would you care to comment if the fusion process through laser-induced fusion will pose any additional problems with neutrons ?

Fowler:

If you're talking about the radioactivity produced, I passed rapidly over that part. The captured neutrons produce radioactivity which is something like 10^9 to 10^{10} curies for a thousand megawatt electric fusion reactor, so that the level of radioactivity due to the neutrons is of the order of magnitude of the level of radioactivity in a fission reactor of the same power level.

Ajzenberg-Selove (U. Penn.):

Are the half-lives similar?

Fowler:

No, the half-lives are shorter so the radioactivity problem -- after a thousand years -- is considerably less.

Ajzenberg-Selove:

How much research is underway on the thorium breeder reactors, either in this country or overseas? It seems like a very interesting thing to pursue further.

Fowler:

That's sort of a loaded question. Do you mean how many cross sections are being measured?

Ajzenberg-Selove:

Is industry interested in pursuing this?

Fowler:

Yes, there is one thorium breeder being designed for the old Bettis reactor. This is being designed perhaps not as a thorium breeder, but as a thorium converter. The nuclear engineers are replacing the fuel elements of a light water reactor in a different configuration in the old Bettis reactor and, so far as I know, this is the limit of the thorium breeder anywhere in the world. I think perhaps the Dutch may be working on a thorium breeder, and also the Canadians. (Inaudible comments from the floor.)Professor Frank, it's been suggested that I ask what the situation is with regard to a thorium breeder in the Soviet Union.

Frank:

I don't know.

Ajzenberg-Selove:

In the case of the ^{6}Li graph you showed at the beginning, there were a bunch of jagged lines over the peak and I didn't understand what they represented. It's the one in which you showed the transuranics and also the lithium.

Fowler:

They are from the Cd filter.

Holm (Northeast Utilities):

About the thorium fuel cycle again: you seem to identify a thorium breeder with a thermal reactor. I wonder if you would expand your comments to talk about fast breeders designed for thorium, and I'm thinking in particular of the helium-cooled reactor.

Fowler:

I think the cross sections are such that a fast breeder with thorium doesn't work very well. I may be wrong.

Wigner (Princeton Univ.):

How much do we know of the η values of the various resonances of ^{233}U?

Fowler:

The low energy ones are known reasonably well, I think. Of course, as one goes higher in energy, you know only the average values of η.

9:00 A.M., FRIDAY, JULY 9, 1976, IN OLNEY 150

MAIN SESSION MK

Chair: H.W. Newson (Duke University, U.S.A.)

Invited Paper: Session MK 1

9.00 a.m., Friday, July 9, 1976

NEUTRONS AND FISSION

A. Michaudon

Service de Physique Nucléaire, Centre d'Etudes de Bruyères-le-Châtel,

Boite Postale No. 61, F-92120 Montrouge, France

RÉSUMÉ

A review is presented of fission processes induced by neutrons. The rôle of the double-humped fission barrier is examined and a survey is conducted of the phenomena, static and dynamic, that have relevance to these considerations.

ABSTRACT

A major break-through occurred in fission this past decade with the discovery of the double-humped fission barrier, which can explain in a coherent manner many aspects of fission. The present situation is briefly reviewed, with special emphasis on the contribution of fission induced by neutrons.

This review includes:

- The calculation of the fission barrier using the Strutinsky procedure and the comparison of measured and calculated barrier heights;
- The fission isomers with the systematics of their half-lives;
- The properties of fission induced by resonance neutrons, with special emphasis on
  (i) properties of ^{235}U and ^{239}Pu fission resonances, as compared to the predictions of the fission channel theory of Bohr, and
  (ii) intermediate structure effects;
- The structure effects in near-threshold fission cross sections, stressing the interest of recent results on the ^{232}Th fission cross section which seem to demonstrate the existence of a third minimum in the fission barrier;
- The dynamical effects in the fission process with special consideration paid to the concept of dynamical fission barriers and damping effects in the low-energy fission of ^{240}Pu.

NEUTRONS AND FISSION

A. Michaudon

Service de Physique Nucléaire, Centre d'Etudes de Bruyères-le-Châtel,
B.P. n° 61, 92120 Montrouge, France

CONTENTS

I - Introduction

II - Fission barriers

II.1 - Introduction .
II.2 - Calculation of fission barriers .
II.3 - General consequences of double-humped barrier shapes .

II.3.1 - Fission isomers .
II.3.2 - Structure effects in the fission cross sections .
II.3.3 - Asymmetry in the fragment mass distribution .

II.4 - Comparison of calculated and experimentally determined fission barriers .

III - Fission Induced by Resonance Neutrons

III.1 - Introduction .
III.2 - Fission channel theory of A. Bohr .

III.2.1 - Examples of fission properties depending on the fission channels .
III.2.2 - ^{239}Pu fission resonances. Evidence of the (n,γf) reaction .
III.2.3 - ^{235}U fission resonances .

III.3 - Intermediate structure effects in sub-barrier fission cross sections

IV - Structure Effects in Fast Neutron Fission Cross Sections

IV.1 - Introduction .
IV.2 - Vibrational resonances in ^{230}Th and ^{232}Th fission cross sections - "Thorium anomaly" - Third minimum in the fission barrier .

IV.2.1 - ^{230}Th + n .
IV.2.2 - ^{232}Th + n .
IV.2.3 - Third minimum in the fission barrier .

V - Dynamical Effects in Fission

V.1 - Generalities .

V.1.1 - Inertia .
V.1.2 - Energy dissipation .

V.2 - Dynamical fission barriers for spontaneous fission .

V.3 - Dynamical effects in the low-energy fission of ^{240}Pu .

VI - Conclusion

I. INTRODUCTION

The discovery of nuclear fission, a little over thirty five years ago[1], opened an important chapter in the study of nuclear physics . Yet, despite the fact that fission is a nuclear phenomenon which has been the subject of many studies, it has grown for a long time almost independently from the general trend of nuclear physics. This situation occured because fission is a complicated process which could not be described by the models and reaction mechanisms developed in low-energy nuclear physics . In fission, the nucleus undergoes a series of large oscillations of such amplitude that the fissioning system is ultimately elongated to the point where it breaks into two strongly deformed fragments of comparable masses , liberating a large amount of energy (about 200 MeV for fission induced by thermal neutrons in ^{235}U). In conventional low-energy nuclear physics, on the contrary, the studies are restricted to nuclear states with properties not too far from those of the nucleus in its ground state . For example, the deformation of such excited states is very close to the ground state deformation ; this is true also for collective excitations since they represent only small deviations from the nuclear shape at equilibrium . Also, the intrinsic excitations that may occur have a configuration which does not differ much from that of the ground state and can usually be described in terms of particle-hole interactions . If nuclear species different from the target nuclei are formed in the nuclear reactions, again, the difference is relatively small compared to the mass division that occurs in fission since only a small number of particles can be transferred in the reaction process . All this explains why the methods developed for the understanding of low-energy nuclear physics could not be successfully applied to describe and explain the manifold properties of the violent collective phenomenon through which fission proceeds . Nevertheless fission, especially neutron-induced fission, has been studied extensively because of the large energy release produced in the process and also because of the possibility provided by the fission neutrons to maintain a self-sustained chain reaction. But, because of the complexity of the phenomenon, these studies were mostly experimental and when models were invented to account for the results in a more orderly and coherent fashion, they did not stem directly from basic nuclear theory but, rather, they were based on phenomenological concepts .

The situation has changed completely in less than a decade both because a major breakthrough has occured in fission during that period and also because the field of nuclear physics is now expanding very rapidly towards heavy-ion induced reactions which show great similarity with fission both in concepts and in experimental techniques .

The breakthrough which happened in fission is now well known and has been described in several review papers (see for example [2,3,4,5,6]). It was due, on one hand, to several puzzling experimental results obtained independently one from the other and which could not be explained with the conventional fission models then available and, on the other hand, to a more sophisticated approach to the calculation

of fission barriers . Such calculations were based on the interplay between macroscopic properties of nuclei which account for most of their potential energy at all deformations, and single-particle effects which appear as a shell-energy correction to the macroscopic values[7]. For actinides, calculations of this type give fission barriers with two humps separated by a second minimum which provides the possibility for very deformed states to exist besides those commonly known with deformations comparable to that of the ground state i.e.of the first minimum.The existence of such strongly deformed states (called also class-II states) in the second well of the fission barrier can explain very well most of the puzzling experimental results referred to earlier ; among them are : fission isomerism, structure in near-threshold fission cross sections and intermediate structure in subthreshold fission cross sections .

Thus,a great step forward has been made in a few years towards a more coherent and fundamental comprehension of fission thanks to several peculiar experimental results and more sophisticated calculations of fission barriers . The combination of macroscopic and microscopic approaches used in fission not only for the calculation of barriers but also for the understanding of viscosity effects now plays also a major role for the treatment of collisions between complex nuclei . In this respect, fission physics has led a pioneering action in the renewal of nuclear macrophysics and is now a full and active member of nuclear physics .

The whole field of fission is far too vast to be reviewed in this paper . In fact, most of the information relevant to the various aspects of fission is contained in the Proceedings of the last two Fission Conferences which were held in Vienna (1969) and Rochester (1973) . But, nevertheless, the more restricted subject of "Neutrons and Fission" is worth being examined in this general context at this Conference . The last worldwide International Conferences on Neutron Physics took place in Antwerp in 1965 and Budapest in 1972 though several other Neutron Conferences were also held during this period but were either oriented towards applications (IAEA Conferences in Paris, 1966, and Helsinki, 1970,) or organised on a regional basis (at Washington, Knoxville or Kiev) or both of them . Therefore, it seems that it is now an appropriate time to review,on a more fundamental basis, what contribution neutrons have made in the last decade to a better understanding of fission, stressing the most recent aspects of this contribution which has been quite important .

These considerations explain the following organisation of this talk . Some general aspects of fission are recalled in Section II with special emphasis given to the double-humped fission barrier situation which is briefly reviewed . The macroscopic-microscopic approach to the calculation of fission barriers is presented together with the general consequences of double-humped barrier shapes ; a comparison is also made between calculated and measured fission barrier parameters.

More specific properties of neutron-induced fission relevant to the barrier shape are discussed in Sections III and IV .

Fission induced by resonance neutrons is examined in Section III with special attention given to properties connected to the Bohr theory of fission exit channels and to intermediate structure effects .

The existence and interpretation of other structure effects, in the near-threshold fission cross sections, are discussed in Section IV .

Fission dynamics, which are ignored in Sections II, III and IV are touched upon in Section V . Some results are presented i) for the spontaneous fission half-lives of even-even nuclei, taking into account more accurate calculations of the mass inertia parameter and ii) for damping effects in the low-energy fission of ^{240}Pu .

In the presentation outlined above, the emphasis is put mainly on the fission mechanism for actinide nuclei and how it varies with the nucleus, its excitation energy and the quantum numbers J, π and K of the fissioning state . In contrast, very little attention is given to a detailed description of the fission properties for a given nuclear state . For this reason, fission induced by thermal neutrons is ignored here, though it has been extensively studied in the past, unless it can help to shed some light in the discussions . In the same manner, the subject of neutrons emitted in fission is not treated as such in this paper which mainly deals with neutrons in the entrance channel for neutron-induced fission .

II . FISSION BARRIERS

II.1 - Introduction .

The fission process is obviously a collective phenomenon which couples an initial state λ to scission . These states λ are usually compound nucleus states which, in favorable cases, can be excited independently one from the other, for example by resonance neutrons, due to the excellent resolution of neutron time-of-flight spectrometers ; but at higher neutron energy or for fission induced by other particles, the resolution function is broader and, rather, a set of several fissioning states λ close in energy is generally populated . The rate of decay by fission of such states is usually expressed by their fission width Γ_f . Their fission properties, including their Γ_f value, are determined by the dynamics of the penetration of the fission barrier .

A complete description of the fission process therefore requires a knowledge of the following three physical quantities :

a) the fission barrier, i.e. the total potential energy of the nuclear system as a function of deformation parameters in a multidimensional space since several deformation coordinates are necessary to describe the nuclear shape along the fission path, especially when the fissioning nucleus is strongly elongated .

b) the mass inertia parameter of the fissioning system, at all deformations, in order to determine the fission path and the fission barrier penetrability .

c) the damping of the fission mode, i.e. its coupling to the other degrees of freedom, especially during the descent from saddle point to scission .

All this needs to be taken into account and in a coherent manner in order to understand thoroughly the mechanism and the properties of the fission process . This is so because i) all these three quantities play a role whose relative importance depends on the initial state λ and on the properties being studied and also because ii) the dynamical and statical aspects of fission may depend one upon

each other. For example, the fission path is determined not only by the fission barrier but also by the mass inertia parameter which seems to vary with deformation thus leading to the concept of "dynamical barrier". In addition, damping effects can modify, through intrinsic excitations of the fissioning system, both the fission barrier and the mass inertia parameter .

The statics and dynamics of fission are far from being known with the same accuracy. Great progress has been made in the calculation of the fission barrier which is now fairly well known. This is due to a new macroscopic-microscopic approach, first developed by Strutinsky for fission barriers and which proves to be very successful [7] . In contrast to the statics, fission dynamics are still poorly known . The mass inertia parameter cannot be calculated with sufficient accuracy though the barrier penetrability depends very critically on its determination . Even less is known about damping or viscosity effects which control the share of the energy available at scission between the kinetic and excitation energies of the fission fragments .

A comprehensive treatment of fission, taking into account all these aspects is not possible at present . This is why the statics (i.e. the fission barrier) are discussed in this Section first and separately from the dynamics which are considered in Section V .

Because of its importance for recent developments in fission, the fission barrier situation is considered here somewhat in detail. The calculation of fission barriers is reviewed in Section II.2 . General consequences of double-humped barrier shapes are given in Section II.3 but some of them are treated in more detail in Section III and IV . Lastly a comparison between calculated and measured fission barrier parameters is made in Section II.4 .

II.2 - Calculation of fission barriers .

The fission barrier of a given nucleus could be obtained if the microscopic wave function of this nucleus could be calculated for any arbitrary shape. The fission path and hence the fission barrier would then be derived. But this is not possible yet, due both to a lack of a precise enough knowledge of the effective nucleon-nucleon interaction in the nucleus and also to computational difficulties both in complexity and length. In addition one would be faced with the problem of properly defining the deformation coordinates .

Nevertheless, it is worth noting that calculation of nuclear properties with constrained self-consistent fields, using Hartree-Fock (H.F) or Hartree-Fock-Bogolyobov (H.F.B) methods, are making rapid progress [8]. In fact , the first H.F. calculations of a fission barrier were first reported for ^{240}Pu at the Rochester Conference [9]. But, despite their interest and the rapid improvements in accuracy, such methods cannot provide as yet realistic barrier shapes .

Single-particle wave functions and energies can easily be calculated from a potential of almost any shape, defined by a set $\{ s \}$ of deformation parameters. But this shell-model approach is not sufficient to obtain fission barriers. It can be shown that the sum $E^{s.p.}(\{s\})$ of single-particle energies up to the Fermi level is not the total potential energy of the nucleus . This sum is given by the following expression :

$$E^{s.p.}(\{s\}) = \sum_{N,P} n_i \, E_i(\{s\}) \qquad (1)$$

where :

- $E_i(\{s\})$ is the energy of orbit i at deformation $\{s\}$,
- n_i is the occupation number of orbit i (n=2 for a completely filled orbit),

and $\sum_{N,P}$ is the sum over neutron and proton orbits .

Expression (1) is incorrect for obtaining deformation energies . It is, in fact, incapable of reproducing a fission barrier with conventional types of potentials since it actually goes to infinity for increasing deformation . But, this energy $E^{S.P}(\{s\})$ is very useful for the derivation of a shell-energy correction in the calculations described below .

It is a well known fact that the general trend of some nuclear properties such as ground-state masses, can be adequately reproduced with a macroscopic model, for example the liquid drop model (LDM). Individual or local properties, on the contrary, strongly depend on the microscopic structure . Combination of these two aspects has been used to determine some properties of nuclei in their ground state, for example their accurate mass and deformation[10] or the systematics of their spontaneous fission half life[11], but this usage was restricted to small deformations only.

The so-called macroscopic-microscopic method, which is generally used now to generate fission barriers, was first developed by Strustinsky[7] who postulated that, for all deformations $\{s\}$ along the fission path from ground state to scission, the total potential energy $E\{s\}$ of the fissioning nucleus can be expressed as the sum of two terms $E_M(\{s\})$ and $E_m(\{s\})$.

$$E(\{s\}) = E_M(\{s\}) + E_m(\{s\}) \qquad (2)$$

In this expression, $E_M(\{s\})$ represents most of the energy, as obtained with a macroscopic model and $E_m(\{s\})$ is a shell-energy correction which is derived from the value of the single-particle level density at the Fermi surface .

The shell-energy correction is given by the following relation :

$$E_m(\{s\}) = 2\int_{-\infty}^{\lambda_o} E\,\overset{o}{g}(E,\{s\})\,dE - 2\int_{-\infty}^{\lambda} E\,\tilde{g}(E,\{s\})dE \qquad (3)$$

where :

- $\overset{o}{g}(E,\{s\}) = \sum_i \delta(E - E_i(\{s\}))$ is the shell-model level density corresponding to a discrete set of levels i having energy $E_i(\{s\})$ at deformation $\{s\}$,
- $\tilde{g}(E,\{s\})$ is a smooth level density obtained by folding $\overset{o}{g}(E,\{s\})$ into a smoothing function having a width of 8 to 10 MeV corresponding to the distance between shells ,
- λ_o and λ are the Fermi energies for the level densities $\overset{o}{g}$ and $\tilde{g}$ respectively and determined so as to conserve the number of particles .

The correction $E_m(\{s\})$ includes both the proton and neutron contributions .

The first calculations of this type were carried out by using the LDM to derive $E_M(\{s\})$ and the Nilsson model with spheroïdal shape to obtain $E_m(\{s\})$ [7] . The barriers so calculated for actinide nuclei displayed the now famous double-humped shape (Fig.1), a result closely connected to the single-particle level density at the Fermi surface. This density fluctuates with increasing deformation, leading to an oscillatory behavior of $E_m(\{s\})$ which is positive or negative depending on whether the density is high (between shells) or low (near shells) respectively . It turns out that, for actinide nuclei, in addition to the first negative shell-energy correction at ground state deformation, there is a second one near the LDM saddle point . This effect is responsible for the existence of a second minimum in the fission barrier. The second shell-energy correction moves from the small deformation side to the high deformation side of the LDM saddle point for increasing mass number, with the consequence that the inner barrier A is lower than the outer barrier B for light actinides whereas the opposite situation prevails for heavy actinides .

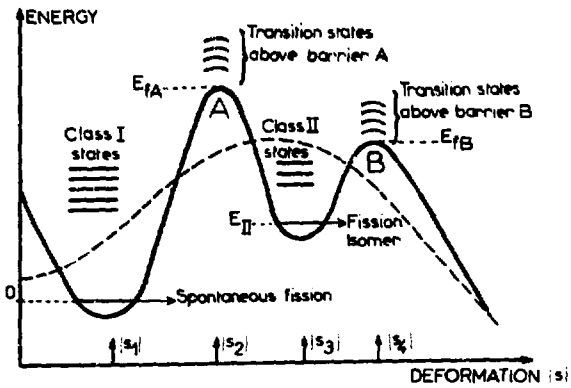

Fig. 1 - Fission barrier (solid line) resulting from shell-energy corrections to the LDM barrier (dashed line). The abscissa {s} gives only an indication of the magnitude of the deformation but does not specify the type of deformation. For certain classes of nuclei, for instance those having neutron number N in the vicinity of 146, the fission barrier presents two humps A and B, at deformation $\{s_2\}$ and $\{s_4\}$ respectively, where the shell-energy corrections are positive . These two humps can be separated by a deep second well, at deformation $\{s_3\}$ where the shell-energy correction is negative. This kind of barrier shape has important consequences (discussed in Section II.3) for the understanding of the fission process .

More sophisticated calculations have followed and these have been reviewed on several occasions[5,12]. Improvements have been made in the three directions discussed below :

a) Parameterization of the nuclear shape

It is important to describe as accurately as possible the deformation of the nuclear system along the fission path. Examples of such basic nuclear shapes are : i) one single perturbed-spheroid in which the spheroidal shape is modified by the addition of Legendre polynomials from third up to sixth order, ii) two spheroids which may have different volumes and deformations and with a possible smooth joining at the neck . With these shapes, provision is made in the parameterization to include axial asymmetry and/or mass asymmetry if necessary, in addition to the usual separation and deformation of the nascent fragments .

b) Macroscopic energy

Great care has to be taken in calculating as accurately as possible this most important part of the total energy of the nucleus . Improvement of the LDM energy can be obtained by using the droplet model in which terms of higher order in $A^{-1/3}$ and $I^2 = \left(\frac{N-Z}{A}\right)^2$ are taken into account in contrast to the LDM where they are eliminated by truncation in the expansion[13] . Nevertheless, this model also fails to reproduce accurately the macroscopic energy for shapes where the surface diffuseness is not small compared to the local size of the droplet, for example if the neck is too narrow . A spurious excess of macroscopic energy may also appear due to ripples or too abrupt irregularities in the nuclear shape .

In order to remove these effects, a simple method has been used recently which takes into account finite-range effects by calculating the macroscopic energy in terms of a double volume integral over a Yukawa function[14] .

c) Shell-energy correction

Many shell-model potentials have been developed to calculate the shell-energy corrections. These include two-center potentials, in addition to the more familiar one-center potentials, in order to reproduce in a more realistic manner the effect of the two nascent fragments in the last stage of fission. Such two-center potentials are also used for the study of heavy-ion reactions . The potentials can be of the harmonic-oscillator type which goes to infinity for increasing radius or, more realistically, of the Woods-Saxon type, with surface diffuseness, which goes to zero for increasing radius. Of the latter type is the folded-Yukawa potential which is obtained by folding a Yukawa function into a nuclear shape having a sharp surface[5].

There can be a large number of combinations of the three aspects discussed above for the calculation of fission barriers ; this is the reason why there are many results now available, all using the Strutinsky procedure .

The same general pattern of barrier shape is obtained in all calculations though the results differ somewhat in numerical values (see Section V.4). The use of a more sophisticated parameterization leads to some change in the detailed shape

of the barrier as is illustrated in Fig. 2 . Axial asymmetry lowers the inner barrier whereas mass asymmetry lowers the outer barrier . This last effect provides a simple explanation for the well-known mass asymmetry in low energy fission of actinide nuclei (see Section II.3.3) .

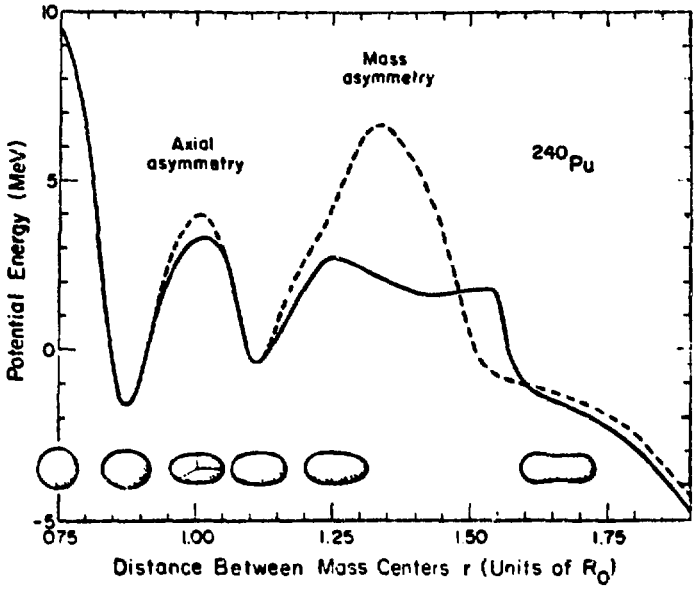

Fig.2 - Effect of axial asymmetry and mass asymmetry on the fission barrier of ^{240}Pu . The dashed curve (which sometimes coincides with the solid curve) gives the potential energy for symmetric deformations as a function of the distance r between the centers of mass of the two nascent fragments . The solid curve gives the potential energy along a path that leads over the axially asymmetric first saddle point and over the mass-asymmetric second saddle point . The lower portion of the figure shows the nuclear shapes corresponding to selected points along this path, namely the sphere, four equilibrium points, and the point of emergence from the barrier in spontaneous fission . (After P. Möller and J.R. Nix[12]).

II.3 - General consequences of double-humped barrier shapes .

The double-humped fission barrier was able to provide a coherent explanation of many different experimental results that could not be interpreted before. Among them, several are relevant to neutron-induced fission (for a comprehensive review, see for example[6]) . A satisfactory explanation of these results was made possible because of specific properties of the double-humped barrier . For example the penetrability of a barrier having such a shape does not present a smooth variation with energy as for a single barrier having a conventional inverted harmonic oscillator shape. This is because the double-humped fission barrier provides the possibility

for strongly deformed states to exist in the second well . The existence of such states, their coupling to the neutron entrance and fission exit channels, can explain many aspects of the fission mechanism .

The general theoretical framework for this study was given by Lynn [3] . Following his approach, it is possible to write the total Hamiltonian of the nuclear system as below :

$$H = H_\beta + \sum_i H_i + \sum_{i<j} H'_{ij} + \sum_i H''_{i\beta} \qquad (4)$$

In this expression, β represents the fission mode and i all the other degrees of freedom. The potential term in H_β is the fission barrier itself . The part of H associated with the degrees of freedom i is the sum $(\sum_i H_i + \sum_{i<j} H'_{ij})$ whereas the interaction between β and the other degrees of freedom i is described by the term $H''_{i\beta}$. This implies that the former term $(\sum_i H_i + \sum_{i<j} H'_{ij})$ corresponds to a fixed deformation β_o ; the variation of this part of the Hamiltonian with β is included in $H''_{i\beta}$.

Eigenfunctions of H_β , called ϕ_ν , correspond to vibrational states in the fission mode. For excitation energies low enough below the inner barrier height E_{fA}, most of the wavefunction ϕ_ν lies either in the first well or in the second well . This renders possible a shape classification of these vibrational states, called class I or class II states depending on whether their wavefunction ϕ_ν is found mostly in the first well or the second well respectively. For energies above E_{fA}, too strong a mixing between class I and class II states prevents the making of such distinctions .

In the same manner as for H_β , it is possible to define class I and class II states for the total Hamiltonian, depending on whether the vibrational part ϕ_ν of the total wavefunction is of the class I or class II type .

Damping of the vibrational states, i.e. their coupling to intrinsic excitations is made possible through $H''_{i\beta}$. At excitation energies usually considered in fission, full damping seems to prevail in the first well . This means that the strength of the fission mode in the first well is uniformly distributed as a function of energy . In contrast, all damping conditions can be found in the second well depending on the nucleus, the barrier shape, the excitation energy and the value of $H''_{i\beta}$. Therefore, fission can proceed through pure, partially or fully damped vibrational states in the second well. Also, rotational bands can be built on vibrational or intrinsic states in the second well and they too can play a role, especially in the absence of damping .

Various damping conditions for the class II states and their effect on fission properties are discussed at different stages in this paper .

The fission isomer situation is briefly reviewed in section II.3.1 because of its own interest though damping of class II states plays no role in this matter . Structure effects in the fission cross sections are introduced in section II.3.2 but are treated in more detail for specific cases in Sections III and IV. The

asymmetry in the fragment mass distribution is touched upon in Section III.3.3 for completeness though it is not exactly a consequence of a double-humped barrier shape but rather a result of the macroscopic-microscopic fission barrier calculations for large deformations .

II.3.1 - Fission Isomers

Historically, the occurence of fission isomers was the earliest manifestation of a barrier effect even before calculations by Strutinsky were available . The first fission isomer was discovered in ^{242}Am when bombarding ^{238}U with Ne ions[15] . Nevertheless, neutron-induced fission has also played a role in this case . It was through the ^{243}Am(n, 2 n) reaction that i) the nucleus exhibiting a 14 msec delayed fission activity was clearly identified as being ^{242}Am, and ii) the excitation energy E_{II} = 2.9 ± 0.4 MeV of the fission isomer was determined, thanks to the steep rise of the cross section at threshold (see Fig. 3) .

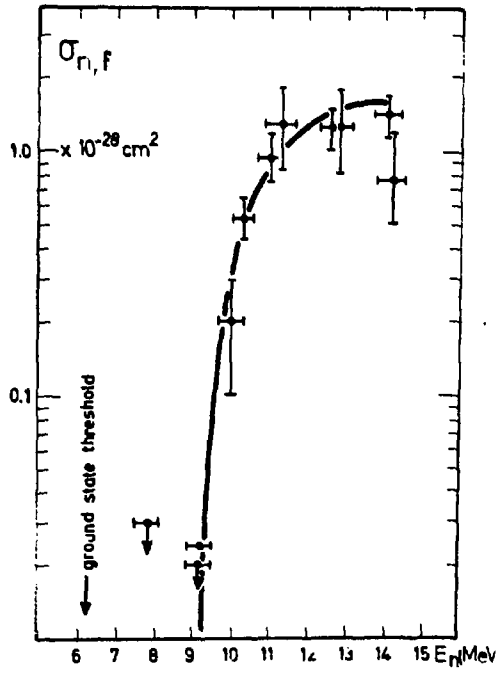

Fig.3 - Excitation function for the production of the ^{242}Am fission isomer through the ^{243}Am(n, 2n) reaction (After G.N. Flerov et al[15]).

This reaction was also very useful in demonstrating that this fission isomer was not a conventional high spin isomer ^{242}Am .

At present, more than 35 fission isomers have been identified in U through Cf elements . These fission isomers are commonly interpreted as being class II states weakly populated in appropriate nuclear reactions . Their decay by spontaneous fission is governed by the outer barrier only and is faster than for the ground state in the first well where the fission rate depends on the whole barrier . Transitions by γ-ray emission to class I states are hampered by the inner barrier . But, such a γ branch has been reported for the 200 ns ^{238}U fission isomer[16] . Fission

isomers can be formed either in the ground state or in a metastable excited state in the second well. In the latter case , there is an additional decay competition by γ-ray emission in the second well . This seems to occur for some even-even fission isomers which, in fact, are thought to be conventional spin isomers, of the type already observed in the first well, but formed this time in the second well where they decay first by γ-ray emission and then by fission . This phenomenon is commonly referred to as "double isomerism" .

The interpretation of the existence of fission isomers, in terms of double-humped fission barrier shapes, was first confirmed by an experiment carried out on the 4 ns ^{240}Pu fission isomer populated by the ^{238}U(α,2 n) reaction[17] . The rotational band associated with this isomeric state was identified by detection of the conversion electrons preceding isomeric fission . The lines observed in the electron energy spectrum were interpreted as being caused by E2 transitions between states of a $K^{\pi} = 0^{+}$ rotational band . The spacing between the lines obeys the expected I dependence and also provides the value $\frac{\hbar^2}{2\mathcal{J}}$ = 3.33 keV for this band, where $\mathcal{J}$ is the moment of inertia (Fig.4) This low $\hbar^2/2\mathcal{J}$ value of , as compared to 7.16 keV for the ground state, gave the first direct confirmation that fission isomers are indeed shape isomers in the second well as predicted by Strutinsky's calculations .

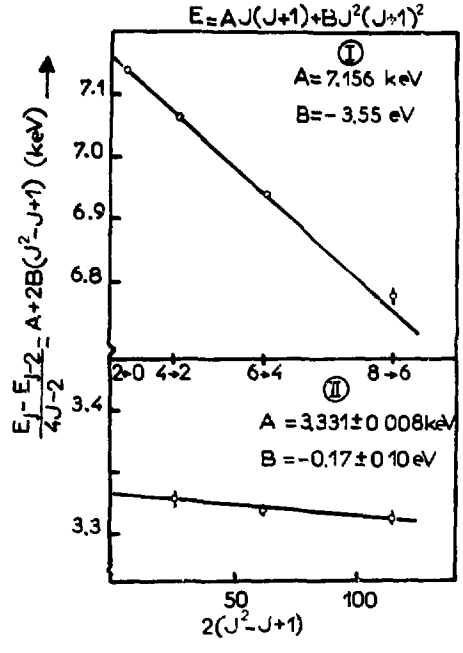

Fig.4 - Fit to the transition energies for the class II rotational band (II) and the ground state rotational band (I) (After H.J. Specht et al.[17]).

An up-to-date version of the systematics of observed half-lives T^i for fission isomers is given in Fig. 5 .

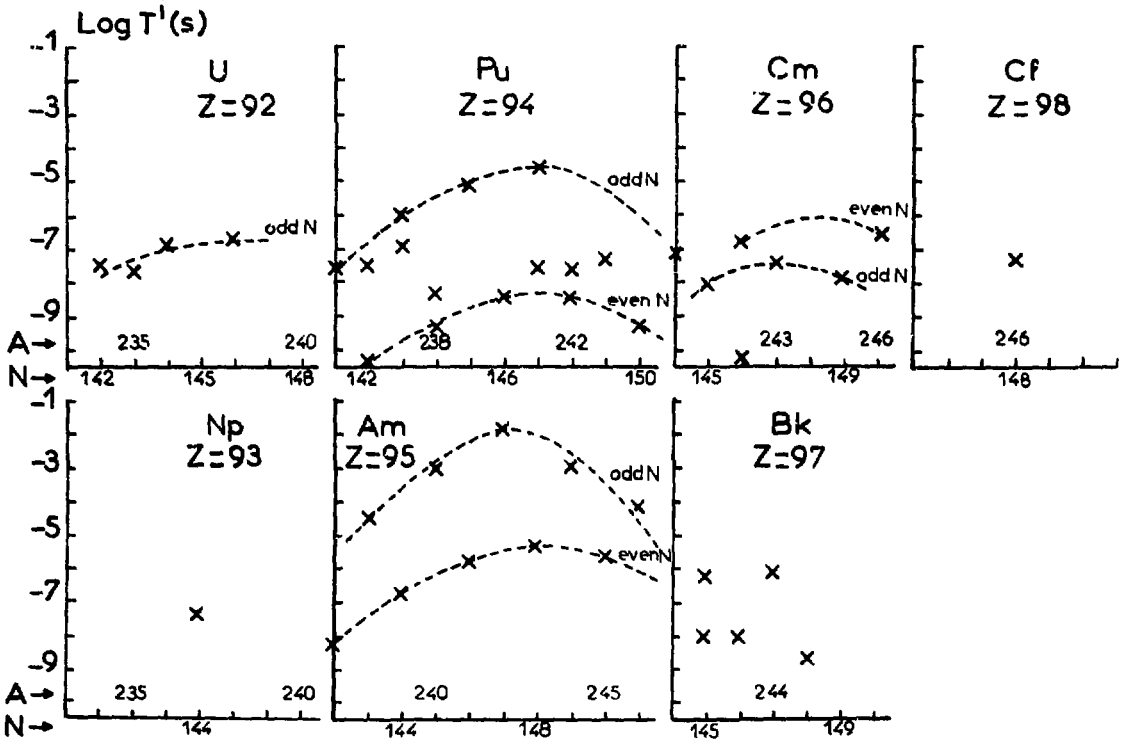

Fig. 5 - Plot of experimental values of the half-lives T^i for the observed fission isomers . The dashed lines are drawn only to illustrate the even-odd effect .

The analysis of these data is rendered difficult for several reasons : i) the nucleus undergoing a delayed fission activity cannot always be identified with certainty though great help is obtained from cross-checks made with different targets and reaction mechanisms ii) the nature of the fission isomeric state (ground state or excited state), its spin and parity are not determined directly, iii) the mode of decay that governs the fission rate (γ -ray emission or fission) is not known accurately . Also, presently available techniques cannot be used to measure half-lives shorter than about 50 ps.

In spite of these ambiguities, the half-life data presented in Fig.5 clearly show that strong odd-even effects are present ; they are commonly interpreted as resulting from the specialization energy and/or to odd-even differences in the mass inertia parameter . The general trend of $T^{\frac{1}{2}}$ versus N also suggests the existence of a neutron shell around $N \simeq 146$ for deformations near that of the second minimum .

Quantitative analysis of available fission isomer data can lead to some fission barrier parameters, in particular to E_{II}, the energy of the second minimum relative to that of the first minimum. In this respect, reactions in which neutrons are emitted prior to fission isomer formation, such as (p, 2 n), (n,n')or (n, 2 n) reactions, are very useful because they present a sharp rise in the cross section at threshold from which the E_{II} value can easily be deduced (see Fig.3 for example)

An up-to-date compilation of experimentally determined E_{II} values is given in Fig. 10 together with other parameters that are discussed in Section II.4 .

It is worth noting at this point that several fission isomers were formed with neutron-induced reactions . This was the case, for example, for ^{234}U, ^{235}U, ^{236}U, ^{240}Pu and ^{242}Am formed with the (n,γ) reaction [18,19] for ^{242}Am formed with the (n, 2 n) reaction[20,21] and for ^{238}U formed with the (n,n') reaction[22] .

In principle, neutrons seem to be appropriate probes to study the properties of fission isomers and, in particular, to identify them without ambiguity. This is because neutrons can be used at relatively low energy and therefore very few reaction channels are possible for the formation of a fission isomer . But, on the other hand, great care has to be taken when performing the experiment, especially if the target nucleus is fissile by slow neutrons . Backscattering of the neutrons from the material surrounding the target can then cause prompt fissions to be induced by those neutrons and to appear delayed in time with the consequence that they can simulate delayed fission induced by the direct neutron beam .

There is generally a good qualitative agreement between fission isomer data obtained with neutrons and those obtained with other reactions. It is nevertheless a little surprising that the ^{235}U and ^{236}U fission isomers have been so far observed with neutron-induced reactions only. Various attempts to form them with (d,p) or (α ,2 n) reactions proved to be unsuccessful.

A recent comparison of fission isomer properties determined from reactions induced by neutrons and other particles was made for the ^{238}U fission isomer which was studied with (d,p n), (γ ,γ') and (n,n') reactions in seven different experiments .

In addition the γ-branch was measured with the (d,p n) reaction . The half-lives measured in all these experiments are plotted in Fig. 6 . The most precise value, T^i = 295 ± 30 ns, comes from a recent ^{238}U (d,p n) experiment[22] and is somewhat greater than the best value T^i = 195 ± 30 ns recommended from data available in 1973[23] . The value T^i = 270 ± 40 ns obtained from the ^{238}U (n,n') reaction[22] is consistent both with the 1973 recommended half-life and the most recent determination from ^{238}U (d,p n) . From that point of view , the neutron experiment does not appear different from the others and it seems that the same fission isomer state is populated in all these cases .

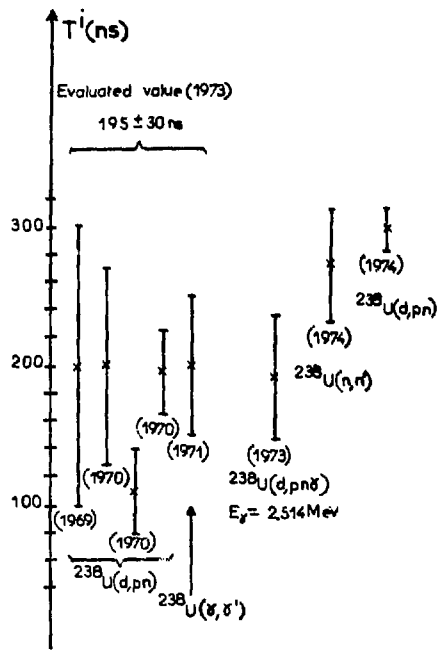

Fig.6 - Plot of the half-life T^i values for the ^{238}U fission isomer as obtained from different experiments .

The situation is different for the determination of the excitation energy E_{II} of the fission isomer, as is illustrated in Fig. 7 . A very precise value E_{II} = 2.559 MeV is obtained from the γ-ray energy E_γ = 2.514 MeV of the transition between the fission isomeric state and the 2^+ state of the ground state rotational band . A good value E_{II} = 2.1 ± 0.1 MeV is also obtained from a fit to the cross section in the case of the neutron experiment because of the steep rise of this cross section just above threshold . But the two values thus obtained for E_{II} are inconsistent : no satisfactory explanation has been provided as yet to account for this discrepancy .

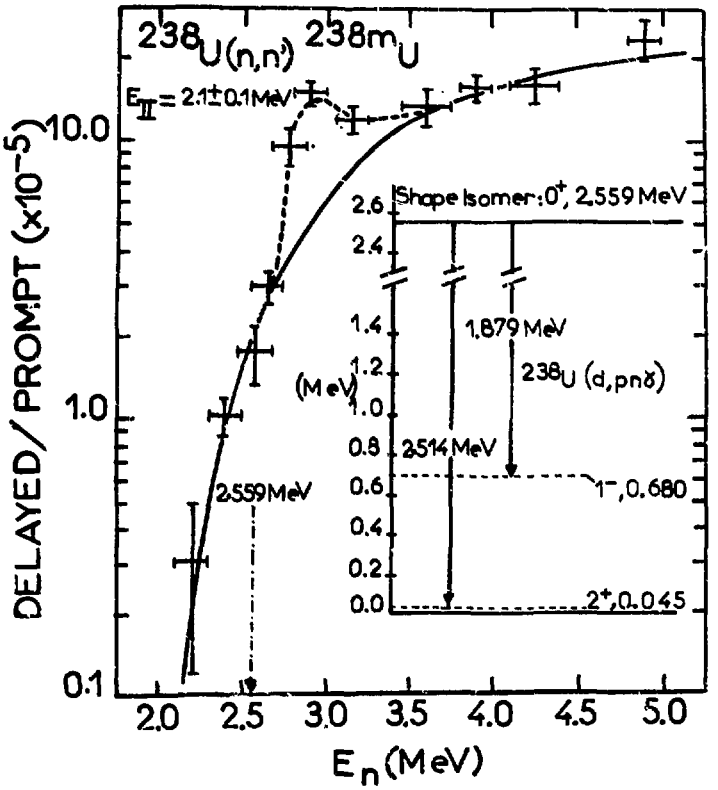

Fig. 7 - Delayed to prompt fission ratio observed when bombarding a high purity ^{238}U target with neutrons and plotted as a function of incident neutron energy E_n .The solid and dashed lines are tentative fits to the data[22] . The diagram showing the γ-ray branch observed in a ^{238}U (d, pnγ) experiment[16] is plotted on the right. Note the difference in E_{II} values as obtained from these two experiments .

II.3.2 - Structure effects in the fission cross sections

Several types of structure effects can be found in fission cross sections σ_f .

Some of them are common to all neutron cross sections. For example, at low incident neutron energy, the cross sections for a heavy nucleus are composed of many closely spaced sharp resonances which can be separated with neutron spectrometers having good resolution . This fine structure in σ_f is considered in Section III (especially in Section III.2) .

Other types of structure effects can appear in σ_f though not being connected to the detailed shape of the fission barrier. For example, even in the single-humped approximation, competition between fission and inelastic scattering can cause structure to show up in the near threshold fission cross section for non fissile nuclei such as ^{238}U. This is because σ_f increases or decreases respectively when a new fission channel (defined in Section II .2) or inelastic neutron channel opens. This aspect is not treated here .

In contrast, several structure effects are closely connected to the specific double-humped barrier shape and they are considerd in more detail in this paper . Such effects are the direct consequences of the existence of the class II states discussed above .

Vibrational levels can cause gross structure in the fission barrier penetrability, hence in σ_f . Damping of these levels plays an important role in the existence and the properties of the gross structure. For example, without damping, the fission mode would exist only at the energies of the vibrational states in the first well and σ_f would be composed of peaks, equally spaced, at these energies . It turns out that, at the excitation energies reached in neutron induced-fission, the class-I vibrational levels are fully damped. This means that the fission mode in the first well is uniformly distributed as a function of excitation energy, above the neutron separation energy S_n in the compound nucleus .

The same situation is not always found in the second well where the total width Γ_{VIB} of the class II vibrational levels can be smaller than their spacing Γ_{II} . This is because i) the first well is deeper than the second one,hence the available excitation energy is correspondingly reduced and ii) the damping width increases rapidly with excitation energy. In such cases, where $\Gamma_{VIB} < \hbar\omega_{II}$, the class II vibrational states cause a gross structure effect in σ_f which is composed of big peaks called "vibrational resonances" (See Fig. 8) .

Fine structure may also appear in these vibrational resonances as a result of different effects. For example, in the absence of damping, the class-II vibrational states can be quite narrow with a width Γ_{VIB} smaller than the spacings between the rotational levels built on them. These rotational levels can thus cause a fine structure within the gross structure . Also, in the presence of coupling of the class II vibrational levels to intrinsic excitations, the class II compound nucleus states can, as do the rotational levels, give rise to a fine structure effect. There are no known examples of a still finer effect which would be produced by the class I compound nucleus states, because the vibrational resonances occur at neutron energies for

which both the overlap of class I resonances and the experimental resolution effects are too important . These types of structure effects are discussed in Section IV .

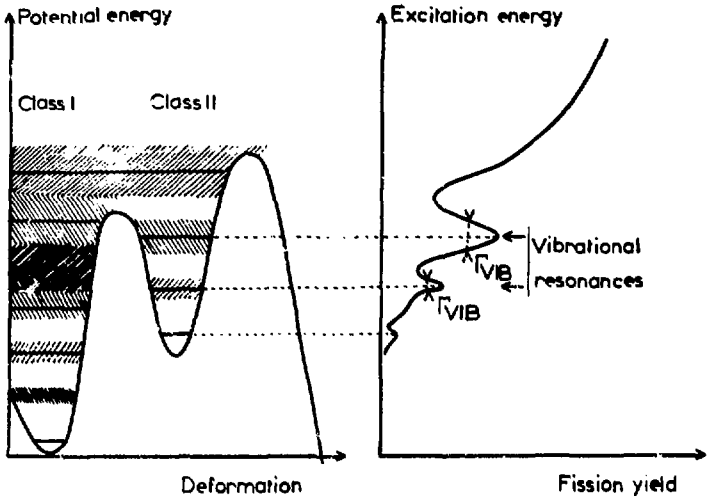

Fig. 8 - Illustration of the fission mechanism in the case of a double-humped fission barrier[2]). Class I and class II vibrational states exist in the first and second wells, respectively (Fig. A). The positions of these states are given by solid lines. Damping of these vibrational levels increases very rapidly with excitation energy and is indicated by hatched areas. The fission yield is plotted qualitatively as a function of excitation energy in Fig. B . The peaks in the fission yield, called "vibrational resonances", have a total width equal to Γ_{VIB} and correspond to class II vibrational states . Fine structure can also exist within these vibrational resonances (See the text) .

In the case of full damping of the vibrational class II states, the fission mode is uniformly distributed as a function of excitation energy . But, nevertheless, another type of structure effect may appear in the sub-barrier fission cross section provided that some suitable conditions are fulfilled. The origin of this structure effect now comes from the coupling between class I and class II compound nucleus states. This type of structure is intermediate between the fine structure of the class I resonances and the gross structure discussed above. For this reason, it is called intermediate structure . Discussion of this last aspect of structure effects in σ_f is given in Section III.3 .

Above the barrier, the structure effects rapidly disappear with increasing energy because of the greater mixing of class I and class II states .

II.3.3 - Asymmetry in the fragment mass distribution

Another interesting aspect to investigate in the potential energy landscape of the fissioning nucleus is the behavior of the surface as a function of odd deformation parameters . It is a well-known fact that low-energy fission presents an asymmetric mass division for most actinides. But, a symmetric component appears in the fragment yields of lighter isotopes (^{227}Ac, for example) ; also, on the heavier side, fission of ^{258}Fm and ^{259}Fm seems to prefer symmetric fragmentation only. Compilation of fragment mass distribution for actinides also shows that, for increasing mass of the fissioning nucleus, the leading side of the heavy fragment peak seems very stable (around Z = 50 and N = 82) whereas the light fragment peak moves towards higher masses. These features seem connected to shell effects but no satisfactory explanation could be provided before extensive fission barrier calculations for odd and even deformation parameters, using the Strutinsky prescription, became available. An illustration of calculations of this type is shown for ^{236}U in Fig. 9, where it can be seen that asymmetry in the fission fragment yields is a consequence of the potential energy surface at scission[24] .

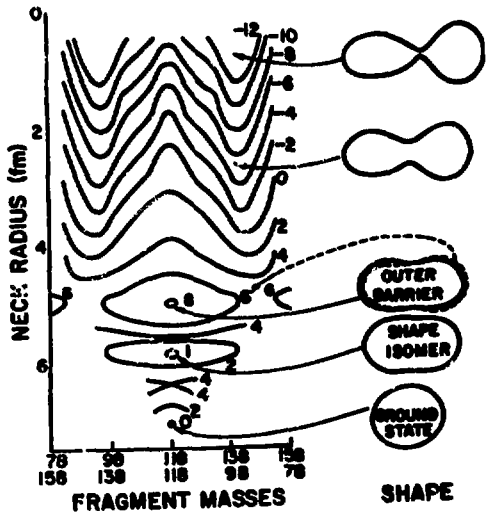

Fig. 9 - Potential energy surface for ^{236}U, as obtained from calculations using the Strutinsky procedure. Contour intervals are 2 MeV except for the shape isomer[24, 84] .

A closer examination of the picture indicates that asymmetry in the nuclear system already appears at the second saddle point, between the shape isomer and scission, where a double valley starts to develop and deepens for increasing deformation as the shell structure of the nascent fragments plays a more important role due to a more pronounced necking-in . Comparison of experimental mass distributions with those obtained from such calculations shows qualitative agreement. In particular, it is of interest to note that, for light actinides (^{226}Ac), the threshold for symmetric fission appears a few MeV higher than that for asymmetric fission [29] . Nevertheless, a quantitative account of the experimental results cannot be obtained from the theory yet [29] .

These potential energy calculations should be supplemented by a more satisfactory theory of fission dynamics which should play an important role in the last stage of fission, i.e. for the determination of the properties of the strongly deformed nucleus at scission .

II.4 - Comparison of calculated and experimentally determined fission barrier parameters

The analysis of various types of fission data in terms of the double-humped fission barrier provides values of some fission barrier parameters for several actinide nuclei . This analysis is generally carried out by assuming simple physical assumptions, for example : parabolic shape of the barrier top, a mass inertia parameter B (or $\hbar\omega$) constant within a given barrier but possibly different from one to the next. With only two exceptions (see Sections II.3 and IV), presently available fission data can provide no information about deformation parameters. The fission data can however give access to the following five parameters :

Three energies (relative to the ground state in the first well): E_{fA} - inner barrier height

E_{fB} - outer barrier height

E_{II} - energy of the ground state in the second well

Two transparency parameters : $\hbar\omega_A$ - inner barrier A

$\hbar\omega_B$ - outer barrier B

Comparison of parameters obtained from experiments and calculations is made in Fig. 10 for the three energies E_{fA} , E_{fB} and E_{II} since values of $\hbar\omega_A$ and $\hbar\omega_B$ are very difficult to determine (see Section V) . Moreover, the comparison is limited to even-even nuclei only in order to avoid the difficulties associated with odd-particle effects .

The E_{fA} and E_{fB} values determined experimentally come from the most recent and comprehensive set of fission barrier parameters, as derived by Lynn [27]. Some E_{II} values obtained from a few other data analyzes are also considered for completeness .

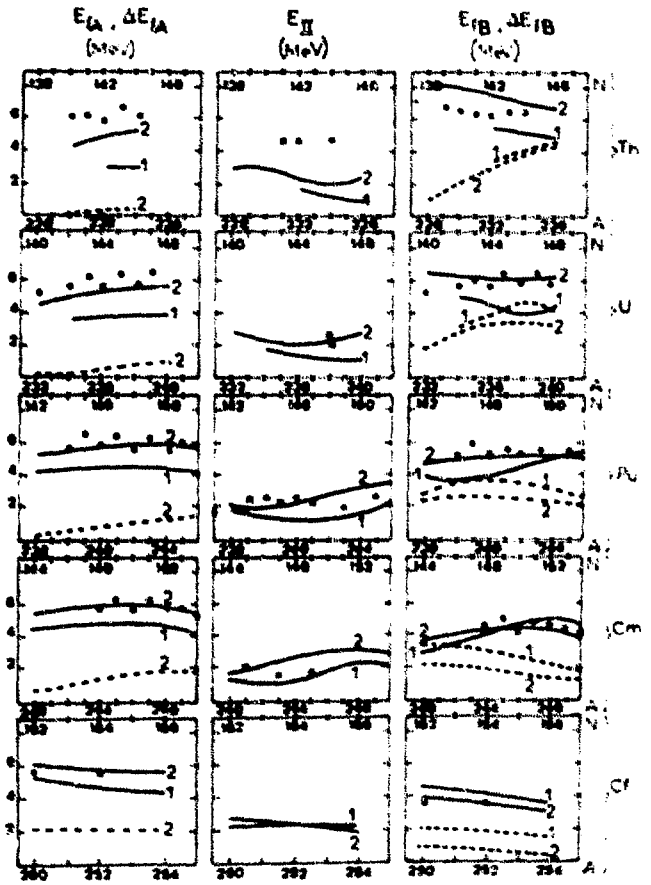

Fig. 11 - Comparison of fission barrier parameters obtained from calculations and analysis of experimental fission data. The calculated values of E_{fA}, E_{II} and E_{fB} are obtained for even-even nuclei only, with the Strutinsky prescription, in which the macroscopic energy is given by the droplet model and the shell-energy correction either by the folded Yukawa potential [28] (solid curve 1) or by the modified harmonic oscillator potential [12] (solid curve 2). Both values of E_{fA} and E_{fB} take into account a zero point energy motion of 0.5 MeV in the first well. The E_{fA} values are reduced by the amount ΔE_{fA} which comes from the effect of axial asymmetry and which is calculated with the modified harmonic oscillator only (dashed curve) . The E_{fB} values are reduced by the amount ΔE_{fB} which comes from the effect of mass asymmetry and which is calculated either with the folded Yukawa potential (dashed curve 1) or with the modified harmonic oscillator potential (dashed curve 2) The values of E_{fA}, E_{II} and E_{fB} obtained from the analysis of experimental fission data are given by open circles (o) [27] or crosses (x) [16,22,23,64,89,90] .

The calculated values are extracted from the most recent and sophisticated studies of fission barriers, using the droplet model for deriving the macroscopic energy and either a modified-harmonic oscillator potential[12] or a folded Yukawa potential[28] for obtaining the shell-energy correction . Both calculations include the effect of mass asymmetry which lowers the top of the outer barrier . The effect of axial asymmetry is calculated only with the harmonic oscillator potential[12] .

It can be seen that the results of the calculations, though in qualitative agreement with each other, show nevertheless significant differences which can amount to almost 2 MeV . Similar differences are also observed between calculated and measured values of the ground state energy which is used as a reference point in Fig. 10 . It has been suggested that the differences in calculated barriers can be caused by a discrepancy in the region of the ground state only[12] though it is difficult to justify why such a discrepancy does not propagate through the whole barrier .

The measured values are in fairly good agreement with the calculations, especially with those reported in[12] . There is nevertheless a noticeable discrepancy for the second well E_{II} of Th isotopes, known as the "Th anomaly". The measured E_{II} value is always greater than the one obtained in all calculations . An explanation is presented in SectionIV in terms of a possible shallow third minimum in the region of the second saddle point .

From this comparison, it appears that the Strutinsky prescription is very successful for the calculation of fission barriers capable of explaining many experimental data . Nevertheless, uncertainties of the order of 1 to 2 MeV are still present in the more sophisticated calculations and seem to be inherent in the method itself . For the accurate calculation of fission data,it would seem preferable to rely on fission barrier parameters derived from experiments[29] .

III - FISSION INDUCED BY RESONANCE NEUTRONS

III.1 - Introduction

The interaction of slow neutrons with nuclei provides one of the best examples of compound nucleus formation. The slow neutron cross section of a heavy nucleus is composed of a multitude of sharply defined resonances, as is illustrated in Fig.11 where the measured ^{239}Pu fission cross section is plotted as a function of incident neutron energy E_n . Each of these resonances is caused by the formation of a compound nucleus state λ having well defined spin and parity quantum numbers J^{π} , an excitation energy E^* and a width Γ equal to the natural width of the resonance . In these data, each resonance is broadened by the Doppler and resolution effects. The small value of Γ demonstrates that the nuclear state λ has a long life time of the order of 10^{-16} s. The energy E^* is equal to $S_n + \frac{A}{A+1} E_n$, i.e.just above the neutron separation energy S_n in the compound nucleus $^{A+1}$ (A + 1), where A is the mass number of the target nucleus (Fig. 12) . This energy is typically from 4.5 MeV to 6.5 MeV depending on whether the neutron number N in the target nucleus is even or odd respectively .

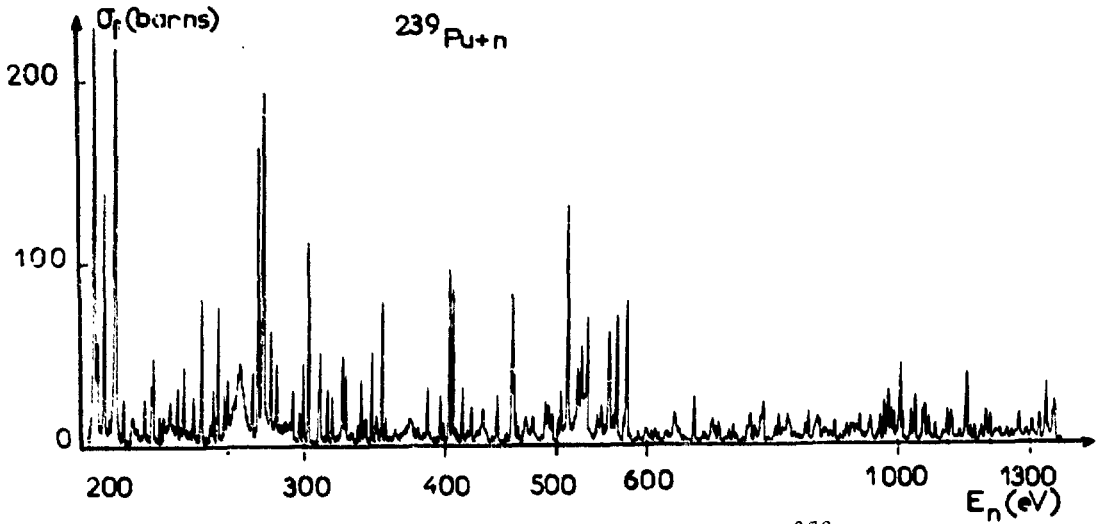

Fig. 11 - High-resolution fission cross section of ^{239}Pu measured with the 45 MeV Saclay linear accelerator used as a pulsed neutron source. The plot of the cross section as a function of neutron energy E_n between 200 eV and 1500 eV shows the extreme complexity of the resonance structure at low neutron energy (After J. Blons et al.[35]).

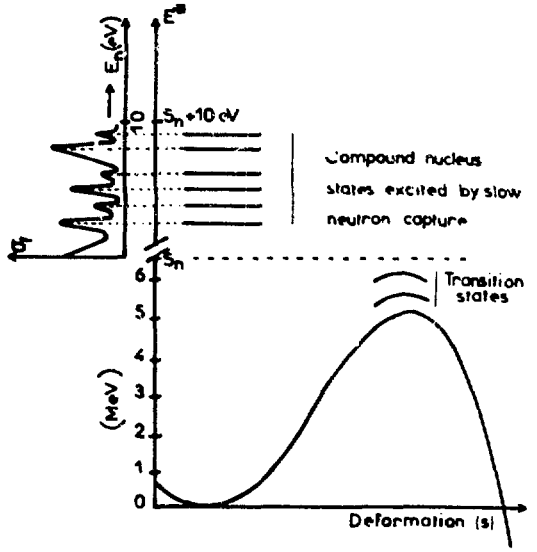

Fig. 12 - Illustration of the fission process induced by resonance neutrons. Note the high density of compound nucleus states excited by slow neutron capture and the scale change at $E^* = S_n$. The fission barrier is drawn with one hump only, for the sake of simplification .

The detailed experimental study of such complex and dense nuclear states at this relatively high excitation energy is made possible thanks to the excellent resolution of neutron time-of-flight spectrometers, as is illustrated in Fig. 13 . At low energy, the individual resonances can be resolved and their shape measured with great accuracy. But the resolution rapidly deteriorates and the Doppler width increases with E_n so that, above a given energy limit E_n^I, level overlap prevents the making of a reliable analysis of individual resonances. Typical values of E_n^I are 3 to 4 keV for even-even actinide nuclei and respectively 1 keV and 100 eV for low spin and high spin odd actinide nuclei .

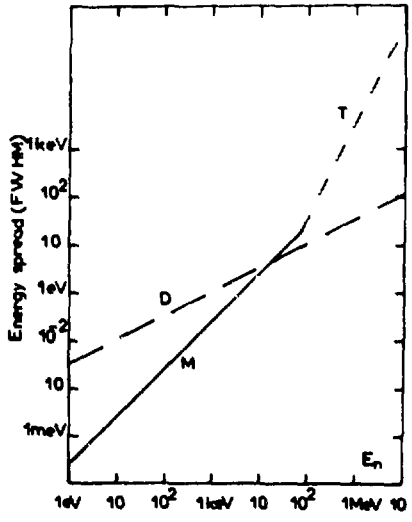

Fig. 13 - Energy spread (FWHM) of neutron time-of-flight spectrometers using white sources .The line D corresponds to the Doppler broadening at room temperature for a heavy nucleus (A = 240) . Line T corresponds to a spectrometer having a resolution of 0.05 ns/m (for example a time resolution of 4 ns and a flight path length of 200 meters) . Line M corresponds to the resolution limited by the moderation time in the neutron source itself (below $E_n \simeq 100$ keV) and to a flight path length of 200 meters .

Only a few J values are possible from the absorption of a slow neutron since the contribution of high angular momentum values is hampered by the effect of the centrifugal barrier . For actinide nuclei, where the "p" wave and "s" wave strength functions are comparable, most of the resonances are due to "s" wave neutrons with a small "p" wave contribution which increases rapidly with neutron energy.

In the resonance region, it is then possible to measure the properties of a well defined process for a large number of states λ and to study i) how these properties vary with J^π , when they are averaged over many states having the same J^π values, and ii) the fluctuations of these properties from resonance to resonance for a given J^π. This requires the lengthy analysis of many resonances, sometimes of the order of one hundred , but, on the other hand,the results that are obtained are very clean, since they are measured for pure states and give a much more detailed

and complete picture than one single measurement, carried out directly for a set of several states λ .

The data are usually analyzed with the single level Breit-Wigner formalism in order to extract the resonance parameters. But, in some cases, especially in fission, level-level interference effects need to be taken into account and a multilevel formalism is sometimes required to fit the shape of the cross section over a wide energy interval containing many resonances . Also, simple level overlap plays a role which may be more important than that of level-level interference[30] . In such cases, analysis of the data with a multilevel formalism, though resulting in a good fit to the cross sections, can lead to parameters without physical meaning .

At the relatively high energy E^* obtained by the absorption of a slow neutron, properties of the states λ usually obey statistical distributions though several interesting non-statistical effects have been identified (see, for example, the Proceedings of the International Conference on Statistical Properties of Nuclei held in Albany (U.S.A.), in 1971) .

For actinide nuclei, the neutron entrance channel does not exhibit any special behavior . Therefore, only the effect of the fission exit channels is considered below when discussing the properties of neutron-induced fission .

The energy E^* is about equal to the height E_f of the fission barrier . In the case of a double-humped barrier, E_f is the height of the higher barrier (inner or outer) . Depending on the odd-even character of N, the energy E^* is either above or below E_f . This reflects the strong effect of pairing on S_n whereas the fission barrier height is less affected by pairing or specialization energy . For even-N nuclei, such as ^{238}U, fission induced by slow neutrons proceeds below the top of the barrier . Assuming a one-humped parabolic barrier top, the penetrability is :

$$P = \left[1 + \exp\left(-2\pi \frac{E^* - E_f}{\hbar\omega}\right) \right]^{-1} \qquad (5)$$

where $\hbar\omega$ is the transparency parameter, related both to the curvature C at the barrier top and to the mass inertia parameter B[31] .

The so-called fission threshold occurs for $E^* = E_f$. But as can be seen from expression (5) fission can also proceed below threshold, with decreasing probability for decreasing E^* . This effect is illustrated in Fig. 14 for the neutron-induced fission of ^{238}U .

Fission properties of slow-neutron resonances are examined below in terms of the fission channel theory of A. Bohr (Section III.2) or of double-humped barrier shapes (Section III.3) .

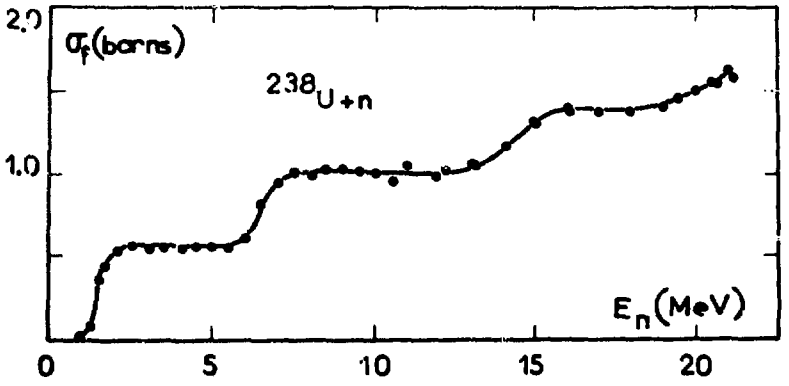

Fig. 14 - Neutron-induced fission cross section of ^{238}U plotted as a function of neutron energy E_n . The general behavior of the fission cross section illustrates the sharp rises which occur at thresholds for first chance fission ($E_n \simeq 1.5$ MeV), second chance fission ($E_n \simeq 6.5$ MeV), etc. This cross section is not meant to show structures which actually appear in more accurate data [6]

III.2 - Fission channel theory of A. Bohr

The fission properties of compound nucleus states could be predicted if their wavefunctions and the fission process were known. But this is far from being the case . The calculation of wavefunctions for compound nucleus states in actinide nuclei at about 6 MeV excitation energy is greatly beyond the present capabilities of nuclear theory and power of computers . But the sheer number and great complexity of the compound nucleus states make it possible to study their properties using statistical assumptions .

A. Bohr showed that many properties of the fission process through these individual excited states could be discussed in terms of a small set of reaction alternatives or channels, even though the number of different fragment pairs is very large in binary fission of a heavy nucleus [32] .

Bohr and Wheeler first introduced the concept of fission exit channels in terms of fission saddle-point configurations which are energetically available [33] . The number N of such "open" fission exit channels is given by the following relation :

$$N = 2\pi \frac{\langle \Gamma_f \rangle}{\langle D \rangle} \qquad (6)$$

where $\langle \Gamma_f \rangle$ and $\langle D \rangle$ are respectively the average fission width and spacing of the resonances. This expression simply comes from the fact that the ensemble of nucleons finds itself in all allowed configurations (including the N fission saddle-point configurations) once every period $\tau \sim 2\pi\hbar / \langle D \rangle$. The life-time τ_f for fission is thus $\tau_f \sim 2\pi\hbar / N \langle D \rangle$ from which the fission width and relation (6) are then deduced .

A. Bohr, in his so-called channel theory of fission, also emphasized the importance of saddle-point configurations for fission properties. For excitation energies slightly above threshold, the fissioning nucleus is "cold" when it passes over the saddle point since most of the excitation energy is then in the form of potential energy of deformation. Therefore, only a few quantum states, called "transition states" i , are energetically available and they are expected to have a spectrum similar to that of the observed low-energy excitations near the ground state . In this situation, there are only a few (say ν) transition states having the same spin and parity J^π , that significantly contribute to the fission decay of compound nucleus states having spin and parity J^π . These transition states play the role of fission exit channels i and, for each of them, there is a specific barrier having penetrability P_i . One can now give a more appropriate interpretation of the number N of fission exit channels defined in (6). Rather than considering the number N of available fission saddle-point configurations, one can define an effective number N_{eff} of fission exit channels, for given spin and parity J^π , which is the sum of the penetrabilities P_i for all the ν channels i having the same spin and parity J^π . Thus :

$$\left(N_{eff}\right)_{J^\pi} = 2\pi \frac{\langle \Gamma_f \rangle_{J^\pi}}{\langle D \rangle_{J^\pi}} = \sum_{i \in J^\pi}^{\nu} P_i \qquad (7)$$

where each P_i has the same expression as in (6) but with a specific value of E_f called E_{f_i} , corresponding to the height of the fission barrier associated with the transition state i .

For common fissile nuclei, the compound nucleus is even-even and the first available transition states, below two-quasi-particle excitations, are of collective character. Their spectrum is sketched in Fig. 15 . Since the neutron separation energy is only slightly larger than the height E_f of the fission barrier for these nuclei, two quasi-particle intrinsic excitations at the saddle point are too high in energy to contribute significantly to fission and their effect is usually neglected . Therefore, at most a few collective transition states, those having the spin and parity J^π of the slow-neutron resonances, need to be considered .

The Bohr theory could be verified, in principle, if fission properties could be measured for well defined fission channels. This is very difficult since fission channels, as such, cannot be identified in the slow-neutron resonances which, on the other hand, have well defined quantum numbers J^π . Common fissile nuclei have a spin I different from zero and therefore, resonances induced by "s" wave neutrons in such nuclei have spin and parity values equal to either $J_+^\pi = (I + \frac{1}{2})^\pi$ or $J_-^\pi = (I - 1/2)^\pi$. Fission channel effects in such fission resonances can be identified only if the channels have sufficiently different properties for the two J_+^π and J_-^π values .

Despite its limitations, the spin determination of the fission resonances is nevertheless essential for the understanding of the fission process in terms of the Bohr theory. This determination is difficult for fission resonances, especially if I is nigh, because i) the two possible values of their statistical factor $g = (2J + 1) / 2(2I+1)$ are quite close and can therefore hardly be distinguished in a scattering measurement ii) both their size and spacing are small ;

this renders difficult their analysis ii.) the prompt-fission neutrons and γ rays which are emitted can seriously hamper the spin determination by means of the yield of scattered neutrons or the spectrum of capture γ rays .

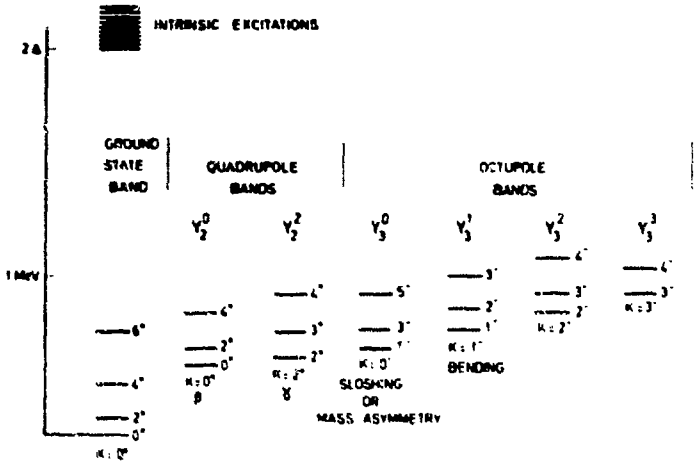

Fig. 15 - Schematic representation of the collective excitations of an even-even nucleus having a quadrupole ground-state deformation . Rotational bands appear associated with the ground state and with quadrupole and octupole vibrations . For each band are indicated the K^{π} value, the spherical harmonics Y_l^m corresponding to the vibration, and also the descriptive names given by various authors . The energy is given for illustration only, but the bands are drawn in the order predicted by Wheeler (After J.S. Fraser and J.C.D Milton [35])

The various methods of spin determination for fission resonances have already been reviewed[34] and are not discussed here .

Some fission properties that may depend on the fission channels and on spin are listed with comments in Section III.2.1 . Examination of the variations of these properties in terms of the fission channel theory of A. Bohr is given in Sections III.2.2 and III.2.3 respectively for ^{239}Pu and ^{235}U fission resonances which are by far the best known of all fissile nuclei . The comparison of fission properties for the neutron resonances of these two nuclei is also of great interest because of the different properties of their fission exit channels [6] .

III.2.1 - Examples of fission properties that may depend on the fission channels

1) Fission widths. This is a direct consequence of equation (7) not only for the average value $< \Gamma_f >_{J\pi}$ but also for the fluctuations of Γ_f that depend on the number of exit channels and on the average value of the partial fission width $<\Gamma_{fi}>$ for each channel i .

2) Mass distribution of the fission fragments

The mass distribution is known to be very asymmetric for low-energy fission of actinide nuclei and is now qualitatively understood thanks to more precise calculations of the potential energy surface of the fissioning nucleus at large deformations (see Section II.3). But the mass distribution may also be slightly influenced by symmetry properties of the transition states. For example, the peak-to-valley ratio of this distribution may be larger for octupole vibrational states (which are asymmetric) than for quadrupole vibrational states (which are symmetric) .

3) Kinetic energy of the fission fragments

This energy is determined by the Coulomb repulsion at scission, with the possible addition of pre-scission kinetic energy which depends on viscosity effects (see Section V) . Since the Coulomb energy is determined by the scission configuration, the total kinetic energy is closely related to the mass distribution . Any change in the latter should be reflected in the former .

4) Average number $\bar{\nu}$ of prompt fission neutrons

Usually, $\bar{\nu}$ measurements are averaged over all mass divisions . But, more detailed studies show that $\bar{\nu}_{A_f}$ for each fragment depends on the mass A_f of this fragment with a kind of saw-tooth behavior . Therefore, as for the kinetic energy, any change in the mass distribution of the fission fragments should be reflected in the overall $\bar{\nu}$ value .

5) Emission probability and energy spectrum of long-range α particles

Though the evidence is not as conclusive as for neutron emission, it seems that the emission probability of long-range α particles varies as a function of A_f . Therefore, as for the other fission aspects discussed above, the properties of long range α particles emitted in fission should also be sensitive to the symmetry properties of the transition states .

6) Angular distribution of the fission fragments

This distribution is another interesting consequence of the Bohr theory, because i) near threshold, only a few transition states are available with specific values of K, the projection of the total angular momentum along the symmetry axis, and ii) from saddle point to scission the passage is assumed to be so rapid that Coriolis forces, which are weak, do not seem to change the value of K . Thus , at scission, the fissioning nucleus keeps the same value of K which, for given values of J and M, governs the angular distribution $W^J_{KM}(\theta)$ of the fission fragments emitted along the symmetry axis . More precisely :

$$W^J_{KM}(\theta) \propto \left| D^J_{KM}(\theta) \right|^2 \qquad (8)$$

where $D^J_{KM}(\theta)$ is the symmetric top wave function and θ is the angle of the symmetry axis relative to the reference axis .

In actual practice, the observed angular distribution $W^J(\theta)$ of the fission fragments, for a given J , has to be compared to a suitably weighted sum of W^J_{KM} functions over K and M values . The summation and the weights on K and M quantum numbers depend on the process under study and on the experimental conditions . Specific examples are given below in Sections II.2.3 and IV.2 .

III.2.3 - ^{239}Pu fission resonances . Evidence of the (n, γ f) reaction

Resonances induced by "s" wave neutrons in ^{239}Pu have $J^\pi = 0^+$ or 1^+ . This situation is quite favorable since the low spin value of the resonances leads to relatively large spacings and neutron widths of these resonances . They are big and well separated and therefore almost all of them can be easily analysed in a given range of incident neutron energies . Moreover, because the two possible g values ($\frac{1}{4}$ and $\frac{3}{4}$) are widely different, the spin determination is possible for more than one hundred resonances below 660 eV .

For the $J^\pi = 0^+$ fission resonances, there is at least one fully open 0^+ fission exit channel, that of the ground state, since it lies about 1 MeV below S_n . Another partially open 0^+ channel may be provided by the $K^\pi = 0^+$ β vibration though this transition state is often excluded from the scheme of transition states since this is the main fission mode . In contrast, no simple 1^+ collective excitation seems to exist below S_n + 1 MeV where two-particle states start to be excited .

The large energy difference between the lowest 0^+ and 1^+ transition states is actually reflected in the fission width distribution plotted in Fig. 16 where two families of resonances are clearly visible[35]. The two groups of narrow and wide fission resonances have been shown, by various methods, to have $J^\pi = 1^+$ and $J^\pi = 0^+$ respectively .

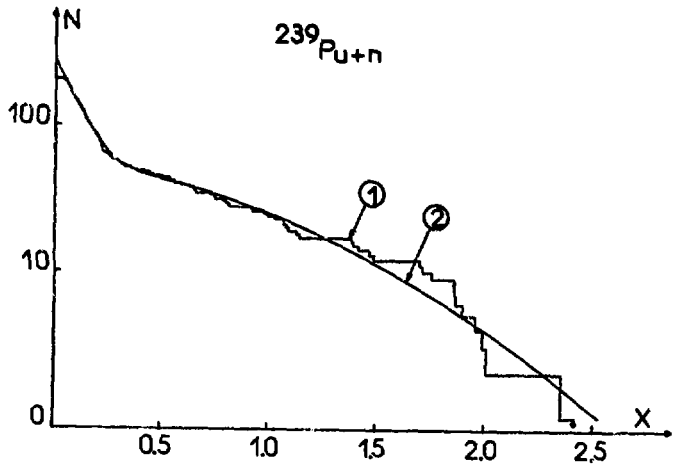

Fig. 16 - Integral distribution of the fission widths Γ_f for the ^{239}Pu neutron resonances that could be analyzed below 660 eV. N is the number of resonances having a value of $\sqrt{\Gamma_f / \langle \Gamma_f \rangle}$ greater than the abscissa X . The average value $\langle \Gamma_f \rangle$ of the fission widths is taken over all the analyzed resonances . The experimental histogram ① is fitted with two chi-squared distributions ②, having the parameters :

$$\langle \Gamma_f \rangle = 0.035 \text{ eV} , \quad \nu = 1$$

$$\langle \Gamma_f \rangle = 2.27 \text{ eV} , \quad \nu = 1.4 .$$

These two distributions are interpreted as corresponding to the two spin states $J^\pi = 1^+$ and $J^\pi = 0^+$, respectively . A constant width of 3.5 meV has been subtracted to remove the calculated contribution of the $(n,\gamma f)$ process (After J. Blons et al. [35]) .

The values of N_{eff} and ν for these two groups are :

$J^{\pi} = 1^+$: $N_{eff} = 0.07$ and $\nu = 1$ (9)

$J^{\pi} = 0^+$: $N_{eff} = 1.48$ and $\nu = 1.4$. (10)

This is in excellent agreement with the theory of A. Bohr provided that a 1^+ transition state, resulting from the coupling of $K^{\pi} = 0^-$ and $K^{\pi} = 1^-$ octupole vibrations, lies at about S_n + 200 keV , well below two-quasi-particle excitations[6].

It turns out that, for ^{239}Pu fission resonances, the two most important 0^+ and 1^+ transition states are quite different not only in energy, as pointed out above, but also in shape since the 0^+ state is symmetric but the 1^+ is asymmetric (combination of octupole vibrations) .

The symmetry character of these transition states seems to appear in the measurements of the mass distribution . The valley-to-peak ratio of this distribution, or more exactly the $^{115}Cd/^{99}Mo$ ratio called R, was measured for more than twenty resonances with the "wheel technique", using an underground nuclear detonation as a single pulse neutron source[36] . As can be seen in Fig. 17, the R values seem to fall into two categories, having average values of R in ratio 3.5, and corresponding to the two spin states 0^+ and 1^+ . As expected from the theory , high-R and low-R groups belong to the 0^+ and 1^+ spin states respectively

Moreover there is also a correlation between the R values and Γ_f , as predicted by the theory (Fig. 18) . The fission widths are larger, on the average, for the high-R group of resonances . In this group, a few resonances are so broad that their spin could not be measured . From their high value of both R and Γ_f, one can deduce that these resonances have $J^{\pi} = 0^+$ and this is confirmed by the multilevel analysis of the total and fission cross sections[37] .

The behavior of $\bar{\nu}$ from resonance to resonance was more difficult to understand for a long time . Several years ago, the two most complete sets of data then available showed definite variations in $\bar{\nu}$, but in opposite directions[38,39] . Moreover, these variations could be correlated with J but in a different manner ; for one data set[38] the high $\bar{\nu}$ values were associated with $J^{\pi}=1^+$, but with $J^{\pi}=0^+$ for the other set[39] . Nevertheless both results could be explained by the Bohr theory. A high value $\bar{\nu}$ for the 0^+ resonances[39] can be justified by postulating that the 1^+ fission barrier remains higher than the 0^+ one all the way to scission . Then, neglecting viscosity effects, the energy difference is found as an increase in the excitation energy of the fission fragments for the 0^+ resonances, hence as a higher prompt neutron emission . Another argument, still derived from the Bohr theory, can be invoked to explain the other data set[38] . Since the 1^+ transition state is asymmetric, it should result in a more asymmetric mass division, as observed, and hence in a higher $\bar{\nu}$ value .

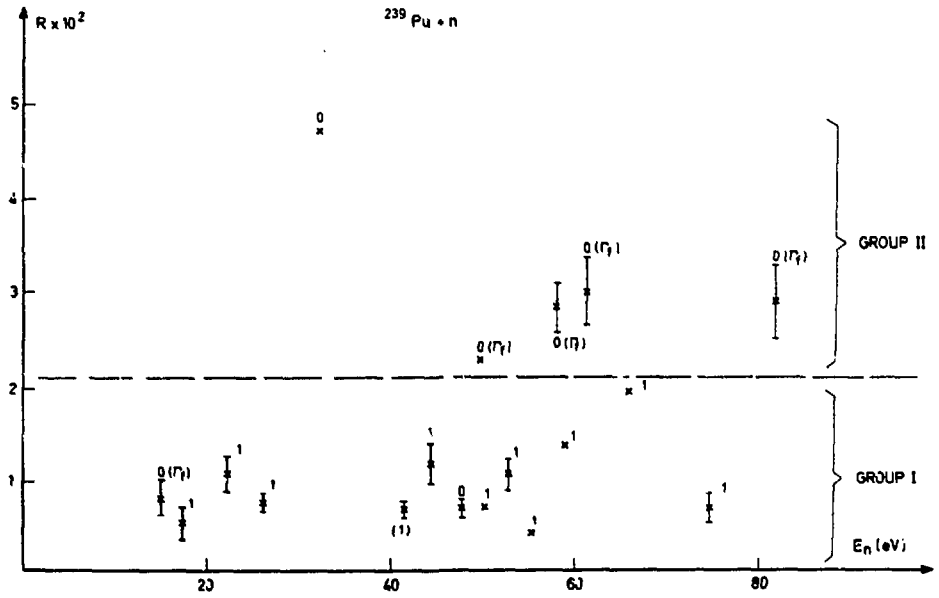

Fig. 17 - The ratio R (multiplied by 10^2) of the yield of ^{115}Cd relative to that of ^{99}Mo produced in fission induced by slow neutrons in ^{239}Pu, as measured by G.A. Cowan at neutron resonances [36], is plotted as a function of resonance energy. The spins J = 0 or J = 1 of the resonances, as determined and compiled by J.Trochon [46] are indicated near the plotted value of R. Spin values J = 0 , marked by 0 (Γ_f), are deduced only from the large fission width of the resonance . There seems to be a clear separation of the resonances (with two exceptions) into two groups corresponding to the two spin states .

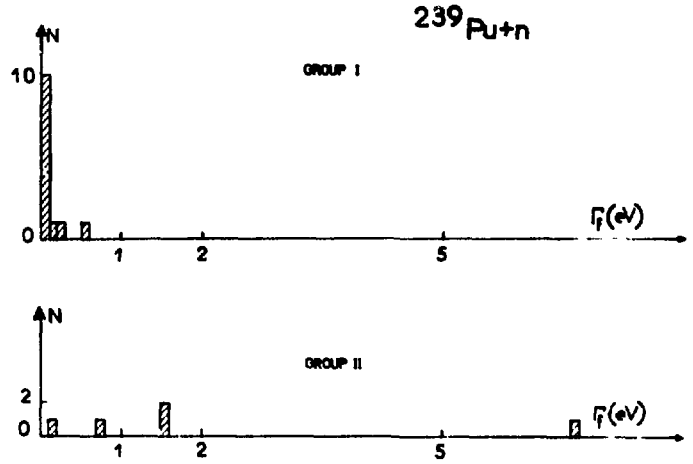

Fig. 18 - Frequency distributions of the Γ_f values for the two groups of ^{239}Pu resonances, as they appear in Fig. 17 . This plot is similar to that drawn by G.A. Cowan [36] but with more recent values of the fission widths [6,37] .

The situation was clarified by recent measurements carried out at Saclay on prompt fission neutron and γ-ray emission .In one experiment, both $\bar{\nu}$ and $\bar{E}_\gamma$ (the mean fission γ-ray energy) were measured for a large number of resonances, using a big Gd-loaded liquid scintillator for the detection of prompt neutrons and γ rays[40] . The results are plotted separately for the 1^+ and 0^+ resonances in Figs. 19 and 20 respectively .

Examination of the data for the 1^+ resonances leads to the following remarks :

First, large fluctuations are observed both in $\bar{\nu}$ and in $\bar{E}_\gamma$ and they are far greater than the error bars. Tests show that there is only a very weak proba - bility ($< 5.10^{-5}$) that these variations come from statistical fluctuations only .

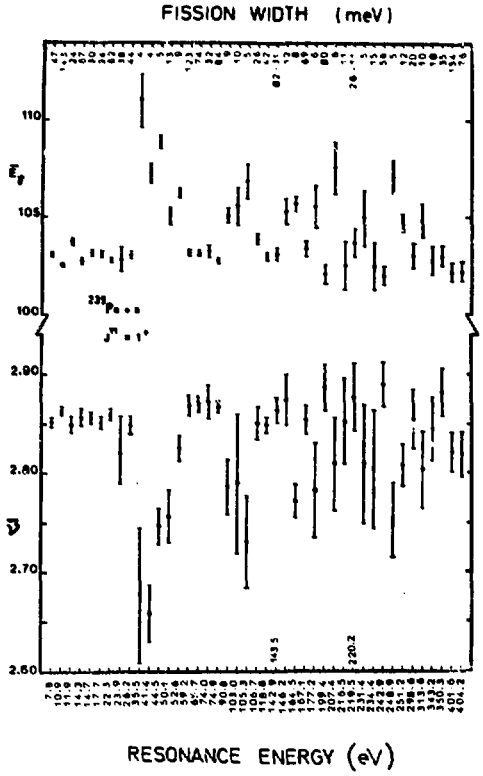

Fig. 19 - Plot of the average prompt fission neutron and γ-ray yields (respectively $\bar{\nu}$ and $\bar{E}_\gamma$, as defined in the text) as a function of the resonance energy for the ^{239}Pu resonances having $J^\pi = 1^+$ and analyzed below 405 eV. The scale for $\bar{E}_\gamma$ is given in arbitrary units. The value of Γ_f is given on the upper horizontal scale for each resonance[40].

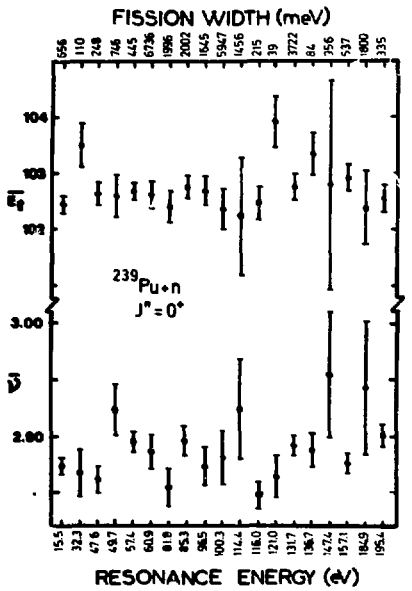

Fig. 20 - Same plot as in Fig. 19 but for the the $J^\pi = 0^+$ resonances that could be analyzed below 200 eV.[40].

Secondly, there is an anticorrelation between the $\bar{\nu}$ and $\bar{E}_\gamma$ variations . For example high $\bar{\nu}$ values are generally associated with low $\bar{E}_\gamma$ values . The correlation coefficient between $\bar{\nu}$ and $\bar{E}_\gamma$ data sets is $- 0.84 \pm 0.12$.

Thirdly, the variations in opposite directions for $\bar{\nu}$ and $\bar{E}_\gamma$ are larger for small Γ_f resonances . This effect appears clearly in Fig. 21 where both $\bar{\nu}$ and $\bar{E}_\gamma$ values are plotted as a function of $(\Gamma_f)^{-1}$.

The same effects also show up for 0^+ resonances but are less pronounced .

Different measurements of $\bar{\nu}_\gamma$, the average multiplicity of fission γ rays, show results having a behavior similar to those for $\bar{E}_\gamma$[41] .

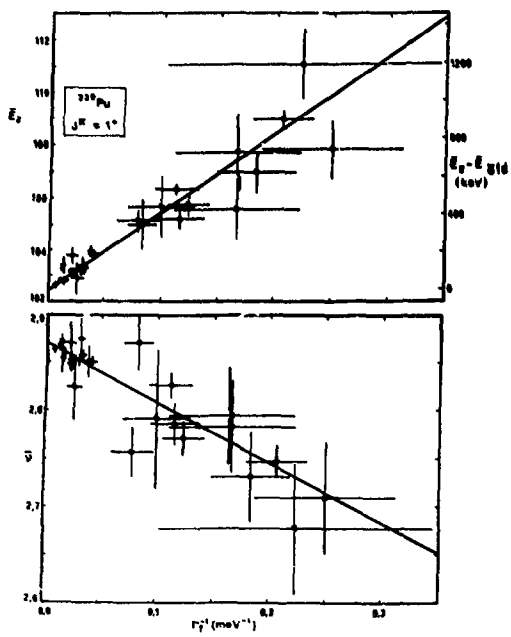

Fig. 21 - Plot of the average prompt fission neutron and γ -ray yields (respectively $\bar{\nu}$ and $\bar{E}_\gamma$, as defined in the text) as a function of Γ_f^{-1} for the ^{239}Pu resonances having $J^\pi = 1^+$ and analyzed below 200 eV . The scale for $\bar{E}_\gamma$ is given in arbitrary units . The difference $(\bar{E}_\gamma - \bar{E}_{\gamma fd})$ between the observed γ -ray energy $\bar{E}_\gamma$ and the estimated γ -ray energy $\bar{E}_{\gamma fd}$ for "direct fission" (defined in the text) is given in keV . The solid lines are least-squares fits to the data[40] .

All these results were interpreted in terms of the (n, γ f) reaction in which a γ ray is emitted after compound nucleus formation, but before scission . This effect was already considered from a theoretical point of view[42] but was not clearly identified before the results mentioned above were available . In the (n,γ f) reaction, compared to "direct fission" called (n, f d), less excitation energy is available at scission, thus resulting in a decreased neutron emission . This is in contrast to the overall γ -ray emission which is larger because, in addition to the γ -ray deexcitation of the fragments below threshold for neutron emission, pre-scission γ -rays are emitted prior to scission . The competition between (n,γf) and (n, f d) reactions is governed by the widths $\Gamma_{\gamma f}$ and Γ_{fd} respectively, with :

$$\Gamma_{\gamma f} + \Gamma_{fd} = \Gamma_f \qquad (11)$$

The $\Gamma_{\gamma f}$ width is expected to be fairly small (a few meV according to calculations[42]) and constant from resonance to resonance since it corresponds to a process with many exit channels for the pre-scission γ rays . In contrast, the width Γ_{fd} is larger but shows large fluctuations due to the small number of transition states . Therefore, the competition between the (n,γ f) and (n, f d) processes should vary from resonance to resonance , with the consequence that Γ_{fd} can become comparable to $\Gamma_{\gamma f}$ for a few of them, more likely to have $J^\pi = 1^+$ than $J^\pi = 0^+$ since $\langle \Gamma_f \rangle_{0^+} \gg \langle \Gamma_f \rangle_{1^+}$.

These consideration lead to the following relations for the average neutron and γ -ray yields in the fission resonances where the (n, γ f) and (n, f d) processes are present .

$$\bar{E}_\gamma = \bar{E}_{\gamma fd} + \bar{e}_\gamma \frac{\Gamma_{\gamma f}}{\Gamma_f} \qquad (12)$$

$$\bar{\nu} = \bar{\nu}_{fd} - \bar{e}_\gamma \frac{\partial \bar{\nu}}{\partial E^*} \cdot \frac{\Gamma_{\gamma f}}{\Gamma_f} \qquad (13)$$

In the above expressions :

. $\bar{\nu}_{fd}$ and $\bar{E}_{\gamma fd}$ are the average yields of neutrons and γrays respectively for the (n, f d) process ,

. $\bar{e}_\gamma$ is the average γ-ray energy of the pre-scission γrays in the (n,γf) process ,

and $\frac{\delta \bar{\nu}}{\delta E^*}$ is the variation of $\bar{\nu}$ with excitation energy E^* of the fissioning system .

Expressions (12) and (13) are derived assuming simple physical assumptions and ignore small effects such as competition between neutron and γ-ray fragment deexcitation above neutron emission threshold[43]. The yields $\bar{\nu}$ and $\bar{E}_\gamma$ derived in (12) and (13) show a linear dependence on $(\Gamma_f)^{-1}$ which is actually observed for the 1^+ resonances (Fig. 21) . The effect is certainly present also in the 0^+ resonances but is masked by their large fission width .

Analysis of the data gives the following values for the product $\Gamma_{\gamma_f} \cdot \bar{e}_\gamma$:

$J^\pi = 1^+$ resonances : $\Gamma_{\gamma_f} \cdot \bar{e}_\gamma = (4.6 \pm 0.4)\ 10^3$ eV^2 (14)

$J^\pi = 0^+$ resonances : $\Gamma_{\gamma_f} \cdot \bar{e}_\gamma = (8.0 \pm 1.9)\ 10^3$ eV^2 (15)

These values are in agreement with recent calculations using conventional sumptions about the γ-ray and fission decays of the compound nucleus[40] . The $(n,\gamma f)$ fect also explains the fact no resonances are observed with a fission width smaller an 4 meV, which is very close to the expected value for Γ_{γ_f} .

After removal of the $(n,\gamma f)$ effect, the neutron and γ-ray yields for rect fission and for the two spin states are :

$$(\bar{\nu}_{fd})_{0^+} - (\bar{\nu}_{fd})_{1^+} = 0.0130 \pm 0.0055 \text{ neutrons} \quad (16)$$

$$(\bar{E}_{\gamma_{fd}})_{0^+} - (\bar{E}_{\gamma_{fd}})_{1^+} = 10 \pm 10 \text{ keV} \quad (17)$$

This results in the following difference in fragment excitation energy E^t_{exc} r the two spin states

$$(E^t_{exc})_{0^+} - (E^t_{exc})_{1^+} = 109 \pm 43 \text{ keV} \quad (18)$$

Therefore, there is a weak spin effect on prompt neutron emission and fragnt excitation and also possibly on prompt γ-ray energy . But, most of the vations observed both in $\bar{\nu}$ and $\bar{E}_\gamma$ are due to the effect of the $(n,\gamma f)$ reaction d not to the fission exit channels, as was postulated previously .

III.2.3 - ^{235}U fission resonances

Resonances induced by "s" wave neutrons in ^{235}U have $J^\pi = 3^-$ or 4^- . This tuation is not as favorable as for ^{239}Pu since the resonances are small in size d closely spaced, with appreciable overlap. Moreover, the two possible values of are so close that spin determination by the elastic scattering method is hardly ssible . Fortunately, recent measurements using polarized neutrons and polarized ^{5}U nuclei were carried out on a large scale, resulting for the first time in unamguous spin determination for a substantial number of resonances[44] .

The transition states have very similar properties for the two spin states ig.15). The only difference appears for the $K^\pi = 0^-$ band which contains a 3^- sabut not a 4^- one . Nevertheless this difference is not expected to play a major le especially since the $K^\pi = 0^-$ contribution is surprisingly weak as discussed below.

The fission width distribution for 124 resonances analyzed with the single-vel formalism below 150 eV is plotted in Fig.22 and can be fitted with one χ^2 faly only[45]. There is no indication of a break which would suggest the existence of o families such as required to fit similar data for ^{239}Pu.

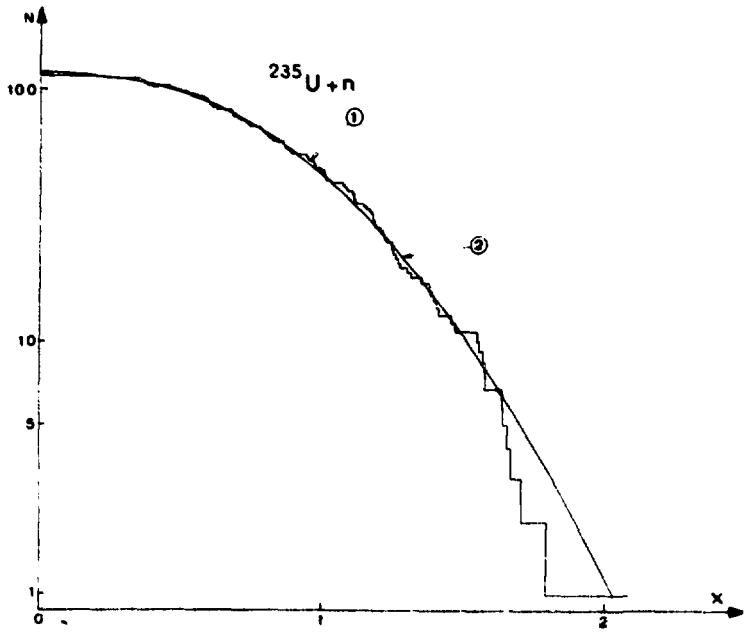

Fig.22 - Integral distribution of the fission widths Γ_f for the ^{235}U neutron resonances that could be analyzed below 150 eV. N is the number of resonances having a value of $\sqrt{\Gamma_f/\langle\Gamma_f\rangle}$ greater than the abscissa x. The average value $\langle\Gamma_f\rangle$ of the fission widths is taken over all the analyzed resonances. The histogram ① shows the extensive fluctuctions of the measured fission widths. The best fit (curve ②) to the experimental histogram with a chi-squared distribution is obtained with the following parameters : $\langle\Gamma_f\rangle$ = 0.073 eV, ν = 2.8 (After J. Blons et al.[45]).

The values of N_{eff} for the two spin states, using spin values given in[45] are the following :

$$J^\pi = 3^- \quad : \quad N_{eff} = 0.43 \qquad (19)$$

$$J^\pi = 4^- \quad : \quad N_{eff} = 0.38 \qquad (20)$$

These two values are very close and also fairly low, taking into account the location of the octupole bands at the saddle point. More exact values of N_{eff} would be obtained if all resonances could be analyzed in a given energy range, but this is not possible with unpolarized neutrons and targets because of level overlap. The resonances that are missed are expected to have, on the average, small neutron widths and large fission widths[46] and their contribution would then tend to enhance the values derived in (19) and (20). This could be especially true for the J = 3 resonances since they are found relatively too few in number in the polarization experiment[44]; several of them, having a large fission width could have been mis-

Larger values of N_{eff} are actually obtained from a multilevel analysis of the cross sections[47]. A good fit to the data is obtained with this type of analysis but this does not mean that the resonance parameters have always a physical meaning, especially for a target nucleus such as ^{235}U where level overlap plays a more important role than level-level interference[30] .

The mass distribution of the fission products was measured for ^{235}U resonances[48] in the same manner as for those of ^{239}Pu. The distribution in R-values obtained from the experiment is narrower than that of ^{239}Pu and it also appears to be composed of two groups of resonances though the separation is not as clear as for ^{239}Pu (see Fig. 23). No correlation seems to exist between R and Γ_f but a weak correlation appears between R and J, as discussed below .

The study of the angular distribution of the fission fragments, when fission is induced by non polarized slow neutrons in aligned ^{235}U nuclei, provided interesting information about the transition states in ^{236}U[49,50]. Under the assumptions derived from the theory of Bohr, the expression (8) can be applied to the case of quadrupole coupling used to align the target ^{235}U nuclei. For a given set of quantum numbers K,J and for the range of temperature employed in the experiment, the angular distribution $W_K^J(\theta)$ of the fission fragments is given by the following expression :

$$W_K^J(\theta) = 1 + A_2 f_2 P_2(\cos\theta) \qquad (21)$$

where :

θ is the emission angle of the fission fragments relative to the c-axis of the crystal,

f_2 is the alignment parameter,

P_2 is the Legendre polynomial of order 2

and $$A_2 = \frac{15}{4} \frac{I}{(I+1)} \left(\frac{3K^2}{J(J+1)} - 1 \right) \qquad (22)$$

The distribution in measured A_2 values[50] shows the absence of the K = 0 contribution which, according to the Bohr theory, should be the most important one (Fig. 24) . The value of K can be obtained with relation (22) for the resonances that have measured values of both A_2 and J . The K values thus derived are comprised between 1 and 2 with the following averages for the two spin states :

$$J^\pi = 3^- \quad : \quad K = 1.51 \qquad (23)$$

$$J^\pi = 4^- \quad : \quad K = 1.60 \qquad (24)$$

These two values are very close, demonstrating that the fission channels have very similar properties for the two spin states. The apparent inhibition of the $K^\pi = 0^-$ band can tentatively be interpreted with the double-humped fission barrier representation, assuming for example that no $K^\pi = 0^-$ class II vibrational state is available in the vicinity of the neutron separation energy .

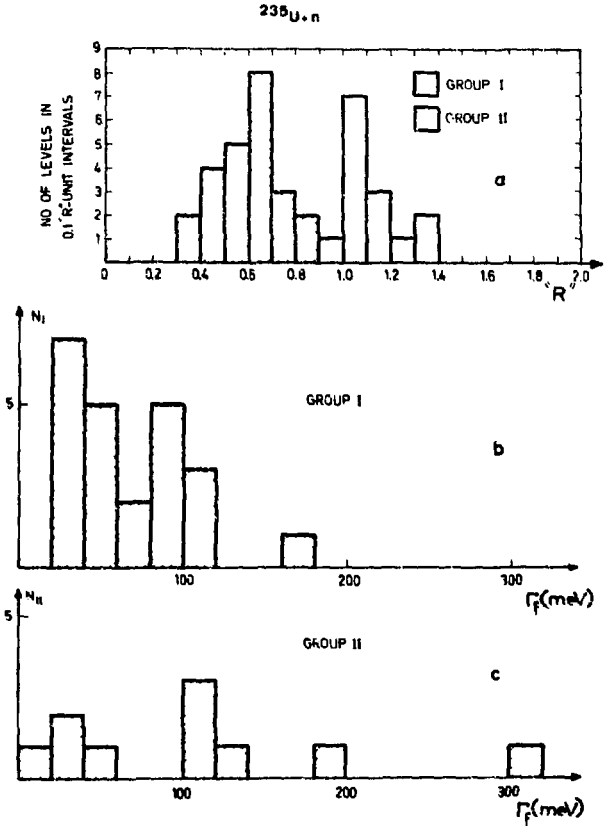

Fig. 23 - Frequency distribution of the "R" values at the measured ^{235}U neutron resonances (a) and of the fission widths associated with Groups I and II (b,c) . "R" is the mass asymmetry parameter R relative to the thermal R value . This figure is similar to that drawn by G.A. Cowan [48] except for the distributions of the fission widths where more recent values have been used [45] .

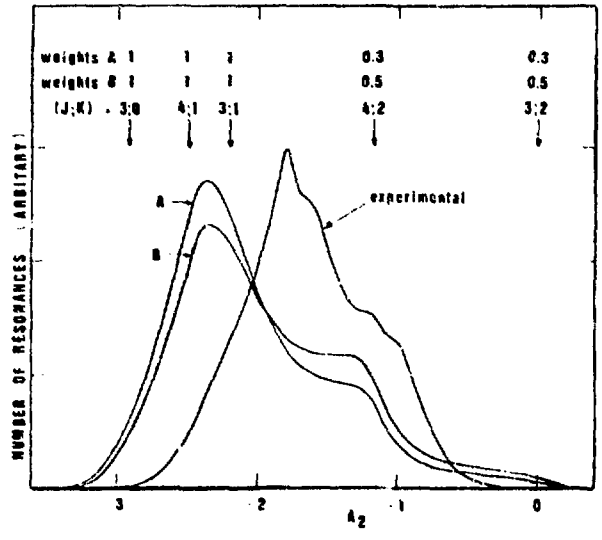

Fig. 24 - Weighted frequency distribution for oberved A_2 values in the ^{235}U resonances (see the text) . Two simulated distributions A and B for A_2 are also shown for comparison with the data . The latter were obtained under the assumptions of equal contributions from the two spin states, a random selection from a Porter-Thomas distribution for Γ_{fK} and assuming relative weights for different channels as indicated in the figure . Positions of calculated A_2 (J,K) values are also shown (except for K = 3 and 4) . (After N.J. Pattenden and H. Postma [50]) .

The knowledge of K for several resonances makes it possible to study the influence of the fission channels on the mass distribution, for example through the dependence of "R" (defined in Fig. 23) and K. A plot of K^2 versus "R" for 16 resonances is given in Fig. 25 . A definite trend is observed showing that on the average a large value of K is associated with a large value of "R".

Some correlation between R and K is expected from the Bohr theory but it is not quite clear why the K = 2 channel should lead to more symmetric fission than the K = 1 channel. In addition to this correlation, a spin effect seems to be present since the plot given in Fig. 25 clearly shows a separation between the results corresponding to J = 3 and J = 4 . Such an effect is still more difficult to understand in terms of the Bohr theory .

Prompt neutron emission was studied on several occasions and the measured $\bar{\nu}$ values actually showed variations from resonance to resonance, but smaller than for ^{239}Pu [39,52,53, 54] . Some of the results were tentatively explained by a spin effect but this interpretation was ruled out later by unambiguous assignments obtained from

a polarization experiment[44]. The experimental discovery of the $(n,\gamma f)$ reaction in the ^{239}Pu fission resonances stimulated the search for a similar phenomenon for ^{235}U. In the same manner as for ^{239}Pu resonances, prompt fission neutron and γ-ray yields were measured for ^{235}U resonances[40]. Definite variations both in $\bar{\nu}$ and $\bar{E}_\gamma$ were observed from resonance to resonance though these variations are not as pronounced as for ^{239}Pu. Analysis of the results for both spin states J = 3 and 4 shows a linear dependence of both $\bar{\nu}$ and $\bar{E}_\gamma$ as a function of $(\Gamma_f)^{-1}$, with opposite signs as for ^{239}Pu though the effect is not as clear-cut. Nevertheless, taking into account the existence of the $(n,\gamma f)$ reaction clearly demonstrated for ^{239}Pu, the results obtained for ^{235}U and analyzed in the same manner as for ^{239}Pu can also be interpreted in terms of the $(n,\gamma f)$ reaction. This analysis gives the following results :

$$\Gamma_f \cdot \bar{e}_\gamma = (1480 \pm 650)\ eV^2 \text{ for } J^\pi = 3^- \qquad (25)$$

and

$$\Gamma_f \cdot \bar{e}_\gamma = (5.140 \pm 3480)\ eV^2 \text{ for } J^\pi = 4^- \qquad (26)$$

After removal of the $(n,\gamma f)$ effect, it is not possible to distinguish a spin dependence of the excitation energy of the fission fragments.

In summary, the fission channel theory of Bohr has provided the Ariadne's thread for the understanding of many aspects of fission induced by resonance neutrons. This theory is generally well verified for the ^{239}Pu fission resonances, which are the best known. This is in contrast to the situation for ^{235}U fission resonances where interpretation is still unclear. The variations of prompt fission neutron and γ-ray yields in the resonances of these two nuclei are very well explained by the effect of the $(n,\gamma f)$ reaction whose existence seems now firmly established from the results obtained for ^{239}Pu. This interpretation renders unnecessary the influence of the fission exit channels which seem to play a minor role in these $\bar{\nu}$ and $\bar{E}_\gamma$ variations.

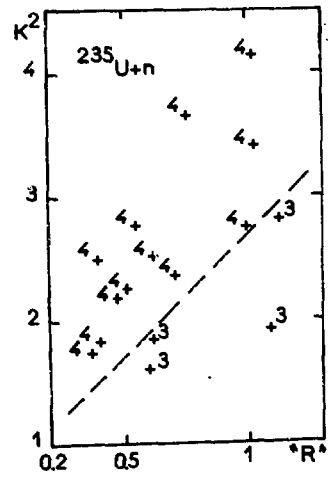

Fig. 25 - Plot of K^2 versus "R" for ^{235}U resonances. The K^2 values are obtained from the angular distribution of the fission fragments[50] and the spin determination of the resonances[44]. "R" is proportional to the valley-to-peak ratio of the fission fragment mass distribution[48]. The spin value (J=3 or 4) is marked near each resonance point. A similar plot was made between K and A_2 (defined in the text)[51].

III.3 - Intermediate structure effects in sub-barrier fission cross sections.

The discovery made about a decade ago of a strong intermediate structure effect in the subthreshold fission cross section of some actinide nuclei is certainly one of the most fundamental contribution of neutron-induced fission to nuclear physics . This dramatic phenomenon came as a surprise in the course of a systematic study of auto-correlations in the cross sections of actinide nuclei where short-range correlations of this type, butweaker, had already been observed for a few fissile nuclei . The improvements in intensity of pulsed neutron sources and in fission detector efficiency made it possible to extend this type of study to non-fissile nuclei for which the fission cross section is very small due to the tunelling through the fission barrier. A strong intermediate structure effect in the fission cross section appeared in the study of ^{237}Np . A similar effect was found later for other non fissile nuclei such as ^{240}Pu, ^{234}U, ^{238}U etc...[6] .

As an illustration of this phenomenon, the ^{237}Np fission cross section is plotted as a function of incident neutron energy E_n in Fig. 26 . Instead of being uniformly distributed as a function of E_n , the fission resonances are grouped in clusters at definite energies : 40 eV, 120 eV etc... About 40 such clusters can be identified up to 2000 eV, with an average spacing $\langle D_{II} \rangle \simeq 50$ eV, roughly 100 times that of the individual resonances observed in the total cross section. Between the clusters, fission resonances are so small that they can hardly be detected .

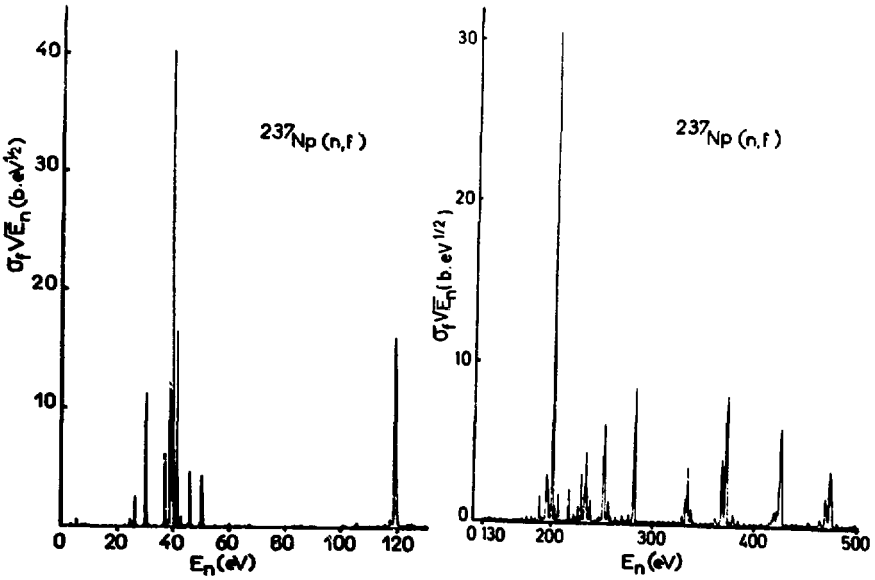

Fig. 26 - The Saclay ^{237}Np fission cross section multiplied by $\sqrt{E_n}$ is plotted as a function of incident neutron energy E_n below 500 eV [62] . The fine structure in the first cluster at 40 eV is resolved but, at higher energy, the experimental resolution smoothes out the fine structure in the clusters and at still higher energy the clusters themselves disappear in the data (see the text in Sections III.3 and IV.1) . This figure shows the best data now available, but the intermediate structure effect was already reported for data obtained earlier[6] .

In the total cross section, the resonances are distributed according to the conventional properties of compound nucleus states. This is illustrated in Fig. 27 where the cumulative sums of the reduced neutron widths $\Gamma_n^o = \Gamma_n E_n^{-1/2}$ and of the fission widths are plotted as a function of E_n . The behavior of these two histograms clearly demonstrates that the intermediate structure effect is not due to the neutron entrance channel but, rather, to the fission exit channels which are more strongly coupled to the compound nucleus states at the cluster energies .

An interpretation of this puzzling phenomenon was given by Lynn[55] and Weigmann[56] in terms of the double-humped fission barrier, as is illustrated in Fig. 28 .According to this interpretation, the large fission yields in the clusters are due to the coupling between class I and class II compound nucleus states. This coupling occurs when class I states are close in energy to a class II state having the same J^π quantum numbers. The fission width $\Gamma_{f_{II}}$ of a class II state is much larger than for a class I state since only the outer barrier and not the whole barrier needs to be penetrated for the fission decay of a class II state .

The class II components in the class I states then cause the fission width of these last states to be much larger than the one which would correspond to the penetrability of the whole barrier, in the absence of coupling to class II states .

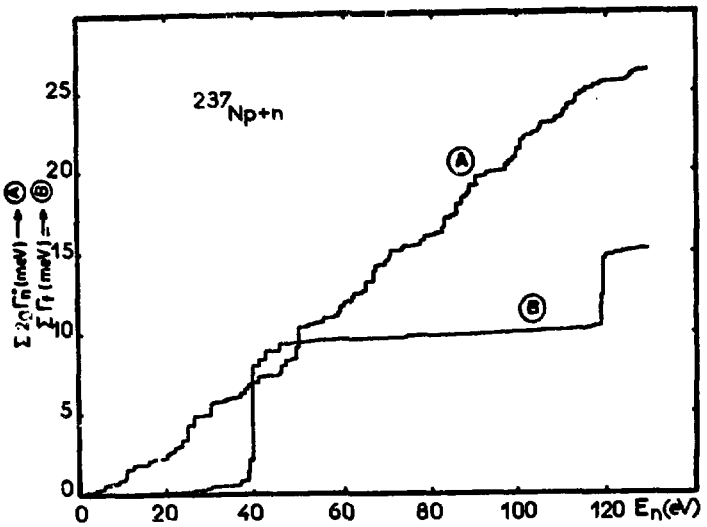

Fig. 27 - The cumulative sums of the reduced neutron and fission widths, for the ^{237}Np resonances that could be analyzed at low energy, are plotted as a function of neutron energy. Histograms A and B correspond to reduced neutron widths and fission widths respectively. This picture demonstrates that the intermediate structure is not caused by the neutron entrance channel but to the fission exit channels [6,87] .

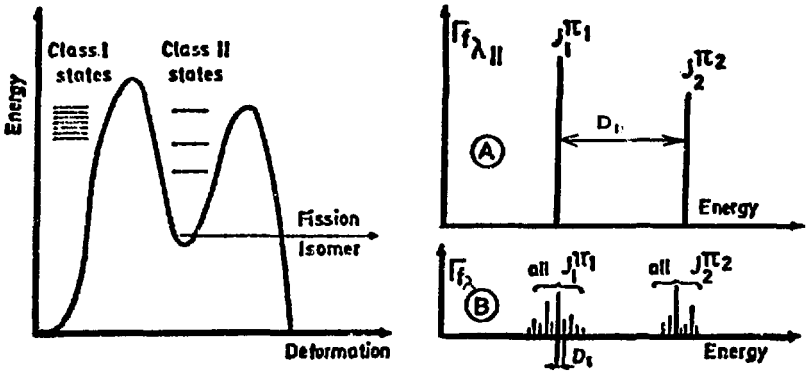

Fig. 28 - Mechanism of intermediate structure in subthreshold fission cross sections . Clusters appear in the fission cross section when energy, spin and parity of a class-II state match those of the class-I resonances (at most two J^{π} values are possible for "s" wave neutrons). The fission widths are drawn at the energy of the respective levels for class-II states (diagram A) and for the observed resonances (diagram B) .

This interpretation was supported recently by the spin determination of the ^{237}Np resonances from a polarization experiment [57] . The results obtained in this experiment are plotted in Fig. 29 for the first cluster at 40 eV . A big difference is noticed between the fission cross sections corresponding to the J = 3 and J = 2 states populated by "s" wave neutrons. All the large fission resonances have J = 3 whereas the J = 2 fission contribution is negligible. These results are quite consistent with the interpretation of the large fission resonances coupled to a J = 3 class-II state in the vicinity of E_n = 40 eV .

The difference in spacings $\langle D_I \rangle$ and $\langle D_{II} \rangle$ simply comes from the fact that, for a given total energy of the nuclear system, less excitation energy is available in the second well compared to the first well since the former is shallower than the latter. Making simple assumptions, the ratio $\langle D_I \rangle / \langle D_{II} \rangle$ yields the energy E_{II}.

Adopting the formalism developed by Lynn, one can write the following expression of the fission width Γ_{f_λ} for the states λ , as they appear in the cross sections :

$$\langle \Gamma_{f_\lambda} \rangle = \Gamma_{f_{\lambda_{II}}} \cdot \frac{\langle D_I \rangle}{2\pi} \cdot \frac{\Gamma_{c\lambda\,II}}{(E_\lambda - E_{\lambda_{II}})^2 + (\Gamma_{\lambda_{II}}/2)^2} + \langle \Gamma^b_{f_\lambda} \rangle \qquad (27)$$

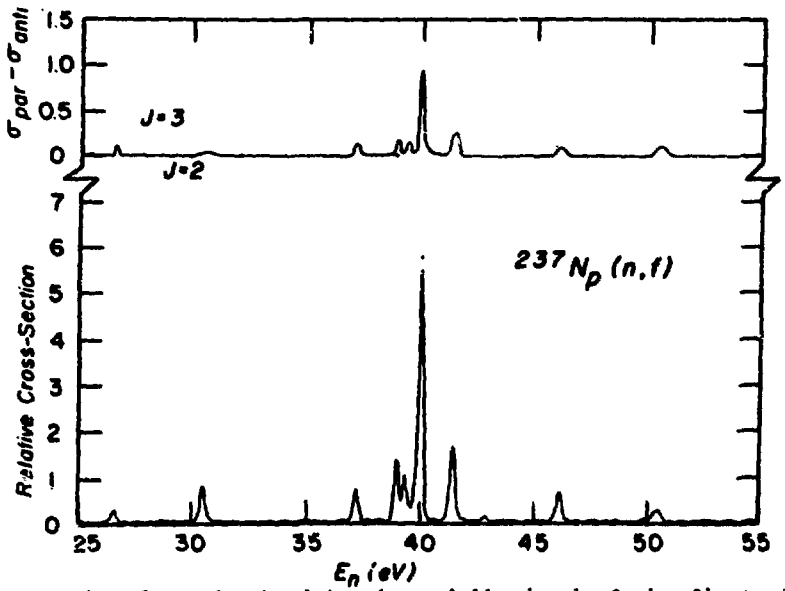

Fig.29 - Fission data obtained in the neighborhood of the first cluster at 40 eV in the ^{237}Np subthreshold fission cross section using a polarized neutron beam and a polarized ^{237}Np target. The upper curve represents the difference between the cross sections measured with beam and target polarizations parallel and antiparallel . These data demonstrate that most of the cross section in this cluster comes from J = 3 resonances[57] .

In this formula :

$\langle \Gamma_{f\lambda} \rangle$ is the average behavior of the width Γ_{f_λ} as a function of the resonance energy E_λ ,

$\Gamma_{c\lambda_{II}}$ is the width of the class-II state λ_{II} corresponding to its coupling to the neighboring class-I states ,

Γ_{f_λ} and $\Gamma_{\lambda II}$ are the fission and total widths of the class-II state λ_{II}, respectively ,

$E_{\lambda II}$ is the energy of the class-II state λ_{II} ,

and $\langle \Gamma^b_{f\lambda} \rangle$ is the average background fission width coming from the direct coupling of the states λ to the fission exit channels, without any effect from class-II states (usually $\Gamma^b_{f\lambda}$ can be neglected compared to Γ_{f_λ}) .

The total width $\Gamma_{\lambda II}$ is given by the following relation :

$$\Gamma_{\lambda II} = \Gamma_{f_{\lambda_{II}}} + \Gamma_{c_{\lambda_{II}}} + \Gamma_{\gamma_{\lambda_{II}}} \qquad (28)$$

where $\Gamma_{\gamma\lambda_{II}}$ is the width for γ decay of the state λ_{II} in the second well .

Expression (27) which is valid only for weak or moderate coupling between class I & classII states shows that $\Gamma_{f\lambda}$, on the average, obeys a Lorentzian energy dependence . But, in addition to this general trend, the actual values of $\Gamma_{f\lambda}$ are subject to Porter-Thomas fluctuations from resonance to resonance due to the great complexity of the compound nucleus states λ .

Similar considerations also apply to the case of the fission widths $\Gamma_{f\lambda_{II}}$. Their energy dependence obeys, on the average, a Lorentzian law having this time a FWHM (full width at half maximum) equal to the width Γ_{VIB} of the vibrational class-II state responsible for the fission strength in the energy range being considered. The actual widths $\Gamma_{f\lambda_{II}}$ exhibit fluctuations from cluster to cluster due to the complexity of the compound nucleus states λ_{II} . The width Γ_{VIB} is usually large because the damping of class II vibrational states is important for most cases where intermediate structure is observed . Therefore the local value of $\langle \Gamma_{f\lambda_{II}} \rangle$ should remain constant in the neutron energy range being considered since this range is much smaller than Γ_{VIB} .

The conditions of the coupling between class I and class II states, at energy S_n, can vary from one nucleus to another depending on the penetrabilities of the barriers A and B . Three types of coupling conditions can be defined though there is no clear-cut separation between them [3] :

a) The very weak coupling situation occurs when the total width $\Gamma_{\lambda_{II}}$ is very small with a value comparable to $\langle D_I \rangle$. This happens when both barriers A and B are high enough above S_n . In that case, each cluster is composed of a few large fission resonances only . Among them, one resonance appears to be mostly of the class II type because its fission width is much larger than that of the other fission resonances belonging to the same cluster. Since this large fission resonance is mostly class II, it has in addition a small neutron width because the coupling of a pure class II state to the neutron entrance channel is essentially zero . This type of coupling seems to apply to the (^{240}Pu+n) case as is illustrated in Fig.30 where the fission widths of all resonances analyzed below 3 keV is plotted as a function of the resonance energy [58]. Four fission widths stick out very clearly at energies of 782, 1405, 1936 and 2700 eV where four narrow class II states are supposed to exist and to be responsible for the intermediate structure effect in this energy range . The neutron widths of these four resonances are very small as should be expected from states where class-II components are predominant .

Analysis of the resonances in each cluster can give the widths $\Gamma_{c\lambda_{II}}$ and $\Gamma_{f\lambda_{II}}$ of the class II state .

For example, perturbation theory which can be applied in this case shows that :

$$\sum_{\lambda} \Gamma_{f\lambda} = \Gamma_{f\lambda_{II}} \qquad (29)$$

The average values of $\Gamma_{c\lambda_{II}}$ and $\Gamma_{f\lambda_{II}}$ can then lead to the penetrabilities of the inner and outer barriers respectively and, consequently, to the values of $(E_{fA} - S_n) / \hbar\omega_A$ and $(E_{fB} - S_n) / \hbar\omega_B$) .

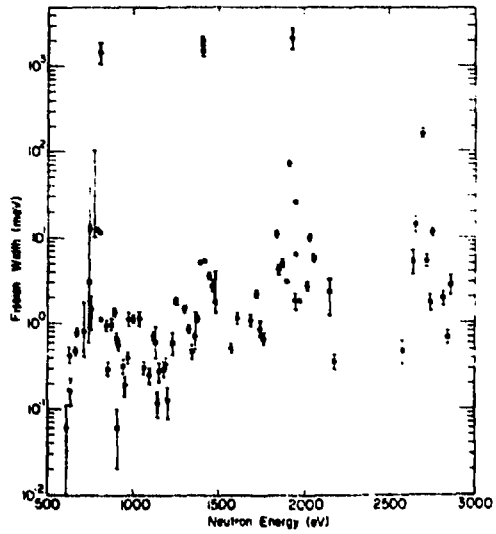

Fig. 30 - Differential plot of the class I fission widths vs resonance energy. Four class II states are clearly visible at 782, 1405, 1936 and ~2700 eV . The width of each state is extremely small and much less than the class I level spacing. The apparent increase in the background fission width with energy is a consequence of poorer resolution at higher energies and therefore a decrease in our sensitivity to weak fission strength resonances [58] .

Another example of very weak coupling seems to be given by the ^{238}U fission cross section .The general behavior of this cross section, as obtained from most recent and accurate measurements[59] , is displayed in Fig. 31 . The now familiar pattern of intermediate structure appears very clearly especially since the good resolution makes the large fission resonances stick out more sharply . The details of the capture and fission cross sections measured simultaneously in the first cluster around 720 eV[60] are shown in Fig. 32 . Examination of these data shows that some capture resonances which appear within the cluster are not seen in fission . This is unexpected in the case of an even-even target nucleus for which all "s" wave resonances have $J^{\pi} = \frac{1^+}{2}$. Interpretation of this apparent anomaly is searched for in terms of Porter-Thomas fluctuations and a "p" wave contribution .

b) The weak coupling to a broad class II state is found when the width $\Gamma_{\lambda II}$ is greater than $< D_I >$ but smaller than $< D_{II} >$ and when barrier B is more easily penetrated than barrier A . Then :

$$\Gamma_{f\lambda II} > \Gamma_{c\lambda II} \qquad (30)$$

The distribution of the fission widths $\Gamma_{f\lambda}$ is also given by expression (27) but, because of the relatively large value of $\Gamma_{\lambda II}$, the cluster is composed of a larger number of resonances than in the very weak coupling case discussed above .

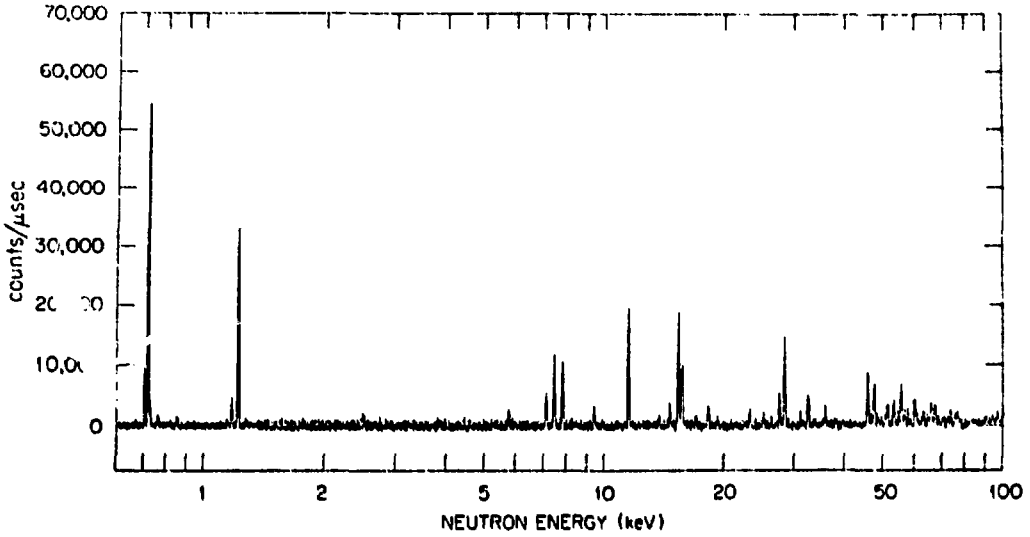

Fig.31 - High resolution fission yields obtained when bombarding ^{238}U with neutrons having energies between 600 eV and 100 keV[59] .

It can be easily shown that the width of the cluster yields $\Gamma_{f\lambda_{II}}$ and that the coupling width is

$$\Gamma_{c\lambda_{II}} = \sum_{\lambda} \Gamma_{f\lambda} \qquad (31)$$

In this expression, the summation over λ runs over all the large fission resonances within the cluster .

This type of coupling seems to apply to the (^{237}Np + n) system[6] .

c) The third type of coupling occurs when a narrow class II state is broadened by moderate coupling to the class I states .

The total width is then dominated by the coupling width, provided that

$$< D_I > \; < \; \Gamma_{\lambda II} \; < < \; D_{II} > \qquad (32)$$

This coupling is found when barrier A is more transparent than barrier B .

The fission widths $\Gamma_{f\lambda}$ in a cluster are also distributed according to a Lorentzian given by expression (27). But, in contrast to the weak coupling case, the widths $\Gamma_{c\lambda_{II}}$ and $\Gamma_{f\lambda_{II}}$ are now obtained from the following relations :

$$\Gamma_{c\lambda_{II}} \neq \Gamma_{\lambda II} = \text{width of the cluster} \qquad (33)$$

$$\sum_{\lambda} \Gamma_{f\lambda} = \Gamma_{f\lambda_{II}} \qquad (34)$$

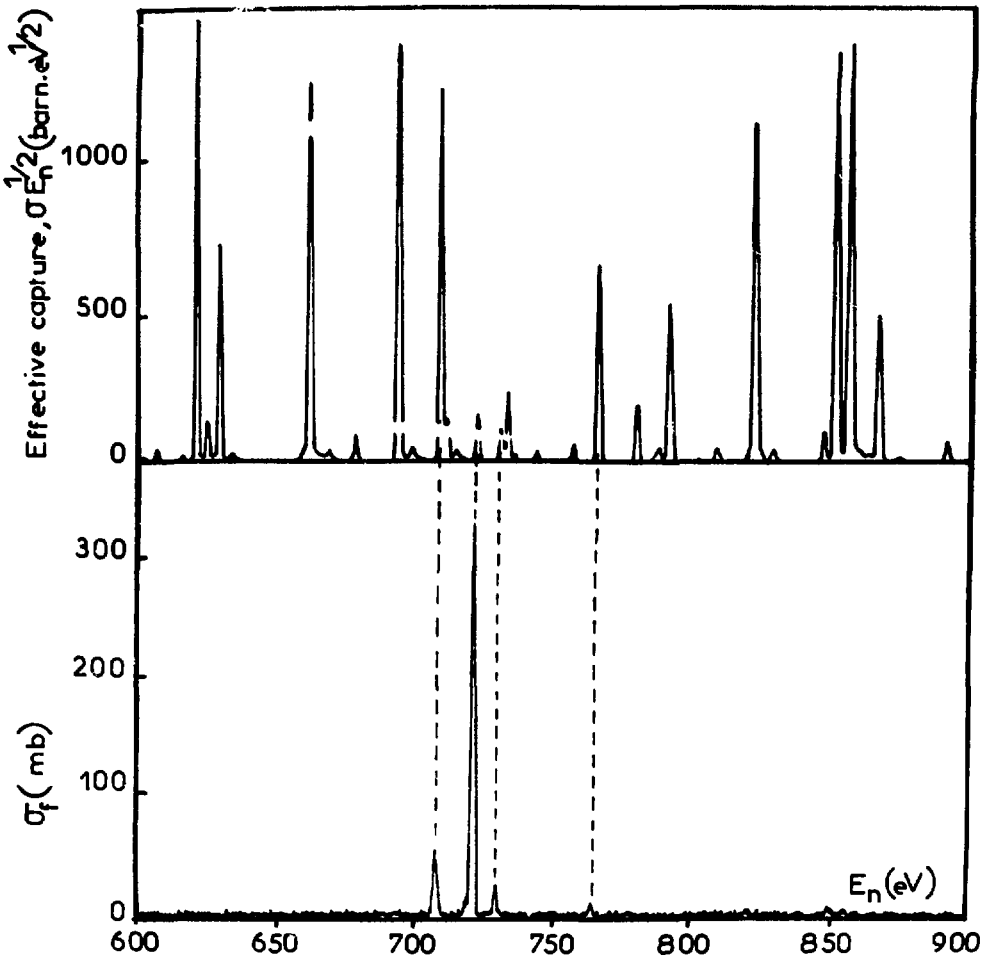

Fig. 32 - High resolution ^{238}U capture and fission cross sections in the neighborhood of the first cluster at 720 eV[60].

This coupling situation seems to apply to the (^{234}U + n) system. From recent and quite accurate measurements, it is possible to extract the fission widths for the most prominent resonances situated below 1500 eV[61]. A plot of the $\Gamma_{f\lambda}$ values versus the resonance energy is given in Fig. 33. A fit to these data can be made with two Lorentzian curves which take into account the fluctuations of $\Gamma_{f\lambda}$ around this average trend. In the same manner as for coupling b) described above, the analysis of the data yields the transparency parameters $E_f/\hbar\omega$ for the two barriers.

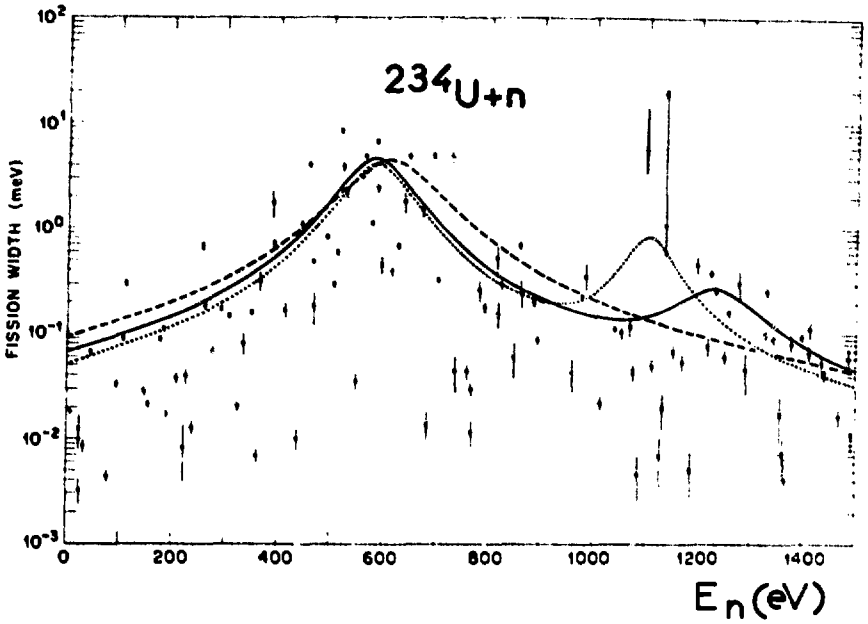

Fig.33 - Energy dependence of the fission widths for the ^{234}U neutron resonances analyzed below 1500 eV . The curves represent the calculated energy dependence of the mean fission width, as defined by Lorentzian functions. The solid line is the preferred fit . It shows the sum of two non interfering Lorentzian curves with parameters deduced by a weighted maximum likelihood method The dashed curve represents a single Lorentzian also derived by a weighted maximum likelihood method . The dotted curve shows the sum of two Lorentzians derived by an analysis in which the contribution from each fission width to the likelihood is not weighted (After G.D. James et al.[61]).

It should be noted at this point that the analysis of the cross sections cannot itself conclude which type of coupling actually applies to the case being studied since formula (27) is symmetric in exchange of the widths $\Gamma_{c\lambda II}$ and $\Gamma_{f\lambda II}$. Other methods need to be used to determine the type of coupling . These methods are not discussed in this paper but are reviewed elsewhere [6] .

In summary, the striking phenomenon of intermediate structure in sub-barrier fission cross sections appears to be one of the consequences of the double-humped barrier shape and can be very well explained as being the effect of intermediate states in the second well. This interpretation is supported by the spin determinations of the ^{237}Np resonances in the first fission cluster . Analysis of the cross sections yields the values of E_{II}, $E_{fA}/\hbar\omega_A$, $E_{fB}/\hbar\omega_B$ provided that the type of coupling between class I and class II states is known .

IV. STRUCTURE EFFECTS IN FAST NEUTRON FISSION CROSS SECTIONS

IV.1 - Introduction

In fission induced by resonance neutrons, individual resonances can be resolved at low energy due to the extremely good resolution of time-of-flight spectrometers, as is discussed in Section III . But, at higher neutron energy, the resolution which varies as $E_n^{3/2}$ rapidly deteriorates for increasing E_n . The broadening of the resolution function results first in the smearing out of the class I states which cannot be resolved above a given energy E_n^I . This value is about 150 eV for ^{237}Np and 1500 eV for ^{234}U . In the presence of an intermediate structure effect in σ_f, the fission clusters can still be separated above E_n^I , because $\langle D_{II} \rangle \gg \langle D_I \rangle$. But, above an energy E_n^{II} greater than E_n^I , the fission clusters themselves cannot be separated because the width of the resolution function then becomes comparable to or larger than $\langle D_{II} \rangle$. This happens at about 5 keV for ^{237}Np and 100 keV for ^{234}U . Above E_n^{II} , the fission cross section should become smooth but with fluctuations having an amplitude decreasing with increasing E_n .

The general behavior of σ_f , in the presence of an intermediate structure effect, should then be the following :

for $E_n \leqslant E_n^I$ both the class I levels and the fission clusters are resolved,

for $E_n^I \lesssim E_n \lesssim E_n^{II}$ the fission clusters are resolved but not the fine structure in each cluster,

for $E_n \gtrsim E_n^{II}$ both the class I levels and the fission clusters are smeared out by the resolution function .

This Section deals essentially with the last case ($E_n > E_n^{II}$).

The general features of σ_f recalled above are actually found in most subbarrier fission cross sections which are smooth in the neighborhood of the threshold and above . Such a behavior is observed for example in the ^{237}Np fission cross section which is featureless near threshold [62] . This is interpreted as evidence that the vibrational class II states are fully damped at such an excitation energy in ^{238}Np .

There are nevertheless a few cases discussed below where σ_f near threshold presents some gross structure which cannot be explained by conventional models (competition theory, for example). These data can tentatively be interpreted in terms of partial damping of the vibrational class II states . In such a case, as already discussed in Section III , the fission strength, averaged over an energy interval ΔE greater than $\langle D_{II} \rangle$ but smaller than Γ_{VIB}, is not uniformly distributed as a function of E_n but varies according to a Lorentzian law having a FWHM equal to Γ_{VIB} .In the presence of partial damping, $\Gamma_{VIB} \ll \hbar\omega_{II}$ where $\hbar\omega_{II}$ is the spacing of vibrational class II levels. In this situation, the following relation is satisfied :

$$\langle D_{II} \rangle \ll \Gamma_{VIB} \ll \hbar\omega_{II} \qquad (35)$$

An example of the possible existence of a partially damped vibrational class II state seems to be provided by the ^{234}U fission cross section in the vicinity of 310 keV[61] (See Fig. 34) . At this energy, a shoulder appears in the data and can tentatively be interpreted as being due to a vibrational class II state having $\Gamma_{VIB} \simeq 50$ keV . The peaks that appear in this 50 keV range do not correspond to resolved class II states since the resolution function is too broad at this energy ($E_n^{II} < 310$ keV) . Rather, they are interpreted as fluctuations due to the contribution of unresolved class II states .

More dramatic examples of structure in the fast neutron fission cross sections are found for ^{230}Th and ^{232}Th . For these two thorium isotopes, gross structure in the form of big peaks is observed in σ_f ; but, fine structure also appears in these big peaks if the experimental resolution becomes sufficiently narrow . These peaks seem to be caused by almost pure vibrational class II states with the contribution of rotational bands built on them . This interpretation is not compatible with calculated double-humped fission barriers, as already pointed out in Section II.4 . In Section IV.2 below, the ^{230}Th and ^{232}Th cases are treated with the presentation of the data, the discussion of the so-called "Th anomaly"and the possible explanation of this anomaly by a third minimum in the fission barrier .

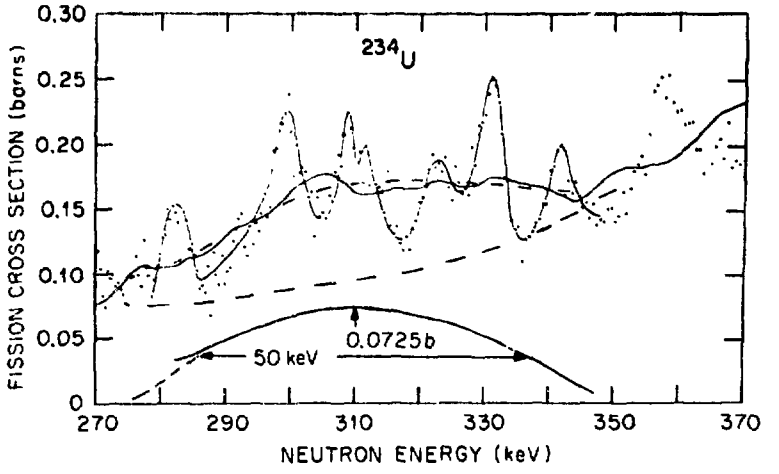

Fig. 34 - The fission cross section of ^{234}U measured between 270 keV and 370 keV is shown by the full circles . Of the two solid lines through the data, one shows a running sum over twenty timing channels and the other is a guide line indicating fluctuations. The presumed contribution of the vibrational level is shown by the dashed lines and again by the diagram below the data [64] .

IV. 2 - Vibrational resonances in ^{230}Th and ^{232}Th fission cross sections - "Thorium anomaly" - Third minimum in the fission barrier

IV.2.1 - $^{230}Th + n$

The first evidence that the fission mode could not be fully damped was provided by the ^{230}Th fission cross section[63] . Below threshold, σ_f for this nucleus presents a strong peak at 720 keV having about 100 mb at the maximum and a width of 30 keV, as is illustrated in Fig. 35[64] . Such a peak could not be explained by competition theory since there are no appropriate inelastic neutron channels adequately located to cause the fall of σ_f on the high energy side of the peak . But, the double-humped fission barrier can provide a qualitative explanation in terms of an almost pure vibrational class II state situated at this energy . Forward peaking in the measured fission fragment angular distribution across the peak indicates that this vibrational state has K = 1/2 with an unknown parity. Nevertheless the shape of the peak and the behavior of σ_f in the vicinity of 720 keV are not consistent with a weakly damped vibrational state having $\Gamma_{VIB} \simeq 30$ keV . Rather the peak can be explained by an almost pure vibrational state whose contribution is broadened by the effect of the rotational band built on it . The energy sequence of a rotational band having a given K value is given by the following relation :

$$\varepsilon_K(J) = \varepsilon_{oK} + \frac{\hbar^2}{2\mathcal{J}} \left\{ J(J+1) - K(K+1) + \delta_{K,1/2}\, a(-1)^{J+1/2} (J+1/2) \right\} \qquad (36)$$

where :

ε_{oK} and $\varepsilon_K(J)$ are the energies of the states having K=J and K>J respectively,

$\mathcal{J}$ is the moment of inertia of the rotating nuclear system,

$\delta_{K,1/2}$ is the Kronecker symbol,

and a is the decoupling parameter .

For $K \neq 1/2$, the energy $\varepsilon_K(J)$ goes up regularly with J but, for $K = \frac{1}{2}$, large a values can bring about level inversion for increasing J values .

The contribution of rotational levels naturally broadens the energy range where the fission strength is enhanced, but the effect of the centrifugal barrier for incident neutrons having angular momentum ℓ rapidly decreases the influence of these rotational levels for increasing spin $J = \ell \pm 1/2$.

Analysis of both cross section and angular distribution data has been made, allowing a and $\mathcal{J}$ to be adjustable in the fitting procedure[64] . A fairly large a negative value is necessary to account for the strong variations in angular anisotropy throughout the peak . A large value of the moment of inertia is also needed to fit the data and this is consistent with a strongly deformed vibrational state .

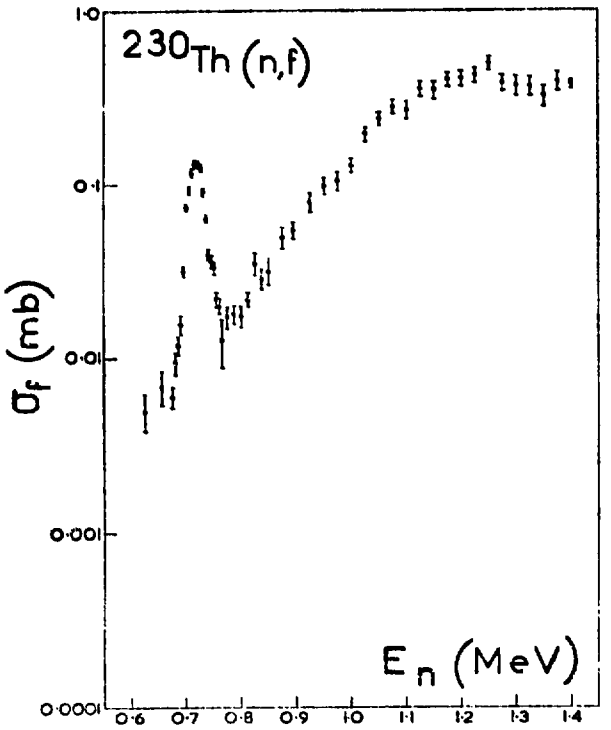

Fig.35 - Fission cross section of ^{230}Th plotted as a function of incident neutron energy. These data show a strong "vibrational resonance" at 720 keV [64] .

This interpretation is supported by a careful examination of higher resolution σ_f data in the neighborhood of 720 keV[65] . Fine structure appears in the vibrational resonance and each peak in this fine structure seems to correspond to a rotational level (see Fig. 36). Unfortunately, accurate angular anisotropy data for each of these peaks are not available yet in order to check the J sequence from one peak to the other .

Despite its interest, this interpretation is not quantitatively substantiated by fission barrier calculations. In order to have negligible damping a shallow second well is needed ($E_{II} \simeq$ 4-5 MeV) together with a fairly high inner barrier height ($E_{fA} \simeq$ 6 MeV). Such high values of E_{II} and E_{fA} are never found in realistic fission barrier calculations using the Strutinski prescription and in which much lower results are obtained (see Fig.6). This is one example of the "Th anomaly" .

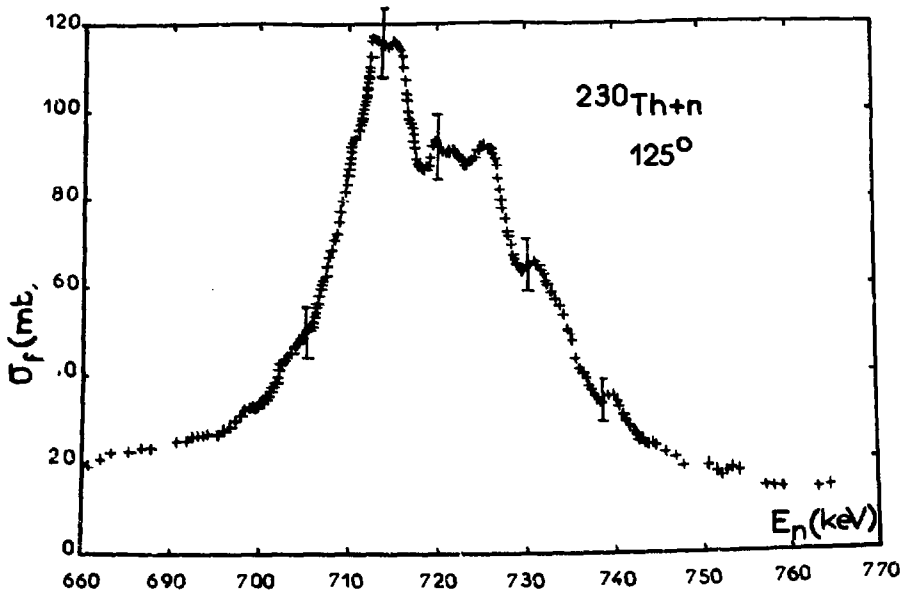

Fig. 36 - Fission cross section of ^{230}Th in the vicinity of 720 keV, as measured with a underground nuclear detonation used as a pulsed neutron source [65]. These data, obtained from fission fragments emitted at 125° relative to the neutron beam, show a fine structure in the big peak at 720 keV (See Fig. 35 for comparison).

IV.2.2 - $^{232}Th + n$

An even more striking example of vibrational resonances with identification of fine structure is provided by the (^{232}Th +n) system. A recent measurement, carried out in the MeV neutron range, with the high nominal resolution of 0.16 ns/m, has revealed the existence of detailed structure in the ^{232}Th fission cross section[66].

A gross structure is confirmed at several energies : 1.4 MeV, 1.5 MeV, 1.6 MeV and 1.7 MeV, which cannot be explained by competition theory but is now thought to be composed of vibrational resonances (see Fig. 37). Angular anisotropy measurements, also made in the same neutron energy range, show a strong contribution of $K = \frac{1}{2}$ at 1.4 MeV and 1.7 MeV and of $K = 3/2$ at 1.5 MeV and 1.6 MeV. But in addition, the high resolution in σ_f measurements now makes sharp peaks stick out in each vibrational resonance.

In the same manner as for the $^{230}Th(n,f)$ cross section, it is tempting to interpret each of these four big peaks as being due to the effect of vibrational class II levels broadened by the contribution of a rotational band built on each of them. The analysis of the $^{232}Th(n,f)$ data is made easier by the clear contribution of each rotational level and also because the a decoupling parameter, which is difficult to determine, plays no role for the two $K = 3/2$ cases. The energy spacing

between two adjacent levels in the fine structure should obey the following relation :

$$\varepsilon_K(J+1) - \varepsilon_K(J) = \frac{\hbar^2}{2\mathcal{J}} 2(J+1) \qquad (37)$$

This law is actually observed for the energy spacing between the sharp peaks in the vibrational resonances at 1.5 MeV and 1.6 MeV (see Fig. 38) . The case of the gross structure having K = 1/2 is not studied here because of the additional complexity of the unknown decoupling parameter a .

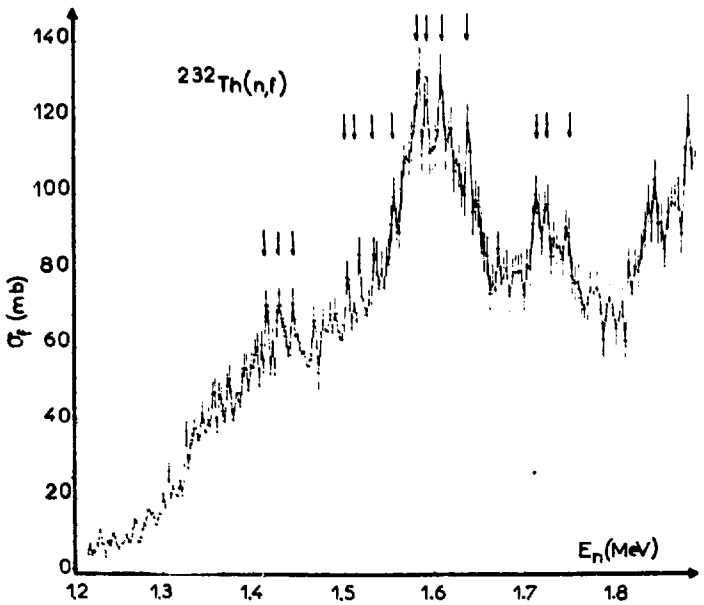

Fig. 37 - Fission cross section of ^{232}Th, as measured with the 60 MeV Saclay linac , showing the structure observed near threshold. The arrows indicate the positions of the sharp peaks corresponding to the fine structure in the big peaks [66].

This analysis confirms that the qualitative interpretation of the data, proposed above, is essentially correct. But, again, the quantitative understanding in terms of calculated double-humped fission barriers proves difficult . From the observed widths of the sharp peaks, it is possible to assert that the rotational levels have a natural width smaller than 10 keV . This is absolutely inconsistent with the energies E_{fA} and E_{II} obtained from fission barrier calculations and which are far too low to explain such narrow levels at $E_n \gtrsim 1$ MeV . This is the second case of the "Th anomaly" .

IV.2.3 - Third minimum in the fission barrier

The "Th anomaly" is perhaps removed by a closer examination of both i) Th fission barrier calculations in the region of the second saddle point and ii) analysis of the (^{232}Th + n) data .

Potential energy calculations around the second saddle point, using the droplet model and a folded Yukawa potential (See Section II.2) , show that this saddle point is actually split by a third minimum at asymmetric distortion and for even Th isotopes[12] . A third minimum continues to appear in similar calculations made i) for odd Th isotopes having all spin states that can be populated in neutron-induced fission and ii) for some U and Pu isotopes[12,68]. This shallow lake in the potential energy surface provides the possibility for vibrational states (called class III states) to exist, in the same manner as for the second well, but with a larger deformation, that of the third minimum .

The analysis of ^{232}Th data given in Fig. 38 can also help one to understand the "Th anomaly" . The parameter $\frac{\hbar^2}{2\mathcal{J}}$ obtained directly from such an analysis is fairly low as is seen below :

$$\frac{\hbar^2}{2\mathcal{J}} = (2.46 \pm 0.11)\ \text{keV for}\quad K_{oK} = 1.505\ \text{MeV} \qquad (38)$$

$$= (2.73 \pm 0.11)\ \text{keV for}\quad K_{oK} = 1.579\ \text{MeV} \qquad (39)$$

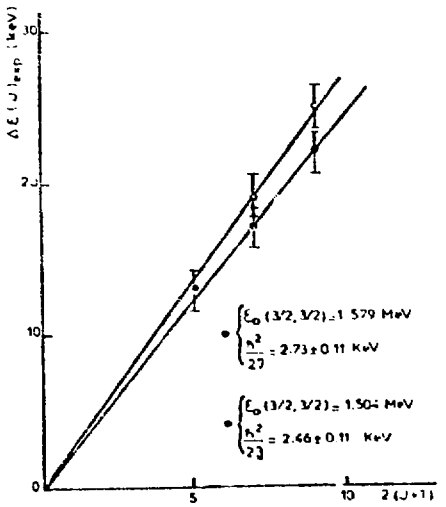

Fig. 38 - Least-squares fits to the energy intervals between the sharp peaks observed in the gross structure at 1.5 and 1.6 MeV (See Fig. 37)[66].

These two values are definitely greater than $\frac{\hbar^2}{2\mathcal{J}}$ = 3.33 keV obtained for the ^{240}Pu fission isomer[17] (See Section II.3.1), but are close to the value $\frac{\hbar^2}{2\mathcal{J}}$ = 2.5 keV calculated for the second saddle point of the ^{240}Pu fission barrier [67]. Though the moment of inertia of ^{233}Th may differ from that of ^{240}Pu at the second saddle point, these results seem to confirm that the third minimum actually exists for ^{231}Th and ^{233}Th and is responsible for the "Th anomaly" according to a mechanism sketched in Fig. 39 .

In order to substantiate this interpretation, more accurate calculations are needed to know better the moment of inertia of ^{231}Th and ^{233}Th as a function of deformation and also the decoupling parameter a for the analysis of K = 1/2 vibrational resonances . The potential energy surface seems also to present a third minimum for a few other nuclei which, in this respect, should be studied more attentively together with the two Th isotopes mentioned above. Accurate angular distribution data are clearly needed in each peak of the fine structure in order to check their individual J value .

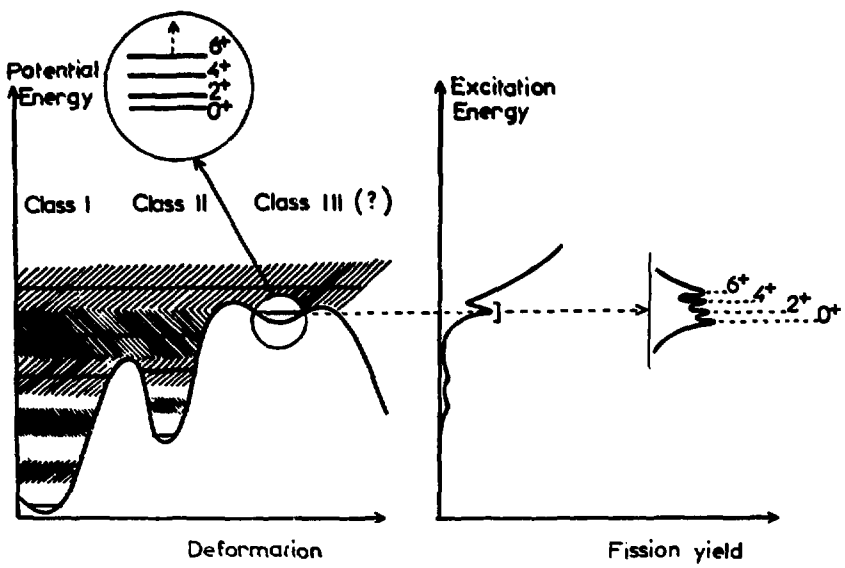

Fig. 39 - Possible explanation of the "Th anomaly" in terms of a third minimum in the fission barrier . The picture is drawn for an even nucleus for clarity but the Th data are actually obtained for odd Th isotopes . At excitation energies obtained by fast neutron capture, class I and class II vibrational states are completely mixed and fully damped ; they cannot cause structure in σ_f . Vibrational resonances could then be due to vibrational levels in the third well (class III) . Since the third well is shallow, the class III vibrational levels are not damped . The rotational band indicated in the circle causes fine structure to appear in the vibrational resonance .

V. DYNAMICAL EFFECTS IN FISSION

V.1 - Generalities

A great deal of attention has been paid to the determination of the potentia energy surface of the fissioning system . Present fission barrier calculations are accurate to ± 1 MeV (See Section II). But, the knowledge of the potential energy, though essential,is not sufficient for a thorough understanding of the fission pro - cess . This is because the equation of motion of the fissioning system, in addition to the potential term,also contains other terms that reflect the dynamical aspects of the motion . More precisely, these terms correspond to energy dissipation and to inertia and are associated respectively with the first and second derivatives of the collective degrees of freedom .

V.1.1 - Inertia gives the manner in which the nuclear system responds to an external force . This effect seems to vary strongly with deformation[69] . At scission, the effective mass μ_{eff} associated with the fission motion is simply equal to the reduced mass μ_o of the two fragments. For symmetric fission $\mu_o = A/4$, where A is the mass of the fissioning nucleus . But much higher μ_{eff} values are obtained for smaller deformations .

For example, the value of μ_{eff} at ground state deformation can be estimated from the properties of the β-vibrational states in the first well, where :

$$\hbar\omega = \hbar (\kappa / \mu_{eff})^{1/2} \simeq 0.8 \text{ MeV} \qquad (39)$$

$$\text{and } V(r) = \frac{1}{2} \kappa (r - r_o)^2 \qquad (40)$$

In these two expressions :

- $\hbar\omega$ is the spacing of the β vibrational levels in the first well,
- κ is the force constant in the potential ,
- V(r) is the potential, supposed to be of the harmonic oscillator type ,

and - r is a deformation paramater, having the value $r=r_o$ at equilibrium

With this parameterization , the deformed nucleus is described as composed of two halves having their centers of mass separated by the parameter r which can be calculated in terms of the usual deformation parameters[70] .

From $\hbar\omega$ = 0.8 MeV and the calculated shape of the fission barrier near the first minimum, the two expressions (39 and (40) give $\mu_{eff} = 40\mu_o$ for the ground state of ^{236}U, a value which is much higher than μ_o at scission .

In a similar manner, expresaions (39) and (40) can also be used at the three other extrema of the double-humped fission barrier where $\hbar\omega$ and V(r) can also be known . This results in a steady decrease of μ_{eff} with increasing deformation from $\mu_{eff} = 40\mu_o$ at ground state deformation to μ_o at scission[69].

The proper determination of the fission path requires, however, a more precise determination of the mass inertia paramaters since it is very sensitive to them. Therefore, the above estimates need to be supplemented by more detailed microscopic calculations for all possible deformations along the fission path . An attempt has been made along this line for ^{240}Pu, and is presented in Section II.2 where the concept of dynamical fission barrier is introduced and discussed .

V.1.2 - Energy dissipation , called also friction or viscosity, corresponds to the coupling of the fission mode to the intrinsic degrees of freedom . This aspect of fission is already considered above in Sections III and IV but attention is limited there only to the damping of class I and class II vibrational levels into intrinsic excitations .

In this Section, attention is focused mainly on energy dissipation effects in the descent from the last saddle point to scission . The fission barrier at the scission point is about 15 MeV below the total energy for slow-neutron-induced fission of light actinides. Viscosity effects control the division of this 15 MeV of available energy between excitation energy E^s_{exc} and pre-scission kinetic energy E^s_{kin} of the system at scission. Along the fission path, including the scission point, the following relation holds :

$$E_{tot} = E_{pot} + E_{kin} + E_{exc} = E^s_{pot} + E^s_{kin} + E^s_{exc} \qquad (41)$$

In the full damping picture, the energy in the fission mode is fully dissipated into internal excitation. At scission, this internal excitation is transmitted to the fragments also in the form of internal excitation . The total kinetic energy TKE of the fission fragments is then just equal to the Coulomb energy V_c at scission since the pre-scission kinetic energy is zero . The opposite situation prevails in the absence of damping. In this case, all the available energy at scission goes into pre-scission kinetic energy E^s_{kin} which, added to the Coulomb energy at scission, gives the total kinetic energy TKE^{kin} of the fission fragments . These fragments are cold but deformed at scission, and their deformation energy E_d is transformed into excitation energy after they have separated .

Whatever the damping situation is, i) the TKE of the fragments is equal to the sum of the Coulomb and pre-scission kinetic energies at scission and ii) the total excitation energy E^t_{exc} of the fragments is equal to the sum of the excitation energy of the system and the deformation energy of the fragments at scission. The overall sum of TKE and excitation energy of the fragments is just the Q value for the fission process . This results in the following relations :

$$TKE = E^s_{kin} + V_c \qquad (42)$$

$$E^t_{exc} = E^s_{exc} + E_d \qquad (43)$$

$$Q = TKE + E^t_{exc} \qquad (44)$$

Very little is known about dissipation effects in the last stage of fission . Theoretical calculations are just starting to be made but, despite their strong interest, they are still preliminary because of the extreme complexity of the problem (see for example[71] . Many experimental results exist for the fragment excitation energy (through measurements of prompt fission neutron and γ-ray yields) and for the total kinetic energy. Most of the results are obtained for the sum of all mass splittings at scission but more and more measurements are made for detailed and specific mass divisions. Despite their number and their value, these fission data are difficult to interpret in a unique manner . This is because the properties of the fission fragments are measured <u>after</u> scission and not <u>at</u> scission . A model is therefore needed to relate the final properties of the fission fragments to those of the scission point .

This ambiguity in the interpretation is illustrated, for example, in the case of ternary fission in which a long range α particle is emitted in addition to the two main fragments. Ternary fission data, including the energy spectrum and angular distribution of the ternary α's, can be explained equally well in terms of strong and weak damping by using different but realistic scission configurations[72,73] .

The TKE data can also be interpreted with contradictory hypotheses . For example the average total kinetic energy $\overline{TKE}$ for all mass divisions is plotted in Fig. 40 for a wide variety of fissioning species as a function of their fissility parameter x . These $\overline{TKE}$ data show a regular $Z^2\ A^{-1/3}$ dependence but their interpretation is somewhat ambiguous.

It would seem, at first sight, that the nearly linear dependence of $\overline{TKE}$ with $Z^2\ A^{-1/3}$ implies that the pre-scission kinetic energy is negligible and that the scission configurations can be specified simply by a separation <u>d</u> of the fragment charge centers proportional to $A^{1/3}$. In this case :

$$TKE = V_c = \frac{e^2}{d} \cdot Z_{f1} \cdot Z_{f2} \qquad (45)$$

where :

- e is the proton charge,

and - Z_{f1} and Z_{f2} are the atomic numbers of the two fragments .

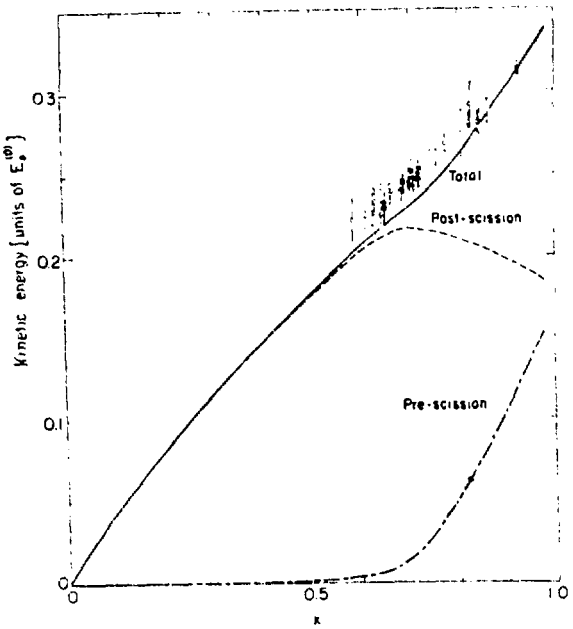

Fig. 40 - Comparison of measured and calculated values of the kinetic energy of the fission fragments for a wide variety of fissioning nuclei as a function of their fissility parameter x. The measured values are for the total kinetic energy $\overline{TKE}$ only. The calculated values are obtained for the Coulomb energy V_c (post-scission) (short-dashed curve), for the pre-scission kinetic energy E^s_{kin} (dot-and-dash curve) assuming absence of damping and for the total kinetic energy $TKE = V_c + E^s_{kin}$ [74].

This interpretation would favor the strong damping hypothesis in which there is no appreciable pre-scission kinetic energy and therefore TKE comes from Coulomb repulsion only .

The above assumption that d varies as $A^{1/3}$ is nevertheless unrealistic because d depends not only on A but also on Z [74] . For higher Z values, the scission configuration is relatively more elongated, thus resulting in larger d values and lowered Coulomb energy . The variation of V_c with x, as obtained from LDM calculations, is plotted in Fig. 40 . For relatively light nuclei, the scission and saddle points are very close and, therefore, the observed $\overline{TKE}$ and calculated V_c values are almost equal, as expected . This is in contrast to the situation for heavy nuclei where the remoteness of the scission point from the saddle point brings about a decrease of V_c compared to a pure $Z^2\ A^{-1/3}$ dependence . In fact the behavior of V_c with x flattens for heavy nuclei as a consequence of the more stretched configuration at scission . The difference between observed $\overline{TKE}$ and calculated V_c values

implies that some pre-scission kinetic energy E^{s}_{kin} needs to be taken into account . If viscosity effects are supposed to be negligible in the descent from saddle point to scission, all the available energy at scission appears in the form of pre-scission kinetic energy which , when added to V_c , results in calculated TKE values in reasonable agreement with the data (Fig. 40) .

In fact, more recent and sophisticated calculations give TKE values which are too high compared to the measured ones especially on the heavier element side[71]. Some damping needs to be introduced to bring the calculated TKE values down to the measured ones . This damping is calculated in terms of either one-body dissipation or two body viscosity. These concepts stem from their analogy with classical fluid dynamics in which the energy dissipation either comes from the interactions between the molecules of the fluid or proceeds through collisions of the particles with the moving boundary of the system. A good fit to the data can then be obtained but uncertainty still persists as to the manner in which the energy dissipation occurs, whether through one-body or two-body processes or both[71] .

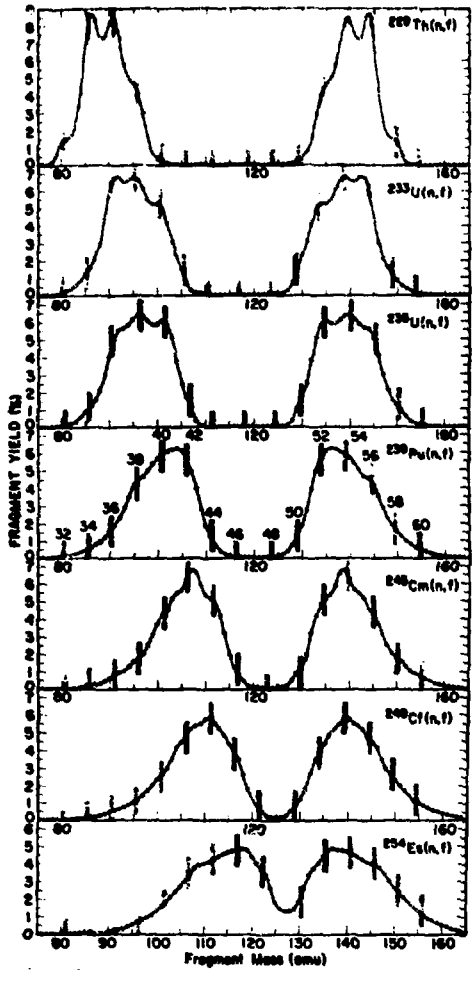

Fig. 41 - Primary fragment mass distribution obtained for thermal-neutron-induced fission . All distributions have been corrected for experimental dispersions . The shaded vertical bars indicate the calculated fragment masses associated with the even nuclear charges shown in the figure for $^{239}Pu(n,f)$ [76]) .

The weak damping hypothesis receives some support from other pieces of data, for example from the mass distribution of the fission fragments[75] . This is illustrated in Fig. 41 where the mass distribution for the primary fragments emitted in thermal-neutron-induced fission is plotted for several fissile nuclei ranging from ^{229}Th to ^{254}Es[76] . A fine structure is observed with peaks corresponding to even charge splittings. This structure which is quite pronounced for the lighter fissioning nuclei fades away when moving to heavier ones . Also, for a given even-even fissioning nucleus such as ^{236}U, the fine structure is enhanced if a selection of high TKE events is made in the data analysis[77]. It is quite possible that a fine structure is also present for the high TKE events of heavy fissioning nuclei for which the total fragment yields lead to a smooth spectrum . Interpretation of these data has been tentatively proposed in terms of superfluid motion in the fission mode[75] . In this type of motion, the nucleons remain coupled by the pairing force and no internal excitation is transmitted to the nuclear system .The peaks at even charge yields imply that some superfluidity is preserved in the descent to scission, otherwise there would be no obvious reason for the fissioning nucleus to prefer even-even division (The even-odd neutron effect in the splitting at scission is not as obvious as for the protons because of the correction for prompt neutron emission needed to obtain the properties of the primary fission fragments) . Intuitively, one is led to think that superfluidity is better preserved if :

i) the TKE is higher. This comes simply from the fact that, for a given Q value, very little is left, in the high TKE events, for the total excitation energy E^t_{exc} of the fragments, as a consequence of relation (44). At scission, the fragments are then deformed but without internal excitation .

ii) the scission point is closer to the saddle point or the exit point for sub-barrier fission . This is because friction forces play a bigger role if the path from descent to scission is longer .

These physical conditions are actually met in the data which are therefore consistent with a contribution of superfluid motion in low energy fission .

The effects of energy dissipation briefly discussed above, are thus far from being completely understood yet . They appear to vary a lot, depending on the nucleus, the mass splitting and the fission events being considered .A comprehensive description of the situation is well beyond the scope of this paper. Rather, in Section V.3 , several experimental data relevant to viscosity effects are presented for the low energy fission of ^{240}Pu where damping of the fission mode seems to vary also with excitation energy .

V.2 - Dynamical fission barriers for spontaneous fission.

A simplified approach to the calculation of the mass inertia parameter consists in assuming that the fission motion is adiabatic until the motion to scission becomes irreversible . In this representation, the barrier penetration proceeds without intrinsic excitation of the system . Different damping conditions may occur after the barrier penetration and they can influence the scission properties, as discussed in Section V.1, but not the fission probability since the process is then

irreversible. This approach is certainly valid for spontaneous fission for which detailed calculations of the fission life-time have been made along this line[4,78].

The probability $\lambda_{s.f.}$ per unit time for decay by spontaneous fission is given by the following relation :

$$\lambda_{s.f.} = 2\pi\omega \; P = \tau_{s.f.}^{-1} \qquad (46)$$

where :

$2\pi\omega$ is the frequency of the zero point motion in the first well ($\hbar\omega \simeq 0.8 - 1$ MeV),

P is the barrier penetrability,

and $\tau_{s.f.}$ is the life-time for spontaneous fission.

The calculation of P is greatly simplified for a one-dimensional fission barrier and a constant mass parameter B . Standard WKB techniques[79] then give :

$$P \simeq \exp\left(-2S/\hbar\right), \text{ if } S \gg \hbar \qquad (47)$$

with

$$S = \int_{s'}^{s''} \left(2\,|\,E - E(s)\,|\,B\right)^{1/2} ds \qquad (48)$$

In expression (48) :

- s is the deformation parameter of the one-dimensional fission barrier

and s' and s" (with s" > s') are the values of s, respectively at the entrance and exit points of the barrier, where the total energy E of the system is equal to that of the barrier (E = E(s') = E (s")) .

Improvements to $\tau_{s.f.}$ calculations have been made by using a more sophisticated approach [4,78] briefly introduced above and described in more detail below where the concept of a dynamical barrier is presented .

It is first considered that the potential energy is known in a multidimensional space, with a set $\{s\} = (s_1, s_2 \ldots s_i \ldots s_j \ldots)$ of deformation coordinates, using the Strutinsky procedure . But the major step forward is to consider that the mass inertia parameter B is no longer constant but can vary with $\{s\}$. This is justified by noting that the shell structure, which is so important in the calculation of the potential energy, also plays a major role in the value of the mass tensor B_{ij} (the indices i and j refer to the deformation coordinates s_i and s_j respectively). Actual calculations of B_{ij} , using the "cranking" formula, show oscillations in these values with deformation quite similar to those of $E_m(\{s\})$ discussed previously. In this multidimensional representation, with possible variations in B_{ij} with $\{s\}$ taken into account explicitly, the expression for S now reads :

$$S = \int_{\sigma'}^{\sigma''} \left(2\,|\,E - E(\sigma)\,|\,B(\sigma)\right)^{1/2} d\sigma \qquad (49)$$

where :

- the deformation parameters s_i, s_j, are assumed to be functions of some arbitrary parameter σ,
- σ' and σ'' are the end-point values of the parameter σ, similar to s' and s" defined for (48), for which $E = E(\sigma') = E(\sigma'')$,

and - $B(\sigma)$ is the effective mass defined by the following relation :

$$B(\sigma) = \sum_{i,j} B_{ij}\,(s_1(\sigma)\ ,\ s_2(\sigma) \ldots s_i(\sigma)\ , s_j(\sigma)\ldots) \frac{\partial s_i}{\partial \sigma} \frac{\partial s_j}{\partial \sigma} \qquad (50)$$

In the adiabatic approximation, the collective motion in the fission mode is supposed to be slow enough so that, for each deformation $\{ s \}$, (or a given σ value) the nucleons have enough time to rearrange themselves . It is then justified to consider the state of the system (including the single-particle states $| m \rangle$) at any deformation $\{s\}$ in the sub-barrier region . In these conditions, it is possible to derive an expression for B_{ij}, in terms of the single-particle states $| m \rangle$, having eigenvalue E_m, using the cranking formula :

$$B_{ij}(\sigma) = 2\hbar^2 \sum_{m \geq 1} \frac{\langle 0 \,|\, \partial/\partial s_i \,|\, m \rangle \langle m \,|\, \partial/\partial s_j \,|\, 0 \rangle}{E_m - E_o} \qquad (51)$$

The calculation of S, with equation (49), can be carried out provided that a trajectory, the fission path, is defined between the two end points σ' and σ'' . If B were constant, the fission path would follow the extremal values of the potential energy surface . This condition defines what is called the "static barrier" . The fission path is no longer the static barrier if B varies with deformation . For example, the fission trajectory may reach higher potential energy if the mass parameter takes there a smaller value. The fission path is then determined by the least-action principle, which leads to the smallest possible value for S and, consequently, for $\tau_{s.f}$. Such a path gives the so-called "dynamical barrier" which is illustrated in Fig. 42 for ^{240}Pu. It is interesting to note that the least-action trajectory does not pass through the "static" saddle points, but prefers a path at a somewhat higher energy . This seems to apply to most of the cases studied so far and appears to be a consequence of a large mass parameter at the saddle point . This effect itself is due to the shell structure which gives a large positive shell-energy correction at that deformation .

These results illustrate clearly that "dynamical barriers" should be considered for the determination of the fission path and the fission probability . A test of the validity of the method has been provided by the comparison between calculated and measured $\tau_{s.f}$ values for a wide variety of nuclei. Good agreement is obtained provided that a delicate adjustment is made for the parameters used in the calculation of macroscopic and microscopic quantities[4,6,78] . A more accurate knowledge of both microscopic and macroscopic properties of the fissioning nucleus as a function of deformation is needed for this type of calculation to be applied quantitatively without too many adjustments of the parameters .

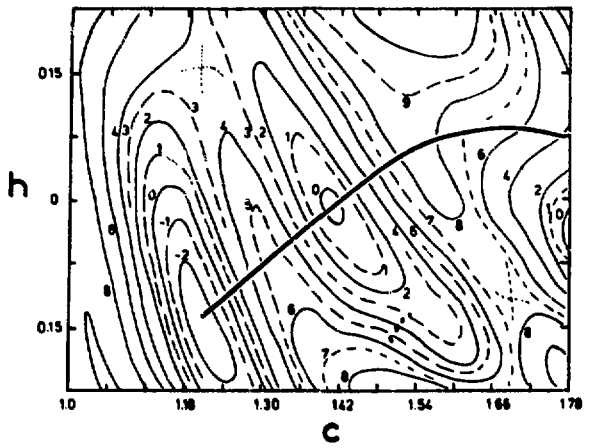

Fig. 42 - The calculated deformation energy of ^{240}Pu versus the two symmetric deformations c (elongation) and h (constriction) is shown as a contour plot . Contour intervals are 1 MeV. The projection of the least action trajectory (see the text) into the symmetric subspace (c,h) is shown by the thick solid line. Note the discrepancy between the static and dynamical barriers [78] .

V.3 - Dynamical effects in the low energy fission of ^{240}Pu

In spite of our poor knowledge of damping effects in the last phase of fission, let us examine how they can play a role by comparing TKE and $\bar{\nu}$ data for spontaneous and neutron-induced fission of some even-even nuclei . Special attention is given here to the ^{240}Pu case for which (d,p f) data are also considered [29,80] .

It can be seen in Fig. 43 that, for a given even-even nucleus, $\overline{TKE}$ is systematically higher for thermal-neutron induced fission than for spontaneous fission . Therefore, the full damping condition is not met for the cases plotted in Fig. 43 since the excess S_n of excitation energy for neutron-induced fission is found, at least partially, in the form of kinetic energy. But the difference $\Delta\overline{TKE}$ in TKE is less than 6 MeV (the approximate value of S_n for such nuclei), implying that some damping can nevertheless occur which causes the rest ($S_n - \Delta\overline{TKE}$) of the excitation energy to appear in the form of dissipation. This is actually reflected in prompt-neutron emission since the $\bar{\nu}$ values, as plotted in Fig. 44, are systematically higher for thermal-neutron-induced fission than for spontaneous fission, in agreement with $\overline{TKE}$ data . From these results, it would seem that moderate damping could apply to the low-energy fission of even-even actinides .

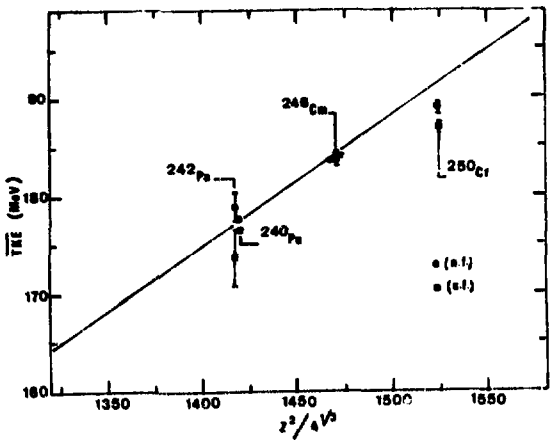

Fig. 43 - Comparison of the total kinetic energy TKE of the fragments for the ground state spontaneous fission (■) and for the thermal-neutron induced fission(o) of some even-even nuclei[76,78]. The solid line is a fit to the available data[76] .

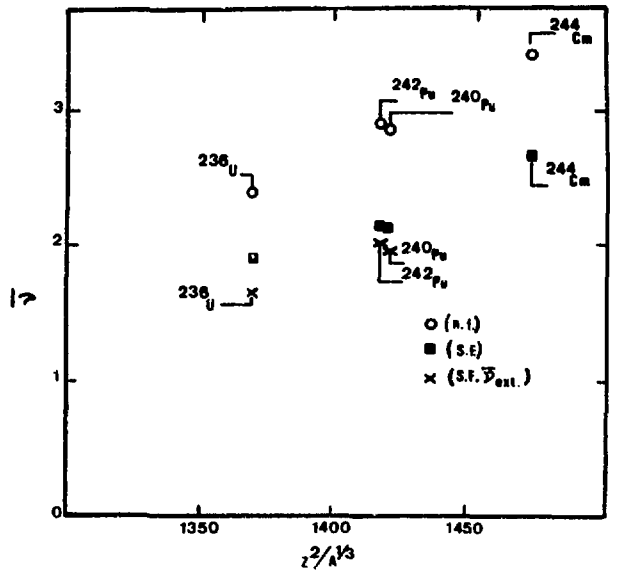

Fig. 44 - Comparison of the average fission neutron multiplicity $\bar{\nu}$ for the ground state spontaneous fission (■) and the thermal-neutron induced fission (O) of some even-even nuclei . The value $\bar{\nu}_{ext.}$ is obtained by extrapolating to zero excitation energy the $\bar{\nu}$-energy dependence observed for neutron-induced fission[29].

A closer examination of neutron-induced fission for a wide range of neutron energies E_n (below the threshold for second chance fission) can help to indicate what fraction of the increase in excitation energy E^* of the fissioning nucleus goes into fragment excitation and how this fraction varies with E^*. Many studies have been made on the variation of $\bar{\nu}$ with E_n for a great variety of actinides[81]. An illustration of this $\bar{\nu}$ energy dependence for ^{240}Pu is given in Fig. 45 where $\bar{\nu}$ shows a rough linear increase with E_n. No attention is paid here to the details of the energy dependence, in particular to the fine structure which may exist at low energy, but rather the gross behavior of $\bar{\nu}$ versus E_n is considered. These results show that the excitation energy E^t_{exc} of the fission fragments increases rapidly with E^*. If this effect, probably due to damping, is supposed to be present in the same manner for all excitation energies below S_n, the linear variation of $\bar{\nu}$ with E_n can be extended down to zero-excitation energy to obtain the extrapolated value of $\bar{\nu}$ (called $\bar{\nu}_{ext}$) for spontaneous fission. Comparison of extrapolated and measured values of $\bar{\nu}$ for ^{240}Pu spontaneous fission shows that the first one is lower than the second one (Fig. 45). This effect is found for all even-even actinides for which relevant $\bar{\nu}$ data are available (Fig. 44). Therefore, it seems that the amount of damping would decrease for $E^* < S_n$.

It is possible to pursue further this type of investigation for low-energy fission of ^{240}Pu since a fairly large number of experimental results is available on the properties of the fission fragments and their variation with excitation energy[80,82]. The variation of the total kinetic energy TKE for the fragments emitted in the low-energy fission of ^{240}Pu is plotted in Fig. 45 which includes data for the spontaneous fission of the ground state (G.S.) and the 4 ns isomeric state (I.S.), for the ^{239}Pu thermal-neutron induced fission and for the ^{239}Pu(d,pf) reaction. Also, the values of $d(TKE)/dE^*$, the slope of the linear variation of TKE with E^*, are given for several groups of fragment mass ratios and for the two types of fission discussed below. Moreover the average mass $\langle m^*_H \rangle$ of the heavy primary fission fragments is plotted as a function of E^* in Fig. 47.

Examination of these data seems to demonstrate the existence of two types of fission. The first one (called type I) includes i) the G.S. and I.S. spontaneous fission and ii) the ^{239}Pu(d,pf) reaction at $E^* = 4.65$ MeV for the fragments emitted at an angle $\theta = 0°$ relative to the recoil axis of the ^{240}Pu compound nucleus. A 200 keV wide resonance appears at $E^* = 4.65$ MeV in the anisotropy data and is interpreted as being due to a vibrational level in the 2nd well of the ^{240}Pu double-humped fission barrier. The second one (called type II) refers to all other ^{239}Pu (d,pf) results and to the ^{239}Pu(n,f) reaction induced by thermal neutrons.

In the fission of type I, the kinetic energy $\overline{TKE}$ increases linearly as a function of E^* with a slope of about + 1. This means that practically all the excitation energy E^* is found as an increase of the kinetic energy of the fission fragments and this holds for all mass divisions (Fig.46). The average mass $\langle m^*_H \rangle$ is the same for the three fission reactions of this type. This strongly suggests that damping, if present, must be very small and the fission of type I may very well be an illustration of superfluid motion already envisaged[69,75]. In this hypothesis, no intrinsic excitation occurs in the descent to scission and the available energy at that point then appears as pre-scission kinetic energy. All increase in E^* is then found entirely as an increase in E^s_{kin} and therefore in TKE since the Coulomb energy

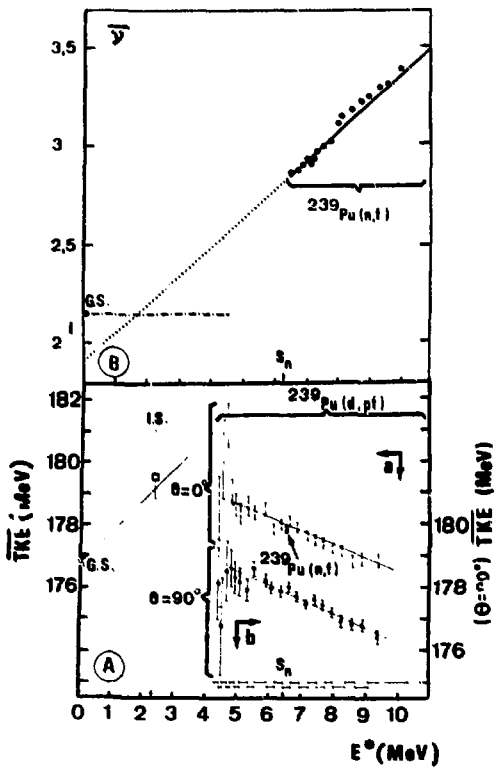

Fig. 45 - Plots of the fragment total kinetic energy $\overline{TKE}$ (graph A) and prompt-neutron yield $\bar{\nu}$ (graph B) for the fission of ^{240}Pu as a function of excitation energy E^* [80].

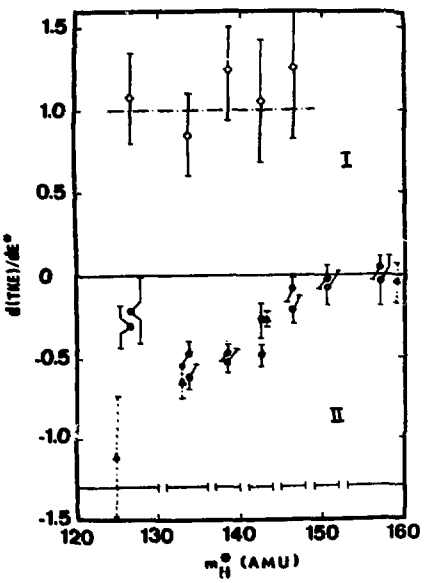

Fig. 46 - The values of $\frac{d\,(TKE)}{dE^*}$, the slope of the linear variation of TKE with E^*, are plotted for several groups of the mass m_H^* of the heavy fission fragment. The plots are made for the two types of fission (I and II) discussed in the text [80].

does not change with E^* in this picture. This applies to all mass divisions since all fission properties but the kinetic energy do not vary with E^* . The experimental results obtained for fission of the type I are consistent with this superfluid motion of the fissioning system .

In the fission of type II, on the contrary, the kinetic energy $\overline{TKE}$ decreases linearly as a function of E^* with a slope of about -0.43 .This is consistent with the increase of $\bar{\nu}$ with E^* observed above S_n . Nevertheless the energy balance in fission calculated with these data leads to a fairly large value $\langle S_n^f \rangle$ of the average neutron separation energy in the fission fragments ($\langle S_n^f \rangle \simeq 8.3$ MeV) . The mass splitting, on the average, is different from that of type I since $\langle m_H^* \rangle$ takes a different value (Fig.47). There does not seem to be a satisfactory interpretation of such a behavior of $\overline{TKE}$ and $\bar{\nu}$ with E^* . Several explanations have been proposed in terms either of damping or variation in stiffness of the fission fragments with E^*[80] . In the first case, the coupling of the fission mode to the other degrees of freedom reduces the pre-scission kinetic energy and induces intrinsic excitations which lead to a greater excitation of the fission fragments, hence to an increase in $\bar{\nu}$ [80]. In the second case, the greater excitation energy reduces the stiffness of the nascent fragments which then become easier to deform . At scission they are more elongated and the increase in the distance d between their charge centers decreases the Coulomb energy[82,83] . In these interpretations, shell effects seem to play an important role in agreement with the experimental results since the rate of decrease $d(TKE)/dE^*$ strongly depends on the fragment mass ratio (Fig. 46) .

The existence of two types of fission having different variations of $\overline{TKE}$ and $\bar{\nu}$ with excitation energy seems justified from these experimental data .

Such a phenomenon needs to be considered when extrapolating fission properties from isolated experimental results. In particular it does not seem adequate to deduce general laws about fission by comparing only spontaneous fission and therral neutron fission for the same nucleus .

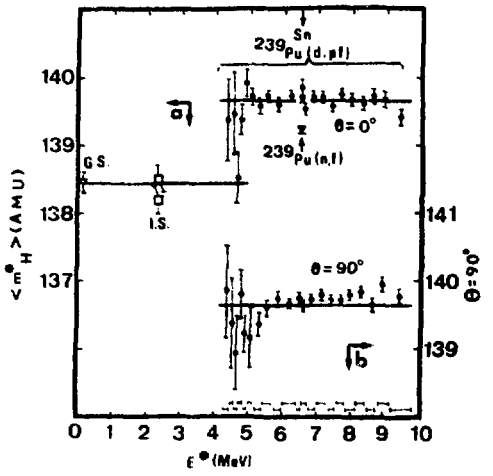

Fig. 47 - Plot of the average mass $\langle m_H^* \rangle$ of the heavy primary fragments emitted in the fission of ^{240}Pu as a function of excitation energy E^* . Note the difference in $\langle m_H^* \rangle$ for the two types of fission discussed in the text [80] .

CONCLUSION

The quantity of material presented in this paper, which is far from being comprehensive, shows obviously that fission is a lively subject. But, the vast amount of data collected about fission, either calculated or measured (but mostly measured) does not always give a clear description of the phenomenon. Though each piece of information adds another patch of color to the painting, the full import is still elusive . Obviously, the picture is not completed and some large surfaces probably still remain blank but, just as for the painting of the Impressionists, full appreciation comes only from afar .In this way, despite the great difficulties arising from the complexity of the process and the abundance of relevant data, general guide-lines can nevertheless be made out .

The neutron contribution to the picture has been significant from the very beginning. The famous patent taken out by Joliot and his collaborators, as early as 1939, on the possibility of self-sustained reactions and their energy applications, resulted from the combination of fission-neutron and neutron-induced-fission properties . More refined aspects of neutron-induced fission could be studied later when more intense neutron sources became available either from nuclear reactors or from nuclear reactions induced by accelerated beams of charged particles . Basic fission properties were then observed with now obsolete equipment such as crystal spectrometers or choppers installed at reactors. This work is probably considered these days by young physicists to have been the odd hobby of eccentrics , now old age pensioners. Nevertheless, the properties of fission induced by neutrons in the thermal and resonance region could be explored under such conditions. It was quite a surprise for instance to find out that fission resonances were not smeared out by their fission width, which was estimated to be quite large. Also, the wide fluctuations of the fission widths from resonance to resonance seemed for quite a while incompatible with the extremely large number of types, and states, of fission fragments, then thought to be the fission channels. The fission channel theory of A. Bohr, introduced about twenty years ago, gave one of the first guide-lines for the understanding of fission at this stage . It proved to be even more useful and fruitful later when hundreds of fission resonances were measured with modern neutron time-of-flight spectrometers installed near powerful pulsed accelerators . Even now, this theory continues to play an important role in neutron-induced fission ; it is verified in many cases , for example for ^{239}Pu resonances, with nevertheless a few obscure areas, such as for ^{235}U fission resonances. When the theory was not apparently verified, this stimulated studies which, in some cases, led to the discovery of new fission aspects, the $(n,\gamma f)$ reaction for example .

Another great step forward, also closely connected to neutron-induced fission, occurred about a decade ago with the advent of the double-humped fission barrier and all its various consequences . Such barrier shapes were first obtained by Strutinsky by an ingenious combination of the macroscopic and microscopic properties of the fissioning nucleus for all deformations along the fission path . The theoretical foundations of the calculational method have not been established as yet but there are presently no other methods of calculating fission barriers with a greater accuracy . Double-humped barrier shapes are obtained for practically all known actinide nuclei and provide a qualitative but unified interpretation of several puzzling experimental results measured independently and otherwise apparently uncorrelated. It is now commonly accepted that these results, encompassing fission

isomers as well as gross structure and intermediate structure in fission cross sections, are consequences of the double-humped shape of the fission barrier. The strength of such an interpretation came, and still comes, from the unified and coherent explanation it gives of so many diverse aspects. Its validity was later confirmed through i) detection of transitions between the rotational levels of the ^{240}Pu fission isomer and ii) spin measurements within the first low energy cluster of the ^{237}Np fission cross section .

Neutrons have also contributed substantially to these last developments . Fission isomers were not discovered with neutrons but the latter played an important role in identifying the first fission isomer, ^{242}Am, in determining its excitation energy and in demonstrating that it was not simply a conventional high spin isomer. But, in contrast, neutrons were solely responsible for the discovery of the now so-called "vibrational resonances" and of the intermediate structure effect in sub-barrier fission cross sections . Furthermore, another neutron experiment confirmed the correctness of interpretation. It is interesting to note that the intermediate states in the fission exit channels were found at the time when, more generally, doorway states were searched for in the neutron entrance channel .

The fine structure observed now in the vibrational resonances of the ^{232}Th(n,f cross section suggests even more complicated shapes of the fission barrier, perhaps with a third minimum .

The whole field of fission, including the description of the process in terms of double-humped barrier shapes, is far from being completely exploited to-day. More complete and accurate fission data are necessary to define more quantitatively the barrier parameters. It is striking, for example, that no direct spin determination for fission isomers has yet been made . Also, the γ branch has been observed only for one fission isomer and the spectroscopy of nuclear states in the second well is still in its infancy. This last aspect would nevertheless give the most interesting possibility of studying very deformed states of nuclear matter .

Neutrons should continue to play an important role for further studies of fission . The low energy fission resonances that can be separated with high resolution neutron time-of-flight spectrometers give the almost unique possibility of studying fission from a large number of pure initial states having well defined and determinable quantum numbers . In this endeavor, the neutron techniques can be challenged only by a few sophisticated charged particle spectrometers used to study reactions such as (d,pf), in which different compound nucleus states are populated with quantum numbers more difficult to measure but with excitation energies covering a wider range, especially below the neutron emission threshold . One natural way for neutrons to continue to contribute would consist in extending current types of measurements to heavier actinides . This would provide valuable information on fission over a wider range of nuclei and thus give better confidence in the predictions of the properties of superheavy nuclei. Of course, it is quite possible that, as was the case many times before, unexpected and exciting results might modify the course of the studies . Also, more intense neutron sources may be needed for extending the measurements to short-lived isotopes available in small quantities only .

Lastly, the fission dynamics that are just starting to be extensively studied, should provide a better knowledge of the fission path and a more thorough understanding ot the later stages of fission, especially at scission . The theoretical calculations that become available can be compared more and more realistically to the experimental results on kinetic and excitation energies of the fission fragments . In this respect and in addition to more sophisticated calculations, detailed measurements of these fission properties for specific mass divisions would be highly desirable for a larger number of different fissioning states . These studies of fission dynamics are closely connected to those also started for heavy ion reactions and this common approach is only the beginning of what could become a strong and long interplay between fission and heavy-ion physics .

Acknowledgements

The author is very grateful to Los Alamos Scientific Laboratory for its hospitality during which a large part of this paper was written . He is also very indebted to those who contributed to the preparation of this work : Drs J.C.D. Milton and S. Plattard for their careful checking and critical reading of the manuscript, Mrs C. Flouret for typing the text and Miss M. Jolibois for making the figures .

REFERENCES

1) O. Hahn and F. Strassmann, Naturwissenschaften, 1939, 27,11 .

2) V.M. Strutinsky and H.C. Pauli, P.C.F.* , p.155 .

3) J.E. Lynn, P.C.F.* , p.249 .

4) M. Brack, J. Damgaard, A.S. Jensen, H.C. Pauli, V.M. Strutinsky and C.Y. Wong, Rev. Mod. Phys., 1972, 44,320 .

5) J.R. Nix, Ann. Rev. Nucl. Sci., 1972, 22, 65 .

6) A. Michaudon, Advances in Nuclear Physics, (Plenum Press), Vol.6, p.1 .

7) V.M. Strutinsky, Nucl. Phys.,1967, A 95, 420 .

8) D. Gogny, Conference on Hartree-Fock and Self Consistent field theories in nuclei (Feb. 24 - March 1 , 1975, Trieste, Italy), (to be published) .

9) H. Flocard, P. Quentin, D. Vautherin. and A.K. Kermann, P.C.F.** ,Vol.1, .

10) A. Bohr and B. Mottelson, Nuclear Structure, (W.A. Benjamin Press), Vol. I .

11) W.J. Swiatecki, Phys. Rev., 1955, 100, 937 .

12) P. Möller and J.R. Nix, P.C.F.** Vol.I, p.103 .

13) W.D. Myers and W.J. Swiatecki, Berkeley Report, 1970, UCRL 19543 - Ann. of Phys. 1969, 55, 395 - Berkeley Preprint, 1973, LBL 1957 .

14) H.J. Krappe and J.R. Nix, P.C.F.**, Vol. 1, p.159 .

15) S. Polikanov, V.A. Druin, V.A. Karnaukhov, V.L. Mikheev, A.A. Pleve, N.K. Skobelev, V.G. Subbotin, G.M. Ter-akop'yan and V.A. Fomichev, Zh. Eksperim. i Theoret. Fiz. 1962, 42 , 1464 ; Sov. Phys. JETP 1962, 15, 1016 .

16) P.A. Russo, J. Pedersen and R. Vandenbosch, P.C.F.**, Vol.1, p.271 .

17) H.J. Specht, J. Weber, F. Konecny and D. Heunemann, Phys. Lett., 1972, 41 B , 43 .

18) A.J. Elwyn, P.C.F.* p. 457 .

19) G.N. Flerov, A.A. Pleve, S.M. Polikanov, S.P. Tretyakova, I. Boka, M. Sezon, I. Vilcov and N.Vilcov, Nucl. Phys., 1967, A 102, 443 .

20) A.F. Linev, B.N. Markov, A.A. Pleve and S.M. Polikanov, Nucl. Phys.,1965, 63 , 173 .

* Physics and Chemistry of Fission (IAEA Vienna, 1969), STI/Pub/234 .

** Physics and Chemistry of Fission (IAEA Vienna, 1974), STI/Pub/347 .

21) G.N. Flerov, A.A. Pleve, S.M. Polikanov, S.P. Tretyakova, N. Martalogu, D. Poenaru, M. Sezon, I. Vilkov and N. Vilcov, Nucl. Phys., 1967, 97 A, 444 .

22) K.L. Wolf and J.W. Meadows, APS Bulletin, 1974, 19 , 595 - Report USNDC, 1974, 11, 31 .

23) H.C. Britt, Atomic and Nuclear Data Tables, 1973, 12 , 407 .
H.C. Britt, M. Bolsterli, J.R. Nix and J.L. Norton, Phys. Rev., 1973, C 7, 801 .

24) M.G. Mustafa, U. Mosel and H.W. Schmitt, Phys. Rev., 1973, C 7 , 1519 .

25) E. Konecny, H.J. Specht and J. Weber, P.C.F.** , Vol. II, p.3 .

26) H.J. Specht, Rev. Mod. Phys., 1974, 46, 773 .

27) J.E. Lynn, Harwell Report, 1974, AERE-R 7468 .

28) P. Möller and J.R. Nix, Nucl. Phys., 1974, A 229, 269 .

29) A. Michaudon, Nuclear Cross Sections and Technology, NSB Special Publication 425 (Oct 1975), edited by R.A. Schrack and C.D. Bowman, Vol. I, p. 202 .

30) D.R. König and A. Michaudon, Journal of Nuclear Energy , 1971 , 25, 273 .

31) D.L. Hill and J.A. Wheeler, Phys. Rev., 1953, 89 , 1102 .

32) A. Bohr, Proc. Int. Conf. Peaceful Uses of Atomic Energy (Geneva 1955) United Nations, New York (1956), Vol. II, p. 220 .

33) N. Bohr and J.A. Wheeler, Phys. Rev., 1939, 56, 426 .

34) A. Michaudon, Nuclear Data for Reactors (IAEA Vienna 1967) STI/Pub/140, Vol.II, p.161 .

35) J. Blons, H. Derrien and A. Michaudon, Nuclear Data for Reactors, (AIEA Vienna 1970) STI/Pub/259, Vol.I, p. 513 .

36) G.A. Cowan, B.P. Bayhurst, R.J.Prestwood, J.S. Gilmore, and G.W. Knobeloch, Phys. Rev., 1966, 144, 979 .

37) H. Derrien, J. Blons and A. Michaudon, Nuclear Data for Reactors, (IAEA Vienna 1970) STI/Pub/259, Vol.I, p.481 .

38) F.L. Shapiro, Nuclear Structure (IAEA Vienna 1968) , STI/Pub/189, p. 283 .

39) S. Weinstein, R. Reed and R.C. Block, P.C.F.* , p. 477 .

40) a) D. Shackleton, J. Trochon, J. Fréhaut and M. Le Bars, Phys. Lett., 1972, 42 B, 344 .

b) J. Fréhaut and D. Shackleton, P.C.F.**, Vol. II, p. 201 .

c) D. Shackleton, D.Sc. Thesis, (Paris 1974) .

d) G. Simon, Thesis (3rd cycle), (Paris 1975) .

41) Y. Ryabov, J. Trochon, D. Shackleton and J. Fréhaut, Nucl. Phys.,1973, A 216, 395.

42) J.E. Lynn, Phys. Lett.,1965, 18, 31 - The Theory of Neutron Resonance Reactions (Clarendon, Oxford, 1968) .

43) H. Nifenecker, C. Signarbieux, R. Babinet and J. Poitou, P.C.F.** ,Vol.II, p.117 .

44) G.A. Keyworth, C.E. Olsen, F.T. Seibel, J.W.T. Dabbs and N.W. Hill, Phys. Rev. Lett., 1973, 31, 1077 .

45) J. Blons, H. Derrien and A. Michaudon, Proceedings of the Third Conference on Neutron Cross Sections and Technology, CONF 710301 Vol. II (Knoxville,1971)p.829 .

46) A. Michaudon, H. Derrien, P. Ribon and M. Sanche, Phys. Lett., 1963, 7, 211 .

47) G. de Saussure, R.B. Perez and W. Kolar, Phys. Rev., 1973, C 7, 2018 .

48) G.A. Cowan, A. Turkevitch, C.I. Browne and L.A.S.L. Radiochemistry Group, Phys. Rev., 1961, 122, 1286 .

G.A. Cowan, B.P. Bayhurst and R.J. Prestwood, Phys. Rev., 1963, 130, 2380 .

G.A. Cowan, B.P. Bayhurst, R.J. Prestwood, J.S. Gilmore and G.W. Knobeloch, Phys. Rev., 1970, 2, 615 .

49) J.W.T. Dabbs, C. Eggermann, B. Cauvin, A. Michaudon and M. Sanche, B.A.P.S. Series II (11), 1968, 13 , 1407 .

J.W.T. Dabbs, C. Eggermann, B. Cauvin, A. Michaudon and M. Sanche, P.C.F.* , p.321

50) N.J. Pattenden and H. Postma, Nucl. Phys., 1971, 167, 225 .

51) M.S. Moore, Statistical Properties of Nuclei, Ed. by J.B. Garg (Plenum Press), p. 55 .

52) L. Weston and J.H. Todd, Proceedings of the Third Conference on Neutron Cross Sections and Technology (Knoxville, USA) 1971, 2 , 861 .

53) Yu. V. Ryabov, So Don Sik, N. Chikov and N. Yaneva, Sov. J. Nucl. Phys., 1972, 14 , 519 .

54) J. Trochon, B. Lucas, A. Michaudon and Yu. V. Ryabov, J. Phys., 1973, 34, 131 .

55) J.E. Lynn, Nuclear Structure (IAEA Vienna 1968), STI/Pub/189 p. 463 - Report AERE Harwell R 5891, 1968 .

56) H. Weigmann, Z. Phys., 1968, 214, 7 .

57) G.A. Keyworth, R.L. Lemley, C.E. Olsen, F.T. Seibel, J.W.T. Dabbs, P.C.F.** Vol. I, p. 85 .

58) G.F. Auchampaugh and L.W. Weston, Phys. Rev., 1975, C 12, 1850 .

59) F.C. Difilippo, R.B. Perez, G. de Saussure, D.K. Olsen and R.W. Ingle, Paper submitted to the Toronto ANS Meeting (June 1976) .

60) G. de Saussure, private communication (1976) .

61) G.D. James, J.W.T. Dabbs, J.A. Harvey, N.W. Hill and R.H. Schindler (to be published) .

62) S. Plattard, J. Blons and D. Paya (to be published in Nuclear Science and Engineering) ; S. Plattard, Y. Pranal, J. Blons , 1975, ANS. Trans., 22, 665 .

63) J.E. Lynn, Nuclear Data for Reactors (IAEA Vienna 1967),STI/Pub/140,Vol.2,p.189 .

64) G.D. James, J.E. Lynn and L. Earwaker, Nucl. Phys., 1972, A 189, 225 .

65) D.W. Muir and L.R. Veeser, Neutron Cross Sections and Technology, (March 15-17 1971, Knoxville), 1 , 292 . - L.R. Weeser, private communication (1976) .

66) J. Blons, C. Mazur and D. Paya, Phys. Rev. Lett., 1975, 35, 1749 .

67) A.Sobiczewki, S. Bjornholm and K. Pomorski, Nucl. Phys., 1973, A 202, 274 .

68) P. Möller, private communication (1976) .

69) W.J. Swiatecki and S. Bjørnholm, Physics Reports, 1972, 4 , 325 .

70) V.V. Pashkevich, Nucl. Phys., 1971, A 169 , 275 .

71) S.E. Koonin and J.R. Nix, Report LA-UR-75-1642 , 1975 .
A.J. Sierk and J.R. Nix, Report LAP-151, 1976 .

72) a) J. Halpern and E.M. Henley, Comments on Nuclear and Particle Physics, 1969, 3, 52 .

b) G.M. Raisbeck and T.D. Thomas, Phys. Rev., 1968, 172, 1272 .

c) Y. Boneh, Z. Fraenkel and I. Nebenzahl, Phys. Rev., 1967, 156, 1305 .

73) P. Fong, P.C.F.* , p. 133 .

74) J.R. Nix, Nucl. Phys., 1969, A 130, 241 .

75) S. Bjornholm, Physica Scripta, 1974, 10 A, 110 .

76) J.P. Unik, J.E. Gindler, L.E. Glendenin, K.F. Flynn, A. Gorski and R.K. Sjoblom P.C.F.**, Vol.II, p. 19 .

77) W.N. Reisdorf, J.P. Unik and L.E. Glendenin, Nucl. Phys., 1973, A 205 , 348 .

78) H.C. Pauli and T. Ledergerber, P.C.F.** , Vol.I, p. 463 .

79) P.O. Fröman and N. Fröman, J.W.K.B. Approximation, Contribution to the Theory North-Holland, Amsterdam , 1965 .

80) a) J. Lachkar, Y. Patin and J. Sigaud, J. de Physique, Lettres 1975, 36, 79 .

b) Journées d'Etudes de la Fission (Cadarache, France 1974) (unpublished)

81) F. Manero and V.A. Konshin, Atomic Energy Review (IAEA Vienna 1972) Vol. 10, (4), p. 637 .

82) E. Konecny, H.J. Specht and J. Weber, Phys. Lett., 1973, 45 B, 329 .

83) W. Nöremberg, P.C.F.* , p. 51 .

84) R. Vandenbosch, Comments on Nuclear and Particle Physics, Vol.5, (6), 1972, p.161 .

85) J.S. Fraser and J.C.D Milton, Ann.Rev. Nucl. Sci., 1966, 16 , 379 .

86) J. Trochon, H. Derrien, B. Lucas and A. Michaudon, Nuclear Data for Reactors (AIEA Vienna 1970) , STI/Pub/259,Vol.I, p. 495 .

87) A. Fubini, J. Blons, A. Michaudon and D. Paya, Phys. Rev. Lett., 1968, 20, 1373 .

88) A.J. Deruytter and G. Wegener-Penning, P.C.F.**, Vol. II, p. 51 .

89) B.B. Back, H.C. Britt, J.D. Garrett, O. Hansen, Phys. Rev. Lett. 1972, 28, 1707

90) B.B. Back, O. Hansen, H.C. Britt, J.D. Garrett, P.C.F.** ,Vol.I, p. 25 .

MK 1 - NEUTRONS AND FISSION - Dr. A. Michaudon (C.E.N.-Bruyères-le-Châtel, France)

Block (R.P.I.):

Comment: In one of the papers yesterday on neptunium-237 from the Géel group, they reported results in which they said that the radiation widths of some of the 40 volt resonances were extremely large — two to three times the average radiation width. As I understand the paper these were the resonances with strong subthreshold fission components. I wonder if you would comment on this.

Michaudon:

Since there are so many parallel sessions in this conference, I was not able to listen to the talks but nevertheless I read the abstract and I'm very surprised by these results because as far as I'm concerned I have no explanation for these results.

Wigner (Princeton Univ.):

I have a very down to earth question. You give for plutonium-240, $\hbar^2/2I$ as 33 keV, for thorium as 2.5 keV, is that really three times larger radius, or what is the reason that the difference is so large, or did I copy it wrong?

Michaudon:

You mean the last results about thorium?

Wigner:

You said it was given as 2.5 keV.

Michaudon:

Yes, those are the figures.

Wigner:

Plutonium-240 as 33 keV ?

Michaudon:

No, 3.33. For plutonium-240 you have this value for the parameter $\hbar^2/2I$.

Wigner:

Then that was a misprint in an earlier graph. That was very much at the beginning of your discussion.

Michaudon:

It's 3.33. Because it gives a low value of this parameter and consequently a large value of the moment of inertia.

Wigner:

What radius does it correspond to?

Michaudon:

It is difficult to make a clear connection between the moment of inertia and the shape of the nucleus because we don't know exactly how to calculate the moment of inertia. But we can say that for the extreme stage of fission, the radii are roughly in the factor of 2. So it's between one and two. I would say maybe 1.5 or 1.6.

Kapoor (Bombay):

I'm referring to one slide you showed in which K^2 was plotted versus the mass asymmetry parameter R. Would you imply from this that there is some indication that the mass-asymmetry is already developed at the outer barrier and the fissioning nucleus remembers the asymmetry up to the scission point?

Michaudon:

I think from the experimental point of view the results are significant. Now, the interpretation is much more difficult because the transition states are octupole-octupole bands and you don't know exactly why the mass asymmetry should vary in this manner as a function of K. You expect a correlation of some kind but you don't know exactly what type of correlation. And also, as I mentioned, you have a skin effect which cannot then be understood, because in the fission channel theory of Bohr, it is the fission channels which matter, not the spin.

Special Contributed Paper MK 2

9.45 a.m., Friday, July 9, 1976

NEUTRON INDUCED FISSION OF ^{233}U, ^{235}U, AND ^{239}Pu.

M. A. Hooshyar

Physics Department, Pahlavi University, Shiraz, Iran.

B. Compani - Tabrizzi and F. Bary Malik*

Physics Department, Indiana University,

Bloomington, Indiana 47401, U.S.A.

RÉSUMÉ

The observed change in the percentage mass yield in the fission of ^{233}U, ^{235}U, and ^{239}Pu as a function of incident neutron energy are successfully analyzed in terms of the statistical model and an additional external barrier between the saddle and the scission points.

ABSTRACT

We have analyzed the observed change in the percentage mass yield and total kinetic energy spectra in the fission of ^{233}U, and ^{239}Pu by incident neutrons of thermal, 7 MeV, and 15.5 MeV energies and in the fission of ^{235}U by incident neutrons of thermal, 7 MeV, 15.5 MeV, and 22.0 MeV energies within the context of the statistical theory of Weisskopf-Ewing-Newton-Ericson and using the recently proposed external barrier between the saddle and the scission points. The transmission functions are calculated using a set of coupled equations in the exit channels and the level density formulas of Gadioli and Zetta. The computed results indicate that the model can account for the observed variation of the percentage mass yield spectra and the total kinetic energy in each case. Furthermore, we have calculated the most probably kinetic energy in the fission of ^{235}U and found it to agree with the observed ones. Our calculation of the same quantities for the spontaneous decay of ^{234}U, ^{236}U, and ^{240}Pu and the associated absolute spontaneous fission half-lives also agree with observation. The prediction of the kinetic energy and percentage mass yield spectra associated with the fission from a isomer state of ^{240}Pu are in accord with the recent measurements and will be presented for the fission from isomer states of ^{234}U and ^{236}U.

* *Presented by F. Bary Malik.*

I. Introduction

One of the most fascinating experimental observations associated with the fission process is the fact that the percentage yields of daughter fragments in nuclear fission process changes dramatically as the energy of the incident projectiles, particularly, neutrons is increased from the thermal to a few tens of MeV. This change is particularly pronounced for the symmetric decay modes which refer to those decay modes having nearly equal masses for each member of a particular daughter pair. For targets such as ^{233}U, ^{235}U, and ^{239}Pu, the percentage yields for the symmetric modes for induced fission by thermal neutrons is a few orders of magnitude less than those for the asymmetric modes defined to be those modes where one member of a daughter pair has nearly twice the mass of the other. This percentage yield of the symmetric fission products becomes on the other hand comparable to those of the asymmetric products for incident neutrons of a few tens of MeV. While this effect was well documented in the past,[1] only the recent development of the solid state detectors has made it possible to study this effect systematically in conjunction with the total kinetic energy released as a function of masses of daughter nuclei. Moreover, the earlier experiments primarily analyzed charged particles induced fission.[2,3] Recently, however, D'yachenko, Kuzminov and their collaborators[4-10] have measured the percentage mass yield and the total kinetic energy simultaneously as a function of mass number for incident neutron energies ranging from the thermal to 22 MeV.

Hooshyar and Malik[11] analyzed successfully the data in terms of a statistical theory of Weisskopf,[12] Weisskopf and Ewing,[13] Newton,[14] and Ericson.[15] The first such application of this statistical model to the fission process was developed by Fong[16] who indeed made a preliminary attempt

to understand this change in the percentage yield curve. The statistical model used in ref. 11 is based on the one proposed by Facchini and his collaborators[17,18] and postulates the existence of an external barrier between the saddle and the scission points. Indeed, the analysis of the then available data led Facchini and his collaboratos to conclude the possibility of the existence of such an external barrier[18] which is similar to one originally proposed by Block and Malik[19] and Block et al.[20] and used extensively by Hooshyar and Malik[21-24] to understand and predict various observables such as half-lives and percentage mass yields etc., associated with the spontaneous fission of even-even actinides. In particular this model postulating the existence of an external barrier between the saddle and the scission points has been able to account for (a) the mass distribution, (i.e., percentage yields of the fragments as a function of mass number) in the spontaneous fission of most of the even-even nuclei from ^{234}U to ^{258}Fm (ref. 21-23), in conjunction with the dependence of the total kinetic energy as a function of mass number (i.e., the total kinetic energy spectrum), (b) the total and partial spontaneous fission half-lives and the associated average kinetic energies of these nuclei, (c) the charge distribution and the average mass associated with each such charge distribution, (d) the absolute half-lives for the fission from the isomeric states of ^{234}U, ^{236}U, ^{240}Pu, and ^{244}Cm. The model further predicted the average kinetic energy and the mass distribution for fission from the isomeric states of ^{234}U, ^{236}U, and ^{240}Pu and since then these predictions have been confirmed by the experiment of Weber et al. (ref. 25).

The possibility of the existence of this external barrier has also been recognized in the calculations based on many body approaches such as the energy

density formalism[20,26] and the Hartree-Fock calculations.[27] This external barrier between the saddle and the scission points in these calculations originates from the fact that the density distribution of a nucleus varies as a function of its radius yielding a surface of about 3 fm thickness which is a substantial fraction of its half density radius which is about 7 fm for actinides. Because of this surface, the density of nuclear matter at the neck connecting a particular daughter pair prior to its scission is substantially lower than the saturation density. Actual calculation based on the energy density formalism indicates that this neck of unsaturated low density nuclear matter yields an effective attraction between the two members of a given daughter pair prior to scission. The Hartree-Fock calculation based on density dependent two nucleon interaction indicates also the possibility for the existence of this barrier.

In this article we extend the work of ref. 11 to incorporate the theoretical prediction of the total kinetic energy spectrum in conjunction with the proper mass distribution within the context of the statistical model using this external barrier. We show that the theoretically calculated kinetic energies lie within a few MeV of the observed ones. In addition, this calculated kinetic energies are sensitive to the actual choice of the parameters of the barrier. We slightly modify the parameters used in ref. 11 in order to achieve a better agreement between the calculated and the observed kinetic energy spectrum while maintaining the same excellent agreement in the percentage mass yield spectrum. In addition, we show that the absence of such a barrier would lead to incorrect kinetic energy spectra.

In view of the ability of the model to calculate the kinetic energy spectrum, we are now in a position to predict most of the observables in the spontaneous and particle induced fission processes.

II. The Model

Following the Facchini and his collaborators,[17,18] the expression for the fission width Γ for the decay channel of relative angular momentum zero is given by

$$\Gamma(A_1,A_2,\ I,U) = \int_0^{\mathcal{E}} \Gamma(A_1,A_2,IUE)dE \qquad (1)$$

Here a compound nucleus of spin I and excitation energy U is undergoing a fission into two fragments characterized by A_1 and A_2. $\mathcal{E}$ is the maximum available energy that could be released in the decay of the compound nucleus at an excitation energy U to a daughter pair A_1 and A_2 in their ground states. E is the total kinetic energy of a fragment pair. The energy balance yields the following relations

$$\mathcal{E} = M(A\text{-}1) + M(n) + E_n - M(A_1) - M(A_2) \qquad (2a)$$

This maximum available energy $\mathcal{E}$ is related to excitation energies of a daughter pair by

$$\mathcal{E} = E + U_1 + U_2 \qquad (2b)$$

where M(A-1), M(n), $M(A_1)$ and $M(A_2)$ are, respectively, masses of the target nucleus, incident neutron and the daughter pair A_1 and A_2 in their respective ground states. E_n is the kinetic energy of the incident neutron.

$\Gamma(A_1, A_2, IUE)$ in (1) is the probability of decay of the parent nucleus in a daughter pair A_1 and A_2 with a total kinetic energy E. The $\Gamma(A_1, A_2, IUE)$ is then given by

$$\Gamma(A_1, A_2, IUE) = T(E) \int_0^{\mathcal{E}-E} \rho_1(U_1)\rho_2(\mathcal{E}-E-U_1)dU_1 \qquad (3)$$

where U_1 is the excitation energy of one member of a given daughter pair and by energy conservation $U_2 = \mathcal{E}-E-U_1$ is the excitation energy of the other member of the daughter pair. T(E) is the transmission function through the barrier.

Experimental measurement of the total kinetic energy associated with a given mass splitting refers actually to the total kinetic energy of those daughter pairs which have maximum yields for that particular mass splitting. Because of this additional piece of information, it is sufficient for us to calculate the partial decay width $\Gamma(A_1, A_2, IUE)$ given by (3). Actually, these are also the decay modes contributing primarily to the integral in (1). To compute $\Gamma(A_1, A_2, IUE)$ we require an appropriate level density function and barrier through which the transmission takes place. We use the level density function reported by Gadioli and Zetta [28] and note the fact that we are to use effective excitation energy V in the level density formula which is related to U by (6). In terms of the effective excitation V, their level density formula is given by

$$\rho(I,V) = \frac{\hbar^3}{24\sqrt{2}}(2I+1)\exp\{-[\frac{I(I+1)}{2\sigma^2}]\}a^{\frac{1}{2}}\Big\{^{-3/2}$$

$$\times \exp[2(aV)^{\frac{1}{2}}]/(V+t)^2; \quad U \geq 5 \text{ MeV}. \qquad (4a)$$

and ρ = δ-function for $V < 5$ MeV (4b)

Here $\mathcal{J}$ is the moment of inertia of the nucleus in consideration. $\sigma^2 = (\mathcal{J}/\hbar^2) \times [(V+t)/a]^{\frac{1}{2}}$ and is the spin cut-off factor regulating the distribution of level spin. a is the characteristic parameter related to the single particle spacing near the Fermi sea. The choice of 5 MeV as the transition from the δ-function to (4a) is arbitrary but our results are thoroughly insensitive to this choice. V, the effective excitation, is related to the nuclear temperature t by

$$V = at^2 - t. \tag{5}$$

The effective excitation energy V is given by

$$V = U - \Delta + (70/A) \text{ in MeV.} \tag{6}$$

The energy gap parameter Δ is the sum of the pairing energy of last proton and neutron pairs. This is tabulated by Cameron.[29] The moment of inertia parameter $\mathcal{J}$ is

$$\begin{aligned} \mathcal{J} &= (0.7) \times \text{Rigid Body Moment of Inertia} \\ &= (0.7)(2/5)A\,R^2, \text{ with } R = 1.5\,A^{1/3} \text{ fm.} \end{aligned} \tag{7}$$

Also, a is the a_3 parameter of Gadioli and Zetta (Their Fig.1) = $0.127A$ (MeV^{-1}).

Insertion of (4a) in (3) leads to

$$\Gamma(A_1,A_2,IUE) = \frac{\sqrt{\pi}\hbar^6}{\rho_c(IU)}(a_1a_2)^{\frac{1}{2}}\frac{1}{(12)^2(2\sqrt{2})}\left(\frac{I}{I_1I_2}\right)^{-3/2}$$

$$\times T(E)\int_0^{\tilde{\epsilon}-E}\frac{(\sigma_1\sigma_2)^3}{(\sigma_1^2+\sigma_2^2)^{\frac{1}{2}}}\times\frac{\exp(2\sqrt{a_1V_1})}{(V_1+t_1)^2}$$

$$\times\frac{\exp(2\sqrt{a_2V_2})}{(V_2+t_2)^2}\,dU_1 \qquad (8)$$

Here $\rho_c(IU)$ is the level density of compound nucleus of spin I at an excitation energy U.

For a given daughter pair characterized by their respective mass and charge numbers and for a given energy E_n of the incident projectile, the decay probabilities are different corresponding to different kinetic energy associated with a daughter pair or stated otherwise the decay probabilities to a particular daughter pair depends on the excitation of each member of the daughter pair.

The calculation of the most probable yield and the corresponding kinetic energy involves evaluating (8) for all available values of E and then looking for the particular E for which $\Gamma(A_1A_2,IUE)$ has maximum yield.

To accomplish this, we are to evaluate the transmission function T(E). This function is calculated for the coupled N-channel decay modes using the formulation of Refs. 21 and 24. The form of the external barrier is given by

$$V_D(R) = \begin{cases} V_I & R < R_c \\ V_O & R_c \le R < R_b \\ V_{Coul}\exp\{(R-R_o)/d\} & R_b \le R < R_o \\ \dfrac{Z_1Z_2e^2}{R} & R_o < R \end{cases} \qquad (9)$$

and the coupling term is given by

$$V_c = \lambda \exp\{-|(R-R_o)/c|^3\} \qquad (10)$$

where $V_I = 200$ MeV, $V_o = V_{Coul} - 60$ MeV, $V_{Coul} = \frac{Z_1 Z_2 e^2}{R_o}$,

$$\lambda = 4.56 + (36.1)\exp(-|(175-A)/75.3|^{9.5}) \text{ in MeV}$$

$$R_c = 8 \text{ fm}, \quad R_b = R_o + d\log(V_o/V_{Coul}), \quad d = 3.2 \text{ fm},$$

$$R_o = r_o(A_1^{1/3} + A_2^{1/3}) + 3.0 \text{ fm}, \quad r_o = 1.3 + 0.13\, g(A_1,A_2,A) \text{ fm},$$

$$c = 4.8 - 0.6\, g(A_1,A_2,A). \quad g(A_1,A_2,A) = \exp\{-.036(|A_1-A_2|-\bar{A}+A)^{1.6}\},$$

where A, A_1, A_2 are the mass number of compound nuclear and daughter pairs, respectively.

Except for the small correction $g(A_1,A_2,A)$ this is the same barrier used in Refs. 21 and 24. In fact, for the fission to asymmetric decay modes $g \to 0$ and we get exactly our old barrier. This slight modification affects, however, the mass yield near the symmetric modes. Obviously the spontaneous half-lives are not influenced by this slight change because they are determined by the asymmetric decay modes accounting for most of the yields. For the same reason, the theoretical mass yield spectra published in Refs. 21 and 24 will not be altered significantly because the yield is very low for the spontaneous fission to symmetric modes. Quite often the experimental mass yield for these cases is less than 0.1 percent, and have considerable uncertainties. However, in neutron induced fission the percentage mass yield to symmetric modes becomes significantly large and is sensitive to the detail of barrier relevant to these yields. Thus, the information obtained in induced fission by neutrons of tens of MeV energy is a significant one in learning about that part of the barrier which is relevant to the decay to symmetric modes. Data on spontaneous fission of this nuclei are not good

enough for this purpose.

The transmission function T(E) is calculated by the JWKB approximation

$$T(E) = \exp(-2\int_1^2 \sqrt{B(V-E)}\, dr) \qquad (11)$$

where B = 2x reduced mass/$\hbar^2$. 1 and 2 refer, respectively, to two classical turning points.

At this point it is appropriate to discuss the domain of integration involved in evaluating the decay width (10) and searching for the most probably kinetic energies. For this purpose, we rewrite the energy balance equation as follows:

$$U = E_n + S_n \qquad (12a)$$

$$\mathcal{E} = E + U_1 + U_2 \qquad (12b)$$

where S_n is the binding energy of the incident projectile.

The point to note is that just prior to the scission the excitation energies of a daughter pair must be such that the second law of thermodynamics is not violated. If we identify the excitation energies of the compound nucleus and the daughter pair as available heat energy H, in order to insure that the entrophy is not diminished just prior to the scission all the available heat of the compound nucleus are to be taken up by the daughter pair who are at thermal equallibrium. We impose the condition at the change in entropy Δs cannot be negative i.e.,

$$\Delta s = \Delta H/t \geq 0. \qquad (13)$$

To ensure this inequality, we set the lower limit of integration in (10) from the condition that $U(t) = U_1(t) + U_2(t)$ where t is the temperature of the compound nucleus. This corresponds to $\Delta s = 0$ which refers to the situation that temperature of the compound nucleus is equal to that of each member of the daughter pair. Similarly, the changing the upper limit to $(E - E-U_2(t)$ ensures that Δs remains positive in the entire domain of integration for our choice of the level density function (see Appendix for a proof). We recognize that while these new limits are sufficient to insure (13), there could be other ways to do this.

While this additional modification in the lower limit of integration does not influence the computation of the most probable kinetic energy for induced fission by low energetic neutrons, its incorporation improves the theoretical prediction of the kinetic energy for projectiles of higher energies, i.e., for $E_n \geq 10$ MeV. Empirical support for this theoretical consideration is evident from the fact that the observed kinetic energy spectra for the fission products do not change significantly with the variation of incident projectile energies implying that the excitation energy of the compound system is converted basically to excite daughter pairs.

Thus in essence, we are using the approach of Facchini and Saetta-Mennichella[18] who indeed concluded from their analysis of the mass yield curve and the information on the kinetic energy for induced fission of ^{235}U by 6.0 and 15.5 MeV neutrons that an external barrier of the type discussed here is indeed needed. Our analysis, however, deviates in details, the most important of which are the consideration of the second law of thermodynamics to determine the domain of integration and the coupled channel approach to compute the transmission function.

This statistical model based on Weisskopf-Ewing-Newton-Ericson's

approach reduces in its general outline to the model of Fong[16,30] if the barrier transmission function is taken to be constant. In addition, Fong uses different approximations to evaluate the integral.

III. Details of the Calculation

Ideally we can calculate the percentage yields, kinetic energies, Q-values and half-lives, once a potential for calculating the transmission fucntion and level density functions are chosen. In practice, however, we face the problems that (i) all known mass formulas used to calculate Q-values have an inherent uncertainties of a few MeV. This is further compounded in our case because parameters of most of the mass formulas are adjusted to reproduce nuclear masses in the valley of stability, whereas, the daughter nuclei in a fission process, being neutron rich, lie quite often away from this valley of stability, (ii) the experimental data on percentage yields and kinetic energy have significant uncertainties, and (iii) the potential chosen here is only a good approximation to an actual one which can only be generated by a complicated superposition of analytical functions.

We, therefore, follow the following procedures: (i) we have first chosen a kinetic energy spectrum consistent with the data for spontaneous fission. Experimental information indicates that there is, usually, no substantial difference between the kinetic energy spectrum associated with the spontaneous fission and the one obtained in thermal neutron induced fission. This is further substantiated by our argument based on the second law of thermodynamics that the additional excitation energy of a parent nucleus is primarily distributed in the excitation of its decay products. (ii) We use this kinetic energy spectrum obtained from the analysis of spontaneous fission for calculating the percentage mass yields in thermal neutron induced fission and allowed ourselves to adjust the Q-values within 5 MeV of the theoretical calculation from Meyers and Swiatecki[31] mass formula to obtain the best fit to the percentage mass yields for thermal

induced fission. (iii) Once the Q-values are fixed for the thermal induced fission for a given target, we use the same Q-values unaltered for the induced fission of the same target by neutrons of higher energies. (iv) For every incident energy, we then determine theoretically using (10) the kinetic energy required to obtain the best fit to observed yields. This is the same method used in Ref. 11 to determine the theoretical kinetic energy spectra. In all cases, we find that these theoretically determined kinetic energies lie within 5 MeV of the observed ones. (v) In addition, we theoretically calculate the most probable kinetic energy associated with a given decay mode. This is done by calculating $\Gamma(A_1A_2, IUE)$ as a function of E and searching for that E which maximizes $\Gamma(A_1A_2, IUE)$. (vi) We repeat the procedure (iii) to (v) for every incident energy. (vi) To test further the choice of the potential we calculate both the spontaneous fission and isomer fission half-lives using equation (28) of Ref. (32) and a preformation probability of 10^{-5} calculated in Ref. 20.

The slight difference between the theoretically determined kinetic energy spectra designated under (iv) in this paper and those in Ref. 11 occurs because we have used here one of the calculated theoretical kinetic energy in (v) as a reference point, whereas Ref. 11 used an observed kinetic energy as a reference point. (Since we do not have a knowledge of absolute mass yield for none of the decay modes, we are forced to use a reference point in all our calculations.

Thus in essence using the same potential, we have reproduced (i) half-lives for spontaneous fission, (ii) half-lives for isomer fission, (iii) percentage mass yields for every incident energies and (iv) the most probable kinetic energy associated with each decay mode without using any free parameter. In Ref. 22 and 32, we have also reproduced correctly the charge distribution

and the average mass associated with each set of charge numbers.

Lastly we want to summarize the coupled channel approach used to calculate the transmission function. The decay of a parent nucleus in this approach is governed by N-coupled channels. Under the assumptions mentioned in Refs. 21 and 24 this set of N-coupled equations can be diagonalized to a set of equations, only three of which are different. Spontaneous fission in this context is governed by the decay through an effective barrier comprising $(V_D + V_C)$ and we have used this in Eq. (10) to compute half-lives, and percentage mass yield for spontaneous fission. The other effective barrier $(V_D - V_C)$ lies lower than the observed kinetic energies and represents the simple scattering process and not a decay process. The last one of these non-identical equations contains only V_D, which is relevant for the computation of half-lives and percentage mass yield for decay from isomeric states. The statistical model for the neutron induced fission assumes the formation of a compound parent nucleus in an excited state. This compound nucleus has a life-time much larger than those pertinent to a simple scattering process, i.e , much larger than 10^{-22} sec. The experiments on mass yields measure then the fastest decay probabilities of this compound system. For this purpose, the relevant potential is V_D and we have used this in our computation of observables related to neutron induced fission. It is, however, interesting to note that in the neutron induced fission, there is, in principle, another decay mode corresponding to a decay through a potential $V_D + V_C$; however, the mass yield through that decay mode is about 10^{28} orders of magnitude less than those reported here and is outside the capabilities of present experimental technique.

We shall also discuss the effect of the choice of the potential on the various computations performed here. For this purpose we designate two

sets of potentials:

Set A: The exact potential (8)

Set B: The potential (8) with d = 5.0 fm (instead of 3.2) and $R_o = r_o(A_1^{1/3} + A_2^{1/3}) + 3.7$ fm with the same value for r_o as in the set A and $g(A_1,A_2,A) = \exp\{-0.036|A_1-A_2|^{1.6}\}$.

Both of these sets are very similar. However, our analysis and calculations are sensitive to the actual choice of the potential and had we chosen another set differing substantially from these, results obtained would be poor. The set A is the one used in Refs. 21 to 24. Although the results obtained[11] by using the set A is about the same as those obtained from the use of the set B, there are some improvements, as discussed below. The main purpose is, however, to demonstrate that a finer adjustment of the potential is capable of reproducing the data perfectly.

IV. Results

In Table I, the calculated total half-lives for the spontaneous and isomer fission of ^{234}U, ^{236}U, and ^{240}Pu are compared with those observed in experiments. Although our barrier is slightly different from the one used previously in Ref. 21, it does not change the previously calculated results in any significant way. As stated earlier, this is expected because these barriers differ from each other significantly for the decay to symmetric modes only. On the other hand, the half-lives for spontaneous fission are primarily determined by the decay probabilities to asymmetric modes because the percentage yields to these asymmetric modes exceed to that to symmetric modes for spontaneous and isomer fission by a few orders of magnitudes. The agreement is good. Both the experimental and theoretical average kinetic energy in Table 1 refer to the maximum energy associated with the decay by fission and the agreement is satisfactory. Our theoretical values for the average kinetic energy reported here differ slightly from those reported in Refs. 21 and 24 (using set A), because in these earlier papers the computed average kinetic energy was defined to be the sum of all (kinetic energies times corresponding percentage mass yield) divided by the sum of all percentage mass yield. Consequently, they were slightly lower than experimental values which, as stated, usually refer to the kinetic energy associated with the maximum of the observed yields.

The theory, further, predicts that the kinetic energy spectrum for the fission from isomer states should be about the same as the one associated with spontaneous fission and this seems to be the case for ^{236}U (Ref. 44) and it will be interesting to test this general prediction of the model for other cases, particularly for ^{234}U and ^{240}Pu. In addition, the model predicts that the average kinetic energy associated with spontaneous and isomer fission

should nearly be equal.

A. (n + ^{239}Pu) and Spontaneous and Isomer Fission of ^{240}Pu

In Ref. 21 we predicted the percentage mass yield spectrum for the fission from the isomer state of ^{240}Pu using the set A. The predictions of these quantities using the set B is almost identical. This prediction in ref. 21 should hold for isomer states at 6.46 MeV excitation energy of ^{240}Pu because it was calculated for fission from isomer states generated by the thermal induced fission of ^{239}Pu. The theoretical prediction implied also that the kinetic energy versus mass spectrum for the fission from the spontaneous and isomer fission states should be nearly the same. The recent measurements of the kinetic energy spectrum and the percentage yield curve from the fission of an isomer state at 2.4 MeV excitation energy of ^{240}Pu by Weber et al.[25] bear out these predictions. In Fig. 1, we have plotted the theoretical prediction of the mass yield curve from the decay of the isomer states along with measurements of Weber et al. (insert c). The corresponding kinetic energy spectrum is the same as that of thermal neutron induced fission. This along with the measured kinetic energy spectrum of fission fragments for thermal neutron induced fission by Neiler et al.[34] is shown on the insert (a) of Fig. 1. The theoretical and experimental[34] percentage mass yield spectrum for spontaneous fission are shown in the insert (b).

Recently Torasker and Melkonian[45] have measured the percentage mass yield curve for the spontaneous fission of ^{240}Pu along with the corresponding kinetic energy spectrum. This shows interestingly enough a significant deviation from the mass yield curve obtained in the thermal neutron induced fission around the heavy mass fragment 130 and 134 (Fig. 1). The difference in

the excitation energy of ^{240}Pu formed as a compound nucleus in the thermal neutron induced fission and ^{240}Pu in ground state is 6.455 MeV. Energy balance requires that this 6.455 MeV more energy is available in the integration of the phase space (the phase space corresponds to the integrand of Eq. (2)), for the thermal neutron induced fission and hence in principle we expect some difference between the percentage mass yields obtained in the spontaneous fission and those obtained in the thermal neutron induced fission. The experimental results plotted for these two cases in Fig. 1 indeed show this difference and the theoretical computation can account for this observed difference. In Fig. 1a, we compare the theoretical kinetic energy spectrum for these two cases with those observed and except for a few modes associated with the spontaneous decay, there is a reasonable agreement. The theoretical prediction for the decay from an isomer state close to the ground state is also plotted in Fig. 1c and this agrees somewhat better with the experimental results.

In Fig. 2, the experimental data for the percentage mass yield and the kinetic energy spectrum are compared to the theoretical computation done with the set B for the case of incident thermal neutrons. The solid line in the kinetic energy spectrum corresponds to the kinetic energies required to obtain the best fit to the yield curve using the Q-values drawn in the same figure. These Q-values are compared with those obtained from Meyers-Swiatecki mass formula and they agree with each other within a couple of MeV which is well within the range of the inherent uncertainty of this mass formula. The kinetic energy spectrum corresponding to the best fit to the yield curve agrees with the observed one within 5 MeV which is about the uncertainty of the experimental measurement. The theoretically calculated most probable kinetic energy, marked by open circle, is within 5 MeV of the

experimental data in most cases. This demonstrates that theoretically computed percentage yield curve and the kinetic energies are in agreement with the observations.

We have now used the same Q-values for computing the percentage mass yields and the kinetic energy spectra for the induced fission of ^{239}Pu by 5.5 MeV and 15.5 MeV neutrons. They are compared with the data in Fig. 3 and 4, respectively. Once again the computed kinetic energy spectrum (solid-line) corresponding to the best fit of the obse ved yield curve lies within 5 MeV of the observed kinetic energies. The theoretically computed most probable kinetic energy (open circles) for each decay mode agrees within a few MeV of the observed one. The same set B has been used for our theoretical computation.

B. $(n + ^{235}U)$ Fission Process

Scientists in Physics and Power Engineering Institute of the U.S.S.R. have recently done a systematic study of the variation of the percentage mass yield spectrum and the kinetic energy spectrum obtained from the neutron induced fission of ^{235}U in the incident energy range between the thermal and 22 MeV.[4-10] Although the change in the yield for the thermal and 22.0 MeV neutron induced fission is very substantial, the data indicate that this change takes place gradually. Consequently, we have chosen to analyze data for thermal, 7 MeV, 15.5 MeV and 22.0 MeV neutron induced fission and our theoretical investigation indicates that the model can account for data at other intermediate energies.

Facchini and Saelta-Menichella[18] attempted to derive the nature of the barrier by analyzing the 6 MeV and 15.5 MeV neutron induced fission of ^{235}U data of Ref. 4 and 6 and came to the conclusion that a barrier similar

to the one used here might be needed. Our successful analysis of their data confirms this conclusion.

In Fig. 5, we present the theoretically calculated and observed percentage mass yields and kinetic energy spectra for the thermal induced fission. The theoretical results using the both sets of potential is almost the same and hence we have shown only one set of curves. In addition, we have presented the theoretical Q-value for the fission of the compound nucleus ^{236}U to the decay of various daughter pairs in their ground states. These Q-values are obtained from the best fit to observed mass yield spectrum. So derived Q-values are in excellent agreement with those calculated from Meyers-Swiatecki mass formula. These same Q-values have been used in subsequent calculation of induced fission of ^{235}U by neutrons of high energies.

Fig. 5 also shows the predicted mass yield spectrum for fission from an isomer state of ^{236}U formed at about 6.5 MeV excitation energy which corresponds to the formation of a compound nucleus by bombarding thermal neutrons to ^{235}U. The kinetic energy spectra are predicted to be the same as the one for the thermal induced fission of ^{235}U. Figs 6, 7, and 8 show the calculated and observed kinetic energy and mass yield spectra for the 7 MeV, 15.5 MeV, and 22 MeV neutron induced fission, respectively.

The solid curves in insert (a) of each of these figures represent the kinetic energy spectra corresponding to the best fit to percentage yield data, using the set B along with limits of integration dictated by (13). These kinetic energy spectra lie very close to those observed. The result obtained using the set A with limits of integration dictated by (13) lie very close to results obtained from the set B hence are not shown. We have also calculated the theoretically maximum probable kinetic energy for each decay mode using both the sets. These calculated values lie very close to

the theoretical kinetic energy values obtained from the best fit to the percentage mass yield spectra. They also lie within 5 to 10 MeV of the observed values. These calculations for the set B are shown as open circles.

The effect of the thermodynamical consideration in determining the lower limit of integration is also evident from these studies. If we set the lower limit to be zero, the calculated kinetic energy is 10 to 15 MeV higher than those observed. Although we have shown these calculated values for the set A, the results using the set B is almost the same.

In Fig. 12, 13, 14, and 15, we present samples of the probability of decay to three important decay modes. The set B is used in calculating Figs 12 and 13 for the thermal and 22.0 MeV neutrons. Fig. 14 and 15 represents calculations using the set A. Experimental determination of these decay probabilities are possible today and will provide important information on the transmission function.

In Fig. 16 and 17, we have done the calculation of the probability of decay to the same decay modes using T = 1 using the domain of integration from $U_1 = U_1(t)$ to $U_1 = \mathcal{E} - E - U(t)$. It is not possible at all to get the maximum of the kinetic energy near the observed value irrespective of our choice of the level density formulas.

Thus within the context of the statistical model discussed here, it is reasonable to assert that it is not possible to predict the most probable kinetic energy without postulating the existence of a barrier between the saddle and the scission points.

The predicted mass distribution for the decay from isomer state of ^{236}U is about the same as the one reported in Ref. (21) and the associated kinetic energy spectrum is the one plotted in Fig. 5.

C. $(n + ^{233}U)$ Fission Process

In Fig. 9 , we have compared for thermal neutron induced fission the theoretical and experimental percentage yields and kinetic energy spectra along with the required set of Q-values corresponding to the best fit to the yield curve. These Q-values once again lie very close to the ones calculated using Meyers-Swiatecki mass formula. This same set of Q-values have been used in the calculation for 5.5 and 15.5 MeV neutron induced fission. Fig. 10 and 11 compare the computed yield curves and kinetic energy spectra with observed data. Once again the theoretical kinetic energies obtained from the best fit of the mass distribution spectra lie very close to those observed. More importantly, theoretically calculated most probable kinetic energies lie within 5 MeV of the observed ones. The predicted mass yield and kinetic energy for the fission from an isomer state is about the same as those published in Ref. 21.

V. Discussion and Conclusion

This analysis conclusively indicates that experimental data on (i) spontaneous fission, (ii) isomer fission and (iii) induced fission can be adequately accounted for in terms of a statistical model employing a barrier between the saddle and the scission points. The theoretical computation can moreover reproduce the following important points:

(i) The mass yield near the symmetric decay modes increases by a few orders of magnitudes with the increase in the incident neutron energies, while the yield of the asymmetric decay modes do not change substantially.

(ii) The kinetic energies of the fragments near the symmetric modes increases significantly while those associated with the asymmetric modes do not.

It is important to document that once the parameters of the potential are chosen to reproduce the half-lives of the spontaneous decay of ^{240}Pu to its fastest decay modes, no other free parameters have been used for the induced fission involving neutrons at idfferent energies. The Q-values used in our calculation are essentially those obtained from Meyers-Swiatecki mass formula.

The agreement between the theory and the observation is all the more impressive because the spontaneous fission data of ^{234}U, ^{236}U, and ^{240}Pu can all be explained essentially by the same potential using the simple dependence of the scission radius R_{SC} on the (1/3) power of the mass number.

It is legitimate to ask the effect of transmission coefficient. In the absence of any barrier between the saddle and the scission points, this coefficient is one. As noted in Ref. 11, it is very difficult to fit both the percentage yields and the kinetic energies for the symmetric decay modes at all incident neutrons energies setting T = 1. But the difficulty is much more pronounced

if we calculate the maximum probable kinetic energies using T = 1 as shown in Fig. 16 - 17. They are in disagreement with experimental values by over 100 MeV! This discrepancy cannot be bridged by twisting the parameters of the level density functions. This analysis therefore strongly suggests the existence of such a barrier.

VI. Acknowledgement

We appreciate the helpful comments of Professor Konopinski. One of us (MAH) is thankful to the physics department of Indiana University for its hospitality. FBM wishes to thank the Inidana University Cyclotron Facility for a travel grant to the conference.

Appendix

At every point of integration of (8), Δs is given by $(U_1/t_1+U_2/t_2-U/t)$, where U_1, U_2, and U are excitation energies of each member of a daughter pair A_1 and A_2, and the compound nucleus A and t_1, t_2, and t are their respective temperatures. Neglecting the slight correction $(-\Delta + 70/A)$ in (6), we have $U = at^2 - t$. Hence

$$\Delta s = 0.127(A_1t_1 + A_2t_2 - At) - 1 \qquad (A.1)$$

where we have used $a = 0.127\ A(MeV^{-1})$ or using $A = A_1 + A_2$, we get

$$\Delta s = 0.127(A_1(t_1 - t) + A_2(t_2 - t)) - 1 \qquad (A.2)$$

However, U_1 in the domain of integration is larger than U_1 used in setting the lower limit ($= U_1(LL)$). The lower limit occurs when $t = t_1 = t_2$. Hence, $t_1 \geq t$ in entire domain of integration. The same holds for t_2 and $t_2 \geq t$.

Since $90 \leq A_1 \leq 150$ we get $\Delta s > 0$ at every point of integration.

References

1. For a summary see Nuclear Fission by R. Vandenbosch and J. R. Huizenga (Academic Press, New York, 1973).
2. H.C. Britt, H. E. Wegner, and J. C. Gursky, Phys. Rev. Letts. 8 (1962) 98; and Phys. Rev. 129 (1963) 2239.
3. J. P. Unik and J. R. Huizenga, Phys. Rev. 134 (1964) B90.
4. V. C. Vorobeva, P. P. D'yachenko, B. D. Kuz'minov, and M. Z. Tarasko, Sov. J. Nucl. Phys. 4 (1967) 234.
5. P. P. D'yachenko, B. D. Kuz'minov, and M. Z. Tarasko, Sov. J. Nucl. Phys. 8 (1969) 165.
6. P. P. D'yachenko and B. D. Kuz'minov, Sov. J. Nucl. Phys. 7 (1968) 27.
7. N. I. Akimov, V. G. Vorob'eva, V. N. Kabenin, N. P. Kolosov, B. D. Kuz'minov, A. I. Sergachev, L. D. Smirenkina, and M. Z. Tarashko, Sov. J. Nucl. Phys. 13 (1971) 272.
8. P. P. D'yachenko, D. B. Kuz'minov, L. E. Kutsaeva, and V. M. Piksaikin, Sov. J. Nucl. Phys. 14 (1972) 266.
9. A. I. Sergachev, N. P. D'yachenko, A. M. Kovalev and B. D. Kuz'minov, Sov. J. Nucl. Phys. 16 (1973) 266.
10. V. M. Surin, A. I. Sergachev, N. I. Rezchikov, and B. D. Kuz'minov, Sov. J. Nucl. Phys. 14 (1972) 523.
11. M. A. Hooshyar and F. B. Malik, Ann. Phys. (N.Y.) to be published.
12. V. F. Weisskopf, Phys. Rev. 52 (1937) 295.
13. V. F. Weisskopf and D. H. Ewing, Phys. Rev. 57 (1940) 472.
14. T. D. Newton, Proc. Symposium on the Physics of Fission (1956) Chalk River, Report CRO-642-A; Report AECL-329.
15. T. Ericsson, Advan. Phys. 9 (1960) 36.

16. P. Fong, Statistical Theory of Nuclear Fission (Gordon and Breach, New York 1969).

17. E. Erba, U. Facchini, and E. Saetta-Menichela, Nucl. Phys. 84 (1966) 595.

18. U. Facchini and E. Saetta-Menichela, Acta Phy. Polonica A38 (1970) 537.

19. B. Block and F. B. Malik, Phys. Rev. Letters, 19 (1967) 239.

20. B. Block, J. W. Clark, M. D. High, R. Malmin, and F. B. Malik, Ann. Phys. (NY) 62 (1971) 464.

21. M. A. Hooshyar and F. B. Malik, Phys. Letters 38B (1972) 495.

22. M. A. Hooshyar and F. B. Malik, Helv. Phys. Acta 46 (1973) 720.

23. M. A. Hooshyar and F. B. Malik, Helv. Phys. Acta 46 (1973) 724.

24. M. A. Hooshyar and F. B. Malik, Helv. Phys. Acta 45 (1972) 567.

25. J. Weber, H. J. Specht, E. Konecny, and D. Heunemann, Nucl. Phys. A221 (1974) 414.

26. I. Reichstein and F. B. Malik, Proc. of Int. Conf. on Nucl. Phys. held in Munich, 1973 eds. J. DeBoer and H. Mang (North-Holland Publishing Co. Amsterdam, 1973) and Ann. Phys. (NY) 55 (1976).

27. D. Kolb, R. Y. Cusson, and H. W. Schmitt, Phys. Rev. C10 (1974) 1529.

28. E. Gadioli and L. Zetta, Phys. Rev. 167 (1968) 1016.

29. A. G. W. Cameron, Cand. J. Phys. 36 (1958) 1040.

30. P. Fong, Phys. Rev. 102 (1956) 434.

31. W. D. Meyers and W. J. Swiatecki, Nucl. Phys. 81 (1966)1.

32. F. B. Malik and P. C. Sabatier, Helv. Phys. Acta 46 (1973) 303.

33. M. A. Hooshyar and F. B. Malik, Phys. Letters 55B (1975) 144.

34. H. W. Newson, Phys. Rev. 122 (1961) 1224.

35. F. Pleasonton, Phys. Rev. 174 (1968) 1500.

36. H. W. Schmitt, J. H. Neiler, and F. J. Walter, Phys. Rev. 141 (1966) 1146.

37. J. H. Neiler, F. Walter and H. W. Schmitt, Phys. Rev 149 (1966) 896.

38. A. J. Elwyn and A. T. G. Ferguson, Phys. and Chem. of Fission (IAEA) 1969 and Nucl. Phys. A148 (1970) 337;
S. M. Polkanov and G. Sletten, Nucl. Phys. A151 (1970) 656 Put an upperlimit of 2.10^{-9} sec.

39. N. L. Lark. G. Sletten, J. Pedersen and S. Bjornholm, Nucl. Phys. A139 (1969) 481;
K. L. Wolf, R. Vandenbosch, P. A. Russo, M. K. Mehta and C. R. Rudy, Phys. Rev. C1 (1970) 2096.

40. H. C. Britt, S. C. Bunett, B. H. Erkkila, J. E. Lynn, and W. E. Stein, Phys. Rev. C4 (1971) 1444;
R. Vandenbosch and K. L. Wolf, Phys. and Chem. of Fission (IAEA) 1969.

41. A. Ghiorso, G. H. Higgins, A. E. Larsh, G. T. Seaborg, and S. G. Thompson, Phys. Rev. 87 (1952) 163.

42. A. H. Jaffey and A. Hirsch, Unpublished data (1949).

43. D. E. Watt, F.J. Bannister, J. B. Laidler and F. Brown, Phys. Rev. 126 (1962) 264.

44. R. L. Ferguson, F. Plasil, G. D. Alam, and H. W. Schmitt, Phys. Letters 31B (1970) 526.

45. J. Toraskar and E. Melkonian, Phys. Rev. C4, (1971) 1391.

Table Caption

Table 1. Comparison of the computed half-lives and the average total kinetic energies for the spontaneous fission with the observation. The theory using both sets predicts that the average total kinetic energies for fission from isomer state lie close to those for spontaneous fission. Columns two through four are, respectively, the observed total kinetic energies $\langle E_{kin} \rangle$ in MeV, observed total half-lives, IFS, in seconds for fission from isomer states, and observed total half-lives in years for spontaneous fission, SF. Columns five through seven refer to the corresponding quantities calculated in this paper using two sets of potentials. (a) through (i) corresponds, respectively, to references 35 to 43.

Table 1

PARENT	EXPERIMENTAL			SET A (theory)			SET B (theory)		
	$\langle E_{kin} \rangle$	IFS	SF	$\langle E_{kin} \rangle$	IFS	SF	$\langle E_{kin} \rangle$	IFS	SF
^{234}U	171.2±2.0(a)	3.5×10^{-8}(d)	1.6×10^{16}(g)	171.2	3.5×10^{-8}	1.0×10^{16}	169.2	1.2×10^{-9}	1.0×10^{1}
^{236}U	171.9±1.4(b)	$(105\pm20)10^{-9}$(e)	2×10^{16} (h)	169.2	2.1×10^{-7}	1.0×10^{16}	167.2	1.3×10^{-9}	1.0×10^{1}
^{240}Pu	177.7±1.8(c)	$(3.8\pm0.3)10^{-9}$(f)	1.34×10^{11}(i)	180.9	4×10^{-9}	1.1×10^{11}	178.9	9.0×10^{-10}	1.0×10^{10}

Figure Caption

Fig. 1:

Solid and dashed lines are theoretical values for the thermal induced fission of ^{239}Pu and spontaneous fission of ^{240}Pu respectively in all three inserts. Insert (a) refers to the total kinetic energy as a function of heavy fragment mass M_H in amu and solid triangles and open rectangles are, respectively, experimental values for the thermal induced fission (ref. 36) and spontaneous fission (ref. 45). Insert (b) represents the percentage mass yield curve as a function of M_H and open rectangles refer to experimental data from ref. 45. Insert (c) refers to the percentage mass yield for fission from isomer states as a function of M_H and solid dots with error bars are experimental observation reported in ref. 25.

Fig. 2:

The total kinetic energy and the Q-values for the thermal induced fission of ^{239}Pu are plotted as a function of the masses of heavy fragments M_H in inserts (a). Solid and dashed curves in insert (a) refer, respectively, to the theoretical values required for the total kinetic energies and the Q-values to fit the yields. Dots and triangles refer, respectively, to the experimentally observed kinetic energy (ref. 36) and Q-values calculated from Meyers and Swiatecki mass formula (ref. 31). Calculated most probable kinetic energies are shown by open circles. Insert (b) refers to the theoretical (solid line) and experimental (dots (ref. 36)) percentage mass yield as a function of M_H. Experimental error bars are shown at the bottom of each insert.

Fig. 3:

The total kinetic energy (insert (a)) and percentage yield (insert (b)) are plotted as a function of the mass of heavy fragments mass M_H for 5.5 MeV neutron induced fission of ^{239}Pu. Theoretical calculations of kinetic

energies corresponding to the best fit to observed yields and calculated most probable kinetic energies are shown in insert (a) by solid lines and open circles, respectively. The solid line in (b) refers to the theoretical yields. Solid dots in (a) and (b) are data from ref. 10. Experimental error bars are shown near the bottom of each insert.

Fig. 4:

The total kinetic energy (insert (a)) and percentage mass yield (insert (b)) are plotted as a function of the masses of heavy fragments M_H for 15.5 MeV neutron induced fission of ^{239}Pu. Symbols are the same as described in the caption of Fig. 3.

Fig. 5:

Insert (a) indicates theoretical kinetic energy (solid line) and Q-values (dashed line) used in fitting the percentage mass yield as a function of masses of heavy fragments for thermal neutron induced fission of ^{235}U. In the same insert dots and solid triangles refer, respectively, to the experimental kinetic energy reported in Refs. 4 and 5 and the Q-values calculated from Meyers and Swiatecki mass formula (Ref. 31). The open circle in insert (a) are theoretically calculated most probable kinetic energies. In insert (b), the calculated (solid line) and experimental percentage mass yield (Ref. 4 and 5) are plotted as a function of heavy fragment masses.

Fig. 6:

The total kinetic energy (insert(a)) and percentage mass yield (insert (b)) are plotted as a function of the masses of heavy fragments M_H for 7.0 MeV neutron induced fission of ^{235}U. Symbols are the same as described in the caption of Fig. 3. Data are taken from Refs. 4 and 5.

Fig. [illegible]:

The tota[illegible] netic energy (insert (a)) and percentage mass yield (insert (b)) are plotted as a function of the masses of heavy fragments M_H for [illegible].[illegible] MeV neutron induced fission of [illegible]U. Data are from ref. [illegible]. Symbols are explained in the caption of Figs. 3 and 6.

Fig. [illegible]:

The total kinetic energy (insert (a)) and percentage mass yield (insert (b)) are plotted as a function of masses of heavy fragments, for [illegible].0 MeV neutron induced fission of [illegible]U. Data are taken from ref. [illegible]. Symbols are explained in the caption of Figs. 3 and 6.

Fig. 9:

Insert (a) indicates theoretical kinetic energy (solid line) and Q-values (dashed line) used in fitting the percentage mass yield as a function of masses of heavy fragments M_H for thermal neutron induced fission of ^{239}U. In the same insert solid dots and triangles refer to, respectively, experimental kinetic energy reported in Ref. 10 and Q-values calculated from Meyers and Swiatecki mass formula (Ref. 21). The open circles in insert (a) are theoretically calculated most probable kinetic energies. In insert (b), the calculated (solid line) and experimental percentage mass yield are plotted as a function of M_H. Experimental error bars are indicated near the bottom of each insert.

Fig. 10:

The total kinetic energy (insert (a)) and percentage mass yield (insert (b)) are plotted as a function of masses of heavy fragments M_H for [illegible].5 MeV neutron induced fission of ^{235}U. Experimental data are taken from Ref. 10. Symbols are explained in the caption of Fig. 3.

Fig. 11:

The total kinetic energy (insert (a)) and percentage mass yield (insert (b)) are plotted as a function of masses of heavy fragments M_H for [illegible] MeV neutron induced fission of [illegible]. Experimental data are taken from Ref. 10. Symbols are explained in the caption of Fig. 7.

Fig. 12:

Calculated values of relative probabilities of decay as a function of total kinetic energies of a particular daughter pair for the thermal neutron induced fission of [illegible]. Masses of daughter pairs are noted next to the relevant plot. Kinetic energies corresponding to maxima of these probabilities are refered as theoretical values for most probable kinetic energies for a particular daughter pairs in Figs. 2 to 11. These calculations are for the set B potential with due consideration to $\Delta s > 0$.

Fig. 13:

The same as in the Fig. 12 except for [illegible] incident neutrons of 22 MeV.

Fig. 14:

The same as in the Fig. 12 but the set A potential has been used.

Fig. 15:

The same as in the Fig. 12 except the set A potential has been used and incident neutron energy is 22 MeV.

Fig. 16:

Calculated values of relative probabilities of decay as a function of total kinetic energies of a particular daughter pair for the case $T(E) = 1$ (i.e., for the case of no barrier). Plots are for thermal neutron induced fission of ^{235}U. Masses of daughter pairs are noted next to the relevant plot. Kinetic energies corresponding to maximum probabilities are most probable theoretical kinetic energies.

Fig. 17:

The same as the Fig. 1(except for incident neutron energy of 22.0 MeV.

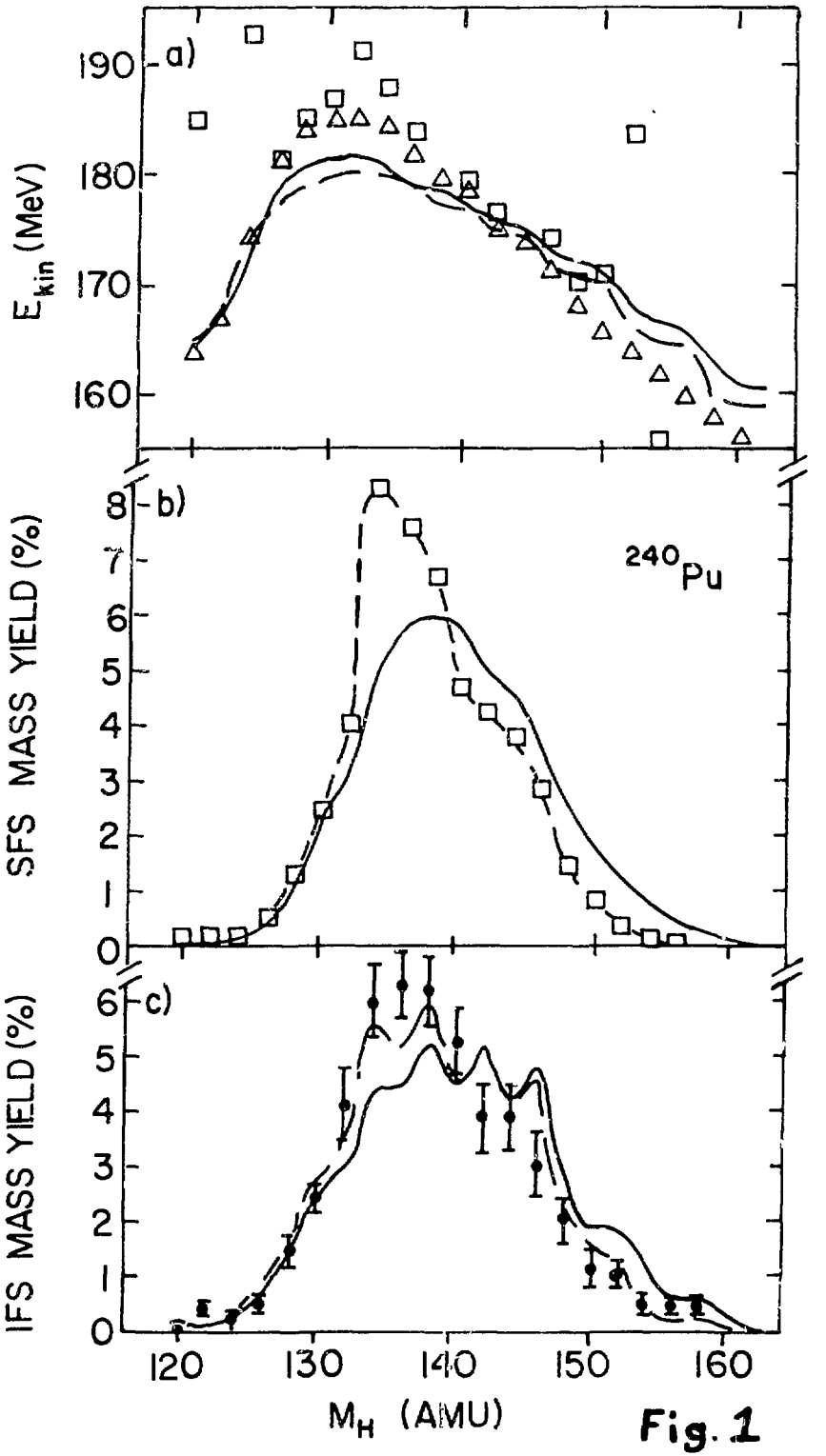
a)
b)
c)
E_{kin} (MeV)
190
180
170
160
SFS MASS YIELD (%)
^{240}Pu
IFS MASS YIELD (%)
0
1
2
3
4
5
6
7
8
120
130
140
150
160
M_H (AMU)

Fig. 1

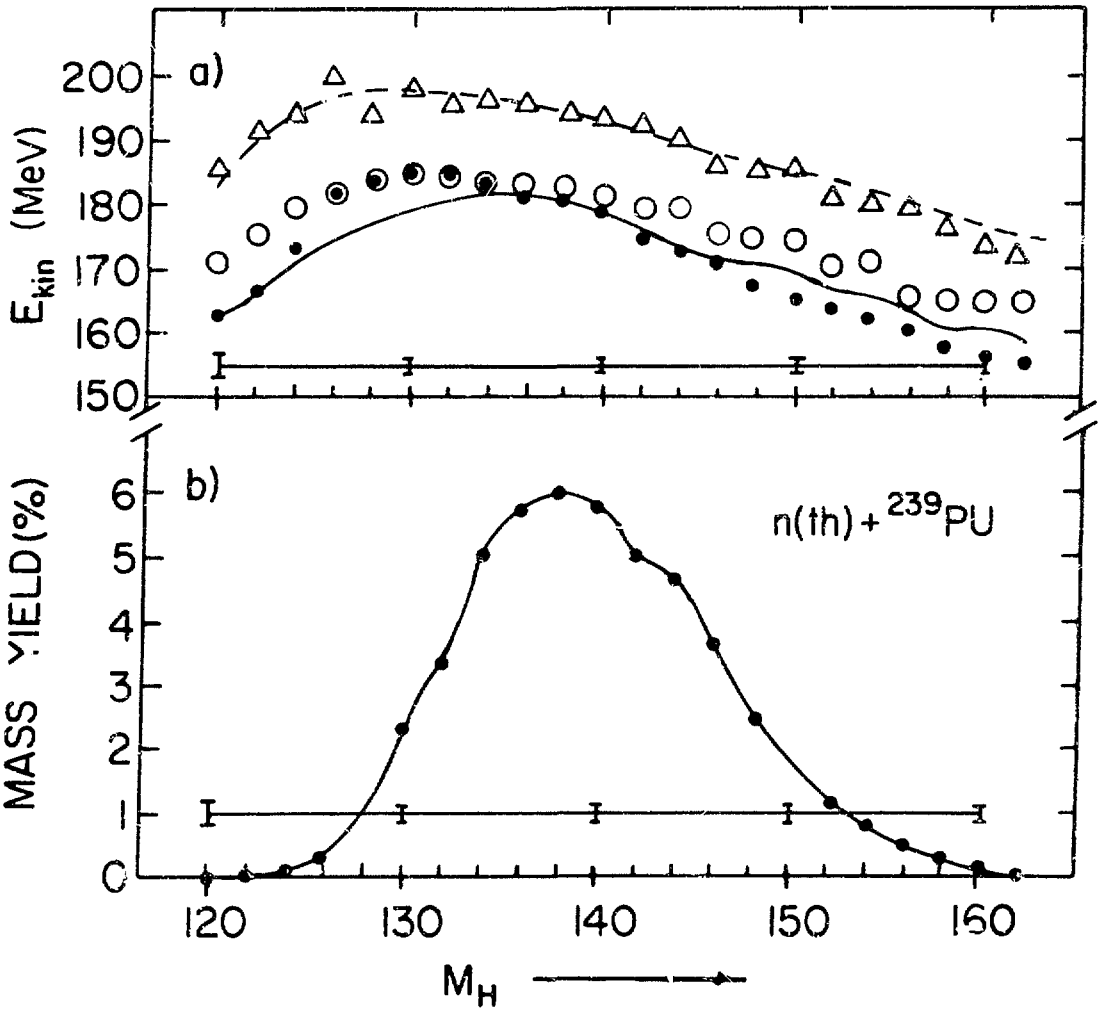
a)
200
190
180
170
160
150
E_{kin} (MeV)
b)
n(th) + ^{239}PU
MASS YIELD (%)
6
5
4
3
2
1
0
120
130
140
150
160
M_H

Fig. 2

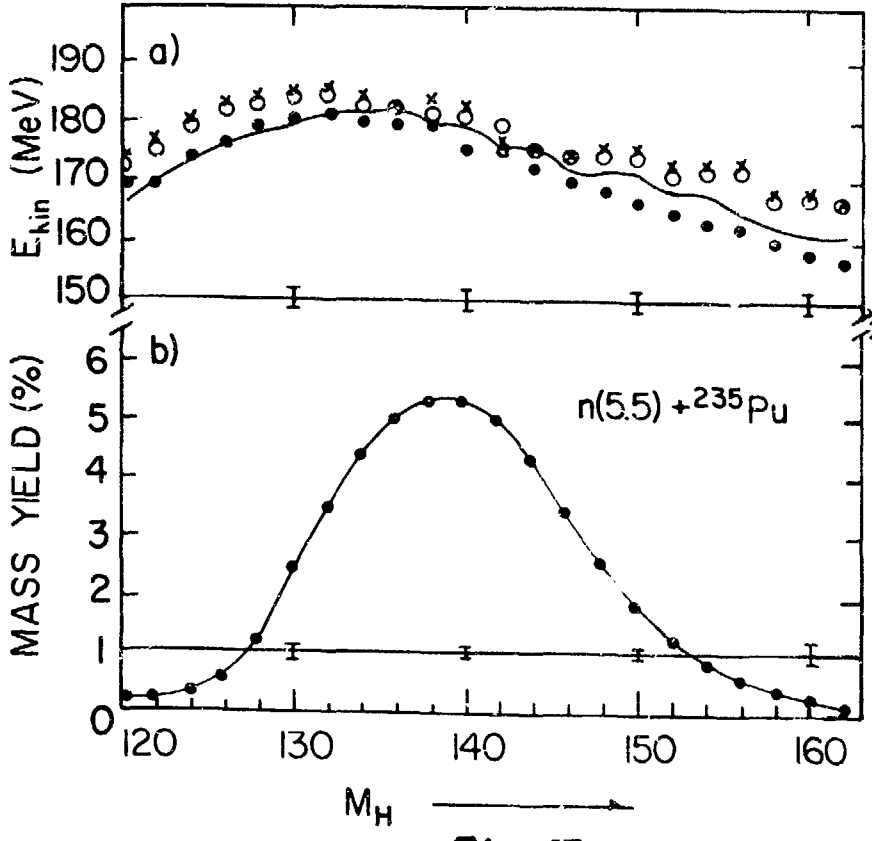
a)
190
180
170
160
150
E_{kin} (MeV)
b)
6
5
4
3
2
1
0
MASS YIELD (%)
n(5.5) + ^{235}Pu
120
130
140
150
160
M_H

Fig 3

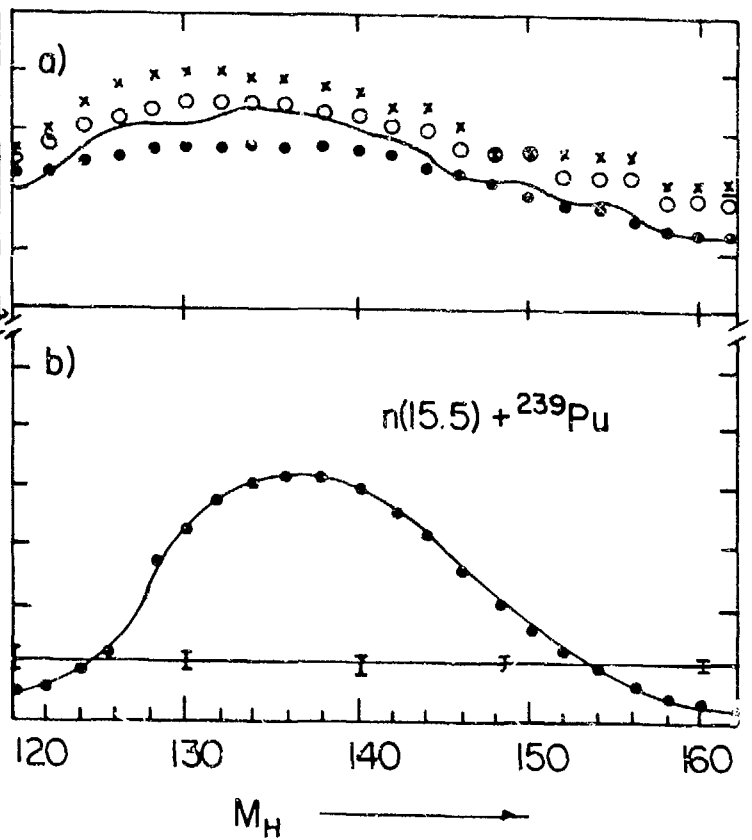
a)
b)
n(15.5) + ^{239}Pu
120
130
140
150
160
M_H

Fig 4

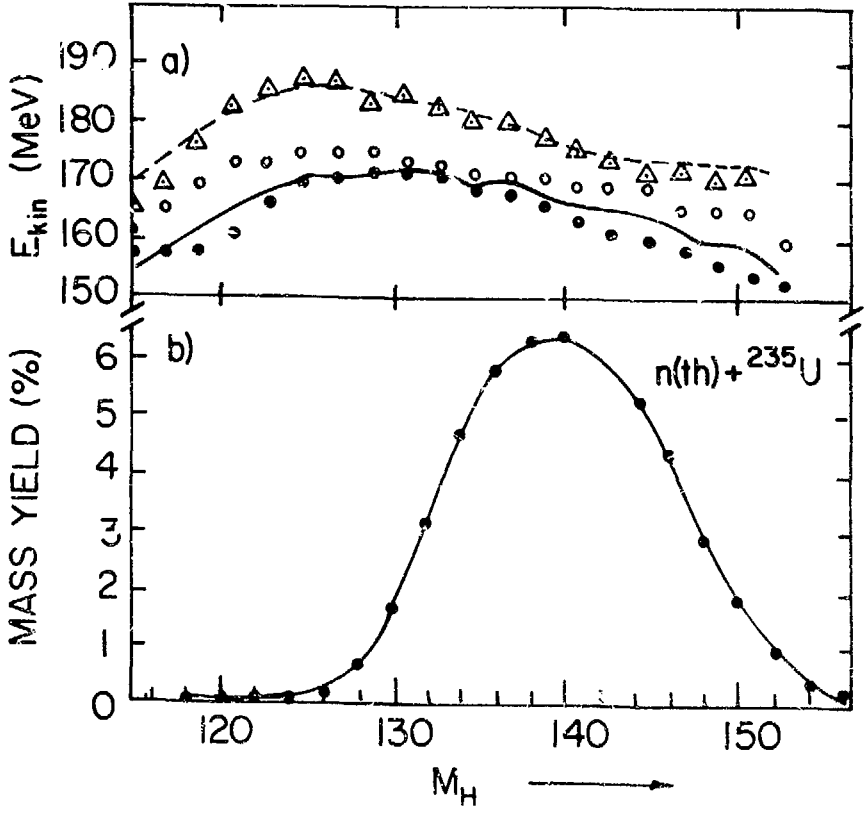
a)
b)
E_{kin} (MeV)
190
180
170
160
150
MASS YIELD (%)
6
5
4
3
2
1
0
120
130
140
150
M_H
n(th) + ^{235}U

Fig. 5

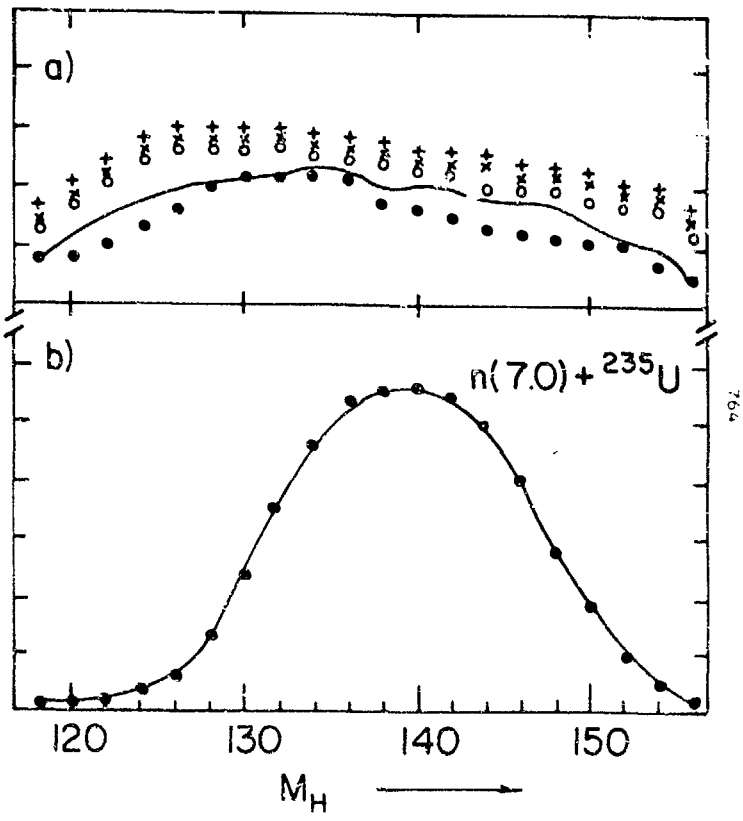
a)
b)
120
130
140
150
M_H
n(7.0) + ^{235}U

Fig. 6

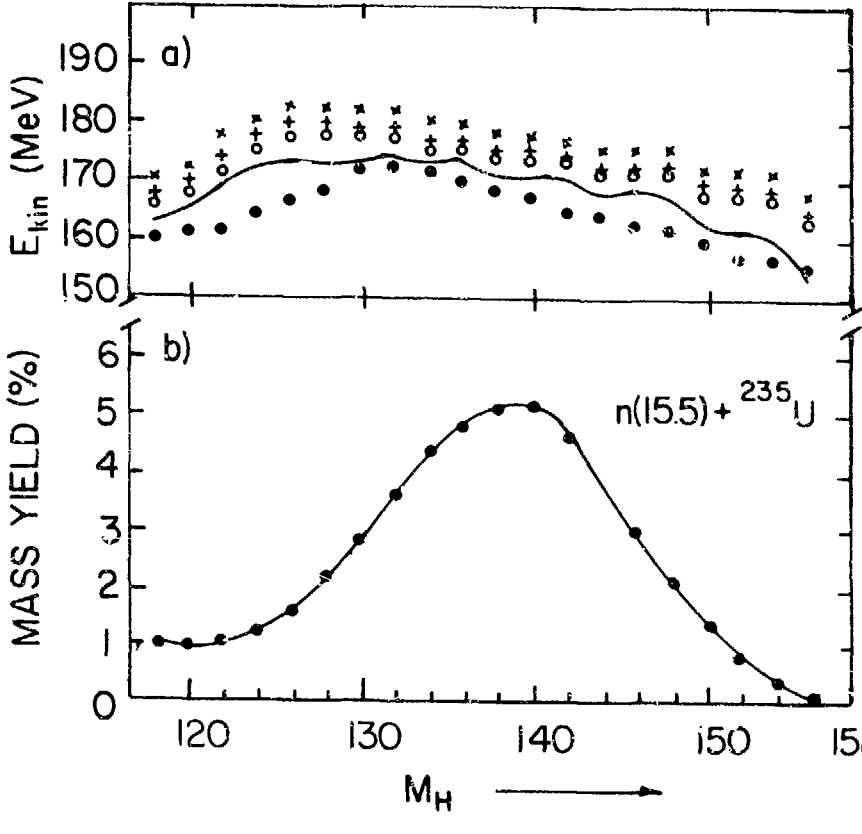
a)
b)
E_{kin} (MeV)
190
180
170
160
150
MASS YIELD (%)
6
5
4
3
2
1
0
n(15.5) + ^{235}U
120
130
140
150
158
M_H

Fig. 7

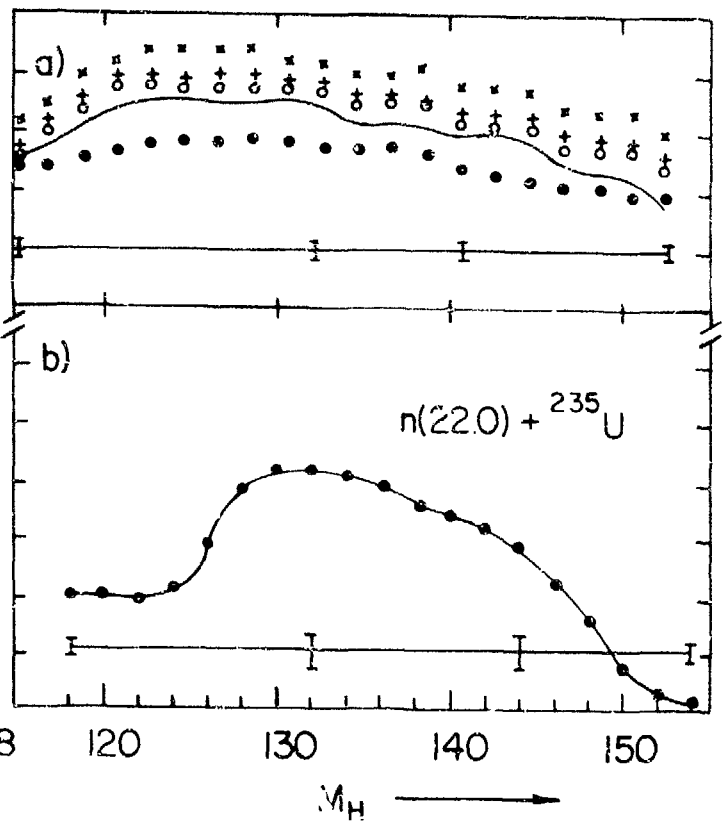
a)
b)
n(22.0) + ^{235}U
120
130
140
150
M_H

Fig. 8

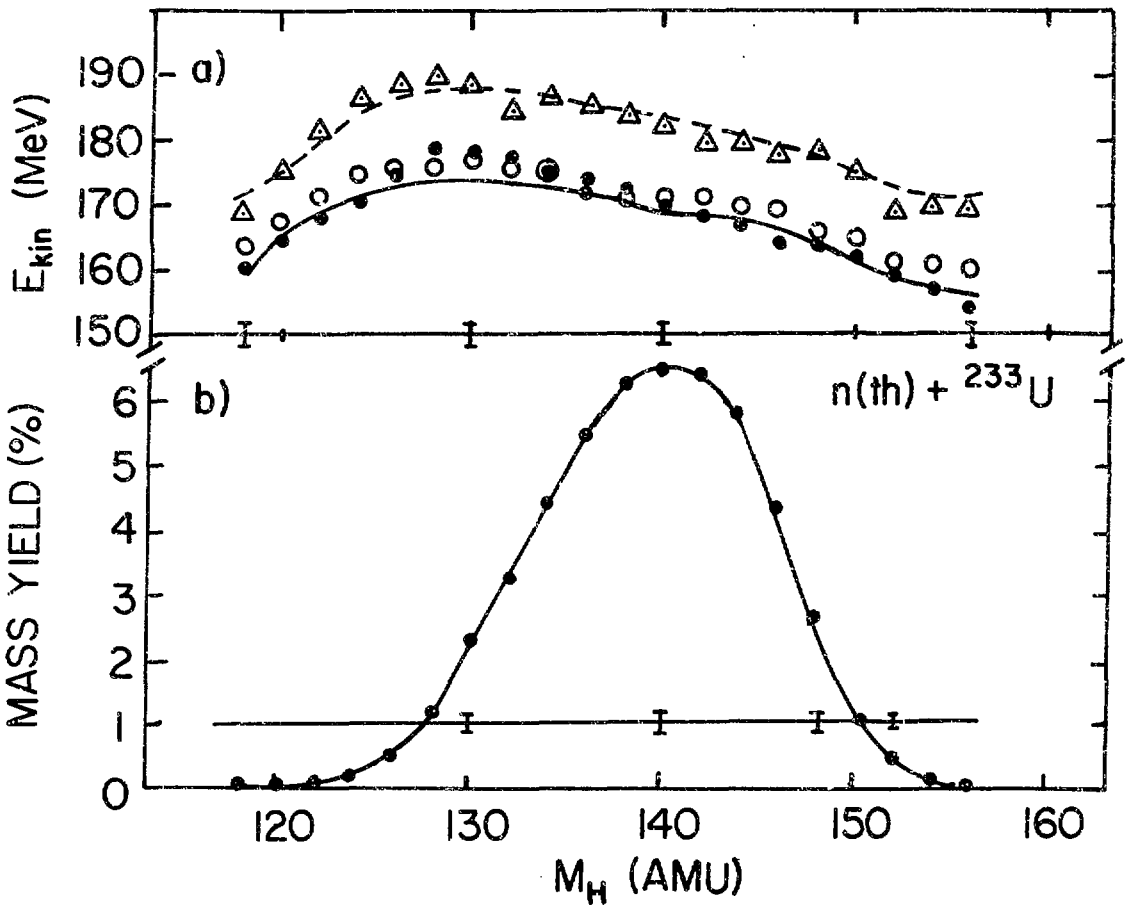
a)
b)
n(th) + 233U
Ekin (MeV)
MASS YIELD (%)
MH (AMU)
190
180
170
160
150
6
5
4
3
2
1
0
120
130
140
150
160

Fig. 9

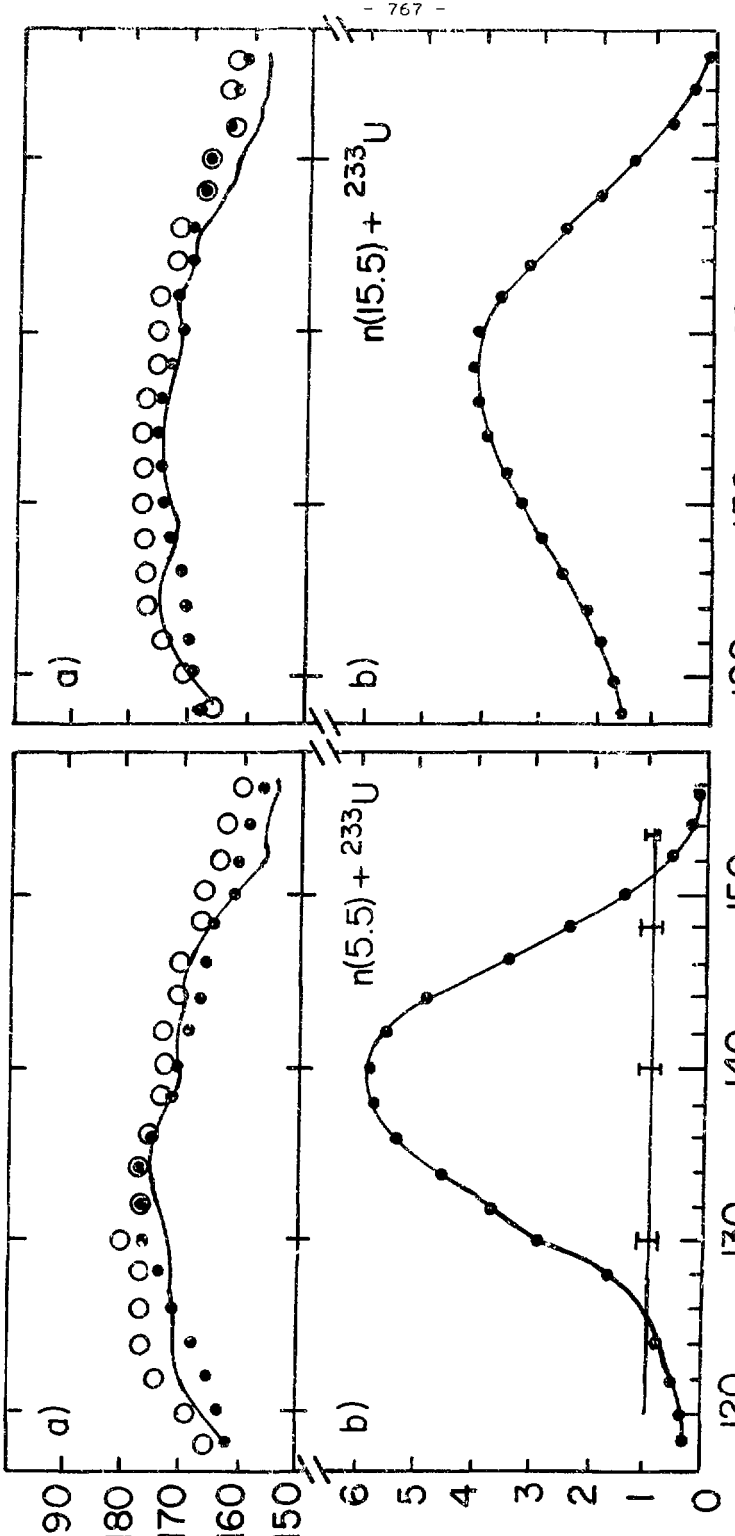

Fig. 10

Fig. 11

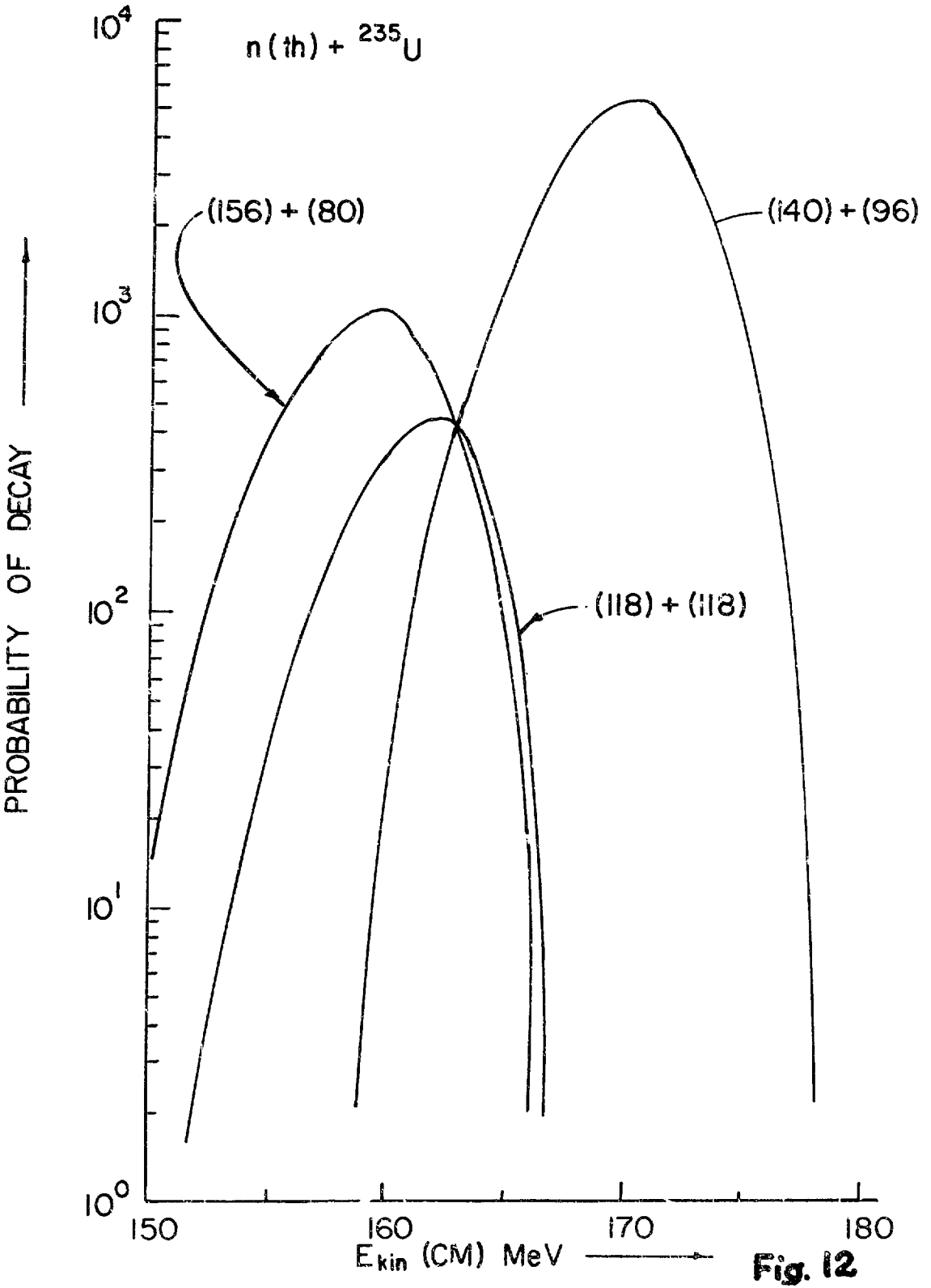
n (th) + 235U
(156) + (80)
(140) + (96)
(118) + (118)
PROBABILITY OF DECAY
10^4
10^3
10^2
10^1
10^0
150
160
170
180
E kin (CM) MeV

Fig. 12

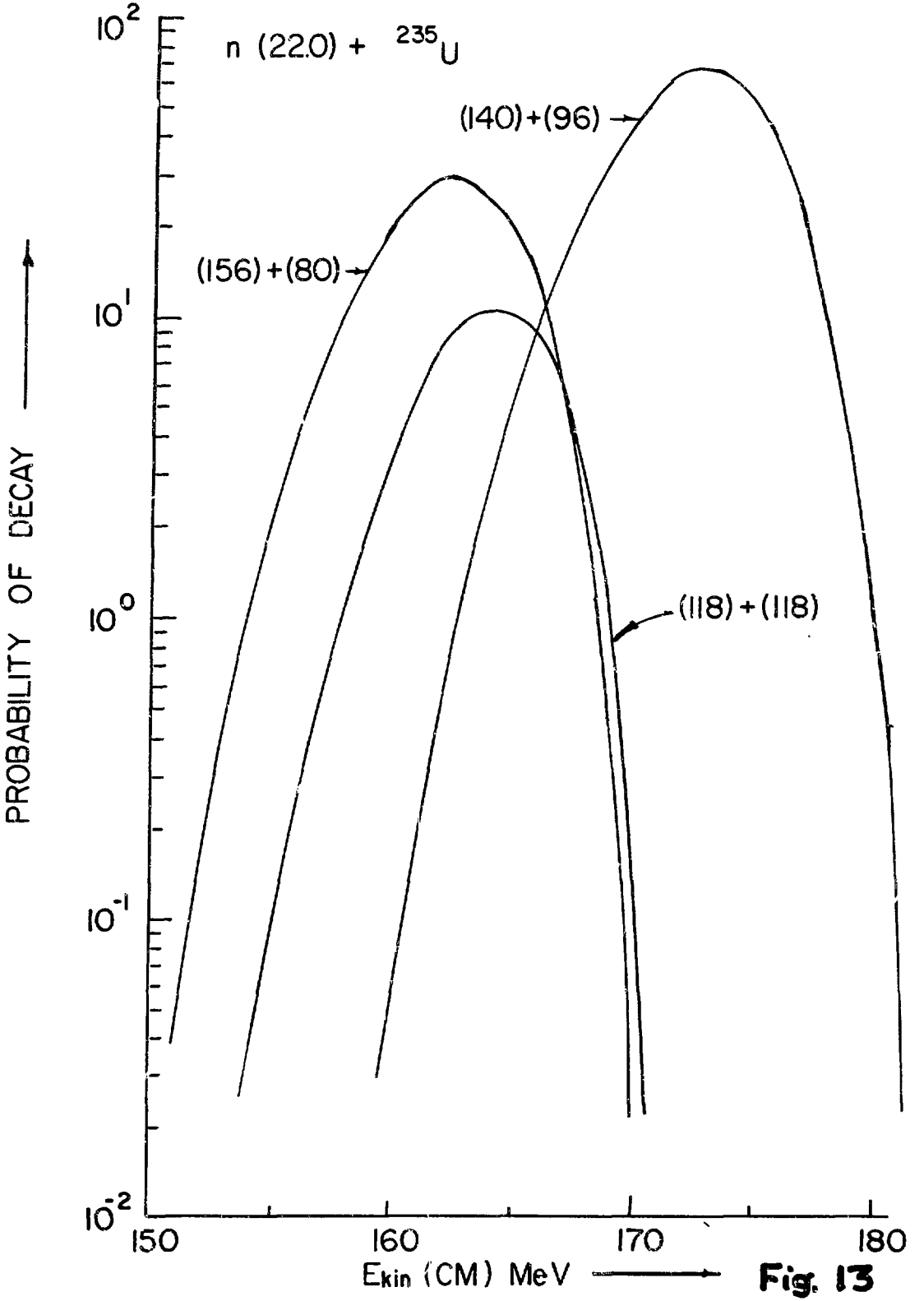
n (22.0) + ^{235}U
(140)+(96)
(156)+(80)
(118)+(118)
PROBABILITY OF DECAY
10^{2}
10^{1}
10^{0}
10^{-1}
10^{-2}
150
160
170
180
Ekin (CM) MeV

Fig. 13

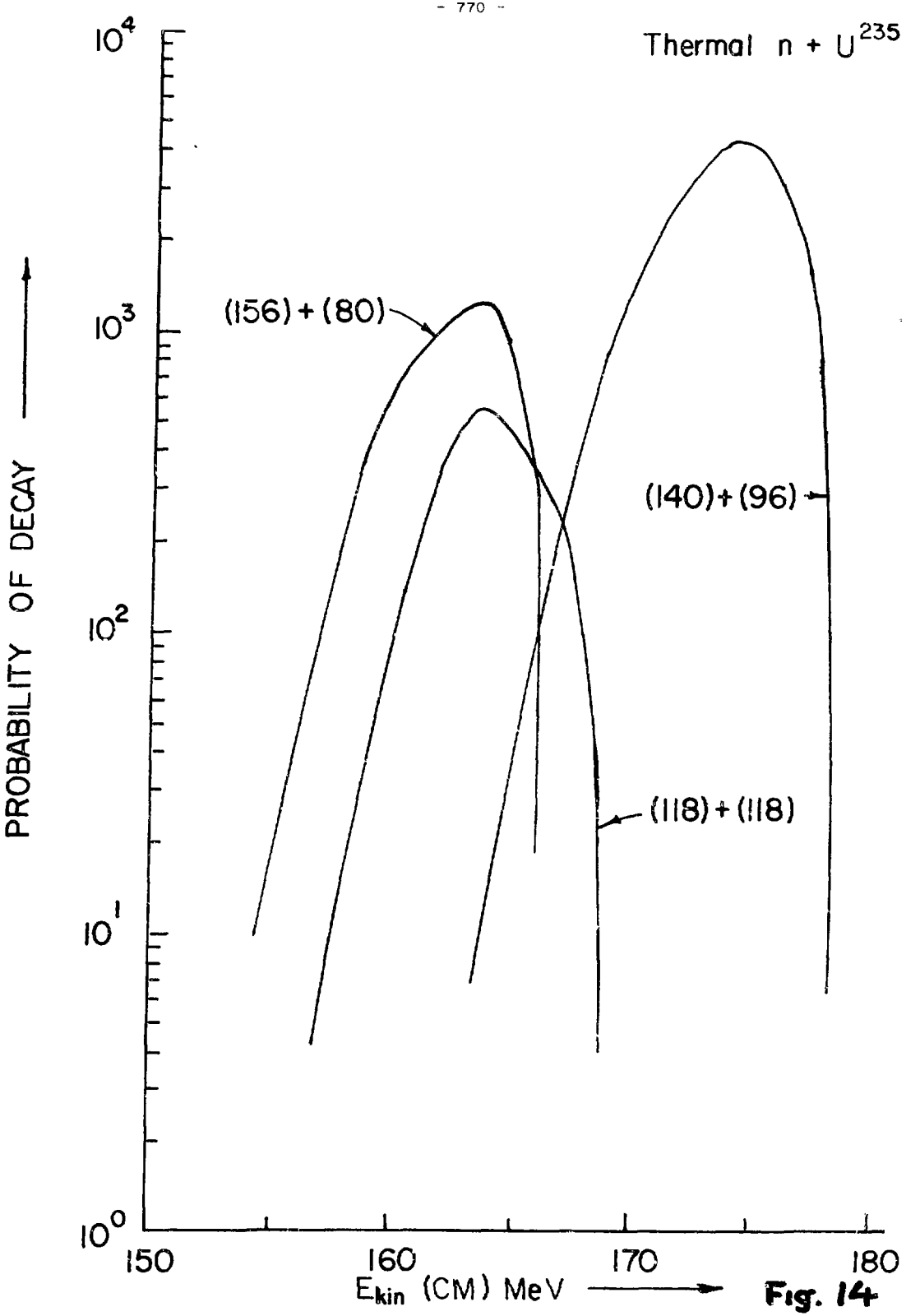
Thermal n + U235
(156) + (80)
(140) + (96)
(118) + (118)
PROBABILITY OF DECAY
10^4
10^3
10^2
10^1
10^0
150
160
170
180
Ekin (CM) MeV

Fig. 14

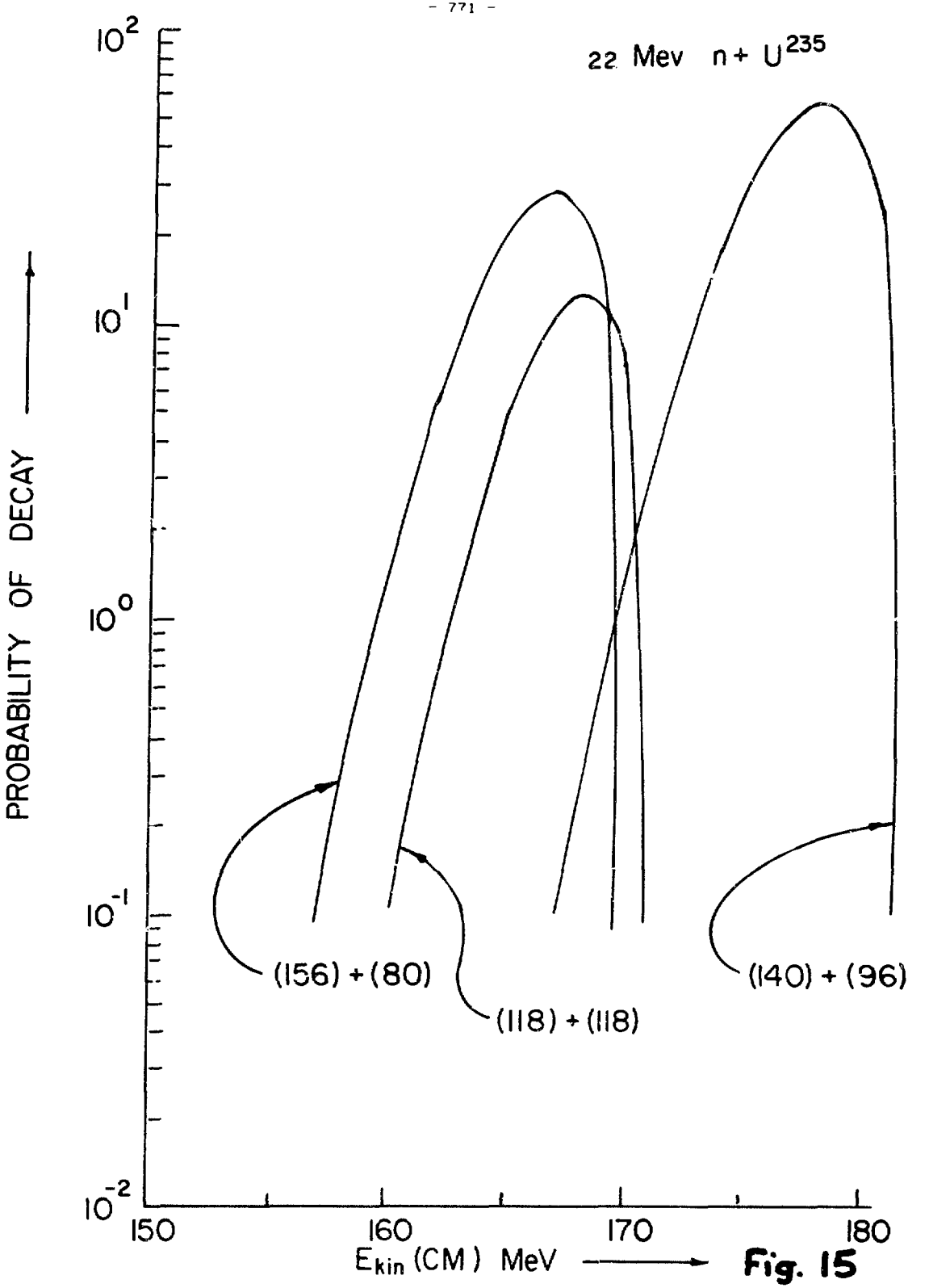
22 Mev n + U235
PROBABILITY OF DECAY
10^2
10^1
10^0
10^-1
10^-2
(156) + (80)
(118) + (118)
(140) + (96)
150
160
170
180
E kin (CM) MeV

Fig. 15

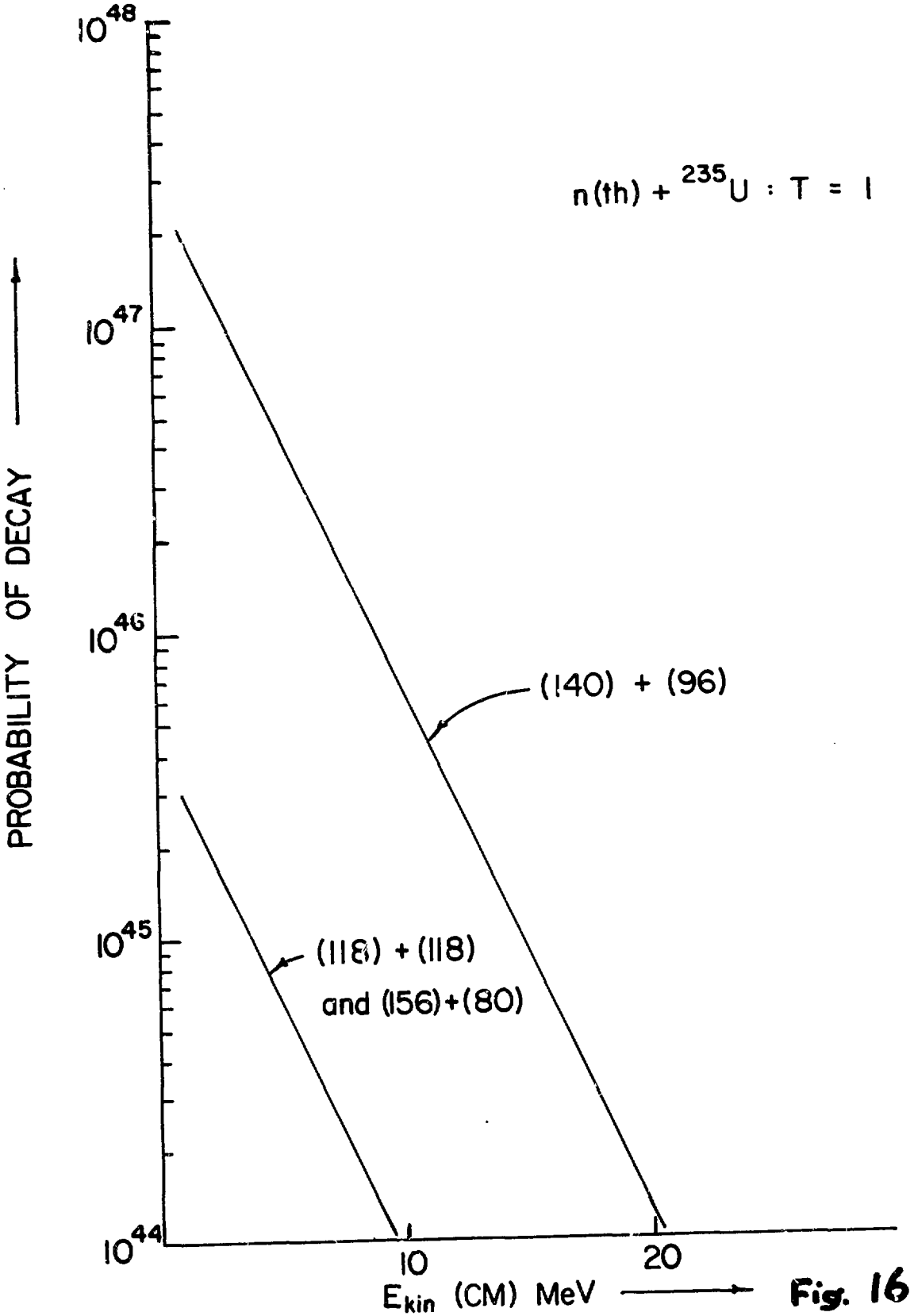
10^{48}
10^{47}
10^{46}
10^{45}
10^{44}
PROBABILITY OF DECAY
n(th) + ^{235}U : T = I
(140) + (96)
(118) + (118)
and (156)+(80)
10
20
E_{kin} (CM) MeV

Fig. 16

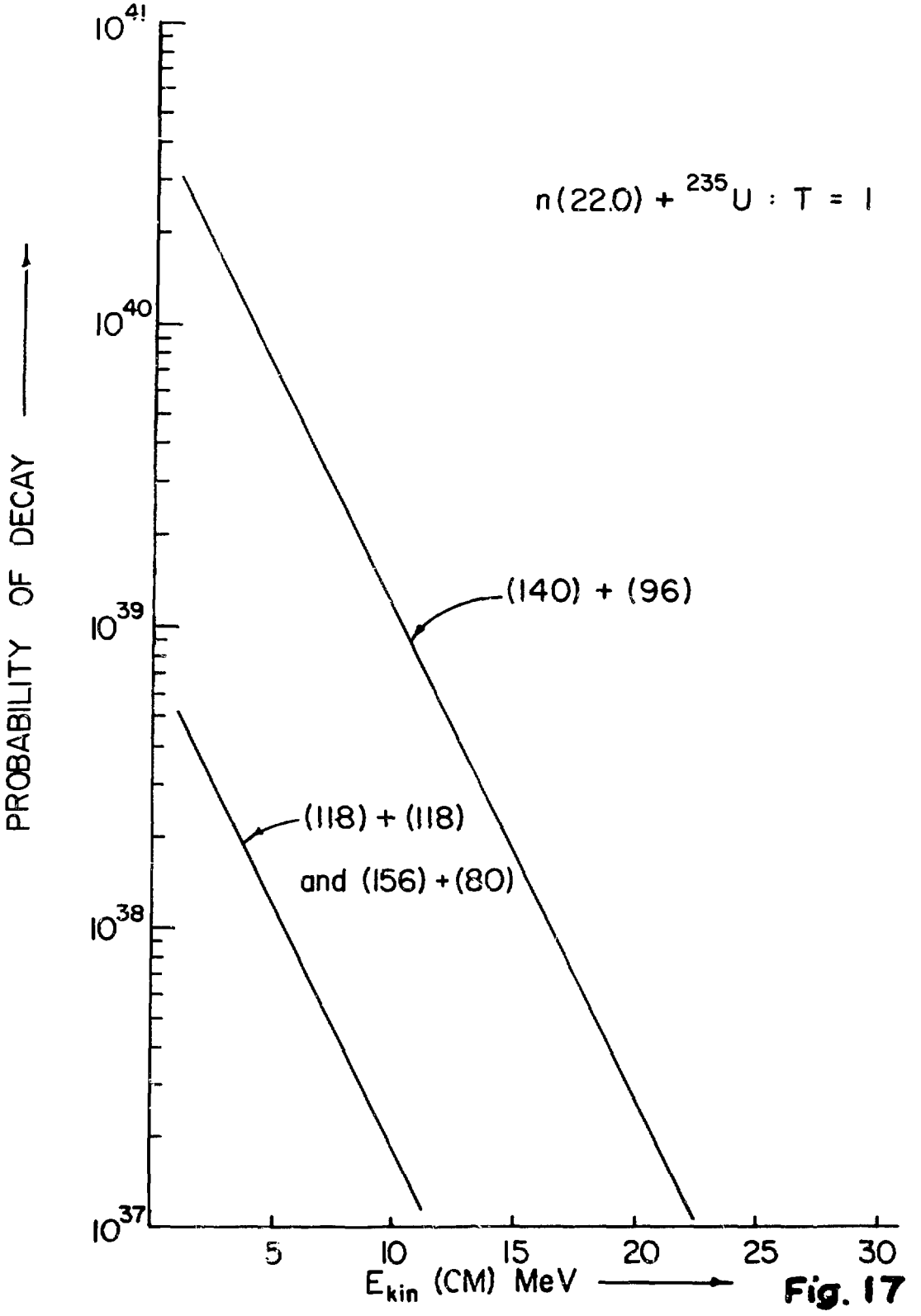
10^{41}
10^{40}
10^{39}
10^{38}
10^{37}
PROBABILITY OF DECAY
n(22.0) + ^{235}U : T = 1
(140) + (96)
(118) + (118)
and (156) + (80)
5
10
15
20
25
30
E_{kin} (CM) MeV

Fig. 17

MK 2 - NEUTRON-INDUCED FISSION OF ^{233}U, ^{235}U, and ^{239}Pu - F. Bary Malik (Indiana)

Wigner (Princeton):

I have again a very trivial question. You mentioned that the kinetic energy of the fragments in the case of the 140 to 80 distribution decreases with increasing energy of the neutrons. That was the second slide, I believe. Where does the extra energy go?

Malik:

When we calculated, and we indeed did so, we find that the excess kinetic energies are going into excitation of the fragments. We find this by integrating the phase space.

Wigner:

And it really is increasing the fragments in that energy so that it goes mostly into gamma rays or into what?

Malik:

Mostly into gamma rays. Sorry, mostly in the neutron; it's in the excitation energy of the fragments and it primarily goes into neutron. Of course it is shared by the gamma rays as well.

Wigner:

But that means that neutron energy is increasing fantastically, because there are only two neutrons --

Malik:

Right. There are only two neutrons at thermal induced fission. At other energies, it is only necessary for us to specify that it is going into internal excitation energy.

Wigner:

What is the final disposition? You see, the internal energy is not the final disposition. Finally it goes either into gamma rays or into neutrinos or into the sky, but something happens to it.

Malik:

Right. The something it is going into are both gamma rays and neutrons.

Michaudon (Bruyères-le-Châtel):

In fact, I wanted to cover this aspect in my talk [MK 1], but I didn't have time to do so. All this depends on the viscosity effects after the saddle point and to scission. You have some available energy which can go either into pre-scission kinetic energy (which, added to the Coulomb energy gives a total kinetic energy of the fission fragments), or it can go into excitation energy of the fragments. So the sharing is thereby controlled by viscosity effects. If viscosity effects are important, all of the available energy goes into excitation energy; if you have superfluid motion, as seems for instance to be the case for the low-energy fission of plutonium-240, the available energy goes into pre-scission kinetic energy. Now, the excitation energy goes mostly into the number of neutrons which are emitted.

Wigner:

The number of neutrons?

Michaudon:

The number of neutrons. There is a slight change in the temperature of the spectrum of fission neutrons which are emitted, but the gross effect is in the neutron number.

Wigner:

And it goes up to about three and a half?

Michaudon:

Oh, it goes up to three. The slope for plutonium-240 is, I think, 0.13 neutrons per MeV of excitation.

Wigner:

Tremendous number.

Michaudon:

Tremendous number, yes.

Wigner:

Have you tested this experimentally?

Michaudon:

The results are obtained experimentally. Now, if you try to understand a qualitative effect, nevertheless, you are slightly in trouble, because you cannot with a binding energy of fission fragments which is slightly too high, something like 8 MeV. But the main effect is there.

Wigner:

Thank you very much.

Kapoor (Bombay):

The observation on the variation of kinetic energy with mass at different excitation energy has also been interpreted earlier as simply a washing out of the shell effects of N = 82 shell. This may also be explained by assuming a scission barrier, as you have done. But since this would involve introduction of additional adjustable parameters, I was wondering whether there is any other way to test your hypothesis of a scission barrier.

Malik:

You are right, that the change in the yield curve was known already in 1940. But the change in the yield curve in conjunction with the asymptotic kinetic energy has been systematically studied, as far as I know, first time in Russia for neutron induced fission. There is some data now available in this country. I haven't come across any theoretical model which can explain

the change in the yield curve in conjunction with the kinetic energy and I will be quite willing to get some information on that.

Kapoor:

One of the recent papers is by Steinberg et al., where he has tried to explain these observations by a different model. I would also like to know whether you have included shell effects on level densities used in your analysis.

Malik:

Yes, Steinberg's paper does not talk about kinetic energy at all. The thing that always bothers me is that how can one talk about a decay probability if one doesn't specify the kinetic energy of the decaying fragments, because the decay probability is the surface area between the kinetic energy and the top of the barrier. So unless the kinetic energy is specified, it can decay in all possible ways and there is an infinite solution to that problem.

Michaudon (Bruyères-le-Châtel):

(Inaudible.)

Malik:

Yes, shell effect does not affect the transmission through the external barrier. It affects the properties near the saddle point.

Michaudon:

As you know, there are strong odd-even effects in the mass distribution of fission fragments and there is a strong tendency, especially in the low energy fission, to have stronger yields for even Z and even N nuclei fragments. How can you explain this with your model?

Malik:

Are you talking about odd-even effect in the yield curve, or odd-even effect in the parent?

Michaudon:

In the yield curve.

Malik:

We can reproduce the yield curve for the odd masses also. We haven't analyzed, on the other hand, the other thing, the decay due to the odd parent nucleus.

).00 a.m., Friday, July 9, 1976 Special Contributed Paper: MK 3

DOUBLY RADIATIVE NEUTRON CAPTURE IN H_2 AND D_2

E.D. Earle, A.B. McDonald, M.A. Lone, H.C. Lee and F.C. Khanna

Chalk River Nuclear Laboratories, A.E.C.L., Chalk River, Ontario, Canada K0J 1J0

RÉSUMÉ

Cross sections for double photon emission following thermal neutron capture in and D_2 and the $^{16}O(n,\gamma)^{17}O$ cross section and branching ratios were measured. The lues are $H_2(\sigma_{2\gamma} = -3 \pm 8$ μb) for 600 keV < E_γ < 1620 keV, $D_2(\sigma_{2\gamma} = 8 \pm 15$ μb) for 0 keV < E_γ < 5500 keV, $^{16}O(\sigma_{n\gamma} = 202 \pm 27$ μb) and (82 ± 3)% for the branching ratio to e 3055 keV level of ^{17}O.

ABSTRACT

The $(n,\gamma\gamma)$ reactions on H_2 and D_2 provide tests (not dominated by the uncer-inties in nuclear structure) of the current theories of the electromagnetic inter-tion of the nucleons. From measurements[1] with two GeLi detectors shielded from ich other (see insert, fig. 1) we obtain $\sigma_{2\gamma} = -3 \pm 8$ μb for the $H(n,\gamma\gamma)D$ reaction or the γ-ray energy range 600 keV < E_γ < 1620 keV. The residual contribution from ie cross registration of the 2.223 MeV γ-rays due to multiple Compton scattering id positron annihilation in flight was calculated[1,2] and subtracted from the bserved yield at 2.223 MeV. This measured limit is larger than the conventional redictions[3] of $\sigma_{2\gamma} = 0.08$ μb, but is smaller than the prediction[3] of 13 μb btained by assuming maximal non-orthogonality of the ^3S np state and the deuteron round state. These $\sigma_{2\gamma}$ have been normalised for the region 600 < E_γ < 1620 keV.

We also measured $\sigma_{2\gamma} = 8 \pm 15$ μb for the $D(n,\gamma\gamma)T$ reaction for the γ-ray energy ange 700 keV < E_γ < 5550 keV. The cross section for $D(n,\gamma\gamma)T$ is expected to be arger than that for $H(n,\gamma\gamma)D$. Detailed calculations are in progress. The double hoton cross sections for H_2O and D_2O were measured relative to the cross section 156 ± 16 μb) of the sum peak from the 870.89 and the 1087.88 keV cascade in ^{17}O as hown in fig. 1. The cross section for this cascade is an average of our results measured relative to the known $D(n,\gamma)T$ cross section of 521 μb) and the results of urney and Motz[4].

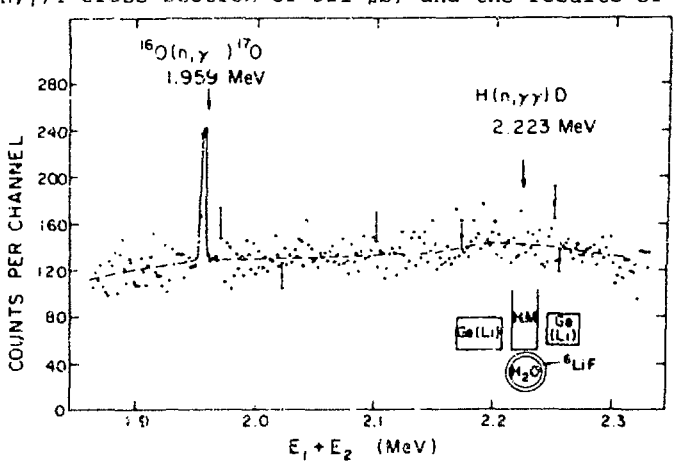

Fig. 1. Sum spectrum with 600 keV < $E_{1,2}$ < 1620 keV

) E.D. Earle, A.B. McDonald, O. Hausser and M.A. Lone, nys. Rev. Letts. 35(1975)908 and o be published.

) H.C. Lee and E.D. Earle, Nucl. Inst. & Meth. 131(1975)199.

) D.P. Grechukhin, Sov. J. Nucl. Phys. 14(1972)62; J. Blomqvist nd T.E. Ericson, Phys. Letters, 7B(1975)117; H. Hyuga and M. ari, Phys. Letters 57B(1975)330; .C. Lee and F.C. Khanna, Phys. etters B, to be published.

) E.T. Jurney and H.T. Motz, ANL-6797, page 236.

DOUBLY RADIATIVE NEUTRON CAPTURE

E.D. Earle, A.B. McDonald, M.A. Lone, H.C. Lee and F.C. Khanna*

Atomic Energy of Canada Limited, Chalk River Nuclear Laboratories,

Chalk River, Ontario, Canada K0J 1J0

* *Speaker*

RÉSUMÉ

Cross-sections for doubly radiative thermal-neutron capture on ^{1}H, ^{2}H, ^{3}He, ^{16}O and ^{208}Pb are calculated to be 118, 26, 1200, 48 and 53 nb. Measured upper limits for this cross-section are -3 ± 8 μb for ^{1}H, 8 ± 15 μb for ^{2}H and 3 ± 19 μb for ^{16}O.

1. INTRODUCTION

Neutron capture in nuclei with the emission of a single photon has been a very important tool for studying the structure of nuclei. It has provided useful information about the gamma-ray strength function[1] and hence details of the tail region of the giant dipole resonance. In this talk we would like to present an interesting companion study - doubly radiative capture, which should provide further understanding of the electromagnetic interactions in the nucleus.

The two photon process[2] has been studied in $0^+ \rightarrow 0^+$ transitions in the nuclei ^{16}O, ^{40}Ca and ^{90}Zr. However extraction[3] of useful information has been difficult since excited 0^+ states have very complicated structures. We shall show that in certain cases the two photon process in thermal neutron capture can be calculated more accurately.

We shall here present some recent advances in the study of doubly radiative capture, first outlining the theory and then summarising the experimental results that we have obtained to date.

2. THEORY

The cross-section for doubly radiative capture is (ignoring recoil of the target)

$$\sigma_{2\gamma} = \frac{1}{2v_n} \frac{(2J_i+1)}{2(2J+1)} \int \frac{d^3\omega_1}{(2\pi)^3} \frac{d^3\omega_2}{(2\pi)^3} \frac{d^3p}{(2\pi)^3} (2\pi)^4 \delta(\vec{\omega}_1 + \vec{\omega}_2 + \vec{p} - \vec{k}) \delta(\omega_1 + \omega_2 - \omega) \sum' |M_{2\gamma}|^2$$

where the factor 1/2 normalises the two photon final state; $J_i(J)$ is the spin of the initial state of the total system (target nucleus): $(2J_i+1)/(2(2J+1))$ is the statistical weight factor; $v_n^{-1} = 1.37 \times 10^5$ is the inverse velocity for thermal neutrons; Σ' sums over the polarisation of the photon and magnetic substates of the final state and averages over those of the angular-momentum-coupled initial state; ω_1, ω_2 are the energies of the two photons; $\omega = \omega_1 + \omega_2$; $\vec{k}(\vec{p})$ is the momentum of the initial neutron (residual nucleus); and $M_{2\gamma}$ is the two photon matrix element. We use units $\hbar = c = 1$. The two photon matrix element is

$$M_{2\gamma} = \sum_{\alpha}' \left[\frac{\langle \psi_f | O(\omega_2) | \alpha \rangle \langle \alpha | O(\omega_1) | \psi_i \rangle}{E_\alpha - E_i} + (\omega_1 \leftrightarrow \omega_2) \right]$$

where $\psi_i(\psi_f)$ is the initial (final) state wavefunction. It has been shown[4] that only the electric dipole (E1) transitions are important. The transition operator is

$$O(\omega) = e\sqrt{\frac{2\pi}{\omega}}\,\vec{\varepsilon}\cdot\vec{r}$$

where $\vec{\varepsilon}$ is the polarisation vector of the photon.

There are three different mechanisms that can contribute to $M_{2\gamma}$.

i) Single-particle direct capture. This is analogous to the direct capture process[5] for one photon emission. The target nucleus is treated as an inert elementary particle. The initial wavefunction is taken to be the s-state scattering wavefunction ($s_{1/2}$) of the thermal neutron which has an asymptotic form (1 - a/r), where a is the neutron scattering length. The intermediate states are taken to be single-particle plane waves. The final wavefunctions are bound s-waves ($s_{1/2}$) in ^{2}H, ^{3}H and ^{4}He and bound d-waves ($d_{5/2}$) in ^{17}O (ground state) and ^{209}Pb (at an excitation of 1.58 MeV). Calculated $\sigma_{2\gamma}$'s are given in Table 1 (in the column labelled single-particle). The result for nH capture is reliable to ∿1%[4]. The uncertainty in all other cases is ∿20%. In n-^{2}H, three body effects increase[6] $\sigma_{2\gamma}$ to 26 nb.

ii) Capture through core excited states. In the case of ^{16}O and ^{208}Pb two processes due to collective excitations of the target could be important. In the first process the intermediate states are the two $3/2^-$ states formed by coupling the giant dipole state (1^-) of the target to $s_{1/2}$ and $d_{5/2}$ respectively. The second process is due to the initial ($1/2^+$) and the final ($5/2^+$) states having components $|(1^- \otimes 1^-)2^+\, d_{5/2};1/2^+\rangle$ and $|(1^- \otimes 1^-)2^+\, s_{1/2};5/2^+\rangle$ respectively. It is found[6] that in the schematic model the matrix element of the second process is twice that of the first process. If these contributions are added coherently to that of the direct capture $\sigma_{2\gamma}$ is increased to 48 and 53 nb for ^{16}O and ^{208}Pb respectively.

iii) Resonance capture. For neutron capture in ^{2}H, ^{16}O, ^{208}Pb there are no resonances at or near thermal energies. The singlet ($^1S_0$) n-^{1}H resonance does not contribute to the cross section for ^{1}H(n,γγ)^{2}H because the electric dipole operator cannot alter the spin wavefunction. In the case of ^{3}He(n,γγ)^{4}He, a broad p-^{3}H resonance underlies the neutron threshold. Consequently the (n,p) cross section is very large (5327 b). This resonance requires the neutron scattering length[7], determined by elastic and inelastic scattering data, to be complex. In calculating $\sigma_{2\gamma}$ the effect of this resonance is included by using the complex scattering length. This results in a large value (1180 nb) for $\sigma_{2\gamma}$, most (1150 nb) of which is due to the resonance.

The final result for all cases is given in column 7 of Table 1. The experimental values for ^{1}H($600 < E_\gamma < 1620$ keV), ^{2}H($700 < E_\gamma < 5557$ keV) and ^{16}O ($1200 < E_\gamma < 2943$ keV) are given in the last column. From the predicted energy spectra shown in Fig. 1, the integrated cross sections for the restricted energy ranges given above are 64, 94 and 53% of the total calculated $\sigma_{2\gamma}$ for ^{1}H, ^{2}H and ^{16}O respectively.

3. EXPERIMENT

The measurements[6,11] of two photon cross sections for ^{1}H, ^{2}H and ^{16}O were performed with 0.009 eV neutrons (∿4 × 10^5 neutrons $s^{-1}cm^{-2}$) obtained by Bragg reflecting a beam of neutrons from the NRU thermal column with a pyrolytic graphite monochromator. The target and detector geometry is shown in the insert in Fig. 2. For the ^{1}H measurement an H_2O target was used. For ^{2}H and ^{16}O measurements a 99.76%

isotopically enriched D_2O target was used. Targets were 50 cm^3 contained in 0.1 mm thick polyethylene bag. Because of the large ratio of scattering to capture cross sections the neutrons were effectively thermalized before capturing.

The detector geometry and the 4.9 cm thick heavy metal (90% W, ρ = 16.7 g/cm) shield were designed to reduce the probability of detecting coincidence events due to gamma-ray scattering between the detectors. The entire target-detector assembly was surrounded by 10 cm of Pb and the neutron beam-tube was constantly flushed with ^4He gas in order to reduce the background from capture in ^{14}N.

Spectra of the summed linear signals from the two detectors, gated by a fast coincidence requirement, were obtained on line with a modular electronic system (^1H measurement) or off line by playback of three parameter data accumulated by a PDP-5 computer. Energy resolution of ∿4 keV FWHM (at 2 MeV in the sum spectrum) and time resolution of 6 ns FWHM were obtained.

The detector efficiencies as a function of energy were determined from the known[12] relative intensities of gamma rays from neutron capture in ^{14}N, ^{12}C and ^7Li. The absolute coincidence efficiencies were determined from the peaks in the sum spectrum due to the well known cascade[6,13] in ^{17}O.

Figure 2 shows a portion of the sum spectrum collected in 600 hours of data accumulation with the H_2O target. This spectrum is composed of events in which the energies observed in the two detectors, E_A and E_B, are greater than 600 keV. Therefore the majority of the cross registration due to pair production and Compton scattering is gated out. For E_γ > 600 keV, cross registration is due to multiple Compton scattering and positron annihilation in flight and is well described by Monte Carlo calculations[14]. For this spectrum, the residual contribution with the heavy metal in place was calculated to be 19 ± 4 counts. The peak at 1959 keV is due to coincidences between 871 and 1088 cascade[6,13] gamma-rays in ^{17}O (σ = 156 ± 16 μb) and was used for normalisation. For an 8 keV region at 2223 keV in this spectrum, the net yield was 11 ± 25 counts. After subtraction of the cross registration contribution, we obtain an upper limit of $\sigma_{2\gamma}$ = -3 ± 8 μb for 600 keV < E_A, E_B < 1620 keV, corresponding to $\sigma_{2\gamma}/\sigma_{1\gamma} = (-0.8 \pm 2.5) \times 10^{-5}$. About 60% of the background in the region of 2223 keV arises from random summing of the Compton tails of two 2223 keV gamma-rays. Unless major improvements are made in time resolution or peak to Compton ratio for the Ge(Li) detectors, this will also constitute a major limitation to future experimental sensitivity. This problem and the problem of cross registration are much less severe in the case of ^2H and ^{16}O because the $\sigma_{1\gamma}$ are lower by a factor of more than 600.

Figure 3 shows the sum spectrum obtained with the D_2O target with the restriction that E_A and E_B > 700 keV. Here the background is due to capture in materials other than D_2O, such as F, N and Ge. From a 14 keV wide region at 6257 keV we obtain an upper limit of $\sigma_{2\gamma}$ = 8 ± 15 μb for $^2H(n,\gamma\gamma)^3H$ in the energy range 700 < E_A,E_B < 5557 keV.

The sum spectrum shown in Fig. 4 was used to obtain a limit of $\sigma_{2\gamma}$ = 3 ± 19 μb for $^{16}O(n,\gamma\gamma)^{17}O$ for the energy range 1200 < E_A,E_B < 2943 keV. The somewhat higher energy limit of 1200 keV in this case was chosen partly to reduce the background at 4143 keV in the sum spectra and also to eliminate the contribution from the 871 + 3272 keV cascade. Triple coincidences from the 871 + 1088 + 2184 keV cascade are negligible in the present measurement and could be excluded completely by not including a small region near 2184 keV in each detector.

4. SUMMARY

Most of the theoretical[4] and experimental[11,15] work in doubly radiative capture has been concentrated on the $^1H(n,\gamma\gamma)^2H$ reaction. The second last column in Table 1 indicates that in the four other cases considered $\sigma_{2\gamma}/\sigma_{1\gamma}$ is expected to be much larger than that for nH capture. The small values of $\sigma_{2\gamma}$ will still present a major experimental problem, but the large two photon branching ratios will reduce a substantial source of difficulty apparent in the $^1H(n,\gamma\gamma)^2H$ measurement. The predicted branching ratio and the absolute $\sigma_{2\gamma}$ are by far the largest in n-^{3}He, making this case appear very attractive. However the competing (n,p) cross-section (5327 b) will present severe problems. The branching ratios in n-^{16}O and n-^{208}Pb are smaller but still almost three orders of magnitude greater than that for nH capture. In both cases, backgrounds due to cascading γ-rays following (n,γ) capture are not expected to pose serious problems provided that energy windows for the two-photon spectra are judiciously chosen.

The present upper limits on $\sigma_{2\gamma}$ are much larger than the calculated values presented in Table 1. Improvements in sensitivity are possible, particularly for ^2H *and* ^{16}O, *by increasing the neutron flux and reducing the background from* (n,γ) *reactions* in materials other than the target. Work to achieve both improvements is in progress.

REFERENCES

1. G.A. Bartholomew, E.D. Earle, A.J. Ferguson, J.W. Knowles and M.A. Lone, Advances in Nuclear Physics, M. Baranger and E. Vogt, Eds., 7(1973)239.
2. B.A. Watson, T.T. Bardin, J.A. Becker and T.R. Fisher, Phys. Rev. Lett. 35(1975) 1333 and references therein.
3. D.P. Grechukhin, Nucl. Phys. 62(1965)273; G.F. Bertsch, Part. & Nucl. 4(1972)237.
4. H.C. Lee and F.C. Khanna, Phys. Lett. 61B(1976)216 and to be published in Phys. Rev. C; J. Blomqvist and T.E.O. Ericson, Phys. Lett. 61B(1976)219 and references cited therein.
5. J.E. Lynn, "The Theory of Neutron Resonance Reactions", (Oxford, 1968).
6. A.B. McDonald, E.D. Earle, M.A. Lone, H.C. Lee and F.C. Khanna; and H.C. Lee, F.C. Khanna, M.A. Lone and A.B. McDonald, to be published.
7. V.F. Sears and F.C. Khanna, Phys. Lett. 56B(1975)1.
8. Y.E. Kim and A. Tubis, Ann. Rev. Nucl. Sc. 24(1974)69.
9. S.F. Mughabghab and D.I. Garber, "Neutron Cross Sections, Vol. 1, Resonance Parameters", BNL-325, 3rd Ed. (USAEC 1973); S. Fiarman and S.S. Hanna, Nucl. Phys. A251(1975)1.
10. D.J. Hughes and R.B. Schwartz, "Neutron Cross Sections", BNL-325, 2nd Ed. (USAEC 1958).
11. E.D. Earle, A.B. McDonald, O. Häusser and M.A. Lone, Phys. Rev. Letts. 35(1975) 908; E.D. Earle, A.B. McDonald and M.A. Lone, to be published.
12. P. Spilling, H. Gruppelaar, H.F. De Vries and A.M.J. Spits, Nucl. Phys. A113 (1968)395; D. Bellman, Atomkernenergie 17(1971)145; E.T. Jurney, quoted in F. Ajzenberg-Selove and T. Lauritsen, Nucl. Phys. A227(1974)1.
13. E.T. Jurney and H.T. Motz, Proc. of Int. Conf. on Nuclear Reactions with Reactor Neutrons, Ed. F.E. Throw, ANL-6797 (1963)236.
14. H.C. Lee and E.D. Earle, Nucl. Instr. and Meth. 131(1975)199.
15. R.G. Arnold, B.E. Chertok, I.G. Schröder and J.L. Alberi, Phys. Rev. C, (1973) 1179; W.B. Dress, C. Guet, P. Perrin and P.D. Miller, Phys. Rev. Lett. 34(1975) 752; N. Wüst, H.H. Güven, B. Kardon and H. Seyfarth, Z. Phys. A274(1975)349.

TABLE I. RESULTS FOR $\sigma_{2\gamma}$

Initial Nucleus	ℓ	a (fm)	ω (MeV)	$\sigma_{1\gamma}$ [d] μb	$\sigma_{2\gamma}$ (μb) single-particle	$\sigma_{2\gamma}$ (μb) Total [e]	$\sigma_{2\gamma}/\sigma_{1\gamma}$	Expt. $\sigma_{2\gamma}$ (μb)
^{1}H	0	5.41	2.22	3.32×10^{5}	0.118	0.118	3.6×10^{-7}	-3 ± 8
^{2}H	0	0.65 [a]	6.14	521 ± 9	0.021	0.026	4.9×10^{-5}	8 ± 15
^{3}He	0	6.1-i4.4 [b]	20.6	60 ± 30	0.030	1.180	3×10^{-2}	
^{16}O	2	5.81 [c]	4.14	190 ± 18 [f]	0.041	0.048	2.7×10^{-4}	31 ± 19
^{208}Pb	2	9.52 [c]	2.36	487 ± 30	0.050	0.053	1.1×10^{-4}	

a) ref. 8; b) ref. 7; c) ref. 9; d) ref. 10;

e) single-particle and collective amplitudes are added coherently; f) refs. 6, 13.

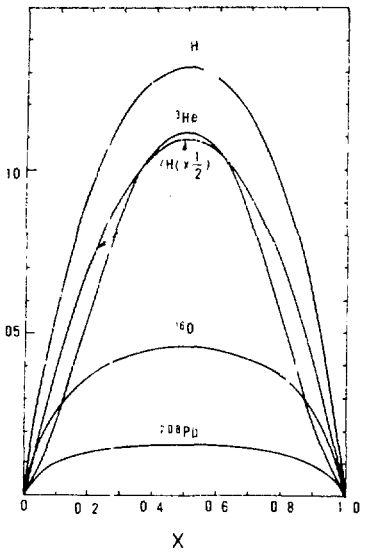

Fig. 1. Calculated energy spectra; x = E_A/E where E_A is the energy of one of the photons and E is the total energy of the two photons.

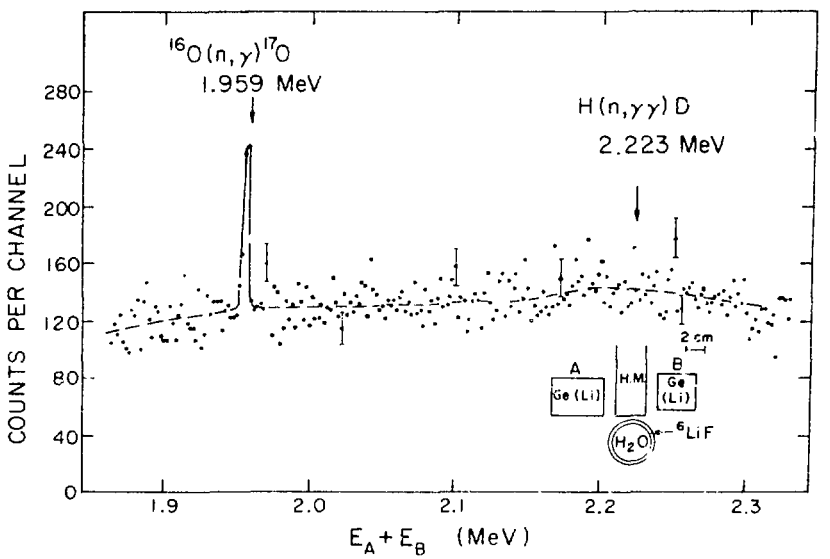

Fig. 2. Spectrum of coincidences summing to an energy $E_A + E_B$, obtained with the H_2O target for a total accumulation time of 600 hours. The inset shows the geometry used in the experiments.

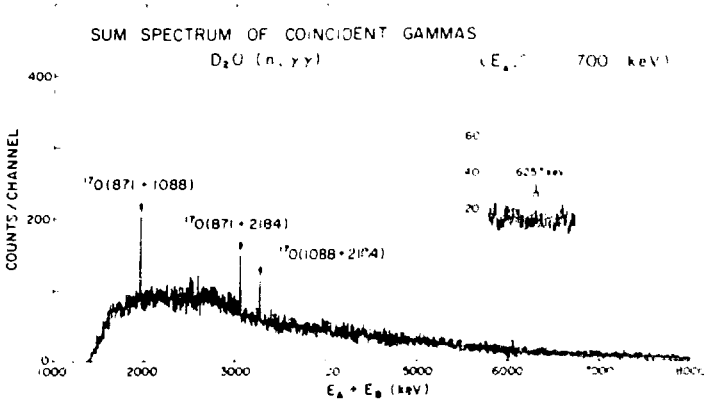

Fig. 3. Sum spectrum obtained with the D_2O target for a total accumulation time of 300 hours. The energies of the γ-rays in detectors A,B have been restricted to the range 700 keV < E_A, E_B. The peaks arise from cascade gamma-rays from the $^{16}O(n,\gamma)^{17}O$ reaction. The insert indicates the region summed to determine $\sigma_{2\gamma}$ for deuterium.

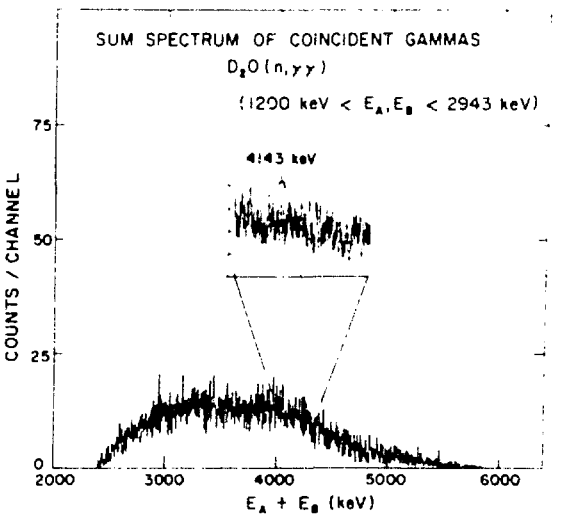

Fig. 4. Sum spectrum obtained as in fig. 3 but with 1200 < E_A, E_B < 2943. The insert indicates the region summed to determine $\sigma_{2\gamma}$ for oxygen.

MK 3 - DOUBLY RADIATIVE NEUTRON CAPTURE IN H_2 AND D_2 - E. D. Earle, A. B. McDonald, M. A. Lone, H. C. Lee and F. C. Khanna (A.E.C.L.-Chalk River, Canada)

Seyfarth (Jülich, Germany):

Perhaps one should mention that we have measured the double radiative capture in hydrogen-2 and that we have a bit of additional information. It wasn't only the sum peak that we measured - in fact, what we really measured was the matrix element between the two single-event peaks, and that means that we measured the differential cross section. We didn't find any significant deviation from the background. Our value for the ratio double radiative decay/single radiative decay is about a factor of 6 higher, but one should remark that our energy region was greater by a factor of 2, i.e., we measured from 40 keV up to about 2.15 MeV.

Khanna:

I am sorry that I did not mention all the people who have done previous work on this doubly radiative capture problem. But you will find them referred to in my talk.

10:45 A.M., FRIDAY, JULY 9, 1976, IN OLNEY 150

MAIN SESSION ML

Chair: P.K. Iyengar (Bhabha Atomic Research Centre, Trombay, Bombay, India)

10.45 a.m., Friday, July 9, 1976 *Invited Paper: Session ML 1*

NEUTRONS AND FUSION

Charles W. Maynard

Nuclear Engineering Department, The University of Wisconsin, Madison, USA

RÉSUMÉ

The D-T fusion process yields 14-MeV neutrons numbering four times as many as those produced in an equivalent fission reactor and carrying seven times the energy of the fission neutrons. A review is undertaken of the associated problems: details of the energy deposition processes and of reactions needed to provide additional tritium are outlined, damage considerations are presented, and a report is given on the status and prospects of data for fusion studies.

ABSTRACT

The production of energy from fusion reactions does not require neutrons in the fundamental sense that they are required in a fission reactor. Nevertheless, the dominant fusion reaction, that between deuterium and tritium, yields a 14 MeV neutron. To contrast a fusion reactor based on this reaction with the fission case, we note there will be 3×10^{20} such neutrons produced per gigawatt of power. This is four times as many neutrons as in an equivalent fission reactor and they carry seven times the energy of the fission neutrons. Thus, they dominate the energy recovery problem and create technological problems comparable to the original plasma confinement problem as far as a practical power producing device is concerned. Further contrasts of the fusion and fission cases are presented to establish the general role of neutrons in fusion devices.

Details of the energy deposition processes are discussed and those reactions necessary for producing additional tritium are outlined. The relatively high energy flux with its large intensity will activate almost any materials of which the reactor may be composed. This activation is examined from the point of view of decay heat, radiological safety, and long-term storage. In addition, a discussion of the deleterious effects of neutron interactions on materials is given in some detail; this includes the helium and hydrogen producing reactions and displacement rate of the lattice atoms. The various materials that have been proposed for structural purposes, for breeding, reflecting, and moderating neutrons, and for radiation shielding are reviewed from the nuclear standpoint. The specific reactions of interest are taken up for various materials and finally a report is given on the status and prospects of data for fusion studies.

Neutrons and Fusion

Charles W. Maynard

Nuclear Engineering Department
University of Wisconsin

Introduction

The use of fusion reactions as a source of energy is a concept currently mentioned in popular media with great regularity and with a general vagueness that indicates how little the general public is aware of how the concept might be implemented. Those within the technical community are likely to have a view of fusion reactors based primarily on the confinement problems which have dominated the field since its beginning. Solutions to the problem of confining the fusing nuclei at the required temperatures vary greatly in size, appearance, and physical basis. However, the fuel cycle is almost always based on the D-T reaction in devices proposed for near term construction. This results simply from the lower confinement requirements and leads to many consequences that are common to a wide range of these devices.

The D-T reaction results in a direct energy release of 17.6 MeV with 14.1 MeV appearing as kinetic energy of the product neutron. This neutron will undergo further reactions which generally yield a net addition to the energy production such that around 20 MeV results per D-T reaction. This can be contrasted with a fission reaction which produces approximately 200 MeV, including about 2.5 neutrons with an average energy per neutron of 2 MeV. Thus, for the same power, there are 4 times as many neutrons produced in a fusion as in a fission reactor. In addition, they carry seven times the energy per neutron. Thus the neutron flux in a fusion reactor is very intense and the spectrum very hard.

This gives rise to a variety of nuclear effects which are in many respects as diverse and intricate as those found in a fission reactor. However, the important behavior is quite different; for there is no eigenvalue problem for neutron multiplication. Further, no single problem dominates the subject like the neutron multiplication problem of fission reactors. Instead, a number of different, but more or less equally important, responses of the system to the neutron flux occur.

The energetic 14 MeV neutrons from the $D(T,n)\alpha$ reaction produce a highly anisotropic angular flux, at the first material wall, which requires a high order transport approximation for its accurate determination. Much new data in

an energy range not previously of great importance is required for this as well as for the system responses. These responses strongly affect the economics of the systems.

Blanket and Shield Functions and Responses

As noted above the various fusion reactor concepts vary in many respects, but all form an intense neutron source in a region generally transparent to the neutrons. This results in an intense high energy flux which must be utilized and attenuated. The first zone surrounding the fusion zone is referred to as the blanket and is followed by a zone called the shield. The functions performed by the blanket are to breed tritium, convert the kinetic energy of the 14 MeV source neutrons into heat, transfer the heat to the external thermal cycle, and provide a vacuum chamber for the fusion zone. A schematic of a representative blanket and shield for a magnetic confinement reactor is given in Figure 1.

The requirement of tritium breeding arises since its instability precludes it from occurring naturally in significant quantities. The only effective reactions for this purpose are the neutron reactions in Li^6 and Li^7. The possibility of producing as much or more tritium that D-T fusion reactions consume is based on capturing most fusion neutrons in Li^6 and loosing very few fusion neutrons to parasitic capture, the production of tritium during inelastic scattering from Li^7, and the multiplication of fusion neutrons by (n,2n) reactions in some materials. The response function required here is simply the sum of the tritium production cross sections of Li^6 and Li^7 weighted by their respective number densities. The actual response can be influenced directly by the lithium density through changes in the lithium bearing materials and the fractional content of structure and other constituents of the breeding zone and by intentionally changing the isotopic composition of the lithium. Indirectly, the response is influenced by wall, structure and other composition influences on the spectral and spatial flux dependence. The feasibility of fusion power is clearly dependent on the possibility of tritium production exceeding its consumption; however, inventory considerations indicate that the ratio of production to consumption (i.e., the breeding ratio) need only slightly exceed unity.

In Figure 1, a first wall is shown which must withstand the most extreme environment in the system since it is exposed to intense radiation of all kinds and must operate at the highest temperatures possible for the sake of system thermal efficiency. A set of performance indices determined by nuclear properties are required for radiation damage analysis. This is most severe in the first wall. While ideally, one would relate the radiation fluxes to the specific material property effects, the phenomena involved are too complex to allow such a direct approach. Instead, one can only determine transmutation and initial displacement rates in the material. Composition changes, due to hydrogen and helium production, can cause deleterious property changes which limit the time during which acceptable material performance can be assured. The transmutation products may influence materials properties, but they may also be radioactive and thus create a new set of problems. For these reasons, cross sections for the various reactions form a set of response functions of great importance. A

slightly different case is the displacement of atoms from their positions in the crystal lattice of the material. The damage due to displacements is complex since many displacements are offset by recombination of the vacant lattice sites with displaced atoms. The degree of recovery and the interaction of vacant sites and displaced atoms with one another and with other lattice imperfections depends on temperature and imperfection densities and is a major study area. The above quantities serve as input to these studies. However, even the initial displacement rate is a complex topic which depends on lattice properties as well as nuclear cross sections. Thus, a desirable response function, the displacement cross section, which gives the displacement rate when multiplied by the flux and integrated, must be based on a model of the displacement process and the various nuclear cross sections. This response function is important enough that it is determined by processing cross sections weighted by primary knock on recoil energies and a model predicting the number of displaced atoms per unit energy of the primary nucleus.

Most of the energy produced is carried by the neutrons. To determine the spatial distribution and the exact total amount of energy produced, neutron energy deposition cross sections known as kerma factors must be available. The energy deposition depends on the reaction Q values as well as the cross sections. Closely related to the kerma factors, the gamma production cross sections complete the energy balance for the reactions and provide the source for gamma transport calculations. Thus, while gamma production is not directly a response function of interest, it is related to energy deposition both through reaction energy conservation and through the eventual energy deposition by the gamma photons.

The shielding effectiveness is measured by energy attenuation. This is not a reaction rate and is not even a volumetric effect. While it is related to all reactions taking place. its determination by subtracting incident energy absorbed from the incident energy would be an awkward procedure. The energy weighted current can be used to determine the attenuation achieved, but the high energy total cross section is the data which most readily indicates the approximate attenuation rate. In any case, the energy leakage represents an important response of the blanket and shield since it measures the energy load to the magnets and thus to the cryogenic refrigerators.

The system responses discussed to this point are required in the technical analysis of reactor performance. Energy production is included above, where the emphasis is on the determination of the energy deposited. However, from an economic point of view, a comparative study of alternative materials and their relative energy production may strongly influence design decisions. Thus, while energy production is not a separate response function, this discussion is introduced to emphasize that a different set of calculations may be important when optimizing the performance than in simply analyzing a particular system.

Materials and Reactions of Interest

The nature of the problem of nuclear analysis of fusion systems is basically like many radiation shielding problems, but with a greater need to know the detailed reaction rates in the zones close to the source than is usual. The blanket clearly contributes to the shielding as it must extract most of the energy release. The high energy neutron capture cross sections are small and likely endoergic in any case; thus, it is necessary to slow the source neutrons down to an energy where they can mostly be absorbed in Li^6 to produce tritium. Fortunately, this reaction is highly exoergic and produces an additional 4.8 MeV for the reactor. The moderation of the energy of the source neutrons is carried out most effectively by inelastic collisions with materials of medium to heavy mass rather than through elastic collisions with light nuclei as in fission reactors. The reason is that at the source energy here, the elastic cross sections have fallen and anisotropic scattering occurs. On the other hand, inelastic events readily occur at these energies and structural materials are generally good for neutron moderation.

The first zone behind the initial wall will contain lithium in some form, a coolant, and structural materials. This may be followed by a reflector region which returns as many neutrons as possible to the lithium bearing zone. Beyond the reflector there may be a coolant zone and then the shield which simply attenuates the neutron and gamma fluxes as rapidly as possible.

In some cases, there is a concern over obtaining adequate tritium breeding. This leads to the introduction of a material called a neutron multiplier because of its relatively large (n,2n) cross section in the part of the blanket near the source. Another consideration of importance for a fusion reactor is the activation of the reactor constituents. The first wall is not expected to last the life of the plant, thus maintenance and replacement will occur in the presence of the radiation by the activated materials.

Materials that have been suggested for the first wall and the structure include steels, alloys of the refractory metals, nickel based alloys, Aluminum, and Zirconium. Each has its merits from the thermal, mechanical, and fabricability points of view. From a neutron physics standpoint, steel, Niobium, and Molybdenum are good neutron moderators, have helpful (n,2n) cross sections, but they activate to long lived products to a significant degree. On the other hand, Aluminum and Vanadium have very low activation cross sections. From the standpoint of radiation damage, there are large uncertainties in all of the materials. This is due primarily to lack of materials studies in the expected radiation environment. To reduce these uncertainties there is a need for nuclear data on helium and hydrogen production as well as data for determining displacements, since the calculated production of these impurities and defects can be correlated with actual material properties.

The coolants that have been favored in most studies have been liquid lithium and helium. Liquid lithium has been given considerable attention since it is a good coolant, lithium must be present in any case, and the technology for handling liquid metal coolants could be borrowed from the fast reactor

development programs. Helium is well-known as a coolant and is innocous from the nuclear standpoint. The reasons for avoiding water as a coolant are the risk of lithium-water reactions in an accident and the difficulty of removing tritium produced in the blanket from the water if leakage or diffusion result in contamination.

If a coolant other than lithium is chosen, then lithium must be introduced in a form suitable for both tritium production and removal. Lithium bearing solid compounds have been proposed for this purpose, with $LiAl_2O_3$ a prominent example. Tritium production is not expected to be a problem at the present time. However, it was considered very carefully since it is essential to sustained energy production from this fuel cycle. The possibility of using a neutron multiplier has been developed. For this purpose berylium has a very large (n,2n) cross section and is clearly the best choice. The expense and availability of berylium have resulted in the evaluation of other materials and several metals have been considered for this function including lead as well as most of the structural materials since they are present in all cases.

Another idea for increasing tritium production is to introduce a reflector behind the lithium bearing zone in analogy to the use of reflectors in fission reactors. The material should have a large scattering cross section, low scattering anisotropy, and a low neutron capture cross section. Carbon meets these criteria well and is often the choice for the reflector. However, it has been observed that if tritium breeding is more than adequate, the use of a reflector may still be desirable as the $Li^6(n,\alpha)t$ reaction is a good energy producer. The reflector material may then be chosen to minimize energy losses in the nonelastic reactions which are often endoergic. For example, there is less energy loss to the system in using a steel reflector compared to a carbon reflector.[1] The inelastic scattering in iron produces a very hard gamma which is eventually absorbed, while the $C(n,3\alpha)$ reaction results in a binding energy loss that is then not available to the reactor.

For an efficient use of the energy, on the order of 99% should be recovered at reasonably high temperature in the blanket. The remainder must be removed by the shield to protect magnets and equipment. The biological shield will be the walls of the containment structure and is treated separately. The region referred to as the shield is constrained by magnet and other equipment costs to be relatively thin and total costs may dictate the use of expensive shield materials if radiation intensity gradients can be enhanced. The most penetrating radiation is the 14 MeV neutron flux. For this reason a heavy material with a large inelastic cross section should be present. Ideally this should produce only soft gammas and not activate to a significant degree. Lead, for example meets this criteria well, but will not support itself. Iron is suitable and in the form of stainless steel is a good relatively inexpensive non-magnetic structural material. Unfortunately, iron produces the previously mentioned very hard gamma which requires a significant amount of high Z material for its attenuation. The heavy materials will only slow neutrons down efficiently at the higher neutron energies and are very inefficient below about 1 MeV. A good material to include for this energy range and for capture of the neutrons is B_4C. The boron and carbon will aid in moderation especially at the lower energies, and the boron capture is an (n,α) reaction preventing (n,γ) capture in other materials which might produce a hard γ. Many materials have been

proposed for the shield and the best choices for different situations are still not settled. The attenuation to be achieved is determined by a number of criteria. The criteria which is limiting varies with the design. Examples of these criteria are the acceptable thermal load to the magnet cryogenic system, radiation damage to the cryogenic thermal insulation or the conductor stabilizing material.

In addition to the above effects, activation of the blanket and shield constituents will result in radiation problems for maintenance operations and for wall replacement.

Cross Sections and Spectra

The neutron spectra at different locations is clearly dependent on the particular system; however, the general trend is not overly sensitive to the particular design since all have the same source, a medium mass structure and lithium. Shield materials also have enough common features to allow a typical spectrum to characterize the behavior. The system shown schematically in Figure 2 has been used to generate the representative spectra of Figure 3. This displays conveniently normalized spectra for the first structural wall, the middle of the lithium zone, the reflector, and in the lithium behind the reflector. The 14 MeV peak is characteristic of the source and is suppressed as the position gets further from the source. The dip extending from a few MeV to the 14 MeV peak results from the source neutrons being scattered below this region by inelastic collisions, with only the elastic collisions moderating the neutrons into this region. In the first zones, a fairly flat region extends to around 10 KeV in which resonances are prevalent but the average cross section remains roughly constant. There is a dip at a few hundred keV which is due to the Li elastic scattering resonance peak. At still lower energy, the flux falls off rapidly to its thermal level except in the reflector with its low thermal capture. The trend is for a softer spectrum further from the source as would be expected.

To illustrate the energy regions of importance, three responses are used here. These are the atomic displacement, the helium production, and the tritium production rates. The time independent neutron transport equation can be written in operator form as

$$L\,\psi = S$$

where L is the transport operator, ψ the angular neutron flux, and S the neutron source distribution. The equation involving the adjoint operator

$$L^{\dagger}\,\psi^{*} = S^{*}$$

with solution ψ^{*} called the adjoint flux can easily be shown to relate to the original problem through the relation

$$\int S^{*}(\underline{r},E,\underline{\Omega})\,\psi(\underline{r},E,\underline{\Omega})\,d\underline{r}dEd\underline{\Omega} = \int S(\underline{r},E,\underline{\Omega})\,\psi^{*}(\underline{r},E,\underline{\Omega})\,d\underline{r}dEd\underline{\Omega}$$

This leads to the interpretation of ψ^{*} as an importance function for a source neutron to contribute to response S^{*} which may be chosen to be a macroscopic cross section resulting in one of the responses of interest. Adjoint sources

equal to the displacement, helium production, and tritium production cross sections are employed to obtain importance spectra. The displacement cross section is obtained as follows. The recoil spectra of atoms from each type of collision is determined and a solid state model employed to give the number of atoms displaced from their lattice positions by the primary knock on. The original cross section is multiplied by the number of displacements and on summing over all collision types, the displacement cross section is obtained. This response cross section is illustrated for several structural metals on Figure 4. [2] It is large at high energies as the number of displacements due to the energetic primary more than offsets any cross section differences. After decreasing with energy, it again increases at low energy where the primary energy is supplied by recoil during reactions an the increase is due to the increase is the reaction cross sections. The helium production cross sections emphasize the high energy region even more as they are usually threshold reactions. It should be noted that the appropriate cross section here is the sum over all cross sections where helium is a product, i.e., (n,α), $(n,n'\alpha)$ $2(n,2\alpha)$, etc. These are shown for the main constituents of stainless steel and for vanadium in Figure 5. The tritium production cross sections are not shown but consist of a very large cross section at low energies in Li^6 and an inelastic scattering event at high energy in Li^7.

Importance spectra are clearly both system and response specific, but give good insight into the energy regions that dominate a given response. Figure 6 shows importance spectra at the same points for which the flux spectra are given for displacement production in the first wall. As would be expected, the high energy range dominates but there is no 14 MeV peak. At the first wall, the top curve, the spectrum follows approximately the cross section itself. However, the remaining spectra become negligible at low energy because they stand little chance of further interaction in the first wall. Figure 7 is a similar plot of the importance spectra for helium production in the first wall. Again the largest spectrum is in the first wall corresponding to point 1 of Figure 2. These spectra emphasize the high energy neutrons in the extreme. Figure 8 shows the importance spectra for total tritium production. The first wall and main breeding zone spectra are almost superposed on top of one another since the first wall neutrons at most energies end up in the breeding zone. At the very lowest energies there is a difference and the first wall spectra is the lowest of the four. The initial drop for the first few MeV below 14 MeV occurs as the energy passes through the Li^7 breeding reaction. The reflector spectrum shows all energies to be of essentially equal importance as most neutrons of any energy in the reflector will end up contributing Li^6 reactions in one of the lithium zones. The low importance, except at the lowest energies, of neutrons in the second lithium zone results from the thinness of the zone so most neutrons will simply leak into the shield.

There is a well developed formalism for determining the effect of data uncertainties on uncertainties in design responses. The information is summarized by a sensitivity coefficient or function. If an uncertainty in cross section for reaction Y, $\delta\sigma_y$ results in an uncertainty δR_x in response R_x, this coefficient is defined as

$$\frac{\delta R_x}{R_x} / \frac{\delta \Sigma_y}{\Sigma_y} .$$

If this is not integrated over energy, a sensitivity profile results which can be determined in terms of δL_y, the perturbation of the transport operator, ψ_x^*, and ψ. This is very specialized information as it is system, response, material, and reaction specific and thus will only be representative for a narrow range of designs. Three examples have been carried out to illustrate the sensitivity concept. The first example considers the tritium breeding of the system of Figure 2, and its sensitivity per unit energy to the stainless steel cross sections in the first wall and in the middle of the breeding zone.

The results are shown in the lower and upper curves respectively for these points. The sensitivity is greater for changes involving the center of the breeding zone as is appropriate for this response. The profile may be either positive or negative depending on whether the source or loss terms of the transport operator containing the cross sections in question dominate. Actually the absolute values are plotted for convenience. In this particular case the upper curve corresponds to positive values to the mark at a few KeV and to negative values above this. Lower values are positive as scattering from the larger flux at higher energy dominates, the losses due to collisions at these low energies. Above the mark the effect is negative as the total cross section is larger than the scattering cross section at higher energy while the spectra are closer to the same value. A large amount of detailed interpretation is possible. For example, the initial drop occurs both due to the source peak and the threshold nature of the breeding reaction in Li^7.

Similar insights are gained from Figures 10 and 11 for the displacements per atom and helium production respectively. Both show the extreme importance of the high energy data compared to the low energy data. The effects illustrated are for the entire contribution of the material in question. One could also do this by individual reaction for even more detailed analysis of the influence of data on design quantities.

Current Status

The interest in this field is indicated by the large division of the American Nuclear Society devoted to controlled thermonuclear research with several sessions at a recent national meeting devoted to the nuclear analysis aspects of fusion power. This interest is widely dispersed geographically and indicates that many nations are starting to look beyond the confinement problem to the reactors. The general technology problems have been the subject of several conferences and have recently been reviewed. [3]

The neutron aspects of fusion divide naturally into the calculational methods and the nuclear data. Both areas have borrowed heavily from the fission reactor development of the past thirty years. The calculational approaches have thus far been completely taken from earlier work. It appears that special methods and computer programs for fusion will require only modest

extensions of those already available. Nuclear data needs extend very significantly the data base needed for fission. The energy range of importance now extends to at least 14 MeV whereas in fission there is only a nominal interest above about 5 MeV. In this higher energy range the number of reactions of consequence increases dramatically. A response function involving these reactions is the energy deposition cross sections or kerma factors which played a very minor role in fusion but are quite important in fusion where the neutrons carry most of the energy. Some of the materials of prime interest are also new. The data needs have been reviewed recently [4] in greater detail.

While the data needs have not always been met, and much data is of rather uncertain quality, the data community has generally been very responsive. Some very good data has been available from the weapons programs and the data files and evaluation procedures developed for fission and other applications have been extended to allow the handling of the needs of fusion. [5] Computerized implementations of nuclear models have been used to fill in some of the needed data. [6] At this point, data is available for fusion power studies and we are just starting the assessment of its adequacy.

Several studies [7,8] have looked at tritium breeding and the lithium cross section data. While the final assessment must await large scale tests; it seems that adequate breeding is possible with existing data uncertainties. The materials degradation by the radiation is very uncertain, but this stems from materials behavior more than from data uncertainty. While materials performance may be a limiting factor in fusion systems, additional nuclear data will have only a small impact on the problem. A possible exception here are the total helium production cross sections which are often not well-known. There are current experimental programs to reduce this problem.

The real importance of better nuclear data on neutron interactions for fusion will be felt in the details of reactor economics. Since competitive power systems will not be reached in the present century, there is no great urgency in carrying out detailed improvements in much of the data. This allows time for a careful appraisal of the results from experimental reactors. Those cross sections of prime importance can be studied using the formalisms developed to date to establish quantitative information on required accuracy. [9,10]

The discussion to this point has not mentioned the fusion-fission hybrid reactor concept in which the fusion neutron source drives a blanket consisting at least in part of fertile and fissile materials. Such a system can amplify the energy production from fusion alone and breed fissile fuel for use in other reactors. A variety of optimizations are possible in such systems. Much of the neutron data needed is well-known from the intensive studies for fission reactors. The higher energies have again not been explored intensively. The interactions of greatest importance in this energy range are the fission, (n,2n), and (n,3n) cross sections. The energy distribution of the secondary neutrons from these reactions will be important to the systems performance. [11]

The neutron data of greatest near term interest is that required for the first large experiments to produce intense fusion neutron sources or simulations of such sources. In order to characterize spectra precisely, dosimetry must be well-developed in the energy range above a few MeV. Since D-Li and other neutron producing reactions are proposed for use in intense neutron sources, spectra extending well above 14 MeV must be characterized to aid in evaluating the appropriateness of each source in simulating effects in a fusion reactor. [12]

Activation data is also of importance in the near term due to its consequences for shielding and maintenance. [13]

Conclusions

Neutron interactions are of great interest for fusion development programs. They will influence many reactor design and operational decisions, and affect plant economics. The crucial tritium breeding reactions possess cross sections that currently seem adequate to assure the fuel supply. The cross section data will play an important role in materials research both as a basis for correlating damage data to the radiation and in characterizing the radiation environment in which studies are carried out. Other data effects are primarily economic and not as urgently needed. A continuing assessment program is necessary to quantify priorities and necessary accuracies.

Acknowledgements

I would like to thank Dr. M Gohar and Mr. E. Cheng and S. Sayegh for their assistance with the calculations. The work was supported by ERDA.

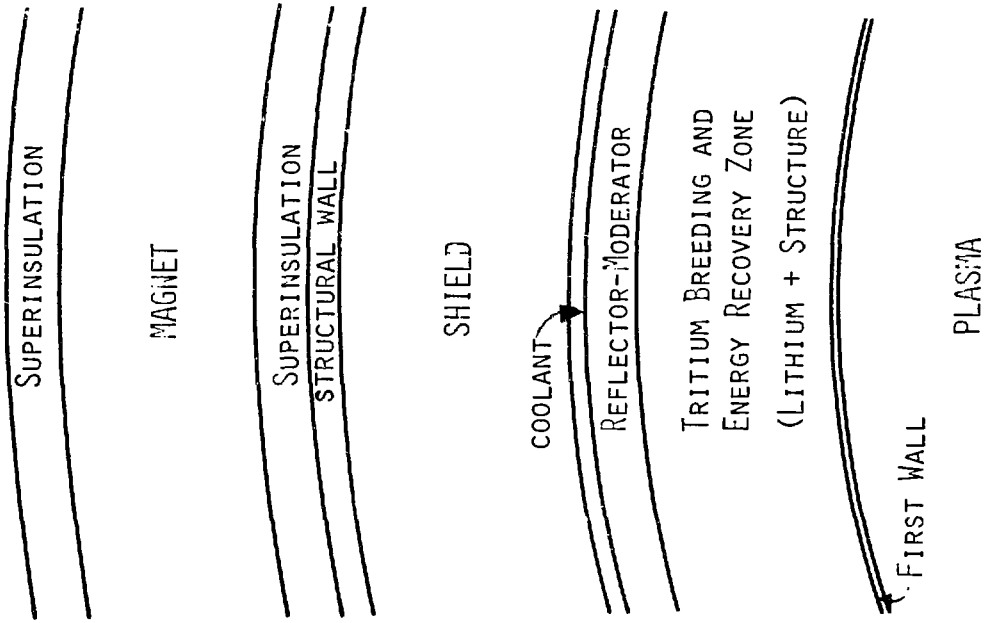

SCHEMATIC OF BLANKET AND SHIELD REGIONS

FIGURE 1

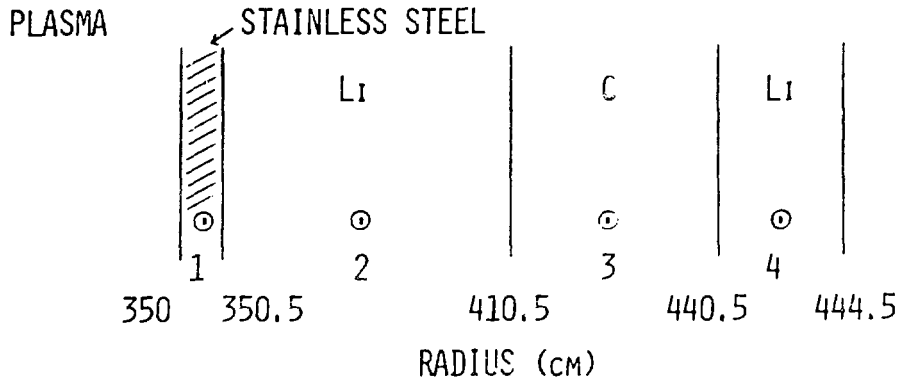

A CYLINDRICAL, 46 ENERGY GROUP, S_4, P_3 CALCULATIONAL MODEL IS EMPLOYED FOR THIS BLANKET SCHEMATIC.

Figure 2

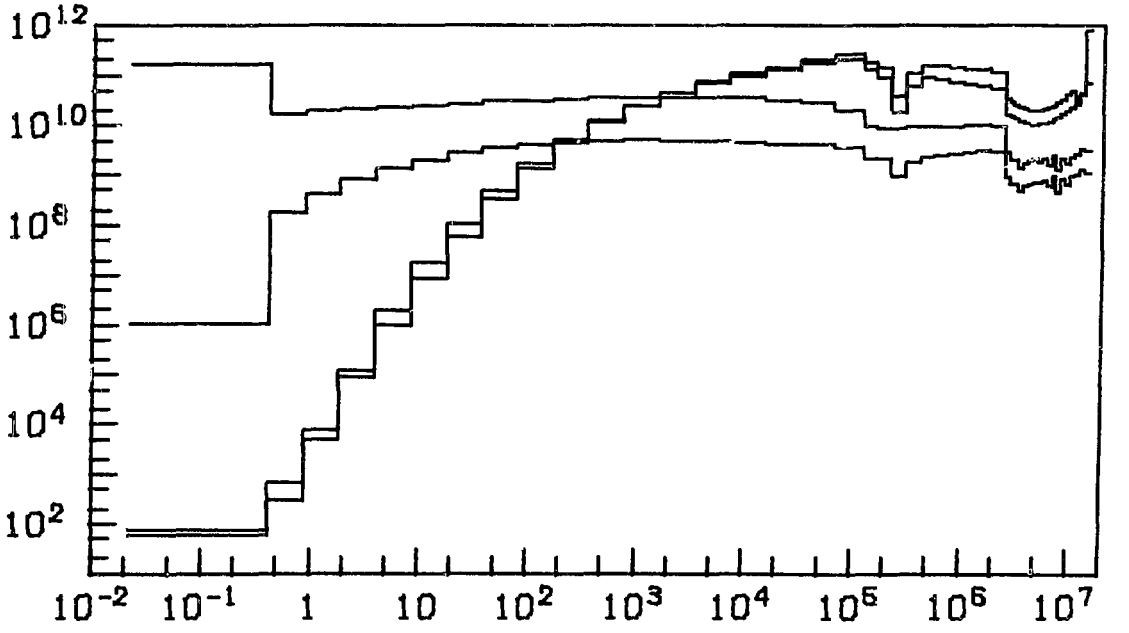

Flux spectra in arbitrary units versus energy. Numbers refer to points designated in Figure 2.

Figure 3

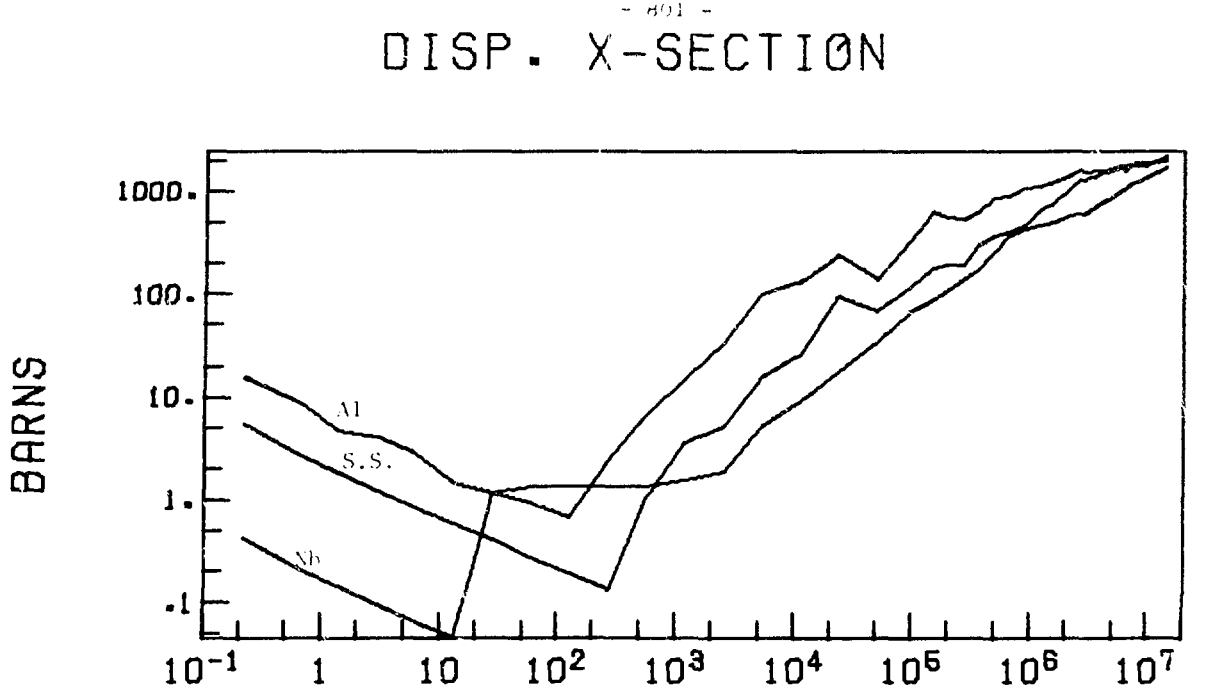

Displacement cross section in barns versus energy in eV for aluminum, stainless steel, and niobium.
Figure 4

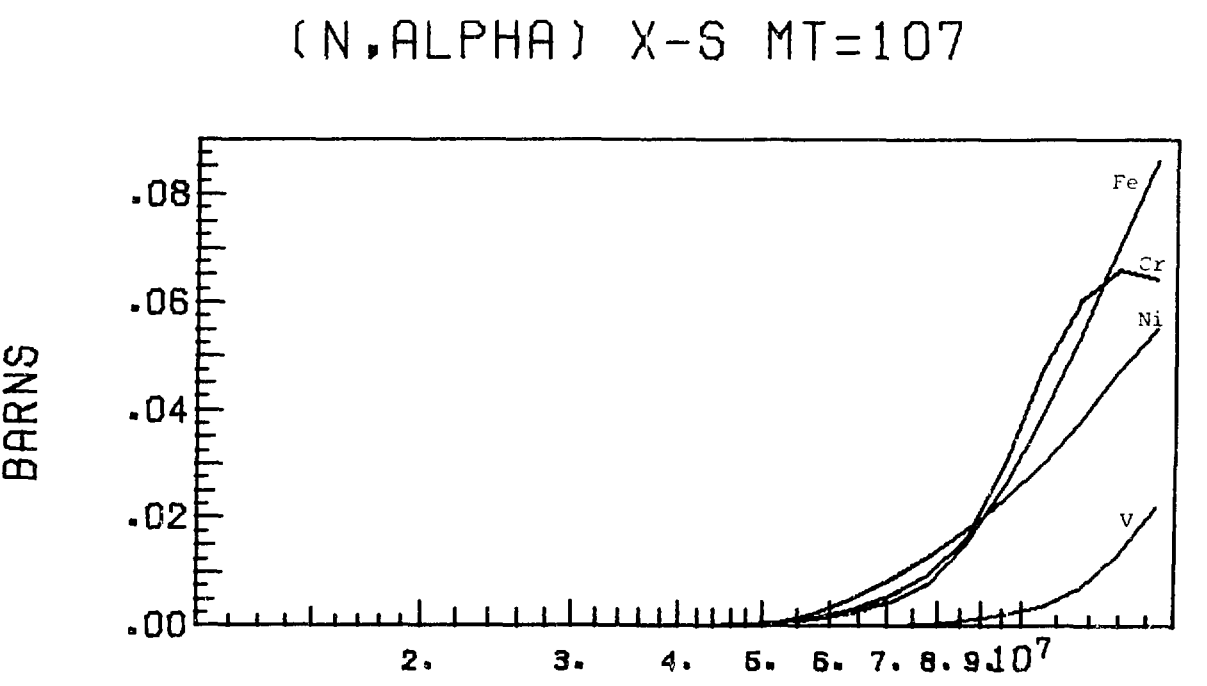

Helium production cross section in barns versus energy in eV for iron, chromium, nickel, and vanadium. Original data from ENDF/B4
Figure 5

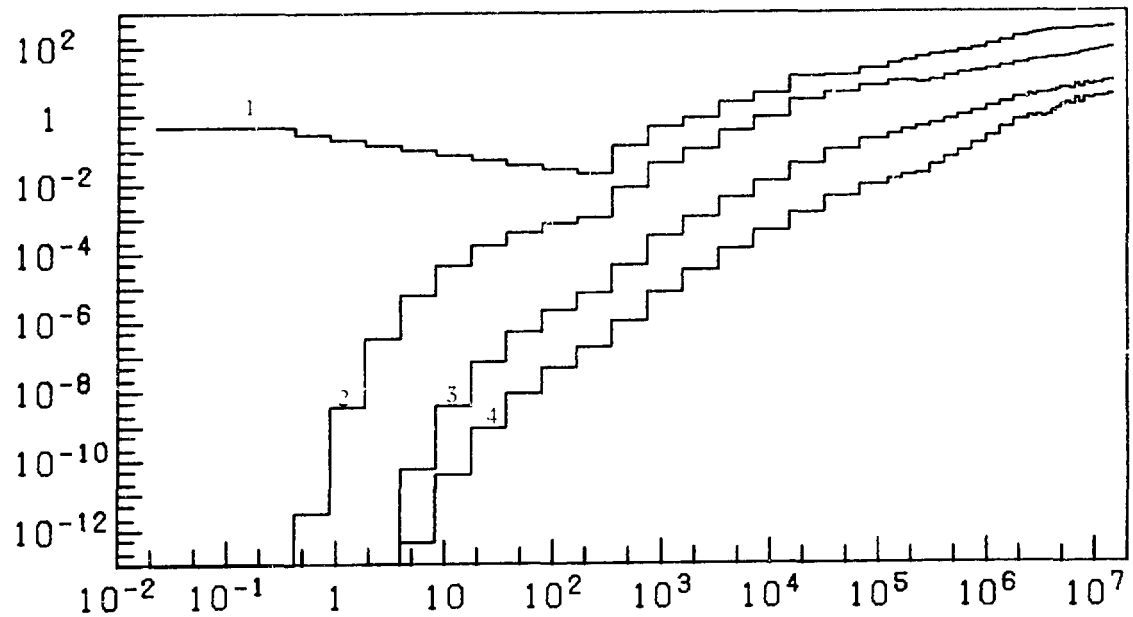

Importance Spectra for displacement production in the stainless steel first wall versus energy in eV at the numbered points of figure 2.

Figure 6

FIRST WALL HELIUM PRODUCTION IMPORTANCE SPECTRA

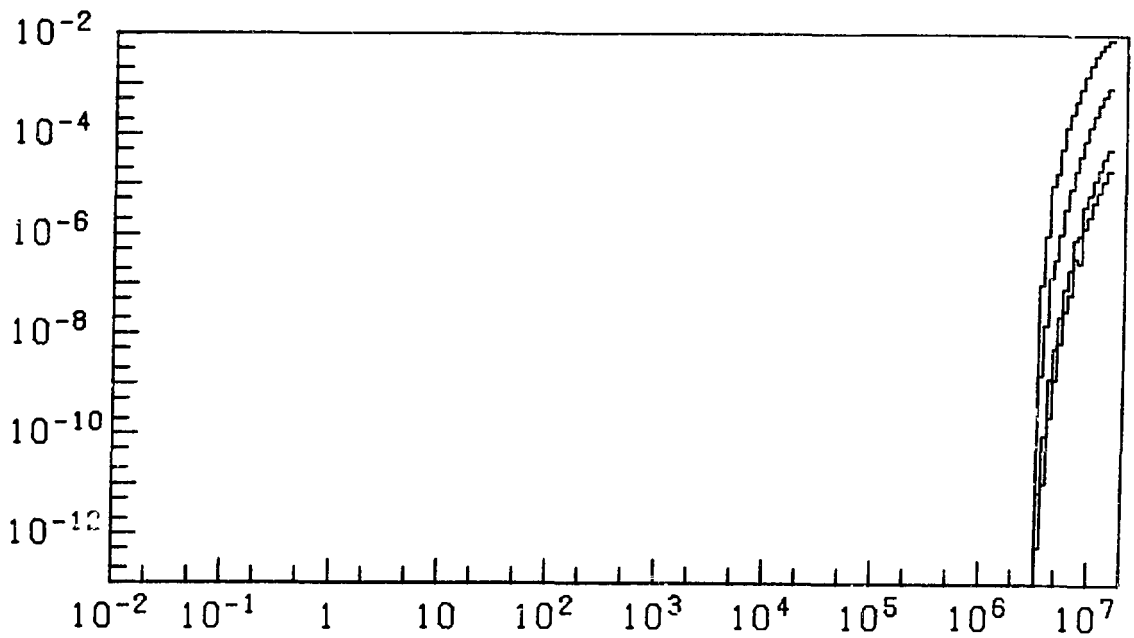

Importance spectra for helium production in the first wall as a function of energy in eV at the points for which flux spectra are given in Figure 2.

Figure 7

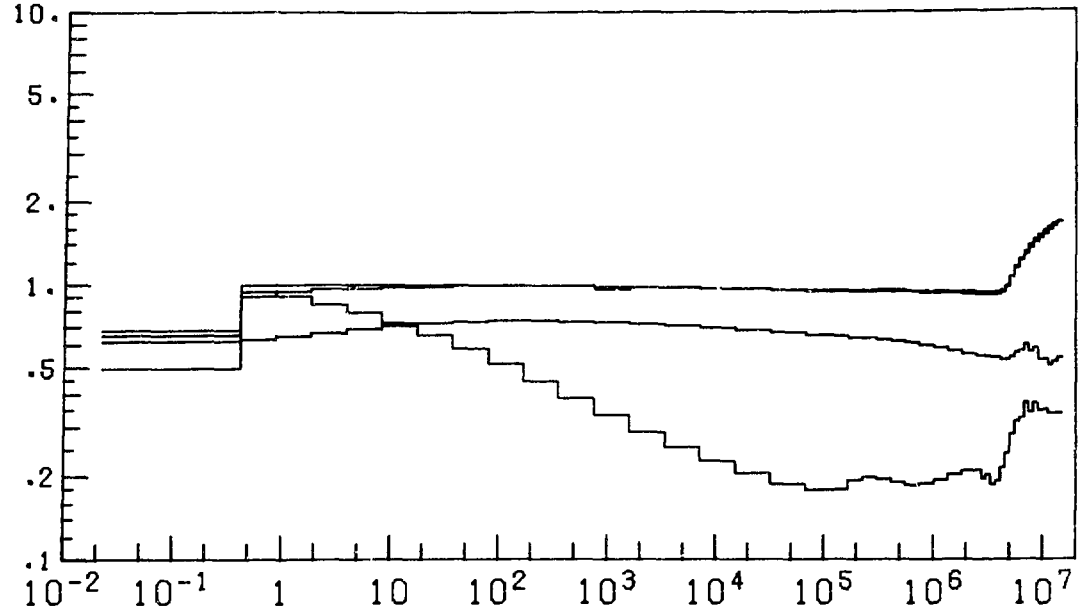

Importance spectra for total tritium production versus energy in eV for the numbered points of Figure 2.

Figure 8

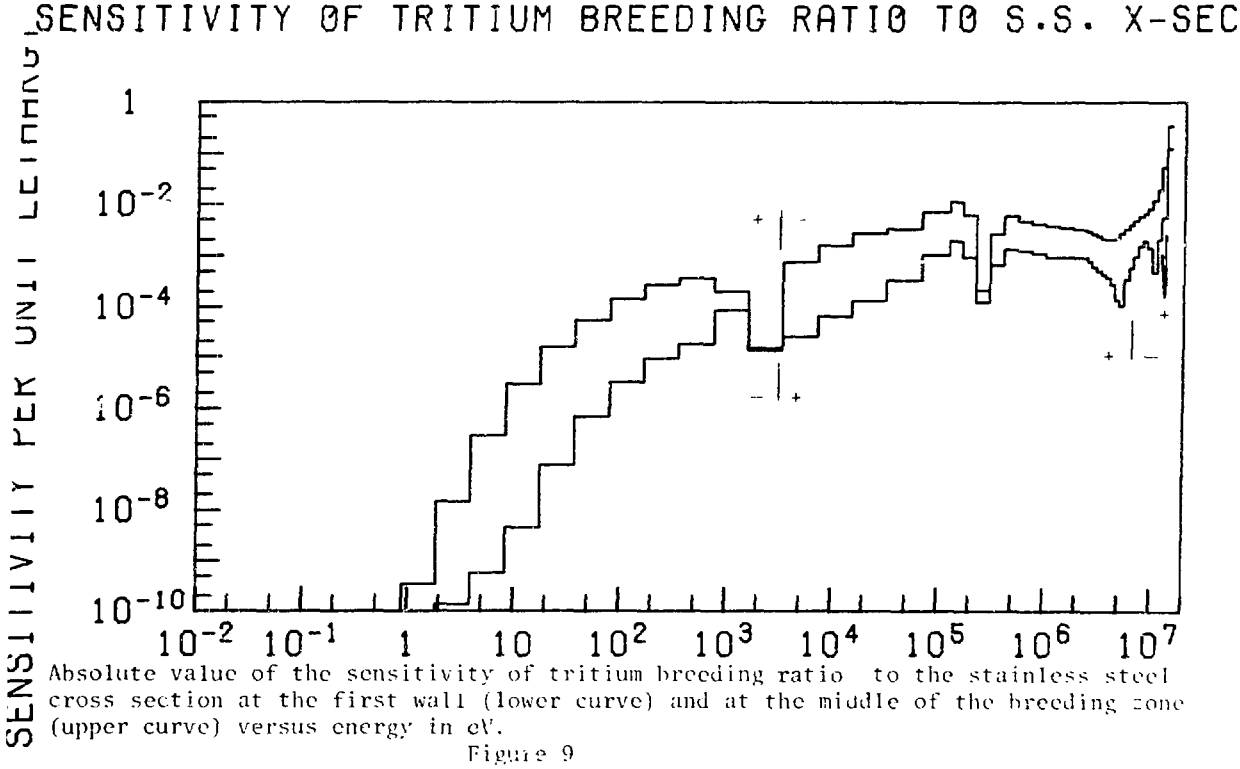

Absolute value of the sensitivity of tritium breeding ratio to the stainless steel cross section at the first wall (lower curve) and at the middle of the breeding zone (upper curve) versus energy in eV.

Figure 9

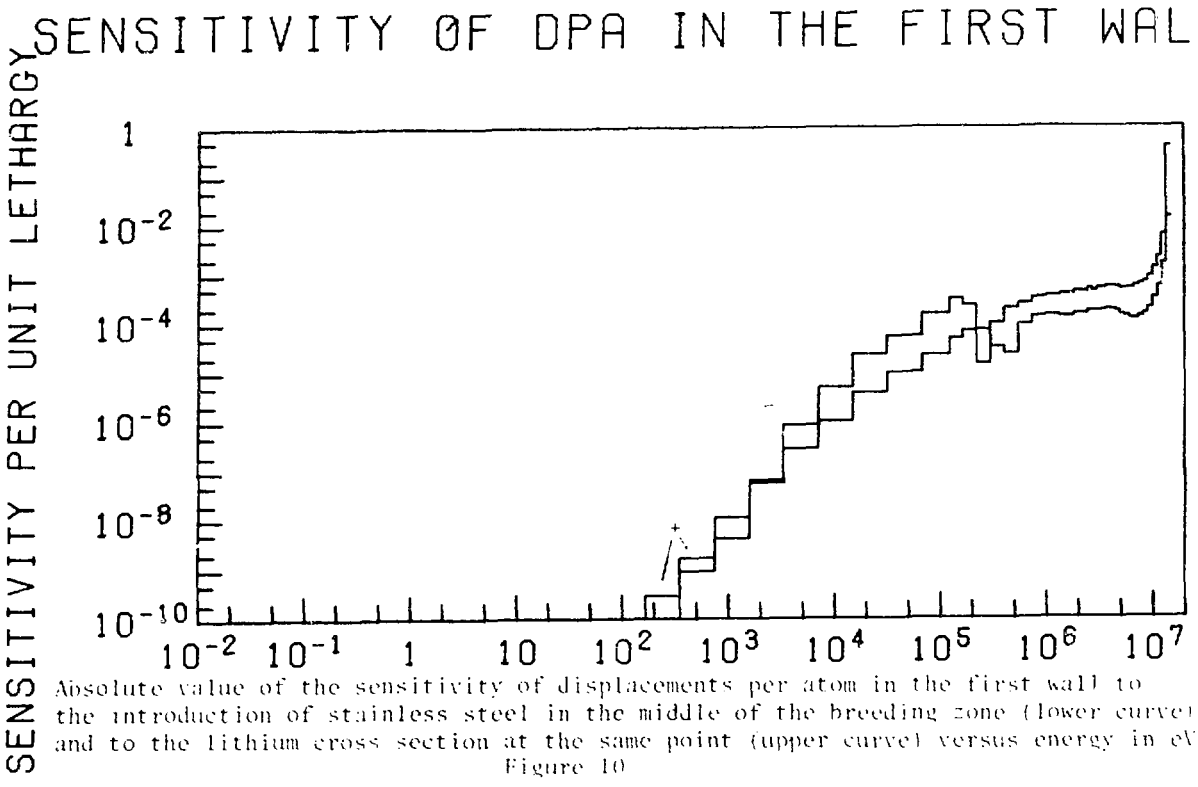

Absolute value of the sensitivity of displacements per atom in the first wall to the introduction of stainless steel in the middle of the breeding zone (lower curve) and to the lithium cross section at the same point (upper curve) versus energy in eV

Figure 10

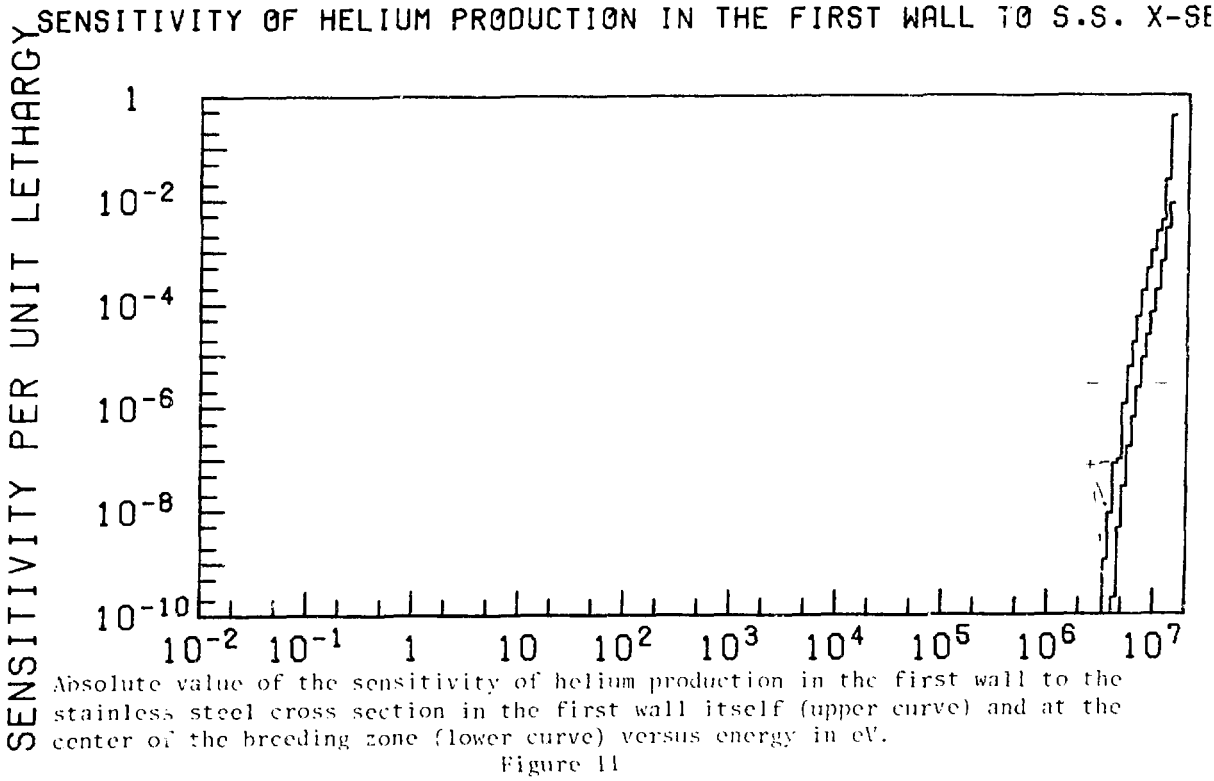

Absolute value of the sensitivity of helium production in the first wall to the stainless steel cross section in the first wall itself (upper curve) and at the center of the breeding zone (lower curve) versus energy in eV.

Figure 11

eferences:

. B. Badger et al, "UWMAK-I A Wisconsin Toroidal Fusion Reactor Design," Fusion Design Memo 68, University of Wisconsin, (March, 1974).

. T.A. Gabriel, J.D. Amburgey, N.M. Greene, "Radiation Damage Calculations: Primary Recoil Spectra, Displacement Rates, and Gas-Production Rates," ORNL-TM-5160 Oak Ridge National Laboratory, Oak Ridge, Tenn. (March, 1976).

. D. Steiner, "The Technological Requirements for Power by Fusion," Nucl. Sci. Engr., 58, 107 (1975).

. D. Steiner, "Nuclear Data Needs for Fusion Reactor Design," Nuclear Cross Sections and Technology, R.A. Schrack and C.D. Bowman, Eds., National Bureau of Standards Special Publication 425, 646 (1975).

. L. Stewart, P.G. Young,"Evaluated Nuclear Data for CTR Applications," Transactions American Nuclear Soceity 23, 22 (June, 1976).

. M.R. Bhat, et al, "Nuclear Data for CTR Related Projects," BNL-19344, Brookhaven National Laboratory (October, 1974).

. D.E. Bartine, et al, "Cross-Section Sensitivity of Breeding Ratio in a Fusion-Reactor Blanket," ORNL-TM-4208, Oak Ridge National Laboratory, Oak Ridge, Tenn. (October, 1973).

. M.L. Tobias and D. Steiner, "Cross-Section Sensitivity of Tritium Breeding in a Fusion-Reactor Blanket: Effects of Uncertainties in Cross Sections of ^{6}Li, ^{7}Li, and ^{93}Nb," ORNL-TM-4200, Oak Ridge National Laboratory (1973).

. G.C. Campbell, J.L. Rowlands, "The Relationship of Microscopic and Integral Data," Nuclear Data for Reactors (Proc. Conf. Helsinki, 1970), 2 IAEA p. 391, Vienna (1970).

10. S.A.W. Gerstl, D.J. Dudziak, D.W. Muir, "A Quantitative Basis for Cross-Section Requirements for a Fustion Test Reactor," Trans. Am. Nucl. Soc. 21, 68 (June, 1975).

11. B.R. Leonard Jr., et al, "A Sensitivity Study of Data Deficiencies, Weighing Functions, and 14 MEV Neutron Source Spectrum Effects in a ^{238}U Fueled Fusion-Fission Hybrid Blanket," Nuclear Cross Sections and Technology, R.A. Schrack and C.D. Bowman, Eds., National Bureau of Standards Special Publication 425, 680 (1975).

12. M.J. Saltmarsh, "D-Li Neutron Sources-Application to the CTR Materials Program," Trans. Am. Nucl. Sci. 23, p 1 (1976).

13. S.A.W. Gerstl, D.J. Dudziak, and D.W. Muir, "Application of Sensitivity Analysis to a Quantitative Assessment of Neutron Cross-Section Requirements for the TFTR: An Interim Report," LA-6118-MS, Los Alamos Scientific Laboratory (1975).

ML 1 - NEUTRONS AND FUSION - C. W. Maynard (University of Wisconsin)

Newstead (Brookhaven):

Could you give us your personal view of the ultimate utility of a laser induced fusion device as opposed to the TOKAMAK type machine you've been discussing?

Maynard:

Well, the difficulty of the problem is that I think if the laser can be had and if you believe their (Hodges and Emicks) codes the laser has great merits. It would allow for smaller modules and I don't see any hard engineering problems. I don't think there will be many serious shock-wave type problems from the pellet explosion so I think laser fusion would be a very fine thing but I guess I have to say it's further down the road at present. They may be able to come along very fast with their bigger lasers, but at the present time they're not as well understood and so we have to keep them as an alterrate for the time being.

Newstead:

I wanted to ask you a second question. One has recently heard about "clean fusion" using more exotic thermonuclear reactions and I wonder if you can comment on whether this is a real possibility.

Maynard:

Are you referring to the advanced fuel cycles?

Newstead:

Yes.

Maynard:

Well, you see, if you use a fuel cycle based on D-D, you get roughly a 2.5-MeV neutron; also, you have the time to get tritium, though. That will result in 14-MeV neutrons and that's not clean. The reaction $d + {}^3He$ gives all charged particles, but you have to wait for your helium-3; it's rather a hard cycle to work with. There are some other cycles like $p + B$ that have been proposed: another charged particle. The problem is you aggravate a confinement problem, and the confinement problem is still extremely difficult. So I'm all for "clean fusion" but I just don't see how it can be done.

Fowler (Oak Ridge):

In calculating the breeding ratio, what do you take as the chemical efficiency for extracting the tritium from the lithium? How much loss is there?

Maynard:

I really don't recall the number. They've assumed fairly small losses, for a number of reasons. First of all, you'll spend enough money to assure yourself that you don't. I can only tell you that there are quite a few chemists, for example, Oak Ridge has some good people in this area, to ensure that you can't afford to lose it because of the environmental problem; also you would hur-

yourself on your economy if you lost it. So I think something less than a tenth of a percent would have to be insisted on.

Qaim (Juelich):

I would like to make a comment on the question asked by Dr. Fowler. Tritium recovery will be a tricky business. The tritium which is produced via (n,t) reactions on lithium will exist in different chemical forms; chemical species like LiT, Li_2T, T, and T_2 have been observed in the vapor phase. We have a group at Juelich Institute of Nuclear Chemistry doing this type of work and our own feeling is that there is no point in getting very accurate data and calculating the breeding ratio of tritium very accurately until and unless one also has some knowledge about some methods of tritium recovery from various blanket materials.

Iyengar (BARC):

If I may ask a question; are there any experimental measurements of these spectra, which you showed?

Maynard:

This is what you refer to as an integral experiment in our end of the business. There are few. They haven't been very extensive. But Nuclear Science and Engineering in a recent issue did contain, I believe it was German work, in which some spectrum measurements were made and they are in the process of receiving more emphasis. ERDA has given Oak Ridge money specifically for this type of experiment.

11.30 a.m., Friday, July 9, 1976

NEUTRON PHYSICS AT LAMPF*

L. C. Northcliffe

Physics Department, Texas A&M University, College Station, Texas 77843

*Supported by the U. S. Energy Research and Development Administration.

RÉSUMÉ

The experimental program in neutron physics at intermediate energies (460-800 MeV) at the Clinton P. Anderson Meson Physics Facility (LAMPF) will be surveyed. Among the reactions studied are n-p elastic scattering, pion-production, (p,n) reactions and neutron-induced reactions in various nuclei.

ABSTRACT

The Nucleon Physics Laboratory at Lampf and the multiwire proportional chamber spectrometer used in neutron physics experiments will be described. The neutron spectra at 0° from proton bombardment of hydrogen, deuterium and numerous other targets at nominal proton energies of 647 and/or 800 MeV have been investigated. While all spectra (except those for $pp \rightarrow np\pi^+$) show a sharp charge-exchange peak at essentially the bombarding energy, the peak for $pd \rightarrow npp$ is intense, narrow and exceptionally well isolated from the background of lower energy neutrons and thus provides the basis for a nearly ideal monoenergetic neutron beam. This beam has been used in precision studies of the differential cross section for n-p elastic scattering in the region $50° < \theta^n_{cm} < 180°$ at 463, 647 and 800 MeV. Values of the pion-nucleon coupling constant derived from the shape in the charge-exchange region are in good agreement with values obtained from pion-nucleon scattering. The experiments also give the angular distribution for the reaction $n + p \rightarrow \pi^\circ + d$ at these energies with high statistical accuracy. In a separate experiment, the cross sections $d^2\sigma/d\Omega dp_\pi$ for production of π^+ and π^- mesons in n-p collisions at 800 MeV have been measured. The monoenergetic neutron beam has also been used in measurements of n-d back-angle elastic and inelastic scattering and in measurements of proton, deuteron and triton spectra from neutron bombardment of other nuclei.

NEUTRON PHYSICS AT LAMPF*

L. C. Northcliffe

Physics Department, Texas A&M University, College Station, Texas 77843

I. INTRODUCTION

More than a decade ago a need was recognized for accelerators of high beam intensity to be used in the accurate investigation of a wide variety of phenomena in the "medium-energy" region, above the threshold for meson production. In response to that need, accelerator facilities identified by the acronyms LAMPF, TRIUMF and SIN have been built in the U. S., Canada and Switzerland. Prominent among the motivations which led to the construction of these "meson-factories" was the need for detailed data on the phenomenon of meson production near threshold and for an accurate determination of the nucleon-nucleon interaction in both elastic and inelastic collisions at medium energy. In particular, despite considerable previous experimental effort, the available data on the n-p interaction have not been sufficiently accurate and comprehensive to permit unambiguous n-p phase-shift analyses for energies above about 400 MeV. A definitive determination of the n-p interaction, elastic and inelastic, for energies up to 800 MeV has been the primary motivation for the program of neutron physics research which has been undertaken at the Clinton P. Anderson Meson Physics Facility (LAMPF) at the Los Alamos Scientific Laboratory (LASL). While this continues to be the long-term objective in the neutron physics program, the instrumentation developed has made possible a number of other experiments involving high-energy neutrons. The purpose of this paper is to present a brief description of the facility and instrumentation for neutron physics research at LAMPF, and a summary of the experimental results obtained thus far. The work has been a collaborative effort involving scientists from LASL and from several universities (see Table I.). It should be noted that papers on some of this work were presented by Mahavir Jain[1] and D. M. Wolfe[2] at the recent International Conference on Few Body Problems in Delhi.

Table I. Collaborators in neutron physics experiments at LAMPF. Asterisks indicate those whose work constitutes PhD thesis research.

Texas A&M U.	U. of New Mexico	U. of Geneva	LASL
M. L. Evans*	H. C. Bryant	D. W. Werren	B. E. Bonner
G. Glass	C. G. Cassapakis*		J. E. Simmons
J. C. Hiebert	B. Dieterle	U. of Texas	Nelson Stein
Mahavir Jain	C. P. Leavitt	C. W. Bjork*	
R. A. Kenefick	W. Thomas*	P. J. Riley	
L. C. Northcliffe	D. M. Wolfe		

II. THE LAMPF EXPERIMENTAL FACILITY

The accelerator is a proton linear accelerator, a half-mile in length, of variable energy (200-800 MeV), designed to provide, simultaneously, H^+ beams of intensity up to 1.0 mA and H^- beams of intensity up to 100 μA. The machine has a macroscopic duty factor of 6%, providing beam pulses of 500 μsec duration at a rate of 120 Hz. Microscopically, the beam comes in bursts of 1/4 nsec duration separated by 5.0 nsec. This time structure can be utilized to some extent in time-of-flight (TOF) measurements. Further optimization for TOF measurements can be achieved by operating the H^- beam in an optional "chopped" mode in which seven out of eight

beam micropulses are eliminated and the micropulse separation becomes 40 nsec.

A view of the experimental areas, Fig. 1, shows how primary (H^+,H^-) and secondary (π,μ,ν,n) beams can be provided simultaneously in a variety of experimental channels, permitting the performance of more than a dozen experiments at the

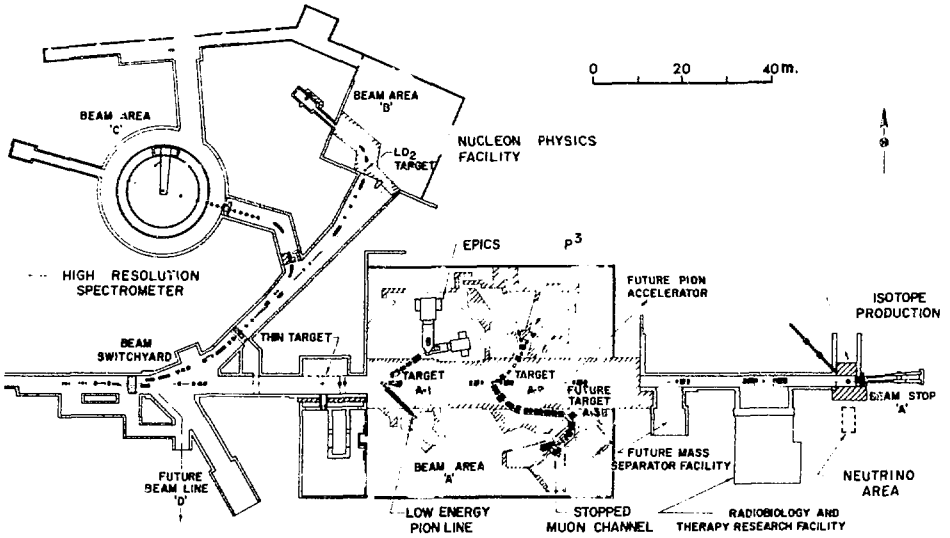

Fig. 1. Plan view of experimental areas at LAMPF. the beam enters from the left. The accelerator is not shown.

same time. The splitting of the beam between lines into beam areas A, B and C is achieved by use of foil strippers to convert fractions of the H^- beam into H^+ and magnets to separate the H^- and H^+ components. During the first two years of operation only the H^- beam from the accelerator was used. Recently, H^+ beams have been accelerated with intensity as high as 110 μA and routine operation with simultaneous acceleration of beams of 35 μA H^+ and 6 μA H^- has been achieved. This mode of simultaneous H^- and H^+ operation will be used in the future, and no major difficulty in increasing the beam intensity is foreseen.

III. THE NEUTRON FACILITY

The neutron experiments are done in beam area B, called the Nucleon Physics Laboratory, which is located at the top of Fig. 1. The neutron beam is generated by passage of the H^- beam through a production target, normally a forced-convection liquid-deuterium (LD_2) target of thickness 1.80 g/cm^2 which is designed to dissipate 100 W of beam power.[3] The H^- beam current is monitored by integration of the output of a toroid beam-current monitor.[4] As shown in more detail in Fig. 2, the neutrons from the $^2H(p,n)2p$ reaction are collimated at 0° (in a cone of half-angle 0.1°) while the proton beam is deflected into a beam stop. Background charged particles are swept from the neutron beam with magnet M_1. In the earlier runs a veto scintillator S_0 was placed in front of the second target so as to eliminate any residual charged-particle contamination, but this was found to be unnecessary and S_0 was eliminated in the later runs. The second target is normally a cell containing liquid-hydrogen (LH_2) of thickness 0.94 g/cm^2. The neutron flux is monitored by N-MON, a polyethylene radiator at the collimator exit viewed by counter

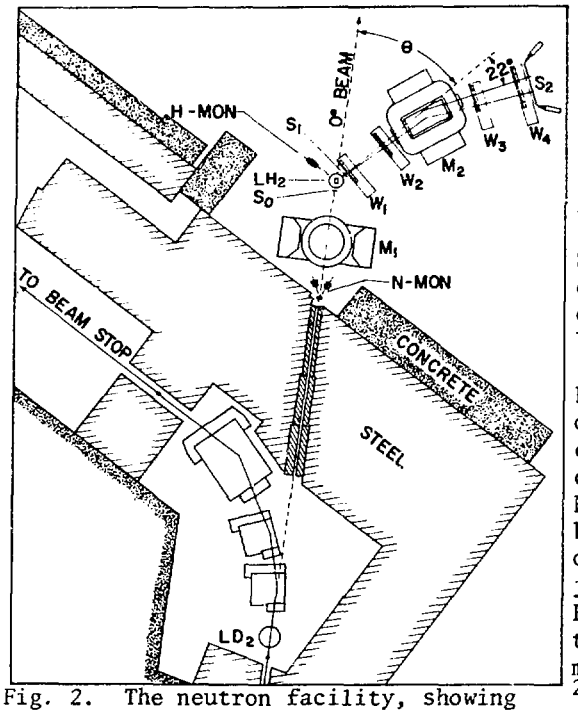

Fig. 2. The neutron facility, showing the production target (LD_2), the 0° neutron line, the reaction target (LH_2) and the MWPC spectrometer.

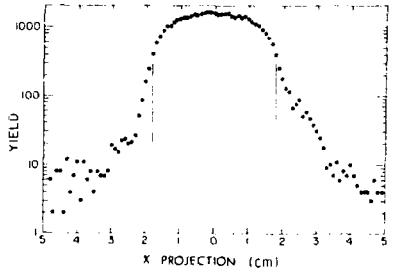

Fig. 3. Beam profile at LH_2 target.

telescopes positioned at 25° to left and right of the beam; another range telescope (H-MON) placed to detect protons recoiling at 45° from the LH_2 target serves to monitor the product of neutron flux and LH_2 thickness. Charged particles produced in the target are analyzed in a multiwire proportional chamber (MWPC) magnetic spectrometer (elements $S_1, W_1, W_2, M_2, W_3, W_4, S_2$ in Fig. 2), which determines the trajectories and momenta of the particles. The spectrometer will be discussed in more detail in Sec. IV.

The properties of the 0° neutron beam are inferred from the distribution of recoil protons from n-p charge-exchange scattering in the LH_2 target, as observed in the MWPC spectrometer. The horizontal distribution of the neutron beam at the midplane of the LH_2 target, obtained by projection of the proton trajectories back to that plane, is shown in Fig. 3. Note that the full width at one-tenth maximum is only ∿4 cm. The neutron momentum distributions observed for the $^2H(p,n)$ reaction at nominal beam energies of 647 and 800 MeV[5] are shown in Fig. 4. These spectra are of special interest because of the comparative isolation of the sharp high-energy peak from the background of lower energy neutrons which makes this reaction almost ideal for generation of monoenergetic neutron beams for use in scattering experiments. This beam is quite intense: at both energies the integrated flux of neutrons in the high-momentum peak is ∿8 x 10^5/sec per μA of proton beam current.

In some experiments, LH_2 is used in the production target or LD_2 is used in the second target or various solid targets are used in one or the other position. Some of the results obtained when this is done will be presented and discussed in Sec. V., below. Of special interest is the first alternative, in which the neutrons come primarily from the $^1H(p,n)p\pi^+$ reaction. The observed spectra[5] are also shown in Fig. 4, for comparison with the $^2H(p,n)$ spectra. The remarkable similarity of the lower-momentum regions of the spectra from the two targets is an indication that similar pion-producing mechanisms may be responsible for this continuum in both reactions.

IV. THE MWPC SPECTROMETER

The spectrometer has been described in more detail elsewhere.[6] It consists of a large magnet (M_2; see Fig. 2), two scintillators (S_1 and S_2) and four MWPC's (W_1-W_4) which give the horizontal and vertical coordinates of four points on the

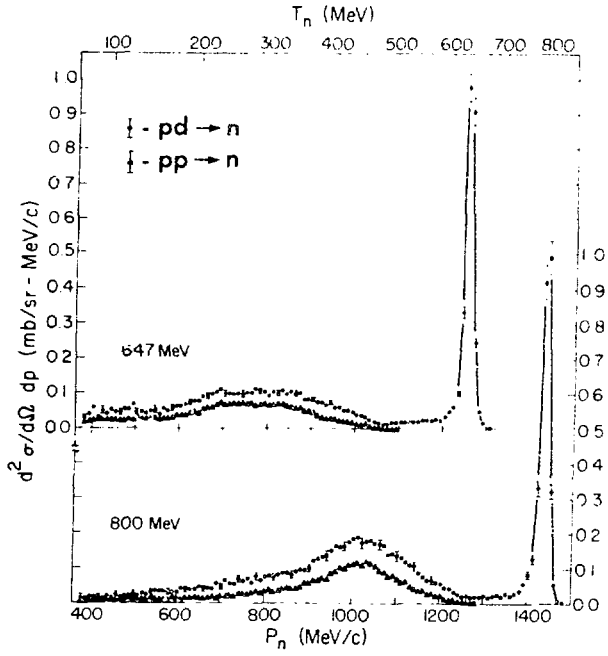

Fig. 4. Neutron spectra at 0° from proton bombardment of deuterium and hydrogen at nominal energies of 647 and 800 MeV. Typical statistical errors are shown.

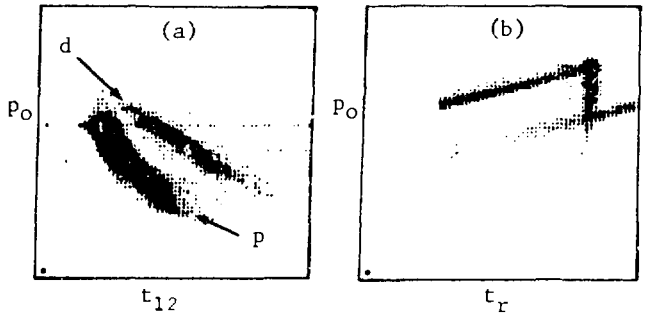

Fig. 5. Examples of important on-line displays. (a) p_o vs t_{12} shows the separation of protons (band p) from deuterons (band d). (b) p_o vs t_r shows the separation of low-momentum recoils caused by low-energy neutrons (slanting bands) from those caused by inelastic reactions in the LH_2 target (vertical band); The separation in this display is enhanced by obtaining the data with "chopped-beam" (40 nsec micropulse spacing).

path of charged particle recoiling from the LH_2 target, determining the path before and after the deflection, from which the momentum and recoil angle of the particle can be determined. Typical deflection angles are $\sim 22°$ and are determined with a precision of $\sim 0.06°$, which gives a momentum determination of accuracy $\sim 0.5\%$. (Actually, multiple scattering and other effects increase this to $\sim 1\%$.) The angular acceptance of the spectrometer in the horizontal plane is $\sim 4°$. In order to measure angular distributions over a wider range, the entire spectrometer system is rotated as a rigid unit about a vertical axis through the center of the LH_2 target. The scintillators S_1 and S_2 are used to measure t_{12}, the TOF of the particle through the spectrometer, which differs for different charged particles (p,d,t, π) of the same momentum and is used to identify them (see Fig. 5(a), below). Independent identification is provided by the pulse height seen in S_2, which differs for particles of the same momentum but different mass. The timing t_r of the S_1 signal relative to the accelerator rf micropulse is also measured since it can be used to distinguish low-energy recoils which are produced by low-energy neutrons from the LD_2 target from those which are produced by inelastic processes in the LH_2 target (see Fig. 5(b)).

When a coincidence between signals from S_1, S_2 and at least three out of four of both horizontal and vertical MWPC's occurs in the absence of a veto from S_0, an event is accepted and analog signals from S_1, S_2, t_{12} and t_r along with digital signals identifying the "hit-wires" in the MWPC's are read via CAMAC and a microprogrammed branch driver[7] into a PDP-11 computer. The data-acquisition program[8] writes all data for each event on magnetic tape for use in subsequent off-line analysis as well as providing live, on-line display of a variety of histograms and two-parameter plots of

the data. The two examples shown in Fig. 5 are of special interest. They are plots of the approximate momentum p_0 (estimated from the angle of deflection) vs. t_{12} and t_r, respectively. Figure 5(a) shows the separation of protons and deuterons into separate bands which is used as one means of particle identification, while Fig. 5(b) shows how low-momentum recoils which are caused by inelastic reactions in the LH_2 target (the vertical band of events) can be distinguished from those due to low-energy neutrons from the LD_2 target (the slanting bands).

A final determination of the momentum p for each event is made in the off-line analysis by starting with the approximate value p_0, computing the path of a particle of this momentum through the spectrometer using a matrix of measured magnetic field values and finding the optimum path and momentum p by a χ^2 minimization procedure.[9] This p value and other data on the event are written on another tape which is used in all further analysis.

The problem caused by the occasional occurrence of multiple "hits" in the MWPC planes is resolved by considering all possible trajectories through individual "hits" in the different wire planes and selecting the one with the best χ^2 value. Events with a missing x or y coordinate due to MWPC inefficiency (typically ~0.3%) caused no problem because three x and three y coordinates determine the particle orbit unambiguously.[9]

The geometric acceptance of the spectrometer is limited vertically by the gap of the magnet and horizontally by the edges of the MWPC's. The vertical limitation can be specified in terms of the polar and azimuthal angles θ_m and ϕ_m in a polar coordinate system fixed in the spectrometer with its polar axis normal to wire-planes W_1 and W_2. With our spectrometer geometry and beam size, particles restricted to the region $\sin\theta_m \sin\phi_m \leq 0.02$ had negligible probability of striking a magnet pole. Imposition of this restriction limits the azimuthal angular acceptance to the fraction $\varepsilon = (2/\pi) \arcsin(0.02/\sin\theta_m)$ when $\sin\theta_m > 0.02$ but eliminates uncertainty about the eclipsing due to the magnet poles. The limitation imposed by the finite width of the MWPC's can be determined empirically from plots of θ_m vs hit-wire position for various momentum bands and all magnet currents. The results are summarized in Fig. 6, in which the limits determined by the left and right edges of the MWPC's are plotted. If an event falls within the shaded region it is sure to have passed through all four MWPC's. Only events within this region which have $\sin\theta_m \sin\phi_m \leq 0.02$ are used in the analysis. Thus the uncertainties due to finite beam size and the geometric limits of the spectrometer are eliminated. From this plot it is seen that the width of the angular region accepted by the spectrometer in the horizontal plane is ~ 4° and that the location of this angular region for particles of a given momentum p changes as the magnet current is changed (i.e., as $\int B \cdot d\ell$ through the magnet is changed, where B is the vertical component of the magnetic field at ele-

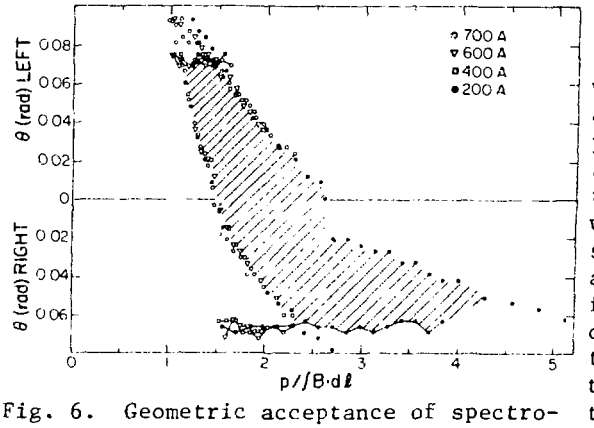

Fig. 6. Geometric acceptance of spectrometer as determined by left and right edges of MWPC's. The dependence on magnet current is eliminated by dividing the momentum p by the magnetic field integral $\int B \cdot d\ell$.

ment of path $d\ell$). Thus, the angular region studied can be changed somewhat without moving the spectrometer if the magnet current is changed.

The sense-wire spacing in the MWPC's is 2.0 mm. The discreteness of the coordinate information gives rise to surprisingly large artificial discontinuities in the θ_m and ϕ_m distributions. This instrumental "granularity" is removed by redistributing the discrete coordinates randomly in accord with a trapezoidal probability distribution which approximates the actual probability that a wire will be triggered as a function of the distance by which the particle misses the wire. This distribution is tailored to reproduce the observed frequency of simultaneous triggering of neighboring wires.

V. EXPERIMENTAL RESULTS

A. Neutron Momentum Spectra

One of our objectives has been to make a systematic investigation of the neutron spectra produced in proton bombardment of a wide range of target nuclei. For these measurements the spectrometer was positioned at the nominal angle $\theta = 0°$ (see Fig. 2) and LH_2 was used as a radiator. In each case the neutron spectrum was derived from the observed spectrum of recoil protons from n-p charge-exchange scattering in the radiator. The proton recoil spectrum was synthesized by merging the results of runs made with several magnet currents (typically four) which spanned different overlapping momentum regions. The spectra were corrected for the slow variation of the n-p charge-exchange cross section with neutron energy. They were also corrected for the inelastic (pion-producing) reactions in the LH_2 target, which also produced protons of reduced energy. The correction was determined in a special set of "chopped" beam runs with the broad spectrum of neutrons produced in the $^{27}Al(p,n)$ reaction at 786 MeV (see Fig. 8, below); while the recoil proton momentum was measured in the spectrometer, the neutron momentum could be inferred from t_r with adequate accuracy to determine whether the recoil protons came from n-p elastic scattering or were associated with pion production (the energies of the latter protons are reduced by at least 135 MeV).

The (p,n) spectra from hydrogen and deuterium at 647 and 805 MeV already have been presented in Fig. 4. (Momentum measurements indicate that the actual energy of the nominal 800 MeV beam was 805 MeV.) The data for hydrogen are reproduced on a larger scale in Fig. 7, along with another spectrum measured at 771 MeV. The reaction in hydrogen is of particular interest because it can only proceed by way of pion production and because the simplicity of the reaction $pp \rightarrow np\pi^+$ makes it a suitable candidate for a theoretical calculation. A first attempt at such a calculation[10] was based on a phenomenological pion-exchange model, dominated by the pion-nucleon interaction in the $\Delta(1232)$ resonant $J = 3/2$, $I = 3/2$ state. While fairly successful in reproducing the spectral shape, the model underestimated the yield in the region where enhancement by the n-p final-state interaction (FSI) was expected. The model has since been improved by including this FSI.[11] As presently constituted it contains four phenomenological parameters: R_{NN} is a length characteristic of the average separation of the two final-state nucleons; f_{NN} is a factor characterizing the attenuation of the final-state N-N interaction caused by the presence of the pion; α_{pr} and α_{sc} account for off-shell effects of the exchanged pion at the production and scattering vertices. These parameters were determined by fitting the 805 MeV data (see Fig. 7), and the success of the model is indicated by the closeness with which the calculation (solid curves) predicts the 647 and 771 MeV spectra when the same values are used for these parameters.

The next simplest (p,n) reaction is that for deuterium. Its spectrum is of interest both because of its similarities to and its differences from the pp → n spectrum (see Fig. 4). The striking difference is the appearance of the intense and narrow peak at approximately the bombarding energy. This peak makes the pd → n reaction the best yet found for the production of monoenergetic neutron beams in this energy region. The mechanism responsible for this peak is quasi-free p-n charge-exchange scattering from the target neutron enhanced by the p-p FSI. The peak can be compared with the predictions of calculations which have been made[12] using both the simple plane-wave Born approximation (BA) and the distorted-wave Born approximation (DWBA) including the FSI of the diproton in the L=0 partial wave. At both energies the integrated cross section in the charge-exchange peak is observed to be ∿29 mb/sr (approximately 58% of the free n-p charge-exchange cross section), whereas the predicted values are ∿25 mb/sr for the BA and ∿60 mb/sr for the DWBA calculations.[12]

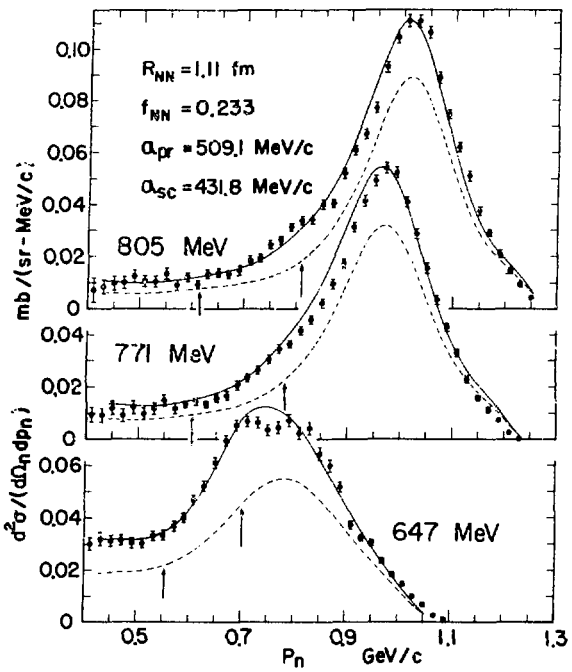

Fig. 7. Neutron spectra at 0° from p-p collisions. The solid line shows the theoretical calculation including the n-p FSI. The dashed line shows the portion not contributed by the n-p FSI in this model. The righthand arrow shows the point in each spectrum at which the n-p FSI is expected to be a maximum. The lefthand arrow shows the point about which there is forward-backward symmetry in the center of mass system.

In the lower-momentum region there is a striking similarity in the shapes of the pp → n spectra and the pd → n spectra, although the distribution is somewhat broadened in the latter case. This is true in both the 647 and 800 MeV spectra. The broadening is expected because of the nucleon motion within the target deuteron.

The remarkable similarity in the shape of the spectra in the low-momentum region leads to the speculation that the same mechanism is operating in both reactions. It seems likely that in the p-d collisions the neutrons of lower momenta are primarily associated with pion production in quasi-free p-p or p-n collisions which proceed through the Δ(1232) channel with the third nucleon as a spectator. This assumption neglects contributions from p-d breakup without pion production as well as pion production which proceeds through π-N isospin 1/2 states in p-n collisions. It leads to the prediction of a 4/3 intensity ratio between the p-d and p-p spectra. The data are reasonably consistent with this prediction.

The (p,n) spectra obtained with more complex targets are shown in Figs. 8 and 9. (The data of Fig. 8 have been published.[13]) All of these spectra are qualitatively similar to the deuterium spectrum, showing both a prominent charge-exchange peak at approximately the bombarding energy and a broad peak associated with pion production in the lower-momentum region. In no case, however, is the isolation of the charge-exchange peak from the background of lower-energy neutrons as good as in the case of deuterium. A comparison of the C and Al spectra at the two energies in

Fig. 8 shows that the integrated intensity in the charge-exchange peak is essentially independent of energy, while the broad peak associated with pion production tends to increase at the higher energy. The same observations seem to hold true for the D spectra in Fig. 4. The systematic trends of some important features of the 800 MeV spectra as a function of mass number A are summarized in Fig. 10. The smoothness of the A-dependences exhibited for the heavier targets is remarkable.

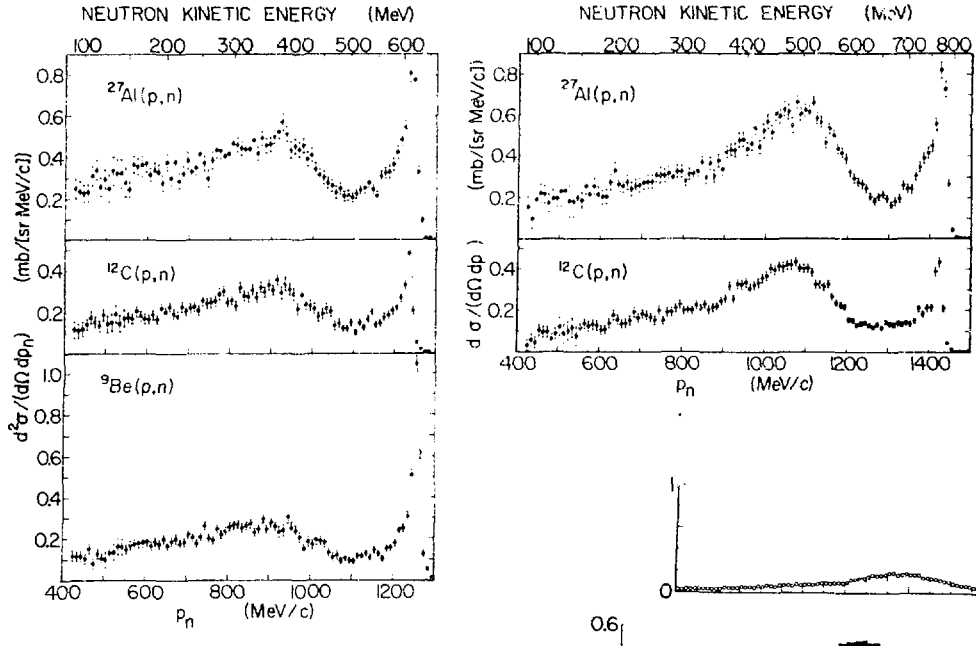

Fig. 8 Neutron spectra observed at 0° in proton bombardment of Be, C and Al. The proton energy was 633 MeV for the spectra on the left and 786 MeV for those on the right.

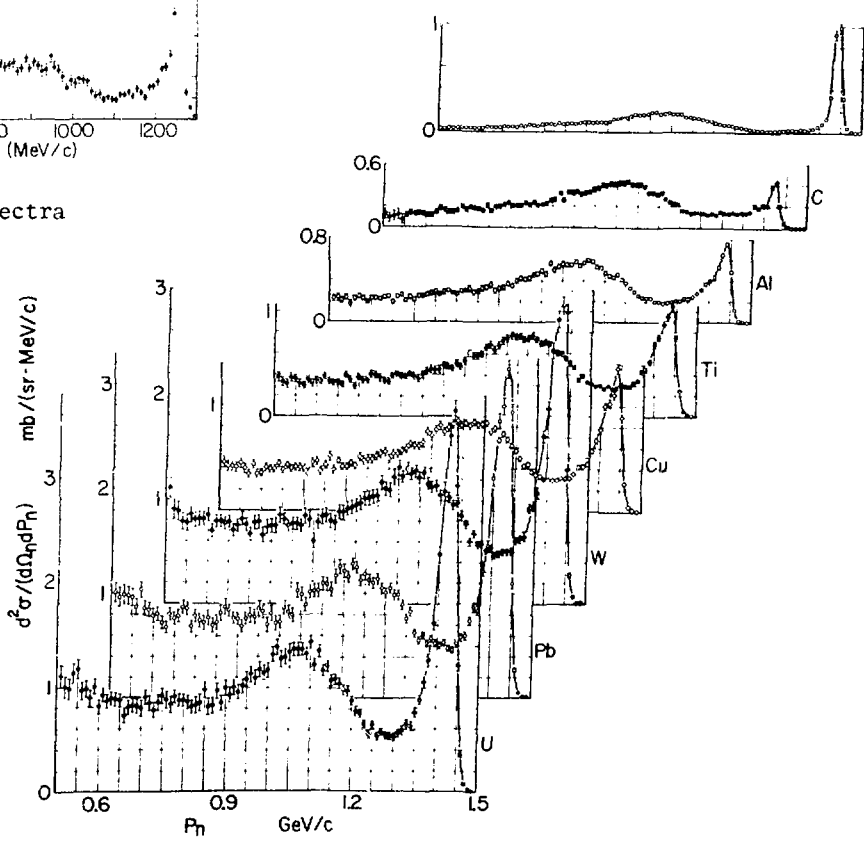

Fig. 9. Neutron spectra observed at 0° in 800 MeV proton bombardment of various targets. (The spectrum for C was obtained at 786 MeV beam energy.

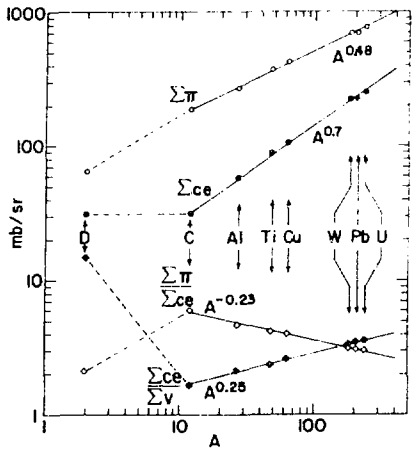

Fig. 10. A-dependence of important features in the spectra of Fig. 9. The curve labeled Σ_π gives the sum over the "pion-production" region (505-1295 MeV/c); that labeled Σ_{ce} gives the sum over the charge-exchange peak (1295-1500 MeV/c); that labeled Σ_{ce}/Σ_v gives the ratio of the sum over the charge-exchange region (1365-1465 MeV/c) to that over the adjacent valley (1245-1345 MeV/c). For the carbon spectrum the momentum windows were adjusted to account for the difference of beam energy.

B. n-p Differential Cross Section

Measurements of the differential cross section $d\sigma/d\Omega$ for n-p elastic scattering have been undertaken at 463, 647 and 800 MeV. The scattering occurs in the LH_2 target (see Fig. 2) and the recoil proton is observed in the MWPC spectrometer. At the same time, deuterons are being produced at forward angles by the reaction $np \rightarrow d\pi^\circ$. The cross section for this reaction is known (with an estimated absolute accuracy of 7%) because by isospin conservation it is one-half the cross section for the $pp \rightarrow d\pi^+$ reaction and the latter cross section is well known.[14] The observation of these deuterons along with the charge-exchange protons provides a convenient means for absolute determination of the neutron flux and thus for absolute normalization of the n-p cross section values.

The 647 MeV data were obtained in two sets of runs, some six months apart. In the first set the spectrometer was fixed at 0° and the θ-acceptance region was varied by making runs with three different magnet currents, giving data of high statistical accuracy on $d\sigma/d\Omega$ for $174.5° < \theta_{cm} < 180°$. In the second set the spectrometer was moved in steps of 4° (lab) from 0° to 60° with magnet current adjusted to compensate for the changing recoil proton momentum, giving data on $d\sigma/d\Omega$ for $50° < \theta_{cm} < 180°$. Every foreground run made with the filled LH_2 target was matched by a background run with the target cell emptied. Relative normalization between runs was provided by both the proton beam integrator and the neutron beam monitor. The absolute normalization was determined from the deuteron yield at forward angles. After background subtraction, the results obtained with different currents in the first set of runs were self-consistent and agreed very well with those obtained in the second set.

The final $d\sigma/d\Omega$ values at 647 MeV were obtained by pooling all of the data and are shown in Fig. 11 along with previously published measurements in the same energy region from Dubna[15] and the Princeton-Penn. accelerator (PPA).[16] A comparison with another recently published measurement from Saclay[17] which covers only the angular region above $\theta_{cm} = 145°$ is shown on an expanded scale in the inset in Fig. 11. (The data shown in the inset have been published.[18]) Our values are seen to fall between those of Dubna and PPA. They are in reasonable agreement with the Saclay values except at extreme backward angles ($\theta_{cm} > 175°$). The plausibility of the shape of the backward peak in the angular distribution can be tested by using the pole-extrapolation method of Chew[19] to extract the pion-nucleon coupling constant from the shape. In this energy region the method is expected to give a reasonably accurate value.[20] When this is done with our 647 MeV data the value obtained is $f^2 = 0.073 \pm 0.003$, in agreement with the value $f^2 = 0.076 \pm 0.003$

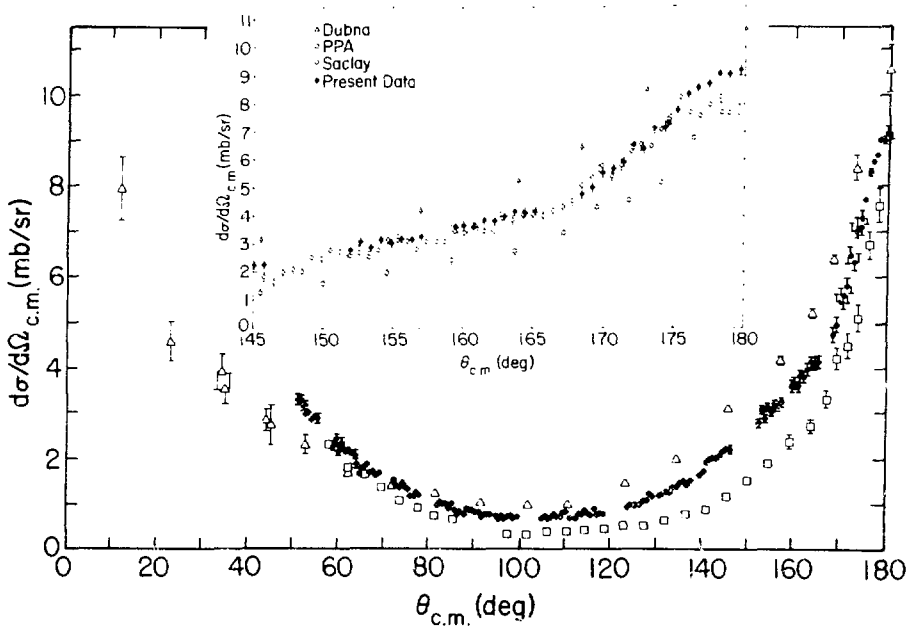

Fig. 11. Differential cross section data for n-p elastic scattering near 640 MeV; Dubna (630 MeV; Ref.15); PPA (649 MeV; Ref. 16); Saclay (649 MeV; Ref. 17); present experiment (647 MeV). The inset shows an expanded view of the back-angle region. For clarity, the Saclay data are omitted from the full angular distribution.

obtained in a phase-shift analysis of p-p scattering data.[21] When the same is done with the Saclay data,[17] a reasonable value for f^2 is obtained only if their back-angle points (175^o) are omitted.

The analysis of the 800 MeV data has recently been completed and the results are being presented here for the first time. They are displayed in Fig. 12 along with data from Saclay[17] and PPA[16] at the nearby energy of 817 MeV. The agreement with the Saclay results is remarkably good. The value of the pion-nucleon coupling constant obtained from our data by the pole-extrapolation method is $f^2 = 0.079 \pm 0.003$, again in good agreement with the value given by the p-p phase-shift analysis.[21]

The analysis of the 463 MeV data has only just begun.

C. $np \to d\pi^\circ$ Angular Distribution

As mentioned in the above subsection, deuterons from the two-body reaction $np \to d\pi^\circ$ are observed at laboratory angles less than $\sim 15°$. In fact, these deuterons serve as the basis for normalization of the n-p differential cross sections. While we cannot determine the absolute differential cross section for the $np \to d\pi^\circ$ reaction from these data (since it is assumed to be half of that for $pp \to d\pi^+$), nevertheless we are able to determine the relative angular distribution with greater accuracy than has previously been achieved, even for the $pp \to d\pi^+$ case. Our results at 647 and 800 MeV are shown in Fig. 13. It has been customary to fit the center of mass differential cross sections with a parameterization of the form[14]

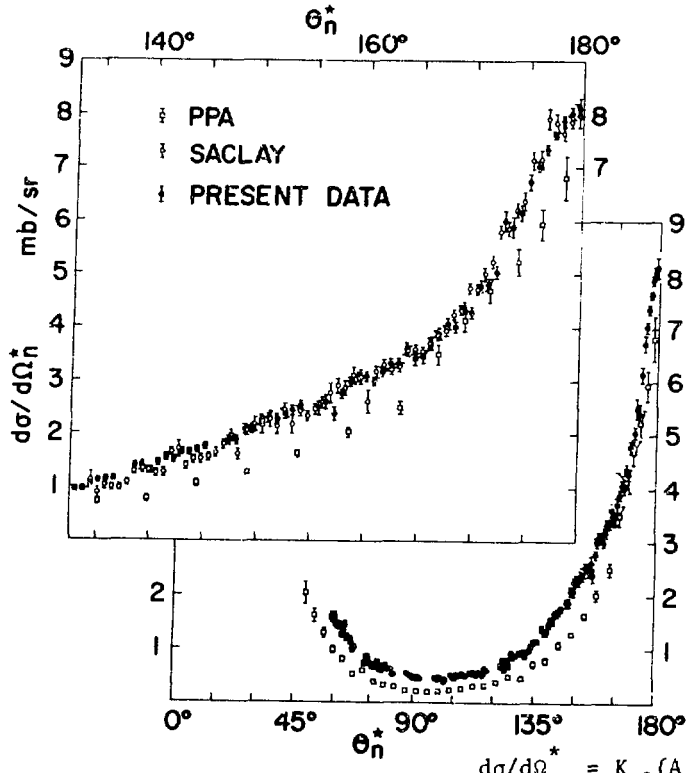

Fig. 12. Differential cross section data for n-p elastic scattering near 810 MeV; PPA (817 MeV; Ref. 16); Saclay (817 MeV; Ref. 17); present experiment (800 MeV). The upper plot shows an expanded view of the back-angle region. For clarity, the Saclay data are omitted from the full angular distribution (lower plot).

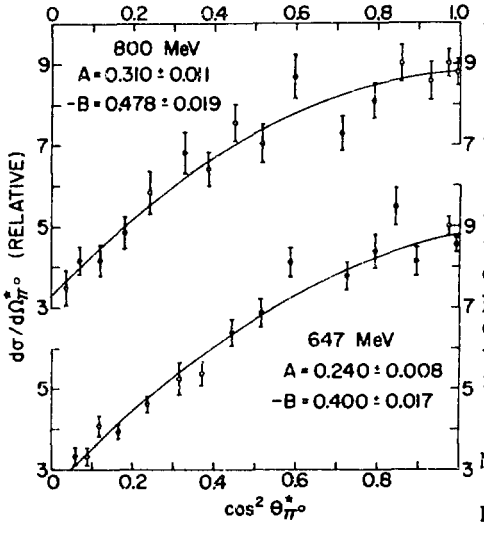

Fig. 13. Relative differential cross sections in the center of mass system for the reaction $np \to d\pi^0$ at 647 and 800 MeV.

$$d\sigma/d\Omega_{\pi^0}^* = K_{\pi^0}(A + \cos^2\theta_{\pi^0}^* - B\cos^4\theta_{\pi^0}^*), \qquad (1)$$

where $\theta_{\pi^0}^*$ is the pion angle in the center of mass system and K_{π^0}, A and B are the fitting parameters. The values of A and B obtained by least-squares fitting of this functional form to the data of Fig. 13 are given in the figure. In Fig. 14 they are compared with all previous determinations of A and B for the $np \to d\pi^0$ reaction in this energy region,[22-25] as well as with the most accurate determinations for the $pp \to d\pi^+$ reaction.[14] It will be noted that the present results are consistent with but more precise than the previous determinations. Also, there is no evidence for violation of charge-independence at this level of accuracy.

Similar data have been obtained at 463 MeV but have not yet been analyzed.

D. $np \to \pi^{\pm}$ Momentum and Angular Distributions at 800 MeV

Data have been obtained on both π^+ and π^- spectra produced at ten laboratory angles in 800 MeV n-p collisions. These data represent a

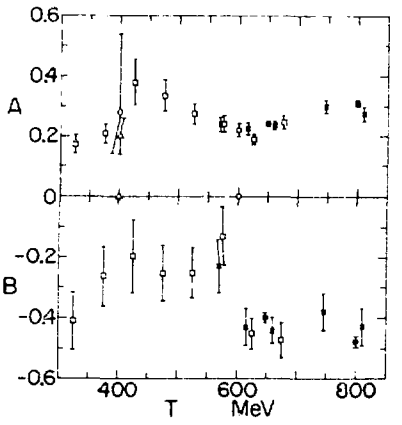

Fig. 14. The coefficients A and B of Eq. 1. Determinations based on the $np \rightarrow d\pi^0$ reaction; open squares - Ref. 22; open triangle - Ref. 23; open diamond - Ref. 24; open circle - Ref. 25; solid circles - present results. The best determinations based on the $pp \rightarrow d\pi^+$ reaction[14] are shown by the crosses. Note that B was assumed to be zero in Refs. 23-25.

considerable improvement over previous studies of these reactions. At present, only a small portion of our data have been analyzed. Preliminary π^- energy spectra obtained at several spectrometer angles are shown in Fig. 15. As more of the data are analyzed, the statistical accuracy of these spectra will be improved.

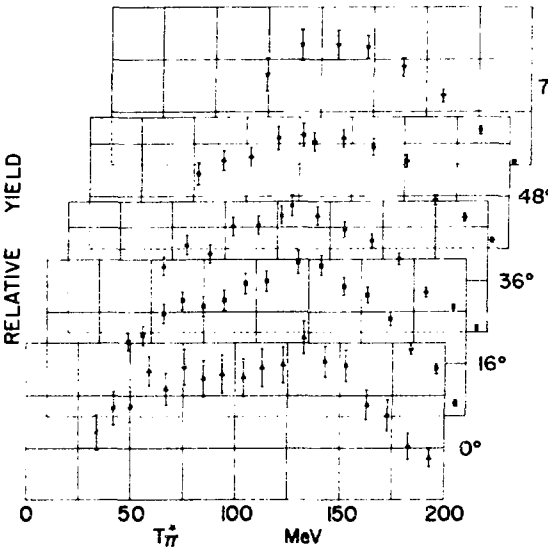

Fig. 15. Center of mass energy spectra for π^- meson production in n-p collisions at 800 MeV. Absolute normalization of the cross sections has not yet been established. The angles quoted are nominal spectrometer laboratory angles. They correspond approximately to center of mass angular regions of 0-3°, 29-35°, 63-73°, 80-90°, and 107-119°, respectively.

E. Neutron Induced Reactions on Deuterium

Proton and deuteron spectra produced in 800 MeV neutron bombardment of deuterium have been measured at spectrometer angles of 0°, 4°, 8° and 16°. The prominent reactions seen include n-d elastic scattering, the quasifree pion-producing reactions $np' \rightarrow d\pi^0$ and $nn' \rightarrow d\pi^-$, and quasifree n-p scattering. While the analysis of the data is incomplete, preliminary results for the quasifree n-p scattering are available and are compared in Fig. 16 with previous data from Harvard[26] at 152 MeV as well as with our measurement of the free n-p cross section at 800 MeV. The free n-p cross section at 152 MeV (the solid line) is that given by the Yale phase-shift prediction YLAN4MP. The quantity t is the square of the exchange four-momentum transfer. In the limit of small t we find the ratio of quasifree to free cross sections to be 0.51, while the ratio was 0.65 at 152 MeV.

F. Neutron Induced Reactions on Heavier Targets

Proton, deuteron and triton spectra produced at 0°, 16° and 24° have been obtained for 800 MeV neutron bombardment of ^{6}Li, ^{7}Li, ^{9}Be, C, ^{27}Al and Cu targets. While preliminary results have been reported[27] the analysis of these data is still incomplete. A sample of the results is shown in Fig. 17.

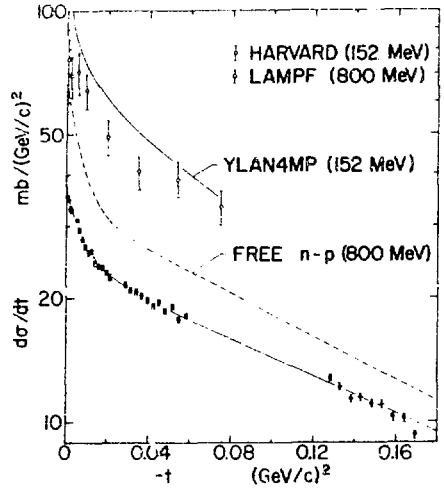

Fig. 16. Differential cross section for $^2H(n,p)$ quasifree scattering. The 152 MeV data and curve have been multiplied by a factor of five so as to displace them upward in an attempt to avoid confusion.

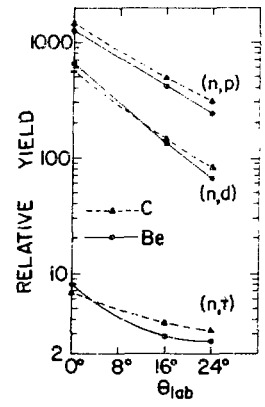

Fig. 17. Relative yields of protons, deuterons and tritons produced in 800 MeV neutron bombardment of Be and C.

VI. ACKNOWLEDGMENTS

A large number of people have made significant contributions to the success of this experimental program. Of particular importance were the assistance of K. D. Williamson, Jr., J. H. Fretwell and J. Novak in cryogenic development, of A. C. Niethammer in programming, of D. Brown in MWPC electronics development, and of S. Cohen in MWPC development. J. Boissevain provided valuable technical support in many areas. The expert efforts of the LAMPF operations personnel have been essential for our success. The important assistance of Mahavir Jain in the preparation of this paper is gratefully acknowledged.

REFERENCES

*This work was supported by the U. S. Energy Research and Development Administration.

1) Mahavir Jain, VII International Conference on Few Body Problems in Nuclear and Particle Physics, Delhi, Dec. 29, 1975-Jan. 4, 1976.

2) D. M. Wolfe, ibid.

3) K. D. Williamson, et al., Advances in Cryogenic Engineering 19, 241 (1974).

4) P. J. Tallerico, Los Alamos Report LA-UR 75-900 (1974).

5) C. W. Bjork, et al., Phys. Letters (to be published).

6) D. W. Werren, et al., Los Alamos Report LA-5396-MS (1973).

7) L. R. Biswell and R. E. Rajala, Los Alamos Report LA-4916-MS (1972).

8) J. C. Hiebert and A. C. Niethammer, Los Alamos Report LA-5609-MS (1974).

9) Mahavir Jain, H. C. Bryant and D. W. Werren, (manuscript in preparation).

10) W. R. Gibbs, et al., Conference on High Energy Physics and Nuclear Structure, Santa Fe and Los Alamos (1975), abstract no. IV.C.12.

11) G. J. Stephenson, et al., (manuscript in preparation).

12) D. S. Ward, PhD Dissertation, University of Texas, Austin (1971;unpublished).

13) C. G. Cassapakis, et al., Phys. Letters (to be published).

14) C. Richard-Serre, et al., Nucl. Phys. B20, 413 (1970).

15) L. N. Glonti, et al., Report P1-6387, Joint Institute for Nuclear Research, Dubna (1972).

16) P. F. Shepard, et al., Phys. Rev. D 10,2735 (1974).

17) G. Bizard, et al., Nucl. Phys. B85, 14 (1975).

18) M. L. Evans, et al., Phys. Rev. Letters 36, 497 (1976).

19) G. F. Chew, Phys. Rev. 112, 1380 (1958).

20) P. Cziffra and M. J. Moravcsik, Phys. Rev. 116, 226 (1959).

21) M. H. MacGregor, R. A. Arndt and R. M. Wright, Phys. Rev. 169, 1128 (1968).

22) S. S. Wilson et al., Nucl. Phys. B33, 253 (1971).

23) R. H. Hildebrand, Phys. Rev. 89, 1090 (1953).

24) R. A. Schluter, Phys. Rev. 96, 734 (1954).

25) V. B. Fliagin et al., J. Exptl. Theoret. Phys. (U.S.S.R.) 35, 854 (1958); translation: Soviet Phys. JETP 8, 592 (1959) .

26) D. F. Measday, Phys. Lett. 21, 66 (1966).

27) P. J. Riley, et al., Bull. Am. Phys. Soc. 21, 586 (1976).

ML 2 - NEUTRON PHYSICS AT LAMPF - L. C. Northcliffe, Jr. (Texas A & M Univ., USA)

Cranberg (TDN, Inc.):

A number of years ago, Professor V. F. Weisskopf, writing in the Scientific American, claimed that one of the spin-offs from high-energy physics is the technology of fast timing. This prompted me to send a letter to the Scientific American pointing out that the origin of nanosecond timing and beam-pulsing technology lay not in high-energy physics, but rather in fast-neutron technology - a point which several colleagues engaged in high-energy physics research have acknowledged. Although this letter was never published, it seemed appropriate to mention this point on this occasion, since this review has felicitously been devoted to both high-energy and neutron physics.

*U.S. GOVERNMENT PRINTING OFFICE: 1976-641-358/20

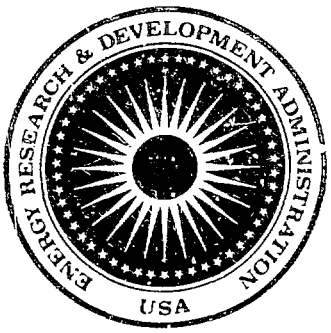
ENERGY RESEARCH & DEVELOPMENT ADMINISTRATION
USA